RIKEN Accelerator Progress Report 2010

vol. 44

BOOK & CD-ROM

独立行政法人理化学研究所　仁科加速器研究センター

RIKEN Nishina Center for Accelerator-Based Science

RIKEN Accelerator Progress Report 2010

vol. **44**

BOOK & CD-ROM

独立行政法人理化学研究所　仁科加速器研究センター

RIKEN Nishina Center for Accelerator-Based Science

Wako, Saitama, 351-0198 JAPAN

GRAVURES & HIGHLIGHTS OF THE YEAR

《Selection process of gravures and highlights》

Gravures and highlights will be selected in two-steps process. In the first step, referee will recommend manuscript for gravure or highlight. With the above recommendation, the editors will then give secondary recommendation.

After the following 1 and 2 are comprehensively considered, the editor-in-chief will draft a manuscript idea which will be thoroughly discussed by the editors for the final decision:

1. Approval based on the editor's judgment as an expert/non-expert in the field (there by agreeing with the referee's recommendation)
2. Additional recommendation based on the editor's expertise.

β-Decay Half-Lives of Very Neutron-Rich Kr to Tc Isotopes†

S. Nishimura,*1 Z. Li,*1 H. Watanabe,*1 K. Yoshinaga,*1,2 T. Sumikama,*2 K. Yamaguchi,*3 M. Kurata-Nishimura,*1 G. Lorusso,*1,5 Y. Miyashita,*2 A. Odahara,*3 J. Chiba,*2 H. Baba,*1 J.S. Berryman,*4,5 N. Blasi,*6 A. Bracco,*6,7 F. Camera,*6,7 P. Doornenbal,*1 S. Go,*8 T. Hashimoto,*8 S. Hayakawa,*8 C. Hinke,*9 E. Ideguchi,*8 T. Isobe,*1 Y. Itou,*3 D.G. Jankins,*10 Y. Kawada,*11 N. Kobayashi,*11 Y. Kondo,*11 R. Krüchen,*9 S. Kubono,*8 H.J. Ong,*12 S. Ota,*8 Zs. Podolyák,*13 H. Sakurai,*1 H. Scheit,*1 K. Steiger,*9 D. Steppenbeck,*1 K. Sugimoto,*2 T. Tachibana,*14 A. Takashima,*3 K. Tajiri,*3 T. Teranishi,*15 Y. Wakabayashi,*16 P.M. Walker,*13 O. Wieland,*6 and H. Yamaguchi*8

[Nuclear structure, unstable nuclei, r-process]

The study of the elemental distribution along the r-process path requires sensitive β-decay related information such as β-decay half-lives, β-delayed neutron-emission probabilities, and nuclear masses. In particular, determination of the timescale that governs matter flow from the r-process "seeds" to the heavy nuclei, as well as the distribution in the r-process peaks, depends sensitively on decay half-lives[1,2)]. Isotopes with extreme neutron-to-proton ratios in the mass region $A = 110 - 125$ have attracted special attention since theoretical r-process yields are found to underestimate isotopic abundances observed in the predicted global abundances by an order of magnitude or more[1,3,4)].

Decay spectroscopy of very neutron-rich nuclei around $A = 110$ was performed at the recently commissioned RIBF facility at RIKEN. A secondary beam, comprised of a cocktail of neutron-rich nuclei, was produced by in-flight fission of a 345-MeV/nucleon ^{238}U beam in a 550-mg/cm^2 Be target. Nuclei in the secondary beam were identified on an event-by-event basis measuring their A/Q and Z (see Fig. 1); these two quantities were deduced by combining the projectile time-of-flight and magnetic rigidity from BigRIPS, and from an energy-loss measurement in an ionization chamber at the end of the ZeroDegree spectrometer (ZDS), respectively.

The nuclei transported through the ZDS were implanted in a nine-layer double-sided silicon-strip detector (DSSSD) system[5)] with a combined thickness of 9×1 mm. Each DSSSD was segmented into 16 strips, horizontally on the front side and vertically on the back, each with a width of 3 mm. The implantation position and timing of the identified nuclei were reconstructed using their momenta and the energy deposited in each strip of the second DSSSD. Due to the relatively large energy deposition of individual nuclei in the second DSSSD, a low-gain readout system with a dynamical energy range above 4 GeV was used in parallel to the one with high gain. The ion implantation rate throughout the 8 hours of beam time was about 8 particles per second[6)]. A decay curve was constructed for each nuclide by measuring the correlation between heavy-ion implantations and subsequent β particles detected within 3.3 mm of each other, and

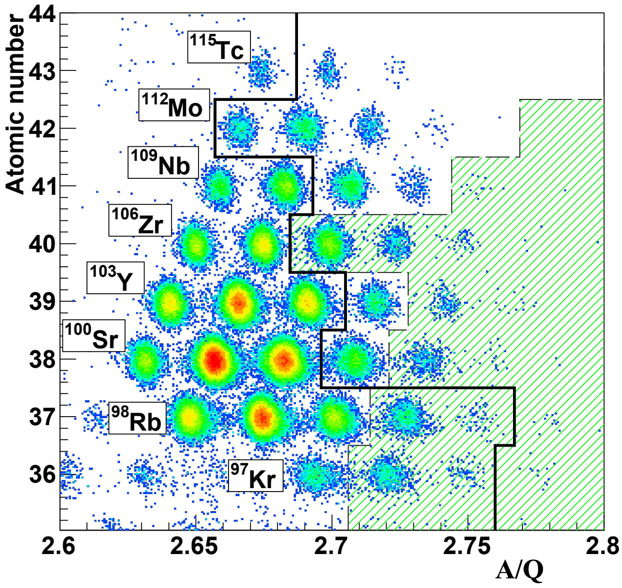

Fig. 1. Particle-identification plot from 8 hours of accumulated beam time. The lowest-mass isotope from each isotopic chain was tagged for reference purposes. Isotopes with previously known half-lives lie to the left of the black solid line. The shaded area represents the r-process waiting points predicted by the ETFSI-Q mass model, within the classical r-process model[9)].

† Condensed article in Phys. Rev. Lett. **106**, 052502 (2011)

*1 RIKEN Nishina Center
*2 Department of Physics, Tokyo Univ. of Science
*3 Department of Physics, Osaka Univ.
*4 Nucl. Sci. Div., LBNL, USA
*5 NSCL, Michigan State Univ., USA
*6 INFN, Sezione di Milano, Italy
*7 Dipartimento di Fisica, Università di Milano, Italy
*8 Center for Nuclear Study (CNS), Tokyo Univ.
*9 Physik Dep., Technische Univ. München, Germany
*10 Department of Physics, Univ. of York, United Kingdom
*11 Department of Physics,Tokyo Institute of Technology
*12 Research Center for Nuclear Physics, Osaka Univ.
*13 Dep. of Phys., Univ. of Surrey, United Kingdom
*14 4 Senior High School of Waseda Univ.
*15 Department of Physics, Kyushu Univ.
*16 Japan Atomic Energy Agency, Ibaraki

in the same DSSSD layer. The maximum-likelihood analysis technique was used to extract β-decay half-lives ($T_{1/2}$) from the decay spectra. All necessary components were taken into consideration during the fitting procedures: the β-detection efficiency, background rate, daughter and granddaughter half-lives, including the nuclides populated by β-delayed neutron emission, and β-delayed emission branches (P_n).

The β-decay half-lives of the very neutron-rich nuclides $^{97-100}$Kr, $^{97-102}$Rb, $^{100-105}$Sr, $^{103-108}$Y, $^{106-110}$Zr, $^{109-112}$Nb, $^{112-115}$Mo, and $^{115-117}$Tc, all of which lie close to the astrophysical r-process path, have been measured for the first time (for 18 nuclei) or their uncertainties have been reduced significantly. The results of the present work are compared to two theoretical calculations that are used to model the astrophysical r-process[4]. The first is the finite-range droplet mass model with the deformed quasiparticle random-phase-approximation (FRDM+QRPA)[7] as well as the new version with the first-forbidden part of β decay taken[1]. The second is KTUY+GT2, i.e., the KTUY mass formula combined with the 2nd generation of the gross theory of β-decay (GT2) without bottom-raising[8].

The half-lives of the Kr to Tc isotopes are displayed as a function of neutron number and compared to the predictions of the two models discussed above in Figs. 2(a)-(h). The KTUY+GT2 model overpredicts

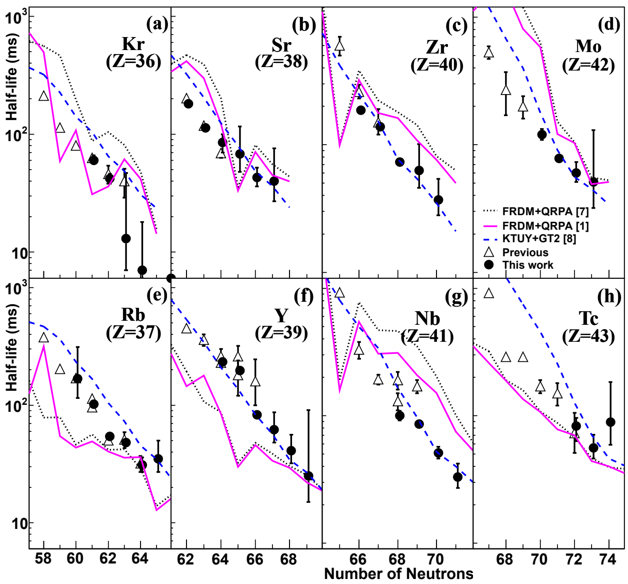

Fig. 2. Neutron number dependence of β-decay half-lives for [top] even-Z (a) Kr, (b) Sr, (c) Zr, and (d) Mo, and [bottom] odd-Z (e) Rb, (f) Y, (g) Nb, and (h) Tc. Filled circles and open triangles represent results from the present work and those from previous studies, respectively.

the $T_{1/2}$ values for Mo and Tc below $N = 70$, but generally reproduces the experimental data more accurately than the FRDM+QRPA calculation does for the other isotopic chains.

The heavier neutron-rich $_{36}$Kr to $_{42}$Mo isotopes measured in this work are proposed as waiting-point nuclei by some models of the r-process[9]. The systematic deviation of the FRDM+QRPA model, which generally underpredicts the half-lives of the odd$-Z$ nuclides and overpredicts those of the even$-Z$ nuclides, seems to improve with increasing neutron richness.

The data suggest that one of the main problems associated with β-decay half-life predictions is related to uncertainties involved with binding-energy calculations and β-strength functions.

As discussed by P. Möller et al.[1], the sum of the half-lives of the r-process nuclei up to the mid-mass region, i.e., around $A = 130$, determines the rate of r-matter flow at $N = 82$. Following this prescription, the relatively short half-lives of the Zr and Nb isotopes deduced in the present study suggest a further speeding up of the classical r-process, and shed light on the issue concerning the low production rates of elements beyond the second r-process peak. The results presented here also make an impact on the abundances of nuclei at the second peak, since the peak position and shape in the solar abundances around $A = 110 - 140$ can be reproduced better by decreasing the half-life of the r-process nuclei by a factor of 2 to 3[2].

In summary, the new results suggest a systematic enhancement of the β-decay rates of the Zr and Nb isotopes by a factor of 2 or more around $A = 110$ with respect to the predictions of the FRDM+QRPA model[1,7]. More satisfactory predictions of the half-lives from the KTUY+GT2 model[8], which employs larger Q_β-values, indicate a shorter timescale for matter flow from the r-process "seeds" to the heavy nuclei.

References

1) P. Möller et al.: Phys. Rev. C **67**, 055802 (2003).
2) S. Wanajo, et al., Astro. J **606**, 1057-1069 (2004).
3) K.-L. Kratz, et al., Astro. J **403**, 216 (1993).
4) J.M. Pearson et al., Phys. Lett. B **387**, 455 (1996).
5) N. Uematsu and S. Nishimura, RIKEN Acc. Prog. Rep. 41 (2008) 151.
6) S. Nishimura: AIP Conf. Proc., Vol 1269, **91** (2010).
7) P. Möller et al.: A. Data N. Data T. **66**, 131 (1997).
8) H. Koura et al: Prog. Theor. Phys. **113**, 305 (2005); T. Tachibana et al.: Proc. of ENAM 95, Int. Conf. on Exotic Nuclei and Atomic Masses, (Editions Frontieres, Gif-sur-Yvette) 763 (1995).
9) H. Schatz, et al. Astrophys. J. **583**, 87 (2003).

Identification of β^+-type Isovector Spin Monopole Resonance via $(t, {}^3\mathrm{He})$ Reactions at 300 MeV/nucleon

K. Miki*1, H. Sakai, T. Uesaka*2, H. Baba, G.P.A. Berg*3, N. Fukuda, D. Kameda, T. Kawabata*4, S. Kawase*2, T. Kubo, S. Michimasa*2, H. Miya*2, S. Noji*1, T. Ohnishi, S. Ota*2, A. Saito*2, Y. Sasamoto*2, M. Sasano*5, S. Shimoura*2, H. Takeda, H. Tokieda*2, K. Yako*1, Y. Yanagisawa, and R.G.T. Zegers*5

[Nuclear structure, giant resonance, spin-isospin response, charge-exchange reaction]

The isovector spin monopole resonance (IVSMR) of the β^+ type has been identified for the first time via the ^{208}Pb, ^{90}Zr$(t, {}^3\mathrm{He})$ reactions at 300 MeV/nucleon. The IVSMR has long been an important topic of interest in the study of spin-isospin responses in nuclei, but it has not been clearly identified, especially for the β^+ side. We measured the double differential cross sections for the ^{208}Pb, ^{90}Zr$(t, {}^3\mathrm{He})$ reactions at 300 MeV/nucleon at $0 \le E_x \le 40$ MeV and $0 \le \theta \le 4°$. The experiment was performed in November 2009 at the RIBF facility using the spectrometer SHARAQ[1]. Details of the experimental setup can be found in Ref.[2]. In this article, we report the results of the experiment, especially the evidence obtained for the β^+-type IVSMR.

We performed multipole decomposition (MD) analysis[3] of the obtained differential cross section spectra in order to extract the monopole ($\Delta L = 0$) component precisely. Figure 1 shows the result of the MD analysis for the ^{90}Zr$(t, {}^3\mathrm{He})$ spectrum measured at 0.27°. A significant amount of the monopole component was observed up to the high-excitation-energy region. Because the IVSM and Gamow–Teller (GT) transitions are both $\Delta L = 0$ transitions, further decomposition is impossible by MD analysis, in principle. Therefore, we separated the GT and IVSM components by comparing the present spectra with the reported (n, p) spectra[4]. Since the $(t, {}^3\mathrm{He})$ reaction has higher sensitivity to the IVSMR than does the (n, p) reaction, the cross section of the IVSMR can be extracted from the difference spectrum between these two reactions. Figure 2 (a) shows a comparison of the monopole cross section between the $(t, {}^3\mathrm{He})$ and (n, p) reactions. The (n, p) spectrum is appropriately normalized so that the GT components contained in the two spectra are the same. A significant amount of enhancement for the $(t, {}^3\mathrm{He})$ reaction was obtained and it should be identified as the IVSMR. Figure 2 (b) represents the IVSM cross section obtained by subtracting the normalized (n, p) component from the $(t, {}^3\mathrm{He})$ cross section, where a small correction was applied by distorted-wave Born approximation calculations. The obtained distribution could be mostly reproduced by the Tamm–Dancoff approximation (TDA) calculations[5] shown by the blue and green lines in Fig. 2 (b). Interestingly, the calculation significantly underestimated the spectrum at $E_x > 30$ MeV.

The existence of the IVSMR (β^+) is also suggested by the obtained ^{208}Pb$(t, {}^3\mathrm{He})$ data.

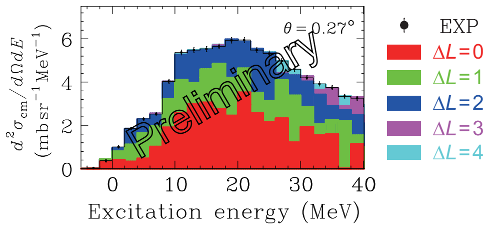

Fig. 1. The result of MD analysis for the ^{90}Zr$(t, {}^3\mathrm{He})$ spectrum measured at 0.27°. A significant amount of the monopole component (red) was found up to the high-excitation-energy region.

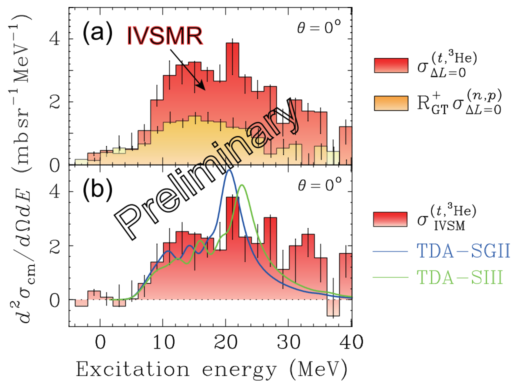

Fig. 2. (a) Comparison of the monopole cross section between the $(t, {}^3\mathrm{He})$ and (n, p) reactions. The enhancement for the $(t, {}^3\mathrm{He})$ spectrum can be identified as the IVSMR. (b) The obtained IVSM cross section and comparison with the Tamm–Dancoff approximation (TDA) calculations for the IVSM strength (arbitrarily normalized).

References
1) T. Uesaka *et al.*: Nucl. Inst. Meth. B **266** (2008) 4218.
2) K. Miki *et al.*: RIKEN Accel. Prog. Rep. **43** (2010) 7.
3) M. Ichimura *et al.*: Prog. Part. Nucl. Phys. **56** (2006) 446.
4) K. Yako *et al.*: Phys. Lett. B **615** (2005) 193.
5) I. Hamamoto and H. Sagawa: Phys. Rev. C **62** (2000) 024319.

*1 Department of Physics, University of Tokyo
*2 CNS, University of Tokyo
*3 JINA, Department of Physics, University of Notre Dame
*4 Department of Physics, Kyoto University
*5 NSCL, Michigan State University

Cb-TDHFB calculation for isovector dipole mode of heavy nucleus

S. Ebata,[*1] T. Nakatsukasa, T. Inakura, K. Yoshida, Y. Hashimoto,[*1,*2] and K. Yabana[*1,*2]

[Nuclear structure, heavy nucleus]

With the availability of new radioisotope beam facilities around the world, it has become possible to generate and measure unstable nuclei over a wide range of nuclear masses. For a systematic theoretical investigation of unstable nuclei, we should take into account the effects of deformation and pairing correlation. A combination of the Hartree-Fock-Bogoliubov method and quasi particle random-phase approximation (HFB+QRPA) is a candidate for such a framework, and it is applicable to a wide range of light and heavy nuclei. However, in this framework, considerable efforts are required for coding the programs, and a significant number of computational resources are necessary[1)].

We propose the canonical-basis time-dependent Hartree-Fock-Bogoliubov (Cb-TDHFB) theory in the three-dimensional coordinate-space representation, which can take into account the effects of nuclear deformation without spatial symmetry restriction while treating the pairing correlation in Bardeen-Cooper-Schrieffer(BCS)-like approximation. The Cb-TDHFB theory can be derived from the full TDHFB equation by utilizing the canonical-basis representation, which diagonalizes the normal density matrix $\rho_{ij} = \langle c_j^\dagger c_i \rangle$, and by introducing a BCS-like pairing functional: $E_{\rm pair} = -\sum_{k,l>0} G_{kl}\kappa_k^*(t)\kappa_l(t)$, where $\kappa_l = u_l v_l$ and u_l, v_l correspond to the time-dependent BCS factors for the canonical pair of states $\phi_l(\boldsymbol{r},t)$ and $\phi_{\bar{l}}(\boldsymbol{r},t)$. The state $\bar{l}$ is not necessarily the time-reversed state of the state l. Details of the Cb-TDHFB equations and the adopted functionals are given in Ref.[2)]. The results for light nuclei have been reported previously[2,3)].

This year, we extended the application of the Cb-TDHFB theory to heavy nuclei. We have confirmed that the Cb-TDHFB theory can be used to describe various properties of heavy and deformed nuclei, thereby reducing the computational cost of the calculation drastically. We show the result for ^{172}Yb as a typical example.

We solve the Cb-TDHFB equations in real time and calculate the linear response of the nucleus. For the linear-response calculation, we consider an external field $\hat{V}_{\rm ext}(\boldsymbol{r},t)$, which is weak and instantaneous in time, $\hat{V}_{\rm ext}(\boldsymbol{r},t) \equiv -k\hat{F}\delta(t)$, where $\hat{F}$ is a one-body operator and $k \ll 1$. In this study, we choose the isovector dipole operator, $\hat{F}_{\rm IVD} = (N/A)\sum_p \hat{z}_p - (Z/A)\sum_n \hat{z}_n$. We calculate the time evolution of the expectation value of $\hat{F}_{\rm IVD}$ and obtain the strength function $S(\hat{F}_{\rm IVD}; E)$ by Fourier transformation[2)].

Figure 1 shows the photo nuclear reaction cross section of ^{172}Yb. The black symbols show the experimental data[4)], and the lines show the results computed using the SkM* parameter set. In this calculation, the ground state of ^{172}Yb shows prolate deformation ($\beta = 0.32$), and both neutrons and protons are in the superfluid phase ($\Delta_{\rm n} = 0.76, \Delta_{\rm p} = 0.55$ MeV). In this calculation, we employ a schematic pairing functional[3)], which is a very good approximation to the HFB+QRPA with a δ-type paring functional[1)]. The computational cost for this Cb-TDHFB calculation is only about 300 CPU hours. This should be compared with the deformed HFB+QRPA calculation proposed by Terasaki and Engel[1)], which requires about 100,000 CPU hours, using ten thousands of processors.

It has been confirmed that the Cb-TDHFB theory describe the dipole resonances of deformed heavy nuclei at a reasonable computational cost. Currently, we are developing a Cb-TDHFB code for parallel computing to facilitate systematic calculations for heavy nuclei. We also plan to use this code to investigate nuclear collision dynamics.

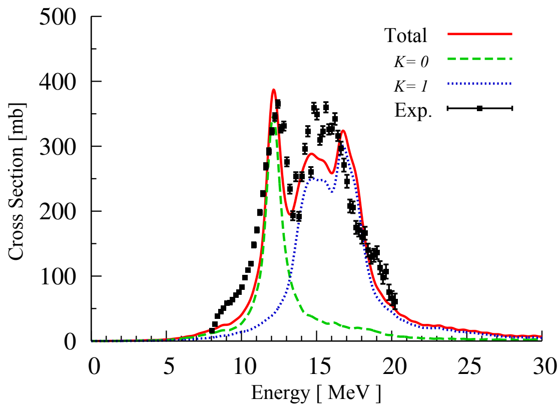

Fig. 1. Photo nuclear reaction cross section of ^{172}Yb. Black symbols show the experimental data[4)]. Solid line shows the total cross section, which can be decomposed into $K = 0$ and $K = 1$. The Skyrme functional of the SkM* parameter set and the smoothing parameter $\Gamma = 1$ MeV are used.

References
1) J. Terasaki and J. Engel: Phys. Rev. C **82**, 034326 (2010).
2) S. Ebata *et al.*: Phys. Rev. C **82**, 034306 (2010).
3) S. Ebata *et al.*: RIKEN Accel. Prog. Rep. **43**, 51 (2009).
4) A. M. Goryachev and G. N. Zalesnyy: Vopr. Teor. Yad. Fiz. **5**, 42 (1976).

*1 Graduate School of Pure and Applied Sciences, University of Tsukuba
*2 Center for Computational Science, University of Tsukuba

Calculations of Branching Ratios for Radiative-Capture, One-Proton, and Two-Neutron Channels in the Fusion Reaction ^{209}Bi+^{70}Zn[†]

T. Ichikawa[*1] and A. Iwamoto[*2]

[Nuclear reaction, Statistical model, Superheavy nuclei]

The syntehsis of superheavy elements is a challenging task and is important for exploring the upper bound of the existence of heavy-mass nuclei. It is necessary to identify the evaporation residue formed when an the excited fusion product is de-excited to a certain stable state by particle or gamma-ray emissions. In experiments, the synthesized elements can be identified by determing the alpha-decay chains to known nuclei.

However, this is not always straightforward in the case of odd-odd evaporation residues because in such alpha-decay chains, one can expect not only ground-state-to-ground-state alpha decay but also the involvement of excited states. It is difficult to directely compare the observed alpha-decay energy and lifetime with the measured values for known products in the decay chain. It is thus desirable to calculate the confidence level with which other reaction channels can be excluded from the reaction mechanism consideration. Here, we investigate the sensitivity of the assignment of the evaporation residue to different model assumptions.

In this study, we focus on the experiment performed by Morita *et al.* to produce element 113[1,2)]. The reaction channel of this experiment for the two observed alpha chains was assigned as the one-neutron (1n) evaporation channel. We therefore estimate the probability of the radiative-capture, two-neutron evaporation, and one-proton evaporation channels relative to the one-neutron evaporation channel in standard theoretical models.

For such estimations, it is difficult to calculate the non-1n reaction by using the Monte Carlo simulation for the de-excitation process because of its extremely low survival probability. Therefore, we employ the "fusion-by-diffusion" (FBD) model[3,4)], which consists of simple analytic expressions. We extend it to the non-1n reaction channels.

One difficulty in the estimation arises from the fact that the de-excitation process is very sensitive to the level-density parameter and the height of the fission barrier. To reduce uncertainties resulting from this sensitivity, we estimate worst-case scenarios for different relative probabilities by substantially varying the level-density parameter and the fission-barrier height.

From the calculated results, we find that the 2n reaction is the main decay branch among the non-1n reaction channels. Figure 1 shows the worst-case scenario for the resulting two-neutron evaporation. The solid and dashed lines indicate the calculated results for the 1n and 2n reaction channels, respectively, obtained with standard parameters. The dashed line shows the result obtained with the level-density parameter $a_n \times 1.1$ for the 2n reaction and a decrease in the fission-barrier height by 1 MeV. The filled arrow indicates the excitation energy corresponding to the experimental incident energy. The light-gray area denotes the incident-energy distribution in the target for the worst-case scenario.

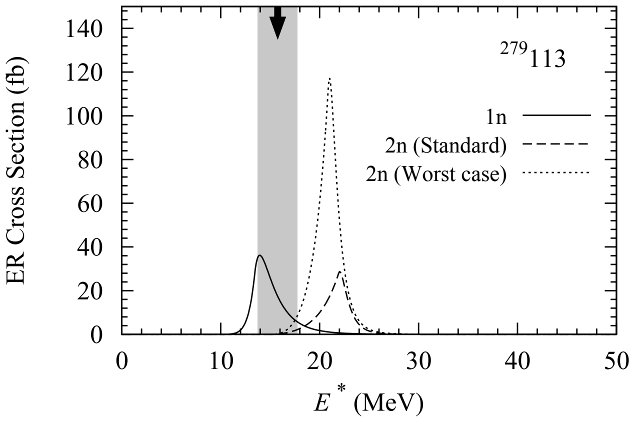

Fig. 1. Evaporation residue cross sections for the 2n and 1n reactions versus excitation energy of the compound nucleus ^{279}113.

We obtain the maximum branching ratios of the one-proton, radiative-capture, and 2n-reaction channels to the 1n-reaction channel, and they are 4.97×10^{-3}, 1.7×10^{-3}, and 7.91×10^{-2}, respectively. For the total non-1n branching ratio, we obtain a probability of 8.51×10^{-2}, which is fairly small.

References
1) K. Morita *et al.*: J. Phys. Soc. Jpn. **73**, 2593 (2004).
2) K. Morita *et al.*: J. Phys. Soc. Jpn. **76**, 045001 (2007).
3) W. J. Świątecki, K. Siwek-Wilczyńska, and J. Wilczyński: Acta Phys. Pol. **34**, 2049 (2003).
4) W. J. Świątecki, K. Siwek-Wilczyńska, and J. Wilczyński: Phys. Rev. C **71**, 014602 (2005).

† Condensed from the article in J. Phys. Soc. Jpn. **79**, 074201 (2010).
*1 Yukawa Institute for Theoretical Physics, Kyoto University
*2 Japan Atomic Energy Agency

Measurement of Single-Spin Asymmetries of W-Boson Production in Polarized $p + p$ Collisions with $\sqrt{s} = 500$ GeV

K. Karatsu*1 from the PHENIX Collaboration

[nucleon spin, W boson, polarized parton distribution]

While the polarizations of valence quarks in the proton have been determined well by DIS (Deep Inelastic Scattering) and semi-inclusive DIS[1)], a large uncertainty pertaining to the polarized parton distribution function (PDF) of sea quarks still exists. One of the main objectives of polarized $p + p$ collisions at RHIC is to measure the polarized PDF of the sea quarks by producing W bosons[2)]. The longitudinal single-spin asymmetry (A_L) in W-boson production is a useful tool for measuring the polarization of the sea quarks since the chirality of the interacting quarks is fixed. It is also possible to identify the flavor of the sea quarks by the charge-separated measurement of W^+/W^-. A_L is given by:

$$A_L = \frac{D}{P} \cdot \frac{N^+ - R \cdot N^-}{N^+ + R \cdot N^-}, \tag{1}$$

where N^+ (N^-) is the number of W events from a beam of positive (negative) helicity and R is the ratio of the luminosity of the positive- and negative-helicity beams. P is the beam polarization and D is the dilution correction to account for backgrounds.

A run held in 2009 at RHIC (RHIC Run 9) was the first that involved collisions with $\sqrt{s} = 500$ GeV. This was also the first opportunity for the PHENIX[3)] to measure significant amounts of W bosons, and an attempt to measure $e^{\pm}$'s produced by W decays was made using the PHENIX central arms ($|\eta| < 0.35$). The W-boson production was measured through the inclusive $pp \to e^{\pm} + X$ production, where $e^{\pm}$'s with transverse momenta of $p_T > 30$ GeV/c are mainly produced by W and Z decays. Since the PHENIX cannot distinguish between $e^{\pm}$'s produced by W decays and those produced by Z decays, the measured A_L includes both these components.

To determine A_L from a sample of high-p_T $e^{\pm}$'s with minimal background contamination, an energy-momentum matching cut (E/p cut) and isolation cut, which requires no jet activity in the vicinity of $e^{\pm}$, are applied. After applying these cuts, there are 42 (13) candidate $W+Z$ decays producing positrons (electrons) with a background of 1.7 ± 1.0 (1.6 ± 1.0) events within a signal region having $30 < p_T < 50$ GeV/c. The backgrounds are extrapolated from the region having $12 < p_T < 20$ GeV/c where the background is dominant. To treat the low-statistics data properly, a likelihood function created from the four-spin sorted yields corresponding to the two polarized beams was used to determine A_L within its physical range $[-1, 1]$. As a result, the measured A_L's are $A_L^{e^+} = -0.86^{+0.30}_{-0.14}$ and $A_L^{e^-} = 0.88^{+0.12}_{-0.71}$. Figure 1 shows a comparison of the measured A_L values with those estimated on the basis of a sample of polarized PDFs extracted from the fits of DIS and semi-inclusive DIS data[4)]. The experimental results were consistent with the theoretical calculations at confidence levels of 6−15% for $A_L^{e^+}$ and 20−37% for $A_L^{e^-}$.

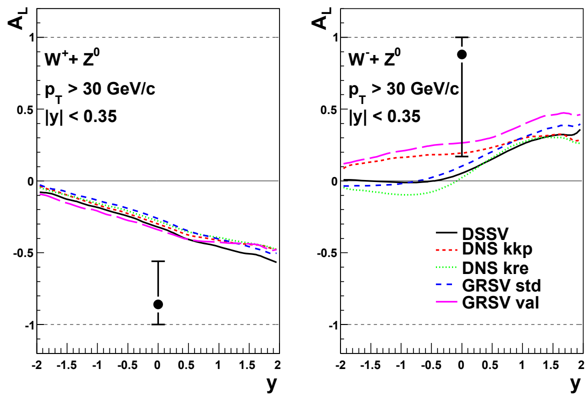

Fig. 1. Single-spin asymmetries for $e^{\pm}$'s produced by W and Z decays. The error bars represent a 68% confidence level. The theoretical curves are calculated using NLO with different polarized PDFs[4)].

The observed asymmetries are sensitive to the polarized PDFs at $x \sim M_W/\sqrt{s} \simeq 0.16$ and directly demonstrate the parity-violating coupling between W bosons and light quarks. The results are consistent with theoretical expectations and similar measurements[5)]. The upgrades for RHIC luminosity and PHENIX detector that are in progress will make it possible in the future to significantly reduce the uncertainties associated with A_L.

References

1) D. de Florian et al.: Phys. Rev. **D80**, 034030 (2009).
2) G. Bunce et al.: Ann. Rev. Nucl. Part. Sci. **50**, 525 (2000).
3) PHENIX Collaboration: Nucl. Instrum. Meth. **A499**, 469 (2003).
4) D. de Florian et al.: Phys. Rev. **D81**, 094020 (2010).
5) STAR Collaboration: Phys. Rev. Lett. **106**, 062002 (2011).

*1 Kyoto University, Kitashirakawa Oiwake-cho, Sakyo-ku, Kyoto 606-8502, Japan

First beam acceleration on new linac injector for RI Beam Factory

K. Yamada, S. Arai, M. Fujimaki, T. Fujinawa, H. Fujisawa, N. Fukunishi, A. Goto, Y. Higurashi, E. Ikezawa, M. Kase, M. Komiyama, K. Kumagai, T. Maie, T. Nakagawa, J. Ohnishi, H. Okuno, N. Sakamoto, Y. Sato,*1 K. Suda, H. Watanabe, T. Watanabe, Y. Watanabe, Y. Yano, S. Yokouchi, and O. Kamigaito

A new linac injector called RILAC2[1] was constructed at the RIKEN Radioactive Isotope Beam Factory (RIBF) in 2010 in order to increase the beam intensity of very heavy ions such as xenon and uranium ions, as well as performing independent RIBF experiments and super-heavy-element synthesis. As shown in Fig. 1, RILAC2 consists of a 28-GHz superconducting ECR ion source (ECRIS)[2], a low-energy beam transport (LEBT)[3] section including a pre-buncher, a four-rod RFQ linac, three drift-tube linac tanks (DTL1-3), a high-energy beam transport (HEBT) section from DTL3 to the RIKEN ring cyclotron (RRC), a rebuncher between the RFQ linac and DTL1 (B2-REB), a rebuncher in the HEBT section (B7-REB), and strong quadrupole magnets placed between the acceleration cavities for transverse focusing. The key features of RILAC2 are the powerful ECRIS, higher extraction voltage of the ECRIS compared to the voltage of the existing injector RILAC to reduce the space charge effect, improvement of the vacuum level to reduce the loss by charge exchange, and the compact equipments yet to be installed in the existing AVF cyclotron vault.

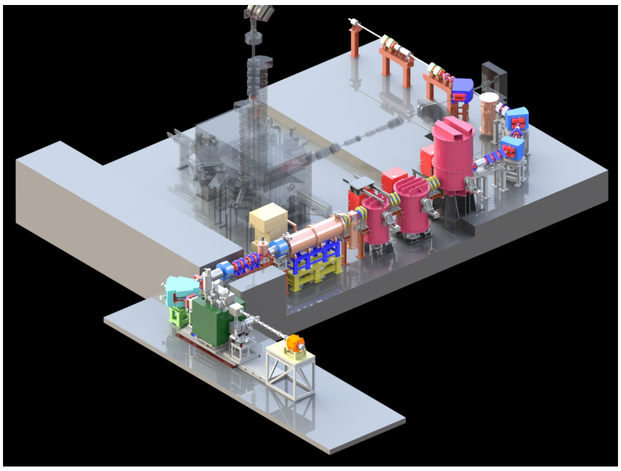

Fig. 1. View of RILAC2, newly built in the AVF cyclotron vault.

The mechanical design of RILAC2 was started in fiscal year 2009, and the acceleration cavity resonators were constructed as described in a previous report[4–6]. After the electrical wiring was completed and water connection was provided for the RFQ linac, a rated voltage of 42 kV was successfully achieved on the RFQ in August 2010. Further tests and modifications were performed for the DTLs in fiscal year 2010 to improve the long-term stability of the DTLs. A noise problem on a crowbar circuit in the DC power supply for the DTL amplifier was overcome. The capacitive rf pickup of the DTLs was modified in order to reject the hard spark on the pickup because the spark could damage the diode detector. An rf-voltage stability of $\pm 0.03\%$ and a phase stability of $\pm 0.15°$ were attained for the DTLs. The two rebunchers were newly designed and fabricated. The structure of the rebunchers is based on the quarter-wavelength cavity resonator with four gaps. The B2-REB was installed in the AVF vault in December 2010, while the B7-REB was installed in January 2011. The B2-REB is described in detail in Ref. 7. Figure 2 shows the internal structure of the B7-REB located in the HEBT section. The drift tubes and inner conductor of the B7-REB were monolithically milled from a copper plate; thereby, the high-precision alignment of the drift tubes was achieved. Two half-cylinders of the outer conductor sandwich the copper-center plate. The total voltage required for the B7-REB is 200 kV, which can be provided by a 3 kW transistor amplifier. The relocation of the ECRIS from the RILAC building to RILAC2, construction of the LEBT and HEBT sections, preparation of the vacuum system, beam diagnosis, and installation of a control system were also performed in fiscal year 2010, as reported in Ref. 8.

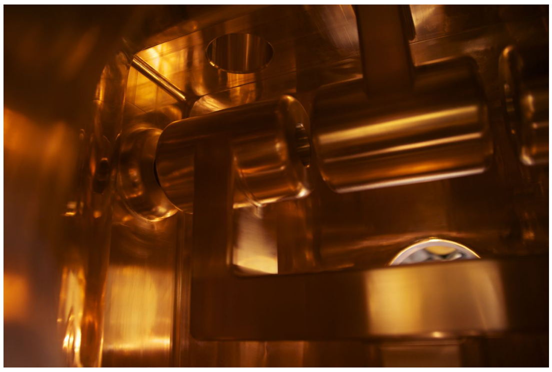

Fig. 2. Internal structure of the rebuncher (B7-REB) located in the HEBT section.

The beam acceleration test of RILAC2 was started on December 21, 2010. At first, the beam was accelerated by using RILAC2 only downstream of the bending magnet (B71) in the AVF vault. The accelerated beam was a $^{124}Xe^{20+}$ beam with an energy of 674 keV/nucleon at B71. After validating each equipment of RILAC2 step by step, we succeeded in accel-

*1 J-PARC Center, KEK

erating the first beam on day one by using all the rf resonators of RILAC2. Figure 3 shows a profile of the first beam at B71, measured by a wire scanner. To reduce the beam loss during machine tuning, the movable slit downstream of the ECRIS was adjusted to decrease the beam intensity to about 10 μA. When the beam intensity downstream of the ECRIS was 9.5 μA, the beam was accelerated and transported to B71 with an intensity of 7.1 μA.

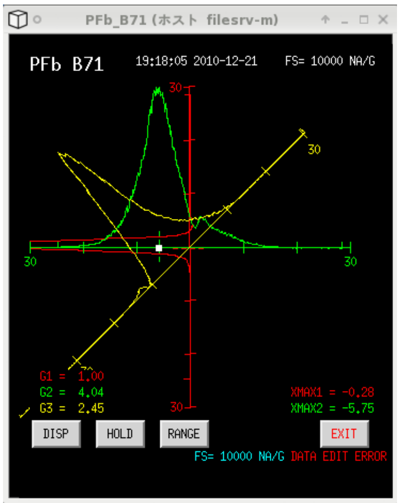

Fig. 3. Profile of the first beam accelerated by using all rf systems. This profile was measured downstream of the 90° bend.

Further tests were performed in January and February 2011 to determine the optimal parameters of the RILAC2 rf resonators. Figure 4 shows the performance of the pre-buncher. The left panel provides the time spectrum measured by a plastic scintillator at B71 for the case where the pre-buncher was not used, while the right panel shows the spectrum for the case where a pre-buncher was used. The RRC is operated at the rf frequency of 18.25 MHz, which is at half the RILAC2 acceleration resonators, and the beam bunch should be compressed to the effective bunch of 18.25 MHz repetition. This result indicates the sufficient effect of the pre-buncher. Figure 5 shows the beam intensity on

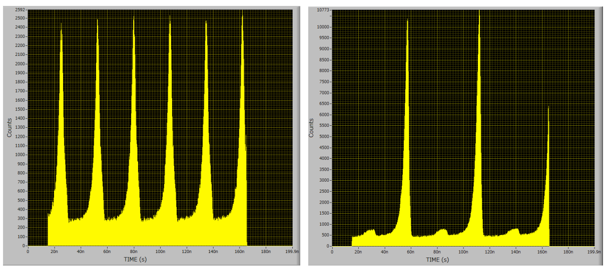

Fig. 4. Time spectra measured downstream of the 90° bend without using/by using the pre-buncher.

each Faraday cup installed in the RILAC2 beam line. The beam intensity was decreased to about 30 μA by using the movable slit, as described above. In the figure, B12 is upstream of the RFQ linac, B22 is upstream of DTL1, and B50 is downstream of DTL3.

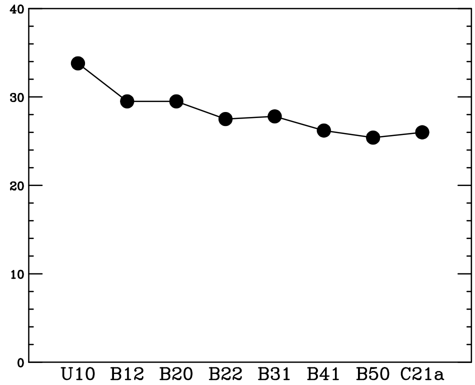

Fig. 5. Beam intensity on each Faraday cup installed in RILAC2.

After the completion of the B7-REB in January, beam acceleration through the fixed-frequency ring cyclotron (fRC) has been performed for a ^{124}Xe beam. The beam energy accelerated by the RRC was 10.75 MeV/nucleon, and the ^{124}Xe beam was charge-stripped by a nitrogen-gas stripper from 20+ to 38+ for the fRC. The ^{124}Xe beam has almost the same magnetic rigidity as the $^{238}U^{73+}$ beam studied in 2006. Although machine tuning was not optimized, we were able to extract the ^{124}Xe beam from the fRC successfully.

In these studies, the beam energy from both RILAC2 and RRC was found to be slightly high and to cause large off-centering on the cyclotrons. After preparing the time-of-flight measurement system, we have to measure the beam energy and longitudinal emittance precisely in order to adjust the acceleration energy and to find the optimal parameters of the rf voltage and the phase of each resonator on RILAC2. We aim to accelerate the ^{124}Xe beam through the superconducting ring cyclotron (SRC) in March 2011.

References
1) O. Kamigaito et al.: Proc. of PASJ3-LAM31, WP78, Sendai, 2006, p.502.
2) T. Nakagawa et al.: Rev. Sci. Instrum. **79**, 02A327 (2008).
3) Y. Sato et al.: Proc. of PASM6, FOBTA01, Tokai, 2009, p.801.
4) K. Yamada et al.: RIKEN Accel. Prog. Rep. **43**, 105 (2010).
5) K. Yamada et al.: RIKEN Accel. Prog. Rep. **43**, 107 (2010).
6) K. Suda et al.: RIKEN Accel. Prog. Rep. **43**, 109 (2010).
7) K. Suda et al.: in this report.
8) Y. Watanabe et al.: in this report.

Low-Z gas stripper as an alternative to carbon foils for the acceleration of high-power uranium beams†

H. Okuno, N. Fukunishi, A. Goto, H. Hasebe, H. Imao, O. Kamigaito, M. Kase, H. Kuboki, Y. Yano, S. Yokouchi and A. Hershcovitch*1

[Charge stripper, Uranium acceleration]

At the RIBF, programs for increasing the intensity of uranium beams (U-beams) are in progress; these programs include the construction of a new 28-GHz superconducting ECR ion source and a new injector linac. However, despite extensive R&D, the most serious problem, i.e., that involving a charge stripper used for U-beams still remains unsolved. This paper describes the possibility of using a low-Z gas stripper to solve a serious problem related to a charge stripper, which plays an essential role in high-power U-beam acceleration.

Figure 1 shows a scheme for accelerating U-beams using two strippers. One stripper is located behind the RRC, where the beam energy is 11 MeV/u, and the other is located behind the fRC, where the beam energy is 51 MeV/u. Carbon foils are used for both the strippers. The typical thicknesses of the foils used for the first and second strippers are 300 μg/cm^2 and 17 mg/cm^2, respectively. The problem associated with the first stripper is very serious. The commercially available carbon foils obtained from ACF-Metals are used for the first stripper. The typical lifetime of these foils is about 12 h for a beam intensity of 1 eμA. Carbon foils that have the same thickness as the foils used in the case of the first stripper are being developed at RIKEN, and the quality of these foils is approaching that of the commercially available foils. Currently, there is no problem associated with the beam intensities for which these foils can be used. However, the intensity will be a serious problem in the future because the intensity of U-beams will be increased by a factor of more than 100 when the aforementioned programs are completed; thus, there will be a requirement for much stronger strippers. A gas stripper is free of lifetime-related problems; however, the equilibrium charge state in the gas stripper is lower than that in a carbon foil because of the density effect.

The equilibrium charge state is determined by the competition between e-loss and e-capture processes of an ion. The capture cross sections depend strongly on the ion velocity V_p as compared to the target electrons. In particular, the e-capture process is highly suppressed because of the poor kinematical matching that occurs when the velocity of the ions significantly exceeds that of the 1s electrons (V_{1s}), which are the fastest target electrons. Such merits motivated us to develop a low-Z gas stripper and thus realize a high charge state in gases. The suppression of e-capture is expected to occur in the case of low-Z targets or at a high ion velocity. This is because V_{1s} is significantly decreased in the case of low-Z targets, since it is approximately expressed as $V_{1s} = Zc/137$, resulting in a high equilibrium charge state. In fact, a significant increase in the equilibrium charge state is indicated by some experimental data on the equilibrium charge state or effective charge at intermediate energies in low-Z regions[3–5]. We measured the loss and capture cross sections for the 1s electron as a function of the charge state of uranium ions to determine the equilibrium charge state from the intersection point of the cross sections.

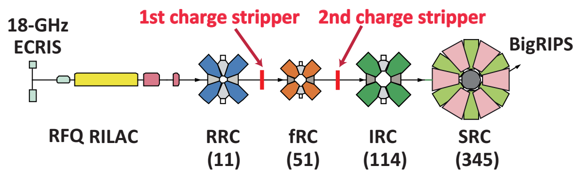

Fig. 1. Scheme for accelerating U-beams using two strippers.

The experiment was conducted at the RIBF using the RILAC and RRC. The following U-beams were extracted from the RRC: $^{238}U^{35+}$ with an energy of 11 MeV/u , $^{238}U^{41+}$ with an energy of 14 MeV/u , and $^{238}U^{41+}$ with an energy of 15 MeV/u. The incoming ions passed through a carbon foil located in front of a bending magnet, which was used to select the individual projectile charge state Q_i. The thickness of the carbon foil was optimized to obtain the maximum intensity for the charge state. Each beam was directed through a windowless, differentially pumped He-gas cell. After emerging from the gas cell, the beams were passed through a second bending magnet into an FC (Faraday cup). The FC measured the intensity of the beam current of the charge state for e-loss (Q_i + 1), e-capture (Q_i - 1), and no reaction (Q_i).

Figure 2 shows the measured cross section as a function of the charge number of the uranium ions at 11, 14, and 15 MeV/u. The data show that the e-capture cross section largely depends on the energy, while the e-loss cross section does not depend significantly on the energy. Because the contribution of multiple-electron

† Condensed from the article in Phys. Rev. ST Accel. Beams **14**, 033503 (2001)
*1 Brookhaven National Laboratory

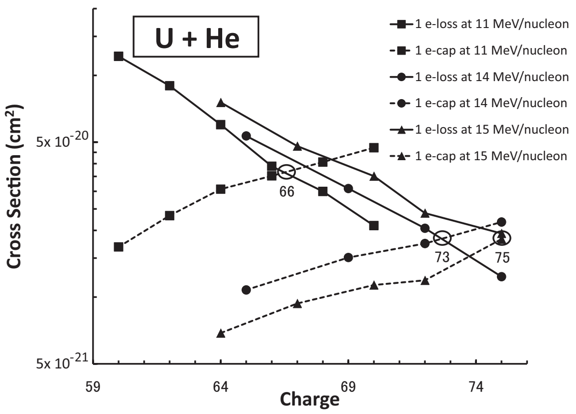

Fig. 2. Measured e-loss and e-capture cross sections as a function of the charge state of uranium ions at 11, 14, and 15 MeV/u in a He-gas cell. The cross sections were determined by assuming the thickness of the gas cell to be 13.27 μg/cm^2.

transfer in He is very small[6], the point of intersection of of the two lines gives a good approximation of the equilibrium charge state. The points of intersection are determined to be 66, 73, and 75 at 11, 14, and 15 MeV/u, respectively. Table 1 lists the equilibrium charge state in He, N_2, and C. The equilibrium charge state in He is clearly higher than that in N_2 by more than 10 and is close to that in C.

Table 1. Equilibrium charge state in He, N_2, and C at 11, 14, and 15 MeV/u. The data for N_2 and C were taken from references[1,2].

Material	Q_e**@11 (MeV/u)**	Q_e**@14 (MeV/u)**	Q_e**@15 (MeV/u)**
He	66	73	75
N_2	56	61	62
C	72	76	77

The measurement results show that a low-Z gas stripper for achieving a high charge state of uranium can be realized. However, the accumulation of low-Z gases is still difficult. The existing gas stripper can accumulate only 0.015 mg/cm^2 (0.7 kPa) of He, while it can accumulate 1.3 mg/cm^2 of N_2. A simple estimation shows that about 1 mg/cm^2 of He or H_2 is necessary to achieve a high charge state; this suggests that a new device must be developed to solve this problem for accumulating the gases. The plasma window invented by Hershcovitch in 1995 can be used for this purpose[7]. The plasma window is a wall-stabilized plasma arc that is used as an interface between accelerator vacuum and pressurized targets. No solid material is introduced into the beam; therefore, the plasma window can transmit a charged particle beam with low loss. The window mainly consists of three cathodes, one anode, and some cooling plates for cooling the

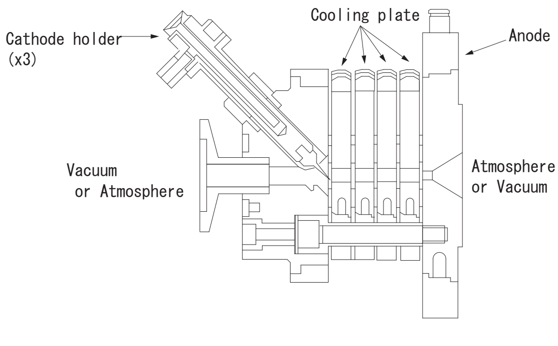

Fig. 3. Schematic of plasma window.

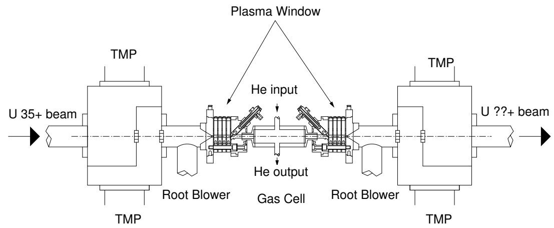

Fig. 4. Conceptual sketch of the low-Z gas stripper with two plasma windows.

plasma arc, as shown in Fig. 3. The arc in the plasma window can generate a pressure difference between its ends; the ratio of the higher pressure to the lower pressure is 600. Hence, it can maintain the pressure inside the gas cell while maintaining vacuum outside. Figure 4 shows a schematic of the low-Z gas stripper that includes two plasma windows; this stripper was proposed by P. Thieberger from BNL at a workshop on the charge stripper for the FRIB in 2009[8]. The low-Z gas is accumulated in the cell, which is sandwiched between the two plasma windows. We are starting R&D programs to test the plasma window in a test stand; we are being assisted in these programs by Hershcovitch.

References

1) H. Kuboki et al.: Phys. Rev. ST Accel. Beams **13**, 093501 (2010).
2) H. Kuboki et al.: Phys. Rev. ST Accel. Beams *to be published.*
3) T. Mizogawa et al.: RIKEN Accel. Prog. Rep. **22**, 62 (1988).
4) R. Bimbot et al.: Nucl. Instrum. Methods Phys. Res., Sect. B **107**, 9 (1996).
5) A. Fettouchi et al.: Nucl. Instrum. Methods Phys. Res., Sect. B **245**, 32 (2006).
6) H. D. Betz: in Appl. At. Coll. Phys. **4**, 1 (1983).
7) A. Hershcovitch: J. Appl. Phys. **78**, 5283 (1995).
8) Facility for Rare Isotope Beams (FRIB), Stripper and Target Technology for High Power Heavy Ion Beams Workshop, East Lansing (2009).

Sympathetic crystallization of CaH^+ in a linear Paul trap

N. Kimura,[*1] K. Okada,[*1] T. Takayanagi,[*1] S. Ohtani,[*2] H.A. Schessler, [*3] M. Wada

[Coulomb crystals, Ca^+, Sympathetic laser cooling]

Cold molecules open up interesting research possibilities, such as precision spectroscopy of vibrational and rotational transitions of cold molecules and the study of chemical reactions at very low temperatures. Recently, a new method was developed for studying the reaction between cold ions and polar molecules[1]. In this experiment, slow polar molecules were produced by a Stark velocity filter and the cold Ca^+ target was prepared in a linear Paul trap by employing laser cooling. This method can be extended to study a multitude of cold reactions if applying sympathetic cooling of molecular ions to produce cold ion target.

We plan to perform such experiments, i.e., analysis of reactions between sympathetically cooled molecular ions and cold polar molecules. In this connection, we investigated the sympathetic Coulomb crystallization of CaH^+ ions produced by a laser-induced reaction through an excited state as follows:

$$^{40}\mathrm{Ca}^+(4p\ ^2P_{1/2}) + \mathrm{H}_2 \rightarrow {}^{40}\mathrm{CaH}^+ + \mathrm{H}. \qquad (1)$$

Figure 1 (a) shows a typical fluorescence image of 290 Ca^+ ions. In this case, the crystal has a cylindrical symmetric shape. After the laser-induced reactions (1), an asymmetric Coulomb crystal as shown in Fig. 1 (b) is observed often. This modified structure can be attributed to the production of CaH^+ ions. The number of two-species crystallized ions, the secular motion temperature, and the structure were determined by performing molecular dynamics simulations[2]. A simulation image reproducing (b) is shown in Fig. 1 (c). CaH^+ ions are found on the upper portion of the image because of asymmetric DC voltages due to the patch effect of the electric charge on the electrodes. The simulation results suggest that the CaH^+ ions were sympathetically crystallized and also show that their secular motion temperature was lower than 10 mK.

This method was used to determine the reaction rate of (1) by studying the fluorescence images of two-species Coulomb crystals by systematically changing the reaction time. An example of the measurement is shown in Fig. 2. The upper images in Fig. 2 were obtained after the indicated reaction time. The numbers of Ca^+ and CaH^+ ions were determined from the observed crystal images by performing molecular dynamics simulations. We obtain the number of each ion species as a function of the reaction time as shown in Fig. 2 in bottom panel. ¿From the decay curve of Ca^+, the reaction rate is determined to be 6.1 ± 0.2)$\times10^{-4}$ s^{-1}. The reaction rate coefficient k is related to γ as $\gamma = k\rho_e n_{\mathrm{H}_2}$, where n_{H_2} and ρ_e are the number density of H_2 molecules and the excited $^2P_{1/2}$ state population, respectively. By using the optical Bloch equation, we determined ρ_e to be approximately 0.09% under the present experimental conditions. Since this measurement was performed while loading H_2 gas at a pressure of 4.8×10^{-6} Pa, a lower limit for the reaction rate coefficient $k = 8 \times 10^{-10}$ cm^3/s was obtained[3].

*1 Department of Materials and Life Sciences, Sophia University
*2 ILS, University of Electro-Communications
*3 Department of Physics, Texas A&M University

References
1) S. Willitsch*et al.*: Phys. Rev. Lett. **100**, 043203 (2008).
2) K. Okada *et al.*: Phys. Rev. A **81**, 013420 (2010).
3) N. Kimura *et al.*: Phys. Rev. A **83**, 033422 (2011).

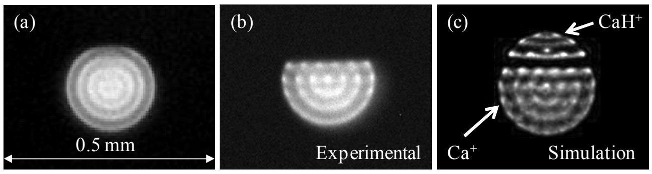

Fig. 1. (a) 290 Ca^+ ions, (b) Two-species Coulomb crystal composed of 134 Ca^+ and $^{40}CaH^+$ ions, and (c) Simulation image reproducing the observed image (b).

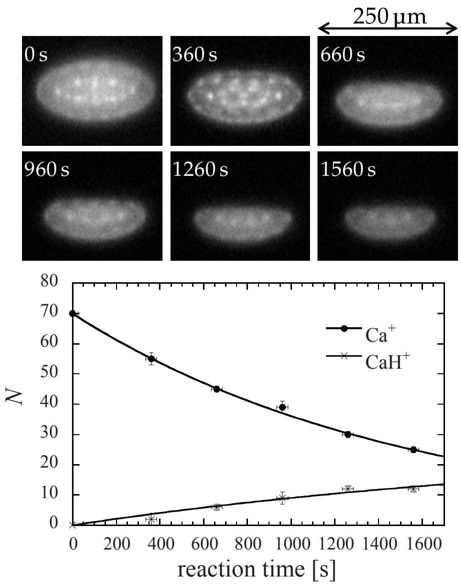

Fig. 2. Reaction rate measurement of the laser-induced reaction (1). See text for the details.

Production and decay properties of ^{265}Sg

H. Haba, D. Kaji, Y. Kasamatsu,[*1] H. Kikunaga, Y. Komori,[*1] H. Kudo,[*2] Y. Kudou, K. Morimoto, K. Morita, K. Ooe,[*1] K. Ozeki, R. Sakai, N. Sato,[*3] A. Shinohara,[*1] T. Sumita, K. Tsukada,[*3] and A. Yoneda

The isotopes of element 106, i.e., ^{265,266}Sg, which were discovered by Lazarev et al.[1)] in the ^{248}Cm(^{22}Ne,xn)$^{270-x}$Sg reactions, have been used for chemical studies of Sg.[2)] Recently, the decay properties of ^{265,266}Sg were reexamined by Düllmann and Türler[3)] in the light of new results on ^{269}Hs. Düllmann and Türler[3)] suggested that all decay events that were previously attributed to ^{266}Sg are caused by ^{265}Sg; moreover, they indicated the presence of isomeric states in ^{265}Sg: ^{265}Sg^{a} (half-life $T_{1/2} = 8.9^{+2.7}_{-1.9}$ s, α-particle energy E_α = 8.80–8.90 MeV) and ^{265}Sg^{b} ($T_{1/2} = 16.2^{+4.7}_{-3.5}$ s, E_α = 8.70 MeV). They, however, also stated that the accuracy of the deduced decay properties of ^{265}Sg^{a,b} is not very good, partly owing to the fact that the analyses of the previous experiments on ^{265}Sg were biased because of the assumptions made for the decay properties of ^{265}Sg; these properties are now known as indefinite. At RIKEN, we plan to start chemical studies of Sg using ^{265}Sg produced by the ^{248}Cm(^{22}Ne,5n)^{265}Sg reaction. In the present study, we investigated production and decay properties of ^{265}Sg in detail by using the gas-jet transport system coupled to the RIKEN gas-filled recoil ion separator, GARIS.[4)]

A $^{248}Cm_2O_3$ target with a thickness of 230 (280)[†] μg cm^{-2} was prepared by electrodeposition onto a Ti foil of thickness 0.91 (0.90) mg cm^{-2}. A $^{22}Ne^{6+}$ ($^{22}Ne^{5+}$) ion beam was extracted from the RIKEN Linear Accelerator, RILAC. The beam energy was 117.8 MeV at the middle of the target, and the average beam intensity was 3 pμA. By using GARIS, the reaction products of interest were separated in-flight from the beam and the majority of the transfer-reaction products. The reaction products were then guided into the gas-jet chamber through a 0.7-μm-thick Mylar window, which was supported by a grid with 84% (72%) transparency. GARIS was filled with He gas at 33 Pa, and the magnetic rigidities ($B\rho$) were 2.07 (1.73, 1.94, 2.04, and 2.16) Tm. The reaction products were then transported by a He/KCl gas jet to the rotating-wheel system, namely, MANON for performing α-spectrometry. In MANON, aerosol particles were deposited on a Mylar foil with a diameter of 20 mm and a thickness of 0.5 μm; forty such foils were set on the periphery of the rotating wheel. The wheel was stepped at 20.5-s or 10.5-s interval to position the foils between seven pairs of Si PIN photodiodes (Hamamatsu S3204-09).

Beam doses of 2.07×10^{18}, 2.34×10^{18}, 6.39×10^{17}, 1.12×10^{19}, and 1.57×10^{18} were accumulated at a $B\rho$ of 1.73, 1.94, 2.04, 2.07, and 2.16 Tm, respectively. We searched for time-correlated α-α and α-SF (spontaneous fission) event pairs in the time window of 226 s and energy range 8.0 MeV ≤ E_α ≤ 9.0 MeV and E_{SF} ≥ 30 MeV. As a result, a total of 18 α-α-α, 43 α-α, and 18 α-SF correlations were obtained. After referring to the decay pattern reported in Ref.,[3)] it was concluded that these correlations were related to ^{265}Sg^{a,b} (18 and 24 atoms, respectively) and to their daughter nuclides ^{261}Rf^{a,b} and ^{257}No. The decay patterns of ^{265}Sg obtained in the present study are shown in Fig. 1. The presence of two isomeric states of ^{265}Sg, i.e., ^{265}Sg^{a,b}, which were proposed by Düllmann and Türler,[3)] was successfully confirmed on the basis of the observed E_α and $T_{1/2}$ values: E_α = 8.84±0.05 MeV, $T_{1/2} = 8.5^{+2.6}_{-1.6}$ s for ^{265}Sg^{a} and E_α = 8.69±0.05 MeV, $T_{1/2} = 14.4^{+3.7}_{-2.5}$ s for ^{265}Sg^{b}. The following decay data were obtained for ^{261}Rf^{b}, which is a daughter nuclide of ^{265}Sg^{a,b}: E_α = 8.51±0.05 MeV, $T_{1/2} = 2.6^{+0.7}_{-0.5}$ s, and SF branch (b_{SF}) = 0.82±0.09; these values are consistent with those obtained in our previous ^{248}Cm(^{18}O,5n)^{261}Rf^{b} experiment (E_α = 8.52±0.05 MeV, $T_{1/2}$ = 1.9±0.4 s, b_{SF} = 0.73±0.06).[4)] The cross sections were evaluated to be 180^{+80}_{-60} pb and 200^{+60}_{-50} pb for ^{265}Sg^{a} and ^{265}Sg^{b}, respectively, by assuming that the transmission of GARIS was 13%, the gas-jet efficiency was 50%, and the gas-jet transport time was 3 s. ^{265}Sg is now ready for chemistry experiments, and its production yield is one atom h^{-1} in a chemistry laboratory.

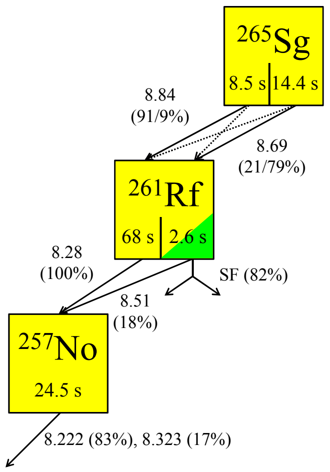

Fig. 1. Observed decay patterns for the chain ^{265}Sg^{a,b} → ^{261}Rf^{a,b} → (^{257}No →). The dominant and weak transitions are indicated with solid and dashed lines, respectively; the intensities are also shown. The data for ^{261}Rf^{a} and ^{257}No were obtained from Ref.[3)]

[*1] Graduate School of Science, Osaka University
[*2] Department of Chemistry, Niigata University
[*3] Advanced Science Research Center, JAEA

[†] The values given in parentheses correspond to a different set of conditions.

References

1) Yu. A. Lazarev et al.: Phys. Rev. Lett. **73**, 624 (1994).
2) M. Schädel: Angew. Chem. Int. Ed. **45**, 368 (2006).
3) C. E. Düllmann and A. Türler: Phys. Rev. C **77**, 064320 (2008).
4) H. Haba et al.: Phys. Rev. C **83**, 034602 (2011).

Development of flowering mutant of cherry blossom by heavy-ion irradiation

S. Ishii, *1 Y. Hayashi, T. Hirano, N. Fukunishi, and T. Abe

The cherry blossom is a symbolic flower in Japan. Most Japanese have a special feeling toward cherry blossoms because of their beauty and flowering habit. Many cherry blossom cultivars in Japan, e.g., Somei-yoshino; require a period under low temperature for dormancy breaking of floral buds. However, in some areas of Japan, global warming has affected winter temperatures, which have not been sufficiently low in recent years. This climate change has resulted in decrease in the number or, occasionally, absence of cherry blossoms in spring.

We used heavy-ion beam irradiation to successfully produce a mutant of cherry blossom that does not require a period under low temperature for dormancy breaking. Ten scions of Keiou-Zakura (*Prunus subhirtella* Miq, Yamagata 13 line) were irradiated in February 2006. The dose of carbon beam irradiation ($^{12}C^{6+}$, 135 MeV/u, LET 22.6 keV/μm) was 10 Gy. The irradiated scions were grafted onto the rootstock (Keiou-Zakura). Of the ten plants, 7 survived for a year after grafting. Two of the surviving plants (C10K13-1 and C10K13-2) were selected for multiplication. The period from grafting to the first bloom is at least 2 years in original Keiou-Zakura. In contrast, most plants from these lines bloomed in autumn of 2007, 9 months after grafting. The flowering rates of plants grown from C10K13-1 and C10K13-2 were 94.1% (16/17) and 88.9% (16/18), respectively. The plants grown from C10K13-1 died after flowering. In contrast, the plants grown from C10K13-2 in a greenhouse bloomed again after 5 months. Subsequently, the blooming time of these plants differed among individuals after continuous cultivation in a greenhouse. Original Keiou-Zakura has one-season flowering. Keiou-Zakura requires exposure to temperatures below 8℃ for 1000 hours to break dormancy. The plants from C10K13-2 grown in a field bloomed twice a year, in spring and in autumn. Exposing the plants to low temperature in winter can synchronize the blooming time in spring. In this case, it produced 3 times more flowers than original Keiou-Zakura (Fig. 1). The flowers bloomed in autumn had more than 4 pistils (Fig. 2) and were sterile. The flowering period of these flowers was twice as long as that of original flowers.

This mutant with a single pink flower was named Nishina Otome. This is the second cultivar of cherry blossom that has been developed after Nishina Zaou[1] by using heavy-ion beam irradiation. Nishina Otome has been available on the market since March 2010.

Reference
1) S. Ishii et al.: RIKEN Accel. Prog. Rep. **42**, xi (2009).

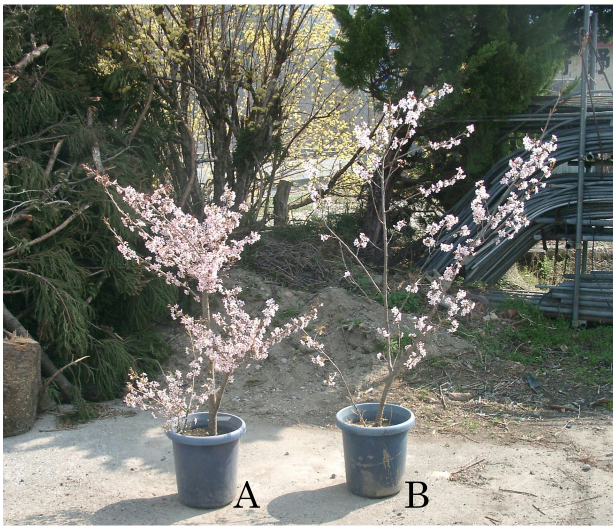

Fig.1 Comparison of the mutant Nishina Otome (A) and the original (B) that bloomed in April 2009.

Fig. 2 Flower of Nishina Otome with 7 pistils that bloomed in October 2008.

*1 JFC Ishii Garden

C O N T E N T S

3. Hadron Physics

7. Instrumentation

III. RESEARCH ACRIVITIES II (Material Science and Biology)

1. Atomic and Solid State Physics (ions)

2. Atomic and Solid State Physics (muon)

I. PREFACE

Preface

On the 11th of March 2011, a massive earthquake hit north-eastern Japan followed by a huge tsunami and subsequently by the Fukushima nuclear disaster. This volume of RIKEN Accelerator Progress Report (APR) compiles the research activities conducted in the calendar year 2010, with all the manuscripts prepared before the disaster. In the light of the huge impact of the disaster, we wish to present a brief status report as of July 2011 when this preface is written. We were very fortunate that the direct damage to RI Beam Factory (RIBF) was kept at a minimum. All the accelerator and experimental components have survived the impact, and RIBF is now ready for a full-scale operation after performing some fixes and tests by beam acceleration. While few problems have been found, they were all fixable within months. Even in this difficult time, we believe our mission is to continue on with the science without hindering the recovery process of the Tohoku area. We are accepting experiments originally scheduled to be performed at the damaged accelerators in Tokai area, sending scores of researchers to Fukushima to perform radiation screening, and collaborating on the soil investigation project.

**** **** **** **** **** ****

RIKEN Accelerator Progress Report (APR) includes research activities conducted in RIKEN Nishina Center for Accelerator-Based Science, or simply RIKEN Nishina Center (RNC). It also contains progress reports submitted by the users of RIBF and RIKEN Muon Facility at Rutherford Appleton Laboratory in UK.

In 2010, the operation performance of RIBF was significantly improved. We have delivered RI beams on a user target for about 70 days, a time span three times longer than the year before. This was achieved by superior technical supports from Accelerator Group, BigRips Team, and many other individuals. The leadership exhibited by W. Henning and H. Sakai who newly joined RNC was also the key behind the achievement. It should be noted that we have asked our Program Advisory Committee (PAC) to not only review but also grade approved experimental proposals. While this has placed extra burden on experimentalists as well as the PAC members, it is extremely useful for the effective beam-time scheduling. We appreciate all the users' understanding on this matter.

To be a user-friendly synergetic-use laboratory, we have been supportive of forming a well-defined international collaboration specifically targeted for a particular large-size experimental apparatus and its physics program. A new collaboration is being formed for SAMURAI, multiple-particle spectrometer with a large acceptance, nearing completion. EURICA (EUro-RIken Crystal Array) collaboration was formed by inviting the European germanium-detector array and its RISING collaboration to RIBF. This type of approaches will be a template for the future experiments of a certain scale.

With regard to the scientific progress of Nishina Center, many achievements have been made last year. Some of them have been specially selected by the editorial committee of RIKEN Accelerator Progress Report to be featured in “Frontispiece” and "Highlights of the Year". Of the selected papers, a special attention should be given to the work by Nishimura *et al.* This research on "β-decay Half-Lives of Very Neutron-Rich Kr to Tc Isotopes" which was released to the press, has shown again the magnitude of power of RIBF. The newly measured 18 isotopes lie close to the astrophysical r-process path, and half-life measurements for the nuclei on the path are the key to understand the process. The results indicate that a shorter timescale is required for the matter flow in the r-process to seed heavier nuclei.

In the APR of the previous year, Kuboki presented his pioneering work for the gas stripper development. This idea was harvested in the work by Okuno *et al*., "Low-Z gas stripper as an alternative to carbon foils for the acceleration of high-power uranium beams". Together with another new progress accomplished by Accelerator Group as reported by Yamada *et al*., in " First beam acceleration on new linac injector for RI Beam Factory (RILAC2)", we believe we have achieved a significant milestone. RIBF will now enter the new stage of high-power uranium-ion delivery.

T. Abe was appointed as the leader of Accelerator Application Research Group in October, 2010. Her group's new invention is called Nishina Otome, as reported by Hayashhi *et al*., "Development of flowering mutant of cherry blossom by heavy-ion irradiation". Amazingly, this new breed of cherry blossom blooms during all four seasons. Moreover, following the tsunami disaster, her group started a collaboration with Tohoku University to test her newly developed salt-resistant rice in the ruined rice field located in the Tohoku seaside area.

Gambare Tohoku.

Hideto En'yo
Director,
RIKEN Nishina Center for Accelerator-Based Science

II. RESEARCH ACTIVITIES I

(Nuclear-Particle Physics)

1. Nuclear Physics

Study of structure of ^{19,21}N nuclei by γ spectroscopy[†]

Z. Elekes, [*1] Zs. Vajta, [*1] Zs. Dombrádi, [*1] T. Aiba, [*2] N. Aoi, H. Baba, D. Bemmerer, [*3] B. A. Brown, [*4] T. Furumoto, [*5] Zs. Fülöp, [*1] N. Iwasa, [*6] Á. Kiss, [*7] K. Kobayashi, [*10] Y. Kondo, [*8] T. Motobayashi, T. Nakabayashi, [*8] T. Nannichi, [*8] Y. Sakuragi, [*5] H. Sakurai, D. Sohler, [*1] M. Takashina, [*9] S. Takeuchi, K. Tanaka, Y. Togano, K. Yamada, M. Yamaguchi, and K. Yoneda

[nuclear structure, unstable nuclei, inelastic scattering]

In the past years, new magic numbers far from stability have been discovered. A new N=14 subshell closure in ^{22}O the strength of which was determined to be 4.2 MeV, was identified. Recently, the disappearance of this N=14 gap in ^{20}C was observed by γ spectroscopy. In this study, we investigated the interaction of an ^{21}N radioactive ion beam with a hydrogen target and a lead target. This allowed us to study the transition along the N=14 line and obtain spectroscopic information on the structure of the lighter neutron-rich nitrogen isotopes.

The experiment was performed at RIKEN Nishina Center by using an ^{40}Ar primary beam with an energy of 63 MeV/nucleon and intensity of 700 pnA. Other details of the setup and particle identification can be found elsewhere[1)].

For all the nitrogen isotopes, Doppler-corrected spectra were recorded using the hydrogen target, at M(multiplicity)=1 and M=2. The ^{18}N spectra were used to cross-check the procedure because the low-energy excited states for this nucleus are well known. Two peaks were found for ^{19}N in the neutron knockout reaction at 529(21) and 1137(26) keV. This result was in good agreement with that reported in Ref.[2)], where these transitions were stated to form a cascade. For ^{21}N, the transition between the first excited and ground states [E_γ = 1140(30) keV] dominated the M=1 proton inelastic scattering spectra, while the M=2 spectra indicated events originating from the transition between the first and second excited states [E_γ = 1210(33) keV]. This observation agreed well with the conclusion drawn in Ref.[2)] for the level scheme, where the two strongest peaks were found at 1177 and 1228 keV.

In addition to the level scheme, the inelastic scattering cross sections were also deduced for ^{21}N, with hydrogen and lead targets. The net counts in the nearby peaks for the spectra with liquid hydrogen were derived by fixing the known peak positions and the peak widths determined previously. The relative intensities deduced from the spectrum, which includes all the multipolarities are as follows: 100(10) for the 1140-keV line and 65(6) for the 1210-keV line. The three excitation cross sections determined are σ(1140, H) = 6.6(8) mb, σ(2350, H) = 12.3(16) mb, and σ(1140, Pb) = 11.4(34) mb.

The cross sections were interpreted in terms of the collective model. The proton and neutron deformation lengths ($\delta_p\, \delta_n$) were determined by the method described in detail in Ref.[3)] and were found to be $\delta_n = 0.95(5)$ fm and $\delta_p = 0.95(15)$ fm. From these values, the quadrupole neutron and proton transition matrix elements $M_n^2 = 110(12)$ fm^4 and $M_p^2 = 28(9)$ fm^4, and the ratio $M_n/M_p = 2.0$ were obtained. This ratio was equal to N/Z, indicating the pure isoscalar character of the transition. The results were similar to those obtained for the ^{22}O nucleus, which has 14 neutrons for which small transition matrix elements and $M_n/M_p = 1.4(5)\ N/Z$ were extracted.

According to the weak-coupling approximation, the sum of the E2 strengths from the ground state to the $3/2^-$ and $5/2^-$ states in the ^{21}N isotope gives the B(E2; $0^+ \to 2^+$) strength in the appropriate core. Under this assumption, the effective B(E2) value of the ground-state transition in the core of ^{21}N can be estimated as 56(18) e^{2}fm^4. The shell model calculations show that the summed strength for ^{21}N is 54 e^{2}fm^4[2)], which is about twice that for ^{22}O value and is between the neighbouring oxygen and carbon B(E2; $0^+ \to 2^+$) values. Shell model calculations give 110 e^{2}fm^4 for ^{20}C, which is much larger than the experimental value (<18 e^{2}fm^4) because of the decoupling of the neutrons from the core in heavy carbon nuclei. This fact shows that the core structure of the nitrogen isotopes is softer than that of the singly closed shell oxygen isotopes; this proposal is consistent with the 1.2 MeV reduction of the N=14 shell closure from ^{22}O to ^{21}N, which is due to the removal of a proton from the $p_{1/2}$ orbit.

References
1) Z. Elekes et al., Phys. Rev. C **82**, 027305 (2010).
2) D. Sohler et al., Phys. Rev. C **77**, 044303 (2008).
3) Z. Elekes et al., Phys. Rev. C **78**, 027301 (2008).

† Condensed from the article in Phys. Rev. C **82**, 027305 (2010)
*1 Institute of Nuclear Research of the Hungarian Academy of Sciences, Hungary
*2 Niigata University, Japan
*3 Forschungszentrum Dresden-Rossendorf, Germany
*4 Michigan State University, USA
*5 Osaka City University, Japan
*6 Tohoku University, Japan
*7 Eötvös Loránd University, Hungary
*8 Tokyo Institute of Technology, Japan
*9 RCNP, Osaka University, Japan
*10 Saitama University, Japan

Proton resonance elastic scattering of ^{34}Si

N. Imai,[*1] Y. Hirayama,[*1] Y.X. Watanabe,[*1] T. Teranishi,[*2] T. Hashimoto,[*3] S. Hayakawa,[*3] Y. Ichikawa, S.C. Jeong,[*1] D. Kahl,[*3] S. Kubono,[*3] H. Miyatake,[*1] H. Ueno, H. Yamaguchi,[*3] K. Yoneda, and A. Yoshimi,

[Nuclear structure, resonance scattering, unstable nuclei]

The $N = 21$ nucleus ^{35}Si is located in the vicinity of the island of inversion. The neutron single-particle structure of the nucleus may shed light on the shell evolution in this region. We investigated the isobaric analog resonances (IARs) of the bound states in ^{35}Si by measuring the proton resonance elastic scattering of ^{34}Si using the thick-target inverse-kinematics method[1]. When isospin symmetry of the nuclear force is assumed, the neutron single-particle configurations of the bound states of ^{35}Si are identical to the configuration of the valence proton in the excited states appearing at high excitation energies in the isobaric nucleus ^{35}P, called IARs. The IAR shape and widths will provide information about the angular momentum l and spectroscopic factor S in the parent state.

The experiment was performed at the accelerator facility operated by the RIKEN Nishina Center and Center for Nuclear Study, University of Tokyo. A secondary ^{34}Si beam was produced by projectile fragmentation of a 63-MeV/nucleon ^{40}Ar primary beam and separated by the fragment separator RIPS. The secondary beams were identified on the basis of the time-of-flight between the timing signals measured by a 0.1 mm thick plastic scintillator located in the second focal plane of RIPS and the cyclotron RF signals. After the particle identification, the energy of the beams was decreased to 4.7 ± 1.2 MeV/nucleon by allowing them to pass through a rotating carbon plate with a thickness of 90 mg/cm^2. The incident energies of the beams on a secondary target were determined by the time difference between the plastic scintillator and two sets of parallel-plate avalanche counters (PPACs) placed upstream of the target. The ^{34}Si beam had a typical intensity of 7×10^4 particles per second.

The secondary target was a 10.9 mg/cm^2 thick polyethylene film. A 12.9 mg/cm^2 thick carbon film was also used to evaluate the protons derived from the fusion evaporation reaction. Outgoing particles were detected by the three layers of silicon semiconductor detectors (SSDs) mounted at 0° in the laboratory frame. The respective thicknesses of SSDs were 1.0, 1.5, and 1.0 mm, and size of the detector was 48×48 cm^2, which covered $\pm 6.2°$. The first-layer SSD double-sided and orthogonally oriented $16 + 16$ strips, allowing for the determination of the scattering angles.

The excitation function of the differential cross section of proton elastic scattering is presented in Fig. 1; this function was obtained by subtracting the carbon contribution from the cross sections measured using the polyethylene target. The cross section at each energy bin was deduced by taking into account the target thickness at which the beam lost the energy of the bin width, and the energy distribution of the beams.

R-matrix analysis was performed to deduce the resonance parameters of the respective resonances. Assuming the ls, the minimum value of χ^2 was searched for by changing the parameters. In the calculation, potential scattering was obtained by using the global optical model potential set[2]. The best-fit curve was obtained with nine resonances, including the four IARs estimated from the parent states. Their ls were assigned the values $0, 3, 2, 2, 1, 0, 3, 2$, and 0, starting from the lowest energy. The resultant curve is also presented in Fig. 1, and it shows good agreement with the data.

The first resonance $l = 0$ should be due to a lower-isospin excitation since the resonance energy is smaller than that expected for the IAR of the ground state, when the Coulomb energy difference between ^{35}Si and ^{35}P is considered. The second resonance $l = 3$ can be assigned to the IAR of the ground state. The deduced S value, 0.78, is consistent with the result of resent g-factor measurements[3]. Further analysis is in progress.

References
1) N. Imai *et al.,* Eur. Phys. J. **A 46**, 157-160 (2010).
2) F.D. Becchetti, Jr., and G.W. Greenless, Phys. Rev. **182**, 1190-1209 (1969).
3) G. Neyens *et al.,* Eur. Phys. J. Special Topics **150**, 149-153 (2007).

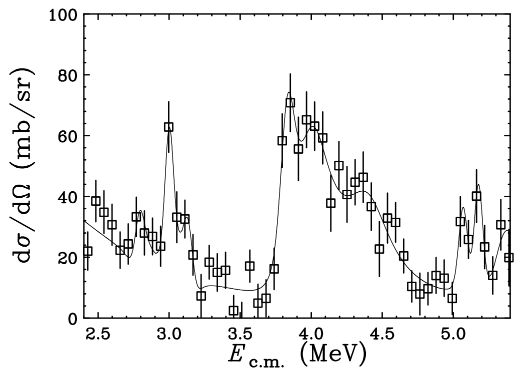

Fig. 1. Excitation function of proton elastic scattering on ^{34}Si.

*1 IPNS, KEK
*2 Department of Physics, Kyushu University
*3 CNS, University of Tokyo

Spherical shell closure at N=16 in ^{24}O

K. Tshoo,[*1] Y. Satou,[*1] T. Nakamura,[*2] N. Aoi, H.C. Bhang,[*1] S. Choi,[*1] S. Deguchi,[*2] F. Delaunay,[*3] J. Gibelin,[*3] T. Honda,[*4] M. Ishihara, Y. Kawada,[*2] N. Kobayashi,[*2] T. Kobayashi,[*5] Y. Kondo,[*2] F.M. Marques,[*3] M. Matsushita,[*4] Y. Miyashita,[*6] T. Motobayashi, Y. Nakayama,[*2] N.A. Orr,[*3] H. Otsu, H. Sakurai, S. Shimoura,[*7] D. Sohler,[*8] T. Sumikama,[*6] S. Takeuchi, K.N. Tanaka,[*2] N. Tanaka,[*2] Y. Togano, K. Yoneda, K. Yoshinaga,[*6] T. Zheng,[*9] Z.H. Li, Z.X. Cao,[*9]

[Nuclear structure, Neutron-rich nuclei, Magic number, Shell structure]

Recently, the first experimental attempt to measure the first 2^+ excitation energy of ^{24}O was made by Hoffman *et al.*[1)] at MSU using the proton removal reaction of a ^{26}F beam. Since no γ-ray decay was observed, they used the invariant mass method to measure the resonance energies of the unbound excited states of ^{24}O. Although the measured high excitation energy of the first excited state of ^{24}O supports the magic nature of this isotope at N=16, no assignment has been made for the spin parity of the state, and the degree of collectivity has still not been experimentally determined.

In order to clarify the magic nature of ^{24}O, the experiment was performed using the proton inelastic scattering in inverse kinematics at 63 MeV/nucleon at RIKEN. The resonance energies of the unbound excited states of ^{24}O were determined by the invariant mass method. The decay energy of ^{24}O* (relative energy between ^{23}O and n) was reconstructed by measuring the four momenta of ^{23}O and n. The resonance energy of the first unbound excited state was extracted to be $E_{\rm r} = 0.56 \pm 0.06$ MeV (preliminary), which corresponded to the excitation energy $E_{\rm x} = 4.65 \pm 0.14$ MeV. This result agreed well with that of the previous measurement made in the proton removal reaction of ^{26}F[1)].

For extracting the deformation parameter, DWBA calculations were performed with the coupled-channel calculation code ECIS97[2)] using the standard symmetric vibrational model with two sets of global phenomenological potentials KD02[3)] and CH89[4)]. The result of DWBA calculation with the potentials KD02[3)] and CH89[4)] were in good agreement with the ^{22}O data that were previously obtained by proton inelastic scattering[5)]. The deformation parameter β_2 in the (p,p') reaction, which is usually denoted as "$\beta_{(p,p')}$", was deduced by normalization of the calculated inelastic cross section $\sigma_{2+}^{\rm DWBA}(\theta_{\rm cm} < 90°)$ to the experimental data $\sigma_{2+}(\theta_{\rm cm} < 90°)$. The extracted deformation parameters were $\beta_{(p,p')}$=$0.14^{+0.06}_{-0.02}$ and $\beta_{(p,p')}$=$0.15^{+0.07}_{-0.02}$ (preliminary) for the KD02[3)] and CH89[4)] optical parameters, respectively. The quoted errors were deduced from the uncertainty in the experimental cross section $\sigma_{2+}(\theta_{\rm cm} < 90°)$. Fig. 1 shows the observed angular distribution for inelastic scattering to the 2_1^+ state (filled circles). The angular distribution was obtained by fitting the decay energy spectrum for each angular bin. The solid and dashed curves represent the angular distributions calculated by the ECIS97[2)] code with $\beta_{(p,p')}$ values of 0.14 and 0.15 for the optical parameter sets KD02[3)] and CH89[4)], respectively. Both the calculated distributions were consistent with the experimental angular distribution, thus supporting the J^π= 2^+ assignment of the first excited state in ^{24}O.

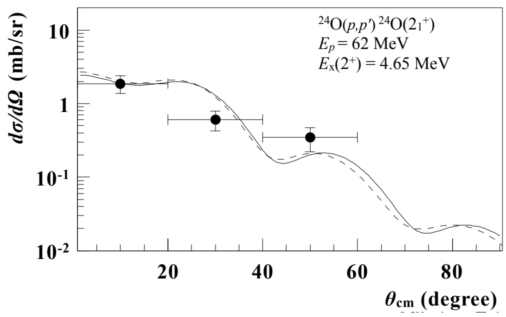

Fig. 1. The observed angular distribution is shown by the filled circles. The vertical errors are statistical errors, and the horizontal errors indicate the angular bin size (±10°).

The high excitation energy of the 2_1^+ state and the small $\beta_{(p,p')}$ value strongly support the spherical shell closure at N=16 for the oxygen isotopes.

*1 Department of Physics and Astronomy, Seoul National University, Korea.
*2 Department of Physics, Tokyo Institute of Technology, Japan.
*3 LPC Caen, ENSICAEN, Université de Caen, CNRS/IN2P3, Caen, France.
*4 Department of Physics, Rikkyo University, Japan.
*5 Department of Physics, Tohoku University, Japan.
*6 Department of Physics, Tokyo University of Science, Japan.
*7 Department of Physics, The University of Tokyo, Japan.
*8 Institute of Nuclear Physics (ATOMKI), Debrecen, Hungary.
*9 School of Physics and State Key Laboratory of Nuclear Physics and Technology, Peking University, Beijing, China.

References

1) C.R. Hoffman *et al.*, Phys. Lett. B **672**, 17 (2009).
2) J. Raynal, coupled channel code ECIS97 (unpublished).
3) A.J. Koning and J.P. Delaroche, Nucl. Phys. A **713**, 231 (2003).
4) R.L. Varner, W.J. Thompson, T.L. McAbee, E.J. Ludwig, and T.B. Clegg, Phys. Rep. **201**, 57 (1991).
5) E. Becheva *et al.*, Phys. Rev. Lett. **96**, 012501 (2006).

Spin-orbit potentials between proton and neutron-rich helium isotopes studied with solid polarized proton target

S. Sakaguchi, T. Uesaka,[*1] T. Kawabata,[*1] T. Wakui,[*2] N. Aoi, Y. Hashimoto,[*3] Y. Ichikawa, K. Itoh,[*5] M. Itoh,[*2] H. Iwasaki,[*4] T. Kawahara,[*6] Y. Kondo,[*3] H. Kuboki, Y. Maeda,[*7] K. Miki,[*4] T. Nakamura,[*3] T. Nakao,[*4] Y. Nakayama,[*3] S. Noji,[*4] H. Okamura,[*8] H. Sakai,[*4] Y. Sasamoto,[*1] M. Sasano, Y. Satou,[*3] K. Sekiguchi, T. Shimamura,[*3] Y. Shimizu, M. Shinohara,[*3] K. Suda, D. Suzuki,[*4] Y. Takahashi,[*4] A. Tamii,[*8] K. Yako,[*4] and M. Yamaguchi

Recently, there has been considerable interest on spin-orbit coupling in unstable nuclei. While there have been extensive discussions on its possible change in neutron-rich nuclei[1–3)], experimental information is rather scarce. To obtain direct information on the spin-orbit interaction between proton and neutron-rich nuclei, we have measured the vector analyzing power of the elastic scattering of protons from ^{6}He and ^{8}He at 71 MeV/A. The experiment was carried out using the RIKEN Projectile-Fragment Separator (RIPS). We used a solid polarized proton target that was specially constructed for radioactive-ion-beam experiments[4,5)].

In order to understand the global nature of $p-^{6,8}$He interactions, we determine optical model potentials that reproduce the data. The obtained potentials are shown in Fig. 1 as functions of the radius. The upper panel shows real (solid) and imaginary (dashed) parts of the central term, while the lower one presents a spin-orbit term (dotted) with error bands (solid) that result from the fitting uncertainty. Here, we focus on the radius and amplitude of the peak of the spin-orbit potentials. We call the radius as "LS radius" and the amplitude as "LS amplitude." Since the spin-orbit potential is approximated by the radial derivative of the density distribution, the LS radius and LS amplitude should be related to the radius and gradient of the density distribution, respectively. The obtained LS amplitudes (1.3 and 2.0 MeV) are remarkably smaller than the global systematics of stable nuclei (5 MeV). This is considered to be a reflection of the diffuse density distribution of neutron-rich helium isotopes.

^{6}He and ^{8}He are known to have an $\alpha + xn$ cluster structure. It has been pointed out that the contribution of valence neutrons to the spin-orbit potential would be one order of magnitude smaller than the contribution of the α core[6)]. From this estimation, the spin-orbit potentials of ^{6,8}He are expected to reflect the spatial distribution of an α core in the nucleus. To be specific, the LS radius should increase with the diffuseness of the α core distribution, while the LS amplitude decreases. The LS radius and LS amplitude of helium isotopes are plotted in Fig. 2 as functions of the radius of the point proton distribution, which represents the spatial distribution of the α core. These radii are deduced from the corresponding charge radii[7,8)] using a relation given in Ref.[8)]. Although the large experimental uncertainty prevents us from making a definite statement, linear relations are indicated as discussed above. Thus, we can infer that the existence of valence neutrons broadens the spatial distribution of an α core in the nucleus and reduces the amplitude of the spin-orbit potential.

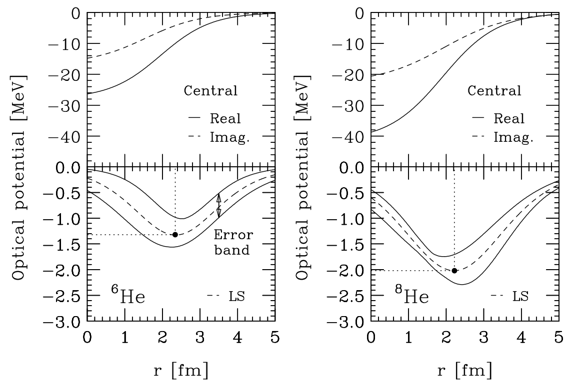

Fig. 1. Phenomenological optical potentials.

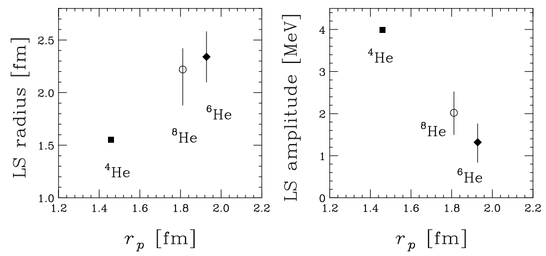

Fig. 2. LS radius and LS amplitude of helium isotopes as functions of the proton radius.

*1 Center for Nuclear Study, University of Tokyo
*2 Cyclotron and Radioisotope Center, Tohoku University
*3 Department of Physics, Tokyo Institute of Technology
*4 Department of Physics, University of Tokyo
*5 Department of Physics, Saitama University
*6 Department of Physics, Toho University
*7 Department of Physics, Kyushu University
*8 Research Center for Nuclear Physics, Osaka University

References

1) J. Dobaczewski et al.: Phys. Rev. Lett. **72**, 981 (1994).
2) G.A. Lalazissis et al.: Phys. Lett. B **418**, 7 (1998).
3) B.S. Pudliner et al.: Phys. Rev. Lett. **76**, 2416 (1996).
4) T. Wakui et al.: Nucl. Instr. Meth. **550**, 521 (2005).
5) T. Uesaka et al.: Nucl. Instr. Meth. **526**, 186 (2004).
6) Y. Iseri et al.: Genshikaku Kenkyu **49**, 53 (2005).
7) I. Sick: Phys. Lett. B **116**, 212 (1982).
8) P. Mueller et al.: Phys. Rev. Lett. **99**, 252501 (2007).

Measurement of the ^{90}Zr(^{12}N, ^{12}C)^{90}Nb reaction at 200 MeV/nucleon

S. Noji[*1], H. Sakai[*2], N. Aoi[*2], H. Baba[*2], G. P. A. Berg[*4], R. Chen[*2], P. Doornenbal[*2], M. Dozono[*3], N. Fukuda[*2], N. Inabe[*2], D. Kameda[*2], T. Kawabata[*5], S. Kawase[*3], Y. Kikuchi[*3], K. Kisamori[*3], T. Kubo[*2], Y. Maeda[*6], H. Matsubara[*3], S. Michimasa[*3], K. Miki[*1,*2], H. Miya[*3], H. Miyasako[*6], S. Sakaguchi[*2], Y. Sasamoto[*3], S. Shimoura[*3], M. Takaki[*3], H. Takeda[*2], S. Takeuchi[*2], H. Tokieda[*2,*3], T. Ohnishi[*2], S. Ota[*3], T. Uesaka[*3], H. Wang[*2], K. Yako[*1], Y. Yanagisawa[*2], N. Yokota[*5], and K. Yoshida[*2]

[SHARAQ spectrometer, nuclear reactions ^{90}Zr(^{12}N, ^{12}C) $E = 200$ MeV/nucleon, exothermic charge-exchange reaction, giant resonance]

The existence of the isovector spin monopole resonance (IVSMR) has long been an issue to be clarified. The IVSMR is a coherent $2\hbar\omega$ $1p$-$1h$ excitation with $\Delta L = 0$ and $\Delta S = \Delta T = 1$ driven by the operator $\hat{O}_{\pm} \equiv \sum_k t_{\pm}(k)\sigma_{\mu}(k)r(k)^2$. The energy centroid and width of the IVSMR can be related to, for example, the isovector spin-incompressibility, the effective interaction in a spin-isospin channel, etc. From the model independent sum rule $\mathcal{S}_- - \mathcal{S}_+ = 3(N\langle r^4\rangle_n - Z\langle r^4\rangle_p)$, with $\mathcal{S}_{\pm} = \sum_{\mu}\sum_m |\langle m|\hat{O}_{\pm}|0\rangle|^2$, one can deduce a quantity $\delta_{np} = \sqrt[4]{\langle r^4\rangle_n} - \sqrt[4]{\langle r^4\rangle_p}$, which is related to the neutron skin thickness and then places a strong constraint on the neutron matter equation of state. Although important, experimental information on the IVSMR has been scarce.

In October 2010, we performed a ^{90}Zr(^{12}N, ^{12}C)^{90}Nb experiment at 200 MeV/nucleon to search for IVSMR in ^{90}Nb. The charge-exchange reaction induced by an unstable heavy ion, here ^{12}N, which we call the exothermic charge-exchange reaction, has the following advantages for the IVSMR study: (1) This reaction can realize high excitation energy transfer with only a small momentum transfer, thanks to the large mass difference (~17 MeV) between the projectile and ejectile. This kinematical condition is preferable for the $\Delta L = 0$ mode. (2) This reaction is sensitive to the surface region because of strong absorption. Therefore IVSMR, whose transition density has a node at the surface, can be strongly excited. (3) This reaction has the selection rule $\Delta S = \Delta T = 1$; thus, it exclusively excites isovector spin-flip modes.

However, this reaction should introduce two types of physical backgrounds: One is because of the β decay of the ^{12}N projectile, whose half-life is 11.0 ms. The other is because of the Fermi transition of ^{12}N to the excited state in ^{12}C at 15.1 MeV, which is the IAS of the ground state of ^{12}N. The transition has a relatively large B(F) value of 2, unlike the transition to the ground state, which has B(GT) = 0.3. This relationship is depicted in Fig. 1. This Fermi transition excites the IAS and the isovector non-spinflip monopole resonance in ^{90}Nb, and the ^{12}C*(IAS) mainly decays to the ground state by γ decay. In this experiment, we aimed to verify the usefulness of the method by employing a setup to remove the backgrounds.

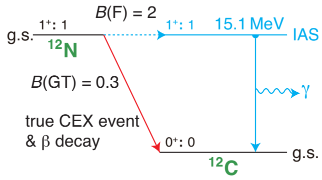

Fig. 1. Energy relationship between ^{12}N and ^{12}C.

We carried out the experiment at the RIBF by using the BigRIPS, the High Resolution Beam Line, and the SHARAQ Spectrometer. The primary beam of ^{14}N, accelerated by AVF, RRC, and SRC up to 250 MeV/nucleon, bombarded the Be target at F0 with a thickness of 5 mm, and the secondary ^{12}N beam was produced via projectile fragmentation. The beam was transported to the target in the dispersion matching mode. A position-sensitive segmented scintillation detector at F3 and two MWDCs at F-H10 were used to measure the trajectories of the beam during the measurement. The reaction target used here was ^{90}Zr with a thickness of 150 mg/cm^2. The reaction product was momentum analyzed by SHARAQ and detected at the focal plane by two CRDCs and a scintillator stack.

For the estimation of the background contribution, we installed a pair of 1 mm-thick plastic scintillators at ~8 mm up- and downstream of the ^{90}Zr target in order to determine the charges of the incoming and outgoing particles and to separate the true charge-exchange events from the β decay events. We also installed the NaI array DALI2 around the target chamber for the detection of γ rays from the de-excitation of ^{12}C*(IAS).

The beam was stable throughout the experiment; the maximum intensity of the primary beam was 400 pnA. The counting rate and the purity of the ^{12}N beam were 1.4 Mcps and 90%, respectively. Double-differential-cross-section data were successfully obtained. Detailed analysis for the IVSMR is currently in progress.

*1 Department of Physics, University of Tokyo
*2 RIKEN Nishina Center
*3 Center for Nuclear Study, University of Tokyo
*4 Joint Institute for Nuclear Physics and the Department of Physics, University of Notre Dame
*5 Department of Physics, Kyoto University
*6 Department of Applied Physics, University of Miyazaki

Coulomb excitation of proton-rich nucleus ^{28}S

Y. Togano, Y. Yamada,[*1] N. Iwasa,[*2] T. Motobayashi, N. Aoi, H. Baba, S. Bishop, X. Cai,[*3] P. Doornenbal, D. Fang,[*3] T. Furukawa, K. Ieki,[*1] T. Kawabata,[*4] S. Kanno, N. Kobayashi,[*5] Y. Kondo, T. Kuboki,[*6] N. Kume,[*2] K. Kurita,[*1] M. Kurokawa, Y. G. Ma,[*3] Y. Matsuo, H. Murakami, M. Matsushita,[*1] T. Nakamura,[*5] K. Okada,[*1] S. Ota,[*4] Y. Satou,[*5] S. Shimoura,[*4] R. Shioda,[*1] K. N. Tanaka,[*5] S. Takeuchi, W. Tian,[*3] H. Wang,[*3] J. Wang,[*7] K. Yamada, and K. Yoneda

[Nuclear structure, Unstable nuclei, Coulomb excitation]

The Coulomb excitation of the proton-rich nucleus ^{28}S was studied by inverse kinematics for deducing the reduced transition probability B(E2) between the ground and first excited state in ^{28}S.

B(E2) for the $0^+_{g.s.} \rightarrow 2^+_1$ transition in an even-even nucleus is one of the important quantities that should be considered to investigate the nuclear collectivity. In addition, the neutron and proton multipole matrix elements M_n and M_p are used to discuss the relative importance between the neutron and proton contributions to the transition, where M_n (M_p) is defined as $M_n(M_p) = \langle J_f||\Sigma_{n(p)} r_i^\lambda Y_\lambda(\Omega_i)||J_i\rangle$. The M_p value, which reflects the motion of protons in the nucleus, is directly related to the B(E2) value as $B(\mathrm{E2}; J_i \rightarrow J_f) = |M_p|^2/(2J_i+1)$. Therefore, the M_p value can be determined via the measurement of the B(E2) value. The M_n value can be obtained by comparing the B(E2) value in the mirror nucleus by assuming isospin symmetry[1)]. The aim of the present study is to determine the ratio M_n/M_p of ^{28}S to discuss the nuclear collectivity of ^{28}S.

An experiment was performed by using the RIPS at the RIKEN Nishina Center. A ^{28}S beam with an energy of 62 MeV/nucleon was produced by the fragmentation of a 115-MeV/nucleon ^{36}Ar beam incident on a 531 mg/cm^2 Be target. The secondary beams were selected by RIPS with the help of an RF deflector system[2)]. The isotopic purity of ^{28}S in the secondary beams was 1.9%. The major contaminants were ^{26}Si, ^{25}Al, and ^{24}Mg. The ^{28}S beam was made to impinge on a ^{208}Pb target with a thickness of 348 mg/cm^2. Particle identification for the secondary beams was performed event by event by means of the time of flight (TOF)-ΔE method and by using the RF signal of the cyclotrons, a 0.1 mm-thick-plastic scintillator and a 0.1 mm-thick-silicon detector located in the final focal plane of the RIPS. Three sets of parallel plate avalanche counters (PPACs) were also placed in the final focal plane to determine the position and angle of the beams at the target position. The scattering angle and the energy of the outgoing ^{28}S particle from the target were measured by a silicon telescope located 62 cm downstream of the target. The detail of the telescope are provided in Ref. 3. A 160 NaI(Tl) scintillator array, DALI2[4)], was placed around the target to measure de-excitation γ-rays from the outgoing ^{28}S particle.

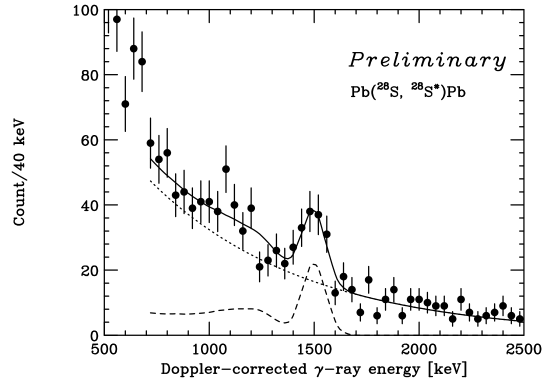

Fig. 1. Doppler-shift-corrected γ-ray spectrum measured in coincidence with ^{28}S. The solid curve represents the best fit obtained with the simulated response function (dashed curve) and the exponential background (dotted curve).

Figure 1 shows the Doppler-shift-corrected γ-ray energy spectrum of the ^{28}S+Pb reaction. The filled circles are the experimental data. The solid curve represents the best fit obtained by using the simulated response function of the DALI2 array and the exponential background, which are shown by the dashed and dotted curves, respectively. The response function was calculated by Monte Carlo simulation using GEANT4. The γ-ray line at 1.5 MeV, which is consistent with a previous result[5)], was clearly observed. Further analysis of a cross section and an angular distribution to obtain the B(E2) value is in progress.

*1 Department of Physics, Rikkyo University
*2 Department of Physics, Tohoku University
*3 Shanghai Institute of Applied Physics, CAS
*4 Center for Nuclear Study (CNS), University of Tokyo
*5 Department of Physics, TITECH
*6 Department of Physics, Saitama University
*7 Institute of Modern Physics, CAS

References

1) A. M. Bernstein et al.: Phys. Rev. Lett. **42**, 425 (1979).
2) K. Yamada et al.: Nucl. Phys. A **746**, 156c (2004).
3) Y. Togano et al.: RIKEN Accel. Prog. Rep. **42**, 11 (2009).
4) S. Takeuchi et al.: RIKEN Accel. Prog. Rep. **36**, 148 (2003).
5) K. Yoneda et al.: Phys. Rev. C **74**, 021303 (2006).

Diproton emission signals from excited ^{22}Mg and ^{23}Al

Y. G. Ma,[*1] D. Q. Fang,[*1] X. Y. Sun,[*1,*2] P. Zhou,[*1,*2] X. Z. Cai,[*1] J. G. Chen,[*1] W. Guo,[*1] W. D. Tian,[*1] H. W. Wang,[*1] G. Q. Zhang,[*1,*2] X. G. Cao,[*1,*2] Y. Fu,[*1,*2] Z. G. Hu,[*3] J. S. Wang,[*3] M. Wang,[*3] Y. Togano, N. Aoi, H. Baba, Y. Hara,[*4] T. Honda,[*4] K. Ieki,[*4] Y. Ishibashi,[*5] Y. Itou,[*5] N. Iwasa,[*6] S. Kanno, T. Kawabata,[*7] H. Kimura,[*8] Y. Kondo, K. Kurita,[*4] M. Kurokawa, T. Moriguchi,[*5] H. Murakami, H. Oishi,[*5] K. Okada,[*4] S. Ota,[*7] A. Ozawa,[*5] H. Sakurai, S. Shimoura,[*7] R. Shioda,[*4] E. Takeshita, S. Takeuchi, K. Yamada, Y. Yamada,[*4] Y. Yasuda,[*5] K. Yoneda, and T. Motobayashi

[C(^{22}Mg, p+p+^{20}Ne)C, C(^{23}Al, p+p+^{21}Na)C, diproton emission, momentum correlation]

The mechanism of proton decays, two-proton radioactivity in particular, is not well understood[1)]. To investigate a two-proton decay mechanism in proton-rich ^{23}Al and ^{22}Mg whose structures are interesting in many aspects[2–5)], we measured the relative momentum and opening angle of two protons emitted from a three-body decay channel corresponding to the excited states of ^{23}Al and ^{22}Mg. Radioactive isotope beams of ^{23}Al and ^{22}Mg were produced and selected using the RIPS facility. A ^{23}Al secondary beam with an incident energy of 72AMeV was produced by the projectile fragmentation of a ^{28}Si primary beam with an energy of 135A MeV by using a ^{9}Be production target. The secondary beam was then transported to a ^{12}C reaction target. The experimental setup and particle identification have been described in Ref. 6.

The relative momentum (q_{pp}) and opening angle (θ_{pp}) distributions of the two protons in the rest frame of the three-body decay channel corresponding to ^{23}Al are shown in Fig. 1 for an excitation-energy (E^*) window $10.5 \leq E^* \leq 15$ MeV. A peak at a q_{pp} value around 20 MeV/c is observed, which corresponds to a peak at a small θ_{pp} value around 30°. In addition, another peak is observed around $q_{pp} \sim 40$ MeV/c, which corresponds to a peak at large θ_{pp}. The peak at a q_{pp} value of 20 MeV/c and small θ_{pp} is consistent with the diproton emission mechanism. On the other hand, a peak at large q_{pp} and θ_{pp} may correspond to sequential proton decay or three-body democratic decay.

A similar analysis was performed for an even-even proton-rich nucleus ^{22}Mg. Fig. 2 shows the q_{pp} and θ_{pp} distributions for the channel ^{22}Mg → p + p + ^{20}Ne for the window $13.5 \leq E^* \leq 18$ MeV. A peak at a q_{pp} value of 20 MeV/c and the corresponding small θ_{pp} were observed. These values are consistent with the diproton emission mechanism.

From this analysis, a peak around $q_{pp} \sim 20$ MeV/c and small θ_{pp} is clearly observed for the above mentioned excitation-energy windows for the three-body decay channel corresponding to ^{23}Al and ^{22}Mg, which can be explained by the ^{2}He-like diproton emission. Considering the probability of a peak around $q_{pp} \sim$ 20 MeV/c and small θ_{pp}, it may be possible that sequential decay is dominant for the odd-Z proton-rich nucleus ^{23}Al, while diproton emission is favorable for the even-even proton-rich nucleus ^{22}Mg. We are collecting more details about the analysis and simulations to be performed.

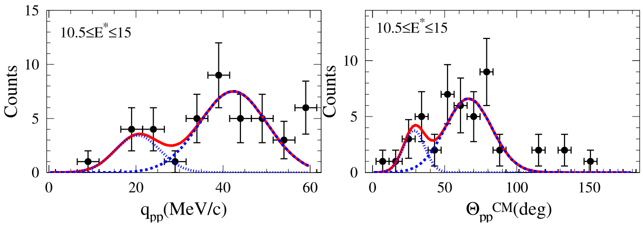

Fig. 1. Left panel: relative momentum distribution of two protons produced by the decay of ^{23}Al into two protons and ^{21}Na for $10.5 \leq E^* \leq 15$ MeV. Right panel: opening angle distribution between the two protons. The short-dotted and long-dashed lines represent two separate Gaussian fits and the solid line represents the summation of the two Gaussian fits.

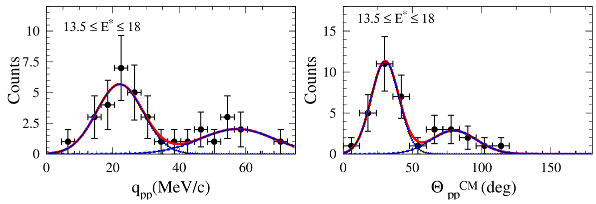

Fig. 2. The same distributions as those shown in Fig. 1 except for the channel p + p + ^{20}Ne corresponding to ^{22}Mg for $13.5 \leq E^* \leq 18$.

References
1) V. I. Goldansky: Nucl. Phys. **19**, 482 (1960).
2) T. Gomi et al.: Nucl Phys. A **758**, 761c (2005).
3) A. Ozawa et al.: Phys. Rev. C **74**, 021301(R) (2006).
4) D. Q. Fang et al.: Phys. Rev. C **76**, 031601(R) (2007).
5) M. Wiescher et al.: Z. Phys. A **325**, 309 (1986).
6) Y. G. Ma et al.: RIKEN Accel. Prog. Rep. **43**, 12 (2010).

*1 Shanghai Institute of Applied Physics, CAS, Shanghai 201800, China
*2 Graduate School of the CAS, Beijing 100039, China
*3 Institute of Modern Physics, CAS, Lanzhou 730000, China
*4 Department of Physics, Rikkyo University, Japan
*5 Institute of Physics, University of Tsukuba, Ibaraki, Japan
*6 Department of Physics, Tohoku University, Japan
*7 Department of Physics, Kyoto University, Japan
*8 Department of Physics, University of Tokyo, Japan

Nuclear Spectroscopy of neutron rich ^{10}He by ^{11}Li (d,^{3}He) transfer reaction

A. Matta,[*1] D. Beaumel,[*1] H. Otsu,[*2] N. Aoi,[*2] M. Assie,[*1] H. Baba,[*2] S. Boissinot,[*3] R. Chen,[*2] F. Delaunay,[*4] N. DeSereville,[*1] S. Franchoo,[*1] J. Gibelin,[*4] F. Hammache,[*1] H. Wang,[*2] N. Imai,[*5] N. Kobayashi,[*6] T. Kubo,[*2] Y. Kondo,[*6] Y. Kawada,[*6] V. Lapoux,[*3] J. Lee,[*2] N. Mizuki,[*2] T. Motobayashi,[*2] T. Nakamura,[*6] L. Nalpas,[*3] E. Nikolski,[*2] A. Obertelli,[*3] E. Pollacco,[*3] T. Sako,[*6] H. Sakurai,[*2] A. Sanchez-Benitez,[*7] J-A. Scarpaci,[*1] I. Stefan,[*1] D. Suzuki,[*8] T. Koutarou,[*6] M. Takechi,[*2] S. Takeuchi,[*2] R. Wolski,[*9] K. Yoneda,[*2]

The ^{10}He nucleus has been firstly studied at Riken by pioneering work [1] using invariant mass method in the 90's. Recent experiment at GSI [2] leads to compatible results for the first resonant state at 1.2MeV but ambiguities remain. A recent experiment using ^{8}He(t,p) reaction [3] shows no evidence of state below 3MeV above the two-neutron threshold. Thus, results for excited of states of 10He remain unclear. A calculations using ACCC method [4] predicted a never observed ground state just above the two neutrons threshold in addition to the 1.2MeV state [4].

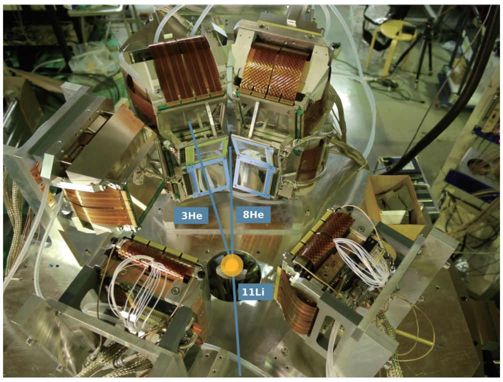

Fig. 1. *Upstream view of the set-up, the forward angle telescopes and thin silicon detectors (blue and green frame) are visible as well as telescopes at backward angle for (d,p) studies*

The missing mass method allows to reconstruct the excitation energy spectrum independently of the decay channel. The experiment was performed at the RIKEN RIPS facility, producing a secondary beam of ^{11}Li at 50A.MeV on a CD2 target. At forward angle, a wall of four MUST2 telescopes [5] were coupled with four 20μm thick silicon detectors (Fig. 1) in order to perform an E-ΔE identification of the light particles, and separation of ^{4}He and ^{3}He. At zero degree, a fifth MUST2 telescope was used for identification of heavy residues of reaction in coincidence. This telescope was protected by a two stages plastic used for E-ΔE identification. It is therefore expected to obtain information on the different decay channels opened for each resonant states. In addition a ^{9}Li beam at 50AMeV was used to perform a reference experiment. The ^{8}He reconstructed spectrum will be used as a validation criteria for the ^{10}He one.

*1 Institut de Physique Nucleaire, Orsay Cedex, France
*2 Riken, 2-1 Hirosawa, Wako, Saitama 351-0198, Japan
*3 CEA/IRFU/SPhN, CEA Saclay, Gif-sur-Yvette, France
*4 LPC, Universite de Caen ,Caen, France
*5 KEK, 1-1 Oho, Tsukuba-shi, Ibaraki-ken, 305, Japan
*6 Tokyo Institute of Technology,O-okayama,Tokyo, Japan
*7 Departamento de FA, Universidad de Huelva, Huelva, Spain
*8 NSCL, Michigan State University, Michigan, USA
*9 Institute of Nuclear Physics, Krakow (Poland)

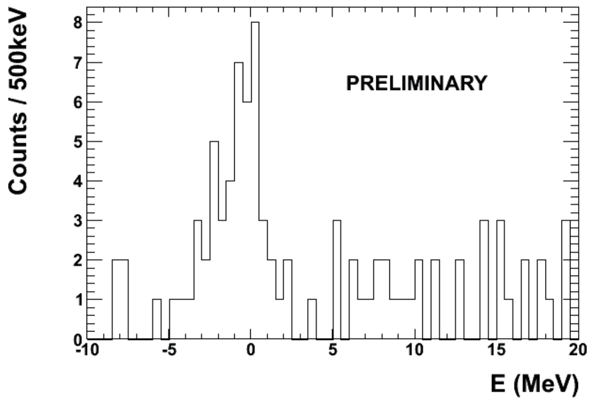

Fig. 2. *Preliminary spectrum of the ^{8}He nuclei.*

The energy and time calibrations have been done for the 128 X and Y strip of each telescopes, as well as the energy calibration of the 20μm thick silicon detector. E-ΔE and Time of Flight (TOF) identification has been performed and the ^{8}He ground state appear clearly (Fig. 2), populated by the ^{9}Li(d,^{3}He)^{8}He reaction, with a reasonably low background. Effect of the energy straggling in the target still need to be improved.

References

1) A.A. Korsheninnikov et al, Phys. Lett. B 326, 31 (1994)
2) H.T. Johansson et al, Nucl. Phys. A Volume 842, 15 (2010)
3) M.S. Golovkov et al, Phys. Lett. B Volume 672, 22 (2009)
4) S. Aoyama, Nucl. Phys. A722, 474 (2003)
5) E. Pollacco et al, Eur. Phys. J. A25, 287 (2005)

RIKEN Accel. Prog. Rep. 44 (2011)

Measurement of interaction cross sections for Mg isotopes

M. Takechi, S. Suzuki,[*1] D. Nishimura,[*2] M. Fukuda,[*2] T. Ohtsubo,[*1] M. Nagashima,[*1] T. Suzuki,[*3] T. Yamaguchi,[*3] A. Ozawa,[*4] H. Ooishi,[*4] T. Moriguchi,[*4] T. Sumikama,[*5] H. Geissel,[*6] N. Aoi, Rui-Jiu Chen, De-Qing Fang,[*7] N. Fukuda, S. Fukuoka,[*4] H. Furuki,[*3] N. Inabe, Y. Ishibashi,[*4] T. Ito,[*1] T. Izumikawa,[*1] D. Kameda, T. Kubo, M. Lantz,[*9] C. S. Lee,[*3] Yu-Gang Ma,[*7] Yu-Gang Ma,[*2] M. Mihara,[*2] S. Momota,[*8] D. Nagae,[*4] R. Nishikiori,[*4] T. Niwa,[*4] T. Ohnishi, K. Okumura,[*4] T. Ogura,[*1] H. Sakurai, K. Sato,[*3] Y. Shimbara,[*1] H. Suzuki,[*4] H. Takeda, S. Takeuchi, K. Tanaka, H. Uenishi,[*2] M. Winkler,[*6] and Y. Yanagisawa

[BigRIPS, interaction cross section, nuclear structure, unstable nuclei]

Over the past 25 years, the nuclear radii of exotic nuclei have been determined through the measurement of interaction cross sections ($\sigma_{\rm I}$), and the anomalous structures of these nuclei, such as skin and halo structures, have been found and discussed[1]. On the other hand, in the 1990s, vanishing of the $N = 20$ magic number in the so-called island of inversion region[2], which includes neutron-rich Ne, Na, and Mg isotopes has been extensively studied and discussed. In those studies, the inversion of amplitudes between the sd-normal and pf-intruder shells was considered along with the nuclear deformation. Presently, an advanced radioactive-beam facility enables us to explore the weakly bound nuclei near the drip line in this island of inversion, and thus, we can investigate the single-particle orbital of the valence nucleons in such nuclei by searching for possible large low-ℓ halo formations caused by the anomalous shell structures.

We have measured $\sigma_{\rm I}$ for $^{24-38}$Mg from the stability line to the vicinity of the neutron drip line, with the aim of searching for halo nuclei in a systematic manner. Measurements were performed at the RI beam factory (RIBF). Secondary beams of the Mg isotopes were produced by projectile fragmentation of a 345 MeV/nucleon ^{48}Ca primary beam on Be production targets. The average intensity of the primary beam in the measurement of $\sigma_{\rm I}$ for ^{37,38}Mg was around 70 pnA. The $\sigma_{\rm I}$ can be assumed to be almost equal to the reaction cross section ($\sigma_{\rm R}$) at the relativistic energies, and can be directly determined using transmission method[5]. Our experimental setup is based on the BigRIPS fragment separator[3,4], as shown in Fig. 1. A wedge-type 1.8 g/cm^2 thick or a homogeneous 3.6 g/cm^2 thick carbon target was located at F5. The incident and outgoing secondary beams were identified by the $B\rho$ - ΔE -TOF method using the BigRIPS beamline from F3 to F5 and from F5 to F7, respectively. For ΔE measurements, Ion Chambers (IC) at F3 and F7 were used. Plastic scintillators located at the F3, F5, and F7 focal planes were used for TOF and $B\rho$ measurements. The position information from the PPACs at F3 was used to apply the appropriate emittance cut for the incident beam, so that all the noninteracting particles could be accurately counted after the reaction target. Empty-target measurements were also performed to measure the nuclear reactions in the detectors and to deduce the reaction rate in the target accurately.

A statistical accuracy of 1∼2 % in $\sigma_{\rm I}$ has been achieved for each Mg isotope. Data analysis is in progress.

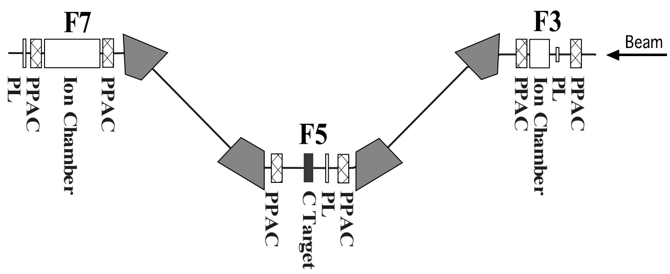

Fig. 1. Schematic drawing of the experimental setup.

References
1) A. Ozawa et al.: Nucl. Phys. **A691**, 599 (2001).
2) E. K. Warburton et al.: Phys. Rev. C **41**, 1147 (1990).
3) T. Kubo: Nucl. Inst. Meth. **B204**, 97 (2003).
4) T. Ohnishi et al.: J. Phys. Soc. Jpn. **77**, 083201 (2008).
5) T. Suzuki et al.: Nucl. Phys. **A630** 661(1998).

*1 Graduate School of Science, Niigata University
*2 Department of Physics, Osaka University
*3 Department of Physics, Saitama University
*4 Institute of Physics, Tsukuba University
*5 Department of Physics, Tokyo University of Science
*6 GSI
*7 Shanghai Institute of Applied Physics, Chinese Academy of Sciences
*8 Faculty of Engineering, Kochi University of Technology
*9 Institutionen för fysik och astronomi, Uppsala University

Single-nucleon removal reactions of ^{30}Ne and ^{36}Mg on a carbon target

J. Lee, H. Scheit,[1] N. Aoi, P. Doornenbal, E. Ideguchi,[2] N. Kobayashi, Y. Kondo,[3] G. Lee,[3] K. Li,[1] M. Matsushita,[4] S. Michimasa,[2] T. Motobayashi, H. Sakurai, D. Steppenbeck, M. Takechi, S. Takeuchi, Y. Togano, and H. Wang,[1]

[Nuclear structure, Island of Inversion, in-beam γ-ray spectroscopy]

Experiments involving nuclei close to the boundary or within the well-known island of inversion, a region where the $N = 20$ shell closure disappears, play a vital role in the understanding of nuclear structure. The enhanced particle-hole excitations due to the broken $N = 20$ shell and large pf-shell occupancy result in the dramatic change in the single-particle structure. Systematic investigation of the structure evolution towards and across the island of inversion is essential to establish the role of intruder configurations and evaluate the effective interactions employed in current shell models.

Single-nucleon removal reaction is known as the powerful technique to study the singe-particle properties. The γ-ray transitions yield the energies of excited states, while the shapes of the longitudinal momentum distributions give the l-values of the knock-out to the individual states in the reaction residues. Coupled with reaction and structure theories, the cross section data provide quantitative information on the details of the nuclear wave functions.

Here, we report on the in-beam γ-ray spectroscopic study performed at the Radioactive Ion Beam Facility, aiming for the determination of level schemes and spin assignments of the populated low-lying excited states of ^{29}Ne and ^{35}Mg via one-neutron knockout reactions from ^{30}Ne and ^{36}Mg. The present work extends the systematic studies to more neutron-rich isotopes from the previous measurements of ^{27}Ne[1)] and ^{29,31}Mg[2)].

A primary ^{48}Ca beam with an average intensity of about 70 particle nA and an energy of 345 MeV/u was impinging on a 15 mm thick rotating Be target mounted at the focus F0 of the fragment separator BigRIPS[3)]. The produced secondary beams were separated and selected in the first stage of BigRIPS, using the standard $B\rho - \Delta E - B\rho$ method with a 15 mm thick and 10 mm thick Al wedge degrader at the F1 dispersive focus of the BigRIPS separator for ^{30}Ne and ^{36}Mg beam respectively. The particles were identified event-by-event in the second stage of BigRIPS using the standard $\Delta E - B\rho -$TOF method. The time-of-flight (TOF) was measured between two plastic scintillators located at the foci F3 and F7, the energy loss (ΔE) was determined with an ion-chamber[4)] located at the focus F7, and the $B\rho$ was obtained from the position measurements with the parallel plate avalanche counters[5)] at the dispersive F5 focus of BigRIPS. The momentum acceptance for the secondary beams passing BigRIPS was ±3%.

The secondary beams ^{30}Ne and ^{36}Mg were transported to the focus F8 and incident on a 2.54 g/cm^2 thick (natural) carbon target at energies of about 250 and 245 MeV/u respectively. The averaged ^{30}Ne and ^{36}Mg rates were about 250 and 80 particles/s and comprised 60 % and 13 % of the respective secondary beams. The emitted de-excitation gamma rays were detected by 186 large volume NaI(Tl) crystals, DALI2 array[6)], with full energy peak efficiency of about 25 % and the expected resolution after correcting the large Doppler shift of about 10 % for a 1 MeV gamma transition. ZeroDegree spectrometer was employed for particle identification and track reconstruction after the secondary target. The standard $\Delta E - B\rho -$TOF method was applied to identify the particles unambiguously event by event. More than 3 hours and 9 hours of data taking were performed for the ^{30}Ne and ^{36}Mg beams on the one-neutron removal channel respectively.

The data currently being analyzed are expected to give information about single-particle properties of the low-lying states in ^{29}Ne and ^{35}Mg. Cross section population of the states in ^{29}Ne would also confirm the components in the ground-state wave function of ^{30}Ne lying inside the Island of Inversion.

References
1) J.R. Terry *etal.*, Phys. Lett. B **640**, 86 (2006).
2) J.R. Terry *etal.*, Phys. Rev. C **77**, 041316 (2008).
3) T. Kubo *et al.*, Nucl. Instr. and Meth. B 204, 97 (2003).
4) H. Otsu *et al.*, RIKEN Acc. Rep. 42, 163 (2009).
5) T. Ohnishi *et al.*, J. Phys. Soc. Jpn. **77**, 083201 (2008).
6) S. Takeuchi *et al.*, RIKEN Acc. Rep. **36**, 148 (2003).

*1 Peking University, China
*2 Center for Nuclear Study, The Univ. of Tokyo
*3 Department of physics, Tokyo Institute of Technology
*4 Department of Physics, Rikkyo University

Spectroscopy of ^{42}Si via two-proton removal reaction

S. Takeuchi, M. Matsushita,[*1] N. Aoi, P. Doornenbal, J. Lee, K. Li,[*2] H. Scheit, D. Steppenbeck, H. Wang,[*2] H. Baba, D. Bazin,[*3] L. Caceres,[*4] H. Crawford,[*5] P. Fallon,[*5] R. Gernhäuser,[*6] J. Gibelin,[*7] S. Go,[*8] S. Grévy,[*4] C. Hinke,[*6] C. Hoffman,[*9] R. Hughes,[*10] E. Ideguchi,[*8] D. Jenkins,[*11] N. Kobayashi,[*12] Y. Kondo,[*12] R. Krücken,[*6] T. Le Bleis,[*13] G. Lee,[*12] A. Matta,[*14] S. Michimasa,[*8] T. Motobayashi, T. Nakamura,[*12] S. Ota,[*8] M. Petri,[*5] T. Sako,[*12] H. Sakurai, S. Shimoura,[*8] K. Steiger,[*6] K. Takahashi,[*12] M. Takechi, Y. Togano, R. Winkler,[*3] and K. Yoneda

[nuclear structure, in-beam γ-ray spectroscopy]

The excited states of a ^{42}Si nucleus have been studied via in-beam γ-ray spectroscopy following two-proton removal reaction to investigate the structure of a ^{42}Si nucleus. Experimental studies on the ^{42}Si nucleus were performed at NSCL[1] and GANIL[2] to measure γ rays from the first 2^+ state. The deformation and disappearance of shell closure at the $N = 28$ have been suggested from the low excitation energy (770 keV) of the first 2^+ state in the ^{42}Si nucleus[2]; however, there are no experimental results on the excited states higher than the 2^+ state which are related to the nuclear shape or information on the shell evolution. In order to study the excited states higher than the 2^+ state, we have measured the two-proton removal reaction of the ^{44}S nucleus.

The experiment was performed at the RI Beam Factory operated by RIKEN Nishina Center and CNS, University of Tokyo. Secondary beams were produced by bombarding a 15-mm-thick Be target with a ^{48}Ca beam at 345 MeV/nucleon with an intensity of around 70 pnA. Various products of projectile fragmentation reactions were analyzed by using the BigRIPS fragment separator[3] to obtain ^{44}S beams. The secondary beam of ^{44}S was identified by the ΔE-$B\rho$-TOF method at the second stage of BigRIPS. Figure 1 shows the identified particles in the secondary beams. The energy and intensity of ^{44}S beam were around 200 MeV/nucleon and around 4×10^4 particles per second, respectively. The ^{44}S beam bombarded a carbon target that was located at the F8 focus and had a thickness of 2.54 g/cm^2. Reaction products following a removal and/or inelastic reactions were analyzed using the ZeroDegree spectrometer[4] by employing the ΔE-$B\rho$-TOF method. De-excitation γ rays were detected by the DALI2 γ-ray detection array[5] in coincidence with the ^{42}Si particles. We observed the prominent peak corresponding to the first 2^+ state in the γ-ray spectrum with high statistics and other γ lines. The analysis of the excited states higher than the 2^+ state is currently in progress.

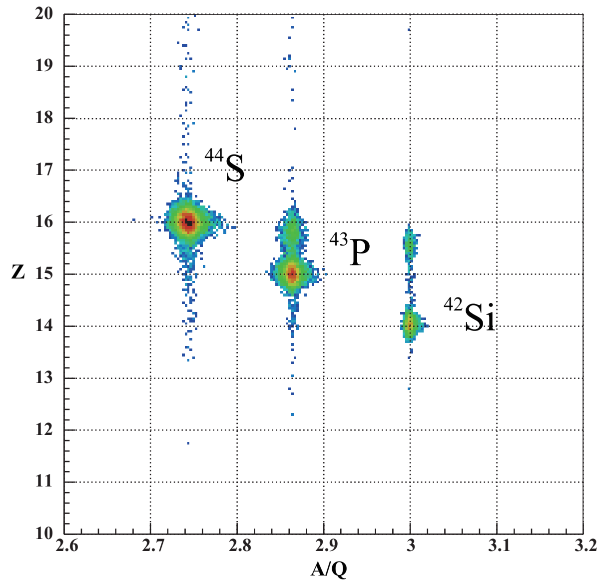

Fig. 1. Particle identification at BigRIPS.

*1 Department of Physics, Rikkyo University
*2 State Key Laboratory of Nuclear Physics and Technology, Peking University
*3 National Superconducting Cyclotron Laboratory (NSCL)
*4 Grand Accélérateur National d'Ions Lourds (GANIL)
*5 Lawrence Berkeley National Laboratory (LBNL)
*6 Physik-Department, Technische Universität München
*7 LPC-ENSICAEN, IN2P3-CNRS et Universite de Caen
*8 CNS, University of Tokyo
*9 Argonne National Laboratory (ANL)
*10 Department of Physics, University of Richmond
*11 Department of Physics, University of York
*12 Department of Physics, Tokyo Institute of Technology
*13 University of Frankfurt/Helmholtzzentrum für Schwerionenforschung GmbH (GSI)
*14 Institut de Physique Nucléaire, Orsay

References
1) J. Fridmann et al.: Phys. Rev. C **74**, 034313 (2006).
2) B. Bastin et al.: Phys. Rev. Lett. **99**, 022503 (2007).
3) T. Kubo: Nucl. Instr. and Meth. B **204**, 97 (2003).
4) Y. Mizoi et al.: RIKEN Accel. Prog. Rep. **38**, 297 (2005).
5) S. Takeuchi et al.: RIKEN Accel. Prog. Rep. **36**, 148 (2003).

In-beam γ-ray spectroscopy of ^{38}Mg

P. Doornenbal, H. Scheit,[1] N. Aoi, E. Ideguchi,[2] N. Kobayashi, Y. Kondo,[3] G. Lee,[3] J. Lee, K. Li,[1] M. Matsushita,[4] S. Michimasa,[2] T. Motobayashi, H. Sakurai, D. Steppenbeck, M. Takechi, S. Takeuchi, Y. Togano, and H. Wang,[1]

[Nuclear structure, Island of Inversion, in-beam γ-ray spectroscopy]

In the region of neutron-rich Ne, Na, and Mg isotopes, a region known as the Island of Inversion, a sudden quenching of the $N = 20$ neutron shell closures occurs, resulting in largely deformed nuclei. Despite enormous interest in discovering the boundaries of the Island of Inversion, the neutron-rich border lines are yet to be established experimentally. Here, we report on the first γ-ray spectroscopy of ^{38}Mg which arose interest after it has been shown that the Island of Inversion extends at least to the neutron number $N = 24$ for the Mg isotopes[1)]. Of particular interest is the energy and two-proton knockout cross-section determination of the $E(2_1^+)$ state, as comparison to shell-model calculations allows for a determination if ^{38}Mg has to be placed inside or outside of the Island of Inversion[1)].

A primary beam of ^{48}Ca with an intensity of 70 particle nA and an energy of 345 MeV/u was impinging on a 15 mm thick Be target located at the F0 Focus of the BigRIPS fragment separator[2)]. From the produced reaction products, secondary beams mainly composed of ^{39}Al and ^{40}Si were selected via the $B\rho - \Delta E - B\rho$ method, putting a 10 mm wedge-shaped Al degrader at the F1 focus position. In order to purify the selected beam cocktail, a second, 5 mm thick Al degrader was put at the dispersive focal point F5. The particles passing BigRIPS were identified with the $\Delta E - B\rho-$TOF method. The energy loss ΔE was measured with an ion-chamber[3)] located at the F7 achromatic focal point. A position measurement at the dispersive focal point F5 was used to deduce the $B\rho$ value. The time of Flight (TOF) was determined from two plastic scintillators located at the focal points F3 and F7. The particle identification plot is shown in Fig. 1. A clear separation in charge Q and the ratio of mass to charge number A/Q can be seen. The momentum acceptance for the secondary beams passing BigRIPS was $\pm 3\%$.

The secondary beams hit a 14.1 mm (2.54 g/cm^2) thick C secondary target at the F8 focal point position. The energies for ^{39}Al and ^{40}Si were 218 and 227 MeV/u in front of the secondary target. To detect γ-rays from decaying excited states in ^{38}Mg after one- and two-proton knockout, the secondary target was surrounded by the DALI2 γ spectrometer[4)]. It consisted of 186 large volume NaI(Tl) crystals and covered inclination angles from 18° to 146° (center of crystals).

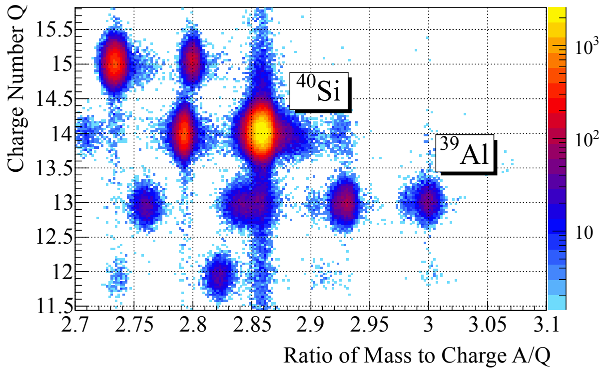

Fig. 1. Particle identification in front of the secondary target. Plotted is the deduced charge number Q against the ratio of mass to charge A/Q.

The full energy peak efficiency of the array was around 20 % for a γ-ray energy of one MeV and the resolution after correcting for the Doppler shift was about 10 %. Reaction products behind the secondary target were identified by the ZeroDegree spectrometer (ZDS). Again the $\Delta E - B\rho-$TOF method was employed to unambiguously identify Q and A/Q by measuring the TOF with two scintillators placed at the focal points F8 and F11, the position at the dispersive focus F9, and the energy loss with an ionization chamber at the focal point F11.

After a measuring time of 15 hours, excited states were observed in ^{38}Mg from the one- and two-proton reaction channels. At present the data are under analysis.

References

1) A. Gade *et al.*, Phys. Rev. Lett. **99**, 112501 (2007).
2) T. Kubo *et al.*, Nucl. Instr. and Meth. B 204, 97 (2003).
3) H. Otsu *et al.*, RIKEN Acc. Rep. 42, 163 (2009).
4) S. Takeuchi *et al.*, RIKEN Acc. Rep. 36, 148 (2003).

*1 Peking University, China
*2 Center for Nuclear Study, The Univ. of Tokyo
*3 Department of physics, Tokyo Institute of Technology
*4 Department of Physics, Rikkyo University

Inclusive breakup measurement of the neutron-rich nuclei ^{29}Ne, ^{33,35,37}Mg, and ^{39,41}Si

N. Kobayashi,*1 T. Nakamura,*1 Y. Kondo,*1 N. Aoi, H. Baba, S. Deguchi,*1 N. Fukuda, G. S. Lee,*1 H. S. Lee,*2 N. Inabe, M. Ishihara, Y. Kawada,*1 R. Kanungo,*3 T. Kubo, M. Famiano,*4 M. Matsushita,*1 T. Motobayashi, T. Ohnishi, N. A. Orr,*5 H. Otsu, R. Barthelemy,*4 H. Sakurai, S. Kim,*2 T. Sako,*1 T. Sumikama,*6 Y. Satou,*2 K. Takahashi,*1 M. Takechi, H. Takeda, S. Takeuchi, R. Tanaka,*1 N. Tanaka,*1 Y. Togano, and K. Yoneda

[Halo nuclei, Coulomb breakup, nuclear structure]

The relationship between the formation of a halo structure and shell evolution in the neutron-rich region has recently attracted considerable attention. A recent study[1] on the Coulomb breakup of ^{31}Ne nucleus found that this nucleus is a halo; this can be attributed only to a change in the conventional shell order. To understand the relationship between halo formation and shell evolution, it is important to collect experimental data on halo nuclei along the drip line towards heavier nuclei.

The aim of this present study is to identify new halo nuclei heavier than ^{31}Ne and to clarify the shell structures on the basis of Coulomb and nuclear breakup. Coulomb breakup is useful in investigating the soft $E1$ excitation, which is a unique property of halo nuclei. Nuclear breakup is also useful in investigating single particle property of the valence neutron, which could form the halo. In the present experiment, we determine the $1n$ removal cross sections (σ_{-1n}) on lead and carbon targets on the basis of the inclusive Coulomb and nuclear breakup. We also determine the momentum distribution for the core fragment in coincidence with the associated γ ray for the carbon target. The combinatorial measurements can be used not only to obtain the evidence for the halo structure but also quantitatively determine the halo structure by evaluating the separation energy and spectroscopic factor of a specific shell configuration.

Here, we focus on the neutron-rich nuclei ^{29}Ne, ^{33,35,37}Mg, and ^{39,41}Si near the drip line around N = 20–28. The separation energies of these nuclei are less than about 2 MeV, although some of the mass values have large uncertainty. According to the conventional shell order, the valence neutrons of these nuclei occupy the high-angular-momentum orbit $f_{7/2}$, which hinders the tunneling effect to form the halo. On the other hand, the shell melting effect may result in the dominance of p or s orbit and thus enhance the halo structure.

*1 Department of Physics, Tokyo Institute of Technology
*2 Seoul National University, Korea
*3 Saint Mary's University, Canada
*4 Western Michigan University, USA
*5 LPC-ENSICAEN, IN2P3-CNRS et Universitè de Caen, France
*6 Department of physics, Tokyo University of Science

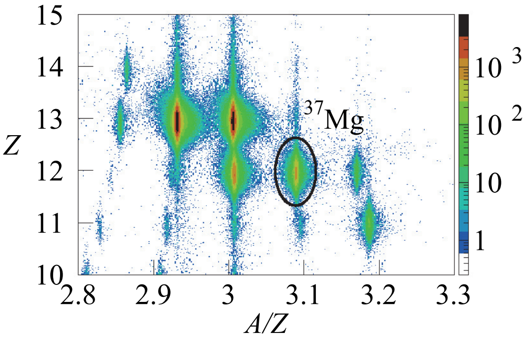

Fig. 1. Particle identification of the secondary beam for ^{37}Mg setting on the basis of the plot of the atomic number (Z) versus the ratio of mass number to atomic number (A/Z)

The experiment was performed at RI Beam Factory (RIBF). ^{29}Ne, ^{33,35,37}Mg, and ^{39,41}Si beams were produced through the projectile fragmentation of a ^{48}Ca beam at 345 MeV/u on a 15-mm-thick Be target. The intensity of a typical ^{48}Ca beam was about 100 pnA. The secondary beams were separated up to the F8 focal plane, which is at the end point of BigRIPS[2,3]. The secondary targets of lead (3.37 g/cm^2) and carbon (2.54 g/cm^2) were installed at F8.

To extract the $1n$ removal cross sections of ^{29}Ne, ^{33,35,37}Mg, and ^{39,41}Si, the beam particle and the fragment particle following the breakup were identified and counted event-by-event using the standard ΔE-TOF-Bρ method. For the beam particle (fragment particle) the ΔE at F7 (F11), TOF between the achromatic foci F3 and F7 (F8 and F11), and position information at the dispersive focus F5 (F9) were combined to determine the atomic number (Z) and the mass number (A). Figure 1 shows an example of particle identification before the secondary target. The data are currently being analyzed.

References
1) T. Nakamura et al.: Phys. Phys. Lett. **103**, 011302 (2009).
2) T. Kubo: Nucl. Instrum. Methods Phys. Res., Sect. B **204**, 97 (2003).
3) T. Ohnishi et al.: J. Phys. Soc. **77**, 083201 (2008).

Spectroscopy of the drip-line nucleus ^{24}O via (p,p') scattering

V. Lapoux,[*1] H. Otsu, S.Boissinot,[*1] H. Baba, R.J. Chen, A. Matta,[*2] E.C. Pollacco,[*1] Y. Blumenfeld,[*2] F. Flavigny,[*1] S. Franchoo,[*2] N. Fukuda, P. Gangnant,[*3] F. Hammache,[*2] Ch. Houarner,[*3] N. Inabe, D. Kameda, J.F.Libin,[*3] C. Louchart,[*1] M. Matsushita, T. Motobayashi, L. Nalpas,[*1] E. Yu. Nikolskii, M. Nishimura, A. Obertelli,[*1] T. Onishi, E. Rindel,[*2] Ph. Rosier,[*2] H.Sakurai, F. Saillant,[*3] M.Takechi, S. Takeuchi, Y. Togano, K.Yoneda, A.Yoshida and K.Yoshida

[Unstable nuclei, shell structure, magic number, inelastic scattering]

The understanding of the properties of the drip-line nuclei is a stringent test for the nuclear theories and their modeling of the nuclear interaction. In the region of the neutron-rich nuclei, around the last bound O isotope, ^{24}O, the neutrons occupy the sd-fp shells and new shell structure effects have been found or predicted, in contrast with the shell occupation of the stable nuclei. Experimentally, N=16 has been indicated as a new possible magic number[1], theoretically interpreted as an enhancement of the neutron shell gap between the 2*s1/2* and the 1*d3/2* shells, driven by the tensor proton-neutron force[2]. To explore these new properties, the spectroscopy of ^{24}O was studied: at GANIL, no gamma-ray associated to ^{24}O was found[3], showing that the excited states are unbound. At MSU, via invariant mass method, possible states were indicated[4] above S_n =4.1 MeV, around 4.5 and 5.3 MeV, but not clearly identified. An alternative technique is to use the (p,p') reactions and the light charge particle spectroscopy to obtain, from the recoil proton and via the missing mass method, the kinematical reconstruction of the (p,p'), and the ^{24}O excitation spectrum (Ex). This can give hints about the N=16 shell gap. From the (p,p) angular distributions, the entrance potential and the matter density features can also be extracted.

Our ^{24}O(p,p') experiment (RIBF57) became feasible with the advent of the intense beams of RIBF. It was done in 2010 using the state-of-the-art particle detector array MUST2[5] and the secondary beams produced by the fragmentation on a Be target of the ^{48}Ca beam at 345 MeV/n, in BigRIPS[6]. ^{24}O was produced at 263 MeV/n with unique intensities, 1100/s on average (maximum 2000 when ^{48}Ca intensity was at 180 particle nA). The reaction chamber was mounted in the F8 area (Fig. 1) with 8 MUST2 detectors. The left block of 4 2-stage (Si+CsI) telescopes was located ~23 cm downstream the 2.7 mg/cm^2-thick CH_2 reaction target, to cover lab. angles between (65-90) deg. Each MUST2 of 10*10cm^2 active area, provides identification, energy and trajectories of the light particles. The (p,p') kinematics were obtained by the correlations of the proton energies with the scattering angle deduced from the proton trajectories and the incident tracks reconstructed by the 3 PPACs in F8. The incident and outgoing particles were identified by Bρ-ETOF-ΔE technique in BigRIPS, and in the ZDS[7], respectively.

*1 CEA Saclay IRFU/SPhN, France
*2 CNRS-IN2P3, IPNO, France *3 GANIL, France

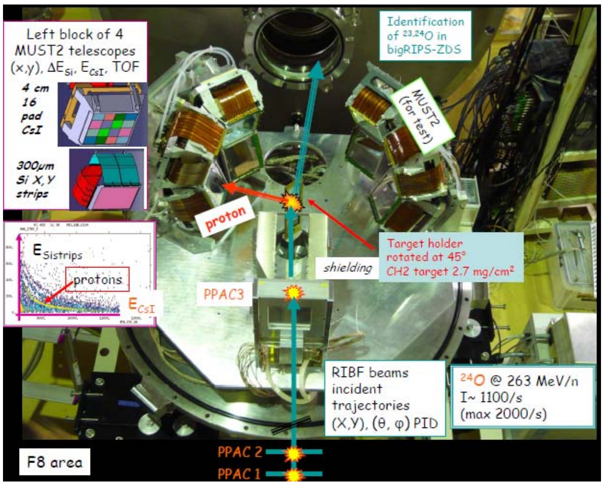

Fig.1.Top view of the set-up inside the reaction chamber.

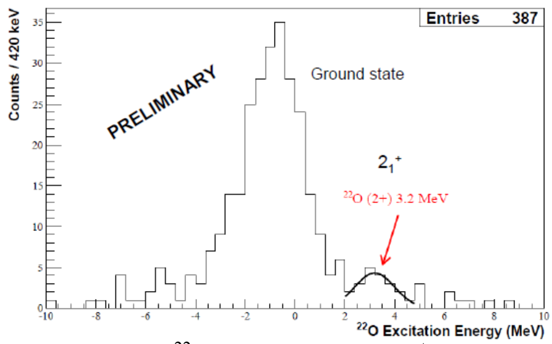

Fig.2.Ex spectrum of ^{22}O, with the known 2_1^+ at 3.2 MeV.

The calibrations have been done for all the energy and time channels of the 128 (X*Y) telescope strips and for the CsI pads; the kinematics were checked on the ^{22}O(p,p') reference measurement done at 262.5 MeV/n. One preliminary Ex spectrum for ^{22}O is shown in Fig. 2. The energy straggling effects in the target remain to be fully taken into account. The analysis is in progress for ^{24}O(p,p').

References

1) A. Ozawa *et al.*: Phys. Rev. Lett. **84,** 24 (2000).
2) T. Otsuka *et al.*: Phys. Rev. Lett. **91**, 179202 (2003).
3) S. Stanoiu *et al.*: Phys. Rev. C **69**, 034312 (2004).
4) C.R. Hoffman *et al.*: Phys.Lett.B **672**,17 (2009).
5) E.C. Pollacco *et al.*: Eur. Phys. J. A **25**, 287 (2005)
6) T. Kubo *et al.*: NIM. in Phys. Res., B **204**, 97 (2003).
7) T. Ohnishi *et al.*: J. Phys. Soc. Jpn. **77**, 083201 (2008).

Production cross sections of neutron-rich isotopes produced by the fragmentation of a ^{48}Ca beam at 345 MeV/nucleon†

N. Fukuda, T. Kubo, T. Ohnishi, N. Inabe, H. Takeda, and D. Kameda

[Projectile fragmentation, Production cross sections]

Since the commissioning of the RIKEN RI Beam Factory in 2007, a variety of radioactive isotope beams have been produced by using the BigRIPS[1)] in-flight separator, and their production cross sections have been determined from the measured production yields. These measured production cross sections are important for designing RI-beam experiments, allowing accurate estimation of the RI-beam intensities. In this article, we will report the measured production cross sections of neutron-rich carbon, oxygen, neon, magnesium, aluminum, silicon, and sulfur isotopes, which are produced by the projectile fragmentation of a ^{48}Ca beam at 345 MeV/nucleon with a beryllium target.

The experimental data that were used to determine the production cross sections were collected during the RI-beam production runs that the BigRIPS team conducted leading to users' experiments from 2008 to 2010. Both the production-target thickness and wedge-shaped energy-degrader thickness were optimized to fulfill users' requirements in the terms of the yield rate and/or purity of an isotope of interest. The target thickness for the users' experiments ranged from 10 to 40 mm. The method of isotopic separation and particle identification is described in Ref[2)].

Total ^{48}Ca beam doses were obtained by measuring the light charged particles that were recoiling out of the target. The transmission efficiency of a fragment was estimated for each setting of the BigRIPS by using the LISE++ code[3)]. The production cross sections thus determined from the measured production yields are shown in Fig.1 along with the EPAX systematics[4)]. The statistical errors are negligible and the systematic errors, which arise mainly due to the uncertainty of the primary beam dose, are estimated to be about 30%. We find that EPAX fairly reproduces the measured cross sections except in the case of the carbon isotopes, ^{41}Al, and ^{42}Si.

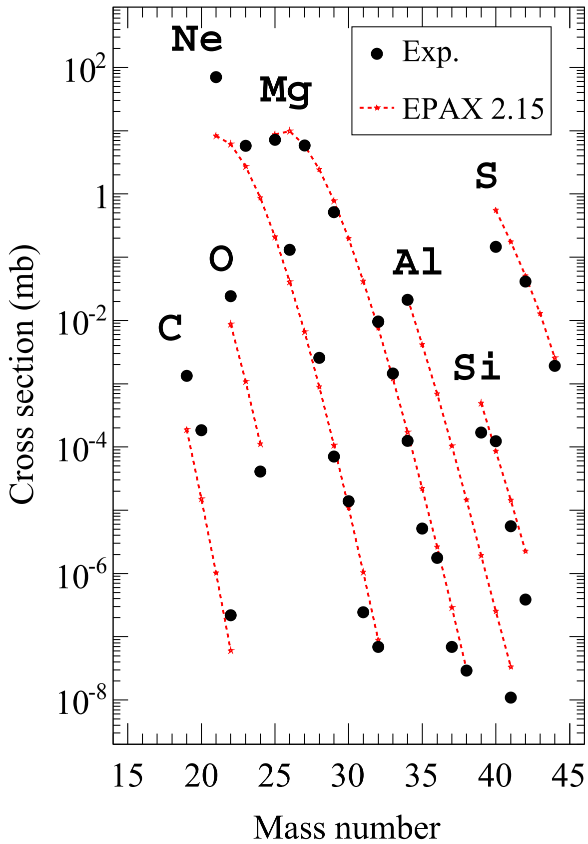

Fig. 1. Production cross sections of the isotopes produced by the projectile fragmentation of a ^{48}Ca beam with a Be target. The cross sections determined from the measured production yields are shown by solid circles. The red stars with the dashed lines show the cross sections calculated from the EPAX systematics.

References

1) T. Kubo: Nucl. Instr. and Meth. **B 204**, 97 (2003).
2) T. Ohnishi et al.: J. Phys. Soc. Jpn. **77**, 083201 (2008).
3) O.B. Tarasov and D. Bazin: Nucl. Instr. and Meth. **B 266**, 4657 (2008).
4) K. Sümmerer and B. Blank: Phys. Rev. **C 61**, 034607 (2000).

Shape evolution for neutron-rich Zr isotopes around $A = 110$

K. Yoshinaga,[*1,2] T. Sumikama,[*1] S. Nishimura,[*2] H. Watanabe,[*2] Y. Miyashita,[*1] K. Yamaguchi,[*3] K. Sugimoto,[*1] J. Chiba,[*1] Z. Li,[*2] H. Baba,[*2] J.S. Berryman,[*4,5] N. Blasi,[*6] A. Bracco,[*6,7] F. Camera,[*6,7] P. Doornenbal,[*2] S. Go,[*8] T. Hashimoto,[*8] S. Hayakawa,[*8] C. Hinke,[*9] E. Ideguchi,[*8] T. Isobe,[*2] Y. Ito,[*3] D.G. Jenkins,[*10] Y. Kawada,[*11] N. Kobayashi,[*11] Y. Kondo,[*11] R. Krüchen,[*9] S. Kubono,[*8] G. Lorusso,[*2,5] T. Nakano,[*1] M. Kurata-Nishimura,[*2] A. Odahara,[*3] H.J. Ong,[*12] S. Ota,[*8] Zs. Podolyák,[*13] H. Sakurai,[*2] H. Scheit,[*2] K. Steiger,[*9] D. Steppenbeck,[*2] S. Takano,[*1] A. Takashima,[*3] K. Tajiri,[*3] T. Teranishi,[*14] Y. Wakabayashi,[*15] P.M. Walker,[*13] O. Wieland,[*6] and H. Yamaguchi[*8]

[Nuclear structure, unstable nuclei]

A drastic shape evolution is expected in neutron-rich Zr isotopes. Sudden onset of deformation has been observed at a neutron number of 60[1]. The degree of deformation increases with neutron number toward $N = 64$[2]. A calculation performed by using the Skyrme density functional predicts a transition to the spherical shape due to the sub-shell closure at $N = 70$[3]. However, the level structure of low-lying states is known only up to $N = 64$. In the present work, we have identified low-lying states in ^{106}Zr and ^{108}Zr by observing the β-decay of ^{106}Y and the isomeric decay of ^{108}Zr at the RIBF.

Neutron-rich nuclei were produced by in-flight fission of a 345 MeV/nucleon ^{238}U beam in a Be target with a thickness of 3 mm[4]. The typical intensities of ^{106}Y and ^{108}Zr beams were 0.1 cps and 0.4 cps, respectively; their purities were 0.15% and 0.62%, respectively. The RI beams were implanted into double-sided silicon strip detectors (DSSDs) placed at the end of the beam line (F11). The DSSDs measured the energy of beam particles and subsequently detected β-rays emitted from the implanted RI. Four Clover-type Ge detectors were placed around the DSSDs to detect γ-rays. Transitions in ^{106}Zr were identified by measuring γ-rays in coincidence with β-rays after implantation of ^{106}Y, while those in ^{108}Zr were identified from γ-rays observed within 4 μs of the implantation of ^{108}Zr. The details of the experimental setup are given in Ref. 5.

For ^{106}Zr, we observed three new γ-lines with energies of 152, 324, and 607 keV. The 152-keV γ-ray was the most intense among them. Thus, the γ-ray was attributed to the transition $2_1^+ \to 0_1^+$ in ^{106}Zr. The 324-keV γ-ray was tentatively attributed to the transition $4_1^+ \to 2_1^+$[5] on the basis of a comparison with the result of a calculation performed by using the interaction boson model[7]. Because the ratio of the energy of the 4_1^+ state to the energy of the 2_1^+ state, $R_{4/2}$, for ^{106}Zr is obtained to be 3.13, ^{106}Zr is most likely well deformed like the lighter Zr isotopes, as shown in Fig.1.

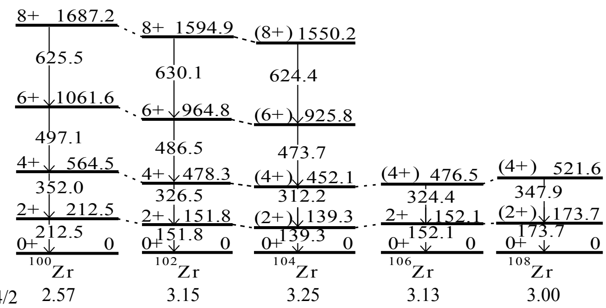

Fig. 1. Ground-state band and $R_{4/2}$ value of neutron-rich even-even Zr isotopes with $N \geq 60$. The energies of ^{100,102,104}Zr are taken from the ENSDF database[6].

For ^{108}Zr, five new γ-ray peaks were observed with energies of 174, 278, 348, 478, and 606 keV. From the systematic trends of $E(2_1^+)$ and $R_{4/2}$ shown in Fig. 1, the 173- and 348-keV γ-rays are tentatively attributed to the transitions of $2_1^+ \to 0_1^+$ and $4_1^+ \to 2_1^+$, respectively, which leads to an $R_{4/2}$ value of 3.0. These results support a well-deformed ground state for ^{108}Zr rather than the spherical shape expected when $N = 70$ is a magic number.

*1 Department of Physics, Tokyo University of Science
*2 RIKEN Nishina Center
*3 Department of Physics, Osaka University
*4 Nuclear Science Division, Lawrence Berkeley National Laboratory, USA
*5 NSCL, Michigan State University, USA
*6 INFN, Italy
*7 Dipartimento di Fisica, Università di Milano, Italy
*8 Center for Nuclear Study (CNS), Tokyo University
*9 Physik Department, Technische Universität München, Germany
*10 Department of Physics, University of York, UK
*11 Department of Physics,Tokyo Institute of Technology
*12 Research Center for Nuclear Physics, Osaka University
*13 Department of Physics, University of Surrey, United Kingdom
*14 Department of Physics, Kyushu University
*15 Japan Atomic Energy Agency

References

1) E. Cheifetz *et al*; Phys. Rev. Lett. **25**, 38 (1970).
2) J. K. Hwang *et al*; Phys. Rev. C **73**, 044316 (2006).
3) M. Bender *et al*; Phys. Rev. C **80**, 064302 (2009).
4) T. Ohnishi *et al*; J. Phys. Soc. Jpn. **79**, 073201 (2010).
5) T. Sumikama *et al*; Phys. Rev. Lett. **106**, 202501 (2011).
6) ENSDF database, http://www.nndc.bnl.gov/ensdf.
7) S. Lalkovski *et al*; Phys. Rev. C **79**, 044307 (2009).

Study of Neutron-Rich Mo and Nb Isotopes around A = 110

K. Yamaguchi,[*1] A. Odahara,[*1] S. Nishimura, H. Watanabe, T. Sumikama,[*2] K. Yoshinaga,[*2] Z. Li, Y. Miyashita,[*2] H. Baba, J.S. Berryman,[*3] N. Blasi,[*4] A. Bracco,[*4,5] F. Camera,[*4,5] J. Chiba,[*2] P. Doornenbal, S. Go,[*6] T. Hashimoto,[*6] S. Hayakawa,[*6] C. Hinke,[*7] E. Ideguchi,[*6] T. Isobe, Y. Ito,[*1] D.G. Jenkins,[*8] Y. Kawada,[*9] N. Kobayashi,[*9] Y. Kondo,[*9] R. Krücken,[*7] S. Kubono,[*6] G. Lorusso,[*10] T. Nakano,[*2] M. Kurata-Nishimura, H.J. Ong,[*11] S. Ota,[*6] Zs. Podolyák,[*12] H. Sakurai, H. Scheit, K. Steiger,[*7] D. Steppenbeck, K. Sugimoto,[*2] K. Tajiri,[*1] S. Takano,[*2] A. Takashima,[*1] T. Teranishi,[*13] Y. Wakabayashi,[*14] P.M. Walker,[*12] O. Wieland,[*4] and H. Yamaguchi[*6]

[Nuclear structure, β decay, unstable nuclei]

Nuclear deformation is one of the important keys to reveal the nuclear structure. Well-deformed prolate nuclei are known to be present in the neutron-rich $A \approx 110$ region. Shape evolution and shape coexistence between prolate, oblate, and asymmetric deformations are also expected.[1,2] Moreover, these neutron-rich nuclei locate on the path of a rapid neutron-capture process (r-process) nucleosynthesis. Therefore, from the aspects of the nuclear deformation and nucleosynthesis, information on β decay of the neutron-rich nuclei with $A \approx 110$ is very important. In the present work, results of the neutron-rich $^{107-110}$Mo were obtained by measuring the β decay of $^{107-110}$Nb isotopes, respectively, as one of the results of the experiment based on the β-γ spectroscopy method at RIBF[3–5].

The experiment was performed at the RIBF facility by using a 345 MeV/u ^{238}U beam with an intensity of approximately 0.3 pnA. Details of the experimental conditions have been provided in Refs. [3-5]. The neutron-rich isotopes ^{107}Nb, ^{108}Nb, ^{109}Nb, and ^{110}Nb with total counts of 1.1×10^5, 1.9×10^5, 2.0×10^5, and 5.0×10^4, respectively, were implanted in a nine-layer double-sided silicon-strip detector (DSSD) system. Event-by-event selection for the β-decay events was made on the basis of the detection of β rays at the same position of the DSSD as that of the implantation of the particle-identified Nb isotopes. Analysis of the β-γ and β-γ-γ coincidence data with particle identification of each Nb isotope was carried out.

Beta-decay half-lives of ^{108}Nb, ^{109}Nb, and ^{110}Nb were deduced from the decay curves, which indicated the time dependence of counts of the β rays coincident with the γ rays in the daughter Mo nuclei. The obtained half-lives of ^{108}Nb, ^{109}Nb, and ^{110}Nb were 190(10), 116(8), and 89(9) ms, respectively. These are shorter than theoretical values, as discussed in Ref. [3].

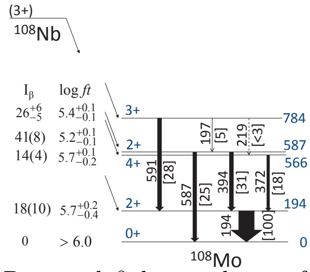

Fig. 1. Proposed β-decay scheme of ^{108}Nb.

Beta decays of the neutron-rich ^{107}Nb, ^{109}Nb, and ^{110}Nb isotopes were studied in this work for the first time, and γ rays in the daughter Mo isotopes were observed. Results for the β decay of ^{110}Nb have been submitted[6] , and those for ^{107}Nb, ^{108}Nb, and ^{109}Nb will be submitted. One of the results is the revised decay scheme of ^{108}Nb, as shown in Fig. 1. Previously reported γ-ray intensities were ambiguous because of the low statistics and high background resulting from the small production rate in the isotopic distribution with $A = 108$ based on the on-line mass separator technique using the proton-induced fission fragments.[7] In the present work, the γ-ray intensity, β-decay branching ratio, and log ft value were much more precisely determined. The spin-parity of the ground state in ^{108}Nb was assigned to be (3^+) as this nucleus decays to the states of 2_1^+, 4^+, 2_2^+, and 3^+ with log ft values of 5.7, 5.7, 5.2, and 5.4, respectively. The ground state of ^{108}Nb was assigned to have the $5/2^+[422]$ and the $1/2^+[413]$ configurations for the valence proton and neutron, respectively. This indicates that ^{108}Nb has a well-deformed prolate shape with $\beta \approx 0.4$.

*1 Department of Physics, Osaka University
*2 Department of Physics, Tokyo University of Science
*3 Lawrence Berkeley National Laboratory, USA
*4 INFN, Italy
*5 Dipartimento di Fisica, Università di Milano, Italy
*6 CNS, University of Tokyo
*7 Technische Universität München, Germany
*8 University of York, UK
*9 Department of Physics, Tokyo Institute of Technology
*10 NSCL, Michigan State University, USA
*11 RCNP, Osaka University
*12 University of Surrey, UK
*13 Department of Physics, Kyushu University
*14 Japan Atomic Energy Agency

References

1) J.Skalski *et al.*: Nucl. Phys. A **617**, 282 (1997).
2) P.Möller *et al.*: Atomic Data and Data Tables **94**, 758 (2008).
3) S.Nishimura *et al.*: Phys. Rev. Lett. **106**, 052502 (2011) and references therein.
4) H.Watanabe *et al.*: Phys. Lett. B **696**, 186 (2011).
5) T.Sumikama *et al.*: Phys. Rev. Lett. **106**, 202501(2011).
6) H.Watanabe *et al.*: submitted to Phys. Rev. Lett.
7) H.Penttilä: Phys. Rev. C **54**, 2760 (1996).

Energy Dependence of π^-/π^+ Ratio Observed in In+^{28}Si Reaction

M. Sako,[*1] T. Murakami,[*1] Y. Ichikawa,[*1] S. Imajo,[*1] R. Sameshima,[*1] E. Takada,[*2] K. Ieki,[*3] M. Matsushita,[*3] J. Murata,[*3] Y. Nakai, S. Nishimura, and H. Sakurai

[Symmetry energy, pion ratio, high density]

The density dependence of nuclear symmetry energy $E_{sym}(\rho)$ is one of the hot topics not only in nuclear physics but also in astrophysics. It is suggested that detailed studies of the pion yield ratio, $Y(\pi^-)/Y(\pi^+)$, in central nucleus-nucleus collisions at intermediate energies would provide significant constraints on $E_{sym}(\rho)$ at high densities ($\rho > \rho_0$)[1]. The transport model calculation (IBUU04)[1] predicted that the incident energy dependence of the pion yield ratio is related to the behavior of $E_{sym}(\rho)$ in the supra-normal density region ($\rho > \rho_0$) and that the pion yield ratio would increase as the incident beam energy decrease toward the pion-production threshold.

Since there is rather few experimental data on the pion yield ratio, we performed a series of measurements of the pion yield ratio in In(^{28}Si, $\pi^{\pm}$)X reactions for beam energies of 400, 600, and 800 MeV/nucleon at HIMAC with a compact centrality filter and a pion range counter[2)3)]. The total number of charged pions was estimated by using ΔE_i-ΔE_j correlations obtained experimentally for π^+ events, since π^+ events were clearly identified by the $\pi^+ \rightarrow \mu^+ + \nu_\mu$ decay when π^+ stops in one of the elements of the range counter.

Figure 1 shows the pion yield ratio as a function of the kinematic energy of the pions in a mid-rapidity frame. the pion yield ratios were measured at 45°, 60°, 90°, and 120° in the laboratory system. It is found that at each incident energy, the data for all measurement angles are on a curve like a exponential function. The curves fitted to the experimental data by using an exponential function are shown in Fig. 1. The slope of the fitted curves decreases with the incident energy, and the pion yield ratio in the lower-energy region increases with decreasing incident energy. This seems to be consistent with the transport model prediction for mass-symmetric collision systems[1)].

Furthermore, the pion yield ratio in Fig. 1 indicates that the charged pions are mainly emitted from a moving source with mid-rapidity and that these ratios may provide information on $E_{sym}(\rho)$ for the high density nuclear matter created by nucleus-nucleus collisions. The distributions observed in Fig. 1 also indicate that the pions emitted at forward angles show higher sensitivity to investigate the beam energy dependence of the pion yield ratio than those emitted at backward angles.

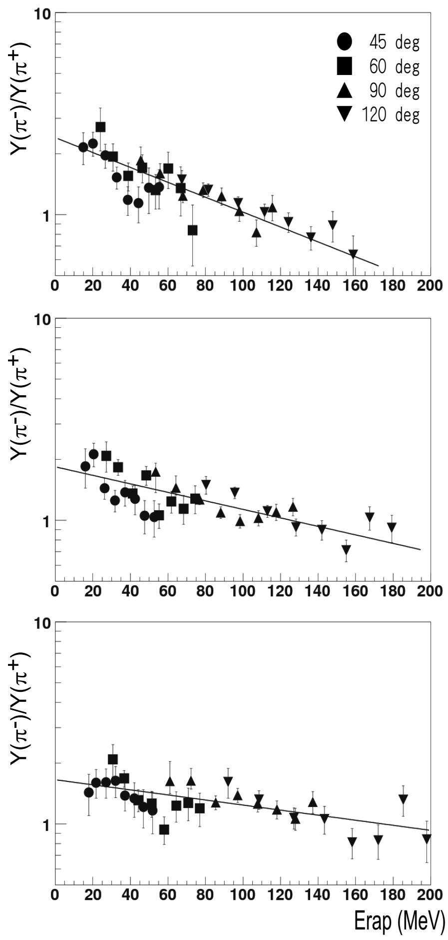

Fig. 1. Pion yield ratio as a function of kinematic energy in a mid-rapidity frame for In+^{28}Si collisions at 400 (upper), 600 (middle), and 800 (bottom panel) MeV/nucleon. Solid lines are curves fitted by using a function of $C\exp(-\alpha x)$. The slope parameters (α) are $(8.5 \pm 1.1) \times 10^{-3}$, $(4.8 \pm 0.9)\times 10^{-3}$, and $(2.9\pm 0.7) \times 10^{-3}$ for 400, 600, and 800 MeV/nucleon, respectively.

*1 Department of Physics, Kyoto University, Kyoto, Japan
*2 Department of Accelerator and Medical Physics, NIRS, Chiba, Japan
*3 Department of Physics, Rikkyo University, Tokyo, Japan

References

1) Bao-An Li, Gao-Chan Yong, and Wei Zuo, Phys. Rev. C **71**, 014608 (2005).
2) T. Murakami et al., RIKEN Accel. Prog. Rep. **43**, 26 (2010).
3) T. Murakami et al., Nucl. Phys. A **834**, 593c (2010) (NN2009 proceedings).

RIKEN Accel. Prog. Rep. 44 (2011)

Production of spin-aligned RI beam via two-step fragmentation

Y. Ichikawa, H. Ueno, Y. Ishii,[*1] T. Furukawa,[*1] A. Yoshimi, D. Kameda, H. Watanabe, N. Aoi, K. Asahi,[*1] D. L. Balabanski,[*2] R. Chevrier,[*3] J. M. Daugas,[*3] N. Fukuda, G. Georgiev,[*4] H. Hayashi,[*1] H. Iijima,[*1] N. Inabe, T. Inoue,[*1] T. Kubo, T. Nanao,[*1] T. Ohnishi, K. Suzuki,[*1] M. Tsuchiya,[*1] H. Takeda, M. Rajabali,[*5] and M. Ishihara

[RI beam, spin alignment, nuclear moment]

In order to produce a radioactive-isotope (RI) beam with high spin alignment, we have developed a novel method – the two-step projectile-fragmentation (PF) method with a technique of momentum-dispersion matching.

Studies on nuclear-electromagnetic moments have been conducted by employing a technique of spin-oriented RI beams through the single-step PF[1,2)]. The magnitude of spin orientation is, however, drastically reduced for the PF implying removals of many nucleons from a projectile. Because of this, accessible nuclei with the conventional method with a single-step PF are limited to those in the neighborhood of the primary beam. In the proposed new method that has been developed to overcome this difficulty, a nucleus of interest is yielded as a tertiary beam in the secondary PF, following the primary PF. Here, the secondary PF is chosen to be the one-nucleon removal reaction so that the tertiary beam can be promisingly spin-aligned as highly as possible. The production yield of the tertiary beam is, however, very low in a simple two-step PF scheme. A technique of momentum-dispersion matching was therefore combined to this method, where the tertiary beam with the same relative momentum to the secondary beam was focused at the same lateral position on a focal plane irrespective of the initial momentum. Satisfying the dispersion-matching condition, we can achieve the enhancement of the yield by extracting the same component of spin alignment from the tertiary beam without any cancellations among the spin alignment with opposite signs.

The experiment to apply the new method to study of ^{32}Al was carried out using BigRIPS[3)] at the RIKEN RIBF facility[4)]. In the primary reaction, ^{33}Al was produced by the PF of a 345-MeV/nucleon ^{48}Ca beam on a primary ^{9}Be target with a thickness of 1.85 g/cm^2 that was chosen to provide a maximum production yield of a secondary beam of ^{33}Al. A wedge-shaped aluminum degrader with a mean thickness of 221 mg/cm^2 was placed at the momentum-dispersive focal plane F1 for the isotope separation. The momentum acceptance at F1 was set to $\pm3\%$. The ^{33}Al secondary beam was bombarded on an aluminum wedge-shaped secondary target with a thickness of 2.70 g/cm^2 placed at the momentum dispersive focal plane F5. Here, ^{32}Al was produced through the one-nucleon removal PF, its isomeric state ^{32m}Al[5)] was populated, and the spin alignment was effectively produced simultaneously in a "one-shot" reaction. The ^{32}Al beam was then transported to the double-achromatic focal plane F7 so that the beam-line between F5 and F7 is dispersion-matched to that between F3 and F5. The momentum acceptance at F7 was set to $\pm0.15\%$ from the center of the momentum distribution.

The magnitude of the spin alignment was determined by employing the time-differential perturbed angular distribution (TDPAD) method, in which the spin-alignment is observed through the change in the anisotropy of the de-excitation γ-ray emission from ^{32m}Al under an external magnetic field $B_0 = 0.259$ T. The spin-aligned ^{32}Al beam was stopped in an annealed Cu crystal stopper with a thickness of 3.0 mm and an area of 30 × 30 mm^2 located between a pair of magnet poles. The 221-keV γ-rays emitted from the isomeric state were detected using four Ge detectors located at a distance of 7.0 cm apart from the stopper and at angles of ±45 and ±135 degrees with respect to the beam axis. Relative detection efficiencies were 35% for one and 20% for three.

Having measured the 221-keV photo-peak counting rates of a pair of adjacent Ge detectors, $N_1(t)$ and $N_2(t)$, we observed an oscillation pattern in an $R(t)$ function representing the anisotropy of the γ-ray emission, defined as $R(t) = (N_1(t)-N_2(t))/(N_1(t)+N_2(t))$. The magnitude of the spin alignment was determined from the amplitude of the oscillation to be $\sim12\%$. Evaluation of the figure of merit for the new method compared with that for the conventional one is in progress.

*1 Department of Physics, Tokyo Institute of Technology, Japan
*2 Institute for Nuclear Research and Nuclear Energy, Bulgarian Academy of Sciences, Bulgaria
*3 CEA, DAM, DIF, France
*4 CSNSM, IN2P3-CNRS, France
*5 Katholieke Univerisiteit Leuven, Belgium

References

1) K. Asahi *et al.*: Phys. Lett. **B 251**, 488 (1990).
2) K. Asahi *et al.*: Phys. Rev. C **43**, 456 (1991).
3) T. Kubo *et al.*: Nucl. Instr. and Meth. in Phys. Res. **B 204**, 97 (2003).
4) Y. Yano *et al.*: Nucl. Instr. and Meth. in Phys. Res. **B 261**, 1009 (2007).
5) M. Robinson *et al.*: Phys. Rev. C **52**, R1465 (1996).

α fine-structure spectroscopy for ^{255g,m}Lr

M. Asai,[*1] H. Haba, N. Sato,[*1] Y. Kasamatsu,[*2] D. Kaji, K. Morimoto, and K. Morita

[Nuclear structure, ^{255}Lr, ^{255m}Lr, α decay]

Energy spacings and order of single-particle orbitals are sensitive probes to investigating shell structure of superheavy nuclei. In particular, energies of the proton orbitals around $Z = 101$, 103, and 105 (Md, Lr, and Db) are interesting because one orbital, $1/2^-[521]$, which originates from the spherical $2f_{5/2}$ orbital lying just above the $Z = 114$ gap comes down to the Fermi level in deformed nuclei around $Z = 101$–105. Experimental assignments of the deformed proton orbitals around $Z = 101$–105 thus give us valuable information on the spherical shell gap energy around $Z = 114$.

Experimental data on the single-particle states in odd-mass Md, Lr, and Db isotopes are, however, very scarce. There is no firm information on excitation energies, spin-parities, and proton configurations of ground- as well as excited states in odd-mass Md, Lr, and Db isotopes except for the ground-state configurations of some Md isotopes.[1)] To study these nuclei, we proposed high-resolution α fine-structure spectroscopy which allows us to identify single-particle configurations only by measuring an α-singles spectrum. We applied this technique to studying the α decay of odd-mass Lr isotopes.[2)] In the present work, we definitely identify the proton single-particle configurations of ^{255g,m}Lr.

^{255g,m}Lr were produced in the ^{209}Bi(^{48}Ca,2n) reaction using the RIKEN linear accelerator RILAC. The beam energy was 219.5 MeV at the center of the target. Reaction products were separated by the gas-filled recoil ion separator GARIS, and then injected into a gas-jet chamber placed at the focal plane of GARIS through a 3.5-μm thick Mylar window. The products stopped in the gas-jet chamber were transported through a 10-m long capillary with a He/KCl jet into a rotating-wheel α detection system, and deposited on a thin foil forty of which were set on the rotating wheel. The wheel periodically rotated at 5.5 s intervals to move the deposited sources to seven consecutive detector stations each of which was equipped with two Si detectors. To achieve a good α-energy resolution and to reduce a low-energy tail of α peaks, Si detectors were set at the distance with a solid angle of 16% of 4π. This setup also reduces the energy sum between the α particles and the subsequently emitted conversion electrons, Auger electrons, and low-energy X rays which distorts the measured α energy spectrum considerably.

Figure 1(a) shows a sum of α energy spectra measured at the 1st and 2nd detector stations. The α energy resolution was ~12 keV FWHM. The most intense α lines observed at 8376 and 8469 keV are the favored α transitions from ^{255g}Lr ($T_{1/2} = 31$ s) and ^{255m}Lr (2.5 s) to one-quasiparticle states in ^{251}Md with the configurations the same as that of ^{255g}Lr and ^{255m}Lr, respectively.[3)] In addition, we have observed new α lines at 8342 and 8408 keV which are considered to be the transitions to the rotational-band members built on the one-quasiparticle states. Taking into account the energy differences and the intensity ratios between the 8342 and 8376 keV α transitions and between the 8408 and 8469 keV ones, we have identified the proton single-particle configuration of $1/2^-[521]$ to ^{255g}Lr and $7/2^-[514]$ to ^{255m}Lr as shown in Fig. 1(b). The observed 8342 keV α peak should be a doublet containing the transitions to the closely lying $3/2^-$ and $5/2^-$ states in the $1/2^-[521]$ band.

References
1) F.P. Heßberger *et al.*: Eur. Phys. J. A **26**, 233 (2005).
2) M. Asai *et al.*: RIKEN Accel. Prog. Rep. **43**, *ix* (2010).
3) A. Chatillon *et al.*: Eur. Phys. J. A **30**, 397 (2006).

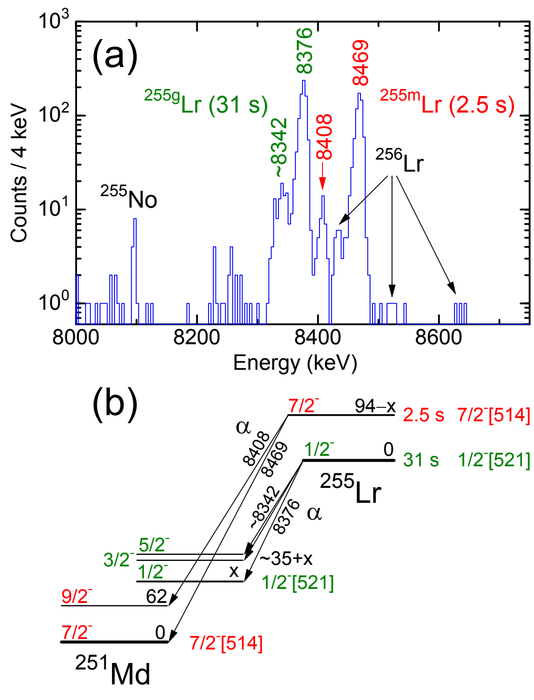

Fig. 1. (a) Measured α energy spectrum for ^{255g,m}Lr. (b) Proposed α decay scheme of ^{255g,m}Lr.

*1 Advanced Science Research Center, Japan Atomic Energy Agency
*2 Graduate School of Science, Osaka University

Magnetic moment of ^{58}Cu measured by means of the β-NMR technique

M. Mihara,[*1] T. Izumikawa,[*2] H. Ueno, K. Matsuta,[*1] D. Nishimura,[*1] T. Nagatomo,[*3] T. Moriguchi,[*4] Y. Ito,[*4] D. Nagae,[*4] M. Fukuda,[*1] A. Yoshimi, K. Yamada, M. Takechi, Y. Ichikawa, S. Momota,[*5] Y. Hirayama,[*6] T. Ohtsubo,[*7] S. Suzuki,[*7] T. Kubo,[*7] Y. Namiki,[*7] A. Ozawa,[*4] Y. Ishibashi,[*4] H. Oishi,[*4] K. Suzuki,[*8] I. Hachiuma,[*9] K. Namihira,[*9] D. Horikawa,[*5] T. Minamisono,[*10] T. Yamaguchi,[*9] T. Kuboki,[*9] T. Suzuki,[*9] K. Satoh,[*9] Y. Kobayashi, K. Asahi,[*8] K. Matsukawa[*11] and K. Shirai[*12]

[Magnetic moment, charge-exchange reaction, unstable nuclei, β-NMR]

As an extension of our previous study on the production of a ^{58}Cu secondary beam[1)], we have performed β-NMR measurements of the short-lived nucleus ^{58}Cu ($I^{\pi} = 1^{+}$, $T_{1/2} = 3.2$ s) in order to determine the electromagnetic moments of ^{58}Cu; the electromagnetic moments are important for the study of the nuclear structure of ^{58}Cu and to develop a spin-polarized ^{58}Cu beam as a new β-NMR probe for use in material science.

Spin-polarized ^{58}Cu nuclei were produced through the charge-exchange reaction of ^{58}Ni. A ^{58}Ni primary beam at 63A MeV was produced by the RIKEN ring cyclotron (RRC) using the RIKEN heavy-ion linac (RILAC) injection with a typical intensity of 200 particle nA, and it was made to impinge on a 0.5-mm-thick Be target. The fully stripped ^{58}Cu^{29+} ions were separated by the RIKEN projectile fragment separator (RIPS). The emerging angle of the ^{58}Cu ions was selected to be between 0.75° and 4.1° to ensure the appropriate nuclear spin polarization of the ions. The momentum window was set at $-(2.5 \pm 2.5)$% in relative momentum, which almost covers the entire distribution. By using an achromatic Al degrader with a thickness of 85 mg/cm^2, a ^{58}Cu purity of a few percent was achieved for the secondary beam. The presence of a large amount of contaminants such as the isotones ^{57}Ni, ^{56}Co, and ^{55}Fe did not affect the β-ray detection of ^{58}Cu because of the long lifetimes and low Q values of isotones. The obtained ^{58}Cu nuclei with an energy of 36$-$40A MeV were implanted in a single-crystal sample of B-doped Si with a B concentration of 10^{16} cm^{-3} at 15 K. The implantation depth was about 600$-$700 μm. The sample was placed in a magnetic field B_0 of 0.93 T to maintain the polarization and detect β-NMR. The ^{58}Cu intensity was a few thousands per second, which resulted in a mean β-ray counting rate of about 200 cps.

Figure 1 shows the β-NMR spectrum of ^{58}Cu in Si, obtained with a total of about 2×10^7 ^{58}Cu ions and a ^{58}Cu magnetic moment $|\mu[^{58}\mathrm{Cu}]|$ of $(0.46 \pm 0.03)\mu_{\mathrm{N}}$ was deduced, which is consistent with results from laser spectroscopy[2,3)]. The spin-lattice relaxation of ^{58}Cu in Si at 15 K was observed, as shown in Fig. 2, and a relaxation rate $1/T_1$ of (0.7 ± 0.6) s^{-1} was estimated.

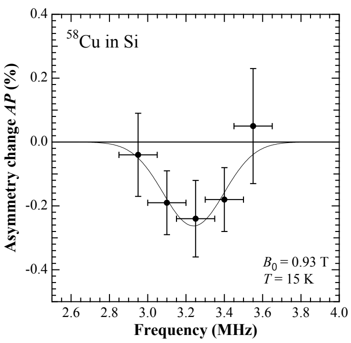

Fig. 1. β-NMR spectrum of ^{58}Cu in Si.

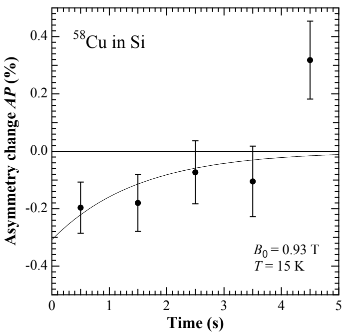

Fig. 2. Polarization of ^{58}Cu in Si vs. time.

*1 Department of Physics, Osaka University
*2 Radioisotope Center, Niigata University
*3 International Christian University
*4 Department of Physics, University of Tsukuba
*5 Faculty of Engineering, Kochi University of Technology
*6 Institute of Particle and Nuclear Studies, KEK
*7 Department of Physics, Niigata University
*8 Department of Physics, Tokyo Institute of Technology
*9 Department of Physics, Saitama University
*10 Department of Applied Nuclear Technology, Fukui University of Technology
*11 Renesas Electronics Corporation
*12 Institute of Science and Industrial Research (ISIR), Osaka University

References

1) M. Mihara et al.: RIKEN Accel. Prog. Rep. **42**, 24 (2009).
2) N. J. Stone et al.; Phys. Rev. C **77**, 067302 (2008).
3) T. E. Cocolios et al.; Phys. Rev. C **81**, 014314 (2010).

A pilot experiment for the precise spectroscopy of pionic atoms with 4×10^{11}/s deuteron beam at RIBF

T. Nishi,[*1] G.P.A. Berg,[*2] H. Geissel,[*3] R.S. Hayano,[*1] N. Inabe, K. Itahashi, S. Itoh,[*1] D. Kameda, T. Kubo, H. Matsubara,[*4] S. Michimasa, K. Miki,[*1] H. Miya,[*4] M. Nakamura,[*5] S. Noji,[*1] S. Ota,[*4] K. Suzuki,[*6] H. Takeda, K. Todoroki,[*1] K. Tsukada, T. Uesaka, H. Weick,[*3] K. Yoshida

[Pionic atom, Precision spectroscopy, MWDC]

We are planning to perform a precise spectroscopy of pionic atoms with BigRIPS at the RI beam factory[1]. The goal is to study the $1s$ and $2s$ pionic states of ^{121}Sn in the ^{122}Sn(d,^{3}He) reaction. The measurement will provide a better understanding of the strong interaction between the pion and the nucleus.

In October 2010, we performed a pilot experiment to construct ion optics for dispersion matching for the (d,^{3}He) reaction and to check the performance of the focal plane detectors, which will be used in the production experiment. The beam used in the experiment was provided by the SRC, and in had an energy of 250 MeV/nucleon and an intensity of $\sim 4 \times 10^{11}$/s. This high-intensity deuteron beam hit the target, 10 mg/cm^2 ^{122}Sn, and produced ^{3}He and a large number of protons of ∼200 kHz as the background in the focal plane. We measured the horizontal position of ^{3}He in the F5 focal plane and the calculated Q-value of the ^{122}Sn(d,^{3}He) reaction from position of ^{3}He. Here, we describe the performance of the detectors under such a high-intensity beam. The characteristics of the beam and the development of optics for dispersion matching will be explained in another paper[3].

We used two multi-wire drift chambers (MWDCs) and a plastic scintillator in the F5 focal plane, and a plastic scintillator in the F7 focal plane. Tracks were measured by MWDCs and identified as ^{3}He from the TOF and the energy loss in the scintillators.

The particle tracks were reconstructed by fitting a line to the MWDC hits. The position resolution of the MWDC was estimated from the residual distribution to be ∼0.13 mm (σ) (see Fig. 1), which is consistent with the design value of 0.3 mm (FWHM). We also verified that the time over threshold (ToT) of MWDC signals is related to the particle species. The pulse height for ^{3}He is about four times as large as those from protons or deuterons. With the ToT, we could identify ^{3}He with 90% accuracy.

Particles were identified from the TOF and energy loss in the F5 scintillator, in addition to the ToT of the MWDCs as described above. Figure 2 shows a plot of the energy loss in the F5 scintillator vs. the TOF between the F5 and F7 scintillators.

We confirmed that all detectors worked in the presence of the high-intensity beam as we had expected. We could measure the track for the designed resolution of the MWDCs and identify ^{3}He against the large background of protons from the TOF and energy loss of the scintillators.

This work is supported by a Grant-in-Aid for Scientific Research on Innovative Areas (No. 22105517).

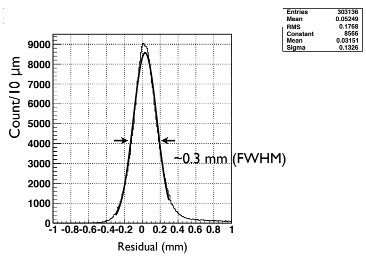

Fig. 1. Residual distribution of MWDC tracks. The residual is calculated as the distance between the position of the track in the plane and the hit position in the plane. The distribution has a width of ∼0.3 mm (FWHM).

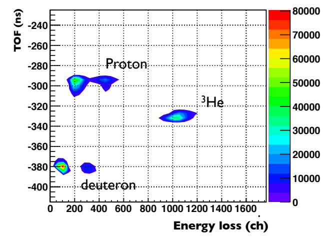

Fig. 2. Particle ID with the energy loss and TOF between F5 and F7 measured by scintillators. The colored areas correspond to protons, ^{3}He, and deuterons as indicated. Protons and deuterons have double hit components due to pile-up events.

*1 Department of Physics, University of Tokyo
*2 JINA and Department of Physics, University of Notre Dame
*3 GSI, Germany
*4 Center for Nuclear Study, University of Tokyo
*5 Department of Physics, Tokyo Institute of Technology
*6 Stefan Meyer Institute, Austrian Academy of Sciences

References

1) K. Itahashi et al.: *RIBF Proposal* **No.054** (2008).
2) K. Suzuki et al.: *Phys. Rev. Lett.* **92**, 072302 (2004).
3) S. Itoh et al.: *RIKEN Accel. Prog.* Rep. **44** 221(2011).

RIKEN Accel. Prog. Rep. 44 (2011)

KISS project and development of schemes for laser resonance ionization of rhenium and iridium

Y. Hirayama,[*1] S.C. Jeong,[*1] H. Miyatake,[*1] H. Ishiyama,[*1] Y.X. Watanabe,[*1] N. Imai,[*1] M. Oyaizu,[*1] K. Niki,[*1] M. Okada,[*1] M. Wada, T. Sonoda, Y. Ito, Y. Matsuo, A. Takamine,[*2] T. Furukawa,[*3] P. VanDuppen,[*4] Y. Kudryavtsev,[*4] and M. Huyse[*4]

[laser resonance ionization, r-process]

The beta-decay properties of the neutron-rich isotopes with neutron numbers $N = 126$, which act as progenitors in the r-process path forming the third peak ($A \approx 195$) in the r-abundance element distribution, are considered critical for clearly understanding astrophysical sites for the production of the heavy elements such as gold and platinum[?]. The proposal for the construction of the equipments of the KEK Isotope Separation System (KISS) that are necessary for conducting the program at RIKEN has been accepted, and the installation of the KISS started in March 2011. We are going to complete the system check of the KISS in FY2011 and will start the experiment in 2012.

Nuclei with $N = 126$ could be obtained via the multi-nucleon transfer (MNT) reactions induced by low-energy ($\sim$7 MeV/nucleon) intense neutron-rich radioactive ion beams, such as ^{140}Xe and/or ^{144}Xe generated at the facility by adopting the isotope separation on-line (ISOL) and post-acceleration scheme. Since such facilities have not been developed in the world so far, as the first step, we are going to produce and study ^{200}W, ^{201}Re, ^{202}Os and ^{203}Ir ($Z = 74$–77, $N = 126$), which have not been produced at any other facilities, by carrying out the MNT reactions between the stable beam ^{136}Xe and target nucleus ^{198}Pt. The energies of the nuclei with $N = 126$ produced as target-like fragments are as low as 1 MeV/nucleon with a wide energy distribution. The emission angle calculated by the GRAGING code varies widely, and the average value of the emission angle is found to be 65° in the laboratory frame.

The characteristics of the MNT reaction products make it difficult to collect the nuclei with $N = 126$ by using an in-flight-type electromagnetic spectrometer. Therefore, we employ a gas catcher to efficiently collect all reaction products, and we adopt the laser resonance ionization technique to select the nuclei with specific atomic numbers Z of collected nuclei and use electromagnetic separator (ISOL) to obtain the nuclei with specific mass numbers A. The selected isotopes are implanted into a tape transport system surrounded by detectors, which allows us to measure their beta-decays.

The gas catcher system and ISOL will be installed at the E2 experimental room, and the detectors will be installed at the E3 experimental room. A test bench of a laser resonance ionization system, which will be moved to J3 room, has been constructed at B1F of the RIBF building. The system can selectively ionize radioactive elements, because the laser wavelengths for ionization are different to each element.

So far, new efficient ionization schemes for stable rhenium ($Z = 75$) and iridium ($Z = 77$) have been successfully developed using two-wavelength (λ_1 and λ_2) tunable dye lasers pumped by excimer lasers and an ionization chamber that contains filament of the specific elements and a channeltron for the detection of ions[?]. The available powers of the dye lasers are 1 mJ/pulse and 10 mJ/pulse for λ_1 (210–350 nm) and λ_2 ($\geq$350 nm), respectively. Figure 1 shows the newly observed auto-ionization states (AIS) of rhenium (left) and iridium (right). We found that the dye laser power required for saturating the ionization of these elements was 0.1 mJ/pulse and 3 mJ/pulse for λ_1 and λ_2, respectively. The study for developing the ionization scheme of other stable elements with $Z = 68$–78 is in progress.

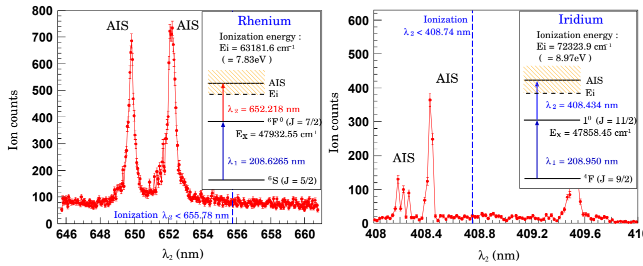

Fig. 1. Excitation spectra of rhenium (left) and iridium (right) as a function of wavelength λ_2.

References

1) S.C. Jeong et al.: KEK Report 2010-2.
2) Y. Hirayama et al.: presentation at LAP2010.

*1 High Energy Accelerator Research Organization (KEK)
*2 College of Science and Engineering, Aoyama Gakuin University
*3 Department of Physics, Tokyo Institute of Technology
*4 Instituut voor Kern-en Stralingsfysica, K.U. Leuven, Belgium

Influence of solid state effects on resonant neutrino scattering†

D. Suzuki,[*1,*2] T. Sumikama,[*3] M. Ogura,[*4] W. Mittig,[*5,*2] A. Shiraki,[*1] Y. Ichikawa,[*1] H. Kimura,[*1] H. Otsu, H. Sakurai,[*1] Y. Nakai and M. S. Hussein[*6,*7]

[Beta decay, neutrino, Mössbauer resonance, solid state]

The feasibility of conducting an experiment to study the resonant scattering of monoenergetic neutrinos was investigated.

Two-body beta decays such as electron capture (EC) decay involve a two-body final state that solely consists of a neutrino and a daughter nucleus. The emitted neutrino is thus monoenergetic. Monoenergetic γ rays from nuclear de-excitations are resonantly absorbed by other nuclei having the same final state, a process known as Mössbauer resonance[1]. Shortly after the discovery of Mössbauer resonance in 1958, Visscher proposed the concept of resonant neutrino scattering: neutrinos from the EC decay are absorbed by the daughter nucleus[2]. An intriguing feature of the resonant neutrino scattering is its enormously large cross section resulting from the long wavelength of the neutrino. The cross section of non-resonant scattering is typically of the order of 10^{-42} cm^2, making the observation of neutrinos difficult. In contrast, a 10-keV neutrino has a cross section of the order of 10^{-17} cm^2.

Atomic processes in experimental environments broaden the extremely narrow width of weak processes and attenuate the resonance. A previous study argued that line broadening by hyperfine interaction causes an attenuation of 10^{-16} or more when one adopts the recoil-less setup conceived by Mössbauer[3]. This paper discusses the effects of the electronic structure of atoms in a solid. The initial and final states of resonant neutrino scattering are the ground state of the whole atom. Only electrons in valence s orbits can contribute to the resonance since the capture of the inner electrons leaves the atom in a highly excited state. Being located close to the Fermi surface, the valence state readily develops a spatial extension. In the Mössbauer setup, the emitting and absorbing nuclei are embedded in a solid crystal to suppress the energy shift resulting from recoil. In solids, electrons in extended states can interact with neighboring atoms and form an electronic band. The discrete levels of the individual atoms are modified into a continuous band. This effect leads to a broadening of the atomic ground state, which attenuates the resonance.

We discuss two cases. One is the EC decay of ^{181}W to ^{181}Ta. The ^{181}W atom has a valence electron in the $6s$ orbit, making it a suitable candidate for resonant scattering. The electronic structures of a pure Ta crystal and a crystal in which one of the Ta atoms is substituted by a W atom were determined. We employed a self-consistent approach and used the Korringa-Kohn-Rostoker Green's-function method based on the local density approximation in the density functional theory[4]. The relativistic effect was taken into account by using the scalar relativistic approximation. The calculated local density of the $6s$ states indicates a conduction band with a width of several electronvolts close to the Fermi surface, which is attributed to hybridization with the $5d$ states of surrounding atoms. The attenuation of the resonant cross section was estimated to be of the order of 10^{-24}.

The other case was the bound-state β decay of ^{3}H to ^{3}He, in which the β electron is emitted into an atomic orbit instead of the continuum. The decay to the atomic ground state of ^{3}He has a finite branching ratio of 5.4×10^{-3}. A recent work[5] proposed a setup with ^{3}H and ^{3}He atoms embedded in Nb metal. The electronic structure of Nb metal was determined for different densities of the impurity ^{3}H and ^{3}He atoms. The level width was found to increase with the impurity density: For a mixture of $2-10\%$, the magnitude of the width was of the order of 1 eV. This is comparable to that in the ^{181}Ta$-^{181}$W case, thus yielding an attenuation of a similar order. The origin of this broadening is attributed to the interaction among the impurities. The increasing concentration of the impurities reduces the mean distance between neighboring impurities, leading to the overlap of the electronic wave functions. This overlap leads to the formation of an impurity band and the broadening of the energy level. In the limit of zero density, the level has a hyperfine linewidth, but the experiment becomes unfeasible because of the lack of statistics.

We concluded that the solid state effect significantly attenuates resonant neutrino scattering.

† Condensed from the article in Phys. Lett. **687**, 144 (2010)

*1 Department of Physics, University of Tokyo
*2 NSCL, Michigan State University, USA
*3 Department of Physics, Tokyo University of Science
*4 Department of Physics, Osaka University
*5 GANIL, CEA/DSM-CNRS/IN2P3, France
*6 Max-Planck-Institut für Physik komplexer Systeme, Germany
*7 Instituto de Física, Universidade de São Paulo, Brazil

References

1) R. L. Mössbauer: Z. Physik. **151**, 124 (1958).
2) W. M. Visscher: Phys. Rev. **116**, 1581 (1959).
3) W. P. Kells and J. P. Schiffer: Phys. Rev. C **8**, 2162 (1983).
4) H. Akai, M. Akai, S. Blügel, B. Drittler et al.: Prog. Theor. Phys. Suppl. **101**, 11 (1990).
5) R. S. Raghavan: Phys. Rev. Lett. **102**, 091804 (2009).

2. Nuclear Physics (Theory)

New description of four-body breakup reaction

Takuma Matsumoto[*1], Kiyoshi Katō,[*1] and Masanobu Yahiro[*2]

[Nuclear reaction, unstable nuclei]

The investigation of unstable nuclei far from the stable line is of considerable importance in nuclear physics. Unstable nuclei have exotic properties such as the halo structure[1–3] and the island of inversion[4]. A feature of reactions induced by unstable nuclei is that the projectile easily breaks up into its constituents. One of the most reliable methods for treating projectile breakup processes over a wide range of incident energies is the continuum-discretized coupled-channels (CDCC) method[5,6].

In this paper, we propose a practical method for obtaining $d\sigma/d\varepsilon$ as a continuous function of ε, which is the excitation energy of a projectile; the method involves the use of the CDCC method and complex-scaling method (CSM). The CSM is a powerful tool for studying many-body resonance and weakly bound states[7], and is suitable not only for resonances but also for continuum states. The smoothing method proposed here is an alternative to the direct calculation of the smoothing factor[8] with the hyper-radial continuum wave function[9,10]. A merit of the present smoothing method is that one can see the fast convergence of the calculated breakup cross section upon extending the model space. In this study, the method is applied to ^{12}C(^{6}He,nn^{4}He) and ^{208}Pb(^{6}He,nn^{4}He) reactions at 240 MeV/A[11], and the data obtained are compared with the experimental data.

In Fig. 1, the breakup cross section $d\sigma/d\varepsilon$ calculated by the present method is compared with the experimental data on ^{6}He + ^{12}C and ^{6}He + ^{208}Pb scattering at 240 MeV/A. These data have already been analyzed by using the four-body distorted-wave Born approximation (DWBA)[12] and the eikonal approximation[13]. Nuclear breakup is dominant in the ^{6}He + ^{12}C scattering, while Coulomb breakup to 1^{-} continuum is dominant in the ^{6}He + ^{208}Pb scattering. For a ^{12}C target, the present theoretical result is consistent with the experimental data, except for the peak of the 2^{+}-resonance around $\varepsilon = 1$ MeV. This overestimation is also seen in the results obtained by using the four-body DWBA, and the problem is partly solved by considering the experimental energy resolution. For a ^{208}Pb target, the present method underestimates the experimental data for $\varepsilon \gtrsim 2$ MeV. A possible cause of this underestimation is that the inelastic breakup reactions are not included in the present calculation. As mentioned in Ref. [12], the effect of inelastic breakup reactions is not negligible, and the elastic breakup cross section calculated with the four-body DWBA also underestimates the data.

In summary, we propose a practical method for calculating the differential breakup cross section as a continuous function of the excitation energy of a projectile: the combination of the CDCC method and the CSM. This method does not require the calculation of the continuum wave functions of the projectile. All we have to do is diagonalize the projectile Hamiltonian and the scaled Hamiltonian with L^2-type basis functions. The method is successful in reproducing the data on ^{6}He + ^{12}C and ^{6}He + ^{208}Pb scattering at 240 MeV/A. In principle, the present formalism is applicable to the many-body breakup reaction, provided the diagonalization of the projectile Hamiltonian and the scaled Hamiltonian is possible.

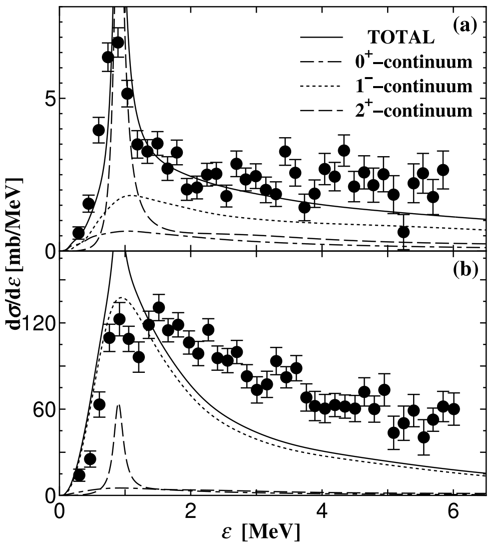

Fig. 1. Comparison of the breakup cross section calculated by the CDCC method (solid line) with experimental data[11] for (a) ^{6}He + ^{12}C scattering at 240 MeV/A and (b) ^{6}He + ^{208}Pb scattering at 240 MeV/A. The dot-dashed, dotted, and dashed lines correspond to contributions of the 0^{+}, 1^{-}, and 2^{+} breakup, respectively.

References

1) I. Tanihata *et al*.: Phys. Lett. B **289**, 261 (1992).
2) I. Tanihata: J. Phys. G **22**, 157 (1996).
3) P. G. Hansen *et al*.: Anuu. Rev. Nucl. Part. Sci. **45**, 591 (1995).
4) E. K. Warburton *et al*.: Phys. Rev. C **41**, 1147 (1990).
5) M. Kamimura *et al*.: Prog. Theor. Phys. Suppl. **89**, 1 (1986).
6) N. Austern *et al*.: Phys. Rep. **154**, 125 (1987).
7) S. Aoyama *et al*.: Prog. Theor. Phys. **116**, 1 (2006).
8) T. Matsumoto *et al*.: Phys. Rev. C **68**, 064607 (2003).
9) B.V. Danilin *et al*.: Phys. Rev. C **55**, R577 (1997).
10) B.V. Danilin *et al*.: Nucl. Phys. A **632**, 383 (1998).
11) T. Aumann *et al*.: Phys. Rev. C **59**, 1252 (1999).
12) S. N. Ershov *et al*.: Phys. Rev. C **62**, 041001(R) (2000).
13) D. Baye *et al*.: Phys. Rev. C **79**, 024607 (2009).

*1 Hokkaido University
*2 Kyushu University

Monopole strength of ^{8}He into five-body scattering states

T. Myo,[*1] R. Ando,[*2] and K. Katō,[*2]

[Nuclear structure, Unstable nuclei, Cluster model, Resonance]

Recently, many experiments on ^{8}He have been reported. Most of the excited states of ^{8}He are located above the ^{4}He+4n threshold energy[1,2].

In this report, we investigate the monopole transition of ^{8}He to clarify the properties of the ^{4}He+4n unbound states. We employ the cluster-orbital shell model of the ^{4}He+n+n+n+n system. We describe the many-body resonances and continuum states under the correct boundary conditions by using the complex scaling method. We employ the Hamiltonian, which reproduces the ^{4}He-n scattering data and the ^{6}He energies. This model can reproduce the energy levels for ^{5}He to ^{8}He[3]. For ^{8}He, we take care of not only five-body resonances, but also all of the residual continuum states of ^{7}He+n, ^{6}He+2n, ^{5}He+3n and ^{4}He+4n.

In Fig. 1, the monopole strengths for isoscalar (IS) and isovector (IV) responses are shown. It is found that two strengths exhibit a similar shape showing the low energy enhancement just above 3 MeV in the excitation energy. There is no clear signature of the 0^+_2 state around its excitation energy of 6.3 MeV in both strengths[3]. In fact, the transition matrix elements from the ground state into the 0^+_2 state are so small in comparison with the total strengths. This result is understood from the configuration of the 0^+_2 state. In the 0^+_2 state, the $(p_{3/2})^2(p_{1/2})^2$ is a dominant configuration of four valence neutrons with 97%, and the mixed $p_{1/2}$ orbit in this state cannot be excited from the $(p_{3/2})^4$ configuration dominated in the ground state by 86% via the monopole operator. As a result, the monopole strength into 0^+_2 becomes negligible. Instead, the continuum strength gives a main contribution.

Among the continuum components, it is found that the IS and IV strengths both dominantly come from the ^{7}He$(3/2^-_1)$+n components which explains the enhancement of the strengths. This selectivity of the continuum states indicates the excitation of the one of the relative motions in ^{8}He by the monopole operator. As a result, the intercluster motion between the ^{7}He cluster and a valence neutron is strongly coupled with the ground state by the monopole excitation. The obtained result also indicates the sequential breakup process of ^{8}He(G.S.) $\rightarrow$ ^{7}He$(3/2^-_1)$+n $\rightarrow$ ^{6}He(G.S.)+n+n. This result is similar to the case of the Coulomb breakup of ^{8}He[4].

In Table 1, the ratios of the integrated strengths into two final states ^{6}He+n+n and ^{4}He+n+n+n+n with respect to the total ones are shown. Dominance of the ^{6}He+n+n state is commonly found in the IS and IV cases and more significant in the IS case[3].

Table 1. Ratios of the integrated monopole strengths into ^{6}He+n+n and ^{4}He+n+n+n+n final states.

	^{6}He+n+n	^{4}He+n+n+n+n
IS	0.939	0.061
IV	0.690	0.310

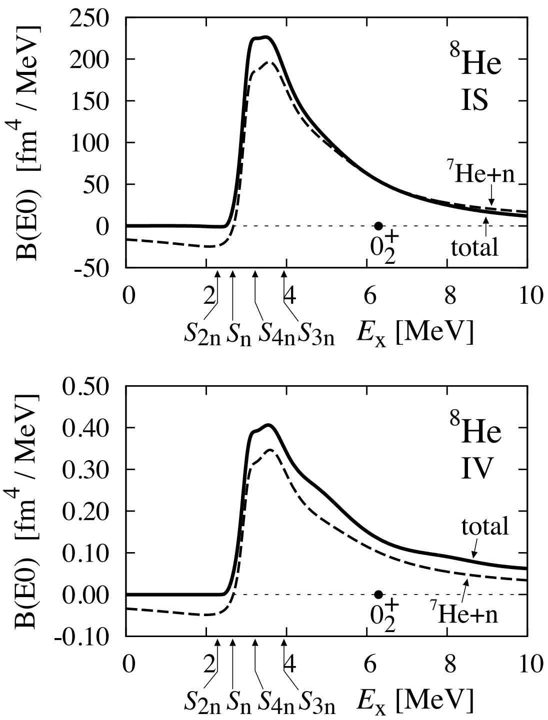

Fig. 1. Monopole transition strengths of ^{8}He as functions of the excitation energy of ^{8}He. The threshold energies of ^{7}He+n, ^{6}He+2n, ^{5}He+3n and ^{4}He+4n are indicated by arrows with S_n, S_{2n}, S_{3n} and S_{4n}, respectively. Position of the 0^+_2 state is shown by dot.

References

1) F. Skaza *et al.*: Nucl. Phys. A**788**, 260c (2007), and references therein.
2) M.S. Golovkov *et al.*: Phys. Lett. B**672**, 22 (2009).
3) T. Myo, R. Ando and K. Katō: Phys. Lett. B**691**, 150 (2010).
4) Y. Iwata *et al.*: Phys. Rev. C**62**, 064311 (2000).

† Condensed from the article in Phys. Lett. B**691**, 150 (2010)

*1 General Education, Faculty of Engineering, Osaka Institute of Technology
*2 Graduate School of Science, Hokkaido University

Triaxial superdeformation in ^{40}Ar†

Y. Taniguchi, Y. Kanada-En'yo[*1], M. Kimura[*2], K. Ikeda, H. Horiuchi[*3], and E. Ideguchi[*4]

[Superdeformation, triaxial deformation]

Superdeformation of light nuclei that have $N \sim Z$ is a topic of great interest in nuclear physics. A particularly interesting topic related to the superdeformed (SD) bands in systems with $A \sim 40$ is the possible triaxial deformation of these bands. For example, a candidate of the $K^\pi = 2^+$ band that adjoins the SD band in ^{44}Ti experimentally observed and theoretically associated with the triaxial deformation.[2] In addition, the triaxial deformation of the SD band in ^{40}Ca has been predicted.[3] Triaxial superdeformations in nuclei whose mass is around 40 region are very important topics.

Recently, an SD band built on the $J^\pi = 0_2^+$ state (2.12 MeV) in ^{40}Ar was experimentally identified to exist up to $J^\pi = (12^+)$ state.[4] An unnatural parity state, $J^\pi = 3^+$, exists at 4.23 MeV. The present study theoretically investigates the structure of the SD band in ^{40}Ar and the possible triaxial deformation of this band by using antisymmetrized molecular dynamics (AMD).

To obtain the wave functions of low-lying states, the parity and angular momentum projections were performed; further the generator coordinate method (GCM) with the deformed-basis AMD wave functions was used. A deformed-basis AMD wave function is a Slater determinant of triaxially deformed Gaussian wave packets. The GCM basis wave functions were obtained by varying the energy of the total system with a constraint on the quadrupole deformation parameter β after the projection to positive parity states was performed; the triaxiality γ was optimized automatically. The Gogny D1S force was used as an effective interaction.

Figure 1 shows the experimental and theoretical excitation energies obtained by the GCM. The $K^\pi = 0^+$ ground state band (GS), $K^\pi = 0^+$ SD band (SD0), and $K^\pi = 2^+$ SD band (SD2) are obtained by the GCM calculations. The observed states, i.e., $J^\pi = 2_5^+$ (3.92 MeV), 3^+ (4.23 MeV), and $(2, 3, 4)^+$ (5.17 MeV) are tentatively assigned to be members of the SD2 band in this study because their excitation energies are similar to the calculated energies of the SD2 band and the candidate states decay to the members of the SD0 band. The dominant components of the SD0 and SD2 bands are triaxially deformed $[(\beta, \gamma) = (0.478, 11.2°)]$. The $|K| = 0$ and 2 components of a single deformed-basis AMD wave function are dominant in the members of the SD0 and SD2 bands, respectively, up to high spin states. Both the SD0 and SD2 bands show rigid rotor-like behavior. The calculated level spacings in the SD0 band members show rotational band spectra; these level spacings and those of the SD2 band members are consistent with the experimental data. The calculated values of $B(E2)$ for the intraband transitions of the GS and SD0 bands are consistent with the experimental data.

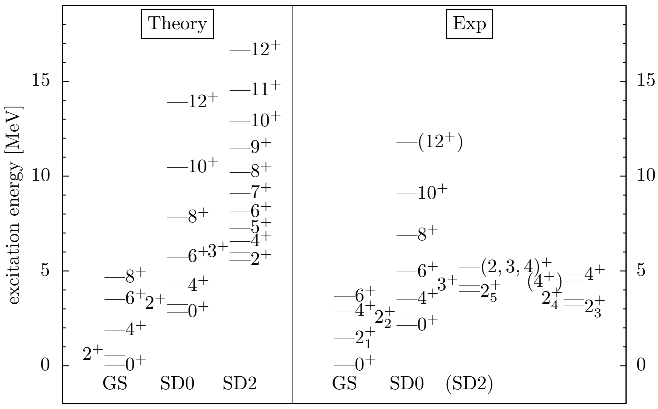

Fig. 1. Level scheme of ^{40}Ar is shown. The experimental data are taken from Refs. 4 and 5. This figure is taken from Ref. 1.

The numerical calculations were conducted on the RIKEN Integrated Cluster of Clusters (RICC) and the supercomputer SX9 at the Research Center for Nuclear Physics, Osaka University.

References

1) Y. Taniguchi, Y. Kanada-En'yo, M. Kimura, K. Ikeda, H. Horiuchi, and E. Ideguchi: Phys. Rev. C **82**, 011302(R) (2010).
2) M. Kimura and H. Horiuchi: Nucl. Phys. A **767**, 58 (2006).
3) Y. Taniguchi, M. Kimura, Y. Kanada-En'yo, and H. Horiuchi: Phys. Rev. C **76**, 044317 (2007).
4) E. Ideguchi et al.: Phys. Lett. B **686**, 18 (2010).
5) J. A. Cameron and B. Singh: Nucl. Data Sheets **102**, 293 (2004).

† Condensed from the article in Ref. 1.

*1 Graduate School of Science, Kyoto University
*2 Creative Research Institution (CRIS), Hokkaido University
*3 Research Center for Nuclear Physics, Osaka University
*4 Center for Nuclear Study, University of Tokyo

Canonical-basis time-dependent Hartree-Fock-Bogoliubov theory and linear-response calculations†

S. Ebata,[*1] T. Nakatsukasa, T. Inakura, K. Yoshida, Y. Hashimoto,[*1,*2] and K. Yabana[*1,*2]

[Nuclear structure, unstable nuclei]

The time-dependent Hartree-Fock-Bogoliubov (TDHFB) theory can describe nuclear phenomena related to pairing correlation. However, there has been no realistic application of the TDHFB theory because the TDHFB calculation needs significant computational resources. Its small-amplitude limit, the quasi-particle random-phase approximation (QRPA), also requires a considerable computational efforts[1,2].

We present simple equations for a canonical-basis (Cb) formulation of the TDHFB theory with an approximation that the pair potential is assumed to be diagonal in the Cb. They are written as

$$i\hbar\dot{\phi}_l(\boldsymbol{r},t) = \big(h[\rho(t)] - \eta_l(t)\big)\phi_l(\boldsymbol{r},t), \quad (1)$$

$$i\hbar\dot{\rho}_l(t) = \Delta_l^*(t)\kappa_l(t) - \Delta_l(t)\kappa_l^*(t), \quad (2)$$

$$i\hbar\dot{\kappa}_l(t) = (\eta_l(t) + \eta_{\bar{l}}(t))\kappa_l(t) + \Delta_l(t)(2\rho_l(t) - 1), \quad (3)$$

where $\phi_l(\boldsymbol{r},t)$ respects single-particle wave functions and $\bar{l}$ denotes a pair of l-state but does not necessarily relate to the time reversal $|\phi_{\bar{l}}\rangle \neq T|\phi_l\rangle$. $\rho_l(t) = |v_l(t)|^2$ and $\kappa_l(t) = u_l(t)v_l(t)$ are occupation- and pair-probabilities in terms of the BCS factor (u,v), $\Delta_l(t) \equiv -\sum_{k>0}\kappa_k(t)\bar{\mathcal{V}}_{l\bar{l},k\bar{k}}$ indicates the pair potential, and $\bar{\mathcal{V}}_{l\bar{l},k\bar{k}}$ respects the antisymmetric two-body matrix elements that are also time dependent because Cb $\{l,\bar{l}\}$ and $\{k,\bar{k}\}$ are time dependent. We also have $\eta_l(t) \equiv \langle\phi_l(t)|h|\phi_l(t)\rangle + i\hbar\langle\frac{\partial\phi_l}{\partial t}|\phi_l(t)\rangle$. These equations conserve the orthonormality of the single-particle wave function, the particle number, and the total energy.

We call Eqs.(1)-(3) the canonical-basis TDHFB (Cb-TDHFB) equations. We apply the Cb-TDHFB to the linear response for light nuclei by using the full Skyrme functional and compare the response with that recently obtained calculations through the QRPA[1,2]. The good agreement observed demonstrates the feasibility and accuracy of the new method.

In numerical calculations, we adopt a schematic pairing functional, $E_{\rm pair} = -\sum_{k,l>0} G_{kl}\kappa_k^*(t)\kappa_l(t)$, where $\kappa_l = u_l v_l$; u_l and v_l correspond to the time-dependent BCS factors for the canonical pair of states $\phi_l(\boldsymbol{r},t)$ and $\phi_{\bar{l}}(\boldsymbol{r},t)$. This pairing functional produces a pair potential that is diagonal in the Cb. Because this functional violates the gauge invariance of the phase degree of freedom of the Cb, we need to choose a special gauge for correctly describing the time evolution of Cb.

We solve the Cb-TDHFB equations in real time and calculate the linear response of the nucleus. We calculate the time evolution of the expectation value of a one-body operator $\hat{F}$ and obtain the strength function $S(\hat{F};E)$ by Fourier transformation.

Figure 1 shows a comparison between the Cb-TDHFB results and those of the QRPA computed by using the SkM* parameter set for the isoscalar quadrupole modes ($K=0$ and $K=2$) of ^{34}Mg. In these calculations, the ground state of ^{34}Mg shows prolate deformation and the superfluid phase only for neutron. Figs.1 (a) and (b) show Cb-TDHFB results with the schematic pairing functional, while (c) and (d) show the results of the QRPA calculated with δ-type interaction for the pairing channel[1,2]. The panels (a) and (c) do not include the residual spin-orbit and Coulomb interactions, while (b) and (d) show fully self-consistent results. These comparisons indicate that the small-amplitude Cb-TDHFB calculations well reproduce the results of the QRPA, except for the height of the lowest peak. We suppose that the mismatch is because of the difference in the pairing functional.

In the near future, the Cb-TDHFB method will provide a useful tool to study heavy-ion collision dynamics beyond the TDHF, for instance, to investigate the dynamical pairing effects for dissipation.

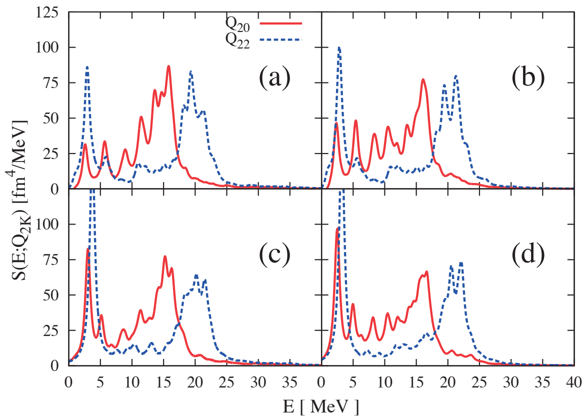

Fig. 1. Calculated isoscalar quadrupole strength distribution for ^{34}Mg: (a) Cb-TDHFB without residual spin-orbit and Coulomb interactions, (b) fully self-consistent Cb-TDHFB results, (c) deformed QRPA without the residual spin-orbit and Coulomb interactions[1)], and (d) fully self-consistent deformed QRPA calculation[2)]. The value of the smoothing parameter of Γ is 1 MeV.

† Condensed from the article in Phys. Rev. C **82**, 034306 (2010).
*1 Graduate School of Pure and Applied Sciences, University of Tsukuba
*2 Center for Computational Science, University of Tsukuba

References

1) K. Yoshida and N. V. Giai: Phys. Rev. C **78**, 064316 (2008).
2) C. Losa *et al.*: Phys. Rev. C **81**, 064307 (2009).

Systematic calculations of electric dipole responses in fully self-consistent Skyrme-RPA approach

T. Inakura,[*1] T. Nakatsukasa,[*1,*2] and K. Yabana[*2,*1]

[Nuclear structure, random-phase approximation, photonuclear reaction]

The systematic calculation covering a wide region of the nuclear chart is expected to helps us to improve our understanding of the nuclear structure. Using an effective interaction typified by the Skyrme interaction, we carried out systematic and fully self-consistent RPA calculations for a wide mass region up to zirconium, for both spherical and deformed nuclei. We focused our attention on the dipole responses. For the electric dipole mode (or the photoabsorption cross section), there are abundant experimental data that have been accumulated over many years, including data on the giant dipole resonances (GDRs).

The upper panel of Fig. 1 shows the evolution of the GDR peak positions, estimated by using the mean energy $E_{\rm mean} = m_1/m_0$ with $m_k = \int d\omega\, \omega^k \sigma(\omega)$, where $\sigma(\omega)$ is the photoabsorption cross section. The peak energies approximately follow the empirical low, $21A^{-1/3} + 31A^{-1/6}$. However, in each isotopic chain, the peak energies in stable nuclei are nearly the highest, and they decrease with an increase in the distance from the stability line. Such behavior on the neutron-deficient side is opposite to the empirical law. The lower panels of Fig. 1 show the dependence of the mean energy on the neutron number and proton number. It is interesting to see a correlation between the GDR peak energies and the neutron number. There are cusps at N =14 and 28, corresponding to the subshell closure of the $1d_{5/2}$ and $1f_{7/2}$ orbitals. In addition, the peak energies at the cusps are almost invariant with respect to the proton number. While the neutron Fermi level is located in the $1d_{5/2}$, $1f_{7/2}$, and $1g_{9/2}$ orbitals, which have the largest angular momentum j in each major shell, the peak energies are roughly constant against the variation in the neutron number. Then, after filling up these highest-j orbitals, the peak energies start to decrease, and they decrese until the major shells are completely filled. On the neutron-deficient side, we may see similar trends; however, the dependence on the proton number is weaker than that on the neutron number.

The correlation between the ground state deformations β_2 and the GDR splitting in deformed nuclei is shown in Fig. 2. In order to evaluate the deformation from the GDR splitting, we define a new deformation parameter[1] $\beta_{\delta E} = (E_{K=1} - E_{K=0})/E_{\rm ave}$, where $E_{K=0,1}$ are the peak positions extracted from

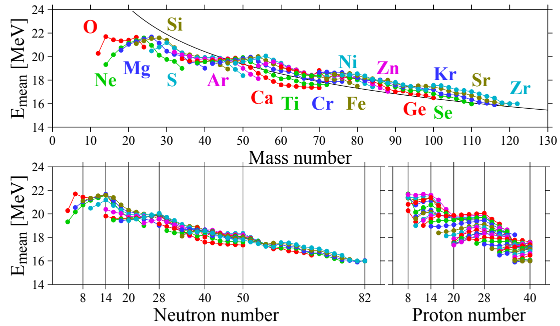

Fig. 1. Evolution of the GDR peak position.

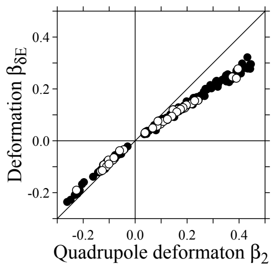

Fig. 2. Correlation between GDR splitting and ground state deformation β_2. Open (filled) circles denotes stable (unstable) nuclei.

the energy-weighted Lorentzian fitting for the $K = 0, 1$ components of the calculated photoabsorption cross section, and $E_{\rm ave} = (E_{K=0} + 2E_{K=1})/3$. The figure clearly shows that the magnitude of the deformation resulting from the GDR splitting $\beta_{\delta E}$ is proportional to the magnitude of the static deformations β_2 , as was pointed out in Ref. 1 and as has been widely recognized. One of the interesting findings in our calculation is that the proton-neutron asymmetry does not influence the GDR splitting. In neutron drip-line nuclei, the root-mean-square radius of the neutron is larger than that of the proton by 0.5 fm. In some nuclei, the protons and neutrons may show different deformations. However, in our systematic calculations, the GDR splitting is found to be characterized only by the gross deformation β_2, which is not sensitive to the proton-neutron asymmetry, and hence $\beta_{\delta E} \propto \beta_2$.

More detailed systematic analyses on dipole responses are under progress.

References

1) A. Bohr and B. R. Mottelson: *Nuclear Structure, vol. II* (W. A. Benjamin, New York, 1975).

[*1] Theoretical Nuclear Physics Laboratory, RIKEN Nishina Center

[*2] Center for Computational Sciences, University of Tsukuba

Photoabsorption cross sections in Nd and Sm isotopes undergoing shape phase transitions†

Kenichi Yoshida and Takashi Nakatsukasa

[Nuclear structure, dipole responses, density functional theory]

Density functional theory has been widely used to describe a variety of quantum many-body systems, including nuclear many-body system. Ground-state properties, including nuclear deformation, are described well by the modern nuclear energy-density functional (EDF) method. It is known that nuclear deformation affects the high-frequency collective modes of excitation, giant resonances (GRs). For instance, the peak splitting of the giant dipole resonance (GDR), which is caused by the different frequencies of oscillation along the long and short axes, has been observed in experiments[1]. A typical example of the shape phase transition from spherical to deformed ground states and the evolution of deformation splitting in GDRs have been observed in Nd and Sm isotopes[2,3]. In this paper we report the first systematic calculation of electric dipole ($E1$) responses of these heavy isotopes undergoing shape phase transition; this calculation is carried out by employing a non-empirical approach with the Skyrme EDF, namely, the quasiparticle random-phase-approximation based on the Hartree-Fock-Bogoliubov ground states (HFB+QRPA)[4].

Figure 1 shows the calculated photoabsorption cross sections in the GDR energy region and the available experimental data[2,3]. The GDR peak energies agree well with experimental values and produce the deformation splitting in ^{150,152}Nd and ^{152,154}Sm. The GDR width calculated by using $\gamma = 2$ MeV is also in good accordance with the experimental values. The QRPA accounts for the Landau damping, corresponding to fragmentation of the GDR strength into nearby two-quasiparticle states, but not for the spreading effect, which corresponds to the fragmentation into more complex states. The nice agreement on the broadening indicates that in these nuclei, the smearing width $\gamma = 2$ MeV is strongly correlated with the spreading width $\Gamma^{\downarrow}$.

The isotopic dependence of the peak broadening is well reproduced, surprisingly, even for transitional nuclei. This broadening effect is commonly interpreted as the effect of coupling to the low-lying collective mode. In the present QRPA calculation, the mode coupling is not explicitly taken into account. However, the QRPA based on the deformed HFB state may implicitly include a part of the coupling effect. Figure 1 shows that the isotopic dependence can be satisfactorily attributed to the gradual increase in the ground-state deformation.

We may notice small disagreement with the oberva-tion in the peak shape: In the spherical nuclei, the calculated GDR peak has a shoulder, and in the deformed nuclei, this shoulder is becoming the third peak. This is due to the Landau fragmentation, however, this feature is not clearly observed in the experiments. We found that the detailed properties of the Landau fragmentation depend on the chosen Skyrme EDF. For instance, the fragmentation effect becomes weak with the SkP functional, and better agreement with the experimental results is achieved.

Systematic calculations by employing the HFB+QRPA for spherical-to-deformed and light-to-heavy nuclei help us not only in understanding and in predicting new types of collective modes of excitation, but also help us in shedding light on the nuclear EDF of new generations.

References
1) B. L. Berman et al.: Rev. Mod. Phys. **47**, 713 (1975).
2) P. Carlos et al.: Nucl. Phys. **A172**, 437 (1971).
3) P. Carlos et al.: Nucl. Phys. **A225**, 171 (1974).
4) K. Yoshida et al.: Phys. Rev. C **78**, 064316 (2008).

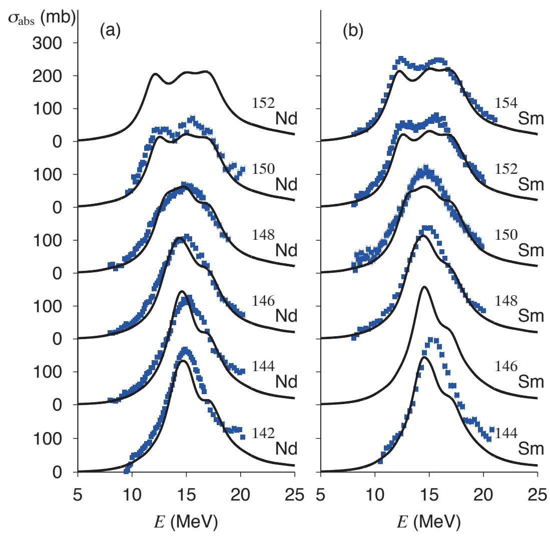

Fig. 1. Photoabsorption cross sections in (a) Nd and (b) Sm isotopes as functions of photon energy obtained by employing the SkM* functional. The filled squares represent the experimental data[2,3]. The calculated cross sections are smeared by a Lorentzian function with a smearing width of $\gamma = 2$ MeV.

† Condensed from article in Phys. Rev. C **83**, 021304R (2011).

Roles of deformation and neutron excess in giant monopole resonance in Zr isotopes†

Kenichi Yoshida

[Nuclear structure, monopole responses, density functional theory, unstable nuclei]

The surface structures of neutron-rich nuclei are very different from those of stable nuclei because of the presence of the loosely bound neutrons in the former. Since collective excitations are sensitive to the surface structure, new exotic excitation modes may appear in neutron-rich nuclei. Furthermore, strong mixing of the isoscalar (IS) and isovector (IV) components associated with the neutron-proton asymmetry may lead to the emergence of the neutron-dominant giant resonance (GR).

GRs are typical collective modes of excitation in nuclei. The effects of nuclear deformation on the GRs have been investigated for long, both experimentally and theoretically. Deformation splitting of the giant dipole resonance (GDR) is one such effect that has been well established. This is due to the oscillation along the major and minor axes. For GRs with high multipolarity, the deformation splitting is less pronounced. The effects of deformation on the giant monopole resonance (GMR) were discussed soon after the GMR concept was established[1)].

We investigate the GMR in neutron-rich medium-mass nuclei around ^{110}Zr, by taking into account the deformation effect and the mixing of the IS and IV components. To this end, we use a nonempirical approach with the Skyrme energy density functional (EDF), namely, the quasiparticle random-phase approximation based on the Hartree-Fock-Bogoliubov ground states[2)].

Figure 1 shows the IS and IV monopole and quadrupole transition strength distributions in Zr isotopes. In the present calculation, the ^{90}Zr nucleus is considered to be spherical, and the other nuclei are prolately deformed. The ISGMR has a two-peak structure in the deformed nuclei. The high-energy peak of the IS monopole excitation seen at around 20 MeV is identified as a primal ISGMR because the ISGMR in ^{90}Zr is located at around 18 MeV, where only one peak is observed.

To understand the origin of the low-energy peak at around 10 MeV, we focus on the $K^\pi = 0^+$ component of the quadrupole transition strength (Figs. 1(k)-1(o)). A peak structure can be seen in the same energy region where the low-energy peak of the ISGMR appears. Thus, the appearance of the low-energy peak is thought to be associated with the coupling to the $K^\pi = 0^+$ component of the IS giant quadrupole resonance (GQR).

† Condensed from article in Phys. Rev. C **82**, 034324 (2011).

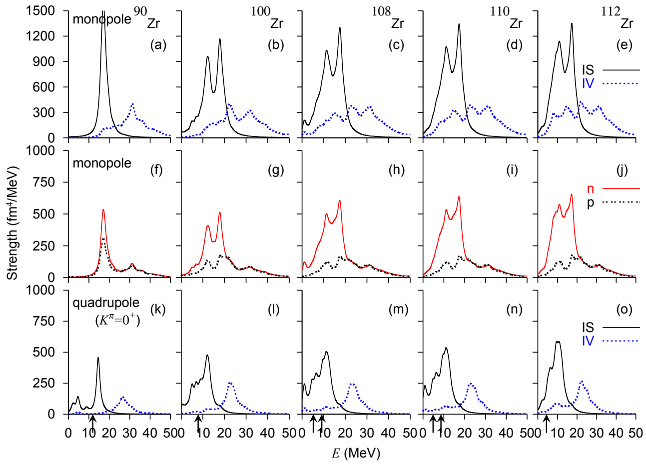

Fig. 1. IS and IV monopole and the $K^\pi = 0^+$ component of the quadrupole transition strengths in ^{90,100,108,110,112}Zr. The neutron and proton transition strengths are also shown for monopole excitation. The transition strengths are smeared by a Lorentzian function with a width of $\gamma = 2$ MeV.

The neutron excitation is found to concentrate in the region of the low-energy peak of the ISGMR. The middle panels in Fig. 1 show the neutron and proton monopole transition strengths. It is seen that the neutron excitation plays a dominant role in increasing the IS transition strengths.

The IVGMR in deformed neutron-rich nuclei has interesting features, because of which a four-peak structure appears, as shown in Fig. 1. This four-peak structure is well pronounced in ^{112}Zr. The highest peak appearing at energies greater than 30 MeV corresponds to a primal IVGMR, as revealed by a comparison of the peak energy with that in the case of ^{90}Zr. A peak structure appears in the 22-23-MeV region, where the IVGQR is seen. Thus, the second highest peak is associated with the coupling to the $K^\pi = 0^+$ component of the IVGQR. In addition, two more peaks appear at energies less than 20 MeV. These peaks may have been shifted to the ISGMR energy region owing to the neutron excess. One of these two peaks is associated with the coupling to the ISGMR, and the other is due to the coupling to the $K^\pi = 0^+$ component of the ISGQR.

References

1) U. Garg et al.: Phys. Rev. Lett. **45**, 1670 (1980).
2) K. Yoshida et al.: Phys. Rev. C **78**, 064316 (2008).

Microscopic description of large-amplitude shape-mixing dynamics with local QRPA inertial functions

N. Hinohara,[*1] K. Sato,[*2,*1] T. Nakatsukasa,[*1] M. Matsuo,[*3] and K. Matsuyanagi[*1,*4]

[Nuclear structure, large-amplitude collective motion, shape coexistence]

On the basis of the microscopic theory of large-amplitude collective motion, we formulate a practical method for deriving the five-dimensional (5D) quadrupole collective Hamiltonian (with the collective potential and three vibrational and three rotational inertial functions), and we illustrate its usefulness by applying it to the oblate-prolate shape coexistence/mixing phenomena in the proton-rich isotopes ^{68,70,72}Se.

To derive the collective Hamiltonian, we start from the two-dimensional (2D) version of the adiabatic self-consistent collective coordinate (ASCC) method.[1)] We determine a 2D collective hypersurface associated with large-amplitude quadrupole shape vibrations by transforming a set of two collective coordinates into the quadrupole deformation variable set (β, γ). The constrained Hartree-Fock-Bogoliubov (CHFB) equation and the local quasiparticle random-phase approximation (LQRPA) equations are derived from the 2D ASCC equations. The central concept of this approach is local normal modes built on CHFB states defined at every point of the (β, γ) deformation plane. These local normal modes are determined by the LQRPA equations that are an extension of the well-known QRPA equations to non-equilibrium HFB states determined by the CHFB equations. The vibrational and rotational inertial functions in the 5D collective Hamiltonian are determined using these modes. The inertial functions determined in this approach include the time-odd terms that arise from the moving mean field, which are ignored in the widely used Inglis-Belyaev (IB) cranking mass.[2)]

As a first step toward calculations using modern energy density functionals, the pairing-plus-quadrupole model that includes the quadrupole-pairing interaction is employed in this work. Inclusion of the quadrupole-pairing interaction is essential since it gives rise to a time-odd mean field contribution to the collective masses. The collective Hamiltonians for the low-lying states of oblate-prolate shape coexistence/mixing phenomena in the proton-rich nuclei of ^{68,70,72}Se are determined (Fig. 1). Figure 2 shows the excitation energies and $B(E2)$ values obtained by numerical calculations. They are in good agreement with recent experimental data[3,4)] for the yrast $2_1^+, 4_1^+$, and 6_1^+ states in the above-mentioned nuclei. The time-odd components of the moving mean field significantly increase the vibrational and rotational collective masses; they also improve the agreement between the theoretical spectra and experimental data. Such agreement with experimental data is not seen in the case of the calculations performed using the IB cranking masses. The present calculation clearly indicates that the low-lying states in the above-mentioned nuclei possess a transitional character between the oblate-prolate shape coexistence and the so-called γ-unstable situation, where large-amplitude triaxial-shape fluctuation plays a dominant role.

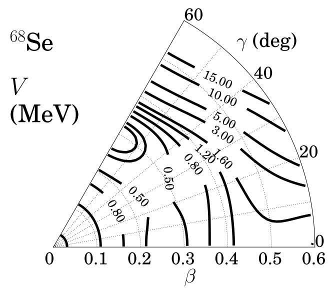

Fig. 1. Collective potential for ^{68}Se.

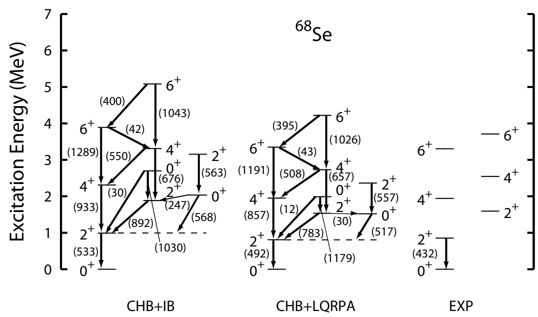

Fig. 2. Theoretical (calculated using IB and LQRPA masses) and experimental excitation spectra and $B(E2)$ values (in units of e^2 fm^4) for low-lying states in ^{68}Se.

References

1) M. Matsuo, T. Nakatsukasa, and K. Matsuyanagi: Prog. Theor. Phys. **103**, 959 (2000).
2) S. T. Beliaev: Nucl. Phys. **24**, 322 (1961).
3) S. M. Fischer, C. J. Lister, and D. P. Balamuth: Phys. Rev. C **67**, 064318 (2003).
4) A. Obertelli et al.: Phys. Rev. C **80**, 031304 (2009).

† Condensed from Phys. Rev. C **82**, 064313 (2010)

*1 Theoretical Nuclear Physics Laboratory, RIKEN Nishina Center
*2 Department of Physics, Kyoto University
*3 Department of Physics, Niigata University
*4 Yukawa Institute for Theoretical Physics, Kyoto University

Triaxial quadrupole deformation dynamics in *sd*-shell nuclei around ^{26}Mg

N. Hinohara and Y. Kanada-En'yo[*1]

[Nuclear structure, large-amplitude collective motion]

Collective deformation grows in the middle of the *sd*-shell region. In contrast to the well-understood prolate deformation in ^{24}Mg and oblate deformation in ^{28}Si, the deformation property of ^{26}Mg is not yet fully understood. Since ^{26}Mg has $N = 14$ and $Z = 12$, neutrons and protons favor different shapes of the nucleus separately. Theoretical calculations suggest extremely soft triaxial potential-energy surfaces.

We analyze the role of triaxiality in connection with the large-amplitude collective motion in the low-lying states of ^{24}Mg, ^{28}Si, ^{26}Mg, and ^{24}Ne. The analysis is performed using a five-dimensional quadrupole collective Hamiltonian calculated with the constrained Hartree-Fock-Bogoliubov plus local quasiparticle random-phase approximation (CHFB + LQRPA) method[1)] in conjunction with the pairing-plus-quadrupole model. The collective Hamiltonian approach is a powerful theoretical tool for investigating the large-amplitude collective motion by taking into account β and γ degrees of freedom.

The calculation reproduces the prolate rotational band and γ-vibrational band of ^{24}Mg, and the oblate rotational band and β-vibrational band of ^{28}Si. In the case of ^{26}Mg and ^{24}Ne, the collective potentials are shown to be soft against β and γ deformations, and large shape fluctuations in the (β, γ) plane are found in the vibrational wave functions of the ground states. The vibrational wave functions of the 0_1^+ state are spread over the triaxial region from the oblate to the prolate areas of the region. Yrast bands show rotational hindrance to shape mixing, and the states localize around the prolate region as the angular momentum increases. Figure 1 shows a comparison between the theoretical and experimental spectra of the low-lying states of ^{26}Mg. The theoretical value of $E_x(4_1^+)/E_x(2_1^+)$ ratio is 2.64, which explains the experimental value of 2.71 very well.

The neutron and proton quadrupole transition matrix elements are analyzed for the systems in which $N \neq Z$. In the mirror nucleus method[2)], the proton matrix element is determined from the $E2$ transition as $B(E2) = M_p^2/(2I+1)$, while the neutron matrix element is determined from the same $E2$ transition of the mirror nucleus as $B(E2)_{\rm mirror} = M_n^2/(2I+1)$. The experimental values of M_n and M_p for the $2_2^+ \to 0_1^+$ transition in ^{26}Mg are 6.05 ± 0.94 e fm^2 and 2.83 ± 0.28 e fm^2, respectively, and the value of the ratio $M_n/M_p/(N/Z)$ is 1.83 ± 0.34. In the simple collective model, the ratio M_n/M_p should be equal to the ratio N/Z, and a large experimental value of the ratio clearly indicates the dominance of the neutron matrix element in this transition.

We obtained M_n and M_p values of 3.19 and 0.234 e fm^2 for a two-major shell, which shows neutron dominance. In this case, the absolute values of M_n and M_p obtained with bare charges are smaller than the experimental values because of a restricted model space. To take into account the effect of core polarization, we introduce a phenomenological polarization charge δe that is equal to 0.5 for both neutrons and protons. The neutron and proton matrix elements are then evaluated to be 4.90 and 1.95 e fm^2. The ratio of these matrix elements is $M_n/M_p/(N/Z) = 2.15$; this value is comparable with the experimental value.

We discussed the mechanism of neutron dominance for $2_2^+ \to 0_1^+$ transition in ^{26}Mg in terms of large-amplitude triaxial shape dynamics. We found that cancellation occurs between the contributions to the matrix elements in the oblate and prolate regions. The proton matrix element is almost completely canceled between the oblate and prolate regions. In the case of neutrons, the contribution to the matrix element is relatively larger in the oblate region than in the prolate region, and this situation produces a large M_n/M_p ratio.

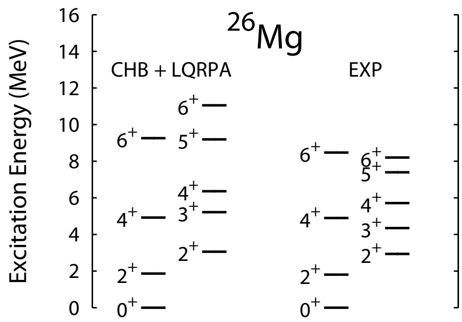

Fig. 1. Theoretical and experimental excitation spectra of low-lying states of ^{26}Mg.

References
1) N. Hinohara *et al.*: Phys. Rev. C **82**, 064313 (2010).
2) A. M. Bernstein *et al.*: Phys. Rev. Lett. **42**, 425 (1979).

† Condensed from Phys. Rev. C **83**, 014321 (2011)
*1 Department of Physics, Kyoto University

Large-amplitude shape mixing dynamics in proton-rich Kr isotopes†

K. Sato,*[1,2] N. Hinohara*[2]

[Nuclear structure, large-amplitude collective motion, shape coexistence]

Atomic nuclei exhibit various shapes depending on their proton and neutron numbers, excitation energies, and angular momentum. Shape coexistence phenomena, in which an excited band whose shape is different from the ground-band shape coexists close to the ground band, are widely observed across the nuclear chart. From the mean-field viewpoint, the shape coexistence implies that there are two equilibrium points in the mean-field potential energy surface. If the potential barrier between the equilibrium points is sufficiently low, the different shapes are largely mixed because of the many-body tunneling effect.

To describe this large-amplitude shape mixing dynamics, we adopt the five-dimensional (5D) quadrupole collective Hamiltonian.[1)] Recently, we have developed a new method[2)] for determining the 5D quadrupole collective Hamiltonian; the method is based on the adiabatic self-consistent collective coordinate method.[3)] This method comprises the constrained Hartree-Fock-Bogoliubov (CHFB) equation at each mesh point in the (β, γ) plane and the local QRPA (LQRPA) equations, which are an extension of the usual quasiparticle random phase approximation (QRPA) equations to the non-HFB-equilibrium points, on top of each CHFB state. Therefore, we call it the CHFB+LQRPA method. One of the advantages of this method is that the collective masses determined with this method contain contributions from the time-odd components of the mean field, unlike the case of the widely used Inglis-Belyaev (IB) cranking formula.

We have applied this method to the oblate-prolate shape coexistence/mixing phenomena in the low-lying states of the proton-rich Kr isotopes ^{72,74,76}Kr. The numerical results are in good agreement with available experimental data, and they indicate a shape transition from the oblate ground band in ^{72}Kr to the prolate one in ^{74,76}Kr. In the calculation, we have employed the pairing-plus-quadrupole model including the quadrupole-pairing interaction. The inclusion of this interaction is essential to obtain the time-odd components of the mean field. We have calculated the vibrational and rotational masses with the CHFB+LQRPA method and found that the time-odd components of the mean field increase these masses more in comparison with the IB cranking masses and that the increase is strongly dependent on (β, γ). Reflecting this enhancement, the excitation energies obtained with the LQRPA masses are lower than those obtained with the IB cranking masses and are in better agreement with the experimental data. The numerical results also show that the low-lying states of these isotopes are located in intermediate situations between the ideal oblate-prolate shape coexistence and γ-unstable limit. The basic features of the low-lying spectra are determined by the interplay among the large-amplitude shape fluctuation in the triaxial degree of freedom, the β-vibrational excitation, and the rotational motion. Furthermore, we have shown that the rotational motion can lead to the increased localization of the vibrational wave function in the (β, γ) plane. Figure 1 shows the excitation energies and $B(E2)$ values calculated for ^{72}Kr. One can see that the interband transition between the initial and final states having the same angular momentum becomes weaker as the angular momentum increases, which is a result of the development of the localization of the wave function mentioned above.

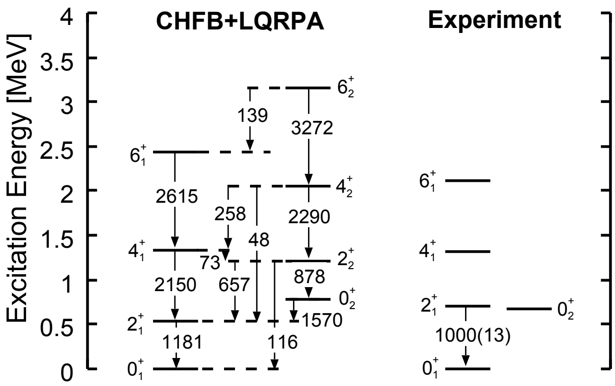

Fig. 1. Excitation energies and $B(E2)$ values calculated for ^{72}Kr with the CHFB+LQRPA method (left) and experimental data (right).[4–6)] In the left spectrum, only $B(E2)$ values larger than 1 Weisskopf unit are shown in units of $e^2\mathrm{fm}^4$.

References
1) A. Bohr and B. R. Mottelson: *Nuclear Structure*, Vol. II (W. A. Benjamin Inc., 1975; World Scientific, 1998).
2) N. Hinohara, K. Sato, T. Nakatsukasa, M. Matsuo, and K. Matsuyanagi: Phys. Rev. C **82**, 064313 (2010).
3) M. Matsuo, T. Nakatsukasa, and K. Matsuyanagi: Prog. Theor. Phys. **103**, 959 (2000).
4) E. Bouchez et al.: Phys. Rev. Lett. **90**, 082502 (2003).
5) A. Gade et al.: Phys. Rev. Lett. **95**, 022502 (2005); Phys. Rev. Lett. **96**, 189901 (2006), Erratum.
6) S. M. Fischer et al.: Phys. Rev. C **103**, 064318 (2003).

† Condensed from Nucl. Phys. A **123**, 129 (2011).

*1 Department of Physics, Kyoto University
*2 Theoretical Nuclear Physics Laboratory, RIKEN Nishina Center

Density dependence of pairing correlations determined by global fitting†

M. Yamagami,[*1] J. Margueron,[*2] H. Sagawa,[*1] and K. Hagino[*3]

[Pairing correlations, Neutron-rich nuclei, Density functional theory]

Information on neutron-rich nuclei is indispensable for understanding the nuclear dynamics in celestial bodies, such as r-process nucleosynthesis, and the reactions in a nuclear reactor. In this study, by using existing experimental data, we aim to develop a density functional theory that will allow us to extend our knowledge to nuclei with large neutron excess.

While extensive efforts have been made for improving the energy density functional (EDF), one of the bottlenecks stems from the pairing part of the EDF (pair-DF). Although the low-energy nuclear properties are strongly influenced by pairing, the standard pair-DF with isoscalar density (ρ) dependence fails to reproduce the dependence of pairing on the mass number A and on the neutron excess ($\alpha = (N-Z)/A$).

We propose the pair-DF $\tilde{h}_\tau(\mathbf{r}) = \frac{1}{2}V_0 g_\tau(\mathbf{r})\tilde{\rho}_\tau(\mathbf{r})$ including the linear[1,2] and quadratic[3] terms of the isovector density ($\rho_1 = \rho_n - \rho_p$) for the α-dependence of pairing[3], in addition to the usual ρ term for the A dependence:

$$g_\tau(\mathbf{r}) = 1 - \eta_0\left(\frac{\rho}{\rho_0}\right) - \eta_1\left(\frac{\tau_3\rho_1}{\rho_0}\right) - \eta_2\left(\frac{\rho_1}{\rho_0}\right)^2.$$

Here, $\tau_3 = 1(-1)$ for $\tau = n(p)$ and $\rho_0 = 0.16\ \mathrm{fm}^{-3}$.

The parameters are determined so as to minimize the rms deviation σ_{tot} between the experimental pairing gaps and the results of the Hartree-Fock-Bogoliubov calculation with the Skyrme force for even-even nuclei in the medium mass region (referred to as Zone 1, and including 159 neutron and 139 proton pairing gaps). We check the performance of our pair-DF for even-even nuclei in the region of $28 \le A \le 254$ (346 neutron and 295 proton pairing gaps).

We show that the ρ dependence can be clarified if and only if the ρ_1 terms are included. The parameter is determined to be $\eta_0 \approx 0.8$ by optimizing σ_{tot} as a function of η_0, η_1, η_2, and V_0 (see Figs.1 and 2). We also point out that the optimal V_0 is close to the strength parameter determined by the neutron-neutron scattering length of the ${}^1S_0$ channel in vacuum if the effective mass of Skyrme force is in the range of $0.7 \le m^*/m \le 0.8$.

We conclude that our pair-DF has the potential to improve the global description of pairing correlations and pairing-sensitive observables, thanks to the reproducibility of the A and α dependence of pairing and the connection between the strength V_0 and the low-density limit.

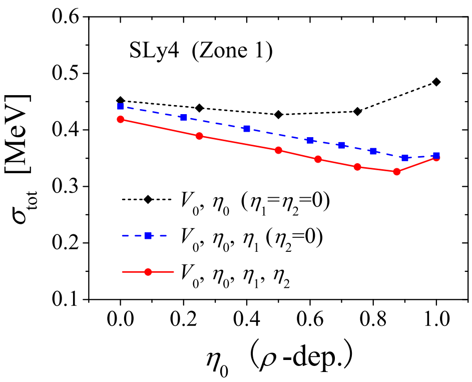

Fig. 1. σ_{tot} values obtained by using pair-DF with 1) only the ρ term, 2) the ρ and linear ρ_1 terms, and 3) all ρ and ρ_1 terms are compared. For each η_0, the other parameters of pair-DF are optimized in Zone 1.

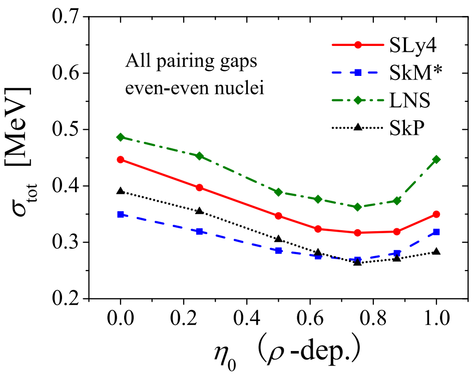

Fig. 2. σ_{tot} values obtained by using pair-DF with all ρ and ρ_1 terms. The results with Skyrme SLy4, SkM*, LNS, and SkP are compared. Available data for even-even nuclei in the region of $28 \le A \le 254$ are considered.

References

1) J. Margueron, H. Sagawa, and K. Hagino: Phys. Rev. C **76**, 064316 (2007).
2) M. Yamagami and Y. R. Shimizu: Phys. Rev. C **77**, 064319 (2008).
3) M. Yamagami, Y. R. Shimizu, and T. Nakatsukasa: Phys. Rev. C **80**, 064301 (2009).

*1 Department of Computer Science and Engineering, University of Aizu, Aizu-Wakamatsu, Fukushima 965-8580, Japan
*2 Institut de Physique Nucléaire, Université Paris-Sud, IN2P3-CNRS, F-91406 Orsay Cedex, France
*3 Department of Physics, Tohoku University, Sendai 980-8578, Japan

A new method for finding the QRPA solution†

P. Avogadro and T. Nakatsukasa

[Nuclear structure, harmonic approximation, unstable nuclei]

At present, many tools are being used to investigate the structure and properties of atomic nuclei. Ab initio calculations can be performed only for low-mass nuclei, while for high-mass nuclei the density functional theory is the best tool available. Quasiparticle random-phase approximation (QRPA) is widely used to study low-energy excitations, including giant resonances.

The QRPA problem is solved when one obtains the X and Y amplitudes that determine the structure of the excitation phonons in the harmonic approximation:

$$Q^{\lambda\dagger} = \frac{1}{2}\sum_{\mu\nu}\left(X^{\lambda}_{\mu\nu}a^{\dagger}_{\mu}a^{\dagger}_{\nu} - Y^{\lambda}_{\mu\nu}a_{\nu}a_{\mu}\right),$$

where a_μ and $a^\dagger_\mu$ denote the quasiparticle operators. Two main difficulties are encountered when finding the solution to the problem, one concerning the calculation of the matrix elements, and the other related to the diagonalization of the resulting matrix. In order to simplify the construction of the problem, we developed an extension of the finite amplitude method (FAM), which was first proposed for the random phase approximation (RPA) problem. In the present research, we take into account the presence of pairing correlations in atomic nuclei for the extension of the FAM.

We consider the time-dependent Hartree-Fock-Bogoliubov (TDHFB) equations in the small-amplitude limit, which are equivalent to the QRPA equations[2]; in this limit, the Hamiltonian of the system can be divided into the HFB Hamiltonian and a time-dependent residual field as $H(t) = H_0 + \eta\delta H(t)$. Similarly, the quasiparticle annihilation operator can be written as $a_\mu(t) = \{a_\mu + \eta\delta a_\mu(t)\}\, e^{-iE_\mu t}$. In the TDHFB theory, the quasiparticle states contain all the information to solve the problem. We can thus insert

$$\delta a_\mu(t) = \sum_{\nu} a^{\dagger}_{\nu}\left(X_{\nu\mu}e^{-i\omega t} + Y_{\nu\mu}e^{i\omega t}\right),$$

into the TDHFB equations and take the small-amplitude limit:

$$i\frac{\partial\delta a_\mu(t)}{\partial t} = E_\mu\delta a_\mu(t) + [H_0, \delta a_\mu(t)] + [\delta H(t), a_\mu].$$

With the help of the FAM, we obtain a set of linear equations for X and Y amplitudes. The residual densities obtained are functions of the QRPA amplitudes, and thus, the resulting problem is self-consistent. To solve this problem, we use the generalized conjugate gradient (GCR) method, in which the solution of a linear system is obtained by successive iterations from a guess choice.

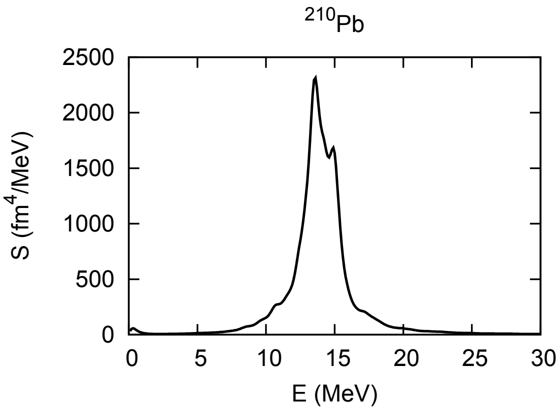

Fig. 1. Monopole isoscalar strength function for the ^{210}Pb nucleus, using the SKM* interaction in the ph channel and a volume-type density-dependent delta interaction in the pp channel; the strength is smeared out with a 0.5 MeV width.

In practice, one needs a Hartree-Fock-Bogoliubov (HFB) code that can be converted into a QRPA code. The FAM is advantageous over the standard procedure because the computer code can be constructed by a simplified procedure, and moreover, all the terms of the Hamiltonian present in the "parent" code are passed to the QRPA code. The FAM allows for the use of the subroutines that are already present in the HFB code to calculate the residual fields in the frequency representation with a numerical derivation.

For trial, we modified the HFBRAD code[3]; this code solves the HFB equations for even-even nuclei in the coordinate space using Skyrme interactions in the ph channel. The time-odd terms of the Skyrme functional are zero in all these cases (hence they are not implemented in the code). However, they have a non-zero effect in the calculation of the excitation of the system. The resulting QRPA code is not completely self-consistent; however, the general behavior of the strength function is reproduced. We are currently implementing the time-odd terms in the QRPA code.

References

1) T. Nakatsukasa, T. Inakura and K. Yabana: Phys. Rev. C 76, 024318 (2007)
2) P. Ring and P. Shuck: *The Nuclear Many Body Problem*, Springer-Verlag, Berlin (1980)
3) K. Bennaceur and J. Dobaczewski: Comp. Phys. Comm. Vol 168(2), 96 (2005)

Fast computation of the Hamiltonian kernel for the Monte Carlo shell model

Y. Utsuno,[*1] N. Shimizu,[*2] T. Otsuka,[*2*3*4] and T. Abe,[*2]

[Nuclear structure, shell model, computational physics]

The Monte Carlo shell model (MCSM)[1)] is a powerful method for performing a shell-model calculation which is not feasible by the conventional diagonalization method because of huge dimensionality of the Hamiltonian. In order to carry out an MCSM calculation on state-of-the-art parallel computers, we are developing a new MCSM code[2)] that is equipped with some novel features such as the extrapolation method for precisely estimating the eigenvalue of the Hamiltonian in the MCSM framework[3)]. Below we report another advancement of the new MCSM code which enables much faster computation than the former MCSM code that has been used in many applications[1)]. The work was carried out in part as a RIKEN-CNS collaboration project on large-scale nuclear structure calculations.

In the MCSM calculation, most of the computation time is devoted to the Hamiltonian kernel given by $\langle V\rangle = \sum_{l_1l_2l_3l_4} \rho_{l_3l_1}\bar{v}_{l_1l_2l_3l_4}\rho_{l_4l_2}$, where $\bar{v}_{l_1l_2l_3l_4} = \langle l_1l_2|V|l_3l_4\rangle$ and ρ is the density matrix[4)]. It is not efficient to directly execute this formula because many of the matrix elements $\bar{v}_{l_1l_2l_3l_4}$ vanish owing to the symmetry of the Hamiltonian. To avoid the operation of the vanishing matrix element, the former MCSM code adopted the so-called list-vector method. In this numerical method, a set of (l_1, l_2, l_3, l_4) with non-vanishing $\bar{v}_{l_1l_2l_3l_4}$ is stored in memory and the summation over l_1 to l_4 takes place in the set only.

We find another method for efficient computing. The symmetry of the Hamiltonian requires that $J_z(l_1) + J_z(l_2)$ should be equal to $J_z(l_3) + J_z(l_4)$ to have non-vanishing $\bar{v}_{l_1l_2l_3l_4}$, equivalent with $J_z(l_3) - J_z(l_1) = -(J_z(l_4) - J_z(l_2))$, where $J_z(l)$ is the z component of the angular momentum of the orbit l. This imposes restriction on the indexes (l_1, l_2, l_3, l_4) to be summed over. In addition, by mapping the set (l_1, l_3) onto a one-dimensional index l_{31}, the expression of $\langle V\rangle$ becomes a sum of $(\text{vector})^{\mathrm{T}}\times(\text{matrix})\times(\text{vector})$, where most of the matrix elements are non vanishing. This is called the matrix method.

In the MCSM, since a number of Slater determinants are superposed, similar calculations with different density matrices should be done at the same time, keeping $\bar{v}_{l_1l_2l_3l_4}$ fixed: to be clearer, the $(\text{matrix})\times(\text{vector})$ operations are now written as $Av_1, Av_2, Av_3, \ldots$, where A is the matrix commonly used and v's are different vectors. By binding those vectors into a matrix, it is equivalent with a product of matrices AU, where $U = (v_1, v_2, v_3, \ldots)$. This is called the matrix method with binding vector.

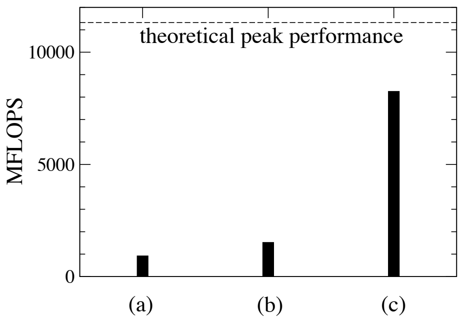

Fig. 1. Performance of computing the Hamiltonian kernel compared among different numerical methods: (a) list-vector method, (b) matrix method, and (c) matrix method with binding vector. See the text for details of the methods. The number of the binding of vectors is 100. The performance is measured on the Intel Xeon E5440 processor and the code is compiled by the Intel Fortran Compiler version 11 and the Intel Math Kernel Library version 10 for matrix calculation.

Figure 1 shows computational performance compared among the numerical methods presented above. It is demonstrated that much higher efficiency, i.e., $\sim 70\%$ of the theoretical peak performance on a recent processor, is achieved by the matrix method with binding vector. This is because the product of matrices needs much less memory access per floating-point operation than the product of a matrix and a vector. Furthermore, numerical libraries highly optimized for the linear algebra are available such as the Intel Math Kernel Library.

References

1) For a review, T. Otsuka, M. Honma, T. Mizusaki, N. Shimizu and Y. Utsuno: Prog. Part. Nucl. Phys. **47**, 319 (2001).
2) N. Shimizu, Y. Utsuno, T. Abe, and T. Otsuka: RIKEN Accel. Prog. Rep. **43**, 46, (2010).
3) N. Shimizu, Y. Utsuno, T. Mizusaki, T. Otsuka, T. Abe, and M. Honma: Phys. Rev. C **82**, 061305(R) (2010).
4) For instance, P. Ring and P. Schuck, *The Nuclear Many-Body Problem* (Springer, New York, 1980).

*1 Advanced Science Research Center, Japan Atomic Energy Agency
*2 Department of Physics, University of Tokyo
*3 Center for Nuclear Study, University of Tokyo
*4 National Superconducting Cyclotron Laboratory, Michigan State University

Shell-model description of N=44 pfg-shell nuclei

M. Honma,[*1] T. Otsuka,[*2,*3] T. Mizusaki,[*4] and M. Hjorth-Jensen[*5]

[NUCLEAR STRUCTURE, shell model]

It has long been a challenging problem for nuclear structure theory to understand two fundamental aspects of nuclear dynamics, the single-particle motion and the collective motion, within a unified framework. Large-scale shell-model calculation can be a possible way to approach this problem. Owing to innovative advances in computer technology as well as developments of novel methods for numerical calculations, the scope of the shell-model calculation is rapidly extending far beyond the magic nuclei, where the collective feature becomes significant.

Recently, we have proposed an effective interaction JUN45 for the shell-model description of nuclei with masses A=56-100 in the model space consisting of single-particle orbits $p_{3/2}$, $f_{5/2}$, $p_{1/2}$ and $g_{9/2}$.[1)] Starting from a microscopic interaction[2)] derived from the Bonn-C nucleon-nucleon potential, we have modified 45 well-determined linear combinations of single-particle energies and two-body matrix elements by fitting to 400 experimental energy data taken from 87 nuclei in this mass region. We have tested this interaction extensively and found it successful for nuclei with $N = 50$ magic number and also for less-neutron cases with $N \geq 45$.

In is expected that, as N decreases from 50 (the number of holes increases on top of the N=50 core), the collectivity gradually develops especially near the middle of the shell with $Z \sim 40$. In order to investigate the validity of the present model space and the effective interaction for such cases, we have carried out shell-model calculations for $N = 44$ isotones. The calculated results for electromagnetic moments of low-lying states show reasonable agreement with available experimental data. In addition, the description of energy levels looks successful even for high-spin states.

As an example, Fig. 1 shows the energy levels of ^{80}Kr. One can find a remarkable correspondence between the experimental band structure[3)] and the shell-model results for both positive and negative parity bands. As for the 2^+_1 state, the calculated magnetic moment is $+0.64\mu_N$ which compares well with the experimental value $+0.76(10)\mu_N$.[4)] The quadrupole moment is not known experimentally. The calculated value $+27e\text{fm}^2$ indicates weak oblate deformation, which is consistent with the prediction based on the Hartree-Fock-Bogolyubov cranking model with a Woods-Saxon potential.[5)] The experimental data suggest the two-quasiparticle alignment for $J > 8$ in the ground-state band, which was interpreted as the alignment of neutrons.[3)] By the analysis of the shell-model wavefunction, we have found that the angular momentum gain around $J \sim 8$ is mainly due to the neutrons in the $g_{9/2}$ orbit.

*1 Center for Mathematical Sciences, University of Aizu
*2 Department of Physics, University of Tokyo
*3 Center for Nuclear Studies, University of Tokyo
*4 Institute of Natural Sciences, Senshu University
*5 Department of Physics and Center of Mathematics for Applications, University of Oslo

References

1) M. Honma *et al.*: Phys. Rev. C **80**, 064323 (2009).
2) M. Hjorth-Jensen *et al.*: Phys. Rep. **261**, 125 (1995).
3) J. Döring *et al.*: Phys. Rev. C **52**, 76 (1995).
4) Data extracted using the NNDC WorldWideWeb site from the ENSDF database.
5) W. Nazarewicz *et al.*: Nucl. Phys. **A435**, 397 (1985).
6) T. Mizusaki: RIKEN Accel. Prog. Rep. **33**, 14 (2000).

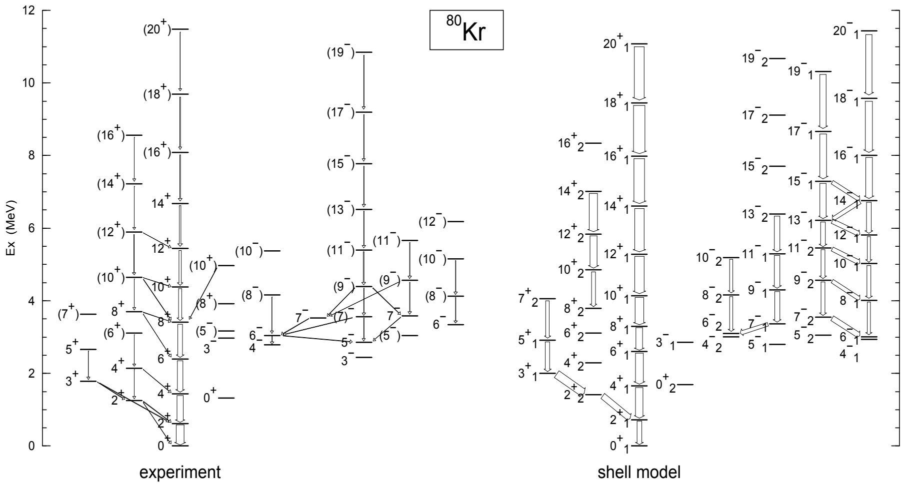

Fig. 1. Comparison of energy levels between the experimental data and the shell-model results for ^{80}Kr. The width of the arrow drawn in the experimental part corresponds to the relative γ-ray intensity, while it stands for the relative B(E2) values in the theoretical part. Experimental data are taken from Refs.[3,4)]. The shell-model results are obtained by using the efficient shell-model code MSHELL[6)].

Extrapolation methods for the low-lying states of nuclei in the *sd* shell and the *pf* shell†

J. J. Shen,*1,*2 Y. M. Zhao,*2 A. Arima,*2,*3 and N. Yoshinaga,*4

[Extrapolation method, Low-lying states, Shell model]

The study of low-lying states is one of the most important topics in nuclear physics, especially in nuclear structure theory. Theoretically, one of the most powerful method for studying low-lying states is the nuclear shell model. However, the main problem is that its model space becomes gigantic when we study heavy nuclei. In this report, we present the extrapolation methods[1,2] of predicting low-lying states.

We denote a matrix of the shell model Hamiltonian with dimension D and spin I by $H^{(I)}$, and its matrix elements by $H_{ij}^{(I)}$. After sorting diagonal matrix elements of the nuclear shell model Hamiltonian, We can rank the configurations on basis states of energies roughly and truncate artificially the matrix $H^{(I)}$ and obtain a series of Hamiltonian $h^{(I)}$ in subspaces with dimension d ($d < D$) where $h_{ij}^{(I)} = H_{ij}^{(I)}$ ($i, j = 1, 2, \cdots, d$). As can be seen in Fig. 1 (a) and (b), the overlaps between the exact ground state wave function (Φ) and the wave functions in the sub-space with and without the first-order perturbation ($\Psi^P(d)$ and $\Psi(d)$) converge very quickly and smoothly with d, thus demonstrating the usefulness of our extrapolation methods.

We can predict the energy levels of low-lying levels by the linear extrapolation method without perturbation[1] and the quadratic extrapolation method with second-order perturbation[2]. In Fig. 1 (c), we present the application of the both extrapolation methods for ^{46}Ti, in which we only diagonalize the Hamiltonian in the sub-space with $d < 0.15D$. Both the methods approximately reproduce the energy levels of the low-lying states. The extrapolation method can also be applied to evaluating the electromagnetic properties such as electric quadrupole moments, magnetic dipole moments and E2 transition rates. In Table 1, we present the application of the extrapolation method on evaluating electromagnetic properties of ^{46}Ti.

To summarize, We investigate the validation and application of extrapolation methods by studying the wave function after sorting the configurations. By truncating the shell model space efficiently after sorting the diagonal elements of the Hamiltonian, we can predict the properties (including energy levels, electric quadrupole moments, magnetic dipole moments and E2 transition rates) of the low-lying states by the linear extrapolation method without perturbation[1] and the quadratic extrapolation method with perturbation[2] through the nuclear shell model calculation.

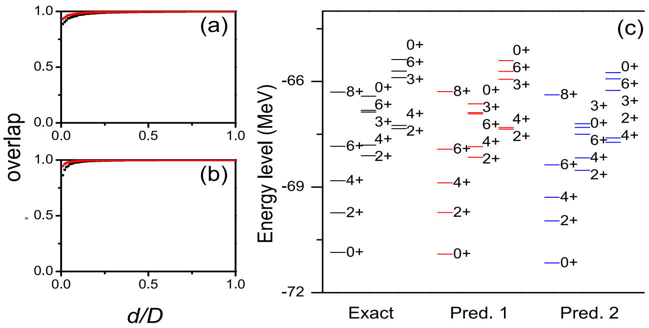

Fig. 1. The overlap $|\langle \Psi^P(d) \mid \Phi \rangle|$ (red points) and $|\langle \Psi(d) \mid \Phi \rangle|$ (black points) versus $\ln(D/d)$ for ^{46}Ti (GXPF1 interaction) with $I^\pi = 0^+$ (panels (a)) and $I^\pi = 2^+$ (panels (b)), respectively. Panels (c) show the energy levels (MeV) of ^{46}Ti evaluating by the diagonalization of $H^{(I)}$ (denoted by "Exact"), the linear extrapolation with perturbation (denoted by "Pred.1"), and the quadratic extrapolation without perturbation (denoted by "Pred.2"). In the predictions, we use up to 15 percents of the full space for each $H^{(I)}$, i.e., $d/D \leq 0.15$.

Table 1. Predicted E2 transition rates (e^2 fm^4), electric quadrupole moments Q (e fm^2), and magnetic dipole moments μ (in μ_N) of ^{46}Ti, in comparison with those calculated by the exact diagonalization (denoted by "Exact"). "Pred.1" and "Pred.2" are based on $\Psi^P(d)$ and $\Psi(d)$, respectively.

^{46}Ti	I^π	Exact	Pred.1	Pred.2
B(E2)	$2_1^+ \to 0_1^+$	62.36	61.01	66.10
Q	2_1^+	-8.90	-7.25	-8.84
μ	2_1^+	0.84	0.90	0.91

*1 Theoretical Nuclear Physics Laboratory, RIKEN Nishina Center, Wako 351-0198, Japan
*2 Department of Physics, Shanghai Jiao Tong University, Shanghai 200240, China
*3 Science Museum, Japan Science Foundation, 2-1 Kitanomaru-koen, Chiyoda-ku, Tokyo 102-0091, Japan
*4 Department of Physics, Saitama University, Saitama 338-8570, Japan

References
1) J. J. Shen, Y. M. Zhao and A. Arima, Phys. Rev. C **82**, 0143309 (2010); N. Yoshinaga and A. Arima, Phys. Rev. C **81**, 044316 (2010).
2) J. J. Shen, Y. M. Zhao, A. Arima and N. Yoshinaga, Phys. Rev. C**83**, 044322 (2011);

Shell model estimate of electric dipole moment in ^{129}Xe†

N. Yoshinaga*1 and K. Higashiyama*2

[Electric dipole moments, Nuclear Schiff moments]

The permanent electric dipole moment (EDM) of a particle or an atom provides us with important information on our fundamental understanding of nature concerning the simultaneous violation of parity (P) and time-reversal (T) invariance. The EDM of a neutral atom is mainly induced by the nuclear Schiff moment, since the electron EDM is very small and the nuclear EDM is shielded by outside electrons owing to the Schiff theorem[1)]. The Schiff moments were theoretically calculated in terms of various mean field approaches[2,3)], but no study has yet been made from the shell model point of view.

In this work, we calculate the nuclear Schiff moment and the EDM for ^{129}Xe arising from the intrinsic nucleon EDM in terms of the pair-truncated shell model. In this model, the collective nucleon pairs with angular momenta of zero and two are its basic ingredients. Systematic studies are carried out for the even-even and odd-mass nuclei in the mass $A \sim 130$ region in terms of the PTSM[4)]. The calculation reproduces well the energy levels and electromagnetic transitions.

The nuclear Schiff moment operator arising from the intrinsic nucleon EDM may be written as[5)]

$$\boldsymbol{S} = \frac{1}{6}\sum_{i=1}^{A} \boldsymbol{d}_i \left({r_i}^2 - \langle r^2 \rangle_{\mathrm{ch}} \right) + \frac{1}{5}\sum_{i=1}^{A} \left[\boldsymbol{r}_i \left(\boldsymbol{r}_i \cdot \boldsymbol{d}_i \right) - \boldsymbol{d}_i {r_i}^2/3 \right], \tag{1}$$

where $\langle r^2 \rangle_{\mathrm{ch}}$ is the mean squared radius of the nuclear charge distribution, $\boldsymbol{r}_i$ indicates ith nucleon position, and $\boldsymbol{d}_i$, the nucleon EDM operator, which is expressed in the non-relativistic approximation as

$$\boldsymbol{d}_i = \frac{1}{2}\left[\left(1+\tau_{iz}\right) d_p \boldsymbol{\sigma}_{ip} + \left(1-\tau_{iz}\right) d_n \boldsymbol{\sigma}_{in} \right]. \tag{2}$$

Here τ_{iz} represents the third component of isotopic operator, d_t is the intrinsic EDM for a proton ($t=p$) or a neutron ($t=n$), and $\boldsymbol{\sigma}_{it}$ represents the spin operator. Then the Schiff moment is calculated as

$$S = \langle \Phi(JJ\eta) | \hat{S}_z | \Phi(JJ\eta) \rangle = \langle \hat{S}_z \rangle, \tag{3}$$

where $|\Phi(JJ\eta)\rangle$ represents a PTSM wave function after diagonalization of the effective Hamiltonian. Here the third component of the Schiff moment operator $\hat{S}_z$ in Eq. (3) is expressed in the second quantized form. Using Eq. (1), the Schiff moment is expressed as

$$S = s_p d_p + s_n d_n, \tag{4}$$

with

$$s_t = \frac{1}{10}\left\langle \hat{\sigma}_{tz} \hat{r}_t^2 \right\rangle - \frac{1}{6}\left\langle r^2 \right\rangle_{\mathrm{ch}} \left\langle \hat{\sigma}_{tz} \right\rangle + \frac{1}{5}\left\langle \hat{z}_t \left(\hat{\boldsymbol{r}}_t \cdot \hat{\boldsymbol{\sigma}}_t \right) \right\rangle, \tag{5}$$

where $\hat{z}_t$ represents the third coordinate component of a proton or a neutron.

The calculated factors s_t for the nuclear Schiff moment of the $1/2_1^+$ state (the ground state) in ^{129}Xe are

$$s_p = +0.0061 \text{ fm}^2, \tag{6}$$

$$s_n = -0.3169 \text{ fm}^2. \tag{7}$$

The factor s_n for neutron is approximately 50 times as large as the factor s_p for proton. Thus the intrinsic EDM for a neutron d_n is dominant in the nuclear Schiff moment. In the previous study[5)], the factors $s_p = 0.20 \pm 0.02$ fm^2 and $s_n = 1.895 \pm 0.035$ fm^2 were reported for the nuclear Schiff moment of ^{199}Hg. This factor s_n is larger than our result for ^{129}Xe in magnitude.

According to V. A. Dzuba et al.[6)] the EDM for neutral ^{129}Xe atom is expressed in terms of the nuclear Schiff moment S as,

$$d\left(^{129}\mathrm{Xe}\right) = 0.38 \times 10^{-17} \left(\frac{S}{e\,\mathrm{fm}^3} \right) e\,\mathrm{cm}. \tag{8}$$

Using the upper limit for the experimental neutron EDM, $|d_n| < 2.9 \times 10^{-26}\ e\,\mathrm{cm}$[7)], and Eqs. (4) and (8), we obtain the upper limit for the EDM for neutral ^{129}Xe atom:

$$\left| d\left(^{129}\mathrm{Xe}\right) \right| < 3.5 \times 10^{-31}\ e\,\mathrm{cm}. \tag{9}$$

Note that in the present study we have estimated the upper limit arising from the nucleon intrinsic EDM. In order to obtain a definite value, we need to take into account the contribution arising from the two-body interaction which breaks P and T invariance.

References

1) L. I. Schiff: Phys. Rev. **132**, 2194 (1963).
2) J. Engel et al.: Phys. Rev. C **68**, 025501 (2003).
3) J. H. de Jesus and J. Engel: Phys. Rev. C **72**, 045503 (2005).
4) N. Yoshinaga and K. Higashiyama: Phys. Rev. C **69**, 054309 (2004).
5) V. F. Dmitriev and R. A. Sen'kov: Phys. Rev. Lett. **91**, 212303 (2003).
6) V. A. Dzuba et al.: Phys. Rev. A **66**, 012111 (2002).
7) C. A. Baker et al.: Phys. Rev. Lett. **97**, 131801 (2006).

† Condensed from an article in Prog. Theor. Phys. **124**, 1115 (2010)
*1 Department of Physics, Saitama University
*2 Department of Physics, Chiba Institute of Technology

Band structure of doubly-odd nuclei around mass 130

K. Higashiyama*[1] and N. Yoshinaga*[2]

[Chopsticks configurations; Pair-truncated shell model; ^{134}La calculated levels]

The study of $\Delta I = 1$ doublet bands in doubly odd nuclei has recently been one of the most interesting subjects in nuclear physics. A number of experimental data have been accumulated in the $A \sim 130$ region, which show nearly degenerate doublet bands built on the $\nu h_{11/2} \otimes \pi h_{11/2}$ configuration[1,2]. From the theoretical side, these bands were extensively investigated in terms of the pair-truncated shell model (PTSM)[3]. This approach successfully describes the properties of the doublet bands. By analyzing the PTSM results, it turned out that the level scheme of these bands arises from different angular-momentum configurations of the unpaired neutron and the unpaired proton in the $0h_{11/2}$ orbitals, chopsticks configurations, weakly coupled with the quadrupole collective excitations of the even-even part of the nucleus. The theoretical results, however, failed to reproduce the relative position of the positive parity and negative parity states.

In order to systematically describe the energy levels and electromagnetic properties for all the even-even, odd-mass and doubly-odd nuclei, we have recently performed an extensive study to find the best effective interaction around mass 130[4]. In this study, the single particle energies and the two-body interaction strengths are changed linearly with the number of the valence particles to give an improved fitting for the odd-mass nuclei. The calculated results are in excellent agreement with the experimental energy levels and electromagnetic properties of the even-even, odd-mass and doubly-odd nuclei.

In Fig. 1, the experimental energy spectrum based on the $\nu h_{11/2} \otimes \pi h_{11/2}$ configuration is compared with

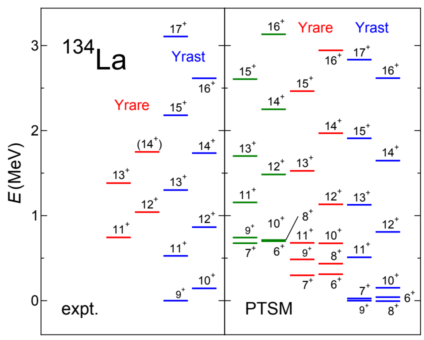

Fig. 1. Comparison of the experimental energy spectrum (expt.) with the PTSM result (PTSM) for ^{134}La.

*1 Department of Physics, Chiba Institute of Technology
*2 Department of Physics, Saitama University

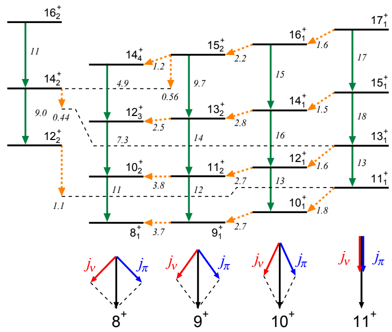

Fig. 2. Partial level scheme of ^{134}La suggested by the PTSM calculation. The narrow arrows indicate $E2$ transitions, and the dotted narrow arrows indicate $M1$ transitions. The numerals on the right side of the $E2$ transitions denote the $B(E2)$ values (in 10^{-2} e^{2}b^2), and those beneath the $M1$ transitions denote the $B(M1)$ values (in μ_N^2).

the PTSM calculation for ^{134}La. The energy levels for the yrast states are almost perfectly reproduced, except that in our calculation the 8_1^+ state is predicted in between the 9_1^+ and 10_1^+ states. Concerning the yrare states, our theoretical result provides a successful description of the energy levels.

The partial level scheme of ^{134}La constructed from the theoretical results of the $M1$ and $E2$ transition rates is shown in Fig. 2. Our model gives five $\Delta I = 2$ $E2$ bands. The states within four $\Delta I = 2$ $E2$ bands with the bandhead states of 8_1^+, 9_1^+, 10_1^+ and 11_1^+ are connected by the strong $E2$ transitions to the same members of the $\Delta I = 2$ $E2$ bands, and by the strong $M1$ transitions to the states in the neighboring $\Delta I = 2$ $E2$ bands. Schematic illustrations of the chopsticks configurations are presented below each $\Delta I = 2$ $E2$ band in Fig. 2. Since quadrupole collectivity plays an important role in describing the $\Delta I = 2$ $E2$ bands, we conclude that the level scheme of ^{134}La arises from the chopsticks configurations of the unpaired nucleons in the $0h_{11/2}$ orbitals, weakly coupled with the quadrupole collective excitations of the even-even part of the nucleus.

References

1) K. Starosta et al.: Phys. Rev. Lett. **86**, 971 (2001).
2) A. A. Hecht et al.: Phys. Rev. C **63**, 051302 (2001).
3) K. Higashiyama, N. Yoshinaga, and K. Tanabe: Phys. Rev. C **72**, 024315 (2005).
4) K. Higashiyama and N. Yoshinaga: Phys. Rev. C **83**, 034321 (2011).

Suppression of the interband transitions among triaxial, strongly deformed bands in even nuclei†

K. Tanabe*1,*2 and K. Sugawara-Tanabe*1,*3

[Nuclear structure, TSD bands, Top-on-top model, Electromagnetic transition rates]

We have developed the "top-on-top model" based on the generic particle-rotor model to describe a nuclear system with one nucleon in a high-j orbital coupled to a triaxially deformed core.[1–3] An algebraic solution[1] is obtained for this model by introducing two kinds of bosons for total angular momentum $\vec{I}$ and single-particle angular momentum $\vec{j}$ by means of the Holstein-Primakoff (HP) transformation.[4] An excellent approximation is obtained by taking into account the next-to-leading order contributions in the HP boson expansion consistent with the D_2 invariance of the system.[1] Such a solution deals with the Coriolis coupling between the single-particle and the total angular momenta, which is not included in the wobbling model.[5] Two kinds of quasiboson numbers, n_α and n_β, that describe the wobbling motion of the rotor and the precession of the single-particle angular momentum, are available for the classification of rotational bands and the derivation of selection rules for the interband and intraband electromagnetic transitions.[1,2]

In the case of triaxial, strongly deformed (TSD) rotational bands in the odd-A nuclei ^{163,165,167}Lu and ^{167}Ta, the observed TSD band levels can be well reproduced by considering common rigid-body moments of inertia and the assumption that one valence proton occupies the $i_{13/2}$ orbital.[1] The same calculation effectively reproduces the experimental ratios between the in-band and out-of-band electromagnetic transitions among the TSD1 and TSD2 bands, $B(E2)_{\rm out}/B(E2)_{\rm in}$ and $B(M1)_{\rm out}/B(E2)_{\rm in}$ in ^{163}Lu[2] and ^{167}Ta.[3]

As a natural extension, we consider the "tops-on-top model" and the same method to describe even-mass nuclei with two valence nucleons occupying two orbitals j_1 and j_2. Our Hamiltonian is given by

$$H = H_{\rm rot} + H_{\rm sp}(\vec{j}_1) + H_{\rm sp}(\vec{j}_2)\,;$$
$$H_{\rm rot} = \sum_{k=x,y,z} A_k(I_k - j_{1k} - j_{2k})^2,$$
$$H_{\rm sp}(\vec{j}) = \frac{V_j}{j(j+1)}\left[\cos\gamma(3j_z^2 - \vec{j}^2) - \sqrt{3}\sin\gamma(j_x^2 - j_y^2)\right],$$

where $A_k = 1/(2\mathcal{J}_k)$ and $\vec{j}$ stands for either $\vec{j}_1$ or $\vec{j}_2$. We introduce three kinds of HP boson representations for $\vec{I}$, $\vec{j}_1$, and $\vec{j}_2$, and we diagonalize the bosonized Hamiltonian by means of boson unitary transformation. For the case of pure rotor (i.e., $V_1 = V_2 = 0$), the eigenvalue of $H_{\rm rot}$ turns out to be

$$E_{\rm rot}(I, n_\alpha, n_\beta, n_\gamma) = A_x R(R+1) - \frac{p+q}{2}n_\alpha^2 + \left(2R\sqrt{pq} + \sqrt{pq} - \frac{p+q}{2}\right)\left(n_\alpha + \frac{1}{2}\right),$$

with $R \equiv I - j_1 - j_2 + n_\beta + n_\gamma$. In the symmetric limit $A_y = A_z$, $E_{\rm rot}$ coincides with the well-known expression $A_z R(R+1) + (A_x - A_z)(R - n_\alpha)^2$. The quasiboson numbers n_β and n_γ describe the precessions of $\vec{j}_1$ and $\vec{j}_2$, and n_α describes the wobbling of the rotor. In the same approximation, the B values for the most dominant transitions from TSD2 with quantum numbers $(n_\alpha, n_\beta, n_\gamma) = (1,0,0)$ to TSD2 with $(0,0,0)$ become

$$B(E2; I, 100 \to I-1, 000) \sim \frac{3}{I}\left(\frac{I - j_1 - j_2}{I}\right)^3 \frac{1}{\eta_+^4},$$
$$B(M1; I, 100 \to I-1, 000) \sim \frac{1}{I}\left(\frac{I - j_1 - j_2}{I}\right)^3 \frac{1}{\eta_+^4}.$$

These quantities gain a factor $[(I - j_1 - j_2)/I]^3$, which is much less than $[(I-j)/I]^3$ for the odd-A case.[2,3] The value of $j_1 + j_2$ is almost 14 owing to the alignment of two particles in the $i_{13/2}$ and $j_{15/2}$ orbitals for an even-A nucleus, and we get $[(I - j_1 - j_2)/I]^3 \sim 0.011$ (even A), while the corresponding ratio for an odd-A nucleus is 0.27 at $I = 37/2$ and $j = 13/2$ (odd A). Thus, we get value of about 0.04 for the relative ratio B(even-A)/B(odd-A), which predicts the suppression of the interband transitions from the TSD2 to the TSD1 band levels in the even-A nucleus. In the case of ^{168}Hf,[6] $j_1 + j_2$ seems to be much larger, e.g., 23, which results in a smaller value of $[(I - j_1 - j_2)/I]^3$; this smaller value makes the observation of the transition from the other TSD partner in the even-A nucleus more difficult.

References

1) K. Tanabe and K. Sugawara-Tanabe: Phys. Rev. C **73**, 034305 (2006); **75**, 059903(E) (2007).
2) K. Tanabe and K. Sugawara-Tanabe: Phys. Rev. C **77**, 064318 (2008).
3) K. Sugawara-Tanabe and K. Tanabe: Phys. Rev. C **82**, 051303(R) (2010).
4) K. Tanabe and K. Sugawara-Tanabe: Phys. Lett. B **34**, 575 (1971).
5) A. Bohr and B. R. Mottelson: *Nuclear Structure*, (Benjamin, Reading, MA, 1975), **II**, Chap. 4.
6) R. B. Yadav *et al.*: Phys. Rev. C **78**, 044316 (2008).

† Condensed from the article in Phys. Rev. C **82**, 051303(R) (2010)

*1 Theoretical Nuclear Physics Laboratory, RIKEN Nishina Center, Wako, Saitama 351-0198
*2 Department of Physics, Saitama University, Sakura-Ku, Saitama 338-8570
*3 Otsuma Women's University, Tama, Tokyo 206-8540

GCM amplitudes in t-band for ^{182}Os

Y. Hashimoto *1 and T. Horibata *2

[HFB, GCM, TAR]

When the shape of a nuclear mean field changes from one with axial symmetry to one without axial symmetry, we expect a general type of nuclear rotational motion in which the rotational axis is not parallel to the principal axis (PA), corresponding to the largest moment of inertia; rather, the rotational axis wobbles around the PA. Such type of collective motion is called wobbling motion.[1,2]

From a theoretical point of view, a more general type of rotation in which the rotational axis is located away from any of the principal axes is expected[3,4]. This type of rotation is called tilted-axis rotation (TAR).[5] The three-dimensional (3D) cranking model plays a central role in the study of the wobbling motion and TAR.

The experimental data that have been accumulated support the theoretical assumptions about the existence of general types of nuclear rotational motion.[6,7]

In recent years, we have studied the wobbling motion and TAR with the aim of understanding the microscopic mechanism behind the complicated general rotational motion. We performed three-dimensional cranked Hartree-Fock-Bogoliubov (3D-CHFB) calculations for ^{182}Os. For our calculations, we introduced the tilt angle ψ that was measured from the x-axis, which was perpendicular to the symmetry axis (z-axis) placed along the prime meridian. The wave function $|\Phi(\psi)\rangle$ that includes ψ was obtained by solving the 3D-CHFB equation with the pairing-plus-quadrupole Hamiltonian $\hat{H}$.

We calculated the signature splitting in the t-band by the generator coordinate method (GCM).[8,9] Since the magnitude of the energy splitting was of the order of a few hundred keV, the solution of the GCM equation was sensitive to the numerical conditions, e.g., choice of the basis states and symmetry conservation.

We paid attention to the symmetry property of the GCM solutions with respect to the inversion of the axis of ψ. In our method for calculating the HFB states along the axis of ψ, the HFB solution for the principal-axis rotation (PAR) is taken to be the initial state and the constraint angular-momentum vector is tilted toward the north as well as the south direction along the meridian of angular-momentum space. Consequently, care must be taken to prevent any numerical error in the tilted HFB solutions.

The signature symmetry of the tilted HFB solutions with respect to the inversion of the axis of ψ may break, and the asymmetry property may appear in the GCM amplitudes. This aberration reduces the numerical accuracy in the calculation of energy splitting of the pair of symmetric and anti-symmetric GCM solutions.

For avoiding the numerical error that leads to asymmetry in the GCM amplitudes, we introduce a new set of basis states by combining a pair of states in the northern and southern hemispheres of angular-momentum space.

In Fig. 1, we show some examples of the GCM solutions with even and odd symmetries for $J = 24\ \hbar$. It can be observed that the strengths of the amplitudes of the solutions with low excitation energies are concentrated around the TAR state with $\psi = 18°$. There is left-right symmetry in the GCM amplitudes, except in the case of one solution (the one with a node in the lowest part of Fig. 1). The numerical refinement of the GCM calculations is now in progress, and the problem will be solved soon.

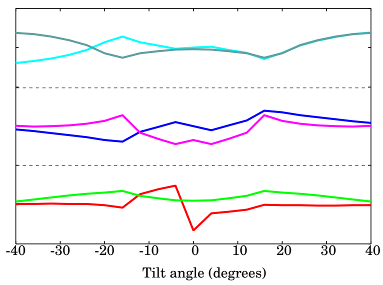

Fig. 1. GCM amplitudes with respect to the tilt angle. The symmetric- and asymmetric-pair solutions are plotted with a common zero axis.

*1 Graduate School of Pure and Applied Sciences, University of Tsukuba, Tsukuba 305-8571, Japan
*2 Faculty of Software and Information Technology, Aomori University, Aomori 030-0943, Japan

References

1) A. Bohr and B. R. Mottelson: *Nuclear Structure*, Vol.II (Benjamin, Reading, MA, 1975).
2) S. Frauendorf: Rev. Mod. Phys. **73**, 463-514 (2001).
3) A. K. Kerman and N. Onishi: Nucl. Phys. A**361**, 179-191 (1981).
4) N. Onishi: Nucl. Phys. A**456**, 279-297 (1986).
5) T. Horibata and N. Onishi: Nucl. Phys. A**596**, 251-284 (1996).
6) P. M. Walker et al.: Phys. Lett. B**309**, 17-22 (1993).
7) S. W. Ødegård et al.: Phys. Rev. Lett. **86**, 5866-5869 (2001).
8) T. Horibata, M. Oi, N. Onishi, and A. Ansari: Nucl. Phys. A**646**, 277-295 (1999); A**651**, 435-436 (1999).
9) Y. Hashimoto and T. Horibata: Eur. Phys. J. A**42**, 571-575 (2009).

Dynamical fusion threshold in heavy-ion reactions

L. Guo and T. Nakatsukasa

[time-dependent Hartree-Fock, fusion reaction, interaction barrier]

Studies of the dynamical fusion threshold in heavy-ion reactions have attracted significant interest in recent years, especially with the experimental progress in the synthesis of superheavy elements and exotic nuclei. Both the macroscopic model[1)] and simplified microscopic model[2)] indicate the need for an extra push over the Coulomb barrier in fusion reactions. The extra push is provided by an additional bombarding energy over the barrier height in order to achieve a fused system. For the heavy nuclei, the repulsive potential energy becomes so large that the system has to overcome, in order to achieve fusion, the saddle point associated with the fission barrier of a compound nucleus. The energy difference between the interaction barrier and saddle point is known as extra-push energy.

Our study aims at investigating whether the microscopic time-dependent Hartree-Fock (TDHF) calculation can quantitatively reproduce the extra-push energy required for the fusion reaction, give the criterion for the combined mass of the projectile and target above which the extra push is needed, and indicate the magnitude of the extra-push energy. We carry out the investigation for heavy-ion fusion reactions by using TDHF theory with the full Skyrme force and without any geometric symmetry restrictions. The dynamical evolution of a nuclear system, denoted by the TDHF equation

$$i\hbar\frac{d\hat{\rho}}{dt} = [\hat{h}, \hat{\rho}], \tag{1}$$

is expressed by the time evolution of one-body density.

We solve the TDHF equation in three-dimensional coordinate space and calculate the low-energy fusion threshold, which is the lowest bombarding energy required to achieve fusion, for the systems ^{16}O+^{16}O, ^{16}O+^{40}Ca, ^{16}O+^{48}Ca, ^{40}Ca+^{40}Ca, ^{40}Ca+^{48}Ca, ^{48}Ca+^{48}Ca, ^{16}O+^{208}Pb, ^{40}Ca+^{90}Zr, and ^{100}Sn+^{132}Sn. The obtained fusion threshold is shown by blue line passing through the filled squares in Fig. 1. Here, we use the effective fissility $(Z^2/A)_{\rm eff}$, defined as[1)]

$$(Z^2/A)_{\rm eff} \equiv 4Z_1Z_2/A_1^{1/3}A_2^{1/3}(A_1^{1/3}+A_2^{1/3}), \tag{2}$$

to represent the combined mass of the projectile and target. In the above equation, Z_1, Z_2, A_1, and A_2 are the atomic and mass numbers of the colliding nuclei.

A good estimation of the interaction potential between the colliding nuclei can be obtained within the energy density functional (EDF) theory by using the frozen density (FD) approximation[3)], assuming that the densities of the projectile and target remain constant and equal to their respective ground state densities ρ_p and ρ_T. By using the FD-EDF method, the interaction potential can be obtained as

$$V_{FD}(R) = \mathcal{E}[\hat{\rho}_{P+T}](R) - \mathcal{E}[\hat{\rho}_P] - \mathcal{E}[\hat{\rho}_T], \tag{3}$$

in terms of the energy functional $\mathcal{E}$. The total density is given as $\hat{\rho}_{P+T}(R) = \hat{\rho}_p + \hat{\rho}_T$, and it is the sum of the projectile and target densities at a given relative distance R.

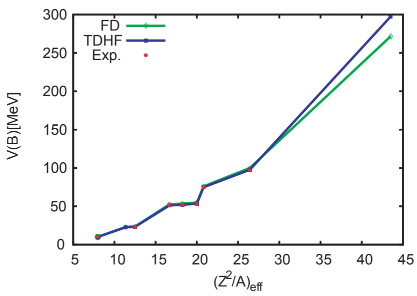

Fig. 1. Low-energy fusion threshold obtained with the TDHF calculation (bule line), interaction barrier determined with the FD-EDF method (green line), and the experimental Coulomb barrier (red points).

Fig. 1 shows the interaction barrier determined with the Skyrme FD-EDF method and the available experimental Coulomb barrier[4)]. It is seen that for light systems, e.g., for an effective fissility $(Z^2/A)_{\rm eff}$ smaller than 30, the TDHF fusion threshold, interaction barrier determined with the FD-EDF method, and the experimental Coulomb barrier show a quite good agreement, which implies extra push is not needed for light systems. However for a heavy system, the TDHF fusion threshhold is higher than the interaction barrier determined with the FD-EDF method. One may conclude that for heavy systems, an extra-push energy above the interaction barrier is needed in order to achieve fusion. In order to confidently answer the issues on the fusion dynamics considered in the present investigation, more systematic calculations for heavy systems are currently under way.

References

1) W. J. Swiatecki: Nucl. Phys. **A 376**, 275 (1982).
2) J. A. Maruhn, K. T. R. Davies, and M. R. Strayer: Phys. Rev. **C 31**, 1289 (1985).
3) K. Washiyama and D. Lacroix: Phys. Rev. **C 78**, 024610 (2008).
4) M. Dasgupta, D. J. Hinde et al.: Annu. Rev. Nucl. Part. Sci. **48**, 401 (1998).

Total reaction cross sections between heavy nuclei

A. Kohama, K. Iida,[*1] K. Oyamatsu,[*2] H. Iwase,[*3] and K. Niita[*4]

[Nuclear reaction, reaction cross section, nuclear radius]

The total reaction cross section (σ_R) of nuclei is one of the most fundamental observables that characterize the geometrical size of nuclei. It is also important in numerical simulations in the fields of accelerator technology, radiotherapy, and space radiation, as well as in many other fields that are related to particle and heavy-ion transport phenomena, because, in the codes for such simulations, one needs to estimate reaction rates systematically by using σ_R for various combinations of colliding particles over a wide energy range. There are several semiempirical parametrizations of σ_R used in the codes. However, since they are too empirical in that they basically express σ_R in powers of $A^{1/3}$ with energy-dependent parameters determined in such a way so as to reproduce available data, the application of such parametrizations to unmeasured processes is accompanied by ambiguities. Thus, the aim of this study is to illustrate such ambiguities and to seek a better way to obtain systematic estimates of σ_R.

In order to systematically estimate σ_R for nucleus-nucleus reactions, one may use the black sphere (BS) cross-section formula.[1)] It was originally constructed by Iida *et al.*[1)] for σ_R of proton-nucleus reactions in the framework of the black-sphere approximation of nuclei, in which a nucleus is viewed as a "black" sphere of radius "a". In this formula, the geometrical cross section, πa^2, is expressed as a function of the mass and neutron excess of the target nucleus and of the proton incident energy, T_p, in a way free from any adjustable T_p-dependent parameter. We deduce the dependence of σ_R on T_p from a simple argument involving the nuclear "optical" depth for incident protons. This formula can be easily extended to nucleus-nucleus reactions by using $\pi(a_P+a_T)^2$, where a_P (a_T) is the black-sphere radius of a projectile (target),[1,2)] and has been shown to reproduce the empirical data for reactions involving light nuclei remarkably well for energies above 100 MeV/nucleon.[1,2)] Note that no Coulomb effect is included. Due to its suitability for systematics, the present formula is being incorporated into the Particle and Heavy Ion Transport code System (PHITS).[3)]

Here, we consider the reactions between heavy nuclei, where the Coulomb dissociation may contribute. For comparison, we adopt Tripathi's formula,[4)] which is one of the most popular semiempirical parametrizations in the codes, because it can reproduce a variety of available data. Note that the Coulomb effect is included in this formula via the distortion of the classical trajectory, which is effective only at very low energies. For reactions involving heavy nuclei, we identify the mass-changing cross section $\sigma_{m.c.}$ with σ_R, which is expected to be valid with a few percent accuracy.[2)] While the value of Tripathi's formula agrees with the empirical values of $\sigma_{m.c.}$ for ^{56}Fe+^{208}Pb, it deviates from those for ^{56}Fe+^{238}U (Fig. 1). On the other hand, the value of our formula, which deviates from the empirical $\sigma_{m.c.}$ for both reactions, agrees with $\sigma_{m.c.}-\sigma_{\rm CD}$, where $\sigma_{\rm CD}$ is the theoretically deduced contribution of the Coulomb dissociation.[5)] These facts suggest that Tripathi's formula may contain terms leading to different energy and/or mass-number dependence from the empirical behavior and that we can expect $\sigma_R(\simeq \sigma_{m.c.}) \simeq \sigma_{\rm BS}+\sigma_{\rm CD}$ to be valid. Further research to pin them down is now in progress.

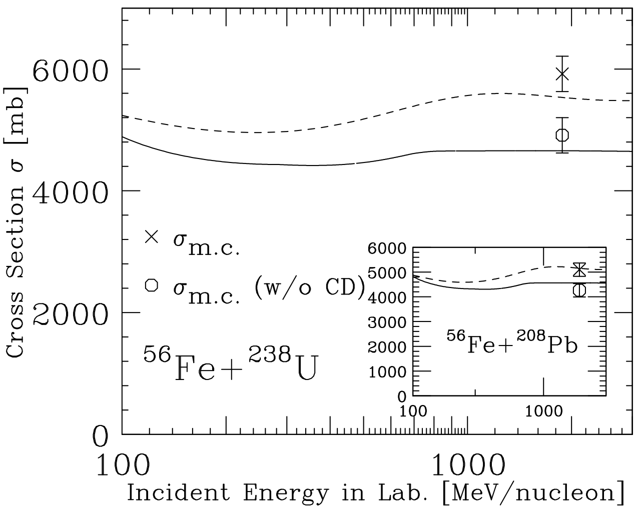

Fig. 1. Comparison of the BS cross-section formula (solid curve) with Tripathi's formula (dashed curve) for ^{56}Fe+^{238}U (^{208}Pb) reactions as a function of the incident kinetic energy. For reference, we plot the measured value of $\sigma_{m.c.}$ and $\sigma_{m.c.}$ with the Coulomb dissociation (CD) contribution[5)] subtracted out.

References
1) K. Iida *et al.*: J. Phys. Soc. Japan **76**, 044201 (2007).
2) A. Kohama *et al.*: Phys. Rev. C **78**, 061601(R) (2008).
3) K. Niita *et al.*: PHITS: Parti. and Heavy Ion Transport code Sys., Ver. 2.23, JAEA-Data/Code 2010-022 (2010).
4) R. K. Tripathi *et al.*: Nucl. Instr. Meth. B **117**, 347 (1997).
5) G. D. Westfall *et al.*: Phys. Rev. C **19**, 1309 (1979).

[*1] Department of Natural Science, Kochi University
[*2] Faculty of Human Informatics, Aichi Shukutoku University
[*3] Radiation Science, KEK
[*4] Research Organization for Informa. Science & Technol.

Thermodynamic properties of hot nuclei within the self-consistent quasiparticle random-phase approximation*

N. Quang Hung, N. Dinh Dang

NUCLEAR STRUCTURE, pairing, superfluid-normal phase transition, BCS theory, self-consistent quasiparticle RPA, Lipkin-Nogami method, canonical ensemble, microcanonical ensemble, exact solution of pairing problem, level density, quantal and thermal fluctuations

Thermodynamic properties of any systems can be studied by using three principal statistical ensembles, namely the grand canonical ensemble (GCE), canonical ensemble (CE) and microcanonical ensemble (MCE). Because the number of nucleons in a hot isolated nucleus is conserved, the use of the GCE in nuclear systems is a good approximation so long as the effect caused by particle-number fluctuations is negligible. From the experimental point of view, the CE and MCE are usually used to extract various thermodynamic quantities of nuclear systems. However, most of present theoretical approaches, derived within the GCE, cannot describe well these data.

Recently we have proposed a method, which has allowed us to construct theoretical approaches within the CE and MCE to describe rather well thermodynamic properties of atomic nuclei[1)]. The proposed approaches have been derived by solving the BCS and self-consistent quasiparticle RPA (SCQRPA) equations with the Lipkin-Nogami (LN) particle-number projection for each total seniority (number of unpaired particles at zero temperature)[2)]. The obtained results are then embedded into the CE and MCE. Within the CE, the resulting approaches are called the CE-LNBCS and CE-LNSCQRPA, whereas they are called the MCE-LNBCS and MCE-LNSCQRPA within the MCE. The results obtained within these approaches are found in quite good agreement with not only the exact solutions of the doubly-folded equidistant multilevel model with monopole pairing interaction, but also the experimentally extracted data for ^{56}Fe isotope. The merit of these approaches reside in their simplicity and feasibility in the application even to heavy nuclei, where the exact solution is impracticable whereas the finite-temperature quantum Monte-Carlo method is time consuming. The present article applies the above-mentioned approaches to describe thermodynamic quantities of ^{94,96}Mo, ^{162}Dy and ^{172}Yb nuclei. A model Hamiltonian, which includes the single particle mean-field described by an axially-deformed Woods-Saxon potential and monopole pairing interaction with parameter G, is adopted. The single-particle energies span a space from the bottom ($1s$ level) to $N = 126$ closed shell. The results obtained show that the CE(MCE)-LNSCQRPA describes quite well the recent experimental level densities, entropies, and heat capacities[3,4)] [See Fig. 1, e.g.]. The better agreement between the predictions of our approaches and the results of Ref.[4)] gives a strong indication to the fact that, to construct an adequate partition function for a good description of thermodynamic quantities, the measured level density should be extended up to very high excitation energy $E^* \sim 180$ MeV or 200 MeV.

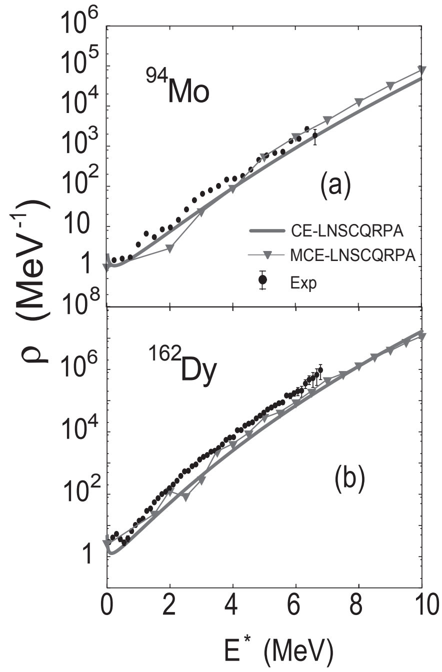

Fig. 1. Level densities as functions of E^* obtained within the CE-LNSCQRPA (solid line) and MCE-LNSCQRPA (triangles) versus the experimental data (circles with error bars) for ^{94}Mo (a) and ^{162}Dy (b).

* Condensed from Phys. Rev. C **81**, 034301 (2010).

References

1) N.Q. Hung and N.D. Dang, Phys. Rev. C **81**, 057302(BR) (2010).
2) N. Quang Hung and N. Dinh Dang, Phys. Rev. C **76**, 054302 (2007); Ibid **77** 029905(E); Ibid **77**, 064315 (2008).
3) E. Melby *et al.*, Phys. Rev. Lett. **83**, 3150 (1999); A. Schiller *et al.*, Phys. Rev. C **63**, 021306 (R) (2001); E. Algin *et al.*, Phys. Rev. C **78**, 054321 (2008); M. Guttormsen *et. al*, Phys. Rev. C **62**, 024306 (2000); R. Chankova *et al.*, Phys. Rev. C **73**, 034311 (2006).
4) K. Kaneko *et al.*, Phys. Rev. C **74**, 024325 (2006).

Shear-viscosity to entropy-density ratio from giant dipole resonances in hot nuclei

N. Dinh Dang

[NUCLEAR STRUCTURE, quark-gluon plasma, shear viscosity, entropy density, perfect fluid, giant dipole resonances, hot nuclei, photoabsorption cross section, thermal pairing, phonon damping model, Fermi liquid drop model]

The recent experimental data from the Relativistic Heavy Ion Collider (RHIC) at Brookhaven National Laboratory and Large Hadron Collider (LHC) at CERN have revealed that the matter formed in ultrarelativistic heavy-ion collisions is a nearly perfect fluid with extremely low viscosity. This has driven the attention to the calculation of the ratio η/s of shear viscosity η to entropy density s. Using the string theory, Kovtun, Son and Starinets conjectured a universal value $\hbar/(4\pi k_B) \simeq 5.24 \times 10^{-23}$ Mev s (the KSS bound or KSS unit) for this ratio as the lowest bound for all fluids [1]. For finite nuclei, the recent calculations by Auerbach and Shlomo within the Fermi liquid drop model (FLDM) estimated η/s within $(4 - 19)$ and $(2.5 - 12.5)$ KSS units for heavy and light nuclei, respectively[2]. The obtained η increases with temperature T up to almost $T \sim 10$ MeV, then slows down to reach a maximum at $T \sim 13$ MeV. Consequently, within the region $0 \leq T \leq 5$ MeV, the damping width of the giant dipole resonance (GDR) predicted by the FLDM increases with T almost quadratically. However, the experimental systematic has shown that the GDR width in heavy nuclei increases with T only within $1 \leq T \leq 2.5$ MeV. Below $T \sim 1$ MeV, it remains nearly constant, whereas at $T > 3$ - 4 MeV the width seems to saturate. The entropy density $s = \rho S/A$ ($\rho = 0.16$ fm^{-3}) has been calculated in Ref.[2] by using a linear temperature dependence $S = 2aT$ with a temperature-independent level density parameter a. This approximation too is rather poor for finite nuclei. Therefore, although by dividing two quantities, both of which increase with T, the obtained result in Ref.[2] for the ratio η/s does decrease qualitatively to a value within one order of the KSS bound, a refined quantitative prediction for this ratio still remains a challenge. The present work uses the Kubo relation and the generalized Nyquist theorem to extract the ratio η/s from the experimental systematic for the GDR widths in copper, tin and lead regions at $T \neq 0$, and compares the results obtained with the theoretical predictions of the phonon damping model (PDM) and FLDM. The PDM was proposed by Dang and Arima to describe the damping of GDR at $T \neq 0$[3]. At $1 < T \leq 3.2$ MeV in these experiments, the empirical η/s is found between (1.7 - 4.4) and (2 - 10.6) KSS units by using $\eta(0) = 0.5u$ and $(0.9 \pm 0.3)u$, respectively, with $u = 10^{-23}$ Mev s fm^{-3} [The former value of $\eta(0)$ is the same as that used in Ref.[2], whereas the latter is obtained by fitting the ground-state giant resonance and fission data]. The PDM describes well these values and also predicts the corresponding values of the limit of $\eta/s \simeq$ (1.4 - 1.6) and (1.7 - 3.8) KSS units at $T = 5$ MeV in agreement with the estimations based on the microscopic definition as well as the Fermi-gas formula for the entropy [Fig. 1]. This is an indication that nucleons inside a hot nucleus at $T \geq 5$ - 6 MeV might behave as closely to a perfect fluid as quark-gluon plasma discovered at RHIC and LHC.

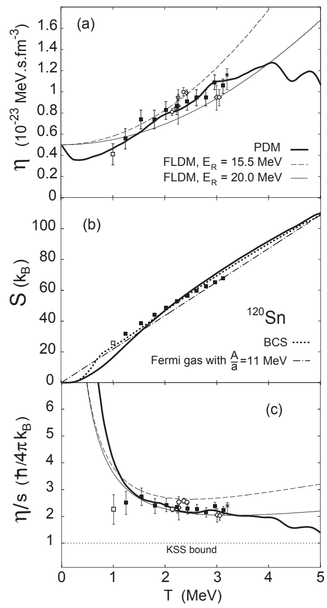

Fig. 1. Shear viscosity η (a), entropy S (b), and the ratio η/s (c) as functions of T for tin region. Data points are empirical values extracted from the hot GDR experimental systematic. The FLDM predictions were obtained by using two values of GDR energy E_R with $A/a = 11$ MeV.

References

1) P.K. Kovtun, D.T. Son, and A.O. Starinets, Phys. Rev. Lett. **94**, 111601 (2005).
2) N. Auerbach and S. Shlomo, Phys. Rev. Lett. **103**, 172501 (2009).
3) N.D. Dang and A. Arima, Phys. Rev. Lett **80**, 4145 (1998).

New empirical formula for an average equilibrium charge of a heavy recoil atom in helium gas

D. Kaji, H. Haba, and K. Morimoto

[GARIS, superheavy, hot fusion, average equilibrium charge]

The average equilibrium charges q_{ave} of heavy recoil ions moving in helium gas were measured by a gas-filled recoil ion separator (GARIS). A new empirical formula was derived for calculating the q_{ave} values of superheavy recoil ions moving with a low velocity .

The GARIS is one of the most active recoil separators used for searching superheavy elements (SHEs). The most important parameter to be considered when operating the GARIS is the average equilibrium charge q_{ave} of a recoil ion moving in a filled gas; this is because the trajectory of the recoil ion is governed by the relation $B\rho = 0.0227 \times A \times (v/v_0)/q_{ave}$, where $B\rho$ is the magnetic rigidity; A, the mass number; and v/v_0, the recoil velocity expressed in Bohr velocity units ($v_0 = c/137$, where c denotes the speed of light). In a previous study, we measured the q_{ave} values of various heavy recoil ions (^{169}Tm, ^{208}Pb, ^{193,209}Bi, ^{196}Po, ^{200}At, ^{203,204}Fr, ^{212}Ac, ^{234}Bk, ^{245}Fm, ^{254}No, and ^{255}Lr) moving in helium gas by using a GARIS and on the basis of the results, derived the following empirical formula for q_{ave} in helium gas[1]:

$$q_{ave} = 0.625 \times (v/v_0) \times Z^{1/3}. \tag{1}$$

This formula is useful in the range $9.0 \leq (v/v_0) \times Z^{1/3} \leq 19.1$. The formula was used to search for the SHE nuclides ^{263,264,265}Hs, ^{271}Ds, ^{272}Rg, ^{277}112, and ^{278}113 produced in cold fusion reactions.

Recently, the measurement of q_{ave} was carried out for superheavy recoil ions produced by actinide-base fusion reactions. Heavy recoil ions were produced in actinide-based fusion reactions: ^{238}U(^{22}Ne,5n)^{255}No [2], ^{248}Cm(^{18}O,5n)^{261}Rf[3], and ^{248}Cm(^{22}Ne,5n)^{265}Sg[4]. The evaporation residues (ERs) were separated from the projectiles, target recoils, and light-charged particles by the GARIS and collected at the focal plane of the separator. The GARIS was filled with helium gas at a pressure of approximately 30 Pa. The optimum magnetic field for maximum transmission was measured by a typical silicon detector system or a GARIS+Gas-jet+MANON system[2]. The q_{ave} value was deduced from the $B\rho$ value corresponding the maximum ER collection. Each q_{ave} value is plotted against $(v/v_0) \times Z^{1/3}$ in Fig. 1. The deviation of the measured q_{ave} from that derived using (1) increased with a decrease in $(v/v_0) \times Z^{1/3}$. Thus, a new empirical formula for determining the q_{ave} value of the recoil ions produced in actinide-based fusion reactions can be derived:

$$q_{ave} = 0.242 \times (v/v_0) \times Z^{1/3} + 2.19. \tag{2}$$

This formula is useful in the range $4.6 \leq (v/v_0) \times Z^{1/3} \leq 6.8$. A change in the slope was also observed in an earlier study on the light recoil ions in helium gas[5]. The atomic shell structure of the recoil ion might influence the charge-exchange process in helium gas. This new formula was used to search for the SHE nuclides ^{266}Bh[6] and ^{262}Db produced in a ^{248}Cm-based fusion reaction.

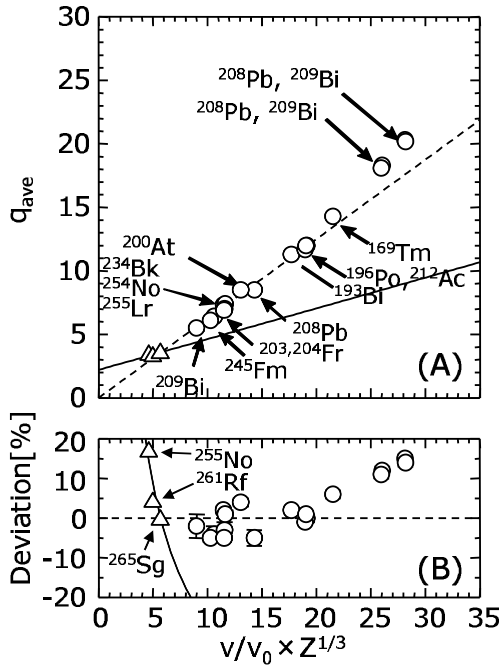

Fig. 1. (A) Measured equilibrium charge q_{ave} of heavy recoil ions moving in helium gas. Circles: values obtained in a previous study[1]: triangles: values obtained in a present study: broken line: $q_{ave} = 0.625 \times (v/v_0) \times Z^{1/3}$: solid line: $q_{ave} = 0.242 \times (v/v_0) \times Z^{1/3} + 2.19$. (B) Deviation from q_{ave} values predicted using eq.(1).

References

1) D. Kaji et al., RIKEN Accel. Prog. Rep. 36, 89(2002).
2) H. Haba, H. Kikunaga, D. Kaji et al., J. Nucl. Radiochem. Sci. 9, 27(2008).
3) H. Haba, D. Kaji et al., Chem. Lett. 38, 426(2009).
4) H. Haba, 7th Workshop on Recoil Separator for Superheavy Element Chemistry (TASCA08), 31 Oct., 2008, Darmstadt, Germany.
5) Yu. Ts. Oganessian et al., Z. Phys. D 21, S357(1991).
6) K. Morita, K. Morimoto, D. Kaji et al., J. Phys. Soc. Jpn. 78, 064201(2009).

Five-body cluster structure of the double-Λ hypernucleus ${}^{11}_{\Lambda\Lambda}$Be†

E. Hiyama M. Kamimura[*1] Y. Yamamoto,[*2] and T. Motoba,[*3]

[hypernuclei, cluster model, hyperon-nucleon interaction]

The $\Lambda\Lambda$ interaction is an important entry into the $S = -2$ baryon-baryon interactions, decisive information about which is obtained from observations of double-Λ hypernuclei and their separation energies for two Λ's separated from a double-Λ hypernucleus, denoted as $B_{\Lambda\Lambda}$. In the KEK-E176/E373 hybrid emulsion experiments, there were observed several events corresponding to double-Λ hypernuclei. Among them was the epoch-making observation of the NAGARA event, which was identified uniquely as ${}^{6}_{\Lambda\Lambda}$He in the ground state with a precise value of $B_{\Lambda\Lambda} = 6.91 \pm 0.16$ MeV[1,2).

A newly observed double-Λ event has been recently reported, called the Hida event[2)]. This event has two possible interpretations: One is ${}^{11}_{\Lambda\Lambda}$Be with $B_{\Lambda\Lambda} = 20.83 \pm 1.27$ MeV, and the other is ${}^{12}_{\Lambda\Lambda}$Be with $B_{\Lambda\Lambda} = 22.48 \pm 1.21$ MeV. It is uncertain whether this is an observation of a ground state or an excited state.

The aim of this work is to interpret the new Hida event on the basis of our theoretical study, adapting the method used for interpreting the Demachi-Yanagi event. At present, the Hida event has two possible interpretations: ${}^{11}_{\Lambda\Lambda}$Be and ${}^{12}_{\Lambda\Lambda}$Be. Here, we assume this event is a ${}^{11}_{\Lambda\Lambda}$Be hypernucleus. It is reasonable to employ an $\alpha\alpha n\Lambda\Lambda$ five-body model for the study of ${}^{11}_{\Lambda\Lambda}$Be, because, as mentioned above, the interpretation of the Demachi-Yanagi event for ${}^{10}_{\Lambda\Lambda}$Be was possible on the basis of an $\alpha\alpha\Lambda\Lambda$ four-body cluster model, and ${}^{11}_{\Lambda\Lambda}$Be is composed of ${}^{10}_{\Lambda\Lambda}$Be plus one additional neutron. We further note that the core nucleus ^{9}Be is well described by using an $\alpha\alpha n$ three-cluster model[3)], and, therefore, it should be possible to model the structure change of ^{9}Be due to the addition of the two Λ particles as a five-body problem. We have succeeded in developing our Gaussian expansion method[4)] in order to perform this five-body cluster-model calculation.

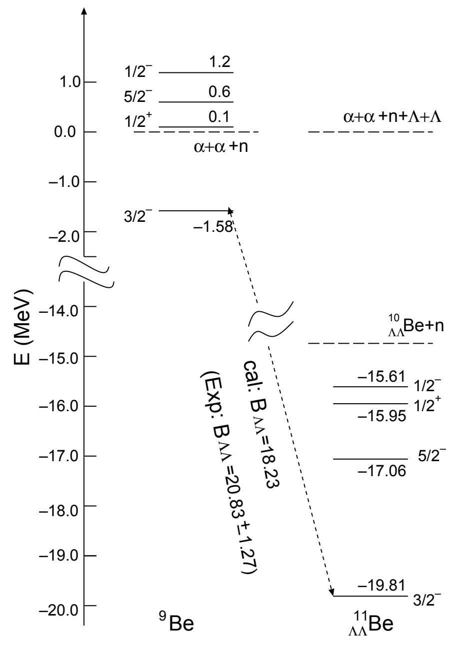

Fig. 1. Calculated energy spectra of the low-lying states of ${}^{11}_{\Lambda\Lambda}$Be together with those of the core nucleus ^{9}Be.

The energy level is illustrated in Fig. 1 together with that of ^{9}Be. The calculated value of $B_{\Lambda\Lambda}({}^{11}_{\Lambda\Lambda}\mathrm{Be})$ is 18.23 MeV for the $3/2^-$ ground state, which for the excited states the $B_{\Lambda\Lambda}$ values are calculated to be less than 15.5 MeV. Therefore, the observed Hida event can be interpreted to be the ground state. When our calculated binding energy is compared with the experimental value of 20.83 MeV with a large uncertainty of $\sigma = 1.27$ MeV, we can say at least that our results does not contradict the data within 2σ. For an alternative interpretation of the Hida event as the ground (or any excited) state of ${}^{12}_{\Lambda\Lambda}$Be, a corresponding six-body $\alpha\alpha nn\Lambda\Lambda$ model calculation is necessary, but such an undertaking is beyond our present consideration. More precise data are needed in order to test our present result quantitatively. In near future, many data for double Λ hypernuclei are expected to be found in the new emulsion experiment E07 at J-PARC.

References
1) H. Takahashi *et al.*, Phys. Rev. Lett. **87**, 212502 (2001).
2) K. Nakazawa *et al.*, Nuclear Physics (The proceedings on the 10th International Conference on on Hypernuclear and Strange Particle Physics (Hyp X), Tokai, Sept.14-18, 2009), in progress and to be submitted to Phys. Rev. C: K. Nakazawa, private communication (2010).
3) K. Arai, P. Descouvemont, D. Baye and W. N. Catford, Phys. Rev. C **68**,014319 (2003);
K. Arai, Phys. Rev. C **69** ,014309 (2004).
4) E. Hiyama, Y. Kino and M. Kamimura, Prog. Part. Nucl. Phys. **51**, 223 (2003).

† Condensed from the article in Phys. Rev. Lett. **104**, 212502 (2010)

*1 Department of Physics, Kyushu University
*2 Physics Section, Tsuru University
*3 Laboratory of Physics, Osaka Electro-Communication University

Energy dependence of K^--"pp" effective potential

T. Koike and T. Harada[1]

To elucidate the nature of antikaon–nucleon ($\bar{K}N$) interactions in high-density nuclear matter, it is important to clarify whether the "deeply bound kaonic nucleus" exists or not. In particular, the $[\bar{K} \otimes \{NN\}_{I=1}]_{I=1/2}$, $J^\pi = 0^-$ bound state, which is referred to as "K^-pp" herein, is suggested to be the lightest and most fundamental kaonic nucleus. Since the existence of the K^-pp bound state has not yet been confirmed, a new experimental search for K^-pp via the ^{3}He(in-flight K^-, n) reaction is planned (J-PARC E15 experiment). We have theoretically discussed the expected inclusive and semi-exclusive spectra for the ^{3}He(in-flight K^-, n) reaction within the framework of the K^-pp single-channel distorted-wave impulse approximation (DWIA) by employing the phenomenological K^--"pp" (complex) effective potential[1–3].

In the single-channel DWIA framework, the spectrum shape can be understood by the "moving pole" picture[3]; the pole position of the K^-pp bound state in the complex energy plane changes with the energy along the real axis, and its trajectory determines the spectrum shape. Therefore, the bound-state peak generally deviates from the standard Breit–Wigner type. Moreover, a cusp-like peak may appear at the $[K^-pp] \to \pi\Sigma N$ decay threshold energy ($E \sim 100$ MeV) in some cases, depending on the K^-pp binding energy.

The trajectory of the moving pole is determined by the energy dependence of the K^--"pp" effective potential, especially its imaginary part. We have used the phenomenological effective potential, which has the form

$$U^{\rm eff}(E;\boldsymbol{r}) = (V_0 + i\,W_0 f(E)\,)\exp[-(\boldsymbol{r}/b)^2], \qquad (1)$$

where $f(E)$ is the phase space factor of the decay channels[4]. To check whether the energy dependence in the form of Eq.(1) is appropriate or not, we developed a numerical method for deriving the K^--"pp" single-channel effective potential from the $(K^-p)p$-$(\pi\Sigma)N$ coupled-channel Green's function. Fig.1 shows an example of the calculated effective potential. The results are summarized as follows.

- Except when the $\pi\Sigma N$ channel has a bound state, the imaginary part strength of the effective potential is proportional to phase space factor $f(E)$, at least, near the $[K^-pp] \to \pi\Sigma N$ decay threshold energy, as shown in Fig.2.

- If the $\pi\Sigma N$ channel has a bound state, the energy dependence of the effective potential differs considerably from that shown by Eq.(1).

Further detailed investigation is underway for confirming these results.

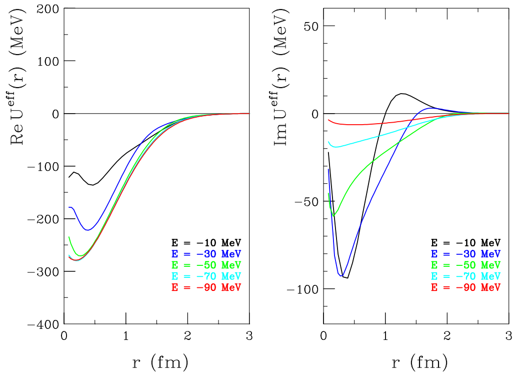

Fig. 1. An example of the calculated K^--"pp" single-channel effective potential derived from the $(K^-p)p$-$(\pi\Sigma)N$ coupled-channel model. The left and right panels show the real and imaginary parts, respectively. The energy E, which is measured from the K^-+p+p threshold, is varied from −10 MeV to −90 MeV.

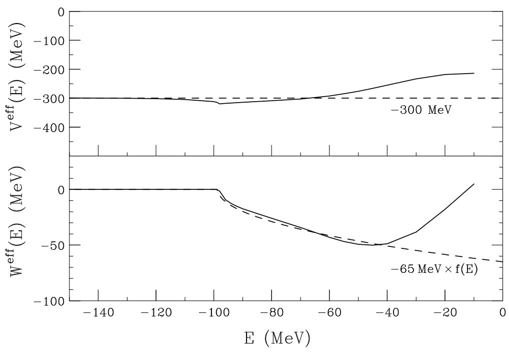

Fig. 2. Energy dependence of the potential strength deduced from the effective potential in Fig.1. The upper and lower panels show the real and imaginary parts, respectively.

*1 Research Center for Physics and Mathematics, Osaka Electro-Communication University

References
1) T. Koike and T. Harada, Phys. Lett. **B652**, 262 (2007).
2) T. Koike and T. Harada, Nucl Phys. **A804**, 231 (2008).
3) T. Koike and T. Harada, Phys. Rev. **C80**, 055208 (2009) .
4) J. Mareš, E. Friedman and A. Gal, Phys. Lett. **B606**, 295 (2005).

Structure and production of *sd*-shell Λ hypernuclei, ${}^{20}_{\Lambda}$Ne

A. Umeya, T. Motoba,*1 and T. Harada*1

Detailed hypernuclear studies have been mainly focused on structures of p-shell systems. In addition to the (π^+, K^+) reaction experiments done for wide mass number region,[1)] the γ-ray measurements[2)] from p-shell hypernuclei provide us with remarkable possibility of high-precision spectroscopic studies on theoretical side.[3)] Recently, also the $(e, e'K^+)$ reaction experiments done at Hall-A and Hall-C of JLab[4,5)] have been proved to be very fruitful in disclosing hypernuclear structure details within the energy resolution of few hundreds of keV. These aspects encourage us to perform theoretical study of *sd*-shell hypernuclear structures, because even the Λ single-particle energies and its interplay with nuclear core excitations are not well known in these medium-mass systems.

As one of the typical *sd*-shell hypernuclei, the positive- and negative-parity energy levels of ${}^{20}_{\Lambda}$Ne are calculated to investigate structures of low-lying states within the shell-model calculations. In addition to the conventional *NN* effective interactions,[6,7)] the Λ*N* *G*-matrix interactions derived from the Nijmegen NSC97f potentials[8)] are employed. The production cross sections of (π^+, K^+) and (K^-, π^-) reactions are estimated using the calculated shell-model wave functions.

Figure 1 shows the calculated energy levels of ${}^{20}_{\Lambda}$Ne, together with the experimental and calculated levels of ^{19}Ne. The calculation for ^{19}Ne well reproduces the experimental energy levels of three low-lying states with $J^{\pi} = \frac{1}{2}^+$, $\frac{5}{2}^+$ and $\frac{1}{2}^-$. For the ${}^{20}_{\Lambda}$Ne nucleus, the calculation by using the NSC97f Λ*N* interaction leads to the 0^+ ground state, which is inconsistent with the previous work[9)] by using the cluster model, where 1^- ground state was predicted.

Figure 2 shows production cross sections of (π^+, K^+) and (K^-, π^-) reactions in DWIA calculations. In the case of ^{20}Ne (π^+, K^+) reaction at $p_\pi = 1.05$ GeV/c and $\theta^{\mathrm{Lab}} = 3°$ in the left panel of Fig. 2, the 2^+, 3^- and 4^+ states are populated at the first, second and third peaks, respectively. On the other hand, in the case of ^{20}Ne (K^-, π^-) reaction at $p_K = 0.80$ GeV/c and $\theta^{\mathrm{Lab}} = 5°$ in the right panel of Fig. 2, the 1^- and 0^+ states are dominant at the second and third peaks. The positions of the second and third peaks in the (π^+, K^+) production are different from those in the (K^-, π^-) production. If the differences are measured, the order of $J = 3^-$ and 1^- states with $0p_\Lambda$ and of $J = 4^+$ and 0^+ states with $0d_\Lambda$ can be determined.

We are now calculating the DWIA production cross sections on the basis of the similar theoretical prescriptions, so that we can have a concrete idea to be utilized in possible J-PARC projects for light *sd*-shell hypernuclear production.

*1 Research Center for Physics and Mathematics, Osaka Electro-Communication University

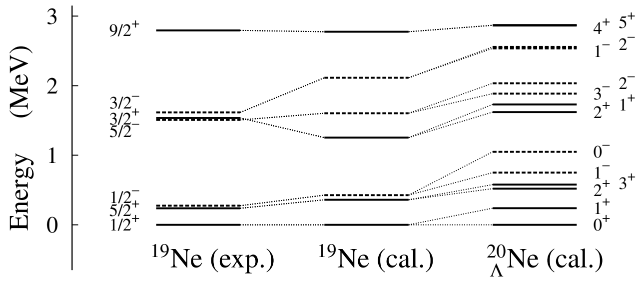

Fig. 1. Calculated energy levels of a ${}^{20}_{\Lambda}$Ne hypernucleus, together with experimental and calculated levels of ^{19}Ne.

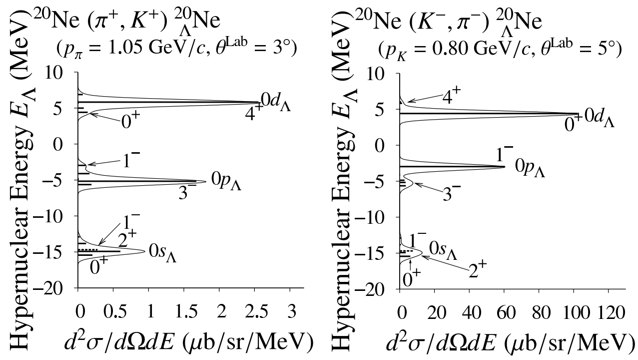

Fig. 2. Production cross sections of ^{20}Ne (π^+, K^+) and ^{20}Ne (K^-, π^-) reactions in DWIA calculations.

References

1) O. Hashimoto and H. Tamura: Prog. Part. Nucl. Phys. **57**, 564 (2006), and references therein.
2) H. Tamura: Nucl. Phys. A **827**, 153c (2009), and references therein.
3) D. J. Millener: Nucl. Phys. A **804**, 84 (2008), and references therein.
4) J. J. LeRose *et al.*: Nucl. Phys. A **804**, 116 (2008); F. Garibaldi *et al.*: Proc. of the Sendai International Symposium on Strangeness in Nuclear and Hadronic Systems (World Scientific, 2010) p.195.
5) O. Hashimoto *et al.*: Nucl. Phys. A **804**, 125 (2008); Y. Fujii *et al.*: Proc. of the Sendai International Symposium on Strangeness in Nuclear and Hadronic Systems (World Scientific, 2010) p.188.
6) T. T. S. Kuo: Nucl. Phys. A **103**, 71 (1967).
7) D. J. Millener and D. Kurath: Nucl. Phys. A **255**, 315 (1975).
8) Th. A. Rijken, V. G. J. Stoks, and Y. Yamamoto: Phys. Rev. C **59**, 21 (1999).
9) T. Sakuda and H. Bandō: Prog. Theor. Phys. **78**, 1317 (1987).

RIKEN Accel. Prog. Rep. 44 (2011)

Toward understanding of nuclear fine-tuning problems

Y Hidaka,[*1] T. Kojo,[*2] L. McLerran,[*2,*3] and R.D. Pisarski[2]

[$1/N_\mathrm{c}$ expansion, axial charge g_A, nuclear forces]

To explain nuclear forces remains a long standing problem in Quantum Chromodynamics (QCD). In phenomenology, it seems to be commonly accepted that 1) at long distance, the pion exchange force is dominant; 2) at intermediate distance, meson exchange forces show subtle cancellations; 3) at short distance, there is a hard core. As a consequence of subtle interplay of these forces and nucleon kinetic energy, a typical nuclear binding energy is kept $\sim 2-16$ MeV, which is astonishingly smaller than the typical QCD scale $\Lambda_{\mathrm{QCD}} \sim 200$ MeV. We call the emergence of such a small nuclear scale *nuclear fine-tuning problem.*

Is the small nuclear scale emerged just accidentally, or are there any reasons? Perhaps the first reasonable step to answer these questions is to examine the relative strength of forces in terms of QCD parameters such as Λ_{QCD} and a number of colors, N_c. The purposes of this work is 1) to emphasize a utility of the $1/N_\mathrm{c}$ expansion for classifications of nuclear forces; 2) to argue phenomenological problems in the pion exchange, which arise in conventional large N_c arguments; 3) to give possible resolutions of pion problems.

In the conventional N_c counting, an intrinsic quark-meson coupling is $\sim N_\mathrm{c}^{-1/2}$. So the nucleon-meson coupling depends on how quark-meson couplings are summed up. If summed additively, we get $N_\mathrm{c}^{-1/2} \times O(N_\mathrm{c}) \sim N_\mathrm{c}^{1/2}$ as a total. If contributions cancel one another, total contributions can be $N_\mathrm{c}^{-1/2} \times O(1) \sim N_\mathrm{c}^{-1/2}$. These factors $O(1)$ or $O(N_\mathrm{c})$ are proportinal to charges of nucleons: quark number of $O(N_\mathrm{c})$, and, isospin and spin of $O(1)$. Since the strength of meson exchange is proportional to (coupling)^2, the $1/N_\mathrm{c}$ expansion distinguishes different meson exchange forces by powers of $1/N_\mathrm{c}^2 \sim 1/10$, and classify parameters in phenomenological nuclear potentials very well[a)].

However, this logic can not be directly applied to the pion exchange, since pions couple to the nucleon axial charge g_A which is not a conserved quantity. Thus we need to know the relationship between internal dynamics of nucleons and the value of g_A. Although its value is experimentally known to be ~ 1.26, how to interpret this value provides dramatic differences in the leading order picture for nucleons.

Conventional arguments suggest $g_A \sim N_\mathrm{c}$ which is regarded as a large quantity. The large axial charge produces a large number of pions, and leads to coherent pion clouds or pionic soliton pictures of nucleons.

This picture, however, is known to produce serious phenomenological problems. Because of many pion exchanges, the long range part of nuclear force becomes $O(N_\mathrm{c})$ which is too strong. Then, even at low density, nulear matter becomes a crystal, instead of a (quantum) liquid which is experimentally supported.

This problem may imply that the $1/N_\mathrm{c}$ expansion is simply not a good guide for nuclear physics, since the leading order picture fails at qualitative level so that the corrections play essential roles. Alternative possibility is that we might have assigned nucleons in a wrong way. We explored the latter possibility.

Our basic strategy is to find candidates of nucleon wavefunctions with g_A of $O(N_\mathrm{c}^0)$ which is small enough to recover the one pion exchange picture. As a first attempt, we try to construct such nucleons in the framework of constituent quark model.

We found one possible candidate. We first pair up $u-d$ quarks in $I=S=0$ channels as a basic building block. When $N_\mathrm{c} = 2n_d + 1$, we put n_d-diquark pairs in the same spatial wavefunction. In this part, contributions to the axial charge exactly cancel one another. However, if we put an unpaired quark, offdiagonal coupling among wavefunctions of diquark pairs and that of unpaired quark generate $O(N_\mathrm{c})$ contributions to the axial charge, since a number of combinations is $O(N_\mathrm{c})$.

This problem can be avoided by putting the unpaired quark into another spatial orbit. Then the total axial charge is merely saturated by that of unpaired quark. Here an obvious question is whether a nucleon with such a small spatial overlap – which costs more kinetic energy – can be the ground state or not. Two mechanisms to overtake such an energetic cost might be possible. One is diquark correlations. Another is based on the hypothesis that the reduction of g_A generate a small pion cloud so that the nucleon mass becomes smaller[1)].

While the present work remains only suggestive, we expect that the $1/N_\mathrm{c}$ classifications would provide one useful portrait of nuclear forces in a simple terminology. Once it turned out to be reasonable picture, it is interesting to extrapolate these simple scheme into the nuclear-quark matter transition region.

References

1) Y. Hidaka, T.Kojo, L. McLerran, and R.D. Pisarksi, arXiv:1004.2261, to be published in Nucl. Phys. A.

*1 Department of Physics, Kyoto University
*2 RIKEN BNL Research Center, BNL, USA
*3 Brookhaven National Laboratory, USA

a) For velocity dependent vertices, discussions become more involved, and will not be argued here.

RIKEN Accel. Prog. Rep. 44 (2011)

N-Body Nuclear Forces at Short Distances in Holographic QCD†

K. Hashimoto,*1 N. Iizuka,*2 and T. Nakatsukasa*3

[Nuclear Force, String theory]

We provide a calculation of N-body ($N \geq 3$) nucleon interactions at short distances in holographic QCD. In the Sakai-Sugimoto model of large-N_c massless QCD, N baryons are described by N Yang-Mills instantons in 5 spacetime dimensions. We compute a *classical* short distance interaction hamiltonian for N 'tHooft instantons. This corresponds to N baryons sharing identical *classical* spins and isospins. We find that genuine N-body nuclear forces turn out to vanish for $N \geq 3$, at the leading order. This suggests that classical N-body forces are always suppressed compared with 2-body forces.

Recent developments in computational nuclear physics reveals that the microscopic description of nucleus in terms of nucleon degrees of freedom requires three-nucleon interactions. The two-body interactions adopted in many-body calculations are determined by the phase-shift analysis of nucleon-nucleon scattering data. However, much less information is available for the N-body forces ($N \geq 3$). Of course, we know that, in principle, the nuclear properties should be derived from QCD[1]. However, QCD is strongly coupled at the nuclear energy scale, which leads to a huge gap between QCD and nuclear many-body problems.

A recent progress in string theory can bridge this gap, analytically. It is called holographic QCD, an application of gauge/string duality[2] to strongly coupled QCD. We apply the holographic QCD to N-body nuclear force ($N \geq 3$).

In holographic QCD, one of the most successful D-brane models is Sakai-Sugimoto model (SS model) [3]. The theory, which is a $U(N_f)$ Yang-Mills-Chern-Simons (YM-CS) theory in a warped 5-dimensional space-time, was conjectured to be dual to low energy massless QCD with N_f flavors, in the large-N_c and large-λ limits ($\lambda \equiv N_c g^2_{\rm QCD}$ is a 'tHooft coupling of QCD). Modes of the gauge fields correspond to meson degrees of freedom and this model reproduces surprisingly well various expected features of hadrons, incorporating very nicely the nature of chiral Lagrangians. Baryons are identified with soliton solutions localized in the spatial 4-dimensions[3]. Quantization of a single soliton in the SS model[4] gives baryon spectra, and also chiral properties such as charge radii and magnetic moments[5]. Short-distance nucleon-nucleon forces were computed[6], which generates a repulsive core with analytic formula for potentials in the large-N_c limit. A key is that the warping can be absorbed into the rescaling of the YM-CS theory and brings the string scale to QCD scale. Furthermore, when two solitons are close to each other, the warping factor is almost constant, therefore the effects of the curved geometry can be ignored so that an exact two-soliton solution is available.

In this letter, we compute N-body nuclear forces for arbitrary N, with *exact* N-instanton solutions, generalizing the method in Ref.[6]. The exact treatment is in contrast to the Skyrmion and other chiral soliton models, in which multi-soliton solutions are quite difficult to obtain.

The leading order of the short-range nuclear force in proper to N-body is expected in SS model as

$$H^{U(1)}_{\rm pot}\Big|_{\rm N-body} = \frac{N_c}{\lambda^{N-1}}\,\mathcal{O}\left(\prod_{i=2}^{N}\frac{1}{X^2_{1i}},\cdots\right). \qquad (1)$$

We prove that for any N this leading contribution vanishes. We have finally found that the N-body nuclear force at short range ($N \geq 3$) is order of $N_c(\lambda r^2)^{-N}$, for nucleons sharing identical *classical* spin/isospins.

This is small compared to the 2-body force which is $\mathcal{O}(N_c(\lambda r^2)^{-1})$ in contrast, and it leads to a hierarchy of the $(N+1)$-body / N-body ratio $V^{(N+1)}/V^{(N)} \sim 1/(\lambda r^2) \ll 1$ for $N \geq 3$, in the unit 949 [MeV] $= M_{\rm KK} = 1$. This suppression is consistent with our empirical knowledge.

Effects of the short-range many-body interaction becomes more prominent for higher-density nuclear matter. Therefore, for physics of neutron stars and supernovae, for instance, properties of N-body interactions such as what is revealed in this letter are important, even if qualitative.

References

1) See for recent lattice QCD analyses, N. Ishii, S. Aoki and T. Hatsuda, Phys. Rev. Lett. **99**, 022001 (2007) [arXiv:nucl-th/0611096].
2) J. M. Maldacena, Adv. Theor. Math. Phys. **2**, 231 (1998) [Int. J. Theor. Phys. **38**, 1113 (1999)] [arXiv:hep-th/9711200].
3) T. Sakai and S. Sugimoto, Prog. Theor. Phys. **113**, 843 (2005) [arXiv:hep-th/0412141].
4) H. Hata, T. Sakai, S. Sugimoto and S. Yamato, Prog. Theor. Phys. **117**,1157 (2007) [arXiv:hep-th/0701280].
5) K. Hashimoto, T. Sakai and S. Sugimoto, Prog. Theor. Phys. **120**, 1093 (2008) [arXiv:0806.3122 [hep-th]].
6) K. Hashimoto, T. Sakai and S. Sugimoto, Prog. Theor. Phys. **122**, 427 (2009) [arXiv:0901.4449 [hep-th]].

† Condensed from the article in Phys. Rev. **D81** 106003 (2010)

*1 Mathematical Physics Lab., RIKEN Nishina Center
*2 Theory Division, CERN
*3 Theoretical Nuclear Physics Lab., RIKEN Nishina Center

A Matrix Model for Baryons and Nuclear Forces[†]

K. Hashimoto,[*1] N. Iizuka,[*2] and P. Yi[*3]

[Nuclear Force, String theory]

We propose a new matrix model describing multi-baryon systems. We derive the action from open string theory on the wrapped baryon vertex D-branes embedded in the D4-D8 model of large N_c holographic QCD. The positions of k baryons are unified into $k \times k$ matrices, with spin/isospin of the baryons encoded in a set of k-vectors. Holographic baryons are known to be very small in the large 't Hooft coupling limit, and our model offers a better systematic approach to dynamics of such baryons at short distances. We compute energetics and spectra ($k = 1$), and also short-distance nuclear force ($k = 2$). In particular, we obtain a new size of the holographic baryon and find a precise form of the repulsive core of nucleons.

Nuclear physics is one of the oldest branches of high energy physics, yet remains one of more difficult. Despite the fact that we know the underlying fundamental theory, *i.e.* QCD, we are still unable to predict, reliably and analytically, behavior of nuclei or even a single proton. In this paper, by using the gauge/gravity duality[1)], we propose a new matrix model for the dynamics of multi-baryons, whereby we compute basic properties of holographic baryons, interaction with mesons, and ultimately nuclear forces.

What matrix? In our matrix model, the number of baryons is represented by the rank of the matrix. Therefore, for k-body baryons, it is a $U(k)$ matrix model. If we path-integrate out the off-diagonal elements of matrices, we are left with k diagonal elements. It is these elements which represents the positions of the k baryons. In addition, there are a pair of complex $k \times N_f$ rectangular matrices whose classical values are related to the size of baryon. Together, they form the well-known Atiyah-Drinfeld-Hitchin-Manin (ADHM) matrix of instantons.

Why matrix? In the large N_c QCD, mesons are open strings and light degrees of freedom, with mass $\sim \mathcal{O}(1)$, while baryons are solitons with large mass $\sim \mathcal{O}(N_c)$. If we embed the large N_c gauge theory into string theory, baryons are described by string theory solitons, *i.e.*, D-branes[2)]. Therefore, the dynamics of multi-baryons are described by a multi-D-brane system, which is nothing but the $U(k)$ matrix model. Our matrix model is along the line of the ADHM construction which is the matrix description for multi-instantons in gauge theory, or equivalently along the line of D0-D4 quantum mechanics.[a)]

The matrix model action we derive is a $U(k)$ quantum mechanics,

$$S = \frac{\lambda N_c M_{\rm KK}}{54\pi}\int dt\; {\rm tr}_k \Big[(D_0X^M)^2 - \frac{2}{3}M_{\rm KK}^2(X^4)^2 + D_0\bar{w}_i^{\dot\alpha}D_0 w_{\dot\alpha i} - \frac{1}{6}M_{\rm KK}^2\bar{w}_i^{\dot\alpha}w_{\dot\alpha i} + \frac{3^6\pi^2}{4\lambda^2 M_{\rm KK}^4}\left(\vec{D}\right)^2 + \vec{D}\cdot\vec{\tau}^{\,\dot\alpha}{}_{\dot\beta}\bar{X}^{\dot\beta\alpha}X_{\alpha\dot\alpha} + \vec{D}\cdot\vec{\tau}^{\,\dot\alpha}{}_{\dot\beta}\bar{w}_i^{\dot\beta}w_{\dot\alpha i}\Big] + N_c\int dt\; {\rm tr}_k A_0\,.$$

Here $\lambda = N_c g_{\rm QCD}^2$ is the 'tHooft coupling constant, and $M_{\rm KK}$ is the unique dimension-ful constant. The dynamical fields are X^M and w, while $\vec{D}$ and A_0 are auxiliary fields. All the fields are bosonic. We claim that this matrix model describes the k-baryon system, according to the holographic principle in string theory.

With this matrix model, we compute the holographic size and the spectrum of the baryon ($k = 1$), and also short-distance nuclear force ($k = 2$). The latter exhibits a repulsive core, which has been quite important in nuclear and hadron physics for long years. We obtaine the central and the tensor forces,

$$\langle V\rangle_{I_1,J_1,I_2,J_2} = V_{\rm C}(\vec{r}) + S_{12}V_{\rm T}(\vec{r}) \qquad (1)$$

with the standard definition $S_{12} \equiv 12J_1^i\hat{r}_iJ_2^j\hat{r}_j - 4J_1^iJ_2^i$ (with $\hat{r}_i \equiv r_i/|r|$), where

$$V_{\rm C}(\vec{r}) = \pi\left(\frac{3^3}{2} + 8I_1^iI_2^iJ_1^jJ_2^j\right)\frac{N_c}{\lambda M_{\rm KK}}\frac{1}{r^2}\,, \qquad (2)$$

$$V_{\rm T}(\vec{r}) = 2\pi I_1^iI_2^i\frac{N_c}{\lambda M_{\rm KK}}\frac{1}{r^2}\,. \qquad (3)$$

This is the short-distance nuclear force obtained from our matrix model. We find there is a repulsive core of nucleons. The repulsive potential scales as $1/r^2$ for the inter-nucleon distance r.

References
1) J. M. Maldacena, Adv. Theor. Math. Phys. **2**, 231 (1998)
2) E. Witten, JHEP **9807**, 006 (1998), D. J. Gross and H. Ooguri, Phys. Rev. D **58**, 106002 (1998)
3) K. Hashimoto, Prog. Theor. Phys. **121**, 241 (2009), JHEP **0912**, 065 (2009)

† Condensed from the article in Journal of High Energy Physics **1010** (2010) 003

*1 Mathematical Physics Lab., RIKEN Nishina Center
*2 Theory Division, CERN
*3 Korea Institute for Advanced Study

a) The relevance of such a matrix model for baryons was previously emphasized by one of the authors[3)].

Three-Body Nuclear Forces from a Matrix Model†

K. Hashimoto,[*1] and N. Iizuka[*2]

[Nuclear Force, String theory]

We compute three-body nuclear forces at short distances by using the nuclear matrix model of holographic QCD proposed in our previous paper with P. Yi. We find that the three-body forces at short distances are repulsive for (a) aligned three neutrons with averaged spins, and (b) aligned proton-proton-neutron / proton-neutron-neutron. These indicate that in dense states of neutrons such as cores of neutron stars, or in Helium-3 / tritium nucleus, the repulsive forces are larger than the ones estimated from two-body forces only.

One of the fundamental ingredients of nuclear physics is the nuclear force with which point-like nucleons interact with each other. A variety of aspects of nuclear forces results in the protean metamorphosis of nuclei, the bound states of nucleons. It is known that in nuclear forces there are forces that can not be explained by two-body forces only, one of which is the three-body force. The three-body forces play important role, for example, in reproducing excitation spectra of light nuclei, or explaining equations of states for high-density baryon matters such as supernovae and neutron stars. However, in spite of the long history of nuclear physics, the bulk properties of three-body nuclear forces are yet to be revealed.

The main obstacle for revealing the various aspects of nuclear forces is obvious: QCD is strongly coupled and thus difficult to solve. In this paper, by using a nuclear matrix model of holographic QCD which we have derived together with P. Yi in[1)], we explicitly compute a three-body nuclear force in a large N_c holographic QCD. The two-body nuclear force was already computed in[1)].

For the derivation of our matrix model[1)] we use the gauge/string duality (the AdS/CFT correspondence)[2)] applied to a D4-D8 system[3)] of a large N_c QCD at a large 'tHooft coupling λ. Precisely speaking, our matrix model is a low-energy effective field theory on baryon vertex D4-branes[4)] in the D4-D8 holographic model of large N_c QCD. The matrix model describes k-body baryon systems with arbitrary k, where the size of the matrix is given by this k, based on the fact that baryons are wrapped D-branes on sphere[4)] in the gravity side of the gauge/string duality. In the previous work[1)], in addition to the derivation of the matrix model, the cases with $k = 1$ (baryon spectrum) and $k = 2$ (two-body nuclear force) were studied. For $k = 2$, it was found that a universal repulsive core exists for any baryon states with two flavors. Since our matrix model is not a phenomenological model for multi-baryon systems, but based on a firm ground of the gauge/string duality in string theory, it is natural to extend the analysis of our matrix model to derive the three-body nuclear forces. In this paper, we continue the analysis to the $k = 3$ case, *i.e.* we study the short-range three-body nuclear force, using the matrix model.

Although generic configurations of three baryons can be treated in the matrix model, as the computations are involved and thus not so illuminating, in this paper we shall concentrate on two particular examples: (a) three neutrons with spins averaged and (b) proton-proton-neutron (and proton-neutron-neutron), both aligned on a line with equal spacings. System with spin averaged is rather typical for dense states of multi-baryons such as cores of neutron stars. We obtain

$$\langle V_{3-\text{body}}\rangle_{\text{nnn(spin}-\text{averaged)}} = \frac{2^{-1/2}3^{15/2}\pi^2 N_c}{\lambda^2 M_{\text{KK}}^3 |r|^4}\,. \quad (1)$$

The latter (b) is related to Helium-3 and tritium nucleus.

$$\langle V_{3-\text{body}}\rangle_{\text{ppn}} = \frac{2^{5/2}3^{9/2}5\pi^2 N_c}{\lambda^2 M_{\text{KK}}^3 |r|^4}\,. \quad (2)$$

For both cases, the resultant three-body potential is positive, *i.e.* repulsive. It scales as $N_c/\lambda^2 r^4$ (where r is the inter-nucleon distance), in contrast to the two-body repulsive core $\sim N_c/\lambda r^2$. As the region of validity is at short range, $1/\sqrt{\lambda}M_{\text{KK}} \ll r \ll 1/M_{\text{KK}}$ (where $M_{\text{KK}} \sim \mathcal{O}(1 \text{ GeV})$), the three-body potential is suppressed compared to the two-body potential by $\sim 1/\lambda(rM_{KK})^2 \ll 1$. However at very short distances, *i.e.* at high dense states of nucleons, three-body forces are not small. The scaling is consistent with our previous findings,[5)].

References

1) K. Hashimoto, N. Iizuka and P. Yi, JHEP **1010** (2010) 003.
2) J. M. Maldacena, Adv. Theor. Math. Phys. **2**, 231 (1998)
3) T. Sakai and S. Sugimoto, "Low energy hadron physics in holographic QCD," Prog. Theor. Phys. **113**, 843 (2005) [arXiv:hep-th/0412141].
4) E. Witten, JHEP **9807**, 006 (1998)
5) K. Hashimoto, N. Iizuka and T. Nakatsukasa, Phys. Rev. D **81**, 106003 (2010)

† Condensed from the article in Journal of High Energy Physics **1011** (2010) 058

*1 Mathematical Physics Lab., RIKEN Nishina Center
*2 Theory Division, CERN

EXFOR Compilation of New RIKEN Data in 2010

K. Tsubakihara[*1] M. Kimura,[*2] N. Otuka,[*3] N. Furutachi,[*1] A. Makinaga,[*1] T. Matsumoto,[*1] and K. Kato,[*4]

[Nuclear reaction, database, NRDF, EXFOR]

The development of a nuclear reaction database is strongly needed for stimulating innovations in nuclear physics as well as for astrophysics and nuclear power engineering. In order to compile the domestic nuclear reaction data into a database, the Nuclear Reaction Data Centre was established on April 1, 2007 as a branch of Faculty of Science at Hokkaido University. It has taken over nuclear database activities from the former Japan Charged-Particle Nuclear Reaction Data Group (JCPRG). Thus, the Nuclear Reaction Data Centre is also referred to as JCPRG, the original abbreviation of the center. We, at the JCPRG, have been providing Japanese nuclear experimental data to the international nuclear physics community.

Furthermore, as a member of International Network of Nuclear Reaction Data Centers, NRDC, the other important task of the center is to create nuclear data entries in EXtended FORmat(EXFOR) in collaboration with the International Atomic Engineering Agency, IAEA. In particular, we have suggested that JCPRG can easily contact and communicate with the domestic authors and can accept the numerical data to be compiled after fruitful discussions with the author. At the NRDC meeting held in April 2010 at the Hokkaido university, this proposal was unanimously accepted. Therefore, we will continue these nuclear data compilation energetically. These results can be accessed through our web site.[1)]

In Table 1, we list the number of papers published in 2010 that were selected by JCPRG for compilation and for conversion into the EXFOR format in 2010. We also list the number of compiled papers in which the reaction data obtained from RIKEN facilities were used. This table shows that the papers reporting RIKEN experiments[2–8)] appear to constitute a majority of NRDF entries and the entries converted to the EXFOR format. Some of the reaction data in the entries[2–5)] are obtained by using radioactive beams with RIPS. They can be accessed on the EXFOR database[9)] using the E-numbers, which are the numbers assigned to each Japanese entries by IAEA and shown in the Reference list. The other entries have to be sent to IAEA.

Recently, the center established a research contract with the RIKEN Nishina Center in order to efficiently include the reaction data obtained by RIBF experiments using RI beams. We now plan to extend the NRDF format and also plan to suggest these change to IAEA in order to compile new experimental data that will be obtained from RIBF experiments. On Aug 6, 2010, JCPRG and RIKEN Nishina Center participated in a RIKEN Mini-Workshop at RIBF Facility to understand the present status of compilation performed by JCPRG and discuss future of the research contract. At the workshop, it was decided that the relationship between JCPRG and RIKEN Nishina Center should be developed further and that effective communication of ideas on efficiently compiling the reaction data of unstable nuclei should be realized by appointing certain contact persons at each center. In addition, Prof. Hideto En'yo, RIKEN Nishina Center Head, and Prof. Hiroyoshi Sakurai were invited on the 1st Asia Africa Science Platform Program Workshop held at Sapporo to confirm our relationship and develop the first step of the future Asian collaboration on nuclear data compilation. The development of the domestic database NRDF in collaboration with experimentalists for compiling all the data obtained from RIKEN and other Japanese institutes is strongly desired.

Table 1. The number of papers chosen for compiling data into the EXFOR database in 2010. All the papers were published in 2010.

	RIKEN	Total
EXFOR Entries	7	20

*1 Nuclear Reaction Data Centre (JCPRG), Faculty of Science, Hokkaido University
*2 Creative Research Institution, Sosei Research Department, Hokkaido University
*3 IAEA Nuclear Data Section
*4 Department of Physics, Faculty of Science, Hokkaido University

References

1) http://jcprg.org/
2) S. Takeuchi et al.: Phys. Rev. C **79**, 054319 (2010) (E2147).
3) Y. Kondo et al.: Phys. Lett. B **690**, 245 (2010) (E2173).
4) K. Tanaka et al.: Phys. Rev. Lett **104**, 062701 (2010) (E2174).
5) E. Yu. Nikolskii et al.: Phys. Rev. C **81**, 064606 (2010) (E2280).
6) J-Q. Faisal et al.: Chin. Phys.Lett **27**, 092501 (2010) (E2286).
7) T. Uesaka et al.: Phys. Rev. C **82**, 021602 (2010) (E2287).
8) K. Tanaka et al.: Phys. Rev. C **82**, 044309 (2010) (E2290).
9) http://jcprg.org/exfor/

3. Hadron Physics

Search for double anti-kaon production in antiproton-^{3}He annihilation at J-PARC

F. Sakuma

[kaonic-nuclei, J-PARC]

The possible existence of anti-kaonic nuclear clusters has been investigated extensively in recent years by adopting both theoretical and experimental approaches. In view of the strongly attractive K^-N interaction, existence of nuclear clusters with more than one K^-, such as K^-K^-NN double anti-kaonic nuclear systems [1], is also predicted. It is predicted that double anti-kaonic nuclear clusters have binding energies up to 300 MeV and extremely high density that is approximately 5 $\sim$ 6 times more than the normal nuclear density $\rho(0) = 0.17$ fm^3; the resulting phase diagram of hadronic kaon condensation phase and color superconducting phase or a precursor of these may be attained. In order to investigate such strong attraction mediated by double anti-kaons, experimental search for double anti-kaonic nuclear systems in $\bar{p} + A$ annihilation have been proposed [2].

The elementary anti-proton annihilation reaction, which produces two pairs of (K^+K^-), is expressed as $\bar{p}+p \rightarrow K^+ + K^+ + K^- + K^- - 98MeV$ with a negative Q-value of 98 MeV; therefore, the elementary reaction is forbidden for stopped antiprotons. However, if a multi kaonic nuclear cluster with deep bounding energy exists, as suggested by Ref. [1], the following $\bar{p}$ annihilation reactions will be possible on He targets [2]:

$$\begin{aligned} &\bar{p} + {}^3\text{He} \rightarrow \\ &K^+ + K^0 + ppK^-K^- + B^{pp}_{KK} - 109MeV. \end{aligned} \quad (1)$$

The formation of this double kaonic nuclear cluster occurs if the binding energy of the two K^- in a ppK^-K^- cluster B_{KK} exceeds 109 MeV. For the reaction in the final state (1), we can determine the missing mass from the K^+K^0 energies and also invariant mass of the decay products, e.g., ppK^-K^- decays into $\Lambda\Lambda$. We need to carry out a detailed theoretical evaluation of the decay branching ratio to the $\Lambda\Lambda$ final state, even though this coherent kaon absorption strength would not be small because of the favored isospin-zero channel.

We propose to perform the experiment at the existing K1.8BR beamline at J-PARC by using the E15 spectrometer that consists of a high-precision beam line spectrometer, a Cylindrical Detector System that surrounds a target, and a forward neutron TOF counter. The expected yield of stopped $\bar{p}$ is 250 per pulse (3.5 s) with a beam momentum of 0.7 GeV/c, beam intensity of 6.5 $\times$ 10^3 at 50 kW beam power, and a stopping rate of 3.8% which is evaluated using the GEANT4 toolkit. With some assumptions of the double-strangeness production yield and branching ratio, the expected sensitivity to the K^-K^-pp production is shown in Fig. 1. For 6 weeks data taking at 50kW beam power and the K^-K^-pp binding energy of 200 MeV, the sensitivity to the K^-K^-pp production is 4 $\times$ 10^{-5} per stopped $\bar{p}$ at the 3σ significance level.

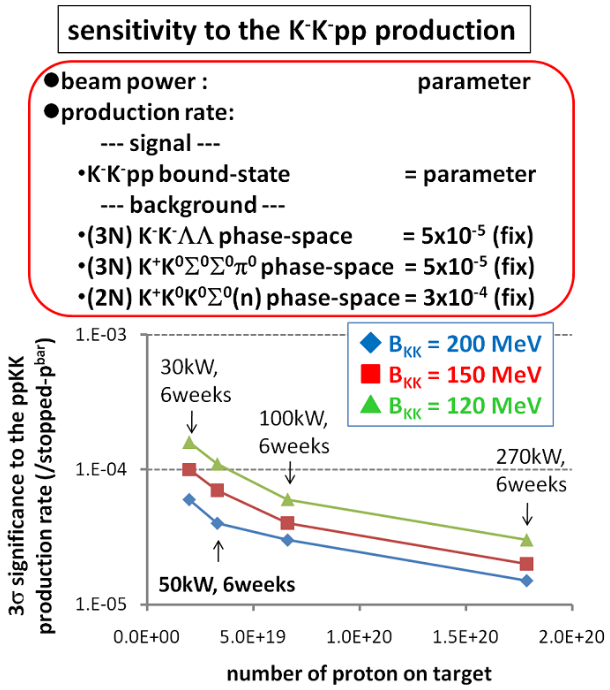

Fig. 1. Sensitivity to the K^-K^-pp signal obtained in exclusive K^+K^0 missing mass measurement in $\bar{p}+^3$He $\rightarrow$ $K^+ + K^0 + \Lambda + \Lambda(+X)$ reaction. The assumptions for the calculation are listed, and 3σ significances are plotted as a function of number of protons on the target for different binding energy of K^-K^-pp. The width of the K^-K^-pp is assumed to be 100 MeV/c^2.

References

[1] Y. Akaishi and T. Yamazaki, Phys. Rev., **C65** (2002) 044005; Y. Akaishi, A. Dote and T. Yamazaki, Phys. Lett., **B613** (2005) 140.

[2] W. Weise, arXiv: nucl-th0507058 (2005); P. Kienle, J. Mod. Phys., **A22** (2007) 365; P. Kienle, J. Mod. Phys., **E16** (2007) 905; F. Sakuma *et al.*, J-PARC LOI, http://j-parc.jp/NuclPart/pac_0907/pdf/LOI_Sakuma.pdf.

E906/SeaQuest Experiment: Probing Flavor Asymmetry of Antiquarks in Proton by Drell-Yan Process

S. Miyasaka*1, Y. Goto, Y. Miyachi*2, K. Nakano*1,
F. Sanftl*1, S. Sawada*3, T.-A. Shibata*1, and S. Takeuchi*1

Currently, in hadron physics, the study of the internal structure of a proton is attracting considerable attention. When the proton is probed at a high-energy scale, a large number of partons, i.e., quarks (q), antiquarks ($\bar{q}$) and gluons (g) are observed. Gluons and antiquarks are dynamically created by the strong force via $q \to q+g$ and $g \to q+\bar{q}$, respectively. Their states in the proton are sensitive to the detailed characteristics of the strong force.

Experiments have revealed that the flavor symmetry is largely broken in the distributions of light antiquarks ($\bar{u}$ and $\bar{d}$). Figure 1 shows the asymmetry, $\bar{d}-\bar{u}$, as a function of Bjorken x. Here Bjorken x is defined as the fraction of the momentum of a parton that is contributed to the proton momentum. The blue circles represent the latest measured results of the E866/NuSea experiment[1]. The measured asymmetry is as large as $\bar{d}/\bar{u} = 170\%$ at $x = 0.1$. The lines in Fig. 1 are the model calculation results that were obtained after the measurement. No models can reproduce the measured asymmetry well, particularly the reversal of $\bar{d} \gtrless \bar{u}$ at $x \sim 0.3$.

The E906/SeaQuest experiment at Fermi National Accelerator Lab (Fermilab) in USA is conducted to evaluate the Drell-Yan process in order to precisely determine the flavor asymmetry at the high x range of 0.25 to 0.45. The Drell-Yan process is, as shown in Fig. 2, a hadron+hadron reaction in which a quark in one hadron and an antiquark in the other hadron annihilate into a virtual photon and then a muon pair is created as follows: $q+\bar{q} \to \gamma^* \to \mu^+ + \mu^-$. Since the Drell-Yan process always involves an antiquark, it is the ideal process for measuring the flavor asymmetry. In the E906/SeaQuest experiment, a 120-GeV proton beam is extracted from the Fermilab Main Injector, and hydrogen and deuterium targets are irradiated with this beam. Further, the Drell-Yan cross sections in $p+p$ and $p+d$ reactions are determined, and the flavor asymmetry is calculated from the ratio of the cross sections. The anticipated accuracy is 10 times better at $x \approx 0.3$ than that achieved in the E866/NuSea experiment.

The first beam for commissioning will be available by the beginning of July 2011, and data acquisition started in summer. Japanese groups (RIKEN, KEK, Tokyo Institute of Technology, and Yamagata University) are in charge of one of three tracking stations. A drift chamber for the station was manufactured in Japan and was shipped to Fermilab in summer 2010. It was installed in March 2011. The detailed description of the drift chamber can be found elsewhere[2,3]. Four sets of trigger hodoscopes were successfully set up by February 2011, and they are ready to measure the rates of signals and backgrounds for the first incoming beam. The construction of a target system was completed in June 2011. The beam experiment will be adjourned halfway for a year to upgrade the Main Injector, and the experiment will be completed in 2014.

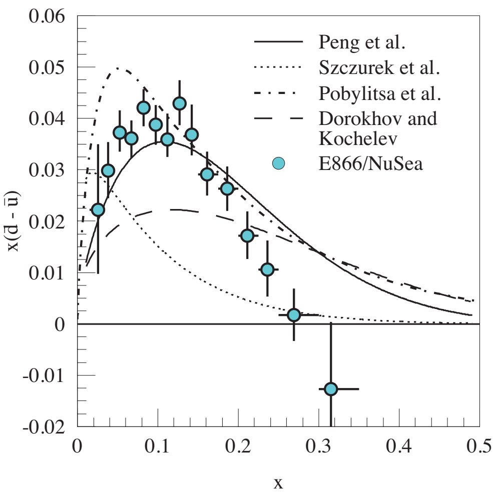

Fig. 1. Flavor asymmetry, $\bar{d}-\bar{u}$, as a function of x.

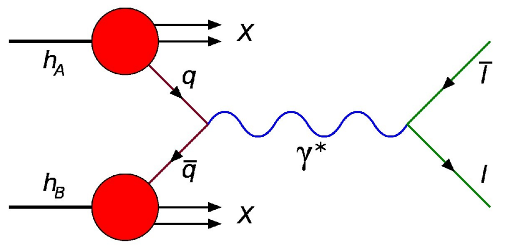

Fig. 2. Diagram of Drell-Yan reaction.

*1 Tokyo Institute of Technology
*2 Yamagata University
*3 KEK

References

1) R. S. Towell *et al.*: Phys. Rev. D **64**, 052002 (2001).
2) K. Nakano *et al.*: RIKEN. Accel. Prog. Rep. **43**, 219 (2010).
3) F. Sanftl *et al.*: RIKEN. Accel. Prog. Rep. **44**, 206 (2011).

Precision Measurements of Charged Hadron Multiplicities in e^+e^- Annihilation at Belle†

M. Leitgab,*1 M. Grosse Perdekamp,*1 R. Seidl, A. Ogawa,*2 and A. Vossen*1*3

[Precision hadron multiplicities, fragmentation functions, Belle, particle identification]

1 Measurement Description

This paper summarizes the status of precision measurements of $\pi^\pm$ and $K^\pm$ (in the following, resolving all particle charges is implied) multiplicities in e^+e^- annihilation at a center of mass energy of 10.52 GeV at the Belle experiment at KEK, Japan[1]. The hadron multiplicities are measured as a function of z which is the hadron energy relative to half of the center-of-mass energy in electron-positron annihilation into quark-antiquark pairs. The measured multiplicity distributions are corrected for particle misidentification and acceptance effects.

2 Motivation

Multiplicity measurements at Belle are motivated by two recent studies on the extraction of unpolarized fragmentation functions[2),3)]. Fragmentation functions describe hadron production from a final-state quark or gluon in processes such as hadron collisions, electron-positron annihilation and deep inelastic scattering of leptons on protons or nuclei. The present measurement is intended to provide high precision datasets as an input to the extraction of fragmentation functions, and thereby significantly lower the uncertainties of these. Precise knowledge of fragmentation functions is required for the extraction of the gluon helicity distribution from spin asymmetries measured in hadron collisions at the Relativistic Heavy Ion Collider[4].

3 Measurement Status and Outlook

For charged hadrons, experimental particle yields need to be corrected for particle misidentification. The correction is performed through an unfolding technique based on inverse 5x5 particle identification (PID) probability matrices. To not rely on the GEANT-based[5] Monte Carlo modeling of the Belle PID performance, the elements of the probability matrices are obtained from reconstructing unstable particles in experimental data with purely kinematical means, forming samples of tracks with known 'real/physical' species $i = \{e, \mu, \pi, K, p\}$. PID probabilities $p_{(i\to j)}$ can be calculated by applying PID likelihood cuts to select particles of species j from the reconstructed samples and forming ratios of the yields obtained with and without PID cuts. Another unfolding correction based on inverse probability matrices is applied to correct for momentum/z smearing introduced by the detector. Smearing matrices have been extracted from about 1.2×10^9 Monte Carlo generated events which have been reconstructed with the GEANT-based[5] Belle detector simulation. Figure 1 shows plots of the smearing probability matrices for π^- and K^+, respectively.

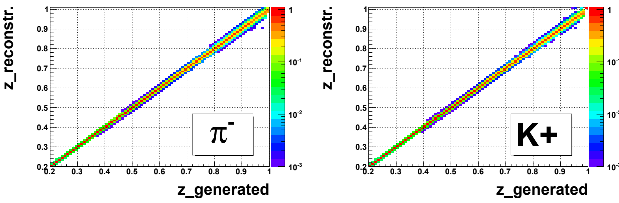

a) b)

Fig. 1. Figures a) and b) show smearing probability matrices extracted from Monte Carlo generated events which have been reconstructed with the Belle detector simulation for π^- and K^+, respectively. The color in each bin indicates the probability that a pion/kaon with generated normalized hadron energy *z_generated* is reconstructed with *z_reconstructed*. White-colored bins represent smearing probabilities smaller than 10^{-3}.

The measurement of hadron multiplicities against z will be performed from about 0.2 to close to 1.0 in z. The systematic uncertainty analysis for acceptance effects will be finalized. The leading uncertainty is expected to arise from the systematic uncertainties connected with the PID correction. The overall systematic uncertainties are expected to remain below 3% (5%) for π (K) spectra for $z < 0.6$, and to increase with z up to 5% (17%) for π (K) spectra for $z \sim 0.9$, respectively.

References
1) A. Abashian et al.: Nucl. Instrum. Methods **A** 479, (2002), pp. 117-232.
2) M. Hirai, S. Kumano, T.-H. Nagai, and K. Sudoh: Phys. Rev. D 75, 114010 (2007).
3) D. de Florian, R. Sassot, and M. Stratmann: Phys. Rev. D 75, 094009 (2007).
4) A. Adare et al.; Phys. Rev. Lett. 103, 012003 (2009).
5) Geant 4 Collaboration: Nucl. Instrum. Methods **A** 506, (2003), pp. 250-303.

*1 University of Illinois at Urbana-Champaign (UIUC), USA
*2 Brookhaven National Laboratory (BNL), USA
*3 Indiana University Bloomington (IUB), USA

Measurement of the interference fragmentation function in e^+e^-

R. Seidl, A. Vossen,[*1] M. Grosse-Perdekamp,[*1] A. Ogawa,[*2], and M. Leitgab.[*1]

[spin dependent fragmentation, transverse spin]

The interference fragmentation function IFF is a chiral-odd fragmentation function first suggested by Collins[1)] acting as an analyzer of transverse quark spin. In contrast to the Collins function[4)], previously also measured in Belle[2,3)], the IFF does not require a transverse momentum dependence relative to the quark axis and collinear factorization can be applied. This allows a model independent extraction of the quark transversity from SIDIS and pp data using the known collinear evolution[5)]. Following Boer[6)], the measurement relies on extracting an azimuthal correlation of the planes spanned by two charge ordered $\pi^+\pi^-$ pairs relative to the reaction plane defined by the incoming leptons and the formed quark-antiquark pair approximated by the thrust axis. The planes and angular definitions are displayed in Fig. 1. The results are obtained from a 672fb^{-1} data sample that contains $711 \times 10^6\,\pi^+\pi^-$ pairs and was collected near the $\Upsilon(4S)$ resonance, with the Belle detector at the KEKB asymmetric energy e^+e^- collider. In events with a clear two-jet like topology as defined by a thrust value larger than 0.8 a $\pi^+\pi^-$ pair is selected in each hemisphere. The azimuthal angular yield of these pairs is normalized by the average yield and fit by several azimuthal modulations, where the $\cos(\phi_1+\phi_2)$ modulation (a_{12}) is proportional to the product of the interference functions $H_1^{\sphericalangle}(z,m)$ of quark side and antiquark side, normalized by the corresponding unpolarized functions. $z = E_{pair}/E_{quark}$ is the fractional energy of the hadron pair and m is its invariant mass. Preliminary results were first shown

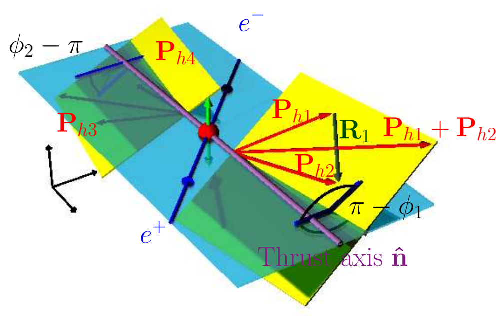

Fig. 1. Azimuthal angle definitions for ϕ_1 and ϕ_2 as defined relative to the thrust axis.

in fall 2009[7)] and the publication of the final results will be submitted in early 2011 after being delayed due to the internal refereeing process within Belle. We observe large asymmetries which are rising with the fractional energy, as can be seen in Fig. 2. The asymmetries are also rising with the invariant mass before leveling off which is not shown here due to space limitations. It is important to note that this mass behavior favors model calculations by Radici[9)] over those by Jaffe[8)] which have predicted a sign change at the ρ meson mass, although the observed kinematical dependences are still rather different from either prediction.

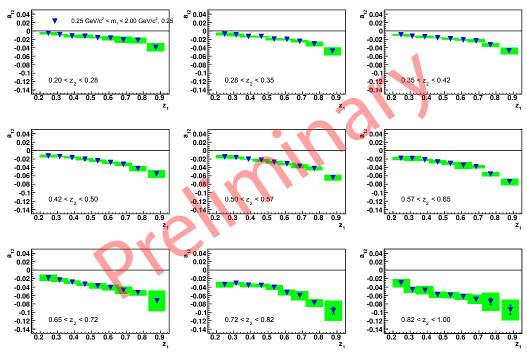

Fig. 2. a_{12} modulations for the 9×9 z_1, z_2 binning as a function of z_2 for the z_1 bins, where $1, 2$ stands for the hemisphere.

The analysis for the extraction of the interference function for other hadron combinations is ongoing.

References

1) J. C. Collins, S. F. Heppelmann and G. A. Ladinsky, Nucl. Phys. B **420**, 565 (1994) [arXiv:hep-ph/9305309].
2) R. Seidl *et al.* [Belle Collaboration], Phys. Rev. Lett. **96** (2006) 232002 [arXiv:hep-ex/0507063].
3) R. Seidl *et al.* [Belle Collaboration], Phys. Rev. D **78**, 032011 (2008) [arXiv:0805.2975 [hep-ex]].
4) J. C. Collins, Nucl. Phys. B **396**, 161 (1993) [arXiv:hep-ph/9208213].
5) F. A. Ceccopieri, M. Radici and A. Bacchetta, Phys. Lett. B **650**, 81 (2007) [arXiv:hep-ph/0703265].
6) D. Boer, R. Jakob and M. Radici, Phys. Rev. D **67** (2003) 094003 [arXiv:hep-ph/0302232].
7) A. Vossen, R. Seidl, M. Grosse-Perdekamp, M. Leitgab, A. Ogawa and K. Boyle, to appear in the proceedings of the Dubna Spin workshop 2009, arXiv:0912.0353 [hep-ex].
8) Jaffe, R.L. and Jin, X. and Tang,J.,Phys. Rev. Lett.**80**,1166, (1998)
9) Bacchetta,A. and Radici,M.,Phys. Rev.,**D74**,114007(2006)

*1 University of Illinois, Urbana Champaign, USA.
*2 Brookhaven National Laboratory, Upton, USA.

Measurement of production cross section of W bosons in proton-proton collisions at $\sqrt{s} = 500$ GeV

K. Okada

W boson production in polarized proton-proton collisions can be used to probe the spin structure of the proton. Because of the parity violating feature of the weak interaction, an asymmetry in W boson production to the helicity of the incoming proton is a probe for the quark and anti-quark polarization in the proton. This report describes how the W production is confirmed by detecting the $e^{\pm}$ from the W decay.

The PHENIX detector has been described in detail elsewhere[1]. The data set was recorded with the EMCal trigger, which has a nominal energy threshold of 10 GeV. In the 2009 run, an integrated luminosity of 8.6 pb^{-1} was recorded for this analysis.

Figure 1 shows the p_T spectra for the positron and electron candidates. The bands represent our estimated background, which are dominated by charged hadrons with hadronic interactions in the EMCal and electrons resulting from photon conversions before the tracking system. In the figure, clear signals of the W decay are seen, as confirmed by the Jacobian peak at $M_W/2 \simeq 40$ GeV. It is noteworthy that our selection is limited to one hemisphere, so that the signal is a combination of the W and Z boson decays.

By counting the events in the signal region ($30 < p_T < 50$ GeV/c), the cross sections are calculated. The systematic uncertainties in the measurement include the uncertainty in the background and a 15% normalization uncertainty due to the luminosity (10%), multiple collision (5%), and acceptance and efficiency uncertainties (10%). To compute the $W^{\pm}$ production cross sections, we performed the next-to-leading-order (NLO) and next-to-NLO (NNLO) calculations to subtract the Z contribution in our sample and to correct for W decays that were outside of the detector acceptance. The contribution from the Z decays was 6.9% for W^+ and 30.6% for W^-. The fraction of the total cross section within $|y| < 0.35$ in rapidity, $p_T > 30$ GeV/c, and $|\Delta\phi| < \pi$ was estimated to be 11.3% of the positrons from W^+ and 7.4% of the electrons from W^-. The theoretical uncertainties were smaller than other sources of systematic uncertainty. In Fig. 2, the obtained results are compared with published LHC, Tevatron and Sp$\bar{p}$S data[2–6].

In summary, W bosons are confirmed to be produced in proton-proton collisions at $\sqrt{s} = 500$ GeV. The cross section is consistent with that determined by the standard model theoretical calculations. RHIC is ready to use W production as a tool to probe the spin structure of the proton.

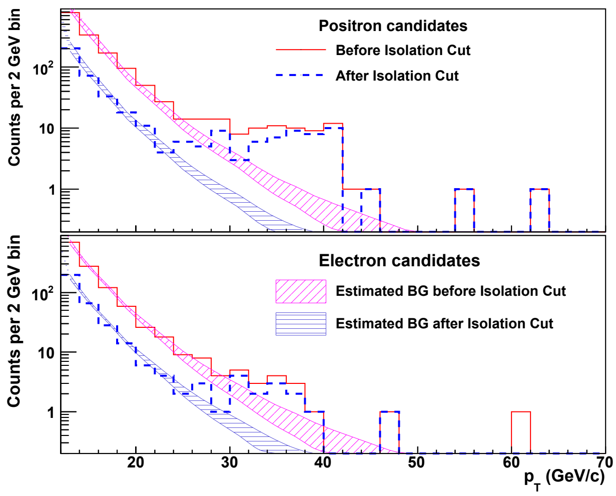

Fig. 1. The spectra of positron (upper panel) and electron (lower panel) candidates before (solid histogram) and after (dashed histogram) an isolation cut. The bands reflect the uncertainty of the background.

† Condensed from the article in Phys. Rev. Lett. 106, 062001 (2011), arXiv:1009.0505

References

1) K. Adcox et al.: Nucl. Inst. Meth. A **499**, 469 (2003)
2) D. E. Acosta et al.: Phys. Rev. Lett. **94**, 091803 (2005)
3) B. Abbott et al.: Phys. Rev. D **61**, 072001 (2000)
4) J. Alitti et al.: Z. Phys. **C47**, 11 (1990)
5) C. Albajar et al.: Z Phys. **C44**, 15 (1989)
6) G. Aad et al.: JHEP **1012**, 060 (2010)

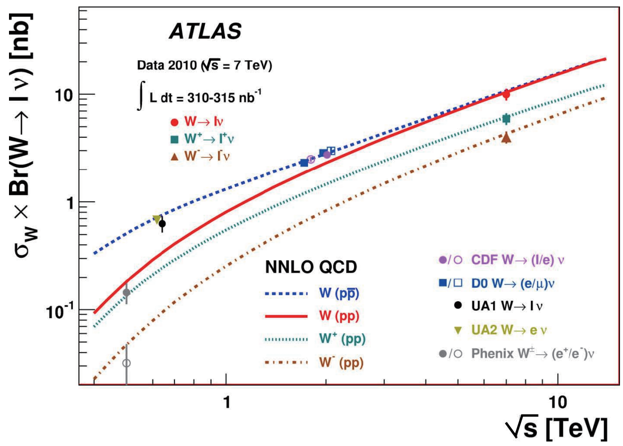

Fig. 2. Leptonic decay channel of this measurement and $\bar{p}p$ measurements[6]. Statistical and systematic uncertainties are added in quadrature. The curves indicate the results of theoretical calculations.

Measurement of Neutral Pion A_{LL} and the Resulting Constraint on the Gluon Polarization

K. Boyle, and A. Manion,[*1]

[Nucleon spin, Polarized Protons]

A primary goal of the RHIC Spin Program is to understand the spin structure of the proton, and in particular the gluon spin contribution (ΔG), through polarized proton collisions. Pions are abundantly produced in proton collisions, and using the PHENIX Electromagnetic Calorimeter, which has fine position resolution and is coupled with a high energy photon trigger, we are able to record a large sample of neutral pions via the $\pi^0 \to \gamma\gamma$. In the measured π^0 transverse momentum (p_T) range, gluon-gluon and gluon-quark scattering dominate. The measurement of the double spin asymmetry in π^0 production, A_{LL}, can be used to determine ΔG. Results from 2005 (Run5) and 2006 (Run6) π^0 A_{LL} data from PHENIX significantly constrained ΔG[1,2]. In the 2009 RHIC polarized proton run (Run9), PHENIX had a sampled luminosity of 14 pb^{-1} with 57% polarization.

Experimentally, we define

$$A_{LL} = \frac{\sigma_{++} - \sigma_{+-}}{\sigma_{++} + \sigma_{+-}} = \frac{1}{P_1 P_2} \frac{N_{++} - RN_{+-}}{N_{++} + RN_{+-}} \qquad (1)$$

where, σ is the cross section, N is the measured yields, P is the RHIC beam polarization, R is the relative luminosity defined as $R = L_{++}/L_{+-}$, L is the Luminosity and '++' ('+−') signifies same (opposite) polarization orientation. The asymmetry is measured for two photon pairs within $\sim 2\sigma$ of the expected π^0 mass peak, as well as separately in two background regions on either side of the mass peak. The background asymmetry, weighted by the fraction of background under the mass peak, is subtracted from the asymmetry in the peak region to extract the π^0 A_{LL}. The preliminary result from Run9, combined with previous published results from Run5 and Run6, are plotted as a function of p_T in Figure 1.

The Run5 and Run6 data have been included in a global analysis of world data for polarized Deep Inelastic scattering (DIS), Semi-inclusive DIS and proton-proton ($p+p$) scattering. The results showed that the $p+p$ data significantly constrained ΔG when included in the fit. The expectation for A_{LL} based on the best fit results (labeled 'DSSV') is shown in Figure 1. Note that this fit includes some of the data included in the plotted points.

The grey band in Figure 1 is the systematic uncertainty from relative luminosity. In 2009, this uncertainty for the preliminary result was 1.4×10^{-3}, which is larger than the statistical uncertainty in the lower p_T bins. Work is continuing to determine the source of this systematic uncertainty in order to reduce it. As was discussed in[3], a rate correction to account for the effect of multiple collisions has been developed and will be applied. Further work will however be necessary, and studies are ongoing.

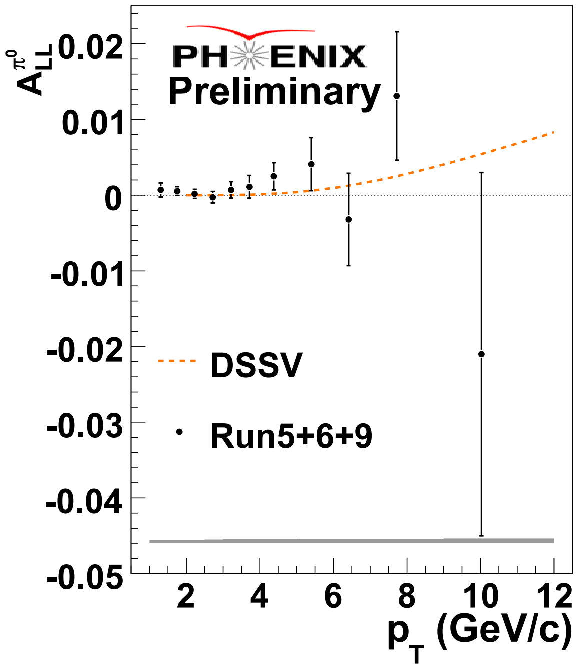

Fig. 1. π^0 A_{LL} as a function of p_T from 2005, 2006 and 2009 data. Fit result from DSSV (incuding 2005 and 2006 data) is also shown.

References
1) A. Adare *et al.*: Phys. Rev. Lett. **103**, 012003 (2009).
2) D. de Florian, R. Sassot, M. Stratmann and W. Vogelsang: Phys. Rev. Lett. **101**, 072001 (2008), D. de Florian, R. Sassot, M. Stratmann and W. Vogelsang: Phys. Rev. D **80**, 034030 (2009).
3) A. Manion, K. Boyle, and A. Deshpande: RIKEN Accel. Prog. Rep. 43 (2010).

*1 Department of Physics and Astronomy, Stony Brook University

RIKEN Accel. Prog. Rep. 44 (2011)

Measurement of double spin asymmetry of single electron production in polarized proton-proton collision on the RHIC PHENIX

K.R. Nakamura*[1] and Y. Akiba, for the PHENIX Collaboration

[proton spin structure, gluon polarization, single electron]

Spin asymmetry measurement of the heavy flavor quark production in a proton-proton collision is an important method of determining the gluon polarization in a proton. In the PHENIX, the heavy flavor quark is detected by detecting single electrons from the semileptonic decays. However, the detected electrons include a large fraction of background electrons.

The dominant background in the single electron detection mainly consists of photonic electron pairs caused by the Dalitz decay of neutral mesons and photon conversion in the material. To remove the background, a Hadron Blind Detector (HBD) was installed in the PHENIX. The HBD is a gas Cherenkov detector and detects electrons. While a single electron leaves a cluster signal on the HBD, the photonic electron pairs leave a merged cluster signal that corresponds to a charge twice that of the single electron cluster because the angles between the photonic electron pairs are quite small. Using this principle, the HBD removes the photonic electron backgrounds effectively on the basis of the respective cluster charges.

To estimate the dilution effect of the spin asymmetry, fractions of single electron clusters in the HBD clusters must be known. In addition to photonic electrons, scintillation lights generated in Cherenkov radiator gas also make background hits on the HBD. To estimate these background fractions, the superposition of charge distributions of single electron clusters, merged clusters, and scintillation hit clusters is fitted to a charge distribution obtained for reconstructed electrons. Fig.1 shows the charge distributions for each component and the fitting result for a distribution obtained for electrons with transverse momentum p_T ranging from 1.00 GeV/c to 1.25 GeV/c. The charge distributions of the single electron clusters and the merged clusters are estimated by using low-mass unlike-sign electron pairs, which include a small fraction of misidentified electrons. The charge distribution for the scintillation lights is estimated from clusters associated with hadron tracks. The charge distribution of the reconstructed electrons can be reproduced by the superposition of the three components excellently.

The fitting was performed with HBD charge distributions measured in other p_T regions, and the yields for the three components were determined in each p_T region. Fig.2 shows the momentum spectra for the three components. The spectrum of the single electron clusters has a lower slope than that of merged clusters. This behavior is consistent with the known cross sections of single electron production and photonic electron production.

The last step in determining the single electron yield is to estimate the actual fraction of single electron tracks in the single electron clusters. Subsequently, the spin asymmetry of the single electron cross section can be estimated.

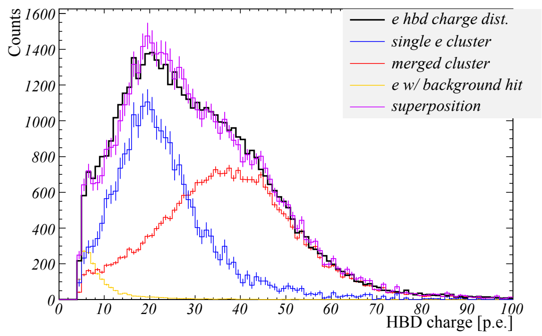

Fig. 1. Charge distribution of HBD clusters associated with reconstructed electrons with a transverse momentum ranging from 1.00 GeV/c to 1.25 GeV/c (black), and the charge distribution for each component, i.e., single electron clusters (blue), merged clusters (red), and scintillation hit clusters (yellow). The superposition of these components is also shown (purple).

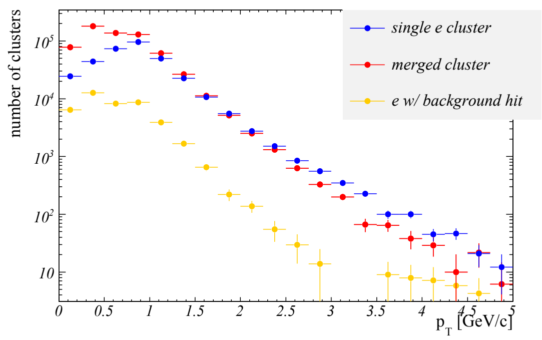

Fig. 2. Momentum spectra obtained for the single electron clusters (blue), merged clusters (red), and scintillation hit clusters (yellow) on one of the HBD sectors obtained by the fitting method.

*1 Department of Physics, Kyoto University, Kitashirakawa-Oiwake, Sakyo, Kyoto, 606-8502, Japan

Probing Transverse Spin Structure using Transverse Single Spin Asymmetries in polarized $p+p$ collisions†

J. Koster,*1

This work was done at the PHENIX Experiment at the Relativistic Heavy Ion Collider. The major goal of the PHENIX collaboration is to determine spin-dependent parton distribution functions. These measurements are carried out by studying collisions between either longitudinally or transversely polarized proton beams. When colliding a transversely polarized proton beam with an unpolarized proton beam, the spin-direction makes it possible to measure azimuthal asymmetries with respect to the spin-direction of the polarized proton beam. This asymmetry is denoted as A_N and is given as:

$$A_N = \frac{\sigma^{\uparrow} - \sigma^{\downarrow}}{\sigma^{\uparrow} + \sigma^{\downarrow}} \tag{1}$$

In the framework of pQCD, this asymmetry was expected to be small at high p_T. Early experiments date back to the 1970's, but they were carried out at an energy below the level for which pQCD has successfully predicted the unpolarized cross-sections. The E704 collaboration continued the measurement of A_N to higher center of mass energies ($\sqrt{s}$=19.4 GeV), and found that, surprisingly, the asymmetries persisted. More recently and at even higher center of mass energies the STAR, BRAHMS and PHENIX collaborations measured these asymmetries and found that the asymmetry magnitude and general behavior does not change. This is surprising since the techniques of perburbative QCD fail to describe hadron production for low $\sqrt{s}$, but succeeds at high $\sqrt{s}$[1]. The asymmetries are typically plotted either versus p_T, the hadron momentum transverse to the initial proton momenta, or versus $x_F \equiv 2p_L/\sqrt{s}$, where p_L is the hadron momenta parallel to the incoming polarized proton momenta.

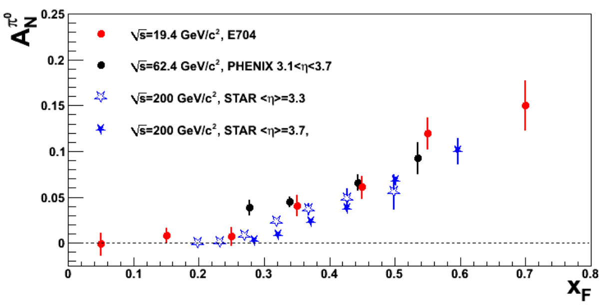

Fig. 1. Forward rapidity π^0 A_N results from the E704[2], PHENIX and STAR collaborations[3].

At present, three theoretical approaches are under active research to explain the origin of single spin asymmetries: the Sivers mechanism[4], the Collins mechanism[5] and higher-twist effects[6].

Two measurements of A_N are presented in this report. The first measurement at forward-rapidity is for $p_T < 5$ GeV/c but $|x_F| > 0.2$ and the second is at high p_T and at $x_F \approx 0$. For the first measurement an electromagnetic calorimeter was built and its first results from $p^{\uparrow}+p$ collisions at $\sqrt{s}$=62 GeV are shown in figure 1.

The second measurement's data collection and analysis procedures closely follows that of an earlier mid-rapidity A_N publication[7]. However, the measurement is expanded to higher p_T and to include both neutral pions and η mesons. Results are shown in figure 2. The previous publication led to constraints being

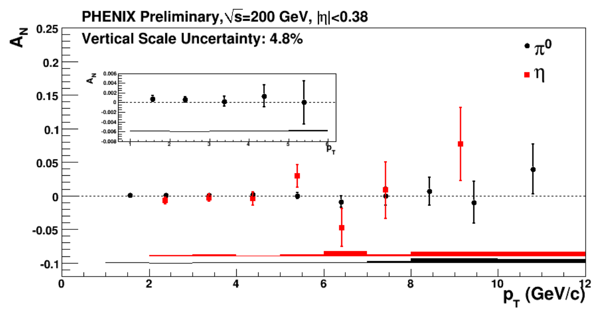

Fig. 2. Mid-rapidity π^0 and η meson A_N results.

placed on the theoretical models. The results were particularly sensitive to gluons due to the production mechanism of neutral pions at low p_T, which is dominated by gluon-gluon scattering. Compared to this previous result, the statistical uncertainties of the new result have been reduced by a factor of 20. Therefore, even greater constraints on the function are expected.

References

1) C. Bourrely and J. Soer, Eur. Phys. J., vol. C36, pp. 371374, 2004.
2) D. Adams et al., Z.Phys., vol. C56, pp. 181184, 1992.
3) B. I. Abelev et al., Phys. Rev. Lett., vol. 101, p. 222001, 2008.
4) D. W. Sivers, Phys. Rev., vol. D43, pp. 261263, 1991.
5) J. C. Collins, Nucl. Phys., vol. B396, pp. 161182, 1993.
6) A. V. Efremov and O. V. Teryaev, Sov. J. Nucl. Phys., vol. 36, p. 140, 1982.
7) S. S. Adler et al., Phys. Rev. Lett. 95, 202001, 2005.

*1 RIKEN BNL Research Center

Production cross section of inclusive charged hadrons in pp collisions at $\sqrt{s}$=62.4 GeV at PHENIX

D. Kawall,[*1,*2] and A. Datta[*2]

[proton-proton interactions, total cross sections]

Introduction

In 2006 the PHENIX collaboration at the Relativistic Heavy Ion Collider (RHIC) recorded data from collisions of polarized protons at $\sqrt{s}$ of 62.4 GeV. From this data the cross section of $pp \to h^{\pm}X$ of inclusive non-identified charged hadrons $h^{\pm}$ at mid-rapidity $|\eta| < 0.35$ has been measured.

Event Selection and Discussion

We examined approximately 214 million pp collisions, corresponding to an integrated luminosity of 15.6 nb^{-1}, selected with a minimum bias trigger formed from a coincidence of hits in two Beam-Beam Counters (BBCs) on either side of the interaction region[1]. Collisions within the acceptance of the PHENIX central arm detectors were examined for charged tracks in the PHENIX drift chamber (DC)[1] with a momentum between 0.5 and 4.5 GeV/c. The tracks were extrapolated to the PHENIX pad chambers (PC3)[1] where we required a closely matching hit.

Several cuts were used to remove particles other than the charged hadrons of interest (K, π, p). To remove $e^{\pm}$ from γ conversion, a veto was placed on the PHENIX Ring Imaging Detector[1] which fires on $e^{\pm}$ above 20 MeV/c, and $\pi^{\pm}$ above 4.7 GeV/c. Particles from the decay in flight of long-lived species such as $\pi^{\pm}$, $K^{\pm}$, K_L^0 are rejected since they originate far from the primary vertex and do not pass the tight matching cuts. Short lived particles such as K_S^0, Λ, Σ, $\Xi, \ldots$ decay close to the primary vertex, yielding an irreducible background of particles that appear to originate from the primary vertex and which pass the matching cuts. This contamination is estimated using PYTHIA[2] and the PHENIX detector simulation to be approximately 7% of the total sample. Corrections for relative offsets of the beam position and DC were applied, as were corrections to the p_T spectrum arising from the finite DC momentum resolution, and fiducial cuts to remove regions of the detector with poor performance. A correction for the change in the trigger efficiency versus particle p_T was also applied.

The efficiency of the cuts for each species, $K^{\pm}$, $\pi^{\pm}$, $p^{\pm}$ was estimated using a single particle detector simulation. The relative fractions of each species was estimated from identified charged hadron data[3]. From the these factors the charged hadron cross-section was estimated from the raw p_T spectrum. The cross sections are plotted and compared with perturbative QCD calculations performed at next-to-leading order (NLO) and next-to-leading-logarithm (NLL)[4] in Fig. 1. The results suggest NLL provides a better description of the data, and should be used in the interpretation of double longitudinal spin asymmetry measurements in the production of charged hadrons at $\sqrt{s}$=62.4 GeV. The results are also useful in the calculation of R_{AA} from mid-rapidity charged hadron production in dAu and $AuAu$ collisions.

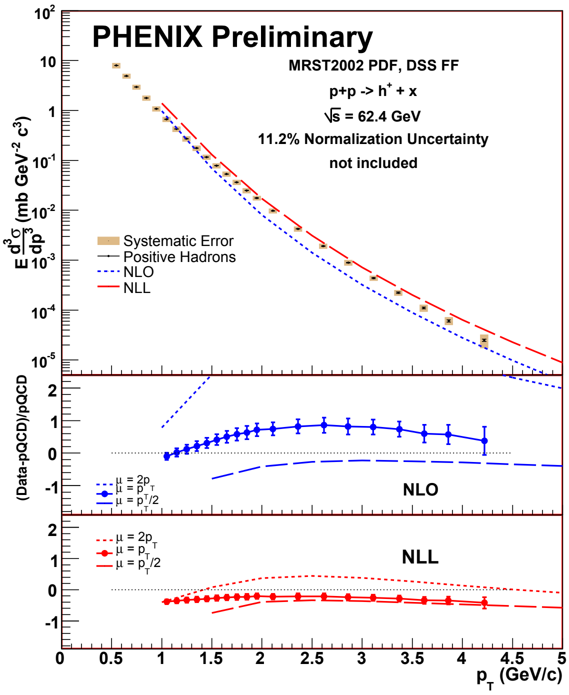

Fig. 1. The invariant cross section for $pp \to h^{+}X$ at $\sqrt{s}$=62.4 GeV is plotted with pQCD predictions[4].

References

1) K. Adcox *et al.* (PHENIX Collab.), Nucl. Instrum. Methods. A **499**, 469-602 (2003).
2) T. Sjöstrand *et al.*, Comput. Phys. Commun. **135**, 238 (2001).
3) A. Adare *et al.*(PHENIX Collab.), arXiv:1102.0753.
4) D. de Florian, W. Vogelsang, and F. Wagner, Phys. Rev. D **76**, 094021 (2007), and private communication.

*1 RIKEN-BNL Research Center, Brookhaven National Laboratory, Upton, NY, USA

*2 Department of Physics, University of Massachusetts, Amherst, MA, USA

RIKEN Accel. Prog. Rep. 44 (2011)

Neutral Pion Production with Respect to the Azimuthal Angle in $\sqrt{s_{NN}} = 200$ GeV Au+Au Collisions at RHIC-PHENIX

Y. Aramaki*, for the PHENIX Collaboration

[Quark Gluon Plasma, Jet quenching, Parton energy loss]

In the most central collisions, the suppression of neutral pion yield at high p_T has been observed, compared to the yield in $p+p$ collisions at $\sqrt{s} = 200$ GeV scaled by the number of nucleon-nucleon collisions in Au+Au at Relativistic Heavy Ion Collider (RHIC). The suppression is a factor of ~ 5 at p_T range of 5–20 GeV/c, while the yield of neutral pion in d+Au are not suppressed. Therefore, the yield suppression in Au+Au is not initial state effect such as Cronin or Shadowing observed in d+Au collisions.

The strong suppression of neutral pion is interpreted as the consequence of parton energy loss with gluon bremsstrahlung in the created dense matter (jet quenching). The magnitude of the energy loss in the created matter depends on the path length which partons pass through. This interpretation of the experimental data is supported by many parton energy loss models. The path length dependence of the energy loss is different formalisms of parton energy loss.

Since the matter created in non-central collision has an almond-shape, path length is strongly associated with azimuthal angle of emitted particles. Some parton energy loss models predict different azimuthal angular dependence of the R_{AA} so that the measurement of the R_{AA} with respect to the azimuthal angle from the reaction plane enables us to understand parton energy loss mechanism more precisely[1)].

In 2006 and 2007, two detectors that can determine the reaction plane precisely, Muon Piston Calorimeter (MPC) and Reaction Plane Detector (RXNP), were installed in RHIC-PHENIX. The determination accuracy for reaction plane was improved by a factor of two compared with the previous measurement at RHIC-PHENIX using MPC and inner RXNP. The $R_{AA}(p_T, \Delta\phi)$ for each azimuthal angle is derived from the $R_{AA}(p_T)$ and azimuthal anisotropy v_2 of π^0.

Recently theoretical models (ASW[2)], HT[3)] and AMY[4)]) to describe parton energy loss mechanism which involve the time-evolution of the medium produced at RHIC have been proposed. Figure 1 shows the comparison of the predictions by the AMY, HT, and ASW models and the measured $R_{AA}(p_T)$ as a function of p_T at centrality 0–5 % and 20–30 %. These models agree with the data well.

Figure 2 shows the R_{AA} as a function of p_T and azimuthal angle for centrality 20-30 % and the prediction by the ASW model which has largest azimuthal angular dependence of R_{AA} in the three models. Since the produced medium after the collisions is assumed to be almond shape, the in-plane path length is shorter than out-of-plane. This difference of the path length is reflected in the R_{AA} with respect to the azimuthal angle. Solid and dashed lines show the theoretical curve for the ASW of in-plane and out-of-plane, respectively.

The parton energy loss models based on pQCD are achieved a certain result that p_T and centrality dependence for R_{AA} is well described, while their models can't reproduce the azimuthal angular dependence of the measured R_{AA}. It indicates that pQCD might not be applicable to the strong-coupled dynamics in the hot and dense matter created at RHIC. Thus, alternate approach which is applicable to the strong-coupled system is needed.

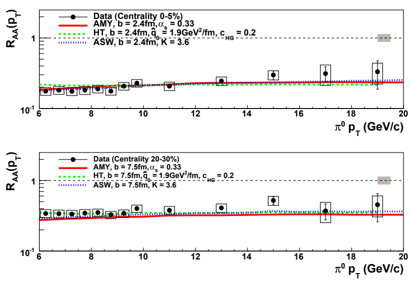

Fig. 1. The R_{AA} as a function of p_T at centrality 0–5 % and 20–30 % and the AMY, HT, and ASW.

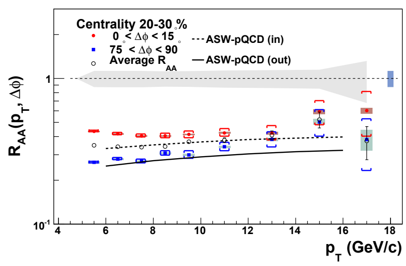

Fig. 2. The in-plane and out-of-plane R_{AA} as a function of p_T at centrality 20-30 % and the ASW.

References
1) S.A. Bass *et al.*: J. Phys. G**35** 104064 (2008).
2) T. Renk *et al.*: Phys. Rev. C**75** 031902 (2007).
3) A. Majumder *et al.*: Phys. Rev. C**76** 041902 (2007).
4) G-Y. Qin *et al.*: Phys. Rev. C**76** 064907 (2007).

* Center for Nuclear Study, Graduate School of Science, University of Tokyo, Japan

Study of K_S production in $\sqrt{s_{NN}} = 200\ GeV\ Au + Au$ collisions at RHIC-PHENIX

M. Nihashi,*1

[Quark gluon plasma, jet quenching, Parton energy loss]

Quantum chromodynamics (QCD) predicts the quark-gluon plasma (QGP) phase at high temperatures of more than 170 MeV[1]. PHENIX has assisted in systematic measurements of the number of hadrons in $Au + Au$ collisions; the results suggest that all meson production is suppressed because of jet quenching which is considered to be an effect of the QGP. Measuring the interactions between scattering partons and the QGP matter is an effective means of understanding its properties; a transport coefficient $\hat{q} = \frac{\mu^2}{\lambda}$, a ratio of the average momentum squared transfer per a scattering μ^2 and the mean free path λ. The interactions can be measured from the nuclear modification factor (R_{AA}), which is the suppression ratio of the particle yield in $Au + Au$ collisions and that in $p + p$ collisions.

One of the models for the jet-medium coupling predicts that the particle yield of particles at a high p_T is significantly changed by the jet conversion process in the QGP matter.

Since there is no valence strange quark in the colliding nuclei the yield of a strange jet at a high p_T is suppressed. Thus if a jet conversion process ($g \rightarrow s + \bar{s}$) occurs, the yield of strange mesons at a high p_T can increase.

We believe that a leading strange parton captures a quark (or quarks) from the QGP medium and becomes a hadron. Light quarks (u, d) are dominant in the QGP, and hence, the leading strange quark at a high p_T is expected to become a K meson. Therefore, the yield of strange mesons such as K_S can be a good indicator of jet conversion. According to a theoretical prediction, R_{AA} of K_S mesons may be twice that of π^0 mesons[2].

In this study, I performed mesurements on K_S mesons (497 MeV) via pion decay mode ($\pi^+\pi^-$, branch ratio is 69.2 %) in $\sqrt{s_{NN}} = 200\ GeV\ Au + Au$ collisions. The first step in the formation of $\pi^+\pi^-$ pairs is to reconstruct charged π meson tracks with drift chambers (wire chamber) in a magnetic field. I calculated the momentum and charge of the particles from these tracks for particle identification (PID) with the time of flight. In this analysis, the background is subtracted by estimating uncorrelated backgrounds from an event-mixing technique. Figure 1 shows the obtained invariant mass spectra of $\pi^+\pi^-$ pairs. I obtained the time of flights from a TOF detector and PbSc EMCal; both the tracks had to go through PID cuts for pions and one had to do not-Kaon PID cuts. The invariant mass spectra for K_S production are shown in Figure 2. Here, the charged track had to be $\pi^+(\pi^-)$ with TOF detector, whose mass was assigned to the charged-pion mass.

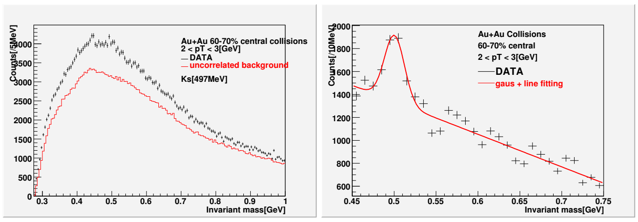

Fig. 1. the $\pi^+\pi^-$invariant mass spectra with two different pion IDs which were obtained by TOF detector and PbSc EMCal. Both PIDs required 2 σ charged pion ID and one required not-Kaon ID too. Red line is uncorreated background obtained by event-mixing technique in the left figure. The right figure shows the result obtained after subtracting uncorrelated backgrounds.

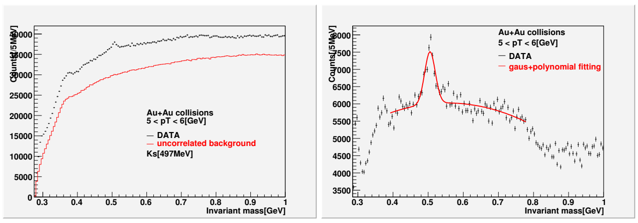

Fig. 2. the $\pi^+\pi^-$invariant mass spectra with TOF PID, which required pion ID only. Red line is uncorreated background obtained by event-mixing technique in the left figure. The right figure shows the result obtained after subtracting uncorrelated backgrounds.

The K_S behavior of R_{AA} has not been clarified. The invariant cross section will be obtained. However, there may be contributions from the hadron interactions in cold nuclear matter (CNM). Thus, CNM effects associated with $d + Au$ collisions must be identified to determine the effect of the interaction between a fast parton and the QGP medium.

References
1) F. Karsch. Lecture Notes in Physics, 2002, Volume 583/2002, 209
2) W. Liu and R. J. Fries. PRC 77, 054902 (2008).

*1 Department of Physics, Hiroshima University

Reconstruction of π^0 pairs in polarized proton-proton collisions at $\sqrt{s} = 200$ GeV at PHENIX

K. Hashimoto,[*1] R. Seidl,[*2] and PHENIX Collaboration

[spin structure of the nucleon, gluon polarization]

1 Introduction

Results from deep inelastic scattering (DIS) experiments show that the quark spin contribution to the proton spin is only about 25 %. In PHENIX, the gluon-spin contribution to the proton spin has been studied for the past 10 years. In recent years, double-helicity spin asymmetries, A_{LL} , have been measured in several production channels ($\pi^0, \pi^\pm$, direct photon, etc). Inclusive π^0 production channel is high statistics and dominant sub-processes are quark-gluon and gluon-gluon scattering.Therefore, π^0 production channel is suitable for studying the gluon spin.

2 Simulation study

The inclusive π^0 production covers a large range of Bjorken x,partonic momentum fraction ($0.02 < x_{Bj} < 0.3$). The goal of our study is to estimate the gluon polarization in a restricted Bjorken x range. In order to restrict the x_{Bj} range of the probed partons,the events with two back-to-back jets in the PHENIX Central Arm acceptance[2)] were selected. As jets cannot be fully reconstructed in the PHENIX electromagnetic calorimeter (EMCAL)[2)], leading π^0s were selected instead. Due to the effect of fragmentation function, probed parton x_{Bj} is more broader than Di-Jets production channel.But still provides a better localized x_{Bj} range. The following procedure was followed:

(1) Select all π^0s in PHENIX Central arms (East arm,West arm) acceptance[2)] in each event.
(2) Select at least one π^0 in each arm.
(3) Select the highest-energy π^0 in each arm per event (labelled π_{east}, π_{west}).

The effect of the π^0 pair selection was studied by performing a simulation. Using the event generator Pythia6[3)] ,the x_{Bj} distribution for the selected π^0 pairs as well as for inclusive π^0 was studied. When the transverse momentum threshold was increased , the mean increased x_{Bj}. x_{Bj} distribution is generally more restricted than the inclusive π^0 channel.

3 Data analysis

Following the simulation, the analysis of the PHENIX 2009 polarized proton-proton data at 200 GeV was performed. First inclusive π^0s were analyzed, and then pairs. To reconstruct π^0s, the PHENIX EMCAL was used, which covers $|\eta| < 0.35$ and $\Delta\phi = \pi/2 \times 2$, and which is located at a distance about 5 m from the collision point. It consists of two calorimeters lead glass (PbGl) and a lead scintillator (PbSc) calorimeters. PbGl is a homogeneous calorimeter made of lead-glass modules whose size is $4.0 \times 4.0 \times 40$ cm^3,and the PbSc is a sampling calorimeter made of alternating tiles of Pb and whose size is $5.535 \times 5.535 \times 37.5$cm^3. The left plot in Fig.1 shows the two-gamma invariant mass spectrum in the East arm vs West arm, the right plot shows the transverse momentum correlation of the selected π^0 pairs. In the left plot in Fig.1, peak position is around π^0 mass (135MeV) in each arm. From the right plot, we can calculate $2\pi^0$ invariant mass as $\sqrt(p_{Teast} \times p_{Twest})$(similar to Di-Jet invariant mass). A preliminary result of the asymmetry A_{LL} will be obtained by the summer 2011. The asymmetry will be plotted against $2\pi^0$ invariant mass. This analysis has been performed at CCJ[4)].

References
1) A. Adare et al.: Physical Review Letters 103 , 012003 (2009).
2) See http://www.phenix.bnl.gov/techpapers.html
3) T. Sjöstrand, L. Lonnblad, S. Mrenna, and P. Skands; PYTHIA 6.3 physics and manual, hep-ph/0308153, (2003).
4) http://ccjsun.riken.jp/ccj/

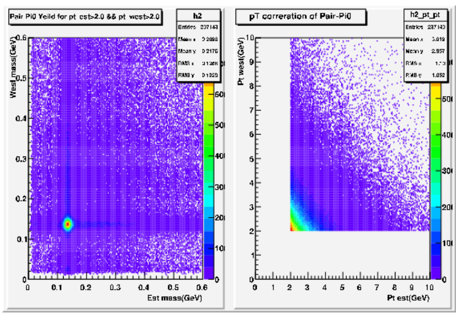

Fig. 1. Left: invariant mass distribution of π^0 pair ; Right: Pt spectrum of π^0 pair

*1 Department of Physics, Rikkyo University, Japan
*2 Riken, Japan

Separation of Charm and Beauty Decays Using the VTX in a Blind Analysis Test

S. Baumgart, Y. Akiba, N. Apdula,[*1] C. Biggs,[*2] S. Chollet,[*3] O. Drapier,[*3] A. Dress,[*1] H. En'yo K. Fujiwara, Y. Haki, K. Hashimoto, R. Ichimaya, Y. Ikegami, J. Kanaya, M. Kasai,[*5] T. Kobayashi,[*4] T. Kondo,[*4] K. Kurita,[*5] M. Kurosawa, J. LaBounty,thanks2 J. Lajoie,[*6] S. Lebedev,thanks6 E. J. Mannel,[*7] Y. Nomiya, R. Nouicer, H. Ohnishi, C. Ogilvie,[*4] Y. Onuki, R. Pak,[*2], C. Pancake,[*1] P. Riedler,[*8] M. Sekimoto, E. Shafto,[*1] S. Shimoda, W. Sondheim,[*10] M. Togawa, A. Taketani, S. Watanabe,[*11] Y. Yamada

The study of heavy flavor and its interactions with the medium as produced by a relativistic heavy-ion collision provide unique insights into the physical nature of the medium. Observables which can be studied via heavy flavor include the total heavy-quark cross-section, collective flow effects, and the nucler modification factor.

The new Silicon Vertex Tracker (VTX)[1] of the PHENIX at RHIC experiment allows the geometric identification of particles from the decays of heavy flavor (charm and bottom mesons). A geometric reconstruction can be either the finding of the decay point of the particle from the intersection of two or more daughter tracks, or it can the distance of closest approach (DCA) of the daughter track (or its extrapolation past its origin point) to the primary collision vertex. The distribution of distances between the primary vertex to the secondary (decay) vertices of a particle species is given by,

$$f(x,p) \propto e^{\frac{-Mx}{\tau |p|}} \tag{1}$$

where x is the distance between the primary vertex and the decay point, M is the mass of the parent particle, τ is the lifetime of the parent, and $|p|$ is the momentum of the parent. Note that separate terms must be added for each additional particle species.

Charm and bottom mesons decay through both semi-leptonic and fully hadronic decay channels. A hadronic decay channel may allow the reconstructed of a particles invariant mass, if all daughters are detected. Semi-leptonic decay analysis rely on the fact that most high-momenta electrons are generated from HF decays [reference]. For electrons, the decay vertex can be reconstructed if a second track is found by the VTX detector. Otherwise, the DCA can be used to identify the particle species.

In order to use the DCAs of daughter tracks to identify the parents, the differences of the DCA distributions of the various particle species is used. A DCA distribution in a particlular pt bin can be parameterized by the following formula,

$$f_i(x) = A_i e^{-\omega_i x^a} \tag{2}$$

where x represents DCA distance, and A and ω are parameters unique to each species. $a \approx 0.58$ is found from fitting the particle distribution in simulation. From simulation it is understood that the ratio of ω parameters from different species is a constant, regardless of the underlying assumptions of the collision. This can be in a combined fit,

$$f_{total}(x) = \sum_{species} A_i e^{-\omega_i x^a} \tag{3}$$

by making assumptions (such as fixing the ratios between the different species of charm mesons like D/D_s), a fit can be made with the charm/bottom ratio as a free parameter. Integration then gives the total yields of charm and bottom decays. In order to use this procedure, an efficiency correction is done using a separate simulation of electron tracks with their transverse momenta and DCAs set to create a flat distribution in both DCA and pt. The DCA procedure has been shown to work for a sample of simulated tracks as shown in Fig. 1.

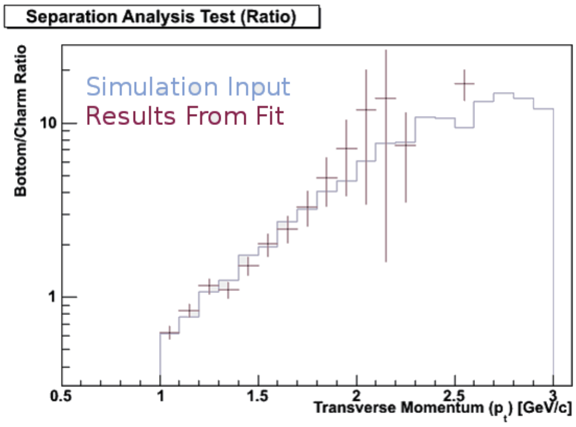

Fig. 1. Bottom and charm yields in a test using a non-blind sample and combined fit.

References

1) Y.Akiba et al.:RIKEN Accel.Prog.Rep.**43** (2010).

*1 Stony Brook University, USA
*2 Brookhaven National Laboratory, USA
*3 LLR, Ecole Polytechnique, CNRS-IN2P3, France
*4 Lawrence Livermore National Laboratory, USA
*5 Rikkyo University, Japan
*6 Iowa State University, USA
*7 Columbia University, USA
*8 European Organization for Nuclear Research, Switzerland
*9 High Energy Accelerator Research Organization, Japan
*10 Los Alamos National Laboratory, USA
*11 Tokyo Metropolitan College of Industrial Technology, Japan

RIKEN Accel. Prog. Rep. 44 (2011)

Simulation and analysis preparations for the PHENIX W→ μ measurements

R. Seidl, Y. Fukao, Y. Imazu, K. Karatsu,[*2] T. Mibe,[*1] T. Murakami,[*2] J. Murata,[*3] K. Nakamura,[*2] I. Nakagawa, S. Park,[*4] N. Saito,[*1] K. Tanida,[*4] and K. Watanabe,[*3]

[proton spin structure, W-boson measurement, sea quark polarization]

The parity violation of the weak interaction connects in real W production to left-handed fermions and right-handed antifermions only. Measuring the W yield for parallel and antiparallel proton polarization states and building the asymmetry one can single out the quark and antiquark helicity distributions. Via the sign of the produced W boson also the quark flavor can be determined as for example W^- are produced from d and $\bar{u}$ quarks. As the PHENIX detector is not a hermetic detector missing transverse momentum tecniques cannot be applied and one measures the Ws inclusively through their leptonic decay electrons or muons. In 2009 the first exploratory proton-proton RHIC run at $\sqrt{s} = 500$ GeV took place which yielded the first result using the central arm and the electron W decay channel[1]. In the forward regions the muon arms were being upgraded[2] and are now ready for the 2011 run. In order to make a successful $W \rightarrow \mu$ cross section and asymmetry measurement one has to understand all possible sources of background. Those contributions could be tested using the 2009 data. The first group of backgrounds are real muons, from heavy flavor decays, however W decay muons in the PHENIX muon arms are dominating over other collision related muon sources in the transverse momentum range of $15 - 40$ GeV and only smearing[3] includes some of them in the signal region. Drell-Yan/Z processes also contribute, but by one order of magnitude lower due to the different branching fractions into muons. The fraction of cosmic muons passing through close to the interaction point was found to be already negligible in dedicated cosmic muon runs and the recently installed RPC's timing[4] will restrict them further. Apart from real muon backgrounds hadrons decaying within the muon tracking volume and mimicking high momentum tracks are the dominant background. Only a small fraction of the hadrons survive the absorbing material upstream of the muon tracking system, but due to the large cross section, especially at the lowest real hadron momenta this contribution is significant. A large effort was undertaken to classify this background and to remove it. The most effective ways turned out to be selection criteria to require tracks to be pointing to a small region around the collision vertex, good agreement of position and angles between the muon tracking system and the muon identifier downstream of it. However even after these selection criteria the yield is still dominating, so another steel absorber was installed to reduce this background by further 80-90%. Some further improvements using the RPC hit information are expected.

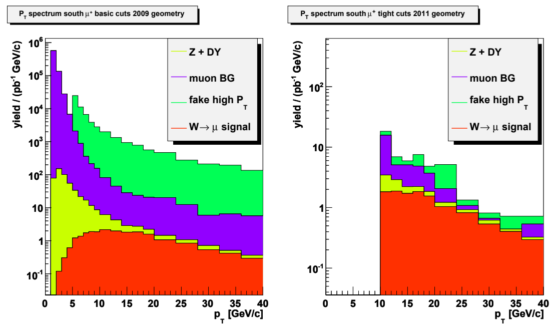

Fig. 1. Stacked, simulated yields for the expected W signal (red) and backgrounds from heavy flavor processes (purple), DY/Z (light green) and false high transverse momentum hadrons(green). The left plot shows the yields after basic selection criteria and the right plot shows tight selection criteria and recently installed additional absorber.

The current simulation results are shown in Fig. 1 which are in agreement with the 2009 data. One clearly sees, that the backgrounds can be reduced by several orders of magnitude and that the yields are now at least comparable above 25 GeV/c with some potential improvements not yet included. For the real muon BG simulations full Pythia + Geant3 detector simulations were performed. The false high transverse momentum backgrounds were obtained using single particle simulations with full detector simulation, scaled according to NLO perturbative QCD calculations.

References
1) A. Adare *et al.* [PHENIX Collaboration], arXiv:1009.0505
2) I. Nakagawa et. al, RIKEN Accel. Prog. Rep. 42 (2009) 216, M. Grosse-Perdekamp, R. Seidl, RIKEN Accel. Prog. Rep. 42 (2009) 219.
3) R. Seidl, B. Meredith and M. Grosse-Perdekamp, RIKEN Accel. Prog. Rep. 42 (2009) 32.
4) M. Grosse Perdekamp, A. Vossen and R. Seidl, for the PHENIX Muon Trigger Upgrade Group, RIKEN Accel. Prog. Rep. 43 (2010) 73.

*1 KEK, Tsukuba, Ibaraki, 305-08011 Japan
*2 Kyoto University, Kitashirakawa-Oiwakecho, Kyoto, 606-8502 Japan
*3 Rikkyo University, Rikkyo, 3-34-1, Nishi-Ikebukuro, Tokyo, 171-8501 Japan
*4 Seoul National University, Seoul, South Korea

4. Hadron Physics (Theory)

RIKEN Accel. Prog. Rep. 44 (2011)

Nucleon Statistics in Holographic QCD : Aharonov-Bohm Effect in a Matrix Model†

K. Hashimoto,[*1] and N. Iizuka[*2]

[Nuclear Force, String theory]

We show that the Aharonov-Bohm effect in the nuclear matrix model[1)] derives the statistical nature of nucleons in holographic QCD. For N_c= odd (even), the nucleon is shown to be a fermion (boson).

The statistics of baryons depends on the number of colors in QCD; in particular for large N_c QCD, as the baryons are bound states of N_c quarks, they are fermions for odd N_c, while bosons for even N_c. The nuclear matrix model[1)] derived in holographic QCD offers a simple effective description of multi-baryon systems, where we can compute baryon spectra, short-distance nuclear forces, and even three-body nuclear forces[2)]. However, since the nuclear matrix model has only bosonic variables, it is natural to ask how the fermionic nature of baryons comes out from the matrix model. In chiral soliton models, this question was answered from the properties of Wess-Zumino term[3)].

To identify the statistics (fermionic/bosonic) of nucleons in the nuclear matrix model, we consider a 2π rotation in the target space of the matrix model. The target space index is carried by X^M and $w_{\dot\alpha i}$. The effect on X^M is trivial, since X decouples from the system in the matrix model for a single baryon ($k = 1$) once the ADHM constraint is solved. However, since we have a nontrivial gauge field A_0, there is a nontrivial effect on the $w_{\dot\alpha i}$ sector. In fact, this gauge field A_0 turns out to be responsible for the statistics of the baryons, as we will see.

In the nuclear matrix model, the terms including the fundamental field $w_{\dot\alpha i}$, except for the ADHM potential terms and the mass term, are

$$S = \frac{\lambda N_c M_{\rm KK}}{54\pi} \int dt\, D_0 \bar{w}_i^{\dot\alpha} D_0 w_{\dot\alpha i} + N_c \int dt\, A_0 \,. \quad (1)$$

$\dot\alpha$ is a spinor index which is for $SU(2) \simeq SO(3)$ spatial rotation in the target space. $i = 1, \cdots, N_f$ is a flavor index. This is a one-dimensional gauge theory whose gauge field is A_0. The covariant derivative is defined as $D_0 w_{\dot\alpha i} \equiv \partial_0 w_{\dot\alpha i} - i w_{\dot\alpha i} A_0$. Note that A_0 is a gauge field for $U(k)$ gauge symmetry of the matrix model, so, for $k = 1$ (single baryon), A_0 does not carry any non-Abelian index.

Let us make a spatial rotation, for example along the x^3 axis, by an angle 2π. Since $w_{\dot\alpha i}$ carries a spinor index of the target space, it is obvious that the spatial rotation acts for the case of the rotation around the x^3 axis with an angle θ, as

$$w_{\dot\alpha i} \to U_{\dot\alpha}^{\ \dot\beta} w_{\dot\beta i} \,, \quad U = \exp\left[i\frac{\theta}{2}\tau^3 \right] . \quad (2)$$

Here τ^3 is the third component of Pauli matrices. Our spatial rotation by 2π means that the angle θ moves in the period $0 \le \theta \le 2\pi$.

As shown in[1)], the vacuum of the matrix model for $k = 1$ is quite simple,

$$w = \begin{pmatrix} \rho_0 & 0 \\ 0 & \rho_0 \end{pmatrix} . \quad (3)$$

After minimizing the hamiltonian, we obtain a certain nonzero value for this ρ_0. So the spatial rotation (2) corresponds to a certain path in the target space of $w_{\dot\alpha i}$. In the following, we would like to compute an Aharonov-Bohm phase with this path.

We are interested in a phase change of a baryon wave function. The argument of the wave function is the moduli of this matrix model, and it is a part of $w_{\dot\alpha i}$ configuration space. If we think of the path of $w_{\dot\alpha i}$ defined by (2), then the phase of the wave function of our concern is in fact an Aharonov-Bohm (AB) phase, for the path (2), as if we regard the lower-right entry of the matrix field $w_{\dot\alpha i}$ as a position of a charged particle. Indeed, since it was shown in[1)] that solving the equation of motion for A_0, gives $A_0 = -27\pi/2\lambda M_{\rm KK}\rho_0^2$, which is a real constant, we could obtain the phase explicitly as

$$\Phi = N_c \pi \,. \quad (4)$$

This AB phase means that, when N_c is odd, the spatial rotation by the angle 2π results in a sign (-1) multiplied to the baryon wave function. Therefore, when N_c is odd (even), the baryon is a fermion (boson).

It is intriguing that a simple mechanism, the AB phase, is encoded in the nuclear matrix model naturally to ensure the baryon statistics in holographic QCD.

References

1) K. Hashimoto, N. Iizuka and P. Yi, JHEP **1010** (2010) 003.
2) K. Hashimoto and N. Iizuka, JHEP 1011 (2010) 058.
3) E. Witten, Nucl. Phys. B **223**, 433 (1983).

† Condensed from the article in Phys. Rev. **D82** 105023 (2010)

*1 Mathematical Physics Lab., RIKEN Nishina Center
*2 Theory Division, CERN

Quark mass dependence of hadron spectrum in holographic QCD[†]

K. Hashimoto,[*1] T. Hirayama,[*2] and D.-K. Hong,[*3]

[Hadron, String theory]

We compute a shift of baryon mass spectra due to quark masses in perturbation, in Sakai-Sugimoto model of holographic QCD. We find the shift for the ground state nucleons to be $\delta M = 4.1\ m_\pi^2\,\mathrm{GeV}^{-1}$, which is consistent with the current lattice QCD result. We predict the same value of the shift for N(1535) and Δ, while a larger value $7.7\ m_\pi^2\,\mathrm{GeV}^{-1}$ for Roper N(1440). We also present some evidences that the shifts of the vector meson masses are suppressed in the large 't Hooft coupling limit.

Recent progress in holographic QCD of string theory enables us to compute the important physical observables of QCD: the hadron masses. QCD has only two kinds of dimension-ful parameters: the prime one is the QCD scale which basically generates all the hadron masses, and the quark masses. For the light quarks, the quark masses can be treated as a perturbation (while heavy quarks have their particular importance in various phases in QCD). In this short paper, we present a computation of the hadron mass shift due to the quark masses, in the Sakai-Sugimoto model[1)] which is the most successful model of holographic QCD so far.

Sakai-Sugimoto model is a holographic dual of *massless* QCD. There proposed two ways to introduce the quark mass to the model: (i) worldsheet instantons[2,3)], and (ii) tachyon condensation of the D8/$\overline{\mathrm{D8}}$-branes[4)]. We are going to use the worldsheet instanton method (i), since the other method (ii) assumes a tachyon "effective" action which is difficult to be validated in any manner in string theory except for using string field theories.

The worldsheet instanton produces the quark mass term in QCD, and the gravity dual of the worldsheet instanton generates a term of the form

$$\delta L = c\,\mathrm{tr}\,[MU] \tag{1}$$

where M is the quark mass matrix of the form $M = \mathrm{diag}(m_\mathrm{u}, m_\mathrm{d})$, and U is the pion field in the standard notation in the chiral perturbation theory: $U \equiv \exp[2i\pi(x)/f_\pi]$. The value c is computed from the worldsheet instanton amplitude, but it turned out to be difficult to evaluate. Except for the pion mass through 1, the contribution of quark masses to other meson masses has not been computed yet.

† Condensed from the article in Phys. Rev. **D81**:045016 (2010)

*1 Mathematical Physics Lab., RIKEN Nishina Center

*2 Physics Division, National Center for Theoretical Sciences, Hsinchu, Taiwan

*3 Department of Physics, Pusan National University

In this paper, we present two computations. First, we compute shift of the baryon mass spectra due to the quark mass, by assuming that the quark mass dependence in the meson effective lagrangian of the Sakai-Sugimoto model appears only in the new term (1), at the leading order in expansion in $1/\lambda$. We also show that shift of the vector/axial vector meson masses is small and at a higher order in $1/\lambda$ expansion.

As noted in[1)] and computed in detail in[5)], the baryon in the Sakai-Sugimoto model is nothing but an instanton-like soliton in the 5-dimensional Yang-Mills-Chern-Simons (YMCS) action describing all the mesons effectively in a unified way. The term (1) can be thought of as a perturbation to the YMCS action, so the mass shift can be computed by just inserting the soliton configuration obtained in[5)] to (1). The resultant correction is evaluated with baryon wave functions of[5)]. Since the parameter c is undetermined, we obtain the baryon mass as a function of the pion mass. Our result for nucleons is in rough agreement with results of lattice QCD. The mass shifts for N(1535) and Δ turn out to be the same as that of the nucleons, while the shift for Roper N(1440) is larger.

Using $M_{\mathrm{KK}} = 949$ [MeV] and $\kappa \equiv a\lambda N_c = 0.00745$ which were used in[1)], we obtain the value of the baryon mass shift for the nucleon as

$$\frac{\delta M_{n_\rho=0}}{m_\pi^2} = 4.11\ [\mathrm{GeV}^{-1}]\ . \tag{2}$$

We can compare our result (2) with numerical results obtained in lattice QCD simulations. For example, a lattice result for nucleons in[6)] shows $\delta M_{\mathrm{nucleon}}/m_\pi^2 = 4 \times 1.02(7)$ [GeV^{-1}].

References

1) T. Sakai and S. Sugimoto, Prog. Theor. Phys. **113**, 843 (2005), Prog. Theor. Phys. **114**, 1083 (2006)
2) O. Aharony and D. Kutasov, Phys. Rev. D **78**, 026005 (2008)
3) K. Hashimoto, T. Hirayama, F. L. Lin and H. U. Yee, JHEP **0807**, 089 (2008)
4) *"Chiral symmetry breaking as open string tachyon condensation,"* Nucl. Phys. B **787**, 98 (2007)
5) H. Hata, T. Sakai, S. Sugimoto and S. Yamato, *"Baryons from instantons in holographic QCD,"* Prog. Theor. Phys. **117**, 1157 (2007) [arXiv:hep-th/0701280].
6) D. Brommel *et al.*, arXiv:0804.4706 [hep-lat].

Tests of running-coupling BK evolution at LHC energies†

A. Dumitru,*1

[QCD, high energy, gluon saturation]

The Balitsky-Kovchegov (BK) equation determines the forward scattering amplitude of a color dipole (in the fundamental representation of large-N_c QCD) on a dilute or dense target. Its accuracy has recently been boosted substantially when running-coupling corrections became available[1)]. These corrections are essential for quantitative phenomenology such as a successfull description of inclusive proton structure functions measured at HERA[2)].

The rcBK evolution equation needs to be supplemented with appropriate initial conditions at some initial scale $x_0 \sim 10^{-2}$. Results shown below and in ref.[3)] were obtained using a McLerran-Venugopalan model initial condition,

$$\mathcal{N}_F(r, x = x_0) = 1 - \exp\left[-\frac{r^2\, Q_{s0}^2}{4}\, \ln\left(\frac{1}{\Lambda\, r} + e\right)\right] . (1)$$

The initial saturation scale Q_{s0} measures the local density of sources with $x > x_0$ at a given point in the transverse plane. For a proton with trivial impact parameter profile, $Q_{s0}^2 \approx 0.2$ GeV^2 leads to a reasonable fit to HERA inclusive structure functions[2)], and also to a good fit of RHIC and LHC multiplicities in heavy-ion collisions (see below). For nuclei, of course, Q_{s0}^2 is enhanced by the number of stacked up nucleons.

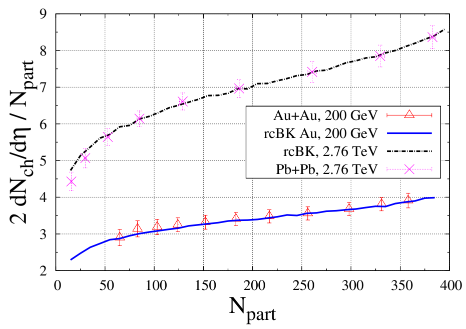

Fig. 1. Centrality dependence of the charged particle multiplicity at midrapidity ($\eta = 0$) for Pb+Pb collisions at $\sqrt{s} = 2.76$ TeV. ALICE data from ref.[4)].

The multiplicity can be calculated from the k_t-factorization formula[3)] if the p_t-integrated parton multiplicity is proportional to that of hadrons, cf. fig.1. The good agreement with the data indicates that the x and A dependence of the saturation scale is reasonably accurate, over at least an order of magnitude in both x and A. It is then interesting to test the theory in the dilute regime, for p_t well above the scale Q_s. At LHC energies the opportunity for particle production *at small-x but with high p_t* arises.

The p_t distribution of charged hadrons (fig.2) has been obtained by a convolution with a $g \to h^{\pm}$ fragmentation function. Clearly, the calculated number of high-p_t hadrons is much too high. We stress that the normalization and the initial saturation scale Q_{s0} is the same as for fig.1 above.

The failure to reproduce the correct number of high-p_t hadrons can be traced back to the hard p_t distribution of gluons predicted by our current approach at TeV energies. We interpret this as a clear indication that the MV-model initial condition (1) is much too flat at $rQ_{s0} < 1$ which demonstrates the excellent reach of LHC into the small-x, high-p_t regime. Somewhat less striking indications for a more rapid drop-off of the initial unintegrated gluon distribution at high k_t have also been reported from DIS fits to HERA.[2)] It will be most interesting to see whether more realistic initial conditions for rcBK evolution agree with the data from LHC.

References

1) Y. Kovchegov and H. Weigert, Nucl. Phys. **A 784**, 188 (2007); I. Balitsky, Phys. Rev. **D75**, 014001 (2007); E. Gardi, J. Kuokkanen, K. Rummukainen, and H. Weigert, Nucl. Phys. **A784**, 282 (2007).
2) J. L. Albacete, N. Armesto, J. G. Milhano, and C. A. Salgado, Phys. Rev. **D80**, 034031 (2009).
3) J. L. Albacete and A. Dumitru, arXiv:1011.5161 [hep-ph]
4) ALICE Collaboration, arXiv:1012.1657 [nucl-ex]
5) V. Khachatryan *et al.* [CMS Collaboration], Phys. Rev. Lett. **105**, 022002 (2010).

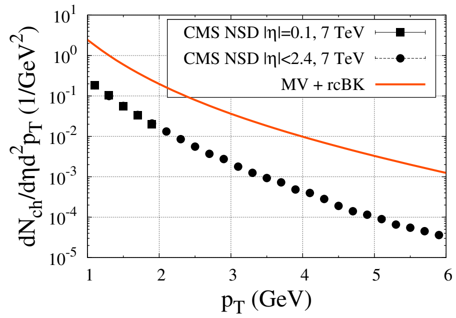

Fig. 2. Charged hadron transverse momentum distribution in pp collisions at $\sqrt{s} = 7$ TeV. CMS data from ref.[5)].

*1 Department of Natural Sciences, Baruch College (CUNY), New York and RIKEN BNL Research Center (RIKEN fellow)

NJL-jet model for quark fragmentation to hadrons†

W. Bentz,*1 H. Matevosyan,*2 and A. W. Thomas*2

[QUARK FRAGMENTATION FUNCTIONS, Semi-inclusive hadron production, Deep inelastic scattering]

In order to describe quark fragmentation processes in semi-inclusive deep inelastic scattering, the NJL-jet model has been developed recently[1)]. In this model, the total fragmentation functions $D_q^h(z)$ are expressed as infinite products of elementary ones, which are calculated in the Nambu-Jona-Lasinio (NJL) model. This product ansatz, which has been formulated first by Field and Feynman[2)], describes multi-fragmentation processes in such a way that the momentum and isospin sum rules

$$\sum_h \int_0^1 dz\, z\, D_q^h(z) = 1\,, \qquad \sum_h \int_0^1 dz\, t_h\, D_q^h(z) = t_q$$

are satisfied naturally without introducing any new parameters into the theory. The physical content of these sum rules is that 100% of the light-cone momentum and isospin of the quark q are converted to hadrons h. Restricting the hadrons h to the primary pions and kaons, this model has been used in Ref.[1)] and[3)] to obtain results which can be compared with the empirical fragmentation functions.

Recently[4)] we have considered an extension of the model, which includes the pion, kaon, nucleon and antinucleon channels, as well as the effects of intermediate rho mesons which subsequently decay into secondary pions. The coupled integral (chain) equations can be solved numerically to obtain the fragmentation functions at the low energy (model) scale. In order to compare with the empirical functions, one has to perform the Q^2 evolution from the model scale to the high energy scale. In this Report, we will show some results at the model scale, and refer to[4)] for the results of the next-to-leading order Q^2 evolution and the comparison with the empirical functions.

Our results for the *favored* fragmentation processes $u \to \pi^+$, $u \to K^+$, $u \to P$ are shown in Fig.1. In this calculation, the elementary NJL fragmentation functions were calculated by using the invariant mass regularization scheme. The model parameters were chosen so as to reproduce the experimental values for the pion mass, the pion decay constant, and the kaon mass. The constituent u and d quark mass was fixed to $M = 300$ MeV. The support of the functions shown in Fig.1 for intermediate and small z comes mainly from the multi-fragmentation processes. The contributions of the various hadron channels to the momentum sum rule are shown in Fig.2. We see that a large part of the light-cone momentum of the u-quark is transferred to pions, followed by kaons, nucleons and antinucleons.

We finally remark that it would be very interesting to extend these calculations to finite baryon density. Since the NJL model has been used already to obtain in-medium quark distributions functions[5)], one could use the model to make predictions for semi-inclusive hadron production processes on nuclear targets.

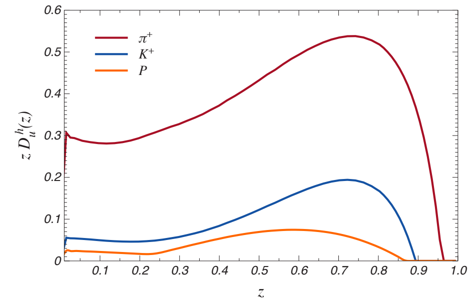

Fig. 1. *Favored* fragmentation functions $zD_u^h(z)$ for the cases $h = \pi^+$, K^+ and P, obtained in the NJL-jet model at the low energy (model) scale.

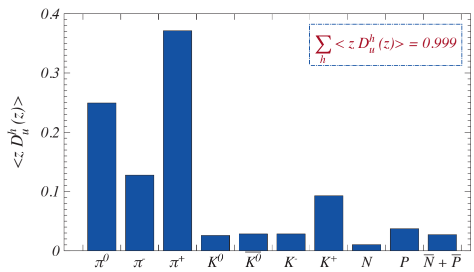

Fig. 2. The contributions $\langle zD_u^h(z)\rangle = \int_0^1 z\,\mathrm{d}zD_u^h(z)$ of various hadrons h to the momentum sum rule for the u quark at the low energy (model) scale.

References

1) T. Ito, W. Bentz, I.C. Cloët, A.W. Thomas, K. Yazaki, Phys. Rev. D **80**, 074008 (2009).
2) R. D. Field and R. P. Feynman, Phys. Rev. D **15**, 2590 (1977).
3) H. Matevosyan, W. Bentz, A.W. Thomas, arXiv:1011.1052 [hep-ph].
4) H. Matevosyan, W. Bentz, A.W. Thomas, to be published (2011).
5) I.C. Cloët, W. Bentz, A.W. Thomas, Phys. Lett. **B 642** (2006) 210.

† Condensed from an article by H. Matevosyan, W. Bentz and A.W. Thomas, to be published (2011).

*1 Department of Physics, Tokai University, Kanagawa, Japan
*2 University of Adelaide, Adelaide, Australia

Neutral B-meson mixing matrix elements

Y. Aoki,[*1] T. Ishikawa,[*2] T. Izubuchi[*3] (for RBC and UKQCD collaborations)

[Lattice QCD, Standard Model, Flavor Physics]

The neutral B-meson mixing matrix elements in the standard model are defined as

$$\mathcal{M}_q = \left\langle \bar{B}_q^0 \right| [\bar{b}\gamma^\mu(1-\gamma_5)q][\bar{b}\gamma_\mu(1-\gamma_5)q] \left| B_q^0 \right\rangle \quad (1)$$

for B^0 $(q=d)$ and B_s^0 $(q=s)$ mesons. Due to the CP violation through Kobayashi-Maskawa mechanism the B^0 and $\overline{B^0}$ mesons acquire different mass. The mass difference in the standard model is expressed using the $\mathcal{M}_q$ and CKM matrix V,

$$\Delta m_q = [\text{known factor}] \cdot |V_{tq}^* V_{tb}|^2 \mathcal{M}_q. \quad (2)$$

The experimental accuracy of the mass difference observed through the oscillation frequency is sub-percent, thanks to Belle, BaBar and Tevatron experiments. This opens up the opportunity to determine the CKM matrix elements precisely and further to search the new physics beyond the standard model through CKM unitarity. The $(V-A)^2$ type four-fermi operator of $\Delta b = 2$ process in Eq. (1) is induced by the one-loop box diagram of the Weinberg-Salam model. Since the interaction is remarkably enhanced for the heavier fermion inside the loop, this process is highly sensitive to existence of the heavy new particle.

The baton for this important physics goal is now passed to the lattice QCD, by which the highly non-perturbative matrix elements $\mathcal{M}_q$ can be determined form the first principles. By historical reason matrix element sometimes is written with mass m_{B_q} and decay constant f_{B_q} being factorized as $\mathcal{M}_q = \frac{8}{3} m_{B_q}^2 f_{B_q}^2 B_{B_q}$, which defines the bag parameter B_q. The difference of the matrix element for d and s is only brought by the mass difference between d and s quarks. In lattice calculation the flavor $SU(3)$ breaking ratio $\xi = f_{B_s}\sqrt{B_{B_s}}/f_{B_d}\sqrt{B_{B_d}} \propto \sqrt{\mathcal{M}_s/\mathcal{M}_d}$ can be obtained more precisely than the each matrix element, since the large fraction of the statistical and systematic errors cancel in the ratio. Through ξ (theory) and $\Delta m_s/\Delta m_d$ (experiment), the ratio $|V_{td}/V_{ts}|$ is determined. $|V_{td}/V_{ts}|$ provides an important constraint on the unitarity triangle. As the error of the ratio from the experiment is small (sub-percent), the error of the lattice calculation of ξ dominates the width of the allowed range of $|V_{td}/V_{ts}|$.

To achieve the required high precision, the full $2+1$ flavor lattice QCD calculation of ξ is indispensable. The RBC/UKQCD collaborations have been trying to calculate the mixing matrix elements employing static approximation in the heavy quark effective theory (HQET) with the $2+1$ flavor domain wall fermions for the light flavors. The $SU(3)$ breaking ratio ξ calculated with two different heavy quark discretization scheme (APE and HYP2) are shown as function of u, d quark mass in Fig. 1 (red and green)[1]. We are improving this results to obtain much more precise number of the matrix element. The key issues to achieve this will be a) to have smaller quark mass for the extrapolation of the u, d quarks to the physical point, where larger physical volume must be used to make the finite volume effect negligible; b) to have better signal/noise ratio, optimization of quark source smearing parameter should be fine-tuned; c) to determine matrix elements and the mixing coefficients of higher dimensional operators to get lid of $O(a)$ discretization error, where a is the lattice spacing; d) to have no discretization error, the second lattice spacing is needed for the continuum extrapolation $a \to 0$. Having accomplished a) and b) a preliminary result have been obtained with better accuracy than the previous study and shown as blue symbol in Fig. 1. The perturbative study has been completed[2] for c). Now the preparation of the continuum extrapolation d) is underway.

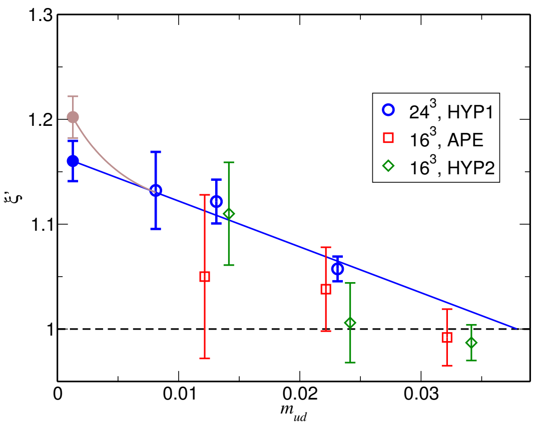

Fig. 1. Ratio M_s/M_d of the $B^0 - \overline{B^0}$ mixing matrix elements $M_q = \mathcal{M}_q m_{B_q}$ renormalized at m_b with $\overline{\text{MS}}$, NDR as functions of m_{ud}. A new preliminary result (24^3, HYP1) is compared to those published[1].

This project is supported in part by US DOE through USQCD collaboration, Japanese MEXT grant Kakenhi No. 21540289, RIKEN RICC.

References

1) C. Albertus, et al., Phys. Rev. D 82 (2010) 014505.
2) T. Ishikawa, et al., arXiv:1101.1072.

*1 Nagoya University, KMI
*2 University of Connecticut
*3 RIKEN-BNL Research Center

Nucleon structure from lattice QCD

Y. Aoki,[*1,*2] T. Blum,[*1,*3] T. Izubuchi,[*1,*4] C. Jung,[*1,*4] M.F. Lin,[*1,*5]
S. Ohta,[*6,*7,*1] S. Sasaki,[*1,*8] and T. Yamazaki[*2]

[Nucleon Structure, Lattice QCD]

The internal structure of nucleon is of great interest for nuclear and particle physics. Many experiments worldwide, like those at the Jefferson (JLab) and Brookhaven (BNL) National Labs, are actively probing the fundamental properties and internal structure of the nucleon. In particular, the RIKEN-sponsored RHIC-Spin experiment at Brookhaven National Laboratory in the US probes the spin structure of the nucleon. Non-perturbative first-principles lattice QCD calculations of nucleon structure will help us gain insight to the strong interactions, and help interpret the experimental data.

While the techniques for lattice calculations of nucleon structure have been well established, one of the remaining issues is that the pion masses in the calculations are heavier than the physical value, and extrapolations to the physical pion mass of 140 MeV are needed to obtain results to be compared with the experiments. To reduce the systematic errors associated with these extrapolations, we recently started nucleon structure calculations with domain wall fermions[1)] at pion masses of 180 MeV and 250 MeV[2)]. These are the first lattice calculations at such light pion masses with chiral fermions, and have the potential to produce results with unprecedented precision.

A precision test of our lattice calculations is to see if we could reproduce the well-known nucleon mass, m_N, of about 939 MeV. Fig. 1 shows our preliminary results for m_N from this and previous lattice calculations done by the RBC and UKQCD collaborations. While no chiral extrapolations have been performed yet, we observe that our results roughly fall on the same curve as the previous lattice calculations with heavier pion masses, and lead smoothly to the experimental result.

Another example of the quality of our data is the isovector vector charge g_V, which sets the overall renormalization of our vector and axial vector form factor calculations. Shown in Fig. 2 is the preliminary result for g_V as a function of the Euclidean time t for $m_\pi = 250$ MeV. Averaging over the plateau region in the middle gives $g_V \approx 1.45$, which is consistent with the value determined from an independent calculation with conserved axial vector current. We are now accumulating data for the determination of isovector nucleon vector and axial vector form factors, nucleon axial charge, isovector momentum and helicity fractions, transversity, and d_1, and expect to have some preliminary results soon.

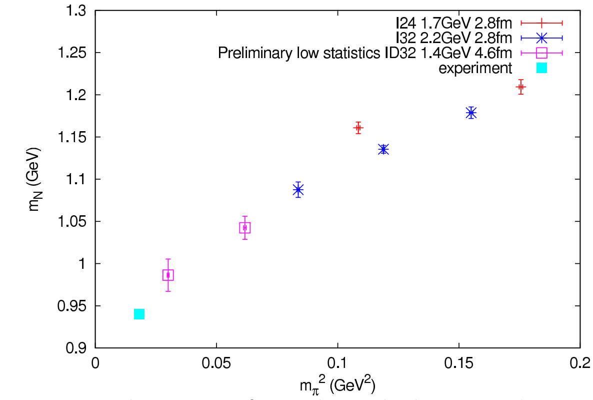

Fig. 1. Nucleon mass from this calculation and previous lattice calculations.

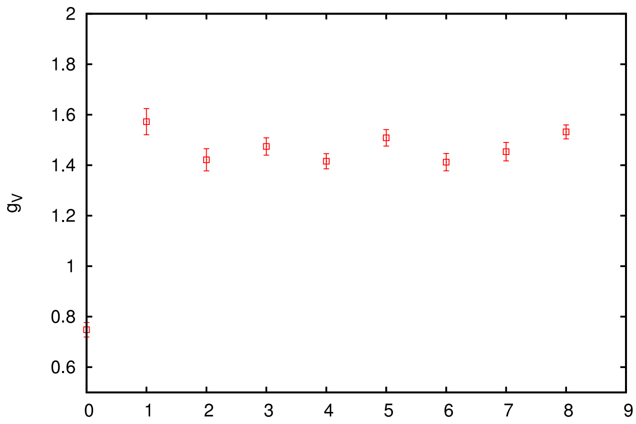

Fig. 2. Nucleon isovector vector charge g_V for the $m_\pi = 250$ MeV ensemble.

These calculations were performed on the RIKEN Integrated Cluster of Clusters (RICC) at the Advanced Center for Computing and Communication, RIKEN. The gluon field configurations used in these calculations were generated by the RBC and UKQCD collaborations[3)] .

*1 RIKEN-BNL Research Center, U.S.A.
*2 Kobayashi-Maskawa Institute for the Origin of Particles and the Universe (KMI), Nagoya University
*3 Department of Physics, University of Connecticut, U.S.A.
*4 Brookhaven National Laboratory, U.S.A.
*5 Department of Physics, Yale University, U.S.A.
*6 Institute of Particle and Nuclear Studies, KEK
*7 Department of Particle and Nuclear Physics, SOKENDAI
*8 Department of Physics, University of Tokyo

References

1) T. Blum *et al.*, Phys. Rev. D **69**, 074502 (2004).
2) S. Ohta [for the RBC and UKQCD Collaborations], PoS **LATTICE2010**, 152 (2010).S. Ohta [for the RBC and UKQCD Collaborations], arXiv:1102.0551 [hep-lat].
3) C. Jung, PoS **LAT2009**, 002 (2009).

Inter-quark and meson-baryon potentials with strangeness on lattice

Y. Ikeda

Strongly interacting systems with the strange quark (s) or the anti-strange quark ($\bar{s}$) are shedding light on new features of hadrons. Since the mass of s-quark is comparable to the typical scale of quantum chromodynamics (QCD), the non-perturbative nature of QCD plays an important role. The non-perturbative dynamics with s- and/or $\bar{s}$-quark is investigated in lattice QCD (LQCD), which provides us with the first principle results of the strong interaction.

One of interest is the inter-quark interaction for the s-$\bar{s}$ system. The inter-quark potentials are usually studied by Wilson loop approach in LQCD. This approach can be applied to the heavy quarks. To study the relatively light quark such as the s-quark, it may be difficult to utilize Wilson loop approach. We propose a new method to extract the inter-quark potentials including the s-quark from the Nambu-Bethe-Salpeter (NBS) wave functions on lattice, which has been used in two-nucleon systems[1]. The NBS wave function $\psi(\vec{r})$ of the $\bar{q}$-q systems are measured on lattice as follows:

$$\psi(\vec{r}) = \sum_{\vec{x}} \langle 0|\, \bar{q}(\vec{x}+\vec{r},t)\Gamma q(\vec{x},t)\overline{\mathcal{J}}_{\bar{q}q}(t_0)\,|0\rangle\,, \qquad (1)$$

and the potentials are calculated with the effective Schrödinger equation:

$$-\frac{\nabla^2}{2\mu}\psi(\vec{r}) + \int d\vec{r'}U(\vec{r},\vec{r'})\psi(\vec{r'}) = E\psi(\vec{r}), \qquad (2)$$

where $\mu(= m_q/2)$ and E denote the reduced mass of the $\bar{q}$-q system and the non-relativistic energy, respectively. We expand the non-local potential in terms of the velocity:

$$\begin{aligned} U(\vec{r},\vec{r'}) &= V(\vec{r},\vec{v})\delta(\vec{r}-\vec{r'}) \\ &= (V_{LO}(\vec{r}) + V_{NLO}(\vec{r})\vec{L}\cdot\vec{S} + \cdots)\delta(\vec{r}-\vec{r'}), \end{aligned} \qquad (3)$$

where the non-locality is determined order by order. By applying this method with the leading order potential $V_{LO}(\vec{r})$, we systematically investigate the inter-quark potentials with different quark masses. As shown in Fig. 1, we obtain the linear confinement potential and the Coulomb potential even for the $\bar{s}$-s system, which is consistent with the string picture of the confinement mechanism. The string tension is comparable to that of Wilson loop approach. On the other hand, the Coulomb interaction is much modified by light s-quark motions[2].

We also study the meson-baryon interactions with strangeness. In this study we focus on the KN scatterings on lattice, because these channels maybe relevant to the recently reported exotic particle Θ^+. The NBS wave functions and the potentials for the KN state with $J^P = 1/2^-$ reveal the scattering states in both $I = 0, 1$ as shown in Fig. 2. Thus, we conclude that the possibility of existing Θ^+ in $J^P = 1/2^-$ is doubtful[3].

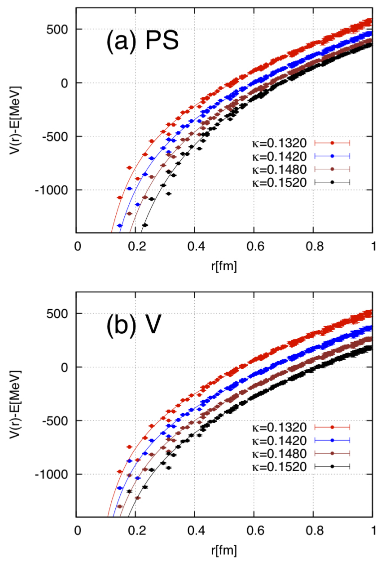

Fig. 1. Inter-quark potentials with various quark masses in pseudoscalar (a) and vector (b) channels.

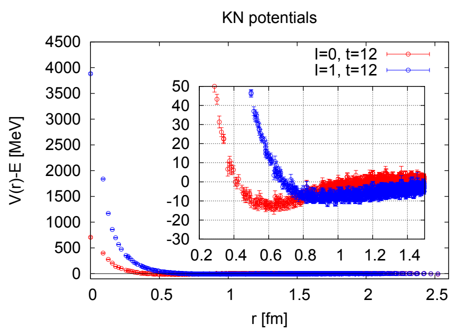

Fig. 2. The KN potentials in $I = 0, 1$.

This work is done in collaboration with H. Iida and by HAL QCD Collaboration.

References

1) N. Ishii, S. Aoki and T. Hatsuda, Phys. Rev. Lett. **99** (2007) 022001; S. Aoki, T. Hatsuda and N. Ishii, Prog. Theor. Phys. **123** (2010) 89.
2) Y. Ikeda and H. Iida, PoS **LATTICE2010** (2010) 143.
3) Y. Ikeda *et al.* [HAL QCD Collaboration], arXiv:1002.2309 [hep-lat]; Prog. Theor. Phys. Suppl. No. 186 (2010) 228.

Meson screening masses at finite temperature and finite density with two-flavor Wilson fermions

H. Iida, Y. Maezawa, and K. Yazaki

Mesons in a medium are expected to have abundant information about the characteristic properties of QCD, such as the deconfinement phase transition at finite temperature and the partial chiral symmetry restoration at finite density[1)]. Here, we report our recent study on meson screening masses at finite temperature and finite density with two-flavor Wilson fermions in lattice QCD. Using gauge configurations generated by WHOT-QCD Collaboration[2)], we calculate the meson correlation functions along the line of constant physics and extract information on the temperature dependence of the meson screening masses from the long-range behavior of the correlators.

First, we show the temperature dependence of meson screening masses. Figure 1 shows the meson screening masses normalized by the temperature, M_0/T, in a PS channel as a function of $T/T_{\rm pc}$, where $T_{\rm pc}$ is the pseudo-critical temperature. The circles (triangles) correspond to the results at $m_{\rm PS}/m_{\rm V}|_{T=0} = 0.65$ (0.80). We can see a concave structure around $T_{\rm pc}$, that is, when the temperature increases, M_0/T decreases below $T_{\rm pc}$, whereas it increases above $T_{\rm pc}$. This implies that the screening masses M_0 are constant below $T_{\rm pc}$, while they monotonically increase above $T_{\rm pc}$. The thermal effect on the meson screening masses becomes apparent in the quark-gluon plasma phase. At high temperatures, M_0/T converges to a constant value of 2π, which implies that the meson becomes a weakly interacting quark-antiquark pair with each quark/antiquark having a thermal mass πT. We also find clear quark-mass dependence, i.e., the magnitude of the screening masses with a lighter quark mass ($m_{\rm PS}/m_{\rm V}|_{T=0} = 0.65$) is smaller than that with a heavier quark mass ($m_{\rm PS}/m_{\rm V}|_{T=0} = 0.80$), similar to the case of the ordinary meson mass measured by temporal correlation. This implies that the screening of the meson spatial correlation becomes weak when the quark mass becomes small.

We also investigate the properties of the screening masses at finite density. The second response of the screening masses $M(\tilde{\mu})$ to the quark chemical potential $\tilde{\mu} \equiv \mu/T$, $M_2 \equiv \partial^2 M(\tilde{\mu})/\partial\tilde{\mu}^2|_{\tilde{\mu}=0}$, is calculated via the Taylor expansion method. Figure 2 shows the temperature dependence of M_2/T in the PS channel, with $m_{\rm PS}/m_{\rm V}|_{T=0} = 0.65$ (circles) and 0.80 (triangles). We find that M_2/T is always positive in the temperature range considered, which implies that the screening masses increase in the leading order contribution of μ. M_2/T increases rapidly at $T_{\rm pc}$, which means that the density effect on the meson screening-masses becomes significant in the quark-gluon plasma phase.

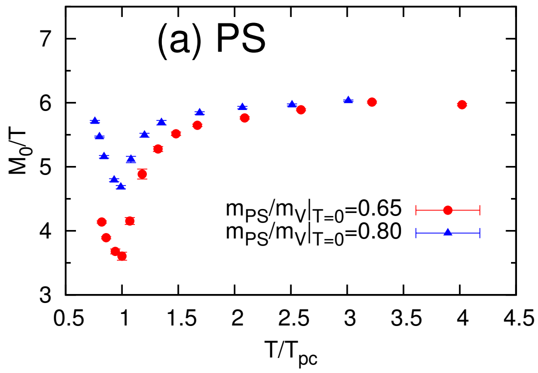

Fig. 1. Meson screening masses M_0/T in the PS channel as a function of temperature.

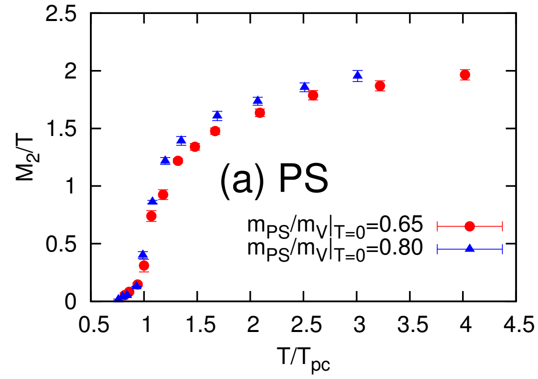

Fig. 2. Second response of the screening masses M_2/T with respect to $\tilde{\mu}$ as a function of $T/T_{\rm pc}$ for the PS channel.

We can also see the quark-mass dependence in the PS channel; the magnitude of M_2/T with a lighter quark mass ($m_{\rm PS}/m_{\rm V}|_{T=0} = 0.65$) is slightly smaller than that with a heavier quark mass ($m_{\rm PS}/m_{\rm V}|_{T=0} = 0.80$). This is similar to the quark-mass dependence of M_0/T, but different from the results of M_2 calculated for the staggered-type quark action[3)]. This difference should be further investigated in simulations by considering a smaller quark mass and a larger volume.

References

1) K. Yagi, T. Hatsuda and Y. Miake: *Quark-Gluon Plasma*, Cambridge University Press, Cambridge (2005).
2) **WHOT-QCD** Collaboration: Y. Maezawa *et al.*, *Phys. Rev.* D**75** 074501 (2007).
3) **QCD-TARO** Collaboration: I. Pushkina *et al.*, *Phys. Lett.* **B609** 265 (2005).

5. Particle Physics

Tenth-order QED contributions to lepton $g-2$

T. Aoyama,[*1] M. Hayakawa,[*2] T. Kinoshita,[*3] and M. Nio

[QED, anomalous magnetic moment, electron, muon]

The anomalous magnetic moment of the electron, $g-2$, plays a central role in testing the validity of quantum electrodynamics (QED). The Harvard team recently reported an astonishing result for the electron anomaly $a_e = (g-2)/2$[1)]

$$a_e(\mathrm{HV}) = 1\ 159\ 652\ 180.73\ (0.28) \times 10^{-12}\ . \qquad (1)$$

At present, the best theoretical prediction in the context of the standard model includes QED corrections of up to the eighth order and hadronic and electroweak corrections. To compare the theoretical prediction with the result of experiment (1), we need the value of the fine structure constant α determined by a method independent of $g-2$. The best value of such an α has been obtained recently from the measurement of h/m_{Rb}, the ratio of the Planck constant and the mass of the Rb atom, along with the very precisely known Rydberg constant and m_{Rb}/m_e[2)]:

$$\alpha^{-1}(\mathrm{Rb}) = 137.035\ 999\ 037\ (91)\ . \qquad (2)$$

With this α, the theoretical prediction of a_e is theoretically predicted:

$$a_e(\mathrm{th}) = 1\ 159\ 652\ 181.13\ (11)(37)(77) \times 10^{-12}, \qquad (3)$$

where the first, second, and third uncertainties come from the calculated eighth-order QED term, the tenth-order estimate, and $\alpha(\mathrm{Rb})$, respectively. Theory (3) is thus in good agreement with the result of experiment (1), proving that QED is valid even at this very high precision.

An alternative test for QED involves comparison of the value of $\alpha(\mathrm{Rb})$ with that determined from the experiment and theory of $g-2$:

$$\alpha^{-1}(a_e) = 137.035\ 999\ 085\ (12)(37)(33), \qquad (4)$$

where the first, second, and third uncertainties come from the eighth-order QED term, the tenth-order estimate, and the measurement of $a_e(\mathrm{HV})$, respectively. Although the uncertainty of $\alpha^{-1}(a_e)$ in (4) is smaller than that of $\alpha^{-1}(\mathrm{Rb})$ by a factor 2, it is not a firm factor since it depends on the estimate of the tenth-order term, which is only a rough guess[3)]. To settle this issue unambiguously, we must evaluate the tenth-order term explicitly. We launched a systematic program several years ago to evaluate the complete tenth-order term.[4,5)]

*1 Kobayashi-Maskawa Institute for the Origin of Particle and the Universe (KMI), Nagoya University
*2 Department of Physics, Nagoya University
*3 Laboratory for Elementary-Particle Physics, Cornell University

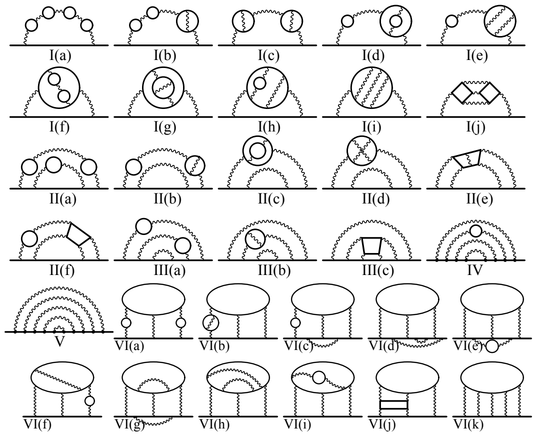

Fig. 1. Feynman diagrams contributing to the tenth-order lepton $g-2$. Typical diagrams from 32 gauge-invariant sets are shown.

There are 12672 vertex Feynman diagrams that contribute to the tenth-order $g-2$. They are divided into 32 gauge-invariant sets, as shown in Fig. 1. The contributions from 17 sets, I(a–f), II(a,b), II(f), VI(a–c), VI(e,f), and VI(i–k), have been previously determined.[5)] The contributions from 10 more sets, I(j), II(e), I(g,h), VI(d,g,h), I(i), and II(c,d) have been recently reported.[6–8)] We are now performing a final check on set III(a,b) and set IV and preparing to publish the results. Numerical evaluation of the remaining two sets, III(c) and V, is in the final stage on RICC, RIKEN's supercomputer system.

We now have obtained the results from all 32 gauge-invariant sets of the tenth-order diagrams, although some of them are still preliminary.

References

1) D. Hanneke, S. Fogwell, and G. Gabrielse: Phys. Rev. Lett. **100**, 120801 (2008).
2) R. Bouchendira, P. Clade, S. Guellati-Khelifa, F. Nez, and F. Biraben: Phys. Rev. Lett. **106**, 080801 (2011).
3) P. J. Mohr, B. N. Taylor, and D. B. Newell: Rev. Mod. Phys. **80**, 633 (2008).
4) T. Aoyama, M. Hayakawa, T. Kinoshita, and M. Nio: Nucl. Phys. B **740**, 138 (2006); **796**, 184 (2008).
5) T. Kinoshita and M. Nio: Phys. Rev. D **73**, 053007 (2006).
6) T. Aoyama, M. Hayakawa, T. Kinoshita, M. Nio, and N. Watanabe: Phys. Rev. D **78**, 053005 (2008).
7) T. Aoyama, K. Asano, M. Hayakawa, T. Kinoshita, M. Nio, and N. Watanabe: Phys. Rev. D **81**, 053009 (2010).
8) T. Aoyama, M. Hayakawa, T. Kinoshita, and M. Nio: Phys. Rev. D **78**, 113006 (2008); **82**, 113004 (2010); **83**, 053002 (2011); **83**, 053003 (2011).

RIKEN Accel. Prog. Rep. 44 (2011)

Supersymmetric non-perturbative formulation of the WZ model in lower dimensions†

D. Kadoh and H. Suzuki

[Supersymmetry, lattice field theory]

Considering the fundamental role played by supersymmetry (SUSY) in particle physics beyond the standard model, it is very important to develop formulations of supersymmetric field theories that facilitate non-perturbative calculation. In this study, we propose a non-perturbative formulation of the Wess–Zumino (WZ) model[1] in two and three dimensions (2D and 3D). Our present formulation possesses desirable features such as manifest SUSY and global symmetries and it is suitable for non-perturbative studies involving Monte Carlo . Further, the 2D $\mathcal{N} = (2, 2)$ WZ model possesses a well-defined Nicolai map. Although the locality is not manifest in our formulation, we can show that there is actually no problem concerning this, at least for all orders of perturbation theory.[a]

Our basic idea is quite simple. The off-shell supermultiplets in the WZ model are expressed by the chiral and anti-chiral superfields Φ and $\Phi^\dagger$.[2] In the momentum space, they yield

$$\tilde{\Phi}(p,\theta,\bar{\theta}) = e^{-\theta\sigma_\mu\bar{\theta}p_\mu}\left[\tilde{A}(p) + \sqrt{2}\theta\tilde{\psi}(p) + \theta\theta\tilde{F}(p)\right],$$
$$\tilde{\Phi}^\dagger(p,\theta,\bar{\theta}) = e^{\theta\sigma_\mu\bar{\theta}p_\mu}\left[\tilde{A}^*(p) + \sqrt{2}\bar{\theta}\tilde{\bar{\psi}}(p) + \bar{\theta}\bar{\theta}\tilde{F}^*(p)\right] \tag{1}$$

as they satisfy the constraints $\bar{D}_{\dot{\alpha}}\tilde{\Phi}(p) = 0$ and $D_\alpha\tilde{\Phi}^\dagger(p) = 0$, where the covariant spinor derivatives are given by $D_\alpha = \partial/\partial\theta^\alpha - \sigma_{\mu\alpha\dot{\alpha}}\bar{\theta}^{\dot{\alpha}}p_\mu$ and $\bar{D}_{\dot{\alpha}} = -\partial/\partial\bar{\theta}^{\dot{\alpha}} + \theta^\alpha\sigma_{\mu\alpha\dot{\alpha}}p_\mu$.[2] On these off-shell supermultiplets in the momentum space, SUSY is linearly realized and super transformations generated by

$$Q_\alpha = \frac{\partial}{\partial\theta^\alpha} + \sigma_{\mu\alpha\dot{\alpha}}\bar{\theta}^{\dot{\alpha}}p_\mu, \quad \bar{Q}_{\dot{\alpha}} = -\frac{\partial}{\partial\bar{\theta}^{\dot{\alpha}}} - \theta^\alpha\sigma_{\mu\alpha\dot{\alpha}}p_\mu \tag{2}$$

do not mix momentum modes with different momenta. Therefore, we can regularize the functional integral of the system by restricting the possible momenta of the off-shell super multiplets as follows:

$$-\Lambda \le p_\mu \equiv \frac{2\pi}{L}n_\mu \le \Lambda, \qquad n_\mu \in \mathbb{Z}, \tag{3}$$

where L denotes the size of an Euclidean box within which the system is defined and Λ is the UV cutoff; this regularization does not break the SUSY and other global symmetries. Specifically, one can derive Ward–Takahashi identities associated with these symmetries within a regularized framework. Since the prescription does not modify the spinorial structure of the WZ model, one may repeat the proof of perturbative non-renormalization theorems[3–5] in this regularized framework. One may also repeat the argument of Ref. 6 because the holomorphy is manifestly preserved. Furthermore, the prescription is suitable for non-perturbative studies involving Monte Carlo simulations.

The above description sounds too good to be true. Actually, prescription (3), which is equivalent to the lattice formulation of the WZ model in Ref. 7 based on the SLAC lattice derivative,[8] *differs* from the conventional momentum cutoff of perturbative Feynman integrals. A resulting concern is that the restriction on the functional integration variables in Eq. (3) could induce the additional dependence of a Feynman integral on external momenta, which cannot be interpreted as an insertion of local operators. (See an analysis in Appendix of the original paper.)

Nevertheless, we can show that all (super) Feynman diagrams in the 3D $\mathcal{N} = 2$ WZ model with the cubic superpotential and the 2D $\mathcal{N} = (2, 2)$ WZ model with an arbitrary superpotential are *absolutely convergent* if the SUSY is manifestly preserved by the regularization. Then, we can show that the finite values of (super) Feynman diagrams are reproduced with prescription (3) in the $\Lambda \to \infty$ limit owing to the good convergence. Thus, our prescription provides a valid non-perturbative formulation of the above-mentioned lower-dimensional WZ models; in the formulation, the locality is guaranteed at least for all orders of perturbation theory.

† Condensed from the article in Phys. Lett. B **684**, 167 (2010)

a) We assume that the Kähler potential is a flat one, $\Phi^\dagger\Phi$, and the superpotential is cubic in the 3D model, so that the model is ultraviolet (UV) finite.

References

1) J. Wess and B. Zumino: Nucl. Phys. B **70**, 39 (1974).
2) J. Wess and J. Bagger: "Supersymmetry and supergravity," *Princeton, USA: Univ. Pr., p. 259 (1992).*
3) K. Fujikawa and W. Lang: Nucl. Phys. B **88**, 61 (1975).
4) P. C. West: Nucl. Phys. B **106**, 219 (1976).
5) M. T. Grisaru, W. Siegel and M. Roček: Nucl. Phys. B **159**, 429 (1979).
6) N. Seiberg: arXiv:hep-th/9408013.
7) J. Bartels and J. B. Bronzan: Phys. Rev. D **28**, 818 (1983).
8) S. D. Drell, M. Weinstein and S. Yankielowicz: Phys. Rev. D **14**, 1627 (1976).

RIKEN Accel. Prog. Rep. 44 (2011)

Supersymmetry restoration in lattice formulations of 2D $\mathcal{N} = (2, 2)$ WZ model based on the Nicolai map†

D. Kadoh and H. Suzuki

[Supersymmetry, lattice field theory]

It is believed that in the case of low energies or at long distances the two-dimensional (2D) $\mathcal{N} = (2, 2)$ Wess–Zumino (WZ) model with a quasi-homogeneous superpotential[a] becomes non-trivial $\mathcal{N} = (2, 2)$ superconformal field theories (SCFT). See §14.4 of Ref. 1 for a review. Although the consistency of this WZ/SCFT correspondence has been tested in various ways, it has been impossible to show this correspondence directly, because the 2D WZ model is strongly coupled at low energies; one needs a powerful tool that can enable non-perturbative calculations in the 2D WZ model.

Recently, Kawai and Kikukawa[2] reanalyzed this problem and numerically computed some correlation functions in the 2D WZ model by employing a lattice formulation developed in the study reported in Ref. 3. They considered the WZ model with a cubic superpotential $W(\phi) = \lambda\phi^3/3$, which should become the so-called A_2 model according to the conjectured correspondence. The central charge of the A_2 model is $c = 1$, and a unique chiral primary field in its Neveu-Schwarz sector, $\Phi_{0,0}$, which should be given by the scalar field of the WZ model at low energies, has the conformal dimensions $(h, \overline{h}) = (1/6, 1/6)$. Finite-size scaling of scalar two-point functions obtained in the study reported in Ref. 2 is remarkably consistent with this conjectured correspondence.

The results reported in Ref. 2 naturally induce one to consider lattice formulations of the 2D $\mathcal{N} = (2, 2)$ WZ model with more general (quasi-homogeneous) superpotentials. It would be interesting to generalize the study repeated in Ref. 2 and take into consideration the superpotential $W(\phi) = \lambda\phi^n/n + \lambda'\phi\phi'^2/2$ with $n \geq 3$, where ϕ and ϕ' are independent scalar fields, which should correspond to the D_{n+1} model according to the WZ/SCFT correspondence. However, before carrying out such a study of physical questions, one has to be sure at least according to the perturbation theory, that symmetries that are broken by lattice formulation, especially supersymmetry (SUSY), are restored in the continuum limit.[b] Somewhat surprisingly, such an argument for symmetry restoration in lattice formulations of the 2D $\mathcal{N} = (2, 2)$ WZ model has not been found in the literature; the only exception has been one for a cubic superpotential with a single supermultiplet. At first glance, in fact, it appears that a rather complicated enumeration of possible symmetry-breaking terms in the effective action is required for the argument.

In the present study, we show that there actually exists a very simple method for showing the symmetry restoration in the continuum limit for lattice formulations[3,5] based on the Nicolai map for general superpotentials with multiple supermultiplets. We can show that SUSY and other symmetries are restored in the continuum limit without fine-tuning to all orders of the perturbation theory. Thus, our study provides a theoretical basis for the application of these lattice formulations.

Our argumentation proceeds as follows (for more details, see the original paper). Lattice formulations of 2D $\mathcal{N} = (2, 2)$ WZ model based on the Nicolai map[3,5] can be expressed in a Q-exact form, where Q is one particular spinor component of the $\mathcal{N} = (2, 2)$ super transformation. Since the fermionic transformation Q is nilpotent, $Q^2 = 0$, the lattice action $S^{\text{LAT}}_{\text{2DWZ}}$ is manifestly invariant under Q transformation, $QS^{\text{LAT}}_{\text{2DWZ}} = 0$. Our key observation is that the local Q-cohomology is trivial. Using the explicit form of the Q transformation and the algebraic Poincaré lemma of Ref. 6, it can be easily shown that if $Q \int d^2x\, X([\varphi]) = 0$ then $X([\varphi]) = QY([\varphi]) + \partial_\mu Z_\mu([\varphi]) + \text{const.}$, where all X, Y, and Z_μ are local polynomials of fields. This shows that in enumerating the possible local terms in the effective action which would break the symmetries other than Q, we could consider only the local polynomials of the fields of the form QY. Then, dimensional counting and a perturbative consideration show that such local terms cannot be induced by radiative corrections.

† Condensed from the article in Phys. Lett. B **696**, 163 (2011)

a) A polynomial $W(\phi)$ of variables ϕ_I ($I = 1, 2, \ldots, N$) is called quasi-homogeneous when there exist certain weights ω_I for each variables such that $W(\phi_I \to \Lambda^{\omega_I}\phi_I) = \Lambda W(\phi)$.

b) There also exists a valid lattice formulation of the 2D $\mathcal{N} = (2, 2)$ WZ model based on the SLAC derivative in which SUSY and other symmetries are manifest.[4]

References

1) K. Hori *et al.*: "Mirror symmetry," *Providence, USA: AMS (2003) 929 p*
2) H. Kawai and Y. Kikukawa: Phys. Rev. D **83**, 074502 (2011) [arXiv:1005.4671 [hep-lat]].
3) Y. Kikukawa and Y. Nakayama: Phys. Rev. D **66**, 094508 (2002) [arXiv:hep-lat/0207013].
4) D. Kadoh and H. Suzuki: Phys. Lett. B **684**, 167 (2010) [arXiv:0909.3686 [hep-th]].
5) N. Sakai and M. Sakamoto: Nucl. Phys. B **229**, 173 (1983).
6) F. Brandt, N. Dragon, and M. Kreuzer: Nucl. Phys. B **332**, 224 (1990).

Geometry dependence of RMT-based methods to extract LECs[†]

C. Lehner,[*1,*2] J. Bloch,[*2] S. Hashimoto,[*3] T. Wettig,[*2]

[epsilon regime, random matrix theory, lattice QCD, geometry dependence]

It is well known that QCD in a finite volume V at small quark masses m simplifies as the Compton wavelength of the pion, m_π^{-1}, becomes large compared to $(V^{1/4})$[1]. In this limit the space-time dependence of the low-energy effective theory is suppressed and the theory is dominated by the constant mode of the pions. The distribution of the low-lying eigenvalues of the Dirac operator can then be calculated in random matrix theory[2]. The low-energy constants (LECs) of chiral perturbation theory are used to map the dimensionful quantities of QCD (or the effective theory) to the dimensionless quantities of RMT. Matching lattice data for the low-lying Dirac eigenvalues to RMT results then allows for a determination of phenomenologically important LECs. In the following we discuss the geometry dependence of such methods.

To be specific we discuss the lattice geometries (a_x) with $L_0 = xL$, $L_1 = L_2 = L_3 = L$ and (b_x) with $L_3 = xL$, $L_0 = L_1 = L_2 = L$, where L_i is the extent of the space-time box in direction i ($i = 0$ denotes the temporal direction to which a chemical potential μ couples) and x is the ratio $\max L_i / \min L_i$.

In Ref.[3] we showed that finite-volume effective coupling constants Υ_i and $\mathcal{H}_2$ are responsible for the systematic deviations from RMT. It is an interesting observation[3] that $\Upsilon_1, \Upsilon_2, \Upsilon_3$ do not depend on the NLO LECs of χPT and depend on the geometry only through a common coefficient γ, i.e.,

$$\Upsilon_1, \Upsilon_2, \Upsilon_3 \propto \gamma \,. \tag{1}$$

The coefficient γ changes under $(a_2) \leftrightarrow (b_2)$[3]. We plot γ for different geometries in Fig. 1. We note that the coefficient γ, and thus a part of the systematic deviations from RMT, can be reduced significantly by choosing the geometry (b_x) instead of (a_x) for the same value of the asymmetry x.

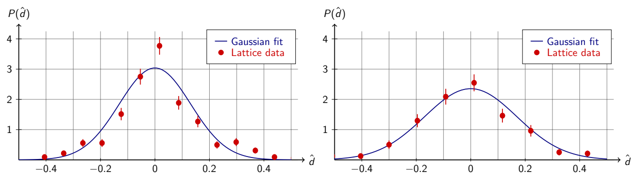

Fig. 2. Fit for $a\mu = 0.01$ with $\hat{d} = d\Sigma V$ in geometry (a_2) (left) and (b_2) (right). The result is given by $F = 50(4)$ MeV with $\chi^2/\mathrm{dof} = 4.2$ for (a_2) and $F = 80(5)$ MeV with $\chi^2/\mathrm{dof} = 0.91$ for (b_2). Results include NLO finite-volume corrections[7].

We check this result against the epsilon-regime run of JLQCD with two dynamical overlap fermions[4,5]. We fit the shift of the lowest-lying Dirac eigenvalue due to a small imaginary chemical potential $i\mu$ in order to extract F as proposed in Ref.[6]. RMT predicts a Gaussian distribution with $\sigma^2 = \mu^2 F^2 V$ for the distribution P of the difference d between the lowest Dirac eigenvalue at zero and at nonzero imaginary chemical potential. In Fig. 2 we show the resulting fits for geometry (a_2) and (b_2).

Note that the respective values for χ^2/dof indicate that the systematic deviations from RMT are significantly reduced in geometry (b_2), in agreement with our analytic discussion[3]. We observe that the geometry dependence of the Dirac eigenvalue distributions at nonzero chemical potential strongly influences the determination of F from RMT fits. Making a judicious choice of the lattice geometry, this dependence can be significantly reduced such that the systematic error on F is kept under control. This makes the RMT-based method a useful alternative to other lattice methods.

† Condensed from the preprint arXiv:1101.5576

*1 RIKEN/BNL Research Center, Brookhaven National Laboratory, Upton, NY-11973, USA
*2 Institute for Theoretical Physics, University of Regensburg, 93040 Regensburg, Germany
*3 High Energy Accelerator Research Organization (KEK), Tsukuba 305-0801, Japan

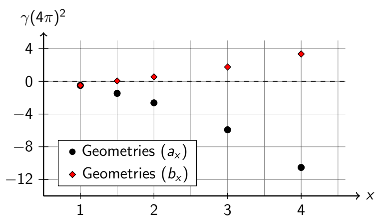

Fig. 1. Coefficient γ for $F = 90$ MeV, $L = 1.71$ fm, and $m_\pi^2\sqrt{V} = 1$. Taken from Ref.[3].

References

1) J. Gasser and H. Leutwyler, Phys. Lett. **B188** (1987) 477.
2) E. V. Shuryak and J. J. M. Verbaarschot, Nucl. Phys. **A560** (1993) 306–320.
3) C. Lehner, S. Hashimoto and T. Wettig, JHEP **06** (2010) 028.
4) JLQCD, H. Fukaya *et al.*, Phys. Rev. Lett. **98** (2007) 172001.
5) H. Fukaya *et al.*, Phys. Rev. **D76** (2007) 054503.
6) P. H. Damgaard, U. M. Heller, K. Splittorff and B. Svetitsky, Phys. Rev. **D72** (2005) 091501.
7) P. H. Damgaard, T. DeGrand and H. Fukaya, JHEP **12** (2007) 060; G. Akemann, F. Basile and L. Lellouch, JHEP **12** (2008) 069; C. Lehner and T. Wettig, JHEP **11** (2009) 005.

Monte-Carlo approach to insulator transition on the Graphene

E. Shintani,*1 T. Onogi,*2

Graphene is a monolayer of Carbon atoms two-dimensional sheet forming hexagonal lattice. The low energy property has been well known in the low-energy expansion of Hamiltonian in tightbinding approximation[1]. From the discovery of Graphene[3] many specific features have been found. Especially Graphene has quiet large electron mobility as order of 10^6 cm^2/V/s, which is more than 100 times larger than ordinary semiconductor of silicon compounds[2], it seems to have a possibility of the next generation of silicon chip. However in order to apply Graphene as a semiconducting material we should understand behavior of the energy density near the Fermi level under various impurities or finite temperature.

In this study we focus on a temperature dependence of energy gap in suspended monolayer Graphene. Through sufficiently strong attractive interaction a bound structure of quasiparticle and quasihole becomes different from dispersion relation of massless Dirac and anti-Dirac fermion. As a result, the massless Dirac fermion has a finite mass when ground semimetal state transitions into insulating state. The coupling of Coulomb interaction between quasiparticle can be described as $\lambda = e^2/(4\pi v_R \varepsilon_0) \sim O(1)$ with Fermi velocity $v_F \simeq 1/300$. In the analysis about semimetal-insulator transition we should make use of non-perturbative method on the strong Coulomb interaction. The prior non-perturbative study with Dyson-Schwinger equation[4] and lattice Monte-Carlo simulation[5] has suggested the instability of the ground semimetal state may exist less than critical coupling λ_c.

We perform Monte-Carlo simulation in strong QED system with magnetic field and velocity of fermion into the lattice QED action which are ignored in Ref [5]. Ignoring both magnetic field and Fermi velocity, which actually appears by moving the electron, are too naive approximation because gauge symmetry does not conserve and renormalization free in[5]. We consider gauge-invariant QED action as 2+1D fermion action and 4D gauge action:

$$S = \int d^3x \bar{q}(x) \sum_{\mu} \Big(\partial_\mu - A_\mu(x,s)\Big)_{\text{fixed:s}} \gamma_\mu q(x) + \int d^3x ds \Big(\beta v_F \sum_i F_{0i}^2 + \beta / v_F \sum_{ij} F_{ij}^2\Big) \qquad (1)$$

with velocity v_F. Here s denotes the perpendicular direction. Dirac fermion $q(x)$ exists on 2D sheet, while gauge field $A_\mu(x,s)$ exists on 3D. γ_μ is Dirac gamma matrix in 2+1 dimension. For the monolayer of Graphene, gauge field in z direction $A_z(x,s)$ does not interact with Dirac fermion, and s means the position of monolayer in z direction. To perform Monte-Carlo integral the above action should be modified to lattice action. We use the staggered type fermion action and plaquette gauge action. In this action global symmetry of fermion field has $U(4)$ which consists with original monolayer Graphene symmetry. The chiral symmetry breaking pattern is $U(4) \to U(2) \times U(2)$. We insert the mass term $m\bar{q}q$ into lattice action and calculate chiral condensate $\langle q\bar{q} \rangle$ as a probe of chiral phase transition.

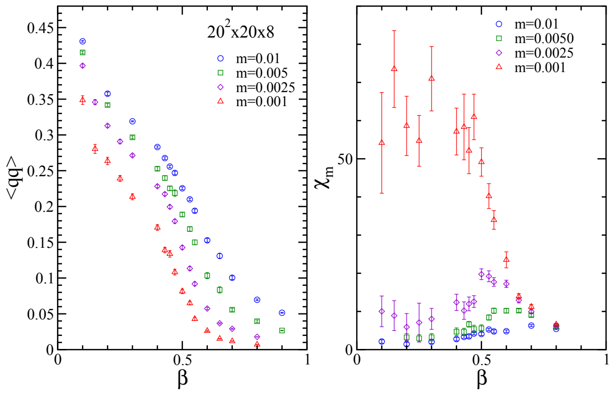

Fig. 1. β dependence of Chiral condensate (left) and chiral susceptibility (right)

Figure 1 shows our present result of chiral condensate and chiral susceptibility in $20^4 \times 8$ lattice size with $v_F = 0.1$. If chiral phase transition occurred, chiral condensate would have discontinuous point and chiral susceptibility would have singular point at critical coupling in the massless limit. In Figure 1 around $\beta = 0.5$ chiral susceptibility blow up in the small quark mass, which is encouraged to exist critical point. To proceed to investigate chiral phase transition, we may use finite size scaling technique. We are searching detailed scaling behavior of chiral susceptibility near such critical point by changing the lattice size with enough statistics under way.

*1 RIKEN-BNL Research Center, Brookheaven National Laboratory
*2 Physics Department, Osaka University

References
1) G. W. Semenoff, Phys. Rev. Lett. **53**, 2449 (1984).
2) K. I. Bolotin, *et al.*, Sol. St. Comm. **146**, 351 (208).
3) A. K. Geim and K. S. Novoselov, Nature material Vol.6, 183 (2007).
4) E. V. Gorber, *et al.*, Phys. Rev. B **66**, 045108 (2002).
5) J. E. Drut and T. A. Lahde, Phys. Rev. Lett. **102**, 026802 (2009); J. E. Drut and T. A. Lahde, Phys. Rev. B **79**, 165425 (2009).

Development of Bound-State Approach to Strangeness in Holographic QCD†

T. Ishii

[String Theory, Gauge/gravity Correspondence, Holographic QCD]

Chiral symmetry is a significant principle for describing the low energy of quantum chromodynamics (QCD). Pions emerge as the Nambu-Goldstone bosons of the spontaneous breaking of the symmetry. However, in real QCD, the chiral symmetry is clearly broken by non-zero quark masses. In particular, the mass of a strange quark should be considered to be large in contrast to the masses of up and down quarks. Here, we focus on the baryons in the Sakai-Sugimoto model of holographic QCD, with strangeness as a massive flavor. The model is originally a holographic dual of massless QCD[1)], but quark masses can be also included.

Let us recall that in the context of the Skyrme model, there is an approach known as the bound-state approach to strangeness[2)]. This approach could be useful when strangeness is considered to be a massive flavor. The idea is to consider a kaon as a fluctuation around a two-flavor Skyrmion, and then, their bound state is identified as a hyperon. This approach appears to be effective.

We would consider this idea in the Sakai-Sugimoto model, in which instanton-like solitons represent baryons. Though the model contains vector mesons as well as pseudo-scalar mesons, here, we consider only the kaon fluctuation which was significant in the case of the Skyrme model. There was another attempt in which the collective coordinate quantization of three flavor baryons was carried out, and the baryon spectra in the presence of massive strangeness was evaluated[3)].

The Sakai-Sugimoto model is a five-dimensional $U(N_f)$ Yang-Mills-Chern-Simons theory in a curved background. In the model, mesons are encoded in gauge fields, and baryons are represented as solitons. The action is

$$S = -\kappa \int d^4x dz \,\mathrm{Tr}\left[\frac{1}{2}h(z)F_{\mu\nu}^2 + M_{\mathrm{KK}}^2 k(z) F_{\mu z}^2\right]$$

and a Chern-Simons term. The functions $h(z) = (1+z^2)^{-1/3}$ and $k(z) = 1+z^2$ inherit the metric of the curved background. The model describes a holographic dual of a large N_c massless QCD, but we can also add a quark-mass term to this action. We will restrict our discussion to the case $N_f = 3$.

The kaon fluctuation can be turned on as small gauge fields around two-flavor baryons which are represented as instanton-like soliton. $SU(2)$ baryon is embedded in 3×3 matrices, and kaon fluctuation a_z, a two-component vector, is turned on at off-diagonal components as follows:

$$A_\mu = \begin{pmatrix} A_\mu^{\mathrm{inst}} & 0 \\ 0 & 0 \end{pmatrix}, \quad A_z = \begin{pmatrix} A_z^{\mathrm{inst}} & a_z \\ a_z^\dagger & 0 \end{pmatrix}.$$

Here a_z is assumed to be decomposed into the four-dimensional kaon field as

$$a_z \propto \begin{pmatrix} K^+ \\ K^0 \end{pmatrix} \phi_0(z),$$

where $\phi_0(z)$ is an eigenfunction in the holographic direction z. By Reducing to four dimensions, we obtain an action in which the kaon is in a potential provided by the background baryon configuration, and the equation of motion of the kaon becomes an eigenvalue problem. The kaon would be bounded to the baryon.

However, after solving the eigenvalue problem, we find no bound-state when the spin and the isospin of a baryon are 1/2 and 1, respectively, and a weak bound-state with the energy-eigenvalue about 490 MeV is found when the spin and the isospin of a baryon are 1/2 and 1, respectively. In the former case, the potential is strongly repulsive unlike in the case of the Skyrme model, in which the potential is strongly attractive and favors a bound-state. In the latter case, the potential is still reasonably repulsive, but there is a large contribution from the $U(1)$ gauge field which forces the kaon wavefunction to localize at the minimum of the potential. Thus, the result seems quite different from that known in the context of the Skyrme model.

It seems that our trial might bind a kaon and a baryon assuming that both of them have concrete identities after they are generated from a quark-antiquark pair or N_c quarks. This point may be related to a prescription in which $\Lambda(1405)$ can be a bound-state of $\bar{K}$ and N. It will be interesting if the systematic treatment of the vector mesons ignored here gives a significant contribution.

References

1) T. Sakai and S. Sugimoto, *Prog. Theor. Phys.* **113**, 843 (2005).
2) C. G. Callan, Jr. and I. R. Klebanov, *Nucl. Phys.* **B262**, 365 (1985).
3) K. Hashimoto, N. Iizuka, T. Ishii, and D. Kadoh, *Phys. Lett.* **B691**, 65 (2010).

† Condensed from the article in Phys. Lett. **B695**, 392 (2011).

Operator matching in the static heavy and domain-wall light quark system with O(a) improvement

Tomomi Ishikawa[*1] for RBC and UKQCD Collaborations

The Cabibbo-Kobayashi-Maskawa (CKM) quark-mixing matrix is one of the important topic in elementary particle physics. Constraints on the matrix elements V_{ts} and V_{td} can be obtained from B_0–$\overline{B}_0$ mixing, where the $SU(3)$ breaking ratio ξ plays an important role. While the lattice Quantum Chromo Dynamics (QCD) simulation on that mixing is quite challenging, there is a difficulty caused by the difference in the energy scales of light quarks and b quarks. One of the strategies for treating this system involves the use of the Heavy Quark Effective Theory (HQET)[1]. The lowest order of this theory, static approximation, is often used as the first step of the simulations. Although static approximation always includes an error of $O(\Lambda_{\rm QCD}/m_b) \sim 10\%$, it gives satisfactory results for the determination of ξ, in which the theoretical uncertainty is suppressed by $(m_s - m_d)/\Lambda_{\rm QCD}$ and is estimated to be about 2%.

For the lattice calculation of physical quantities, matching factors which correlate the lattice and continuum theories are needed. To match these theories, we adopt the following matching procedure:

i We first perform matching between continuum QCD (CQCD) and the continuum HQET (CHQET) in the $\overline{\rm MS}$(NDR) scheme at a scale of $\mu = m_b$. We perform calculations on the basis of the perturbation theory.

ii We use renormalization group (RG) running in the CHQET to move to a lower scale at which the HQET matching between continuum and lattice is done. We employ two-loop anomalous dimension calculations.

iii We perform matching between the CHQET and the lattice HQET (LHQET) at a scale of $\mu = a^{-1}$, where a denotes lattice spacing. We employ the domain-wall quark formalism for the lattice light quarks. We perform the calculation by taking into account $O(pa, ma)$ discretization errors in the lattice, where p and m are the momentum and mass of the light quark, respectively.

The operator mixing pattern is analyzed by the following symmetries:

i Chiral symmetry in the light quark action

ii Heavy-quark spin symmetry in the static action

iii Spatial rotational symmetry

iv Discrete symmetries ($\mathcal{P}$, $\mathcal{T}$, $\mathcal{C}$)

These symmetries dominate the operator relations between the CHQET and the LHQET. The relation for the axial-vector current is

$$A_\mu^{\rm CHQET} = Z_A \left[A_\mu + c_A a A_\mu^{(pa)} + b_A a A_\mu^{(ma)} \right]^{\rm LHQET} \quad (1)$$

with $A_\mu = \bar{h}\gamma_\mu\gamma_5 q$, $A_\mu^{(pa)} = \bar{h}\gamma_\mu\gamma_5(\gamma_i \vec{D}_i)q$, and $A_\mu^{(ma)} = m\bar{h}\gamma_\mu\gamma_5 q$, where h and q denote the static-heavy and light quark fields, respectively. Z_A is the overall matching factor, and c_A and b_A are the $O(pa)$ and $O(ma)$ improvement coefficients, respectively. The relation for the $\Delta B = 2$ four-quark operator is

$$O_L^{\rm CHQET} = Z_L \left[O_L + c_L a O_L^{(pa)} + b_L a O_L^{(ma)} \right]^{\rm LHQET} \quad (2)$$

with

$$O_L = [\bar{h}\gamma_\mu^L q][\bar{h}\gamma_\mu^L q],$$
$$O_L^{(pa)} = 2[\bar{h}\gamma_\mu^R(\gamma_i \vec{D}_i)q][\bar{h}\gamma_\mu^L q] + 4[\bar{h}P_R(\gamma_i\vec{D}_i)q][\bar{h}P_L q],$$
$$O_L^{(ma)} = m(2[\bar{h}\gamma_\mu^R q][\bar{h}\gamma_\mu^L q] + 4[\bar{h}P_R q][\bar{h}P_L q]),$$

where $\gamma_\mu^L = \gamma_\mu P_L$ and $\gamma_\mu^R = \gamma_\mu P_R$. Z_L is the overall matching factor, and c_L and b_L are the $O(pa)$ and $O(ma)$ improvement coefficients, respectively.

Matching is performed by one-loop calculation of the transition amplitudes, introducing external momenta, for example,

$$\langle {\rm f}|A_\mu|{\rm i}\rangle = \langle h(p')|A_\mu|q(p)\rangle, \quad (3)$$
$$\langle {\rm f}|O_L|{\rm i}\rangle = \langle h(p_2'), q(p_2)|O_L|h(p_1'), q(p_1)\rangle, \quad (4)$$

in which the equations of motion are imposed on the external quarks according to the on-shell improvement program. The transition amplitudes are expanded around zero in the external light quark momenta and the light quark mass up to the first order, resulting in $O(pa, ma)$ effects. The $O(p'a)$ effects always vanish because of the on-shell condition $p' = 0$.

A part of the results of this study was applied to an actual simulation at a smaller volume[2]. The quality of the simulation data was not sufficiently high to show the effect of inclusion of the $O(pa, ma)$ improvement. The on-going simulation with a larger volume and high statistics could be useful for demonstrating the validity of our matching strategy. For high-precision calculation, we must attempt the use of nonperturbative matching with the Rome-Southampton regularization independent momentum subtraction renormalization scheme (RI/MOM).

References

1) E. Eichten and B. R. Hill: Phys. Lett. B **234**, 511 (1990).
2) C. Albertus *et al.* [RBC and UKQCD Collaborations]: Phys. Rev. D **82**, 014505 (2010).

† Condensed from the article in arXiv:1101.1072 [hep-lat].
*1 University of Connecticut

6. Accelerator

Design and construction of the first rebuncher for RILAC2

K. Suda, K. Yamada, M. Fujimaki, E. Ikezawa, H. Imao, O. Kamigaito, M. Kase, R. Koyama,*1 N. Sakamoto, and Y. Watanabe

The cavity of the first rebuncher (B2 REB) for the new injector RILAC2 has been designed and constructed between the RFQ[1] and DTL1[2]. The required total gap voltage for the rebuncher is 100 kV. We had originally planned to modify the existing cavity with three gaps[3]; however, the required gap voltage could not be achieved because of the low shunt impedance and high dissipation power ($\sim$ 5 kW). Therefore, we decided to construct a new cavity. The structure of the cavity is based on that of the quarter-wavelength resonator (Fig. 1). The rebuncher has four gaps and operates at the second harmonic frequency (36.5 MHz). It consists of a beamline chamber, three drift tubes and two end drift tubes, outer and inner conductors, upper and lower plates for the outer conductor, a capacitive coupler, and a capacitive trimmer. The basic parameters for the rebuncher are listed in Table 1. The distance between the gaps was calculated to be $\beta\lambda/2 = 60$ mm. Since the original cavity had three gaps, in which the length of each gap was 20 mm, we fixed the outer and inner length of the beamline chamber at 200 mm and 160 mm, respectively. However, in order to achieve the desired gap voltage, one more gap had to be inserted in the limited space. To accomodate four gaps in the chamber, the inner length of the beamline chamber was increased to 180 mm, and the gap lengths of the first and fourth gaps were set at 10 mm, and those of the second and third gaps 20 mm. The cavity was designed by using the CST Microwave Studio 2010 (MWS). First, the inner diameter of the outer conductor was fixed at 360 mm. Next, the capacitance of the gaps was increased so that the height of the outer conductor decreased to around 1 m. Then, the diameter of the inner conductor was determined to be 70 mm, so that the shunt impedance becomes maximim.

Table 1. Basic parameters for the rebuncher.

Frequency (MHz)	36.5
Duty (%)	100
Mass-to-charge ratio (m/q)	7
Input energy (keV/u)	100
$\beta\lambda/2$ (mm)	60
Inner diameter of outer conductor (mm)	360
Diameter of inner conductor (mm)	70
Gap number	4
Gap length (mm)	10, 20, 20, 10
Gap voltage (kV)	25
Drift-tube aperture diameter (mm)	35
Frequency range (MHz)	36.304–36.618
Input power (81% Q: kW)	0.696
Power amp. (maximum: kW)	1.0

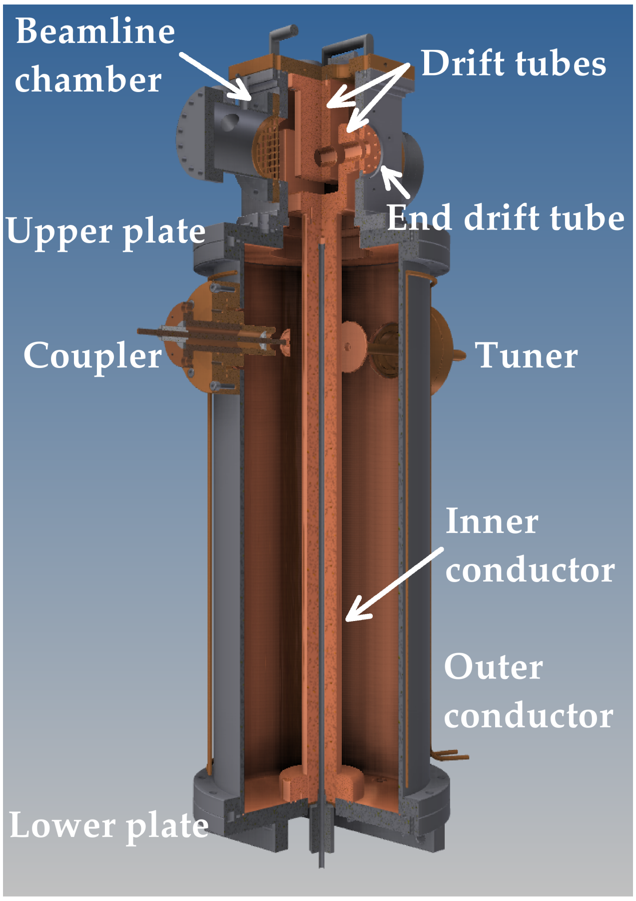

Fig. 1. Schematic view of the first rebuncher for RILAC2 (B2 REB).

*1 SHI Accelerator Service Ltd.

The beamline chamber and outer conductor were made of aluminum (A5052) and stainless steel (SUS304), respectively, and were copper plated to a thickness of 50 μm. A part of the coupler and trimmer was reused from the existing cavity mentioned above. The diameters of the coupler and tuner plates were 70 and 95 mm, respectively. The stroke of the trimmer was designed to be in the range of 30 to 90 mm from the center of the cavity. The tunable range of the resonant frequency was estimated to be 0.84% by MWS calculations.

All the parts were assembled, and vacuum and low-power tests were performed in November 2010. Two turbomolecular pumps (TMPs) with exhaust velocities of 350 and 220 ℓ/s were positioned on either side of the beamline chamber. The tunable frequency range was measured to be 36.304–36.618 MHz (+0.32%/−0.54%). The measured loaded-Q value (Q_L^{meas}) was 3470, whereas the calculated unloaded-Q value (Q_0^{calc}) was 8540. The ratio $2Q_L^{meas}/Q_0^{calc}$ was 81.3%. The shunt impedance was measured by a perturbation method with a bead of ϕ12 mm and $\varepsilon_r = 137$. The bead was moved by a step of 3.5 mm along the beam axis. The measured impedance was 7.181 MΩ, which was 80.6% of the calculated value (8.914 MΩ). The ratio of the measured and calculated shunt impedances was very close to the Q-value ratio, with a difference of less than 1%. A dissipation power required was 696 W. The desired gap voltage was successfully achieved by the end of November, and the cavity was installed in the AVF hall in early December. The rebuncher operated stably during the beam commissioning of RILAC2 in the end of December 2010 and January 2011[4]. The vacuum pressure was typically 1.5×10^{-5} Pa. We are planning to improve the vacuum pressure by replacing one of the TMPs with a cryopump.

References

1) K. Yamada et al.: RIKEN Accel. Prog. Rep. 43 (2010), p. 105.
2) K. Yamada et al.: RIKEN Accel. Prog. Rep. 43 (2010), p. 107.
3) O. Kamigaito et al.: Proc. PASJ6 (2009), p. 38.
4) K. Yamada et al.: In this report.

Design of an electrode of a prebuncher in a new injector linac for RI-Beam Factory

H. Okuno

[Beam dynamics, buncher]

A new injector linac system has been developed to increase the beam intensity of uranium ions. A prebuncher placed upstream of an Radio Frequency Quadrupole (RFQ) linac is an effective system for bunching Direct Current (DC) ion beams extracted from a new powerful 28-GHz superconducting Electron Cyclotron Resonance (ECR) ion source that has a fundamental frequency of 18.25 MHz. The value of the product of velocity β and wave length λ ($\beta\lambda$) for a low-energy ion beam extracted from the ion source at 22.8 kV is as low as 43.6 mm; thus, a small voltage gap is required for effective bunching. However, a small votage gap gives rise to a less uniform electric field distribution in the radial direction. Therefore, two parallel grids are used to achieve uniform field distributions with small voltage gaps in many cases of bunching of low-energy ion beams. However, we have decided to use a gridless bunching system because a high-power uranium can beam easily destroy the grids.

We have selected a bunching system that has a drift-tube structure with two gaps, whose intervals are adjusted to be $3/2\beta\lambda$. The side cross section of the prebuncher is shown in Fig. 1. The aperture diameter is 40 mm and the voltage gap is 20 mm. The axial field distribution obtained from FEM simulation is shown in Fig. 2. The difference between the axial and off-axial field distributions (r = 1 cm) is about 1%, which is allowable for beam bunching. The transit time factor is obtained to be around 0.2 by integrating Ez cos(kz) over the length of the prebuncher, as shown in Fig. 2. A beam dynamics simulation code, TRACK[1], is used to simulate the bunching effect of the prebuncher in the Low Energy Beam Transport (LEBT) line designed by Y. Sato et al.[2]. Figure 3 shows that a DC beam can be bunched at a prebuncher voltage of 1.1 kV. The simulation includes the RFQ that operates at the second harmonic to ensure that a beam is captured in the proper buckets of the RFQ. Figure 4 shows the results when the capture ratio is about 80%.

The rebuncher that was in use for RILAC injection was modified to realize the prebuncher. Y. Watanabe et al. assembled the modified electrodes shown in Fig. 1. The prebuncher was excited by K. Suda et al. and was first used for beam commissioning in Dec. 2010.

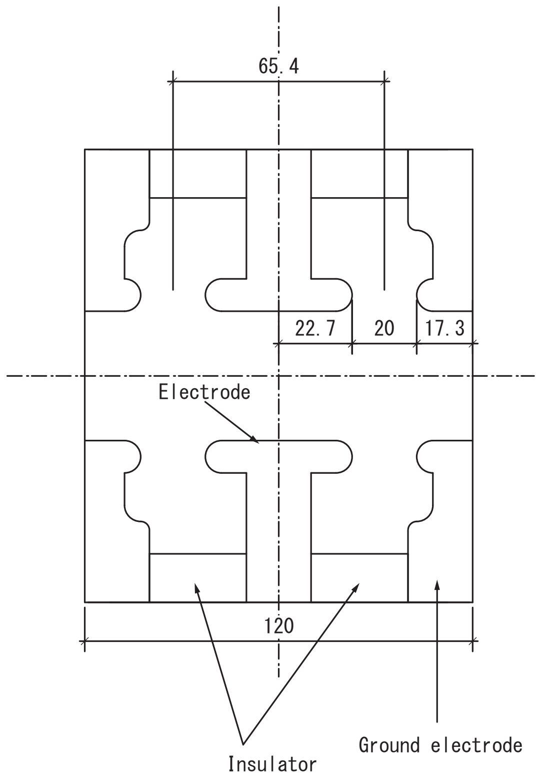

Fig. 1. Side cross section of the electrodes of the prebuncher.

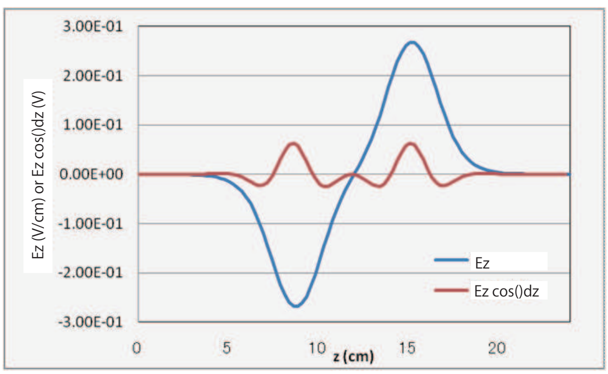

Fig. 2. Axial field distribution and Ez cos(kz) in the prebuncher.

References

1) P. N. Ostroumov, V. N. Aseev, and B. Mustapha: Phys. Rev. ST Accel. Beams **7**, 090101 (2004).
2) Y. Sato, et al.: RIKEN Accel. Prog. Rep. **43**, 119 (2010).

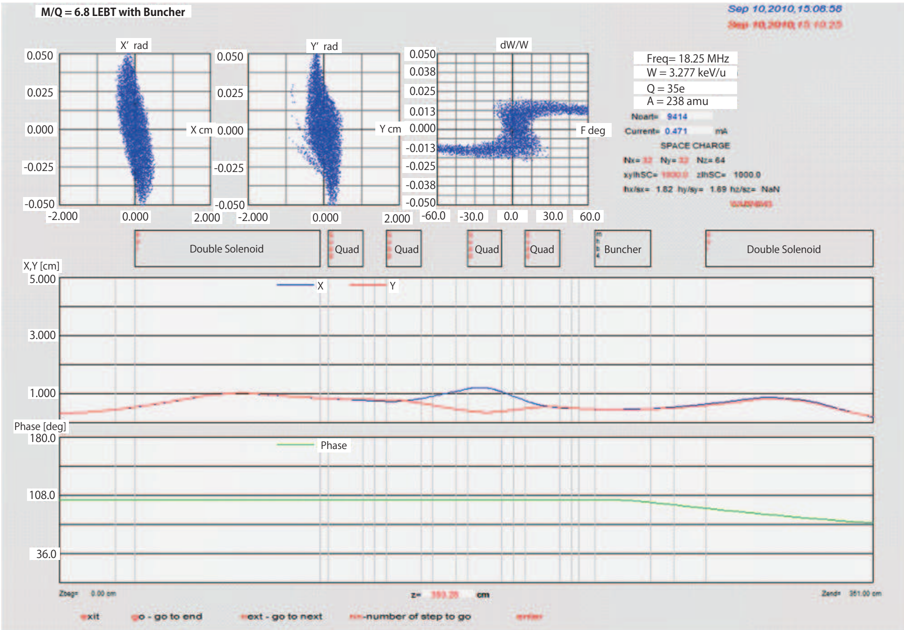

Fig. 3. Simulation results for beam bunching by the prebuncher in the LEBT line. The three graphs in the upper part of the figure show the beam plots in the horizontal (X-X′), vertical (Y-Y′), and longitudinal (F-dW/W) directions at the end of the LEBT. The beam envelopes and phase width are also shown along the beam line.

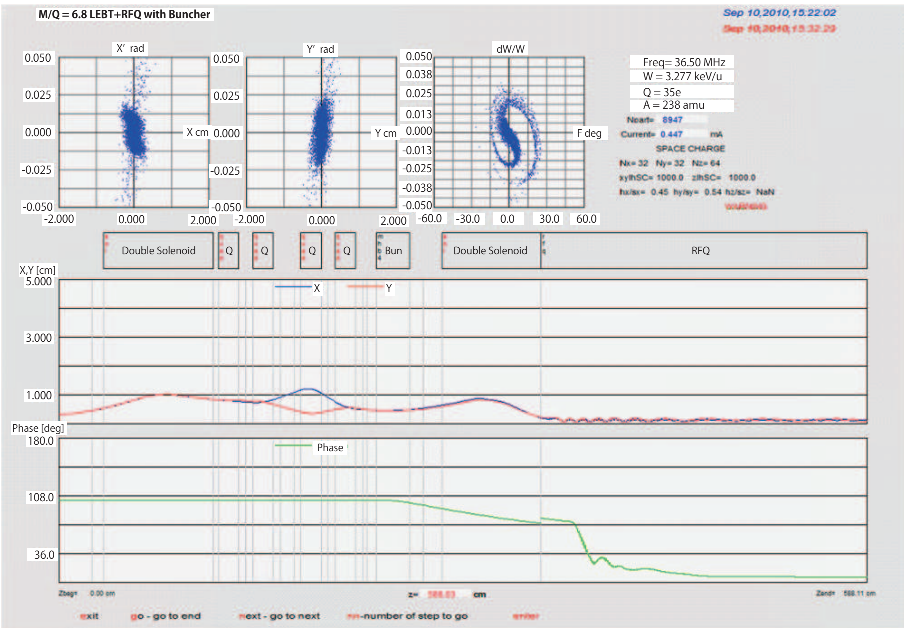

Fig. 4. Simulation results for LEBT+RFQ. The three graphs in the upper part of the figure show the beam plots in the horizontal (X-X′), vertical (Y-Y′), and longitudinal (F-dW/W) directions at the end of the RFQ. The beam envelopes and phase width are also shown along the beam line. The phase width in the RFQ is calculated at the second harmonic of the fundamental frequency (18.25 MHz) while the phase width in the LEBT is calculated at the fundamental frequency.

Water-Cooling System for RILAC2

Takeshi Maie, Eiji Ikezawa, Yutaka Watanabe, Masayuki Kase, Osamu Kamigaito
RIKEN Nishina Center
2-1 Hirosawa, Wako, Saitama 351-0198, Japan

1. Introduction

In March 2010 , a water-Cooling system （Fig.1） was installed at the RIBF in addition to a cooling system intalled exclusively for the RIBF in 2004. this cooling system was installed exclusively for the new injector RILAC2 , which is under construction , because of the high-intensity beams produced by the RIBF.
The cooling method in this system does not use a cooling tower to cool the devices. Instead, it uses cold water generated by an absorption chiller.
This system has the following advantages: 1. Because neither a cooling tower nor a circulating pump is used, the production cost is greatly reduced. 2. The running cost is reduce. 3. Cooling water having a stable temperature can be supplied any time. The cooling method is different from the method used by a cooling tower that depends on the weather, air, etc. this is a big advantage.

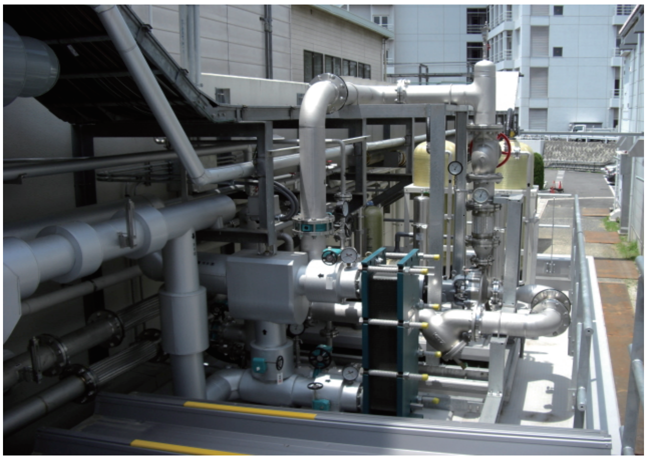

Fig.1: Photograph of the RILAC2 water-cooling system

2. RIBF water-cooling system

It is RIBF water cooling system (Fig.2) that easily showed the supply destination of cooling water in each system. Fig.3 is an overall view of RIBF water-cooling system. The SHARAQ water-cooling system was constructed the SCRIT water-cooling system respectively in 2008 and began operating in 2009 as a cooling installation only for the pilot machine.

Water-cooling system for RIBF

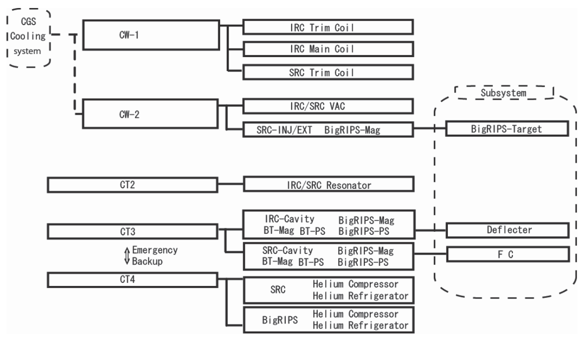

Fig.2: Figure of the RIBF water cooling System diagram

Fig.3: Photograph of the RIBF water-cooling system

3. Water-cooling system for RILAC2 and accelerator cooling water pump with motor

A block diagram of the water-cooling system for RILAC2 is shown in Fig.4.

The system supplies cooling water to the following equipment: compressoron on the superconducting 28-GHz ECR ion source , solenoid coil , RFQ, DTL (drift tube linac)1,2,3, rebuncher , BT-Mag such as a Q-magnet and steering magnet, power supply, beam-diagnosis system such as faraday cup, etc. All this equipment is installed at the supply destination of the RILAC2 water- cooling system.

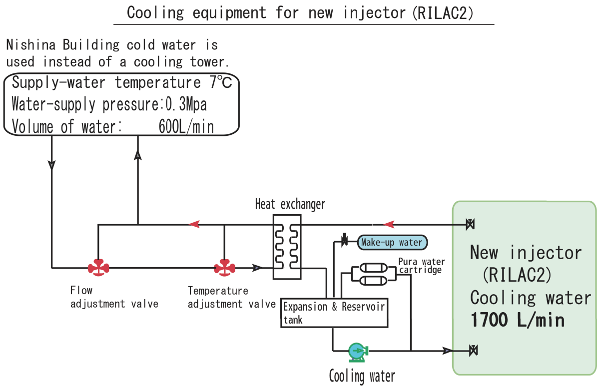

Fig:4 Block diagram of the RILAC2 water-cooling system

Specifications of the Water Cooling System forRILAC2

The primary water-cooling pump
Flow Rate: 1700L/min
Lift :100m
Motor: Highly effective 2 poles
Voltage: Three-phase 400V AC
Output: 55kW
Electric motor start method:Inverter start method
Heat exchanger: Plate type
Heat exchange ability:787kW （Max）
Cooling water flow rate and temperature
Primary:Purified water 1700L/min
IN28C/OUT 34.7C
Secondary:Cool Water 600L/min
IN 7.0C/OUT 25.8C
Temperature control:Electric three-way valve
ThermometerPiping-insertion type Pt resistance thermometer bulb and digital instruction adjustment meter (R36)
Measurement error: ± 0.5C(Actual measurement value)
Water-purifying apparatuses:Ionicexchangeresin cartridge type (pure water machine ×2, make-up water ×1)

The motors (Fig.5) used in the RILAC2 water-cooling system and most of those used in the RIBF cooling-water system are highly effective motors with an efficiency of 93.5%, compared to a normal motor whose typical efficency is 91%. There fore, the system is designed to save energy.
We use low-noise and low-vibration devices and inverter circuits to drive the motors. The inverter- start method is adopted to avoid “water hammering”, which may damage the equipment such as piping, hoses, coupling, and valves and cause leak of water leakage.

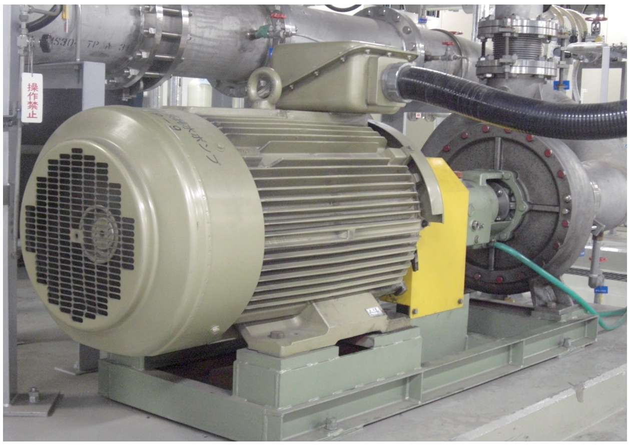

Fig.5: Photograph of the accelerator water pump with a highly effective motor (JIS Standard C4212)

5. Summary

The continuous operation of the water-cooling system started in December 2010 for the commissioning of RILAC2. This system supplies water-coolingto the superconducting ion source also.

RILAC2 Magnet System

K. Kumagai , N. Fukunishi, and Y.Watanabe

The RILAC2 consists of an ion source, a low-energy beam transport line (LEBT), a radio frequency quadrupole (RFQ), a drift tube linac (DTL), and a high-energy beam transport line (HEBT), which are all connected to the AVF-RRC beam line [1)]. The length of RILAC2 is approximately 23 m.

The magnet system of RILAC2 is composed of 3 dipole magnets, 20 quadrupole magnets, 8 steering magnets, and 2 solenoid magnets. Furthermore, doublet quadrupole magnets are added to the existing AVF-RRC beam line in order to keep the beam envelope small along the beam line. Table 1 lists the magnets and power supplies of the RILAC2. The arrangement of the magnets on the RILAC2 is shown in Fig. 1. Some of the magnets and the power supplies had been part of the medium-energy beam transport line (MEBT) of the RILAC and had been reused, and the others were newly constructed.

Because there was not enough space to place the power supplies in the magnet power supply room close to RILAC2, the power supplies were scattered in the AVF mezzanine room, the power supply room D, the polarized ion source room, the junction room, and the No. 2 ion-source room.

The new power supplies for the 10 quadrupole magnets in the DTL zone and the 2 solenoid magnets in the LEBT zone are switching-type power supply using IGBT devices, and the required current stability is about $\pm5\times10^{-4}$. Since the required stability is not very high, the power supplies use DCCTs in the current feedback circuit with relatively lower specification than that for the power supplies used for cyclotrons. Further, the current feedback circuit does not have a temperature-controlled box for current detection resistance and digital-analog converters (DAC).

General-purpose power supplies were used for all steering magnets and the four quadrupole magnets of the LEBT zone. They are controlled by a programmable logic controller (PLC, YOKOGAWA, FA-M3 series) with a CPU module (F3RP61, YOKOGAWA). This CPU module is operated by a Linux OS and is compatible with EPICS that is used for accelerator control in RIBF. Since each power supply does not have enough input/output signals to monitor the status of magnet-power supply system and to operate safely as a component of an accelerator system, a programmable relay unit (ZEN V2 series, OMRON) was introduced between the PLC and the magnet. Safety interlocks can be established by the relay unit regardless of the remote control. Figure 2 shows a block diagram of the control system for these power supplies.

The other power supplies are controlled with the EPICS via the NIO or the SIM-DIM interface system.

Table 1. List of magnets and power supplies for RILAC2

Zone	Magnet Name	Type	Number of Magnets	Magnet	Power Supply	Current Max. (A)	Voltage Max. (V)	Control	Location of Power Supplies (*)
Ion source room	SOU0	Solenoid	1	Existing	Existing	250	60	F3RP61	I2
	STU0	Steering	2	Existing	New	10	60	F3RP61	I
	BM−U10	Dipole	1	Existing	Existing	330	60	NIO	AVF−M
	STU10	Steering	2	Existing	New	10	60	F3RP61	I
	SOU11ab	Solenoid	1	New	New	300	60	NIO	AVF−M
LEBT	QQB12abcd	Quadrupole	4	Existing	New	50	16	F3RP61	I
	STB12a	Steering	2	Existing	New	10	60	F3RP61	I
	STB12b	Steering	2	Existing	New	10	60	F3RP61	I
	SOB13ab	Solenoid	1	New	New	300	60	NIO	AVF−M
DTL	QDB21ab	Quadrupole	2	New	New	300	60	NIO	AVF−M
	STB21a	Steering	2	Existing	New	10	60	F3RP61	I
	STB21b	Steering	2	Existing	New	10	60	F3RP61	I
	QDB22ab	Quadrupole	2	New	New	300	60	NIO	AVF−M
	QTB31abc	Quadrupole	3	New	New	300	60	NIO	AVF−M
	QTB41abc	Quadrupole	3	New	New	300	60	NIO	AVF−M
HEBT	STB50	Steering	2	Existing	New	7.7	70	NIO	J
	QTB51abc	Quadrupole	3	Existing	Existing	260	18	CIM−DIM	D
	DMB6	Dipole	1	New	Existing	300	150	CIM−DIM	D
	QSB61	Quadrupole	1	Existing	Existing	260	18	CIM−DIM	D
	STB61	Steering	2	Existing	New	7.7	70	NIO	J
	DMB7	Dipole	1	New	Existing	300	150	CIM−DIM	D
	QDB71ab	Quadrupole	2	Existing	Existing	260	21	NIO	J
AVF−RRC Beamline	QDS23ab	Quadrupole	2	Existing	Existing	260	21	NIO	J

I2: Second ion source room, I: Polarized ion source room, AVF−M: Mezzanine AVF vault, D: D power supply room, J: Junction room

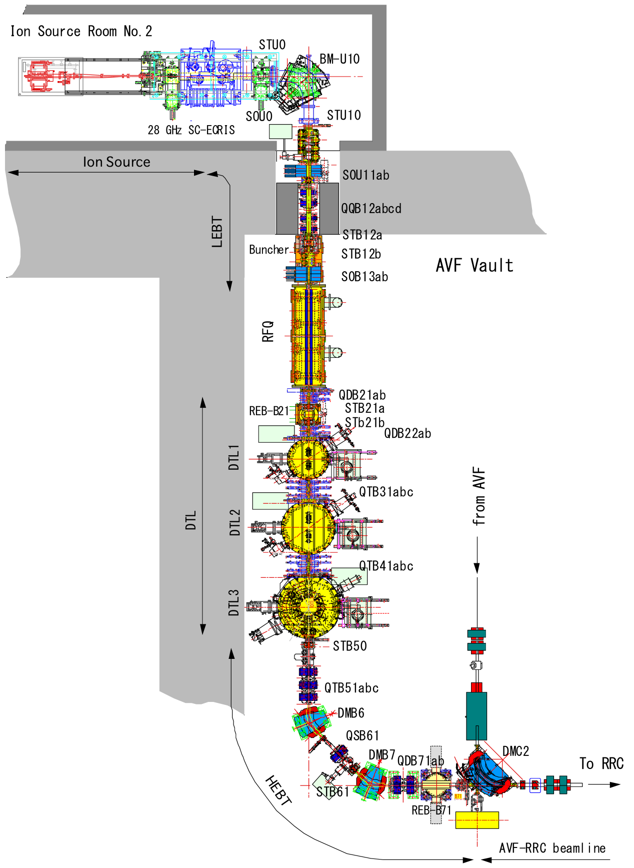

Fig. 1. Arrangement of the magnets on the RILAC2.

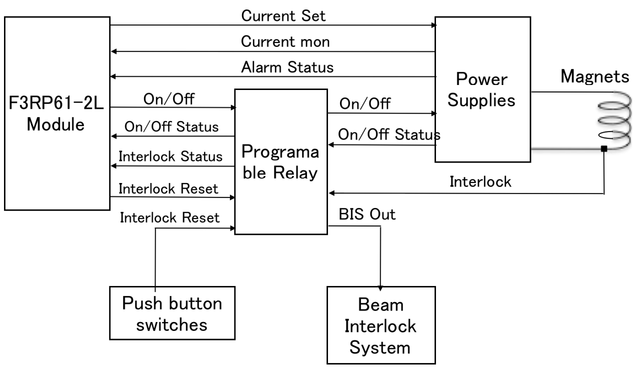

Fig. 2. Block diagram of the control system for steering magnets and the quadrupole magnets.

Two dipole magnets with a 45° deflection angle on the HEBT were designed to produce the magnetic field of 1.5 T by using the maximum current of the existing power supplies. The measured excitation curve at the center of the dipole magnet is shown in Fig. 3. Figure 4 shows the measured magnetic field distribution along the beam orbit with a coil current of 300 A.

The four quadrupole magnets of the LEBT were placed in the middle of a radiation shield wall with a thickness of 1.5m of the AVF cyclotron vault (see Fig. 1). Since the space around the air-cooled magnets has been filled with radiation shielding, overheating of the air-cooled magnet coils is one of the problems. Currently, the excitation current is limited so that the temperature rise will be less than 35 ℃. The coil temperature is continuously monitored to maintain the interlock of the power supplies.

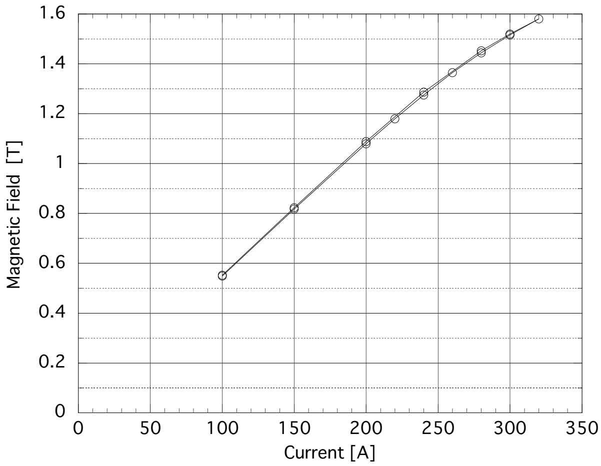

Fig. 3. Excitation curves of the DMB6 dipole magnet. DMC1-7 power supply was used for the measurements. The magnetic field was measured while increasing the current and then measured while decreasing the current.

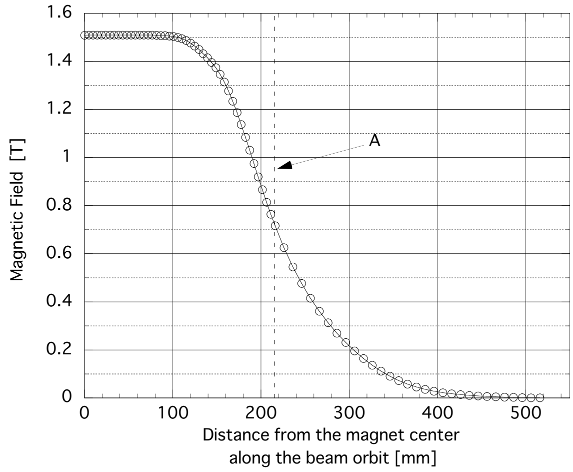

Fig. 4. Magnetic field distribution of DMB6 magnet along the beam orbit at a current of 300 A. Line A indicates the edge of the magnet.

Remained tasks for the improvement of the RILAC2 magnet system are as follows: remaking the steering magnets around the buncher B12 of the LEBT and the re-buncher B21 of the DTL because they are temporarily placed because the space is very narrow to place the existing magnets, installing the magnetic-field-measurement device into the dipole magnet DMB6 or DMB7 in the HEBT, and monitoring the magnetic field anytime in order to determine the beam energy during the operation.

References

1) Y. Watanabe et al.: In this report.

Construction of a new building for the RILAC2 ion source

H. Yamasawa, Y. Watanabe, J. Ohnishi, and M. Kase

The layout of the new injector, RILAC2, is shown in fig. 1. The ion source (28-GHz superconducting ECRIC) would be located outside the Nishina Memorial Building, northwest of the AVF cyclotron vault. It is necessary to construct a small shed that can house the ion source, and this shed would be named "second ion-source room". A special controlled area for nuclear fuel material will be reserved in the room, because uranium ions are mainly produced by the ion source.

The construction area is the narrow pass (6 m in width) between the Nishina Memorial building and the Ring-linac power station building. Two problems arise from this construction.

First, the new construction is located along an important access route to the AVF and RRC vaults, because the entrances to the AVF and RRC vaults are at the far end of the pass. An access that is at least 3 m width is planned; this width is not sufficient for the transportation of large cyclotron parts, which weigh around 20 ton, but is sufficient for the transport of materials (several tons) for the normal maintenance of these cyclotrons.

Second, the important lifelines connecting the east section of the accelerator site and the main part of RIKEN are located underground. Five kinds of pipes are buried in the construction area (three drains for rainwater, household effluents and experimental wastewater, and two supplies for city water and well water used in cooling towers). All these pipes were shifted outside the construction site in the summer of 2010.

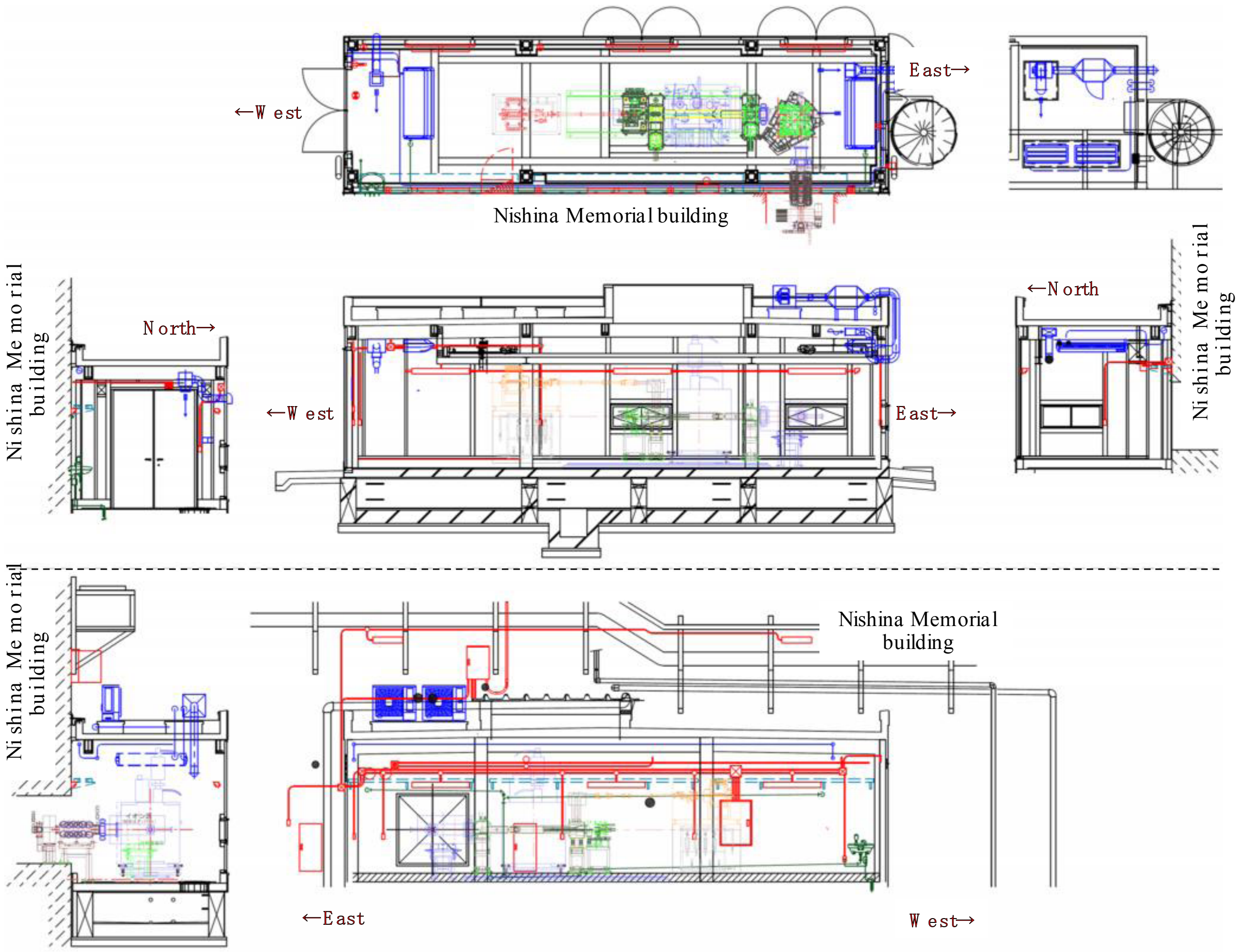

Fig. 1. Layout of ion-source room for RILAC2.

The construction was commenced in September 2009 and completed in February 2010. The new building (the second ion-source room) is, as shown in fig. 2, a steel-framed one-story house with an area of 50 m^2, 12 m (width) × 3.5 m (length), and a height of 3.5 m. The foundation is a solid base, which is sufficiently strong to support the entire ion source system, whose weight is around 10 ton. On the roof of the building, a machine hatch (2.85 m × 1.81 m) is built for installing the ion source, a 6-ton superconducting magnet. A photograph of the installation using a crane truck is shown in fig. 3.

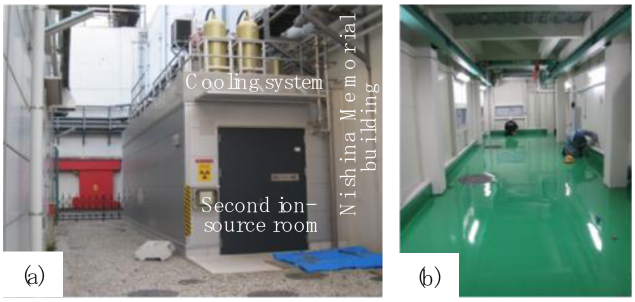

Fig. 2. (a) Outer view of the ion-source room for RILAC2. (b) Inner view of the room before installation of the ion source.

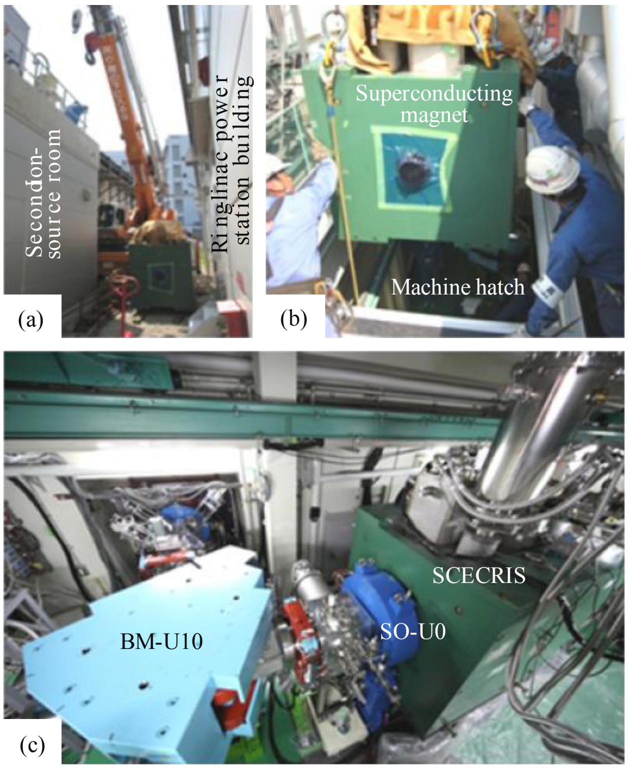

Fig. 3 SCECRIS. (a) Rough-terrain crane (max. lifting capacity: 65 ton); (b) transport of ion source through the machine hatch; (c) the installed SCECRIS (taken by Mr. N. Miyauchi [User support office]).

The superconducting magnet in the ion source and a 3-ton analyzing magnet were carried to the new building by a rough-terrain crane. A crane with a lifting capacity of 65 ton (SL-650R) was selected because of the long distance (12 m) between the crane parked in the narrow pass and the machine hatch and the large magnet weight (6 ton).

Since this building act as a nuclear fuel control room, it must be equipped with special ventilation and drain systems. The ventilation (third category) system maintains the inside air at a negative pressure, so that direct leakage of air to the outside environment is prevented. All the air is filtered and released to the outside. The water from the drain is disposed along with the wastewater from the Nishina Memorial building. The drain pipe in the ion-source room penetrates the 2-m-thick concrete wall and joins the RI drain system in the Nishina Memorial building. The floor is covered with epoxy-resin-type paint.

Because a steel frame structure is employed, the rooftop is strong, thus facilitating the installation of the main parts of the cooling system for RILAC2, as shown in fig. 4. For access to the rooftop, a spiral staircase made of aluminum is attached to the east portion of the building.

A 28-GHz RF transmitter will be used to energize plasma in the near future. An additional X-ray shield surrounding the building may be required.

References

1) O. Kamigaito, et al., Proc. PASJ3 (2006), Sendai, Aug. 2-4, 2006.
2) O. Kamigaito, et al., Proc. PASJ6 (2009), Tokai, Aug. 5-7, 2009.
3) Y. Higurashi, et al., Proc. PASJ7, Himeji, Aug. 4-6, 2010, in press.
4) Y. Watanabe, et al., J. PASJ, Vol.**7,** No.4 (2010), p.37-45.
5) T. Maie, et al., Proc. PASJ7, Himeji, Aug. 4-6, 2010, in press.

Fig. 4 Cooling facility on the roof (taken by Mr. T. Maie).

Production of highly charged U-ion beam from RIKEN SC-ECRIS

Y. Higurashi, T. Nakagawa, J. Ohnishi, H. Haba, M. Fujimaki, M. Komiyama, T. Aihara[*1], M. Tamura[*1], A. Uchiyama[*1], M. Kase, A. Goto and O. Kamigaito

In 2008, we successfully produced a 345 MeV/u U beam (0.4 pnA on target). Even though such a low beam intensity was used for the experiment, more than 40 new isotopes were produced.[1)] It shows that a high-enegy U beam is a strong tool for producing very neutron rich nuclei. In 2008 we produced only 2-4 eμA U^{35+} beams with the RIKEN 18 GHz ECRIS[2)] which was much lower than the beam intensity required (1 pμA on target) for the RIKEN RIBF. To meet this requirement, we constructed a new SC-ECRIS that has the optimum magnetic field strength for 28 GHz.[3)] In the autumn of 2009, we produced the first beam of U^{35+} from the RIKEN SC-ECRIS with 18 GHz microwaves.[4)] Since then, we have continued our efforts to increase the beam intensity of highly charged U-ion beams. In this report, we present the results of a test experiment performed in 2010 to produce a highly charged U-ion beam.

Details of structure of the SC-ECRIS and the first test experiment were presented in ref. 3. Figure 1 shows a photograph of the RF-injection side of the ion source. We used the sputtering method for U beam production. As shown in Fig. 1, the metal uranium rod was placed on the off-center axis. The rod was supported by a supporting rod. The position of the rod was remotely controlled. The supporting rod was water-cooled for minimizing the possibility of a chemical reaction between the uranium metal and the material of the uranium holder at high temperatures. The rod position and high voltage used for sputtering were optimized for maximizing the beam intensity of highly charged U ions. Figure 2 shows the charge distribution of the highly charged U ions when O_2+Ar gas was used. The RF power was 980 W. The extraction voltage was 17 kV.

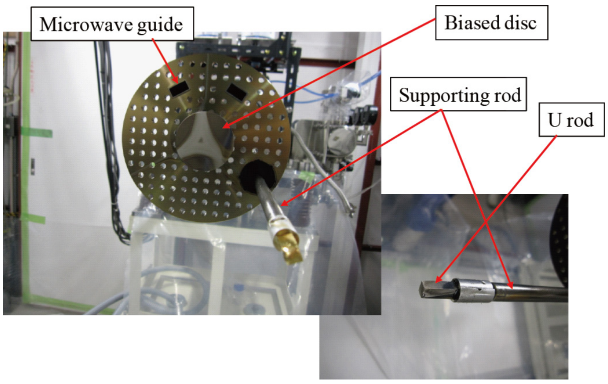

Fig. 1. Photograph of the RF-injection side of the ion source used for sputtering method.

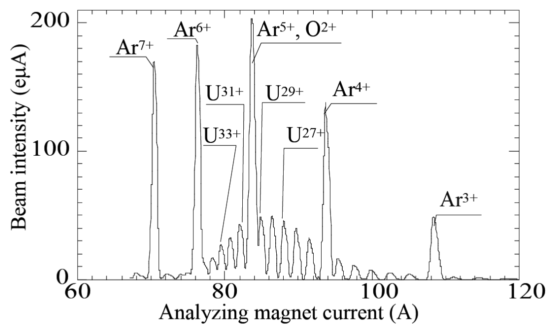

Fig. 2. Charge state distribution of U ions when O_2+Ar gas was used as the ionized gas.

The beam intensity of U^{35+} as a function of the rod position and high voltage used for the sputtering is shown in Figs. 3 and 4, respectively. The RF power was about 900 W. The extraction voltage was 15 kV. B_{inj}, B_{min}, B_{ext},and B_r were 2.3, 0.5, 1.2, and 1.3 T,respectively. The beam intensity increased linearly with the high voltage used for sputtering. The beam intensity also increased with the proximity of the rod to the ECR zone, as shown in Fig. 3.

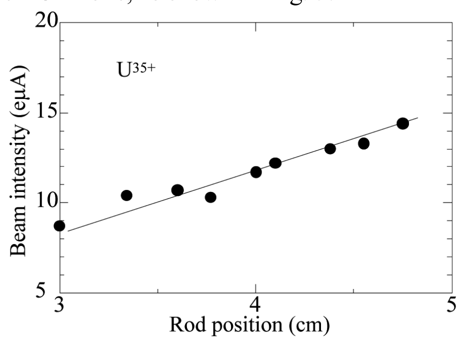

Fig. 3. Beam intensity of U^{35+} as a function of the rod position. The sputtering voltage was 4 kV.

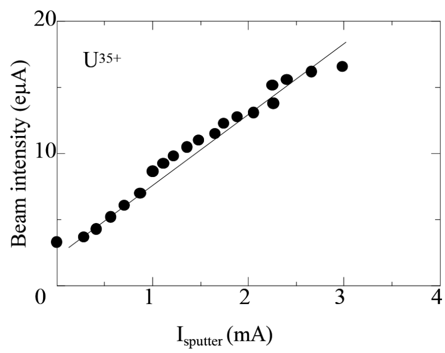

Fig. 4. Beam intensity of U^{35+} ion as a function of the sputtering voltage. The rod position was 4.8 cm.

*1 SHI Accelerator Service Ltd.

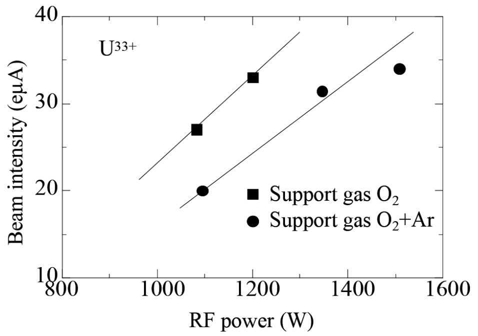

Fig. 5. Beam intensity of U^{33+} as a function of the RF power when O_2(closed squares) and O_2+Ar (closed circles) gases were used as the ionized gas.

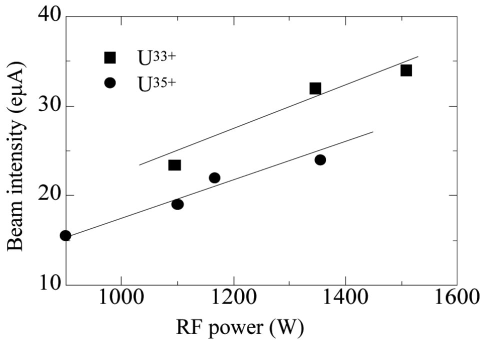

Fig. 6. Beam intensity of $U^{33+}$and U^{35+} as a function of the RF power, when O_2 gas was used.

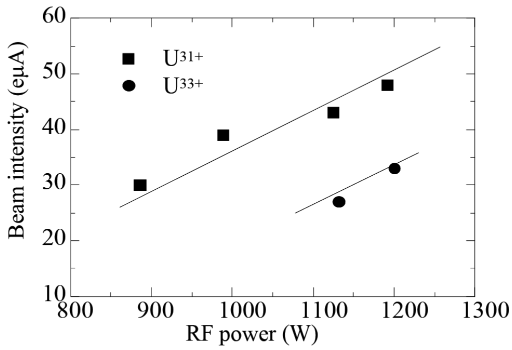

Fig. 7. Beam intensity of U^{31+} and U^{33+} as a function of the RF power when O_2+Ar gas was used.

It has previously been reported that the supporting gas strongly affects the beam intensity of highly charged heavy ions in many laboratories (gas mixing method).[5] For investigating the effect of the gas on the beam intensity, we used O_2 and O_2+Ar gases the an ionized gas. Figure 5 shows the beam intensity of U^{33+} as a function of the RF power. The beam intensity in the case of O_2 gas was always higher than that for O_2+Ar for a given RF power. However, for lower charge states of heavy ions (<31+), for example, the beam intensity of U^{31+} with O_2 gas at the RF power of 1.2 kW was 33 eμA, which was lower than that (48 eμA) with O_2+Ar gas. Figure 6 shows the beam intensities of U^{33+} and U^{35+} as a function of the RF power in the case of O_2 gas. In figure 7, beam intensities for lower charge states of U ions (31+,33+) in the case of O_2+Ar gas are shown. We obtained about 50 eμA of U^{31+} at the RF power of 1.2 kW.

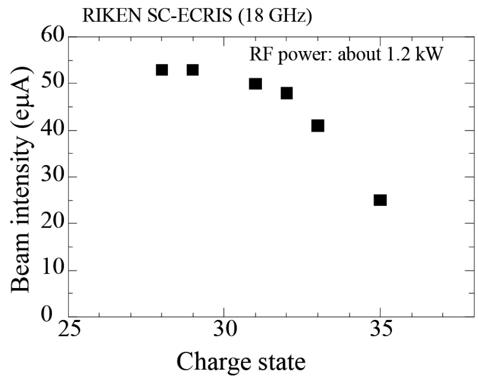

Fig. 8. Beam intensity of highly charged U ions at an RF power of about 1.2 kW.

Figure 8 shows the beam intensity of highly charged U ions at the RF power of about 1.2 kW. It is to be noted that the beam intensities were not saturated in this test experiment, as shown in Figs. 3-7. Because the of RF power density was very low (about 100 W/L). We may obtain a higher beam intensity at a higher sputtering voltage and higher RF power.

References

1) T. Ohnishi et al.: J. Phys. Soc. Jpn. **77**, 073201(2010).
2) Y. Higurashi et al.: RIKEN Accel. Prog. Rep. **42**, 117 (2009).
3) T. Nakagawa et al.: Rev. Sci. Instrum. **81**,02A320(2010).
4) Y. Higurshi et al.: RIKEN Accel. Prog. Rep. **43**, 114 (2010).
5) R. Geller: Electron cyclotron resonance ion sources and ECR plasma, (IOP, London, 1996)p.286.

Emittance measurements for RIKEN SC-ECRIS

Y. Higurashi, T. Nakagawa, J. Ohnishi, H. Haba, M. Fujimaki, M. Komiyama, T. Aihara[*1], M. Tamura[*1], A. Uchiyama[*1], M. Kase, A. Goto and O. Kamigaito

To increase the beam intensity on the target, we have to reduce the emittance and increase the beam intensity. In particular, we need an intense beam of highly charged heavy ions (a few tenth of pμA) from the ion source to meet the requirement (1 pμA on the target). In this case, the space charge strongly affects the beam quality (increase in emittance etc.). To reduce the emittance, we need to not only study the effect of the main parameters of the ion source (magnetic field configuration, gas pressure, etc.) on the emittance for the optimization fo the emittance, but also find a new method .

It is well-known that the so-called "gas mixing" increases the intensity of highly charged heavy ion beams[1] For example, when we produce highly charged Xe ions (e.g., Xe^{30+}), the beam intensity increases upon adding a lighter gas (e.g., O_2 gas) to the plasma.[1] Furthermore, the beam stability of highly charged heavy ions is also affected by the addition of the gas. From these results, we assume that the mixing gas may affect the beam quality. In this paper, we report the effect of the mixing gas on the emittance of a highly charged U-ion beam.

The detailed structure of the SC-ECRIS and the first test experiment were described in ref. 2. In this test experiment, B_{inj}, B_{min}, B_{ext}, and B_r were fixed at 2.3, 0.5, 0.12, and 1.3 T, respectively. The RF power was 970 W. The extraction voltage was 15 kV. For the production of U-ion beam, we used the sputtering method.[2] When using the sputtering method, we have to supply a gas for producing plasma, which functions as a mixing gas for the production of the U-ion beam. We used O_2 or O_2+Ar gas for plasma production.

Figure 1 shows a typical X emittance of U^{35+} at the extraction voltage of 15 kV when using O_2 gas is used. The measured rms X emittance was 134π mm mrad. Figure 2 shows the rms Y emittance as a function of the extracted current when O_2 gas (open circlcles) and O_2+Ar gas (closed circles) are used. It appears that the emittance increased with the extracted current. The emittance increase may be due to the space charge effect. Furthermore, the emittance O_2+Ar gas was smaller than that for O_2 gas for the same extraction current. Using O_2+Ar gas may be the good method for reducing the emittance size. To confirm these observations and the understanding mechanism, further investigations are required.

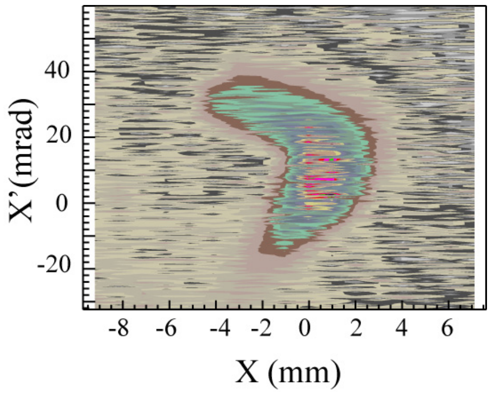

Fig. 1. Typical X emittance of U^{35+} at the extraction voltage of 15 kV. B_{inj}, B_{min}, B_{ext}, and B_r were 2.3, 0.5, 0.12 and 1.3 T, respectively. The RF power was 970 W. For the production of U-ion beam, we used the sputtering method and O_2 gas for plasma production.

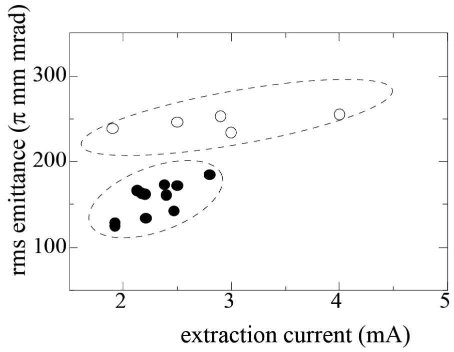

Fig. 2. Y emittance (rms) of U^{35+} when O_2 gas (open circles) and O_2+Ar gas (closed circles) were used.

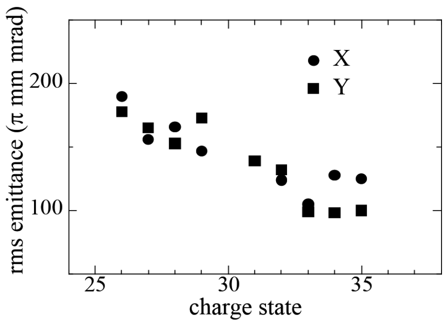

Fig.3. Emittance (rms) for highly charged U ions.

---

*1 SHI Accelerator Service Ltd.

Figure 3 shows the X and Y emittance (rms) for highly charged (U^{26+}-U^{35+}) ions when O_2+Ar gas was used for plasma production. The extracted current was about 2 mA. The emittance decreased with an increase in the charge state for the same extraction voltage. In this experiment, we obtained an rms emittance smaller than 140π mm mrad for U^{35+}. This was smaller than the acceptance of the accelerator of the RIKEN RIBF (about 160π mm mrad). This obsevation implies that we may accelerate almost all the U^{35+} beam (~20 eμA) produced by the RIKEN SC-ECRIS. This intensity is about 10 times higher than the intensity for the RIKEN 18 GHz ECRIS.

References

1) R. Geller: Electron cyclotron resonance ion sources and ECR plasma, (IOP, London, 1996) p.286.

2) T. Nakagawa et al.: Rev. Sci. Instrum. **81**,02A320(2010).

Extraction System of the 28-GHz Superconducting ECR Ion Source and Beam Emittance

J. Ohnishi, Y. Higurashi, and T. Nakagawa

The 28-GHz superconducting ECR ion source[1] was installed at the high-voltage terminal located upstream of the RILAC in 2009; this ion source provided uranium beams to the RIBF in December 2009.[2] In 2010, the ion source was moved to the newly constructed second ion source room to be used as an ion source for RILAC2, which was commissioned with the $^{124}Xe^{20+}$ beam from this source in December 2010.[3] Until now, the ion source has been operated with an 18-GHz microwave source because the 28-GHz source is under testing.

Figure 1 shows the arrangement of the ion source and the extraction system, the magnetic elements of which consists of a solenoid coil, a 90° analyzing dipole, and two steering magnets. The design of the analyzing dipole is the same as that of the VENUS ion source at the LBL.[4] The pole face of the dipole has a three-dimensional shape, and it produces an azimuthally varying sextupole magnetic field to reduce the aberration for large beams. The beam optics is a double-focus system, and the focus point is around 1 m downstream of the exit point of the dipole. Horizontal and vertical slits (SL-U10) are positioned at the focus point, and the slit for emittance measurements, two beam profile monitors (PF-U10a and PF-U10b), and a Faraday cup (FC-U10) are positioned after these slits. This arrangement is almost the same as that at the high-voltage terminal of the RILAC. The beam orbits shown in Fig. 1 are for the Xe beams and are calculated with SCALA,[5] which is a 3d tracking calculation code that takes into account the space –charge effect for multiple ions.

Figure 2 shows the configuration of the extraction region of the ion source. The extraction hole is 10 mm in diameter. The extraction electrode is movable, and its usual gap is 30–40 mm. The extraction voltage is 21.3 kV for $^{238}U^{35+}$ and $^{136}Xe^{20+}$. This ion source is only used to generate beams of very heavy ions such as uranium and xenon ions because it is an ion source for the RILAC2.

Figure 3 shows the emittance plots of the $^{238}U^{35+}$ beam. The emittance measurements were performed before the movement, and the scanning slit located 1.1 m downstream of the exit point of the analyzing dipole and the beam profile monitor 0.2 m downstream of the slit were used. The rms emittance values were calculated using the equation

$$\varepsilon_{rms} = 4\sqrt{<x^2><x'^2> - <xx'>^2},$$

where <> indicates the average value within the square frame shown in the figure. The heap in the lower right area is due to the beams that do not pass through the slit. In this case, the rms emittances were 161π and 134π mmmrad in the horizontal and vertical directions, respectively.

Figure 4 shows the rms beam emittances measured for the beams extracted from this ion source so far. In this figure, the beams are divided to four groups: $^{134}Xe^{20+}$, $^{124}Xe^{20+}$, and two kinds of $^{238}U^{35+}$ beams. Although the operation conditions for the ion source differ in each emittance measurement, the general conditions for each group are given in Table 1. Since the extraction voltage also differs, the emittance values are converted to those corresponding to a RILAC2 injection energy of 3.28 keV/u. The following observations are made from this figure. 1) The smallest horizontal emittance is 140π mmmrad for Xe and 100π mmmrad for U. Overall, the emittance of the Xe beam is 30–40% larger than that of the U beam. 2) The

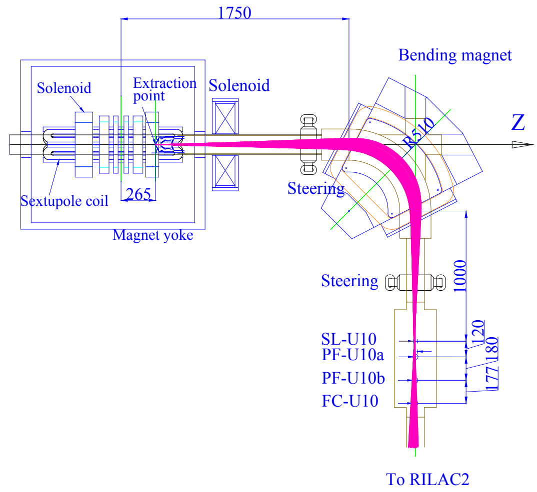

Fig. 1. Arrangement of the extraction system of the 28-GHz superconducting ion source.

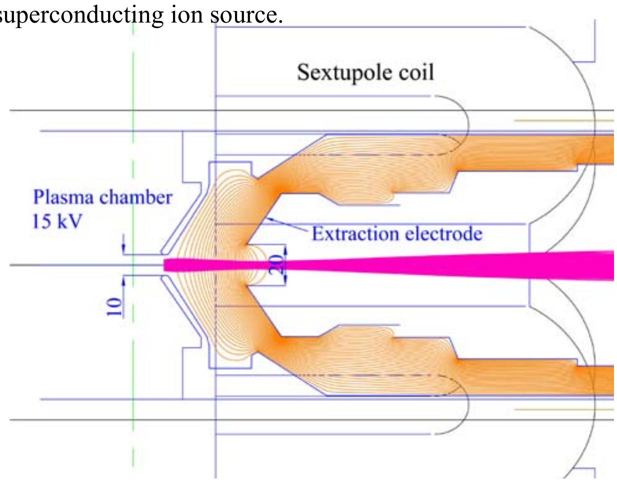

Fig. 2. Configuration of the extraction region.

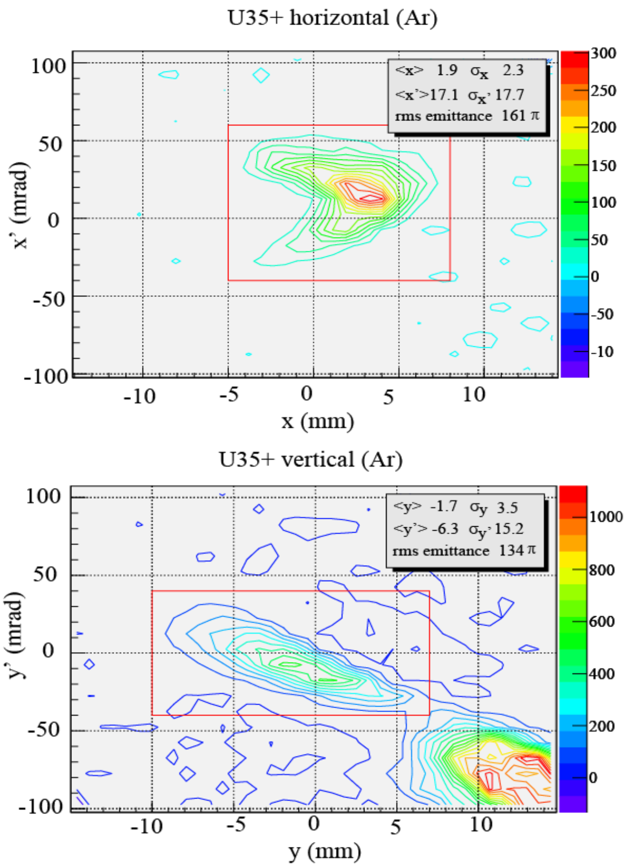

Fig. 3. Measured emittance plots for the U^{35+} beam.

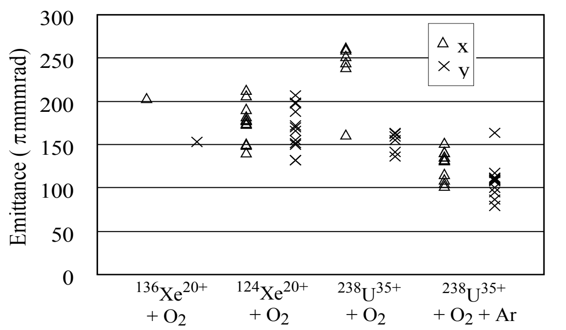

Fig. 4. Measured emittances for the beams extracted from the ion source. The values are converted into those corresponding to the RILAC2 injection energy 3.28 keV/u.

Table 1. Operation conditions for emittance measurements shown in Fig. 4.

	$^{136}Xe^{20+}$	$^{124}Xe^{20+}$	$^{238}U^{35+}$	$^{238}U^{35+}$
Beam current (μA)	78	40 – 60	9 – 15	7 – 13
Support gas	O_2	O_2	O_2	Ar or O_2 +Ar
Extraction voltage (kV)	17	15 – 20	15	15
Drain current (mA)	2.5	1.2 – 1.8	2.5 – 4	1.9 – 2.8
RF power (W)	600	450 – 500	900 – 1000	900 – 1000

emittances of the U beam, which uses Ar or Ar + O_2 as the supporting gas, are smaller than those of the U beam, which uses O_2. In particular, the horizontal emittances are larger than the vertical emittances when O_2 is the supporting gas. This emittance difference depending on the supporting gas can be simulated with SCALA.[6] Namely, according to the SCALA calculation, the beam size in the analyzing dipole increases with the beam current because of the space charge, and the horizontal emittance also increases. Although the reason for this has not yet been clarified, it is presumed that this effect is caused by the maldistribution of the space charge, because the beams are bent with different angles depending on the charge number and aberration is induced for large beams. In this calculation, neutralization by electrons is not considered.

The beam transport line to the RRC is designed with a beam emittance of 6π mmmrad. Since the velocity gain of the RILAC2 is 14.2, this value is equal to 85π mmmrad at the ion source. Although the real beam acceptance seems to be larger than this design value, the beam emittance in this ion source is larger than the acceptance, and hence, the beam loss is expected to occur. When the ion source is operated with a 28-GHz microwave source, the beam current may increase. However, the beam emittance is also expected to increase owing to the space-charge effect. Therefore, it is very important to investigate and improve the operation conditions for the ion source and the extraction structure.

References

1) Y. Higurashi et al.: Proc. IPAC 2010, p. 4191.
2) J. Ohnishi et al.: RIKEN Accel. Prog. Rep. **43**, 117 (2003).
3) K.Yamada et al.: in this report.
4) C. M. Lyneis et al.: AIP Conf. Proc. **600**, 219 (2001).
5) http://www.vectorfields.com/.
6) J. Ohnishi et al.: Proc. IPAC 2010, p. 4194.

Modification of the central region of RIKEN AVF cyclotron for acceleration at the first harmonic (h = 1)

S.B. Vorozhtsov*[1], V.L. Smirnov*[1], and A. Goto

The preparation of a detailed plan for upgrading the RIKEN AVF cyclotron is currently under way[1,2,3].

As reported in the last Progress Report[3], we modified the central region of the AVF cyclotron in the summer of 2009 in order to increase the maximum available energies of $^{16}O^{7+}$ and $^{6}Li^{3+}$ ion beams to 12 MeV/nucleon. In the past one year, we dedicated to further modify the central region geometry. The main aim of the modification is to increase the maximum available energy of protons to 30 MeV. For achieving this, the acceleration should be carried out at the 1st acceleration harmonic (h = 1) instead of the currently used 2nd acceleration harmonic (h = 2). Since the existing structure of the central region was designed only for h = 2 and not for h = 1, for which higher dee voltages are required, the main limitation in increasing the proton energy to 30 MeV is the available maximal dee voltage of approximately 50 kV; with this voltage, the particles are not able to clear the central electrode structure at the 1st turn. Therefore, it is necessary to redesign the central-region geometry.

Several configurations were scrutinized to obtain good centering and transmission for both a 30 MeV proton beam (h = 1) and ions accelerated at h = 2. The new central-region geometry thus designed is shown in Fig. 1. The shaded areas indicate the newly designed geometry, while the white lines indicate the existing geometry. The modifications are as follows: 1) the size of the RF shield covering the inflector was reduced substantially, 2) the position of the inner tip of the second dee electrode, dee 2, was shifted towards smaller radii accordingly, and 3) the position of the second gap of the first dee electrode, dee 1, was shifted downstream.

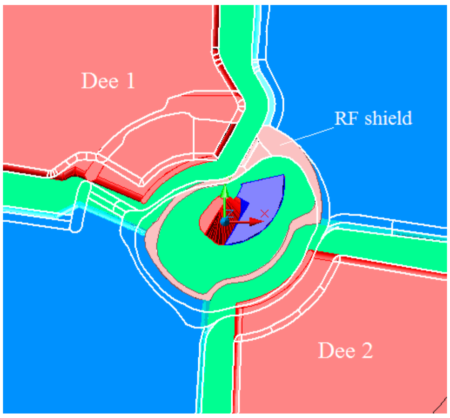

Fig. 1: Newly designed central region geometry (shaded). The white lines indicate the existing geometry.

*[1] Joint Institute for Nuclear Research, Russia.

Figure 2 shows the acceleration performance of the AVF cyclotron. The three shaded areas reflect the increase in the acceleration energy for various ions. The green one indicates the area that is expected to be available with the present design, while the yellow and blue ones indicate the areas corresponding to the original design and the previous modification, respectively.

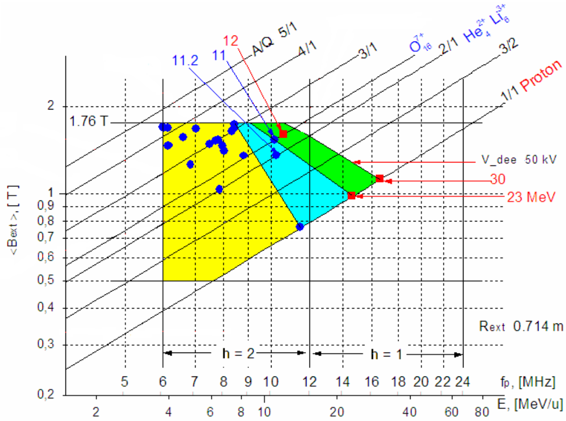

Fig. 2: Acceleration performance of the RIKEN AVF cyclotron. The yellow, blue, and green areas correspond to the original, existing, and newly designed geometries, respectively. Here, the boundaries of the green and blue areas on the high-energy side are given by assuming that the maximum dee voltage of 50 kV is available for the entire range of RF frequencies from 12 to 24 MHz. It is to be noted that the boundaries in the region of the h = 2 mode should be shifted towards lower energies because the actually available dee voltages (V_dee) are less than 50 kV for frequencies higher than around 20 MHz, e.g., 12.6 MeV/nucleon for $^{6}Li^{3+}$ ions. In the figure the following denotations are used: E – particle energy, $<B_{ext}>$ - mean magnetic field at extraction, f_p –rotation frequency of ion, R_{ext} – extraction radius, and A/Q – mass-to-charge ratio of ion.

Simulations of particle trajectories starting from the initial particle distribution in the 6D phase space upstream of the inflector showed that particle losses in the central region occurred mainly in the vertical direction. Figure 3 shows such losses by dots for 30 MeV protons; a total of 43 % of the injected particles are lost, three-fourths of which results from the particles hitting the upper and lower walls of the RF dee electrodes or beam chamber.

There is an attractive proposal[4] for mitigating the loss: modification of the inflector electrode surface (a "bent" inflector). In the "bent" inflector, as shown in Fig. 4, the surface of the electrodes is not smooth as in the classical spiral inflector but bent at some optimal angle with the "valley" along the central line of the electrode surface. The "bent" inflector permits the vertical focusing in the inflector to be increased at the expense of the horizontal focusing, which is degraded. The simulation with the "bent" inflector confirmed that the inflector substantially reduces the axial beam emittance at its exit and increases somewhat the radial emittance. Further optimization of the inflector electrodes is now under way.

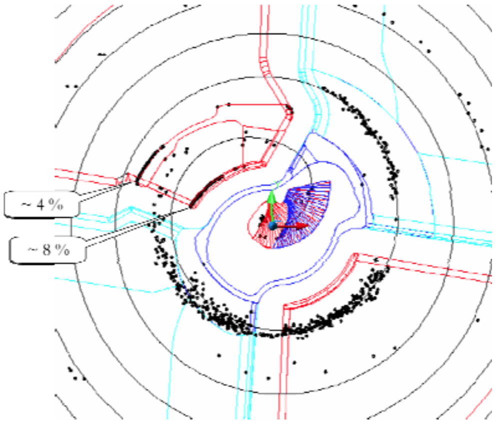

Fig. 3: Losses of the particles in the central region simulated for 30 MeV protons. Dots indicate particles that are lost by hitting the walls of the channel, RF dee electrode, beam chamber, etc. The total loss is 43 %, of which the losses in the vertical and horizontal directions are 31 % and 12 %, respectively.

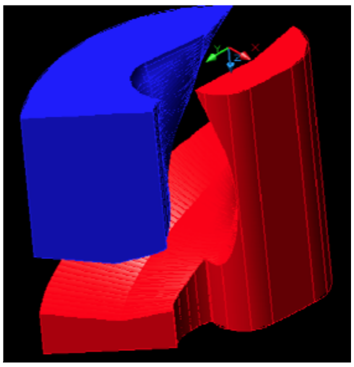

Fig. 4: "Bent" inflector.

The effect of the RF flat-top (FT) system on the energy spread in the beam was also studied for the h = 1 acceleration mode. In order to suppress the energy spread of the extracted beam, in the FT system, a wave at the third harmonic frequency was superimposed on the main (fundamental) wave so as to achieve a flat distribution in the top region, as in the case of the h = 2 mode. It was found, however, that for the h = 1 mode the superposition should be performed so as to achieve a sharp distribution (sharp-top, ST) instead of the flat one. This is because the dee angle is approximately 90°, and accordingly, in the h = 1 mode, the particles are accelerated at an RF phase of approximately 45° not at the top, as shown in Fig. 5. Since the bunch does not sit at the top of the RF wave, the energy gain obtained by particles in the head and tail of the bunch substantially differs at the entrance of the dee. At the exit of the dee, however, the energy spread obtained at the entrance of the dee gets compensated for the same reason. The remnant energy spread in the bunch can be explained by the nonlinear dependence of the dee voltage on time. The linearization of the dee voltage performance can be achieved by the ST system, and therefore, the energy spread and horizontal emittance at the final radius can be reduced substantially (by an order of magnitude for the energy spread) compared with the case where only the main wave is considered, despite an increase in particle losses.

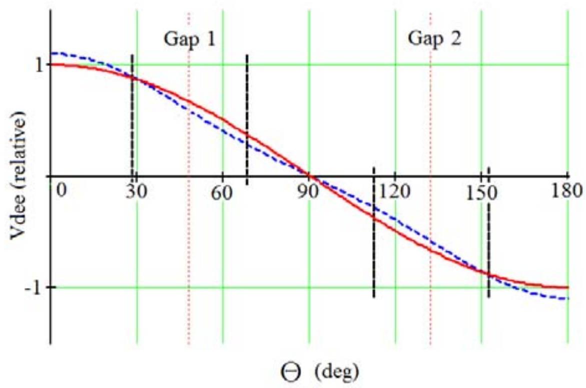

Fig. 5: RF waves and the bunch positions at the two gaps of the dee. The solid and dashed lines indicate the main (fundamental) wave and ST wave, respectively. In the figure the following denotations are used: V_{dee} – dee voltage, and Θ – RF phase.

References

1) S. B. Vorozhtsov et al.: RIKEN-NC-AC-2, RIKEN, Nishina Center for Accelerator-Based Science, June, 2009.
2) S. Vorozhtsov et al.: Proc. 6th Annual Meeting of Particle Accelerator Society of Japan, Tokai, Japan, August 5-7, 2009, p. 240.
3) A. Goto et al.: RIKEN Accel. Prog. Rep. **43**, 127 (2010).
4) B. N. Gikal et al.: Proc. RuPAC 2008, Zvenigorod, Russia, 28 Sept.– 3 Oct. 2008, p.127.

Mechanism of formation of a round beam by space-charge forces in cyclotrons

A. Goto

Experiments and simulations have shown that in isochronous cyclotrons, a bunch of very high intensity beams becomes round[1-4], as shown in Fig. 1. Simulations have shown that this phenomenon occurs because of extremely strong space-charge forces. However, very few research groups[5-7] have investigated the beam formation mechanism; moreover, in these papers, there are no explicit formulae that describe the process of round-beam formation through a galaxy shape (S-shape). In the present study, the beam formation mechanism is elucidated by formulating the motion of a particle in the space-charge-dominated beam bunch.

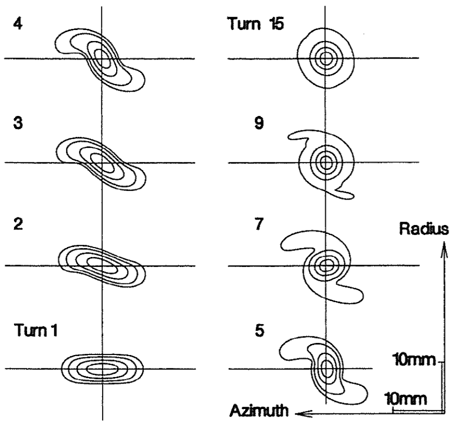

Fig. 1: Simulation of round-beam formation in the PSI Injector II (from Ref. 1).

To estimate the displacement of a particle by the space-charge forces in a bunch, we decompose the force E into radial and azimuthal (longitudinal) components, E_r and E_θ, respectively. The displacement in the radial direction after one revolution, ΔR, is then obtained as follows:

$$\begin{aligned}\Delta R &= \frac{R}{\nu_r^2}\frac{\Delta p}{p} \\ &= \frac{R}{\nu_r^2}\frac{qE_\theta \frac{2\pi}{\omega}}{mR\omega} \\ &= \frac{2\pi q E_\theta}{m\omega^2\nu_r^2} \\ &= \frac{E_\theta}{\nu_r^2 f\langle B\rangle},\end{aligned}$$

where p is the momentum of the particle; Δp, the change in the momentum due to E_θ; R, the orbit radius; ν_r, the radial betatron tune; and $\langle B\rangle$, the average magnetic field. m and q are the mass and charge of the particle, respectively. f and ω are the revolution and angular frequencies of the particle, respectively. The above equation implies that the azimuthal (longitudinal) component of the space-charge force allows the particle to shift in the radial direction (in the outward direction for the leading particles and in the inward direction for the lagging particles) by the amount of the displacement proportional to the magnitude of the space-charge force. On the other hand, when the average shift of the equilibrium orbit for one revolution due to E_r, $\langle x\rangle$, is given by

$$\frac{d^2x}{d\theta^2} + \nu_r^2 x = \frac{qE_r}{m\omega^2},$$

$$\langle x\rangle = \frac{qE_r}{m\omega^2\nu_r^2},$$

the displacement of the particle in the azimuthal (longitudinal) direction after one revolution, Δs, is obtained as follows:

$$\begin{aligned}\Delta s &= -2\pi\langle x\rangle \\ &= -\frac{2\pi q E_r}{m\omega^2\nu_r^2} \\ &= -\frac{E_r}{\nu_r^2 f\langle B\rangle}.\end{aligned}$$

The above equation implies that the radial component of the space-charge force allows the particle to shift in the azimuthal (longitudinal) direction (the outer particles shift toward the tail, and the inner particles shift toward the head) by the amount of the displacement proportional to the magnitude of the space-charge force. Thus, the net displacement of the particle after one revolution due to E, ΔX, is given by

$$\Delta X = \frac{E}{\nu_r^2 f\langle B\rangle}.$$

It can be deduced that the particle moves perpendicular to the direction of the space-charge force by the amount of the displacement proportional to its strength, as shown in Fig. 2.

Accordingly, the mechanism of formation of a round beam can be explained in the following manner. When the azimuthal (longitudinal) charge distribution of a cylindrical beam at the injection is assumed to be Gaussian, the space-charge force is nonlinear: the force increases with the distance from the bunch center, reaches a peak, and finally decreases. Since the displacement velocity of each particle is proportional to the force exerted on the particle, the cylindrical beam begins to get distorted, as shown in Fig. 2. When this process proceeds, the bunch assumes a galaxy

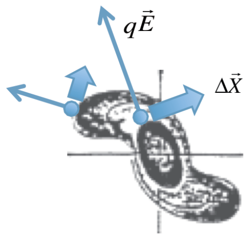

Fig. 2: Motion of a particle due to space-charge force. The displacement of the particle is perpendicular to the direction of the force and proportional to the strength. Here, the beam moves to the left.

shape and finally becomes round (see Fig. 1). Once a round beam is formed, its shape and size become constant[6]; each particle then performs vortex motion,[5] as shown in Fig. 3, and the angular velocity, v, depends on the strength of the space-charge force:

$$v = \frac{E}{v_r^2 \langle B \rangle}.$$

This round-beam formation can occur in any isochronous cyclotron, irrespective of the energy, if the beam is space-charge-dominated.

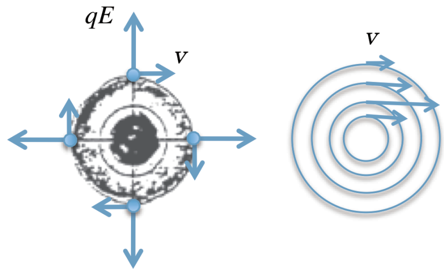

Fig. 3: Vortex motion of particles in a round beam.

References
1) S. Adam: Proc. Cyclotrons'95 (1995) 446.
2) Y. J. Bi et al.: Proc. Cyclotrons'10 (2010) MOPCP045.
3) H. Okuno et al.: RIKEN Accel. Prog. Rep. **44** (2011).
4) M. Seidel et al.: Proc. IPAC10 (2010) 1309.
5) M. M. Gordon: Proc. Cyclotrons'69 (1969) 305.
6) A. Chabert et al.: Proc. Cyclotrons'75 (1975) 245.
7) C. Chasman et al.: Nucl. Instrum. Meth. **219** (1984) 279.

Round-beam formation from high-power uranium beam at low-energy cyclotron in RIBF

H. Okuno, and A. Adelmann[*1]

[Space charge, High-intensity cyclotron]

The increase in the intensity of the uranium beam in the RIBF accelerator complex motivated us to study the vortex motion in cyclotrons. The longitudinal space-charge force causes an increase in the acceleration of the head particles and deceleration of the tail particles. The accelerated and decelerated particles move to higher and lower radii, respectively, because of the isochronous conditions in the cyclotron, and this causes rotation of the ion bunch. The nonlinearity of the space-charge force causees a spiral-shaped halo around the bunch, which finally turns into a rotating sphere. These vortex-motion phenomena were theoretically studied, as shown in the reference[1)], and experimentally verified at PSI Injector II.

Since 2009, we have been studying beam dynamics for high-power uranium beam acceleration in the RRC, where the vortex-motion phenomena are expected to be more prominent because of the use of a low-energy cyclotron at RIBF. OPAL-cycl[2)], which is one of the flavors of the Object Oriented Parallel Accelerator Library (OPAL) framework, is used for the study. OPAL-cycl is a new 3D PIC-based self-consistent numerical simulation code that takes into account neighboring-bunch effects. The self-consistency of the code is clarified by an electrostatic approximation. A more detailed description of the OPAL framework and the OPAL-cycl code can be found in the User's Reference Guide[3)]. A previous report on this study describes the results for single-particle tracking and multi particle tracking for up to 10 turns[4,5)], suggesting the possibility of the formation of a round beam at high intensities such as 0.5 emA. This paper reports the results of multi particle tracking up to the final turn in the RRC, which was performed to confirm round-beam formation.

The RRC consists of four sector magnets and two double-gap rf resonators. Figure 1 shows the top view of single-particle tracking of the reference particle up to the final turn in the RRC. Table 1 summarizes the main parameters for the simulation of multi particle tracking. Figure 2 shows the beam plots in the r-θ plane at the final turn for 0.0, 0.005, 0.05, and 0.5 mA. Except for the beam intensity, the initial conditions are the same foa all the cases. The beam plot in the case of 0.0 mA is typical of that obtained for the cyclotron, indicating maximum acceleration of rf-field. On the contrary, the plot in the case of 0.5 mA clearly shows the formation of round beams after vortex motion. The plot in the case of 0.005 mA is similar to that for 0.0 mA, but is slightly tilted owing to the space-charge force, whose linear component is dominant. The plot for 0.05 mA shows the formation of an almost round beam with tailing. The tail-to-core ratio is appproximately 1/100. Figure 3 shows the rms beam width in the horizontal plane for 0.0 mA and 0.5 mA, through the length of the reference trajectory. The longitudinal width in the case of 0.0 mA increases as the particles are accelerated. However, the longitudinal width in the case of 0.5 mA remains almost constant,

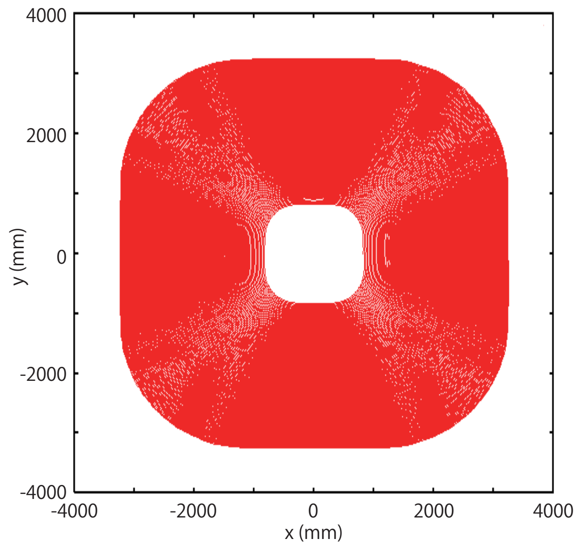

Fig. 1. Top view of single-particle tracking of the reference particle up to the final turn in the RRC.

Table 1. The main parameters used for the simulations.

Item	Value
Frequency	18.25 MHz
Harmonics	9
RF voltage	60 kV
Injection Energy	0.67 MeV/u
Initial R	818.3 mm
Initial θ	0°
Pr/P	0.3 mrad
Transversal emittance	2.5 π mm mrad
Bunch width (σ)	2.0°
Eigenellipse (radial)	X/X' = 5 mm/8 mrad
Eigenellipse (vertical)	Z/Z' = 5 mm/4.2 mrad
Test particle	10000
Beam current	0.0, 0.005, 0.05, 0.5 mA

[*1] Paul Sherrer Institut (PSI)

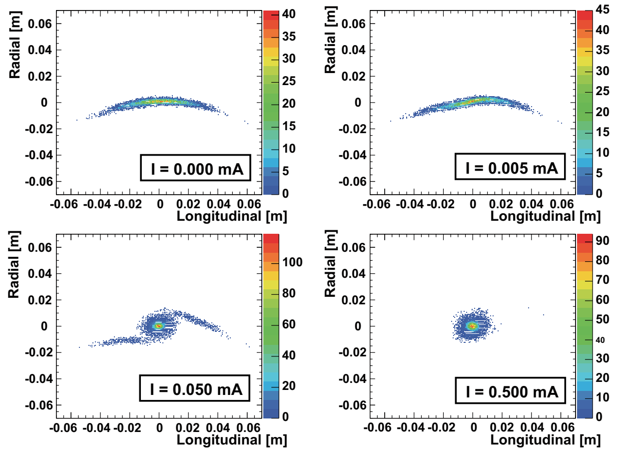

Fig. 2. Beam plots in the r - θ plane at the final turn for 0.0, 0.005, 0.05, and 0.5 mA.

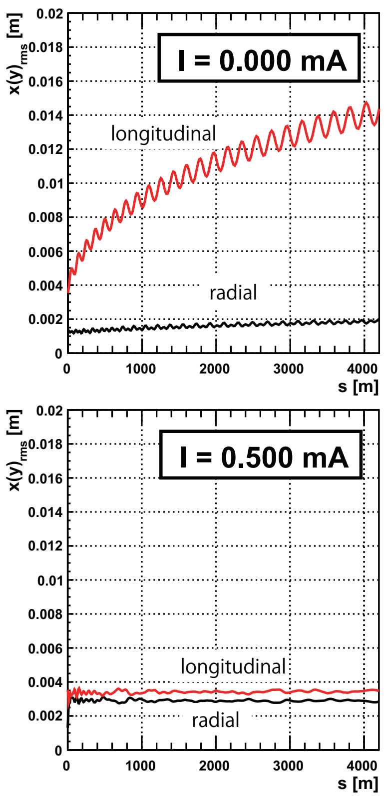

Fig. 3. Development of the beam width in the radial and longitudinal directions at 0.0 mA and 0.5 mA.

which indicates that the round beam is formed at a very early stage of the acceleration. Figure 4 shows the current dependence of the xy rms width of the beam at the final turn, suggesting a strong bunching effect and round-beam formation.

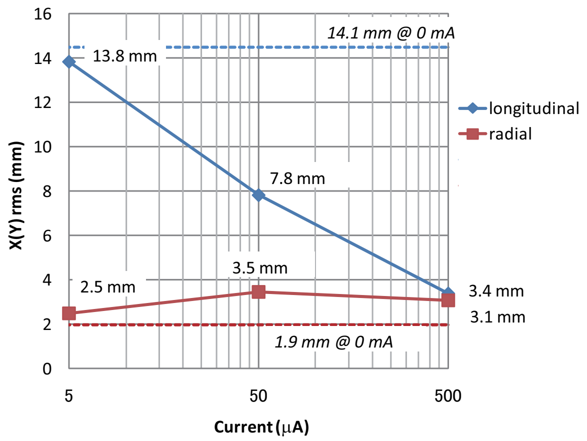

Fig. 4. Current dependence of the rms beam width in the radial and longitudinal directions at the final turn.

In summary, we carried out beam dynamics simulations for up to the final turn in the low-energy cyclotron at RIBF (RRC) for 0.0, 0.005, 0.05 and 0.5 mA, using a 3D PIC-based self-consistent numerical simulation code, OPAL-cycl. The results show that the round beam is definitely formed in the case of 0.5 mA. The simulation results will be compared with measurement results obtained for the real acceleration at a high intensity upgraded by the 28-GHz superconducting ECR ion source and the new injector.

References

1) S. Adam: IEEE Trans. on Nuclear Science 32, 2507 (1985).
2) J. Yang, A. Adelmann, M. Humbel, et. al.: Proc. of HB2008, in press, August 2008, Nashville.
3) A. Adelmann, et. al.: Tech. Rep. PSI-PR-09-05, Paul Sherrer Institut (2009).
4) H. Okuno, et al.: RIKEN Accel. Prog. Rep. 43, 129 (2010).
5) H. Okuno, et al.: Proc. of ICAP09, August 2009, San Francisco, 336 (2009).

RIKEN Accel. Prog. Rep. 44 (2011)

Output impedance of the power tube of the final-stage amplifier for the Superconducting Ring Cyclotron

N. Sakamoto*[1]

The power amplifier for the main cavity of the superconducting ring cyclotron (SRC) was basically same as the amplifier designed for the RIKEN ring cyclotron (RRC)[1]. The acceleration voltage of 600 kV/gap is generated with an rf power of 150 kW from the power amplifier. The amplifier is based on a tetrode (THALES/SIEMENS RS2042SK) with a grounded-grid circuit. As the cavities are frequency tunable, the amplifier has tuning devices which are the STUB (variable inductance) with a moving short plate and the OUTCAP (matching capacitor) with variable capacitance to realize a wide frequency band from 18 to 38.2 MHz (see Fig.1). The main part of the output plate circuit of the amplifier is represented as a simplified electric circuit diagram in Fig. 2. The output impedance of the plate electrode (Z_p) is defined as a ratio of voltage (V) to current (I).

$$Z_p = 1/Y_p = V/I.$$

The admittance at the left-side port of the simplified diagram of Fig. 2 is obtained as follows.

$$\begin{aligned} Y &= j\omega C_\mathrm{p} + 1/j\omega L_\mathrm{s} + 1/(1/j\omega C_\mathrm{m} + Z_\mathrm{cav}) \\ &= \frac{\omega^2 C_\mathrm{m}^2 Z_\mathrm{cav}}{1+\omega^2 C_\mathrm{m}^2 Z_\mathrm{cav}^2} \\ &\quad + j(\omega C_\mathrm{p}(1+\frac{C_\mathrm{m}/C_\mathrm{p}}{1+\omega^2 C_\mathrm{m}^2 Z_\mathrm{cav}^2}) - 1/\omega L_\mathrm{s}). \end{aligned}$$

Here, ω is the angular frequency of V and I. Note that the capacitance of the DC blocker in Fig. 1 is large enough to be neglected, and Z_cav is tuned to be 50 Ω. The inductance of the STUB is tuned to cancel the imaginary part and the matching capacitor is set so that the output admittance of the amplifier matches 1/50 Ω^{-1}. The Z_p of the real amplifier was measured for the frequencies from 27.4 to 36.5 MHz by using a network analyzer¡. The rf output port was terminated by a 50 Ω terminator instead of being connected to the cavity. In Fig. 3, sets of tuning parameters, i.e. capacitance of the OUTCAP and the short plate position of the STUB are plotted. The dotted lines are the constant impedance lines obtained from measurements. The parameters obtained by a high-power dummy load test are located along the bold dotted line, and they employed for usual operation because the plate losses are rather small though the currents of the screen grid became large. When the amplifier is operated with a cavity, the Z_p must be chosen to be such that it corresponds to a plate loss and screen grid current that are within the maximum ratings to prevent a critical damage to the power tube. To choose the parameters the results of the low-power test (Fig. 3) is helpful.

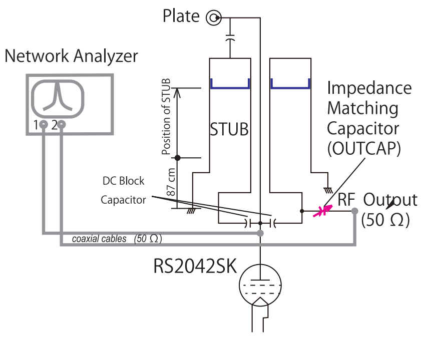

Fig. 1. Schematic of the main amplifier circuit.

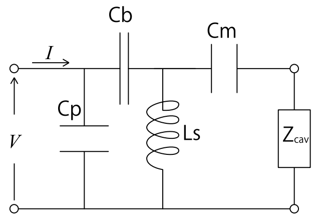

Fig. 2. Simplified diagram of the main part of the output plate circuit amplifier. Cp: plate capacitance; Cb: capacitance of the DC blocker;Ls: inductance of the variable STUB; Cm: capacitance of the variable matching capacitor(OUTCAP) ; Z_cav: impedance of the cavity

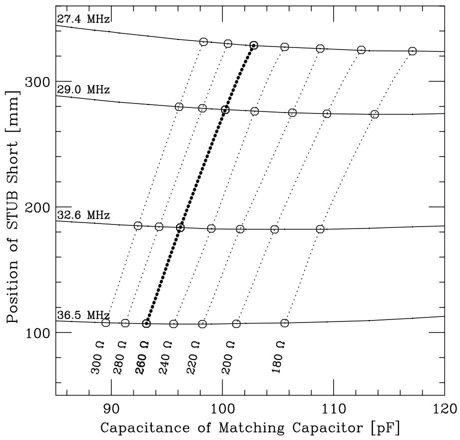

Fig. 3. Tuning parameters of the plate circuit.

References
1) T. Fujisawa et al., Sci. Papers I.P.C.R.80(1985).

*1 nsakamot@ribf.riken.jp

Charge-state distribution of ^{238}U in nitrogen gas and carbon foil at 14 and 15 MeV/nucleon†

H. Kuboki, H. Okuno, H. Hasebe, S. Yokouchi, N. Fukunishi, Y. Higurashi, J. Ohnishi, T. Nakagawa, H. Imao, O. Kamigaito, A. Goto, M. Kase, and Y. Yano

The charge states of heavy-ion beams play a very important role in the performance of heavy-ion accelerators. For efficiently accelerating heavy ions such as uranium ions up to high energies, it is essential to predict their charge states, especially for ions with energies in the range 10–20 MeV/nucleon where charge strippers are commonly used[1]. We measured the charge-state distributions of uranium (^{238}U) ions with energies of 14 and 15 MeV/nucleon by using N_2-gas and C-foil charge strippers to improve the empirical formulas used for the prediction of the equilibrium charge states in gases and C-foils; the formulas were used in the energy range 10–20 MeV/nucleon. Additional data were obtained for ions with an energy of 11 MeV/nucleon to examine the validity of previous results[1,2].

The experiments were performed at the RIKEN RI Beam Factory[3]; ^{238}U beams were accelerated through the RIKEN heavy-ion linac (RILAC), a booster linac (CSM), and the RIKEN ring cyclotron (RRC). Highly charged ^{238}U ions were provided by the superconducting electron-cyclotron-resonance ion source (SC-ECRIS) placed on the high-voltage terminal of the Cockcroft-Walton preinjector of the RILAC. Depending on the RRC output energy, we tuned parameters such as the charge states of ^{238}U, acceleration voltage before the RILAC, RF frequencies, and RRC harmonic number. The values of these parameters are listed in Table 1. ^{238}U beams with energies of 11, 14, and 15 MeV/nucleon were transported to the N_2-gas[2,4] and C-foil charge strippers shown in Fig. 1. The C-foils were ACF foils purchased from ACF-Metals, Inc.[5]. The incident beam intensities were measured using the Faraday cup D17 (A01a) and were 47 (57), 3.8 (2.8), and 8.6 (10) particle nA in the case of the gas (C-foil) stripper for energies of 11, 14, and 15 MeV/nucleon, respectively. In both cases, the charge states were analyzed using a couple of dipole magnets located downstream of the strippers. In the case of the gas (C-foil) stripper, the intensities of the stripped beams were measured using the Faraday cup F41 (A11) (see Fig. 1).

The charge-state distributions of ^{238}U in the N_2-gas and C-foil strippers are shown in Figs. 2 and 3, respectively. The equilibrium values of the most probable charge states in N_2 gas (C-foil) are 56.0 (72.4), 60.8 (75.8), and 62.4 (76.7) for energies of 11, 14, and 15 MeV/nucleon, respectively. The thicknesses necessary to attain 99% of the equilibrium charge states in N_2 gas (C-foil) are 118 (454), 188 (617), and 235 (728) μg/cm^2 for energies of 11, 14, and 15 MeV/nucleon, respectively.

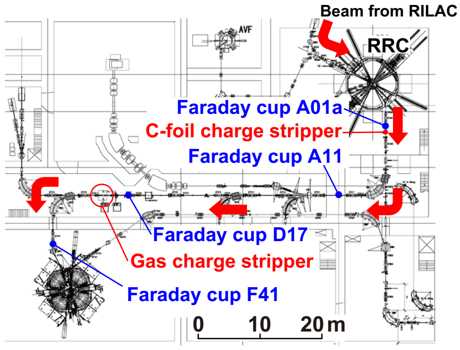

Fig. 1. Schematic view of the charge strippers (gas and C-foil) and Faraday cups.

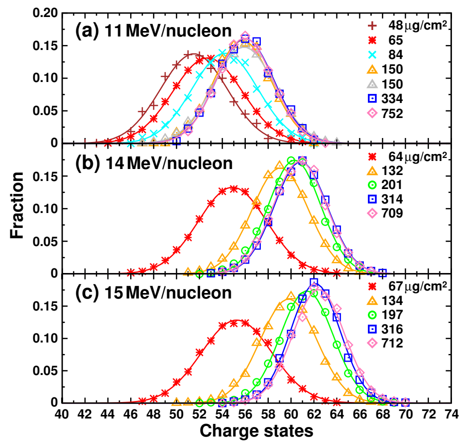

Fig. 2. Charge-state distributions of ^{238}U for the energies of (a) 11, (b) 14, and (c) 15 MeV/nucleon measured using N_2-gas strippers with different thicknesses.

Empirical formulas were derived by fitting the data sets obtained in this study as well as data obtained previously in the energy range 1–20 MeV/nucleon[1,2,6–9]. The data are plotted along with the empirical formulas for (a) gases and (b) C-foils in Fig. 4. In the case of gases, the solid and open squares represent the data obtained in this study and that obtained by past measurements[2], respectively. The open circles denote other data available for gases[6,7]. The new formula for the equilibrium charge state derived in this study is $q_{\rm eq} = Z\big[1 - 0.784\ \exp\big\{-(v/v_0)^{1.63} Z^{-1.17}\big\}\big]$, where

† Condensed from the article in Phys. Rev. ST Accel. Beams, Vol.14, 053502 (2011)

Table 1. Parameters for uranium-beam acceleration.

RRC output energy (MeV/nucleon)	11	14	15
RF frequency of RILAC and RRC (MHz)	18.25	18.25	19.00
RF frequency of CSM (MHz)	(not used)	36.50	38.00
RRC harmonic number	9	8	8
Charge state at SC-ECRIS	35	41	41
Beam intensity at SC-ECRIS (electric μA)	10–12	1.5–2.0	2.4–2.6
Total voltage at entrance of RILAC (kV)	127	109	118

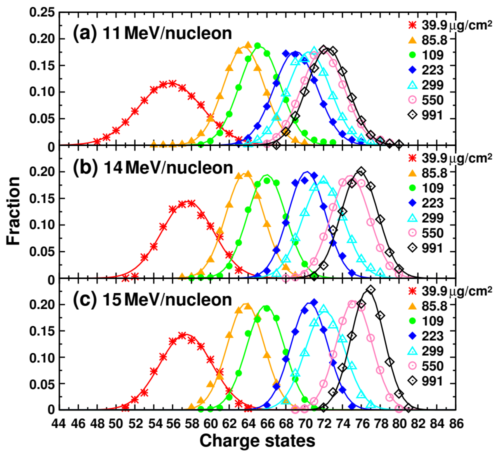

Fig. 3. Charge-state distributions of ^{238}U for the energies of (a) 11, (b) 14, and (c) 15 MeV/nucleon measured using C-foil strippers with different thicknesses.

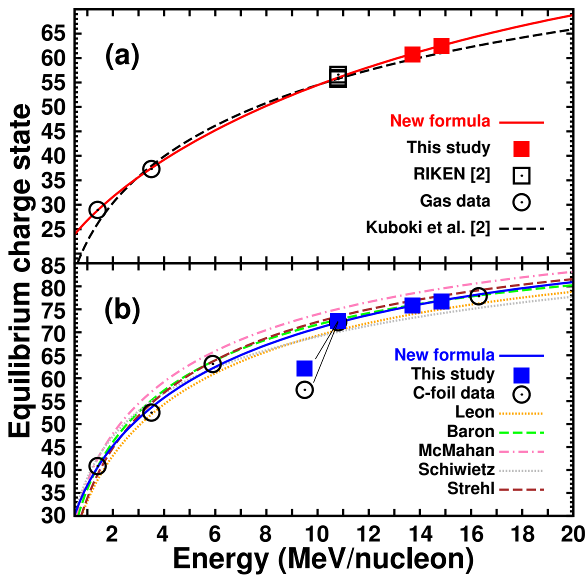

Fig. 4. Data pertaining to the equilibrium charge states of uranium ions in the energy range 1–20 MeV/nucleon in (a) gases[2,6,7] and (b) C-foil [1,6–9] along with empirical formulas. Please refer to the text for details. Two data points are overlapping at 11 MeV/nucleon, which are indicated by drawing two lines from these points and labelling them with the symbols denoting the two data sets.

q_{eq}, Z, v, and v_0 denote the equilibrium charge state, projectile atomic number, projectile velocity, and Bohr velocity 2.188×10^8 cm/s, respectively. This new formula is denoted by the solid curve. The dashed curve represents the empirical formula proposed in Ref. 2. In the case of C-foils, the data obtained in this study are shown by solid squares. The open circles denote the data available for C-foils[1,6–9]. The data for an energy of 11 MeV/nucleon obtained in this study are in good agreement with previous data[1]. The blue solid curve represents the new formula for C-foils; this new formula is $q_{eq} = Z\left[1 - \ 0.835 \exp\left\{-(v/v_0)^{1.20} Z^{-0.736}\right\}\right]$. The orange, green, magenta, gray, and brown curves represent the formulas proposed by Leon[11], Baron[12], McMahan[13,14], Schiwietz[15], and Strehl[16], respectively. The difference between the charge state calculated from previous data and that calculated by the new formula for gases (C-foil) in the energy range 10–20 MeV/nucleon was 0.23 (0.21) charge units on average.

References

1) H. Ryuto et al.: Proc. of 18th Int. Conf. on Cyclotrons and their Applications, Giardini Naxos, Italy, 2007, p. 314.
2) H. Kuboki et al.: Phys. Rev. ST Accel. Beams **13**, 093501 (2010).
3) Y. Yano: Nucl. Instr. Meth. B **261**, 1009 (2007).
4) T. Kishida et al.: Nucl. Instr. Meth. A **438**, 70 (1999).
5) ACF–Metals, Arizona Carbon Foil Co. Inc., http://www.techexpo.com/firms/acf-metl.html.
6) B. Erb: GSI Report, P-7-78 (1978).
7) A. N. Perumal et al.: Nucl. Instr. Meth. B **227**, 251 (2005).
8) K. Shima et al.: At. Data Nucl. Data Tables **34**, 357–391 (1986).
9) B. Franzke: Ann. Isr. Phys. Soc. **4**, 111 (1981).
10) H. D. Betz: Applied Atomic Collision Physics, Academic Press Inc. **4** p. 1 (1983).
11) A. Leon et al.: At. Data Nucl. Data Tables **69**, 217–238 (1998).
12) E. Baron et al.: Nucl. Instr. Meth. A **328**, 177–182 (1993).
13) M. A. McMahan and B. Feinberg: LBL-29758, (1992).
14) K. Shima et al.: Nucl. Instr. Meth. A **200**, 605 (1982).
15) G. Schiwietz and P. L. Grande: Nucl. Instr. Meth. B **175–177**, 125 (2001).
16) P. Strehl: Handbook of Accelerator Physics and Engineering, World Scientific Press, p. 555 (1999).

Status of the development of the large C-foil with rotating-cylinder device

H. Hasebe, H. Kuboki, H. Okuno, H. Imao, N. Fukunishi, O. Kamigaito A. Goto, M. Kase, and Y. Yano

Generally, a carbon foil (C-foil) is used as a charge stripper in a heavy-ion accelerator such as the RIKEN RI-Beam Factory (RIBF). A C-foil with thickness of 0.3 mg·cm^{-2} has been used to strip uranium (U^{35+}) beams to U^{71+}. The intensity of the U^{35+} beam is planned to be increased steadily during FY 2011. The lifetime of the C-foil stripper is a crucial problem considering the irradiation damage to the C-foils by increased U beam intensity.

First, we tested static C-foils mounted on a fixed holder. In 2005, we started the development of polymer-coated carbon foils (PCC-foils) coated with multiple layers of polymer[1]. The maximum lifetime of these foils was approximately 10 h even when the foils were irradiated with U beams having a beam intensity of less than 0.4 eμA. The lifetime of a diamond-like C-foil manufactured by TRIUMF[2] was 9 h under similar beam conditions.

Second, with the aim of increasing the lifetime of C-foils by enlarging the irradiated area, we developed a rotating-cylinder stripper device[3] with a large C-foil having a diameter of 100 mm attached on a holder. The lifetime of multi-layer PCC-foils attached on the rotating-cylinder stripper device was first measured in May 2008[4]. The rotation speed was 100 rpm (rotations per minute). However, the results showed lifetimes of 25 min and 10 min that were considerably shorter than the lifetimes of fixed C-foils.

Third, we improved the holder for the C-foil. We designed a holder with four small windows, as shown in Fig. 1, since we thought that the short lifetime was because of the large irradiated area without supporting frames. The lifetime of four pieces of C-foils were determined by irradiating the foils with U beams in March 2009. The beam intensity was 0.4 eμA. Three of those four pieces of C-foils cracked immediately. One possible reason for this was the centrifugal force generated because of the high rotation speed of 1000 rpm. The other reason was inappropriate beam-chopper timing. The beam should be stopped by the beam-chopper when the frames pass the beam spot. The temperature of the thick frames with more beam-energy-loss than that of C-foils increases, and this shortens the lifetime of the C-foils.

Fourth, we tested a smaller frame-less C-foil attached on the holder with a small aperture with 80-mm diameter. This C-foil was a diamond-like C-foil prepared by TRIUMF, and its results were compared with the previous results obtained in 2008. The C-foil was irradiated with the U beam, and the lifetime was tested in June 2009. First, the static C-foils were irradiated with U beams to compare the lifetimes of rotating C-foils with those of static C-foils. However, the C-foil cracked significantly after being irradiated for several minutes before the maximum intensity. Then, five points on the C-foil were irradiated for 3 h without rotating the C-foils. The surface condition of the C-foil is shown in Fig. 2. The beam intensity was 0.4–0.6 eμA. The position of the irradiated point was changed manually. The energy of the beam irradiating the C-foil changed depending on the irradiated positions, and further, the thickness of the C-foil changed depending on the position. The deviation of the thickness was up to 17%. Although some additional equipment to compensate the energy spread will be necessary for practical use as mentioned later, each different point on the C-foil could be used as a stripper with a total lifetime of more than 15 h. Thus, we concluded that the lifetime of a large frame-less C-foil rotating at a low speed would be longer than that of a C-foil rotating at a high speed.

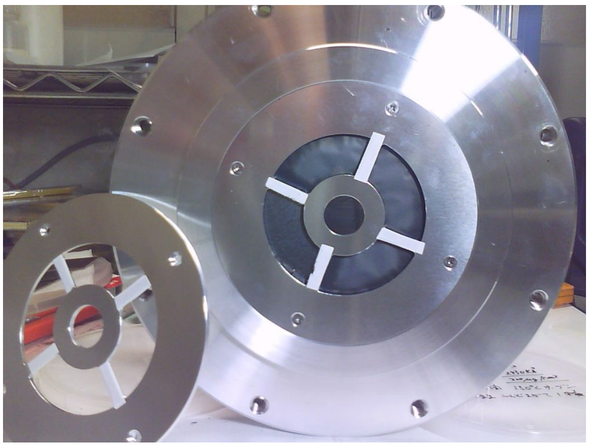

Fig. 1. Four pieces of C-foils were attached to the holder with four windows.

Recently, the rotation speed became adjustable from 0.05 to 1 rpm as a result of the remodeling of the rotating-cylinder stripper device in November 2009. More over, a new high-vacuum evaporation system was installed at the RIKEN heavy-ion linac (RILAC) building in August 2009 to fabricate C-foils with longer lifetimes and high-quality surfaces. This new evaporation system made it possible to fabricate C-foils with single-layer polymer coating (single-layer C-foils). The lifetime of the new single-layer C-foils were approximately 3–5-times longer than those of multi-layer PCC-foils[5].

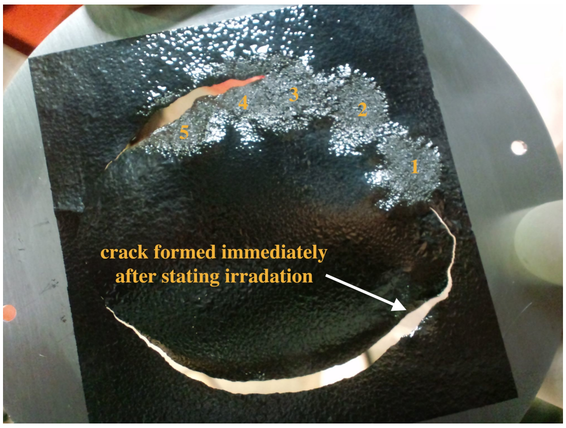

Fig. 2. The C-foil tore immediately after beam irradiation was stated. The five irradiated points are also shown marked by the corresponding number.

Fig. 3. Single-layer C-foil attached to a holder.

A large single-layer C-foil with a thickness of 0.4 mg·cm^{-2} was attached to a holder with an aperture of 80 mm. The C-foil was irradiated with strobe light before mounting it on a rotating-cylinder stripper devices[6] as shown in Fig. 3. It was experimentally observed that strobe-light irradiation reduced the C-foil thickness by 0.1 mg·cm^{-2}. Therefore, the C-foil with a thickness of 0.4 mg·cm^{-2} was used before strobe-light irradiation. The lifetime of this C-foil was tested in April 2010 by irradiating it with U^{35+} beams having 11 MeV/nucleon energy and 1.7 eμA intensity. The beam spot had a diameter of 5 mm. The rotation speed of the device was 0.05 rpm. During a limited irradiation period of 38 h, which corresponds to a total electric charge of 230 mC, no significant damage of the foil was observed (Fig. 4). The total area of the C-foil irradiated by the beam in the case of the rotating-cylinder stripper device was at least 48-times larger than that of the static stripper. Moreover, the average intensity and the spatial distribution of the beam stripped by the single-layer C-foil did not change during the irradiation period. The lifetime of the single-layer C-foil was 91-times longer than those of multi-layer C-foils described above (25 min) and more than 4-times longer than the lifetime in the case of fixed stripper configuration[5]. We concluded that the centrifugal force acting on the foil undergoing fast rotation might severely damage the C-foil. However, the beam intensity downstream of the C-foil changed periodically along with the foil rotation (the average intensity did not change). Since strobe-light irradiation wrinkles the foil, the effective thickness of the stripper changed depending on the position of the C-foil (because the thickness was non-uniform). The energy of the ions was as well spread downstream of the C-foil. Thus, the transmission of the beam was changed along with C-foil rotation. Additional equipments such as a rebuncher will have to be installed to prevent the energy spread during the beam transport.

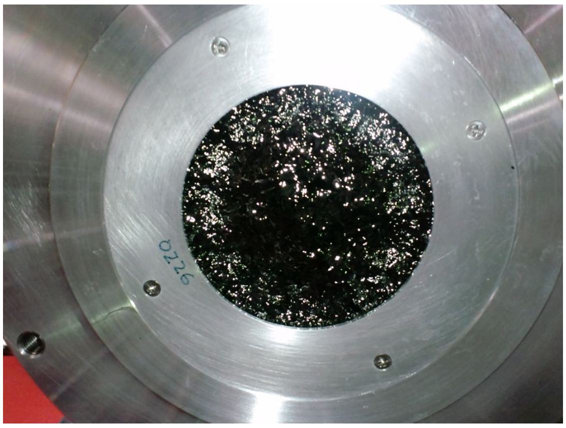

Fig. 4. Large single-layer C-foil mounted on the rotating-cylinder stripper device. The C-foil was irradiated by the U beam for 38 h.

References

1) H. Hasebe, H. Ryuto, N. Fukunishi, A. Goto, M. Kase, Y. Yano: Nucl. Instr. and Meth. A **590** 13, (2008).
2) TRIUMF. URL:<http://www.triumf.ca/>
3) H. Ryuto, H. Hasebe, N. Fukunishi, S. Yokouchi, A. Goto, M. Kase, and Y. Yano: Nucl. Instr. and Meth. A **569**, 697 (2006).
4) H. Hasebe, H. Okuno, H. Kuboki, H. Ryuto, N. Fukunishi, O. Kamigaito, A. Goto, M. Kase, and Y. Yano: Nucl. Instr. and Meth. A **613** 453, (2010).
5) H. Hasebe, H. Okuno, H. Kuboki, N. Fukunishi, O. Kamigaito, A. Goto, M. Kase, and Y. Yano: RIKEN Accel. Prog. Rep. **43,** 125 (2010).
6) H. Hasebe, M. Kase, E. Ikezawa, Y. Miyazawa, M. Hemmi, T. Aihara, T. Ohki, and H. Yamauchi: Proc. The 24th Linear Accelerator Meeting in Japan, Sapporo, Japan, 1999-7, p. 287.

RIKEN Accel. Prog. Rep. 44 (2011)

Prototype charge stripping system with thick low-Z gas

H. Imao,[*1] H. Okuno,[*1] H. Kuboki,[*1] S. Yokouchi,[*1] N. Fukunishi,[*1] O. Kamigaito,[*1] H. Hasebe,[*1] T. Watanabe,[*1] A. Goto,[*1] M. Kase,[*1] and Y. Yano[*1]

A charge stripping method involving the use of low-Z (Z: atomic number) gas is a possible candidate for charge stripping of future high-intensity very-heavy-ion beams. In the present study, a prototype charge stripping system with thick H_2 and He gas targets has been developed.

A key component to realize a massive low-Z gas charge stripper is a windowless connection between the high-vacuum beamline ($\approx 10^{-3}$ Pa) and the high-pressure target region. The differential pumping performance is reduced tremendously for H_2 and He gas in comparison with that for ordinal medium-Z gases like N_2. In a previous experiment involving the use of a differential-pumping gas-cell system[1–3], the maximum thickness for He gas that could be realized while maintaining a tolerable beamline vacuum was found to be 0.015 mg/cm^2. However for N_2 gas, a thickness of 1.1 mg/cm^2 could easily be achieved. The lower electron-loss (EL) and electron-capture (EC) cross sections for ^{238}U colliding with a low-Z gas, in comparison to those for ^{238}U colliding with N_2 leads to a larger mean free path of the injected ions, which results in slow equilibration. A simple estimation of the charge evolution using theoretical EL and EC cross sections for He[3] indicates that a thickness greater than 1 mg/cm^2 is required for 10.8 MeV/u ^{238}U beams to attain the maximum charge state. However, a value of only 0.4 mg/cm^2 is required for N_2[2]. This means that a gas thickness greater than 100 times that in the previous system is required to obtain the maximum charge state for low-Z gas.

To overcome these difficulties, two drastic improvements were made to the gas accumulation method in the present study: (1) a long gas stripper ($\sim$8 m) in which the low-Z gas was directly accumulated in the beamline was used and (2) the design of the differential pumping systems was optimized and improved. For accumulating thick gas in a high-vacuum beamline, a long gas-filled region with small aperture sizes of the conductance limiting tubes is favorable. However, a long stripper increases the lateral spread of the beam. Further, the narrow apertures intercept part of the beam. The design of the gas charge-stripping system was optimized by considering these constraints and the calculated beam trajectories.

The charge stripping system mainly consists of two huge differential pumping systems located at both ends of the 8-m charge stripping section and a gas inlet line connected to the gas-handling system (Fig. 1). In the differential pumping systems, the conductances among the vacuum chambers are limited by the diameters of the tubes, which are in the range 6−10 mm (UAP1-3 and DAP1-4). In the current setup, the gas-cell system used in the previous system[1,2] was fully devoted to one-side evacuation as a differential pumping system on the downstream side (DDP) (Fig. 1).

For the upstream system, a new tube-separated three-stage differential pumping system was designed and constructed (UDP). The design performance was optimized not only for use in the present system, but also for a variety of potential applications, e.g., "short" low-Z gas strippers or "extremely-thick" ($\sim$20 mg/cm^2) medium-Z gas strippers. The vacuum in stage 1 of the UDP was achieved by using a powerful mechanical booster pump backed by a rotary oil pump. A high throughput turbomolecular pump was used in stage 2, and an ordinal one was used in stage 3. Flow-disturbing plates were placed between UAP1 and UAP2. They were specially designed to slow the flow of the supersonic gas jet from UAP1 to UAP2 (Fig. 2).

The differential pumping systems were tested at the beam distribution corridor (D-room) at RIBF (RIKEN RI-Beam Factory). For safety reasons (e.g., to avoid explosion hazards), the evacuated H_2 gas (less than 20 SLM) was released outside the room via a dedicated disposal line (ϕ85 mm) and was mixed with N_2 gas (300 SLM). A sensitive H_2 leak detector was fixed to the ceiling of the D-room to detect unexpected leaks.

In the test experiment, the chambers and the beamline were first evacuated to approximately 10^{-5} Pa. H_2 or He gas was then supplied to the charge stripping region of the beamline via the gas inlet. Performance tests of the UDP and DDP were separately performed by shutting down the system not being tested. The measured pressure distributions for H_2 and He gas in the UDP and the DDP are shown in Fig. 3. For the UDP, data for N_2 and Ar are also shown for comparison. The UDP showed high differential pumping ability. The performance of the UDP was more than three times that of the DDP. Although the length of the UDP was as small as 1 m and the diameter of the beam passage was more than 6 mm, a pressure transition from 15 kPa for He (3 kPa for H_2) to $10^{-2}\sim10^{-4}$ Pa was achieved. The pressure of the upstream beamline was one order of magnitude lower than the third-stage pressure. For a medium-Z gas, gas pressures achievable with the UDP are as high as 50 kPa. This performance suggests that it may be possible to use systems like the UDP in the second charge stripper after fRC (fixed-frequency ring cyclotron), e.g., a thick N_2 gas charge stripper with a thickness of around 20 mg/cm^2

*1 RIKEN Nishina Center for Accelerator-Based Science

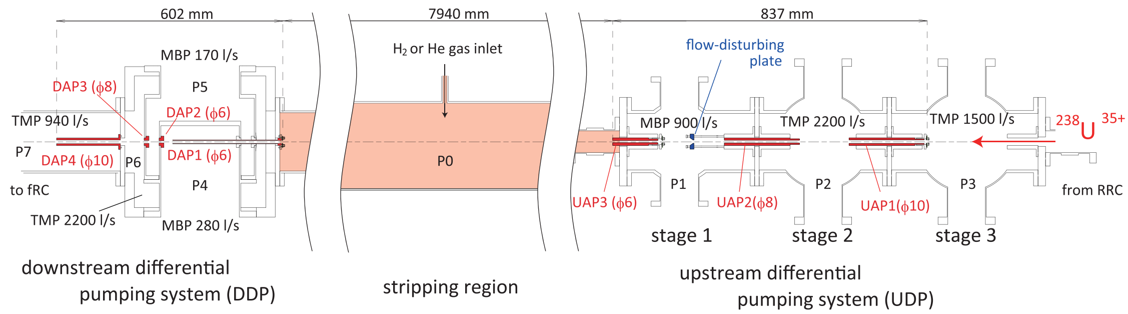

Fig. 1. Cross-sectional view of the charge stripping system.

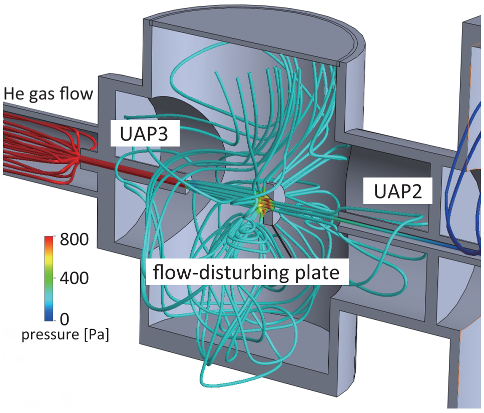

Fig. 2. Simulated gas flow between the first stage and the second stage using Solidworks flow simulation (software based on the finite element method; Dassault Systemes Solidworks, Concord, MA, USA).

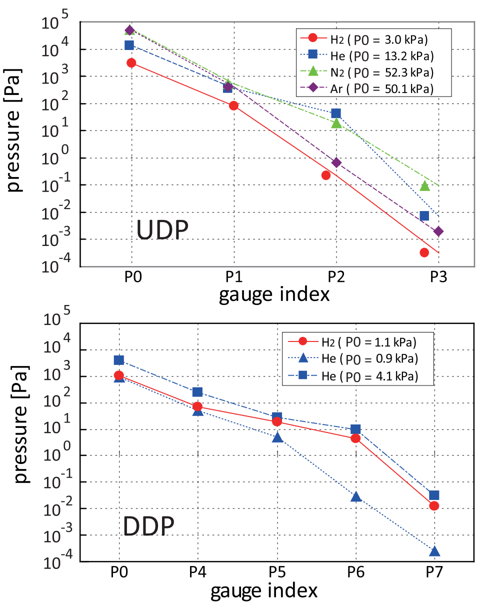

Fig. 3. Pressure distributions in the UDP and DDP.

and a length less than ~50 cm long. In the current 8-m charge stripping system, a thickness of 1 mg/cm^2 for H_2 and 5 mg/cm^2 for He was achieved while maintaining a tolerable beamline pressure. These are reasonable values for achieving the maximum charge state for 10.8 MeV/u ^{238}U beams. The achievable gas pressure in the case of the two differential pumping systems is limited by the performance of the DDP. The H_2 gas pressure is also limited by the flow limit of 20 SLM, which has been determined on the basis of the safety regulation standards of the facility.

The effect of the flow-disturbing plates on the differential pumping performance is shown in Table 1. Note

gauge index	P0 [kPa]	P1 [Pa]	P2 [Pa]	P3 [Pa]
w/o disturber	6.3	104.5	56.0	8.2×10^{-3}
with disturber	16.2	433.0	46.5	5.4×10^{-3}

Table 1. Effect of the flow-disturbing plates.

that the maximum gas pressure is greater by a factor of approximately three in the presence of the plates.

The result of a charge stripping experiment performance recently by using the present system[4] indicates that a helium gas stripper with a thickness of around 1 mg/cm^2 is a good candidate for the first stripper of the future uranium beam at RIBF. Such a stripper can be shortened to approximately 40 cm by adopting UDP for both ends of the stripper section. The development of a system involving the helium-gas recycling system is under way.

The authors would like to thank Dr. Y. Uwamino, Mr. N. Yamagishi, and Dr. T. Kishida for their helpful instructions for the safe handling of hydrogen gas.

References

1) T. Kishida *et al.*: Nucl. Instrum. Methods Phys. Res. **A 438**, 70 (1999).
2) H. Kuboki *et al.*: Phys. Rev. ST Accel. Beams **13**, 093501 (2010).
3) H. Okuno *et al.*: Proc. of HB2010, 2010.
4) H. Imao *et al.*: in this report.

Status of RIBF control system

M. Kobayashi-Komiyama, A. Uchiyama,[*1] M. Hamanaka,[*1] M. Fujimaki,
E. Ikezawa, M. Nagase, T. Nakamura, [*1] N. Fukunishi and M. Kase

The RIBF control group carries out two types of activities every year: one is for the development of new applications and systems of the RIBF control system, and the other is for the maintenance and renewal of the old controllers of the RIBF components. This year, we report three major activities related to the RIBF control system. The first is development of the control system for a new injector of RIBF, RILAC2. Since the first beam commissioning of RILAC2 was scheduled in December 2010, we had been developing the injector as a top priority. The second is related to system maintenance. We have replaced some old controllers in RILAC and AVF. The third is the development of a new archive system to get, store, and display almost all data of RIBF components simultaneously.

The control system of RILAC2 is divided into two parts: one part functions as a system for a new 28GHz superconducting ECR ion source and the other as a system for the accelerator part of RILAC2. The former is developed using EPICS-embedded system on F3RP61-2L (RP). [1] RP is a new PLC-CPU module running a soft real-time Linux, and installation of EPICS on it has been carried out in collaboration with the KEK control group since 2008. The control logic for a system using RP is developed by using EPICS sequencer instead of traditional ladder programs. We adopted the basic I/O modules of PLC such as DI, DO, AI, and AO modules for the control system. For the first time, we adopted EDM instead of MEDM for GUI development. Both EDM and MEDM are applications for developing GUI and are supported by EPICS collaboration. The advantage of using EDM for developing the GUI of the control system of the ion source is that its build-in XY plot tool is convenient in illustrating the charge-stage distribution produced by the ion source. Since we control only simple I/O signals, the control system of the ion source has been operating smoothly and no serious problems have been encountered since we started its operation. In addition, its response speed is sufficiently high for enabling an operator to control every component in the ion source.

The latter consists of two groups. One is a group of devices whose controller is already in operation in the RIBF control system. The beam diagnostic devices and vacuum systems are controlled by N-DIM. More than half of the magnet power supplies present in the beam transportation line of RILAC2 are controlled by NIO or DIM. To control magnet power supplies by NIO, we set an additional VME station at the junction building between RILAC and RRC.

The other group is a group of new devices. Two new beam emittance slits have been introduced in the beam transport line. Beam emittance at the exit of the ion source is measured by using these slits and a beam-profile monitor.

In addition, new types of 16 magnet power supplies have been introduced. For their control, we adopted RP with basic I/O modules of PLC, as in the control system of the new ion source. The system has been operating without any serious problems since we started its operation.

The second activity of this year is related to the renewal of old controllers, GMACS in RILAC control system and DIM in AVF control system. Our policy of renewal of various old controllers aims to unify them into four types of controllers; DIM will be replaced by N-DIM, and various controllers of magnet power supplies except DIM will be unified to NIO or RP, while others will be replaced by RP or PLC.

GMACS has been in operation in the RILAC control system for more than 30 years. It controls the power supplies of quadrupole magnets installed in RILAC drift tubes, a part of RILAC RF, and magnets in the injection beam transport line to the RILAC. We completed the unification of the first group of controllers to RP in the summer of 2010. Along with other RP systems, basic I/O modules were included, and the control system of the RILAC drift tubes has been operating without any serious problems since operation was started. The unification of remaining part to RP is scheduled in 2011.

We changed the control of a differential probe of AVF cyclotron from DIM to N-DIM. Differential probes used in all the other cyclotrons are controlled by two types of controllers: PLC for motion control and N-DIM for current measurement. However, the N-DIM for AVF main probe performs both tasks. Therefore, by this replacement, we succeeded in unifying the controllers for beam measurement of all differential probes in RIBF.

The third activity is the development of a new application for data archive system. At present, three different types of data archive systems are in operation at the RIBF control system. One of the data archive systems is the application, "Channel Archiver," which is presented by EPICS collaboration. [2] We can archive data from EPICS IOC by using this application. We applied it to a vacuum system of cyclotrons and beam transport lines, magnet power supplies, and so on. Channel Archiver stores data in its custom-format files instead of using relational database. We can view the data easily by using the application, "Archive Viewer," which is also developed using EPICS. [3] It is easy to display archive data in chart; however, we have to

*1 SHI Accelerator Service Ltd.

develop a program to present the data in a text file or common spreadsheet software like Excel.

The second data archive system is "Zlog," which was originally developed by KEKB control group. [4] It is a system for recording operation actions. A program for obtaining data from EPICS IOC has been developed by using python, and the system stores the obtained data to a relational database, PostgreSQL. Its GUI program for operator interface has been developed by using Zope.

The third data archive system is MyDAQ2, which was originally developed by Spring-8 control group. [5] RIBF has two components, one is controlled by EPICS and the other is controlled by a non-EPICS system. At present, MyDAQ2 is taking data from non-EPICS systems. For example, it takes data of temperature of cooling water, electric power at switch board of the facility and so on. MyDAQ2 was developed to store data into a table of MySQL. We can view stored data in chart at a GUI of MyDAQ2 easily as well as in a text file.

At present, we can record any data of RIBF by using one of above three applications as long as a controlled object is connected to either the EPICS network or the internal network of the Wako campus. However, a system that can record and display all RIBF data independent of the type of network will be the most convenient system for us. "Channel Archiver" and "Archive Viewer" were at first developed as EPICS applications, and therefore, it is difficult to apply them to our non-EPICS components. Furthermore, "Channel Archiver" does not work stably in our system. This could be due to some mismatch between our system and "Channel Archiver"; however, it is difficult to solve this problem because the EPICS community does not support these applications anymore. Further, we also studied MyDAQ2. When we introduced MyDAQ2 to our control system a few years ago, we tried to apply it to EPICS IOC. MyDAQ2 can obtain data from EPICS IOC, however, it is not possible to obtain a huge amount of data like that of the current of a thousand magnet power supplies in a period of 10 s. MyDAQ2 was developed for users who perform experiments at one of Spring-8 beam lines and not the whole control system of Spring-8. Thus, we stopped attempting to apply MyDAQ2 to our EPICS control system.

Due to the above reasons, since October 2009, we have started developing a system that satisfies all our requests- the RIBF Control data Archive System (RIBFCAS). The RIBFCAS consists of an application server, a database server, and a client-PC, and these are connected to the EPICS-LAN. The role of each component is as followings:

- Database server: It executes a program to take data from EPICS IOCs. Further, it manages the data by using a DataBase Management System (DBMS). In our system, Linux (CentsOS 5.2) was selected as the OS and PostgreSQL 8.4.1-1 was selected as the DBMS.
- Application server: It executes the tasks for responding to the requests from client-PCs.
- Client-PC: The client application is executed on Adobe AIR runtime. GUI with a chart that displays data and some selection buttons has been developed for the client application.

We tried to archive about 3000 parameters of various components of RIBF from 21 EPICS IOCs such as VME, CAMAC-CC/Net, Linux IOC, and RP. We tried to start its operation in January 2010; however, a system problem was encountered a few minutes after we started the programs. The major reasons for this are as follows: the first reason is the excess number of connections between the server and an IOC. The program was written to maintain a connection between them after taking data without releasing. The program should facilitate the connection between the server and an IOC before data taking, and after that, it should disconnect as soon as possible. The second reason is the problem of EPICS Channel Access client library for Java (JCA) itself. The program for data taking from IOCs was based on JCA, which was supported by EPICS collaboration. It is reported that JCA has problems of instability and of vulnerability of the codes. It does not maintain thread safety.

Therefore, we started studying about another solution as a library for Java instead of JCA, and we found a new compact Java channel access library, Java Channel Access Light Library (JCAL), which had been developed in J-PARC linac and RCS control system. [6] The main advantage of JCAL is that it is based on single threaded architecture for thread safety and user thread can be multi-threaded. The main part of the library is designed to function in a single thread, with the other threads for the monitor call-back. After a JCA-based program was changed to a JCAL-based program, we started its test operation since January 2011. At the moment, we have succeeded in obtaining about 3000 data from IOCs every 10 s.

The GUI on a client PC shows data in two manners. One is to monitor real-time data and the other is to show past data of any period. In both cases, a user can select any number of any data, and a result on a chart can also be outputted in a text file or JPEG file.

The major remaining contents of the development of the RIBFCAS are as follows:

- Program development of cooperation with MyDAQ2.
- Development of a mechanism of process and data management.

We have already analyzed a mechanism to get and display data from MyDAQ2 on the GUI of RIBFCAS without merging the databases of RIBFCAS and MyDAQ2. Next, a mechanism is required to manage a large amount of stored data in the database. We plan to complete the development and begin employing the mechanism in 2011.

References

1) M. Komiyama et al.: Proc. ICALEPCS 2009, Kobe, 2009-10, p. 275.
2) 3) http://www.aps.anl.gov/epics/extensions/index.php
4)http://www-acc.kek.jp/KEKB/Control/Zlog_Archive/Zlog_System_Archive.html
5) T. Hirono et.al.: Proc. PCaPAC 2008, Ljubljana, Slovenia, 2008-10, p55.
6) H. Sako et al.: Proc. ICALEPCS 2009, Kobe, 2009-10, p. 842

Development of "BTmap": Online visualization of beam-transport status

R. Koyama*[1] and A. Uchiyama*[1]

The accelerator complex for RI beam factory (RIBF) consists of four ring cyclotrons and three injectors, including a new-injector linac (RILAC2). In addition, we have 13 beamlines in the RIBF. In other words, we have a large number of possible variations for the acceleration mode. On the other hand, we did not have a method to show the online status of the accelerators to the users, which sometimes caused inconvenience. To solve this problem, we developed a status indicator shown in Fig. 1, which facilitates online visualization of the beam-transport (BT) conditions (hereinafter referred to as "BTmap").

The BTmap program consists of a channel access (CA) client for monitoring the Experimental Physics and Industrial Control System (EPICS) records and LabVIEW for visualizing the BT status. The RIBF control system is constructed using EPICS[1)]. EPICS is a set of open-source software tools, libraries, and applications that have been developed collaboratively, and they are used worldwide to construct distributed soft real-time control systems for scientific equipment such as particle accelerators, telescopes, and other large scientific equipment. EPICS uses client/server and publish/subscribe techniques to communicate between the various computers. Most servers (called input/output controllers or IOCs) perform real-world I/O and local control tasks, and they provide this information to clients using the CA network protocol[2)].

The CA client communicates with IOCs of devices such as Faraday cups via EPICS records and outputs their statuses to text files. For example, the CA client returns "0" and "1" when the Faraday cups are inserted and when they are not inserted, respectively. LabVIEW indicates the BT lines and experiment room on its front panel (BTmap); the BT lines are denoted in red color and white color to show the parts where the beam is transported and where it is not transported, respectively. LabVIEW operates logically the status data of the Faraday cups obtained from the CA client. The relative intensities at the target are also plotted on the BTmap and stored in a log file as time-series data. The data are used for the analysis of the stability of the beam intensity. In addition, the experimental condition, position of the radial probe in the cyclotron, on/off status of the acceleration voltage, and ratio of the beam attenuator are indicated on the BTmap. The

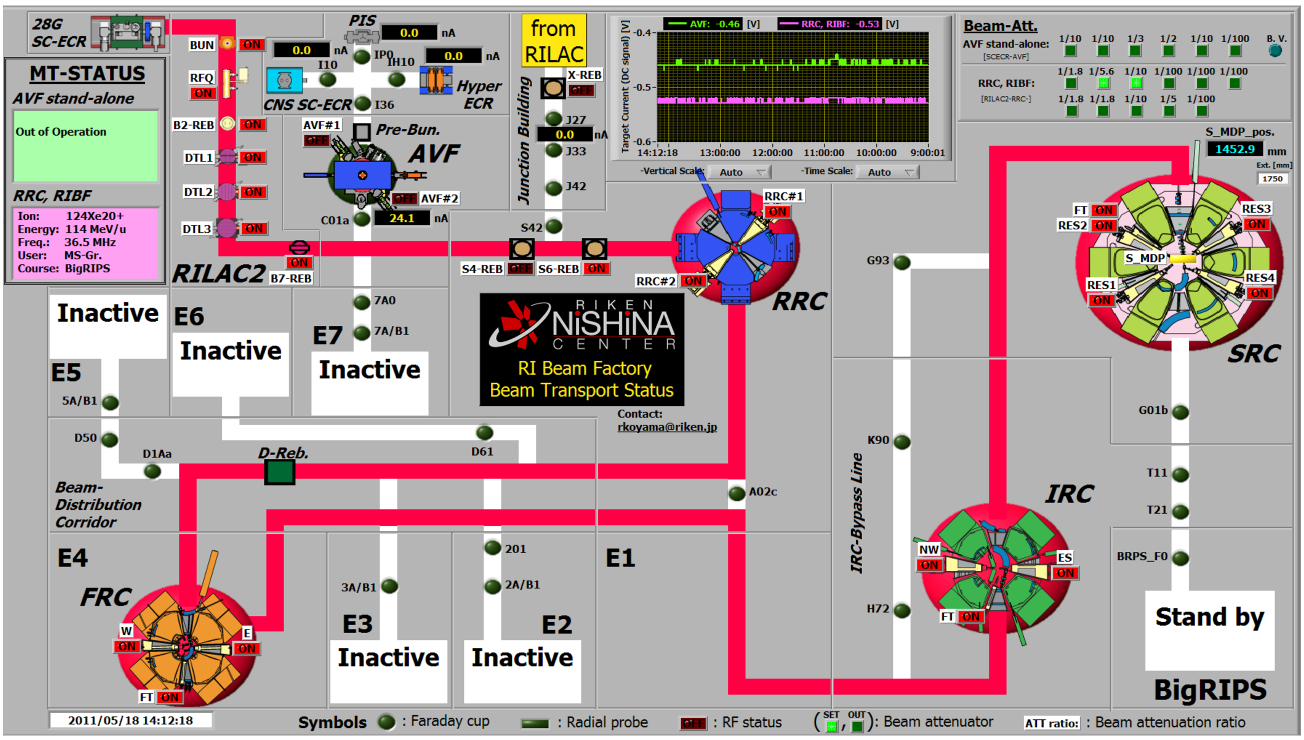

Fig. 1. Screen capture of "BTmap"(LabVIEW front panel).

*1 SHI Accelerator Service, Ltd.

refresh cycle of the status indicator is approximately 1 s. The program chart is schematically presented in Fig. 2.

The BTmap is provided as a PNG image on the network for an EPICS-based control system of the RIBF (EPICS network) by using the Web Publishing Tool contained in LabVIEW. A reverse proxy server has been constructed[3] to allow the RIBF users access to the BTmap on the EPICS network from the RIKEN intranet; the reverse proxy server is constructed since the RIBF users on the RIKEN intranet are disconnected from the EPICS network to ensure that the information is secure. This enables the RIBF users to keep track of the operating conditions of the RIBF on a Web browser from the RIKEN intranet. The network diagram used for providing the BTmap image is shown in Fig. 3.

Since we have just started providing the BTmap image on the Web, the network traffic to the server used for the BTmap is low and there is no problem in browsing. However, we have to examine the adequacy of the performance of the server and be prepared for the expected increase in the number of users in the future. We plan to add the RILAC region, RF status of D-rebuncher, and radiation level of each accelerator room to the existing BTmap. We will also modify the BTmap in response to requests from users since we want to make it more user-friendly.

References

1) M. Komiyama et al.: Proc. of ICALEPCS07, Knoxville, Tennessee, USA, 2007, p.187
2) http://www.aps.anl.gov/epics/index.php (Last accessed on April 1, 2011).
3) A. Uchiyama et al.: in this report.

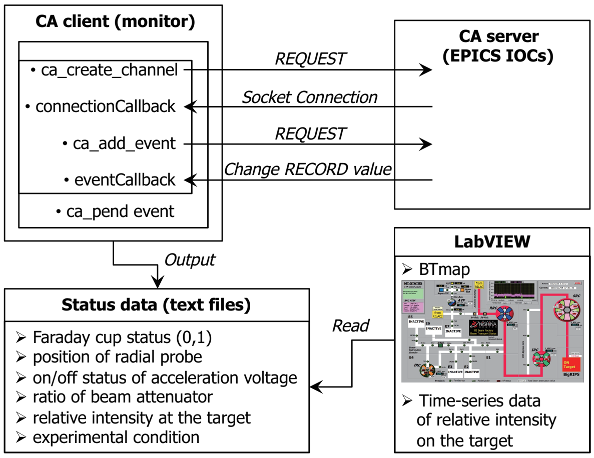

Fig. 2. Program chart of BTmap.

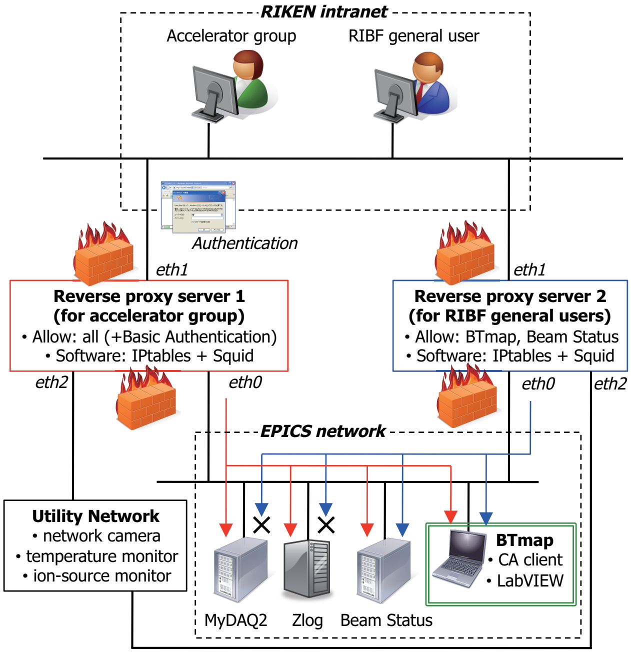

Fig. 3. Network diagram used for providing the BTmap image via a reverse proxy server.

Secured Access to RIBF Control Network from RIKEN VLAN

A. Uchiyama, *[1] M. Kobayashi-Komiyama, R. Koyama, *[1] M. Fujimaki, and N. Fukunishi

The RIKEN RIBF control system is constructed systematically by using Ethernet. The control system comprises two different systems: a system for controlling accelerator operation on the basis Experimental Physics and Industrial Control System (EPICS), and the other is a system for non-EPICS-based utility control (see figure 1). The controllers, servers, and client PCs are installed on the same network system for EPICS-based distributed system (EPICS network)[1]. On the other hand, some digital measurement instruments, video servers, and network cameras are connected to the network for non-EPICS-based utility control (utility network). Thus, the control system network with Ethernet for controlling accelerator operation consists of the two types of network system, EPICS network and utility network. The data traffic of video server and network camera in utility network show that the tow networks are independent network systems without any connection with each other.

E-mail and Internet access for tasks unrelated to accelerator operation usually require RIKEN virtual LAN (VLAN) as office LAN. From the viewpoint of information security, we decided to separate the control system network from the Internet and operate it independently with no connection between the control system network and the VLAN (Fig. 1). Because the number of network-based devices is increasing in the control system, it is difficult to maintain perfect network security in both the network systems by employing limited man power.

Therefore, as our laboratory policy, the control system network was a completely independent stand-alone system and was not connected to the VLAN. However, it was inconvenient for users from the following reason; it was unable to monitor the information and the status of accelerator operation from a user's office in a real-time fashion. The users needed to carry a storage device, such as USB flash memory for logged data to the accelerator control room on occasion. To improve this situation, we have constructed a secure system which allows the users to get the accelerator information from VLAN to control system network, while preventing outsiders from having access to the information.

To allow access to inside control system network over the network from VLAN, the following risks are taken into consideration.

1. Illegal computer access using SSH, HTTP, and other client protocol for servers inside control system network, for example, denial-of-service (DOS) attack.

2. Illegal accelerator operation from outside EPICS network by remote control.

3. Leak of raw accelerator data, operational log, and other critical information about accelerator condition.

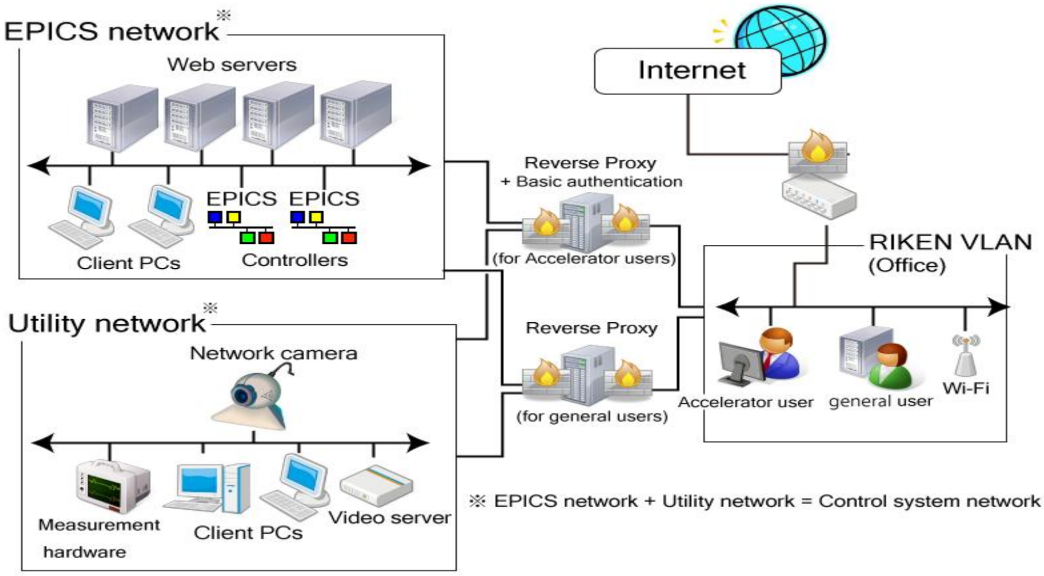

Figure 1. Network diagram of our system.

*1 SHI Accelerator Service, Ltd.

Since a gateway with a firewall is installed between the VLAN and wide area network (WAN), even if a server is assigned both of private IP addresses for VLAN and control system network, a direct attack from WAN to the control system network is protected for certain. However, other laboratories and guest users can have access to the network inside the gateway via Wi-Fi in almost RIKEN's offices. For this reason, the firewalls should be installed in between the control system network and VLAN to be closed all the ports other than proxy. Further, because of the difficulty in system management and system construction, web communication is a suitable method for providing the accelerator information to a large number of people. To satisfy the above mentioned requirements for the system, a combined system with a reverse proxy server for web communication and a firewall has been constructed for providing accelerator information to VLAN with secured access. The system chart and basic concepts are shown in figure 2. In general, a reverse proxy server is used as a proxy server, which is installed in front of web servers in a server network for security and caching. The proxy server is often used to transport requests for web services, when the Internet is accessing using the LAN via a web browser. In other words, the difference between a proxy server and reverse proxy server is in the direction in which a request is forwarded from a browser to web servers.

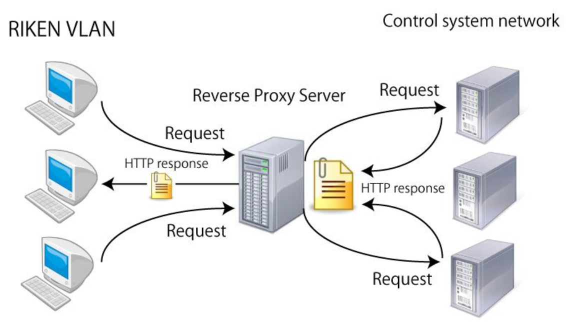

Figure 2. System chart for reverse proxy server.

In order to implement the system, CentOS 5.5, Redhat Enterprise Linux clone distribution, has been used as the operating system. Further, Iptables[2] for the firewall and Squid[3] for the reverse proxy server, the standard package of CentOS 5.5, are installed. The significant feature of our system is improved web security in accessing from VLAN by masking the web servers behind the reverse proxy servers. As a result, our system prevents HTTP attack such as DOS. In addition, it reduces the system load in static web sites by cache management of Squid.

In order to protect the leakage of accelerator operation log and raw data and to restrict the access to critical information to users, we have adopted an authentication system. As a result, the reverse proxy server for accelerator users requires a basic authentication based on username/password before all WebPages inside a control system network can be visited using a web browser. For controlling the access of users by authentication, our system consists of two reverse proxy servers. To manage the username/password, and deny or allow hosts easily, accelerator users and general users use different reverse proxy server. Therefore, the environments that allow users to access web sites are different for accelerator users and general users because the content of information is different. Specifically, general users can access only some specific website without the authentication, while accelerator users can access all of web sites in control system network with basic authentication. Consequently, single sign-on (SSO) authentication, which has a mechanism whereby a single action of user authentication and authorization can permit a user to access all computers and systems, has been achieved by choosing the accessible reverse proxy server for the accelerator users.

Before constructing this system, the following web sites inside control system network can be used.

- Zlog (Operational Log System)[4]
- MyDAQ2 (DAQ System)[5]
- Wiki based log system for 28G-SCECRIS[6]
- Axis video server
- Sony network camera
- Beam transport condition (BTmap)[7]

We attempted to test access all web sites including the ones listed above in the control system network from VLAN. As a result, it was succeeded to access the web sites via the reverse proxy servers without some modern digital oscilloscopes that have web applications written in Java as their user interface.

When the number of users increases in full-scale implementation, it will be necessary to confirm the system load because, so far the number of users accessing has not been very large. In the future, we will develop EPICS client applications using XML technology. After formalization of an XML file created by a web application for a value of EPICS record, EPICS client applications, which run outside the EPICS network via the reverse proxy servers, can be developed.

The authors wish to thank Dr. T. Ichihara for his helpful comments and suggestions.

References

1) M. Komiyama et al.: Proc. ICALEPCS09, Kobe, Japan, 2009, p. 275.
2) http://www.netfilter.org/
3) http://www.squid-cache.org/
4) K. Yoshii et al.: Proc. ICALEPCS07, Knoxville, Tennessee, USA, 2007, p. 299.
5) T. Hirono et al.: Proc. PCaPAC08, Ljubljana, Slovenia, 2008, p. 55.
6) A. Uchiyama et al.: RIKEN Accel. Prog. Rep. **43**, p. 133, 2009.
7) R. Koyama et al.: in this report.

Confinement of laser plasma by solenoid field for laser ion source†

T. Kanesue, *1 M. Okamura, *2 and K. Kondo, *2

A laser ion source produces intense plasma by means of a pulsed high-power laser focused onto a solid-state target. Because laser-produced plasma adiabatically expands in the direction perpendicular to the target surface, the plasma pulse width becomes proportional to the plasma drift distance L (the distance between the target and ion extraction point) and the plasma current density becomes proportional to L^{-3}. To obtain a longer pulse width at a high current density, transverse plasma expansion should be suppressed.

Previously, we tested the confinement of laser-produced plasma of singly charged carbon by a solenoid field and we obtained an ion current that was enhanced by a factor of 40 under a field of 20.9 mT [1]. Although strong current enhancement was verified at the exit of the solenoid magnet, the ion behavior downstream of the solenoid magnet was unknown. Therefore, we measured the transverse ion distribution along the beam axis downstream of a solenoid magnet.

We used an aluminum target and the second harmonics of a Nd:YAG laser with a wavelength of 532 nm (0.56 J/6 ns). The estimated density of laser power on the target was 3.5×10^{8} W/cm^2. At this laser power density, more than 95% of ions are singly charged ions [2].

A 482-mm–long solenoid magnet with an inner diameter of 76 mm was installed at a distance of 326.5 mm from the target. We used a detector that had nine ion probes aligned perpendicular to the beam axis at 5-mm intervals. Each probe had an aperture with a diameter of 0.75 mm. We applied a voltage of -100 V to the probes to avoid the detection of electrons.

Figure 1 shows the peak current measured on the beam axis at a point 22.5 mm downstream of the solenoid magnet. The current is plotted as a function of the solenoid field. As the solenoid field was increased from 0 to 15.4 mT, the peak current increased almost linearly and was saturated at a current enhancement factor of eight. This factor was smaller than that measured in the previous experiment (40). This can be explained by the increased distance between the target and the solenoid magnet. The longer distance results in a smaller solid angle. Figure 2 shows the peak current of the probes at 15.4 mT as a function of the radial position with respect to the beam axis for different distances from the end of the solenoid magnet. The transverse ion distribution at 0 mT at a point 22.5 mm downstream of the solenoid magnet is plotted in this figure.

As the distance from the solenoid magnet increased, the measured current decreased. However, the decrease in the current was smaller than that in the solenoid field. This indicates that ions do not travel along the magnetic field line.

We confirmed the strong enhancement of the ion current by the solenoid field within 27 mm in the transverse direction and 142.5 mm in the longitudinal direction from the end of the solenoid magnet. We will continue our attempts to understand the behavior of laser-produced plasma confined by the solenoid in order to improve the performance of the laser ion source.

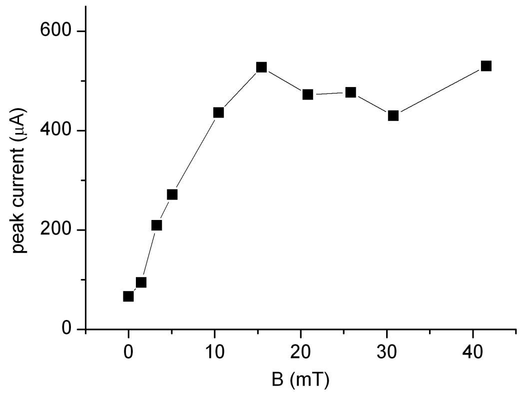

FIG. 1. Peak current measured on the beam axis, as a function of the solenoid field.

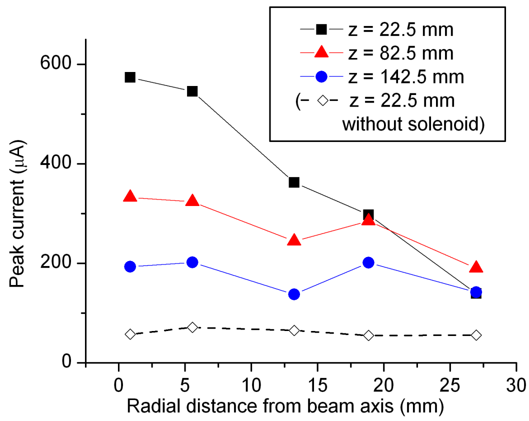

FIG. 2. Transverse ion distribution for solenoid fields of 0 and 15.4 mT at different distances z from the end of the solenoid magnet.

References

1) M. Okamura et al.: Rev. Sci. Instrum. **81**, 02B726 (2010).

2) K. Kondo et al.: Rev. Sci. Instrum. **81,** 02A511 (2010).

† Condensed from the article in Proceedings of IPAC'10, Kyoto, Japan, 2010, p. 4235

*1 Department of Applied Quantum Physics and Nuclear Engineering, Kyushu University

*2 Collider Accelerator Department, Brookhaven National Laboratory

Angular distribution of laser ablation †

M. Okamura,*1 K. Kondo*1 and T. Kanesue,*2

A laser ion source (LIS) is a powerful source that enables us to utilize high-current, high-charge-state heavy ions. However, it is difficult to control the ion pulse duration since the pulse duration can be adjusted only by changing the distance between the laser target and the ion beam extraction point, in other words, plasma drift length. If the plasma drift length is varied, the ion current density at the extraction point changes drastically and the optimum extraction conditions cannot be preserved. Recently, we developed a new technique to control the ion pulse duration by using a solenoidal field. An axial magnetic field traps the expanding plasma from a laser ablation source, and the ion current density can be adjusted independently. As a result, the plasma drift length can be appropriately chosen to the desired ion beam pulse width. However, this solenoid scheme poses a new problem. Conveniently, in a laser ion source, only the central part of the expanding plasma is used as an ion beam. On the other hand, when applying a solenoid field, the divergence of the expanding plasma can be corrected more efficiently. In this case, the characteristics of the off-centered plasma become more important. In this article, the angular distribution of a laser-ablated plasma is reported.

Silver was used as the laser target material. To simplify the experiment, single-charge-state ions were created by focusing a low-density laser beam on the target. The laser spot diameter was measured to be 4.5 mm. A Nd-YAG laser with a second-harmonic crystal (wavelength: 532 nm) having a laser power of 416 mJ was used. The laser pulse duration was measured to be 6.1 ns. The estimated laser power density was 4.3×10^{8} W/cm^2. Eleven Langmuir probes were used to detect the ion currents in the expanding plasmas. Each sensing area was circular with a diameter of 3.33 mm. The probes were biased at -50 V, and the measured signals were within the ion saturation region. The array was installed horizontally, and the detectors were positioned at points 9° apart, as explained in Figure 1. The induced voltages at a 50-Ω terminator are shown in Figure 2. On the vertical scale, a reading of 1 V corresponds to 230 mA/cm^2. At position "K," the normal position, the maximum current was observed, as expected. At an angle of more than 15°, the current was significantly reduced. The plasma expansion velocity was lower at lower angle position.

Current enhancement by a solenoid is strongly affected by the solenoid position. To minimize the effect of the solenoid, the aperture at the solenoid entrance must be made to cover the solid angle of the ablation plasma emission. For Ag$^+$ ions, the solonoid entrance must cover ±15° from the laser irradiation point.

In 2011, we plan to carry out test beam extraction and beam acceleration in order to confirm the obtained results.

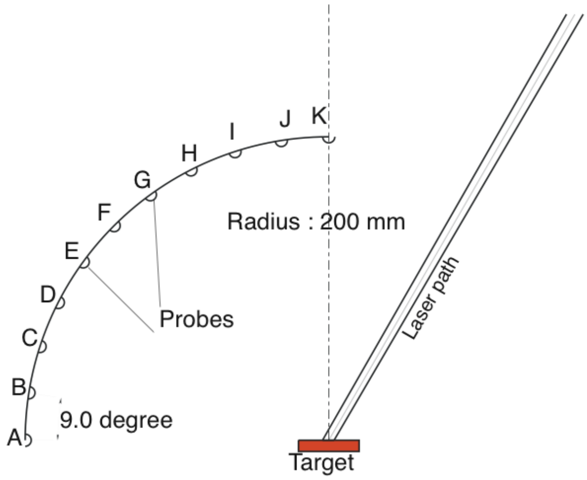

Figure 1 Positioning of the probes and the silver target.

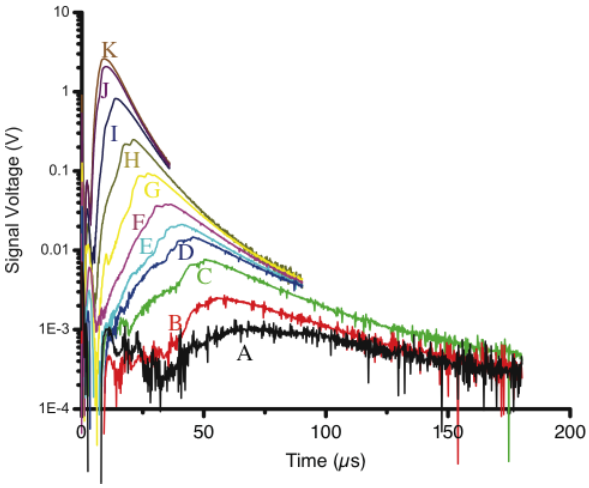

Figure 2 Ion current at each angle.

References
1) M. Okamura, A. Adeyemi, T. Kanesue, J. Tamura, K. Kondo, and R. Dabrowski, Review of Scientific Instruments, 02A510 (2010).
2) T. Kanesue, J. Tamura, and M. Okamura, Proceedings of EPAC 08, 2008 p. 421.
3) T. Kanesue, R. Dabrowski, M. Okamura, and K. Kondo, Proceedings of IPAC 2010, THPEC077.

† Condensed from the article in Proceedings of IPAC'10

*1 Collider-Accelerator Department, Brookhaven National Laboratory
*2 Department of Applied Quantum Physics and Nuclear Engineering, Kyushu University

LIS at low power density for RHIC-EBIS†

K. Kondo,*1 T. Kanesue,*2 and M. Okamura*1

[Laser ion sorce, Electron beam ion source, Relativistic heavy ion collider]

A laser ion source (LIS) has powerful potential for use as a primary ion source for RHIC-EBIS[1)2)] because it use a defocused Nd:YAG laser and has a low charge state, low emittance, and high ion yield[3)]; moreover, a design study has been performed in a solenoid field[4)]. Practically, the LIS must be used in 5-Hz operations in RHIC-EBIS for several months, but there is very little information on long-time operations. We investigated the beam properties and target consumption at different laser power densities with a repetition rate of 5-Hz for 1-h operation.

In this experiment, an Al target placed in a vacuum chamber was irradiated by a Nd: YAG laser at 1064 nm with a pulse length of 7 ns. We used different three laser power densities; 2.2×10^8, 2.8×10^8, and 3.1×10^8 W/cm^2. We assumed that all the supplied ions were singly charged at these laser power densities, on the basis of the results of a previous experiment[5)]. A Faraday cup (FC) with a 5-mm aperture was positioned 1.95 m away from the Al solid target to measure the beam current.

The relationship between the number of ion particles from the FC and the operation time is shown in Figure 1 for the three densities. At the high power density of 3.1×10^8 W/cm^2, the number of ion particles was significantly reduced, by 50%, with an increase in the operation time. A decrease in the ion yield was also observed at 2.8×10^8 W/cm^2. On the other hand, the ion particle number was constant over the 1-h operation at a low power density of 2.2×10^8 W/cm^2. At 2.8×10^8 and 3.1×10^8 W/cm^2, the beam current and beam pulse width, too, decreased with an increase in the operation time. These experimental results showed that low-laser-power-density conditions are suitable for ensuring stable beam properties .

The Al target surfaces after 1-h operation at 2.2×10^8 W/cm^2 and 3.1×10^8 W/cm^2 are shown in Figure 2. The surface is rougher at the high power density than at the low power density, where the beam properties can be maintained stable for long operation time. The surface conditions make the ablation plasma conditions different, which in turn causes changes in the properties such as number of ion, current, and beam pulse width.

We investigated the beam properties of the laser ion source under 5-Hz laser irradiation for 1-h. The ion particle number at a high power density decreased with an increase in the operation times. After the experiment, many bubbles were observed on the Al surface, especially at a high laser power density. These experimental results showed that the ablation plasma profile is sensitive to the target surface conditions. For RHIC-EBIS, the laser power density must be as low as possible.

† Condensed from the article in Proceedings of IPAC'10

*1 Collider-Accelerator Department, Brookhaven National Laboratory
*2 Department of Applied Quantum Physics and Nuclear Engineering, Kyushu University

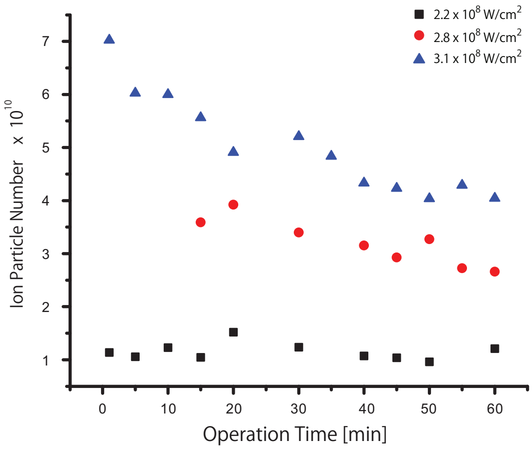

Fig. 1. Ion particle number vs. operation time for three laser power densities and a repetition rate of 5-Hz.

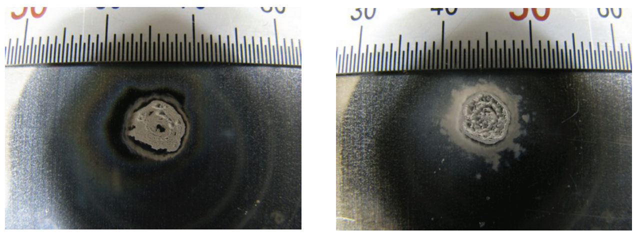

(a) 2.2×10^8 W/cm^2 (b) 3.1×10^8 W/cm^2

Fig. 2. Al surface conditions after 1-h operation at 5-Hz.

References

1) J. G. Alessi, D. Barton, and E. Beebe, *et al.,* Rev. Sci. Instrum. **81**, 02A509 (2010).
2) J. Alessi, D. Barton, and E. Beebe, *et al.,* Proceedings of LINAC 2006, 2006 p. 385.
3) T. Kanesue, J. Tamura, and M. Okamura, Rev. Sci. Instrum. **79**, 02B102 (2008).
4) K. Kondo, T. Kanesue, J. Tamura, and M. Okamura, Rev. Sci. Instrum. **81**, 02A511 (2010).
5) T. Kanesue, J. Tamura, and M. Okamura, Proceedings of EPAC 08, 2008 p. 421.

7. Instrumentation

Fluctuations in beam-spot temperature on a water-cooled rotating disk target at BigRIPS

Atsushi Yoshida, Yoshiyuki Yanagisawa and Toshiyuki Kubo

Since 2007, a water-cooled high-power rotating disk target[1] has been in operation at the BigRIPS. The beam-spot temperature on the rotating tungsten (W) disk target was measured and reported in a previous study[2]. Temperature fluctuations were observed at the beam spot. Further investigation was performed using the same beam and target setup, and a possible explanation for the fluctuations is presented here.

A W disk with a thickness of 2.1 mm thickness was irradiated by a 345-AMeV ^{48}Ca beam, up to 200 pnA (3.3 kW in beam power), which is the most intense beam presently available at our facility. The beam-spot diameter was 2 mm. The heat deposit in the W disk was 0.60 kW. The rotation speed of the disk was 100~300 rpm (rotations per minute). At the beam-spot position, a comet-shaped temperature distribution clearly evolved (Fig.1). The observed beam-spot temperature almost saturated within a few minutes after beam irradiation started. We observed temperature fluctuations at the beam spot in the temperature trend graph (Fig.2). The Ca beam from the SRC cyclotron was a DC beam, and its intensity was stable during these measurements. When we stopped beam irradiation, the beam-spot temperature decreased rapidly but the fluctuations remained. Upon changing the rotation speed, the beam-spot temperature showed periodic fluctuations in the approximate range of ±5 to ±15 °C, and the periodicity of the fluctuations was well synchronized with the rotation speed .

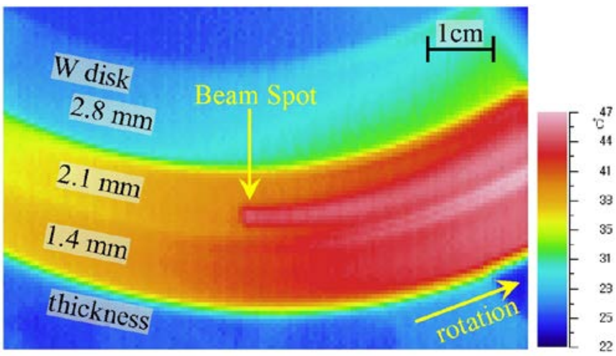

Fig.1. Observed temperature image of W disk target rotating at 150 rpm and irradiated with a ^{48}Ca beam of 185 pnA. The W disk has different thicknesses of 1.4, 2.1, and 2.8 mm at its outer edge.

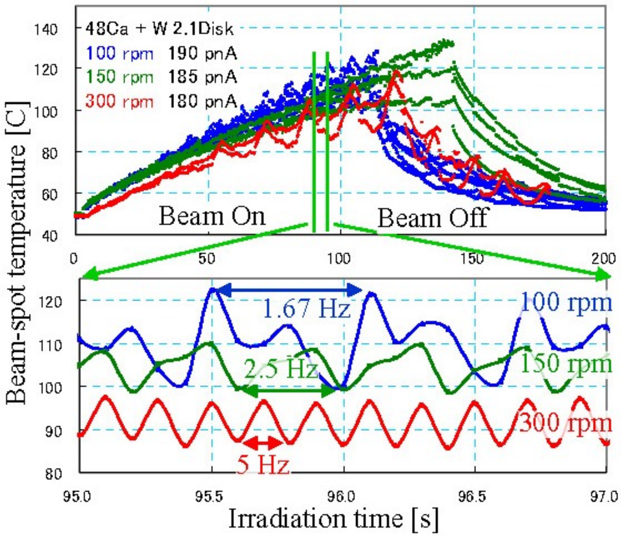

Fig.2: Beam-spot temperature along with the irradiation time for different rotation speeds. A magnified plot (lower graph) shows the periodic temperature fluctuations observed, which were well synchronized with the rotation speed.

A possible explanation for the fluctuations is that it may arise because of the structure of the cooling disk attached to the W-target disk. Since a cooling-water channel runs at the outer rim inside the cooling disk, it could well be that the fluctuation reflects the temperature difference between the outlet and the inlet of the cooling-water channel.

Details of the structure of the target disk unit have been explained in Ref.3. Here, details of the internal structure of the cooling disk are presented in Fig.3. The cooling water is introduced through a double-piped rotating shaft. The water channel is then separated to flow in two directions at the outer rim inside the cooling disk. Water in one channel runs in the clockwise direction, while water in the other channel runs in the counterclockwise direction. The two channels are then merged together and back through the shaft. For a rotating disk target with water cooling, it is essential to position the water-cooling channel as close as possible to the beam spot. Ideally, a one stroke water channel might be preferable to avoid unnecessary turbulence in the merging section. However, the present water channels are designed by considering weight balance during high-speed rotation.

To check the position dependence of the beam-spot temperature, an additional test was performed. In order to know the position of the inlet and outlet water channels in an infrared image, marking tapes whose emissivity is close to black-body emission were attached to the water-cooling disk (Fig.4). An infrared imaging camera[1,2] took infrared images of 256×256 pixels with a frame rate of 1/30 s. The rotation speed of the disk was 120 rpm (2 rotations per second), so that the disk made one rotation for every 15 frames. With this high-speed image data transfer rate involving the use of IEEE-1394 link, missing frames were sometime observed. But, those wrong frames were easily recognized by checking the position of the marking tapes in each image frame, and they were removed manually in the analysis.

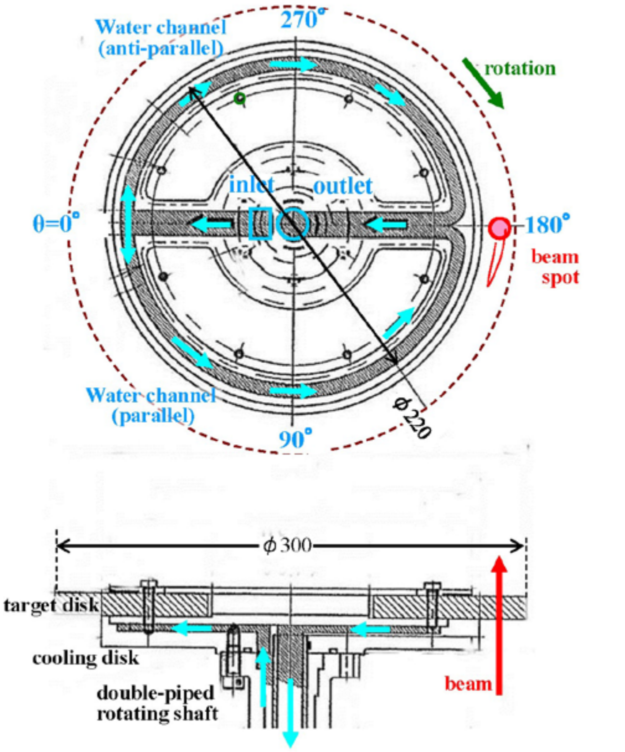

Fig.3. Inner structure of the cooling disk (upper figure). Cross-sectional view of the cooling disk mounted with a target disk (lower figure).

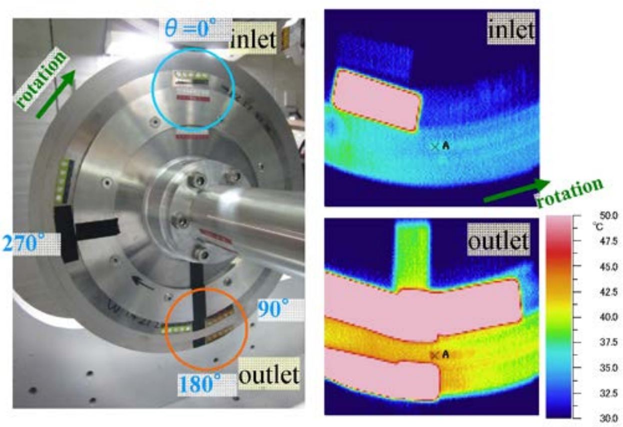

Fig.4. Marking tapes were attached to the cooling disk (left). Infrared image near the inlet and outlet water channels rotating in 120 rpm (right). Here, "A" indicates the beam-spot position.

The obtained trend graph of the beam-spot temperature along the cooling-water channel is shown in Fig.5. The temperature near the water inlet showed the minimum value. The temperature in the half-circle area where the cooling water runs in the same direction as the rotating direction was lower than the other half-circle area. Here, the flow velocity in the water channel was 2.3 m/s, which was slightly greater than the circumferential velocity of 1.4 m/s at the outer rim of the cooling disk. In a rest frame on the cooling disk, the beam spot is rotating around the cooling disk in one direction, whereas the cooling water runs parallel or anti-parallel to the beam spot. The interaction time of heat exchange between the cooling water and the high-temperature area near the beam spot is shorter in the anti-parallel section (θ = 180~360°), resulting in a larger thermal gradient between them and improving the heat exchange efficiency. This is the so-called counter-current heat exchange, which has larger heat exchange efficiency than that of the parallel flow. Thus, the beam-spot temperature fluctuations can be explained by the difference in the heat-exchange efficiency between the anti-parallel section and the parallel section (θ = 0~180°). Consequently, the direction of the cooling water should be the same as the target-disk rotation.

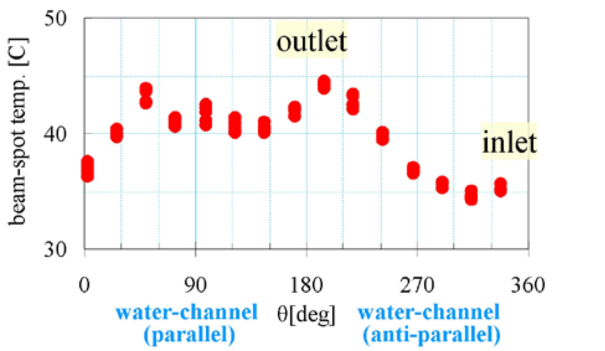

Fig.5. Obtained beam-spot temperature along the cooling-water channel.

Thus, the fluctuations in the beam-spot temperature could be explained quantitatively, but a further qualitative analysis using ANSYS-code simulations is necessary. More precise data analysis taking into account the actual cooling channel structure and the thermal diffusion parameters in the cooling channel is under way. According to the simulation result, some improvements are necessary to achieve more effective water cooling.

References

1) A.Yoshida et al.: RIKEN Accel. Prog. Rep. **41**, vii (2008).
2) A.Yoshida and Y. Yanagisawa: proceedings of INTDS-2010, TRIUMF, Sep.12-17, 2010, to be published in NIM-A.
3) A.Yoshida et al.: Fig. 4 of Nucl. Instrum. & Methods Phys. Res. A, 590, 204 (2008).

Radiation-transport calculation of heat load and radiation damage for superconducting magnets at BigRIPS

T. Ohnishi, K. Kusaka, and T. Kubo

[Radiation transport calculation, Radiation heat load, Radiation damage, PHITS code, Heavy ion beams, ^{48}Ca beam, In-flight RI beam separator, Superconducting magnet]

At RIBF, the goal intensity of heavy ions including uranium is about 1 pμA (6×10^{12} particles/s) for producing radioactive isotope (RI) beam to study unstable nuclei. Using intense beams, many high-energy light charged particles and neutrons are produced mainly at the production target and the beam dump. These particles hit the beam line devices and cause several serious problems such as heat load to the magnets and radiation damage to the beam line devices.

In the BigRIPS[1)] separator, the superconducting triplet quadrupole magnet STQ1[2)] and STQ2[3)] are located just after the production target and downstream of the beam dump, respectively. These STQs are cooled by the cryogenic plant[4)], which has an extra cooling capacity of about 300 W at 4 K. If the total heat load to these STQs exceeds its cooling capacity, the operation of the cryogenic plant becomes unstable, and the resulting high-heat load density at the coil of the STQ changes the superconducting state of the coil. In addition, some parts inside the STQs are made of organic materials, and radiation damage to these parts reduces the lifetime of the STQs.

A radiation-transport calculation is used to estimate the heat load and radiation damage to devices during RI beam production. The calculation for the BigRIPS separator is required to consider both light particles and heavy ions produced along the beam line. PHITS (multi purpose Monte Carlo Particle and Heavy Ion Transport code System)[5)] is a calculation code that takes into consideration the reaction processes of heavy ions as well as light particles and uses the cross sections for low energy process from evaluated nuclear data libraries. The PHITS code transports not only the primary beam and fragments produced in the target but also neutrons, protons, and light charged particles produced along the beam line of the BigRIPS separator. In this report, we present the calculated heat load of STQ and compare it with the result of measurement performed in 2008 and 2010 using an intense ^{48}Ca beam at 345 MeV/nucleon.

The calculated model includes the production target, the beam dump, the superconducting triplet quadrupole magnets (STQ1–STQ4), the normal conducting dipole magnets (D1 and D2), the vacuum chambers (F1 and F2), the concrete shields around the magnet, and the concrete walls. A prototype beam scraper[6)] was installed at the entrance of STQ1 inside the beam bore tube in order to reduce the heat load to STQ1. The beam scraper was a 126-mm-long copper block with a collimation hole that had a diameter of 36 mm.

In the calculation, the shape of the magnetic field of the quadrupole and the dipole was assumed to be a sharp edge shape, and the correction of the effective length was applied to the magnetic field of the quadrupole. The strength of the magnetic field used in the calculation was set according to the experimental values. Gaussian shape of the primary beam was applied to the beam-spot position and angular distribution obtained from the experimental data.

The ^{31}Ne and ^{32}Ne isotope experiments in 2008 and the ^{24}O and ^{33}Al isotope experiments in 2010 were performed using an intense ^{48}Ca^{20+} beam at 345 MeV/nucleon. Table 1 summarizes the conditions of these experiments and the measured heat load to the STQ1 cryostat. The settings used in the ^{31}Ne, ^{32}Ne, ^{24}O, and ^{33}Al isotope experiments are named as Settings 1, 2, 3, and 4, respectively. The beam currents were measured by a fast current transformer in Settings 1 and 2. In Settings 3 and 4, the phase probe at the exit of the accelerator was used. These beam-current monitors were calibrated using the current measured by a Faraday cup. The beam scraper located just after the production target were used in Settings 3 and 4. The heat load to the STQ1 cryostat was accurately determined by comparing the heater power of STQ1 with and without the beam irradiation. To maintain the liquid helium level in the cryostat, the heater power of the cryostat was controlled. The heat load was deduced from the measurement of the heater power. More details about the heat-load analysis of STQ are provided in Ref. 7. The systematic error of the measured heat load is estimated to be about 30%; this is mainly based on the averaging of the heater power and the measurement of the beam intensity.

The calculation was carried out at the RIKEN Integrated Cluster of Clusters facility in order to obtained sufficient event sources and achieve fast computation, and it was performed by generating about a million event sources. The heat load to the STQ1 cryostat was calculated using the experimental settings listed in Table 1, and the results are listed in Table 2. All the results listed in Table 2 are normalized with a ^{48}Ca^{+20} primary beam having an intensity of 20 μA. The total 4 K heat load was calculated by integrating the heat density over each part of the STQ1 component.

Table 1. Experimental conditions and measured heat load to the STQ1 cryostat

Setting	1	2	3	4
Target isotopes	^{31}Ne	^{32}Ne	^{24}O	^{33}Al
Bρ of fist dipole [Tm]	8.2	8.4	8.1	7.0
Be target thickness [mm]	15	20	15	10
Average current [μA]	0.52	2.25	3.5	3.7
Beam scraper	None	None	Used	Used
Measured heat load [W]	11.9	42.6	32.7	26.8

Table 2. Heat load estimated by PHITS calculation

Setting	1	2	3	4
Liquid He	22.1	28.0	12.8	9.01
First coil	23.5	28.7	9.14	6.58
Second coil	11.1	13.7	7.33	5.35
Third coil	4.31	5.24	3.88	2.89
First coil case	121	151	45.9	31.4
Second coil case	27.3	33.5	17.9	12.9
Third coil case	16.3	20.0	13.8	9.30
Inner flanges	18.6	23.0	8.14	5.80
He vessel	208	263	143	102
(Sub total 4 K load)	452	567	262	186
80 K shield vessel	42.5	55.0	30.3	22.0
Inner vacuum duct	87.2	116	68.8	50.9
Outer vessel (upstream wall)	21.1	26.6	7.13	5.08
Outer vessel (others)	8.88	11.0	5.97	4.29
Scraper	0	0	293	186

All values have the unit W. The results are calculated using a beam with an intensity of 20 μA.

The statics error of the total heat load calculated by the Monte Carlo method is estimated to be less than 0.01%. On the basis of the experimental beam intensity, the total heat load to the STQ1 cryostat was estimated to be 12.0, 63.8, 45.9, and 34.4 W for Settings 1, 2, 3, and 4, respectively. The calculation estimates the measured heat load within a factor 1.0–1.5.

The heat load distribution around the STQ1 in the case of Setting 1 is shown in Fig. 1. In Fig. 1, the heat load is mainly distributed within the inner duct of the STQ1 close to the production target. The light charged particles, mainly protons, hit the inner duct of STQ1, because their ion optics are different from those of the objective isotopes. The heat load around the first coil is larger than that around other coils, because the first coil is close to the production target.

The effect of the beam scraper is evaluated by comparing the calculated heat load with and without it. Using Setting 1, the calculated total heat load at 4 K with the beam scraper was about 271 W, which is 40% less than that without the beam scraper. This effect is confirmed using the measured heat load in Settings 1 and 3, because the experimental condition was almost same. Using the measured values and scaling the beam intensity, the beam scraper reduces the total heat load by about 59%, and this result almost agrees with the calculation.

To estimate the radiation damage, the peak value of

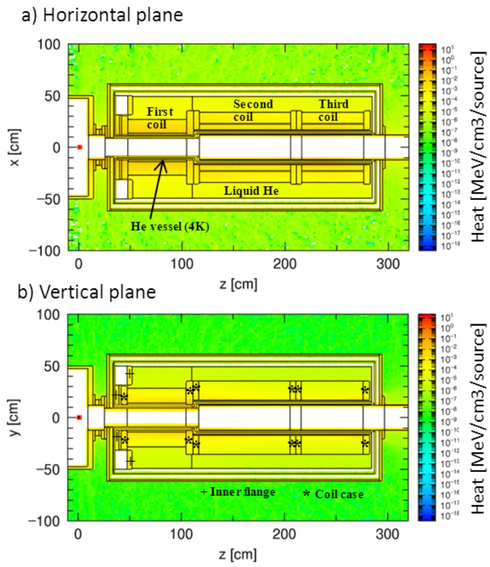

Fig. 1. Heat load distribution around STQ1 in Setting 1. The upper and lower panels show the distribution in the horizontal and vertical cross section, respectively. The normalization factor "per source" means "caused by one nucleus of primary ^{48}Ca beam."

the absorbed dose at the first coil of STQ1 was determined from the calculated heat load distribution. The epoxy resin insulation, which has radiation tolerance of about 10^7 Gy, is used in the coil of the STQ. If the coil is fabricated using only epoxy resin, the calculated peak heat-load density and absorbed dose are 0.75 mW/cm^3 and 0.61 Gy/sec/cm^3, respectively, in Setting 3. Using these values, the lifetime of the epoxy resin insulation is estimated as about 2 years when the beam intensity is 20 μA and the beam time period per year is 10^7 s.

In summary, we have performed the radiation transport calculation using the PHITS code. The heat load to the STQ1 cryostat at the BigRIPS separator was estimated and compared with the measured values in several experimental settings using an intense $^{48}Ca^{20+}$ beam at 345 MeV/nucleon. The PHITS code reproduces the measured heat load within a factor of 1.5. This results will be used for the final design of the beam scraper at STQ1 to reduce heat load and radiation damage.

References

1) T. Kubo et al.: Nucl. Instr. and Meth. **B 204**, 97 (2003).
2) K. Kusaka et al.: IEEE Trans. Appl. Superconductivity, **18**, 240 (2008).
3) K. Kusaka et al.: IEEE Trans. Appl. Superconductivity, **14**, 310 (2004).
4) T. Kubo et al.: IEEE Trans. Appl. Superconductivity, **17**, 1069 (2007).
5) K. Niita et al.: Rad. Measurement **41**, 1080 (2006).
6) A. Yoshida et al.: RIKEN Accel. Prog. **43**, 153 (2010).
7) K. Kusaka et al.: IEEE Trans. Appl. Superconductivity, **21**, 1696 (2011).

RIKEN Accel. Prog. Rep. 44 (2011)

Status of the Control System of BigRIPS

K. Yoshida

This year, two modifications have been made to the control system of BigRIPS[1,2], which is based on the experimental physics and industrial control system (EPICS)[3]. One of the modifications is that support has been provided to MobileCorder MV100, which is manufactured by Yokogawa Electric Corp. MV100 is an all-in-one portable recorder with integrated display, recording, and communications functions. It provides the functionality of a measuring server, which facilitates the transmission of measured data through Ethernet. A software routine to receive the data from MV100 has been developed and included in the control system of BigRIPS. The routine was written as the device support for the asynDriver, which is the one of the support libraries of EPICS. The routine sends a command packet to MV100 through Ethernet and receives response packets from MV100 in a synchronous way. The measured data extracted from the response packet is transferred to the EPICS record and used in EPICS. In BigRIPS, two MV100 devices are used to measure the temperatures of the wall of the target chamber, the beam scraper, and the beam duct between the target and the first dipole magnet D1.

The other modification is the improvement of the user interface of the control display. The new display is capable of indicating a change in the value of an input field. In the control display, generally, the button should be pressed to set the input values of the actual devices. This mechanism is useful in preventing the wrong input being set in the devices; however, if operators forget to push the set-button, the devices retain the old setting despite the input field showing a new value. In order to indicate such a condition, the display is modified to indicate a change in the value through the display of different colors. The characters in the input field change their color to orange if a new value is entered, and they return to the normal color (black) when the input value is set in the devices. Thus, operators easily recognize the input fields for which the set-buttons should be pressed.

New EPICS records were introduced in order to facilitate such recognition. The records corresponding to the input fields were doubled, and one of them was used to store the old value. The other record was connected to the input field and its value was immediately updated when a new value was entered in the input field. The stored record was updated only when a new value was set in the devices. The flag was set depending on whether the two records were identical or not. The flag was used to change the color of the characters in the input field. Unfortunately, the display manager *dm2k*, which is used as the display manager of the control system of BigRIPS, does not support changes in the color of the characters in the input fields. It can change only the character color in the monitor field. The code of *dm2k* was modified so that it could support changes in the color of the characters in the input fields. The code for changing the color was taken from the routine of the monitor field and was introduced in the routine of the input field. The input/output routines of the configuration file of *dm2k* were also modified so that the necessary information to change the color was stored in the configuration file. By utilizing the modified *dm2k* and the newly introduced records, it became possible to indicate a change in the input.

References

1) K. Yoshida et al.: RIKEN Accel. Prog. Rep. **41**, 127 (2008).
2) K. Yoshida et al.: RIKEN Accel. Prog. Rep. **43**, 155 (2010).
3) http://www.aps.anl.gov/epics/

Neutron dose around the BigRIPS

K. Tanaka, N. Inabe, and T. Kubo

[Radiation dose, neutron, BigRIPS]

The radiation-shield system of the BigRIPS was designed according to a simple model estimation. In this study, a realistic distribution of the radiation dose was measured and evaluated using the Monte Carlo calculation code to verify the accuracy of the previous estimation.

Eq. 1 shows the effective dose formula of the simple model used to estimate the radiation dose resulting from the neutrons outside a shield material[1]. The neutron is assumed to be generated by nuclear reaction and it pass through the radiation shield.

$$E = \frac{E_0(\theta) \times exp\{-t/\lambda\}}{L^2} \qquad [Sv/h\ cm^2], \qquad (1)$$

where E is the effective neutron dose rate; $E_0(\theta)$, the angular distribution of effective dose of the generated neutron; t, the shield thickness; λ, the shielding power of the material; and L, the distance from the neutron source. To design the BigRIPS shielding system, this formula was applied by considering a fixed value for the λ parameter. The fixed λ parameter is available when the energy of generated neutron is higher than 150 MeV.

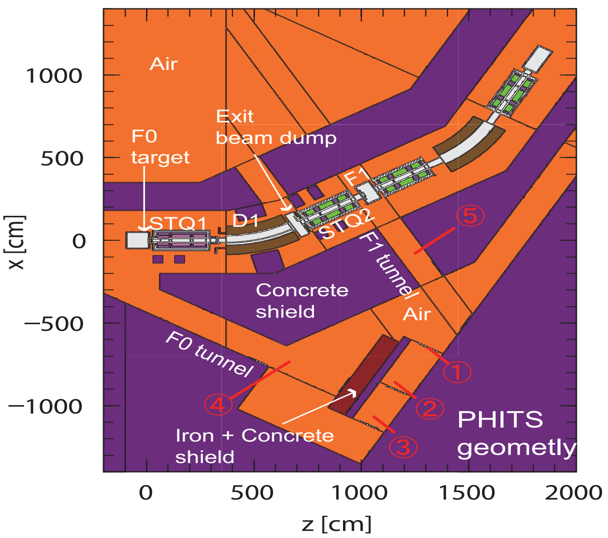

Fig. 1. Geometry of the BigRIPS used in the PHITS calculation. Measurement points for the neutron dose are indicated by numbers 1–5.

Since the simple formula dose not take into account the energy dependence and streaming effect of the neutron, we performed a radiation transport calculation for the BigRIPS setup with the Particle and Heavy-Ion Transport code System (PHITS)[2] by using the

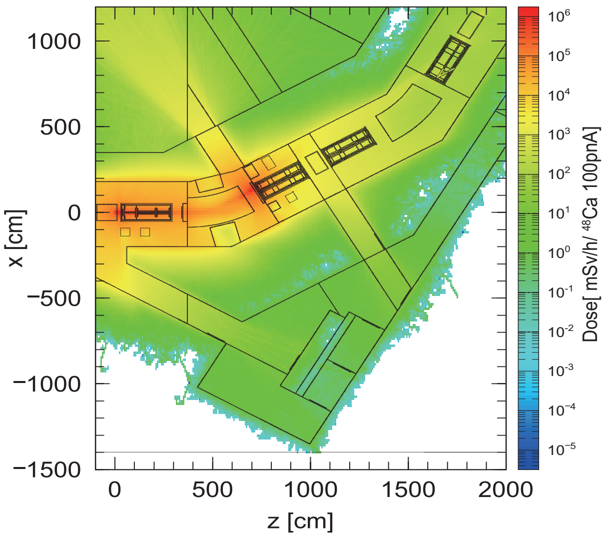

Fig. 2. Neutron dose around the BigRIPS calculated using the PHITS code for a ^{48}Ca beam with an intensity of 100 particle nA. The doses in the figure are values averaged from the floor to a height of 2.5 m.

RIKEN Integrated Cluster of Clusters (RICC) facility. This calculation involves the consideration of the energy dependence and streaming effect of the neutron. Figure 1 shows the top cross-sectional view of the BigRIPS geometry used in the PHITS calculation. Figure 2 shows the calculated neutron-dose distribution. The conditions considered in the calculation are described below. The beam was a 345 MeV/nucleon ^{48}Ca beam with an intensity of 100 particle nA. The production target at F0 (see Fig. 1) was 15-mm-thick Be, and Bρ1 was 8.1 Tm. In the calculation, 2 million ^{48}Ca ions were injected into the target. Neutron streaming was considered to occur through the F0 and

Table 1. Summary of neutron dose (mSv/h) determined by calculation and measurement. The beam intensity was normalized to 100 particle nA.

Measurement point	Simple model (^{84}Kr)	PHITS (^{48}Ca)	Measurement (^{48}Ca)
1	0.1–1 mSv/h	2	2
2	0.02	0.5	0.2
3	0.002	0.4	0.2
4	∼1	5–50	30*
5	≥1	10–100	100*

* preliminary result

F1 tunnels and up to the exterior of the concrete shield.

The neutron dose around the BigRIPS was measured in 2010 under the same conditions as those in the PHITS calculation described above. We used the neutron-survey meter TPS-451C manufactured by ALOKA Co Ltd. The measurement range for the neutron energy was from 0.025 eV to 15 MeV. The measurement points are shown in Fig. 1. The results of the measurements and calculations are listed in Table 1 along with the simple model calculation result for a ^{84}Kr beam performed by K. Yoshida[3]. A ^{84}Kr beam was supposed to generate the highest neutron dose and was therefore employed to design the BigRIPS shielding system. Owing to neutron streaming through the F0 and F1 tunnels, which is not considered in the simple model, the dose level calculated with the PHITS is much higher than that obtained by using the simple model. The PHITS calculation reproduces the measurement well.

The neutron dose level around the rear of the iron + concrete (points 1–3 in Fig. 1) was found to be higher than that expected from the simple model calculation. The electrical circuit of the BigRIPS setup at point 3 was affected by neutron radiation when a 100 particle nA ^{48}Ca beam was provided. In future, more intense beams will be provided. It is therefore necessary to develop more effective shields.

References

1) Y. Uwamino et al.: RIKEN Accel. Prog. Rep. **35**, 321 (2001).
2) K. Niita et al.: JAEA-Data/Code **2010-022**, (2010).
3) K. Yoshida: private communication.

Residual-radiation measurement around the BigRIPS

K. Tanaka, N. Inabe, and T. Kubo

[residual dose, gamma ray, BigRIPS]

Owing to the irradiation of high-intensity beams on the BigRIPS, maintenance and improvement works are performed under high-radiation environment of γ-rays. It is necessary to predict the residual radioactivity by considering the beam intensities and cooling time. This prediction is useful for planning the maintenance and improvement works and for reducing the dose exposure. The time dependence of the residual radioactivity at several spots around the BigRIPS has already been reported[1]. In the previous studies, dose reductions were evaluated only for those cases in which cooling was performed between one and five months after the beam irradiation, except for the beam-dump chamber. In this paper, the dose reduction during several days after the beam irradiation and the evaluation of the long-term estimation of the residual dose around the BigRIPS are reported.

The short-term time dependence of the radiation dose was measured. When troubles occur owing to high radiation and radiative heating on setups, in particular, around the F0 target and beam-dump chamber, it is possible to access the setups and work only for a short time just after beam irradiation. In such a situation, the radiation level is supposed to be high, and the reduction rate of the radiation is also high. Therefore, to plan any urgent maintenance work, the evaluation of the short-term time dependence of the residual radioactivity is necessary. The time dependence of the residual radioactivity at several spots around the BigRIPS was measured using the Teletector 6112D GM survey meter, which can remotely measure the doses, after the beam irradiation has stopped.

Figure 1 shows the spots for the radiation-dose measurement. Spot 1 is on the surface of a concrete wall across the F0 chamber. Spot 2 is on the surface of the aluminum F0 chamber. Spot 3 is on the side of a pillow seal[2] made of stainless steal (SUS304: Fe, 70–74%; Ni, 8–10%; Cr, 18–20%). The aluminum F0 chamber and an iron magnet are surrounding spot 3. Spot 4 is around the beam-dump chamber and a local shield. The beam-dump chamber is made of SUS316 (Fe: 67–72%; Ni: 10–14%; Cr: 16–18%; Mo: 2–3%) and the local shield is made of concrete.

Several experiments using a ^{48}Ca beam with a Be target were performed in December 2009. Figure 2 shows the relative time dependence of the residual γ-

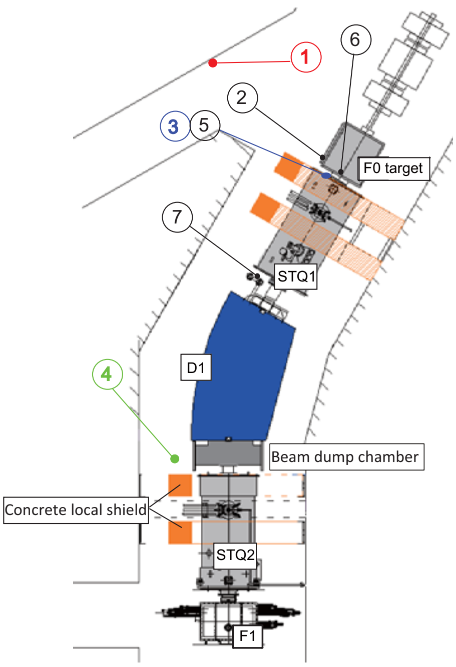

Fig. 1. Spots for γ-ray measurements around the BigRIPS. The measurements at spots 1–4 were performed using a GM survey meter, and those spots 5–7 were performed using a Ge detector.

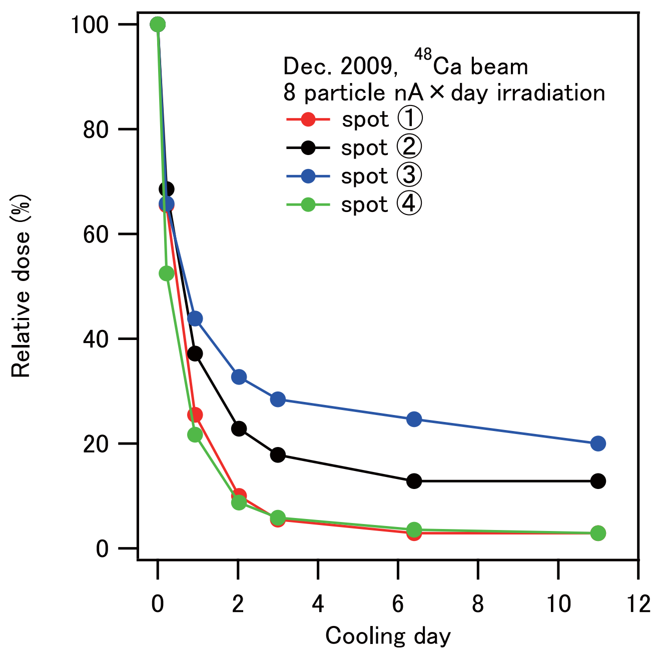

Fig. 2. Time dependence of residual radioactivity. These measurements were performed 10 min after the ^{48}Ca-beam irradiation has stopped. The spots for each plot are shown in Fig. 1.

Table 1. Nuclei identified from the γ-ray spectrum obtained from the F0 pillow seal (spot 5). The spectrum was measured on 29th September, 2010. The radiation dose at the same position at measured by a γ-ray survey mater on 24th September was 2.3 mSv/h.

Nuclide	Energy (keV)	Half life	Dose ratio (%)
^{54}Mn	835	312 d	38.6
^{58}Co	811	70.8 d	15.3
^{56}Co	846, 1038, 1238, 1771, 2598, etc.	77.3 d	13.4
^{46}Sc	889	84 d	8.0
^{60}Co	1173, 1332	5.3 y	5.3
^{48}V	984, 1312	16.0 d	2.5
^{59}Fe	1099, 1292	44.5 d	1.3
^{51}Cr	320	27.7 d	1.0
^{57}Co	122, 136	272 d	0.8
^{22}Na	1275	2.6 y	0.7

Table 2. Nuclei identified from the γ-ray spectrum obtained from the F0 scraper (spot 6). The spectrum was measured on 29th September, 2010. The radiation dose at the same position measured by the γ-ray survey mater on 28th September was 100 mSv/h.

Nuclide	Energy(keV)	Half life	Dose ratio(%)
^{58}Co	811	70.8 d	42.1
^{56}Co	846, 1038, 1238, 1771, 2598, etc.	77.3 d	29.4
^{54}Mn	835	312 d	11.1
^{60}Co	1173, 1332	5.3 y	7.4
^{46}Sc	889	84 d	3.7
^{59}Fe	1099, 1292	44.5 d	3.2
^{22}Na	1275	2.6 y	1.4

ray dose. A relative dose of 100% suggests an initial dose at each spot. The initial dose was measured 10 min after the end of the experiment. In general, the major radioactive nuclide in concrete at spot 1 and aluminum at spot 2 is ^{24}Na ($T_{1/2}$ = 14.96 h). The major nuclides in the SUS material used around spots 3 and 4 are ^{56}Mn ($T_{1/2}$ = 2.58 h), ^{57}Ni ($T_{1/2}$ = 35.6 h), ^{52}Mn ($T_{1/2}$ = 5.59 d) and several other nuclides. ^{24}Na is also supposed to exist in the concrete shield near spot 4.

To predict long-term residual dose, the identification of radioactive nuclides is necessary. A γ-ray spectrum and the radioactive nuclides around the beam-dump chamber identified using a Ge detector have already been reported[1]. In this study, the radiations at several spots were measured. Spot 5 in Fig. 1 indicates the pillow seal installed downstream of the F0 chamber. Spot 6 indicates a copper scraper installed downstream of the F0 chamber. Spot 7 is the space between STQ1 and D1, which was 50 cm apart from an aluminum chamber, a SUS304 duct and iron magnets. A Ge detector surrounded by a Pb collimator was used to obtain the γ-ray spectra on 29th September, 2010. ^{48}Ca 2050 particle nA×day was irradiated on a 15-mm-thick Be target from 14th May to 11th June, 2010, and ^{18}O 540 particle nA×day was then irradiated on a 60-mm-thick Be target from 22nd June to 1st July, 2010. Residual radioactive nuclides were identified from the γ-ray spectra, and results are listed in Tables 1–3. By using the photo-peak area of the spectra, efficiency of the Ge detector, and the γ-ray energy, the relative values of the effective doses of the γ-ray radiated from the identified nuclei were calculated using the conversion coefficients of the γ-ray energy[3]. The calculated effective doses are also listed in Tables 1–3 as the values relative to the values of the total dose at each spot. The future radiation levels can be estimated from these tables.

Table 3. Nuclei identified from the γ-ray spectrum obtained from the STQ1-D1 (spot 7). The spectrum was measured on 29th September, 2010. The radiation dose at the side of the D1-chamber flange measured by the γ-ray survey mater on 24th September was 1.1 mSv/h. The radiation dose in the space was about 1/4th of this value.

Nuclide	Energy (keV)	Half life	Dose ratio (%)
^{54}Mn	835	312 d	37.1
^{56}Co	846, 1038, 1238, 1771, 2598, etc.	77.3 d	21.0
^{46}Sc	889	84 d	14.2
^{58}Co	811	70.8 d	11.2
^{60}Co	1173, 1332	5.3 y	8.8
^{48}V	984, 1312	16.0 d	5.0
^{59}Fe	1099, 1292	44.5 d	1.6
^{51}Cr	320	27.7 d	0.8

The short- and long-term time dependence of the residual dose can be estimated using the evaluations performed in this study and the previous studies.

References

1) K. Tanaka et al.: RIKEN Accel. Prog. Rep. **43**, 163 (2010).
2) K. Tanaka et al.: RIKEN Accel. Prog. Rep. **43**, 161 (2010).
3) ICRP, ICRP Publication 74: Conversion Coefficients for use in Radiological Protection against External Radiation (Elsevier, Amsterdam), 199 (1996).

Details of 3D magnetic-field analysis and its adoption for magnet control system

H. Takeda, T. Kubo, K. Kusaka, T. Ohnishi, N. Fukuda, D. Kameda, and N. Inabe

Superconducting in-flight fragment separator BigRIPS is a next-generation separator that was developed with the aim of efficiently producing radioactive isotope (RI) beams. It is characterized by large angular and momentum acceptances and large magnetic rigidity. These features facilitate efficient transmission of RI beams even when in-flight fission of uranium beams occurs as a production reaction. Large-aperture superconducting triplet-quadrupole (STQ) magnets are used to realize large acceptances. Ion optical calculation with realistic magnetic field maps are necessary for achieving high resolution in A/Q, which is one of the most important quantities in particle identifications because in the range of energies at RIBF, RI beams, especially heavy RI beams, with several charge states are produced.

3D field maps in the cylindrical coordinate can be decomposed into multipole components as follows (skew components are omitted here for simplicity);

$$\begin{aligned} B_r(r,\theta,z) &= \sum_n B_{r,n}(r,z)\sin n\theta, \\ B_\theta(r,\theta,z) &= \sum_n B_{\theta,n}(r,z)\cos n\theta, \\ B_z(r,\theta,z) &= \sum_n B_{z,n}(r,z)\sin n\theta, \end{aligned}$$

where $n = 1, 2, 3, \cdots$ correspond to dipole, quadrupole, sextupole, $\cdots$ components. These components are expressed as

$$\begin{aligned} B_{r,n}(r,z) &= \left(\frac{r}{r_0}\right)^{n-1} \sum_m b_{n,m}(z) \left(\frac{r}{r_0}\right)^{2m}, \\ B_{\theta,n}(r,z) &= \left(\frac{r}{r_0}\right)^{n-1} \sum_m \frac{n}{n+2m} b_{n,m}(z) \left(\frac{r}{r_0}\right)^{2m}, \\ B_{z,n}(r,z) &= \left(\frac{r}{r_0}\right)^{n} \sum_m \frac{r_0}{n+2m}\frac{\partial}{\partial z} b_{n,m}(z) \left(\frac{r}{r_0}\right)^{2m}. \end{aligned}$$

By using the recursive equation,

$$b_{n,m}(z) = -\frac{r_0^2}{4m(n+m)}\frac{n+2m}{n+2(m-1)}\frac{\partial^2}{\partial z^2} b_{n,m-1}(z),$$

all $b_{n,m>0}$ can be expressed only by $b_{n,0}$ distributions, which are used in the COSY ion optical calculation. The scale radius r_0 is an arbitrary number with the dimension of length and is selected as a warm bore radius of 0.12 mm in our analysis.

We have measured the field maps of the STQs along the beam axis at various excitation currents from 20 A to 165 A.[2)] Discrete Fourier transformation of the measured field maps have been performed to decompose

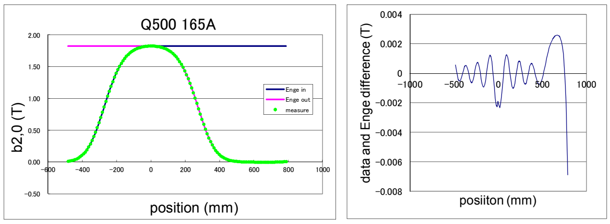

Fig. 1. Enge function fitting for Q500 magnet at 165A is shown as an example. The left panel shows comparison of $b_{2,0}$ data and Enge functions. The difference between the data and the Enge functions is plotted in the right panel.

them into multipole components at each z point according to the first set of equations. The obtained $B_{r,n}, B_{\theta,n}$ distributions are analyzed by using the second set of equations and final recursive formula to deduce the $b_{n,0}$ distributions. The fringe field fall off is approximated by Enge function

$$F(\zeta) = \frac{1}{1 + e^{a_1 + a_2\cdot(\zeta/D) + \cdots + a_6\cdot(\zeta/D)^5}},$$

where ζ is the distance from the field boundary along the beam axis and D is the full aperture of the magnet. The coefficients $a_{1,\cdots,6}$ are selected to fit with the data for both edges of magnets. An example of fitting is shown in Fig. 1. The measured $b_{2,0}$ data are plotted with the Enge functions in the left panel of the figure, while the difference between the measured data and the Enge functions are plotted in the right panel. Fitting is performed for each excitation current. The data and Enge functions agree within approximately 0.2% for all currents, but a relatively large difference can be seen at the tail region (position: approximately 700 mm). The reason for this difference is the undershoot behavior of the measured data, which cannot be expressed by the Enge function. In the future, we need to modify the fitting function in order to improve the agreement of the data. Figure 2 shows the excitation-current dependence of the Enge coefficients. The six upper figures show the coefficients $a_{1,\cdots,6}$ for the entrance side, and the six lower ones show the coefficients for the exit side. The results from measurements in 2006 and 2008 are represented by different symbols. These coefficients are linearly interpolated between the measured results in the COSY calculation at this moment. Although the measured data of 2006 and 2008 agreed each other with the maximum difference being on the order of 0.1%, very small systematic errors of the measured data result in large differences in the

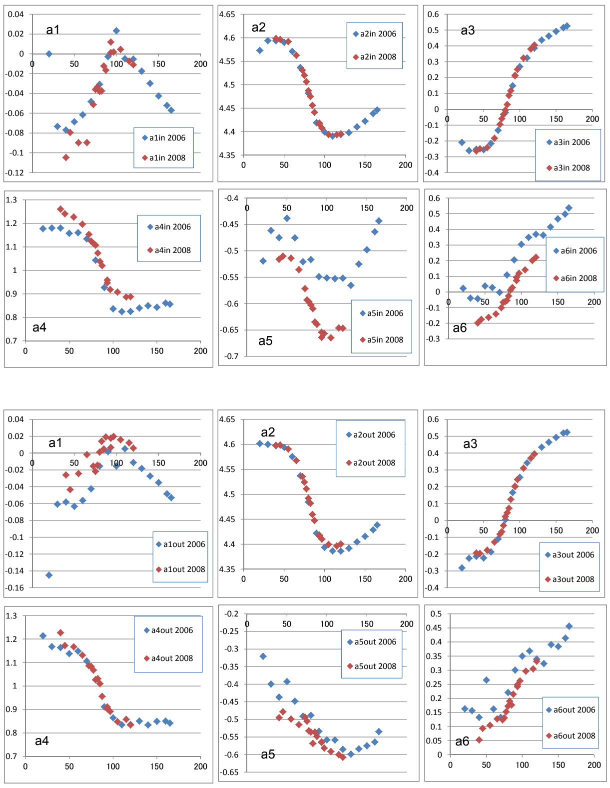

Fig. 2. Excitation-current dependence of Enge coefficients of Q500 magnet. The six upper and lower panels show the coefficients for entrance and exit sides, respectively.

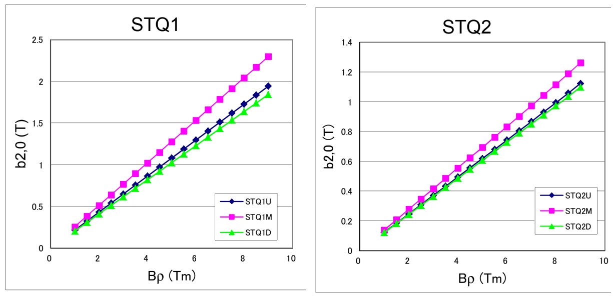

Fig. 3. Example of Bρ scan results.

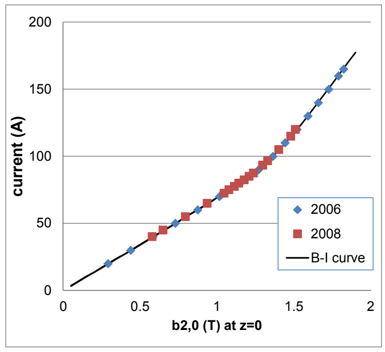

Fig. 4. B-I excitation curve of Q500 magnet. Symbols are data in 2006 and 2008 measurements. Solid curve is a function fitted to the data, which is implemented in the control system.

higher-order coefficients because the Enge function is less sensitive to the higher-order coefficients. The Enge function with four parameters (*i.e.* $a_5 = a_6 = 0$) may be sufficient in our case.

Implementation to the magnet control system[3] is performed as follows. The BigRIPS beamline is divided into some sections, usually separated by the foci F1, F2, etc. The strengths of all magnets in the section are calculated on the basis of the fringing field distributions in order to achieve the suitable optical conditions for the section (achromatic/dispersive focus, etc.) in some steps of magnetic rigidity $B\rho$ of reference particles. Figure 3 shows examples of this $B\rho$ scan results in the standard optics mode for the F0-F1 section. The $b_{2,0}$ values at the center are plotted as functions of $B\rho$. The three lines in the left panel of the figure correspond to the results for the quadrupoles in STQ1, while the ones in the right panel correspond to the results for the results for the quadrupoles in STQ2. The parameter set for determining the lines is prepared for each optics mode. A user can select the optics mode by choosing a configuration file containing the parameter set. The excitation currents to be set are determined according to the B-I curves obtained in the field map measurements. In Fig. 4, the excitation current of Q500 is plotted as a function of the $b_{2,0}$ value at the magnet center ($z = 0$). Both Bρ-B and B-I functions are implemented in the magnet control system. Finally, the field strengths of all magnets are set by applying the $B\rho$ values for the sections.

References

1) T. Kubo: Nucl. Instr. and Meth. **B 204**, 97 (2003).
2) Y. Yanagisawa et al.: RIKEN Acc. Prog. Rep. **41**, 125 (2008), H. Takeda et al.: RIKEN Acc. Prog. Rep. **43**, 157 (2010).
3) K. Yoshida et al.: RIKEN Acc. Prog. Rep. **41**, 127 (2008), K. Yoshida et al.: RIKEN Acc. Prog. Rep. **43**, 155 (2010).

Focal-Plane Detector System of SHARAQ Spectrometer

S. Michimasa,[*1] H. Tokieda,[*1] S. Noji,[*2] S. Ota,[*1] S. Shimoura,[*1] T. Uesaka,[*1] H. Sakai, P. Roussel-Chomaz,[*3] J.-F. Libin,[*4] P. Gangnant,[*4] and C. Spitaels[*4]

[SHARAQ spectrometer, cathode-readout drift chamber]

The SHARAQ spectrometer[1] and the high-resolution beam line[2] have been constructed at the RI Beam Factory (RIBF) at RIKEN. In March and May 2009, we performed a beam study to examine dispersion-matching ion optics and to evaluate the performance of the installed detectors. Through the beam study, we have obtained valuable information on the high-resolution spectrometer system. This report discusses the basic performance of the detector system installed in the dispersive focal plane of SHARAQ.

Figure 1 shows the detector setup in the final focal plane of the SHARAQ spectrometer; the setup was used in the beam study. Two tracking detectors and three plastic scintillators were installed. The focal plane is located 3.04 m downstream of the exit of the SHARAQ D2 magnet and inclined at 35° with respect to the central orbit. A beam is passed through the tracking detectors installed in vacuum, and it passes through a 10-mm-thick aluminum window. The plastic scintillators were placed downstream of the window.

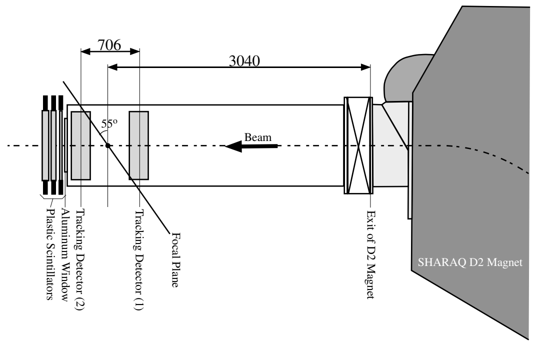

Fig. 1. Detector setup in the dispersive focal plane of SHARAQ. Two tracking detectors and two plastic scintillators were installed for the beam study.

The plastic scintillators were used to determine the timings passing through the focal plane, and to measure energy deposits. The three-layer configuration of the scintillators is efficient in rejecting cosmic-ray events. Each scintillator is read out by two photomultiplier tubes attached to both sides. The effective area of each plastic scintillator is 650 (H) × 400 (V) mm^2. Their thicknesses are 5 mm, 10 mm, and 20 mm. Charge and timing data of the scintillators were obtained by utilizing the charge-to-time conversion (QTC) technique and multi-hit TDC modules[3].

Tracks of beam particles were measured by the cathode-readout drift chambers (CRDCs)[4]. The CRDCs were manufactured in fiscal year 2008 in collaboration with an experimental group of GANIL. Their detailed structure is described in Ref.[5]. In this study, we examined their performance with isobutane gas at 15 and 30 torr. The CRDC has two signals from the anode wires and two multiplexed signals from the cathode pads. The anode signals were utilized to deduce the drift time and the charge of secondary electrons in the CRDC. Preamplifiers for the anode signals were of the charge-sensitive type and were set to have a gain of 0.9 V/pC and a time constant of 20 μs. Since the anode signal is generated when avalanche occurs around the anode wires, the drift time is determined by the difference between an anode timing signal and the timing signal of the plastic scintillator. For the calibration of drift velocities of secondary electrons in the CRDCs, a plastic scintillator with horizontal slit apertures was installed in the focal plane. Slits were located at intervals of 10 mm and their width was 0.2 mm. By using the plastic scintillator, the drift velocities were estimated to be 5.9 cm/μs with an 83.3 V/cm drift field at 15 torr and 5.3 cm/μs with a 140 V/cm drift field at 30 torr. These values are consistent with those obtained by using the GARFIELD code[6].

The horizontal hit position is determined by the charge distribution induced on the cathode pads. The charge signals from the cathode pads were read out by GASSIPLEX chips[7], which have high multiplexing capability. The charge signals from 256 cathode pads can be transmitted through a single signal line and read out with a CAEN sequencer with a CRAM module[8]. In this study, the generation of track-and-hold signals for the GASSIPLEX chips were triggered by the timing of anode signal of the CRDC under a concurrence condition with the signals of the plastic scintillators and the anode.

Figure 2 shows the detection efficiencies for 250 MeV/u ^{14}N particles for 15- and 30-torr operations as a function of the high voltage supplied to the anode wires. We achieved 100 % efficiency at 15 torr, although the gas amplification at 15 torr was roughly five times smaller than that at 30 torr at the same anode voltage. Therefore, we inferred that 15-torr gas was sufficient for tracking nitrogen particles or heavier elements.

Detection efficiencies for light particles are shown in Fig. 3. The three panels show data for ^{9}Li, ^{6}He,

*1 Center for Nuclear Study, University of Tokyo
*2 Department of Physics, University of Tokyo
*3 CEA-Saclay, France
*4 GANIL, France

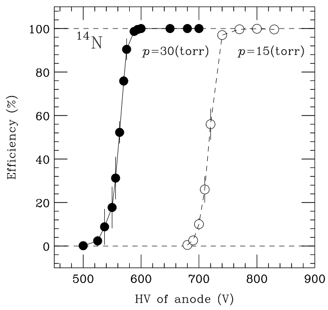

Fig. 2. Detection efficiencies of the anode for the 15-torr and 30-torr operations for 250 MeV/u ^{14}N particles. The horizontal axis shows the high voltage supplied to the anode wires.

and triton. In each panel, the solid (dashed) line indicates the detection efficiency of the anode (cathode) as a function of the high voltage (HV) supplied to the anode wires. The detection efficiency is estimated by considering the coincidence ratio of outputs of two anode (cathode) layers from one CRDC and the output of plastic scintillators installed downstream. The dif-

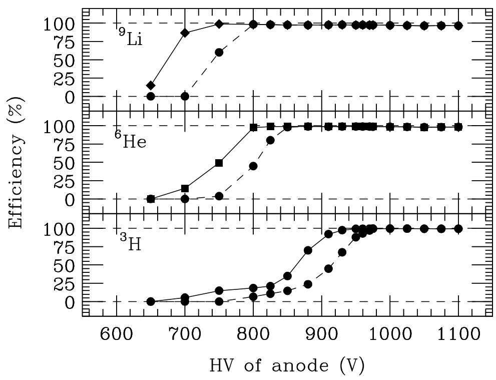

Fig. 3. Detection efficiencies of the anode (solid lines) and cathode (dashed lines) for the 30-torr operations for t, ^{6}He, and ^{9}Li particles with an energy of around 200 MeV/u. The horizontal axis shows the high voltage supplied to the anode wires.

ference between the detection efficiencies of the anode and cathode arises because of a small mismatch in their preamplifier gains. The CRDCs of SHARAQ achieved 100 % detection efficiency through low-pressure operation for light ions such as tritons.

The potential wires located between anode wires to generate a strong field around the anode wires are provided only in the upstream tracking chamber (CRDC1). The downstream one (CRDC2) has no potential wires. The difference in the configuration results in a difference in the avalanche gains, as described in a previous report[5]. Figure 4 (a) shows the pulse height distribution of anode signals. The black histogram was obtained by using CRDC1 at 950 V, while the red one was obtained by using CRDC2 at

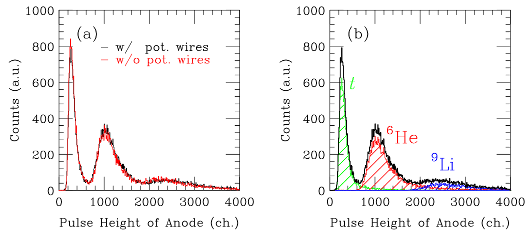

Fig. 4. (a) Pulse height distributions of anode signals. The black (red) histogram was obtained by the upstream (downstream) tracking detector with 950-V (970-V) anode HV. (b) Anode pulse-height spectrum decomposed by passing particles, t, ^{6}He and ^{9}Li.

970 V. Despite the difference in the supplied voltages, the pulse height distributions were almost the same. Therefore, although the potential wires helped achieve the required avalanche gain by decreasing the anode HV, they did not improve the energy resolution of the CRDCs as a function of the avalanche gain. Figure 4 (b) shows the pulse height spectrum decomposed by passing particles; each particle was identified by the plastic scintillator installed downstream. The energy resolution of CRDCs for the 30-torr operation was estimated to be 50% (FWHM). This resolution is suitable for the identifications of light particles such as those with Z = 1–3, but the identification of the beryllium and heavier particles is difficult.

The achieved position resolution of the tracking detectors has been discussed by Tokieda *et al.*[9].

In summary, we performed a beam study using light radioactive isotopes at 200A–250A MeV and examined the detector system installed in the final focal plane of the SHARAQ spectrometer. All the detectors operated successfully, even for Z = 1 particles, and we obtained basic data on their performance in order to optimize the detectors' parameters and to improve the data analysis algorithm.

References

1) T. Uesaka *et al.*: Nucl. Instrum. Methods Phys. Res. B **266**, 4218 (2008).
2) T. Kawabata *et al.*: Nucl. Instrum. Methods Phys. Res. B **266**, 4201 (2008).
3) S. Ota *et al.*: CNS-REP-83, 57 (2010).
4) M.H. Tanaka *et al.*: Nucl. Instrum. Methods Phys. Res. A **362**, 521 (1995).
5) S. Michimasa *et al.*: CNS-REP-80, (2009) 55; CNS-REP-83, 55 (2010).
6) R. Veenhof: GARFIELD, CERN Program Library W5050.
7) The GASSIPLEX is a redesigned chip of the AMPLEX by J.C. -Santiard of CERN. The AMPLEX is described in E. Beuville *et al.*, Nucl. Instrum. Methods Phys. Res. A **288**, 157 (1990).
8) V551 C.A.E.N sequencer User Guide, V550 C.A.E.N CRAM User Guide.
9) H. Tokieda *et al.*: CNS Annual Report 2010 (2011).

Current status of SAMURAI

K. Yoneda, T. Isobe, N. Iwasa,[*1] T. Kawabata,[*2] T. Kobayashi,[*1] Y. Kondo,[*3] T. Kubo, K. Kusaka, Y. Matsuda,[*1] T. Motobayashi, T. Murakami,[*2] T. Nakamura,[*3] J. Ohnishi, T. Ohnishi, H. Okuno, H. Otsu, H. Sakurai, H. Sato, Y. Satou,[*4] K. Sekiguchi,[*1] Y. Shimizu, and Y. Togano

This report describes the current status of construction of the experimental apparatus, SAMURAI (Superconducting Analyzer for MUlti-particles from RAdio Isotope beams with 7 Tm of bending power), a large-acceptance multiparticle spectrometer under construction at the RIBF. The main component of SAMURAI is a large-gap (80 cm) superconducting dipole magnet with a maximum bending power of 7 Tm. This magnet will be used for the analysis of heavy projectile fragments and projectile-rapidity protons with a large momentum and angular acceptance. The large gap also facilitates the measurement of projectile-rapidity neutrons with a large angular acceptance in coincidence with heavy projectile fragments.

SAMURAI can be used in a variety of purposes in experiments involving RI beams provided at the RIBF. When used in experiments on the breakup of neutron-rich or proton-rich nuclei, SAMURAI's large acceptance will facilitate efficient heavy ion(HI)-neutron and HI-proton coincidence measurements that are required for invariant-mass spectroscopy. SAMURAI will also be suitable for missing-mass spectroscopy, in which the measurement of charged particles after the reaction provides information about the decay modes as well as the tagging of the reaction channels, because of the multiparticle detection capability. SAMURAI can also be used to scrutinize reactions of few-nucleon scattering systems such as polarized deuteron scattering on protons, in order to understand fundamental nucleon-nucleon interactions, including three-nucleon force effects. We also plan to install a time projection chamber in the large gap of the SAMURAI magnet, which will be used mainly for reaction studies such as the investigation of the density dependence of the asymmetry term in the nuclear equation of state.

The major part of SAMURAI's construction was funded over four years, beginning from fiscal year (FY) 2008. The construction of the magnet and detectors is underway, and the experimental setup shown in Fig. 1 is expected to be ready in early 2012, when the first experiments are expected to be performed. In the following, an overview and the current status of the detectors and experimental devices are presented. An outline of the detector system has also been given in a previous report [1)].

[*1] Department of Physics, Tohoku University
[*2] Department of Physics, Kyoto University
[*3] Department of Physics, Tokyo Institute of Technology
[*4] Department of Physics and Astronomy, Seoul National University, Korea

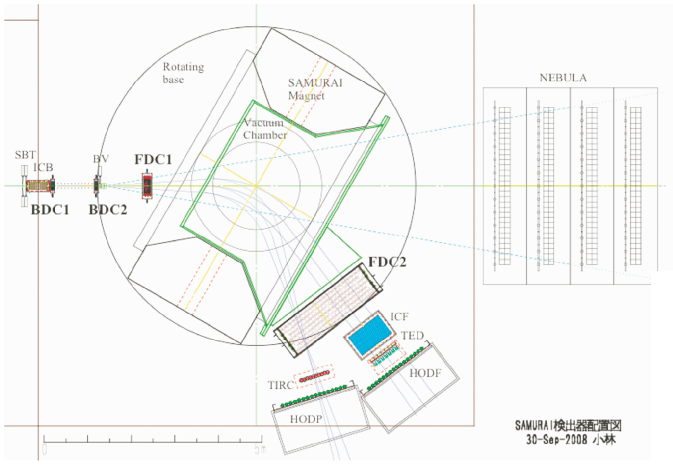

Fig. 1. Schematic image of the SAMURAI system; the first experiment is expected to be performed in early 2012. SAMURAI consists of a large bending magnet surrounded by particle detectors. The magnet is a superconducting dipole magnet with a maximum bending power of 7 Tm and a large pole gap of 80 cm. Heavy-ion detectors and neutron detectors will be installed at the time of the first experiment.

- Bending Magnet
  The magnet is an H-type dipole with cylindrical poles of diameter 2 m. Each pole is surrounded by a superconducting coil that generates a magnetic field of about 3 T at the center of the magnet, leading to 7 Tm of field integral along the particle trajectory. Construction of the magnet is underway at the site, and is expected to be completed in May 2011. Additional details of the magnet are given by H. Sato *et al.* in a separate report in this volume [2)].
- Vacuum System
  A built-in vacuum chamber is planned in the gap of the bending magnet, so that particles after reactions will pass through the vacuum region. The design of the vacuum connection to the upstream beamline has been completed [3)], and the large vacuum window at the exit of the vacuum chamber is being designed. The window will cover an area as large as 2940 mm $\times$ 800 mm. Currently, tests are being performed with Kevlar textile and polyethylene. Details of the window tests are given by Y. Shimizu *et al.* in a separate report in this volume [4)].
- Beam Detectors
  The beam particles will be detected in front of the

target to generate a trigger signal and to provide information required for PI and the beam profiles. The beam timing will be measured by the plastic scintillators (SBT). Each scintillator has an active area of 100 mm × 100 mm and is coupled to PMTs at both ends.
An ion chamber (ICB) will be installed in the beamline to measure the energy loss of the beam particles. The ICB has an active area of 150 mm × 150 mm, is 420-mm thick, and possesses multiple cathodes and anodes that are perpendicular to the beamline.
Beam profiles will be measured by two multiwire drift chambers (BDC1, BDC2) or two multiwire proportional chambers (BPC1, BPC2; not shown in the figure). The active areas of the BDCs and BPCs are 80 mm (V) × 80 mm (H) and 150 mm (V) × 240 mm (H), respectively.
These beam detectors have already been fabricated, and they will be ready for use after the completion of the required performance tests.

- Tracking Detectors
  The HI tracking detectors (FDC1, FDC2) that are to be placed in front of and behind the magnet have been constructed. FDC1 will be installed between the target and magnet. FDC1 has an active area of 340 mm (V) × 620 mm (H). This size was decided so as to allow projectile-rapidity neutrons to pass through the detector aperture.
  FDC2 is to be placed behind the magnet in order to measure HI tracks. Particles will spread in the space behind the magnet, and hence, FDC2 is designed to cover a large area (810 mm (V) × 2230 mm (H)).
  FDC1 has already been built and tested. FDC2 is now being constructed, and it will be ready for tests in March 2012.
- Detectors for PI and TOF measurement
  Plastic scintillator hodoscopes (HODF, HODP) will be used for TOF measurement. Each hodoscope consists of 16 plastic scintillators (1200 mm (V) × 100 mm (H), 10 mm thick). Both ends of the scintillators are coupled to the PMTs. Velocity measurements can also be performed by using total-internal-reflection-type Cherenkov detectors (TIRCs).
  An ion chamber for reaction fragments (ICF) is to be installed for measuring the energy loss of HIs. The ICF has an active area of approximately 400 mm (V) × 700 mm (H). Pure CsI scintillators are prepared for use as total energy detectors (TEDs). The crystal size is 100 mm × 100 mm × 50 mm, and the crystal is coupled to a PMT (Hamamatsu R6233ASSY).
  At present, TIRC and TED are being assembled, and all the detectors will be ready for use in FY2011.
- Neutron Detectors
  A neutron detector system, called NEBULA (NEutron Detection system for Breakup of Unstable Nuclei with Large Acceptance), will be placed at forward angles. NEBULA covers an area of 1800 mm (V) × 3600 mm (H), which corresponds to the angular acceptance of ±5° (V) and ±10° (H). Details of NEBULA detectors are given by Y. Kondo *et al.* [5] in a separate report in this volume. The detectors have been delivered, and tests with cosmic rays are being conducted.
- Proton Detectors
  The TOF of protons will be measured by the hodoscope (HODP), which has been described earlier. A tracking detector that is to be placed after the magnet (PDC, not shown in the figure) is being fabricated separately so that proton-HI coincidence measurement can be carried out. The fabrication of the PDC will be completed by September 2011.
  A tracking detector will be placed before the magnet. This detector should be capable of detecting protons even when both protons and HIs hit the detector. For this purpose, stacks of silicon strip detectors will be installed between the target and magnet. Here, a large dynamic range that covers both proton signals and HI signals that are about 2500 times larger than proton signals must be attained for a large number of channels (∼2500). These requirements are to be realized by developing a new electric circuit that will be coupled to a multichannel circuit designed in collaboration with a US group. We plan to conduct the first HI-proton experiments in early 2013. Additional details are given by Y. Togano *et al.* in a separate report [6].

The magnet construction in Room E18 in the RIBF building will be completed in May 2011. The detectors and electronics are being fabricated in parallel. After some tests and commissioning, we plan to have everything ready for the first SAMURAI experiment in early 2012.

References

1) K. Yoneda *et al.*: RIKEN Accel. Prog. Rep. **43**, 178 (2010).
2) H. Sato *et al.*: RIKEN Accel. Prog. Rep. **44**, 144 (2011).
3) Y. Shimizu *et al.*: RIKEN Accel. Prog. Rep. **44**, 152 (2011).
4) Y. Shimizu *et al.*: RIKEN Accel. Prog. Rep. **44**, 154 (2011).
5) Y. Kondo *et al.*: RIKEN Accel. Prog. Rep. **44**, 126 (2011).
6) Y. Togano *et al.*: RIKEN Accel. Prog. Rep. **44**, 146 (2011), and references therein.

Development of SAMURAI-TPC for the Study of Nuclear Equation of State†

T. Isobe, A. Taketani, T. Murakami,[*1] M.B. Tsang,[*2] W.G. Lynch,[*2] M. Famiano,[*3] and H. Sakurai for the SAMURAI-TPC Collaboration

[Nuclear equation of state, symmetry energy, unstable nuclei]

The nuclear Equation of State (EoS) is a fundamental property of nuclear matter and describes the relationships between the parameters of a nuclear system, such as energy and temperature. Understanding the nuclear EoS has been one of the major goals of nuclear physics. This understanding can help us to learn the properties of the nucleus and dense nuclear matter, and to learn the nature of neutron stars.

The energy per nucleon in the isospin asymmetric nuclear matter is usually expressed as $E(\rho, \delta) = E(\rho, \delta = 0) + E_{sym}(\rho)\delta^2 + O(\delta^2)$, where ρ is the baryon density ($\rho = \rho_n + \rho_p$), δ is the relative neutron excess ($\delta = (\rho_n - \rho_p)/(\rho_n + \rho_p)$), $E(\rho, \delta = 0)$ is the energy per nucleon in the symmetric nuclear matter, and $E_{sym}(\rho)$ is the bulk nuclear symmetry energy ($E_{sym}(\rho) = \frac{1}{2}\frac{\partial^2 E(\rho,\delta)}{\partial \delta^2}|_{\delta=0}$). Experimental information, such as the particle flow in heavy-ion collisions and nuclear giant monopole, impose constraints on the symmetric term of the nuclear EoS ($E(\rho, \delta = 0)$). However, the experiments are performed only with stable nuclei, and there are no strong constraints on any of the EoS terms, depending on the isospin asymmetry($E_{sym}(\rho)$).

An international collaboration, the so-called Symmetry Energy Project, for studying the nuclear EoS has been formed in FY2009. The collaboration planned to install a Time Projection Chamber (TPC) into the SAMURAI dipole magnet installed at the Radioactive Ion Beam Facility (RIBF). At the RI beam energy levels that can be achieved at the RIBF, a nuclear density of $\rho \sim 2\rho_0$ is expected to be achieved. In addition, stronger constraints on the EoS isospin asymmetry term would be obtained[1].

With the TPC, we plan to perform experiments for measuring charged pions, protons, and light ions concurrently as probes for studying the asymmetric nuclear matter. In transport calculations, the π^+/π^- ratios are expected to give strong constraints on the EoS asymmetry term at supra-normal density[2].

Figure 1 shows a schematic view of SAMURAI-TPC. The design is based on EOS-TPC used at the BEVALAC accelerator[3]. We are planning to employ Multi-Wire Drift Chamber (MWDC) type wire amplification with a cathode-pad readout for the induced signals for obtaining good position resolution. The target will be located near the TPC entrance. Table 1 lists the specifications of SAMURAI-TPC.

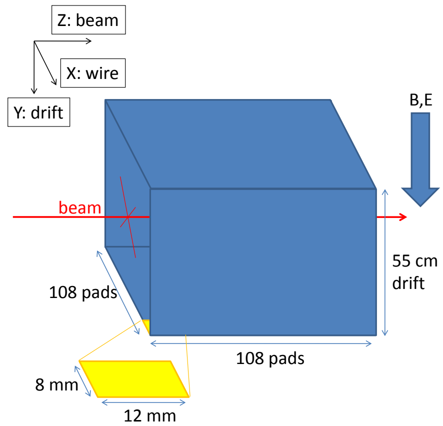

Fig. 1. Schematic view of SAMURAI-TPC.

SAMURAI-TPC is designed to measure ions ranging from pions to oxygen ions, corresponding to a wide range of stopping powers and, consequently, a wide range of induced signals on the pads. RHIC-STAR readout electronics[4] with more than 10k channels will be employed for the first commissioning of SAMURAI-TPC. The dynamic range of the STAR electronics is 10 bit, which will be upgraded to 12 bit for performing the simultaneous measurement of pions and charged fragments. After using the STAR electronics for the first SAMURAI-TPC experiment, it will be replaced with GET (General Electronics for TPC, 12 bit ADC).

To optimize the design of SAMURAI-TPC, a simulation scheme has been developed. The simulation scheme consists of five parts: event generation, detector response, digitization, track reconstruction, and

Table 1. Specifications of SAMURAI-TPC

pad size	8 mm × 12 mm
number of pads	11664 (108 × 108)
drift length	55 cm
chamber gas	P10 (Ar-90% + CH_4-10%)
magnetic field	0.5 T
pressure	∼1 atm
electric field for drift	120 V/cm

*1 Department of Physics, Kyoto University
*2 National Superconducting Cyclotron Laboratory, Michigan State University, United States
*3 Physics Department, Western Michigan University, United States

analysis of output. We have employed two event generators. One generator is the Particle and Heavy Ion Transport code System (PHITS)[5], which was developed by JAEA. The other generator is an empirical generator that has been developed on the basis of the experimental data on heavy-ion collisions collected previously in the GSI-FOPI experiment[6]. The empirical generator has been developed only for the most central collisions. In the case of the most central collisions, the number of charged particles has been estimated to be approximately 70 on an average. For the simulation of the detector response, GEANT4[7] has been used to simulate the secondary particles, multiple scattering, and deposit energy in TPC. The deposited energy determined by GEANT4 is a physical number, which has to be converted to raw data that should be recorded by the readout electronics. A digitization software, which was developed for the ACTAR simulation, has been employed for the digitization of the SAMURAI-TPC simulation data. To reconstruct the particle tracks by using the digitized data, a reconstruction software has been developed. This reconstruction software consists of hit and track reconstructions. The hit patterns for each layer, which is a plane perpendicular to the beam axis, are first reconstructed by using the charge centroid method. The tracks of the charged particles are then reconstructed by using the Kalman filter method. The Kalman filter is a point-by-point fitting algorithm and is suitable for the reconstruction of tracks that have been distorted by multiple scattering. Since SAMURAI-TPC should be operated at unit atmosphere, the effect of multiple scattering is not negligible and an algorithm for considering such an effect is necessary. Figure 2 shows the correlation between dE/dX and reconstructed track rigidity, where the minimum-bias collisions of ^{132}Sn + ^{124}Sn are simulated. While there is a large number of proton tracks, the tracks of charged pions, deuterons, helium ions and tritons are also well reconstructed. The dE/dX resolution of each particle can be observed in Fig. 3. With the current design, dE/dX resolutions of approximately 16 % and 14 % are expected for 140 MeV/c pions and 210 MeV/c protons, respectively. This performance is enough to identify low-momentum (~100 MeV/c) charged pions and protons with a signal-to-noise ratio of more than 100.

References
1) L. W. Chen et al.: Phys. Rev. Lett. **94**, 032701 (2005).
2) G. C. Yong et al.: Phys. Rev. C **73**, 034603 (2006).
3) G. Rai et al.: IEEE Trans. on Nucl. Sci. **37**, 56 (1990).
4) M. Anderson et al.: Nucl. Inst. and Meth. A **499**, 679 (2003).
5) K. Niita et al.: JAEA-Data/Code **2010**, 022 (2010).
6) W. Reisdorf et al.: Nucl. Phys. A **781**, 459 (2007).
7) S. Agostinelli et al.: Nucl. Inst. and Meth. A **506**, 250 (2003).

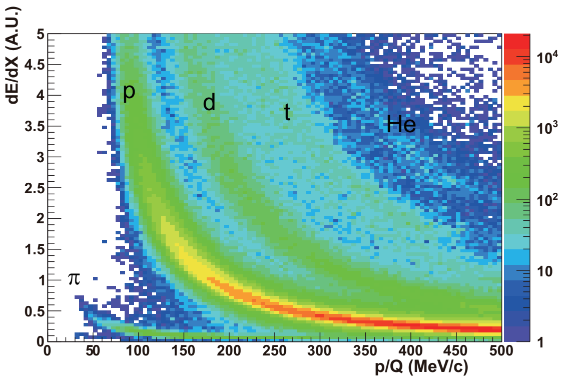

Fig. 2. Correlation between dE/dX and particle rigidity. Minimum-bias collisions of ^{132}Sn + ^{124}Sn are simulated. Most particles are protons.

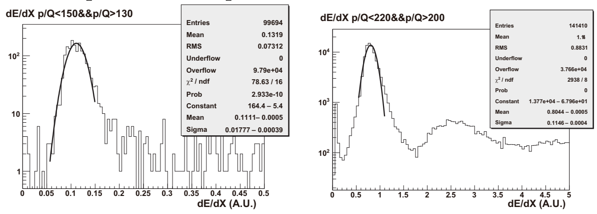

Fig. 3. dE/dX distribution for each rigidity range (Left panel: 130-150 MeV/c, Right panel: 200-220 MeV/c).

Construction of SAMURAI magnet

H. Sato, T. Isobe, N. Iwasa,[*1] T. Kawabata,[*2] T. Kobayashi,[*1] Y. Kondo,[*3] T. Kubo, K. Kusaka, T. Motobayashi, T. Murakami,[*2] T. Nakamura,[*3] J. Ohnishi, T. Ohnishi, H. Okuno, H. Otsu, H. Sakurai, Y. Satou,[*4] K. Sekiguchi,[*1] Y. Shimizu, Y. Togano, and K. Yoneda

A large-acceptance spectrometer named SAMURAI is under construction at the RIKEN RI Beam Factory (RIBF).[1–3] The SAMURAI spectrometer consists of a large-gap superconducting dipole magnet with a large vacuum chamber[4], heavy-ion detectors, neutron detectors, and proton detectors. The purpose of the spectrometer is to perform kinematically complete measurements of multiple particles emitted in reactions induced by a RI-beam. The superconducting dipole magnet is required to have a rigidity resolution of about 1/700 (rms) at $P/Z = 2.2$ GeV/c, which corresponds to a magnetic rigidity $B\rho$ of 7.3 Tm, where P is the momentum and Z is the atomic number. It should also be able to identify particles having mass numbers up to 100.

In the previous report[5], we presented the design of the superconducting dipole magnet in terms of magnetic field calculations. In this report, the present status of the construction of the magnet and some detailed specifications are presented.

The construction of the magnet started at the RIBF site in October 2010. The superconducting magnet is built on a rotatable base. The rotatable base consists of six circular rails, a main frame, and a sub-frame with a circular stage made of iron (Figs. 1 and 2). The stainless steal plates are set between the yoke and the main frame so that the yoke does not come in contact with the main frame magnetically. Similarly, the yoke does not come in contact with the circular stage.

The magnet yoke consists of 58 iron plates, including four pole parts. They are stacked on the main frame and fixed by using stud bolts (Fig. 1). The assembling of the yoke started in December 2010 and ended in January 2011 (Fig. 2).

Two superconducting coils with cryostats were manufactured in TOSHIBA factory. Cooling and excitation tests were also performed there after manufacturing. As a result, the heat load into the cryostat (4.2 K) was about 1 W per coil, which corresponds to an evaporation rate of 1.4 L/h. The prepared cryocoolers have sufficient cooling power for this heat load. The list of the cryocoolers for one coil are shown in Table 1. Thus, a total of 14 cryocoolers are used for the magnet.

During the excitation test, a quench happened on one of the two coils at 450 A (85% of full excitation). After that, the two coils were fully excited successfully with a current of 530 A, which generates the same amount of magnetic force at the coil position as that

*1 Department of Physics, Tohoku University
*2 Department of Physics, Kyoto University
*3 Department of Physics, Tokyo Institute of Technology
*4 Department of Physics and Astronomy, Seoul National University, Korea

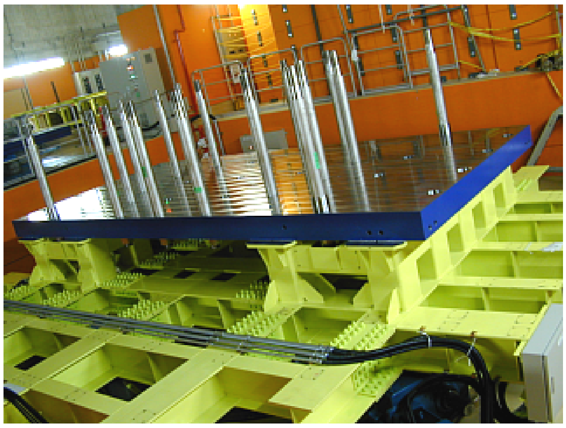

Fig. 1. Main frame of the rotatable base (green) and first layer of the yoke (blue) with stud bolts. (13/12/2010)

Fig. 2. The magnet yoke on the rotatable base with the circular stage. A part of the stage was temporarily removed for coil assembling. (25/01/2011)

Table 1. List of the cryocoolers for one cryostat. The value of heat load (third row) is the estimated value.

	liquid-He vessel	thermal shield 20 K	thermal shield 80 K	current lead
cryocooler	GM-JT ×2	GM ×2	GM ×2	GM ×1
cooling power	3.5 W @4.3 K	5 W @20 K	45 W @40 K	60 W @40 K
heat load	4.11 W	4.96 W	78.22 W	53.94 W

generated in the actual usage with the yoke. The cooling and excitation tests on the coils will be performed again at the RIBF site after assembling them.

After the previous report was published[5], the operation policy of the magnet, especially for quench protection, was defined. An excitation circuit of the magnet is shown in Fig. 3. A quench detector is introduced in the circuit, and it monitors the difference between the voltages of the coils ($V_u - V_d$). The detector recognizes a quench when the difference is more than 1 V, and is sustained for more than 0.5 s. When a quench happens, the quench detector sends a signal to a power supply and DC-cut breaker (DCCB) cuts of the power supply to the coils. As a result, the current flows in the closed circuit of a heater, diodes, and the superconducting coil. Then, the current is discharged by the coil and temperature of the coil will increase.

The change in the temperature of the coil after the quench was estimated. Figure 4(a) shows the result of the estimation. The direction of the quench is from the outer layer ($\theta 10$) to inner layer ($\theta 1$) (Fig 4(b)). In this calculation, the velocity of the quench propagation in the radial direction was set to 0.05 m/s. This value is decided on the basis of experimental data of the KEK-SKS superconducting dipole magnet. In the case of KEK-SKS, the velocity of the quench propagation was 0.01 m/s, and the coil has liquid He channels between layers. In our case, the coil does not have such a cooling mechanism, and therefore, the velocity is higher than that in the case of KEK-SKS. The initial current was 560 A, which is the maximum current defined in the specification, and it corresponds to 33 MJ of stored energy. The results show that the average temperature of the coil becomes 100 K (red curve) after 30 s. The recovery of the superconducting coils (for re-filling, about 1000 L of liquid helium will be needed) will take about two days. When problem with the power supply is encountered, the power supply is spontaneously switched off and the current is dumped through diodes mounted in the power supply. In this case, the superconducting coils are not quenched.

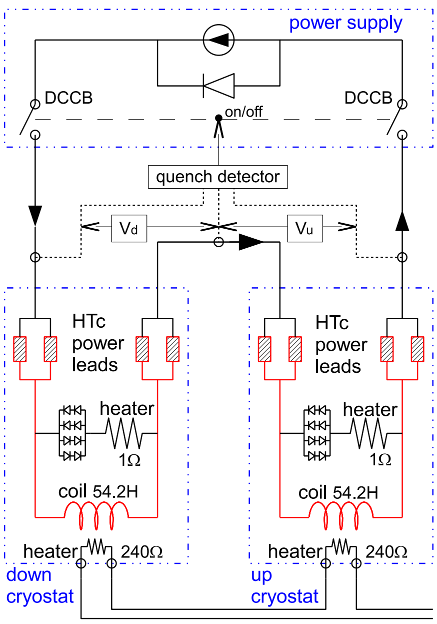

Fig. 3. Excitation circuit of the superconducting magnet. The red lines indicate superconducting wires. The filled arrows show the direction of current flow.

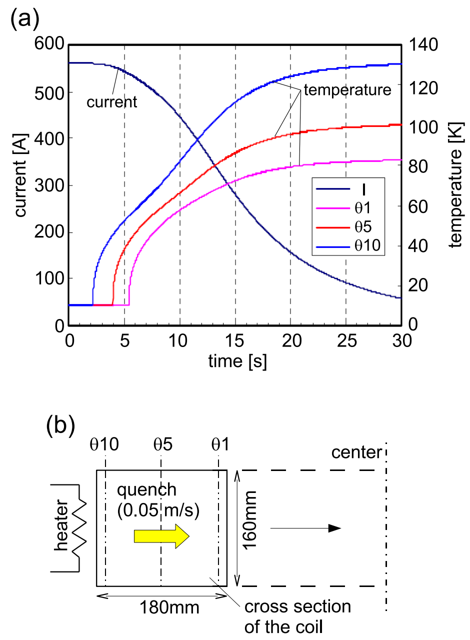

Fig. 4. (a) Current decay and temperature rise after quench of the superconducting coil. (b) Definition of the layer numbers.

The superconducting coils with the cryostats and the liquid helium vessels with the cryocoolers were separately delivered to the RIBF site in January 2011. The cryostats and the helium vessels were re-attached to each other by welding and set into the magnet yoke.

Another main component of the SAMURAI spectrometer, a large vacuum chamber[4], was delivered at the end of February 2011. The cooling and excitation test was performed from April to May, and the construction of the magnet was completed in June 2011.

References

1) K. Yoneda et al.: RIKEN Accl. Prog. Rep. **42**, 26 (2009).
2) K. Yoneda et al.: RIKEN Accl. Prog. Rep. **43**, 178 (2010).
3) K. Yoneda et al.: RIKEN Accl. Prog. Rep. **44**, 140 (2011).
4) Y. Shimizu et al.: RIKEN Accl. Prog. Rep. **44**, 154 (2011).
5) H. Sato et al.: RIKEN Accl. Prog. Rep. **43**, 180 (2010).

Development of SAMURAI Si-tracking detector system for protons and heavy ions

Y. Togano, K. Yoneda, M. Kurokawa, H. Murakami, A. Taketani, K. Kurita,*1 H. J. Ong,*2 A. Takuma,*1 S. Yoshida,*1 and T. Motobayashi

A tracker consisting of silicon strip detector (SSDs) is being developed to obtain the trajectories of protons and heavy ions that are emitted from the Coulomb dissociation reaction on a proton-rich nuclei.

It is important to obtain the trajectories of the reaction products between the reaction target and the SAMURAI magnet[1)] for achieving sufficient resolution for the relative energy between the reaction products. The relative-energy resolution between two reaction products (δE_{rel}) is determined by the resolutions of the momentums of the two reaction products (p_1, p_2) and the opening angle between the two reaction products (θ_o) as

$$\delta E_{rel} = \sqrt{\left(\frac{\partial E_{rel}}{\partial \theta_o}\right)^2 \delta\theta_o^2 + \sum_{i=1,2}\left(\frac{\partial E_{rel}}{\partial p_i}\right)^2 \delta p_i^2}. \quad (1)$$

The relative-energy resolution is almost governed by the opening-angle resolution because the contributions of the two momentum resolutions are relatively small when we consider the designed momentum resolution of the SAMURAI system[1)]. In the most extreme case, the disintegration of the proton-rich Sb isotope produces proton(s) and a heavy ion whose atomic number Z is approximately 50, leading to the generation of signals that are approximately 2500 times stronger than the proton signals; a detector should be capable of detecting protons as well as heavy ions. We are aiming to achieve reasonable opening-angle resolution and capacitate the measurement of the large output-signal difference by using a tracker consisting of SSDs. This article reports the present status of the development process of the tracker for protons and heavy ions.

The tracker consists of the two sets of the two SSDs, with the sets separated by approximately 30 cm as shown in Fig. 1. The system will be operated in vacuum. The system is assumed to be located 50 cm downstream of the secondary target. The silicon detectors have an active area of 89.5×89.5 mm^2 and a thickness of 0.3 mm.

A detector has 384 aluminum strip electrodes with a pitch of 0.228 mm on the p side. The full depletion voltage of the detector is 90 V. These detectors were originally designed for the Fermi Gamma-ray Space Telescope[2)].

The opening-angle resolution is determined by the angular resolution of the detector system and the angular spread of the heavy ions and protons due to multiple scattering in the secondary target. Considering 200 mg/cm^2 thick lead as the secondary target for the Coulomb dissociation reaction, the angular spread due to the multiple scattering of 250-MeV protons is about 4 mrad, which is much larger than that in the case of the heavy ions (≤ 0.1 mrad for Sn isotope). The strip pitch corresponding to 4 mrad is about 1.9 mm; thus, a strip pitch less than 1.9 mm does not have a large effect on the opening-angle resolution. Therefore, we ganged the three strip electrodes together to reduce the number of channels from 384 to 128. This ganging does not affect the effect of the strip pitch on the opening-angle resolution even if a proton target, for which the multiple scattering effect is minimum, is used as a secondary target.

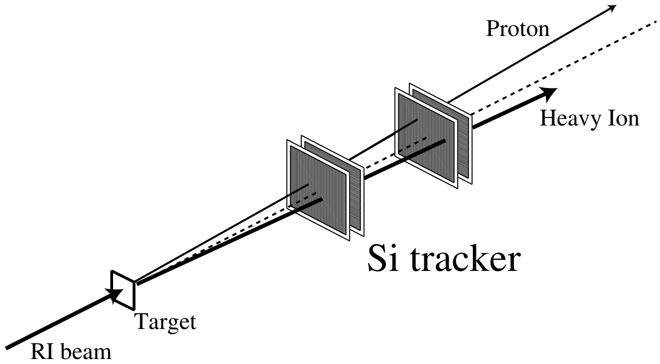

Fig. 1. Schematic view of the tracker for obtaining the trajectories of protons and heavy ions. The tracker is located in front of the SAMURAI magnet. Two sets of two silicon detectors are used to obtain the trajectories of the reaction products. The two silicon detectors in a set measure the horizontal and vertical positions of the reaction products.

The detector is placed on a 146×146 mm^2 PCB frame. The pads of each electrode are connected to the print pattern on the PCB by wire bonding. The signals from the three electrodes are ganged together using the print pattern on the PCB. The 128 lines from the detector are connected to four USL-series right angled connectors fabricated by KEL Corporation[3)]. The USL connector has 40 pins of 0.4 mm pitch, which facilitate the handling of high-density signals and enable the connector to be connected to micro-coaxial cables (AWG#42); this connection helps in minimizing the signal interference during signal transfer through the cables. A photograph of the USL connector with the

*1 Department of Physics, Rikkyo University
*2 Research Center for Nuclear Physics, Osaka University

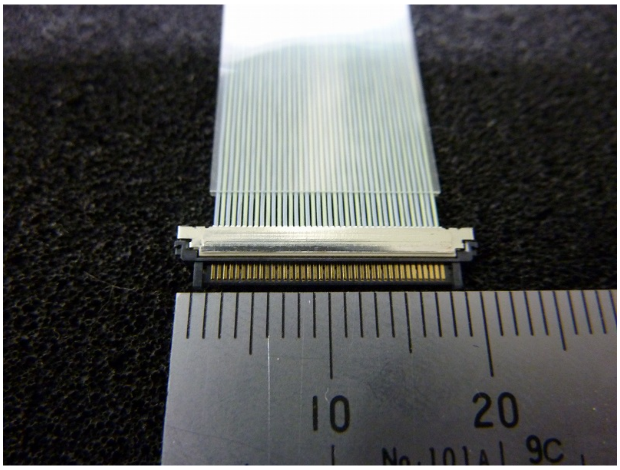

Fig. 2. Photograph of the USL connector clamping 40 micro-coaxial cables. A scale is shown alongside the connector for reference.

micro-coaxial cables is shown in Fig. 2. A bias voltage can be applied to the n side of the detector or the bias ring of the detector. The n side is grounded through a 4.7-μF capacitor to minimize signal interference between the electrodes. The PCB design has been finalized. The fabrication of the PCB and the bonding of the silicon detector to the PCB will be completed in August 2011.

The detectors will be connected to the front-end electronics that are being developed, which can be handle signals from protons as well as heavy ions. ASIC-based electronics are being developed by a collaboration with KEK[4]. The input charges are unsymmetrically divided into two channels and are then fed to two charge-sensitive preamplifiers. The side having a greater charge has a saturation compression circuit. A prototype of the electronics has been developed to measure more than ten thousand times different input charge without saturation of the circuits. A second prototype with improved noise characteristics is undergoing testing.

In addition, a low noise preamplifier with compressive gain characteristics is also being developed in collaboration with Rikkyo University[5]. The square-root response of the gain characteristics are determined by using the prototype circuit. The temperature dependence of the gain will be examined.

The multichannel integrated circuit HINP16C[6] will be used as a pulse-shaping amplifier. HINP16C contains 16-channel charge-sensitive preamplifiers, pulse shapers, peak-sampling circuits, constant-fraction discriminators, and time-to-voltage converters. The outputs from the detector system will be connected to the HINP16C card in air. HINP16C will be operated in collaboration with Texas A&M group.

In 2012, the silicon detectors will be tested with the prototype circuits. The ASIC-type front-end circuit will be mass-produced in 2012. The whole tracker system will be ready for use in 2013; the tracker system will be used for Coulomb dissociation experiments involving the SAMURAI magnet.

References

1) K. Yoneda et al.: RIKEN Accel. Prog. Rep. **43**, 178 (2010).
2) T. Ohsugi et al.: Nucl. Instr. Meth. A **541**, 29 (2005).
3) http://www.kel.jp/english/product/FinePitch/usl.html
4) M. Kurokawa et al.: RIKEN Accel. Prog. Rep. **43**, 182 (2010).
5) A. Takuma and S. Yoshida et al.: RIKEN Accel. Prog. Rep. **44**, (2011).
6) G. L. Engel et al.: Nucl. Instr. Meth. A **573**, 418 (2007).

A preamplifier ASIC with a wide dynamic range

M. Kurokawa, H. Baba, T. Gunji,[*1] H. Hamagaki,[*1] S. Hayashi,[*1] T. Motobayashi, H. Murakami, A. Taketani, M. Tanaka,[*2] Y. Togano, and K. Yoneda

An array of silicon strip detectors will be installed between a secondary target and Superconducting Analyzer for MUltiparticles from RAdioactive Isotope beam (SAMURAI) for experiments performed to study the Coulomb breakup reaction of proton-rich nuclei[1]. We are developing a preamplifier that can provide a required dynamic range of around 10^4 in an energy measurement. Here, the dynamic range is defined as the ratio of the maximum and minimum limits of detection. To handle the enormous number of signal channels of the detectors, application-specific integrated circuit (ASIC) technologies are used in the preamplifier. This article reports the ASIC architecture and the results of the tests that have been conducted on the first prototype of the IC. This study is supported by the High Energy Accelerator Organization for the promotion of collaborative research programs in universities.

ASIC was fabricated by a 0.5-μm CMOS process of Taiwan Semiconductor Manufacturing Company (TSMC). We employed a dual-gain system consisting of two charge-sensitive preamplifiers (CSAs). Identical specifications were adopted for the two CSAs except for an FET that was installed in the high-gain channel[2]. The dual-gain function was implemented by applying capacitive division to the input charge $Q_{\rm in}$[3]. The charge can be divided asymmetrically in proportion to the capacitance ratio of the two coupling capacitors, if the ratio of an input impedance of a CSA to that of the relevant capacitor is negligibly small. When compared with a single-channel system providing a maximum (minimum) detection limit of $L_{\rm max}$ ($L_{\rm min}$), the dual-gain system has a significantly larger maximum detection limit given by $L_{\rm max}(C_{\rm h} + C_{\rm l})/C_{\rm l}$, where $C_{\rm h}$ and $C_{\rm l}$ ($\leq C_{\rm h}/10$) denote the coupling capacitances of the high- and low-gain channels, respectively. On the other hand, the minimum detection limit shows a small increase from $L_{\rm min}$ to $L_{\rm min}(C_{\rm h} + C_{\rm l})/C_{\rm h}$ under the assumption that the connection between the two CSAs induces a negligible increase in the noise. Therefore, the range of the dual-gain system can be greater than that of the single-channel system by $C_{\rm h}/C_{\rm l}$.

We applied a single-ended folded-cascode configuration for the CSA. A feedback capacitance $C_{\rm f}$ (=1.8 pF) was determined by the maximum output voltage and maximum input charge obtained under actual experimental conditions. Another component of the feedback loop was the Krummenacher circuit that functioned as a feedback resistance $R_{\rm f}$[4]. The decay constant given by the product of $R_{\rm f}$ and $C_{\rm f}$ was set to 90 μs.

The output-pulse shapes of the dual-channel CSAs were recorded with an oscilloscope for different input charges and external coupling capacitances. The pulse shapes of the high- and low-gain channels were fed to channels 1 and 2, respectively. The pulses from the preamplifier were also analyzed with shaping amplifiers, and the pulse heights were then recorded with an 11 bit-ADC as a function of $Q_{\rm in}$ (Fig. 1). Two channels of the ADC were required to study the performance of the single-channel CSA across its entire dynamic range.

The pulse shapes are shown in Fig. 2 to demonstrate the proper operation of the capacitive division. In the case of the pulses from the low-gain channel, bumps were formed at the rising edge because each channel had a different argument, which is the angle made by the resistive and reactive components of the channel impedance. The effects of the bumps were ignored because their frequency components could be removed by a subsequent analysis involving a longer time constant. When $Q_{\rm in}$ was 3.2 pC (Figs. 2a and 2c), the pulse-height ratios between the two channels had linear dependences on the capacitance ratios. When $Q_{\rm in}$ exceeded the maximum limit of the high-gain channel and was 16 pC (Figs. 2b and 2d), plateaus were observed in the case of the pulses of the high-gain channel. The reason for the origin of the plateaus was not saturation. An excess charge was flowing as a drain current of the extra FET during the time period corresponding to the plateau width. The capacitive division and the resultant gain linearity of the low-gain channel were realized because of this flow.

The output voltage of a shaping amplifier is shown as a function of $Q_{\rm in}$ in Fig. 3. For the single-channel system, the equivalent noise charge σ was 0.4 fC, which corresponds to a minimum detection limit of 2.0 fC (=5σ) for the present definition. The linearity between $Q_{\rm in}$ and the pulse height degrated at a $Q_{\rm in}$ value of around 5.6 pC, which resulted in a dynamic range of 2.8×10^3. The range of the dual-channel system was obtained in a similar way and was 2.7×10^4. The implementation of the dual-gain system successfully increased the range by about ten times as intended.

References
1) Y. Togano et al.: RIKEN Acc. Prog. Rep. **44** (2011).
2) M. Kurokawa et al.: RIKEN Acc. Prog. Rep. **43**, 182 (2010).
3) N. Uematsu et al.: RIKEN Acc. Prog. Rep. **41**, 151 (2008).
4) F. Krummenacher: Nucl. Instrum. Meth. in Phys. Res.

*1 Center for Nuclear Study (CNS), University of Tokyo
*2 Institute of Particle and Nuclear Studies, High Energy Accelerator Organization

A**305**, 527 (1991).

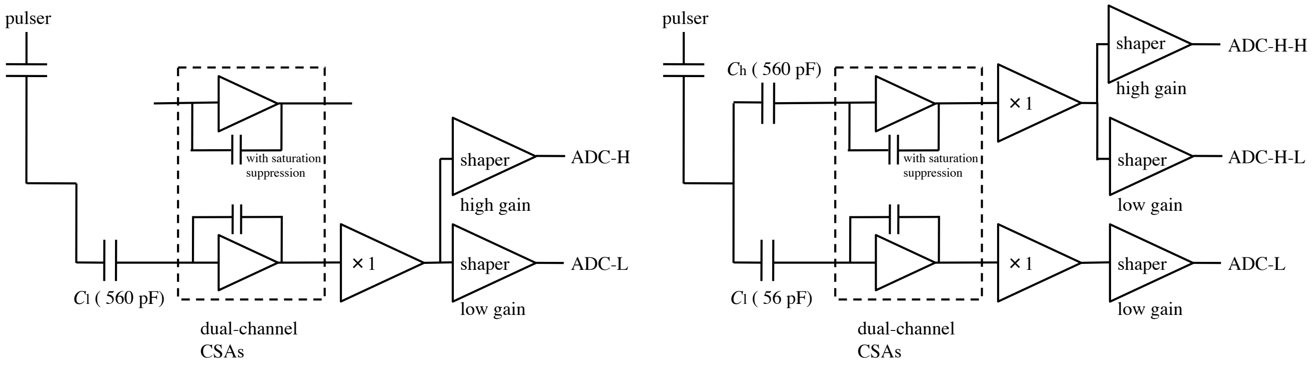

(a) (b)

Fig. 1. Simplified block diagram of the circuits used for the measurement of the dynamic range of the (a) single-channel system and (b) dual-channel system.

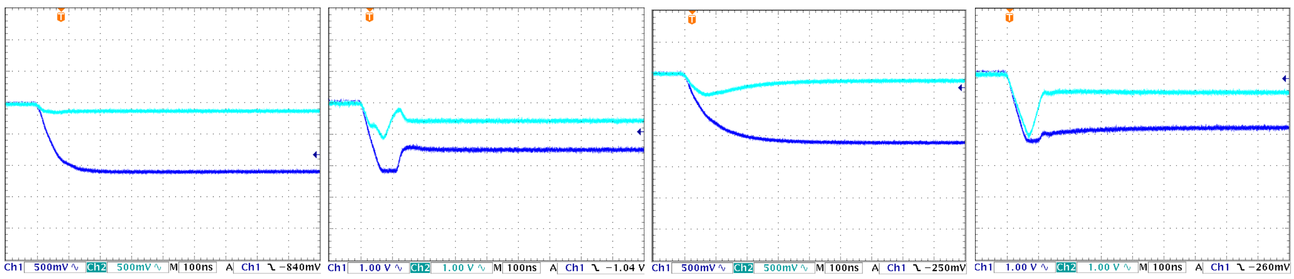

(a) (b) (c) (d)

Fig. 2. Output-pulse shapes of the dual-channel CSAs recorded by an oscilloscope for different input charges and coupling capacitances C_h and C_l (see the text): (a) 3.2 pC, 560 pF, 56 pF; (b) 16 pC, 560 pF, 56 pF; (c) 3.2 pC, 4.7 nF, 470 pF; and (d) 16 pC, 4.7 nF, 470 pF. Larger (smaller) pulses correspond to outputs with high (low) gain.

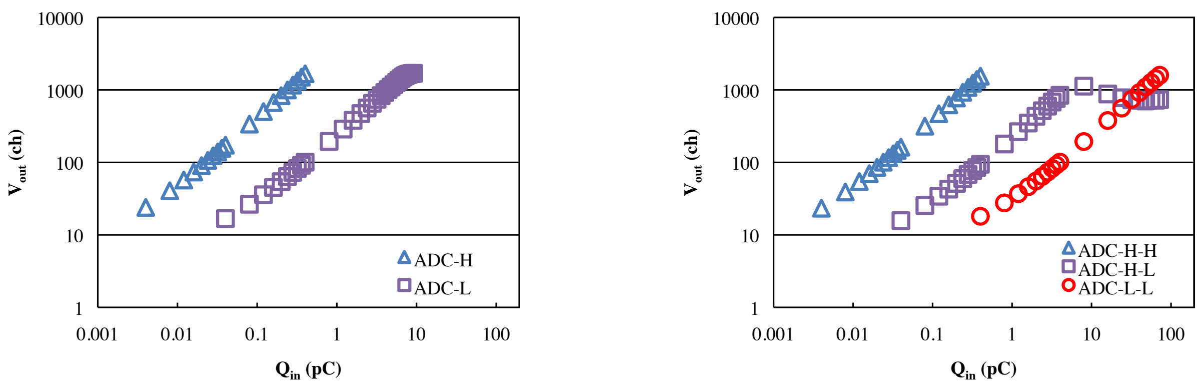

(a) (b)

Fig. 3. Output voltage of a shaping amplifier is shown as a function of input charge $Q_{\rm in}$.

NEBULA (Neutron Detection System for Breakup of Unstable Nuclei with Large Acceptance)

Y. Kondo,*1 T. Nakamura,*1 Y. Kawada,*1 T. Sako,*1 R. Tanaka,*1 S. Deguchi,*1 N. Kobayashi,*1 G. S. Lee,*1 K. Takahashi,*1 N. Tanaka*1 and Y. Satou*2

[SAMURAI, NEBULA, neutron counter]

The neutron detector array NEBULA (Neutron detection system for breakup of unstable nuclei with large acceptance) is being constructed as a key element of the SAMURAI facility at RIBF. NEBULA is utilized for the measurement of four-momentum vectors of fast neutrons at about 100−300 MeV emitted in a small cone as a result of kinematical focusing following the breakup reaction of a neutron-rich projectile. The momentum vectors are then used to reconstruct the invariant mass of the excited unbound system of the projectile that is of interest.

NEBULA is designed such that the following can be realized: (1) large acceptance ($> 50\%$) sufficient for the detection of neutrons emitted in the breakup reactions of neutron-rich unstable nuclei up to the relative energy of 8 MeV; (2) intrinsic efficiency higher than 60% for one-neutron detection and 20% for two-neutron detection; (3) good relative energy resolution ($\Delta E_{\rm rel} \approx 300$ keV at $E_{\rm rel} = 1$ MeV, $\Delta E_{\rm rel} \approx 1$ MeV at $E_{\rm rel} = 10$ MeV) for obtaining a reasonably good energy spectrum with the invariant mass spectroscopy; and (4) multiple-neutron-detection capability. The goal is that NEBULA should be able to unambiguously detect four neutrons in coincidence with 5% intrinsic efficiency.

The specifications of NEBULA are summarized in Table 1. NEBULA consists of neutron detectors (NEUT) and charged-particle veto detectors (VETO). Each NEUT and VETO consists of a rectangular plastic scintillator (BC-408, Saint-Gobain) and two photomultiplier tubes (R7224ASSY, Hamamatsu) that are at the ends of the scintillator via light guides. The dimensions of a NEUT scintillator are 12 cm (horizontal), 180 cm (vertical), and 12 cm (thickness), and those of a VETO scintillator are 32 cm (horizontal), 190 cm (vertical), and 1 cm (thickenss). Currently, 120 NEUTs (half of the total number of NEUTs) and 48 VETOs are available, and the resulting intrinsic detection efficiency for one-neutron detection is 41%.

Neutron events are identified by requiring (1) no signal from VETO and (2) pulse height larger than threshold value ($E_{\rm th}$) of 5 MeVee (electron equivalent) to eliminate γ ray events. Momentum vector of a projectile-like neutron is derived on the basis of the time of flight (TOF) and position measurement by NEUT. The TOF is determined from the time difference between a trigger counter and the average of the timing measured by the top and bottom photomultiplier tubes (PMTs) of NEUT. The horizontal hit position of a neutron is determined by the segmentation of NEUT, and the vertical position is determined on the basis of the time difference between the two PMTs.

The timing information from PMTs is obtained using a combination of VME modules, leading-edge discriminator (CAEN V895), ECL 500 ns logic delay (REPIC RPV-090), and TDC (CAEN V775). The analog information is collected by VME ADC modules (CAEN V792) through 500 ns cable delays and attenuators. VME modules are controlled by a crate controller, SBS Model 618-3. The NIM coincidence modules (Technoland N-RS 413) are used for generating logic signals for a trigger of data acquisition. The high voltages of PMTs are maintained by CAEN SY1527LC system with A1535SN boards.

Two possible configurations are presumed for the NEBULA setup, (1) two-wall setup and (2) four-wall setup. The detectors are now being configured according to the two-wall setup. In the two-wall setup, the 120 NEUT modules are arranged into two walls, located about 1 m apart (minimum distance between the rear face of the 1st wall and the front face of the 2nd wall is 610 mm). Each wall consists of 30 modules × 2 layers with a layer of VETOs (12 pieces). This is considered to be the primary setup and is used in an experiment detecting one and two neutrons. The intrinsic efficiency for one neutron detection is estimated by KSUVAX code[1)] to be 41% for $E_{\rm th} = 5$ MeVee.

For two-neutron detection, neutron crosstalk events must be eliminated. This is done by the causality analysis, which was successfully used in the Coulomb breakup of ^{11}Li.[2)] In the analysis, position information is used when two hits occur on the same wall, resulting in deficiency for events with $E_{\rm rel} \approx 0$ MeV. When two hits occur on different walls, timing information is used. In this case, possible crosstalk events due to the scattering of a neutron in the 1st wall are excluded, if the velocity determined from the 2nd wall is faster than that determined from the 1st layer. Thus, two-neutron events with $E_{\rm rel} \approx 0$ MeV can be measured.

In the four-wall setup, the 120 NEUT modules are arranged into four walls, which are located about 1 m

*1 Department of Physics, Tokyo Institute of Technology
*2 Department of Physics and Astronomy, Seoul National University

Table 1. Specification of NEBULA

Plastic scintillator	BC-408 (Saint-Gobain)
	12 cm (H) × 180 cm (V) × 12 cm (T) (NEUT)
	32 cm (H) × 190 cm (V) × 1 cm (T) (VETO)
Photomultiplier tube	R7724ASSY (Hamamatsu)
Number of available detectors	120 modules (NEUT)
	48 modules (VETO)
Effective area	3.6 m (H) × 1.8 m (V)
Intrinsic efficiency	41% for one-neutron detection ($E_{\rm th}$ = 5 MeVee)

Fig. 1. Photograph of NEBULA.

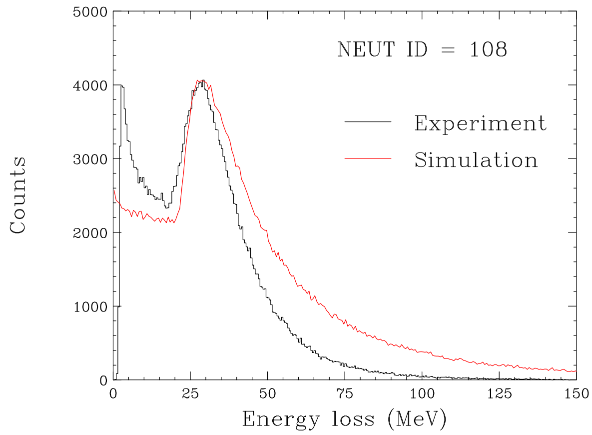

Fig. 2. Energy loss of cosmic-ray muons at a NEUT. The black histogram and red curve correspond to the measured and simulated distributions, respectively.

apart from each other (the minimum distance between the rear face of the 1st layer and the front face of the 2nd layer is 730 mm). Each wall consists of 30 modules with a layer of VETOs (12 pieces). This setup is used primarily for experiments requiring four-neutron detection.

Fabrication of scintillators, PMTs, and light guides has been almost completed. Three scintillator rods for NEUT were defective. They will be replaced with new ones that will be delivered after fabrication. Signals from PMTs and light leakages have been checked for all the assembled modules. Four detector frames have already been fabricated. Sixty NEUTs (30 modules × 2 layers) can be mounted on each detector frame with a layer of VETO in front of the NEUT layers. The whole frame can be moved by using a crane without dismounting the detectors, cables, and electronics. Existing detectors have already been mounted in the two detector frames for the two-wall configuration (Fig. 1). Half of the cables and electronics have been manufactured. Connection of cables for the first wall has been completed. It is planned that a detector test using several NEUT and VETO modules will be performed at the HIMAC facility in the fiscal year 2011 by using a fast neutron beam produced by the ^{7}Li(p, n)^{7}Be(g.s.+0.43 MeV) reaction at 230 MeV to evaluate the one-neutron detection efficiency and timing resolution.

Half of the 1st wall is now being tested using cosmic rays to establish a calibration method. Figure 2 shows the energy loss of cosmic-ray muons measured by NEUT, where a Landau distribution can be seen. The energy loss distribution of muons is simulated by a Monte Carlo method using the known angular dependence of muon flux; this angular dependence is calculated by a simple parametrization.[3] The most probable energy loss of muons is about 30 MeV; this value can be used for the calibration of the analog information of the PMT signals. The difference between the simulated and measured distributions may be due to the insufficiency of the simulation. For example, the angular distribution of muons is affected by the materials surrounding NEBULA such as the RIBF building. This influences the energy loss distribution because the flight length of a muon in the scintillator depends on the incident angle. Further study is currently in progress.

References

1) R. A. Cecil et al.: Nucl. Instrum. Methods **161**, 439 (1979).
2) T. Nakamura et al.: Phys. Rev. Lett. **96**, 252502 (2006).
3) D. Reyna: arXiv:hep-ph/0604145 (2006).

Vacuum System for SAMURAI

Y. Shimizu, H. Otsu, T. Kobayashi,[*1] T. Motobayashi, H. Sato, and K. Yoneda

SAMURAI project aims to open a new research field in nuclear physics by the use of a large acceptance spectrometer for kinematically complete measurements of multiple particles emitted in RI-beam induced reactions[1–3]. The SAMURAI spectrometer consists of a large gap superconducting dipole magnet[4], heavy ion detectors, neutron detectors, and proton detectors. With an effective combination of these equipments, the SAMURAI system allows us to perform various experiments. Vacuum instruments are also expected to be layout depending on the experimental requirement as well as possible. In a designing phase, common instruments were distinguished from other instruments required by individual experimental setups. The common instruments are beam line, SAMURAI vacuum chamber, vacuum pumping system. Individual instruments are considered to be target chamber, connected duct, extended duct, and others which are needed in the other configurations. Figure 1 shows the layout of the vacuum system for SAMURAI. Present status of each instrument is described in the following sections.

Beam line

For the beam line, a target chamber at the focus F13 of the beam line have to be connected with vacuum duct from an existing vacuum chamber at F12. Distance between F12 and F13 is 15.2 m. Beam duct size is compatible with JIS 250, outer diameter of 267.4 mm, which is the same size of upstream beam duct. At present, the superconducting triplet quadrupole magnet STQ25 is located just upstream of the target chamber. A stand for the STQ25 is designed to be adjustable or movable along to beam direction. Vacuum duct should be adjusted depending on the place of the STQ25.

Target chamber

Target chamber configuration will be changed depending on the experiments. Beam line detectors, target itself, and the drift chamber for forward scatterd particle detection (FDC1) are contained in the target chamber. For studies for heavier isotopes, the target section has better to be covered by a γ ray detector array because residual particles do not always stay on ground state. Detail designing for early phase of experiments will be started soon.

Connected duct

At the downstream of the target chamber, a gate valve and a connected duct are located to connect with the entrance window of the SAMURAI vacuum chamber at the magnet gap section. Since scattered particles pass through this section, the connected duct has to be designed to cover as much solid angle as possible. The connected duct should be prepared for each typical angles due to constructional impossibility in making it correspond from 0 to 90 degrees by one mechanism. The connected duct is divided into an individual part and a common part. Figure 2 shows an example of 30 degree setup, which is used for the (γ, n) type experiments. Since the entrance region of the SAMURAI vacuum chamber is cut off at gap inside 750 mm from outer face of field cramp, an entrance flange of the SAMURAI vacuum chamber cannot be easily accessed. So, the common part of the connected duct is designed to be mounted almost permanently. The individual part is designed to be changed for several settings with comparative ease. For EOS (equation of state) experiments, the SAMURAI spectrometer is set with 0 degrees. In this case, beam particles pass through the pipe of the connected duct which is the same size of the upstream beam line. Between the upstream beam line and the connected duct, we plan to separate vacuum section with a large rectangular gate valve.

SAMURAI vacuum chamber

The SAMURAI vacuum chamber is located on the center region of the magnet gap and tapered to downstream along to the magnet return yokes. The entrance region is cut off at gap inside 750 mm from outer face of field cramp in order to realize a finite angle injection up to 45 degrees. On the entrance window, a flange with two windows is mounted to separate between beam entrance window and vacuum pump connected window. These two windows are 300 mm offset for enlarging the beam entrance window, which enables us to adjust various configurations from 0 to 45 degrees of the magnet relative to beam axis. On the side faces at magnet center, two pipes with ϕ390 mm toward 90 and 270 degrees are arranged. The pipe at 90 degrees is utilized for the (γ, p) type experiment with high momentum resolution mode. Scattered particles are led through the pipe to magnet center. The pipe at 270 degrees is invested to auxiliary usages. A vacuum pumping system is mounted here at 90 degree configuration. Laser is introduced to the time projection chamber for position calibration through this pipe. On the top, bottom and saide face, several numbers of screw holes are layout for fixing items inside the vacuum chamber. On the exit window, a flange with two windows with symmetrical configuration is mounted. These two windows are used for combination of scattered particles spatially separated as heavy ions and neutrons or protons. The exit window flange is tightly pressed on the magnet field cramp with special screws in order to prevent the chamber collapsed inside by

*1 Department of Physics, Tohoku University

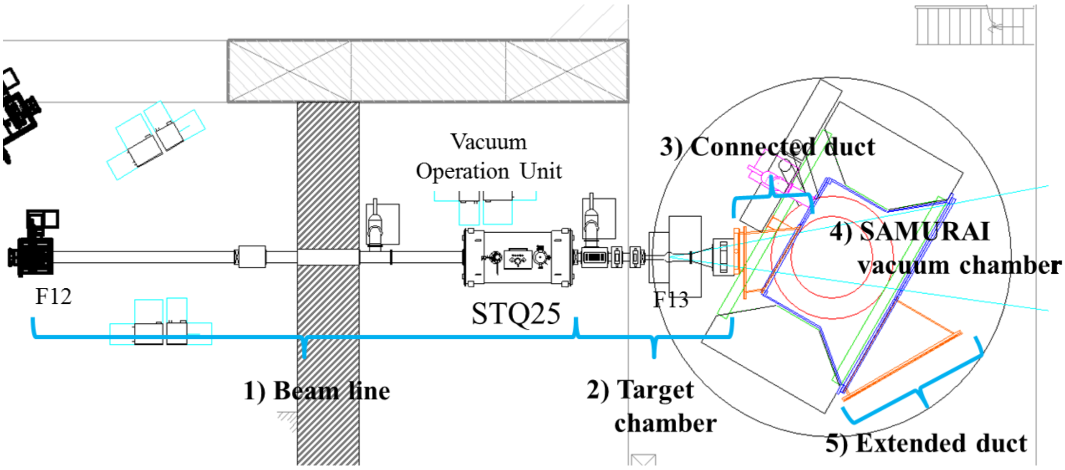

Fig. 1. Layout of the vacuum system.

vacuum pressure, especially for the downstream skirt region.

Extended duct

In order to maximize the performance of the FDC2, the FDC2 should be layout on perpendicular geometry with particle trajectories as well as possible. Supposing to detect 60 degrees bending heavy ions on 30 degree configuration, an extended duct enables us to inject particles on the position sensitive detectors with the perpendicular direction on central trajectory. For this purpose, the extended duct is needed especially for the (γ, n) type experiments. In order to cover the large bending angle region from 34.4 to 82.4 degrees, the extended duct is designed as a shape of right triangle as shown in Fig. 3. The extended duct may also be helpful for other type of experiments. The vacuum pumping system is mounted on this extended duct at (γ, n) type configuration. The FDC2 has been considered to place in the air by partitioning with thin foil window from vacuum. The vacuum partition window is under study for feasibility, which is given in Ref. 5.

Vacuum pumping system

Four sets of vacuum pumping systems are prepared and ready. Two of them consist of 1100 l/s TMP followed by a rotary pump and two vacuum gauges covering from low vacuum to 10^{-4} Pa or lower. The other two consist of 2400 l/s TMP with the same peripherals. The vacuum pumping systems with the 1100 l/s TMP will be mounted on beam line and the target chamber. The two of 2400 l/s TMP systems will be mounted on the SAMURAI vacuum chamber from upstream and downstream, respectively. The layout will be changed depending on the experimental setup, especially for the second 2400 l/s pump station.

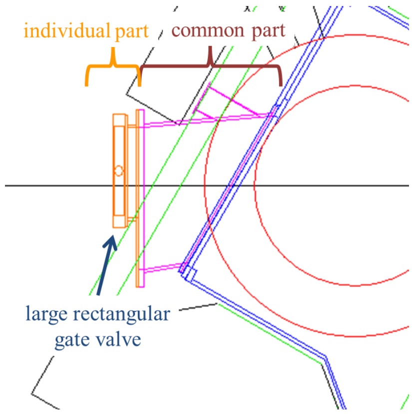

Fig. 2. Connected duct for 30 degree configuration.

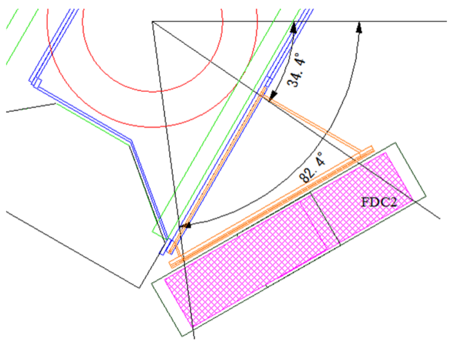

Fig. 3. Extended duct for (γ, n) type experiment.

References
1) K. Yoneda *et al.*: RIKEN Accel. Prog. Rep. **42**, 26 (2009).
2) K. Yoneda *et al.*: RIKEN Accel. Prog. Rep. **43**, 178 (2010).
3) K. Yoneda *et al.*: RIKEN Accel. Prog. Rep. **44**, 140 (2011).
4) H. Sato *et al.*: RIKEN Accel. Prog. Rep. **43**, 180 (2010).
5) Y. Shimizu *et al.*: RIKEN Accel. Prog. Rep. **44**, 154 (2011).

Test of large exit window for SAMURAI spectrometer

Y. Shimizu, H. Otsu, T. Motobayashi, H. Sato, and K. Yoneda

SAMURAI project aims to open a new research field in nuclear physics by the use of a large acceptance spectrometer for kinematically complete measurements of multiple particles emitted in RI-beam induced reactions[1–3]. The SAMURAI spectrometer consists of a large gap superconducting dipole magnet[4], heavy ion detectors, neutron detectors, and proton detectors. Vacuum system is one of the most important infrastructures for nuclear physics to provide primary or secondary beam particles on target and to measure scattering particles without being disturbed by materials for energy deposit or multiple scattering. Present status of the vacuum system for SAMURAI is described in Ref. 5. Details of the test of the charged particle window are given in this paper.

The vacuum area and air have to be separated by vacuum partitioning windows for neutrons and charged particles, which are triggered by plastic scintillator hodoscopes located on the air circumstance. For charged particles, it is required to realize lower multiple scattering and lower energy loss difference for beam rapidity heavy ions on the partition window foil material. The area to be covered is 2940 × 800 mm^2. The window material makes penetrating particles deflect by multiple scattering and makes them energy fluctuation by energy losses. Required momentum resolution of 1/700 gives upper limit of the amount of the material as radiation length of $L/L_R \sim 10^{-3}$. In the same time, it is necessary to ensure the strength to hold the vacuum.

Vacuum window foil for trial consists of Kevlar fiber textile for supporting pressure and polyethylene foil for vacuum separation. From the vacuum side toward air circumstance, Kevlar textile and polyethylene foil are located. The Kevlar textile made of K49 fiber called as #500. The weight per unit area is 163 g/m^2. The thickness is accounted to 0.28 mm. The reason of the selection is that roll of the textile with 1270 mm width are available on a commercial basis. Polyethylene foil with 100 μm thickness and 1300 mm width is also selected because of availability. On the contrary, the polyethylene foil is very easy to be defeated by being scratched. If some of commercial maker provided a roll of Mylar of Kapton foil with more than 1200 mm width, we would choose them. The physical properties of K49 fiber and polyethylene foil are listed in Table 1.

At present, the foil combination with the Kevlar textile and the polyethylene fiol is in test whether it can support the vacuum sufficiently. The geometry of the test vacuum chamber window is 2800 × 1000 mm^2, which is about 20 % larger in length than those of the real exit window. Window support frames are made of aluminum A5056 with 3050 × 1250 mm^2 of area. The trial foil is sandwiched by the window support frames. An O-ring can be attached on the vacuum side of the window support frame. Several conditions have been tested as just sandwiched without gluing, glued with 4 mm, 30 mm or 50 mm width of the Araldite. Results are summarized in Table 2.

Table 1. Physical properties of K49 fiber and polyethylene foil.

Physical properties	K49	polyethylene
Density (g/cm^3)	1.44	0.96
Young's modulus (GPa)	112.4	1.7 ∼ 4.2
Poisson's ratio	0.35	0.34
Tensile strength (MPa)	3000	290 ∼ 570
Break elongation (%)	2.4	10 ∼ 45

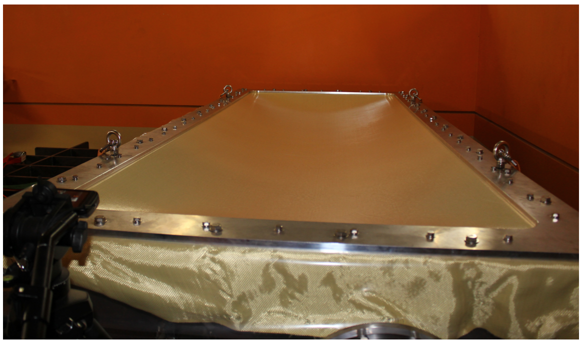

Fig. 1. Shape of the vacuum window at 10 kPa. Distance to the deepest face is about 20 cm.

On the first test, the achieved vacuum level was 42 kPa due to the vacuum leakage. The Kevlar textile was dragged into the test chamber inside due to the fixation without gluing and the polyethylene foil was scratched at the same time. On the second test, the Kevlar textile was fixed on the window frame with gluing of 5 mm width. Since the gluing was not sufficient and several part was removed from the window frame, collapse occurred. On the third test, the Kevlar textile was fixed on the window frame with gluing of 30 mm width. The Kevlar textile was not removed in this condition. The achieved vacuum level was 22 kPa due to the vacuum leakage occurred on screw holes. On the fourth test, the plastic glue was added around screw holes. The Kevlar textile was the same as last time. Since the plastic glue could not adequately penetrate on the window frame through the Kevlar textile, the achieved vacuum level was 10 kPa. The maximum deflection around the center region at 10 kPa was approximately 20 cm as shown in Fig. 1. On the last test, the Kevlar textile was fixed on the window frame with

Table 2. Results of foil test.

Condition	Achieved vacuum	Comment	Date
Without gluing	42 kPa	leak	12/Mar/2010
Gluing, 4 mm width	30 kPa	collapse	03/Jun/2010
Gluing, 30 mm width	22 kPa	leak	28/Jun/2010
Gluing, 30 mm width addition around screw holes	10 kPa	leak	23/Jul/2010
Gluing, 50 mm width including around screw holes	8 kPa	collapse	05/Nov/2010

gluing of 50 mm width including around screw holes. Figure 2 shows the time evolution of the achieved vacuum for last three trials together with the result with iron window. The result of the last test behaved similarly as the result with iron window. Vacuum leakage seems to be improved due to arrangement of gluing at inner region of the screw holes. The achieved vacuum level was 8 kPa and then collapse occurred. The reason why the collapse occurred on last test seems that the strength of the Kevlar textile called as #500 is insufficient. As a next step, two-ply Kevlar textile is in test whether it can support the vacuum sufficiently.

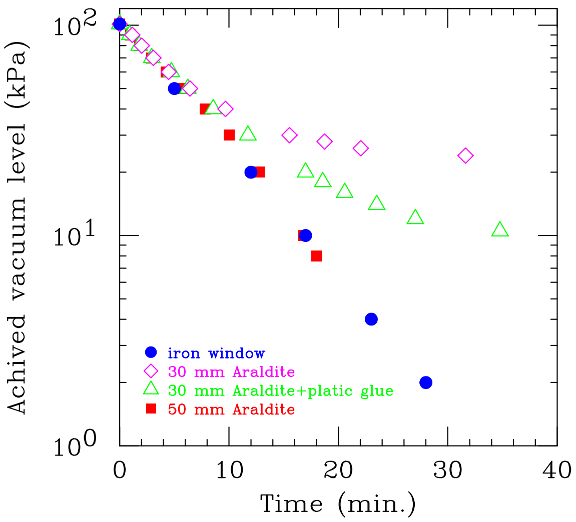

Fig. 2. Time evolution of the achieved vacuum. Blue circles show result with iron window. Magenta diamonds, green triangles, and red squares show results with glued with 30 mm width of the Araldite, glued with 30 mm width of the Araldite and the plastic glue, and glued with 50 mm width of the Araldite, respectively.

From practical point of view, it was found that the most important point is to fix the Kevlar textile on the window frame with gluing more than 30 mm width. So, important point to support vacuum pressure is gluing the Kevlar textile sufficiently. It was also found that the Kevlar textile with thickness of 0.28 mm could not hold the vacuum. A thicker Kevlar textile is necessary to support the vacuum sufficiently. However, a thicker Kevlar textile reduces the momentum resolution. When collapse of the window occurred in the SAMURAI configuration, almost all instruments would be damaged including upstream accelerators. So, we have to establish the way to hold the vacuum by using a thicker Kevlar textile at the cost of the momentum resolution. The final goal of this trial is to achieve pressure of 10^{-4} Pa, while we have to improve and confirm methods step by step.

References

1) K. Yoneda *et al.*: RIKEN Accel. Prog. Rep. **42**, 26 (2009).
2) K. Yoneda *et al.*: RIKEN Accel. Prog. Rep. **43**, 178 (2010).
3) K. Yoneda *et al.*: RIKEN Accel. Prog. Rep. **44**, 140 (2011).
4) H. Sato *et al.*: RIKEN Accel. Prog. Rep. **43**, 180 (2010).
5) Y. Shimizu *et al.*: RIKEN Accel. Prog. Rep. **44**, 152 (2011).

Development of amplifier with wide dynamic range for Si detector in RIBF SAMURAI spectrometer

S. Yoshida,*[1] A. Takuma,*[1] H. Murakami, K. Kurita,*[1] A. Taketani,*[2] K. Yoneda,*[2] T. Togano,*[2] H.J. Ong,*[3] M. Kurokawa,*[2] and T. Motobayashi*[2]

In an experiment of the breakup reaction of proton-rich nuclei, a tracker composed of silicon strip detectors[1)] is installed between the secondary target and SAMURAI[3)]. The tracker must detect nuclei whose atomic number is in the range 1 to 50(from proton to Sn), the pulse height of a Sn nucleus is 2500-times larger than that of a proton. In order to realize the detection capability, a wide dynamic range of more than 2500 is required.

A dual gain amplifier that satisfies requirement for the dynamic range has been already developed[2)]. However, it requires twice as many channels for the following electronics. We propsed an amplifier whose V_{out} is proportional to the square root of V_{in}. We call it the square root amplifier.

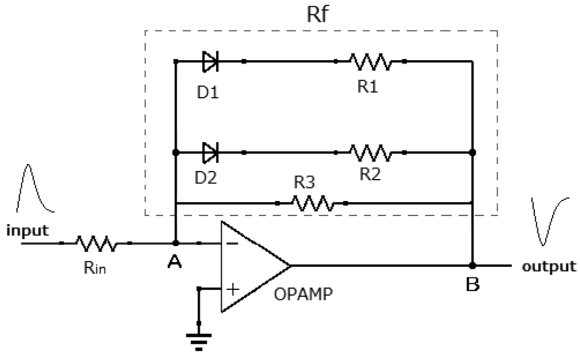

Fig. 1. Diagram of square root amplifier

Figure. 1 shows the diagram of the square root amplifier developed by us. This circuit is an amplifying circuit with negative feedback. The gain decreases as the feedback resistor is lowered. The behavior of this circuit is described using the following three cases. V_{TH1} is the turn-on voltage of D1 and V_{TH2} is the turn-on voltage of D2.

Case 1:$(0 < V_{AB} < V_{TH1})$ When the applied forward voltage is less than the turn-on voltage of a diode, it behaves as a high-resistance devices. Thus, $Rf \simeq R3$ because R1 and R2 considered disconnected.

Case 2:$(V_{TH1} < V_{AB} < V_{TH2})$ When the applied forward voltage is approximately equal to or more than the turn-on voltage of a diode, it behaves as a low-resistance device. In case 2 , $Rf = R1//R2$ because only R3 is considered to be disconnected.

Case 3:$(V_{TH2} < V_{AB})$ In case 3 , $Rf = R1//R2//R3$, because both R1 and R2 are considered to be connected in parallel.

The symbol // means a parallel connection. Rf decreases as V_{AB} increases and square root shape can be approximated by selecting the proper resistors $R1 \simeq R3$

Pulse voltage was applied at the input and the wave pulse voltage at output was measured. Figure. 2 shows the input (V_{in}) and output (V_{out}) voltages correlation. The cross points represent the measured values; the dotted curve is the expected curve for the circuit, and $V_{out} = \sqrt{V_{in}}$ is indicated by the dotted line. They actual and expected values agree quite well. When V_{in} is small and V_{out} is large, the data points are not really consistent with square root. This is because we are approximating the function by joining basically three straight lines in the decreasing-slope order. We conclude that our square root circuit will satisfy the requirements of the SAMURAI Si tracker readout.

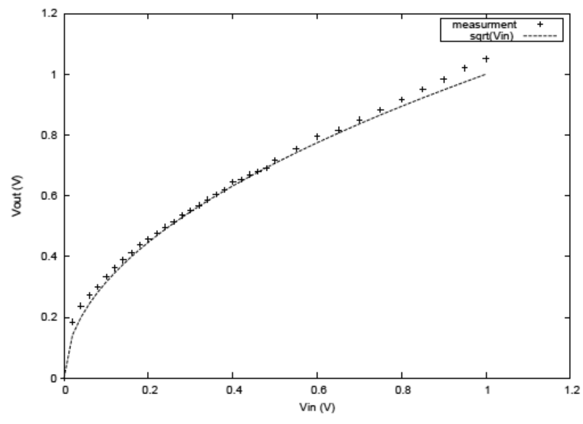

Fig. 2. Correlation between V_{in} and V_{out}.

References
1) Y.Togano et al.: RIKEN Acc. Prog. Rep. B(2011).
2) M.Kurokawa et al.: RIKEN Acc. Prog.Rep. B(2009).
3) K.Yoneda et al.: RIKEN Acc. Prog. Rep. B(2009).

*1 Department of Physics, Rikkyo University
*2 RIKEN
*3 Research Center for Nuclear Physics,Osaka University

Development of ultrafast-response kicker system for Rare-RI Ring

Y. Yamaguchi, A. Tokuchi,[*1*2] S. Fukuoka,[*3] W. Jiang,[*1] T. Kikuchi,[*4] D. Nagae,[*3] A. Ozawa,[*3] T. Sasaki,[*4] and M. Wakasugi

We adopt a unique injection method, the so-called self-trigger individual injection method, for the Rare-RI Ring. Figure 1 shows the concept of our injection method. When a particle passes through a timing detector at F3 of the BigRIPS, a trigger signal is generated. The trigger signal is transmitted to a kicker system by using a high-speed coaxial transmission cable. The kicker magnet is then immediately excited by a thyratron switch. In the meanwhile, the particle goes through the BigRIPS and an injection line and is injected into an equilibrium orbit of a cyclotron-like storage ring by using septum and kicker magnets. To establish our injection method, it is necessary to excite the kicker magnet before the particle arrives at the kicker. The response time of the kicker power supply plays a key role in shortening the time taken for kicker excitation. In a basic design of the Rare-RI Ring[1)], the distance between F3 and the kicker is about 161 m. Then, the flight time of the particle with an energy of 200 MeV/u is about 950 ns, whereas the time taken for kicker excitation is expected to be about 560 ns, excluding the response time. Therefore, it is necessary to reduce the response time to less than 390 ns. Recently, we have succeeded in shortening the response time by the required amount. In this paper, we report the results.

We used a model kicker system[2)] to measure the response time. Figure 2 shows a block diagram of the model kicker system. Trigger pulses of charge and discharge are generated by using a pulse generator during the measurements. A control unit adjusts the timing of the pulses. The duration of flat-top is fixed by the length of the pulse-forming line. An appropriate grid pulse for a thyratron is formed in the thyratron gate unit. The thyratron is a high-peak-power electrical switch. It consists of a cathode, an anode, a ground grid, a control grid, an auxiliary grid, a cathode heater, and a reservoir heater. CTout denotes the current transformer output of the thyratron.

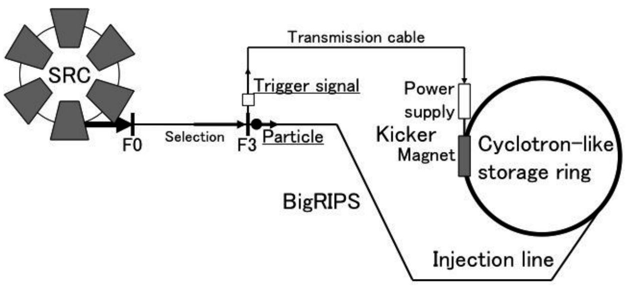

Fig. 1. Concept of our injection method.

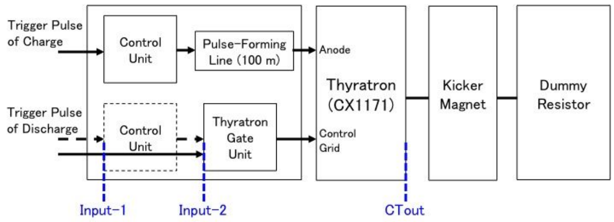

Fig. 2. Block diagram of model kicker system.

We first checked the original condition of the model kicker system. The response time (between Input-1 and CTout) is about 2.67 μs when the charging voltage is 20 kV and reservoir-heater voltage is 5.3 V. Here, measurement timing is defined as 10 % of the full strength of each signal. In our method, the control unit for discharge is not necessary for injection. Therefore, we can directly send the trigger pulse of discharge to the thyratron gate unit. The response time (between Input-2 and CTout) is 550 ns when the charging voltage is 20 kV and reservoir-heater voltage is 5.3 V. However, this value of the response time does not satisfy our requirement.

We constructed a new thyratron gate board to replace the original thyratron gate unit. Figure 3 shows the block diagram of the model kicker system with the new thyratron gate board and a photograph of this

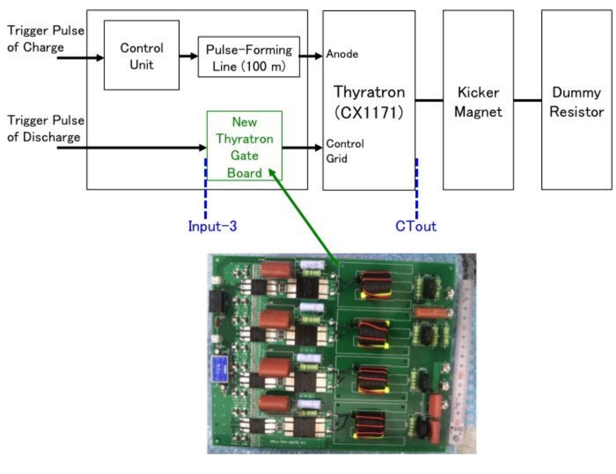

Fig. 3. Block diagram of model kicker system with new thyratron gate board and photograph of this board.

*1 Extreme Energy-Density Research Institute (EDI), Nagaoka University of Technology
*2 Pulsed Power Japan Laboratory Ltd.
*3 Institute of Physics, University of Tsukuba
*4 Department of Electrical Engineering, Nagaoka University of Technology

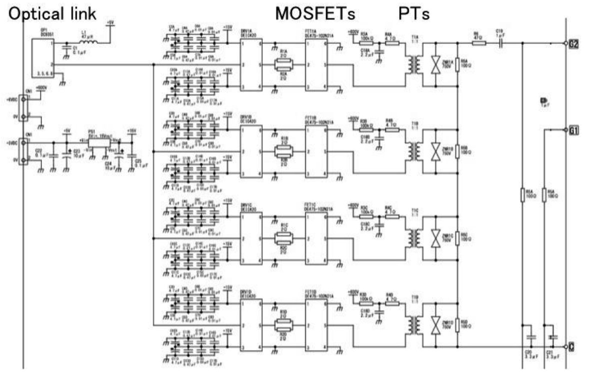

Fig. 4. Circuit diagram of new thyratron gate board.

board. It mainly consists of four MOSFETs and four Pulse Transformers (PTs). To shorten the rise time of the PTs, four PTs are used in parallel for the primary side and in series for the secondary side. Figure 4 shows the circuit diagram of the new thyratron gate board.

For the model kicker system shown in fig. 3, we achieved a response time of about 275 ns between Input-3 and CTout for the same value of charging and reservoir-heater voltages as mentioned before. The pulse takes about 30 ns to cross the optical-link part. A time period of about 75 ns is required to form an appropriate grid pulse. The driving time of the thyratron is about 170 ns. Consequently, the response time shortens to the required value.

Figure 5 shows the response time between Input-3 and CTout as a function of the charging voltage. The response time depends on the charging voltage and steadies when the charging voltage is 20 kV or more.

The propagation time between CTout and the start of flat-top is also important for shortening the time taken for kicker excitation. We check the propagation time by using a model kicker magnet, which is based on a distributed kicker magnet. In our measurement, the kicker magnet is connected to the thyratron by using a 5 m long coaxial cable. To check the magnetic field, we use a long search coil. The long search coil is a one-turn coil with a width of 2 mm and a length of 470 mm. The output voltage is measured with a 1/103.7 attenuator. The waveform of the magnetic field is obtained by integrating the induced voltage. As a result, a propagation time of about 115 ns is obtained between CTout and the start of flat-top. Since this propagation time is short enough, we will adopt the same type of kicker magnet.

Our kicker system will be used not only for injection but also for extraction. The interval between injection and extraction is about 0.7 ms. For injection and extraction, the duration of flat-top should be about 200 ns. Thus, it is necessary to make the flat-top as much uniform as possible. Furthermore, the repetition of charge must be less than 0.7 ms. We will study the feasibility of these requirements by using the model kicker system.

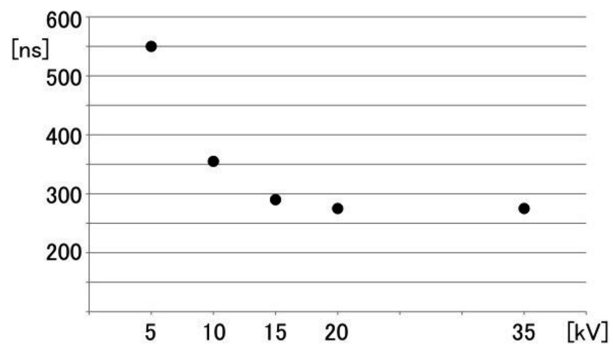

Fig. 5. Response time between Input-3 and CTout as function of charging voltage.

References

1) Y. Yamaguchi et al.: RIKEN Accel. Prog. Rep. **44** (2011).
2) T. Ohkawa et al.: Nucl. Instrum. Meth. Phys. Res. A **547**, 287 (2005).

Status of Rare-RI Ring

Y. Yamaguchi, H. Suzuki,[*1] T. Fujinawa, A. Goto, T. Moriguchi,[*1] D. Nagae,[*1] A. Ozawa,[*1] M. Wakasugi, T. Yamaguchi,[*2] and Y. Yano

We redesigned an injection line and a cyclotron-like storage ring with a momentum acceptance of 1%. We report on their present status.

Figure 1 shows the arrangement plan for the injection line and the cyclotron-like storage ring. The floor level is same as that for the SHARAQ spectrometer. The injection line, which starts from the end of the final focal plane of SHARAQ, is much shorter than that in the previous design[1]. It consists of ten quadrupole magnets, which have been obtained from the KEK proton synchrotron (KEK-PS), and one dipole magnet with a 15° bend. This dipole magnet has been obtained from the cooler synchrotron TARNII[2]. The cyclotron-like storage ring consists of six magnetic sectors, and each magnetic sector consists of four dipole magnets of TARNII. The TARNII Dipole (TARNII-D) is a rectangular bending magnet with a radially homogeneous magnetic field, but it is not acceptable in our isochronous field design. In order to generate an appropriate first-order isochronous field, we scrape the pole of TARNII-D diagonally. Furthermore, we install trim coils in TARNII-D to tune higher-order isochronism. This remodeling, which is optimized to 200 MeV/u, will be performed for two outer dipoles among the four dipoles in each magnetic sector. Some specifications and calculation results for the storage ring are summarized in Table 1. The normalized gradient value, tune values, TWISS parameters, and dispersion are calculated by using the MAD program in 1st order.

In order to evaluate the isochronism of the storage ring in more detail, we use our simulation program[3].

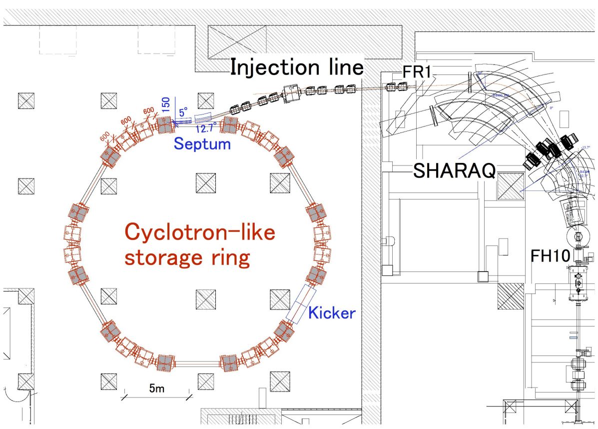

Fig. 1. Arrangement plan for injection line and cyclotron-like storage ring.

Table 1. Specifications and calculation results for the storage ring.

=BEAM CONDITION=
Energy: 200 MeV/u
$B\rho$: 6.43 Tm ($a/q = 3$)
Lorentz factor (γ): 1.2147
=STORAGE RING=
Circumference: 60.3507 m
Length of straight section: 4.02245 m
Length of bending section: 6.036 m
Momentum acceptance: 1%
Harmonics: 13
Revolution frequency: 2.82 MHz
Revolution time: 355 ns
=DIPOLE (TARNII-D)=
Inner two dipoles: 12 flat-pole magnets
Outer two dipoles: 12 gradient-pole magnets
Bending angle: 15°
Radius of curvature: 4.045 m
Magnetic strength: 1.6 T
=CALCULATION RESULT=
Normalized gradient: 0.074 m^{-2}
Transition γ_{tr}: 1.2146
Tune: Q_x 1.22, Q_y 0.88
Max. β function: β_x 8.3 m, β_y 12.5 m
Dispersion of straight section: 66.91 mm/%

We track particles in the magnetic sector by assuming that the particles revolve in circular orbits within a small spatial segment. The magnetic sector is divided into 210 sub-sectors, and the calculated TOFs of particles converge. The field at every segment is deduced from the results of a TOSCA simulation. Figure 2 shows the emittance in the horizontal direction for 2000 turns as a function of the position and angle at the injection point (kicker end) when the isochronism

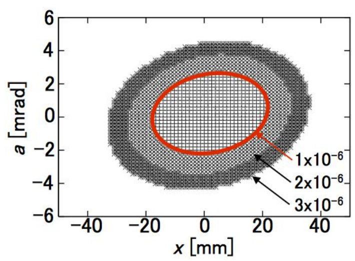

Fig. 2. Emittance in the horizontal direction when the isochronism of the storage ring is maintained. Inside the red circle represents the isochronism region with a precision of 10^{-6}.

*1 Institute of Physics, University of Tsukuba
*2 Department of Physics, Saitama University

of the storage ring is maintained. The emittance of the isochronism region is determined with a precision of 10^{-6}, and it is found to be about 50π mm mrad for any momentum of the particle under ideal conditions. In the next step, we have to take misalignment, stability of the power supply, etc, into consideration to study the tolerance. Trim coils are designed simultaneously with study the tolerance.

Third-order optical calculation for an injection beam with $a/q = 3$ is performed by using the COSY-INFINITY and MOCADI programs. For instance, Fig. 3 shows the horizontal beam trajectories from the F0 production target section of BigRIPS to the FR1 dispersive focal plane. The FR1 is just an optical plane after the SHARAQ. The initial condition is $a_0 = \pm 15$ mrad with $\delta p/p = \pm 0.5\%$. The red line corresponds to $\delta p/p = -0.5\%$, the green line corresponds to $\delta p/p = 0\%$ and the blue line corresponds to $\delta p/p = +0.5\%$. The angular acceptance of the BigRIPS and SHARAQ part is sufficiently wider than that of the injection line part. The optical transmission efficiency of this part is nearly 100% without the momentum dependence, even if 3rd-order aberrations are considered.

Figure 4 shows the horizontal beam trajectories from the FR1 to the kicker part via the septum. The angular acceptance of the injection line is narrow, so the beam emittance is limited here. However, the beam emittance is larger than that in the previous design because of the shorter injection line and the absence of vertically bending magnets.

We adopt a single-turn injection by using the septum and the kicker. The phase advance from the septum end to the kicker center is about $3\pi/2$. The septum, which is operated as a DC magnet, is divided into two magnets (septum-1 and septum-2) to reduce the load exerted on it. The bending angles of septum-1 and septum-2 are 12.7° and 5°, respectively. After passing through septum magnets, a particle is injected into the storage ring from outside ($x = 150$ mm). The injected particle is transported to the kicker, and it is then kicked ($\theta_k = 19$ mrad) into the equilibrium ring orbit with the dispersion and emittance matching. We describe a feasibility study on the kicker system with our injection method in Ref. 4) because the kicker system is important for our injection method.

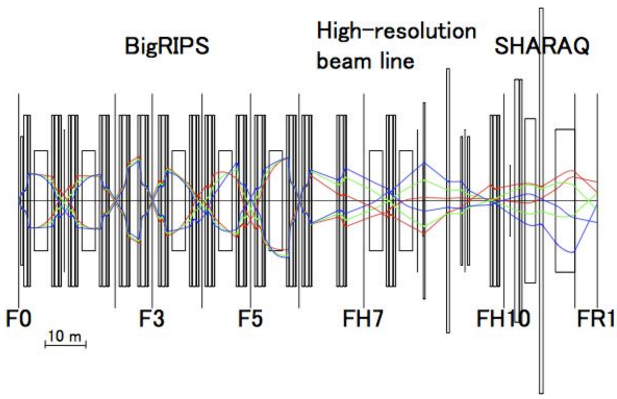

Fig. 3. Horizontal beam trajectories from the F0 production target of BigRIPS to the FR1 dispersive focal plane for $a_0 = \pm 15$ mrad with $\delta p/p = \pm 0.5\%$ in 3rd-order optical calculation.

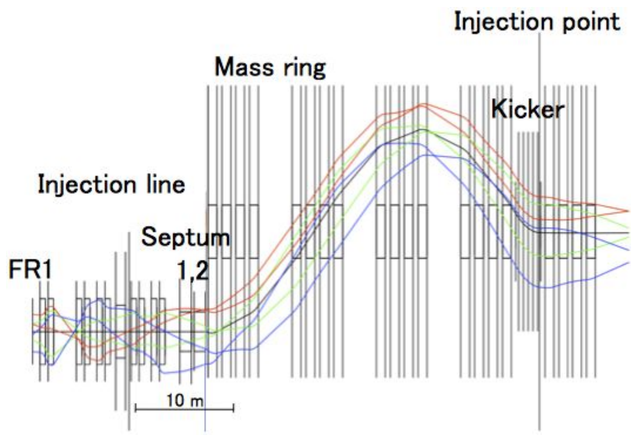

Fig. 4. Horizontal beam trajectories from the FR1 to the kicker part via the septum for $a_0 = \pm 15$ mrad with $\delta p/p = \pm 0.5\%$ in 3rd-order optical calculation.

The efficiency of optical transmission from F0 of BigRIPS to the kicker part is shown in Fig. 5. High optical transmission efficiency is achieved on the large momentum side. On the other hand, the optical transmission efficiency on the small momentum side is not enough. The bottleneck lies in some part of the injection line and septum. Evaluation of the condition for the emittance matching is still in progress.

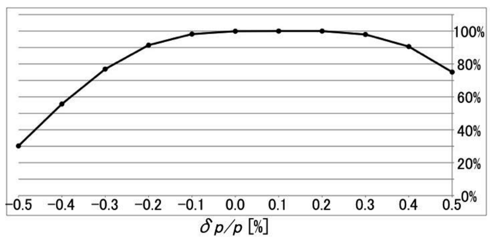

Fig. 5. Momentum dependence of the efficiency of optical transmission from F0 of BigRIPS to the kicker part.

References

1) Y. Yamaguchi et al.: Nucl. Instrum. Methods Phys. Res. B **266**, 4575 (2008).
2) T. Katayama et al.: Particle Accel. **32**, 105 (1990).
3) H. Suzuki et al.: RIKEN Accel. Prog. Rep. **43**, 186 (2010).
4) Y. Yamaguchi et al.: RIKEN Accel. Prog. Rep. **44**, (2011).

A cooling and transport device for online mass measurements to be performed with a MRTOF mass spectrograph

Y. Ito,[*1] M. Wada, P. Schury,[*1] T. Sonoda, A. Takamine,[*2] S. Naimi, H. Wollnik,[*3] A. Ozawa,[*1] and S. Nakamura [*1]

[Mass measurements, unstable nuclei, low-energy beam]

We are planning to use a Multi-Reflection Time-of-Flight Mass Spectrograph (MRTOF-MS) for the online mass measurement of radioactive ions (RI) at RIKEN Projectile fragment Separator (RIPS)[1,2]. Our group has developed a prototype slow RI facility (SLOWRI) that consists of a long helium gas cell, an RF carpet, a carbon octupole ion guide (carbon OPIG), and an MRTOF-MS with a novel preparation trap[3–5]. The setup is shown in Fig. 1 The gas cell produces a low-energy RI beam. The gas cell stops the high-energy RI beam separated by RIPS and accumulates the low-energy RIs on the RF carpet, which transports the low-energy ions to a higher vacuum. After extraction from the gas cell, the ions are converted into a pulsed beam and are injected into the MRTOF-MS where their mass can be determined.

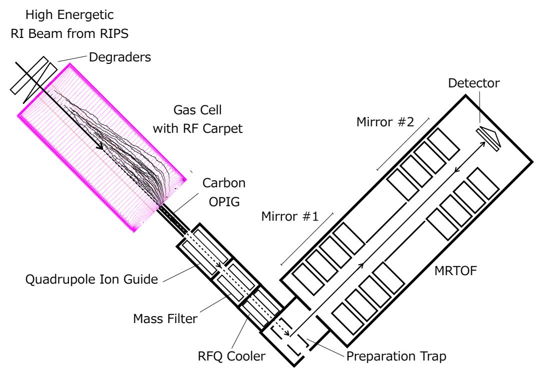

Fig. 1. Schematic of MRTOF system

Because the ions coming out from the gas cell have several mass numbers, they could reduce the efficiency of the MRTOF-MS and preparation trap and the mass precision. Furthermore, it is important to inject only isobars into the MRTOF-MS to avoid any difficulty in the analysis. Therefore, we have developed a quadrupole mass filter (QMF) and a tapered RF quadrupole (RFQ) precooler for separating the mass and initial cooling of the ions, respectively. The QMF and RFQ precooler are installed before the preparation trap. In this report, we will present some simulation results pertaining to the QMF and RFQ precooler.

Fig. 2(a) shows a schematic of the beam-transport line that consists of the RFQ ion guide, QMF, and tapered RFQ precooler. The pressures listed represent approximate values that are evaluated from the calculated conductance. The preparation trap is filled with He buffer gas at a pressure on the order of 10^{-3} Torr to accumulate and cool the ions efficiently. The tapered RFQ precooler is at the same pressure as that of the trap and has an effective electric field in the direction of the trap; therefore, it is considered as a part of the trap. The geometry of the RFQ precooler is shown in Fig. 2(b).

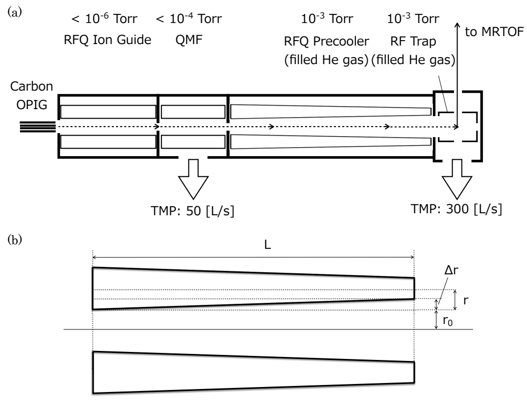

Fig. 2. (a) Schematic of transport system (b) Schematic of tapered RFQ precooler

To evaluate the performance of these devices, we simulated them using SIMION 3D[6]. In these simulations, we employed a collision model with buffer gas; this model was based on the Hard-Sphere model. The QMF can separate the mass of the ions by oscillating them using RF and DC electric fields, which may heat the ions. Therefore, it is preferable to install the QMF just before the precooler to cool the ions immediately. As a result, the region surrounding the QMF is not high vacuum; rather, the pressure in this region is on the order of 10^{-4} Torr. Fig. 3 demonstrates the expected mass spectra of the ions for various gas pressures. In this figure, at 10^{-4} Torr, the QMF has about 90% transmission and enough high mass resolution.

In Fig. 4, the transmission profiles in the RFQ precooler are shown as functions of Mathieu's q-value[7]. The Mathieu's q-value is defined at $\Delta r = 0$. Under this condition for straight-rod geometry of the precooler, some of the ions will stop in the middle of the precooler. The lower transmission of the straight-type precooler shown in the figure results from this effect. However,

*1 University of Tsukuba, Ibaraki, Japan
*2 Aoyama Gakuin University, Tokyo, Japan
*3 University of Gießen, Gießen, Germany

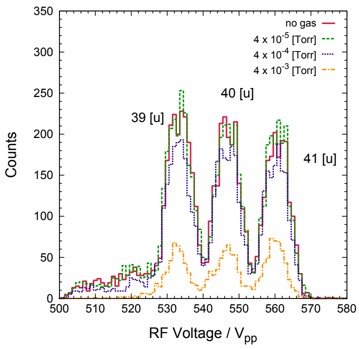

Fig. 3. Performance of QMF in single mass resolution mode for various gas pressures. Note the reduction in efficiency for pressures exceeding for 4×10^{-4} Torr.

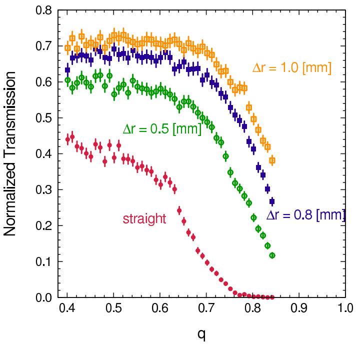

Fig. 4. Transmission curves as functions of Mathieu's q-value for various precooler geometries

the tapered-type precoolers show better transmission because they do not stop the ions owing to an effective electric field. Instead of an increase in the transmission, the beam size becomes larger since the pseudo-potential well becomes shallower. Fig. 5 shows the beam size as a function of Δr. Because the trap has

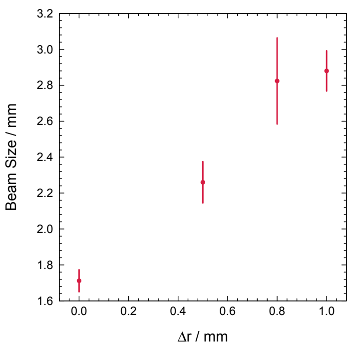

Fig. 5. Beam size after precooler for various geometries

only a 4-mm gap, it is important for the beam size to be smaller than this gap. Even when Δr is 1.0 mm, the beam size is lower than 4.0 mm, which matches the acceptance of the trap. The longitudinal kinetic energy of the ions affects their ability to accumulate efficiently in the trap. Fig. 6 shows the distribution of the longitudinal kinetic energy of the ions after the RFQ cooler. For an ion to be accumulated in the trap,

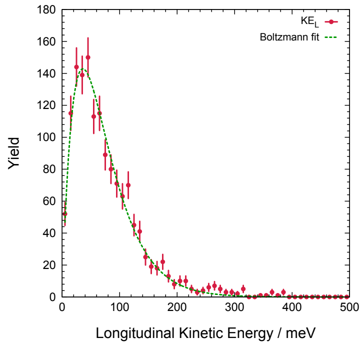

Fig. 6. Distribution of longitudinal kinetic energy after precooler for $\Delta r = 1.0$ mm

it is necessary for the ion to lose sufficient longitudinal kinetic energy in one pass such that its longitudinal kinetic energy at the far side of the trap is lower than the electric potential; otherwise, the ion will pass through the trap. The energy distribution after the precooler is calculated to be a Boltzmann distribution corresponding to the buffer gas temperature. This is sufficient to accumulate the ions in the trap.

The RIs that we want to measure are very short-lived, e.g., $T_{1/2}(^{14}\mathrm{Be}) = 4.84$ ms, $T_{1/2}(^{17}\mathrm{B}) = 5.08$ ms, and $T_{1/2}(^{19}\mathrm{C}) = 49$ ms. Therefore, these ions must not remain for too much time in the precooler. The average time required to pass through the precooler is around 500 μs, which is short compared to the half-lives of the RIs that we are interested in.

We are presently constructing a precooler system based on the simulation results. We have started the offline test of this system early this year.

References

1) Y. Ishida, M. Wada and H. Wollnik: Nucl. Instrum. Meth. B **241**, 983 (2005).
2) Y. Ishida, M. Wada and H. Wollnik: RIKEN Accel. Prog. Rep. **40**, 150 (2007).
3) M. Wada et al.: Nucl. Instrum. Meth. B **204**, 570 (2003).
4) P. Schury et al.: Eur. Phys. J. A **42**, 343 (2009).
5) P. Schury et al.: RIKEN Accel. Prog. Rep. **42**, 189 (2009).
6) SIMION program, available at www.simion.com
7) P. H. Dawson: *Quadrupole Mass Spectrometry and Its Applications*, AIP Press, Woodbury, New York (1995).

Stable high-voltage supplies for MRTOF mass spectrograph

M. Wada, P. Schury[*1]

[Mass spectrograph, High voltage supply]

A multi-reflection time-of-flight mass spectrograph (MRTOF-MS) has been developed for precision mass measurements of short-lived nuclei.[1)] This device essentially consists of a pair of electrostatic mirrors, and stored ions move back and forth between the mirrors multiple times. In order to achieve a high mass resolving power, the potentials of the mirror electrodes should be stably and accurately maintained.

The voltage configuration of our MRTOF-MS is shown in Fig. 1. Since the ion trap is placed at the ground potential for convenient interface with the upstream device, the base potential of the MRTOF-MS is at the negative acceleration voltage ($-V_{\rm acc} \approx -2$ kV). All high-voltage supplies for mirror electrodes are placed on this high-voltage platform. Many ring electordes for static mirror potentials are provided by a single voltage-radder and a single high-voltage supply ($V_{\rm mtof}$); in addition, two special electrodes – one at the injection side and the other at ejection side – having *open* and *close* phases are independently supplied from four high-voltage modules ($V_{\rm injC}, V_{\rm injO}, V_{\rm ejeC}, V_{\rm ejeO}$) with two fast switches. A lens voltage supply ($V_{\rm lens}$) is also independently controllable.

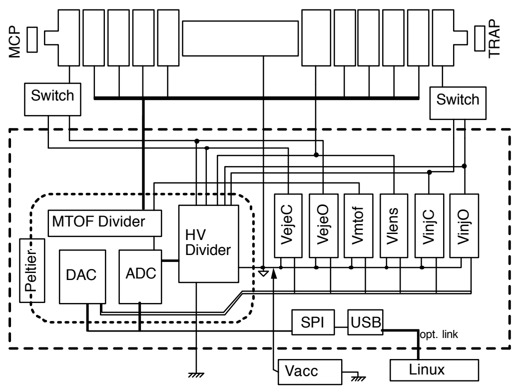

Fig. 1. Diagram of the high-voltage power supplies. The components in the dashed box are on the high-voltage platform, while those in the dotted box are enclosed in a temperature-controlled box. Vxxx represents high-voltage power supply modules.

All the high-voltages including $V_{\rm acc}$ are monitored by a high-precision 24-bit ADC with a single precision voltage reference and precision voltage dividers.[2)] The voltage dividers and the ADC board as well as a DAC board are enclosed in a temperature-controlled box. The voltage dividers are composed of precision high-voltage resisters, RU2A (Japan Finechem) and zero-TCR metal foil resisters (Alpha Electronics). The temperature coefficients of the resisters are ±10 ppm/K and ±0.15 ppm/K, respectively. The voltage radder for mirror electrodes are composed exclusively of zero-TCR metal foil resisters. The ADC boards contains a $\Sigma - \Delta$ 24-bit ADC, LTC2449 (Linear Technology) and a voltage reference, MAX6350 (Maxim). The temperature coefficient of the reference chip is 1 ppm/K. The temperature of the box is monitored by using a LM135 sensor and controlled by using a 15-W Peltier cooler/heater (SL-3FF from Nippon Blower) in which convection flow occurs.

The actual high voltages ($V_{\rm mtof}$, $V_{\rm injC}$, $V_{\rm injO}$, $V_{\rm ejeC}$, $V_{\rm ejeO}$ $\leq$5 kV, and $V_{\rm lens}$ $\geq$ -10 kV) are provided by HPMR series modules (Matsusada Precision) that are placed outside the temperature-controlled box. The reference voltages for the modules are provided from pseudo 22-bit DACs on the DAC board[2)] enclosed in the box.

The periodically measured voltages are transferred to a host PC and the values are compared with setting values and then fed back to the DAC according to a simple PID algorithm. Figure 2 shows the measured voltage fluctuation of the setup. The rms width is less than 10 ppm for most supplies. The actual drift at the TOF spectrum indicated that the high-voltage supplies are suitable for maintaining long-term stability.

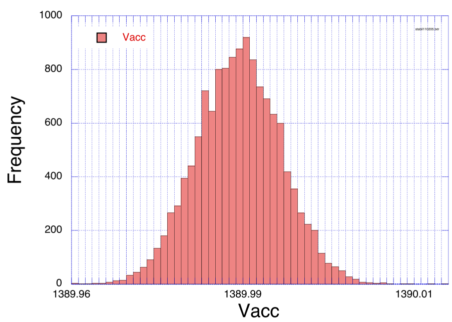

Fig. 2. Fluctuation of the acceleration voltage. The setting voltage was 1390 V and the standard deviation was 4.3 ppm in a 4 h operation.

[*1] Institute of Physics, Tsukuba University

References

1) P. Schury *et al.*: RIKEN Accel. Prog. Rep. **43** 189 (2008).
2) M. Wada and P. Schury: RIKEN Accel. Prog. Rep. **43** 226 (2010).

Status of the resonance ionization laser ion source at SLOWRI II

T. Sonoda, M. Wada, Y. Matsuo, T. Kubo, H. Tomita,[*2] T. Shinozuka,[*3] T. Wakui,[*3] Y. Hirayama,[*4] N. Imai,[*4] H. Ishiyama,[*4] Y. Watanabe,[*4] H. Miyatake,[*4] S. Jeong,[*4] Y. Itou,[*5] P. Schury,[*5] S. Nakamura,[*5] T. Furukawa,[*6] K. Okada,[*7] A. Takamine,[*8] M. Huyse,[*9] Yu. Kudryavtsev,[*9] P. Van Duppen[*9]

A study for developing a laser ion source based on resonance photoionization in a gas cell[1)] is in progress. There are two major objects for the development of the laser ion source: one is the parasitic production of low-energy RI beams from RI garbage by a projectile fragment separator. Since beam time allocation of the fragment separator for one experiment is very limited, we have previously proposed a novel method, named PALIS (PArasitic Laser Ion Source)[2,3)], to enhance the usability for low energy RI beam experiments and save the experimental cost by recycling unused RI beams simultaneously produced by projectile fragmentation or in-flight fission. A PALIS gas cell can be located in the vicinity of the second slit of BigRIPS to capture the unused RI beams. The thermal ions are quickly neutralized in high-pressure Ar gas and transported by gas flow toward the exit of the cell. They can be selectively re-ionized by resonance laser radiations in the vicinity of the exit. They are further purified by an electromagnetic mass separator and transported to the low-energy experimental room.

The other objective is for in-gas cell or in-gas jet laser spectroscopy for nuclear structure studies. During the resonance ionization processes inside the gas cell, the hyperfine splittings as well as the isotope shifts can be measured to determine the nuclear spins, moments, and charge radii. Compared with a similar method in a hot-cavity ion source, much better resolution can be expected, especially for ionization in a supersonic jet behind the nozzle of the cell[4,5)].

In order to confirm the principle of the laser ion source based on resonance photoionization in a gas cell, we carried out the following steps: (1) resonance ionization in vacuum for testing the ionization scheme, (2) resonance ionization in a gas cell for testing a realistic setup, including a beam extraction device, and (3) laser spectroscopy of the hyperfine structure of stable Cu isotopes for carrying out feasibility studies.

In the first step, we performed resonance ionization for stable Ni atoms in a vacuum chamber, as shown in Fig. 1 (left side). The Ni atoms were produced by a filament as vapor, and they were effused to the ionization place, where the lasers were introduced between two electrodes. The Ni atoms were excited stepwise by laser photons until they reached the autoionization states. The partial atomic level scheme for the resonance ionization of Ni[6)] is shown in Fig. 1 (right side). The laser ionized-ions were accelerated by an electric field to a channeltron, where ions were detected. First, an ultra-violet laser was scanned to find the first step resonance from the ground state. Since the strength of the laser was high enough, a fraction of atoms in the excited state could be ionized by capturing the second photon. In this way, we confirmed that the wavelength for the first step was 232.003 nm. Second, we applied an additional green laser to reach the autoionization from the first excited state. Figure 2 shows a resonance spectrum for the second laser. The wavelengths agreed with the values in the literature.

For performing the resonance ionization in a gas cell,

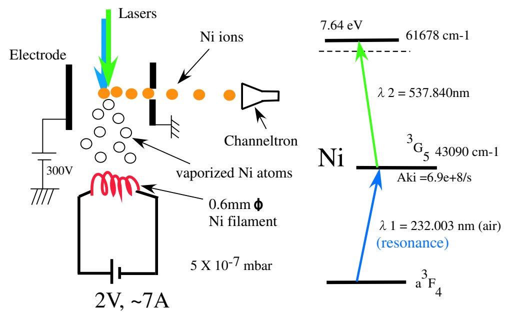

Fig. 1. The experimental setup for resonance ionization in vacuum and the ionization scheme used for Ni[6)].

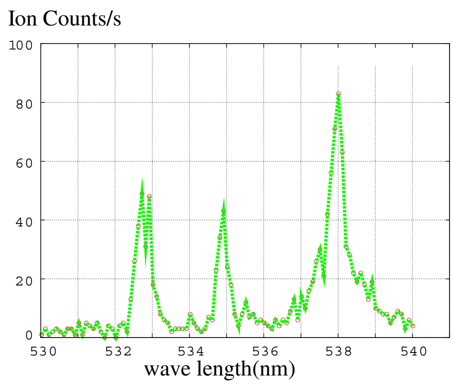

Fig. 2. Resonance spectrum of Ni atoms in vacuum. The first step laser was fixed at 232.003 nm and the ion counting rate was plotted as a function of the wavelength of the second laser.

*1 Department of Physics, Tokyo Institute of Technology
*2 Faculty of Engineering, Nagoya University
*3 Cyclotron and Radioisotope Center, Tohoku University
*4 High Energy Accelerator Research Organization (KEK)
*5 Department of Physics, Tsukuba University
*6 Department of Physics, Tokyo Institute of Technology
*7 Department of Physics, Sophia University
*8 Department of Physics, Aoyama Gakuin University
*9 Nuclear Spectroscopy, IKS, K.U. Leuven (Belgium)

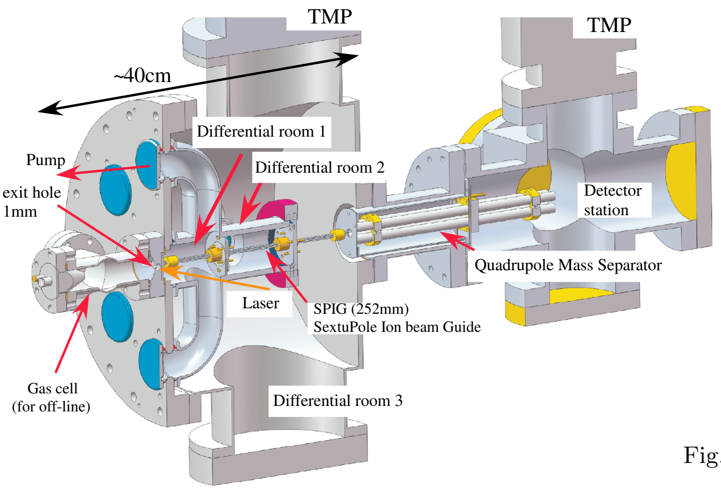

Fig. 3. The setup of a laser ion source based on resonance photoionization in a gas cell.

we built a prototype gas cell and a beam extraction device, as shown in Fig. 3. This setup is composed of four parts: a gas cell, a differential pumping system, a mass separator and a detector station. In the production of low-energy RI beams, the gas cell plays an important role in decelerating high-energy RI beams; the deceleration occurs through collisions with Ar buffer gas, and high energy RI beam are finally thermalized and neutralized. The neutralized atoms are transported by gas flow to the exit hole, and they are then re-ionized by lasers. For the present off-line test, we used the gas cell with an exit nozzle 1 mm in diameter and two feedthroughs to provide an electric current to the filament. The differential pumping system is extremely compact than that in a typical IGISOL (ion guide isotope separator on-line) setup. In order to provide a high pressure, about 500 hPa, inside the gas cell with a large exit hole, a large pumping capability is necessary. In the present setup, however, the pumping load is divided by a few scroll pumps and a turbomolecular pump at individually separated small volumes. Differential pumping capability from a 50000 Pa cell to a 10^{-2} Pa in front of the quadrupole mass filter achieved in three stages, as shown in Fig. 4. The ions from the gas cell could be efficiently transported by SPIG (SextuPole Ion beam Guide)[7–9]. So far we have tested the part up to the end of the SPIG, and a quadrupole mass filter and ion detector will be installed soon. In a series of off-line experiments, we have confirmed the resonance ionization of stable Cu atoms in the gas cell. These atoms were produced by vapor from a filament placed inside the gas cell. Figure 5 shows the resonance spectra of Cu detected by a Faraday cup behind the exit of cell, when dye laser was installed etalon. We can see the hyperfine structure splittings of Cu atoms even with a mixture of naturally abundant isotopes.

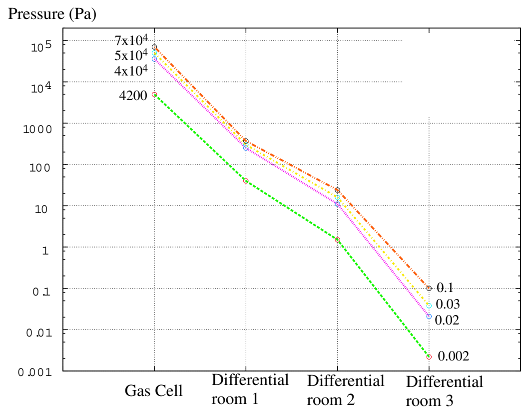

Fig. 4. Schematic diagram of the differential pumping system.

The transmission efficiency of the 252-mm-long SPIG through differential pumping was evaluated to be 80%.

We have confirmed the proof of principle of a laser ion source based on resonance photoionization in a gas cell. An on-line test experiment will be performed at BigRIPS in 2011 to evaluate the overall efficiency of this setup as well as to measure the hyperfine splittings of neutron-rich Cu isotopes.

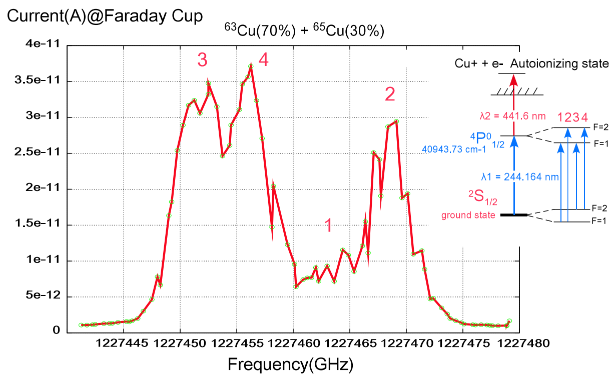

Fig. 5. Observation of the hyperfine splitting of stable ^{63,65}Cu without isotope separation by in-gas cell laser spectroscopy.

References
1) L. Vermeeren *et al.*: Phys. Rev. Lett. **73**, 1935 (1994).
2) T. Sonoda *et al.*: AIP Conf. Proc. **1104**, 132 (2009).
3) M. Wada *et al.*: Hyp. Int. **196**, 43 (2010).
4) T. Sonoda *et al.*: Nucl. Inst. Meth. B **267**, 2918 (2009).
5) T. E. Cocolios *et al.*: Phys. Rev. Lett. **103**, 102501 (2009).
6) Yu. Kudryavtsev *et al.*: Nucl. Inst. Meth. B **114**, 350 (1996).
7) H. J. Xu *et al.*: Nucl. Inst. Meth. A **333**, 274 (1993).
8) P. Van den Bergh *et al.*:Nucl. Inst. Meth. B **126**, 194(1997).
9) P. Karvonen *et al.*: Nucl. Inst. Meth. B **266**, 4794 (2008).

Third Report on Progress of the Portable Multi-Reflection Time-of-Flight Mass Spectrograph for SlowRI†

P. Schury,*1 Y. Ito,*1 S. Nakamura,*1 S. Naimi, A. Ozawa*1 V. A. Shchepunov.*2 T. Sonoda, A. Takamine, M. Wada, and H. Wollnik*3

[Mass measurements, unstable nuclei, low energy beam]

We continue the development of a multi-reflection time-of-flight (MRTOF) mass spectrometer for use with radioactive ion (RI) beams at the future SlowRI facility. To bridge between the current, existing prototype SlowRI system at RIPS and the future SlowRI at BigRIPS, the MRTOF will initially be attached to its own dedicated gas stopping cell, allowing the system-as-designed to be portable and providing flexibility in commissioning the device by making it possible to use RI sources wherever available. We have achieved mass resolving powers which are competitive with Penning trap mass spectrometry (PTMS). These resolving powers were achieved much faster than could be done by PTMS, allowing us to access very short-lived nuclei.

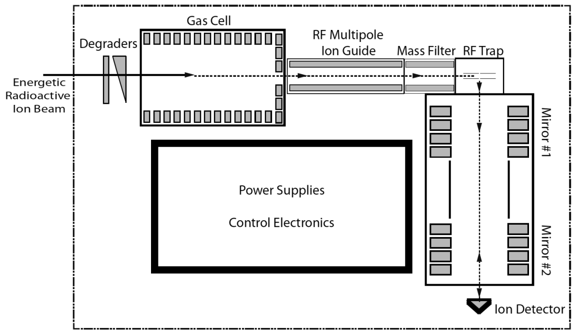

Fig. 1. Planned layout for the portable MRTOF system.

Figure 1 provides a sketch of the system. Energetic ions will be slowed from ≈80 MeV/A to ≈5 MeV total by a solid degrader and further reduced to thermal energies by collision with helium gas. Thermalized ions will then be extracted from the gas cell using a proven RF-carpet technique[1)], then transfered into a radio-frequency (RF) multipole ion beam guide to be transported through a differentially pumped region following the gas cell. An RF quadrupole mass filter selects for a specific ion mass number, removing non-isobaric ions. The isobaric ion ensemble is then cooled in a low-pressure gas-filled RF ion trap before being injected into the MRTOF. The system has been described in detail previously[4,5)].

Initial offline studies have been rather successful, although room for improvement still exists. Using a thermal ion source we can introduce K^+, Rb^+ and Cs^+ ions into the MRTOF to study the behavior in a large range of masses. We find that resolving powers of $R_m = \frac{m}{\Delta m}$ = 140,000 can be achieved for e.g. $^{85}Rb^+$ in ≈8.4 ms. With such a resolving power, it is possible to achieve a relative mass precision of $\frac{\delta m}{m} \approx 2.5\times10^{-7}$ with 1,000 detected ions. It should be noted that a 92 T magnet would be required to achieve a similar precision in the same time using PTMS. Figure 2 provides a typical peak shape for ^{85}Rb.

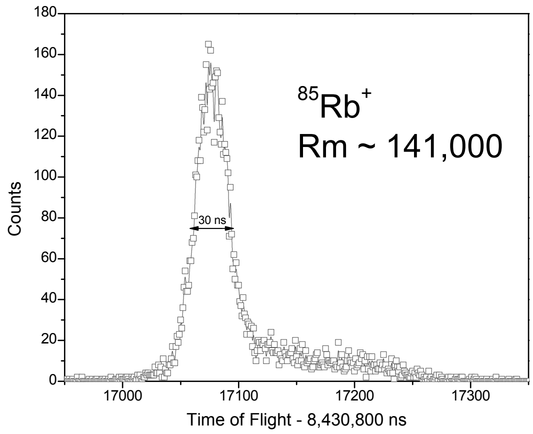

Fig. 2. Typical spectra for ^{85}Rb showing mass resolving power of $R_m \approx$ 141,000.

Approximately 10% of the ions are found in the long tail. This tail is caused by an imperfect tune of the isochronicity of the MRTOF electrostatic mirrors. Within the energy spread acceptance of the mirrors, ions of differing energy penetrate the mirrors to differing depths such that all have the same time-of-flight. The current tune has a smaller than optimal energy spread acceptance, resulting in higher energy ions penetrating more deeply than we desire, leading to these ions having a slightly *increased* time-of-flight. We continue to improve the tune towards achieving the highest possible energy spread acceptance.

Figure 3 shows the equivalent magnetic field required to achieve R_m = 140,000 in the same time as our MRTOF, based on measurements of the alkali elements K, Rb, and Cs from our thermal ion source. As can clearly be seen, we have a large advantage, particularly for heavier nuclei. We believe this will prove to be very useful in a campaign to measure nuclear masses

*1 Tsukuba University, Ibaraki, Japan
*2 SRL, Manchester, England
*3 University of Gießen, Gießen, Germany

of important r-process nuclei – which tend to be both heavy and short-lived. It may also prove very beneficial for the study of very heavy transuranium isotopes or even bio-molecules.

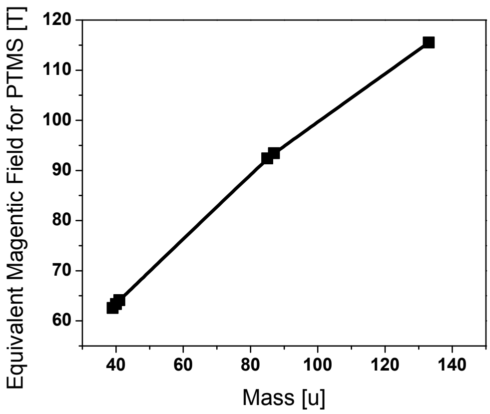

Fig. 3. Equivalent magnetic field required for PTMS to achieve mass resolving powers of $R_m \approx 141{,}000$ in the same time as our MRTOF. In the case of ^{133}Cs, this is 10.5 ms, suitable for very short-lived heavy nuclei.

In order to account for a possible constant offset in the relationship between mass and time-of-flight, such as would be introduced by differing lengths of cables between start and stop signals, two references are needed in order make a measurement. In some cases, such as very light ions and very heavy ions, it may not be easy to find two isobaric references. For this reason we conducted a study of the feasibility of using non-isobaric reference masses. As natural Potassium has three isotopes, it provided an ideal test case for this. We used the abundant isotopes ^{39}K and ^{41}K as references for the very scarce ^{40}K (0.012%). This measurement yielded a deviation from the 2003 Atomic Mass Evaluation[8] of $\Delta m = 40(3)$ keV. This indicates that using non-isobaric references may limit our accuracy to a level of 1 ppm. We believe this error to be caused by ions of differing mass experiencing slightly different electric fields as a function of time. Since the sum difference of experience should be a function of mass difference, it can be inferred that using isobars, which generally have mass differences of less than $0.01u$, as references should allow for an accuracy (though not necessarily precision) on the order of $\frac{\delta m}{m} \approx 10^{-8}$.

Another concern is the possibility that the peak might drift during long-term measurements, such as in the case of very low-yield nuclei. We have developed a PID-based control system to stabilize the bias potentials[6,7] in order to mitigate such possible problems. Figure 4 shows the results of a long duration stability test. As can be clearly seen, the drift is rather small – no more than 4×10^{-7}/hr. This stability is on

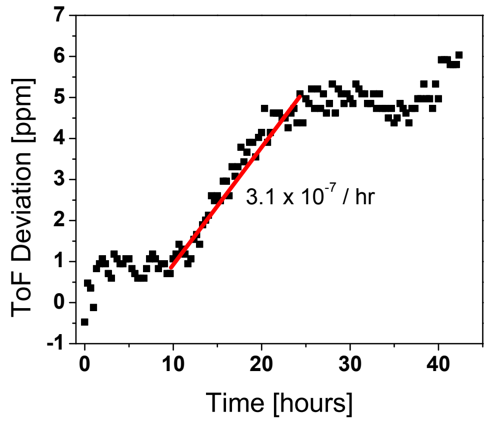

Fig. 4. Measured long-term stability of the MRTOF. The measured average drift of $\approx 1.2\times10^{-7}$/hr is similar to the long-term stability of PTMS. The "fast drift" of 3.1×10^{-7}/hr could indicate a 0.5°C temperature increase in the titanium support structure.

par with the inherent drift in PTMS caused by the magnetic field decay. While the drift is not constant, it is smooth and slow changing and thus we should be able to compensate for it by making reference measurements every few hours, allowing us to perform precision measurements on even the lowest yield nuclei.

One possible source for the measured drift could be thermal expansion of the Titanium support structure for the MRTOF electrodes. Titanium has a thermal coefficient of linear expansion of 8.6 ppm/°C. If thermal expansion we the source of the drift, the observed drift would correspond to a 0.5°C increase in the temperature of the support structure over a 12 hour period. To further stabilize the system, we are studying the effect of all non-PID regulated electronics and may consider how to better maintain the temperature of the electrodes and support structure.

References

1) M. Wada et al., Nucl. Instrum. Methods **B204**, 570 (2003)
2) Y. Ishida, M. Wada and H. Wollnik: Nucl. Instrum. Methods and Phys. Res. **B241**, 982 (2005).
3) Y. Ishida, M. Wada and H. Wollnik: RIKEN Accel. Prog. Rep. **40**, 150 (2007)
4) P. Schury, et al.,Eur. Phys. J. A **42**, 343-348 (2009)
5) P. Schury et al., RIKEN Accel. Prog. Rep. **42**, 189 (2009)
6) M. Wada and P. Schury, RIKEN Accel. Prog. Rep. **43**, 226 (2010)
7) M. Wada et al, RIKEN Accel. Prog. Rep. **44**, (2011)
8) A.H. Wapstra, G. Audi, C. Thibault, Nucl. Phys. A 729: 337-676 (2003)

Status of SCRIT Electron Scattering Facility

M. Wakasugi, Y. Miyashita, M. Togasaki, H. Takehara, T. Hori, M. Hara, S. Ichikawa, H. Takahashi, S. Tamaki, K. Koizumi, M. Moriya, K. Urano, S. Hanada, R. Kitazawa, K. Kurita, T. Suda, T. Tamae

The SCRIT (Self-Confining RI Ion Target) electron scattering facility is now under construction at the Nishina Center. It is consists of electron accelerators, a SCRIT device, an ion transport system, an ISOL system including an RI ion source, and a detector system. Commissioning of the electron storage ring started at the beginning of this year, and it has been continued up to the end of August 2010. We obtained an accumulated beam current greater that 400 mA with a lifetime of 1 AH in the electron storage ring (SR2: SCRIT-equipped RIKEN Storage Ring[1)]), which was constructed in the last fiscal year. After the completion of the first commissioning we installed the SCRIT device and related equipments in SR2. In this paper, details of the accelerator commissioning, SCRIT installation, and status of the facility are reported.

A 150-MeV electron beam accelerated by the RTM (Race-Track Microtron) is injected into SR2, and the beam is accelerated to 700 MeV, which is the maximum energy, in the ring. In February 2010, the commissioning of SR2 was started. The first beam accumulation at the maximum energy of 700 MeV was achieved at February 8, 2010. While the first accumulated beam current was only 0.16 mA, this was the first time that synchrotron light was produced at the Nishina Center (see Fig. 1). Subsequently a machine-tuning procedure aimed at increasing the accumulated beam current was started, and it continued up to the end of August 2010.

Fig. 1. First observed synchrotron light from SR2 on February 8, 2010.

One of the major purposes of machine tuning was to determine good operation points, where stable beam accumulation and acceleration can be achieved. It was also important to optimize the parameters related to the ring components such as the inflector, perturbator, and rf-cavity conditions. In the beam-injection process, the amplitude and synchronization of the pulse magnets were optimized to increase the injection efficiency. The betatron tune values found by adjusting eight quadrupole magnets belonging to two families were ν_x/ν_y = 1.621/1.570 and 1.613/1.565 at the energies of 150 MeV and 700 MeV, respectively. The ramping patterns of the magnets, two 180° bending magnets and eight quadrupole magnets, were determined so that the tune values varied between the above-mentioned tune values during acceleration. RF cavity tuning is quite important for not only achieving higher injection efficiency but also to ensure beam stability during accumulation. It was done by adjusting the position of three tuners and by studying the characteristics[2)] and the response feature of the resonance modes of the three tuners. The machine parameters obtained by the tuning procedure are shown in Table 1, where the stored current is the record value. Figure 2 shows a typical time structure of accumulated beam current. Beam injection to achieve a 400-mA accumulation takes a few minutes and acceleration takes a few minutes; thereafter the beam current decays slowly with a lifetime of about 1 AH. The accumulated beam current was gradually increased after the first commissioning, and it exceeded 400 mA. The integrated beam dose has now reached 64 AH.

Table 1. SR2 machine parameters.

Circumference	(m)	21.95
Beam energy	(MeV)	150-700
Magnetic field	(T)	0.5-2.7
Bending radius	(m)	0.87
Betatron tune	(h/v)	1.62 / 1.57
RF frequency	(MHz)	191.244
Harmonic number		14
RF power at 700MeV	(kW)	20
RF voltage	(kV)	130
Stored current	(mA)	460
Beam emittance	(πmm mrad)	0.4
Lifetime	AH	~1
Total Beam dose	AH	64

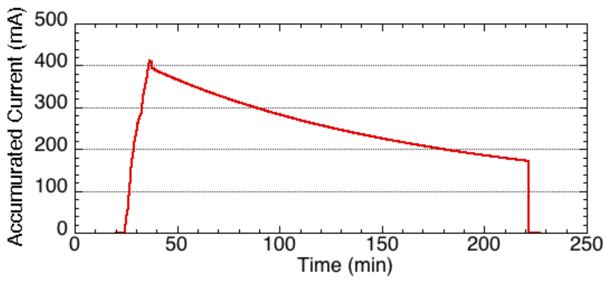

Fig. 2. Time structure of the accumulated beam current for one cycle of injection, acceleration, and accumulation.

While the beam current attained satisfies the requirement of electron scattering experiments, the vacuum level during high-current accumulation still falls short of the target value of 10^{-8} Pa. It is required to maintain a vacuum of 10^{-8} Pa for an accumulated current greater than 300 mA. The vacuum condition can be gradually improved by degassing the inner surface of the vacuum chambers using irradiation with synchrotron radiation. This is the only way to improve the vacuum condition.

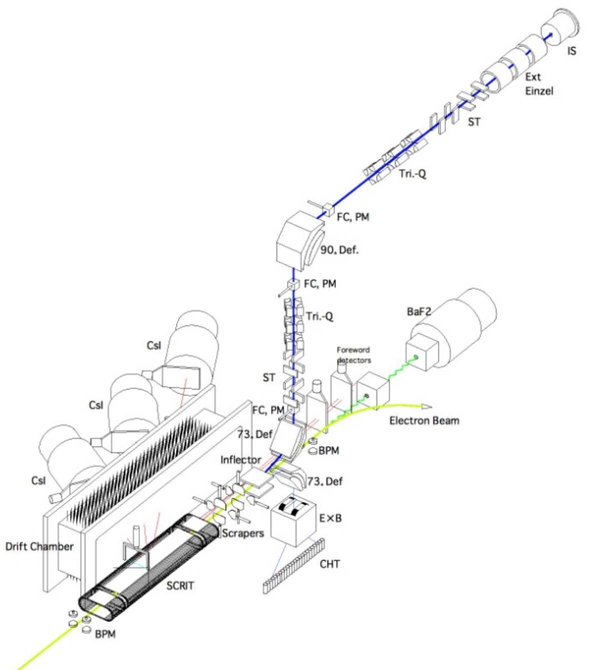

Fig. 3. Schematic view of the SCRIT devices installed in SR2. The ion beam from the ion source (IS) is accelerated by the extractor (EX) and transported in the beam line consisting of steering electrodes (ST), quadrupole lenses (Q), and spherical deflectors (Deff). The beam is merged with the electron beam by using the inflector electrode and is injected into the SCRIT.

We started the installation of the SCRIT devices in the straight section of SR2 at the end of September 2010. The SCRIT system is schematically shown in Fig. 3 and a photograph is shown in Fig. 4. It consists of SCRIT electrodes, a scraper-type beam-monitoring system, an ion analyzer including an E×B filter, an ion-injection beam line, and an ion source for test experiments. Every device placed along the electron-beam axis is two-dimensionally movable. Thus, the overlap between the electron-beam axis and device axis is adjustable by using data from two BPMs placed upstream and downstream of the SCRIT device. While the scraper-type monitor is destructive, it can measure the positions of both the electron beam and injected ion beam. Thus, it is used for fine tuning the injected ion orbit. The ion-beam injection line consists of electrostatic elements such as spherical-shape deflectors, quadrupole lenses, and steering electrodes. Faraday cup and ion profile monitors with a CsI(Th) scintillator, which have been newly developed, are inserted at the focal point of the beam line. This monitor can measure the ion beam current and the profile simultaneously. Details of the ion beam line have been reported in Ref 3. Ions trapped in the SCRIT are extracted and injected into the analyzer in which the ions are separated on the basis of their mass and charge state by the E×B filter. Details of this analyzer system have been reported in Ref. 4. For test experiment aimed at evaluating the performance of the SCRIT system, a stable ^{133}Cs ion source is installed at the end of the ion beam line. The performance of each device in the SCRIT system has already been checked, and the vacuum level of the SCRIT chamber has reached a level of the 10^{-8} Pa, which is identical to in SR2. The SCRIT system is now ready for test experiment, which is planned to start shortly.

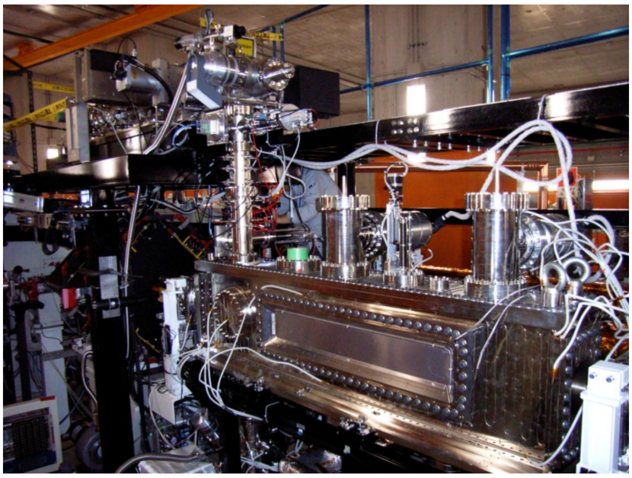

Fig. 4. Photograph of the SCRIT system

Another important apparatus needed at the SCRIT electron scattering facility is an RI ion source and an ISOL system. We plan to construct a photofission RI ion source by using an UCx target, that is driven by a 150-MeV electron beam from the RTM, which is used as an injector for SR2[1]. The ion source is now being constructed and it will be installed in the ISOL system. The test experiment for the ISOL system will start in 2011. Details of the ion source have been reported in Ref. 5.

References

1) M. Wakasugi et al.: RIKEN Acc. Prog. Rep. **43**, 1 (2009).
2) K. Urano et al., in this report.
3) M. Togasaki et al., in this report.
4) Y. Miyashita et al., in this report.
5) Y. Miyashita et al., in this report.

Trapped-ion mass analyzer for SCRIT experiment

Y. Miyashita, M. Togasaki,[*1] H. Takehara,[*2] S. Tamaki,[*1] K. Kurita,[*1] and M. Wakasugi

To realize electron scattering experiments for short-lived nuclei, we have developed a novel internal-target-forming technique named SCRIT (Self-Confining Radioactive Isotope Target). Feasibility studies of the SCRIT technique have been performed using a prototype device in an electron storage ring, i.e., the Kaken Storage Ring (KSR), Kyoto University[1,2].

The SCRIT technique is based on the ion-trapping phenomenon that occurs in an electron storage ring. In this phenomenon, injected RI ions are trapped by a potential well created by a stored electron beam. These trapped ions are used as targets in electron scattering experiments. However, ionized residual gas molecules such as those of H^+, C^+ O^+ H_2O^+ are also trapped in this potential well by electron beam in a vacuum chamber. It is very important to perform the mass and quantitative analyses of the ions trapped in the SCRIT chamber for optimizing the operation of the SCRIT devices. These analyses are used to estimate the purity and yield of the scattering RI target. In the SCRIT experiments, ions are injected into the SCRIT device and are trapped. The trapped ions are extracted by a pulsed electrostatic electrode after a periodic measurement time, and the ions are then mass-separated by an analyzer and are detected by ion detectors.

In a feasibility study conducted at KSR, a prototype SCRIT device was equipped with a mass analyzer component that consisted of one permanent magnet and nine channeltron ion detectors. The prototype SCRIT device was used to check whether the injected ions were trapped by using the SCRIT technique. However, the performance of the analyzer was still unsatisfactory during the mass analysis of the trapped ions. It did not allow to the mass separation of the residual gas molecules and high-charge-state of the injected ions.

An electron accelerator system, a SCRIT target system, and an ISOL system are now under construction at the RIKEN Nishina Center[3]. Moreover, a newly built mass analyzer system has been installed. The new analyzer system consists of an $E\times B$ velocity filter and channeltron ion detectors shown in Figs. 1 and 2, respectively. The $E\times B$ velocity filter has been constructed the basis of a Colutron velocity filter (model 600-B)[4]. The filter consists of magnetic poles and electrostatic electrodes. The electrostatic electrodes consist of 11 plate electrodes and are mounted between the magnetic poles to produce an electric field $\boldsymbol{E}$ perpendicular to the magnetic field $\boldsymbol{B}$. The electrodes and poles are mounted in a vacuum chamber and are designed to be bakeable up to 200 °C. The maximum value of E and B are set to 16,800 V/m and 3,000 gauss, respectively. The ions that are mass-separated by the filter are detected by 44 channeltron detectors; effective detection area of each detector is 4 mm × 15.75 mm. The detectors are located 260 mm downstream of the filter.

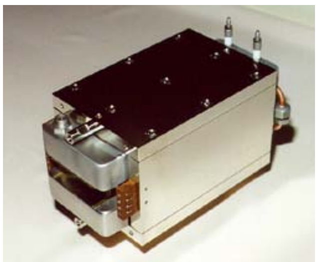

Fig. 1. Photograph of the $E\times B$ velocity filter

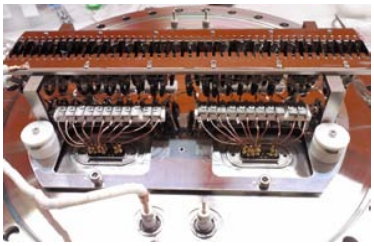

Fig. 2. Photograph of the channeltron ion detectors

The results of a simulation performed by using the SIMION 3D code[5] is shown in Fig. 3. It has been estimated that the mass separation of the $^{132}Sn^+$ ions and highly charged ^{132}Sn ions and other ions that originate in the residual gas is possible by using the new analyzer system.

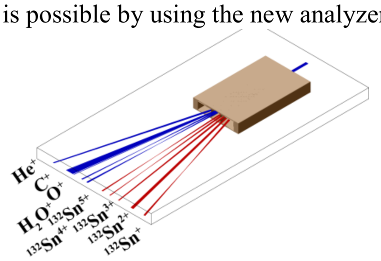

Fig. 3. Simulation results obtained by using the SIMION 3D code. The channeltron detectors are positioned at the left side of the box.

*1 Department of Physics, Rikkyo University
*2 Department of Electrical Engineering, Nagaoka University of Technology

References

1) M. Wakasugi et al.: Phys. Rev. Lett. **100**, 164801 (2008).
2) T. Suda et al.: Phys. Rev. Lett. **102**, 102501 (2009).
3) M. Wakasugi: in this report.
4) L. Wahlin: Nucl. Instr. and Method. **27**, 55 (1964).
5) D.A. Dahl, et al.: Rev. Sci. Instrum. **61**, 607(1990).

Design and Construction of Target/ion Source for ISOL at SCRIT Electron-Scattering Facility

Y. Miyashita, M. Togasaki,[*1] K. Kurita,[*1] T. Suda,[*2] M. Wakasugi and S. Ichikawa

For electron-scattering experiments involving neutron-rich isotopes produced by the photofission of uranium by using the Self-Confining RI Ion Target (SCRIT) technique[1], an Isotope Separation On-Line (ISOL) system is now under design and construction. This new system consists of a target/ion source, an acceleration chamber, and a mass-analyzing magnet. The acceleration chamber contains an extraction electrode and acceleration gap operated at 30 kV and 50 kV maximum, respectively, with respect to the ion-source. An einzel lens is connected mechanically to the extraction electrode, so that the whole assembly can move along the beam axis when the extraction distance is needed to be changed.

The target/ion source is one of the key devices for the ISOL system. For realizing a target/ion source with a wider capability, a Forced Electron Beam Arc Discharge (FEBIAD) type[2] ion source that has been used at ISOLDE at CERN[3] and Holifield Radioactive Ion Beam Facility (HRIBF) at Oak Ridge National Laboratory[4] facilities will be used as the first ion source. Disk-type uranium-carbide (UC_x) will be used as the reaction-target material because of its low vapor pressure at high temperatures and fast release time for radioactive atoms. Figure 1 shows a schematic of the target/ion source at RIKEN. The target container is made of graphite and is designed to have a length of 60 mm with an inner diameter of 15 mm. About 40 g of the UC_x target material with a density of 3.5 g/cm^3 is put in the container, which is attached to a tantalum vaporizer. The photofission distributions in the UC_x target are calculated with the GEANT3 Monte-Carlo simulation[5] and are shown in Figs. 2 and 3.

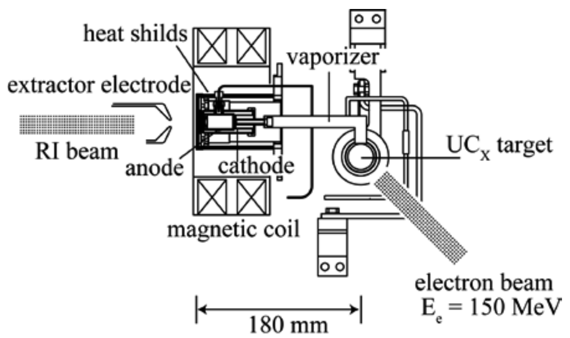

Fig. 1 Schematic of the target/ion source.

*1 Department of Physics, Rikkyo University
*2 Research Center for Electron Photon Science, Tohoku University

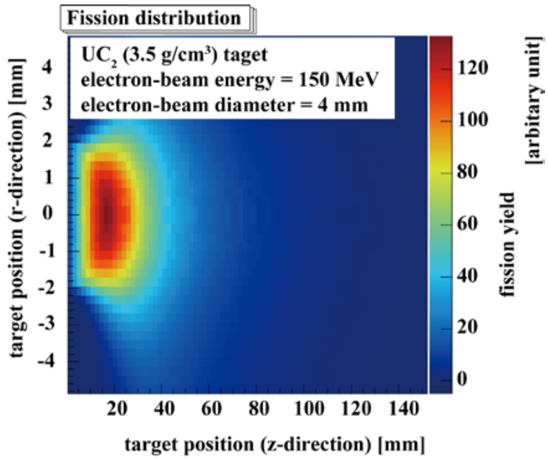

Fig. 2 Fission distributions in the UC_x target for an electron beam with an energy of 150 MeV as calculated by the GEANT3 Monte-Carlo simulation. The diameter of the incident electron beam is 4 mm. The calculated values of the diameter and length of the target are 8 mm and 150 mm, respectively.

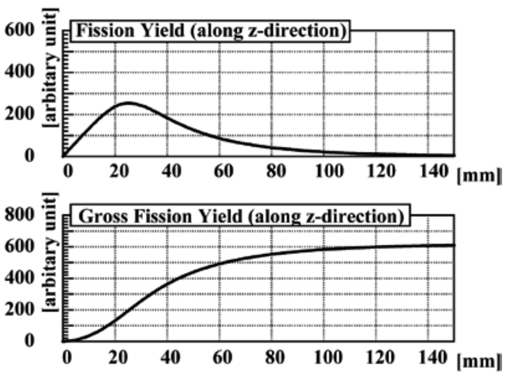

Fig. 3 Fission distributions in the UC_x target along the z-direction as calculated by the GEANT3 Monte-Carlo simulation.

The fission rate in our target system is estimated to be about 2×10^{11} fissions/s for an electron bean with a current of 6.7 μA and energy of 150 MeV. In electron-RI scattering experiments using the SCRIT technique, doubly magic nuclei ^{132}Sn is chosen as the target for the first experiment. According to Frenne[6], the independent yield of ^{132}Sn is estimated to be about 1% of the total fission yield. In addition the separation efficiency of ^{132}Sn isotopes produced by the proton-induced fission of ^{238}U with a FEBIAD-type ion source is measured to be 6.3%[7]. Therefore, the separation yield of ^{132}Sn with our target/ion source is expected to be on the order of 10^8 particles/s.

The target/ion source is assembled into an ion-source housing. A self-contained unit of the target/ion source is connected to the acceleration chamber with a linear-motion carriage having a clamping device by a remotely controlled pneumatic actuator mechanism. The current feedthrough, gas lines, and cooling water connections are simultaneously plugged in/out with this mechanism. The side view of the target/ion source and acceleration chamber is shown in Fig. 4. This system has been installed in the end of FY 2010 in a small room surrounded by a 2-m-thick concrete wall for providing a radiation shield. This small room is in the E21 experimental room at the RIBF (see Fig. 1 in Ref. 8). For the secure maintenance of the highly radioactive contaminated target/ion source, a compact remote-handling system, which consists of a simple transport device and storage section, will be constructed.

References

1) M.Waksugi et al.: Nucl. Instr. and Meth. A **532**,216(2004).
2) R. Kirchner and E. Roeckl: Nucl. Instr. and Meth. **133**, 187(1976).
3) T. Bjornstad et al.: Nucl. Instr. and Meth. B **26**, 174(1987).
4) H.K. Carter et al.: Nucl. Instr. and meth. B **126**, 166(1997).
5) GEANT Detector description and simulation tool,
CERN Program Library Long Write-up W5013, CERN, Geneva, 1994.
6) D. De Frenne et al., Phys. Rev. C **29**, 1908(1984).
7) A. Osa et al.: Nucl. Instr. and Meth. B **266**, 4394 (2008).
8) M. Waksugi et al.: RIKEN Accel, Prog. Rep. **43**, i (2010).

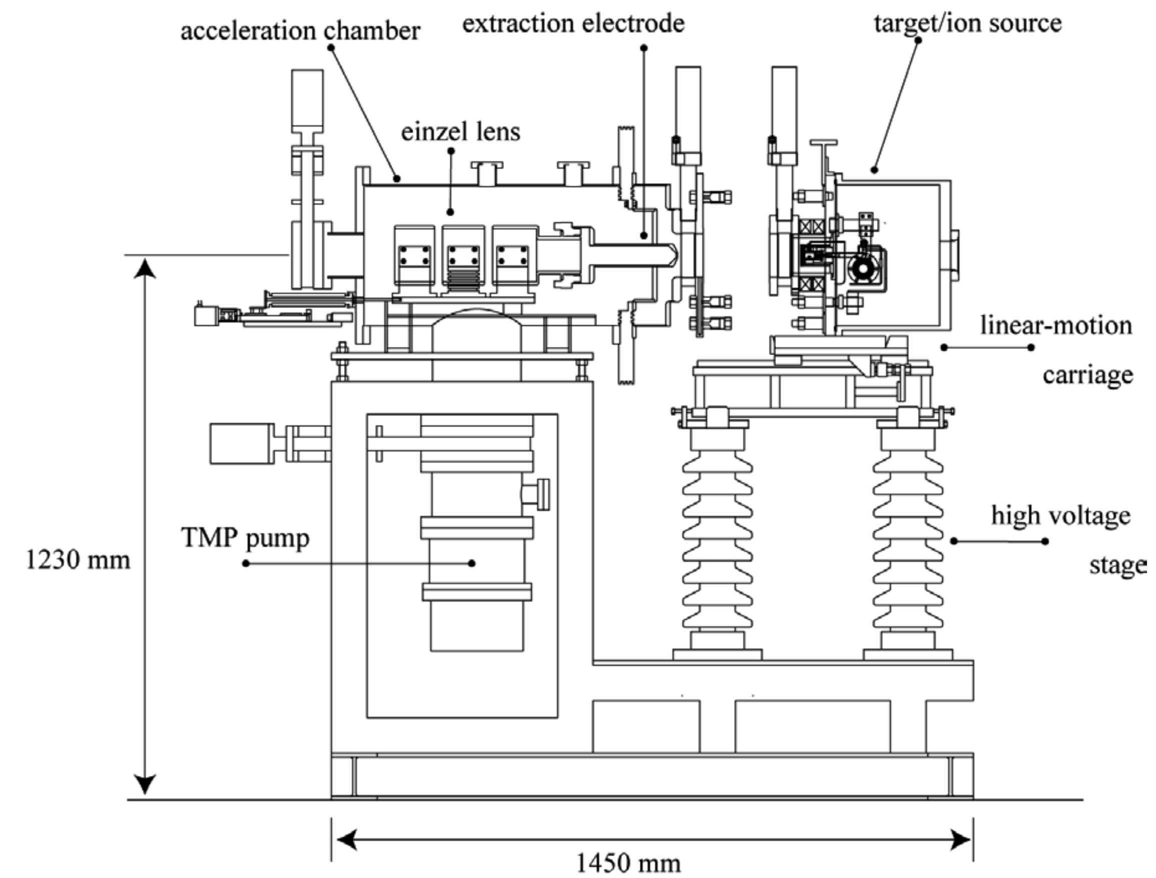

Fig. 4 Side view of the ISOL system assembly.

Development of an Ion-Beam-Profile Monitor for Use in the SCRIT Experiment

M. Togasaki,*1 M. Wakasugi, Y. Miyashita, H. Takehara,*2 and K. Kurita*1

A new experimental system named SCRIT (Self-Confining Radioactive Isotope ion Target)[1,2], which will make electron scattering off short-lived nuclei possible, has been established in our previous researches [3,4]. Encouraged by the success of this new method, we have proposed a new electron storage ring named SR2 (SCRIT-equipped RIKEN Storage Ring)[5]. We are now commissioning the SCRIT experimental system at RIKEN. In this report, we describe the development of an ion-beam-profile monitor installed in an ion-beam transport line for injecting heavy ions, which are internal targets for electron scattering, into the SCRIT.

Figure 1 shows an ion-beam transport line constructed for the performance assessment test of our new SCRIT experimental system. We use a stable nucleus of ^{133}Cs as the ion source. The acceleration energy of ions is 10 keV. In Figure 1, "IBPM" is han ion-beam-profile monitor. Three ion-beam-profile monitors are installed in this beam line as shown in the figure. Figure 2 shows the details of the monitors. They consist of a meshed Faraday cup (aperture ratio : 50%), a CsI(Tl) scintillator, an optical prism, and a CCD camera. The ions that pass through the mesh enter the CsI(Tl) scintillator, and the scintilla-

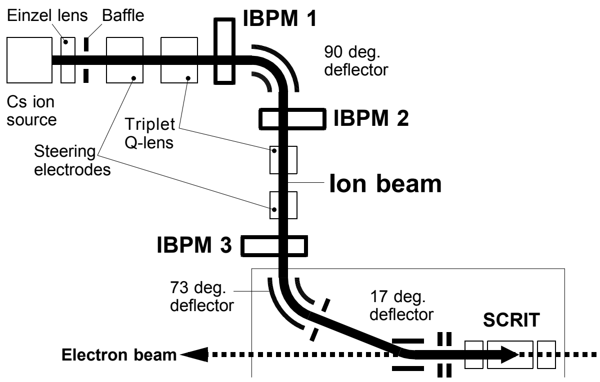

Fig. 1. Ion-beam transport line into the SCRIT. "IBPM" is the ion-beam-profile monitor detailed in Fig. 2.

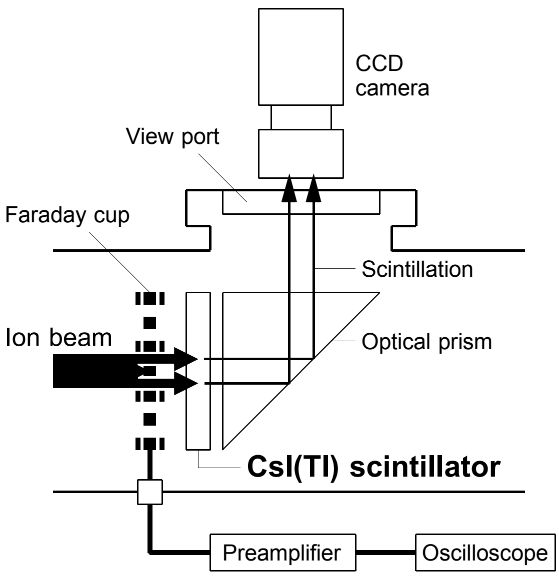

Fig. 2. Ion-beam-profile monitor. This monitor consists of a meshed Faraday cup, a CsI(Tl) scintillator, an optical prism, and a CCD camera.

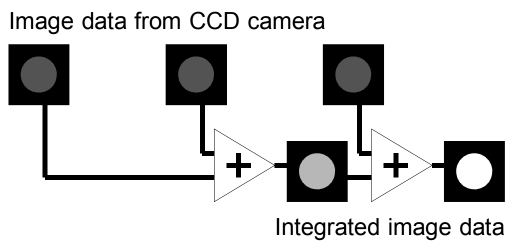

Fig. 3. Conceptual diagram of image data processing. Some dark images obtained from the CCD camera are integrated and a brighter image is created.

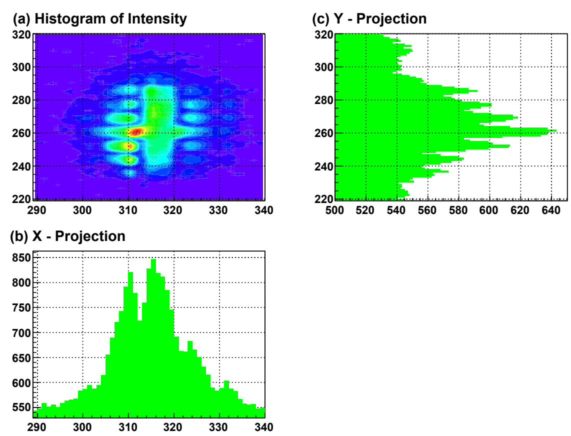

Fig. 4. (a) shows the typical spectra of the ion-beam-profile monitor. (b) and (c) shows the projections of the spectra shown in (a) on X-axis and Y-axis, respectively.

*1 Depertment of Physics, Rikkyo University
*2 Department of Electrical Engineering, Nagaoka University of Technology

tion light emitted by those ions is bent by the prism at right angles and injected into the light-shielded CCD camera that is installed outside the vacuum chamber.

A semi-online analysis of the image data obtained from the camera is performed. Some dark images of the scintillation light are integrated as shown in Figure 3, and a brighter image is created. Because of this process, the beam optical element, such as the triplet Q-lens, can be tuned and a low-intensity ion beam can be transported smoothly while observing the size, shape, or current value of the ion beam.

Figure 4(a) shows the typical spectra of the ion-beam-profile monitor. Figures 4(b) and (c) show the projections of the spectra shown in (a) on X-axis and Y-axis, respectively. The beam current measured by the meshed Faraday cup is 2.7 nA. The image data pertaining to Figure 4 are created from the integration of 60 images, and the time taken to create the image is 60 s. This clearly shows the mesh structure of the Faraday cup and the beam-intensity distribution of the ion beam. The scale of the image is $(0.50\ \mathrm{mm})^2$ per aperture of the mesh. When similar measurements are performed by decreasing the beam current, the shape of the beam can be observed down to about 130 pA.

However, the intensity of an unstable ion beam is expected to be even lower, and thus the performance of the profile monitor is required to be higher. The noise arising during data transfer is the largest. Thus, we are seeking ways to reduce this noise and to obtain a clearer image of ion beams.

References

1) M. Wakasugi, T. Suda, and Y. Yano: Nucl. Instrum. Meth. Phys. Res., Sect. A **532**, 216 (2004).
2) Y. Yano: Nucl. Instrum. Meth. Phys. Res., Sect. B **261**, 1009 (2007).
3) M. Wakasugi et al.: Phys. Rev. Lett. **100**, 164801 (2008).
4) T. Suda et al.: Phys. Rev. Lett. **102**, 102501 (2009).
5) M. Wakasugi et al.: RIKEN Accel. Prog. Rep. **43**, i (2010).

Analysis of the RF cavity in an electron storage ring for SCRIT

K. Urano,*1 M. Moriya,*1 M. Hara, T. Hori, K. Kurita,*1 and M. Wakasugi

An electron-accelerator system is now under conditioning at the RIKEN Nishina Center. The aim of our project is to realize electron-scattering experiments for short-lived unstable nuclei by using the SCRIT technique[1)]. This accelerator system consists of a racetrack microtron injector and a compact synchrotron storage ring. A few components of this system got damaged when it was being moved from the Tanashi works of Sumitomo Heavy Industries. Thus, repair and reconditioning were required for the components. The actual measurements of higher order mode(HOM) of the existing RF cavity and an MW STUDIO©™(MWS) simulation were performed to find a way to avoid the effects of HOMs. For the RF cavity, the RF frequency is 191.2 MHz and the gap voltage is 220 kV.

The renewed storage ring, which is called SR2 (SCRIT-equipped RIKEN Storage Ring), has been designed to accelerate bunched electron beams up to 700 MeV[2)]. The electrons which circulate along the SR2 ring are accelerated by energies of the RF cavity in the ramp-up mode and are compensated for the energy that is lost in the synchrotron-radiation-storage mode. The operation frequency of the RF cavity is chosen to be a harmonic of the beam-revolution frequency. This is done to synchronize the phase of the accelerating field with the beam timing. Furthermore, the suppression of HOMs of the cavity, which are excited by the wakefield of the circulating electrons, is of considerable importance. Some HOMs can be excited by an electromagnetic wave generated by the electron-beam current itself. Though there are theoretically innumerable HOM frequencies possible for the driving RF frequency, the highest excitable HOM frequency is determined by the bunch length. The bunch length can be estimated by performing a Fourier transformation of the crossing time of the electron bunch at the RF cavity.

RF reflection characteristics were measured with a network analyzer and the results were compared with those obtained by MWS simulation. The SR2 cavity is equipped with one auto-tuner and two adjustable tuners. Figure 1 shows the measurement results of the tuner-position dependence of one of the HOM frequencies around 573 MHz. It was found that the maximum change in the HOM frequency was less than half a percent. During the measurements, the auto-tuner was allowed to move for keeping the fundamental frequency fixed at the driving RF frequency. If this specific HOM showed a strong resonance, we could avoid its strength by varying the tuner positions although the tunable range was limited.

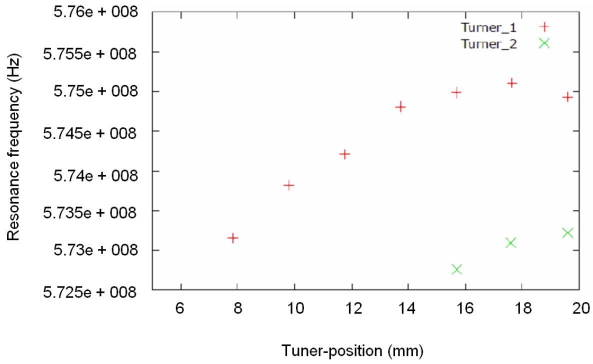

Fig. 1. Tuner-position dependence of a HOM frequency around 573 MHz. When tuner_1-position dependence was measured, tuner_2 was fixed at 12 mm. When tuner_2-position dependence was measured, tuner_1 was fixed at 11 mm. The auto-tuner was allowed to move for keeping the fundamental frequency fixed at the driving RF frequency.

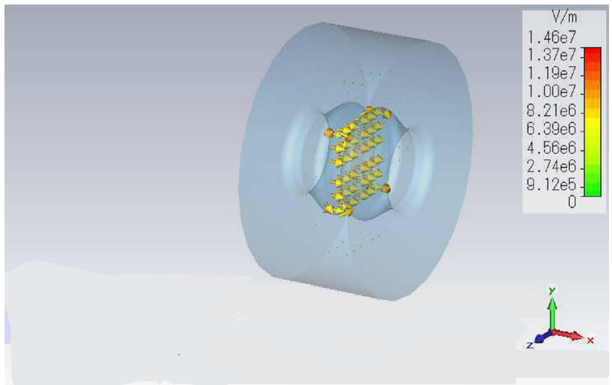

Fig. 2. E-field at RF frequency

Figure 2 shows the electric-field distribution set the beam direction at the driving RF frequency. This distribution was calculated by the MWS simulation. The resonant frequencies of HOMs were roughly searched with a simplified RF-cavity model and a few HOMs were obtained by the MWS simulation.

Table 1 shows a comparison between the resonance frequencies obtained by the measurements and simulation. Four HOMs were obtained by measurements but only two corresponding HOMs were discovered by the simulation. The simulation model needs some refinement for obtaining a better understanding of the HOM structure, considering the discrepancies in the

*1 Rikkyo University

measurements [MHz]	simulation [MHz]
191	194.589 (TM_{010})
573	—
895	862.117 (TM_{020})
916	—
990	974.528 (TM_{210})

Table 1. Comparison of resonance frequencies obtained by the measurements and simulation.

frequencies obtained by the measurements.

Mode TM_{mnp}/TE_{mnp}	Frequency [MHz]	Q values
TM_{010}	194.464	18369
TM_{020}	861.165	25131
TM_{210}	974.093	31746
TM_{221}	1089.701	26753
TM_{011}	1142.764	30138

Table 2. Q values for each HOM as obtained by the MWS simulation.

Table 2 shows the Q values calculated for each HOM by the MWS simulation. Since the bunch-crossing interval is 5.23×10^{-9} sec, an accumulation of electromagnetic energy will occur when the excitation conditions are met. Therefore, the strength of each resonance should be investigated further in detail.

References

1) M. Wakasugi et al.: Phys. Rev. Lett. 100, 164801 (2008).
2) M. Wakasugi et al.: RIKEN. Accel. Prog. Rep. 43, i (2009).

Development of Data-Monitoring System for Pixel Detector of PHENIX Silicon Vertex Tracker†

R. Akimoto,*1 Y. Akiba, A. Taketani, H. Asano,*2 S. Baumgart, O. Drapier,*3 K. Fujiwara,*4 F. Gastaldi,*3 T. Hachiya, J. Kanaya, M. Kasai,*5 J. Koster,*6 K. Kurita,*5 M. Kurosawa, E. J. Mannel,*7 R. Pak,*8 C. Pancake,*9 H. Sako,*10 S. Sato,*10 M. Sekimoto,*11 E. Shafto,*9 W. Sondheim,*12
and the PHENIX VTX group.

A heavy quark (charm and bottom) is one of the key probes used to study the properties of the Quark Gluon Plasma (QGP). A silicon vertex tracker (VTX) has been developed mainly for the measurement of the heavy quarks. The VTX enables the measurement of the tracks of charged particles precisely enough to evaluate the yields of charm and bottom individually. Therefore, the VTX is an essential tool for studying the behavior of charm and bottom inside the QGP.
The VTX has been successfully installed for use in the RHIC-PHENIX experiment and the preparation for operating the VTX has also been completed.
An online data-monitoring system, which is one of the important tools for operating the VTX, has been developed. In this article, the monitoring system for the VTX-pixel detector[1)], which consists of two inner barrels out of four barrels of the VTX, will be described in detail.

The VTX is installed around the PHENIX beam pipe. The first and second barrels of the pixel detector are installed 2.5 cm and 5.0 cm away from the beam axis, respectively. The pixel detector is constructed of two arms, i.e., the west and east arms. In each arm, there are five modules in the first barrel and ten modules in the second barrel. The pixel detector utilizes ALICE1LHCB chips[2)] as readout chips, and a pixel module has 16 of these chips.

The monitoring system is intended to check noisy and dead channels and to optimize the threshold value of the readout chips. The output of the pixel detector, which is binary hit information, is monitored for sampled events during a physics run.
Simulation data were used for the development of the monitoring system. The data used were those per-

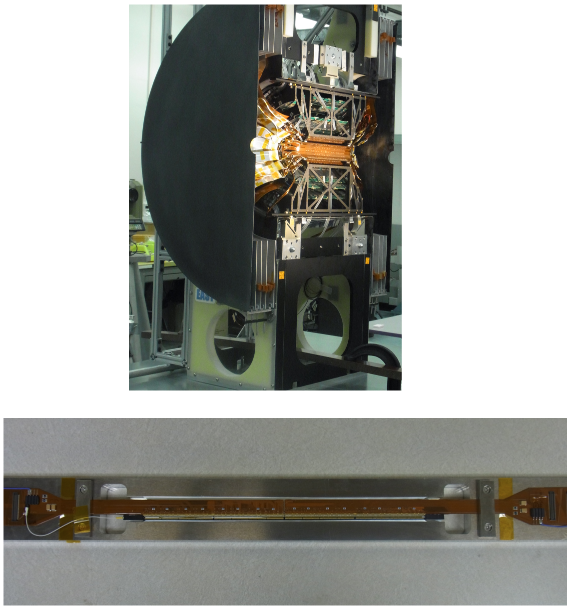

Fig. 1. The upper panel shows an arm of the VTX. The lower panel shows a VTX-pixel module.

taining to $p + p$ events with $\sqrt{s} = 200$ GeV generated using the PYTHIA code[3)], and the detector response was simulated with GEANT3. The noisy and dead channels were not taken into account and the threshold values in the data were set properly. The number of events was 10000.

The noisy channels can be detected by a two-dimensional accumulated hit map, shown in Fig.2. The hit counts of the noisy channels per triggered event are larger than those of the normal channels at the same chip. The left and right panels in Fig.2 show the examples of hit maps of all the pixel modules in the first and second barrels of the west arm, respectively. The horizontal and vertical axes show the channel position in the beam and azimuthal directions, respectively. The labeled numbers on the horizontal and vertical axes represent the readout chips and pixel modules, respectively.
The dead channels can also be detected by the map.
It can be confirmed that the threshold value is optimum for the total hit count of the chips and average cluster size. The upper and lower panels in Fig.3 show the total hit counts of the chips (black) in the first and

*1 Center for Nuclear Study, Graduate School of Science, University of Tokyo, Japan
*2 Kyoto University, Japan
*3 LLR, Ecole Polytechnique, CNRS-IN2P3, France
*4 Tokyo Metropolitan Industrial Technology Research Institute, Japan
*5 Physics Department, Rikkyo University, Japan
*6 RIKEN BNL Research Center, USA
*7 Columbia University, USA
*8 Brookhaven National Laboratory, USA
*9 Stony Brook University, USA
*10 Japan Atomic Energy Agency, Japan
*11 High Energy Accelerator Research Organization, Japan
*12 Los Alamos National Laboratory, USA

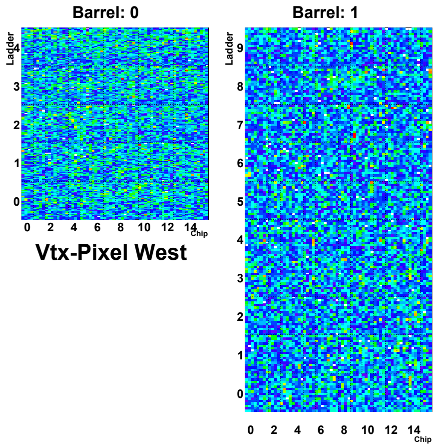

Fig. 2. The left and right panels show the hit maps of the pixel modules in the first and second barrels of the west arm of the pixel detector, respectively.

second barrels of the west arm, respectively. The horizontal axis shows the readout chips and the labeled numbers represent the pixel modules of the readout chips. In this figure, the hit count of the channel that is the hottest in a chip (red) is also shown since extremely noisy channels should be excluded in the evaluation of the total hit counts. The error bar represents the statistical error.

The upper and lower panels in Fig.4 show the average cluster size in each of the chips in the first and second barrels of the west arm, respectively. The horizontal axis shows the readout chips and the labeled numbers represent the pixel modules of the readout chips. The error bar represents the standard error associated with the mean cluster size.

Although the cluster size may be less sensitive to the threshold value than the total hit count, it should be monitored since a large cluster size causes degradation of the position resolution, which is the most important performance parameter for the VTX.

As an outlook, an offline monitor that can analyze the reconstructed track data is being planned to make. This monitor is intended to plot the preliminary results for the VTX performance, such as primary vertex position and the distribution of the distances between the reconstructed track and primary vertex.

References

1) A. Taketani et al.: Nucl. Instr. and Meth. A **623**, 374 (2010).
2) W. Snoeys et al.: Nucl. Instr. and Meth. A **466**, 366 (2001).
3) http://home.thep.lu.se/∼torbjorn/Pythia.html

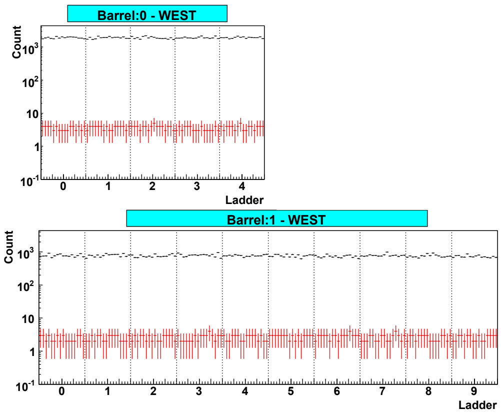

Fig. 3. The upper and lower panels show the total hit counts of the readout chips (black points) and the hit counts of the hottest channels in the chips (red points) in the first and second barrels of the west arm of the pixel detector, respectively.

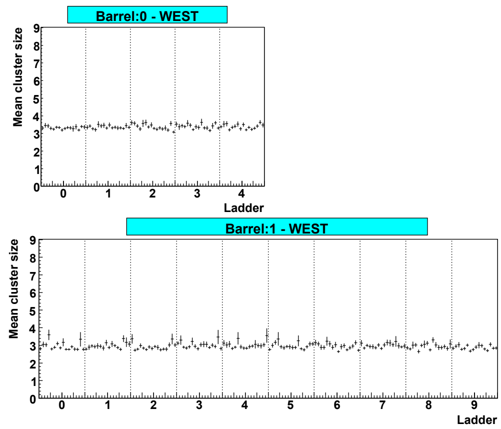

Fig. 4. The upper and lower panels show the average cluster size in the readout chips of the pixel modules in the first and second barrels of the west arm of the pixel detector, respectively.

Construction and Installation of the PHENIX Silicon Vertex Tracker

T. Hachiya, Y. Akiba, R. Akimoto *1, H. Asano, S. Baumgart, O. Drapier, K. Fujiwara *2, F. Gastaldi *3, J. Kanaya, M. Kasai *4, J. Koster, K. Kurita *4, M. Kurosawa, B. Lewis *5, E. Mannel, R. Pak, C. Pancake, B. Sahlmuller *5, H. Sako *6, S. Sato *6, M. Sekimoto *7, E. Shafto, W. Sondheim, M. Stepanov *8, and A. Taketani

A silicon vertex tracker (VTX) was constructed and installed for use in the PHENIX experiment to measure the production of heavy (charm and bottom) quarks in Au + Au and polarized $p+p$ collisions. The production of heavy quarks is a powerful tool for studying the properties of dense partonic matter created in high-energy heavy-ion collisions and for studying the gluon contribution to the spin structure of the proton in polarized $p+p$ collisions. Since heavy quarks are mainly produced by gluon fusions in initial-state hard scattering, the production of heavy quarks is sensitive to the initial states of both the heavy ion and the polarized $p+p$ collisions. In addition, the medium effect can be studied by a comparison between the heavy quark production during Au + Au and $p+p$ collisions.

The heavy quark production was measured in the PHENIX experiment via the measurement of single electrons produced by the semileptonic decays of heavy flavors in Au + Au and polarized p+p collisions[1)]. Suppression of the electron yield was observed at a high transverse momentum in the central Au + Au collisions. There are some models that explain the heavy quark energy loss and the resultant suppression[2)3)]. For the verification of these models, the charm and bottom contributions have to be separated. During the polarized $p+p$ collisions, the separation of charms and bottoms also enables the study of the gluon contributions to the proton spin in different "x" regions.

The VTX is designed to have the capability of measuring the charm and bottom contributions separately [4)5)]. The B meson has a longer lifetime than the D meson; where the flight-path length ($c\tau$) is 122.9 μm for D^0 and 457.2 μm for B^0. The VTX can distinguish between the D and B meson contributions by measuring the displaced vertices of their decays. Therefore, the VTX design requires a vertex-measurement resolution of less than 50 μm.

The VTX consists of four layers of a barrel detector and covers $|\eta| < 1.2$ in pseudorapidity and almost 2π in azimuth. Two inner layers consist of silicon pixel detectors with a pixel size of 50×425 μm^2 and the two outer layers consist of silicon stripixel detectors[6)]. We call a unit of the detector module a "ladder". The detector layers comprise 10, 20, 16, and 24 ladders that are placed around the beam pipe with radii of 2.5, 5.0, 11.7, and 16.6 cm, respectively. A ladder contains silicon sensors, on-board electronics, and a readout bus stacked on a carbon composite stave in which a cooling tube is embedded. The ladders are mounted on carbon barrel supports. We call these supports "barrel mounts". Figure 1 shows a cutaway view of the VTX. The areas surrounded by the red dots and blue dashed lines correspond to the pixel and stripixel layers, respectively. The gray supports are the barrel mounts.

The VTX was constructed and installed into the PHENIX detector in the shutdown period in 2010. The procedure for constructing the VTX was as follows: (1) construction of the four layers individually, (2) assembly of these four layers into the support structure, and (3) a survey of the spatial position of the detector.

In step (1), the ladders were installed into the barrel mounts one by one. There are four barrel mounts holding these four layers individually. During the ladder installation, the barrel mounts were held by a temporary fixture made from an aluminum frame. Figure 2 (a) shows a barrel mount with four installed ladders and the temporary fixture holding the barrel mount. During the installation of a ladder, the edge of the ladder where no sensor was installed was held gently to prevent any accidental contact with the silicon sensor. Cooling tubes and thermal couples were then hooked up to all the ladders to control and monitor the ladder temperature since the silicon sensor is sensitive to temperature and the VTX is required to operate at a low temperature.

A series of "big wheels" which are fan-shaped aluminum plates was attached to the side of the detector. A big wheel is a fixture used for holding and cooling the readout electronics boards. The ladders and readout boards were connected by a bus extender. Figure 2 (b) shows the temporary frame with the installed ladders and big wheels. After the ladder installation, we checked whether the ladder were working properly by measuring their noise and the response to a test pulse.

In step (2), the four layers assembled on the barrel mounts were dismounted from the temporary structure and mated to the support structure individually. The support structure is shown in Figure 2 (c).

In step (3), three-dimensional space positions of all the ladders were determined by a geometrical survey. The survey was performed by triangulation using four identical optical telescopes. After completing steps (2)

*1 Center for Nuclear Study, University of Tokyo
*2 Tokyo Metropolitan Industrial Technology Research Institute
*3 Ecole Polytechnique, France
*4 Rikkyo University
*5 Stony Brook University, USA
*6 Japan Atomic Energy Agency
*7 KEK, High Energy Accelerator Research Organization
*8 University of Massachusetts, USA

and (3), we performed a second check whether all the ladders were working properly. Figure 3 shows a photograph of the fully constructed VTX.

In December 2010, the fully constructed VTX was installed into the PHENIX detector. The optical fibers used for signal readout were connected to front-end electronics boards and the power cables were hooked up. A cooling system was set up and an interlock system was constructed. The interlock system monitors the temperatures of the ladders and the flow rate of the circulating coolant for implementing emergency stop for the VTX. In addition to the interlock system, the humidity inside the VTX and its current consumption were measured for the detailed monitoring. After the installation, we performed a third check of the ladders and examined the cable connections. Then, we confirmed that 96% of both the pixel and stripixel detectors were working properly.

In summary, we completed the construction and installation of the VTX successfully. We started taking the data for the commissioning of the VTX. The new results from the heavy quark measurement by the VTX will come soon.

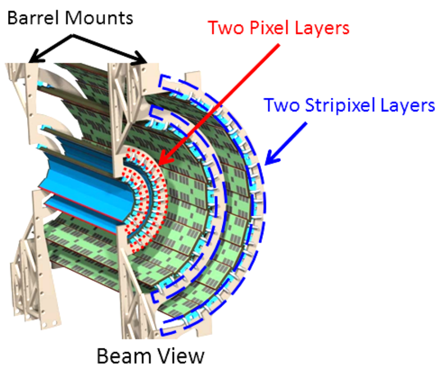

Fig. 1. A cutaway view of the VTX showing the pixel and stripixel ladders. These components are explained in this article.

References
1) A. Adare et al.: Phys. Rev. Lett. **98**, 172301 (2007).
2) Y. L. Dokshitzer and D. E. Kharzeev: Phys. Lett. **B 519**, 199 (2001).
3) M. Djordjevic: Phys. Rev. **C 74**, 064907 (2006).
4) Y. Akiba et al.: RIKEN Accel. Prog. Rep. **44**, 183 (2011).
5) A. Taketani et al.: RIKEN Accel. Prog. Rep. **44**, 181 (2011).
6) R. Nouicer et al.: JINST **4**, P04011 (2009).

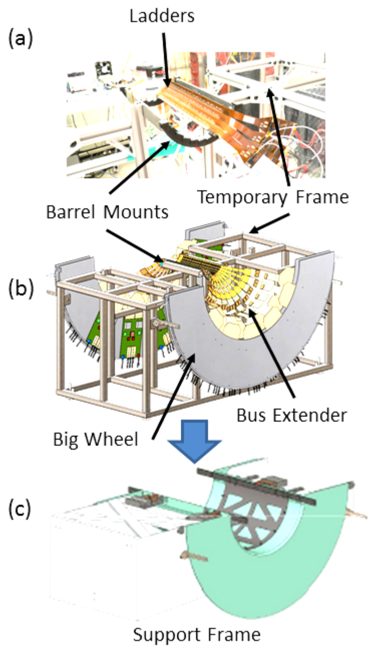

Fig. 2. (a) The ladders installed into the barrel mounts. (b) One of the temporary structures holding the barrel mount. (c) The support structure.

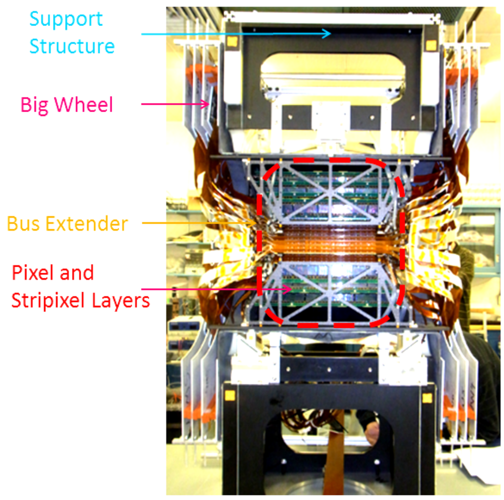

Fig. 3. The constructed VTX detector. All the readout boards, the thermal couples, and cooling tubes are installed.

Completion of Silicon Pixel Detector construction for PHENIX Vertex Tracker†

A. Taketani, Y. Akiba, R. Akimoto,*1 H. Asano,*2 S. Bathe, S. Baumgart, J. Bowen,*3 J. Bryslawskyj,*4 O. Drapier,*5 K. Fujiwara,*6 F. Gastaldi,*5 T. Hachiya, Y. Haki,*7 K. Imai,*8 J. Kanaya, M. Kasai,*7 D. Kawall,*9 J. Koster, K. Kurita,*7 M. Kurosawa, B. Lewis,*10 E. J. Mannel,*11 H. Nishio,*7 C. Oglivie,*3 R. Pak,*12 C. Pancake,*10 P. Riedler,*13 B. Sahlmuller,*10 H. Sako,*8 S. Sato,*8 M. Sekimoto,*14 A. Shaver,*3 E. Shafto,*10 W. Sondheim,*15 M. Stepanov,*9 and the PHENIX VTX group

The pixel detector in PHENIX Vertex Tracker (VTX) at Relativistic Heavy Ion Collider (RHIC) has been constructed in December 2010. The VTX is used to enhance the physics capability in spin and heavy-ion programs. The VTX has four layers of silicon sensors and hence covers $|\eta| \leq 1.2$ and $\Delta\phi \sim 2\pi$.[1)] The VTX is installed 2.5 cm away from the beamline, which is located just outside a beam pipe with a radius of 2 cm. The VTX can be used to identify whether the heavy quarks or light quarks are porduced, because it can track the displaced vertex corresspoinding to long-lived charm mesons and bottom mesons, whose $c\tau$ values are in the range 100 to 400 μm. Further, the jet can can be determined by measuring the momentum of the charged track within the large acceptance of the VTX. In the VTX, pixel detectors are located on the two inner layers, and stripixel detectors[2)] are located on the two outer layers. This article describes the completion of the pixel detector construction.

The pixel ladder consists of four sensor hybrids, a support stave, and two readout buses. The pixel size of the sensor is 50×425 μm^2. Each sensor has $256 \times 32 \times 4$ pixels and is connected to four ALICELHCB1 chips by bump bonding. Signals from the sensor are converted to binary hit pattern data by a preamplifier and a discriminator. These binary data are then transmitted as digital signals to a silicon pixel readout (SPIRO) board via a pixel bus and an extender. The SPIRO board multiplexes the data from eight ALICELHCB1 chips and transmits the data to a front-end module (FEM) through 1.6Gbps serial optical links.

The pixel ladders are mounted on carbon fiber structures, barell mounts. The barrel mounts hold the ladders and attach the enrtire VTX structure. They have four major part, inner west, outer west, inner east, and outer east. The SPIRO boards are mounted on the six aliminum plates, so called big wheels. The big wheels are located at fowared region ($1.2 \leq |\eta| \leq 2.4$). The reigion can be used only for the detection of high momentum muons.

Thirty of the pixel ladders were fabricated and tested in Japan.[3)] Because of the time constraints, we shipped one to five ladders together to BNL when they were fabricated and tested. The first few ladders were shiped to BNL in June 2010, and the last one was reached BNL in October 2010. The ladders were in BNL tested using same the procedure followed in Wako. The ladders that passed the test were mounted on the barrel mount and tested again. The five ladders were installed on the inner-west barrel mount and the big wheels with ten SPIROs were attached. The oute-west barrel mount was assembled with ten ladders and twenty SPIROs. The inner and outer east were assembled in the same manner. All the assembled barrel mounts were moved to another building for final assembly into the VTX. The inner-west and outer-west were merged. Then, the pixel detectors were merged with stripixel detectors. In each step of the assembly process, we confirmed the proper functioning of the ladders ladders working properly by using test benches identical to these at Wako. Quality assurance tests were carried out at the three different satges: just after the arrival of the ladders at BNL, after assembling the on barrel mounts, after assembling in the VTX. The assmbling process including the quality assurance and geometrical survey took nearly two months.[5)] Finally the west-half VTX was moved to the PHENIX experimental hall and installed in the PHENIX detector in December 2010,[4)] as shown in Fig. 1. After the installation, cooling tubes, low-voltage supply lines (LV), bias-voltage supply line (HV), and optical fibers for data acquisition were hooked up. The LV and the HV were controled with an interlock system, which monitors the temperature of the pixel and stripixel ladders. It is necesarry to monitor the detector performance during the physics run. For this purpose, an online monitoring software has been developed.[6)] Moreover, semi-automatic has been developed to determine the threshold level of the discrimnator.

Since the hardwares is installed, the pixel detectors are turned on during beam collision runs. The HV current

*1 University of Tokyo, Japan
*2 Kyoto University, Japan
*3 Iowa State University, USA
*4 Baruch College, City University of New York, USA
*5 LLR, Ecole Polytechnique, CNRS-IN2P3, France
*6 Tokyo Metropolitan Industrial Technology Research Institute, Japan
*7 Rikkyo University, Japan
*8 Japan Atomic Energy Agency, Japan
*9 University Massachusetts, USA
*10 Stony Brook University, USA
*11 Columbia University, USA
*12 Brookhaven National Laboratory, USA
*13 European Organization for Nuclear Research, Switzerland
*14 High Energy Accelerator Research Organization, Japan
*15 Los Alamos National Laboratory, USA

has a nominal value and operatable.

In summary, the pixel detector was constructed and installed in the PHENIX detector system in December 2010. Currentlt, it is under commissioning with the stripixl detector. The system will be operated and will be used to obtain new physics results..

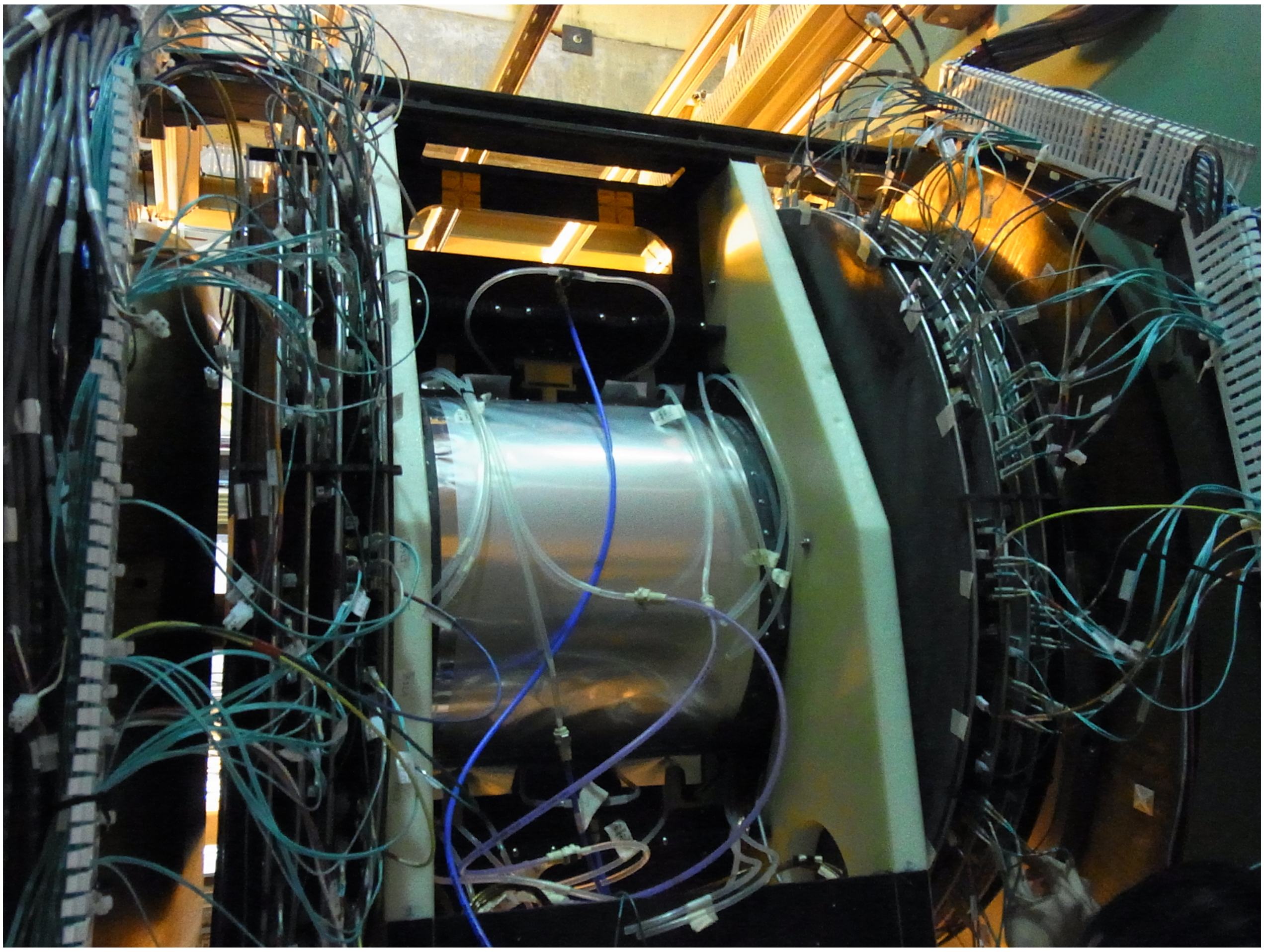

Fig. 1. Installed VTX detector at the center of the PHENIX detector.

References

1) Y. Akiba et al.: RIKEN Accel. Prog. Rep. **44**, 183 (2011)
2) Z. Lee et al.: Nucl. Instr. Meth. A **466**, 366 (2001)
3) M. Kurosawa et al.: RIKEN Accel. Prog. Rep. **44**, 184 (2011)
4) T. Hachiya et al.: RIKEN Accel. Prog. Rep. **44**, 179 (2011)
5) H. Asano et al.: RIKEN Accel. Prog. Rep. **44**, 186 (2011)
6) R. Akimoto et al.: RIKEN Accel. Prog. Rep. **44**, 177 (2011)

PHENIX Silicon Vertex Tracker (VTX)

Y. Akiba, R. Akimoto,[*1] H. Asano,[*2] S. Baumgart, K. Boyle,[*3] V. Cianciolo,[*4] A. Deshpande,[*3,*5] O. Drapier,[*6] A. Enokizono,[*3] K. Fujiwara,[*7] F. Gastaldi,[*6] T. Hachiya, J. Kanaya, M. Kasai,[*8] J. Koster,[*3] K. Kurita,[*8] M. Kurosawa, A. Lebedev,[*9] E. J. Mannel,[*10] R. Nouicer,[*11] C. Ogilvie,[*9] R. Pak,[*11] C. Pancake,[*5] H. Sako,[*12] S. Sato,[*12] M. Sekimoto,[*13] E. Shafto,[*5] W. Sondheim,[*14] A. Taketani, and the PHENIX VTX group

We have constructed a silicon vertex tracker (VTX) for the PHENIX experiment at RHIC. The primary purpose of the detector is to carry out precise measurements of heavy-quark (charm and beauty quarks) production in $A+A$, $p(d)+A$, and polarized $p+p$ collisions. The main physics topics that can be studied by using the VTX are as follows.

- Probing high-density partonic matter
  - Energy loss of heavy quarks (charm and bottom quarks) in dense matter
  - Elliptic flow of heavy quarks in dense matter
  - Open heavy-quark production
  - Medium-induced modification of jets
- Measurement of the gluon spin polarization $\Delta G(x)$ of the nucleon
  - $\Delta G(x)$ through heavy-quark production
  - $\Delta G(x)$ through γ-jet measurement
- Nucleon structure in nuclei
  - Gluon shadowing over a broad x range

The above mentioned measurements are key measurements that are required for future RHIC programs, both for the study of quark-gluon plasma (QGP) in heavy-ion collisions and for the measurement of the nucleon spin-structure functions.

The VTX detector consists of two inner layers of silicon pixel detectors[1)] and two outer layers of silicon strip detectors. The detector covers $|\eta| < 1.2$ in pseudorapidity and $\Delta\phi \approx 2\pi$ in azimuth. The project is funded by RIKEN, the US DOE, and Ecole Polytechnique. The US side of the project commenced in US FY2007. The total budget is US \$4.7 million for the four years FY2007-FY2010. RIKEN is responsible for the inner pixel detectors, while the US DOE is responsible for the strip detectors and mechanical structure.

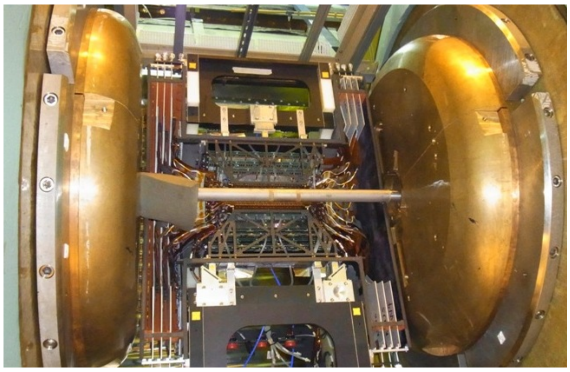

Fig. 1. A photograph of the West VTX detector installed in the PHENIX IR. The interior of the detector can be seen. The two inner layers are pixel detectors and the two outer layers are strip detectors

Each layer of the VTX detector is made of basic building blocks called ladders. Each ladder was fabricated and tested, and the good ladders were then assembled into half-layers of VTX. These half-layers were then assembled together into the East- and the West-half VTX detectors. Construction of the two half-detectors was completed in November 2010, and they were installed in the PHENIX IR by Decdember 1, 2010. Figure 1 shows a photograph of the West VTX detector installed in the PHENIX. VTX will record its first physics data in RUN11 of RHIC, which started in January 2011 and will continue up to the end of June, 2011. Details of the farbricaiton of pixel ladders[2)], the assembly of the VTX detector[3)], commissioning[4)] and online data monitoring[5)] of the pixel subsystem and the offline software[6)] are described in other reports in this volume.

*1 CNS, University of Tokyo, Japan
*2 Kyoto University, Japan
*3 RIKEN BNL Research Center, USA
*4 Oak Ridge National Laboratory, USA
*5 Stony Brook University, USA
*6 LLR, Ecole Polytechnique, CNRS-IN2P3, France
*7 Tokyo Metropolitan Industrial Technology Research Institute, Japan
*8 Rikkyo University, Japan
*9 Iowa State University, USA
*10 Columbia University, USA
*11 Brookhaven National Laboratory, USA
*12 Japan Atomic Energy Agency, Japan
*13 High Energy Accelerator Research Organization, Japan
*14 Los Alamos National Laboratory, USA

References

1) A. Taketani et al.: RIKEN Accel. Prog. Rep. **44**, 181 (2011).
2) M. Kurosawa et al.: RIKEN Accel. Prog. Rep. **44**, 184 (2011).
3) T. Hachiya et al.: RIKEN Accel. Prog. Rep. **44**, 179 (2011).
4) H. Asano et al.: RIKEN Accel. Prog. Rep. **44**, 186 (2011).
5) R. Akimoto et al.: RIKEN Accel. Prog. Rep. **44**, 177 (2011).
6) S. Baumgart et al.: RIKEN Accel. Prog. Rep. **44**, 71 (2011).

Completion of mass production of silicon pixel ladder for PHENIX†

M. Kurosawa, Y. Akiba, R. Akimoto,*1 H. Asano,*2 K. Fujiwara,*4 T. Hachiya J. Kanaya, M. Kasai,*5 J. Koster,*3 K. Kurita,*5 K. Ninomiya,*5 H. Nishio,*5 C. Pancake,*6 H. Sako,*7 S. Sato,*7 M. Sekimoto,*8 E. Shafto,*6 B. Stephen, and A. Taketani

The PHENIX experiment is aimed at elucidating the spin structure of nucleons and studying the hot and dense matter at Relativistic Heavy Ion Collider (RHIC), Brookhaven National Laboratory (BNL). With the aim of enhancing the physics capability of PHENIX for spin and heavy-ion programs, this detector was upgraded with a silicon vertex tracker (VTX) in Dec 2010. The VTX comprises a four-layer barrel detector built from two inner silicon pixel detectors and two outer silicon strip detectors. The mail roles of the VTX are precision measurements of the decay position of heavy-flavor decays and the precision reconstruction of jet axis with its large acceptance.

The silicon pixel ladder is the basic component of a silicon pixel detector. The two inner layers of the silicon pixel detectors are made of 30 silicon pixel ladders. Mass production of the silicon pixel ladders were commenced by the end of 2009 and completed in Oct 2010. In the first stage of the mass production, a few minor changes were made to the assembly procedure for enhancing the production yield. Furthermore, the silicon pixel ladders were subjected to quality assurance (QA) tests in order to ensure operation, before the construction of the silicon pixel detectors. This report presents the improved assembly procedure and a summary of the QA test results for the fabricated silicon pixel ladders.

The structure of a silicon pixel ladder is shown in Fig. 1 The ladder consists of four silicon sensor modules, two readout buses, and a cooling support. Each component is glued with Araldite 2011. The silicon sensor module is an assembly of a silicon pixel sensor and four readout chips[2)] (ALICE1LHCb) bump-bonded to the sensor (bonded by VTT Technical Research Centre of Finland) using bumps with diameters of 25 μm. Each readout chip is electrically connected to the readout buses via bonding wires.

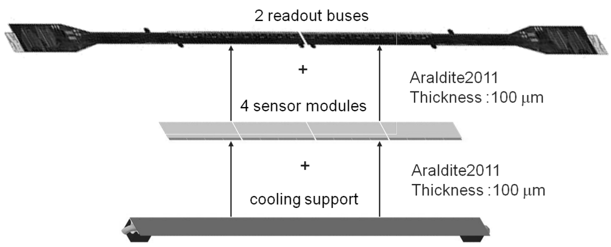

Fig. 1. Structure of the silicon pixel ladder.

The basic procedure of the ladder assembly is described in previous articles[3)4)]. In the assembly process, two issues were identified. The adhesive layer between the sensor modules and the carbon staves had to be flat and thin less than 100 μm thick. First, we used a programmable robot and a compressed-air-controlled syringe with a needle. The adhesive was loaded in to the syringe, and the syringe was moved along the length of the cooling support, all the while spreading a layer of adhesive on the support surface. The uniformity of the applied adhesive layer was maintained by keeping the distance between the tip of the needle and the surface of the cooling support constant. However, the adhesive layer was not sufficiently flat because the surface of the cooling support was slightly distorted and the distance between the needle and the support surface changed. To ensure that the adhesive layer was uniform, a metal mask of 100 μm thickness was used, as shown in Fig. 2. By using the metal mask, the thickness of the applied adhesive layer was maintained at 90 μm.

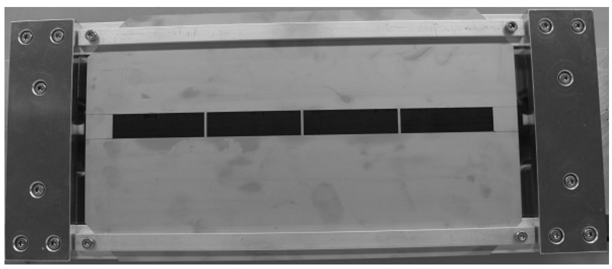

Fig. 2. Metal mask of 100 μm thickness. The part to which the adhesive had to be applied cut out.

Second issue is that the cooling support was not completely glued to adherends. The adherends for the cooling support were readout chips. Since each readout chip had a large power dissipation of 1 W, heat had to be removed by conduction between the readout chip and the cooling support, and the resistance to heat conduction had to be to sufficiently low. Two jigs, a turn jig and a support jig, were used to glue four sensor modules to the cooling support with 25 μm accuracy. The four sensor modules and the cooling support were fixed with the turn jig and the support

*1 Department of Physics, Tokyo University
*2 Department of Physics, Kyoto University
*3 RIKEN BNL Research Center
*4 Tokyo Metropolitan Industrial Technology Research Institute
*5 Department of Physics, Rikkyo University
*6 Department of Physics and Astronomy, Stony Brook University
*7 JAEA
*8 KEK

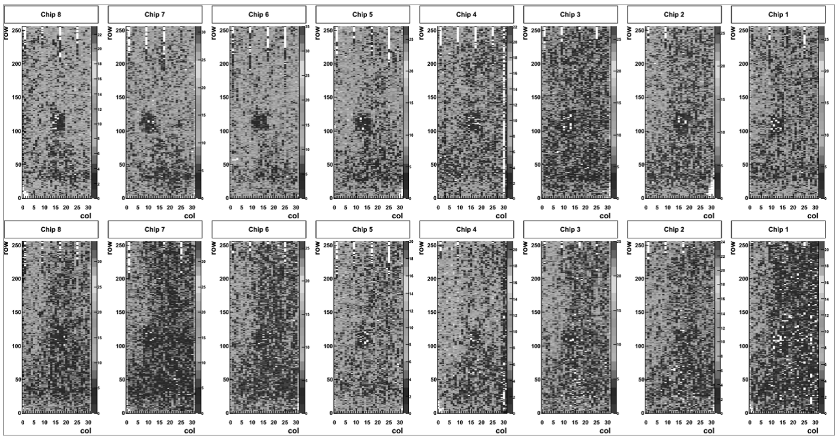

Fig. 4. Response of the pixel ladder to a β source. The horizontal and vertical axes are the pixel position in the column and row directions, respectively. Low gray levels represent a low number of hits.

jig by vacuum contact, respectively. The gap between the sensor module surface and the cooling support surface was controlled by the micrometers mounted on the turn jig. By adjusting the gap width to be almost equal to the adhesive layer thickness with the help of the micrometers, the sensor modules can be adhered to the cooling support if each adherend surface is uniformly flat. However, a few readout chips were distorted by about 20 μm and hence could not be adhered uniformly. In order to minimize such distortions, the four sensor modules were released from the turn jig after they close to the cooling support so that the adhesive could easily spread on the surface of the readout chip by self-weight and surface tension. After optimizing the procedure, 31 ladders could be assembled with a production yield of 95 %.

The bonding wires between the readout chip and the readout bus were encapsulated with a silicon elastomer to avoid damage by the resonant vibrations induced by the Lorentz force in the magnetic field[5]. The maximum resonant violation of the wire was observed at around 6 kHz, which was close to the typical trigger rate. QA tests were performed on all the fabricated ladders before and after the encapsulation. Since rebonding of the wires was impossible after encapsulation, possible problems had to be identified in the QA test before the encapsulation process. The main test items are described in a previous article[3]. The setup for the QA test is shown in Fig. 3 The assembled ladder is connected to Silicon PIxel Read-Out (SPIRO) modules. The SPIRO modules provide electricity and control the readout chip of the sensor module and read out the pixel data. The front-end module (FEM) is an interface between the SPIRO modules and the data acquisition system. NOVEC HFE-7200 was used to cool the readout chips. The ladder was placed in a test-bench container filled with N_2 gas to prevent water condensation due to humidity. Furthermore, an

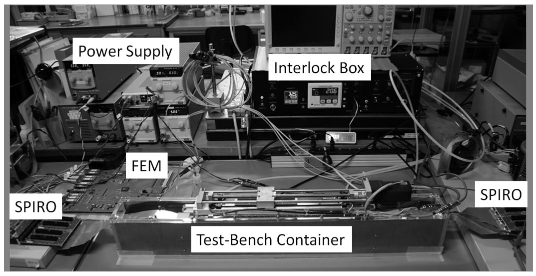

Fig. 3. Setup for QA test.

interlock system was installed to prevent damages to of the ladder by heat and water condensation. All the power supplies for the ladder can trip off under conditions of low flow rate, high flow temperature, and high humidity in the container.

The typical response of the pixel ladder with 16 readout chips to the β source is shown in Fig. 4. Totally, 97 % of the readout chips used for 31 pixel ladders functioned accurately.

In summary, the mass production of the silicon pixel ladder has been completed with a yield of 95 %. QA tests have been performed on the 31 assembled ladders, and 97 % of the readout chips used have been found to function accurately.

References
1) Y. Akiba et al.: RIKEN Accel. Prog. Rep. **44**, 183 (2011).
2) M. Kurosawa et al.: RIKEN Accel. Prog. Rep. **43**, 208 (2010).
3) M. Kasai et al.: RIKEN Accel. Prog. Rep. **41**, 167 (2008).
4) Y. Onuki et al.: RIKEN Accel. Prog. Rep. **40**, 171 (2007).
5) Y. Onuki et al.: RIKEN Accel. Prog. Rep. **42**, 209 (2009).

Commissioning of the Pixel Detector at PHENIX Silicon Vertex Tracker

H. Asano,*1 Y. Akiba, R. Akimoto,*2 J. Koster, D. Oliver, K. Fujiwara,*3 F. Gastaldi, J. Kanaya, M. Kasai,*4 K. Kurita,*4 T. Hachiya, M. Kurosawa, M. Sekimoto,*5 B. Stephen, H. Sako,*6 S. Sato,*6 and A. Taketani

The PHENIX experiment at the Relativistic Heavy Ion Collider (RHIC) at Brookhaven National Laboratory has been upgraded by installing a Silicon Vertex Tracker (VTX).[1)] The VTX consists of two detector sub-systems, a pixel detector and a stripixel detector, and it has been developed for heavy flavor (charm and bottom) measurements; it will take physics data from RUN 11 (RHIC experiment performed in 2011). The pixel detector consists of two layers. The first layer has 10-pixel full ladders and the second layer has a 20-pixel full ladder. ALICELHCb1 chips are used for the readout of pixel signals.[2)] Since the VTX is operated for the first time, commissioning and performance optimization of the pixel detector as well as the stripixel detector is necessary .

Before beginnig the pixel detector commissioning, a cooling system, power supply systems and interlock systems were constructed and checked. Since ALICELHCb1 chips generate heat (1W/cm^2), it is necessary to provide flow (3M NOVEC 7200A) to remove heat from the chips and the readout board on the support structure (BH) (Fig.1). The nominal temperature of the coolant around the detector is 8 °C.
The flow of the coolant is monitored by a flow meter. The temperature of ladders and BHs is measured by thermocouples. Both of them are connected to the interlock system. If the cooling system does not provide enough coolant flow to remove the heat and if the ladder temperature does not increase increase, the associated low voltage (LV) and bias voltage (HV) are removed. The LV and HV systems are controlled by the Graphical User Interface. Their voltage and current are monitored. After the entire cooling and interlock systems were confirmed to work properly, the LV and the HV were applied. An internal analog test pulse was provided to the preamplifier of the ALICELHCb1 chips and the output data were obtained. The chips were confirmed to work properly with real readout electronics, including optical fibers. The dead area of the VTX should be less than 10% of the area of a layer of the pixel detector in acceptance of PHENIX central arm. After testing all ladders,it was found that 97% of the 480 ALICELHCb1 chips were working and the VTX satisfied the required operation condition.

The next step in the commissioning is the calibration of each pixel ladder. The performance of each readout chip is optimized by tuning a subset of the 42 internal Digital-to-Analog Converters(DACs), and adjusting for the best values by using the internal test pulse. Once parameters of the DACs are fixed, noise can be detected by using the self-trigger mode and noisy pixels can be identified and masked. The calibration procedure also includes the determination of the minimum readout threshold value; this is also set by the internal DACs. An automatic threshold scan is carried out for all pixel ladders. Online monitoring and calibration tools have been developed for this scan.

Commissioning of the pixel detector can also be performed by using beam from a 500 GeV p+p collision(Fig.2). The performance with p+p beams will be also studied. The timing of the trigger will be tuned to optimize the detector efficiency. Alignment is also important because precise tracking is required in the VTX to identify primary and secondary vertex reconstruction. We need to know the ladder positions with a precision of 10 μm. The position and orientation of each of the 120 pixel sensors in space are defined by the translation vector and rotation matrix. To align each sensor, survey measurements have been carried out and the translation vector and rotation matrix have been calculated. These data are used as input for the software alignment method. This method uses the p+p collision without any magnetic field and involves the global or local minimization of hit residuals. This procedure is performed and tested with simulation data.

The VTX detector has been successfully installed and the first phase of the detector commissioning has been completed. The plan is to complete the entire commissioning including alignment analysis ,10 weeks of the p+p run and to confirm its tracking capability. The goal is to collect physics data during Au+Au run that will start in April 2011.

*1 Department of Physics,Kyoto University, Japan
*2 Center for Nuclear Study, Graduate School of Science, University of Tokyo, Japan
*3 Tokyo Metropolitan Industrial Technology Research Institute, Japan
*4 Physics Department, Rikkyo University, Japan
*5 KEK, Japan
*6 Japan Atomic Energy Agency, Japan

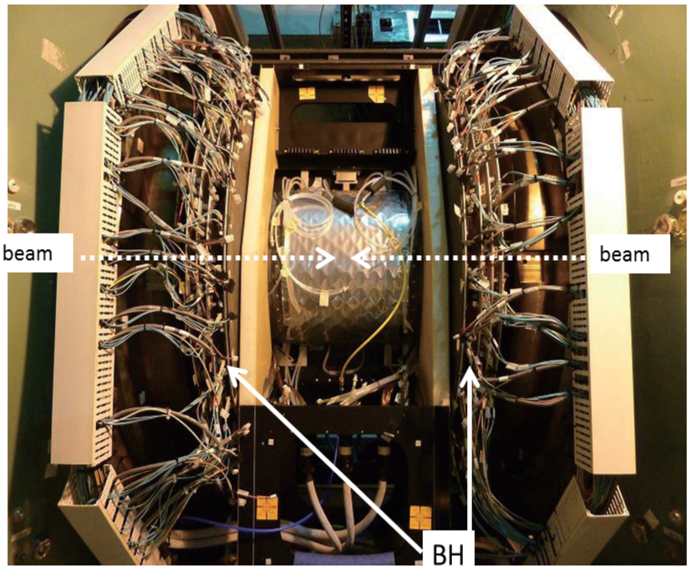

Fig. 1. VTX installed in the PHENIX experiment.

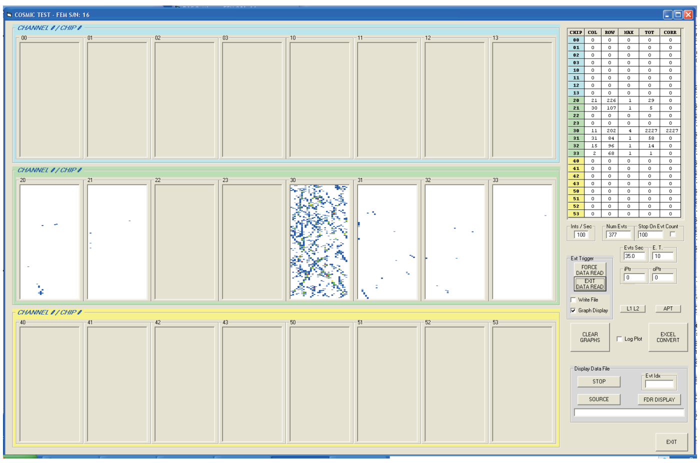

Fig. 2. Hit pattern of pixel ladders in for the beam from the p+p beam collision. In this figure, only one readout chip is enabled to accept a trigger signal. This GUI framework has been developed for the commissioning of the pixel ladder, not for a physics run.

References

1) Proposal for a Silicon Vertex Tracker (VTX) for PHENIX Experiment, 2006
2) A. Taketani et al., Nucl. Instr. and Meth. A 623 (2010) 374

Muon Trigger Performance as Part of RHIC-PHENIX Experiment

Y. Fukao, Y. Imazu, K. Karatsu,[*2] T. Mibe,[*1] T. Murakami,[*2] J. Murata,[*3] K. Nakamura,[*2] I. Nakagawa, S. Park,[*4] R. Seidl, N. Saito,[*1] K. Tanida,[*4] and K. Watanabe,[*3]

[nucleon spin, W boson, polarized parton distribution, electronics, trigger, cathode chamber]

The PHENIX experiment aims to directly investigate the contribution of sea quarks to proton spin by performing measurements of single helicity asymmetry in W boson production. In order to effectively record the W boson production events, we are developing a new trigger system for the PHENIX muon arm.[1)] This trigger system is designed to sort out events with high momentum tracks, which are expected to be muons resulting from W boson decays, by performing online rough momentum measurements. The new trigger system consists of two major upgrades, as shown in Figure 1. One addition is the Muon-Tracker Front-End Electronics Upgrade (MuTRG-FEE) and the other is the Resistive Plate Chamber (RPC). MuTRG-FEE is the additional readout electronics for the muon-tracking chamber, and realizes fast signal transmission for producing the trigger. The RPC provides momentum-sensitive position information and excellent timing resolution. An overview of the trigger system is provided elsewhere.[2)] Half of the MuTRG-FEE (north side) was installed and it was commissioned using proton-proton collisions in 2009. The resulting performance was reported in[3)]. The entire MuTRG-FEE hardware was installed by the end of 2009. In this report, we focus on the results of MuTRG-FEE performance evaluation conducted during the 2010 run of heavy ion collisions and the cosmic ray data taking carried out subsequently. Related articles are provided in this report.[4–6)]

Figure 2 shows the efficiency of the south MuTRG-FEE as a function of track momentum. The efficiency measured with beam is 95% at the plateau. It is consistent with the results of the north side obtained in 2009. The plateau efficiency with cosmic ray becomes 99%. A small discrepancy in the plateau efficiency implies that the data sample includes fake tracks corresponding to muons resulting from hadron decay in the tracking volume or that the efficiency of the MuTRG-FEE decreases depending on the hit rate. The study for analyzing this phenomenon is in progress. The turn-on point of the efficiency in the cosmic ray data is lower than that in the beam data, and this can be attributed to the polar angle distribution of the tracks and the polar angle dependence of the magnetic field strength.

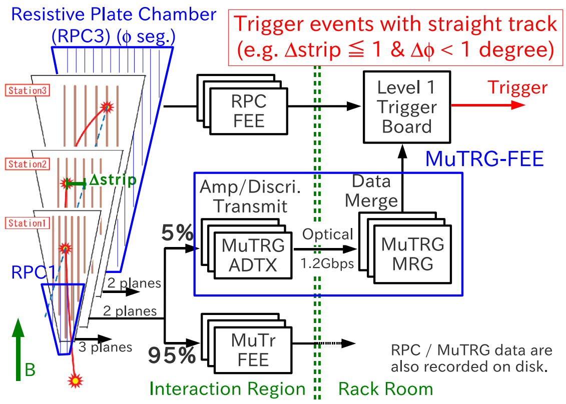

Fig. 1. Schematic of the new W trigger.

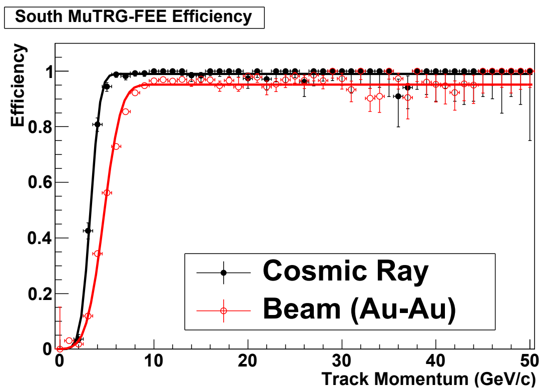

Fig. 2. Efficiency of MuTRG-FEE as a function of track momentum.

We confirmed that the MuTRG-FEE on the south side as well as the north side were operating efficiently. The performance of the MuTRG-FEE was evaluated in the 2010 run and was found to be consistent with that in the 2009 run. The integration of the MuTRG-FEE and the RPC is being developed for the 2011 polarized proton-proton physics production run with 500 GeV in which the new W trigger will become fully operational.

[*1] KEK, Tsukuba, Ibaraki 305-08011, Japan
[*2] Kyoto University, Kitashirakawa-Oiwakecho, Kyoto 606-8502, Japan
[*3] Rikkyo University, Rikkyo, 3-34-1, Nishi-Ikebukuro, Tokyo 171-8501, Japan
[*4] Seoul National University, Seoul, South Korea

References
1) PHENIX collaboration: Nucl. Instrum. Meth. **A 499**, 537 (2003).
2) I. Nakagawa et al.: RIKEN Accel. Prog. Rep. **42** (2009).
3) Y. Fukao et al.: RIKEN Accel. Prog. Rep. **43** (2010).
4) Y. Imazu et al.: RIKEN Accel. Prog. Rep. **44** (2011).
5) R. Seidl et al.: RIKEN Accel. Prog. Rep. **44** (2011).
6) K. Watanabe et al.: RIKEN Accel. Prog. Rep. **44** (2011).

Enhanced Production of Direct Photons in Au+Au Collisions at $\sqrt{s_{NN}} = 200$ GeV and Implications for the Initial Temperature†

Y. Akiba, A. Toia,[*1,*2] Y. Yamaguchi,[*3] for the PHENIX Collaboration

Experimental results obtained from the Relativistic Heavy Ion Collider (RHIC) have established the formation of dense partonic matter in Au + Au collisions at $\sqrt{s_{NN}} = 200$ GeV[1]. The large energy loss of light quarks, gluons, and heavy quarks indicates that the formed matter is very dense. The strong elliptic flow of light and charmed hadrons indicates rapid thermalization. Such a hot, dense medium should emit thermal radiation; the partonic phase has been predicted to be the dominant source of direct photons with $1 < p_T < 3$ GeV/c in Au + Au collisions at RHIC[2].

However, the measurement of real direct photons in such a low p_T range is very difficult due to a large background of photons from hadron decays. To overcome this problem, PHENIX instead measured low-mass high-p_T electron pairs, *i.e.* quasi-real virtual photons. By measuring the electron pairs just above the π^0 mass, the background contribution from π^0 decays is eliminated, reducing the background by a factor of five. Details of the analysis have been published[3,4].

Figure 1 shows[3] the p_T distribution of direct photons obtained in this analysis, together with the direct photon data at higher p_T obtained by real photon measurements using an electromagnetic calorimeter[5,6]. The direct photon spectrum in $p+p$ agrees well with the results of perturbative Quantum Chromo-Dynamics (pQCD) calculation. The direct photon spectrum in Au+Au shows significant excess over the spectrum in $p + p$ scaled with the number of binary collisions. The photon spectrum in Au+Au is fit by an exponential plus binary-scaled photon spectrum in $p+p$. The fitting results are shown by the solid curves in Fig. 1. In central Au+Au collisions, the inverse slope obtained from the fit is $T = 221 \pm 19 \pm 19$ MeV. If the excess direct photons in Au+Au collisions are thermal photons from the hot medium, the inverse slope T is related to the initial temperature $T_{\rm init}$ of the matter. The value of $T_{\rm init}$ is 1.5 to 3 times T due to space-time evolution.

Several hydrodynamical models of thermal photon emission can reproduce the central Au+Au data within a factor of two. In these models the formation of a hot QGP with $T_{\rm init} = 300$ MeV at thermalization time $\tau_0 = 0.6$ fm/c to $T_{\rm init} = 600$ MeV at τ_0=0.15 fm/c is assumed, and the thermal photon emission throughout the space-time evolution of the system is calculated. Lattice QCD predicts a phase transition from hadronic phase to quark gluon plasma at that $T_c \simeq 170$ MeV.

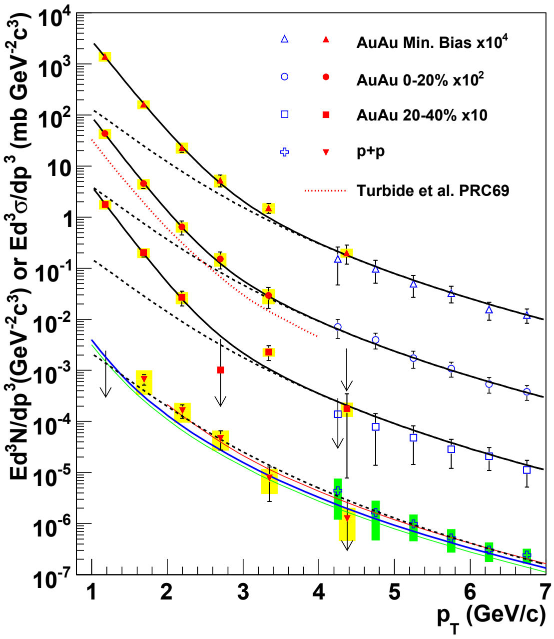

Fig. 1. Invariant cross section ($p + p$) and invariant yield (Au + Au) of direct photons as a function of p_T. The filled points are from this analysis and open points are from previous PHENIX measurements[5,6]. The three curves on the $p+p$ data represent NLO pQCD calculations, and the dashed curves show a modified power-law fit to the $p+p$ data, scaled by $T_{\rm AA}$. The dashed (black) curves are exponential plus the $T_{\rm AA}$ scaled $p+p$ fit. The dotted curve near the 0–20% centrality data is a theory calculation[2].

References

1) K. Adcox et al.: Nucl. Phys. A754, 184 (2005).
2) S. Turbide et al.: Phys. Rev. C69, 014903 (2004).
3) A. Adare et al.: Phys. Rev. Lett. 104, 132301 (2010).
4) A. Adare et al.: Phys. Rev. C81, 034911 (2010).
5) S.S. Adler et al.: Phys. Rev. Lett. 94, 232301 (2005).
6) S.S. Adler et al.: Phys. Rev. Lett. 98, 012002 (2007).

† Condensed from Ref.[3]. This work was also selected for a *Viewpoint* in Physics 3, 28 (2010).

*1 Stony Brook University, USA
*2 Present address: European Organization for Nuclear Research, Switzerland
*3 CNS, University of Tokyo, Japan

Development of wide dynamic readout pad for Time Projection Chamber

K. Fujiwara,[*1] T. Kobayashi,[*1] A. Taketani and T. Isobe

We are developing a readout pad for the Time Projection Chamber (TPC) in the Superconducting Analyser for Multi-Particle Radio-Isotope beam (SAMURAI) spectrometer. It will be located inside the superconducting magnet and will identify various nuclei by measuring dE/dx and determining their momentum. Since the charge induced by an incident charged particle is proportional to the square of the particle's charge, the TPC should have wide dynamic range readout to identify particles with atomic numbers Z in the range 1 to 10.

The TPC is divided into a drift region, gas amplification region, and readout pad region. In principle, the drift and gas amplification parts have good linearity and small crosstalk. However, the readout pad part may have large crosstalk, and accordingly the next input to the pad for a larger signal induced by a higher-Z particle may be a fake signal. Therefore, we started to develop a low-crosstalk readout pad design. The requirement was that the crosstalk level on an adjacent transmission line should be less than 0.5%. This report describes the development of a wide dynamic range TPC pad in a collaborative work involving the Tokyo Metropolitan Industrial Technology Research Institute (TIRI) and RIKEN.

The TPC readout pad is fabricated by the Printed Circuit Board (PCB) technology using the Flame Retardant Type 4 (FR-4) substrate. Its typical structure is shown in Figure 1. The readout pad is connected to the connector through signal lines and holes.

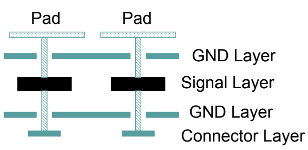

Fig. 1. Cross section of the TPC pad.

The development process consists of the following steps. First, the simplest simulation models are prepared. They are constructed for evaluating the transmission behavior, and therefore, they do not have TPC pads. Figure 2 shows three types of models used in the simulation. Model 1 is a microstripline. Model 2 has signal lines between two ground planes. Model 3 has an additional ground plane between the signal lines in Model 2.

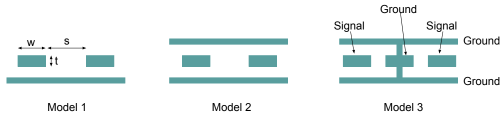

Fig. 2. Cross section of simulation models.

A comparison of the radio-frequency characteristics of the models is presented later. Second, an electromagnetic simulation using the method of momentum[1)] is performed. For the simulation, we use the Advanced Design System (ADS, Agilent Technology). Scattering parameters, which are frequency dependent are calculated in the simulation. Third, the crosstalk level on an adjacent line is evaluated by a simulation. In the simulation, a test pulse is injected into a transmission line and the crosstalk level on a neighboring line is evaluated. Fourth, a test board is fabricated to measure both S_{11} (reflection characteristics) and S_{21} (transmission characteristics) parameters and to evaluate the crosstalk level and line impedance by Time Domain Reflectometry (TDR)[2)]. Finally, the TPC pad is designed by considering the result of the above evaluations.

In the electromagnetic simulation, the width, space, and length of the transmission line are 100 μm, 100 μm, and 36 mm, respectively. This width is required for a realistic TPC configuration. In the RF measurement, SMA connectors and a 50 Ω strip line are built on the boards. The FR-4 substrate is ELC-4762, manufactured by Sumitomo Bakelite Co., Ltd.[3)]. The physical parameters of that are considered are the conductivity ($\sigma = 5.8 \times 10^7$ S/m), relative dielectric constant ($\epsilon = 4.2$), and loss tangent ($\tan\delta = 0.015$). The frequency response of reflection for S_{11} and of transmission for S_{21} are determined in the range 10 MHz to 2.5 GHz. In order to evaluate the crosstalk level on an adjacent line, a test pulse with rise and fall times of 10 ns, a 50 ns pulse width, and a 1 V pulse height is injected into the circuit model with the desired frequency response.

Figure 3 shows the setup for crosstalk measurement. The pulse generator was AFG3252 (Tektronix) and the oscilloscope was DSO80304B (Agilent Technology), which has an analog bandwidth of 3 GHz. When the test pulse was injected into the A line, the crosstalk induced on the B line was measured by using the oscilloscope. In order to measure the lowest crosstalk level, the height of the injected pulse for the A line was set to 4 V instead of 1 V in the simulation.

*1 Electronics Group, Tokyo Metropolitan Industrial Technology Research Institute

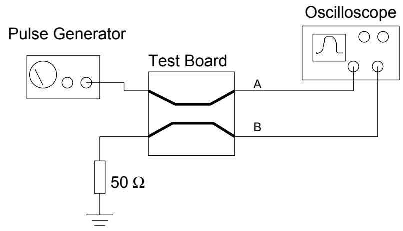

Fig. 3. Setup of crosstalk measurement.

Table 1 shows the result of the simulation and measurement of crosstalk for Model 1, Model 2, and Model 3. Evaluation boards for Model 2 and Model 3 were prepared because of the worst crosstalk level in Model 1. The result of the measurement of crosstalk in Model 2 and Model 3 is shown in Figure 4. The crosstalk level is defined as the value of the maximum signal level on a neighboring line divided by the pulse height of the injected pulse.

Table 1. Crosstalk level for Model 1, Model 2, and Model3.

	Model1	Model 2	Model 3
Simulated	-35.5 dB	-50.2 dB	-61.9 dB
Measured	-	-57.2 dB ± 1.8%	-60.8 dB ± 3.0%

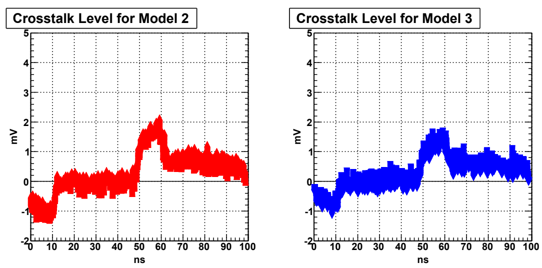

Fig. 4. Crosstalk measurement result for Model 2 and Model 3.

Figure 5 shows the result of the impedance measurement for Model 2 and Model 3. The rise time of the step pulse was set to 35 ps in the simulation and TDR measurement.

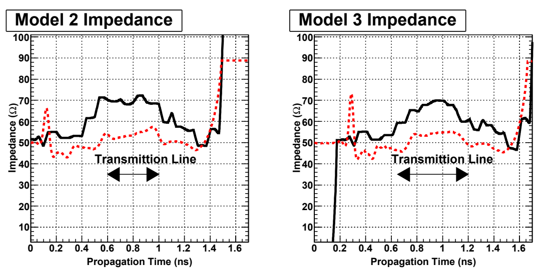

Fig. 5. Impedance measurement result for Model 2 and Model 3 in the time domain. The solid and dashed lines show the simulation and TDR measurement, respectively.

The impedance behavior observed in measurements is very similar to that seen in the simulation, and the measured line impedances of the Model 2 and Model 3 are 55 Ω and in the range 52 Ω to 55 Ω, respectively. The propagation time in the line is approximately 0.5 ns, so that the physical length determined by TDR measurement is consistent with the designed length of 36 mm. The relationship between the physical length (l) and propagation time (t_{pr}) is described by the following equation.

$$l = \frac{c}{\sqrt{\epsilon_r}} \times \frac{1}{2} \times t_{pr} \qquad (1)$$

Here, c is the velocity of light and the ϵ_r is the relative dielectric constant of the FR-4 substrate. The measured physical length is consistent with the designed line length.

Thus, the crosstalk level and the line impedance stability (55 Ω) in Model 3 are better than these in Model 2 because the ground line in Model 3 plays blocks the mutual coupling between two signal lines.

In summary, we are developing a wide dynamic range TPC pad by using the ADS and RF measurement tools. The crosstalk level on an adjacent line is predicted by using the ADS simulator and is evaluated with the pulse generator and oscilloscope. We prepared two evaluation boards for both Model 2 and Model 3, and we found that Model 3 has better crosstalk level (-60.8 dB ± 3.0%). The next step is to design the final TPC pad by considering the obtained result. In February, we will evaluate the final TPC pad by using RF measurement tools.

This work was supported by the collaborative research A at the Tokyo Metropolitan Industrial Technology Research Institute.

References

1) R. F. Harrington: "Field Computation by Moment Method", IEEE Press, New York, 1993.
2) K. Fujiwara: RIKEN Accel. Prog. Rep. **43**, 210, (2010).
3) Sumitomo Bakelite Co., Ltd, http://www.sumibe.co.jp/product/circuitry-electric/circuitry/common/files/catalog001.pdf

Performance of Gas Electron Multiplier with Deuteron Gas

H. Tokieda,*1 S. Ota,*1 T. Hashimoto,*1 S. Michimasa,*1 M. Dozono,*1 H. Matubara,*1 Y. Kikuchi,*1 T. Gunji,*1 H. Yamaguchi,*1 D. M. Kahl,*1 R. Akimoto,*1 H. Hamagaki,*1 S. Kubono,*1 and T. Uesaka*1

1 Introduction

We are developing an active target by using a Gas Electron Multiplier (GEM). The active target is of the "beam transparent type" and is intended for the study of nuclear structures through the measurement of the Gamow-Teller strength in the (d,^{2}He) reaction by using intense (10^6–10^7 Hz) unstable beams of iron group nuclei; inverse kinematics and missing mass spectroscopy will be used in the study. We need to measure the position of the recoiled particle ^{2}He, which decays into two protons instantly, with a low kinetic energy.

The structure of the active target is optimised so as not to measure the beam particles for high beam rates up to 10^7 Hz and with a high incident energy in the range 150–200 MeV/u. Figure 1 shows a photograph (left) and a schematic view (right) of the active target.

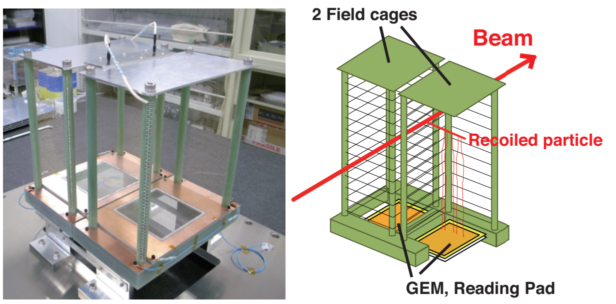

Fig. 1. Photograph (left) and schematic view (right) of the active target. The structure is optimised so as not to measure the beam particles.

The required gas gain, angular resolution, energy resolution, and operation beam rate for this active target to successfully be used in studies are approximately 10^4, 7.5 mrad in the lab frame, 10%, and 10^7 Hz, respectively. This report describes the basic performance of the GEM with D_2 gas at 1 atm.

2 Performance Test

The GEM used in the performance test was a CNS-GEM (for details, see, e.g., [1]). It was 100 μm thick and consisted of an insulator Liquid Crystal Polymer (LCP) and copper. The pitch and diameter of the holes were 140 μm and 70 μm, respectively. Performance test were carried out with a single GEM layer and a double GEM layer mounted in a chamber. We used D_2 gas as the counter gas and CO_2 as the quencher gas at 1 atm.

Figure 2 shows two schematic views of the performance test setup with the single GEM layer mounted in the chamber. The upper panel shows the position of the GEM relative to the 3-compound α source. The lower panel shows the resistive chain to which a high-voltage (HV) is applied.

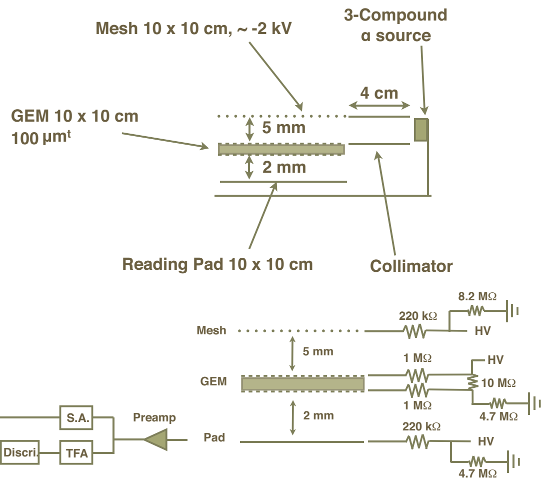

Fig. 2. Two schematic views of the performance test setup for the single GEM layer. The upper panel shows the position of the GEM relative to the 3-compound α source. The lower panel shows the resistive chain to which a HV is applied.

Figure 3 shows a schematic view of the performance test setup with the double GEM layer mounted in the chamber. This view shows the voltage divider resistive chain to which a HV is provided.

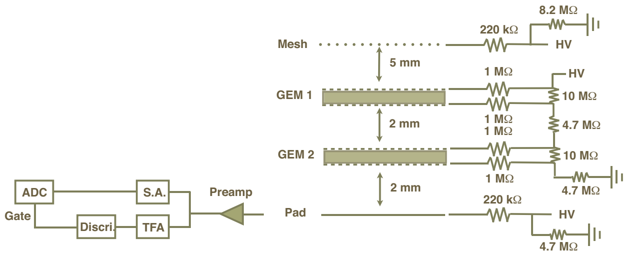

Fig. 3. Schematic view of the performance test setup with the double GEM layer. This view shows the HV being supplied to the resistive chain.

*1 Center for Nuclear Study, Graduate School of Science, University of Tokyo

The distance between the mesh and the top of the GEM and that between the bottom of the GEM and the pad are 5 mm and 2 mm, respectively. In the case of the double GEM layer, the distance between the GEM layers is 2 mm. The size of the mesh, GEM, and pad is the same, 10×10 cm^2. The HV applied to the mesh, GEM, and pad is supplied from a separate HV source. The voltage between the mesh and GEM is denoted by V_f. During our measurement, V_f and the HV applied to the pad were kept at about 300 V and 50 V, respectively.

The voltage applied between the GEM electrodes is denoted by V_{GEM}. We measured the gas gain of the GEM with D_2 gas, as well as the discharge-starting voltage.

Pure D_2 gas and D_2 (95%) + CO_2 (5%) gas were used in this test at 1 atm.

The signal was read out from the pad and input to a preamp (*ORTEC 142AG*) and a shaping amplifier (SA, *ORTEC 572A*). The data were recoded by an ADC (*CAEN V785*). A trigger was provided through a timing-filter amplifier (TFA, *ORTEC 474*) by using the signal read out from the pad.

3 Results

3.1 Pure D_2 Gas

When the V_{GEM} was more than 600 V for pure D_2 gas, discharges occurred. Hence, we were not able to obtain sufficient data to evaluate the gas gain.

3.2 D_2 (95%) + CO_2 (5%) Gas

We measured the gas gain for the single GEM layer and double GEM layer for D_2 (95%) + CO_2 (5%) gas at a pressure of 1 atm. In the single GEM layer, the data were recoded at V_{GEM} values of 710, 716, 720, 730, 740, 750, and 760 V. When the V_{GEM} was 760 V, discharges started. In the double GEM layer, the data were obtained at V_{GEM} values of 600, 625, 650, and 675 V. When the V_{GEM} was 675 V, discharges started.

Figure 4 shows preliminary values of the gas gain as a function of V_{GEM} for the single GEM layer and double GEM layer for D_2 (95%) + CO_2 (5%) gas at a pressure of 1 atm. The highest gas gain for the two GEM layers was about 20 and 280, respectively.

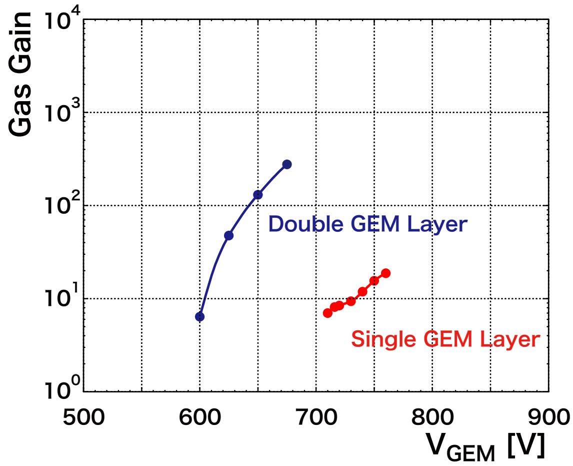

Fig. 4. Preliminary values of the gas gain as a function of V_{GEM} for the single GEM layer and double GEM layer for D_2 (95%) + CO_2 (5%) gas at a pressure of 1 atm.

4 Summary

We measured the gas gain for a single GEM layer and a double GEM layer for D_2 (95%) + CO_2 (5%) gas at a pressure of 1 atm. The highest gas gain for the two types of GEM layers was about 20 and 280, respectively. V_{GEM} at which discharges started was 760 V and 675 V for the single GEM layer and double GEM layer, respectively.

In this test, we were not able to obtain sufficient data to evaluate the gas gain for pure D_2 gas owing discharges at the V_{GEM} value of 600 V.

Data analysis is currently in progress.

References

1) Y. L. Yamaguchi *et al.*: CNS-REP-**69**(2005) 83–84.

Development of resistive-plate-chamber based time-of-flight system for the J-PARC E29 experiment

H. Ohnishi M. Niiyama and N. Tomida

The main aim of the J-PARC E29 experiment is to investigate the interaction between a ϕ meson and nucleons via the ϕ meson nucleus bound state, which is thought to exist[1)] but has not been found experimentally. After the intensive investigation to answer the question how to identify the ϕ meson nucleus bound state we found that the clear missing-mass spectrum for the ϕ meson bound state can be obtained efficiently by $(\bar{p}, \phi)$ spectroscopy when Λ and K^+ are required in the final state. The detailed description of the experiment, including the expected signals over the background, can be found elsewhere[2)] .

The detector is designed to detect forward-going a ϕ meson efficiently with a large acceptance for the decayed particles from the ϕ meson bound state. The conceptual design of the spectrometer is shown in Figure 1. The target is placed at the center of a large dipole magnet under a magnetic field 0.5 T. A cylindrical drift chamber (CDC) surrounds the target to maximize the acceptance for the decay particles, namely K^+ and/or Λ, and the forward-going kaons from the ϕ meson decay. The Time-of-Flight (ToF) wall will be installed immediately outside the CDC for trigger and particle identification (PID). To achieve a separation of more than 2 σ for pions and kaons up to a momentum of 700 MeV/c, the time resolution of the ToF wall must be less than 100 ps. Moreover, a part of the ToF detector system will be in the region of the magnetic field. Hence, the experiment cannot be performed without developing a ToF wall that has good time resolution and can work in a high-magnetic-field environment. To achieve such a high time resolution in the high magnetic field, we selected a resistive plate chamber (RPC) as a candidate for our detector. In this paper, we discuss a resent R&D project for the ToF wall development for the J-PARC E29 experiment.

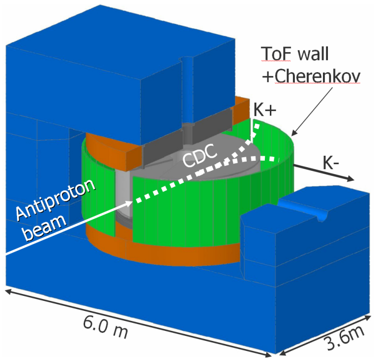

Fig. 1. The conceptual design for the spectrometer.

RPCs made of glass and metal electrodes, with accurately spaced gas gaps of a few hundred micrometers, are known to afford time accuracies of less than 50 ps σ and efficiencies exceeding 95%. This type of detector, which operate at atmospheric pressure with non flammable gases, seems to be well suited for large-area TOF system, and its performance would be comparable to that of the existing scintillator-based TOF detector but the price per channel is significantly lower. The cross section of the prototype MRPC is shown on the left side in Figure 2. The two outer plates are 1-mm-thick pieces of soda-lime glass (resistivity of $\sim 10^{12}$ Ω cm). The four inner plates are also made of soda-lime glass and are 0.5 mm thick. The glass plates have an area of 7×2 cm^2; the size of the electrodes used to apply high voltage is 5×2 cm^2 and they are fabricated using self-adhesive conductive carbon tape. On top of the carbon tape, a 200-μm Polyethylen terephthlate(PET) film is fixed as an insulator layer, and conductive copper tape is attached to the insulator stet signals from the detector. The gas gaps are 280 μm. Normal fishing lines with diameters of 280 μm are used as spacers between the inner plates. The device is mounted in a gas-tight box flushed with a mixture of 5% SF6, 5% normal butane, and 90% $C_2F_4H_2$.

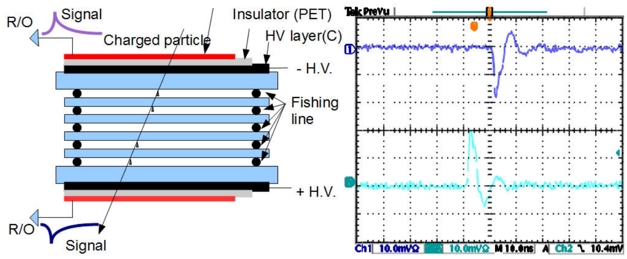

Fig. 2. (Left) Cross section of RPC. (Right) Typical signal from RPC in a cosmic ray event

The first prototype detector has been produced, and the typical signals from the anode and cathode pickup electrodes are shown on the right side in Figure 2. Detailed study of the detector performance is being performed using cosmic rays.

References
1) J. Yamagata-Sekihara *et al.*, Prog. Theor. Phys. 124(2010)147
2) H. Ohnishi *et al.*, J-PARC E29 proposal, http://j-parc.jp/NuclPart/pac_0907/pdf/Ohnishi.pdf, http://j-parc.jp/NuclPart/pac_1007/pdf/KEK_J-PARC-PAC2010-02.pdf

Research on the GEM substrate

K. Komiya,[*1] M. Wakabayashi,[*1] K. Fujiwara,[*1] T. Kobayashi,[*1] H. Hamagaki,[*2] and A. Taketani

The Gas Electron Multiplier(GEM) is a micro-pattern gas detector. In general, polymid[1](PI) and liquid crystal polymers (LCPs) have been successfully used as the substrate materials. However, PI and LCPs have the problem of breakdown during operations. We think that this problem is caused by the degradation of voltage resistance. The problem may to be solved by replacing PI and LCPs with other types of films. Therefore we have evaluated several films by using the methods of Japanese Industrial Standards (JIS) etc. In this article, we describe the results of the evaluation.

Usually, the GEM consists of PI and LCP films. Both PI and LCPs are used in flexible printed circuits (FPCs). They have the advantages of heat hardiness and the films are sold in metal-deposited states. PI and LCP films can be easily procured from the market , but they are expensive. Therefore, we propose polyethylene terephtalate[2](PET) and polyethylene naphthalate[3] (PEN) films as replacements for PI and LCP films. PET and PEN have similar properties, except for the heat hardiness. These films are easily obtainable, but are not available in metal-deposited states. Because of their low heat hardiness, it is difficult to deposit a metal on both sides without thermal damage. However, we suspect that by using low-temperature deposition, a metal can be deposited on both sides of PET and PEN. The characteristics of PI, PET, and PEN are summarized in Table 1. The heat hardiness of GEM is not important because GEM substrates do not get heated to high temperatures during the operation of GEM. We also examined the volume resistivity and characteristics of sputtered copper for films of the three materials, and we evaluated whether those films can be used as GEM substrate materials.

Table 1. Characteristics of PI, PET, and PEN.

	PI	PET	PEN
Cost	×	○	○
Heat hardiness (°C)	>500	258	269
Water absorption (%)	2.9	0.4	0.3
Chemical properties	○	○	○

○: Good, ×: Poor

For comparing the basic characteristics of the three films, we evaluate the volume resistivity of these films by using a JIS. The volume resistivity measurement is carried out in accordance with JIS C2318[4]. The test instruments are a HP4329 High Resistance Meter and a 16008A Resistivity Cell. In JIS C2318, the applied voltage is 100 V during the measurement. However, we measure the volume resistivity with an applied voltage of 1000 V because GEM is usually operated with an applied voltage in the range 1000 V to 3000 V. The measured volume resistivity values are given in Table 2. The volume resistivities of PET and PEN are higher than that of PI at the applied voltage of 1000 V. So we are of the view that PET and PEN could be good GEM substrate materials.

Table 2. Results of volume measurements (Ω·cm).

Applied voltage	PI	PET	PEN
100 V	4.3×10^{17}	2.2×10^{17}	6.1×10^{17}
1000 V	4.3×10^{17}	7.1×10^{17}	7.1×10^{17}

Next, we evaluated films of the tree materials coated with the copper. The presence of a sputtered copper coating on the films was confirmed by Electron Cyclotron Resonance (ECR) sputtering. The ECR sputtering system used was EIS-220 (Elionix Co., Ltd.). An oxygen-free copper target with a purity of 99.99% was sputtered on the films with dimensions of 50 mm × 50 mm. The conditions of the sputtering process ware as follows: The acceleration voltage was 1.8 kV and the microwave power was 100 W. The Ar flow rate was set at 0.7 sccm (standard cubic centimeter per minute). The sputtering duration was 30 min. The monitored beam current during the operation was 0.45 μA/cm^2 under these conditions. We could deposit copper without melting or bending the films. Scanning electron microscopy (SEM) images of the surfaces of the films are shown in Figure 1.

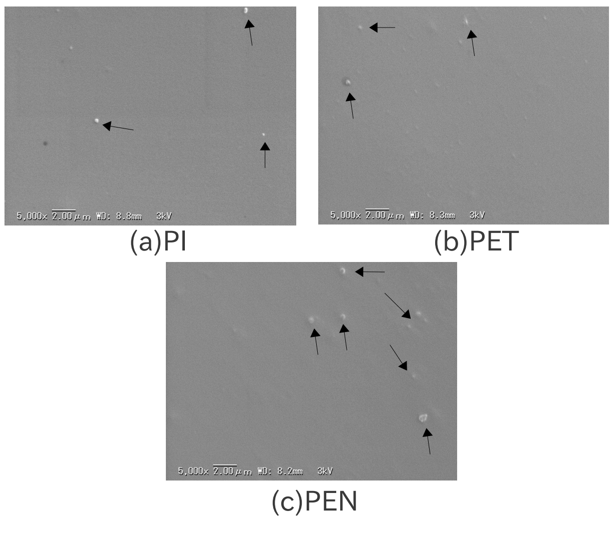

(a)PI (b)PET (c)PEN

Fig. 1. SEM images of the metal-deposited films. The arrows indicate contamination after the sputtering.

*1 Electronics Group, Tokyo Metropolitan Industrial Technology Research Institute
*2 Center for Nuclear Study, University of Tokyo

The contact resistance of the copper coating was measured by the Kelvin method[5]. The test equipment used was a contact resistance meter (CRS-113-AU, Yamasakiseki Co., Ltd.). The configuration of the measuring devices is schematically shown in Figure 2. The contact resistance was obtained from measurements of the current and voltage preformed using probe needles. The distance between the voltage probe (Probe A) and the current probe (Probe C) was 10 mm and the diameter of the probes was 0.5 mm. In the test, we applied a contact load of 50 gf. The contact resistance values obtained are shown in Table 3. The conductivity of the films was improved by ECR sputtering process.

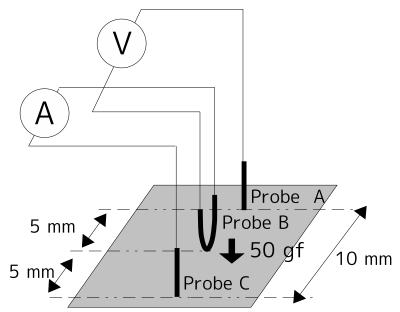

Fig. 2. Configuration used for the contact resistance measurements

Table 3. Contact resistance values.

	PI	PET	PEN
Contact resistance	0.83 Ω	0.68 Ω	0.57 Ω

We measured the peel strength in accordance with JIS H8504[6]. This method is specified for the adhesion evaluation of a metal-coated surface. The measuring points and the method are schematically shown in Figure 3. First, a grid pattern with hundred 1mm × 1mm squares was formed by using a craft knife on the copper-coating side. Second, a tape (Nichiban Co., Ltd. Type #18 mm) was put on the surface. The tape was then pulled by maintaining the angle between the tape and substrate surface at 90°. Finally, by counting the number of peeled cells, we evaluated the peel strength. In this study, the peeling test was not carried out for many samples of the substrate materials. The peel strength of the copper coating on all films was similar.

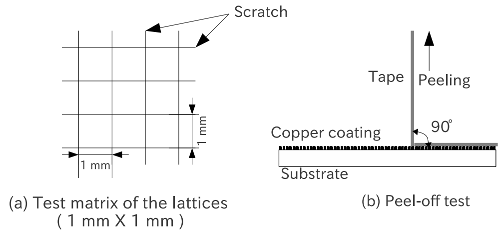

Fig. 3. Schematic of the peel strength test.

In summary, the evaluation of the volume resistivity, contact resistance, and peel strength of PI, PET, and PEN films by JIS methods shows that these films have similar properties. It is confirmed that the PET and PEN films are potential GEM substrate materials. In the next step, we shall try to fabricate a prototype of GEM with these films and test the films in a real setting. We will examine the effects of the volume resistivity, contact resistivity, and peel strength on the film stability.

References

1) The technical data sheet of Kapton, Du Pont-Toray Co., Ltd.
⟨http://www.td-net.co.jp/kapton/index.html⟩
2) The technical data sheet of Tetoron, Teijin Dupont Films Co., Ltd.
⟨http://www.teijindupontfilms.jp/product/name/pet/index.html⟩
3) The technical data sheet of Teonex, Teijin Dupont Films Co., Ltd.
⟨http://www.teijindupontfilms.jp/product/name/pen/index.html⟩
4) JIS C2318 Balanced biaxially oriented polyethylene terephthalate films used for electrical purposes, Japanese Industrial Standards.
5) The instruction manual of CRS-113-AU, Yamasakiseki Co., Ltd.
6) JIS H8504 Methods of adhesion test for metallic coatings, Japanese Industrial Standards.

Development of ionization chamber for superheavy elements

K. Ozeki, T. Sumita,[*1] K. Morimoto, K. Morita, and A. Yoneda

In the superheavy element laboratory, we have been developing an ionization chamber (IC) to determine the mass numbers of superheavy elements. This IC is intended to measure the kinetic energies that are less than 100 keV/nucleon. A detailed configuration of the IC and the voltage applied to each of its components are described in Ref. 1. The stand-alone tests conducted for the IC are reported in Ref. 2.

In the present study, the mass number (A) is obtained from the total kinetic energy (E) and Lorentz factor (γ) of a particle, which are measured by the IC and a time of flight (TOF) detector. A is derived using the relation

$$A = \frac{E}{m_u(\gamma - 1)},$$

where m_u is the atomic mass unit. The experimental setup is shown in Fig. 1. A ^{28}Si beam from the Pelletron[3] passes through the TOF detector and stops in the IC. Ethane gas was filled in the IC. A terminal voltage of 1.3 MV was applied. Two ^{28}Si beams with energies of 6.5 MeV and 7.8 MeV were extracted simultaneously.

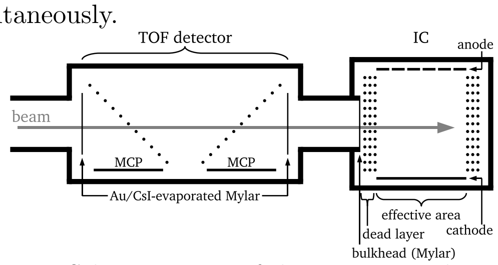

Fig. 1. Schematic view of the experimental setup.

A two-dimensional plot of $m_u(\gamma_{TOF} - 1)$ and E_{msr} is shown in Fig. 2, where γ_{TOF} is γ obtained from the TOF measurement, and E_{msr} is E measured by the IC. We cannot derive actual mass numbers from the pair of E_{msr} and γ_{TOF} values obtained here, since the beam energy decreases because of the energy loss in the materials between the TOF detector and effective area of the IC. These materials are the downstream Mylar film of the TOF detector, bulkhead, and dead layer of the IC.

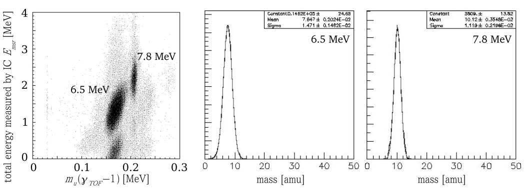

Fig. 2. Left panel: Two-dimensional plot of $m_u(\gamma_{TOF} - 1)$ and E_{msr}. Center and right panels: Mass distributions obtained from E_{msr} and γ_{TOF} for beam energies of 6.5 MeV and 7.8 MeV.

By using the procedure described below, we derived the mass numbers consistently. In other words, $A_{as} = A_{ob}$ was achieved, where A_{as} is the assumed A for estimating the energy loss and A_{ob} is the obtained A. The energy loss was estimated using the Stopping and Range of Ions in Matter (SRIM) code[4].

(1) Obtain E_{TOF} (the energy in the TOF detector) from γ_{TOF}, assuming A_{as} for each locus.
(2) Estimate the energy loss in the aforementioned materials, assuming that the energy of $^{A_{as}}$Si is equal to E_{TOF}. E_{IC} (the energy at the entrance of the effective area of the IC) is then obtained.
(3) Obtain γ_{IC} (γ at the entrance of the effective area of the IC) from E_{IC}.
(4) Obtain A_{ob} from E_{msr} and γ_{IC}.

A two-dimensional plot of $m_u(\gamma_{IC} - 1)$ and E_{msr} is shown in Fig. 3. The absolute values of mass obtained are 26.9 [amu] and 28.4 [amu] for the beam energies of 6.5 MeV and 7.8 MeV, respectively. The widths of mass distribution (rms) are 1.7 [amu] and 1.4 [amu] for the beam energies of 6.5 MeV and 7.8 MeV, respectively. The reason for a lower mass obtained for a lower energy is considered to exist in the energy dependence of the average ionization energy (W-value). It reduces the sensitivity of the IC for dE/dx just before a particle stops. Therefore, E_{msr} is less than the actual energy by a certain amount, and the difference is not negligible when the total energy is few hundred keV/nucleon. Thus, a W-value-correction method is required.

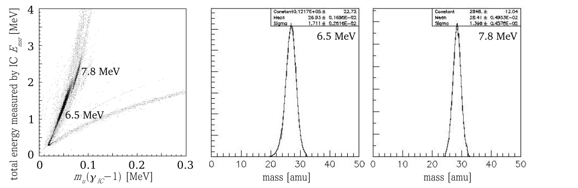

Fig. 3. Left panel: Two-dimensional plot of $m_u(\gamma_{IC} - 1)$ and E_{msr}. Center and right panels: Mass distributions obtained from E_{msr} and γ_{IC} for beam energies of 6.5 MeV and 7.8 MeV.

The mass resolution improves for higher energies (20∼30 MeV in the superheavy region), because the loci shown in Fig. 3 recede from the origin. On the other hand, the increase in energy straggling with the increase in the mass number degrades the mass resolution. For measuring the masses of heavier nuclei, the influence of these conflicting effects on the mass resolution must be examined. For this purpose, test experiments using ^{197}Au are being planned.

*1 Faculty of Science and Technology, Tokyo Univ. of Science

References

1) K. Ozeki et al.: RIKEN Accel. Prog. Rep. **42** (2009).
2) K. Ozeki et al.: RIKEN Accel. Prog. Rep. **43** (2010).
3) http://www.pelletron.com
4) http://www.srim.org

Development Restoring Capacitor Clamp Board

K. Watanabe,*3 Y. Fukao, Y. Imazu, K. Karatsu,*2 T. Mibe,*1 T. Murakami,*2 J. Murata,*3 K. Nakamura,*2 I. Nakagawa, S. Park,*4 N. Saito,*1 K. Tanida,*4

[nucleon spin, W-boson, polarized parton distribution, Electronics, trigger, cathode chamber, cross talk]

1 ReCap concept

The Restoring Capacitor Clamp board (hereafter referred to as the ReCap Board) was developed to improve existing anode circuit in the PHENIX muon cathode strip chambers. Originally, the anode cards were equipped with surface mounted capacitors which were later discarded because moisture being trapped between them and the anode cards, and caused frequent high voltage trips. As a side effect of missing capacitors, the relevant path to the ground for the positive charge generated in anode wire is lost. As a consequence, the charge finds relatively easy path in adjacent strips which share the anode wire. This phenomenon called cross talk. Because cross talk signal interfere with real signal, it will create the unexpected high hit-multiplicity and degrade the position resolution of the tracker. For this reason, we have developed the ReCap board with non-surface type capacitors to be used in lieu of the original capacitors. Its structure will be discussed in this paper whereas the its performance will be addressed in another.

2 Requirement

We reuse the pad which used to be soldered surface mount capacitors, as a contact target of the new clamp. There are following mechanical constraints and requirements to be accounted in terms of designing of ReCap boards. They must be able to be installed within the very limited space between the chambers. Conventional soldering cannot be done, thus electrical contacts between existing pads and capacitor have to be established without soldering. Any remaining protective coating must be removed from the pads of the anode card. Its usability should be reconsidered after 10 years of operation. It must be coated to be protected from moisture. Must not produce dark current on the anode cards. Must to able to withstand a high voltage bias of 1950V. With these requirements in mind, the ReCap board has been designed with three major components. 1 Contact part : This is the part where firm contact is established with the pad of the anode cards. 2 Print board : This is a base board which mounts capacitors and shaped like "comb". 3 Support structure : This clamps around the anode card and hold them together. Good contact between the contact part and the pad of card is required : There are residual solder and an irregular surface so that print part must be able to absorb there bumpy structure by a channel by a channel. Accordingly, this shape has become like "comb". The support structure is then hold the print board on to the anode card. The print board is warped on purpose to push the probes onto the anode surface and secure the contact.

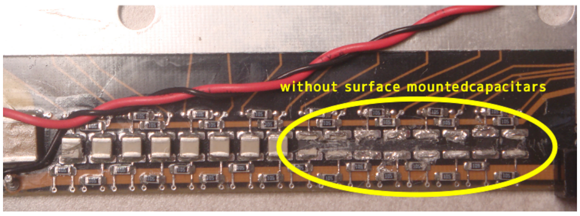

Fig. 1. The condition of the anode card without capacitors. There are some surface structure remained of pads. The bottom side pads is GND line and opposite is HV line.

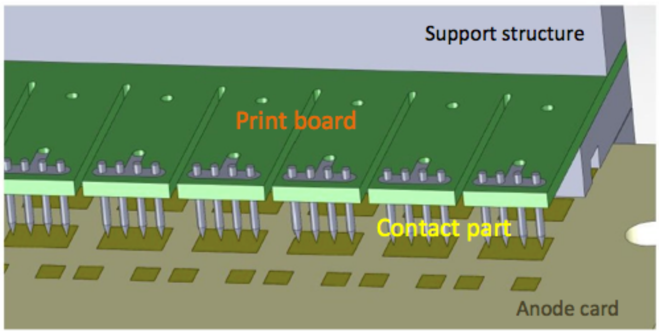

Fig. 2. The three major components of the ReCap board. Contact part is 4pin type.Print board likes "comb"

3 Contact part

Presently we are developing three different type of contact probes. And we must select carefully the best one. First, contact parts are sorted by the material of probe. One is conductive rubber probe and another is pin probe. Followings are described about these per-

*1 KEK, Tsukuba, Ibaraki, 305-08011 Japan
*2 Kyoto University, Kitashirakawa-Oiwakecho, Kyoto, 606-8502 Japan
*3 Rikkyo University, Rikkyo, 3-34-1, Nishi-Ikebukuro, Tokyo, 171-8501 Japan
*4 Seoul National University, Seoul, South Korea

formances and these advantages and disadvantages.

- Conductive rubber probe -

This type is made of conductive rubber. The rubber can absorb some surface structure of pads. On the other hand, the value of resistance can be varied depends on its compression from channel to channel. Although the variety is within the acceptable range, further disadvantage is that coating must be removed from anode cards before installing this one.

- Pin probe -

The probe of this type is made of 1 pin or 4 pins. Its advantage is unnecessariness to remove the existing coating of the anode cards, because the pin can penetrate the coatings and contact to the anode cards directly. This type of probe has a drawback. It may not have enough flexibility to absorb bumpy surface structure of pads unlike the rubber case.

This pin probe is further classified into two models: one with 1 pin par channel and the other with 4 pin per a channel.

- 1 pin type -

This type of probe only makes contact with the pad of the anode card using 1 pin, which has a lower probability of making contact than the 4-pin probe. It is, however, safer to use than the 4-pin model which we will describe later.

- 4 pins type -

The 4-pin probe has a higher chance of making contact, but it is suspected that should one or more of the pins do not, which means these pins are energized but floating in the air, may act as a corona discharge source.

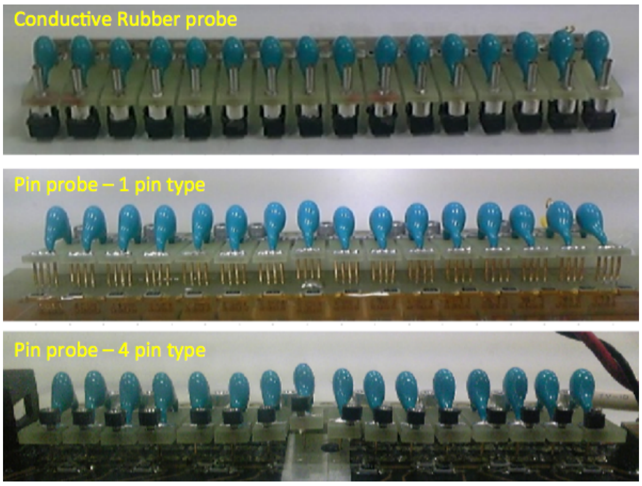

Fig. 3. contact parts : rubber type, 4-pins type, 1-pin type

4 Coating to the board

These ReCap board must be coated by insulator in order to be protected against moisture. The way to be coated is different by the probe type. The rubber type must not be coated the contacting surface because it does not have penetration power. Therefore, this type is suspected it may be weak against moisture. In the pin type case : it has penetration power, so this type can be fully coated. It is enough penetration power to penetrate oneself coating when it is pressed by the print board. Pin type is better insulator coating than rubber type.

5 Confirm the contacts

When ReCap board is installed, these ReCap boards must be confirmed how much fraction of the channels succeed to contact by a channel by channel. For that reason, ReCap board is equipped with voltage readout sockets. Plugging in readout cables, one can measure the finite voltage if the probe is in contact with the pad.

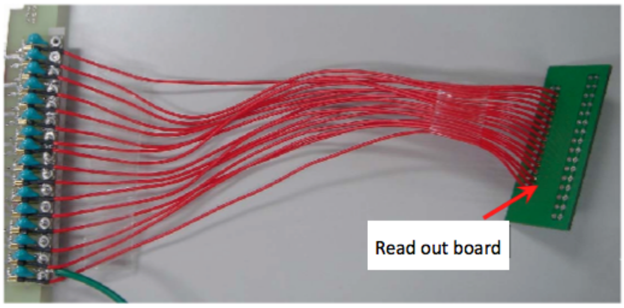

Fig. 4. readout cable

6 Installing

Towards the end of 2010, these prototype ReCap boards (3 pieces/type) have been installed to the cathode chambers in PHENIX to evaluate the performance. These ReCap board cleared the constraints of installation. The major clarifications of the prototype install are confirming 1) not introduce additional dark current 2) be able to withstand a high voltage bias of 1950V in the long run. In the result of that test : Approximately 90% of total channels were confirmed that the electrical contacts are established. The reason for remaining 10% unsuccessful contact is most likely originated from the problem in anode card (e.g. missing target pads). Now, we also confirmed the clamps didn't introduce new dark current and holds HV at 1950V. The final optimization of clamp types will be made based on their performance thru Run11.

Appreciation.

D. Reynolds: Stony Brook University, New York, America

T. Yanagawa: RinEiPrecisionInstruments Company, Japan

References

1) Y. Imazui: Jpn. J. Appl. Phys. **40**, L1299 (2011).

Evaluation of the Impact of Circuit Restoration on the Cross-Talk Effect

Y. Imazu, Y. Fukao, K. Karatsu,[*2] T. Mibe,[*1] T. Murakami,[*2] J. Murata,[*3] K. Nakamura,[*2] I. Nakagawa, S. Park,[*4] D. Reynolds,[*5] N. Saito,[*1] K. Tanida,[*4] and K. Watanabe[*3]

[nucleon spin, W-boson, polarized parton distribution, electronics, trigger, cathode chamber, cross talk]

1 Introduction

Several observations obtained from the 2009 and 2010 runs[1)] made clear that there is unexpected high hit multiplicity in the current muon-tracking chamber at PHENIX. This effect is now considered as the result of a cross-talk effect over read-out cathode strips through shared anode wires.

Because of several operational reasons, the read-out circuits at the anode-wire end had been kept ungrounded during operation over the years. The ungrounding of the anode-wire end causes reflection of the charge generated in the anode wire. This charge then tends to escape from the cathode strips that share the same anode wire, because the impedance of these strips is relatively less than that of the ungrounded end. This mechanism is shown by the blue arrows in the upper panel of Fig. 1. As a result, the charge deposited in the tracking chamber is detected as associated readout signals of negative polarity spread over the cathode strips (blue signals in the upper panel of Fig. 1), in addition to principal signals with normal (positive) polarity (a red signal in the same figure).

This cross-talk phenomenon leads to a loss of independence between the cathode read-out signals. As a result, this cross-talk phenomenon not only gives rise to unexpected high hit multiplicity but more importantly, it can also degrade the position resolution of the tracker by a baseline shift of the normal signal generated by the spreading negative undershoot. It is now predicted that, as the beam luminosity increases, the cross-talk effect will increase and the effect will become a more serious issue especially in the areas of physics research that require a high tracker performance[2,3)].

2 Evaluation of the Impact of the Circuit Restoration

Several countermeasures against the cross-talk effect have been discussed in Ref. 4. These measures have been partially adopted for the 2011 run involving the current tracker. The basic principle of these measures is to restore the anode-end circuit to be properly grounded, as shown in the lower panel of Fig. 1. Along with the discussion, we conducted a pilot study involving a test bench that imitated the PHENIX muon tracker. The study was conducted to evaluate the impact of the circuit restoration on the cross-talk effect and to optimize the circuit parameters (capacitance and resistance in 1).

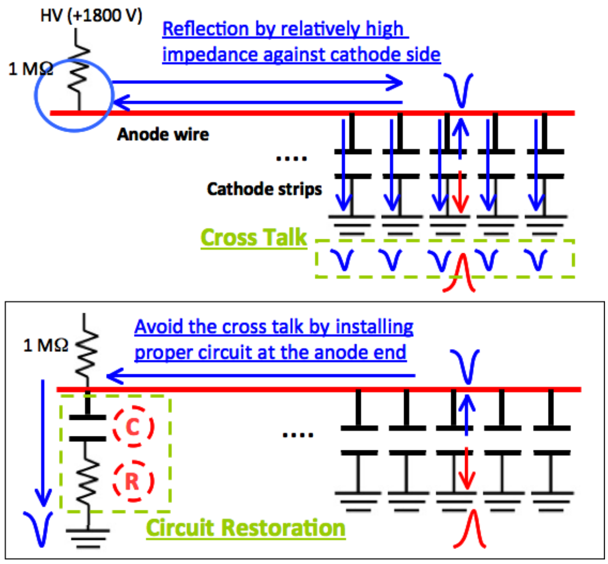

Fig. 1. The cross-talk effect in the cathode strips through the shared anode wire and the circuit restoration at the anode end to avoid the effect.

For the evaluation, we investigated the strength of the correlation between the magnitude of the principal readout signal left in a certain strip and those of the associated signals in other strips away from this strip under different circuit conditions. We clearly observed an expected negative correlation between the ADC values of these signals when the circuit was not restored, as shown in Fig. 2. We then compared the strength of the correlation, the correlation slope to be precise, by installing the anode-end circuit and varying its parameters. Figure 3 shows the results of the comparison. The black bullets represent the results under a condition without the circuit restoration and the red triangles, for example, represent those for the circuit restoration with a set of parameters.

[*1] KEK, Tsukuba, Ibaraki 305-08011, Japan
[*2] Kyoto University, Kitashirakawa-Oiwakecho, Kyoto 606-8502, Japan
[*3] Rikkyo University, Rikkyo, 3-34-1 Nishi-Ikebukuro, Tokyo 171-8501, Japan
[*4] Seoul National University, Seoul, South Korea
[*5] Stony Brook University, New York, USA

We observed that the cross-talk effect over the cathode strips was suppressed by a factor of 1/10 by choosing an appropriate combination of the parameters, which can be observed in Fig. 3. The chosen parameters resulted in an almost reasonable configuration for effective suppression, considering the chamber-side impedance determined by the possible local capacitance between the anode wire and cathode strip. From this observation, we finalized the configuration of the restoring circuit for those parameters.

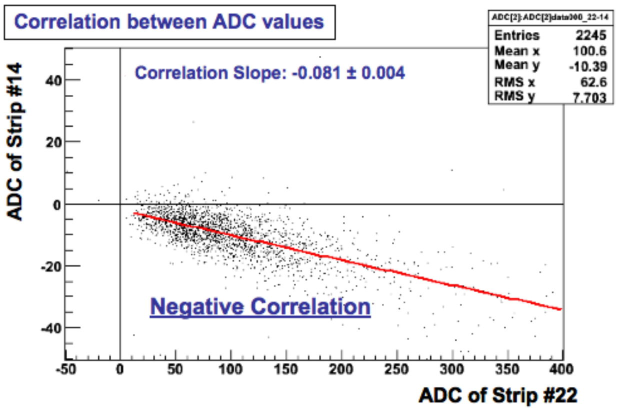

Fig. 2. The negative correlation between the ADC values of distant strips observed during measurements performed on the test bench without the restoration circuit, where the strip #22 provided a principal signal.

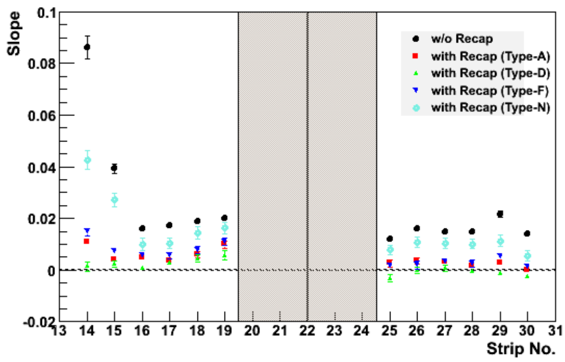

Fig. 3. The observed negative correlations for distant strips where strip #22 provided a principal signal. Here, the strength of the negative correlations were converted to the size of the negative slopes in the ADC-value correlations (refer to Fig. 2). The different markers correspond to different circuit conditions, e.g., the black points represent that no restoration circuit is present.

From the investigation, we have found that circuit restoration can have a large impact on the suppression of the cross-talk effect. We will qualitatively determine the actual impact of the restoration on the suppression and on the improvement in the position resolution of the tracker in operational conditions by applying the analysis method developed in this study to the data to be obtained from the 2011 run.

References

1) T. Mibe et al. *RIKEN Accel. Prog. Rep.*, 42, 2009.
2) Y. Fukao et al. *RIKEN Accel. Prog. Rep.*, 44, 2011.
3) R. Seidl et al. *RIKEN Accel. Prog. Rep.*, 44, 2011.
4) K. Watanabe et al. *RIKEN Accel. Prog. Rep.*, 44, 2011.

RIKEN Accel. Prog. Rep. 44 (2011)

Development of a TGEM TPC for the J-PARC E15 experiment

M. Tokuda,*[1] and F. Sakuma members of the J-PARC E15 Collaboration

[TGEM, TPC, J-PARC E15]

The J-PARC E15 experiment aims to determine the simplest kaonic nuclear bound state $K^- pp$ by the in-flight $^3He(K^-,n)$ reaction[1]. The dedicated detector system consists of a beam line spectrometer, a cylindrical detector system (CDS), and a neutron time of flight (TOF) counter. The goal of this measurement is accurate identification of Λ and Σ decays in the CDS by their secondary vertex reconstruction, because the expected decay modes of $K^- pp$ are $p\Lambda/p\Sigma^0$ and $p\pi\Sigma$. For these measurements, we have been developing a thick gas electron multiplier (TGEM[2]) time projection chamber (TPC) as an inner tracker for the E15 upgrade. The spatial resolution of the TPC in the beam direction should be less than 1 mm, and the material budget of the detector acceptance should be minimized.

The TPC is cylindrical with inner and outer diameters of 170 mm and 280 mm, respectively, and is filled with P-10 gas at atmospheric pressure. The drift length is 30 cm, and field cages are assembled from double-sided flexible printed circuit (FPC) sheets with staggered strip electrodes. A photograph of the TPC is shown in Fig. 1. A double-TGEM structure is used for amplification, and signals are read out with 4-mm-long and 20-mm-wide pads on a PCB. The TGEM is fabricated in an economical manner by the standard PCB technique; holes with diameters of 0.3 mm are drilled into a double-clad 400-μm-thick FR4 plate. For the TPC performance to be sufficiently high, an effective gain of $\sim 10^4$ is required for the readout. Using TGEMs for the TPC is advantageous because the TGEM does not require any support frame for its installation. On the other hand, standard GEM foils of 50 μm thickness[2] have to be tensioned by 1-cm support frames.

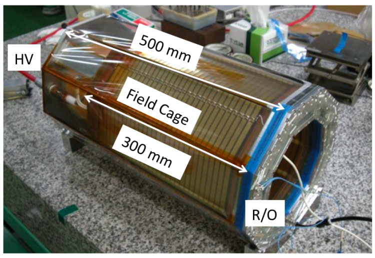

Fig. 1. A photograph of the TPC.

We have fabricated standard TGEMs that have chemically etched rims (30 μm) around each hole. We also have developed carbon-TGEMs that have resistive carbon cathodes ($20 \sim 40\Omega/\mathrm{cm}^2$) instead of copper cathodes;the use of these resistive cathodes helps in preventing electrical discharge. To evaluate the performance of the TGEM, we used prototype TGEMs having an active area of 10 × 10 cm^2, which were produced by REPIC Corp., Japan. Figure 2 shows a prototype TGEM and a nonagonal TGEM for the TPC. Measurements were carried out with the double-TGEM configuration using a test bench consisting of a gas chamber cascade operation, a voltage divider with a resistive chain, and a readout pad with a charge-sensitive preamplifier. All the TGEMs showed a sufficiently high effective gain of more than 10^4 (Fig. 3). The fabrication of TGEMs whose sixes are large than 10 *times* 10 cm^2 was very difficult owing to various production-related problems. Consequently, nonagonal TGEMs by be been successfully produced. In the case of carbon TGEMs, the problem of poor reproducibility was solved by using glass-paper insulators instead of FR4.

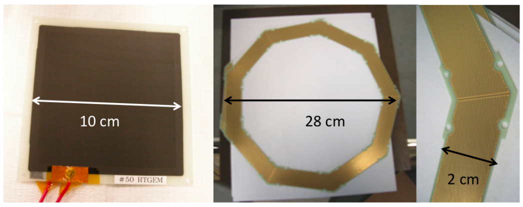

Fig. 2. Prototype carbon TGEM (left) and nonagonal TGEM (right).

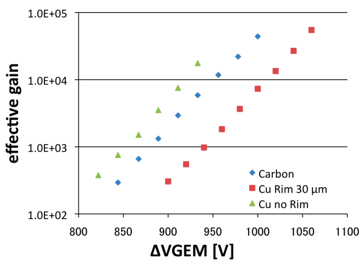

Fig. 3. Effective gain of the double-TGEM structure.

*1 Department of Physics, Tokyo Institute of Technology

References

1) E15 proposal, http://j-parc.jp/NuclPart/pac_0606/pdf/p15-Iwasaki.pdf
2) R. Chechik, et al., Nucl. Instrum. Meth.**A 535**, 303 (2004).
3) F. Sauli, Nucl. Instrum. Meth. **A 386**, 531 (1997).

Commissioning of Cylindrical Detector System for J-PARC E15 Experiment †

Y. Sada,*1 for J-PARC E15 Collaboration

[Nuclear physics, strangeness]

1 Introduction

The J-PARC E15 experiment was proposed to search for the simplest kaonic nuclear bound state "K^-pp" by using the in-flight (K^-, n) reaction on ^{3}He. In this experiment, we can measure the missing mass in the in-flight (K^-, n) reactions and the invariant mass for decays such as $K^-pp \rightarrow \Lambda p \rightarrow p\pi p$, simultaneously [1]. The main E15 spectrometer has four components: a beam-line spectrometer, cylindrical detector system (CDS) with a liquid ^{3}He target, beam-sweeping magnet, and neutron time-of-flight (TOF) wall. Forward neutrons whose flight length is approximately 15 m are detected by the TOF wall.The incident kaons that pass through the target are deflected by the beam-sweeping magnet placed immediately after the CDS. The decay particles from the expected decay $K^-pp \rightarrow \Lambda p \rightarrow p\pi p$ are detected by the CDS.

The CDS mainly consists of a solenoid magnet whose magnetic field can range up to 0.7 T, cylindrical drift chamber (CDC) that has 15 layers, cylindrical detector hodoscope (CDH) that surrounds the CDC for the trigger counter, and particle identification hodoscope. The CDS has already been constructed and installed at the J-PARC K1.8BR experimental area. The K^-pp binding energy from theory[2)6)] are varies from 20 MeV/c^2 to over 100 MeV/c^2. When we assume the K^-pp binding energy to be 100 MeV/c^2, the expected spectrometer performance for the K^-pp measurement is 9.2 MeV/c^2(σ) for the missing-mass resolution and 16 MeV/c^2 for the invariant-mass resolution. The current status of the CDS is reported in this article.

2 Commissioning of CDS

We started commissioning of the CDS in 2010. In May-June 2010, we performed the excitation test of the solenoid magnet and collected cosmic-ray data for the check of CDS performance in the presence of a magnetic field. We confirmed that all detectors works properly in the presence of a magnetic field, and we can successfully reconstruct the tracks (Fig1). In Oct 2010, we completed the commissioning by using a secondary beam of 0.9 GeV/c π^+ for checking momentum resolution of the CDS by $p\pi$ elastic scattering. Moreover we accomplished 0.9 GeV/c K^- data in order to compare the reconstructed invariant mass of Λ and K_s^0 with the simulated values. For this purpose, we used polyethylene (0.5g/cm^2), carbon (0.9g/cm^2), and copper (0.9g/cm^2) target in the CDS. The total collected data comprised 1.9×10^6 and 6.8×10^6 triggered events for the π^+ and K^- beams, respectively.

We confirmed that the achieved efficiency of the CDC is over 98% in all layers and the residual distribution of each layer is about 200-250 μm. Moreover, we can successfully reconstruct the Λ and K^0s peaks in the invariant mass of $p\pi^-$ and $\pi^+\pi^-$, respectively, as shown in Fig 2. Further analysis is in progress.

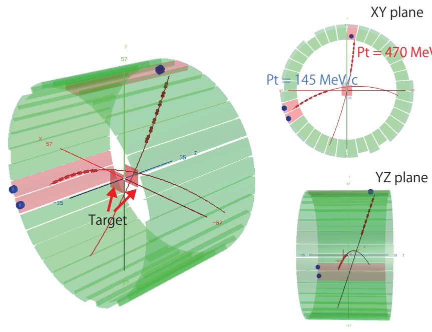

Fig. 1. Example of tracks reconstructed using the CDS.

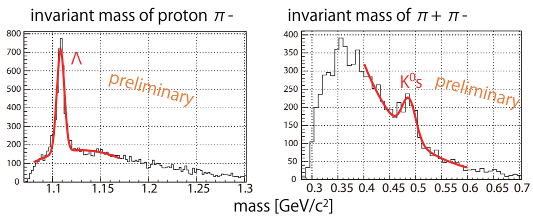

Fig. 2. Invariant masses of $p\pi^-$(left) and $\pi^+\pi^-$(right).

References
1) M. Iwasaki *et al.*: Proposal of J-PARC 50-GeV PS (2006).
2) T. Yamazaki and Y. Akaishi: Phys. Lett. B **535**, 70 (2002).
3) N. V. Shevchenko, A. Gal, J. Mares and J. Revai: Phys. Rev. C **76**, 044004 (2007).
4) Y. Ikeda and T. Sato: Phys. Rev. C **76**, 035203(2007).
5) A. Doté, T. Hyodo, and W. Weise: Nucl. Phys. A **804**, 197 (2008).
6) S. Wycech and A. M. Green: Phys. Rev. C **80**, 045207 (2009).

†

*1 Department of Physics, Kyoto University, Japan

Development of a fluorescence detection system for new nuclear laser spectroscopy in superfluid helium

A. Sasaki,[*1] T. Wakui,[*1] T. Furukawa,[*2] S. Izumi,[*1] T. Kobayashi, T. Shinozuka,[*1] and Y.Matsuo

We are developing a fluorescence detection system for performing nuclear laser spectroscopy of radioisotope (RI) atoms that are stopped in superfluid helium (He II). The Zeeman and hyperfine structures of atoms are determined accurately by using a laser RF/MW double resonance technique to determine the nuclear spins and moments of the atoms. The project of the nuclear laser spectroscopy using He II is named Optical RI-atom Observation in Condensed Helium as Ion-catcher (OROCHI) and is aimed at performing laser spectroscopy for unstable nuclei that are produced in a small amount.[1)] To observe laser-induced fluorescence (LIF) in the low-yield RI atoms, the photon detection efficiency must be maximized and the background count rates must be minimized simultaneously.

In the OROCHI project, one of the key tasks is to develop a fluorescence detection system with a large solid angle and well-reduced background. A set of Fresnel lenses with large diameters and short focal lengths are useful for the collection of LIF with a large solid angle. The use of wavelength-separation filters can greatly reduce the background, which mainly originates from the excitation laser, since there is a considerable difference between the fluorescence and excitation wavelengths in He II.[2)]

Figure 1 shows a schematic diagram of the fluorescence detection system. It consists of three Fresnel lenses, one pair of slits (parallel and perpendicular to the laser light), wavelength filters, and a photomultiplier tube (PMT). The light emitted by the atoms is collected and focused on the slits by the first Fresnel lens (Lens 1). The light that has passed through the slits is collimated with the second lens (Lens 2); thus, the light enters the wavelength filter at normal incidence, resulting in the perfect separation of wavelengths. The light is then focused on the photoelectric surface of the PMT by the third lens (Lens 3).

The fluorescence detection system is used not only to observe fluorescence in atoms with unstable nuclei but also to detect the emission of light from a plastic scintillator, which is placed in a cryostat and is used for adjusting the stop position of the RI beam in He II. A test experiment shows that when a ^{2}H beam with 9.1 A MeV is used, our fluorescence detection system (FDS 1) is useful for determining the stop position at the light emitted from the scintillator.[3)]

However, the OROCHI experiment requires a system that can detect both LIF and scintillator emission with high efficiency. For this purpose, we have designed and constructed a new fluorescence detection system (FDS 2) that can control the position of lenses and slits externally by using electric actuators. On the bases of optical-simulation results, the fluorescence detection system is set to have the optimum configuration at a wavelength of 793 nm (LIF in the case of Rb atoms) or 425 nm (emission from the plastic scintillator). The estimated light-collection efficiencies of FDS 2 at 793 nm are 8.0 % and 1.9 % for incident-beam diameter 1 mm and 10 mm, respectively. Likewise, the efficiency at 425 nm is estimated to be 0.4 %. Thus, the calculated efficiency results in a photon count rate of 2.5×10^5 /s for LIF at 793 nm and Rb-beam injection of 10^5 /s with a diameter of 1 mm; this result is obtained when FDS 2 is irradiated with an excitation laser with a power of 400 mW and a diameter of 2 mm.

FDS 2 was used for an experiment using a stable ^{87}Rb beam with 66 A MeV at the RIKEN RIPS beam line. LIF photons emitted by the Rb atoms were successfully observed with a count rate of approximately 0.8×10^5 /s; this result was in good agreement with the above-mentioned estimation.[4)] Attempts to increase the signal-to-noise ratio by reducing the background count rate caused by stray laser light are in progress.

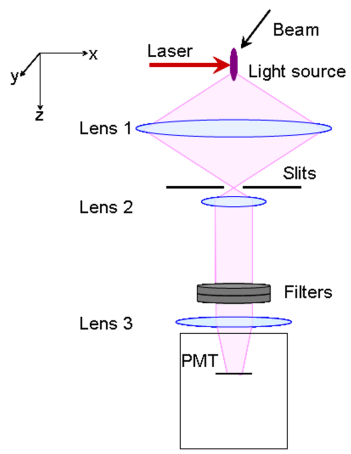

Fig. 1. Schematic of the fluorescence detection system

References
1) T. Furukawa et al.:Riken Accel. Prog. Rep. **41**, 153 (2008).
2) Y. Takahashi et al.: Phys. Rev. Lett. **71**, 1035 (1993).
3) A. Sasaki et al.: RIKEN Accel. Prog. Rep. **42**, 193 (2009).
4) T. Furukawa et al.: RIKEN Accel. Prog. Rep. **44**, 205 (2011).

*1 Cyclotron and Radioisotope Center, Tohoku University
*2 Department of Physics, Tokyo Institute of Technology

First observation of photons from stopped ^{87}Rb atoms injected into superfluid helium for nuclear laser spectroscopy of rare radioisotopes

T. Furukawa,[*1] T. Wakui,[*2] A. Sasaki,[*2] S. Izumi,[*2] Y. Ichikawa, A. Yoshimi, K. Tajiri,[*3] Y. Ishii,[*1] N. Yoshida,[*1] Y. Matsuura,[*4] Y. Kato,[*4] Y. Yamaguchi,[*4] K. Imamura,[*4] M. Makuta,[*5] A. Hatakeyama,[*5] M. Wada, T. Sonoda, Y. Ito,[*6] T. Nanao,[*1] T. Kobayashi,[*7] S. Nishimura, M. Nishimura, Y. Kondo,[*1] N. Aoi, K. Yoneda, S. Kubono,[*8] Y. Ohshiro,[*8] H. Ueno, T. Shimoda,[*3] T. Shinozuka,[*2] K. Asahi,[*1] and Y. Matsuo

[Nuclear laser spectroscopy, Electromagnetic moments, Nuclear Spin]

To measure the spins and moments of low-yield exotic radioisotopes (RIs), we develop a new nuclear laser spectroscopy method using superfluid helium (He II), called "Optical Radioisotope atom Observation in Condensed Helium as Ion-catcher" (OROCHI). In the OROCHI, He II liquid is adopted as the stopping material for RI beams and as host material for the introduced RI atoms for in situ laser spectroscopy. In view of the characteristic features of the atoms immersed in He II[1)], such as the blue-shifting and broadening of the absorption spectra because of the pressure of the surrounding helium liquid, it will be feasible to measure spins and moments of extremely low yield RIs.

In a past study, we have successfully demonstrated that we can deduce the nuclear spins and moments with stable Rb, Cs, Ag, and Au isotopes introduced into He II by laser sputtering method[2)]. As the next step, we planned to observe atoms from intermediate energy beams stopped in He II. We carried out the first experiment by using a ^{87}Rb beam, aiming to evaluate the beam intensity required for the observation.

Figure 1-a) shows a schematic of our experimental setup. The ^{87}Rb beam (energy: 66 AMeV; spot size: ϕ3 mm) is injected into He II, and the number of injected Rb is counted one by one with a plastic scintillator placed in front of the cryostat. Aluminum foils with thicknesses ranging from 0 μm to 800 μm ("Energy degraders" in Fig. 1) reduce the beam energy injected for adjusting the stopping range of ^{87}Rb in He II at the center of the cryostat (7 mm from the injection window). The stopped ^{87}Rb atoms are subjected to irradiation with the CW pumping laser light (Ti:Sapphire laser; power: 200 mW; spot size: ϕ5 mm). The wavelength of the pumping laser light is tuned to the D1 absorption line of Rb atoms in He II (780 nm). The LIF photons from the laser-excited ^{87}Rb atoms are collected, wavelength-separated, and then detected with a photodetection system[3)].

Figure 1-b) shows a typical time evolution of the observed photon intensity with the ^{87}Rb beam switched on and off. The observed intensity increases upon the injection of the ^{87}Rb beam, and the intensity then becomes constant with the number of injected and escaped atoms being balanced. After that, it decreases with the stopping of the beam injection. From the difference in counting rates, the observed LIF intensity is 0.8×10^5/s, with the injected ^{87}Rb intensity being 1.7×10^5/s. The obtained intensity is consistent with the expected intensity of $\simeq1.0\times10^5$/s deduced from the photoabsorption cross section of atoms in He II[4)] and the overall photodetection efficiency of our present setup. The background in Fig.1-b), the rate being comparable to the LIF intensity as typically 1.0×10^5/s, is mostly due to stray laser light. Because of the large background counts, the minimum beam intensity for the measurement is now limited to 10^4/sec. Note that the limitation can be improved to less than 10/s by planned upgrades of the overall photodetection efficiency and background reduction.

In parallel with the upgrades, we plan to measure the hyperfine structure of unstable ^{84,86}Rb isotopes (yield: 10^5/s). In the near future, we will apply the OROCHI to measure the spins and moments of rare isotopes.

a) b)

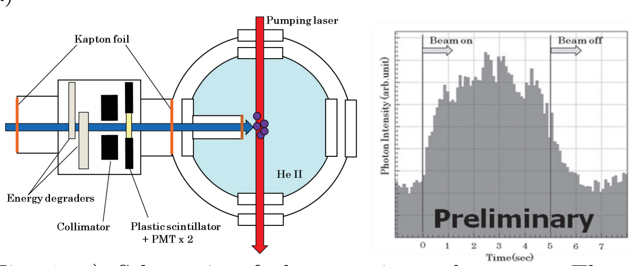

Fig. 1. a) Schematic of the experimental setup. The ^{87}Rb beams (66 AMeV) were injected into the cryostat through two energy degraders and a plastic scintillator. b) Time evolution of the LIF intensity with the turning on and turning off of the beam injection (see text).

[*1] Department of Physics, Tokyo Institute of Technology
[*2] Cyclotron Radioisotope Center, Tohoku University
[*3] Department of Physics, Osaka University
[*4] Department of Physics, Meiji University
[*5] Department of Applied Physics, Tokyo University of Agriculture and Technology
[*6] Department of Physics, University of Tsukuba
[*7] RIKEN Advanced Science Institute
[*8] Center for Nuclear Study, University of Tokyo

References

1) P. Moroshkin et al.: Low. Temp. Phys. **32**, 981 (2006).
2) T. Furukawa et al.: Hyp. Int. **196**, 191 (2010).
3) A. Sasaki et al.: RIKEN. Acc. Prog. Rep. **42**, 193 (2009).
4) T. Furukawa et al.: RIKEN. Acc. Prog. Rep. **41**, 153 (2008).

RIKEN Accel. Prog. Rep. 44 (2011)

Status of the Station-3 Drift Chamber for the E906/SeaQuest Experiment †

F. Sanftl[*1], Y. Goto, K. Nakano[*1], Y. Miyachi,[*2], S. Miyasaka[*1], S. Sawada[*3], T.-A. Shibata[*1] and S. Takeuchi[*1]

1 Introduction

E906/SeaQuest is a fixed-target experiment that has been constructed in the KTeV hall at Fermilab in USA. In this experiment a 120-GeV proton beam extracted from the Fermilab Main Injector is used. The E906/SeaQuest detector is a forward spectrometer designed to be sensitive to the Drell-Yan process, $q\bar{q} \to \gamma^* \to \mu^+\mu^-$, in proton-nucleon reactions; this detector can easily detect the final-state muon pair. The main goal of this experiment is to investigate the flavor asymmetry of sea quarks ($\bar{u}$ and $\bar{d}$) in the proton[1)]. In particular, it focuses on the asymmetry of sea quarks at large x_{Bj} ($\gtrsim 0.25$), where x_{Bj} is the momentum fraction carried by the scattered anti quark with respect to the target nucleon.

2 The E906/SeaQuest Detector

The E906/SeaQuest spectrometer is so designed that it can not only detect muon pairs from the Drell-Yan process, but also eliminate the huge number of low-momentum charged particles, particularly muons from J/Ψ decays.

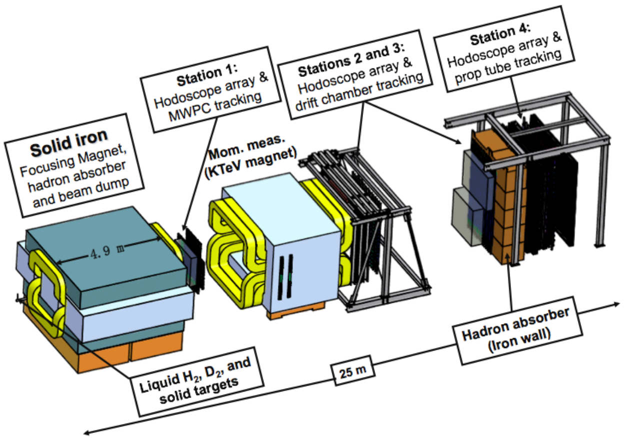

Fig. 1. Schematic drawing of detector setup in side-top view.

Figure 1 shows the setup of the E906/SeaQuest detector, where the proton beam is incident from the left side. The target materials are liquid hydrogen, liquid deuterium, and several solid targets, such as C, Ca and W, which are stored in a cryogenic target cell. A focusing magnet labeled as "Solid iron" condenses high-p_T muons into the detector acceptance region and sweeps out low-momentum background muons. A large iron block inside the focusing magnet serves both as a hadron absorber and as a beam dump. Stations 1, 2, and 3 are multi layer drift chambers (DCs); Station 3 is divided in a Top and Bottom DC. They identify the hit positions of the passing muons in order to reconstruct the tracks and momenta of the muons. The momenta are determined by an analyzing magnet labeled as "KTeV magnet" which bends muons in the horizontal direction. Station 4 consists of alternating layers of drift tubes and iron absorbers. It identifies high-momentum muons by being sensitive only to particles that penetrate the complete spectrometer including its absorbers because it is located at the far end of the detector array. Each station is sandwiched between hodoscope arrays to trigger di-muon events.

The proton beam will be available in summer 2011. Data will be recorded intermittently for the next three years. The E906 Japanese group has constructed the Station 3 Top DC, and it is in charge of the operation of Station 3. This article reports on the commissioning status of the Station 3 Top DC at Fermilab.

3 The New Station 3 Top Drift Chamber

The dimensions of the Station 3 Top DC are 3.2 m (horizontal) × 2.2 m (vertical). In order to maximize the acceptance, this station is placed 19 m away from the target. The required position resolution at Station 3 is less than 400 μm. Station 3 is required to provide a muon pair detection efficiency close to 100% at background rates corresponding to 5 kHz/cm^2. The background rate has been evaluated using the GEANT detector simulator[2)].

Figure 2 shows the cell structure of the Station 3 Top DC. This chamber consists of six layers labeled as U, U', X, X', V, and V'. All the wires are vertically arranged, whereas the wires of the U/U'- and V/V'-layers are tilted by ±14°. In total, the number of sense wires, and thus the number of readout channels, is 768, and the number of field and guard wires is 4368.

The construction of Station 3 Top DC was finalized in February 2010. After basic operational tests at RIKEN during spring and summer 2010 it was shipped to Fermilab in July 2010.

*1 Tokyo Institute of Technology
*2 Yamagata University
*3 KEK

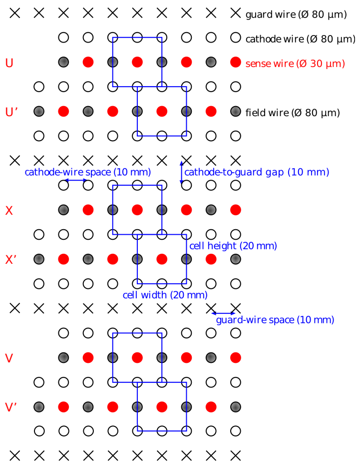

Fig. 2. Cell structure (unit cell in blue boxes) of the new Station 3 Top DC.

4 Commissioning - The First Steps

We present the first studies on the Station 3 Top DC performance. The measurements were commenced in August 2010 at Fermilab National Accelerator Laboratory. For all the studies, eight neighboring sense wires were read out in an Ar:CO_2 (80%:20%) gas mixture.

As the first step, the gas amplification gain for different high voltage (HV) values was measured. Raw signals caused by cosmic rays were recorded, and the corresponding gas gain was evaluated. By GARFIELD simulations[3)], the gas amplification gain was predicted to be $\mathcal{O}(10^5)$. On the one hand, we estimated the order of magnitude of the gas gain accurately, on the other hand, we systematically overestimated the gas gain by a factor of 2 (cf. Fig. 3). Further studies must investigate the ionization process in more detail.

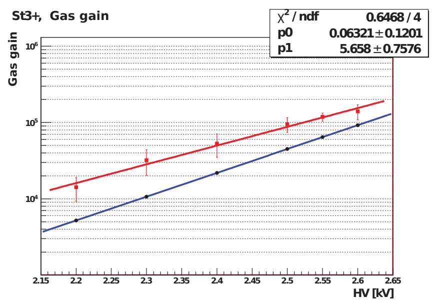

Fig. 3. Measured (red line) and simulated (blue line) gas gains for the Ar:CO_2 (80%:20%) gas mixture.

Furthermore, the one-layer efficiency curve was determined. Two plastic scintillators served as cosmic-ray triggers for the measurement. Figure 4 shows the efficiency curve for two different discriminator thresholds. For the high threshold, more than 99% detection efficiency was achieved at HV ≈ 2.5 kV. This was sufficient because the nominal operational HV of the Station 3 Top DC is 2.8 kV.

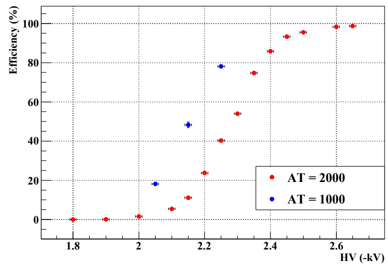

Fig. 4. Efficiency curve for low (blue points) and high (red points) discriminator thresholds.

Finally, the preliminary TDC distribution was measured with a common-stop trigger signal. Since only single hit events (red line in Fig. 5) were considered, the measurement was in good agreement with the result of our Garfield simulations. The width of the TDC distribution was 150 TDC counts, which corresponds to 300 ns. The right side of the TDC distribution corresponded to a shorter drift time, and the number of hits exceeded that on the left side by a factor of 3. According to our simulation, this difference can be explained by the fact that the drift velocity is $2-3$ times higher near the sense wire than at the cell edge.

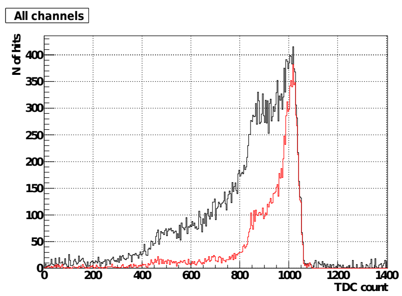

Fig. 5. TDC distribution of 8 neighboring sense wires for multiple hits (black line) and single hits (red line).

5 Conclusion and Outlook

We have reported the preliminary performance measurements carried out on the new Station 3 Top DC at the E906/SeaQuest experiment at Fermilab. The operation and behavior of the chamber are well understood, and they meet our expectations. More detailed performance measurements will be possible as soon as the setup of the full DAQ system is completed.

References
1) J. Arrington *et al.*, Proposal of E906 Experiment, http://www.phy.anl.gov/mep/drell-yan/proposals/
2) CERNLIB Webpage, http://cernlib.web.cern.ch/cernlib/
3) Garfield Webpage, http://garfield.web.cern.ch/garfield/

Development of efficient photocathode for Hadron Blind Detector Used in the J-PARC E16 experiment

K. Aoki, for the J-PARC E16 Collaboration

[HBD, GEM, Cherenkov detector, chiral symmetry, mass modification, vector meson]

1 Introduction

Spontaneous breaking of chiral symmetry is considered to be responsible for hadron mass. The broken symmetry is expected to be partially restored in hot or dense matter, which leads to a reduction in the hadron mass. Experimental observation of chiral symmetry restoration is attracting considerable attention in the field of hadron physics.

The J-PARC E16 experiment[1] has been proposed to measure the in-medium properties of vector mesons. The vector mesons are produced in the $p + A$ reactions, and the invariant mass is reconstructed using e^+e^- decay. Therefore, electron identification is crucial in the experiment. We choose Hadron Blind Detector (HBD)[2], which is a mirrorless and windowless Cherenkov detector. We use CsI-evaporated Gas Electron Multiplier (GEM) as a photocathode for the HBD. CF_4 gas is used as Cherenkov radiator and amplification gas.

We have constructed a prototype of HBD and performed a test experiment using positron beam at the Research Center for Electron Photon Science, Tohoku University[3]. We have successfully observed Cherenkov radiation from the positron beam. However, the number of photoelectrons was only 5−6 and not enough to require 16 photoelectrons at the trigger level for achieving a pion rejection factor of 100[2]. About 22 photoelectrons were observed with a similar setup at BNL. A loss of 30% was due to the absorption of UV light by oxygen and water vapor contamination, which is expected to be reduced in the real experiment. The rest of the discrepancy is considered to be due to the low efficiency of the photocathode.

To produce a photocathode with better quantum efficiency (QE), we have prepared an evaporator at RIKEN to control evaporation parameters. In this article, the QE of a recently produced photocathode is reported and this QE is compared with that of the old one and to that at BNL.

2 CsI photocathode

The photocathode is prepared by vacuum evaporation. The evaporator is pumped out to approximately 5×10^{-6} Torr. CsI crystals are heated with a Mo boat by applying a current of about 40 A and are evaporated on top of a GEM. The thickness of the CsI layer is about 350 nm. The photocathode is left in vacuum for more than 12 hours after evaporation since QE enhancement was reported[4]. The old photocathode was evaporated by Hamamatsu photonics.

For QE measurement, we use the parallel-plate mode (pp mode). Figure 1 shows the setup for the pp mode. An electric field is applied between the mesh and the top of the GEM, and photoelectrons drift toward the mesh to be read out. The current can be read out without amplification in pp mode.

3 Measurement of quantum efficiency

Figure 2 shows a schematic of the experimental setup. A deuterium lamp is used as a UV light source. The light is injected into a monochrometer (Shinku-kogaku VMK-200), and wavelength-selected light is transmitted to a half mirror (Monotech). The light is split and transmitted to a reference PMT (Hamamatsu R6836) and CsI-GEM. The light is transferred to CsI-GEM through a MgF_2 window and CF_4 gas. The distance between the lamp and the CsI-GEM is about 670 mm. The QE of the CsI-GEM is calculated on the basis of the reference PMT. Since vacuum ultraviolet light is of interest, the monochrometer system is pumped out to about 10^{-3} Torr.

The QE of CsI-GEM Q_{CsI} is calculated as follows:

$$Q_{\mathrm{CsI}} = \frac{1}{(T/R)_{\mathrm{hm}} T_{\mathrm{win}}} \cdot \frac{1}{T_{\mathrm{mesh}} A_{\mathrm{GEM}}} \cdot \frac{I_{\mathrm{CsI}}}{I_{\mathrm{PMT}}} \cdot Q_{\mathrm{PMT}}, (1)$$

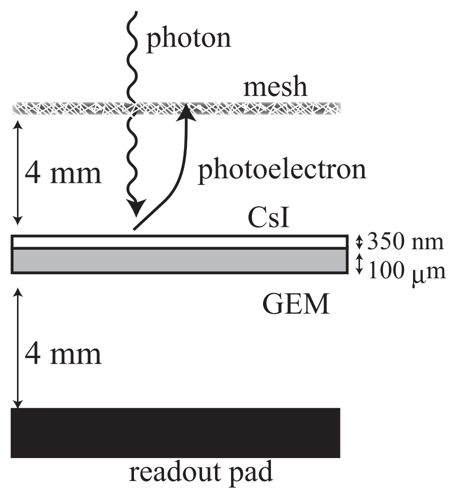

Fig. 1. Schematic view of CsI-GEM read out in parallel-plate mode.

where $(T/R)_{\mathrm{hm}}$ is the transmittance-reflectance ratio of the half mirror, T_{win} denotes the transparency of $\mathrm{MgF_2}$ window, T_{mesh} represents the transparency of the mesh, A_{GEM} is the electrode area ratio of the GEM, and I_{CsI} ($I_{(\mathrm{PMT})}$) is the measured current of the CsI-GEM (PMT). The current of PMT and CsI-GEM were read without amplification. Therefore, the measurement is free from gain uncertainties. Q_{PMT} is supplied by the manufacturer. $(T/R)_{\mathrm{hm}}$ and T_{win} are measured by replacing the CsI-GEM with another PMT. $(T/R)_{\mathrm{hm}}$ and T_{win} are measured twice by swapping the two PMTs. The difference between the results is used to estimate systematic uncertainty of the measurement.

4 Results

Figure 3 shows the measured QE as a function of photon energy. The open and closed circles represent the measured QE of the new photocathode evaporated at RIKEN. The difference between these two curves is a measure of the above mentioned systematic uncertainty. The triangles show the QE of an old photocathode evaporated by Hamamatsu photonics. The red square represents the QE of the BNL photocathode[5]. The number of photoelectrons from Cherenkov radiation, N_{pe}, is proportional to

$$N_{pe} \propto \int_{6\ \mathrm{eV}}^{11.5\ \mathrm{eV}} Q_{\mathrm{CsI}} dE. \qquad (2)$$

The right hand side of the equation is the area of the plots in Fig. 3. At low photon energies (less than

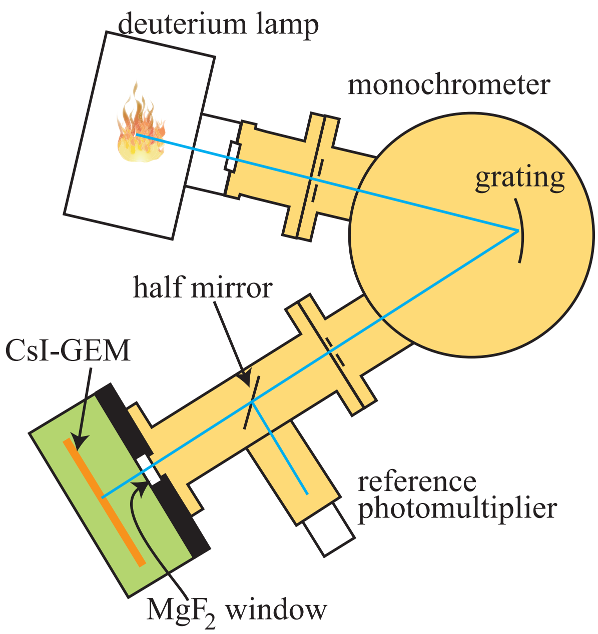

Fig. 2. Experimental setup for quantum efficiency measurement.

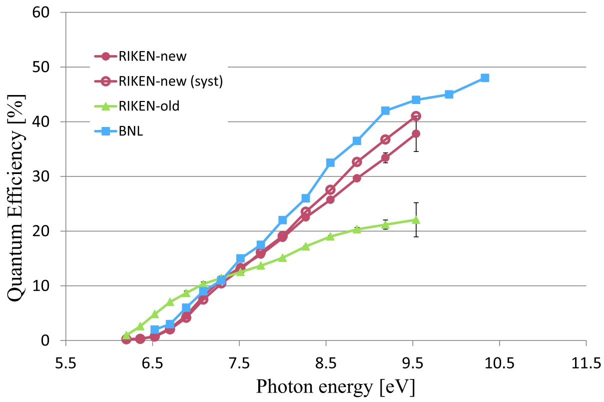

Fig. 3. Quantum efficiency as a function of photon energy.

7.3 eV), the QE of the new RIKEN photocathode is lower than that of the old one, however, the QE becomes considerably higher at higher photon energy. The photon-energy dependence of the new RIKEN photocathode is similar to that of the BNL photocathodes.

The measured photon-energy range is limited by the photon flux of the deuterium lamp, whose yield decreases with increasing photon energy. The range can be extended, for example, with a focusing mirror that is utilized at BNL. However, it cannot be extended in a straight forward way beyond ~10.5 eV since the QE of reference PMT is not known.

Further improvement of QE could be possible by changing the parameters and conditions. One possibility for improvement is heating the GEM after evaporation[4], and such an improvement is also planned.

5 Summary

We have successfully prepared a highly-efficient photocathode for the HBD. The number of photoelectrons for Cherenkov radiation cannot be calculated because of the limited energy range. It has to be measured by carrying out a beam test, and it is planned that this beam test will be conducted in March 2011.

References

1) `http://ribf.riken.jp/~yokkaich/paper/jparc-proposal-0604.pdf`
2) A. Kozlov et al.: Nucl. Instrum. Meth. **A 523**, 345 (2004).
Z. Fraenkel et al.: Nucl. Instrum. Meth. **A 546**, 466 (2005).
3) K. Aoki: RIKEN Accel. Prog. Rep. **43** (2010).
4) M. Durham: private communication.
5) B. Azmoun et al.: IEEE Trans. Nucl. Sci. **56**, 1544 (2009).

Performance of Low-Pressure Multiwire Drift Chamber in High-Intensity Heavy-ion Beam

H. Miya,[*1] S. Ota,[*1] H. Matsubara,[*1] S. Noji,[*2] S. Kawase,[*1] Y. Kikuchi,[*1] K. Kisamori,[*1] M. Takaki,[*1] S. Michimasa,[*1] K. Miki,[*2,*3] T. Uesaka,[*1] and S. Shimoura,[*1]

We are developing low-pressure multiWire drift chambers (LP-MWDCs) for tracking light radioactive isotope (RI) beams(isotope mass number: ± 10 ; beam energy: 100–300 MeV/nucleon). These LP-MWDCs are used as tracking detectors in BigRIPS and the high-resolution beamline at the RI Beam Factory (RIBF). The past development of the LP-MWDCs has been reported elsewhere[1)].

In high-resolution experiments performed with the SHARAQ spectrometer[2)], the secondary target should be sufficiently thin so that the overall energy resolution is not disturbed. This in turn necessitates the use of a high-intensity beam. RI beams at a rate as high as 1–2 MHz are transported to the target in the actual experiments[3,4)]. Although those experiments have beens conducted under lateral and angular dispersion matching condution, the beam tracks on the target had to be measured at an angular resolution of 1 mrad (FWHM) in order to correct the angular spread of the RI beams. A position resolution of 500 μm (FWHM) was necessary to determine the beam track when using two drift chambers. The new LP-MWDCs were developed to achieve the required resolution for the light RI beams at the rate of 1–2 MHz.

Table 1 shows the specifications of the new LP-MWDC. The wire in the X plane is stretched in the vertical direction. The wires in the U and V planes are tilted by 30° and −45° with respect to the vertical, respectively. With this configuration, the counting rate per cell can be reduced for the beam with a large width. The cell size and effective area are 9 mm × 9 mm and 216 mm × 144 mm, respectively. The counter gas is pure isobutane at a pressure of 10 kPa. By maintaining the gas pressure at a low value, the effect of multiple scattering can be diminished.

Table 1. Specifications of LP-MWDC

Configuration	C-AU(−45°)-C-AV(30°)-C-AX(90°)-C
Effective area	216 mm×144 mm
Cell size	9 mm × 9 mm
Number of channel	24 ch (AX), 24 ch (AU), 16 ch (AV)
Anode wire	Au-W, 20 μm^{ϕ}
Potential wire	Cu-W, 75 μm^{ϕ}
Cathode foil	Al-PET, 1.5 μm
Operation gas	pure isobutane, around 10 kPa

*1 Center for Nuclear Study, University of Tokyo
*2 Department of Physics, University of Tokyo
*3 RIKEN Nishina Center

The position resolution of the LP-MWDCs was measured using un ^{12}N beam with an energy and intensity of 200 MeV/nucleon and 1 kHz–1.5 MHz, respectively. The cyclotron radiofrequency was 13.7 MHz. The two LP-MWDCs were installed at a distance of 500 mm from each other in order to cover the focal plane of F-H10. The anode signals from the LP-MWDCs were amplified and discriminated by REPIC RPA-130/131. The timing information for the leading and trailing edges was recorded by using CAEN V1190 multihit TDCs. Plastic scintillators were placed at F-3 and F-H10, whose thicknesses were 1 mm and 3 mm, respectively. The scintillator at F-3 was used as a trigger counter. The time zero for the drift chamber was determined by the scintillator at F-H10. The signals from the scintillators at F-3 and F-H10 were discriminated by Lecroy 623B and Iwatsu QTC[5)], respectively. The discriminated signals were fed to the TDC and digitized.

The data, which were obtained at a beam rate of ∼1 MHz, were analyzed. The events were selected by determining the timing obtained from the scintillator and LP-MWDC. Figure 1(a) shows the spectrum of the timing for the scintillator at F-H10. The timing was selected to be within the range 605–615 ns. Figure 1(b) shows the drift time distribution acquired from the anode wires of one layer at a bias voltage of 1000 V. In the following analysis, the drift time within the range −−35 to 90 ns were used.

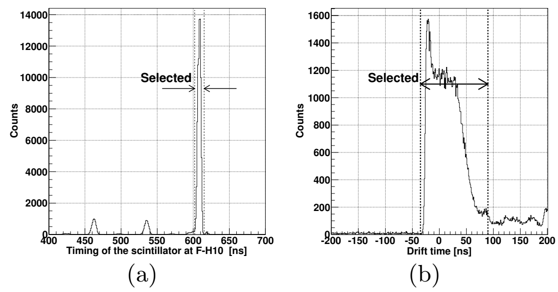

Fig. 1. (a) Timing obtained from the scintillator at F-H10 and (b) drift time distribution in X plane for an ^{12}N beam at a rate of ∼1 MHz.

Next, the event in which only one heavy ion passed through F-H10 for a single trigger was selected in order to obtain the best position resolution under the given beam conditions. Information about the pulse width, which is related to the energy loss of the beam in the gas, enables us to select the single-heavy-ion

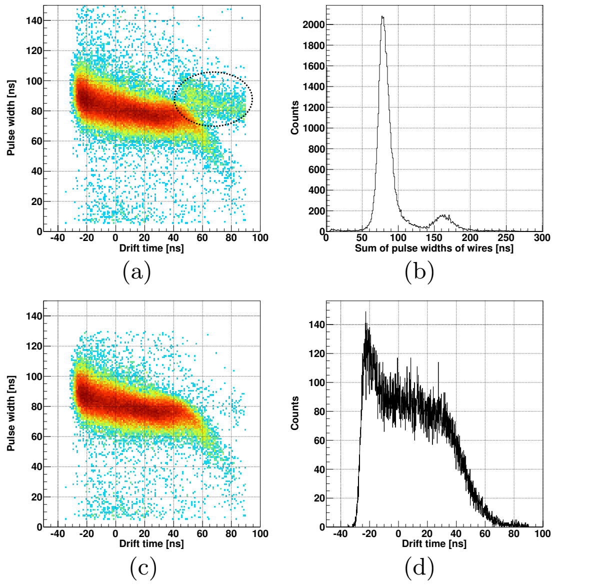

Fig. 2. (a) Relation between pulse width and drift time acquired from the wires in one plane (b) spectra of the sum of the pulse widths, and obtained (c) relation between the pulse width and the drift time and (d) the spectra of the drift time by selecting the sum of the pulse widths.

event. Figure 2(a) shows the relation between the pulse width and the drift time for the wires with the maximum pulse width on an event-by-event basis in the X layer for the ^{12}N beam. In Fig. 2(a), the locus indicated by the dashed circle shows the event where multiple heavy ions pass in one trigger. Figure 2(b) shows the spectra of the sum of the pulse widths over all the wires in one layer. The peaks at around 80 ns and 160 ns were considered to be due to single-heavy-ion hit events in one trigger and double-heavy-ion hit events, respectively. In the following analysis, the events in the range 0–130 ns were considered. Figure 2(c) shows the relation between the pulse width and the drift time. From this figure, it could be senn that the double-heavy-ion events were discriminated from the single-heavy-ion events. Figure 2(d) shows the spectrum of the drift time distribution after the cut. On the basis of the drift time distribution, the beam hit position was calibrated for all anode planes.

In order to estimate the position resolution, the distribution of $U_{\mathrm{U}} - U_{\mathrm{XV}}$ was investigated. Here, U_{U} is a hit position in the U layer, and U_{XV} is a hit position along the U axis and is determined from the hit positions in layers X and V. The geometrical configuration of the planes helps in unambiguous determination of the hit position. Figure 3 shows the residual distribution of $U_{\mathrm{U}} - U_{\mathrm{XV}}$. Considering the error propagation, the position resolution is estimated to be 340 μm (FWHM), which is sufficient for achieving the required

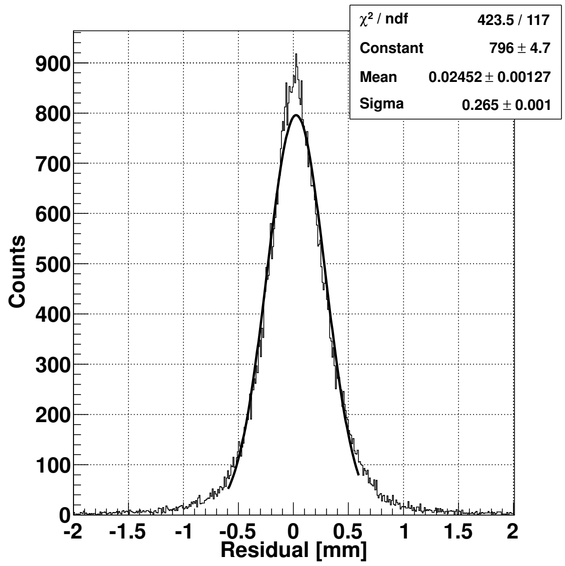

Fig. 3. Residual distribution of $U_{\mathrm{U}} - U_{\mathrm{XV}}$.

performance. Further analysis is now in progress.

References

1) H. Miya et al.: RIKEN Prog. Rep. **43** (2010) 192.
2) T. Uesaka et al.: AIP Conf. Proc. **1235** (2010) 308.
3) Y. Sasamoto et al.: RIKEN Prog. Rep. **44** (2011).
4) S. Noji et al.: RIKEN Prog. Rep. **44** (2011).
5) S. Ota et al.: RIKEN Prog. Rep. **44** (2011).

Development of new online analysis system for Short-range gravity experiment using FPGA

K. Ninomiya,[*1,*2] H. Nishio,[*1] N. Ogawa,[*1] A. Taketani[*2] and J. Murata[*1]

According to the large extra dimension model (ADD model)[1)], a deviation from Newton's inverse square law is expected at below sub millimeter range. We have started test of Newton's inverse square law aiming to search for extra dimension[2)]. In addition, composition dependence of gravitational constant G is also tested at a millimeter scale, motivated to test the weak equivalence principle[2)]. In our experiment, gravitational force is measured using a torsion pendulum and an online image analyzing system. Angular displacement different gravity source (attractor) position is measured as the gravitational signal. The data taking system was originally developed for the PHENIX experiment at RHIC (Relativistic Heavy Ion Collider) at Brookhaven National laboratory, as an optical alignment system (OASys)[3)]. By applying this system, we developed digital image analyzing system using digital video camera[3,4)].

We developed online digital analysis system using analog capture board in 2008. This system can compress data size into 1/180 and reduce analyzing time into 1/1000 compared with offline analysis system developed in 2003[5)]. As a result, we succeeded to test the Newton's inverse square law at cm scale with 5% accuracy (Newton SC experiment). In addition, we also succeeded to confirm the weak equivalence principle at the shortest scale (Newton II experiment).

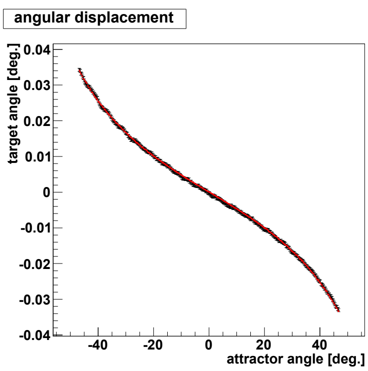

Fig. 1. Result of the test of Newton's Inverse square law in 2009. Red line is Newton's gravitational prediction.[6)]

This year, in order to utilize the full frame rate of CCD and improve the statistic precision, we have started to develop a new online analysis system using FPGA at RIKEN. In order to compress the data size and improve the analyzing speed, original online system developed in 2008 was designed to be composed

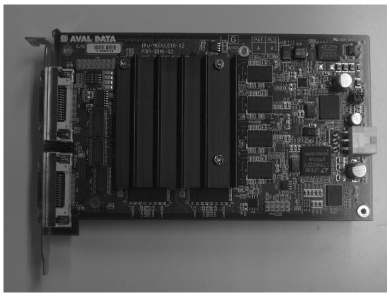

Fig. 2. New image processing board. this board is attached capture board. FPGA is mounted under heatsink.

by a DV camera(canon IXY DV M2) and a video capture board (Interface LPC-530115). By a direct access to the capture board, image data are obtained without being recorded into a video image file. Intensity data are sent to PC, then, a linear line fitting is applied on the intensity data. However, this system can not utilize full ability of CCD. For instance, in spite of frame rate of the DV camera is 30 fps, that of the current online system is limited to below 15 fps. It is because analyzing time depends on the processing speed of CPU. FPGA can execute all the process from data taking to determination of the angular displacement of the torsion pendulum without depending on CPU power.

That is why, we have started developing new online system using FPGA made by Altera. Image processing board is shown fig.2. Analyzing code is written in VHDL. Analyzing speed is finally dependent on the frame rate of CCD. However, analyzing speed of FPGA can be expected over 100fps. By developing this new system using FPGA, we can expect improvement of the statistical precision by factor 1/10.

References

1) Nima Arkani-Hamed, Savas Dimopoulos, Gia Dvali, Phys. Lett. B 429 (1998) 263-272.
2) M. Hata et.al., Journal of Physics: Conference Series 189 (2009) 012019
3) J. Murata, IEEE Nuclear Science Symposium Conference Record 675 (2005).
4) J. Murata et. al., Nucl. Instrum. Meth. A 500(2003) 309-317.
5) K. Ninomiya et.al., Journal of Physics: Conference Series 189 (2009) 012026
6) K. Ninomiya, Master thesis, Rikkyo University (2010)

*1 Department of Physics, Rikkyo University, Japan
*2 RIKEN Nishina Center,Japan

Logic Unit for Programmable Operation

H. Baba, T. Ichihara, T. Ohnishi, S. Takeuchi, K. Yoshida, Y. Watanabe, S. Ota,[*1] and S. Shimoura[*1]

Logical circuits in nuclear physics experiments are now shifting to the use of Field Programmable Gate Array (FPGA) from single-function NIM modules. FPGA can help in constructing large-scale logical circuits and its firmware can be replaced easily. By using the FPGA, a logic unit for a programmable operation (LUPO) module has been developed. To realize a time-stamping system in RIBF DAQ[1)], firmware for the time stamper has been developed[2)]. The specification for the LUPO module is described in a previous paper[2)]. The LUPO module can be used for the time stamper as well as other purposes. Here, we report developed firmwares. Firmware development is based on VHDL language, which is commonly known as hardware description language. Simple VHLD modules that have basic functions such as "Interrupt," "Scaler," and "Coincidence" have been developed. By combining VHDL modules, firmware for the LUPO module can be developed easily (Fig. 1). For example, the firmware of the I/O and Interrupt register contains "Input," "Output," "Interrupt," and "Coincidence" VHDL modules.

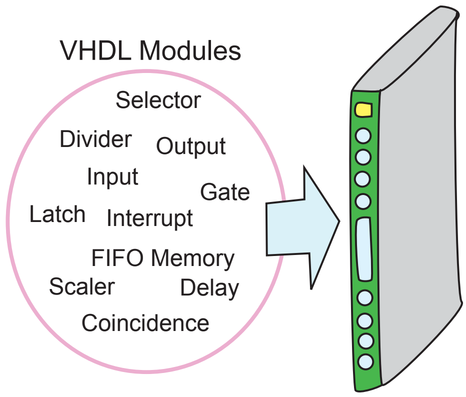

Fig. 1. By combining simple VHDL modules, a LUPO can perform a variety of integrated circuits.

I/O and Interrupt register

This firmware performs the functions of input, output, coincidence, and interrupt registers. LVDS and NIM input registers return the status of inputs (high or low). NIM/LVDS coincidence registers return a pattern that reflects the coincidence between each input and a NIM gate input. Depending on the interrupt input, CAMAC LAM (VME IRQ) is generated. The time between the interrupt input and the actual interrupt generation can be varied (20 ns step, maximum is about 1.3 ms). In an output register, level and pulse signals can be generated. The pulse width is also variable (20 ns step, maximum is about 1.3 ms).

Scaler

The scaler firmware can be used as a 20-channel simple scaler. Inputs are 4 NIM and 16 LVDS. The scaler depths are 24 bits for CAMAC and 32 bits for VME. NIM input 3ch can be configured as a veto input, which inhibits counting. The LUPO module can generate clock signals of several frequencies. This firmware generates 1 MHz, 10 KHz, and 1 KHz clock signals, and the clock counts can be read out. The bandwidth of NIM and LVDS inputs are more than 200 MHz.

DAQ Master

The firmware of "DAQ Master" is designed to cover the operations of conventional circuits for a stand-alone DAQ system. To extract detector data by using CAMAC/VME systems, logical circuits for coincidence, gate, latch, scaler, interrupt, and output are required. Usually these functions are performed by standard NIM and CAMAC (VME) modules; however the firmware can process these functions with only one LUPO module. The firmware contains the functions of the scaler, logical AND/OR gates, variable outputs, and internal trigger circuits. The scaler counts the number of NIM inputs, clocks, and ungated/gated triggers. By registering logical AND/OR gates, the trigger signal is defined as trigger = NIM 0ch AND NIM 1ch. The internal trigger circuit includes the veto and interrupt circuits. The veto circuit inhibits trigger generation, and the number of ungated (generated) and gated (accepted) triggers can be read out through the scaler function. There are four NIM outputs, and these can be configured as an output register, ungated/gated triggers, veto, and clock signals. As shown above, this "DAQ Master" firmware provides the functions of all necessary logical circuits for a stand-alone DAQ system.

In addition, firmwares for "Time Stamper," "Trigger Selector," and "Gate and Delay generator" have been developed. VHDL modules of fundamental functions shown in Fig.1 facilitate easy development for users. And the LUPO module can implement more complex circuits. These features are very powerful and can be used to construct a customized integrated circuit. The LUPO module will be used for various measurements.

*1 Center for Nuclear Study, University of Tokyo

References
1) H. Baba et al.: Nucl. Inst. Meth. A **616** (2010) 65.
2) H. Baba et al.: RIKEN Accel. Prog. Rep. **42** (2009) 222.

Parallel Acquisition and Control Intelligent system for Femto-frontIer Collaboration (PACIFIC)

S. Ota,[*1] S. Shimoura,[*1] H. Baba, E. Ideguchi,[*1] M. Kurokawa, H. Tokieda,[*1] S. Kawase,[*1] S. Go,[*1] and T. Otsuka,[*1,*2]

[Data acquisition system, Digital signal processing, Charge-to-time converter]

Nuclear physics experiments for studying the structures and properties of unstable nuclei have increased in scale because of the number of detectors, reaction rate, and geometrical setup. On the other hand, the scale of the dead time is required to be as small as possible. Recently, a data acquisition system named BABIRL has been developed with the objective of reducing the dead time during data collection.[1)] In this system, the data acquisition subsystem of the detectors are combined by a master event builder. The acquisition time of most of the subsystems has been kept comparable to or smaller than that of the preceding data acquisition system. However, there still remains the task of improving analog signal processing to facilitate dead-time-less data acquisition.

We are developing the Parallel Acquisition and Control Intelligent system for Femto-frontIer Collaboration (PACIFIC). The PACIFIC consists of a high-speed signal processing and parallel data acquisition system. The three main parts of the PACIFIC have the following functions:

(1) analog signal processing for fast signals (QTM)
(2) digital signal processing for slow signals (APU7110-P)
(3) asynchronous control and data collection (e-RT3) for monitoring the status of the experimental setup

In this report, we describe the principle and components of each part.

The QTM module (Fig. 1) is a newly developed generic charge-to-time converter (QTC) module fabricated by Iwatsu Test Instruments Corporation; this modules converts the total charge of the input signal to a pulse width. When we detect the timing of the leading and trailing edge of the output pulse, we can obtain the timing and charge information simultaneously. The timing of the input signal is determined by leading-edge discrimination; the leading edge is the trigger for the charge correction. The time window for the charge correction can be set by using some registers and can be less than 1 μs. Therefore, typical conversion time, *i.e.*, dead time, is only 1 μs, which enables us to perform fast signal processing by using a multi-event non stop TDC module such as the V1190/1290 module (CAEN).

*1 Center for Nuclear Study, University of Tokyo
*2 Department of Physics, University of Tokyo

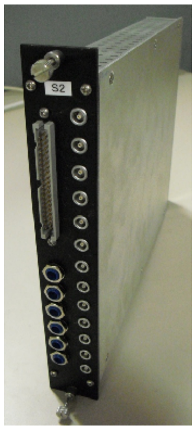

Fig. 1. Photograph of the QTM module

The QTM module is a one-span NIM module involving six preamplifiers (but it is optional and can be bypassed), two QTC chips, and one register controller. The QTC chip has been made by Iwatsu. This chip accepts the charges up to around 50 pC and contains 3×3 charge integrators. The input signal is divided into three identical signals, and two of these signals are attenuated by factors of 1/7 and 1/49. The overall input dynamic range then increases up to approximately 2.5 nC. The QTM module has 6 inputs with 50-Ω termination and 18 LVDS outputs that are grouped into three categories according to the dynamic range.

To evaluate the basic performance of the QTM module, we measure the time and charge resolution at medium gain (50-350 pC). The typical time resolution is 110 ps for charge above 200 pC when using the multi-hit TDC V1190 module, while the resolution is 40 ps when using the V775 TDC module. The difference between these resolutions is because of the least significant bit of each module. The typical charge resolutions measured by using the charge sensitive ADC V792 and a combination of QTM and V1190 were approximately 1% and approximately 3%, respectively, for a charge above 50 pC. Although the resolution in the case of the QTM is lower, this resolution is suitable for not only measurements performed with a the plastic scintillator but also measurements performed the non-organic scintillator. The details are described in some references[2,3)].

The QTM modules have been utilized in experiments performed at the BigRIPS-SHARAQ course at the RIBF. Figure 2 shows a plot for particle identification in the final focal plane of SHARAQ. The horizontal and vertical axes show the time of flight between the target and final focal plane, and the charge, respectively, both the time of flight and charge are measured by using the QTM.

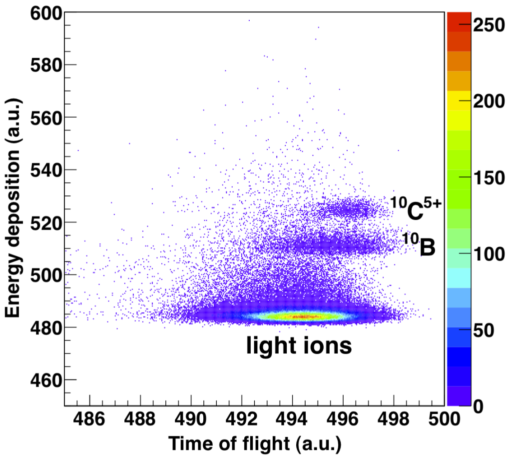

Fig. 2. Plot for particle identification in the final focal plane of SHARAQ. The horizontal and vertical axes indicate the time of flight and energy deposition in the plastic scintillator, respectively.

The APU7110-P (Fig. 3) module has been developed for a γ-ray detector array, namely GRAPE, to extract the energy, timing, and position of incident γ rays by using digital pulse shape analysis. The pre-amplified 2×9 signals from a nine fold segmented germanium detector are digitized using the pipeline process by an FADC. In addition, the digital signals are numerically processed by using an FPGA to determine their energy and timing by applying slow trapezoidal shaping and constant-fraction discrimination, respectively.

To determine the three-dimensional position of incident γ rays, we are developing a new algorithm that is the pipeline processing[4].

To perform the experiment safely and expeditiously, the parameters for each device, for example, the gas pressure, and rate of gas flow and high voltage supplied to the beam-line detectors, vacuum in the chambers, and current supplied to each magnet should be monitored and controlled during the experiment. Moreover, knowledge of the values of the parameters is also important to achieve better resolutions; better resolutions are achieved by correcting the effect of the temporal changes in the parameters. The devices are monitored and controlled by using a programmable logic controller (PLC) for the beam-line detectors and a network I/O controller (NIO) for the magnets.

Although general PLCs are programmed in a very specific and difficult language running on a sequence

Fig. 3. Photograph of the APU7110-P module

CPU, a new PLC module, which has been available since the summer of 2008, enables us to program the PLCs in a more familiar language, namely C, by using a normal Linux operating system running on PowerPC. Experimental Physics and Industrial Control System (EPICS) is chosen as the control software because it is widely used in the field of accelerator operation and is a freeware developed by the Argonne National Laboratory. The operating system and EPICS I/O controller are loaded to each PLC from the main server via a network boot protocol, and the management of PLCs is simplified.

The NIO is a VME module for controlling the power supplied to the magnets. We have developed drivers and software for the Linux operating system to drive the NIO modules; the drivers are based on the drivers for VxWorks that runs on PowerPC. The magnet control system consists of a VME CPU board and NIO-C, NIO-B, and NIO-S boards. The operating system and control programs are loaded from the main server as well as the PLC module. The NIO-S board directly controls and monitors each power supplied to the magnet, and the NIO-C board sequentially controls all the NIO-B boards via the NIO-B hub board.

The data collected from the devices will be merged asynchronously with the physics data via the BABIRL protocol and the combined data will be used for analysis and will be stored in a database; the stored data will be used as an example of the data in a typical experimental setup and will be used for reference in future experiments.

References

1) H. Baba et al.: Nucl. Instrum. and Methods A **616**, 65 (2010)
2) S. Ota et al., CNS Annual Report 2008 (2010)
3) S. Kawase, S. Ota et al., CNS Annual Report 2009 (2011).
4) S. Go et al., CNS Annual Report 2009 (2011).

Radiation analysis for large, thin solid hydrogen target

Y. Matsuda,[*1] H. Sakaguchi,[*2] J. Zenihiro,[*2] S. Terashima,[*3] K. Kamei,[*1] H. Otsu

Proton elastic scattering at intermediate energies has been used to determine the density distributions of nuclei[1–3)]. Therefore, elastic scattering of protons with RI beams (ESPRI) is expected to be measured. Until now, however, it has been difficult to fabricate large, thin solid hydrogen targets (SHTs) for ESPRI measurements because thermal radiation from the hotter surroundings causes sublimation at the center of the target[4,5)]. Recently, we studied this thermal problem in detail and succeeded in developing large, thin SHTs that were 30 mm in diameter and 1 mm thick[6)]. In this report, we describe the estimation of thermal radiation.

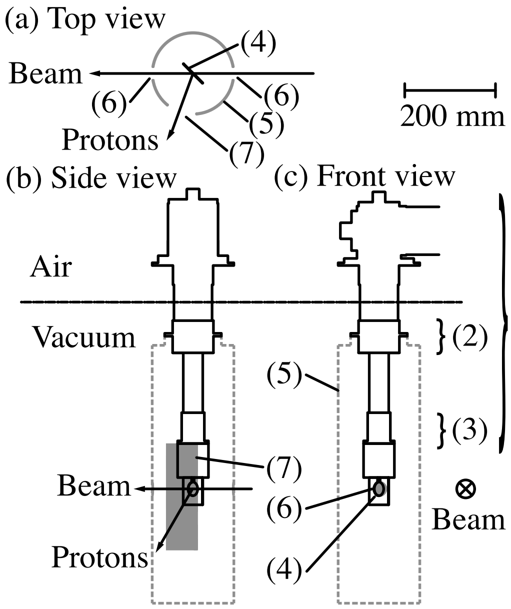

Fig. 1. Schematic view of the cryogenic system. (a) top, (b) side and (c) front views. (1) Two-stage Gifford-McMahon-cycle refrigerator; (2) first stage of the refrigerator; (3) second stage of the refrigerator; (4) target cell; (5) radiation shield; (6) beam window; (7) recoil window. The target chamber and laying pipes are not shown.

In order to estimate the heat transfer to the SHT, we employed the network model[7,8)]. In this model, two potential nodes are connected with a resistance, where heat flows as the current. The resistances are represented by the areas, shape factors, reflectivities, and transmittivites of the network elements. This type of network is equivalent to electrical networks; hence, the laws applicable to electrical circuits can be applied to the present network as well.

Table 1. Assumed conditions for each surface. They are rough approximations for the feasibility study. The emissivity of the SHT ϵ_{SHT} is a parameter

	T [K]	Emissivity	Transmittivity	Reflectivity
SHT	4	ϵ_{SHT}	$1-\epsilon_{\mathrm{SHT}}$	0
RS	50	0.1	0	0.9
BW	300	1	0	0
RW	300	1	0	0

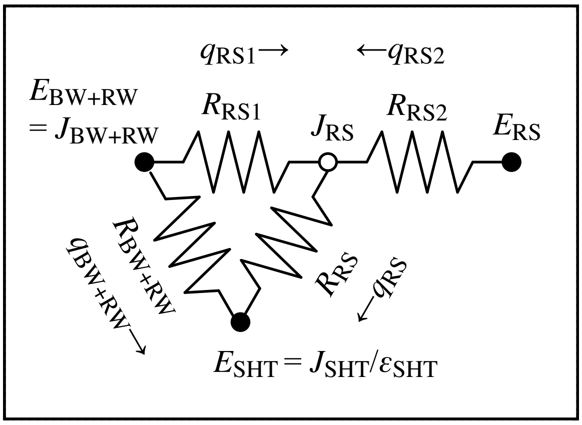

Fig. 2. Radiation network of the system. q_i, E_i, J_i, and R_i (i = BW+RW, RS, SHT, RS1, RS2) are the heat exchange, blackbody emissive power, radiosity, and thermal resistance in each network element, respectively. Closed circles: boundary nodes where the temperatures are constant; open circles: floating potential nodes.

On the basis of the cryogenic system shown in Fig. 1 and the properties listed in Table 1, we constructed a model of a radiation network, as shown in Fig. 2. The beam window, recoil window, and radiation shield are abbreviated as BW, RW, and RS, respectively. BW+RW implies the combination of the BW and the RW. q_i, E_i, J_i, and R_i (i = BW+RW, RS, SHT, RS1, RS2) imply the heat exchange, blackbody emissive power, radiosity, and thermal resistance in each network element, respectively. The blackbody emissive power is given by $E_i = \sigma T_i^4$, where σ (5.7 $\times 10^{-8}$ W/m$^2\cdot$K^4) is the Stefan-Boltzmann constant. In this model, the RS1 element is caused by the heat exchange between BW+RW and the RS; the RS2 element is caused by the finite reflectivity of the RS. Because the reflectivities of BW+RW and SHT are zero, $J_{\mathrm{BW+RW}}$ and J_{SHT} are equal to $E_{\mathrm{BW+RW}}$ and $\epsilon E_{\mathrm{SHT}}$, respectively. Considering that the SHT and the RS are attached to the refrigerator, we fixed the

*1 Department of Physics, Tohoku University
*2 Department of Physics, Osaka University
*3 GSI, Darmstadt, Germany

temperatures as well as that of BW+RS. Since q_i, E_i (J_i), and R_i correspond to the current, voltage, and resistance of electrical circuits, the heat flow $q_{\mathrm{BW+RW}}$ from BW+RW to the SHT is calculated by the formula $(E_{\mathrm{BW+RW}}-E_{\mathrm{SHT}})/R_{\mathrm{BW+RW}}$. The other heat flows are calculated similarly. Here, we considered the following two assumptions to calculate the shape factors easily: (a) the route transmitting radiation through the SHT is ignored in R_{RS1} because of the small SHT; (b) the BW and RW are parallel to the SHT and are hidden from each other. Therefore, the thermal resistances are written as

$$R_i = \frac{1}{\epsilon_{\mathrm{SHT}} A_i F_{i,\mathrm{SHT}}},\ i = \mathrm{BW}+\mathrm{RW}, \mathrm{RS}, \qquad (1)$$

$$R_{\mathrm{RS1}} = \frac{1}{A_{\mathrm{BW+RW}} F_{\mathrm{BW+RW,RS}}}, \qquad (2)$$

$$R_{\mathrm{RS2}} = \frac{1-\epsilon_{\mathrm{RS}}}{\epsilon_{\mathrm{RS}} A_{\mathrm{RS}}}, \qquad (3)$$

where A_i, $F_{i,j}$, and ϵ_i (i,j = BW+RW, RS, SHT) are the areas of medium i, the shape factors from medium i to medium j, and the emissivity of medium i, respectively. The concrete sizes relating the areas and the shape factors are provided elsewhere[6]. Considering that $R_{\mathrm{BW+RW}}$ can be divided into the thermal resistances of R_{BW} and R_{RW}, $1/R_{\mathrm{BW+RW}} = 1/R_{\mathrm{BW}} + 1/R_{\mathrm{RW}}$, we can obtain the heat exchanges as functions of ϵ_{SHT}:

$$q_{\mathrm{BW}} = \frac{E_{\mathrm{BW+RW}} - E_{\mathrm{SHT}}}{R_{\mathrm{BW}}} = \frac{\sigma 300^4 - \sigma 4^4}{27000/\epsilon_{\mathrm{SHT}}}\ [\mathrm{W}],$$

$$q_{\mathrm{RW}} = \frac{E_{\mathrm{BW+RW}} - E_{\mathrm{SHT}}}{R_{\mathrm{RW}}} = \frac{\sigma 300^4 - \sigma 4^4}{4700/\epsilon_{\mathrm{SHT}}}\ [\mathrm{W}],$$

$$\begin{aligned} q_{\mathrm{RS}} &= \frac{1/R_{\mathrm{RS}}}{1/R_{\mathrm{RS}} + 1/R_{\mathrm{RS1}} + 1/R_{\mathrm{RS2}}} \left(\frac{E_{\mathrm{BW+RW}} - E_{\mathrm{SHT}}}{R_{\mathrm{RS1}}} + \frac{E_{\mathrm{RS}} - E_{\mathrm{SHT}}}{R_{\mathrm{RS2}}} \right) \\ &= \frac{\epsilon_{\mathrm{SHT}}/2200}{\epsilon_{\mathrm{SHT}}/2200 + 1/60 + 1/26} \left(\frac{\sigma 300^4 - \sigma 4^4}{60} + \frac{\sigma 50^4 - \sigma 4^4}{26} \right) [\mathrm{W}]. \end{aligned}$$

The heat exchanges and the sum are shown in Fig. 3. The RW is the largest source of heat because it is the largest opening to an area at room temperature. The radiation from the RS is negligibly small; therefore, the radiation from the RW reflected on the RS accounts for most of the radiation from the RS. Judging from a guess that the emissivity of the SHT is less than 0.5 and the size of the sublimated area in the SHT[4], the heat transfer rate can be several tens of milliwatts. Therefore, in order to prevent the sublimation of the SHT, the heat transfer rate should be an order smaller than that of the present system[6]. This is, however, infeasible because inserting any material into the path of the recoil protons would decrease the excitation energy resolution and/or the solid angle. Consequently, we must improve the heat transfer in the SHT instead of decreasing the thermal radiation.

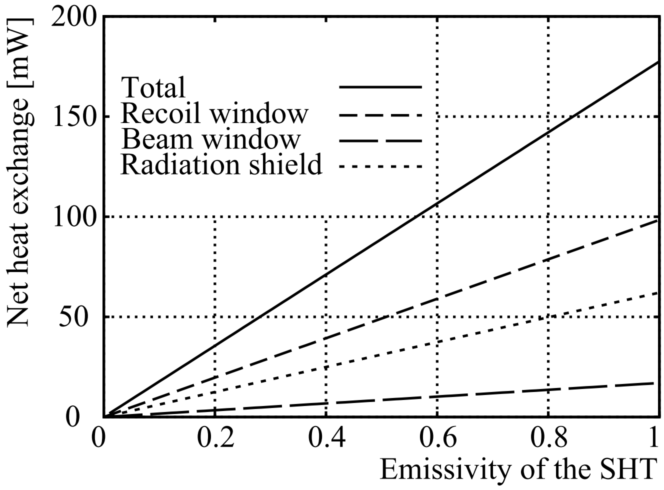

Fig. 3. Heat transfer to the SHT as a function of SHT emissivity. The dashed, long-dashed, and short-dashed lines correspond to the heat transfer from the RW, BW, and RS, respectively. The solid line indicates the sum of the heat transfers.

In conclusion, to investigate the feasibility of fabricating a large, thin SHT for ESPRI measurements, we estimated the thermal radiation from the surroundings to the SHT by employing the network model. From the analysis results, we found that the heat transfer rate is several tens of milliwatts and that the main source of heat is the RW. Because the experimental conditions for ESPRI make it difficult to reduce the thermal radiation, we conclude that the heat transfer in the SHT must be improved in order to prevent the sublimation at the center of the target. A possible solution to the radiation problem is the use of para-hydrogen, which has high thermal conductivity at low temperatures. The development is reported in an our previous paper[6].

References

1) V.E. Starodubsky and N.M. Hintz: Phys. Rev. C **49** 2118 (1994).
2) S. Terashima et al.: Phys. Rev. C **77** 024317 (2008).
3) J. Zenihiro et al.: Phys. Rev. C **82** 044611 (2010).
4) H. Takeda et al.: RIKEN Accel. Prog. Rep. **40** 161 (2006).
5) K. Tanaka et al.: RIKEN Accel. Prog. Rep. **41** 144 (2008).
6) Y. Matsuda et al.: Nucl. Instr. and Meth. A **643** 6 (2011).
7) A.K. Oppenheim et al.: Trans. ASME **78** 725 (1956).
8) J.P. Holman: Heat Transfer, Sixth Edition (McGraw-Hill, New York, 1986).

Development of the cryogenic system CRYPTA for a deuterium gas target

M. Kurata-Nishimura, Y. Kondo,*[1] N. Tanaka,*[1] K. Takahashi,*[1] N. Kobayashi,*[1] A. Matta,*[1],*[2] and D. Beaumel*[2]

[Cryogenic target, unstable nuclei]

The cryogenic proton and alpha target system (CRYPTA)[1)] is advantageous for studying unstable nuclei because of high density and low background. Several experiments have been performed successfully by using liquid hydrogen[2)] and liquid helium[3)] at the RIKEN facilities.

In a previous experiment performed in July 2010, the CRYPTA was employed for studying structure of ^{10}He utilizing the proton transfer reaction with MUST2 telescope arrays[4)]. For achieving an adequate angle and energy resolution, the deuterium-gas (D_2) target with a thickness less than 5.5 mm and a window foil made of a thin and a low atomic number material foil were required. The pressure of the D_2 gas was chosen to be 0.5 atm at 25 K and it had a gain that was 1.5 times that of a CD_2 foil. A 12-μm-thick luminor, whose physical properties were similar to those of the aluminized mylar, was prepared, for use as a separation window of the gas cell in vacuum.

Since we had no experience of using such a thin mylar foil for a cryogenic target, so far, the deflection of the window foil was of siginificant concern. In this experiment, the heat shield, which prevents heat transfer from the surrounding material to the target cell by radiation, was removed to prevent any reduction in the acceptance of a recoil particle. It was necessary to evaluate the effect of the removal of the heat shield.

In this paper, significant results obtained in our development have been presented and discussed.

The target cell consisted of a 3-mm-long aluminum body and two window frames with a 40-mmϕ hole on each side. The luminor foils were glued to the window frames with epoxy (Stycast 1266A). The target cell was installed in a vacuum chamber on which a cryogenic pumping system was mounted.

The target cell was cooled to the cryogenic temperature by using a copper rod connected to the cryogenic system. Two silicon diode sensors (Scientific Instruments, Si410AA) were installed to measure the temperature of the target cell; one was installed at the edge of the copper rod where the target cell was connected (TOP), and the other was installed at the bottom of the target cell (BOTTOM). For maintaing a stable temperature, an automatic temperature controller (Lake Shore, 331S) was used.

*[1] Department of Physics, Tokyo Institute of Technology
*[2] Institut de Physique Nucleaire, IN2P3-CNRS, Universite de Paris Sud, F-91406 Orsay, France

To evaluate the degree of deflection, the curvature of the window-foil surface was measured with a laser displacement sensor (Keyence, LK-500). As shown in Fig.1, the surface of the foil was expanded like that of a balloon at a gas pressure of 0.2 atm at 300 K. The maximum height of the expansion, which is illustrated in Fig.1, is called swelling height.

The pressure dependence of the swelling height was measured at the temperatures of 300 K and 30 K. In Fig.2, the values of the swelling height at 300 K and 30 K are shown as closed circles and closed squares, respectively. It can be observed that the swelling height increased much more at 300 K than at 30 K. These values were compared with those obtained by the following theoretical formula[5)];

$$w = 0.662a(Pa/Eh)^{1/3}, \tag{1}$$

where, w, a, P, E and h are the swelling height, radius, pressure, Young's modulus and thickness of the foil, respectively. The open circles show the calculated values for the case of 12-μm-thick mylar, which has a Young's modulus of 4 GPa[6)]. At 300 K, the calculated value agree well with the experimental value at 0.2 atm and is lower than the experimental value at other pressures. It indicates that gas pressures greater than 0.2 atm are beyond the yield point of the 12-μm-mylar foil at 300 K.

In contrast, the values of the swelling height at 30 K were much smaller than the calculated values, but the slope was similar to that of the calculated values. If we

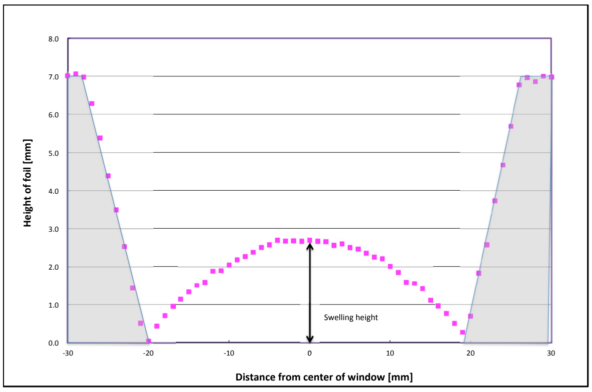

Fig. 1. Deflaction of the window foil. The inner gas pressure was 0.2 atm and the temperature was 300 K. The gray-colored regions indicate the support frames.

compare the experimental results with the calculated results for a Young's modulus of 8 GPa, the calculations reproduce the experimental results very well, as shown by the dotted line in Fig.2.

These observations indicate that at the cryogenic temperature, not only the mylar foil's stiffness increases by a factor of two but its yield point also increases.

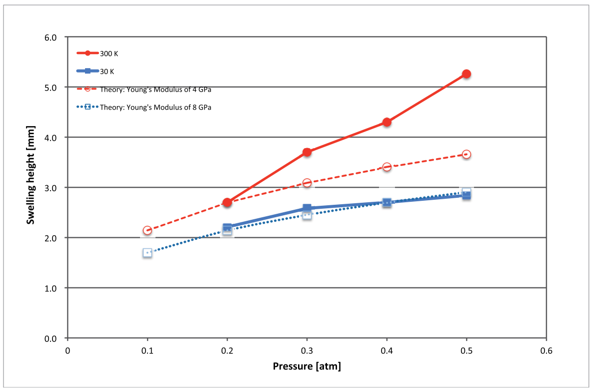

Fig. 2. The swelling height as a function of the pressure. The closed circles and closed squares correspond to 300 K and 30 K, respectively. The dashed line indicates the theoretical calculations for 12-μm-Mylar. The dotted line shows the same calculations for a foil with twice the stiffness.

The minimum achievable temperatures were measured with and without the heat shield. The temperatures at TOP and BOTTOM are listed in Table 1. The shield effect was apparent for the comparison between the two cases, i.e. with and without the heat shield. When the heat shield was not used, a higher minimum temperature and a large difference between the two points were observed, which indicated a larger thermal gradient on the target cell. The temperature gradient increased when the target cell was installed in the reaction chamber. This is because of the modification of the thermal absorption on the surface of the target cell, since the surface of the target cell was contaminated by oil in the reaction chamber. Owing to the large thermal gradient, the system was operated at temperature above 30 K because below 18 K, D_2 gas solidified in an installation tube. It is a crucial problem for the gas target to operate at high temperature, since, for instance, the target becomes thinner by 1.5 times owing to reduced density when the temperature is increased from 20 K to 30 K.

A cryogenic D_2-gas target was developed for the MUST2 experiment at RIPS. The stiffness of the mylar foil at 30 K was two times larger than that of the mylar foil at room temperature. The importance of a heat shield was noted especially for the cryogenic gas target.

Table 1. The minimum achievable temperature with and without the heat shield. The temperature was measured at two positions: TOP and BOTTOM. i.e., at the edge of the copper rod where the target cell was connected and the bottom of the target cell that was the far side of the copper rod, respectively.

Configuration	TOP	BOTTOM
without Shield	17.0 K	24.8 K
with Shield	9.9 K	10.3 K

References

1) H. Ryuto et al.: Nucl. Inst. Meth. **A 555**, 1 (2005); K. Tanaka et al.: RIKEN Accel. Prog. Rep. **39**, 151 (2006).
2) Y. Yanagisawa et al.: Phys. Lett. **B 566**, 84 (2003); S. Kanno et al.: RIKEN Accel. Prog. Rep. **38**, 66 (2005).
3) S. Michimasa et al.: Pys. Rev. **B 638**, 146 (2006).
4) E. C. Pollacco et al.: Eur. Phys. J. **A 25**, 287 (2005).
5) S. P. Timoshenko and S. Woinowsky-Kreiger: Theory of Plates and Shells, McGraw Hill Higher Education, (1964)
6) http://www.toray.jp/films/products/pdf/mictron.pdf.

Development of a polarized target for future spin-structure study of the proton in the SeaQuest experiment

Y. Goto, N. Doshita,[*1] Y. Fukao, S. Ishimoto,[*2] H. Matsuda,[*1] Y. Miyachi,[*1] I. Nakagawa, K. Nakano,[*3] S. Sawada,[*2] and T.-A. Shibata[*3]

The SeaQuest experiment, which is aimed at detecting muon pairs from the Drell-Yan process, is scheduled to begin in early 2011 at Fermilab [1]. In this experiment, a 120-GeV unpolarized proton beam extracted from the Fermilab Main Injector and unpolarized proton and deuterium targets will be used to study the flavor symmetry violation of antiquark distributions in the proton. In this experiment, we will be able to study the spin structure of the proton by using a polarized proton target. The single-spin asymmetry (SSA) of the Drell-Yan process will help in precision measurement of one of the transverse-momentum-dependent distribution functions, the so-called Sivers function[2]. The Sivers function represents a correlation between the proton transverse spin and the parton transverse momentum, and it is closely related to the orbital angular momentum in the proton.

For measuring the SSA of the Drell-Yan process, we need a sufficiently large amount of the material to be used as the polarized proton target because the cross section of this process is small. Hence, a large polarized proton target that can be used with the high-intensity beam from the Main Injector must be developed for the spin-structure study of the proton in the SeaQuest experiment. In order to operate the polarized proton target and preserve the polarization, it is important to stabilize the target at a low temperature by removing the heat from the injected high-intensity beam.

We will develop the polarized proton target from a 3-cm-long irradiated-ammonia polarized target at KEK. Irradiated ammonia has good radiation tolerance, which is also required for polarized-target operations with a high-intensity beam. The target was originally developed by Michigan University and operated in a 5-T magnetic field at 1 K[3]. The target underwent 85% polarization on an average, and it was used in BNL-AGS experiments. Presently, the target is located in the KEK-PS North Counter Hall, as shown in Fig.1. Before operating the "Michigan" target, we must rebuild the polarized proton target system. We have built a 1-K helium pipe, a support structure, and a vacuum insulation system before starting the test operation of the 1-K cryostat and 5-T magnet. Also important is obtaining the desired shape of the target material. We will investigate the cooling performance by heating the target holder artificially.

We will also develop other target materials by using the polarized target system at Yamagata University. One candidate target material is polyethylene fiber. When using fibers, we can obtain a large surface area that would yield a large cooling power. Fibers also show high deformation performance, and they facilitate easy manufacturing of the target. To improve the stability of the cryostat, we are constructing a new cryostat and cooling tests are underway. Development of the target material will be commenced soon after the new cryostat is ready.

This research is supported by the JSPS Grant-in-Aid for Scientific Research (B) 22340070.

References
1) Y. Goto *et al.*: RIKEN. Accel. Prog. Rep. **43**, 80 (2010).
2) D. W. Sivers: Phys. Rev. **41**, 83 (1990).
3) D. G. Crabb *et al.*: Phys. Rev. Lett. **64**, 2627 (1990).

Fig. 1. "Michigan" target located in the KEK-PS North Counter Hall.

*1 Yamagata University
*2 KEK
*3 Tokyo Institute of Technology

Beamline optics for pionic atom spectroscopy at RIBF

S. Itoh,[*1,*2] G.P.A. Berg,[*3] H. Geissel,[*4] R.S. Hayano,[*1] N. Inabe,[*2] K. Itahashi,[*2] D. Kameda,[*2] T. Kubo,[*2] H. Matsubara,[*5] S. Michimasa,[*5] K. Miki,[*1] H. Miya,[*5] M. Nakamura,[*6] T. Nishi,[*1] S. Noji,[*1] S. Ota,[*5] K. Suzuki,[*7] H. Takeda,[*2] K. Todoroki,[*1] K. Tsukada,[*2] T. Uesaka[*5] H. Weick[*4] and K. Yoshida[*2]
for the pionic atom factory collaboration.

[Pionic atom, precision spectroscopy, dispersion matching]

We are planning to carry out precision pionic atom spectroscopy experiments[1)] at the RI beam factory (RIBF). Dispersion matching[2)], which nullifies the effect of the momentum spread of the primary beam, is a key technique that helps achieve high resolution in pionic atom spectroscopy at RIBF. In October 2010, we performed a pilot experiment to construct the ion optics of the beam transfer line (from the SRC to the target) and that of the BigRIPS spectrometer[3)] (from the target to the F5 focal plane), with the aim of realizing dispersion matching under identical conditions to a production experiment with a deuteron beam and a ^{122}Sn target.

The dispersion matching condition is described as

$$b_{16}s_{11} + b_{26}s_{12} + Cs_{16} = 0, \qquad (1)$$

where b_{ij} and s_{ij} denote the R-matrix elements of the beam transfer line and the spectrometer, respectively, and C is the the kinematic factor of the (d,^{3}He) reaction at the target. The kinematic factor is 1.3 for the pionic atom reaction. The elements s_{ij} were selected to achieve a resolving power of 3500, such that $s_{11} = -1.8$, $s_{12} = 0.0$ mm/mrad, and $s_{16} = 64$ mm/%. The elements b_{ij} were selected to satisfy the matching condition specified in (1), such that $b_{16} = 46$ mm/% and $b_{26} = 0.0$ mrad/%.

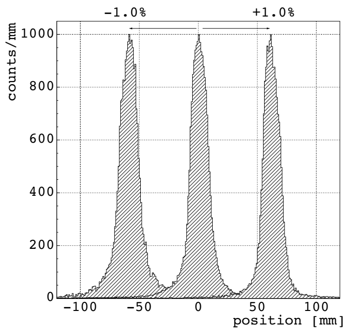

Fig. 1. Histograms of the position in the F5 focal plane. The left and right histograms were measured after scaling magnets by −1% and +1%, respectively.

*1 Department of Physics, University of Tokyo
*2 RIKEN Nishina Center, RIKEN
*3 JINA, University of Notre Dame
*4 GSI, Germany
*5 Center for Nuclear Study, University of Tokyo
*6 Department of Physics, Tokyo Institute of Technology
*7 Stefan Meyer Institute, Austrian Academy of Sciences

For focus tuning of the BigRIPS optics, we used an ^{14}N beam with an energy of 250 MeV/nucleon and a 16-mm-thick Cu target. The target thickness was chosen by considering two requirements: i) filling up the full phase space of the spectrometer and ii) simulation of the ^{3}He rigidity in the production experiment. The beam positions and the beam angles in each focal plane were measured by parallel plate avalanche counters. The momentum dispersion was deduced from the shift of the beam position caused when scaling the BigRIPS magnets (see Figure 1). The dispersion at the F5 focal plane was found to be 60.9 mm/%.

To study the optics of the beam transfer line in the production experiment, we used a deuteron beam with an energy of 500 MeV. The beam profiles at several positions were measured by beam profile monitors. The momentum dispersion at each profile monitor was measured by scaling all the magnets in the beam transfer line. The dispersion at the BRF0G profile monitor was deduced to be 34.3 mm/% (see Figure 2). The total dispersion between the SRC and the target was estimated to be 43.8 mm/%.

Thus, we constructed the BigRIPS optics by using an ^{14}N beam and a thick Cu target and confirmed that the optics of the beam transfer line was consistent with the designed optics.

This work is supported by a Grant-in-Aid for Scientific Research on Innovative Areas (No. 22105517).

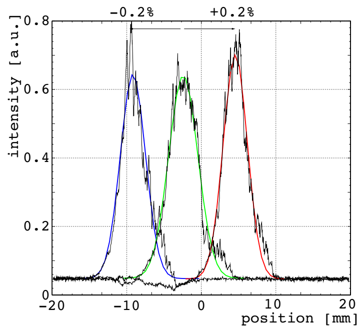

Fig. 2. Beam profiles measured by the BRF0G profile monitor after scaling magnets by −0.2%, 0.0%, and +0.2%.

References
1) K. Itahashi *et al.*, RIBF proposal No.054 (2008).
2) T. Wakasa *et al.*, Nucl. Inst. Meth. A **482**, 79 (2002).
3) T. Kubo *et al.*, Nucl. Inst. Meth. B **204**, 97 (2003).

Installation of a new injector RILAC2 for RIKEN RIBF

Y. Watanabe, E. Ikezawa, H. Imao, J. Ohnishi, H. Okuno, T. Kageyama, M. Kase, O. Kamigaito, H. Kuboki, K. Kumagai, A. Goto, M. Komiyama, N. Sakamoto, K. Suda, T. Nakagawa, M. Nagase, H. Hasebe, Y. Higurashi, N. Fukunishi, T. Fujinawa, M. Fujimaki, T. Maie, K. Yamada, S. Yokouchi, H. Yamasawa, T. Watanabe, H. Watanabe, S. Arai, Y. Uwamino and H. Fukuda[*1]

The RILAC2 has been constructed as the third injector for the RIKEN Ring Cyclotron (RRC) in order to increase the intensity of the uranium beam at the RIKEN RI beam factory[1-3]. The RILAC2 consists of a superconducting ECR ion source (SCECRIS)[4] with an operational frequency of 28 GHz and a linac system (radiofrequency quadrupole (RFQ)[5] followed by three drift-tube linacs, DTL1, DTL2, and DTL3[5-6]), as shown in Fig. 1. Installation of the RILAC2[2-3] involves infrastructure improvement and installation of the relevant components. Table 1 shows the installation schedule. First, we had to improve the infrastructure before the installation of the individual components. Then, we had to install numerous RILAC2 components in a very small area under serious time constraints because of the beam time schedule.

Infrastructure improvement

A new SCECR ion source room (second ion source room; steel construction, one-story building, 3.5 m (length) × 12 m (width) × 3.5 m (height))[7] was constructed outside Nishina building in the winter of 2009/2010. The machine hatch for shifting various components in and out of the building was installed on the roof. Before the construction of the second ion source room, the existing utilities (drain pipes for experimental wastewater, rainwater, and household wastewater, piping for tap water and ground water) in the RIBF building and the Linac laboratory were removed from the construction area in the summer of 2009. Then, many openings (holes)[7] were made in the wall and floor to install the low-energy beam transport (LEBT) line and lay cables, in the winter of 2009/2010. However, drilling mud accumulated in the AVF vault and E7 room on the three different occasions because some of the buried cables in the wall and floor were cut by the boring drill during boring. Boring was carried out in the area between the second ion source room and the AVF vault, between the AVF vault and the E6 room, between the second ion source room and the E6 room, between the second stage and the third stage in the AVF vault, and so on.

In addition, in November 2009, a mezzanine was constructed in the E6 room to install some control panels and amplifiers for DTL and RFQ. AC power cables were constructed with distribution boards in fiscal year 2009, and they were connected to the generating line of the cogeneration system (CGS) as well as the commercial generating line[9].

Finally, after the construction of the second ion source room, a water-cooling system (circulating water amount: 1700 L/min; Lift: 100 m; electric motor output: 55 kw; capacity of plate-type heat exchanger: max. 787 kW)[8] was newly constructed on the roof of the second ion source room in March 2010. The new water-cooling system mostly uses cold water from the CGS system.

Installation of the RILAC2 components

The SCECRIS was installed in the second ion source room in July 2010, after being tested in the high-voltage terminal of the RILAC pre-injector. The superconducting

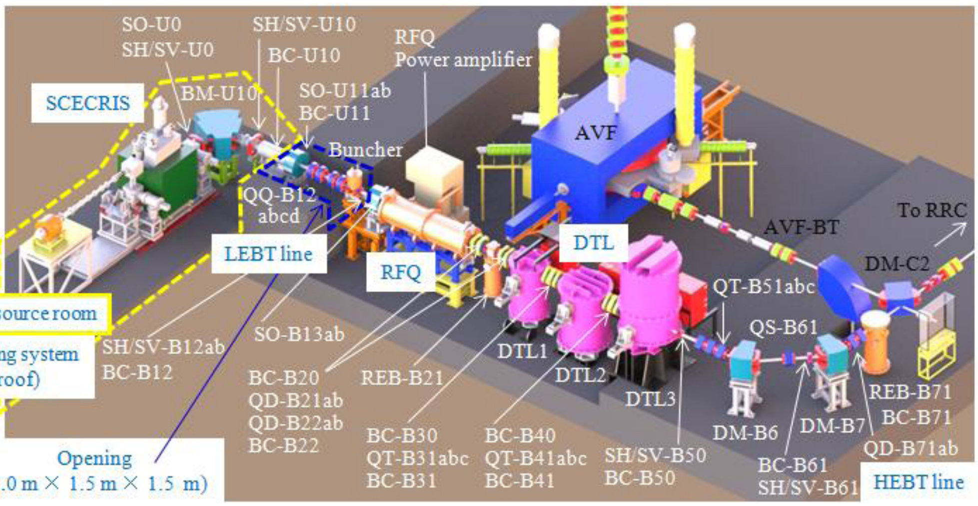

Fig. 1 Layout of the RILAC2 (illustration by Mr. M. Nishida [SHI Accelerator Service Ltd.]).

[*1] Japan Environment Research Corp.

magnet and dipole magnet (BM-U10) were carried to the second ion source room through the machine hatch by using a rough terrain crane (max. lifting capacity: 65 ton). The new components are a superconducting magnet (superconducting coils and a cryostat), microwave sources with an operational frequency of 28 GHz, a plasma chamber, a dipole magnet BM-U10, two steering magnets SH/SV-U0・SH/SV-U10, a solenoid magnet SO-U0, a beam chamber BC-U10, and a gate valve GV- U10.

The LEBT line[10] was installed in between a pair of solenoid magnets, SO-U11ab and SO-B13ab. It was important to install one-half of the LEBT line in an opening (wall thickness: 2.0 m, 1.5 m (width) × 1.5 m (height)) between the second ion source room and the AVF vault and to shield this section of the LEBT line (QQB12abcd) in the opening. The surroundings of QQB12abcd were shielded using shielding materials (concrete, silicone rubber, and plastic) of 1.1 m thickness. The LEBT line was installed between the summer and autumn of 2010, after the installation of the RFQ. The installation was made several times because of three areas (opening, shield, and AVF vault). The components were a modified buncher that was previously used in an old line, two new pair of solenoid magnets SO-U11ab・SO-B13ab, four quadrupole magnets QQ-B12abcd transferred from the CNS, two steering magnets SH/SV-B12ab used in an old line, two new beam chambers BC-U11・BC-B12, and a new gate valve GV-U11.

The RFQ was installed between May and September 2010 after its operation frequency was slightly adjusted. Special jigs were fabricated for the alignment of the RFQ and used to confirm the center of the four vane electrodes with high accuracy. The components were the modified RFQ transferred from Kyoto University and a new amplifier.

The installation of DTL (DTL1, DTL2, and DTL3) was commenced in fiscal year 2009, excluding the rebuncher REB-B21. The amplifiers were built into each DTL tank, and ten strong quadrupole magnets were installed between the acceleration cavities for transverse focusing. Four beam chambers with a special shape were constructed between the acceleration cavities. The components were a new DTL1, a new DTL2, DTL3 (the modified charge-state multiplier system CMS-D1 from the small irradiation room), a new rebuncher REB-B21, ten new quadrupole magnets QD-B21ab・QD-B22ab・QD-B31abc・QT-B41abc, and four new beam chambers BC-B20・BC-B21・BC-B30/B31・BC-B40/B41.

The high-energy beam transport (HEBT) line was installed between the steering magnet SH/SV-B50 and the beam chamber BC-B71 in the autumn of 2010, excluding the rebuncher REB-B71. The components were two new dipole magnets DM-B6・DM-B7, a dipole magnet DM-C2 (modified), six quadrupole magnets QT-B51abc・QS-B61・QD-B71ab transferred from the CNS, two steering magnets SH/SV-B50・SH/SV-B61 used in an old line, a new rebuncher REB-B71, three beam chambers BC-B50・BC-B61・BC- B71 used in an old line, and three gate valves GV-B50・GV- B60・GV-B71 used in an old line.

The rebunchers REB-B21・REB-B71 were newly fabricated because of change in the design. REB-B21 was installed in December 2010, and REB-B71 was installed in January 2011.

Beam commissioning with a Xe beam was commenced at the end of 2010[2]. The intensity of the uranium beam is expected to improve significantly by the autumn of 2011.

References

1) O. Kamigaito, et al., Proc. PASJ6, Tokai, Aug. 5_7 2009, p.38_41.
2) K. Yamada, et al., in this report.
3) Y. Watanabe, et al., J. PASJ Vol.7 No.4 (2010), p.37_45.
4) Y. Higurashi, et al., IPAC'10, Kyoto, May 23_28 2010, p.4191_4193.
5) K. Yamada, et al., IPAC'10, Kyoto, May 23_28 2010, p.789_791.
6) K. Suda, et al., Proc. IPAC'10, Kyoto, May 23_28 2010, p.3726_3728.
7) H. Yamasawa, et al., in this report.
8) T. Maie, et al., Proc. PASJ7, Himeji, Aug. 4_6 2010, in press.
9) T. Fujinawa, et al., in this report.
10) H. Watanabe, et al., in this report.

Table 1 Installation schedule for RILAC2

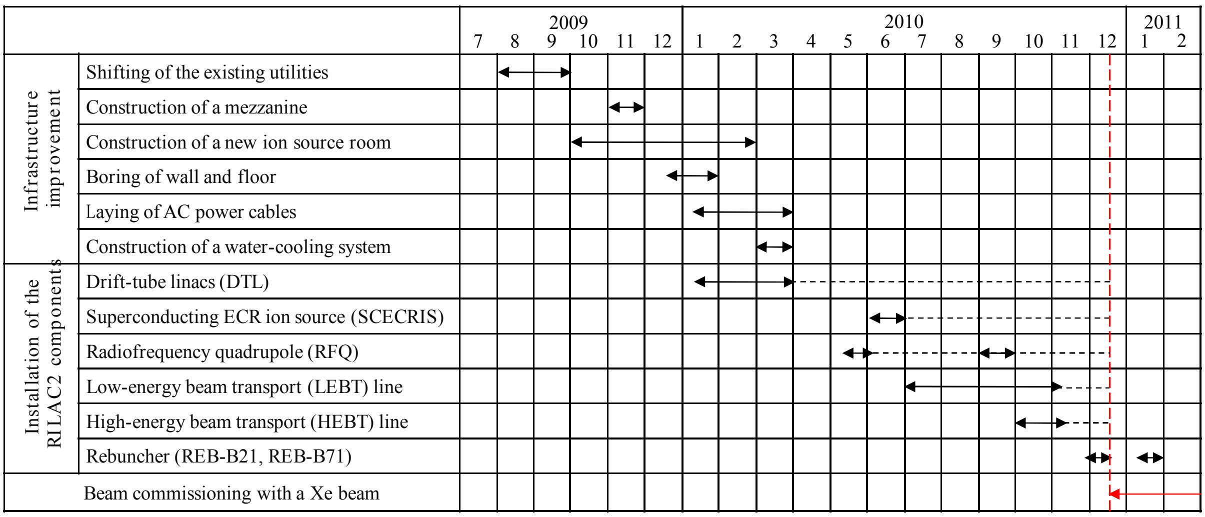

Radiation shielding for the LEBT magnets installed inside the shielding wall of RILAC2

H. Watanabe, Y. Watanabe, K. Kumagai, H. Fukuda, Y. Uwamino, and M. Kase

RILAC2 has the following layout: an ion source (28-GHz Superconducting ECR) outside the Nishina building, accelerators inside the building, and the AVF cyclotron room[1]. The LEBT (low-energy beam transport) line, connecting above mentioned components should penetrate a shielding wall (thickness: 2 m). A quartet of quadrupole magnets should be installed inside the wall. For an easy installation, alignment, and future maintenance, a hole measuring 1500×1500 mm^2 was made for installing these magnets, as shown in Fig. 1. After the magnet installation, a shielding was required around the magnets for ensuring that people can stay inside the ion-source room during the AVF operation.

Fig. 1 Wall hole for installing quadrupole magnets.

Under the licensed acceleration conditions, a 15.1-MeV/nucleon 50-particle-μA deuteron beam from the AVF produces the secondary neutron field with the highest intensity. In fact, the new heavy-ion beams from RILAC2 rarely produce a field with such intensity even for the beam current with the highest intensity (10 particle μA), since the energies of these beams are as low as 0.5 MeV/nucleon. Under these conditions, an ordinary concrete shield of thickness at least 110 cm is necessary to decrease the dose rates at the outer surface of the shield to 25 μSv/h, which is the legal upper limit inside a radiation-controlled area. This shield can also decrease the dose rate outside the second ion-source room to 2.6 μSv/h, which is the legal upper limit at the boundary of a radiation-controlled area. For the estimation performed in this study, an effective hole of 15-cm diameter was assumed to penetrate the 110-cm thick shield, and the dose of leakage radiation was considered in the estimation. The neutron production by the deuteron beam at a beam-loss point in the cyclotron and a beam dump was estimated from a previous experimental result[2]. A neutron- and photon-transport code, ANISN[3], and a group cross-section set, HILO86R[4], were used for calculating the radiation penetration.

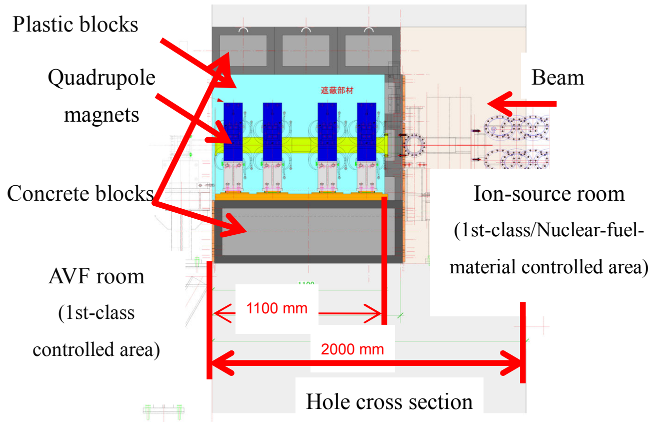

Fig. 2 Hole cross section.

Concrete blocks equivalent to the 110-cm-thick shield were constructed around the quartet, as shown in Fig. 2. The size of the hole first decreased to 900 mm × 700 mm in the portion where the quartet would be located by putting several concrete blocks of a size 300 mm × 400 mm × 1200 mm.

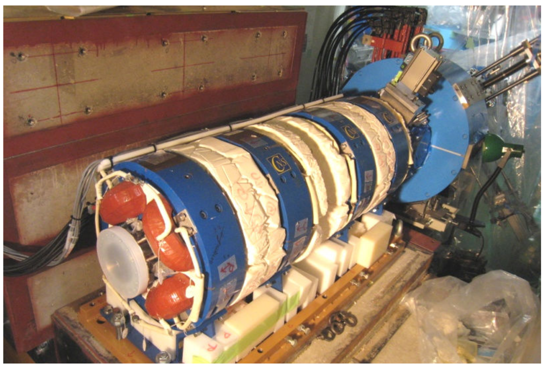

Fig. 3 Quadrupole magnets filled with silicone shield materials.

On the other hand, the gaps inside each magnet, for example, between the copper coils and iron yoke, were filled with silicone shield materials including boron (ASK SANSHIN Engineering Co., Ltd., Neutron Stop (LE)) solidified from liquid one. The copper and iron materials act as fast neutron moderators. Boron absorbs thermal neutrons. The four quadrupole magnets were aligned with each other and fixed on an iron base plate, forming a quartet. The spaces between any two quadrupole magnets were also filled in the same way as shown in Fig. 3.

The quartet was then installed in the hole together with the iron base and was aligned with the RILAC2 beam axis. Finally, the remaining open space between the quartet and concrete blocks was filled as completely as possible with plastic (polyethylene) blocks and/or sheets. Polyethylene is more effective in the shielding (1.4 times) than concrete. The final view of the shield is shown in Fig. 4.

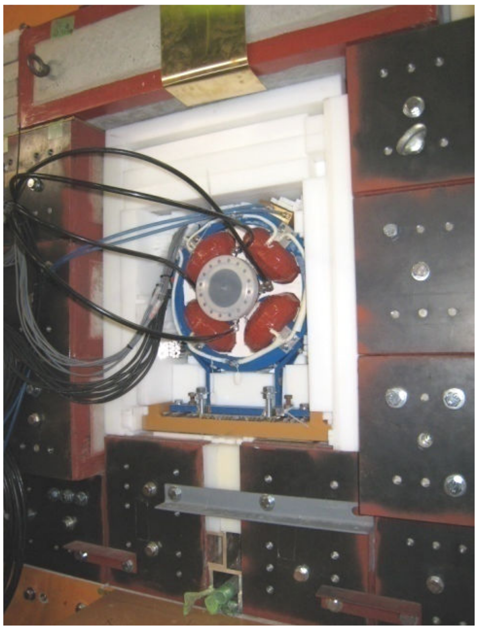

Fig. 4 Final view of wall hole.

Leakage radiations were measured at the outer surface of the refilled shield with survey meters manufactured by Applied Engineering Inc. (AE-133V) for photons and Aloka Co., Ltd. (TPS-451C) for neutrons. A 14-MeV 15-μA proton beam was accelerated during the measurements, and the dose rates for photons and neutrons were found to be 1.5 μSv/h and 0.01 μSv/h, respectively. The total dose rate converted to that for licensed acceleration conditions was estimated to be 5.9 μSv/h, which is much lower than the legal limit. On the other hand, the calculated dose in the case of a 1.2-m-thick shield is 8.1 μSv/h, and the difference is not large. The dose rate at the wall of the second ion-source room was below the detection limit.

Because the quadrupole magnets were of the naturally-cooled type, the magnet coils covered by the shield materials could overheat during operation. Thus, it was necessary to perform forced cooling. Therefore, the coils were indirectly cooled by a water-cooled beam duct installed in the quadrupole magnets and water-cooled yoke. Additionally, an air flow was maintained trough small gaps around the magnets by a blower. It was confirmed that the flow could keep the coil temperature below 80 ^{o}C during nomal magnetization of the magnets.

References

1) Y. Watababe et al.: J. PASJ, Vol. **7**, No. 4, 37 (2010).
2) K. Shin et al.: Phys. Rev., C **29**, 1307 (1984).
3) W. W. Engle Jr.: K-1693, ORNL Gaseous Diffusion Plant (1967).
4) H. Kotegawa et al.: JAERI-M 93-020, Japan Atomic Energy Research Institute (1993).

GARIS-II commissioning #1

D. Kaji, K. Morimoto, H. Haba, Y. Kudou, K. Ozeki, T. Sumita,*1 A. Yoneda, N. Sato,*2 Y. Wakabayashi,*2 M. Murakami,*3 F. Tokanai,*4 S. Namai,*4 and K. Morita

[GARIS-II, superheavy, new element, hot fusion]

Installation and magnetic field measurement

We designed and constructed a new gas-filled recoil ion separator GARIS-II[1], and installed into an experimental hall at RIKEN heavy-ion linear accelerator (RILAC) facility at March 2009 as shown in Fig.1. This separator is developed for study on actinide(An)-based fusion reaction, including superheavy element (SHE) chemistry. This device consists of 5 magnets in a Q_v-D-Q_h-Q_v-D configuration. Total path length is 5.1 m from a target position to a focal point.

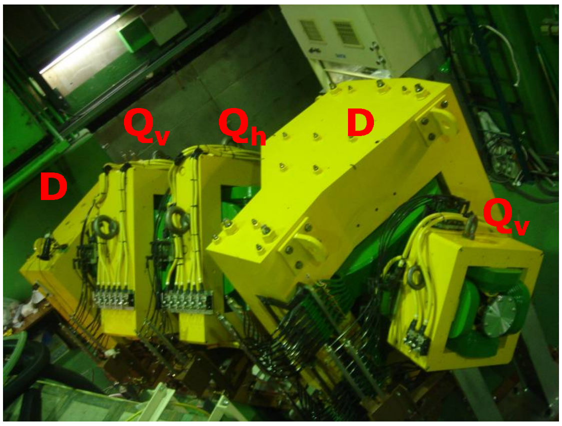

Fig. 1. Photograph of GARIS-II.

After the installation, we measured the magnetic field strength B as a function of current I for all magnets. As a typical example, excitation curves (I-B) for each magnet are shown in Fig. 2, where a central magnetic filed is given for each dipole magnet and a maximum field gradient at the bore radius is given for each quadrupole magnet. A solid line is design values calculated by the code OPERA-3D/TOSCA[2], and circles are measured ones. Measured values well reproduced with design ones for all magnets. The Effective field boundary (EFB) also agrees within 5.2% or less. Then, actual ion-optical characteristics were re-analyzed by the code TRANSPORT[3] in the case of taking this change of EFB and drift space into consideration, where higher-order geometric effects is not included in this analysis. The beam envelope is given in Fig.3. Maximum angular acceptances for horizontal and vertical are 47 and 110 mrad, respectively. So, the solid angle is expected to be 18.5 msr approximately 1.5 times higher than that of GARIS[4].

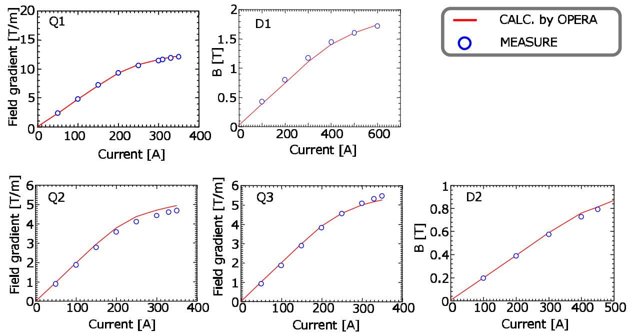

Fig. 2. I-B curves for all magnets.

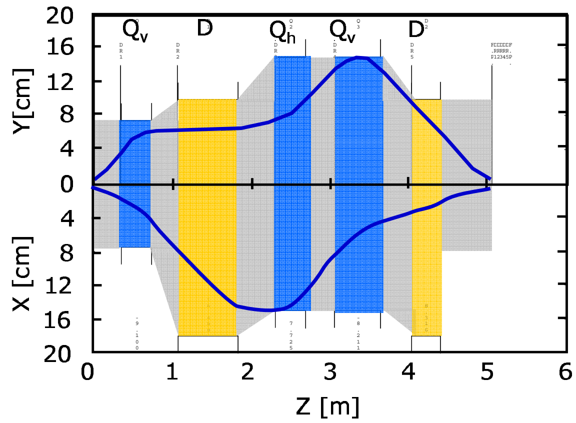

Fig. 3. Beam envelope calculated by TRANSPORT code.

R&D around GARIS-II

A gas-cooled rotating target system for GARIS-II was developed. The system consists of a differential pumping section and a target section as well as GARIS[5]. This situation enables windowless operation of GARIS-II and gas-cooling of the target. The gas-cooling effect plays an important role for SHE synthesis in which a high beam intensity such as 10 pμA is required.

The differential pumping section is installed at an upstream of the target chamber. Each pumping section is connected by ϕ25 mm orifices in a diameter. Using one mechanical booster pump (280 l/s) and two turbo

*1 Faculty of Science and Technology, Tokyo University of Science
*2 Advanced Science Research Center, Japan Atomic Energy Agency
*3 Graduate School of Science & Technology, Niigata University
*4 Department of Physics, Faculty of Science, Yamagata University

molecular pumps (350 l/s) , a vacuum becomes good gradually from target chamber to accelerator side. As a results, the vacuum at an accelerator side can keep at a pressure of P <10^{-3} Pa.

The target for GARIS-II will use two systems according to the experiment purpose. One is for stable isotope target, and the other is for An-target including ^{248}Cm. The target system for the former was already constructed, but the latter is under developing. We will be able to easily change these two independent chambers by a quick-coupling connector. We can commonly use 300 mm wheel in a diameter developed for GARIS[5].

A double side silicon detector (Micron DSSD, W1-1000, Active area = 50×50 mm^2, 16 strip×16 strip) was tested as a focal plane detector for a commissioning experiment of GARIS-II. The typical energy resolution was 35 keV (FWHM) for 5.48 MeV α-particles from ^{241}Am source.

Commissioning #1

Two basic experiments were performed as the 1st commissioning of GARIS-II. One is a standard source experiment, and the other is an accelerator experiment. In both experiments, we checked the image at the focal plane of GARIS-II with changing the balance of magnetic field strength.

A standard source of ^{241}Am with about 21 kBq was set to the target position of GARIS-II. Then, alpha particles moving from the target position to the focal plane were measured by DSSD. A typical result is shown in Fig. 4. From this measurement, solid angle was found to be 18.2 msr, which well agrees with expected value by TRANSPORT code.

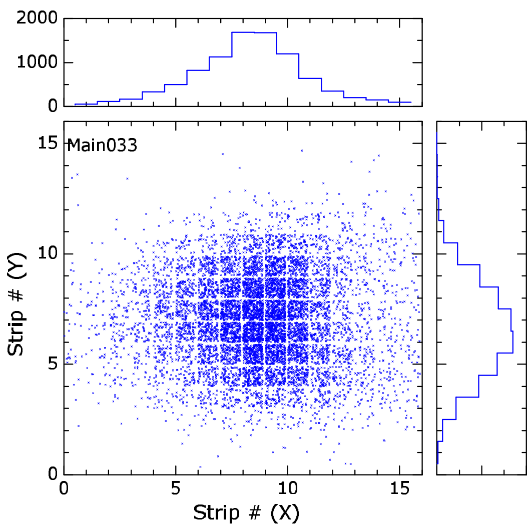

Fig. 4. X-Y scattered plot at the focal plane of GARIS-II.

The GARIS-II will be mainly used for an An-based fusion study. The recoil velocity of SHE nuclide produced by the An-based fusion reaction is low in the typical region of $1.0 < v/v_0 < 2.4$ due to the low momentum transfer. On the other hand, that in the case of Pb, Bi-based fusion is in $2.4 < v/v_0 < 3.5$. Transmission of the gas-filled typed recoil separator becomes low for recoil atom with low recoil velocity, because of multiple scattering with the filled gas. Thus, we checked the image at the focal plane of GARIS-II by using zero degree target recoils of ^{208}Pb with two different velocities (v/v_0=3.36 and 1.93 in a unit of the Bohr velocity $v_0 = c/137$) as low energy ion-sources. The intensity distributions were measured by changing a pressure of a filled-gas (He) as shown in Fig. 5. A dashed curve shows a fit to data points with a Gaussian function. As a result, we obtained the peak center and the width parameter of $\Delta B\rho/B\rho$. With increasing the pressure of the filled-gas, the peak center is shifted to a part of low magnetic field, and the width of the peak is found to be sharp. These results show image size becomes sharp by a charge-exchanging process between the recoil atom and the filled-gas atoms. The GARIS-II give the almost same transmission between these two recoil atoms with v/v_0=3.36 and 1.93. Therefore, it is found that GARIS-II is useful for An-based fusion study. Further measurements are planed for heavier SHE nuclides with lower recoil velocities.

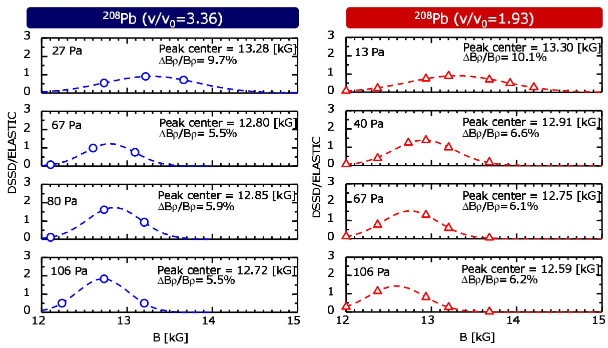

Fig. 5. Intensity distributions of zero degree target recoils of ^{208}Pb with two different velocities (v/v_0=3.36 and 1.93).

References

1) D. Kaji et al.: RIKEN Acc. Prog. Rep. **42**, 179 (2009).
2) http://www.ces-kbk.com/sdi-sp/vf/index.htm
3) K. L. Brown et al.: SLAC Report **No. 91** Rev. 1, 1974.
4) K. Morita et al.: Nucl. Instr. and Meth. **B70**, 220 (1992).
5) D. Kaji et al.: Nucl. Instr. and Meth. **A590**, 198 (2008).

CCJ operation in 2009-2010

S. Yokkaichi, H. En'yo, Y. Goto, T. Ichihara, Y. Ikeda, T. Nakamura, K. Shoji, Y. Watanabe

1 Overview and current configuration

The CCJ[1–3] (RIKEN Computing Center in Japan for the RHIC[4] physics) started operations in June 2000 as the largest off-site computing center involved with the PHENIX[5] experiment at RHIC. CCJ was initially planned to perform three roles in the PHENIX computing, 1) as a simulation center, 2) as the Asian regional center, and 3) as a center for the study of spin physics. Around 2005, 4) DST (Data Summary Tape) production from raw data has become more important, especially for the p+p data. Out of the many off-site computing facilities of PHENIX, only CCJ is currently capable of handling several hundred TBs of raw data in use of HPSS (High Performance Storage System)[6]. In 2005, 2006 and 2008, 2-300 TB of raw-data files were sent from RCF (RHIC Computing Facility)[7]to CCJ and analyzed. Recently, the CPU power of RCF has been increased and DST production can be performed at RCF without any help. Thus, we sent only nDST, which is the name of a summary data file at PHENIX, from RCF to CCJ in 2009 and 2010.

A joint operation with RSCC (RIKEN Super Combined Cluster System) was started in March 2004 and completed in June 2009. In July 2009, RICC (RIKEN Integrated Cluster of Clusters)[8] was launched, and the joint operation was continued. Twenty PC nodes have been assigned to us for dedicated use, and the PHENIX computing environment is being shared.

Many analysis and simulation projects are being carried out at CCJ. They are mentioned on the Web page `http://ccjsun.riken.go.jp/ccj/proposals/`. As of June 2010, CCJ has been contributed 23 published papers and more than 30 doctoral theses.

1.1 Calculation nodes

We have 18 PC nodes (HP ProLiant DL180 G5 with dual Xeon E5430 (2.66 GHz 4 cores), 16 GB memory and 10 TB local SATA data disks for each node) for the data-oriented analysis nodes; these were installed in February 2009[2] and have been used for the analysis of the PHENIX nDST using the local disks. The details of the data-oriented analysis system are presented in some reports[2,9]. Some old nodes, *i.e.*, 36 nodes of IBM server (with 10 TB local SCSI data disk) and 18 nodes of LinuxNetworx server (with no local data disk), were also present in our machine room 258/260 in the RIKEN main building. New data-oriented analysis nodes (HP ProLiant DL180 G6 with dual Xeon X5650 (2.66GHz 6 cores), 24 GB memory and 20 TB local SATA data disks for each node) have been delivered in March 2011 and replaced the 54 old nodes.

The OS upgrade from SL (Scientific Linux)[10] 4.4 to SL 5.3 was performed in April 2010 for the calculation nodes at CCJ, and the same upgrade was performed in May 2010 for the 20 nodes used by us at RICC. After the upgrade, VMWare ESXi is no longer used on the RICC nodes[2] and the OS is running natively. As a batch-queuing system, LSF 7.0.2[11] and Condor 7.4.2[12] were operated in CCJ and RICC nodes, respectively, as of February 2011. Upgrade to LSF 8.0.0 was performed at CCJ in March 2011. Two old LSF server nodes were discarded.

1.2 Data servers

Five data servers (SUN Fire V40) were used to manage the RAID disks, which contained the user data and nDST files of PHENIX. The disks were not NFS-mounted from the calculation nodes to prevent the performance degradation by the congestion of processes and network. These disks can be accessed only by using the 'rcpx' command, which is the wrapper program of 'rcp' developed at CCJ and has an adjustable limit for the number of processes on each server.

The server ccjnfs11 (with 6.8 TB FC-RAID and 8.9 TB-SATA RAID) was discarded in March 2010. Further, three data servers ccjnfs12 (with 10 TB FC-RAID) and ccjnfs14/15 (with 18 TB SATA-RAID for each) were discarded in March 2011. After the discarding, we have a data server ccjnfs13 (with 10 TB FC-RAID). A new data server ccjnfs16 (HP ProLiant DL180 G6 with 20 TB SATA raw disks) is undergoing tests to replace ccjnfs12.

The DNS, NIS, NTP, and NFS servers are operated on the server ccjnfs20 (SUN Enterprise M4000 with Solaris 10) with a 10 TB FC-RAID where users home and work regions are located. In October 2010, the NFS-write operation from the calculation nodes to the work region was prohibited in order to prevent the performance degradation in the interactive usage of the home region due to the heavy writing operation by user jobs. The home and work regions are formatted VxFS 5.0[13], which has a bug in the quota system. When a large file whose size is more than 2GB is deleted, the quota count is not decreased; thus, the count gets piled up and reaches the limit without the user using up all the allocated space. A superuser should be called to resolve the pile-up. The version upgrade of VxFS will solve this problem.

1.3 HPSS

Since December 2008, the HPSS servers and the tape robot are located in our machine room, while they are owned and operated by the RIKEN IT division. The

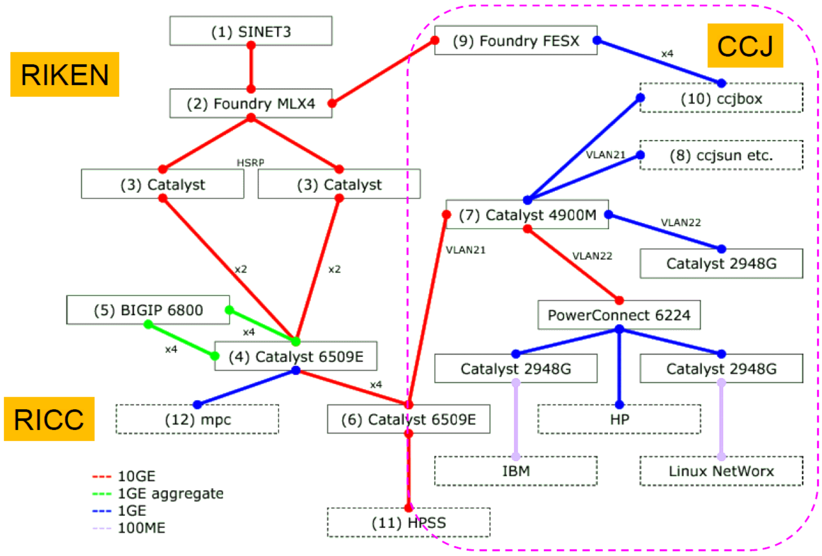

Fig. 1. Schematic view of the network configuration as of June 2010.

specifications of this hardware can be obtained in the literature[3]. The version upgrade of HPSS from version 6.2 to 7.1 was performed in January 2010 and upgrade to 7.3 was performed in March 2011. The amount of data and the number of files archived in the HPSS were approximately 1.5 PB and 2 million files, respectively, as of February 1, 2011.

1.4 PHENIX software environment

Two PostgreSQL[14] server nodes are operated for the PHENIX database, whose data size was 64 GB as of February 2011. The data is copied from RCF daily and is served to the users.

In November 2010, two AFS[15] client nodes operated to copy the PHENIX software environment were combined to one node. Recently, the automatic token-feed system is showing signs of a glitch. It should be fixed or the token should be fed manually and weekly.

1.5 Network configuration

The configuration of the network linking CCJ, RICC and RIKEN IT division has been detailed previously[2]. The topology is shown in in Fig. 1.

2 A big earthquake and a power cut

In March 11, 2011, 'the 2011 off the Pacific coast of Tohoku Earthquake' destroyed a nuclear power plant of TEPCO (Tokyo Electric Power Company). Due to the power limitation caused by the disaster, TEPCO announced to perform the scheduled daily power cut (2-3 hours in a day) from March 14 to April. CCJ was shutdown emergently in the night of March 13, while no actual power outage occurred at RIKEN Wako campus. For salvage of user data and the LSF upgrade, a few servers were temporarily operated in March 18-19 and 28-29. Finally, TEPCO and RIKEN announced in March 29 that the power outage was ended at Wako. Thus, the recovery of CCJ was started and all the system was opened for users in April 4. The recovery of DB and AFS including copying the data took the six days.

CCJ was caused no damage by the earthquake itself.

3 Outlook

In 2011, hundreds TB of nDST from the PHENIX Run-11 will be sent from RCF to CCJ and will be stored on the local disks on the HP calculation nodes. Two old UPS modules, one old data server, and one old login server should be replaced in JFY 2011.

References

1) `http://ccjsun.riken.go.jp/ccj/`
2) T. Nakamura et al., RIKEN Accel. Prog. Rep. **43**, 167 (2010).
3) S. Yokkaichi et al., RIKEN Accel. Prog. Rep. **42**, 223 (2009).
4) `http://www.bnl.gov/rhic/`
5) `http://www.phenix.bnl.gov/`
6) `http://www.hpss-collaboration.org/`
7) `http://www.rhic.bnl.gov/RCF/`
8) `http://ricc.riken.jp/`
9) T. Nakamura et al., Journal of Physics: Conference Series, in press (2011).
10) `https://www.scientificlinux.org/`
11) `http://www.platform.com/products/LSF/`
12) `http://www.cs.wisc.edu/condor/description.html`
13) Veritas file system, provided by Symantec Corporation.
14) `http://www.postgresql.org/`
15) `http://www.openafs.org/`

Possible Slow Polarized Negative Muon Source For Cold g–2 Experiment

K. Nagamine[1,2]

Recently, by using the polarized slow positive muon (μ^+) produced by laser resonant ionization of thermal muonium (Mu, atomic state of μ^+ and an electron)[1], next-generation muon g-2 experiment is under preparation at J-PARC[2]. There, after producing intense ($\geq 10^6$) and slow (below 1 eV) μ^+, acceleration of the μ^+ beyond 100 MeV and store in a compact ring without electric field confinement is considered. It is interesting and important to conduct the same experiment for the μ^- for the purpose of a high precision examination of the CPT theorem. For this purpose, generation of advanced μ^- beam source with high intensity ($\geq 10^4$), low energy (below keV) and high polarization (above 30 %) is required. So far, there is no idea of such advanced μ^- beam production. Here is the first proposal.

So far, two types of proposal exist to produce unpolarized slow μ^- such as 1) in-flight cooling like cyclotron trap developed at PSI[3] and 2) re-emission from the muonic atom with disappearing core nuclei such as ^5He in muon catalyzed D-T fusion[4]. Unfortunately, spin polarization is completely lost in these slow μ^- production processes.

In the case of g-2 application, the polarized cold μ^- will be used eventually at high energy. Therefore, it is allowed to use polarized slow μ^- bound in the muonic atom of light nuclei such as μ^-He followed by free μ^- generation at some stage during acceleration. The slow μ^- production along this line was proposed for the $\mu^{-3}He$ emitted by a particle-decay of $d^3He\mu$ molecule formed as an intermediate state in the transfer process from d to ^3He for the μ^- in D_2 and ^3He (up to 500 ppm) mixture[5]. By taking the geometry shown in Fig. 1, conversion efficiency from MeV μ^- to 3.2 keV $(\mu^{-3}He)^+$ was estimated to be 6 %[5], satisfying the present intensity requirement.

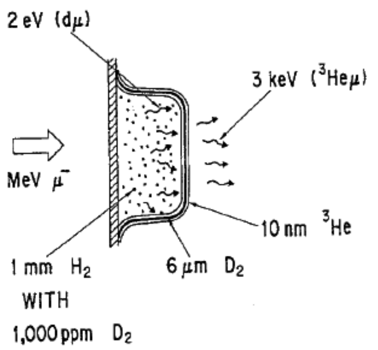

Fig. 1.Target arrangement originally considered for the slow $(\mu^{-3}He)$ production from ^3He coated on H_2/D_2 layer[5].

The next problem is how to polarize μ^- in $\mu^{-3}He$. Here, we follow the results of experiment at LANL[6], the original goal of which was to polarize μ^- in $\mu^{-3}He$ with optically pumped polarized ^3He nuclei by the re-polarization method developed by the group of present author[7]. Unexpectedly, after neutralization of $(\mu^{-3}He)^+$ with CH_4, optically-pumped polarized Rb electron was experimentally found to polarize electron in $(\mu^{-3}He)^+e^-$ which polarize μ^- directly[6].

The polarized slow $(\mu^{-3}He)^+$ source (Fig. 2) will be realized by using the target system consisting of the following components on cold (4.2 K) metallic substrate: 1) Solid H_2 with 1000 ppm D_2, 1 mm thick, to convert MeV μ^- to 2 eV (dμ); 2) Solid D_2 layer, 6 μm, to thermalize 2 eV (dμ); 3) Solid ^3He layer, 4 nm, to form $d^3He\mu$ followed by keV $(\mu^{-3}He)^+$ ion emission. Within the cryostat, there will be a 200 C chamber containing the CH_4 neutralizer and the spin polarized Rb (4×10^{14} atoms/ cm^3) by optical pumping, which will polarize μ^- in $(\mu^{-3}He)^+e^-$. The exit window will detach e^- to produce slow polarized $(\mu^{-3}He)^+$ beam. Confinement optics and acceleration should be optimized.

The properties of produced $(\mu^{-3}He)^+$ beam will be expected as follows: energy (width); 1 keV (0.5 keV), intensity for 10^8/s MeV μ^-; $\geq 10^6$/s; polarization$\geq$ 50 %.

The proposed source will be used for the g-2 experiment in the following scheme: polarized $(\mu^{-3}He)^+$ source; 1 MeV pre-accelerator for dissociation energy of 10 keV$\times 4 \times 9$, wire or foil $(\mu^{-3}He)$ dissociator, 300 MeV linac same as μ^+ g-2 and g-2 ring. Optimized design is required for dissociator.

1) K. Nagamine et al., Phys. Rev. Lett. **74**, 4811 (1995).
2) N. Saito et al., J-PARC Proposal (2009).
3) P. DeCecco et al., Nucl. Instr. **A394**, 287 (1997).
4) K. Nagamine, Proc. Japan Academy **65B**, 225 (1989).
5) K. Nagamine, Hyp. Interaction **82**, 539 (1993)
6) A.S. Barton et al., Phys. Rev. Lett. **70**, 758 (1993)
7) R. Kadono et al., Phys. Rev. Lett. **57**, 1847 (1986).

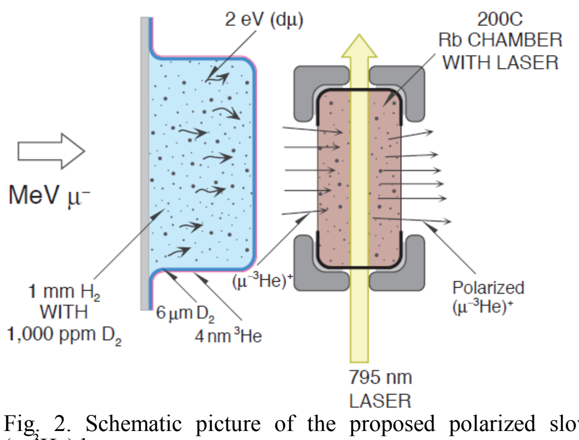

Fig. 2. Schematic picture of the proposed polarized slow $(\mu^{-3}He)$ beam source.

Jointly,
*1 Physics & Astronomy, University of California, Riverside
*2 Muon Science Laboratory, IMSS, KEK

RIKEN Accel. Prog. Rep. 44 (2011)

Pulse-structure dependence of proton-polarization rate

T. Kawahara,[*1] T. Uesaka,[*2] Y. Shimizu, S. Sakaguchi, A. Shibusawa[*1] and T. Wakui[*4]

A polarized solid proton target for RI beam experiments has been developed at the Center for Nuclear Study, University of Tokyo[1]. Protons are polarized through the transfer of the electron population difference in the photoexcited triplet states of pentacene[4]. By using this method, proton polarization of approximately 20% has been achieved in a low magnetic field of 0.1 T and at a high temperature of 100 K. Although this target has been successfully used in RI beam experiments[2,3], further improvement in proton polarization is desirable for future applications. To enhance the photoexcitation power, we examined the pulse-structure dependence of the proton polarization rate.

At present, the photon number of the photo-excited light is the bottleneck in realizing improved polarization because the photon number is smaller than the electron number of the pentacene. For simply increasing the photon number, the best laser light would be continuous wave. However, a problem isencountered the lifetimes of the magnetic sub-levels in triplet states are different. The sublevel with the largest population decays with the shortest lifetime. Therefore, by irradiating with laser light for long time, electron polarization decreases, while the photon number increases. Hence, photo-excited light must be pulsed.

For the optical excitation of pentacene molecules, an Ar ion laser (Coherent TSM25) with a wavelength range of 454.5 nm to 528.7 nm and a total maximum output power of 25 W is used. Since this laser is a continuous wave (CW) laser, light can be mechanically pulsed by using an optical chopper (Fig. 1). The duty factor can be easily varied by adjusting the degree of the overlap of two chopper blades. The frequency of the laser pulse can be changed by changing the rotating speed of the optical chopper.

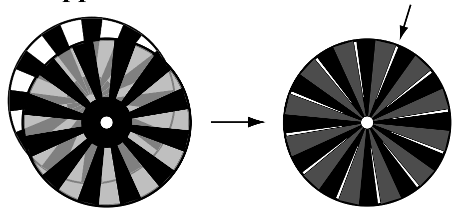

Fig. 1. Optical chopper blades

With the help of this optical system,we can change the duty factor from 5% to 50% and the repetition frequency from 0.75 to 10.5 kHz. When the duty factor, which is the product of widt and repetition frequency of the pulse, is increased, the polarization can be decreased by expanding the pulse width. Therefore, we examine the extent of improvement of proton polarization stet both the duty factor and the repetition frequency are changed to increase.

Measurements were carried out under the following condition. We used a single crystal naphthalene doped with pentacene (0.001 mol%) as the material to be polarized . The crystal was 14 mm in diameter and 2.5 mm in thickness. Protons were polarized at a temperature of 100 K and in a magnetic field of about 80 mT.

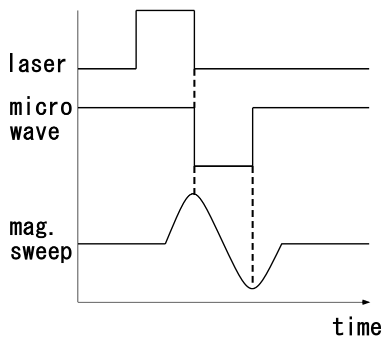

Fig. 2. Timing chart of polarization. When the crystal is irradiated by the laser, electron polarization occurs. Immediately after laser irradiation, microwave irradiation is effected, and the magnetic field is swept in order to transfer the electron polarization to the protons.

Figure 2 shows the typical timing chart of polarization process. In the first step, crystal is irradiated using the laser. In the second step, just after the irradiation, we irradiated the crystal using the microwave and swept the magnetic field in order to transfer the electron polarization to the protons. These steps were repeated at a typical frequency of several kHz.

We measured the polarization after 10-min build up by employing the pulse NMR method. The magnitude of polarization is defined as the proton polarization rate. The result is shown in Fig. 3 where the proton polarization rate is plotted as a function of the duty factor. In a previous study[1], the repetition frequency and the duty factor were 2.5 kHz and 5%, respectively. The measured data are normalized using the data of previous studies. At a high frequency limit, the polarization rate is proportional to the duty factor. In the present study, we found that the proton polarization rate is maximum when the repetition frequency and the duty factor were 10.5 kHz and 50%, respectively. The polarization rate was stet by a factor of 7.5 com-

*1 Department of Physics, Toho University
*2 Center for Nuclear Study, Graduate School of Science, University of Tokyo
*3 Cyclotron and Radioisotope Center, Tohoku University

pared with that achieved in the previous studies. From this result, one can expect that the polarization can be improved by increasing the duty factor and repetition frequency.

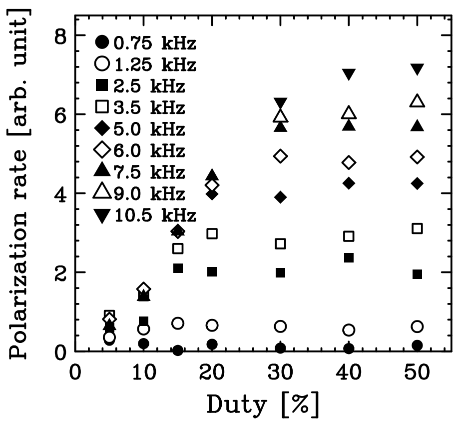

Fig. 3. Polarization rate measured by changing the duty factor and repetition frequency. The measured data are normalized using the data of the previous studies.

We measured the build-up curve of polarization by changing the duty factor and the repetition frequency as summarized in Table 1. Measured data are shown in Fig. 4.

Table 1. The polarization conditions when the build-up curve is measured by changing the duty factor and the repetition frequency.

name	Duty factor	Repetition freq.
Set-5	5%	2.5 kHz
Set-15	15%	5.0 kHz
Set-30	30%	9.0 kHz
Set-50	50%	9.0 kHz

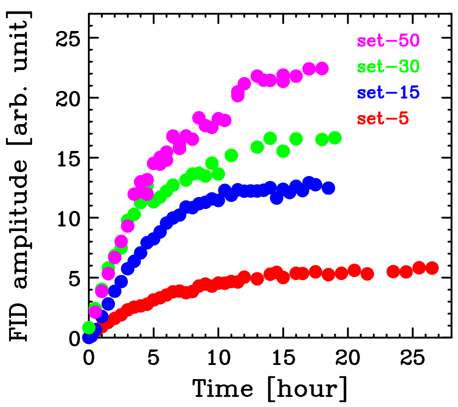

Fig. 4. Build-up curve of polarization measured by changing the duty factor. The measured data are normalized using the data of the previous studies.

The build-up curve of Fig. 4 is represented as

$$P(t) = \frac{A}{A+\Gamma}(1-\exp(-\Gamma t)), \tag{1}$$

where A is the proportional to polarization rate, and Γ is the relaxation rate of polarization. The saturated polarization is described as

$$P(\infty) \propto \frac{A}{A+\Gamma}. \tag{2}$$

Therefore, the saturated polarization is determined on the basis of the balance between A and Γ. From the figure, it can be seen that the magnitude of saturated polarization with a duty factor of 50% (set-50) is stet by a factor of 4 when compared with that of set-5.

References

1) T. Wakui *et al.*: Nucl. Instr. Meth. A **550** (2005) 521.
2) M. Hatano *et al.*: Eur. Phys. J. A **25** (2005) 255.
3) S. Sakaguchi *et al.*: Proc. of ISPUN07, World Scientific (2009) 245.
4) M. Iinuma: Ph. D thesis, Kyoto University, (1997).

Superallowed Fermi-type charge-exchange reaction for studying the isovector non-spin-flip monopole resonance

Y. Sasamoto,[*1] T. Uesaka,[*1] S. Shimoura,[*1] S. Michimasa,[*1] S. Ota,[*1] S. Noji,[*2] K. Miki,[*2] K. Yako,[*2] H. Tokieda,[*1] H. Miya,[*1] S. Kawase,[*1] Y. Kikuchi,[*1] K. Kisamori,[*1] M. Takaki,[*1] M. Dozono,[*1] H. Mathubara,[*1] H. Sakai, T. Kubo, Y. Yanagisawa, H. Takeda, K. Yoshida, T. Ohnishi, N. Fukuda, D. Kameda, N. Inabe, N. Aoi, S. Takeuchi, T. Ichihara, H. Baba, S. Sakaguchi, P. Doornembal, W. He, C. Ruijiu, Y. Shimizu, T. Kawahara,[*3] T. Kawabata,[*4] N. Yokota,[*4] Y. Maeda,[*5] H. Miyasako,[*5] and G. P. A. Berg[*6]

[SHARAQ spectrometer, charge-exchange reaction (^{10}C,^{10}B), giant resonance]

Isovector non-spin-flip monopole resonance (IVMR) is a topic of particular interest because it is an oscillation mode of the isovector density $\rho_{\rm IV}$ $(= \rho_n - \rho_p)$; the energy and width of IVMR are should be closely related to the properties of asymmetric nuclear matter[1)]. In spite of its importance, however, experimental data on IVMR are scarce. To establish a heavy-ion charge-exchange (HICE) probe that is selective to the isovector non-spin-flip ($\Delta T = 1, \Delta S = 0$) mode, we performed the ^{90}Zr(^{10}C,^{10}B(IAS)) experiment at 200 MeV/u.

Our idea of establishing a HICE probe for isovector non-spin-flip ($\Delta T = 1, \Delta S = 0$) states is based on the use of a superallowed Fermi transition between isobaric analog states of the projectile. The analog state of the ground state of ^{10}C is locates at $E_x = 1.740$ MeV in ^{10}B, as shown in Fig.1. The transition from the ground state of ^{10}C to the 1.740-MeV state of ^{10}B can be experimentally verified by observing the emitted 1.022 MeV γ-ray. Thus, the coincident detection of ^{10}B and 1.022-MeV γ-rays in the final state can be a clear identification of the $0^+ \rightarrow 0^+$ transition in the projectile and, consequently, of the non-spin-flip excitation in the target.

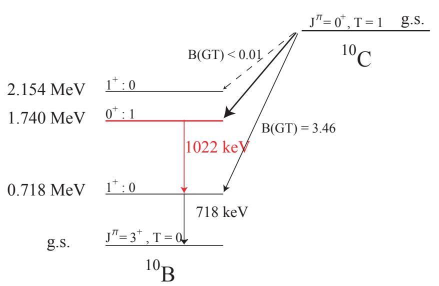

Fig. 1. Energy levels for ^{10}B.

The experiment was performed at the RIBF facility at RIKEN. The secondary ^{10}C beam was produced as fragments of 250 MeV/u ^{14}N from a ^{9}Be target with a thickness of 20-mm positioned at BigRIPS-F0. A purity of approximately 95% was achieved for ^{10}C by using an Al wedge with thickness of 810 mg/cm^2. The intensity of the ^{10}C beam was approximately 2×10^6 pps at the secondary target. The beam trajectories were measured at F3 and the SHARAQ target to determine the position and angle of the beam. The magnetic setting of the high-resolution beamline was that of the dispersion-matching mode so as to cancel the effect of energy spread of the beam itself[2)]. A secondary ^{90}Zr target with a thickness of 150 mg/cm^2 was used. For verifying the non-spin-flip transition, the emitted 1.022-MeV γ-rays were detected by using the NaI detector array (DALI2[3)]) located near the secondary target.

Figure 2 shows the Doppler-corrected γ-ray spectrum, obtained by DALI2, coincident with ^{10}B particles in the SHARAQ focal plane. The 1.022-MeV peak can be clearly observed. Since this γ-ray is emitted from the 0^+ state at $E_x = 1.74$ MeV in ^{10}B, the non-spin-flip transition can be deduced by gating this peak. A detailed analysis to deduce the monopole transition by using the scattering angle is now in progress.

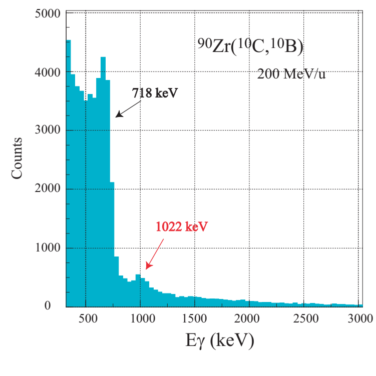

Fig. 2. Doppler-corrected γ-ray spectrum of ^{90}Zr(^{10}C,^{10}B) obtained by DALI2.

*1 Center for Nuclear Study, University of Tokyo
*2 Department of Physics, University of Tokyo
*3 Department of Physics, Kyoto University
*4 Department of Physics, Toho University
*5 Department of Physics, Miyazaki University
*6 Department of Physics and Joint Institute for Nuclear Astrophysics, University of Notre Dame

References

1) G. Colo and N. Van Giai: Phys. Rev. C **53**, 2201 (1996).
2) T. Uesaka et al.: In this report.
3) S. Takeuchi et. al.: RIKEN Accel. Prog. Rep. **36**, 148 (2003).

Computing and Network Environment at RIKEN Nishina Center

T. Ichihara, Y. Watanabe, and H. Baba

We have been operating Linux/Unix NIS/NFS cluster systems[1,2] at RIKEN Nishina Center. The major parts of the systems are installed in the 1F server room of the RIBF building, and some others are installed in the 1F network and server room of the Nishina Memorial building.

Figure 1 shows the current configuration of the Linux/Unix servers at the Nishina Center. We have adopted Scientific Linux[3] as the primary operating system; this operating system has been developed at the Fermi National Laboratory and is widely used in accelerator research facilities worldwide,as well as by the nuclear physics and high-energy physics communities.

We have installed a Web server *RIBF-RESULT*, which provides information about preprints and publications from RIKEN Nishina Center. With *RIBF-RESULT*, electric preprints can be used instead of paper preprints.

The host *RIBF.RIKEN.JP* is used as the mail server, NFS server of the user home directory /rarf/u/, and NIS master server. This is a core server for the Linux/Unix cluster of Nishina Center. Approximately 500 user accounts are registered on this server. The current size of /rarf/u is approximately 1.7 TB.

Since more than six years have lapsed since the launch of the /rarf/u RAID system and five years since the launch of the *RIBF.RIKEN.JP* server, the RAID of user home directory /rarf/u and *RIBF.RIKEN.JP* server must be replaced. Therefore, we have prepared highly reliable 16-TB RAID6 using SAS-HDDs for the new /rarf/u home directory and 17-TB economical SATA RAID6 for its backup system. The size of the new user home directory /rarf/u/ is 16-TB which is corresponding to approximately nine times larger than the previous system. This replacement enables the handling of many large-size file systems in the user home directory on RIBF Linux/UNIX clusters and mail servers.

The planned replacement is as follows. We will first install new the *RIBF.RIKEN.JP* server and then connect it to the new RAID6 (16-TB SAS and 17-TB SATA) systems. The we will carefully create the mail/NFS/NIS environment on the new server. When the new environment is ready and detailed analysis is complete, we will copy the contents of the user home directory /rarf/u and NIS maps (user accounts) from the old server to the new server and then use the new *RIBF.RIKEN.JP* server and RAID. This procedure is very secure and does not disturb the the date analysis by the *RIBF.RIKEN.JP* mail users and all the RIBF/LINUX cluster users.

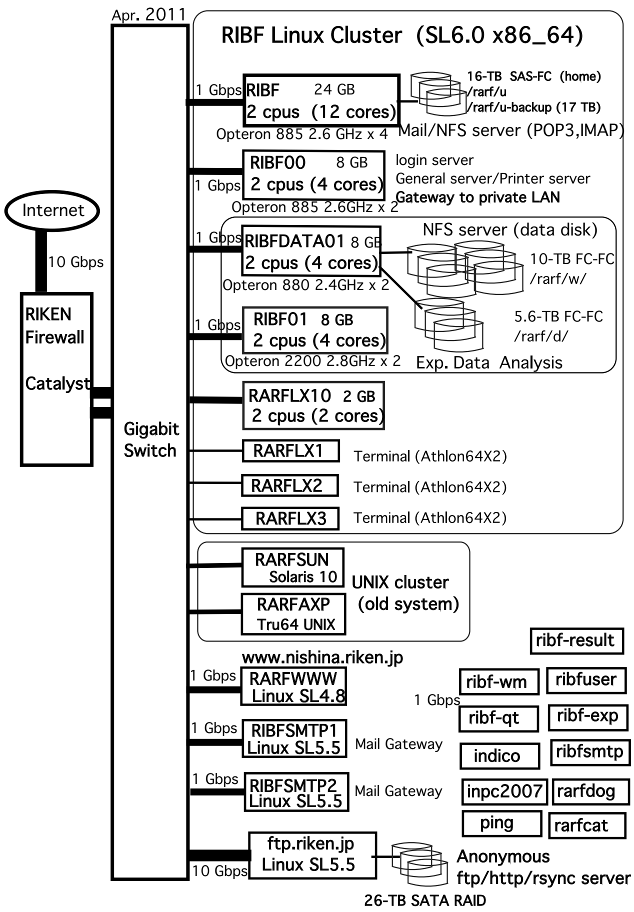

Fig. 1. Configuration of RIBF Linux cluster.

We are planning to start using the new *RIBF.RIKEN.JP* server and RAID in the summer of 2011.

Fiber-channel RAIDs with capacities of 10 TB and 5.6 TB having with fiber-channel hard disk drives /rarf/w/ and /rarf/d/ are connected to the *RIBF-DATA01* server for data analysis and raw data storage in the RIBF experiment. We are planning to add a new RIBFDATA02 server and new RAID systems in JFY2011, since amount of the RIBF experimental raw data has increased very rapidly this year, and /rarf/d is almost full (86% usage). Therefore, we need new and reliable RAID6 system for storing experimental raw data and a RAID6 work area for data analysis.

The host *RIBF00* is used as an ssh login server to provide access to users from the outside the Nishina Center; it is also used as a general-purpose computational server, printer server, and a gateway to the RIBF intranet.

The hosts *RIBFSMTP1/2* are mail front-end servers, and they are used for tagging spam mails and isolating virus-infected mails. Sophos Email Security and Control (PMX) was installed on these servers in March 2008, and it has been functioning well to the intended purposes. Figure 2 shows the spam blocking bu PMX at *RIBFSMTP1* from August 2010 to January 2011. In this figure, we noticed that more than 80% of the incomming mails are spams and that most of them are blocked by the IP blocked capability of PMX on the basis of blacklisted IP addresses of the spam senders hosts.

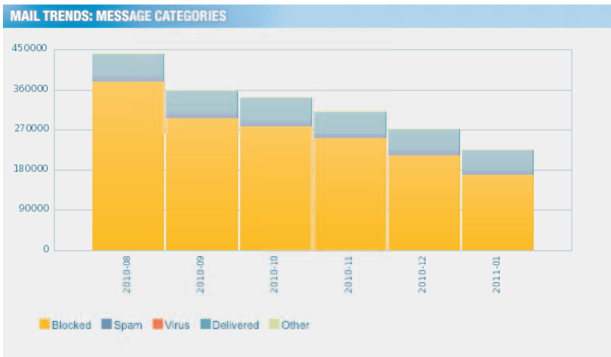

Fig. 2. Spam blocking at RIBFSMTP1 for 6 months.

An anonymous ftp server, *FTP.RIKEN.JP*, is managed and operated at RIKEN Nishina Center. This server is installed in the network server room of the Nishina Memorial building. This server has been working very stably, and Major Linux distributions, which include Scientific Linux, CentOS, Ubuntu, Fedora, Debian, OpenSUSE, Mandrake, Slackware, and Vine, are mirrored daily at the ftp server for facilitating high-speed access to the users. Figure 3 shows the annual network traffic of *FTP.RIKEN.JP*.

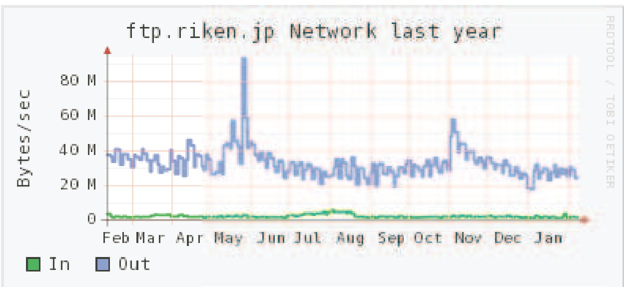

Fig. 3. Annual network traffic of ftp.riken.jp.

We have two server rooms for our computers and network equipments. One is located in the Nishina Memorial building and the other is located at the RIBF building. Emergency power supply and UPS systems (20 kVA each) are installed in both server rooms. However, there is only one air-conditioning system in the server room of Nishina Memorial building, and this failed during the vacation, between the end of 2010 and the beginning of 2011. During that period, room temperature exceeded 30°C, as shown in Fig.4.

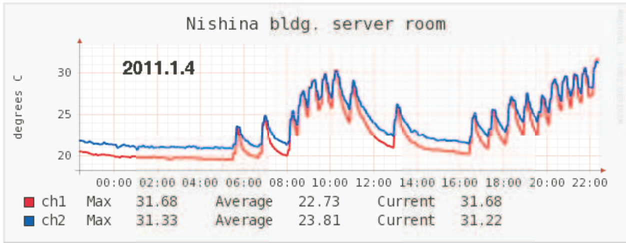

Fig. 4. Temperature in server room, Nishina building

Fortunately, the accelerator operators in the control room noticed this after the alarm went off and opened the door and ventilated the room with a large-scale fan. Therefore no serious damages was cased to our computer and network equipments. To prevent such incidents, we installed backup air-conditioning system in the server room of the Nishina Memorial building in February 2011.

The development of the RIBF data acquisition system (DAQ) is described elsewhere.[4)]

Most of the users at Nishina Center have e-mail addresses of one of the following forms:

username@ribf.riken.jp or *username@riken.jp*.

The former represents the e-mail address at mail server (*RIBF*) of the RIKEN Nishina Center, while the latter represents an e-mail address of the mail server (*POSTMAN*) at RIKEN Advanced Center for Computing and Communication.

References
1) http://ribf.riken.jp/
2) T. Ichihara et al.: RIKEN Accel. Prog. Rep. 43, 221 (2010).
3) https://www.scientificlinux.org/
4) H. Baba et al.: In this report.

III. RESEARCH ACTIVITIES II

(Material Science and Biology)

1. Atomic and Solid State Physics (ion)

Evaluation of single-event effect tolerance of p-channel power MOSFETs

N. Ikeda, S. Kuboyama, Y. Yano,*[1] H. Muto, H. Otomo, O. Shimada, H. Ozono,*[2] and T. Kambara

A power MOSFET (Metal-Oxide-Semiconductor Field-Effect Transistor) is a key device in a power circuit to attain high efficiency. A MOSFET to be used for space applications is required to have radiation hardness. Protons, heavy ions, and other particles in space could cause single-event effects and lead to a malfunction or failure to semiconductor devices. Single-Event Gate Rupture (SEGR) is a major concern in the case of p-channel power MOSFETs. Figure 1 shows the two-dimensional cross section of a power MOSFET.[1)] SEGR is triggered by a heavy ion passing through the neck region of a gate oxide. A dense column of charge is generated along the ion track and charges are collected toward the gate oxide due to the applied voltage, which produces a high electric field in the gate oxide. Breakdown occurs when the produced electric field exceeds the breakdown field. Since the occurrence of SEGR could lead to not only the loss of the power system but the entire spacecraft, it must be prevented.

Currently, JAXA (Japan Aerospace Exploration Agency) is developing p-channel power MOSFETs for space use. The radiation tolerance of prototypes was evaluated by using accelerators in RIKEN. Furthermore, the failure mechanism caused by a heavy ion was studied since the observed failure cannot be explained by the conventional theory. Prototypes of 100 V and 200 V p-channel power MOSFETs designed for space application were tested by using ^{84}Kr ions with the energy of around 700 MeV. Linear energy transfer (LET) and projected range of the ions are 33 to 34 MeV/(mg/cm^2) and 80 to 90 μm, respectively. Figure 2 shows the result of in-situ measurement of the gate current on a 100 V power MOSFET. The failure criteria for this measurement is a gate current greater than or equal to 10 μA. Although an increase in the gate current was observed under the condition of drain voltage (VDS) of 100 V and gate voltage (VGS) of 7.5 V, it is was only 4 μA, and the gate current was at the background level at a gate voltage of 5 V. The results for other MOSFETs were the same, and it was shown that these power MOSFETs have enough tolerance to the single-event effect.

During the irradiation, the gate current showed a step-like increase. Each step seems to correspond to damage to a certain area. The change in electrical characteristics after the irradiation implies that some part of the channel region shown in Figure 1 was damaged by the irradiation. This location cannot be explained by the conventional theory that says SEGR occurs in the neck region. This fact may imply a new failure mechanism, and further studies must be carried out with enough experimental data. We will continue our study to clarify the mechanism, and the result will be used for the development of robust power MOSFETs in the future.

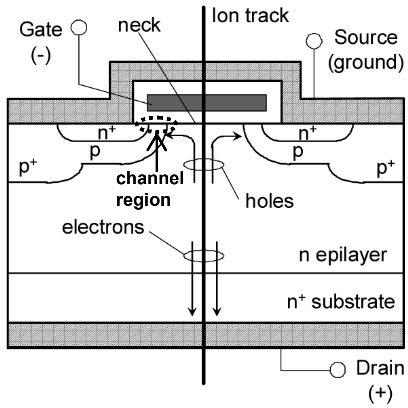

Figure 1. Two-dimensional cross section of a power MOSFET (n-channel) during an ion strike. The polarity and the type of semiconductor (p and n) are the opposite for a p-channel MOSFET.

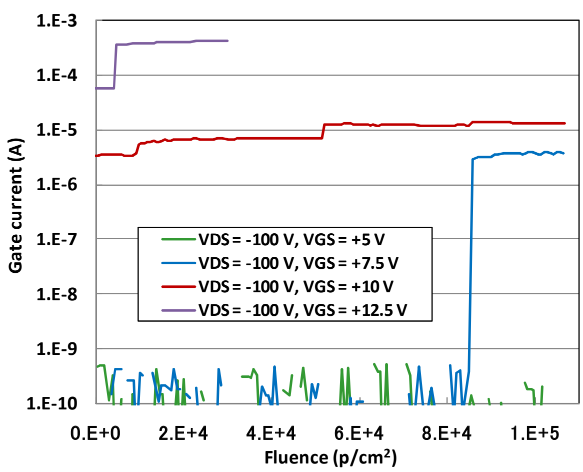

Figure 2. Change in gate current during the irradiation for a prototype of a 100 V p-ch power MOSFET.

References

1) L. Scheick and L. Selva: NSREC Radiation Data Workshop, p.82 (Quebec City Canada, 2009).

*1 Japan Aerospace Exploration Agency
*2 Ryoei Technica Corporation

Charge evolution of ^{238}U beam injected at 10.8 MeV/u in hydrogen and helium gas†

H. Imao,*1 H. Okuno,*1 H. Kuboki,*1 S. Yokouchi,*1 N. Fukunishi,*1 O. Kamigaito,*1 H. Hasebe,*1 T. Watanabe,*1 A. Goto,*1 M. Kase,*1 and Y. Yano*1

[charge stripping, uranium ion, low-Z gas]

A charge stripper using low-Z (Z: atomic number) gas is a possible candidate replacing carbon foil strippers[1)] for high-intensity ^{238}U beams in the future. Because of the suppression of the electron capture process, it is expected that the low-Z gas will give the high-equilibrium charge states maintaining the intrinsic robustness of gas[2)]. However, direct data about the charge evolution for H_2 and He gas was not available because of the difficulty in preparing thick windowless gas targets. Furthermore reliable charge-changing cross sections for ^{238}U colliding with a low-Z gas at energies around 10 MeV/u are not yet available. In the present study, the maximum mean charge state (the mean charge state reaching a maximum gradually becomes lower because of energy attenuation) and the charge evolution of ^{238}U beams injected at 10.8 MeV/u have been investigated using thick H_2 and He gas.

In the experiment, the 8-m-long low-Z gas-charge-stripping system[3)] was located in the D-room at RIBF. The 0.68-MeV/u U^{35+} beams extracted from RILAC are accelerated to 10.8 MeV/u using RRC. The extracted beams from RRC (100−200 enA in the present measurements) go through the 8-m-long gas charge stripper. The charge distribution of the beams passing through the stripper was analyzed with the subsequent two dipole magnets and the faraday cup.

The fraction, $F(q_i)$, of the charge state, q_i, was determined by using the same procedure as that used in previous measurements[4)]. We used the measured injected-beam currents $I_{\rm inj}$ and the analyzed ones $I_{\rm ana}$ with a dipole magnet to deduce $F(q_i)=1/N\{(I_{\rm ana}/q_i)/(I_{\rm inj}/q_{ini})\}$, where N and q_{ini} are normalized factor and the initial charge state (equal to 35^+), respectively. Gaussian functions were fitted to the obtained $F(q_i)$ for H_2 and He gas to determine the mean charge states, q_{mean}. The mean charge q_{mean} for the H_2 and He strippers are plotted as functions of the calculated gas thicknesses (Fig. 1). For comparison with the previous measurements[4)], plots for N_2 and Ar are also shown.

The charge states for H_2 and He strippers gradually increased with thickness up to a thickness of 1 mg/cm^2, and then at higher thicknesses, they remained constant. As expected, the obtained charge states with low-Z gas strippers are considerably higher than those obtained with medium-Z strippers. For the analysis of the charge-state evolution, we used a Monte Carlo method with the EL cross sections for ^{238}U that was based on the binary encounter model[5)] and Schlachter's semiempirical EC cross sections[6)]. The charge-dependent energy-loss cross-sections calculated using the CasP code, which was based on the unitary-convolution approximation[7)], were used in our simulation. The maximum mean charge state for He, which is around 65^+, agrees well with the calculated one, but the required thickness for the equilibration was greater than the calculated value. The slow equilibration could be attributed to the reduced charge-changing cross sections. These tendencies were consistent with the results of the measurements performed using thin He gas targets[2)]. For H_2 gas, the maximum mean charge, which was around 65^+, was significantly lower than the calculated value, which was around 70^+. Unexpectedly, the measured maximum mean charge state for H_2 was almost same as that for He. Further investigations are being carried out to determine the nature of charge stripping in low-Z gas.

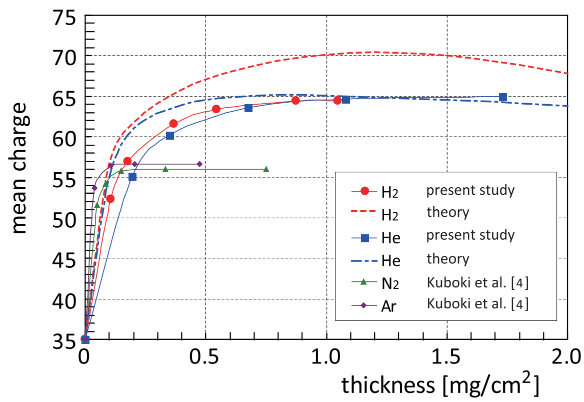

Fig. 1. Measured and calculated charge state evolution.

*1 RIKEN Nishina Center for Accelerator-Based Science

References

1) H. Hasebe et al.: Nucl. Instrum. Methods Phys. Res. Sect. **A 613**, 453 (2010).
2) H. Okuno et al.: Proc. of HB2010, 2010.
3) H. Imao et al.: in this report (2011).
4) H. Kuboki et al.: Phys. Rev. ST Accel. Beams **13**, 093501 (2010).
5) M. Gryzinski et al.: Phys. Rev. **A138**, 305 (1965).
6) A. S. Schlachter et al.: Phys. Rev. **A27**, 3372 (1983).
7) P. L. Grande and G. Schiwietz, Phys. Rev. **A 58**, 3796 (1998).

H_2 and toxic-gas sensitivity of sensors using ePTFE irradiated with 4MeV/nucleon ^{84}Kr beam

Y Suzuki, T. Tanaka, T. Kobayashi, K. Takahashi, T. Kambara, F. Saito,*1 T. Hyodo,*1 S. Hamago,*2 Y. Nagashima,*2 K. Okamura,*3 S. Uchikoshi,*3 N. Nakano,*3 A. Iwase,*4 S. Morisaki,*5 D. Mano,*5 and Y. Shiga*5

Amperometric gas sensors have been widely used for industrial purposes and in environmental monitoring for the detection of hydrogen, hydrogen sulfide, nitrogen oxides, and some other gases [1]. In this study, we attempted to perform ion beam irradiation on expanded polytetrafluoroethylene (ePTFE) membranes for improving the gas permeability characteristics of the sensor electrode. Ion beam implantation through the membrane influences the gas permeability [2]. We have already reported the structure and gas sensitivity of ePTFE irradiated with a 5 MeV/nucleon ^{14}N beam [3], [4]. The CO sensitivity increased with ion irradiation fluence. However, the maximum I_g / I_0 value was only 212%. The sensitivity of the sensors that used the Kr^+-ion-beam-irradiated membranes was tested for CO, H_2, and some other toxic gases, with the aim of investigating the effectiveness of ion beam irradiation for ePTFE modification. The pore size, porosity, and thickness of the ePTFE membranes (Sumitomo Denkou, Japan) used were 0.3 μm, 34%, and 0.2 mm, respectively. The membranes which were squeres with a side of 30 mm, were irradiated at room temperature with 4 MeV/nucleon Kr^{29+} ions from the AVF cyclotron, with fluences ranging from 1×10^{12} to 5×10^{12} ions/cm^2. Au ion plating (BMC800, SHINCRON, Japan) was carried out on the ion-implanted ePTFE membrane surfaces to fabricate gas-permeable electrodes. The plating rate was 0.1 nm/s under an Ar gas pressure of 2.3×10^{-2} Pa. The thickness of the Au-ion-plated was about 370 nm.

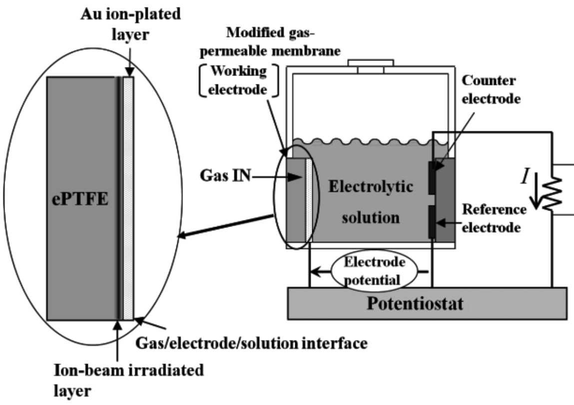

Fig.1 Schematic of the electrochemical gas sensor and the ion-implanted gas-permeable electrode.

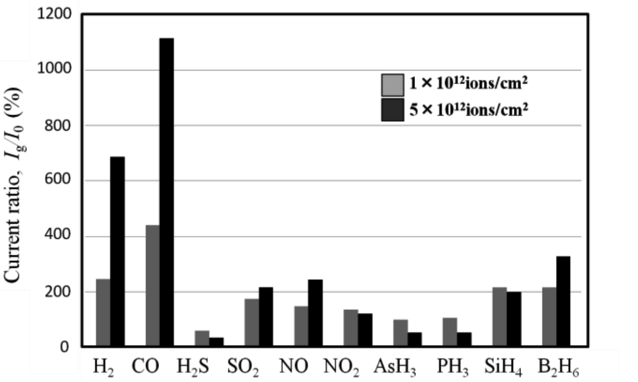

Fig.2 Gas detection current ratio for ion-beam-irradisted ePTFE (I_g) /non-irradiated, ePTFE (I_0) as a function of ion fluence.

The sensor structure is shown in Fig. 1. The gas-permeable working electrode used was 28 mm in diameter. The counter electrode and the reference electrode were Au black electrodes, and the electrolyte solution was 9 mol/dm^3 H_2SO_4; the applied electrode potential was 50 mV vs. the reference electrode. The flow rate of the sample gas was 0.25 dm^3/min. The current-time curves were recorded by a pen recorder, and the variation in the current 2 min after the gas was introduced into the sensor was measured as the characteristic current (I_g) for the sample gas. Fig. 2 shows the relationship between the current ratio, I_g / I_0, and the ion fluence, where I_g and I_0 are the characteristic currents of the sensors using the ion-beam-irradiated ePTFE membrane and the control (non-irradiated ePTFE), respectively. This is clear that I_g for H_2 and CO dramatically increased upon ion beam irradiation at a fluence of 5×10^{12}. The maximum I_g/I_0 was approximately 1113%, which suggested that Kr^+-ion-beam modification of the ePTFE membrane helps enhance the sensitivity for CO sensing. The relationship between surface the characteristics and the gas sensitivity is being investigated.

References

[1] T. Ishiji, T. Iijima, and K. Takahashi, Denki Kagaku (1996) 1304
[2] K. Okamura, T. Ishiji, M. Iwaki, Y. Suzuki, and K. Takahashi, Surface & Coatings Technology 201 (2007) 8116
[3] Y. Suzuki, et. al. RIKEN Accelerator Progress Report, Vol.42 (2009) 226
[4] Y. Suzuki, et. al. RIKEN Accelerator Progress Report, Vol.43 (2010) 232

*1 University of Tokyo
*2 Tokyo University of Science
*3 Riken Keiki Co.Ltd.
*4 Osaka Prefecture University
*5 Meiji University

Site change of hydrogen in niobium on alloying with oversized Ta atoms†

E. Yagi,[*1] M. Yoshii,[*2] Y. Okada,[*2] H. Matsuba,[*2] K. Miyahara,[*2] S.Koike,[*3] T. Sugawara,[*4] T. Shishido,[*4] and K. Ogiwara

An interaction of hydrogen with solute atoms is one of the fundamental subjects in disordered alloys, because it affects various properties of hydrogen. One of the noticeable effects is the change of terminal solubility of hydrogen (TSH) on alloying in the group Va metals in the periodic table (V, Nb and Ta). For undersized metal solutes, *e.g.*, Nb in Ta and V in Nb, the TSH increases rapidly with increasing solute concentration up to a certain solute concentration, whereas for oversized metal solutes the TSH again increases, but less rapidly. Matsumoto et al. proposed, from X-ray diffraction and NMR studies on Nb alloyed with undersized solutes V or Mo or oversized solutes Ta, that the enhancement of the TSH on alloying with V or Mo in Nb is due to trapping of hydrogen by solute atoms. On the other hand, Peterson et al. reported that evidence of trapping could not be observed in the studies on the isopiestic solubility of hydrogen and hydrogen diffusion in V-based alloys (V-Nb, V-Cr and V-Ti) for a wide range of solute concentration. In order to clarify the trapping of hydrogen, direct information on its lattice location is highly required. However, such microscopic information has been extremely limited, because of experimental difficulties. To locate hydrogen dissolved in metals the channelling method utilizing a resonance type of nuclear reaction $^{1}H(^{11}B,\alpha)\alpha\alpha$ with a ^{11}B beam of about 2 MeV has been developed.[1)] In this method, hydrogen can be detected by measuring emitted α particles of energies ranging up to about 5 MeV.

We have already observed that, in Nb, hydrogen is located at tetrahedral (*T*) sites, and that, in 97 at.% Nb–3 at.% Mo alloys ($Nb_{0.97}Mo_{0.03}$), hydrogen is located at sites displaced from *T*-sites by about 0.6 Å towards their nearest neighbour lattice points at room temperature, whereas at 373 K hydrogen is located at *T* sites, clearly indicating the trapping of hydrogen by undersized Mo atoms at room temperature.[2)] There exists a strong attractive interaction between hydrogen and undersized Mo atoms. In the present study, in order to clarify a difference in hydrogen interaction with oversized solutes and with undersized solutes, the site occupancy of hydrogen in Nb alloyed with 5 at.% of oversized Ta atoms has been investigated at room temperature for hydrogen concentrations of 0.018 or 0.025 at a hydrogen-to-metal-atom ratio, C_{H}, $Nb_{0.95}Ta_{0.05}H_{0.018}$ or $Nb_{0.95}Ta_{0.05}H_{0.025}$, by the channelling method with a $^{11}B^{+}$ beam of 2.03 MeV. The atomic radii of Nb, Mo and Ta atoms are 1.43, 1.36 and 1.44 Å, respectively.

†Condensed from the article in J. Phys. Soc. Jpn. **78,** 064601 (2009)

*1 RIKEN and The School of Sci. and Eng., Waseda University
*2 The School of Sci. and Eng., Waseda University
*3 Department of Physics, Tokyo University of Science
*4 Institute for Materials Research, Tohoku University

Figure 1 shows the obtained channelling angular profiles. Different from the result on hydrogen in $Nb_{0.97}Mo_{0.03}$ alloys, H atoms are distributed over *T* sites and *d-T* sites which are displaced from *T* sites by about 0.25 Å towards their nearest neighbour octahedral (*O*) sites. Higher the H concentration, the larger the portion of H atoms located at the *d-T* sites, as indicated by the difference in the angular profiles between Figs. 1(a) and 1(b). In both specimens approximately the same concentration of H atoms of $C_{\mathrm{H}} \approx 0.006$ are located at the *T* sites and the remains are at the *d-T* sites, indicating that the *T* site is more favourable. Hydrogen preferentially occupies the *T* sites, but the number of available *T* sites is limited, and excess H atoms occupy the *d-T* sites. In contrast to a strong attractive interaction between hydrogen and undersized Mo atoms, there exists no such a strong attractive interaction between hydrogen and oversized Ta atoms. The *d-T* site is considered to be a stable site in a slightly distorted lattice around Ta atoms. It is considered that trapping of hydrogen by undersized solute atoms is effective to the large enhancement of the TSH on alloying with undersized solute atoms, at least, in the low solute concentration region.

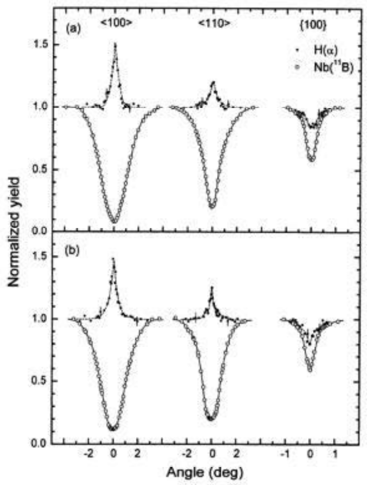

Fig. 1. Channelling angular profiles of yield of α-particles and yield of ^{11}B ions backscattered by Nb and Ta atoms obtained for (a) $Nb_{0.95}Ta_{0.05}H_{0.018}$ and (b) $Nb_{0.95}Ta_{0.05}H_{0.025}$.

References

1) E. Yagi, T. Kobayashi, S. Nakamura, Y. Fukai, and K. Watanabe: J. Phys. Soc. Jpn. **52**, 3441 (1983).
2) E. Yagi, S. Nakamura, F. Kano, T. Kobayashi, K. Watanabe, Y. Fukai, and T. Matsumoto: Phys. Rev. B**39**, 57 (1989).

Stark velocity filter for producing slow polar molecules

T. Suganuma,[*1] K. Okada,[*1] T. Takayanagi,[*1] S. Ohtani,[*2] H. A. Schessler,[*3] M. Wada

[polar molecules, Stark velocity filter, cold molecules]

In the field of astrochemistry, the reaction-rate coefficients of cold chemical reactions and the reaction-network model of interstellar clouds are of interest to understand the chemical evolution of these clouds. Therefore, a database of chemical reactions related to astrochemistry has been set up[1)]. However, the information stored in this database is not detailed enough to reproduce specific molecular abundance. In fact, it has been pointed out that the rate coefficients of ion-polar molecule reactions are not sufficiently well known to understand the chemical evolution of interstellar clouds[2)].

We plan to perform measurements of reaction-rate coefficients for cold ion-polar molecule reactions by using the sympathetic laser cooling method and a Stark velocity filter[3,4)]. In this paper, we report a brief summary of a newly developed Stark velocity filter and the results of an experiment conducted for studying the production of cold ND_3 molecules.

Since the principle of filtering polar molecules by using Stark velocity filter has been described in detail[3)], we present a brief summary of the principle. In spatially nonuniform electric fields such as linear quadrupole fields, slow polar molecules whose the rotational-energy levels increase linearly with the field intensity (that is, "low field seekers") are trapped transversely since the Stark energy must be counterbalanced by reducing the translational energy of the molecules. Therefore, linear quadrupole rods can be used as molecular beam guides for polar molecules. To select longitudinally slow molecules, the quadrupole electrodes are bent by 90°.

Figure 1 shows a schematic drawing of the Stark velocity filter. The molecular beam guide consists of four stainless steel rods with a diameter of 2 mm. The distance between the rods is 1 mm. We placed a quadrupole mass spectrometer (QMS) in front of the filter exit to detect slow molecules. Through the gas inlet, a polar molecular gas is passed through a ceramic gas nozzle with a diameter of 1.5 mm. The back pressure of the nozzle is controlled to be lower than 13.3 Pa by using a variable leak valve. The nozzle temperature can be varied from room temperature to 50 K by simultaneously driving a 10 K cryocooler and a ceramic heater fixed on the nozzle mount. The maximum high voltage (HV) applied to the electrodes is ±3 kV, and a trapping fields of about 60 kV/cm is generated. To obtain the time-of-flight (TOF) signal of the slow molecules, the HV is switched on and off at a high speed (10 ns/kV).

An example of a TOF signal of slow ND_3 molecules is shown in Fig. 2. The HV is switched on at $t = 0$ and the switching period is 200 ms. The QMS signal of the slow molecules starts increasing with a time delay after switching the HV on. During this time delay, the fastest molecules travel in the beam guide. The signal then reaches a steady state; in the steady state, the intensity depends strongly on the HV applied to the electrodes since the maximum filtering velocity increases with increasing the electric field.

The velocity distribution of the detected molecules can be obtained by the time differentiation of the TOF signal. As shown in Fig. 2(b), the peak velocity is about 30 m/s, which corresponds to a thermal energy of about 2 K. In addition to ND_3, we have successfully produced slow NH_3, CH_2O and CH_3CN molecules using the present setup.

*1 Department of Materials and Life Sciences, Sophia University
*2 ILS, University of Electro-Communications
*3 Department of Physics, Texas A&M University

References

1) J. Woodall et al.: A&A **466**, 1197 (2007).
2) V. Wakelam et al.: A&A **451**, 551 (2006).
3) S. A. Rangwala et al.: Phys. Rev. A **67**, 043406 (2003).
4) S. Willitsch et al.: Phys. Rev. Lett. **100**, 043203 (2008).

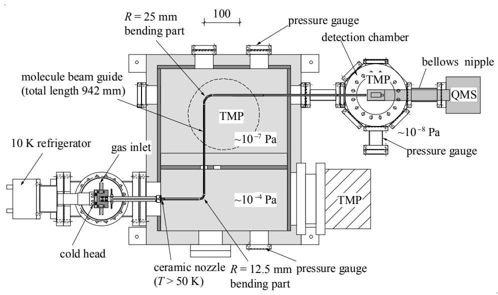

Fig. 1. Schematic drawing of a Stark velocity filter.

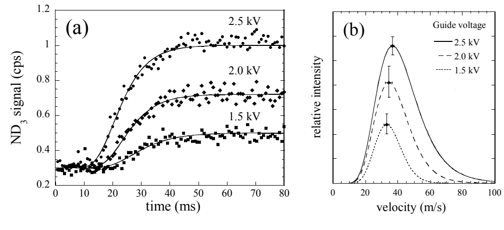

Fig. 2. Time-of-flight signal of slow ND_3 molecules at the nozzle pressure of 5.3 Pa.

Excitation spectra of In and Ga atoms in superfluid helium

Y. Kato,[*1] T. Furukawa,[*2] Y. Matsuura,[*1] T. Kobayashi, Y. Yamaguchi,[*1] K. Imamura,[*1] A. Hatakeyama,[*3] M. Tachikawa,[*1] and Y. Matsuo

We are developing a technique for performing optical pumping and laser RF/MW (radiowave / microwave) double-resonance spectroscopy of atoms in superfluid helium (He II). The developed method is expected to be effective in determining the spin and moment of low-yield unstable nuclei.[1)] By determining the nuclear spins and electromagnetic moments of stable alkali atoms (Cs, Rb) in He II, we have shown the potentiality of this method.[2)] We are planning to perform the optical pumping of atoms of non-alkali elements, such as In and Ga atoms.

In general, the excitation spectra of atoms in He II are broader and more blue-shifted than those of atoms in vacuum. Using this principle, a single-frequency laser can be used to excite all the atomic sublevels of non-alkali atoms that have complex electronic energy levels. Therefore, we can expect large atomic polarization for non-alkali metals by optical pumping with a single laser. For optical pumping to be efficient, we need to tune the laser wavelength to the peak of the excitation spectrum. Here, we report the measurement of the excitation spectra of In and Ga atoms in He II.

The experiment is performed in a cryostat having an internal temperature of approximately 1.6 K (Fig.1). An open-top quartz cell is filled with He II. Clusters of In or Ga, which are generated by the laser ablation of a solid sample placed 1 cm above the He II surface, are immersed in He II and further dissociated by a dissociation-laser. This is a useful method for immersing atoms in He II with less convection flow. Then, the atoms are excited with a pulsed dye laser (probe-laser) and they emit LIF (Laser Induced Fluorescence). A monochromator is set to the emission wavelength of In or Ga to discriminate LIF from the scattered laser light. The LIF photons are detected by a PMT (photomultiplier tube). The signal is accumulated with a gated integrator and recorded in a computer. The LIF intensity is expressed by

$$I \propto \sigma \times N \times P \qquad (1)$$

where I is the LIF intensity, σ is the absorption cross section, N is the number of atoms in the observation region, and P is the probe-laser power. By scanning the wavelength of the probe-laser, we can measure the excitation spectra from the LIF intensity. It is to be noted that the measured spectra are normalized for variation in P because P is dependent on the laser wavelength.

It is also to be noted that N fluctuates because the ablation condition changes with time. To eliminate the effect of this fluctuation, we introduce another pulsed dye laser (reference-laser) set to 370 nm (excitation wavelength of both In and Ga in He II). Because σ and P are constant, the LIF of the reference-laser is proportional only to N. The reference-laser beam is radiated about 30 ns after the probe-laser irradiation. Hence, the number of atoms residing in He II is almost the same for the probe- and reference-laser shots. By recording the LIF of probe- and reference-lasers simultaneously, we can correct the excitation spectrum by normalizing N.

In this experiment, we measured the excitation spectra for In (370 nm peak and 14 nm FWHM) and Ga (367 nm peak and 13 nm FWHM). Figure 2 shows the excitation spectrum for In. By introducing the reference-laser, we have obtained more accurate spectra than those previously reported, which were not normalized by N and which had small peaks owing to fluctuations in N.[3)] As the next step, we are planning to perform the optical pumping In and Ga in He II.

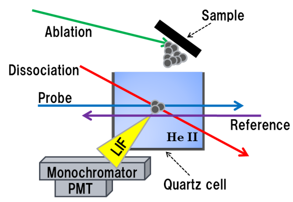

Fig. 1. Experimental setup.
The quartz cell and sample are set in the cryostat.

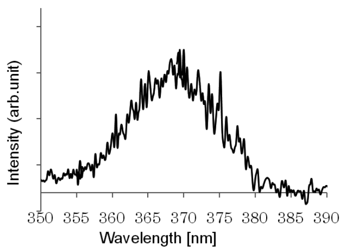

Fig. 2. Excitation spectrum of In atoms.

References
1) T. Furukawa et al.:Riken Accel. Prog. Rep. **38**, 99 (2005).
2) T. Furukawa et al.: Phys. Rev. Lett. **96**, 095301 (2006).
3) A. Sasaki et al.: RIKEN Accel. Prog. Rep. **42**, 231 (2009).

*1 Department of Physics, Meiji University
*2 Department of Physics, Graduate School of Science and Technology, Tokyo Institute of Technology
*3 Department of Applied Physics, Tokyo Univ. Agr.Tech.

2. Atomic and Solid State Physics (muon)

Progress in beam commissioning with new multichannel μSR spectrometer CHRONUS

D. Tomono, T. Kawamata, Y. Hirayama*[1], M. Iwasaki*[1], I. Watanabe, K. Ishida and T. Matsuzaki

An intense pulsed muon source at RIKEN-RAL is used in a variety of studies on condensed matter and particle physics. For detecting decay positron, a new spectrometer named CHRONUS (multiCHannel Riken muON Universal Spectrometer) has been developed. We designed 606 spindle counters (10 mm × 10 mm, 50 mm-length) fabricated in homogeneous magnets. The total muon rate per pulse at a target is approximately 10^4 counters. The decay positron hit rate in a counter is expected to be less than 2 counts per pulse. The positrons that penetrated the spindle counter through 50 mm-length were preferably observed by setting an appropriate threshold level for each output signal. If this spindle counter was directed to the target, positrons emitted at incident angles of 7 ° from the target could be selectively observed. This mechanism was verified by performing a feasibility test[1,2]. A counter mold, iron and permalloy magnetic-field shield, fiber light-guide, modified photomultiplier tube[3,4], and dedicated data-acquisition system[5] have been developed and have already been installed in Port-4.

Figure 1 (a) shows a schematic view of positron counters. The 303 counters were installed in each forward and backward mold inside the bore of the longitudinal magnets. The counters were positioned 136-mm away from the target and covered approximately 26% of the total solid angle viewed to the target. In order to test the "fiducial volume" sensitivity, we observed the muon spin asymmetry with the spectrometer using three types of targets in the transverse field of 20 G.

A silver plate (150 mm × 150 mm, 1 mm-thickness) was first mounted at the center of the spectrometer. The beam was collimated using the 16 mmϕ beam collimator. A spin asymmetry spectrum is shown in Fig. 2 (a). In silver, the muon spin rotates while maintaining the polarization. The spin polarization is approximately 16.3%. This value indicates the initial spin asymmetry with the 16 mmϕ collimator in the present counter setup. In the next step, a holmium plate (150 mm × 100 mm, 1 mm-thickness) is placed instead of the silver plate. Another silver plate (30 mm×30 mm, 1 mm-thickness) is mounted onto its center. If the muons stop at the holmium plate, the asymmetry gradually decreases with a time constant of approximately 500 ns due to depolarization of the muon spin even in the transverse field of 20 G. Fig. 2 (b) shows the asymmetry of 15.6%, which is consistent with in Fig. 2 (a). This indicates that most of the muons still stopped at the silver target. Finally, the 16 mmϕ beam collimator was removed. The beam size of 40 mmϕ was employed. The same target was used. Some of the muons stopped at not only the silver plate but also the holmium plate. If we observed muons which stopped at holmium, the asymmetry may decrease exponentially with a time constant of 500 ns. However, the asymmetry was measured to be 15.4%, as shown in Fig. 2 (c). These fact shows that, even if the beam size is large, the counter can preferably observe positrons emitted from the silver target at the center of the fiducial volume.

In summary, we successfully observed actual asymmetry spectra using the silver and holmium targets at the center of the fiducial volume. The remaining part of the beam commissioning test will be completed by the end of 2011.

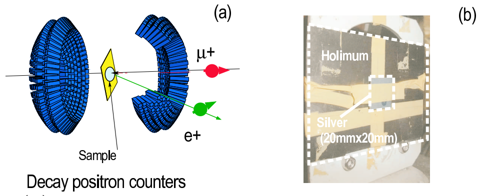

Fig. 1. (a) Schematic view of the counters. The 303 forward and backward counters are mounted. Approximately 26% of a sample is covered by the counters. (b) Photograph of the target. A silver plate (15 mm×15 mm, 1 mm-thickness) is attached to a holmium plate(150 mm×100 mm, 1 mm-thickness).

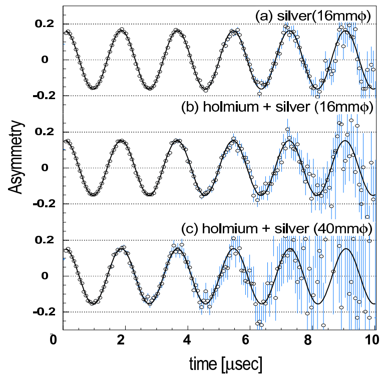

Fig. 2. Asymmetry spectra. Muons were stopped at the (a) silver and (b) and (c) small silver target attached to the holmium plate as shown in Fig. 1 (b). The values within parentheses in each condition denote the beam size.

*1 Department of Physics, Tokyo Institute of Technology

References

1) Y. Hirayama et al.: RIKEN Accel. Rep. **41**, 195 (2008).
2) D. Tomono et al.: Nucl. Inst. Meth. A **600**, 44 (2009).
3) D. Tomono et al.: RIKEN Accel. Rep. **42**, 237 (2009).
4) D. Tomono et al.: RIKEN Accel. Rep. **43**, 237 (2010).
5) T. Kawamata et al.: RIKEN Accel. Rep. **42**, 238 (2010).

Upgrade of the Lyman-α laser system at the RIKEN-RAL muon facility

K. Yokoyama, P. Bakule, N. Saito, O. A. Louchev, M. Iwasaki and S. Wada

The RIKEN-RAL muon facility has been involved in the development of a pulsed low-energy muon (LE-μ^+) source since the 1990s because this source has superior features such as narrow energy spectrum, short pulse, and a small beam size, all of which make it an ideal probe for surface and sub-surface physics studies[1]. LE-μ^+ also has potential applications in the measurement of the anomalous magnetic momentum of muons, which makes the above mentioned development an urgent need. However, the overall generation efficiency achieved so far at the facility, ~15 LE-μ^+/s, is not sufficient for these applications. To generate LE-μ^+, we illuminated the muonium (Mu) atoms in vacuum with Lyman-α (Ly-α) laser light (122 nm), which excites the Mu atoms from the 1s state to the 2p state, and photoionized the atoms by 360nm UV light [1]. Therefore, to improve the yield, it is crucial to generate higher Ly-α power, although it is not trivial because light conversion takes place in the two-photon resonant four-wave mixing process in Kr gas. For this purpose, we are upgrading the existing laser system[1] at RIKEN-RAL so that power generation is increased tenfold and studying how the yield follows with the intense Ly-α light without having any saturations.

The existing Ly-α laser system is constructed using three Nd:YAG lasers to produce ω_1 (212.55 nm) and ω_2 (820 nm) by the optical parametric oscillators (OPOs) and nonlinear frequency conversion in optical crystals[1]. Then ω_1 and ω_2 pump the wave-mixing process in Kr atom to generate $\omega_{Ly\text{-}\alpha}$. To generate ω_1 the system first generates 850 nm light, which is converted to ω_1 as the fourth harmonic. However the grating-based single longitudinal mode (SLM) OPO (Continuum Mirage 800) for 850 nm has always been a problem because of mode hopping and the skewed beam profile with hot spots. Hot spots induced in the spatial mode may heat up the nonlinear crystal and eventually decrease the conversion efficiency because the full mode volume cannot be used. To solve this problem we replaced the OPO with an injection-seeded optical parametric generator/amplifier (OPG/OPA), as shown in Fig. 1. The cw laser light at 850 nm is amplified by down-conversion of the second harmonic of Nd:YAG (532 nm) in the nonlinear crystals. This scheme has three major advantages: 1) the wavelength of the amplified pulse is stable when the 532-nm pump and 850-nm seed light are in SLM operation; 2) the beam profile is drastically improved because of single-path amplification; and 3) the power output is more stable than that when using the OPO because there is no lasing threshold. Fig. 1 shows the calculated parameters for obtaining a 1 mJ/pulse at 850 nm, which is considered sufficient for a tenfold improvement in the Ly-α power generation efficiency.

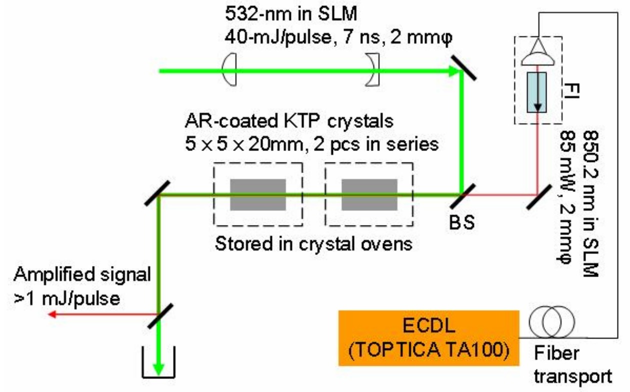

Fig. 1 Nanosecond OPG/OPA system layout.

The SLM 850-nm seed light is emitted from an external-cavity diode laser and transported through a polarization-maintaining single-mode fiber. In this manner, the beam profile is made to be in the ideal Gaussian mode so that uniform OPG/OPA amplification occurs. The key feature of this scheme is the use of two KTP crystals to obtain a gain as high as 10^6 just by single-path amplification. The KTP crystal has a large nonlinear coefficient d_{eff}, and it can grow up to a couple of centimeters long. To obtain a gain of 10^6, it is also necessary to increase the intensity of the pump laser to 120 MW/cm^2. The KTP crystal, however, is not stable in a high laser field because it develops the so-called gray tracking, which may lead to permanent damage along the beam path. Although the actual microscopic mechanism underlying this gray tracking is unknown, the practical solution to prevent this would be to increase the temperature of the crystal. By heating the crystals to 90 ℃ in our home-made crystal ovens and temperature controllers, we could pump the crystal to 120 MW/cm^2 for several hours without the development of gray tracks. Another important feature of the system is the walk-off compensation achieved by placing KTP crystals adjacent to each other to cancel out the relatively large walk-off angle. This increases the spatial overlap of two beams and effectively enhances the gain.

The OPG/OPA system has been developed inside Mirage 800 so that the original Ti:Sapphire amplification stages can be reused. Although the system is still under development, the expected gain can be observed in the low-pumping regime. When the pump power is increased, however, parasitic lasing occurs because of cavity formation between the surfaces of the KTP crystals. We plan to solve this problem by creating wedge angles on the crystal faces and focus on Ly-α generation with the improved beam profile and power.

1) P. Bakule et al.: Nucl. Instr. Meth. B **266**, 335 (2008).

Completed measurement (R379) of muonium reactivity with state selected $H_2^*(v=1)$ molecules at 300 K

D.G. Fleming,[*1] P. Bakule,[*2,*3] F.L. Pratt,[*3] K. Ishida,[*2] O. Sukhorukov,[*4] and T. Momose,[*5]

Using a pulsed muon beam combined with a nanosecond laser at the RIKEN-RAL Muon Facility at ISIS (UK) we have made for the first time an accurate measurement[1,2] of the reaction rate of muonium (Mu) with H_2 molecule in a selected vibrational excited state (v=1). Such a type of experiment allows for accurate and important tests of the thermal rate theory. Historically, there are many measurements of the reaction rates for H+H_2 type reactions in the gas phase, including reactions with hydrogen isotopes such as H + D_2, D + H_2[3,4], Mu + H_2[5], mostly with the reactants in the ground state (mainly v=0). The schematic diagram of the reaction path of Mu + H_2 reaction vs the reaction coordinate 's' for an assumed collinear transition state is shown in Fig. 1. This diagram clearly demonstrates that with H_2 in its v=1 state one can expect a huge enhancement of the reaction rate - by a factor of 10^7(!) - since in this case the barrier height, denoted as $E_a(1)$, is reduced to ≈0.06 eV. For comparison, an earlier report of the reaction rate measurement from vibrationally excited H_2 in the D + H_2(v=1) reaction, determined the reaction rate constant as $k_D(1) = (1.0\pm0.4)\times10^{-13}\mathrm{cm^3s^{-1}}$, an enhancement of 300 compared to its reaction with H_2(v=0). The huge enhancement expected for the Mu + H_2(v=1) reaction makes such a measurement possible even with a relatively low concentration of H_2(v=1) compared to H_2(v=0). Additionally, the reaction is particularly interesting one to study and compare with theory because of pronounced quantum tunnelling of the light Mu atom through the low barrier.

Using the process of stimulated Raman pumping by 532 nm photons we were able to excite up to 4×10^{17} H_2 molecules to the v=1 state and determine their concentration from measurements of the number of Raman shifted red photons at 683 nm and the profile of the laser beam. The stopping distribution of the Mu atoms in the H_2 gas and the overlap with the excited H_2(v=1) was determined from GEANT4 Monte Carlo simulation of the surface μ^+ beam stopping in the reaction cell. The GEANT4 model was validated by comparison with the observed Mu spin rotation asymmetry amplitude, A_{Mu}, measured as a function of thickness

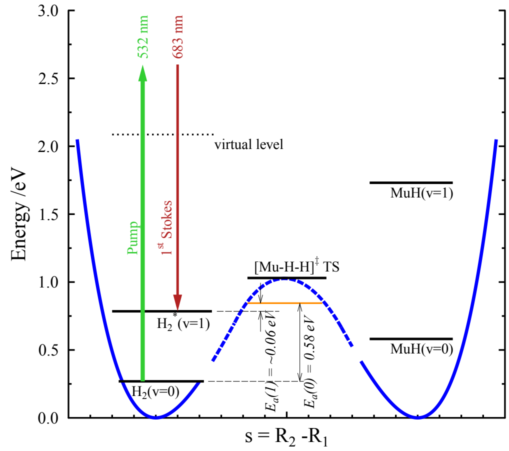

Fig. 1. Schematic of the reaction path for the Mu+H_2 reaction showing also the stimulated Raman pumping processes relevant to selectively populating H_2(v=1) state.

of the muon entrance window (stopping range curve). The muon spin relaxation technique (μSR) was used to measure the reaction rate though observation of an increased relaxation of the spin rotation asymmetry signal of spin polarized Mu, since each Mu undergoing reaction can no longer contribute to the spin rotation signal of the polarized Mu ensemble. By detailed data analysis, taking into account additional sources of Mu spin relaxation and also the collisional relaxation (λ_c) of $H_2(v = 1)$ population, we were able to determine the reaction rate constant at T=300 K. The fitted experimental results are linearly dependent on λ_c as $k_{Mu}[10^{13}\mathrm{cm^3s^{-1}}]=18.57\lambda_c[\mu s^{-1}]+7.20$. The de-excitation rate constants for H_2(v=1)+H_2 collisions have been measured in[6,7], giving an averaged value of $\lambda_c=0.145\pm0.015$ μs^{-1} at 50 bar. This allows us to determine $k_{Mu}=(9.9[-1.2][+1.4])\times10^{13}\mathrm{cm^3s^{-1}}$ at T=300 K. With the technique and methodology for this type of accurate measurement now established, we are planning to measure the temperature dependence of k_{Mu}, particularly below room temperature in order to study in detail contributions from quantum tunnelling confirming the high accuracy of the theory in the process.

*1 TRIUMF and Department of Chemistry, University of British Columbia, Vancouver, Canada
*2 Advanced Meson Science Laboratory, RIKEN Nishina Center, Wako, Saitama 351-0198, Japan
*3 Science and Technology Facilities Council, ISIS, Rutherford Appleton Laboratory, Didcot, OX11 0QX, United Kingdom
*4 Chemistry Dept., Univ. of Alberta, Edmonton, Canada
*5 Depts. of Chemistry and Physics, University of British Columbia, Vancouver, Canada

References

1) D.G. Fleming et al.: RIKEN Acc. Prog. R. **42**, 236 (2009).
2) D.G. Fleming et al.: RIKEN Acc. Prog. R. **43**, 241 (2010).
3) S.L. Mielke et al.: Phys. Rev. Lett. **91**, 063201 (2003).
4) S.L. Mielke et al.: J. Chem. Phys. **122**, 224313 (2005).
5) I.D. Reid et al., J. Chem. Phys. **86**, 5578 (1987)
6) M.M. Audibert et al.: Chem. Phys. Lett., **25**, 158 (1974).
7) M.M. Audibert et al.: Chem. Phys. Lett., **31**, 232 (1975).

Response of negative muonium to conduction electron spin polarization induced by lasers in *n-type* GaAs under longitudinal fields

K. Yokoyama[1], K. Nagamine[1,2], K. Shimomura[2], H.W.K. Tom[1], R. Kawakami[1], P. Bakule[3], Y. Matsuda[4], K. Ishida, K. Ohishi, F.L. Pratt[3], I. Shiraki[5] and E. Torikai[5]

In the research field of spintronics, a spin-dependent exchange scattering of a polarized electron in ortho muonium (ortho-Mu, μ^+e^-, atomic state of μ^+ and an electron with the spins aligned in the same direction) has been proposed to detect the conduction electron spin polarization (CESP) in semiconductors[1]. A feasibility study of this muon method was carried out in strain-free *n*-type GaAs containing 3×10^{16} cm^{-3} Si by measuring the change in the μ^+ spin polarization against a change in the polarization direction of the CESP under zero field (ZF)[2, 3]. The CESP was induced by circularly polarized (CP) lasers[4].

The muon states in *n*-GaAs have been studied. The existence and properties of Mu$^-$ ($\mu^+e^-e^-$, a diamagnetic bound state of μ^+ containing two singlet electrons) in *n*-GaAs with $\geq10^{16}$ doping have been known. As summarized in Fig. 1, before laser irradiation, the μ^+ in *n*-GaAs takes the three states which have characteristic polarization recovery against longitudinal fields (LF); Mu$^-$ with Kubo-Toyabe relaxation function, Mu at body-centered site (BC-Mu) with an exponential one and T-Mu without relaxation.

In the ZF "Para-Anti" effect[3], the Mu$^-$ was found to respond to the change of laser CP, while the BC-Mu is insensitive to the laser irradiation. In Mu$^-$ response, the CESP characteristics consistent with optical data[5] were obtained appearing in 1) the laser wavelength dependence reflecting band-gap and 2) laser-power dependence for electron correlation effect on CESP.

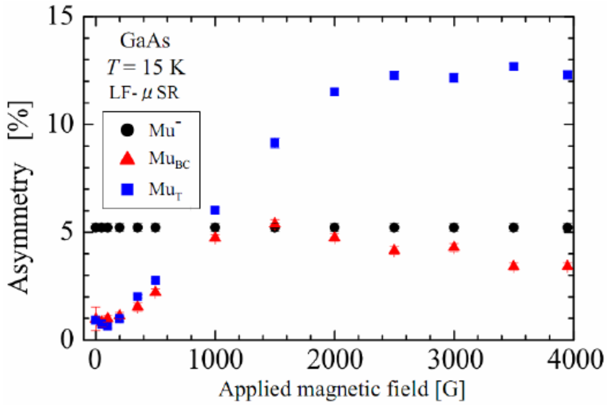

Fig. 1. Asymmetry recovery without lasers under longitudinal fields of the BC-Mu component, T-Mu component and a diamagnetic Mu$^-$ component in *n*-GaAs at 15 K.

[1]Physics & Astronomy, University of California, Riverside
[2]Muon Science Laboratory, IMSS, KEK
[3]ISIS, Rutherford Appleton Laboratory
[4]Arts and Science, University of Tokyo
[5]Medicine and Engineering, University of Yamanashi

The present measurement was conducted under various LF at Port 2 of the RIKEN-RAL by using a pulsed 4-MeV positive muon beam and the 831 nm CP laser light under pulse-to-pulse CP control by the Pockel's cell[4]. The result for the *n*-GaAs at 15K is seen in Fig. 2. The following observations have been made.

1) Both the BC-Mu with exponential relaxation and the T-Mu with characteristic LF decoupling patterns (Fig 1) do not take any changes against laser irradiation in neither "On-Off" nor "Para-Anti" effects. Insensitive nature of both BC-Mu and T-Mu against lasers is confirmed both under ZF and LF. The Mu$^-$ state only responds to the laser.

2) Both "On-Off" and "Para-Anti" effects have peaks at around 1 kG and tend to disappear above 3 kG. At higher LF, the hyperfine magnetic field from the bound electron becomes decoupled so that the polarization change of the bound electron(s) in the Mu$^-$ does not affect μ^+ polarization. This result should be considered as a key information to understand the origin of the unexplained strange phenomena of the spin-dependent response of the Mu$^-$ to the CESP. The observed decoupling manner suggests the involvement of the Mu-like intermediate state in the Mu$^-$ response.

References

1) E. Torikai *et al.*, *Physica B* **289-290**, 558 (2000).
2) K. Yokoyama *et al.*, *Physica B* **404**, 856 (2009).
3) K. Yokoyama *et al.*, *RIKEN-APR* **42**, 234 (2008); *Nature* to be submitted (2010).
4) P. Bakule *et al.*, *RIKEN-APR* **42**, 233 (2008).
5) J.M. Kikkawa *et al.*, *Phys. Rev. Lett.* **80**, 4313 (1998).

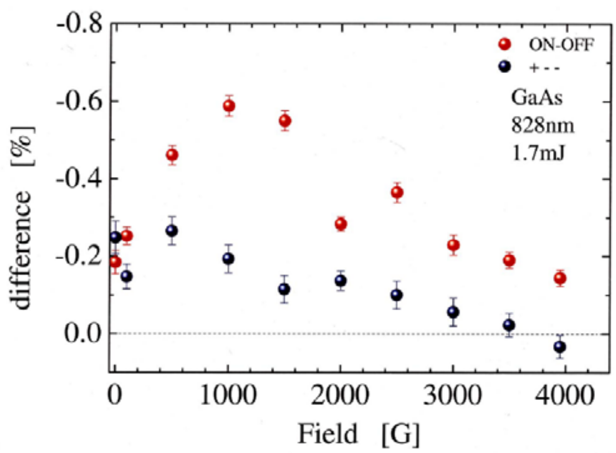

Fig. 2. Summary of laser irradiation effects under various LF, where "+" is for Para and "-" is for Anti between μ^+ and CESP in *n*-GaAs at 15 K.

μSR study of flux-line lattice state in newly discovered antiperovskite-type superconductor ZnN_yNi_3

K. Ohishi, T. U. Ito,[*1] W. Higemoto,[*1] T. Yamazaki,[*2] A. Uehara,[*2] K. Kozawa,[*2]
Y. Kimishima,[*2] and M. Uehara,[*2]

Since the discovery of superconductivity in $MgCNi_3$ at $T_c \sim 8$ K[1)], antiperovskite superconductors have attracted much interest because the ferromagnetic correlation is considered to be associated with the superconductivity in $MgCNi_3$. Band structure calculations indicate the presence of a large peak in the density of states, located just below the Fermi surface, leading to a predictions of a quantum phase transition to a ferromagnetic ground state with hole doping[2,3)]. The emergence of ferromagnetism has been observed in carbon-deficient (Mg,Zn)C_yNi_3 ($y < 0.7$)[4)]. Recently, Uehara *et al.* have discovered a new antiperovskite-type superconductor ZnN_yNi_3, which is the first antiperovskite nitride superconductor[5)]. In order to clarify the superconducting gap symmetry in the newly discovered ZnN_yNi_3, we have performed muon spin rotation (μSR) measurements.

The polycrystalline samples used in this study were synthesized in an NH_3 gas atmosphere. The inset in Fig. 1 shows the temperature dependence of susceptibility at $H = 2$ mT after zero-field cooling and field cooling for the present sample. The superconducting transition temperature T_c was estimated to be $\simeq 2.6$ K. μSR experiments down to 20 mK were performed at the M15 beamline at TRIUMF, Vancouver, Canada, and at RIKEN-RAL Muon Facility, Didcot, UK.

Figure 1 shows the muon spin relaxation rate σ_v observed in the transverse field of 50 mT, obtained in a fit to a Gaussian damping $\exp[-(\sigma_v^2 + \sigma_n^2)/2]$, where σ_n is the relaxation rate due to the nuclear dipole field (0.134(2) μs^{-1}). σ_v is related to the magnetic penetration depth λ and n_s/m^* (superconducting carrier density/effective mass): $\sigma_v \propto \lambda^{-2} \propto n_s/m^*$. σ_v increases with decreasing temperature below ~ 2.3 K, owing to the formation of the flux-line lattice. According to the empirical two-fluid model, which is approximately valid for conventional Bardeen-Cooper-Schrieffer (BCS) superconductors, we have $\sigma_v(T) = \sigma_v(0)\,[1 - (T/T_c)^n]$ with $n = 4$. Fitting analysis by the same formula with an arbitrary power when T_c is used as a free parameter yields $\sigma_v(0) = 0.74(1)$ μs^{-1}, $T_c = 2.3(1)$ K, and $n = 2.2(1)$. The result is shown by the solid curve in Fig. 1. We estimate the penetration depth at 0 K to be $\lambda(0) = 362(2)$ nm, which is consistent with that estimated from H_{c1}[5)]. As shown in Fig. 1, it is apparent that the temperature dependence of σ_v is different from that in the case of conventional BCS superconductors ($n = 4$, dotted curve). Temperature dependence of relaxation rate with $n = 2$ is expected in superconductors having line nodes with impurity scattering or the nonlocal effect. The strongly suppressed specific heat jump and the deviation from the exponential temperature dependence of the electronic specific heat[5)] suggest that ZnN_yNi_3 is an unconventional superconductor. On the other hand, we must consider a broad distribution of the transition temperature $\Delta T_c \sim 1$ K, as shown in the inset of Fig. 1, because such a distribution may decrease the value of n. For example, when we fit the data for the temperature range below 1.5 K, data are well described by two-fluid model with $n = 4$ (see dotted line in Fig. 1), suggesting a conventional superconductor. At this stage, we cannot exclude the possibility that this is conventional superconductor. In order to clarify this problem, we need to study magnetic field dependence of penetration depth in the future.

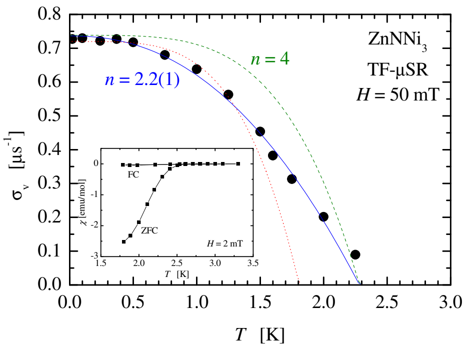

Fig. 1. T dependence of σ_v in ZnN_yNi_3 at $H = 50$ mT. The solid curve shows the result of fitting by the relation $\sigma_v \propto 1/\lambda^2 \propto 1 - (T/T_c)^n$, with n and T_c being free parameters. The dashed curve is obtained when $n = 4$. The dotted curve shows the result of fitting for temperatures below 1.5 K with $n = 4$. Inset shows the temperature dependence of magnetic susceptibility at $H = 2$ mT.

References
1) T. He *et al.*, Nature 411 (2001) 54.
2) J. H. Shin *et al.*, Phys. Rev. B 64 (2001) 180510(R).
3) H. Rosner *et al.*, Phys. Rev. Lett. 88 (2002) 027001.
4) M. Uehara *et al.*, J. Phys. Chem. Solids 68 (2007) 2178.
5) M. Uehara *et al.*, J. Phys. Soc. Jpn. 78 (2009) 033702.
6) E. H. Brandt, Phys. Rev. B 37 (1988) 2349.

† Condensed from the article submitted to Physica C
*1 Advanced Science Research Center, Japan Atomic Energy Agency
*2 Department of Physics, Faculty of Engineering, Yokohama National University

Fe-substitution effects on the Cu-spin correlation in the La-214 high-T_c superconductors

T. Adachi,[*1] K. Suzuki,[*1] Y. Tanabe,[*1*2] H. Sato,[*1] Risdiana,[*3] Y. Ishii,[*3] T. Suzuki,[*3*4] I. Watanabe,[*3] and Y. Koike[*1]

Although the mechanism of superconductivity in the high-T_c cuprates has not yet been clarified, the mechanism based upon dynamical stripe correlations of spins and holes[1)] is one of probable candidates. Formerly, we have found from zero-field (ZF) μSR measurements in $La_{2-x}Sr_xCu_{1-y}Zn_yO_4$ with $x = 0.10 - 0.30$ that the Cu-spin correlation tends to be developed by the Zn substitution and moreover, a magnetic order is formed at low temperatures for $x \leq 0.15$ and $y \sim 0.03$, suggesting the formation of the stripe order through the Zn substitution.[2–5)] In th overdoped regime, on the other hand, the development of the Cu-spin correlation becomes weak due to a lot of doped holes, preventing us from investigating the relationship between the Cu-spin correlation and superconductivity in the whole superconducting (SC) regime.

Recently, Fujita *et al.* have revealed from the elastic neutron-scattering experiment that incommensurate magnetic and nuclear peaks are observed through the partial substitution of Fe with a large magnetic moment for Cu in $La_{2-x}Sr_xCu_{1-y}Fe_yO_4$ (LSCFO) at $p \sim 1/8$.[6)] As the superconductivity is strongly suppressed through the Fe substitution around $p = 1/8$, it is suggested that the Fe substitution is effective for the stabilization of the charge-spin stripe order at $p \sim 1/8$. In fact, we have found in the overdoped regime of LSCFO that the electrical resistivity exhibits a pronounced upturn at low temperatures and that the SC transition temperature is anomalously depressed at $x \sim 0.22$.[7)] Therefore, in order to investigate the Fe-substitution effects on the Cu-spin correlation, we have performed ZF-μSR measurements in the whole superconducting regime of LSCFO. Polycrystalline samples of LSCFO were prepared by the ordinary solid-state reaction method. The ZF-μSR measurements were carried out at temperatures down to $\sim$ 2 K at RIKEN-RAL.

Figure 1 shows the p dependence of the magnetic transition temperature, T_N, estimated from the temperature dependence of the initianl asymmetry of ZF-μSR time spectra for LSCFO with $p = 0.05 - 0.22$ and $y = 0.005$, 0.01, together with formely obtained data of $y = 0$.[2–5)] Here p is defined as $p = x - y$ due to the substitution of trivalent Fe^{3+} for divalent Cu^{2+}. Through the Fe substitution, it is found that T_N increases in the whole p regime and that, in particular, T_N appears for $p > 0.115$. For $y = 0.01$, T_N exhibits the local maximum at $p \sim 0.115$. Surprizingly, for $p > 0.115$, the decrease in T_N with increasing p is found to be weak, resulting in the higher T_N for $p > 0.115$ than that for $p < 0.115$. This is far from the common understanding in the high-T_c cuprates that the Cu-spin correlation tends to be weakened with increasing p. Therefore, the present results suggest that the nature of the Cu-spin correlation induced by the Fe substitution may change at $p \sim 0.115$ in which the stripe order is fairly stabilized by Fe.

In summary, we have found from ZF-μSR measurements that the Cu-spin correlation is developed in the whole SC regime through the Fe substitution in LSCFO. In particular, the Cu-spin correlation is much enhanced for $p > 0.115$ than $p < 0.115$. Therefore, the nature of the Cu-spin correlation induced by the Fe substitution, that is, the nature of the Fe-induced stripe order may be different between $p > 0.115$ that $p < 0.115$.

*1 Department of Applied Physics, Tohoku University
*2 WPI-AIMR, Tohoku University
*3 Advanced Meson Science Laboratory, RIKEN Nishina Center
*4 College of Liberal Arts, International Christian University

References
1) J. M. Tranquada et al.: Nature **375**, 561 (1995).
2) I. Watanabe et al.: Phys. Rev. B **65**, 180516(R) (2002).
3) T. Adachi et al.: Phys. Rev. B **69**, 184507 (2004).
4) Risdiana et al.: Phys. Rev. B **77**, 054516 (2008).
5) T. Adachi et al.: Phys. Rev. B **78**, 134515 (2008).
6) M. Fujita et al.: J. Phys. Chem. Solids **69**, 3167 (2008).
7) T. Adachi et al.: J. Phys. Soc. Jpn. **78**, 025002 (2009).

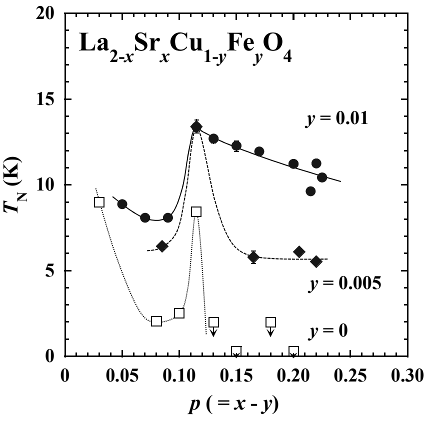

Fig. 1. Hole concentration, p, dependence of the magnetic transition temperature, T_N, estimated from zero-field μSR time spectra for $La_{2-x}Sr_xCu_{1-y}Fe_yO_4$ with $p = 0.05 - 0.22$ and $y = 0.005$, 0.01, together with formerly obtained data of $y = 0$.[2–5)]

Evidence for Horizontal Line Node in KFe_2As_2 Probed by μSR

H. Fukazawa,[*1,*5] T. Saito,[*1] Y. Kohori,[*1,*5] K. Ohishi,[*2,*5] Y. Ishii,[*2,*5] I. Watanabe,[*2,*5] K. Miyazawa,[*3,*4] N. Takeshita,[*3,*5] P. M. Shirage,[*3] K. Kihou,[*3,*5] C.-H. Lee,[*3,*5] H. Kito,[*3,*5] A. Iyo,[*3,*4,*5] and H. Eisaki[*3,*5]

[Iron-based superconductors, μSR, line node, multiple-gap superconductivity]

The discovery of superconductivity at $T_c = 26$ K in $LaFeAsO_{1-x}F_x$[1)] has stimulated a tremendous research effort to elucidate the superconducting pairing mechanism and symmetry in iron pnictide superconductors. In oxygen-free system of $Ba_{1-x}K_xFe_2As_2$, the superconductivity arises when the antiferromagnetically ordered phase has been suppressed by K substitution. One of the important features is that superconductivity occurs even for $x = 1$, although T_c itself is much lower ($T_c \sim 3.5$ K) than the optimum $T_c =$ 38 K. Recent studies have suggested that the superconducting gap in KFe_2As_2 has line nodes[2–4)], in contrast to the nodeless gap suggested in $Ba_{1-x}K_xFe_2As_2$ ($x \sim 0.4$). We have performed muon spin rotation (μSR) measurements in single crystalline samples of $Ba_{1-x}K_xFe_2As_2$ ($x = 0.25$ and 1) in order to observe the both T and H dependence of penetration depth λ and to clarify the superconducting gap mechanism. Especially, we have observed the T dependence of λ for both $H//c$ and $H \perp c$-axis down to 20 mK in KFe_2As_2 to clarify the existence of line node.

High quality single crystalline samples were grown by a self-flux method[5)]. The μSR measurements were conducted both at M15 beamline at TRIUMF, Vancouver, Canada and at RIKEN-RAL Muon Facility in the Rutherford Appleton Laboratory, Didcont, UK. Transverse field (TF) μSR measurements were performed at temperatures between 20 mK and 5 K.

In $x = 0.25$, we found that T dependence of $1/\lambda^2$, which is proportional to the superfluid density, can be completely reproduced by a two-full-gap model. This result is consistent with that observed by ARPES, NMR, and other μSR, suggesting that the multiple fully gapped $s_{\pm}$-wave Cooper pairing is realized. On the other hand, we have found that T dependence of $1/\lambda^2$ in KFe_2As_2 with $H//c$ and $H \perp c$ are completely different. While the temperature dependence of $1/\lambda^2$ observed with $H//c$ is well fitted by a two-full-gap model, T-linear behavior is clearly observed below $\sim T_c/2$ with $H \perp c$, suggesting the existence of line node. The latter dramatic result was obtained at RIKEN-RAL Muon Facility. This result is seemingly contradictory behavior, however, it is well interpreted when we take into account the horizontal line node (line node in ab-plane) in KFe_2As_2[6,7)]. For example, T dependence of $1/\lambda^2$ in UPt_3 observed in B-phase[8)], which has line node in *ab*-plane and point node along *c*-direction, behaves T^α with $\alpha \simeq 2.4$ and 1 for $H//c$ and $H \perp c$, respectively. Theoretical approach also suggests the different T dependence of $1/\lambda^2$, i.e., T^3 and T-linear behavior for $H//c$ and $H \perp c$, respectively, when horizontal line node exists[9)]. The power of exponent depends on the relation between the direction of applied field and that of line node. These results are the first experimental evidences for the existence of horizontal line node in KFe_2As_2.

*1 Department of Physics, Chiba University, Japan
*2 Advancend Meson Scienece Laboratory, Nishina Center for Accelerator-Based Science, RIKEN, Japan
*3 National Institute of Advanced Industrial Science and Technology, Japan
*4 Department of Applied Electronics, Tokyo University of Science, Japan
*5 JST, TRIP, Japan

References
1) K. Kamihara et al., J. Am. Chem. Soc. **130**, 3296 (2008).
2) H. Fukazawa et al., J. Phys. Soc. Jpn. **78**, 083712 (2009).
3) K. Hashimoto et al., Phys. Rev. B **82**, 014526 (2010).
4) J. K. Dong et al., Phys. Rev. Lett. **104**, 087005 (2010).
5) K. Kihou et al., J. Phys. Soc. Jpn. **79**, 124713 (2010).
6) S. Graser et al., Phys. Rev. B **81**, 214503 (2010).
7) Y. Suzuki et al., J. Phys. Soc. Jpn. **80**, 013710 (2011).
8) C. Broholm et al., Phys. Rev. Lett. **65**, 2062 (1990).
9) F. Gross et al., Z. Phys. B **64**, 175 (1986).

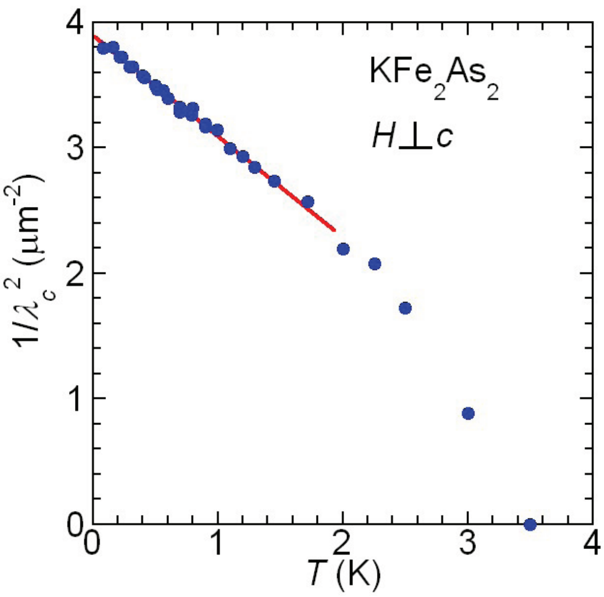

Fig. 1. Temperature dependence of $1/\lambda^2$ with $H \perp c$-axis obtained at RIKEN-RAL Muon Facility. Solid line is a guide to the eye.

Field-Induced Spin Freezing in a Two-Coordinate Fe Complex

I. Watanabe, Y. Ishii, Y. Kobayashi, T. Matsuo, M. Ito, K. Tamao, K. Sedlak[1)], and R. Scheuermann[1)]

Two-coordinate iron complexes of open-shell transition metals are often involved in intriguing chemical reactions and show unique physical properties. So far, a few Fe(II) derivatives have been studied [1,2]. One interesting example of a two-coordinate iron complexes is $Fe[N(t\text{-}Bu)_2]_2$. This system has almost perfect linear coordination of the Fe atom with an angle of 180° [3]. An interesting feature of this system is its magnetism magnetic fields. It has been reported from a Mössbauer measurement that the doublet Mössbauer absorption line splits to form the sextet line at low temperatures in a field of 1 kG. This fact suggests the possibility that the Fe spins are in the paramagnetic state in zero field but transform to be in a static magnetically ordered one upon the application of a longitudinal field (LF). Such a magnetically ordered state induced by a low field is unusual for iron complexes, and therefore we have carried out a μSR measurement on this system in order to confirm the field-induced magnetically ordered state.

The LF-μSR experiment was conducted in the ALC area of the Paul-Scherrer Institute (PSI) in Switzerland by using a continuous DC muon beam. The ALC superconducting magnet was used to apply LFs up to 45 kG. The sample was cooled down to 5 K by using a flow-type cryostat. Time spectra were analyzed by taking into account changes in the background and the zero point of the muon-spin polarization caused by the LF. Time spectra were measured at some temperature points by changing the LF from zero to 45 kG. Muon-spin precession, which shows the appearance of a long-range ordered state of Fe spins, was not observed at any temperature and LF range. The exponential function $A_0e^{-\lambda t}$ was used to analyze the time spectra.

Figure 1 shows the LF dependence of the total muon-spin polarization at 5 K up to the field of 45 kG. The full muon-spin polarization could not be observed in zero field even within the minimum time resolution of the ALC setup of 625 ps. The total asymmetry remains up to an LF of around 3 kG, starts to recover with increasing LF, and saturates above 20 kG.

Figure 2 indicates the LF dependence of the muon-spin depolarization rate measured at 5 K up to the field of 45 kG. The muon-spin depolarization rate increases with the LF strength. After showing a peak around 1 kG, the depolarization rate decreases to a smaller value of around 0.02 μs^{-1}, which is almost equal to the minimum detectable value with the ALC setup.

The absence of LF dependence of the total asymmetry, which was observed up to around 3 kG, is a typical behavior in the case of strongly fluctuating internal fields at the muon site, which are responsible for the dynamic muon-spin depolarization behavior. Since Fe spins are in the paramagnetic state in zero field, the muon spin depolarizes within the order of the minimum time resolution of the ALC setup because of the strongly fluctuating Fe spins, and a part of the muon-spin polarization is lost within the minimum time resolution of the ACL setup of 625 ps. On the other hand, the recovery of the total muon-spin polarization observed for an LF above 3 kG is a typical behavior in the case where muon spin depolarizes because of static internal fields distributed at the muon site. In addition, the peak depolarization rate observed at an LF of 1 kG indicates the appearance of the critical slowing down behavior of Fe-spin fluctuations. Both results indicate that a static ordered state of Fe spins appears above 1 kG and that this transition is the second-order phase transition. Since no muon-spin precession has been observed, the static magnetically ordered state would not be a coherent ordered state but a distorted one.

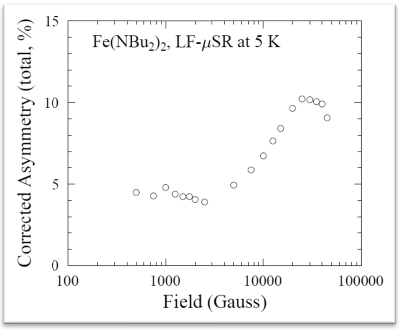

Figure 1: Longitudinal-field dependence of the total asymmetry measured at 5 K.

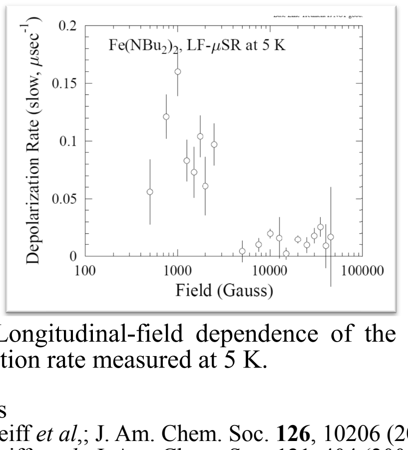

Figure 2: Longitudinal-field dependence of the muon-spin depolarization rate measured at 5 K.

References
[1] W.M. Reiff *et al*,; J. Am. Chem. Soc. **126**, 10206 (2004).
[2] W.M. Reiff *et al*.; J. Am. Chem. Soc. **131**, 404 (2009).
[3] W.A. Merrill *et al*.; J. Am. Chem. Soc. **131**, 12693 (2009).

*1 Bulk Muon Group, PSI, Villigen, Switzerland.

RIKEN Accel. Prog. Rep. 44 (2011)

Coherent Magnetically Ordered State in $V_4S_9Br_4$ Confirmed by μSR

I. Watanabe, B. Adiperdana, T. Waki[1)], T. Tomioka[1)], Y. Tabata[1)], H. Nakamura[1)], I.A. Dharmawan[2)], R.E. Siregar[2)], K. Sedlak[3)], and R. Scheuermann[3)]

The presence of nearly degenerate metal and insulating states and the interplay between structural and electronic degrees of freedom are responsible for the strain-induced self-organized inhomogeneities associated with a nanoscale phase separation. In mixed-valence cluster magnets, which consist of aggregations of a small number of metal atoms sharing unpaired *d* electrons, new exotic phenomena different from those of itinerant-electron and localized-electron systems are expected. In particular, in magnetic cluster compounds where clusters are exchange-coupled with each other, the intercluster interaction leads to a variety of magnetic properties.

The new vanadium cluster compound $V_4S_9Br_4$, whose synthesis was recently reported by Mironov *et al.*[1], shows spontaneous phase separation between high-spin and low-spin cluster states at low temperatures [2]. This system forms a tetragonal structure with the space group *P4/nmm,* in which tetranuclear square planer $[V_4S_9]^{4+}$ clusters are bridged by Br ions. The magnetic susceptibility shows the Curie-Weiss behavior and indicates an effective moment of 1.77 μB/V and a Weiss temperature of 10 K. On the other hand, the magnetic susceptibility deviates from the Curie-Weiss behavior below 15 K and in the case of a cooling process, decreases drastically [2]. Since this system has been newly synthesized, the magnetic ground state is still unclear, especially since there have only been a small number of studies on its magnetism. In order to clarify the magnetic ground state of V spins, we have carried out mSR measurements.

A zero-field (ZF) mSR experiment was conducted in the ALC area of the Paul-Scherrer Institute (PSI) in Switzerland by using a continuous DC muon beam. The superconducting ALC magnet was used for this experiment. The sample was cooled down to 5 K by using a flow-type cryostat. ZF-mSR time spectra, including changes in the background resulting from the length of a sample holder of the cryostat changing with the temperature, were analyzed.

Figure 1 shows ZF-mSR time spectra measured at several temperature points. The time spectrum showed a typical Kubo-Toyabe shape [3] at high temperatures and suddenly changed below about 15 K, and the muon-spin precession behavior appeared thereafter. This result was repeatable against heat cycling. These results prove that the ground state is a coherently aligned state of V spins and that the coherent ordered state appeared in the whole nanoclusters.

The muon-spin precession shows beating. This means that there are some muon-stopping positions in the system. From the Fourier transform analysis of the muon-spin precession components, it is found that there are four muon-precession components. Figure 2 shows the temperature dependence of the internal field at one of 4 muon sites. This site shows the 2^{nd} largest internal field, with a saturation value of about 650 G. The internal field decreases with increasing temperature and vanishes around 15 K. This temperature is the same as that where the magnetic susceptibility deviates from the Cuie-Weiss law with decreasing temperature [2]. Thus, the magnetic anomaly observed around 15 K by the susceptibility measurement [1] is a magnetic transition temperature where the V-spin system assumes the coherent magnetically ordered state. Currently, a dipole-field simulation study is in progress in order to determine the spin structure in the magnetically ordered state; the study is being conducted in collaboration with the University of Padjadjaran, Indonesia.

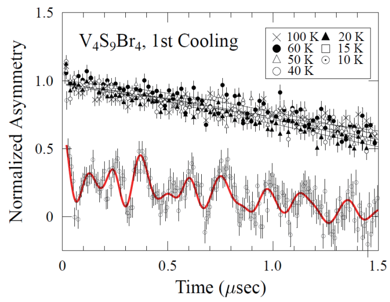

Fig. 1: Time spectra measured at some temperatures. The solid red curve is the best fit result of the time spectrum at 10 K.

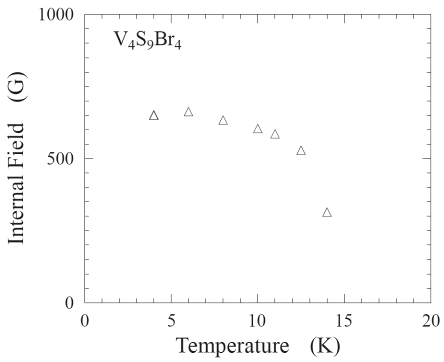

Fig. 2: Temperature dependence of one of internal fields measured at the muon site.

References
(1) E. Dagotte *et al*. "Nanoscale Phase Separation and Colossal Magnetoresistance: The Physics of Manganites and Related Compounds" (Springer-Verlag, Berlin, Heidelbelg 2010).
(2) T. Waki *et al*. (in preparation).
(3) Y.J. Uemura et al. Phys.Rev.B 31 (1985) 546.

1 Department of Engineering, Kyoto University, Kyoto Japan.
2 Department of Physics, University of Padjadjaran, Jatinangor, Indonesia.
3 Bulk Muon Group, PSI, Villigen,Switzerland.

RIKEN Accel. Prog. Rep. 44 (2011)

Change in magnetic ground states in nonmagnetic-impurity-doped spin-gap systems $TlCu_{1-x}Mg_xCl_3$ proved by muon spin relaxation†

T. Suzuki,*1 M. Yamada,*2 Y. Ishii, I. Watanabe, T. Goto,*3 H. Tanaka,*2 and K. Kubo,*1

[spin gap, impurity, magnetic order]

Impurity effects and impurity-induced magnetic orderings on spin gap systems are old-yet-new problems in magnetism, and are still attracting much interest from the view point of a key to the quantum nature of these systems. So far, no little experimental and theoretical studies have been reported for various systems. Recently, Bobroff *et al.* proposed a new common framework to explain the generic low-temperature impurity-induced spin-freezings in low-dimensional spin-gap systems[1]. However, the proposed model can not be applied to the system of S = 1/2 dimers. $TlCuCl_3$, which is the parent material of the subject compound in this study, is a three-dimensionally coupled Cu-3d S = 1/2 spin dimer system, and has a magnetic ground state of the spin singlet. The impurity-induced magnetic ordering has been reported in the Mg-doped $TlCu_{1-x}Mg_xCl_3$[2]. The magnetic phase transition to an ordered state is observed by magnetization and specific heat measurements in the zero-field limit. A remarkable point is that a finite spin gap still remains below the magnetic phase transition temperature T_N[3]. In order to investigate the microscopic properties of the impurity-induced magnetic phases in the spin gap system, we carried out zero- and longitudinal-field muon spin relaxation (ZF-, and LF-μSR) measurements in $TlCu_{1-x}Mg_xCl_3$ single crystals at the RIKEN-RAL muon facility.

In the case of $x = 0.0047$, no evidence for any static internal magnetic field $H_{\rm int}$ was observed down to 20 mK although the specific heat indicated the magnetic phase transition at $T_N = 0.70$ K as previously reported[4]. Figure 1 shows ZF- and LF-μSR time spectra in $x = 0.007$. As for ZF-μSR time spectra, drastic change in the time spectrum is observed with decreasing temperature, and a loss of the initial asymmetry is seen below T_N. All the time spectra are well analyzed using the function of $A(t) = A_1e^{-\lambda_1 t} + A_2e^{-\lambda_2 t}G_{\rm KT}(\Delta, H_{\rm LF}, t)$. λ_1 and λ_2 are muon-spin-relaxation rates, and $G_{\rm KT}(\Delta, H_{\rm LF}, t)$ is the static Kubo-Toyabe function, where Δ/γ_μ is the distribution width of nuclear-dipole fields at the muon sites. γ_μ is the gyromagnetic ratio of the muon spin, and $H_{\rm LF}$ is the applied external longitudinal-field. In order to confirm that the fast relaxation originates from a static $H_{\rm int}$, the LF-μSR measurements are carried out at the lowest temperature. Implanted muon spins in materials are decoupled by $H_{\rm LF}$ from the static $H_{\rm int}$ at the muon sites, and it leads to a revival of the vanished initial asymmetry. This change in time spectra is represented by an increase in A_2, and $H_{\rm int}$ at the muon sites is deduced using the formula $A_2(H_{\rm LF}) \propto \frac{3}{4} - \frac{1}{4x^2} + \frac{(x^2-1)^2}{8x^3}\ln\left|\frac{x+1}{x-1}\right|$, where $x = H_{\rm LF}/H_{\rm int}$. The deduced $H_{\rm int}$ and the saturated value of A_1 are summarized in Fig. 2. The saturated A_1 corresponds to the volume fraction of the spin frozen region. Above $x = 0.006$, the existence of a static $H_{\rm int}$ is confirmed by LF-μSR, and with increasing x, $H_{\rm int}$ and the volume fraction of a spin frozen region where the static $H_{\rm int}$ appears increase simultaneously. These results suggest that the magnetic ground state changes from the spin singlet state to a spin fluctuating state, and to a spin frozen state by the impurity doping, and also suggest there exist a threshold doping ratio at which a static staggered moment appears in S = 1/2 dimer systems.

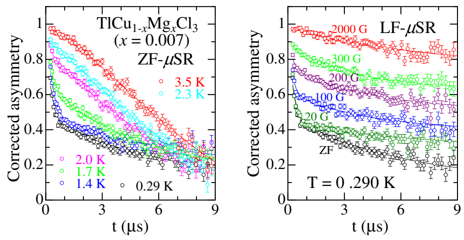

Fig. 1. ZF- and LF-μSR time spectra in $TlCu_{1-x}Mg_xCl_3$ with $x = 0.007$. Solid lines are fitted results.

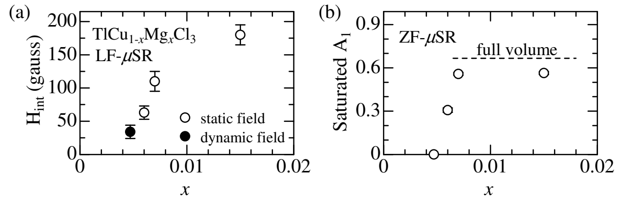

Fig. 2. (a) $H_{\rm int}$ deduced from LF-μSR measurements. (b) The saturated value of the fast relaxation component amplitude A_1 in ZF-μSR time spectra.

† Condensed from the article accepted to Phys. Rev. B.

*1 Graduate School of Arts and Sciences, International Christian University
*2 Department of Physics, Tokyo Institute of Technology
*3 Faculty of Science and Technology, Sophia University

References

1) J. Bobroff *et al.*, Phys. Rev. Lett. **103** (2009) 047201.
2) A. Oosawa *et al.*, Phys. Rev. B **67** (2003) 184424.
3) A. Oosawa *et al.*, Phys. Rev. B **67** (2003) 184424.
4) T. Suzuki *et al.*, J. Phys. Soc. Jpn. **78** (2009) 074705.
5) T. Suzuki *et al.*, Phys. Rev. B **80** (2009) 064407.

μSR Study of Proton Dynamics in 9-Hydroxyphenalenone Derivatives

T. Mochida,[*1] T. Sugawara,[*2] I. Watanabe, Y. Ishii, T. Suzuki, T. Kawamata, and T. Matsuzaki

Molecular crystals of 9-hydroxyphenalenone derivatives are interesting materials for investigating hydrogen/deuterium dynamics and its consequences on phase transitions in hydrogen-bonded ferroelectrics.[1,2] At room temperature, the molecules undergo rapid tautomerization coupling with intramolecular hydrogen transfer between the two oxygen atoms (Fig. 1). The phase sequences of the 5-bromo compound (**1**-*h*; X = Br, Fig. 1) and its deuteroxy analogues (**1**-*d*; X = Br) have been examined in detail:[3–5] **1**-*h* exhibits no phase transition, but **1**-*d* exhibits successive phase transitions at T_I = 34 K and T_C = 22 K. The absence of a phase transition in **1**-*h* has been ascribed to hydrogen tunneling.[4,5] By applying *μ*SR, we try to investigate the distribution or the degree of order-disorder of the hydrogen/deuterium along the hydrogen bond and how it is correlated with the phase transitions.

Previously, preliminary μSR measurements for **1**-*h* and **1**-*d* have been performed, and the relaxation time has been evaluated for both compounds. The temperature dependence of the relaxation rate for **1**-*d* under zero magnetic field displays a significant increase at low temperatures, which may reflect the ordering of the deuterium associated with the phase transition. Relaxation rates measured for a longitudinal magnetic field at 4000 G show marked enhancement of the relaxation rate at approximately 200 K. In contrast, **1**-*h* exhibits no such enhancement.

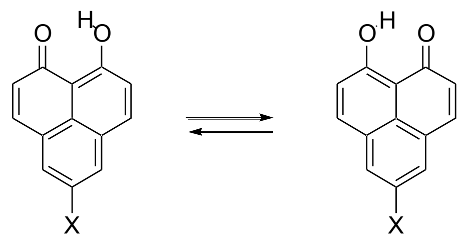

Fig. 1. Tautomerization of 9-hydroxyphenalen-1-one derivatives (X = Br, Me).

The observed difference in the behavior between **1**-*d* and **1**-*h*, particularly the enhancement of the relaxation rates for the deuterated compound, is interesting. However, considering the timescale of μSR measurements, it is unlikely that the proton/deuteron dynamics is the origin of the difference. To check these results in detail, we performed *μ*SR measurements on the samples of **1**-*h* and **1**-*d* carefully prepared under identical conditions. For these samples, no significant isotope effects were observed, and they exhibited similar temperature dependence with comparable relaxation rates. In particular, enhancement of the relaxation rates for **1**-*d* at low temperatures was not observed for longitudinal magnetic fields. These results suggest that the enhancement observed in the previous measurements possibly originates from the motion of residual solvent molecules that may be partly co-crystallized with **1**-*d*.

Since these materials are the organic version of KDP(potassium dihydrogen phosphate)-like ferroelectrics, investigations of their proton dynamics are expected to provide essential information on the role of hydrogen dynamics in hydrogen-bonded ferroelectrics. However, observation of the isotope effect for 9-hydroxyphenalenone derivatives turned out to be difficult with *μ*SR spectroscopy.

References

1) T. Mochida, D. Kuwahara, S. Miyajima, and T. Sugawara: J. Phys. Chem. B. **107**, 12315 (2003).
2) T. Mochida, A. Izuoka, T. Sugawara, Y. Moritomo, and Y. Tokura: J. Chem. Phys. **101,** 7971 (1994).
3) Y. Moritomo, Y. Tokura, T. Mochida, A. Izuoka, and T. Sugawara: J. Phys. Soc. Jpn. **64**, 1892 (1995).
4) T. Matsuo, K. Kohno, A. Inaba, T. Mochida, A. Izuoka, and T. Sugawara: J. Chem. Phys. **108**, 9809 (1998).
5) T. Matsuo, K. Kohno, M. Ohama, T. Mochida, A. Izuoka, and T. Sugawara: Europhys. Lett. **47**, 36 (1999).

*1 Kobe University
*2 The University of Tokyo

μSR study of quasi two-dimensional $S = 1/2$ triangular antiferromagnet, $EtMe_3Sb[Pd(dmit)_2]_2$

Y. Ishii, I. Watanabe, T. Suzuki[*1], T. Matsuzaki and R. Kato

Magnetic ground states of two-dimensional triangular Heisenberg antiferromagnetic (AF) systems are of considerable interest. Magnetic frustration due to the triangular lattice structure is expected to suppress the long-range magnetic ordering (LRMO). The quantum spin state without either LRMO or lattice symmetry breaking, resulting from this magnetic frustration, is named the quantum spin liquid (QSL) state. A candidate material for a QSL is the organic conductor κ-$(BEDT\text{-}TTF)_2Cu_2(CN)_3$[1]. This compound has the 2D triangular lattice structure of $S = \frac{1}{2}$ dimeric unit of BEDT-TTF molecules and shows no LRMO down to 35 mK. However, an anomalous field-induced magnetism has been observed at low temperatures by means of C^{13}-NMR[2]. Very recently, a TF-μSR study showed a linewidth broadening above the critical field $H_{\rm cr}$, suggesting the existence of a gap in the spin-excitation spectrum[3]. Thus, the ground state nature of this material is still a controversial issue. Another candidate material is a salt of a metal complex, $EtMe_3Sb[Pd(dmit)_2]_2$. This material has almost regular triangular exchange networks of $S = \frac{1}{2}$ dimeric units with exchange interaction J in the range $220 \simeq 250$ K and shows no LRMO or lattice symmetry breaking, down to 20 mK ($\leq 0.1\%$ of J)[4–7]. We have performed ZF- and LF-μSR measurements of this $EtMe_3Sb$ salt to investigate the ground state nature of the QSL state.

μSR experiments were carried out by using the ARGUS spectrometer installed at the RIKEN-RAL Muon Facility in the UK. The $EtMe_3Sb[Pd(dmit)_2]_2$ sample was prepared by the air oxidation method. The obtained small plate-like single crystals were wrapped with a silver foil that had a thickness of 12.5 μm. The total mass of the sample was about 100 mg. Additional silver foils with a total thickness of 75 μm were used as a degrader so as to stop injected muons at the sample position efficiently.

Figure 1 shows ZF-μSR time spectra of the $EtMe_3Sb$ salt at temperatures of 80 K and 0.3 K. All the spectra can be described by the expression

$$P(t) = A\exp(-\lambda t) \times G_{\rm KT}(\Delta, t, H_{\rm ext})$$

where λ is the muon depolarization rate associated with the electron spin fluctuation and $G_{\rm KT}$ is the Kubo-Toyabe function that indicates the existence of randomly oriented nuclear magnetic moments. Overall shapes of the μSR time spectra were almost identical and the Δ and λ values were almost constant below 100 K. Thus, we found that there was no sign of any kind of magnetic ordering down to 0.3 K. This result suggests that the effect of electron spin fluctuation may be strong in the temperature range $0.3 \leq T \leq 100$ K. LF-μSR measurements can provide detailed information on electron spin fluctuation, and therefore, we also carried out LF-μSR measurements. LF-μSR time spectra of $EtMe_3Sb[Pd(dmit)_2]_2$ at 0.3 K are shown in fig. 2. It is apparent that the λ value was finite even at the high field of 3950 G, suggesting the existence of electron spin fluctuation, which can be detected by a μSR time window.

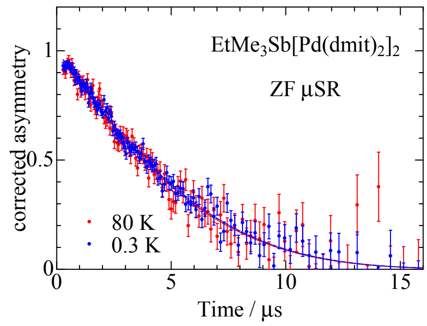

Fig. 1. Zero-field μSR time spectra of $EtMe_3Sb[Pd(dmit)_2]_2$ at selected temperature.

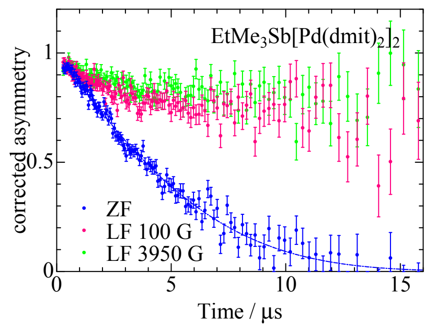

Fig. 2. Longitudinal-field μSR time spectra of $EtMe_3Sb$ salt measured at 0.3 K.

References
1) Y. Shimizu et al., Phys. Rev. Lett., **91**, 107001 (2003)
2) Y. Shimizu et al., Phys. Rev. B **73**, 140407(R) (2006)
3) F. L. Pratt, Private Communications.
4) R. Kato, Chem. Rev., **104**, 5319-5346 (2004)
5) T. Itou et al., Phys. Rev. B **77**, 104413 (2008)
6) T. Itou et al., J. Phys.: Conference series **145**, 012039 (2009)
7) T. Itou et al., Nature Physics, **6**, 673 (2010)

*1 Graduate School of Arts and Sciences, International Christian University.

Microscopic phase separation in frustrated-quantum-spin magnet κ-(BEDT-TTF)$_2$Cu$_2$(CN)$_3$†

S. Nakajima*1, T. Suzuki*2, Y. Ishii, K. Ohishi, I. Watanabe, T. Goto*1
N. Yoneyama*3, N. Kobayashi*3, F. L. Pratt*4 and T. Sasaki*3

The ground state of the quantum-spin system κ-(BEDT-TTF)$_2$Cu$_2$(CN)$_3$ with a triangular lattice, in which a simple antiferromagnetic order is inhibited because of the geometrical frustration, is attracting considerable interest, because two recent reports on thermal conductivity and specific heat have presented completely contradictory results regarding the system's ground state; according to one report, the ground state is gapped, while according to the other, it is gapless.

So far, ^{1}H/^{13}C-NMR[1] and the specific heat measurements[2] have shown that there is no magnetic order at low temperatures greater than 20 mK, which is much lower than the exchange interaction $J/k_B \approx 250$ K, even though the ground state remains gapless. This result has been believed to be quite probable because the frustration effect may suppress a possible magnetic order. However, quite recently, M. Yamashita *et al.*[3] found that temperature dependence of the thermal conductivity is thermal-activation-type, suggesting a gapped ground state. This means that results of experiments in which different techniques are employed are different from each other. Furthermore, an anomalous slowing down of charge-distribution fluctuation has been reported at $T = 6$ K [4]. Because of these contradictory observations, the nature of the ground state still needs to be conclusively determined.

We would like present here our latest μ-SR results that clearly reveal the microscopically phase-separated ground state and also present a model for the spin state; this model resolves the problem of the contradictory results reported in previous papers [1-3]. We have investigated the ground state of the system at zero-field from a microscopic point of view by employing the μSR technique, which probes the magnetic field and its dynamics inside crystals on the basis of the depolarization rate of muon spin polarization. Single crystals of approximately 50 mg have been used for LF-μSR measurements that have been carried out at Riken-RAL Muon Facility in the U.K. using a spin-polarized pulsed surface-muon (μ^+) with a momentum of 27 MeV/c. The incident muon beam was injected perpendicularly into the *bc* plane of crystals.

At $T > 3$ K, depolarization curves can be represented by a function with a single exponential component. At temperatures below 300 mK, the depolarization curves change into those that can be represented by a two-component function with depolarization rates λ_1 and λ_2.

Figure 1 shows the LF-dependence of λ above 3 K, and λ_1 and λ_2 below 300 mK. The behavior of λ_2 is the same as in the high temperature paramagnetic region, while λ_1 shows quite anomalous LF-dependence — λ_1 increases with increasing LF and then decreases above 10 Oe.

Using these experimental results, we develop a model for the spin state in this system. At high temperature of $T > 3$ K, the system is homogeneous and all the spins fluctuate paramagnetically. When the charge fluctuation slows down around 6 K[4], the averaged position of each spin on the dimer is also decentered, following the charge redistribution. This brings the random spatial modulation to the effective exchange interaction J and thus transforms the nearly equilateral triangular lattice to the random lattice. This randomness may cause microscopic phase separation in the system at lower temperatures. The phase corresponding to λ_2 is found to be the paramagnetic phase at high temperatures, and the newly appeared λ_1 phase is considered to be a spin singlet because its LF-dependence is very similar to that of typical spin-gap quantum magnets [5]. Note that phase separation does occur at zero field, which is in a contrast to the reported field-induced inhomogeneity observed by NMR[1]. This observation also resolves the disagreement over the results based on thermal conductivity and specific heat. Since heat energy is present only in the paramagnetic phase of λ_2, it is reasonable that the specific heat contributed from the λ_2 phase exhibits the gapless-type temperature dependence. The gapped-type temperature dependence of thermal conductivity is also reasonable, because the barrier of λ_1 phase surrounding around each island blocks the heat transport that is indispensable to the thermal conductivity.

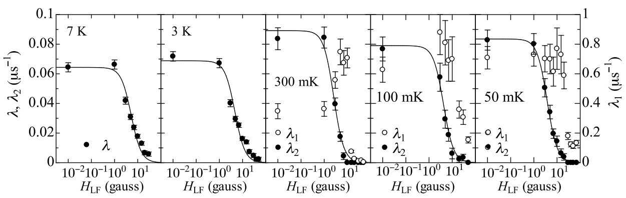

Fig. 1 The dependence of muon-spin depolarization rate on the longitudinal field H_{LF} at various temperatures.

References
1. Y. Shimizu *et al.* Phys. Rev. Lett. 91, 107001 (2003); Phys. Rev. B 73, 140407R (2006).
2. S. Yamashita *et al,* Nature Phys. 4, 459 (2008).
3. M. Yamashita *et al,* Nature Phys. 5, 44 (2009).
4. M. Abdel-Jawad *et al.* Phys. Rev. B82, 125119 (2010).
5. W. Higemoto et al. Phys. Lett. A243, 80-84 (1998); Physica B289-290, 172 (2000).

† Submitted to Phys. Rev. B.

*1 Physics Division, Sophia University
*2 Graduate School of Arts and Sciences, International Christian University
*3 Institute of Material Research, Tohoku University
*4 ISIS Facility

μSR study of structure-dependent electron radical dynamics in polythiophene and its derivatives

Risdiana,[*1,3] L. Safriani,[*1] A. Bahtiar,[*1] Fitrilawati,[*1] R. E. Siregar,[*1] R. Hidayat,[*2] A. A. Nugroho,[*2] M. O. Tjia,[*2] and I. Watanabe[*3]

Studies of polythiophene (PT) and its derivatives have been attracting considerable attention because of the chemical and thermal stability of the compounds, as well as their applications, both existing and emerging, in various fields. In particular, poly(3-alkylthiophene) (P3AT) has being intensively studied because its physical and chemical properties can be effectively modified by varying the alkyl-side-chain length. The optical, electrical, and mechanical properties of P3AT show strong dependence on the molecular structure of the compound, such as the alkyl length and regioregularity (regioregular (RR) and regiorandom (Rdm)).

We have previously studied the microscopic charge-transport processes in RR-poly(3-hexylthiophene-2,5-diyl) (RR-P3HT), Rdm-poly(3-hexylthiophene-2,5-diyl) (Rdm-P3HT), and RR-poly(3-octylthiophene-2,5-diyl) (RR-P3OT) by performing longitudinal-field (LF) μSR measurements[1]. Herein, we report the temperature-dependent spin diffusion dynamics of the charge-carrying polarons in RR-poly(3-butylthiophene-2,5-diyl) (RR-P3BT). The diffusion dynamics were studied by the LF-μSR method for determining the relative contributions of intrachain hopping and interchain coupling to the charge-transport process in RR-P3BT[2]. Similar to previous studies, all the time spectra could be well fitted by the following two-component function:

$$A(t) = A_1 exp(-\lambda_1 t) + A_2 exp(-\lambda_2 t), \qquad (1)$$

where A_1 and A_2 are the initial asymmetries and λ_1 and λ_2 are the depolarization rates for fast and slow components, respectively. The LF dependence of λ reflects the dimensionality of the diffusion of the spin-excited state. That is, λ is proportional to $H^{-0.5}$ for one-dimensional (1D) intrachain diffusion and to C-$H^{0.5}$ for three-dimensional (3D) interchain diffusion[3].

Figure 1 shows the LF dependence of λ_1 in RR-P3BT at the temperatures of 10 K, 25 K, 50 K, 75 K, and 300 K. The data for 25 K, 50 K, 75 K, and 300 K are shifted by multiplication with the factors 2, 4, 50, and 100, respectively. At the low temperatures 10 K, 25 K, and 50 K, λ_1 indicates the $H^{-0.5}$ field-dependent characteristics of 1D intrachain diffusion, implying that the charge transport is dominated by the mobility of the charge carriers along the polymer chain. With an increase in temperature, the charge carriers, which initially follow 1D intrachain diffusion, move by 3D interchain diffusion, which is characterized by the field dependence of λ_1; this field dependence can be well fitted by the C-$H^{0.5}$ curve, as shown for the high temperature of 300 K. The initial change in the carrier mobility appears to occur around 50 K to 75 K. A similar behavior is observed in the LF-dependent variation of λ_2. However, the values of λ_2 are two orders of magnitude smaller than those of λ_1. While the diffusion coefficients are not available in the present analysis, the results show that the dominant charge transport alternates between intra- and interchain charge transport, which depends on the temperature. From a comparison between RR-P3BT and RR-P3HT, which shows a similar change in the carrier mobility at around 25 K to 50 K, it is found that interchain diffusion transport in the RR-P3BT system requires a high temperature. This difference may be due to the high concentration of P3BT rods, which leads to a strong vertical phase separation[4], implying the requirement of higher thermal energy to support interchain hopping.

[*1] Department of Physics, Padjadjaran University, Indonesia
[*2] FMIPA, Bandung Institute of Technology, Indonesia
[*3] RIKEN Nishina Center for Accelerator-Based Science

References

1) Risdiana *et al.*: RIKEN-RAL Facility Report Vol. **9**, 47 (2009).
2) Risdiana *et al.*: Submitted to Physics Procedia (2011).
3) M. A. Butler *et al.*: J. Chem. Phys. **64**, 3592 (1976).
4) B. Friedel *et al.*: Chem. Mater. **22**, 3389 (2010).

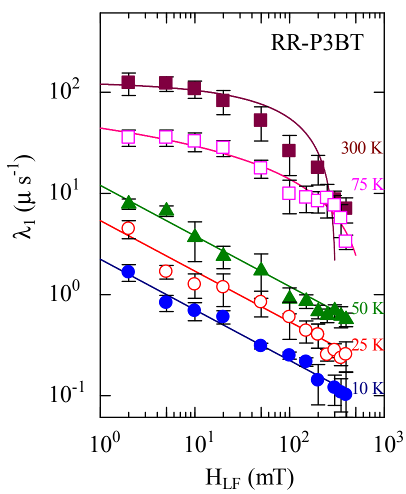

Fig. 1. Longitudinal-field dependence of λ_1 of RR-P3BT at various temperatures. The data for 25 K, 50 K, 75 K, and 300 K are multiplied with the factors by 2, 4, 50, and 100, respectively.

Dynamic change in the H-μ-H bond at the structural phase transition of $NaBH_4$

J. Sugiyama,[*1] H. Nozaki,[*1] T. Noritake,[*1] S. Towata,[*1] M. Månsson,[*2] H.-W. Li,[*3] S. Orimo,[*3] K. Ohishi, and I. Watanabe

[order-disorder transition, H-μ-H bond]

In order to use the HμH system as a unique probe of both structural and dynamics/kinematics properties of H in the $M(BH_4)_n$ system, which is one of the most promising materials for the hydrogen storage material in the future fuel cell[1,2], we have initiated a μ^+SR experiment on the $M(BH_4)_n$ systems below ambient temperature (T) in TRIUMF since 2008. The nature of the "hydrogen bond" between μ^+ and anions has been extensively investigated since the discovery of the $F^-\mu^+F^-$ (or "FμF") ion in metal fluoride crystals such as LiF, NaF, CaF_2 and BaF_2[3]. The FμF system is easily identified *via* its characteristic muon spin oscillation signal in a ZF-μ^+SR spectrum, due to a dipole-dipole coupling in the collinear ^{19}F-μ^+-^{19}F spin system. Similar hydrogen bond systems with other anions *e.g.* "Hμ^+H" and/or "Hμ^{+}" have been reported in $NaAlH_4$[4], which was studied as a hydrogen storage material for fuel cells.

We found the formation of the HμH system in $LiBH_4$, $NaBH_4$, KBH_4, and $Ca(BH_4)_2$, but not in $Mg(BH_4)_2$. It was also found that the normalized asymmetry for the HμH signal ($=A_{H\mu H}/A_0$) varies with the electronegativity (χ_P) of M[5]. This is because, when the χ_P of M is small, BH_4 should be more negative, resulting in an increase in the electron-density of H^- ions. Therefore, the normalized $A_{H\mu H}$ increases with decreasing χ_P.

Furthermore, we found a dynamic change in the HμH signal accompanying a structural phase transition of $NaBH_4$ at T_c =189.9 K from a low-T tetragonal phase to a high-T cubic phase due to an order-disorder transition of the BH_4 tetrahedra[6,7]. The HμH system is stable in the ordered state, but would be unstable in the disordered state due to the rotation of the $[BH_4]^-$ group. In fact, the ZF-spectrum was fitted by a combination of HμH and Hμ signal[8], suggesting that μ^+ forms a "$H^+[BH_4]^-$"-like μBH_4 molecule at high T.

In contrast to $NaBH_4$, KBH_4 keeps a cubic symmetry even at 90 K[9]. In order to know the dynamic nature of the H-μ-H bond in KBH_4, we have measured the ZF-spectrum until 20 μs up to 500 K in the Riken-RAL facility. Interestingly, it is found that the ZF-spectrum of KBH_4 changes drastically with T, particularly in the T range between 200 K and 300 K. Note that such change is very similar to that for $NaBH_4$ around 100 K. This implies a structural change in KBH_4 around 200 K, while neutron measurements supported the absence of a phase transition between 90 and 300 K[9]. In order to explain the whole results, we could consider competition between the electrostatic attractive force of the $[BH_4]^-$-μ^+-$[BH_4]^-$ bond and the rotation of the BH_4 tetrahedra.

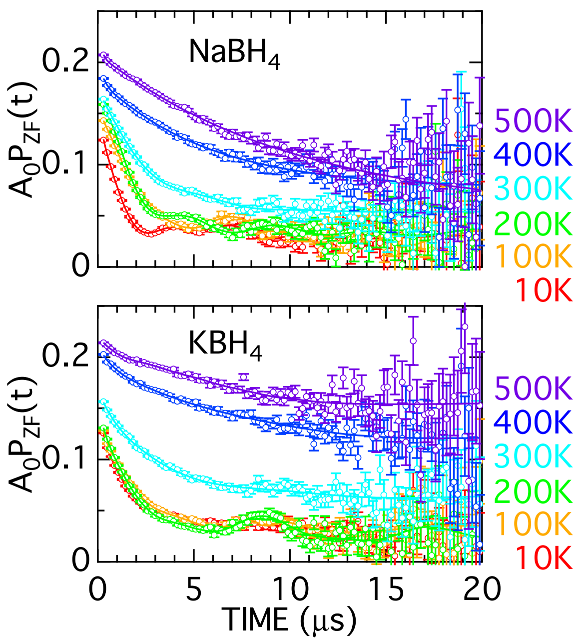

Fig. 1. T variation of the ZF-time-spectrum for (a) $NaBH_4$ and (b) KBH_4. For $NaBH_4$, the spectrum has a maximum around 7 μs at 100 K, indicating the appearance of a μBH_4 molecule. For KBH_4, on the contrary, such maximum is observed around 9 μs at 200 K.

*1 Toyota Central Research and Development Labs., Inc.
*2 Paul Scherrer Institut
*3 Tohoku University

References

1) L. Schlapbach and A. Züttel, Nature **414**, 353 (2001).
2) S. Orimo *et al.*, Chem. Rev. **107**, 4111 (2007).
3) J. H. Brewer, *et al.*, Phys. Rev. B **33**, 7813(R) (1986).
4) R. Kadono, *et al.*, Phys. Rev. Lett. **100**, 026401 (2008).
5) J. Sugiyama *et al.*, Phys. Rev. B **81**, 092103 (2010).
6) H. L. Johnston and N. C. Hallett, J. Am. Chem. Soc. **75**, 1467 (1953).
7) P. Fischer and A. Züttel, PSI Annual Report (2001).
8) K. Nishiyama *et al.*, Physica B **326**, 41 (2003).
9) D. G. Allis and B. S. Hudson, Chem. Phys. Lett. **385**, 166 (2004).

Lithium diffusion in $LiCoO_2$

J. Sugiyama,[*1] H. Nozaki,[*1] M. Månsson,[*2] K. Ohishii, and I. Watanabe

[Lithium diffusion, battery]

The principle behind the operation of Li-ion batteries is a reversible Li^+ ion intercalation to (deintercalation from) electrode materials, i.e., Li-transition metal oxides as a cathode and carbon-graphites as an anode[1]. In order to optimize/improve the total performance of the Li-ion batteries, we should know a diffusion coefficient of Li^+ (D_{Li}) in the materials, particularly for all solid-state batteries.

Although D_{Li} is usually estimated by measurements of spin-lattice relaxation time (T_1) in ^{7}Li-NMR, such measurement is difficult for the materials containing magnetic ions due to an additional relaxation process through electron-spin[2]. We have, therefore, attempted to detect D_{Li} from the hopping rate (ν) of a dynamic Kubo-Toyabe signal in μ^+SR, because muons are unlikely to see a rapidly fluctuating magnetic field in a paramagnetic state, but are likely to see the Li^+ dffusion.

In fact, it was found that μ^+SR provides very consistent D_{Li} for $Li_{0.73}CoO_2$ and $Li_{0.53}CoO_2$[3], compared with the prediction by an electrochemical "common sense" and first principles calculations[4].

In order to clarify the relationship between D_{Li} and x in Li_xCoO_2, we have measured weak transverse field (wTF-), zero field (ZF-) and longitudinal field (LF-) spectra for $LiCoO_2$.

Despite the paramagnetic nature of $LiCoO_2$ confirmed by susceptibility measurements, wTF asymmetry (A_{TF}) exhibits a complex temperature (T) dependence [see Fig. 1(a)], probably due to a contribution of electron-spin in Co^{3+} ions to the μ^+SR parameters. As a result, it is difficult to know the increase in ν caused by Li^+ diffusion, although ν is likely to increase with T in the T range between 250 and 300 K [Fig. 1(b)].

Following the studies on $LiCoO_2$, we also measured μ^+SR spectra for an olivin-type compound, $LiFePO_4$, which had been investigated extensively as a cathode material for the next-generation Li-ion battery[5]. As seen in Fig. 2, ν clearly increases with T above 150 K, and reaches a maximum around 260 K, and then decreases with further increasing T. Since there are no structural and/or magnetic transitions above T_N(= 52 K) for $LiFePO_4$[6], the increase in ν is most likely to be caused by Li diffusion. However, in order to check a possible displacement of oxygen ions with T, particularly in the T range between 150 K and 350 K, we plan to perform a precise structural analysis using a synchrotron radiation X-ray source.

*1 Toyota Central Research and Development Labs., Inc.
*2 Paul Scherrer Institut

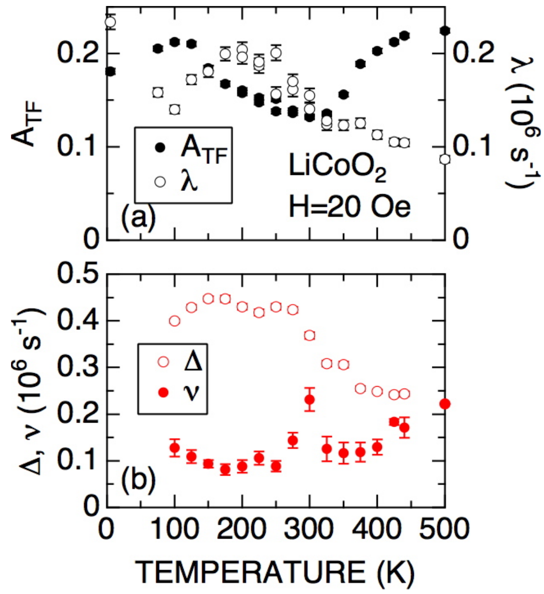

Fig. 1. T dependences of (a) wTF asymmetry (A_{TF}) and its relaxation rate (λ_{TF}) and (b) field distribution width (Δ) and hopping rate (ν) for $LiCoO_2$.

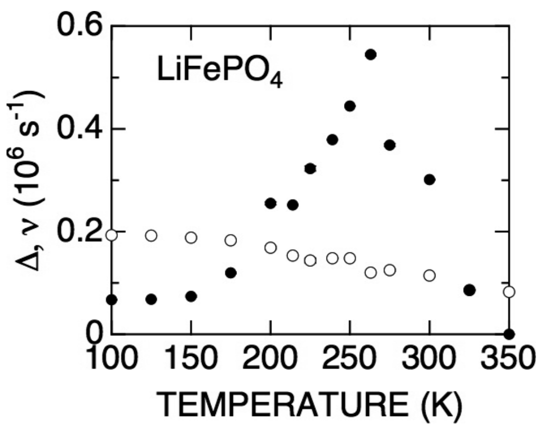

Fig. 2. T dependences of Δ and ν for $LiFePO_4$.

References
1) K. Mizushima *et al.*, Mater. Res. Bull. **15**, 783 (1980).
2) K. Nakamura *et al.*, Solid State Ionics **121**, 301 (1999); *ibid* **135**, 143 (2000); *ibid* **177**, 821 (2006).
3) J. Sugiyama *et al.*, Phys. Rev. Lett. **103**, 147601 (2009).
4) A. Van der Ven and G. Ceder, Electrochem. Solid-State Lett. **3**, 301 (2000).
5) A. K. Padhi *et al.*, J. Electrochem. Soc. **144**, 1188 (1997).
6) G. Rousse *et al.*, Chem. Mater. **15**, 4082 (2003).

Focusing effect of MeV muon beam in the tapered-capillary method

D. Tomono, T.M. Kojima, K. Ishida, T. Ikeda, Y. Iwai, M. Tokuda*1, Y. Kanazawa*2, Y. Matsuda*3, T. Matsuzaki, M. Iwasaki*4, and Y. Yamazaki*5

Generation of a high-density muon beam is an important issue in μSR studies and in muonium formation for the slow-muon project at RIKEN-RAL. Since the size of the sample or target used in these studies is usually much smaller than the muon beam size of approximately 40 mm (full width at half maximum), most of the muons in the beam do not hit the target. The beam is usually cut to match the target size by a collimator at the end of the beamline. In order to increase the beam density available for these experiments, the use of a tapered capillary method is planned. When a tapered tube (capillary) is inserted along with the beam , a certain fraction of the muon beam can be focused by scattering at the inner wall surface of the tube. In a recent experiment[1], we demonstrated this focusing effect by using a pulsed muon beam at RIKEN-RAL. For detailed particle-by-particle study, a new experiment was performed at TRIUMF, Canada, using a continuous muon beam[2]. For simplicity, the narrowing plates were employed instead of the tapered tube above mentioned. to investigate the interaction between the inner-wall surface and the muons. The experimental setup and preliminary results have been already reported[3]. In this article, we will report the result of the beam density enhancement effects observed at an initial momentum of $p_\mu = 35$ MeV/c.

Figure 1 shows the energy spectra obtained when the central momentum of the muon beamline is set at $p_\mu = 35$ MeV/c (5.6 MeV). These spectra were observed with the SSD (lithium drifted silicon detector) fixed 10 mm downstream of the outlet when polished copper plates, rough copper plates, gold-coated copper plates, glass plates, and the corresponding slits were inserted. The entries of each spectrum were normalized by the number of muons incoming to the T1 counter, for comparing the yields under the above mentioned conditions. Each vertical axis was scaled to a relative yield to the slit data, namely, the peak value of the slit data was set to 1.0. These spectra indicated that the beam was focused by the narrowing plates. The muon yield at the SSD increased with the plates when the number of initial muons injected was the same. The increase component included the contribution from muons with slightly lower energy than that of the initial muons when compared to the slit data. Some muons were scattered downstream of the surface of the plates and hence, the lost their kinetic energy.

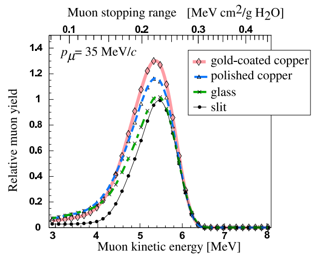

Fig. 1. Energy distributions of the outgoing muons at $p_\mu = 35$ MeV/c (5.6 MeV) when gold-coated copper plates, polished copper plates, glass plates, and the corresponding slit were inserted.

The maximum density enhancement: $\xi_{\rm gold} \sim 1.3$ was obtained with the gold-coated copper plates. The peak widths of energy distribution with the narrowing plates are greater than those with the slits by 5 % because the enhancement was included the contribution by scattered muons, which lost a small amount of their energy. In addition, although the surface of gold-coated copper was approximately more than 10 times rougher than that of polished copper and glass, the enhancement observed with the glass plates was smaller than that with the plates made of metal. The spectrum of the polished copper plates was almost identical to that of the rough copper plates. These facts indicated that the focusing effect is independent of the surface roughness. For the tubes, the enhancement is expected to be nearly the square of the enhancement obtained with the narrowing plates since the focusing effect in the vertical direction is added to that in the horizontal direction.

When this method is applied to muonium formation in vacuum, the muonium density may increase in a small area by a factor of 1.3 if the thickness of a muonium formation target is optimized for the muon stopping range corresponding to the peak position in the enhanced muon energy distribution. The stopping range is shown on the top in Fig. 1. This simple method is expected to be a powerful tool for increasing the muon density. We are planning to apply this method for a slow-muon project at RIKEN-RAL[4] and for the development of a new cold muon source in the precision measurement in the muon g-2 project at J-PARC[5].

References

1) T.M. Kojima, et al.: J. Phys. Soc. Jpn. **76**(2007)093501.
2) D. Tomono, et al.: J. Phys. Soc. Jpn. **80**(2011)044501.
3) D. Tomono, et al.: RIKEN Accel. Rep. **43**(2009)261.
4) P. Bakule, et al.: Nucl. Inst. Meth. B **266**(2008)335.
5) N. Saito, M. Iwasaki, et al.: P34 proposal at J-PARC.

*1 Dept. of Physics, Tokyo Inst. of Tech. and RIKEN
*2 Dept. of Physics, Sophia University
*3 Graduate Sch. of Arts and Sci., Univ. of Tokyo
*4 RIKEN and Dept. of Physics, Tokyo Inst. of Tech.
*5 RIKEN and Graduate Sch. of Arts and Sci., Univ. of Tokyo

Search for a muonium-emitting material as a source of an ultracold muon beam for new J-PARC muon g-2 experiment

Y. Fujiwara,[*1,11] P. Bakule,[*6] G. Beer,[*12] M. Esashi,[*7] S. Hirota,[*11] H. Iinuma,[*4] K. Ishida,[*1] M. Iwasaki,[*1,8] T. Kakurai,[*11] H. Kawai,[*3] N. Kawamura,[*4] G. Marshall,[*2] H. Masuda,[*9] Y. Matsuda,[*10] T. Mibe,[*4] Y. Miyake,[*4] K. Ohishi,[*1] H. Ohnishi,[*1] A. Olin,[*2] N. Saito,[*4,11] K. Shimomura,[*4] P. Strasser,[*4] M. Tabata,[*3,5] D. Tomono,[*1] K. Tsukada,[*1] K. Ueno,[*1] K. Yokoyama,[*1] S. Yoshida[*7]

The anomalous muon g-factor (g-2) provides a good testing ground for the standard model. The measured value of muon g-2 measured to 0.54 ppm precision and it has been more than three standard deviations larger than that predicted by the standard model.[1)] A new J-PARC muon g-2 experiment is aimed at measuring the muon g-2 with a precision of 0.1 ppm by storing a high-intensity ultracold muon beam in a highly uniform magnetic field.[2)]

The ultracold muon beam is generated by the laser ionization of thermal muonium (Mu) by using the method developed at KEK-MSL and RIKEN-RAL.[3)4)] Muons with energies around 4 MeV are decelerated and thermalized as Mu in a target material. Some Mu are evaporated from the surface of the material and are ionized by a laser to be used as a cold muon source for further acceleration. Hot tungsten and silica powder are known as good muonium emitting materials. However, we cannot use hot tungsten because we require a muon source with the lowest possible energy for use in the muon g-2 measurement. In addition, silica powder may cause handling difficulties in clean high-vacuum conditions. Therefore, we started the search for a better target material in an experiment (S1249) at the TRIUMF muon channel.

The first stage of the search was measuring the formation of Mu and its release from a material. The measurement was performed using Mu spin precession and relaxation in the magnetic field of 6 G. If Mu is formed and emitted from a material, the Mu spin will relax by interacting with oxygen spin when a small amount of oxygen is added to the target. We prepared silica powder (Cab-O-Sil, 0.03 g/cm^3), nanogel, silica aerogels (0.03, 0.05, and 0.10 g/cm^3), porous silica (pitch:10 μm; hole diameter:8 μm), porous alumina (pitch:100 nm; hole diameter:68 nm), and fused silica. The nanogel and all silica aerogel targets showed a large Mu yield and faster spin relaxation in the presence of oxygen. This observation was similar to that in the case of silica powder. On the other hand, we did not observe any Mu signal in the porous alumina target or any increased relaxation in the porous silica target in the presence of oxygen.

In the second stage of the search, we measured the decay vertex of Mu to study the Mu yield that escaped from the target volume and to study the time evolution of the Mu spatial distribution in vacuum. We used MWDC and NaI detectors to detect the positrons produced by the muon decay. In addition, we used a microchannel plate (MCP) to detect the electrons left after the muon decay. The measurement was completed only for one silica aerogel sample (0.03 g/cm^3) because the beam time ended suddenly owing to a beamline failure. A space-time distribution of Mu is shown in Fig. 1. The movement of the emitted Mu away from the target can be clearly observed. The evaluation of the Mu yield and other parameters such as the average Mu velocity is in progress. We have planned to perform measurements for other aerogel samples in 2011 for studying the effects of target density.

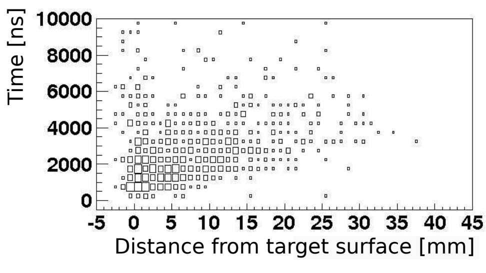

Fig. 1. Space(X)-time(Y) distribution of Mu candidate points. The number of Mu candidates is expressed by the box size (log scale).

*1 RIKEN Nishina Center, Japan
*2 Canada's National Laboratory for Particle and Nuclear Physics (TRIUMF), Canada
*3 Department of Physics, Chiba University, Japan
*4 High Energy Accelerator Research Organization (KEK), Japan
*5 Japan Aerospace Exploration Agency (JAXA), Japan
*6 Rutherford Appleton Laboratory, UK
*7 Advanced Institute for Materials Research (WPI-AIMR), Tohoku University, Japan
*8 Department of Physics, Tokyo Institute of Technology, Japan
*9 Division of Applied Chemistry, Tokyo Metropolitan University, Japan
*10 College of Arts and Sciences, The University of Tokyo, Japan
*11 Department of Physics, The University of Tokyo, Japan
*12 Department of Physics, University of Victoria, Canada

References

1) G. W. Bennett et al.: Muon G-2 Collaboration, Phys. Rev. D. **73** 072003 (2006).
2) J-PARC muon g-2 proposal.
3) K. Nagamine et al.: Phys. Rev. Lett. **74** 4811 (1995).
4) P. Bakule et al.: NIM. B. **266**, 355 (2008).

3. Radiochemistry and Nuclear Chemistry

Measurement of excitation functions of rutherfordium isotopes in ^{248}Cm + ^{18}O reaction

S. Goto,[*1] M. Murakami,[*2] H. Murayama,[*2] H. Kudo,[*3] D. Kaji,[*4] K. Morimoto,[*4] Y. Kasamatsu,[*5] Y. Kudou,[*4] and K. Morita[*4]

[Rutherfordium, excitation fuction, superheavy elements]

^{261}Rf is the most widely used isotope in Rf experiments because it has a relatively long half-life, 68 s[1)], and it decays by the emission of α-particles with an energy of 8.3 MeV. ^{261}Rf is produced by the ^{248}Cm + ^{18}O and ^{244}Pu + ^{22}Ne reactions. In these reactions, a spontaneous-fission nuclide, which had a half-life of a few seconds[2)] was formed, and it was thought to be ^{262}Rf.[3)] On the other hand, it was also reported that ^{261}Rf in the decay chain of ^{277}Cn and ^{269}Hs decays by spontaneous fission and by the emission of α-particles with energy higher than 8.3 MeV.[4)] However, this assignment was made on the basis of the assumption that the decay in the ^{277}Cn chain is entirely α-decay. Therefore, it has not been confirmed whether the nuclide with a half-life of a few seconds is ^{261}Rf. In this study, to confirm that the above mentioned nuclide is ^{261}Rf, the excitation function of the Rf isotopes produced in the ^{248}Cm + ^{18}O reaction was measured. In this paper, the ^{261}Rf isomers having half-lives of 68 s and a few seconds are represented as ^{261a}Rf and ^{261b}Rf, respectively.

Experiments were performed at RIKEN Linear Accelerator facility (RILAC) using the gas-filled recoil separator (GARIS). Rf isotopes were produced by the ^{248}Cm(^{18}O$, xn)^{266-x}$Rf reaction. ^{18}O beams with a current of 6 pμA were irradiated on rotating targets, which were 230 μg cm^{-2} thick ^{248}Cm$_2$O$_3$ targets electrodeposited on a Ti backing foil with a thickness of 0.91 mg cm^{-2}. In order to cool the targets, the target wheel was rotated at 1000 rpm during the irradiation. The beam enegies were 88.2, 90.2, 94.9, and 101.3 MeV at the center of the target. The evaporation residues recoiling from the target were separated from the beam and the byproducts using GARIS, and the residues reached a focal plane of the GARIS. At the focal plane, a position-sensitive detector (PSD) surrounded by four side detectors. Each side detector was composed of four PIN photodiodes which were mounted so as to be square. The beam was periodically changed between the ON and OFF modes to avoid the background of beam components, and the activity grown in the ON mode was measured after the beam was turned off. The ON/OFF period was set at 6 s for the nuclide whose half-life was a few seconds and 0.1 s for ^{262}Rf, whose half-life was 47 ms.[3)]

The α-spectra and spontaneous fission events were observed under very low background conditions. In the α-spectra, ^{261a}Rf and the daughter, ^{257}No, were clearly observed at each beam energy. After normalization of the cross section of Rf as 13 nb[5)] for a beam energy of 94.9 MeV, the constructed excitation function of ^{261a}Rf was in agreement with that reported previously.[5)] In the 0.1-s measurement, the spontaneous fission events were founded to decay within a few seconds. The half-life analysis is shown in Fig. 1. The half-life was found to be 3.1 ± 0.4 s, which was in good agreement with that in recent reports.[6,7)] The excitation fuction of this 3-s nuclide was very similar to that of ^{261a}Rf, indicationg that the nuclide was ^{261b}Rf. Analysis of other Rf isotopes is in progress.

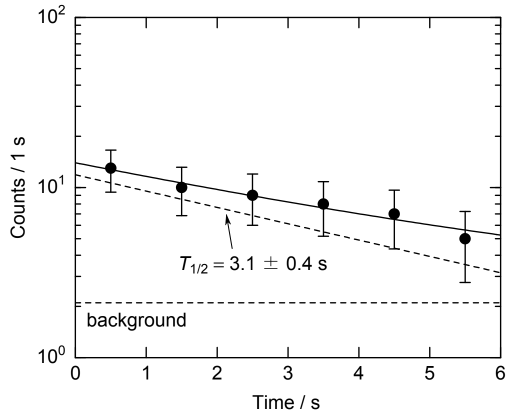

Fig. 1. Decay analysis of the spontaneous fission events for 0.1-s measurement at a beam energy of 94.9 MeV.

*1 Center for Instrumental Analysis, Niigata University
*2 Graduate School of Science and Technology, Niigata University
*3 Fuculty of Science, Niigata University
*4 Nishina Center, RIKEN
*5 Graduate School of Science, Osaka University

References

1) M. Asai:Oral presentation at the 3rd International Conference on the Chemistry and Physics of the Transactinide Elements, TAN07, Sep. 23–28, 2007, Davos, Switzerland.
2) D. C. Hoffman et al.:Phys. Rev. C **24**, 495 (1981).
3) M. R. Lane et al.:Phys. Rev. C **53**, 2893 (1996).
4) Ch. E. Düllmann and A. Türler: Phys. Rev. C **77**, 064320 (2008).
5) Y. Nagame et al.: J. Nucl. Radiochem. Sci. **3**, 85 (2002).
6) A. Gorshkov et al.: GSI Sci. Rep. 2008, 140 (2008).
7) H. Haba et al.: Seventh Workshop on the Chemisty of the Heaviest Elements, Meinz, Germany (2009).

FIA-based continuous extraction system for superheavy element chemistry

Y. Kudou, H. Haba, Y. Kasamatsu[*1], and K. Morita

An online extraction system based on the flow-injection analysis (FIA) principle has been developed to investigate the chemical properties of superheavy elements (SHEs, atomic number $Z \geq 104$).[1] The FIA technique has been widely used for solvent extraction. Typically, when a Teflon® tube is used as the extraction coil, the aqueous segment is excluded from the tubing surface, while the organic phase freely wets the inner wall of the tube. The excluded aqueous segment forms a plug that is completely surrounded by the organic phase. Therefore, the contact area between the aqueous phase and the organic phase is increases. Moreover, mass transfer across the interface is accelerated by the internal circulating flow in the segments.[2] However, since the segments commonly used in FIA are large (about a few microliters) and spread out the extraction tube, the specific interfacial area decreases. Consequently, a long time is taken to attain equilibrium. For this reason, the nornal FIA extraction method is hardly used for SHE experiments. In a previous paper, [1] we reported an FIA system that included a polytetrafluoroethylene (PTFE) tube packed with PTFE chips as an extraction unit for accelerating the extraction process. We also evaluated the performance of the FIA system and studied its applicability in SHE chemistry. The results indicated that optimization of the extraction unit was necessary. This report describes the optimization of the filling material used in the extraction unit and the applicability of the online extraction system.

Firstly, we evaluated the effects of various filling materials on the distribution ratios of Zr and Hf, which are homologs of Rf (Z = 104). PTFE chips and PTFE powders were used as the filling materials. The PTFE chips were made from chopped PTFE tubes (*ca*. 0.5 × 0.5 × 0.5 mm and *ca*. 1.0 × 1.0 × 0.5 mm), while the PTFE powders comprised irregularly sized particles (*ca*. 0.1 × 0.1 × 0.1 mm). A 10-cm-long PTFE tube (i.d.: ϕ 1 mm) packed with PTFE chips or PTFE powder was used as the extraction unit. Test experiments were performed using the radiotracers ^{88}Zr ($T_{1/2}$ = 83.4 d) and ^{175}Hf ($T_{1/2}$ = 70.0 d) produced in the ^{89}Y(p, 2n)^{88}Zr and ^{nat}Lu(p, xn)^{175}Hf reactions, respectively. The proton beam was provided by the RIKEN K70 AVF cyclotron. Solutions of the aforementioned tracers in 11 M HCl were prepared and stored in polypropylene containers. For solvent extraction, the HCl solutions were used as the aqueous phase, while 50 wt% tributyl phosphate (TBP) in toluene was used as the organic phase. The desired HCl solution and TBP/toluene solution were propelled by a double-plunger pump at a flow rate of 0.5 cm^3 min^{-1}. A solution containing ^{88}Zr and ^{175}Hf was introduced into the aqueous phase by switching the flow channel using a six-way valve. The solutions were mixed in a T-connector, and the mixture was introduced into the extraction unit packed with PTFE chips or PTFE powder. After the extraction, these phases were separated by a phase separator via a PTFE membrane filter with a pore size of 0.8 μm. Pressure regulators were installed downstream of the phases for efficient phase separation. Then, the aqueous and organic effluents were separately collected in separate polyethylene tubes and subjected to γ-ray spectrometry.

The distribution ratios D was calculated by the conventional radiometric method.[3] The results showed D values were consistent with the results of a batch experiment performed using small PTFE chips and PTFE powders comprising small particles. However, it was difficult to carry out continuous extraction when using the PTFE powder because of the high back pressure generated in this case. For this reason, the extraction unit was packed with PTFE chips (*ca*. 0.5 × 0.5 × 0.5 mm) in this flow system.

Second, we examined the FIA-based extraction system by online experiments. A short-lived zirconium isotope, ^{89m}Zr ($T_{1/2}$ = 4.16 min), was produced in the ^{89}Y(p, n)^{89m}Zr reaction. The reaction products recoiling from the target were transported by a He/KCl gas-jet transport system to the chemistry laboratory. The products were continuously deposited at the collection site of a dissolving apparatus for 2 min and dissolved in 11 M HCl propelled by the double-plunger pump at flow rates of 0.5 and 1.0 cm^3 min^{-1}. The toluene solution was also propelled at the same flow rate as the aqueous phase. The solutions were mixed in a T-connector, and the mixture was introduced into the extraction unit packed with PTFE chips. The lengths of the extraction units were 5, 7.5, and 10 cm. The mixture eluting from the extraction unit was collected in a polyethylene tube for 1 min and separated the aqueous phase and the organic phase using a pipette. After the separation, the mixture was analyzed by γ-ray spectrometry. The dependence of the extraction percentage on the extraction-unit length is shown in Fig.1. The results agree with those obtained for the batch extraction even when a short extraction unit of 5 cm was used, i.e, when the contact time was 4 s at a flow rate of 1.0 cm^3 min^{-1}. This fast extraction system can be used to study SHEs having half-lives of several tens of seconds, by connecting the phase separator to a liquid scintillation counting system.[4]

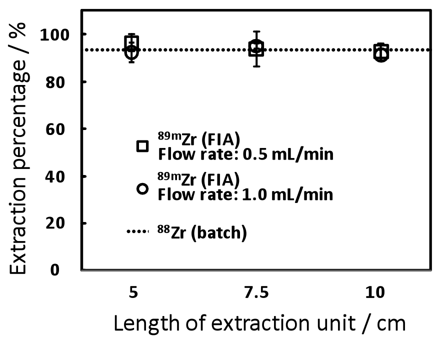

Fig.1. Dependence of the extraction percentage of ^{89m}Zr on the extraction-unit length (number of samples: n = 3).

References
1) Y. Kudou et al.: RIKEN Accel. Prog. Rep. **43**, 273 (2010).
2) L. Nord and B. Karlberg: Anal. Chim. Acta. **164**, 233 (1984).
3) D. F. Peppard et al.: J. Inorg. Nucl. Chem. **3**, 215 (1956).
4) Y. Komori et al.: RIKEN Accel. Prog. Rep. **43**, 267 (2010).

*1 Graduate School of Science, Osaka University

4. Radiation Chemistry and Biology

Possible *in-situ* monitoring of molecular biological effects in proton therapy with muon spin probes†

K. Nagamine[1, 2]

Excellent feature of radiation therapy by high energy protons is clear; a significant radiation effect at the specific position near stopping called Bragg peak and a reduced radiation effect before stopping. The Bragg peak of accelerated proton in human body takes a monotonic change against energy. Here, we propose that the polarized positive muons (μ^+) originating from the same proton beam are able to stop at proton Bragg peak and to be used as a monitor of important radiation biological effect at proton Bragg peak, providing a new insight of radiation therapy.

The 250 MeV proton whose range and Bragg peak in water is at around 35 cm produces positive pions (π^+) at the entrance-surface region of the human body within the depth of 10 cm. The π^+ produced at forward angle by these protons with light nuclei takes energy distribution around 72 MeV up to 80 MeV with a double differential cross section of around 0.006 (mb/sr/MeV)[1], where produced π^- is negligible. Thus, in 10 cm water 1/(5 $\times 10^4$) of the proton becomes π^+ of around 75 MeV in forward direction ($\pm$30 degree open angle). Most of 75 MeV π^+ stops at 19 cm depth from the birth position.

Here, let us consider a pion-to-muon decay during slowing-down process inside the matter (PMSD).

Pion slowing-down time τ_{SD} can be estimated by using the range-energy relation $R\ (E_\pi)$. The 75 MeV π^+ takes 1.5 ns in water.

Fraction of PMSD is the ratio between τ_{SD} and pion lifetime with γ_π correction; 3.3 % for 75 MeV π^+.

Properties of the produced muons can be estimated by the relativistic two-body decay of $\pi^+ \rightarrow \mu^+ + \nu_\mu$. The μ^+ produced by the forward-decay of 75 MeV π^+ are inside the cone of 15 degree with the energy of 98 MeV. These forward μ^+ are highly polarized and stop at 35 cm from the surface, exactly the same as the proton Bragg peak position

For 10 nA 250 MeV proton which is most frequently employed at the proton cancer therapy, we can expect 810/s polarized forward μ^+ stopping at the proton Bragg peak. By using the e^+ spectrometer with acceptance solid angle of 1/5 for decay positrons, event rate of 160/s can be expected, enabling one μ^+SR data-taking in a few minutes.

By detecting charged-particle events delayed by ≥10 ns from the muon (proton) pulse, the prompt high-energy backgrounds occurring at the proton pulse such as protons, alphas, neutrons, pions, electrons, etc can be eliminated. Thus, decay e^+ events from μ^+ required for the μ^+ spin imaging can easily be obtained.

The delayed e^+ are also coming from the stopped μ^+ from other origins. By placing optimally shaped Pb shield against 50 MeV e^+, these backgrounds in delayed positrons can be eliminated. Also by a telescope of two 2-dimensional position sensitive detectors such as segmented plastic scintillators, it is possible to make a e^+ ray-tracing and determine the e^+ emitting position, μ^+ stopping position with a spatial resolution of 5 mm. A possible layout of the detection system is schematically shown in Fig. 1.

Since the μ^+ spin probe (μ^+SR) is a sensitive microscopic magnetic probe to explore non-invasively the phenomena of molecular radiation biology at proton Bragg peak during a process of particle radiation therapy e.g. cancer treatment. Typical examples are as follows.

<u>Radical density determination</u> The radical formation and reaction can be probed by spin relaxation of muonium (Mu、H-like atom of μ^+ and e^-) in water which is known to be highly sensitive to the presence of paramagnetic impurities such as radicals in ppb to ppm level.

<u>Probing Hypoxia</u> Hypoxia, or low oxygenation, is known to be an important factor in tumor biology and response to cancer treatment[2]. The μ^+SR for molecular level magnetism can be used as a new probe for the measurement of dissolved paramagnetic molecular oxygen[3] for monitoring hypoxia. By the forward μ^+ with pulsed time structure, the sensitivity range of the muon spin probes for the oxygen tension in water is matching to the range of Hypoxia.

Development of medical proton accelerator with optimized time-structure for *in-situ* μ^+SR such as rapid-cycling synchrotron or FFAG is called for.

1) J. Matensson et al., Phys. Rev. C, **62** 014610 (2000).
2) J.L.Tatum et al., Int. J. Radiat. Biol., **82**, 699(2006).
3) E. Roduner et al., J.Chem. Soc. Faraday Tran., **91**, 1935 (1995).

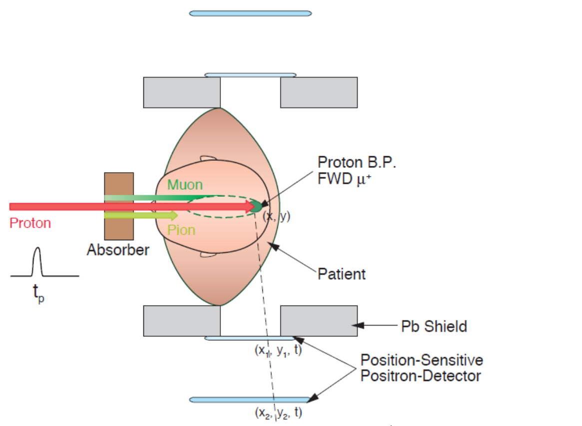

Fig. 1. Layout of the system to detect the μ^+SR signal from the μ^+ stopped at the proton Bragg peak for radiation therapy.

† Condensed from the article submitted to Proc. Japan Academy Ser. B.

Jointly,
*1 Physics & Astronomy, University of California, Riverside
*2 Muon Science Laboratory, IMSS, KEK

Enhancement of radiosensitivity by trichostatin A after heavy-ion irradiation in human cancer cells

M. Izumi and T. Tsukada

In eukaryotes, DNA is associated with histones and packaged into nucleosomes, which are in turn arranged into various higher order structures to form chromatin. The chromatin structures are regulated by chromatin-associated factors and histone modifications such as acetylation, methylation, and phosphorylation, and thereby contribute to the formation of domains, such as euchromatin and heterochromatin in the genome. The chromatin structures are involved in many aspects of DNA metabolism including DNA replication, repair, recombination, and transcription. However, it is not fully understood how repair reactions and checkpoint responses are regulated by the chromatin structures. It is also unknown how the distribution of damage caused by ionizing radiation is different between euchromatin and heterochromatin.

Recently, a number of histone deacetylase (HDAC) inhibitors have been developed and screened for use as anticancer drugs[1]. The anticancer effects of HDAC inhibitors are attributable, in part, to the accumulation of acetylated histones that loosens the chromatin structure and activates the expression of tumor suppressor genes. In addition to their intrinsic anticancer activity, several HDAC inhibitors enhance the radiosensitivity of tumor cells[2),3)], although the mechanism of enhancement remains unknown.

To examine the role of chromatin structures in DNA repair and investigate the potential use of HDAC inhibitors in radiotherapy where heavy-ion irradiation is used, we focused on the damage response after cells are treated with trichostatin A (TSA), a potent HDAC inhibitor. Our previous studies have shown that the phosphorylation of histone H2AX, which is a hallmark of double–strand breaks, is facilitated by trichostatin A in a dose-dependent manner[4),5)].

In this report, we examined whether TSA changed the sensitivity of human cancer cells to heavy-ions. Human HeLa S3 cells were irradiated with a graded dose of X-rays or carbon ions after the pretreatment with 0.1 μM TSA for 10 h. Following the post-treatment with TSA for 14 h, survival fraction was estimated by colony formation (Fig. 1A). The treatment with TSA before and after irradiation resulted in an increase radiosensitivity to X-ray by 1.5-fold at 3 Gy and 2.3-fold at 5 Gy, respectively. TSA also enhanced radiosensitivity to carbon ions by 2.4-fold at 3 Gy and 1.6-fold at 5 Gy, respectively. Therefore, TSA enhanced radiosensitivity at the dose which is usually used in therapy. Our previous analysis showed that the pretreatment of TSA increased the phosphorylated histone H2AX by 2.5-fold 1 hour after irradiation[4)]. On the other hand, the amount of phosphorylated histone H2AX decreased by 80-90% in following 4 hours in the presence of TSA as well as in the absence of TSA[4)]. These results suggest that the sensitivity was enhanced by inducing more damage on DNA, not by suppressing the cellular DNA repair response (Fig. 1B), although it is necessary to directly quantify the amount of DNA damage to draw a conclusion.

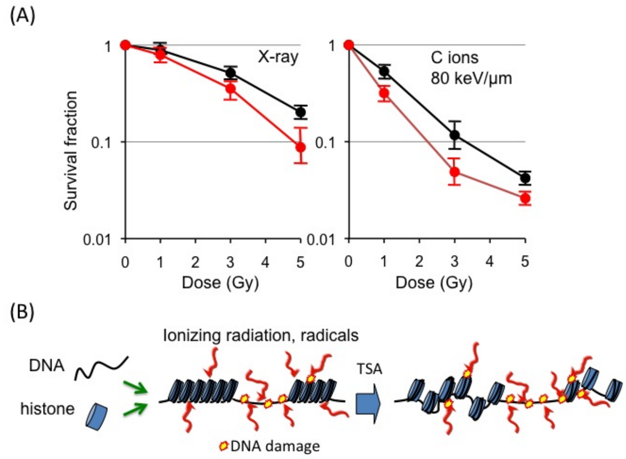

Fig. 1 The effects of trichostatin A (TSA) on HeLa cell radiosensitivity. (A) HeLa cells were trypsinized and plated as single cells in TSA-free media. After allowing 24 h for attachment, cells were pre-treated with TSA (0.1 μM) for 10 h and irradiated with 1, 3, 5 Gy of X-ray using Radioflex (Rigaku) or carbon ions at 80 keV/μm. Then the cells were cultured for additional 14 h in the presence of TSA, and the radiosensitivity was estimated by the colony-forming efficiency 14 days later. The black and red circles indicate the survival in the absence and presence of TSA, respectively. Values represent the mean ± standard deviation obtained from three independent experiments.
(B) A model for the role of chromatin structures in radiosensitivity. The open chromatin structure is more susceptible to the attack of ionizing radiations.

References
1) R. L. Piekarz et al: Blood **103,** 4636 (2004).
2) Y. Zhang, et al: Radiat. Res. **161,** 667 (2004).
3) K. Camphausen et al: Clin. Cancer Res. **10,** 6066 (2004).
4) M. Izumi: RIKEN Accel. Prog. Rep. **42,** 275 (2009).
5) M. Izumi: RIKEN Accel. Prog. Rep. **43,** 275 (2010).

Comparison of the killing effect irradiation with different heavy-ion beams on DSB repair-deficient mutants of *Neurospora*

L. Q. Ma,* S. Tanaka,* Y. Kazama, T. Abe and S. Hatakeyama*

Heavy-ion beam irradiation can induce DNA double-strand breaks (DSBs), which are a severe threat to cell survival. If the induced DSBs are not repaired, they can lead to cell death. Even in cells that survive after DSB induction. DNA mutations may occur because of the low fidelity of error-prone DSB repair system(s). DSBs are mainly processed by the following 2 repair pathways: non-homologous end-joining (NHEJ) and homologous recombination (HR); the former is thought to be error-prone, and the latter, error-free. Previously, we reported the killing effect of C-ion beam irradiation on DSB repair-deficient mutants of the filamentous fungus *Neurospora crassa.* In that study, the fungal cell preferably used the NHEJ system to repair DSB induced by low dose irradiation and the HR system to repair DSBs induced by high-dose irradiation. In this study, we investigated whether these tendencies are observed for irradiation with other types of beams—Fe-ion, Ar-ion, and X-rays.

We examined 2 DSB repair-deficient mutants of *N. crassa*, *mei-3* and *mus-52*, having mutation in the genes that are homologous to of budding yeast *RAD51* (belonging to the HR system) and *YKU80* (belonging to the NHEJ system), respectively. Wild-type C1-T10-28a was used as the control strain. All strains were cultured in glycerol complete medium at 30˚C for 8 days. Conidia were collected, and we prepared suspensions of 3.2×10^7 conidia per ml of phosphate buffer. Irradiation samples were prepared explained below. For irradiation with C-ion beam and X-ray, 8 ml of conidial suspension was poured into a 15 ml centrifuge tube. Fe- and Ar-ion beams, irradiation, 3 ml of conidial suspension was enclosed a hybridization bag, which was sectored in the 5×5 cm quadrangle. These samples were irradiated with Fe- ($^{56}Fe^{24+}$; 90 MeV), Ar- ($^{40}Ar^{17+}$; 95 MeV), and C- ($^{12}C^{5+}$; 135 MeV) ion beams generated by a RIKEN cyclotron at doses from ranging 25 to 200 Gy. As for the physical properties of the Fe-, Ar-, and C-ions, their mean linear electron transfer (LET) for *N. crassa* were estimated as 641, 286.5, and 30 keV/µm, respectively. X-ray irradiation was performed at 250 kV; the LET value was estimated as 2 keV/µm. After irradiation, the samples were diluted with phosphate buffer and plated at a density of 2×10^3 conidia per agar plate. The number of surviving colonies on each plate was counted after 3 days of incubation at 30 ˚C.

The beams used in this experiment are categorized into 2 groups according to their LET values, *i.e.* high-LET and low-LET groups. The high-LET group consisted of Fe-, Ar-, and C-ion, and the low-LET group consisted of X-ray. Figures 1—3 show the sensitivity of the tested strain for different ion beams. As expected, the 4 types of ion beams had different killing effects. Sensitivity to X-rays (low-LET) was the lowest for all the strains. Although the LET value of the Ar-ion beam is lower than that of Fe-ion beam, the killing effect of the Ar-ion beam was higher than that of the Fe-ion beam. This phenomenon can be explained by the fact that the number of Ar-ion particles are approximately twice the number of Fe-ion particles at the same dose. Hence, the irradiation dose of Fe should be greater than that of Ar in order to obtain the same effect for both Fe- and Ar-ion beam. We think that high-LET beams have a greater killing effect than low-LET beams, and these effects are largely dependent of the genetic background of the strains used in this experiment except for the gene deficiency in *mus-52*. Results of previous study showed that the *mus-52* strain was resistant to irradiation with C-ion beam at doses higher than 100 Gy (Fig. 3). In this study, the same tendency was observed for X-ray irradiation, but not for irradiation with Fe- and Ar-ion beams (Fig. 3). Although C-ion beam belongs to the high-LET group, it is interesting that the killing effect of C-ion on the *mus-52* strain is similar X-ray (low-LET group). It is unclear whether the above-mentioned observation is dependent on the level of LET. To understand, the *mus-52* strain should be irradiated with the same ion source, *e.g.* C-ion, at different levels of LET.

Currently, we are analyzing the mutation frequencies and types of survivors. This will add to our knowledge of different modes of repair of DNA damage induced by different heavy-ion beams.

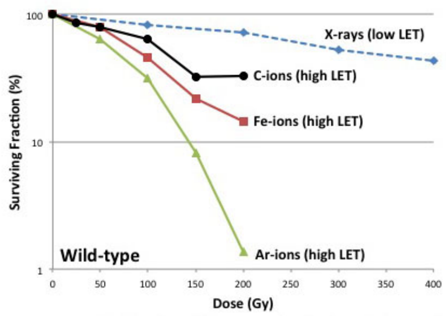

Fig. 1 Percent survival for the wild-type strain after irradiation with different ion-beams

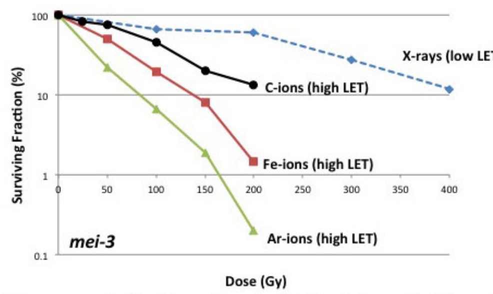

Fig. 2 Percent survival for the *mei-3* strain after irradiation with different ion-beams

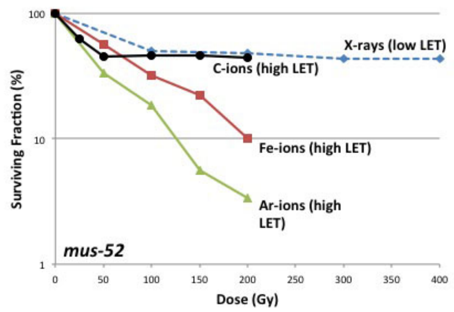

Fig. 3 Percent survival for the *mus-52* strain after irradiation with different ion-beams

* Laboratory of Genetics, Faculty of Science, Saitama Univ.

RIKEN Accel. Prog. Rep. 44 (2011)

Immunofluorescence of γ-H2AX in a root tip of *Arabidopsis thaliana* after the irradiation of X-ray

K.Takagi*[1], T.Hirano, Y. Kazama, T.Tsukada, Y. Hayashi, and T. Abe

Most of mutations are caused by results of inappropriate repair of DNA damages. Because of its difficulty of restoration, DNA double strand break (DSB) is thought to have greater tendency to cause mutation than other types of DNA lesion.

Heavy-ion-beams have a greater relative biological effectiveness than other radiations such as X-ray and γ-ray. In the case of plant breeding, irradiation of heavy-ion-beams is thought to bring higher mutation rate, wider spectrum of mutation, and large deletions of DNA sequences. Reasons of these phenomena are still exactly unknown. DNA damages specifically induced by the ion-bemas should be one of the causes of them. Specific pattern of energy deposition along the tracks of ions is thought to evoke concentrated DSBs and/or cluster lesions. Therefore, the localization of DSBs in a nucleus is a very important information to recognize effects of ion-beams on cells.

In animal cells and yeast, it is known that one of the variants of histone 2A, called H2AX, is phosphorylated at a serine residue near the carboxyl terminal when a DSB is generated nearby it. One DSB brings phosphorylation of H2AXs within the length of several kilobases of DNA adjacent to the DSB, making a focus structure under the light microscopic observation. Therefore, the distribution of phosphorylated H2AX (γ-H2AX) is thought to reflect the distribution of DSBs[1].

In the present report, we tried to detect γ-H2AX in a model plant, *Arabidopsis thaliana*, by means of immunofluorescent chemistry to establish the method for visualizing the localization of DSBs in *Arabidopsis* cells. To detect Arabidopsis γ-H2AX, polyclonal antibody against synthetic polypeptide of *Arabidopsis* H2AX, that includes phosphorylated serine residue of putative phosphorylation site, was generated. Arabidopsis has 2 kinds of H2AX in its genome[2]. This antibody cannot distinguish each of them, because of the same amino acid sequence near the putative phosphorylation site.

Figure 1A, B and C show cells of the same root tip of an unirradiated *Arabidopsis* seedling (3 days after sowing on 1/2 MS with 2% sucrose). Apparent immunofluorescence of α-tubulin (Fig. 1B, E, and H) excluded the possibility of failure in intrusion antibody molecules into cells. Except the background fluorescence, there was no apparent immunofluorescence of γ-H2AX in an unirradiated root tip. Meristematic region revealed weak immunofluorescence of it (Fig. 1A). On the other hand, in root tips, fixed at 30 min after the X-ray (150 kVp) irradiation, strong immunofluorescence of γ-H2AX (Fig. 1D and G) appeared in almost all nuclei. The intensity of fluorescence was greater in a root tip, irradiated 10 Gy of X-ray, than in that, irradiated 15 Gy of X-ray. Preincubation of primary antibody with phosphorylated polypeptide antigen totally abolished the fluorescence on nuclei of irradiated root tips, indicating the specificity of the antibody (data not shown). These results suggest that phosphorylation of H2AX is specifically occurred after the irradiation, and intensity of the phosphorylation has a dose dependence.

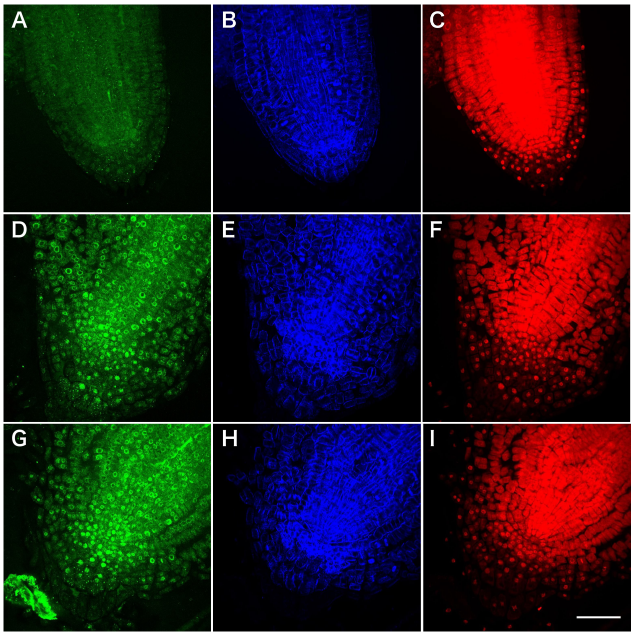

Fig.1. Immunofluorescence of γ-H2AX in root tips of *Arabidopsis* seedlings. A-C: Control, D-F: 10 Gy of X-ray, G-I: 15 Gy of X-ray. A, D,G: immunofluorescence of γ-H2AX, B,E,H: immunofluorescence of α-tubulin, C, F,I: fluorescence of propidium iodide. Scale bar = 50 μl

It is expected that ion-beam-specific effects on plant cells first appear on the distribution of DNA damages. Therefore, we further intend to investigate detail localization of γ-H2AX in Arabidopsis after the irradiation of various ionizing radiations.

References

1) E. Rogakou et al.: J. Biol. Chem. **273**, 5858 (1998).
2) J. D. Friesner et al.: Mol. Biol. Cell 16, 2566 (2005)

*1 The Wakasa Wan Energy Research Center

Mutation frequency analysis of M_1 plants irradiated with heavy-ion beams

Y. Kazama, T. Hirano, S. Ohbu, Y. Shirakawa, and T. Abe

Heavy-ion beam is a high-LET radiation, and its LET values are selectable in RIBF. We are studying the LET effect on mutation induction by using a model plant *Arabidopsis thaliana*. In a previous study, we irradiated dry seeds of *A. thaliana* with with-LET (22.5 keV/μm, 30.0 keV/μm, 61.5 keV/μm, 290 keV/μm, and 640 keV/μm) heavy-ion beam, and investigated the incidence of albino mutation the M_2 generation. The result indicated that irradiation with LET of 30.0 keV/μm was the most effective for mutation induction in the M_2 generation.[1)] To determine the most effective value for mutation induction, more detailed examination of LET values is needed. However, the analysis of mutation frequency in the M_2 generation is time consuming. Here, we report the development of a method for analyzing the mutation frequency in the M_1 generation.

To analyze the mutation frequency in the M_1 generation, we focused on a specific gene locus. The *Arabidopsis APG3* gene is involved in chloroplast development.[2)] Homozygous mutants of *APG3* (*APG3*$^{-/-}$) show albino or pale-green leaves, whereas heterozygous mutants (*APG3*$^{+/-}$) and wild-type plants (*APG3*$^{+/+}$) have green leaves. We studied the heterozygous mutants to determine mutation frequency. In heterozygous plants in which intact alleles underwent mutation induced by mutagens, leaves showed white sectors (Fig. 1). An allele of *APG3*, which was obtained inserting T-DNA harboring a BASTA-resistant gene (bar), enabled the preparation of a heterozygous seedling (*APG3*$^{+/-}$). When plants were grown on a BASTA-containing medium, the wild-type plants showed growth inhibition, and the homozygous (*APG3*$^{+/+}$) or the heterozygous (*APG3*$^{+/-}$) plant showed normal growth. Therefore, the heterozygous plant could be selected as a green seedling with BASTA-resistance.

The seeds of *APG3* heterozygous plants were obtained from the Arabidopsis Biological Resource Center, and were a mixture of segregated *APG3*$^{+/+}$, *APG3*$^{+/-}$, and *APG3*$^{-/-}$ seeds. The seeds were irradiated with C-ion beams with LETs of 22.5 keV/μm and 30.0 keV/μm; their radiation doses were 450 Gy and 400 Gy, respectively. These doses, at each LET, were most effective for inducing the albino in the M_2 generation.[1)] The irradiated seeds were incubated on 1/2 MS agar medium containing 2% sucrose and BASTA (2 μg/mL) at 4°C in the dark for 3 days for vernalization and then at 23°C under a long day condition (16h light) for 5 days. The selected *APG3*$^{+/-}$ plants were transplanted on BASTA-free 1/2 MS agar medium and grown at 23°C under the long day condition. Eight days after transplantation, the plants were examined for the presence of white sectors. Some irradiated heterozygous plants showed a white sector in the first or second true leaf (Fig. 2). Such sectors were not observed in the non-irradiated heterozygous plants (data not shown), indicating that the sectors formed because of the mutation in the *APG3* gene. This result shows that the mutation frequency in the M_1 generation can be monitored by using this system.

Table. 1 shows the results of white sector counting. On irradiation with LET of 30.0 keV/μm, the frequency of the occurrence of the white sector was 2 times higher than that observed in cases of irradiation with 22.5 keV/μm. This tendency is in accordance with that observed in a previous mutation frequency analysis performed for the M_2 generation.[1)] We concluded that the mutation frequency in the M_1 generation should be at least one indicator for determining the LET effect on mutation induction. More detailed analysis with different LETs is in progress.

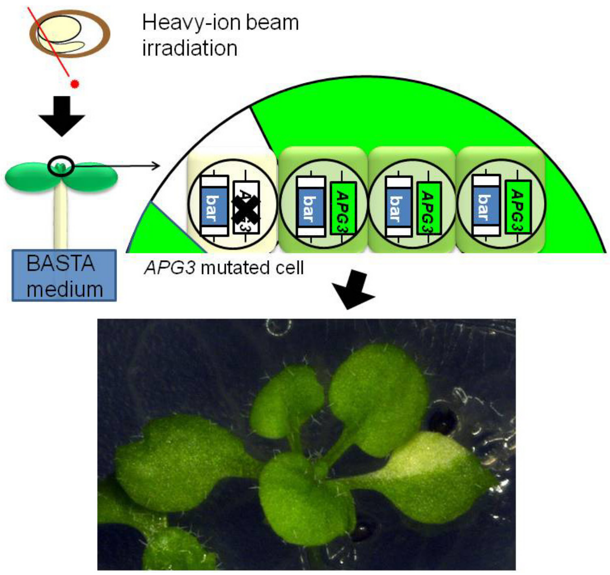

Fig. 1. Conceptual diagram of white sector formation. Mutation in the shoot apical meristem of the *APG3*$^{+/-}$ plant leads to the development of white sectors.

Table 1. Mutation frequency observed in the M_1 generation.

LET (keV/μm)	Dose (Gy)	No. of *APG3*$^{+/-}$ plants	No. of plants with sectors	Mutation frequency (%) ± SE
22.5	450	255	8	
		320	9	
		274	9	3.08 ± 0.14
30.0	400	317	29	
		384	23	
		283	17	7.05 ± 1.05

References
1) Y. Kazama et al.: Plant Biotech. **25**, 115 (2008).
2) R. Motohashi et al.: Plant Mol. Biol. **64**, 481 (2007).

Effect of LET on mutation induction by heavy-ion beam irradiation in imbibed seeds of *Arabidopsis thaliana*

T. Hirano, Y. Kazama, S. Ohbu, Y. Shirakawa, and T. Abe

Linear energy transfer (LET) is an important parameter for mutation induction by using heavy-ion beam irradiation. In dry seeds of *Arabidopsis thaliana*, heavy-ion beam irradiation at 30 keV/μm is the most effective method for mutation induction[1]. Moreover, when imbibed seeds of rice are exposed to C- and N-ion beams, the highest mutation frequency is observed at an LET of 60–70 keV/μm[2]. It is, however, unclear whether this difference between *Arabidopsis* and rice with respect to the most effective LET is caused by the difference in these plant species or the seed conditions such as dry and imbibed. To clarify the difference, we irradiated imbibed seeds of *A. thaliana* with C-ion beams at different LETs and evaluated the effect of LET on mutation induction.

Dry seeds of *A. thaliana* ecotype Columbia were surface sterilized with a sodium hypochlorite solution (1% available chlorine) containing 0.1% Triton X-100 for 10 min. The sterilized seeds were sown on 0.7% agar-solidified MS medium with 1.5% sucrose and were placed at 4˚C in the dark for 24 h. Then, the seeds were exposed to C-ion beams at an LET range of 30–60 keV/μm in combination with a dose range of 0–125 Gy. Seed germination and plant growing were performed as previously described[1]. Flowering rate was determined 1 month after transferring the plants to soil and was calculated by dividing the number of flowering plants by the total number of irradiated M_1 seeds. M_2 seeds were collected and incubated under the same conditions used for germinating M_1 seeds. The mutation frequency of the induction of albino plants was calculated as the ratio of albino plants to the total number of M_2 seedlings that germinated after culturing the seeds for 5 days at 22˚C.

Flowering rates of the plants that developed from the irradiated imbibed seeds decreased when the radiation dose was increased from 75 to 125 Gy (Fig. 1). LET had an observable effect on the decrease in flower rates: in the plants exposed to 100-Gy irradiation, the flowering rates did not decrease at an LET of 30 keV/μm, but the rates decreased at LET of 50 and 60 keV/μm. When dry seeds of *A. thaliana* were irradiated with C-ion beams at LET of 22.5 and 61.5 keV/μm, the flowering rates began to decrease at radiation dose of 500 and 300 Gy, respectively[1]. Acomparison of dry and imbibed seeds in rice and *Murraya paniculata* showed that survival rate decreased in the M_1 plants that developed from imbibed seeds exposed to a low dose of radaition[2),3)]. Therefore, it is indicated that the difference of the dose response is due to the water content and/or the active and inactive state of the cells.

In the M_2 generation, we measured the mutation frequency (Fig. 2). The highest mutation frequencies at LETs of 30, 50, and 60 keV/μm were 0.98% at 75 Gy, 1.01% at 100 Gy, and 0.79% at 75 Gy, respectively. In the dry seeds, heavy-ion beam irradiation at an LET of 30 keV/μm and a radiation dose of 400 Gy was the most effective for induction of the albino mutants, and the highest value (3.28%) was higher than that the LET of 61.5 keV/μm at a radiation dose of 150 Gy (1.35%)[1]. In the imbibed seeds, LETs of 30 and 50 keV/μm were more effective than an LET of 60 keV/μm to induce the mutants. These results lead to the speculation that the effective LET value for the imbibed seeds of *A. thaliana* is similar to that of the dry seeds rather than the imbibed seeds of rice. To confirm this speculation, we will repeat the experiments.

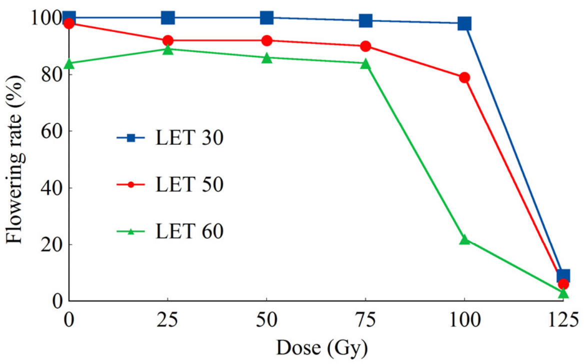

Fig. 1 Flowering rate in M_1 plants that developed from the imbibed seeds irradiated with the carbon-ion beam.

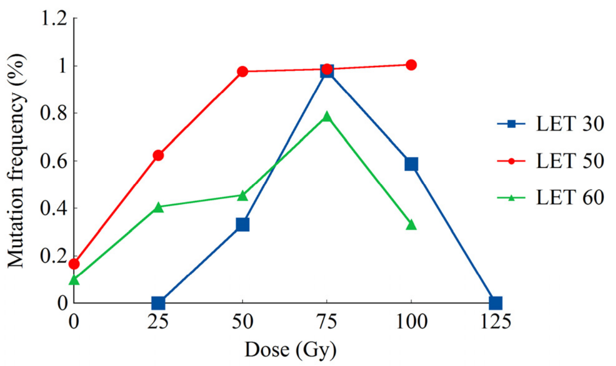

Fig. 2 Effects of LET and dose on mutation frequency in M_2 plants.

References
1) Y. Kazama et al.: Plant Biotech. **25**, 115 (2008).
2) Y. Hayashi et al.: Proc. 18th Int. Conf. on Cyclotrons and their Applications, 237 (2007).
3) T. Hirano et al.: RIKEN Accel. Prog. Rep. **43**, 287 (2009).

Chromosomal rearrangement induced by Fe ions in *Arabidopsis thaliana*

K. Nishihara, Y. Kazama, T. Hirano, S. Ohbu, S. Kawano,* and T. Abe

The ion species and linear energy transfer (LET) values used for heavy-ion beam irradiation can be varied according to own needs. Previous studies on the microbe *rhizobium* have shown that Fe ions induced larger deletions than C ions.[1] In *Arabidopsis*, irradiations with LET values of 290 and 640 keV/μm induced large deletions of over 1 kbp and other mutations such as insertions.[2] Here, we identified DNA mutations caused by Fe-ion irradiation to understand the relationship between high LET values and the different types of mutation.

Dry seeds of *Arabidopsis* were irradiated with Fe ions (90 MeV/nucleon, LET: 640 keV/μm) at a dose of 50 Gy. This irradiation dose was most effective for inducing the formation of albino plants.[3] The germination and culture of M_1 seeds were performed using the same method as that used in a previous study.[4] We collected M_2 seeds from 2,893 M_1 plants and screened mutants from 29,176 M_2 progenies.

We screened mutants that were easily distinguishable on the basis of morphology and leaf color: mutants with elongated hypocotyls (*hy*), mutants in which trichomes were absent (*gl*), mutants with narrow leaves (*nl*), and mutants with pale green leaves (*pg*). From 29,176 M_2 progenies, we isolated 2 *hy* mutants, 1 *gl* mutant, 2 *nl* mutants, and 41 *pg* mutants. We performed PCR amplification and sequencing of the mutated genes and successfully identified DNA mutations in the 4 mutants (Table 1).

First, we identified a point mutation in a *hy* mutant Fe-87-hy1. This mutant had a 2-bp deletion, which caused a frameshift mutation in the second exon of the *HY3* gene.

Among the *pg* mutants, we observed a mutant Fe-148-pg1, which had siliques that pointed downward. We considered this as a *brevipedicellus* (*bp*) mutant and tried to amplify a DNA fragment containing the responsible gene *BP1* (3.3 kbp). However, no PCR product was obtained. We expanded the search range but failed to amplify the region that was 69-kbp upstream and 12-kbp downstream of the *BP1* gene by using PCR. Therefore, we concluded that this mutant had a deletion of around 90 kbp.

When PCR and electrophoresis was performed for the mutated genes of the *nl* mutants, we found that a longer DNA fragment was amplified from a *nl* mutant Fe-88-nl1. Sequencing of the fragment containing the *ANGUSTIFOLIA* (*AN*) gene showed that a 178-bp fragment was tandemly repeated. Sequencing of the cDNA of the *AN* gene revealed the insertion of an 82-bp fragment. A 5-bp micro homology was detected just before and at the end of the duplicated fragment. This duplication was assumed to be caused by synthesis-dependent strand annealing (SDSA), a type of homologous recombination (Fig. 1).

The *gl* mutant Fe-67-gl1 showed a large deletion of around 13 kbp. We performed TAIL-PCR to investigate the ligation of the deleted ends. The results revealed that DNA fragmentation and rearrangement had occurred at the *GL1* gene and its surrounding regions within chromosome 3 (Fig. 2).

To our knowledge, this is the first report of partial duplication and complicated chromosomal rearrangement in *Arabidopsis thaliana* that was induced by heavy ions. Since such mutations have not been reported in C ion-derived mutants, they may have been attributed to the high LET value or broad ion track of Fe ions.

Table 1. A list of identified mutations that were induced by Fe ions.

Mutant	Mutated Gene	Type of Mutation	Mutation Size
Fe-87-hy1	*HY3*	Deletion	2 bp
Fe-88-nl1	*AN*	Insertion	178 bp
Fe-67-gl1	*GL1*	Deletion	13 kbp
Fe-148-pg1	*BP1*	Deletion	90 kbp

* Graduate School of Frontier Sciences, The University of Tokyo.

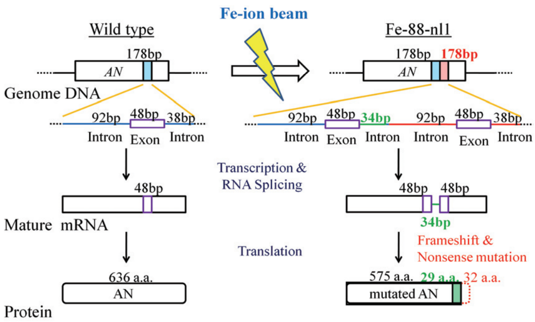

Fig. 1. Partial tandem duplication of the *ANGUSTIFOLIA* (*AN*) gene in the Fe-88-nl1 mutant.

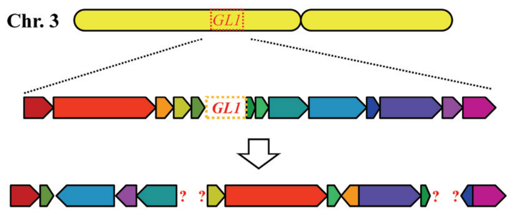

Fig. 2. Chromosomal rearrangement in the Fe-67-gl1 mutant. The pentagons that point to the left indicate inverted fragments.

Reference

1) H. Ichida et al.: Mut. Res. **639,** 101 (2008).
2) Y. Kazama et al.: RIKEN Accel. Prog. Rep. **43**, 284 (2010).
3) Y. Kazama et al.: Plant Biotech. **25**, 113 (2008).
4) H. Saito et al.: RIKEN Accel. Prog. Rep. **37**, 147 (2004).

Heavy-ion beam-mediated screening to evaluate leaf-size control in *fugu5* mutant of *Arabidopsis thaliana*

M. Katano,[*1] Y. Kazama,[*2] T. Abe,[*2] and A. Ferjani[*1,*2]

The way in which the number and size of cells in an organ are determined poses a central challenge in our understanding of organ-size control.[1)] Compensation, whereby reduction of cell proliferation below a threshold level triggers enhanced post-mitotic cell expansion in leaf primordia, suggests an interaction between these cellular processes during organogenesis and provides clues to understand organ-size regulation[1, 2)]. Among the compensation exhibiting *Arabidopsis thaliana* mutants (*fugu1*-*fugu5*) that we have isolated[3)] and characterized,[4)] here, we focused on *fugu5*. Germination of *fugu5* mutant seeds in inorganic media showed oblong cotyledons that showed strong compensation; compensation recovered completely on sucrose supplementation. However, the mechanism of sucrose action and the triggering factor for compensation in this mutant remained unclear. FUGU5 is the vacuolar type H^+-pyrophosphatase (V-PPase) that has 2 functions, hydrolysis of cytosolic pyrophosphate (PPi) and vacuolar acidification. ATP is the main molecule for storage and transfer of biochemical energy in all living organisms. However, its hydrolysis in cells by ~200 known biochemical reactions releases PPi that becomes a metabolic inhibitor at high concentrations and that must be hydrolyzed by V-PPase.

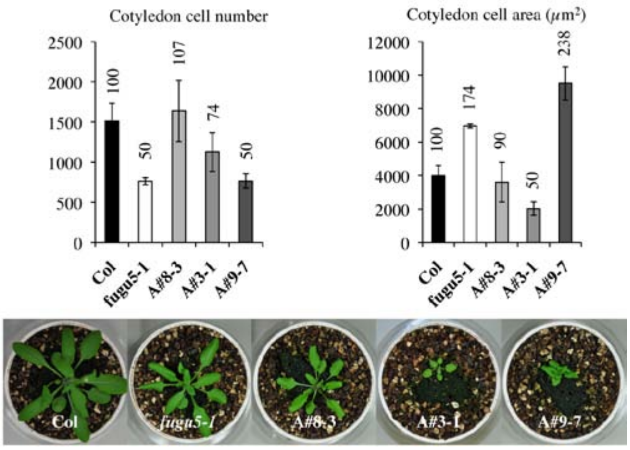

Fig. 1. Cellular phenotypes (top) and gross morphology (bottom) of the newly isolated mutants. Numbers on the top of the columns indicate relative values compared to the WT.

*1 Department of Biology, Tokyo Gakugei University
*2 RIKEN Nishina Center

To elucidate the biological role of V-PPase in plants, we adopted a unique approach that consisted of separate analyses of V-PPase functions. Importantly, we discovered that the cytosolic inorganic pyrophosphatase IPP1 of *Saccharomyces cerevisiae* was enough to rescue *fugu5* mutant phenotypes. Further in-depth analysis of seed lipids and protein reserve mobilization led us to finally conclude that *fugu5* mutants are compromised in gluconeogensis (*de novo* synthesis of sucrose from seed oil reserves), which is known to provide carbohydrates essential for sustaining post-germinative development in oil seed plants. Thus, we showed, for the first time, that PPi hydrolysis, rather than vacuolar acidification, is the major role of FUGU5 *in vivo*, and therefore, removal of cytosolic PPi produced in active cellular metabolism is a prerequisite for proper resumption of post-germinative development.

The following procedures were performed on the basis of our previous results. In order to further understand the importance of V-PPase in plant development, *fugu5* seeds were irradiated with $^{12}C^{6+}$ heavy-ion beam (linear energy transfer (LET), 30 keV/μm; 400 Gy); then, we conducted a large-scale screening of enhancers, repressors, and suppressors of compensation. Following a primary screening of 6088 M_1 seeds, we successfully identified 17 lines of interest in M_2 plants. Interestingly, in the secondary histological screening, we identified 3 mutant lines — A#8-3, A#3-1, and A#9-7 — that affected the *fugu5* mutant phenotype in different ways (Fig. 1). We found that the A#8-3 mutation terminated compensation by restoring cell number and size to the wild type (WT) levels. On the other hand, the A#3-1 mutation inversely affected cell number and size. Indeed, in the A#3-1 line, despite a slight recovery in the number of cells, cell size was reduced by about 60% compared to the original cell size in the *fugu5* mutant. The A#9-7 mutation further enhanced the compensated cell enlargement to more than 2-fold (238%) of that in the WT. To gain further insights into the functions of the genes in which these 3 mutations occur, rough mapping will be carried out using map-based cloning approach, followed by fine mapping using next-generation sequencing technologies or other useful tools. The identification of the above-mentioned mutant genes should further clarify the mechanisms underlying cellular dynamism during leaf organogenesis and should enhance our understanding of leaf-size regulatory mechanisms.

References

1) A. Ferjani et al.: In Plant Cell Monographs: Plant Growth Signaling, L. Bögre and G.T.S. Beemster, eds. (Springer Berlin Heidelberg, Berlin, Heidelberg), pp. 47-62 (2008).
2) A. Ferjani et al.: Plant Morphology 22, pp. 65-71 (2010).
3) G. Horiguchi, U. Fujikura, A. Ferjani, N. Ishikawa, and H. Tsukaya: Plant J. 48, 638-644 (2006).
4) A. Ferjani et al.: Plant Physiol. 144, 988-999 (2007).

Production of bisexual flower-producing mutants of the dioecious plant, *Silene latifolia*, by using γ-ray and the heavy-ion

W. Aonuma,[*1] K. Ishii,[*1] C. Torii,[*1] N. Fujita,[*1] Y. Shimizu,[*1] K. Nishihara,[*1] Y. Kazama, T. Abe, and S. Kawano[*1]

The dioecious plant *Silene latifolia* has XY-type sex chromosomes. Dioecious plants are thought to have evolved from plants with bisexual flowers through the acquisition of male and female sterility. A bisexual flower-producing mutant would be an ancestor-type plant and would be useful in evolutionary research of dioecious plants. Such a bisexual flower-producing mutant of *S. latifolia* has been produced by using γ-ray and X-ray irradiation in a previous study.[1)] Often, the viability of such mutants is reduced, leading to a loss of their self-fertilization ability. A possible reason for this could be that the deletion region was very large.

We aimed to produce bisexual flower-producing mutants that can undergo self-fertilization and have small regions of damage in thier genome by using C-ion beam irradiation. Pollen grains were irradiated with γ-rays (dose range, of 10—80 Gy) and C-ion beam (dose range of 5—40 Gy). The irradiated pollen grains were used to pollinate wild-type female flowers.

The results obtained after screening for mutants are shown in Table 1. We isolated 4 bisexual flower-producing mutants after both γ-ray and C-ion beam irradiation. GP1, GP4, GP6, and GP7 were obtained from the γ-ray-irradiated pollen grains. GP2, GP3, GP5, and GP8 were obtained from pollen grains irradiated with the C-ion beam. GP1 and GP7 could neither develop a complete stamen nor produce pollen grains. All the other bisexual flower-producing mutants except GP1 and GP7, were able to normally develop a fertile stamen. Figures 1A and 1B show sterile and fertile bisexual flower-producing mutants, respectively. In sterile mutant GP1, the ovary did not turn green. The tendncy of γ-ray irradiation to produce sterile mutants was more than that of C-ion beam irradiation. To identify the deleted regions on the Y chromosome, we mapped the 8 mutants by using primers for 15 sequence–tagged site markers on the Y chromosome (Fig. 2). In the mutants obtained after C-ion beam irradiation, only a domain in the neighborhood of the MK17 marker near the gynoecium-suppressing function (GSF) domain were deleted. These results show that irradiation with heavy-ion beams results in the deletion of only small regions of the chromosome; thus it does not adversely affect the viability and fertility of the mutants. Heavy-ion beam irradiation may be used to produce mutants in which deletions affects that only a limited numberof functions.

Table 1. Bisexual flower-producing after γ-ray and C-ion beam irradiation.

Dose (Gy)	γ -ray Irradiated plants	γ -ray Bisexual mutants	C-ion beam Irradiated plants	C-ion beam Bisexual mutants
5			58	0
10	12	0	141	2
20	325	1	90	2
40	193	3	75	0
60			11	0
80	27	0		
Total	557	4	375	4

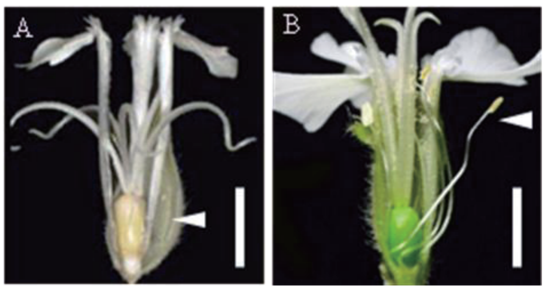

Fig. 1. Sterile and fertile bisexual flower-producing mutants. (A) GP1 was obtained after γ-ray irradiation. (B) GP3 was obtained after C-ion beam irradiation. Bar = 1 cm., The arrowhead indicates the position of the stamen.

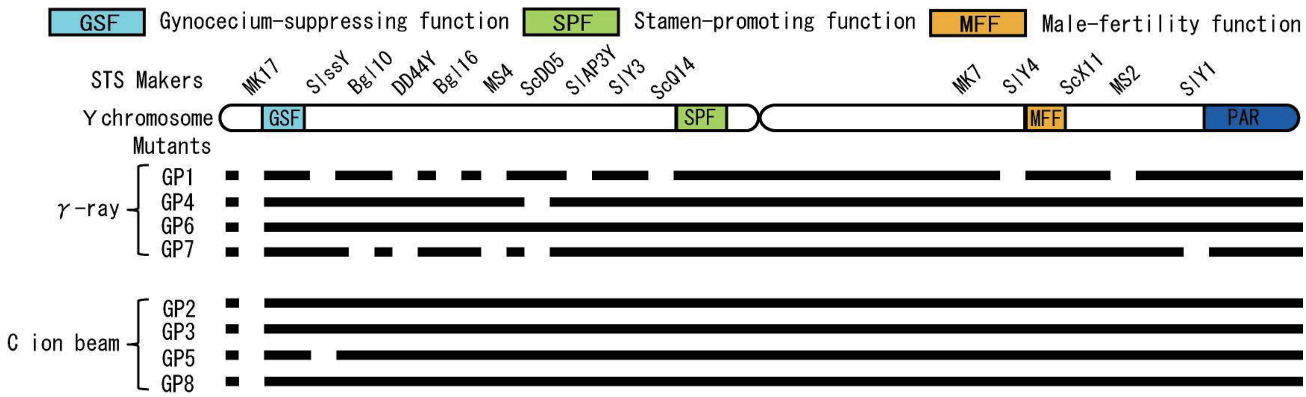

Fig. 2. A deletion map of the Y chromosome of the bisexual flower-producing mutants after γ-ray and C-ion beam irradiation. Blank areas indicate the deletions detected after performing polymerase chain reaction for the Y chromosome sequence-tagged site markers.

[*1] Department of Integrated Biosciences, The University of Tokyo

References

1) Zluvova,J. et al.: Genetics. **177**,375 (2007).

2) Koizumi, A. et al.:Plant Cell Physiol. **48**,1450 (2007).

Development of libraries for mutations induced by heavy-ion-beam irradiation in 'Micro-Tom' tomato†

S. Imanishi*, A. Noguchi*, N. Yokotani*, Y. Kazama, T. Hirano, Y. Hayashi, K. Tsuji*, I. Honda*, and T. Abe

Mutant plants are useful tools not only as parents of new cultivars but also as materials for assessing physiological mechanisms. Tomato (*Solanum lycopersicum*) is an excellent model system to study plant mechanism, such as fruit development and ripening, which cannot be easily studied in *Arabidopsis* or rice. To obtain information on these mechanisms, we induced mutations in the tomato cultivar Micro-Tom by irradiation with accelerated heavy ions. Irradiation with accelerated heavy ions is more effective in inducing mutations in plants on a per-dose basis than irradiation with other sources on a per-dose basis. Further, it is suggested that mutagenesis induced by irradiation with accelerated heavy ions can be a unique approach for studying both forward and reverse genetics in plants.

The determinate miniature *S. lycopersicum* Micro-Tom is well suited for large-scale experiments because of its small size and rapid life cycle. Dry or imbibed seeds of Micro-Tom were irradiated by ^{12}C or ^{20}Ne-ion beams accelerated to 135 MeV/nucleon with RIKEN Ring Cyclotron within the dose range of 1–300 Gy. The linear energy transfer values of the ^{12}C and ^{20}Ne ions were 22.7 and 64.2 keV/μm, respectively.

The irradiated seeds were sown in a greenhouse and transplanted to the field after 3 weeks. M_2 seeds were collected from individual plants to generate independent lines. In the M_2 generation, 5–8 seeds from each line were sown and transplanted to the field; the phenotype was determined on the basis of morphological characteristics. Overall, about 35,000 plants were grown in the field and subjected to phenotypic analysis. M_3 seeds of the lines that were segregated on the basis of visible mutation were collected from each plant. Seeds of the other lines were collected in bulk from the sibs to create large seed resources for further experimentation. A total of 4,642 lines have been screened to date (Table 1), and 789 candidate mutant lines have shown variation in one or more phenotypic characteristics (Fig. 1). To test the genetic nature of the mutants in the libraries, we sowed a selected subgroup of 50 mutants that were identified in the M_2 generation and scored the M_3 generation plants for mutations. Out of these 50 mutants, 33 showed the same phenotype as in the M_2 generation.

Table 1-1 Composition of liblaries of dry seeds irradiated with heavy-ion-beam.

		Radiation Dosage (Gy)								total		
		1	3	10	30	50	100	200	300			
Ne	M_2 lines stock[a]	131	414	495	1,488	1,015	732	157	0	4,432		
	M_2 lines tested		24	268	526	150	216	50			1,234	
	M_3 families stock[b]		24	263	518	149	213	49				1,126
C	M_2 lines stock[a]	119	366	1,037	1,392	542	819	149	63	4,487		
	M_2 lines tested		24	314	568	175	243	75	25		1,424	
	M_3 families stock[b]		24	308	563	175	240	73	24			1,407
										8,919	2,658	2,533

Table 1-2 Composition of liblaries of imbibed seeds irradiated with heavy-ion-beam.

		Imbibed Time - Radiation Dosage (Gy)									total		
		6 h - 5	12 h - 5	24 h - 5	6 h - 10	12 h - 10	24 h - 10	6 h - 20	12 h - 20	24 h - 20			
Ne	M_2 lines stock[a]	83	91	81	84	75	74	25	27	19	559		
	M_2 lines tested	60	87	74	83	68	66	18	22	15		493	
	M_3 families stock[b]	58	85	73	80	68	66	17	16	14			477
		6 h - 10	12 h - 10	24 h - 10	6 h - 20	12 h - 20	24 h - 20	6 h - 40	12 h - 40	24 h - 40			
C	M_2 lines stock[a]	343	330	171	367	360	183	74	40	81	1,949		
	M_2 lines tested	280	284	160	226	253	150	51	28	59		1,491	
	M_3 families stock[b]	280	276	101	218	150	87	50	24	29			1,215
											2,508	1,984	1,692

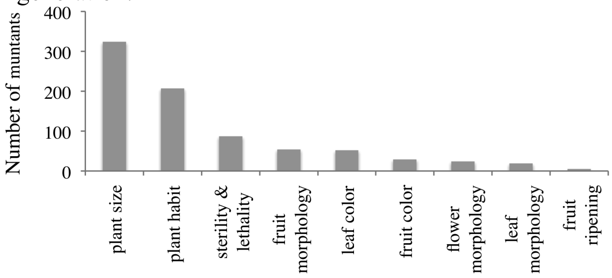

Fig. 1. Distribution of phenotypic characteristics of the candidate mutant lines.

In this study, we introduce the concept of developing comprehensive tomato mutant libraries, which can serve as resources for functional genomic studies. In comparison with libraries of mutants obtained by using ethyl methane sulfonate and fast-neutron mutagenesis, the libraries of mutants obtained by using our approach showed lower rates of sterility and lethality and a different spectrum of mutations[1]. Because our libraries of mutations induced by heavy-ion-beam irradiation could include various types of novel alleles, successive examination of the mutants for effective mutagenesis will contribute to an understanding of the physiological mechanisms of plants.

† A part of this study was carried out under the NIVTS Priority Research Program and Strategic Promotion Program for Basic Nuclear Research by the Ministry of Education, Culture, Sports, Science and Technology of Japan.

* National Institute of Vegetable and Tea Science (NIVTS), National Agriculture and Food Research Organization (NARO)

References

1) N. Menda et al.: Plant J. **38**, 861 (2004).

Identification of deletion mutants for the apomixis-controlling genomic region induced by ion-beam irradiation

M. Takahara*[1], M. Ebina*[1], K. Iimura*[1], R. Morita, Y. Kazama, T. Abe, T. Takamizo*[1], and H. Nakagawa*[2]

Apomixis is an asexual mode of reproduction in which progenies can be produced as maternal clones through seed. Guinea grass (*Panicum maximum* Jacq.), a major tropical forage grass, has both facultative apomicitc lines and obligate sexual lines. We have been working towards the isolation of the gene(s) controlling apomixis in guinea grass by using a map-based cloning method. Recent studies have suggested that recombination is suppressed at the apomixis-controlling locus in guinea grass. Extremely large deletion in a genome can be induced by using ion-beam irradiation with an appropriate value of linear energy transfer (LET).[1)] Therefore, to narrow down the apomixis-controlling genomic region, we developed deletion mutants for this region by using ion-beam irradiation.

Our first step was to determine the optimum dose of ion-beam irradiation for the experiment. We measured the germination and survival rates of guinea grass seeds after ion-beam irradiation. Dry seeds of guinea grass (4 apomicitic cultivars) were irradiated with $^{12}C^{6+}$ (23 keV/μm), $^{20}Ne^{10+}$ (63 keV/μm), or $^{56}Fe^{24+}$ (624 keV/μm) ions at a dose range of 0~600 Gy, 0~400 Gy, and 0~80 Gy, respectively. The irradiated M_1 seeds were placed on agar plates. Then, they were grown at 25°C under long-day condition (16-h light/8-h dark). Their germination and survival rates were measured 3 weeks after sowing.

The germination rates of M_1 seeds did not decrease, similar to that of the untreated control (0 Gy), irrespective of the dose range of ion-beam irradiation (Fig. 1A, C, E). In contrast, the survival rates of the seeds decreased after ion-beam irradiation (Fig. 1B, D, F). In the case of Ne ions, the survival rates of the seeds decreased from 75~92% at 200 Gy to 5~38% at 300 Gy (Fig. 1C). All the 4 cultivars showed a similar trend in survival rate. These results suggested that the LD_{50} value was 400~550 Gy for C, 250~270 Gy for Ne, and 35~55 Gy for Fe.

To obtain deletion mutants, 188 and 145 M_1 plants obtained from seeds (cv. Natsukaze) irradiated with Ne-ions at 150 and 200 Gy, respectively, were grown in a field. Panicles were collected from 3 independent ears for each mutant, and DNA was extracted and purified using the cetyltrimethylammonium bromide (CTAB) method. Then, they were subjected to polymerase chain reaction (PCR) screening by using apomixis-specific sequence-tagged-site (STS) markers, which we have recently developed for the apomixis-controlling genomic region. To date, 30 deletion lines have been obtained by using 40 markers (Fig. 2). The number of lost markers for each line ranged from 2 to 13.

We still need to confirm the phenotypes and transmission of the mutations by using M_2 progeny. To determine the genomic deletion size of each mutant and to identify candidate genes for apomixis, we have initiated whole genome sequencing of the apomixis-controlling genomic region using next generation sequencing.

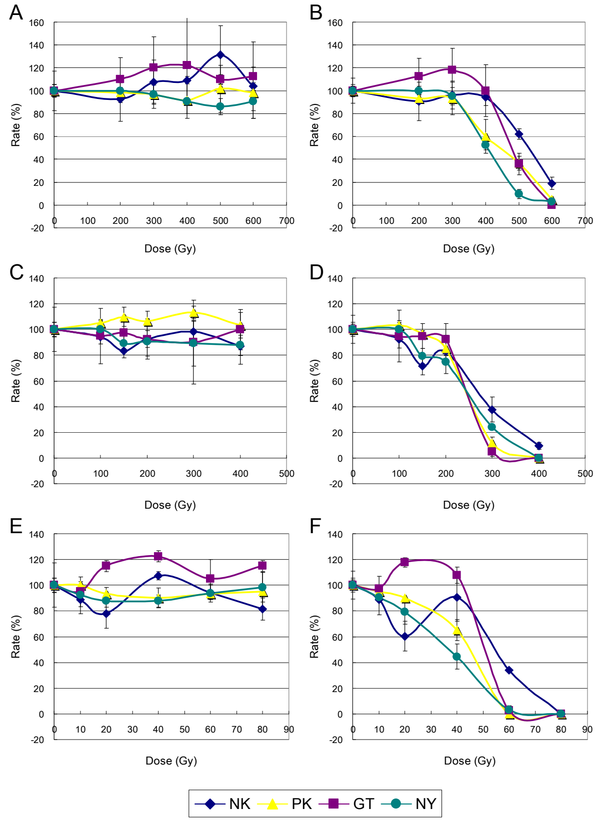

Fig. 1 Effects of different doses of ion-beam irradiation in guinea grass seeds. Germination (A, C, E) and survival (B, D, F) rates were determined after irradiation with C (A, B), Ne (C, D), Fe (E, F) ion beams. The relative rates for 0-Gy irradiation are defined as a rate of 100%. The 4 cultivars used in this study are as follows: NK, Natsukaze; PK, Paikaji; GT, Gatton; and NY, Natsuyutaka.

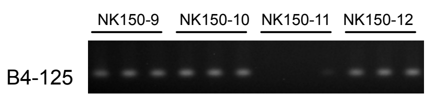

Fig. 2 Detection of a deletion mutant by using apomixis-specific STS markers. In this example, one of the mutants (NK150-11) has lost the marker B4-125.

Reference

1) Y. Kazama et al.: RIKEN Accel. Prog. Rep. **43**, 284 (2010).

*1 National Institute of Livestock and Grassland Science, NARO
*2 Biomass Research & Development Center, NARO

Molecular characterization of *plastochron 1* mutation induced by heavy-ion-beam irradiation in rice

R. Morita, Y. Hayashi, H. Tokairin, T. Sato*[1], and T. Abe

Mutations in plants are powerful tools, not only for their use in the analysis of plant gene function, but also for developing new plant varieties by mutation breeding. Irradiation with heavy-ion beams is thought as an effective method for inducing mutations in plants. To elucidate the DNA mutation induced by heavy-ion beams in rice plants, we irradiated rice (*Oryza sativa* L. cv. Nipponbare) with heavy-ion beams. We have screened the mutants, the causative genes of which were already identified. One such mutation was *plastochron* (*pla*). The *pla* mutants showed rapid leaf emergence and small leaf blade size. Three causative genes, *PLA 1*[1,2], *PLA 2*[3] and *PLA 3*[4] had been already identified.

We isolated 2 *pla*-like mutants, 6–49 and 13–14. 6–49 was induced by C-ion irradiation (40 Gy, 22.5 KeV/μm) of imbibed seeds, whereas 13–14 was induced by C-ion irradiation (50 Gy, 30 KeV/μm) on dry seeds. PCR analysis was performed using the primers specific to the *PLA 1*, *PLA 2,* and *PLA 3* genes. All the coding regions of these genes for both the mutants were amplified, which suggested small deletions or base substitutions in one of these genes. Sequence analysis of the *PLA 1* gene revealed that the 6–49 and 13–14 mutants contained 1- and 9-bp deletions in their respective 2nd exons (Fig. 1). 6–49 possessed 1bp deletion at position 1 in codon 541, resulting in a frame-shift mutation. The 9-bp deletion in the 13–14 occurred from at position 1 in codon 398 to position 3 in codon 400, which resulted in a loss of 3 amino acid residues, Met-Pro-Tyr (Fig. 2). The *PLA 1* gene encodes cytochrome P450 protein and exhibits the similarity to the maize CYP78A1 and Arabidopsis CYP78A7[2]. Amino acid sequence alignments revealed that not only the deleted regions in 13–14 but also the surrounding regions were highly conserved in the 3 species (Fig. 2). This observation suggested that the deleted region may be functionally important in both the *PLA 1* gene and the orthologous genes. Further experiments such as the complementation test would be required to confirm these findings.

The deletion induced by γ-ray irradiation in rice was either small (1–16 bp) or large (9.4–129.7 kb)[5]. The sizes of the deletions described in this paper are similar to those induced by γ-ray irradiation. It is necessary to investigate more number of mutants to characterize mutations induced by heavy-ion-beam irradiation in rice. Studies of the other mutations induced by heavy-ion-beam irradiation are currently in progress.

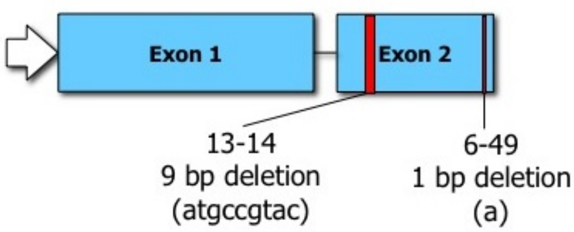

Fig. 1. Position of mutations in the 6–49 and 13–14 in the *PLA 1* gene.

Boxes and a line indicate exons and an intron, respectively. The transcriptional orientation is denoted by an arrow. Mutation sites are shown in red. The deleted sequences are shared inside parentheses.

References

1) J. Itoh et al.: Plant Cell 10, 1511 (1998)
2) K. Miyoshi et al.: PNAS 101, 875 (2004)
3) T. Kawakatsu et al.: Plant Cell 18, 612 (2006)
4) T. Kawakatsu et al.: Plant J. 58, 1028 (2009)
5) R. Morita et al.: Genes Genet. Syst. 84, 361 (2009)

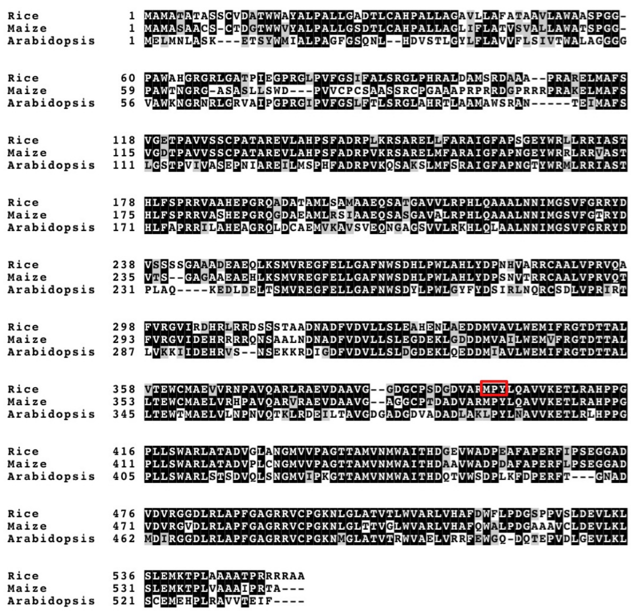

Fig. 2. Sequence alignments of the PLA1 protein with the most closely related cytochrome P450.

PLA1 (Rice), CYP78A1 (Maize), and CYP78A7 (*Arabidopsis*) are shown. The 3 deleted amino acid residues in the 13–14 are shown in a red box. Multiple sequence alignments were performed using the ClustalW and the BOXSHADE programs.

---

*1 Graduate School of Life Sciences, Tohoku University

Mutation breeding of orchids by using heavy-ion beam irradiation

M. Chaya[*1], K. Tachiko[*2], T. Hirano, Y. Hayashi, and T. Abe

Mutation breeding by heavy-ion beam irradiation is associated with a high frequency of mutant induction and a wide range of mutations[1]. Generally, cross-breeding in orchid takes long time. Therefore, we aimed to shorten the time required for developing new cultivars in orchids and conducted mutation breeding in the 2 genera, *Dendrobium* and *Spathoglottis*, by using heavy-ion beam irradiation.

Plantlets of 11 cultivars of phalaenopsis-type *Dendrobium* grown in vitro were irradiated with a C-ion beam of 22.5 keV/μm with a dose range of 5–20 Gy. Survival rate and flowering rate of each cultivar about 2.5 years after irradiation are shown in Table 1. Among the plantlets exposed to 5-Gy irradiation, the survival rates of 'Burana Emerald' and 'Burana Pink' were 86 and 100%, respectively. We did not observe a remarkable decrease in the survival rates of these plants. However, the survival and flowering rates decreased with the increase in dose from 10 to 20 Gy. None of the cultivars that were exposed to radiation at 20 Gy survived, except for 2 cultivars ('Burana Stripe' and 'Burana Fire Ball'). 'Burana Pearl' and 'Burana Pearl Beauty' showed low survival and flowering rates after irradiation at 10 Gy. These results suggest that the *Dendrobium* cultivars used in the present study showed different sensitivities to radiation. Mutant screening for flower color and flower morphology was performed in the 299 flowing plants after irradiation. We obtained 9 mutants with paler flower color, 5 mutants with deeper flower color, and 11 mutants with smaller flowers than that of the original variety (Table 1). Mutation frequency calculated on the basis of the flower mutation was 10% at 10 Gy and 14% at 20 Gy. The survival rate of the plants irradiated at 20 Gy decreased; therefore, we thought that the irradiation dose of 10 Gy was suitable for efficient screening of the mutants. However, none of these mutants were marketable.

Table 1 Survival rate, flowering rate, and mutant phenotypes in the *Dendrobium* cultivars irradiated with a C-ion beam.

Cultivars	Dose (Gy)	Survival rate (%)	Flowering rate (%)	Number of flower mutants		
				Pale color	Deep color	Small flower
'Burana Emerald'	0	100.0	93.3	-	-	-
	5	100.0	93.3	-	-	-
	10	92.3	84.6	-	-	-
	20	0.0	0.0	-	-	-
'Burana Pink'	0	100.0	93.3	-	-	-
	5	85.7	78.6	-	-	-
	10	85.7	71.4	1	-	-
	20	0.0	0.0	-	-	-
'Burana Crystal Pearl'	10	57.1	46.4	-	2	-
	20	0.0	0.0	-	-	-
'Burana Fire Ball'	10	100.0	64.2	-	-	-
	20	77.8	16.7	-	-	-
'Burana Mini Crystal'	10	98.3	45.8	-	-	-
	20	0.0	0.0	-	-	-
'Burana Pearl'	10	35.5	35.5	-	-	-
	20	0.0	0.0	-	-	-
'Burana Pearl Beauty'	10	32.1	26.8	-	-	-
	20	0.0	0.0	-	-	-
'Burana Princess'	10	63.0	46.3	1	1	3
	20	0.0	0.0	-	-	-
'Burana Red Stripe'	10	79.2	54.2	2	1	2
	20	0.0	0.0	-	-	-
'Burana Rosy Pink'	10	80.0	67.3	2	1	4
	20	0.0	0.0	-	-	-
'Burana Stripe'	10	82.1	53.6	3	-	1
	20	33.3	22.2	-	-	1

-: No plant showed mutant phenotypes.

In vitro plantlets of the *Spathoglottis* sp. were irradiated with a C-ion beam of 22.5 keV/μm at a dose range of 5–20 Gy. Twenty plantlets were irradiated with the C-ion beam at each dose. Survival and flowering rates were measured after 12 months cultivation. The survival rates of these mutants decreased with the increase in dose: the plantlets exposed at 5 and 10 Gy showed 80 and 15% survival, respectively. The flowering rate showed a similar tendency to the survival rate, and the flowering rates of plantlets exposed to irradiation at 5 and 10 Gy were 50 and 10%, respectively. When the phenotype of the plants that survived was investigated, 3 dwarf mutants were obtained and were derived from plants exposed to irradiation at 5, 10, and 20 Gy (Fig. 1). Leaf length of the mutants was about 30 cm, which was half the size of the leaves of the original cultivar (60 cm). Such foliage mutants showed normal flowers. Thus, we considered that these mutants can be marketed as pot plants. Currently, we are propagating the mutants, and we will evaluate the stability of the dwarf phenotype.

Fig.1 Dwarf mutants of *Spathoglottis* sp. derived after C-ion beam irradiation. Bar = 10 cm.

Reference

1) T. Abe et al.: in Plant Mutation Breeding and Biotechnology (Shu, Q.Y., ed.), The Joint FAO/IAEA Programme, pp. 95-102 (2010)

*1 Nagasaki Agricultural and Forestry Technical Development Center
*2 Tachiko Orchids

Induction of mutations in chrysanthemum by using C-ion beam irradiation

K. Tamaki[*1], M. Yamanaka[*1], Y. Koyama[*1], Y. Mizutani[*1], Y. Hayashi, and T. Abe

Chrysanthemum is one of the important cut flowers in Hyogo Prefecture. It is cultivated in the central and southern parts of Hyogo Prefecture. Farmers usually grow chrysanthemums in open fields. In chrysanthemums, flowering varies for each cultivar. Chrysanthemum cut flowers are sold in the market as bundles consisting of flowers of 3 colors, namely, pink, white, and yellow. Therefore, synchronicity of the flowering time of flowers of these 3 colored varieties is a prerequisite for the production of chrysanthemum cut flowers. Flowering changes with the weather. The objective of this study was to obtain mutants that have similar cultivation characteristics, except for flower color.

We irradiated 3-cm cuttings of 34 cultivars of chrysanthemums with C-ion beam (Energy, 135MeV/nucleon; LET 23 keV/μm) at doses of 2, 4, 6, and 8 Gy. The irradiation doses were determined on the basis of a previous study[1)]. After irradiation, the cuttings were planted cell-trays containing soil. One month later, these cuttings were transplanted to an experimental field or a green house. Cultivation condition is no pinch and no picking the bud. The other conditions used for cultivation were standard. At the time of full bloom, all the flowers were observed.

Survival rates were expressed as the number of growing plants/the number of irradiated cuttings × 100 (%). The survival rates were not affected when the irradiation dose was less than 4 Gy. However, survival rates decreased when the irradiation dose was higher than 6 Gy (data not shown). An irradiation dose of 8 Gy inhibited growth in all cultivars and delayed flowering time by over 2 weeks.

Among the 34 cultivars used in this study, 18 cultivars showed flower-color, flower-shape, leaf-color, and leaf-shape mutations（Table 1）.

Mutation frequency was expressed as the number of mutants/the number of growing plants × 100 (%). At an irradiation dose of 2 Gy, the mutation frequency was high for the “Kincha-nirin” and “Benichidori” cultivars. Flower-color mutants were obtained for both these cultivars, whereas a leaf-shape mutant was obtained only for “Kincha-nirin.”

For 4-Gy irradiation, the mutation frequency was high for all the 18 mutant cultivars. These 16 cultivars, except for “Ki-shuho” and “Jinba,” showed mutations in flower color and flower shape. “Ki-shuho,” “Jinba,” “Asayuki,” “Tenshukaku,” and “Itogo” had mutations in leaf color or in leaf shape. With 4-Gy irradiation, we observed mutation frequencies higher than 20% in 9 cultivars; the highest mutation frequency was 26.7% in “Chorus.”

In the present study, we obtained 45 mutants from 649 plants belonging to 34 cultivars, and subsequently, we selected 19 mutants (12 cultivars) that showed mutations in flower color or in flower shape. Further we cultured the petals of the chimeric plants in order to obtain plants with selected characteristics.

*1 Hyogo Prefectural Research Institute for Agriculture, Forestry and Fisheries

Reference

1) K. Suzuki et al.: RIKEN Accel.Prog.Rep.**37**, 152 (2004)

Table 1. The mutation frequencies of the irradiated cuttings*

Flower type	Cultivars	Dose (Gy) 2	4	6	8
Large mum	“Ki-shuho”	-	1/21 (4.8%)	-	1/23 (4.3%)
	“Kincha-nirin”	2/9 (22.2%)	2/8 (25.0%)	-	-
	“Asayuki”	-	2/8 (25.0%)	-	0/3 (0.0%)
	“Jinba”	-	2/10 (20.0%)	-	-
	“Hanakotoba”	-	2/8 (25.0%)	-	-
	“Tenshukaku”	-	2/14 (14.3%)	-	-
	“Kajin”	-	2/13 (15.4%)	0/4 (0.0%)	-
Spray mum	Kobe line	-	1/6 (16.7%)	1/6 (16.7%)	0/2 (0.0%)
	“Chorus”	-	4/15 (26.7%)	-	-
Small mum	“Komame”	-	2/9 (22.2%)	-	-
	“Kanhakuto”	0/17 (0.0%)	2/20 (10.0%)	-	-
	“Hiroshimabeni”	0/13 (0.0%)	2/17 (11.8%)	-	0/5 (0.0%)
	“Komurasaki”	0/8 (0.0%)	2/20 (10.0%)	1/7 (14.3%)	0/9 (0.0%)
	“Benichidori”	1/11 (9.1%)	2/21 (9.5%)	0/4 (0.0%)	0/5 (0.0%)
	“Benitsuki”	0/20 (0.0%)	3/32 (9.4%)	0/1 (0.0%)	0/8 (0.0%)
	“Itogo”	0/10 (0.0%)	3/13 (23.1%)	0/1 (0.0%)	-
	“Naomi”	0/13 (0.0%)	3/19 (15.8%)	-	0/3 (0.0%)
	“Hanazome”	0/7 (0.0%)	2/9 (22.2%)	-	0/1 (0.0%)

* The numbers in the table indicate the followings:

number of mutants/number of growing plants (mutation frequency)

\- Not tested

Flower-color mutation in chrysanthemum induced by C-ion beam irradiation

K. Tamaki[*1], M. Yamanaka[*1], Y. Koyama[*1], Y. Mizutani[*1], Y. Hayashi, and T. Abe

Chrysanthemum is a popular cut flower in Hyogo Prefecture. The deep pink-colored chrysanthemum, commonly called “red” chrysanthemum, is referred to as “pink” chrysanthemum in this report. The cut chrysanthemum flowers are sold in the market as bundles formed of flowers of 3 colors, namely, pink, white, and yellow. Therefore, synchronicity of flowering time of the varieties producing flowers of these 3 colors is prerequisite for cut flower production of chrysanthemum. In this study, we aimed to develop colored varieties of chrysanthemum.

We used 3 yellow (including “Kincha” color in which 2 colors (yellow and brown) are present in the same petal), 1 orange, 17 white, and 13 pink flower cultivars as starting materials. We obtained 24 flower-color mutants from 14 cultivars by using C-ion beam irradiation (LET 23 keV/μm, 2 Gy, 4 Gy, and 6 Gy).

Table 1 shows the flower color of the original cultivars and their resultant mutants. Three mutants with yellow color were induced from “Kincha-nirin.” Mutants showing other colors were not obtained.

Two mutants were induced from “Komame.” One of those mutants had yellow flowers, and the other had deep orange flowers; the color of the deep orange flowers faded gradually. So, it is necessary to improve this character.

Six mutants were induced from 4 white flower cultivars. Two mutants induced from “Tenshukaku” and “Kanhakuto” had yellow flowers (Fig. 1). Two kinds of mutants were induced from “Asayuki” and “Chorus.” Especially, the cream yellow and light pink color segments were present on 2 different flowers on the same mutant from “Asayuki”.

Thirteen mutants were induced from 7 pink flower cultivars. The flower color of 5 of the mutants from “Komurasaki” and “Naomi” changed to wine red; 1 mutant from “Kajin” changed to much deeper pink; and the other 5 mutants from “Hanakotoba,” “Benichidori,” “Benitsuki,” and “Hanazome” changed to white. Two mutants from the Kobe line changed to pale dull orange and lemon yellow. The mutants from the pink cultivars produced flowers with the widest range of colors.

In this study, we obtained various flower-color mutants. We observed a directionality in the mutation pattern of the flower colors (pink > white > yellow or pink > orange > yellow). We did not obtain yellow-flower mutants from pink-flower cultivars. However, we were able to induce yellow-flower mutants from orange- or white- flower cultivars. Therefore, we think that we can induce yellow-flower mutants from the orange or white-flower mutants developed from pink-flower cultivars. Moreover, we think that pink has the widest mutational spectrum for flower color.

* Hyogo Prefectural Research Institute for Agriculture, Forestry and Fisheries

Fig. 1 The flower of “Kanhakuto”
Top: original flower
Bottom: mutant flower

Table 1 The mutation pattern of flower-color mutants

Flower type	Cultivar	Flower color: Original	Flower color: Mutant	No. of flower color mutants
Large mum	“Kincha-nirin”	Kincha	Yellow	3
	“Asayuki”	White	Cream yellow Light pink	1
	“Tenshukaku”	White	Yellow	1
	“Hanakotoba”	Pink	White	1
	“Kajin”	Light pink	Deep pink	1
Spray mum	“Chorus”	White	Pale dull pink Cream yellow	3
	Kobe line	Pale pink	Pale dull orange Lemon yellow	2
Small mum	“Komame”	Orange	Yellow Deep orange	2
	“Kanhakuto”	White	Yellow	1
	“Komurasaki”	Pink	Wine red	3
	“Benichidori”	Pink	White	1
	“Benitsuki”	Pink	White	1
	“Naomi”	Pink	Wine red	2
	“Hanazome”	Pink	White	2

Characteristics of fruit appearance mutations induced by heavy-ion-beam irradiation in Satsuma mandarin (*Citrus unshiu* Marc.)

T. Teraoka,* K. Kamiya,* I. Sawano,* T. Nakajima,* H. Kagami,* A. Kamio,* N. Hamabe,*

Y. Hayashi, H. Ryuto, N. Fukunishi, and T. Abe

Satsuma mandarin (*Citrus unshiu* Marc.) is a major fruit tree crop in Shizuoka Prefecture. Many cultivars of Satsuma mandarin have been discovered since bud mutations occur naturally in fields. These cultivars sometimes have advantageous characteristics such as high sugar content and early maturation. Although mutation breeding provides new citrus cultivars, discovering naturally occuring bud mutations is very difficult. Recently, heavy-ion-beam irradiation has been reported as a practically viable technique for inducing artificial mutation. There are a few reports on the effect of irradiation on citrus[1]. In this study, we investigated the types and rate of visible mutation in Satsuma mandarin, and studied the quality of the fruit.

From 2000 to 2005, dormant scions from the hard branches of 2 cultivars and 2 lines of Satsuma mandarin were irradiated with $^{12}C^{6+}$ (135 MeV/n, 22.5 keV/μm), $^{14}N^{7+}$ (135 MeV/n, 26.3 keV/μm), and $^{20}Ne^{10+}$ (135 MeV/n, 61.1 keV/μm) at doses of 10, 20, 30, 40, and 50 Gy(table 2). After irradiation, the scions were grafted on to *Poncirus trifoliata* to produce the VM1 (Vegitative Mutant 1) generation. After sprouting, the treetops were cut back at least 3 times. From 2006 to 2008, mutation could be visually observed in flowers, leaves, and fruits. Quality of the fruit was investigated by harvesting 5 fruits from each tree. Fresh weight, specific gravity, sugar content (degrees Brix), and citric acid content of the fruits were measured. Shape index of the fruits was calculated as a ratio of the horizontal and vertical diameters. The tendency of peel puffing was rated as 0 (null), 1 (slight puffing), 2 (medium), 3 (heavy). The index of color development in the peel was rated as 0 (before coloring) to 10 (coloring completed).

Leaves with abnormal shapes were observed immediately after sprouting. After performing cutting back thrice, almost all the new leaves were observed to be normal. Hence, the first abnormally shaped leaf was maybe a transient effect of irradiation. We regarded the continued variation in appearance for 3 years as a stable mutation. Mutation caused by irradiation with $^{20}Ne^{10+}$ ion beam was observed in flowers, leaves, and fruits, and the rate of fruit appearance mutation was, 1.1% with 20- Gy dose, 0% with 10- and 50-Gy doses (table 1). A dose of 20 Gy was concluded to be effective for mutation induction in the fruit. The types of fruit mutation were coloring, peel smoothness, and fruit shape. In some cases, a chimeric structure in the peels was observed. Nine mutants were selected from 1397 VM1 trees, and the mutation rate was about 0.6% (table 2). The sugar content was observed to be higher in the compressed mutant than in the control, whereas it was lower in the oblate mutant. On the other hand, the citric acid content was higher in the oblate mutant and lower in the compressed mutant. The color development was slower in the oblate mutant. The peel puffing index was higher in the compressed mutant than in the control (table 3).

These results indicate that heavy-ion-beam irradiation can induce various visible mutations in the Satsuma mandarin. In the case of irradiation with the $^{20}Ne^{10+}$ beam, the putative rate of fruit mutation was about 0.6%. Furthermore, the quality of the citrus fruit could vary according to the heavy-ion-beam irradiation. In order to analyze the stability of the mutation, we are presently growing VM2 lines from the VM1generation by using the grafting technique.

*Fruit Tree Res. Center, Shizuoka Res. Inst. of Agric. and For.

Table 1. Rate of visible mutation induced by irradiation with $^{20}Ne^{10+}$ ion beam[Z]

Dose (Gy)	No. of plants irradiated[Y]	No. of leaf mutants	No. of flower mutants	No. of fruit mutants
10	420	2 (0.5)[X]	1 (0.2)	0
20	460	2 (0.4)	0	5 (1.1)
50	50	0	0	0

[Z]Data were recorded in 2008; [Y]1 cultivar and 2 lines were used (nucellar seedling (NS) of 'Aoshima Unshiu', NS of 'Miyagawa wase', 'Jutaro Unshiu'); [X]Mutation rate (%)

Table 2. Types of fruit appearance mutation by heavy-ion-beam irradiation[Z]

Cultivar or Line	No. of plants irradiated	No. of mutants	Ion	Dose (Gy)	Fruit appearance
Aoshima Unshiu	357	2	N	10	Delay in color development
			N	10	Compressed shape
Aoshima NS[Y]	240	5	Ne	20	Oblate shape
			C+N[X]	20+20	Compressed shape
			Ne	20	Delay in color development
			Ne	20	Smooth peel
			Ne	20	Chimeric peel
Miyagawa NS	400	1	Ne	20	Chimeric peel
Jutaro unshiu	400	1	Ne	10	Chimeric peel
Total	1397	9			

[Z]Data were recorded in 2008. Data were gathered in the same cultivar or line, from different ions and dose; [Y]NS: nucellar seedling; [X]2 kinds of ion beams were used sequentially.

Table 3. Qualities of fruit appearance mutants[Z]

Type of mutation	Ion	Dose (Gy)	Shape index	Fruit wt. (g)	Specific gravity	Peel puffing	Coloring	Sugar (degrees Brix)	Citric acid content(%)
Oblate	Ne	20	131	122	0.87	0.0	8.6	9.6	1.24
Compressed	C+ Ne[Y]	20+ 20	150	112	0.80	1.4	10.0	11.3	0.97
Control			143	133	0.87	0.1	9.6	10.8	0.90

[Z]Data were recorded in 2010. 5 fruits per tree from 2 mutants of Aoshima NS line have been shown; [Y]2 kinds of ion beams were used sequentially for irradiation.

Reference

1) H. Kagami et al: RIKEN Accel. Prog. Rep. **36**, 136 (2003)

Induction and isolation of pigmentation mutants of *Porphyra yezoensis* (Bangiales, Rhodophyta) by heavy-ion beam irradiation†

K. Niwa,*1 Y. Hayashi, T. Abe, and Y. Aruga

The life cycle of the marine crop *Porphyra yezoensis* involves a heteromorphic alternation of generation, with gametophytic haploid blades and sporophytic diploid filaments called conchocelis. Thus, haploid blades could be suitable for inducing mutation in *Porphyra* because recessive mutations would appear directly in the phenotype. In addition, *P. yezoensis* propagates by an asexual subcycle through archeospores (monospores) released from gametophytic blades. Therefore, if an archeospore released from a mutated cell cluster developed into a mature blade, a pure line (complete homozygous conchocelis strain) of the mutation genotype could be easily established by self-fertilization.

To induce mutation, the gametophytic blades of *P. yezoensis* were put into centrifuge tubes (15 mL) containing seawater and irradiated by $^{12}C^{+6}$ beams (135 MeV/nucleon) in an automatic irradiation system at the E5B beam line. The linear energy transfer (LET) of ions corresponded to 23 keV/µm. After approximately 1.5 months of culture, the clonal blades from the archeospores were irradiated with the $^{12}C^{+6}$ beams at doses of 25, 50, 100, 150, 200, 300, and 400 Gy, and the survival rate of gametophytic cells 1 day after heavy-ion beam irradiation was found to be more than 97% even at 400 Gy. However, the survival rate 2 weeks after irradiation decreased at 200, 300, and 400 Gy. Furthermore, the blades irradiated at ≦150 Gy grew normally, but those irradiated at ≧200 Gy did not grow well (Fig. 1). These results suggest that a dose of ≦150 Gy is suitable to induce mutation at an LET of 23 keV/µm with $^{12}C^{+6}$ beams for isolating mutants of *P. yezoensis*.

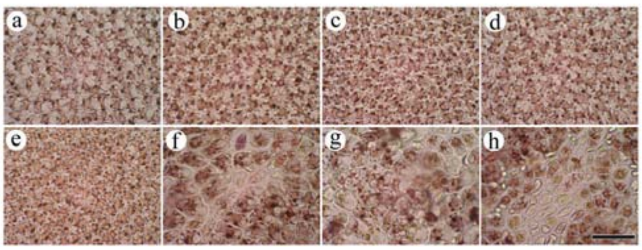

Fig. 1. Gametophytic cells of *Porphyra yezoensis* 20 days after heavy-ion beam irradiation. (a) Control (no irradiation). (b) Irradiation at 25 Gy. (c) Irradiation at 50 Gy. (d) Irradiation at 100 Gy. (e) Irradiation at 150 Gy. (f) Irradiation at 200 Gy. (g) Irradiation at 300 Gy. (h) Irradiation at 400 Gy. Scale bar: 50 µm in h; also applies to a-g.

Small cell clusters with mutation colors were found in several irradiated blades observed under a light microscope about 20 days after irradiation (Fig. 2), and the method used for isolation of the artificial pigmentation mutants of *P. yezoensis* is shown in Fig. 3. The procedure after other mutagenic treatments, such as chemical mutagenesis and gamma ray irradiation, is basically the same. The blade piece containing a mutated cell cluster was cut out from the irradiated blade. This piece was cultured in a flask, and vinylon monofilaments were placed in the flask for the attachment of archeospores that were released from the mutated cell cluster. The archeospore germling grew to a single colored blade, which was a clonal blade that developed from the mutated cell. This blade was cultured in a flask until maturation. After self-fertilization, the mutant strain was established as a conchocelis strain. Using the above-mentioned method, we succeeded in isolating 2 genetically stable pigmentation mutants of *P. yezoensis*.

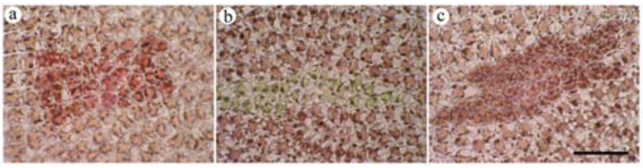

Fig. 2. Small cell clusters with mutation colors in gametophytic blades of *Porphyra yezoensis* about 20 days after heavy-ion beam irradiation at 50 or 100 Gy. (a) Cluster of red cells. (b) Cluster of green cells. (c) Cluster of deep reddish brown-colored cells. Scale bar: 50 µm in c; also applies to a and b.

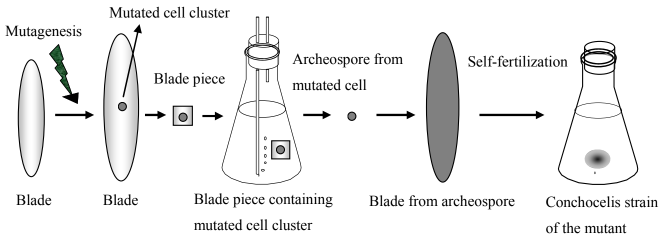

Fig. 3. Isolation method of the artificial pigmentation mutant of *Porphyra yezoensis* after mutagenic treatment.

† Condensed from the article in Phycol. Res. **57**, 194 (2009)

*1 Fisheries Technology Institute, Hyogo Prefectural Technology Center for Agriculture, Forestry and Fisheries

Isolation of Ar-ion-induced mutants of the moss *Funaria hygrometrica*

M. Itouga,[*1] Y. Kato,[*1] S. Kawakami,[*2] Y. Kazama, Y. Hayashi, T. Abe, and H. Sakakibara[*1]

We found that the wild-type moss *Funaria hygrometrica* has very high capacity of adsorption of lead and gold from some aqueous water environments.[1] We are currently developing unique bio-sorption systems that include water contaminated with heavy and/or rare metals, by making use of this property of *F. hygrometrica*. We have also created effective mutant cells by ion-beam irradiation for use in sustainable applications in future bio-sorption systems. Recently, we isolated Ar-ion-induced mutants of the moss *F. hygrometrica*. In this report, we show that Ar-ion-induced mutants can be used as practical standard cells in future bio-sorption systems that use the moss *F. hygrometrica*.

Protonemal cells of wild-type Fh01 were cultured on an agar plate overlaid with cellophane. The cells were irradiated by $^{40}Ar^{17+}$ (LET 280 keV/μm) at a dose of 75Gy, which is the optimum condition[2] for *Funaria* moss mutation breeding. The Ar ions were accelerated to 95 MeV/nucleon by RIKEN Ring Cyclotron. Then, the cells were collected and inoculated on a new agar plate and cultured for 40 days.

We selected 6 mutants that were visually distinguishable from Fh01 (Fig. 1). A high mutation frequency of about 6% was observed. These mutants could be characterized by no-bud formation. Thus, these were named as NB mutants. The filamentous growth performance of the NB mutants was sufficient for our bio-sorption system (Fig. 2). We succeeded in maintaining the protonemal cell state. Thus, we could develop a stable moss production system.

Next, we checked the total chlorophyll content, because each colony of NB mutants was deep green in color. The photosynthetic pigments were extracted with 80% acetone, and their levels were determined spectrophotometrically.[3] Absorption spectrum analysis was performed using a UV-vis spectrophotometer (U-1900, Hitachi Co., Japan). The total chlorophyll and carotenoid contents and the pigment ratio are summarized in Table 1. The chlorophyll-carotenoid weight ratio of mutants was significantly higher than that of Fh01 (Table 1). Recently, we selected NB01 mutant cells from NB mutants, because the growth performance of NB01 was better than that of the other NB mutants. Off cause, the lead and gold adsorption capacities of NB01 were similar to those of Fh01. Thus, we conclude that heavy-ion beam irradiation can be used to produce effective mutation cells from *F. hygrometrica* for future bio-sorption systems.

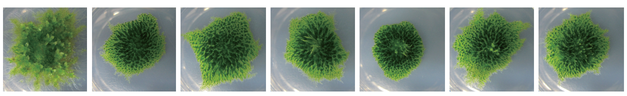

Fig. 1. Comparison of radial growth of the colony. Leafy gametophytes are not formed from mutants (NB01 06).

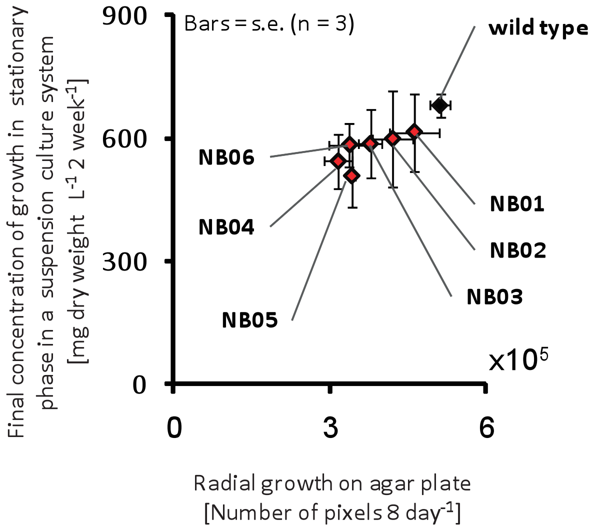

Fig. 2. Characterization of filamentous growth performance of the moss *Funaria hygrometrica*. Final concentration of the growth in the stationary phase in a suspension culture system and radial growth on solid media are measured for wild type and mutants.

Table 1. Chlorophyll and carotenoid contents and pigment ratio for the moss *Funaria hygrometrica*. Data show mean (n = 3). Single asterisk indicates a significant difference between the wild type and the mutant under the same growth conditions at the $p < 0.05$ level, as confirmed by Welch's t test. a + b: total chlorophyll a and b; x + c: xanthophylls and carotenes (total carotenoids).

Type	Culture name	a + b (mg/g dw)	x + c (mg/g dw)	Pigment ratio	
				a/b	(a + b)/(x + c)
Wild	Fh01	28.3	4.10	1.54	6.91
Mutant	NB01	33.3	4.08	1.79*	8.16*
Mutant	NB02	30.2	3.65	1.71	8.28
Mutant	NB03	29.4	3.36	1.70	8.76*
Mutant	NB04	30.8	3.53	1.75	8.73*
Mutant	NB05	29.2	3.32	1.75	8.80*
Mutant	NB06	29.9	3.44	1.72	8.70*

*1 RIKEN, Plant Science Center
*2 DOWA ECO-SYSTEM CO., LTD., Environmental Protection Lab.

References

1) M. Itouga et al.: Regulation of Plant Growth & Development 45, 64-72 (2010).
2) M. Itouga et al.: RIKEN Accel. Prog. Rep. 43, 278 (2010).
3) H. K. Lichtenthaler and C. Buschmann: Current Protocols in Food Analytical Chemistry F4.3.1-F4.3.8 (2001).

IV. OPERATION RECORDS

1. Operation of RIBF

Operations of RIBF ring cyclotrons (RRC, fRC, IRC, and SRC)

K. Kobayashi,[*1] M. Kase, T. Aihara,[*1] M. Fujimaki, N. Fukunishi, S. Fukuzawa,[*1] A. Goto, M. Hamanaka,[*1] H. Hasebe, Y. Higurashi, E. Ikezawa, S. Ishikawa,[*1] H. Imao, T. Kageyama, O. Kamigaito, M. Kidera, M. Komiyama, Y. Kotaka,[*1] R. Koyama,[*1] H. Kuboki, K. Kumagai, T. Maie, M. Nagase, T. Nakagawa, T. Nakamura,[*1] M. Nishida,[*1] M. Nishimura,[*1] T. Ohki,[*1] Y. Ohshiro,[*2] H. Okuno, K. Oyamada,[*1] N. Sakamoto, J. Shibata,[*1] K. Suda, M. Tamura,[*1] N. Tsukiori,[*1] A. Uchiyama,[*1] H. Watanabe, Y. Watanabe, K. Yadomi,[*1] K. Yamada, S. Yamaka,[*2] H. Yamauchi,[*1] and S. Yokouchi

[*1] SHI Accelerator Service Ltd.

[*2] Center for Nuclear Study, the University of Tokyo

The 2010 operation statistics of the four ring cyclotrons (RRC, fRC, IRC, and SRC) at the RIBF are summarized in Table 1. In particular, the annual operation time of the RIKEN ring cyclotron (RRC), which is always the first energy booster in every acceleration mode, was 4069 h in 2010.

In 2010, a series of experiments involving the use of the ^{48}Ca beam were scheduled twice, in spring and autumn, in order to satisfy the large number of requests for the use of the beam. Actually, at the beginning of 2010, the backlog list showed a total of 275 days of experiments that had been approved by the Nuclear Physics Program Advisory Committee, and around 30% of these were the ^{48}Ca beam experiments. Consequently, an amount of 36% of the available operation time in 2010 was devoted to the ^{48}Ca beam operation, as shown in Table 2.

The first ^{48}Ca campaign, from May to June, was carried out very smoothly. A 345MeV/u ^{48}Ca beam with an intensity of around 200 particle nA could be delivered to the BigRIPS for a long duration of 26 days with an availability exceeding 90%. In the series of experiments, those involving the detector MUST2 were carried out in collaboration with French groups.

On the other hand, the second ^{48}Ca campaign, from October to November, faced constraints and resulted in a relatively low availability (around 60%); nevertheless, the accelerator condition was exactly the same as before. Many machine-relatited problems were faced in various places one after another. For example, serious vacuum leaks occurred twice in the RRC due to beam-loss damage in its extraction devices (the MDC2 casing and the EBM beam pipe), the two power supplies (T9-trim coil and G2 bias for the NW rf amplifier) of the IRC failed one after the other, and one of the cryogenic vacuum pumps in the IRC suddenly developed problems in its compressor and had to be was replaced. In addition, ac power lines for the injector system of the SRC was heated and disconnected due to the loosening of a screw bolt on the cable terminal. A total of 330 hr was spent in troubleshooting these problems. The ^{48}Ca beam condition was not satisfactory. The beam intensity had to be limited to less than 100 particle nA and the instability due to some power supplies all the time effected on the extracted beam in SRC. Although all the scheduled experiments were not carried out, the several remarkable results were obtained from some experiments.

Table1. Operation hours of the RRC, fRC, IRC, and SRC.

Years / Cyclotrons	2008	2009	2010
RRC	3961	4359	4069
fRC	1273	1079	72
IRC	2052	1487	1900
SRC	1308	2543	2421

After the ^{48}Ca beam experiments, in June, a 345 MeV/u ^{18}O beam was accelerated and experiments were carried out by using the Kappa magnet. Close to the end of the beam time, a serious vacuum leak suddenly occurred in the vicinity of the BigRIPS target, and the experiment was cancelled.

Thirty-seven percent of the RRC operation time was devoted to ordinary experiments in the Nishina Building, as listed in Table 2. In 2010, unlike 2009, the acceleration mode of RILAC-CSM-RRC (h8) was used frequently since the AVF operation was limited because of the installation of RILAC2, a new injector linac. ^{20}Na, ^{40}Ar, ^{58}Ni, ^{48}Ca, and ^{58}Fe beams with an energy of 63MeV/u were used at RIPS. In summer, a test of 66 MeV/u ^{87}Rb beam was made successfully and in September the beam was used in RIPS for Mossbauer experiment for the first time. A 100 MeV/u ^{18}O beam was used at RIPS for thirteen days in July for an experiment involving MUST2; this was the second experiment after that in the BigRIPS in June, which involved the use of the ^{48}Ca beam.

As shown in Table 1, the fRC was operated very few times in 2010 because there were no experiments involving a ^{238}U beam was not carried out at all. The experiments are will be scheduled after the intensity of the ^{238}U beam is increased in the new acceleration mode, RILAC2- RRC-fRC-IRC-SRC.

From January to March 2010, RILAC2 was installed in the AVF cyclotron vault. At the end of 2010, an acceleration test was successfully carried out with a xenon beam. Operation in the new acceleration mode of RILAC2-RRC- fRC-IRC-SRC is expected to be ready shortly, and the intensities of Xe and U beams are expected to increase drastically.

To prepare for a further increase in the ^{238}U beam intensity, a gas stripper with large differential pumping was tested in the D-room by using the RRC output beam, and a promising result was obtained.

Table 2. The statistics of operation corresponding to beams.

INJ	Ring cyclotrons	Particle	Experiment Course	Energy (MeV/u)	Beam tuning (hr)	Total Experiment Duration (hr)	Fractioin2 (%)
AVF	RRC	^{87}Rb	M. S.	66	17		16.6%
		^{87}Rb	RIPS	66	25	32	
		^{18}O	RIPS	100	14	331	
		^{13}C	RIPS	100	9	38	
		^{56}Fe	E5B	90	18	7	
		^{20}Ne	E5B	135	18	8	
		^{13}C	E5B	100	12	3	
		^{12}C	E5B	135	52	28	
		^{14}N	E3A	135	10	53	
	RRC-SRC	^{14}N	BigRIPS-SHARAQ	250	54	372	12.8%
		d	BigRIPS	250	43	53	
RILAC	RRC	^{58}Ni	RIPS	63	17	107	20.9%
		^{58}Fe	RIPS	63	14	132	
		^{48}Ca	RIPS	63	16	129	
		^{40}Ar	RIPS	63	18	133	
		^{23}Na	RIPS	63	31	60	
		^{238}U	E5A	8.4	24	11	
		^{84}Kr	E3A	36	19	25	
		^{84}Kr	E3A	38	31	83	
	RRC-IRC-SRC	^{48}Ca	BigRIPS-ZD	345	916	578	46.7%
		^{18}O	BigRIPS-ZD	345	196	210	
	RRC-(fRC)	^{238}U	M. S.	10.8	3	16	3.0%
		^{238}U	M. S.	10.8	15	39	
		^{70}Zn	M. S.		49		

Total operation time= 4069hr 100.0%

RIKEN Accel. Prog. Rep. 44 (2011)

RILAC operation

Eiji Ikezawa, Ohki Tomonori,* Kase Masayuki, Takahide Nakagawa, Naruhiko Sakamoto, Hiroki Okuno, Nobuhisa Fukunishi, Masaki Fujimaki, Makoto Nagase, Tadashi Kageyama, Shigeru Yokouchi, Misaki Kobayashi-Komiyama, Masanori Kidera, Yoshihide Higurashi, Tamaki Watanabe, Kazunari Yamada, Takeshi Maie, Hiroo Hasebe, Hironori Kuboki, Kenji Suda, Yutaka Watanabe, Toshimitsu Aihara,* Hiromoto Yamauchi,* Akito Uchiyama,* Kazuyuki Oyamada,* Masashi Tamura,* Akira Goto, and Osamu Kamigaito

* SHI Accelerator Service Ltd.

The RIKEN heavy-ion linac (RILAC) has been operating steadily throughout the reporting period and has been supplying various ion beams for various experiments, beam acceleration tests, and beam commissioning. Some statistics on the RILAC operation from January 1 to December 31, 2010, are given in Table 1. The total beam-service time of the RILAC accounted for 87.9% of its operation time. The two operation modes of the RILAC, namely, the stand-alone mode and the injection mode, in which the beam is injected into the RIKEN Ring Cyclotron (RRC), accounted for 34% and 66% of the total beam-service time of the RILAC, respectively.

For the beam experiments of the RI Beam Factory (RIBF), a 2.68-MeV/nucleon ^{48}Ca-ion beam accelerated by the RILAC was injected into the RRC between May and June 2010 and between October and December 2010. In addition, a 2.65-MeV/nucleon ^{18}O-ion beam was injected into the RRC between June and July 2010.

Table 2 lists the beam-service times in the stand-alone

Table 1. Statistics on the RILAC operation from January 1 to December 31, 2010.

Operation time of the RILAC	5577.0	h
Mechanical trouble	149.0	h
Stand-alone mode of the RILAC	1666.5	h
Injection mode into the RRC	3236.5	h
Total beam-service time of the RILAC	4903.0	h

Table 2. Beam-service times in the stand-alone mode of the RILAC allotted to each beam course in target rooms No. 1 and No. 2 of the RILAC in 2010.

Beam course	Total time (h)	%
e2	63.0	3.8
e3	1475.5	88.5
e4	49.5	3.0
e6	78.5	4.7
Total	1666.5	100.0

Table 3. Operation statistics on the two ion sources (18G-ECRIS and 28G-SCECRIS) in 2010; the statistics include preliminary work time. The durations for which the 28G-SCECRIS was in operation are indicated in parentheses.

Ion	Mass	Charge state	Total time (h)	
O	16	5	59.5	(0.0)
O	18	5, 6	755.5	(0.0)
Ne	22	6	130.0	(0.0)
Na	23	7	156.0	(0.0)
Ar	40	9, 11	277.5	(0.0)
Ca	48	10	2681.5	(0.0)
Ni	58	13	177.0	(0.0)
Fe	58	13	206.0	(0.0)
Zn	70	16	1568.0	(0.0)
Kr	84	19, 20	218.0	(0.0)
Xe	136	27	81.0	(0.0)
Os	188	24	126.5	(0.0)
U	238	35, (35, 41)	123.0	(442.5)
		Total	6559.5	(442.5)

mode of the RILAC allotted to each beam course in the RILAC target rooms in 2010. The e2 beam course in target room No. 1 was used in the machine study of a new gas-filled recoil ion separator (GARIS-Ⅱ). The e3 beam course in target room No. 1 was used in research experiments involving the heaviest elements and the study of the physical and chemical properties of these elements with the GARIS. The e4 beam course in target room No. 1 was used in studies in radiation chemistry. The e6 beam course in target room No. 2 was used in studies pertaining to accelerator mass spectrometry.

This year, research experiments on the heaviest elements were carried out for 18 days in March, 16 days in September, and 19 days in October.

Statistics on the operation times of an 18-GHz ECR ion source (18G-ECRIS) and a new 28-GHz superconducting ECR ion source (28G-SCECRIS), both of which use the 18-GHz microwave power source, in 2010 are listed in Table 3. Ion beams of the 13 elements listed in the table were used for various experiments, beam acceleration tests, and beam commissioning.

We carried out the following improvements and overhauls during the reporting period.

1) All devices, including the 28G-SCECRIS, were removed from the high-voltage terminal of the Cockcroft-Walton preinjector for the RILAC and were reinstalled in the new ion-source room for a new injector linac (RILAC2) of the RIBF in June 2010. Therefore, the beam transport line used for injecting beams into the RILAC was partly dismantled.
2) An electrical transformer embedded in the DC power supply of the mirror coil magnet of the 18G-ECRIS was replaced with a new one because it was worn out after many years of operation. In addition, the DC power supply was overhauled.
3) To control the injector system for the RILAC consisting of the prebuncher, FC-RFQ, and rebuncher with an experimental physics and industrial control system (EPICS), a remote-control system that uses a programmable logic controller was introduced.
4) The remote-control interface of the power supplies of the quadrupole magnets embedded in the drifts of cavities No. 4, No. 5, and No. 6 was replaced with a programmable logic controller because it was worn out after many years of operation.
5) To divide the RF reference signal of the RF amplifiers appropriately, the RF signal divider was replaced with a directional coupler.
6) The water flow switches for lower-limit flow detection in power amplifiers No. 3 and No. 4 were replaced with new ones because they were worn out after many years of operation.
7) In the RF systems, the power supplies that were in their final and intermediate stages of operation were subjected to annual inspection. In addition, the major components of mechanical parts were subjected to simple inspection.
8) Five water pumps of the water-cooling system for the ion source and the RILAC RF system were overhauled. The other water pumps were subjected to simple inspection. Three heat exchangers of the deionized water-cooling circuit for the ion source, the FC-RFQ, and devices used for experiment were overhauled. All cooling towers were subjected to monthly inspection and annual cleaning.
9) The vacuum control systems of RILAC cavities No. 1 and No. 2 were replaced with new ones.
10) All vacuum pumps were subjected to annual inspection.

We experienced the following mechanical problems during the reporting period.

1) Water had been splashed on a cavity of the FC-RFQ because of leakage from cooling pipes on the outside wall of the cavity; we repaired the pipes with a repair material as a stopgap measure.
2) Water had been splashed on RF power amplifier No. 2 because of leakage from a water joint inside the grid stub; we repaired the joint.
3) In RF power amplifier No. 2, the control-grid contact fingers that were used for electric contact with the final vacuum tube melted because of poorly fitting electrical contacts; we replaced a component with the spare component.
4) In RF power amplifier No. 5, a junction piece of the power amplifier for the RF power feeder generated abnormal heat because of poorly fitting electrical contacts; we repaired the junction piece.
5) The final vacuum tube of the FC-RFQ final RF amplifier had a problem; we replaced it with a new one.
6) The contact fingers of the shorting plate embedded in the FC-RFQ final RF amplifier were damaged in an accident when the limit switch of the shorting plate malfunctioned; we repaired the fingers.
7) There were problems in the RF power amplifier systems, the DC power supplies, the low-level controllers, the wide-band amplifiers, a programmable logic controller, a driving motor, and an air-cooling fan; we replaced each component with spare components.

AVF Operation

K. Yadomi,[*1] M. Kase, M. Fujimaki, N. Fukunishi, S. Fukuzawa,[*1] A. Goto, M. Hamanaka,[*1] H. Hasebe, Y. Higurashi, S. Ishikawa,[*1] T. Kageyama, O. Kamigaito, K. Kobayashi,[*1] M. Komiyama, Y. Kotaka,[*1] R. Koyama,[*1] H. Kuboki, K. Kumagai, T. Maie, M. Nagase, T. Nakagawa, T. Nakamura,[*1] M. Nishida,[*1] M. Nishimura,[*1] Y. Ohshiro,[*2] H. Okuno, N. Sakamoto, J. Shibata,[*1] K. Suda, N. Tsukiori,[*1] K. Yamada, S. Yamaka,[*2] and S. Yokouchi.

[*1] SHI Accelerator Service Ltd.

[*2] Center for Nuclear Study, the University of Tokyo

In table 1, the operation statistics of the K70 AVF cyclotron (denoted by AVF hereafter) from 2009 to 2010 are listed. The total operation time of AVF in 2010 amounted to 3339h, which was less the operation time in 2009 by 15%. The main reason for this was the fact that the operation of AVF was completely stopped during three months from January to March in 2010 because of the preparation and installation work for the new injector RILAC2.

RILAC2 was installed in the AVF room, along the narrow space between AVF and the west wall. The big hole (1500 mm × 1500 mm) in the 2m-thick wall at the north of the AVF room was made in January 2010, which is required for installing the LEBT (low-energy beam transport) of the RILAC2. In January and February 2010, the piping and cabling inside the room were replaced to ensure the coexistence of AVF and the new system. The installation of the RILAC2 Drift-Tube Linac cavities was started in February and finished in March 2010. On 23rd March, the official visited to inspect the change of building around AVF, especially the effect of the LEBT hole made in the shielding wall. After the inspection was over, AVF started operation in April 2010.

An output-beam line of RILAC2 merges the existing beam lines from AVF to RRC at an analyzer dipole magnet (DMC2). The simultaneous operations of the AVF and the RILAC2 are possible. The standalone operations of AVF (AVF-C03, AVF-CRIB, and AVF-E7b) can be performed together with the operation of RILAC2 for the RIBF applications. However, the effect of a transient magnetic field during the cycling of AVF magnetization on the RILAC2 beam will possibly be appreciable, although it was estimated to be small.

Table 1. The statistics of AVF operation in 2009 and 2010

	2009		2010	
Total operation time	3870		3339	
Beam tuning	701	18.1%	1016	30.4%
Injection to RRC	782	20.2%	511	15.3%
injection to RRC-SRC	547	14.1%	507	15.2%
AVF standalone	1894	48.9%	1304	39.1%
Beam course (AVF standalone)				
E7a	817	43.1%	734	56.3%
E7b	302	15.9%	74	5.7%
C03	622	32.8%	385	29.5%
Machine study	153	8.1%	110	8.4%

The AVF-RRC-SRC acceleration, which was started in 2009, was performed for 507 h in 2010. In October 2010, a nitrogen beam and a polarized deuteron beam were accelerated and injected into the RRC-SRC, and delivered to BigRIPS; the final energy of the beam was 250 MeV/u.

During the standalone operations of AVF in 2010, a total time of 734 h was dedicated to CRIB experiments, which have been managed by CNS, the University of Tokyo. This value is decreasing every year. This decrease is partly due to the fact that the CRIB experiments have been efficiently performed in the past and the number of experiments on the backlog list is small.

As part of annual university curriculum, three sets of one-day experiments were scheduled in autumn and another one was scheduled in January 2011. They were conducted smoothly by students from the University of Tokyo. The beam course was then changed from E7a (near the CRIB target) to E7b, so that the experiments could be carried out even immediately just after a CRIB experiment. So far, the residual activity was a problem for these experiments sometimes. Elastic scattering experiments involving the use of a 6-MeV/u α-beam were performed in a new vacuum chamber that was temporarily installed in the E7b course.

A vacuum leak occurred frequently in the AVF chamber after a shutdown. The leak location might have been an O-ring seal between the lower pole of the magnet and the vacuum chamber. After turn-off, a leak occurred because of the cooling effect of the magnet.

In 2010, the Hyper ECR ion source successfully produced three kinds of solid metal ions: $^{87}Rb^{+20}$ in August, $^{28}Si^{+20}$ in June, and $^{7}Li^{+3}$ in December. For producing Rb and Si ions, a Ta crucible that was heated by the ECR plasma was used. The Li and Si ions, accelerated in AVF, were used in the CRIB experiments. On the other hands, the Rb beam was accelerated in the AVF-RRC up to 66 MeV/n and delivered to RIPS where they was used in the Mossbauer experiment for the first time.

Since a 14-GHz, 1-kW klystron microwave power supply had some problem in its transmitter circuit, it was replaced with a 14-GHz TWTA power supply, which was used for the second ion source, the superconducting ECR ion source. A reserve 18-GHz klystron was used for the second ion source in summer. After tuning, the 18-GHz super conducting ECR ion source, started producing light ions: protons and He beams. It was being tuned for the production of heavy-ion, such as C, N, O, and Ar, so that it can be used as a backup for the Hyper ECR ion source in 2011.

PAC Meetings for Nuclear Physics, and Material and Life Science

H. Ueno, K. Ishida, Y. Kobayashi, and H. Sakai

Two Program Advisory Committees (PACs) are responsible for reviewing submitted proposals in the fields of nuclear physics (NP-PAC) and material and life science (ML-PAC). Each PAC holds the meetings twice a year, and reviews the proposals. The NP-PAC is co-organized by RIKEN Nishina Center and CNS, Univ. of Tokyo. The ML-PAC reviews experimental programs at RAL and RIBF.

NP-PAC

The 7th and 8th NP-PAC meetings were held Jun. 14-15 and Dec. 3-5, 2010, respectively [1]. Professor Tribble was elected chair. A new grading scale has been adopted since 7th NP-PAC, where the approved proposals were ranked with S, A, or B. Table 1 shows summary of these two PAC meetings.

ML-PAC

The 6th and 7th ML-PAC meetings were held June, 2010 and Jan. 11-12, 2011, respectively [2]. The summary of the meetings are shown in Table 2. In the 6th PAC, only proposals for RIBF experiments were called and reviewed, where discussions were made through emails. In the 7th PAC, both RAL and RIBF proposals were reviewed.

PAC members

NP-PAC: R. Tribble (Texas A&M, the chair), B. Fulton (Univ. of York), T. Glasmacher (MSU), I. Hamamoto (Lund Univ.), M. Huyse (KU Leuven), T. Kishimoto (RCNP), K. Langanke (GSI), M. Lewitowicz (GANIL), W. Liu (CIAE), T. Nakamura (Tokyo Tech.), T. Noro (Kyushu Univ.), A.A. Ogloblin (Kuchatov Institute), A. Ono (Tohoku Univ.), T. Shimoda (Osaka Univ.), K. Yabana (Univ. of Tsukuba)

ML-PAC: J.-M. Poutissou (TRIUMF, the chair), A. Amato (PSI), G.A. Beer (Univ. Victoria), F. Hanaoka (Gakushuin Univ.), R. Kato (RIKEN), K. Komaki (Univ. of Tokyo), K. Kubo (ICU), D.E. MacLaughlin (UC Riverside), S. Maekawa (JAEA), K. Nagamine (UC Riverside, RIKEN, KEK), N. Nishida (Tokyo Tech.), K. Nishiyama (KEK), F.L. Pratt (RAL), I. Yamaguchi (Tokyo Univ. of Agri.), J. Zmeskal (SMI)

References
1) http://www.nishina.riken.jp/UsersGuide/NP-PAC/
2) http://www.nishina.riken.jp/UsersGuide/ML-PAC/

Table 1. Summary of the 7th and 8th NP-PAC meetings. The sum of the proposals ranked with S, A, and B are displayed in the "approved" columns.

	7th NP-PAC (June 14-15, 2010)				8th NP-PAC (December 3-5, 2010)			
	proposals		beam time (days)		proposals		beam time (days)	
	requested	approved	requested	approved	requested	approved	requested	approved
GARIS (RILAC)	0	0	0	0	0	0	0	0
CRIB (AVF)	1	1	17	17	3	3	46	46
RIPS (RRC)	0	0	0	0	1	1	8.5	8.5
BigRIPS/ZDS	2	1	16	8	11	8	92.5	64
SHARAQ	1	1	8.5	8.5	3	3	26	26
Construction	0	1	–	–	2	2	–	–
Total	5	4	41.5	33.5	20	17	173	144.5

Table 2. Summary of the 6th and 7th ML-PAC meetings.

	6th ML-PAC (June, 2010)				7th ML-PAC (January 11-12, 2011)			
	proposals		beam time (days)		proposals		beam time (days)	
	requested	approved	requested	approved	requested	approved	requested	approved
RAL	–	–	–	–	21	20	128	59
RIBF	7	7	58	42	3	3	10.5	10.5
Total	7	7	58	42	24	23	138.5	69.5

Beam time statistics for user experiments

H. Ueno and H. Sakai

In this report, statistics related with the beam time (BT) are presented.

In FY2010, RIBF BT operation was planned to reduce large backlogs of the BigRIPS-based experiments to an appropriate amount, 1.5~2 years. The following four measures were considered:

i) To maximize the available BT for BigRIPS-based experiments, a series of experiments with the same primary beams was scheduled as much as possible.
ii) To push further the measure i), a tentative two-year plan of the primary-beam delivery, given in Table 1, has been introduced to promote efficient beam-time allocation for BigRIPS-based experiments.
iii) A parasitic BigRIPS BT was planned when main experimental groups approve.
iv) A new grading scale has been introduced by the NP-PAC, which allows efficient beam-time allocation under the limited operation budget. In fairness to past proposals, the already approved backlog experiments were also re-evaluated using the new grading scale.

The beam time and number of users' experiments in FY2010 were shown in Fig. 1. They are categorized by the accelerator operation modes. Due to the improvement of accelerator stability and the above noted BT measures, the users' beam times of BigRIPS-based experiments drastically increased in FY2010, as shown in Fig. 2, compared with that in FY2009.

Table 1. A tentative two-year plan of the primary beam for BigRIPS-based experiments. LCI denotes a light charged ion delivered with the AVF injection.

Year	Season	Primary beam
2010	Autumn	^{48}Ca & LCIs
2011	Spring	^{124}Xe & LCIs
	Autumn	^{238}U & Xe
2012	Spring	(open)

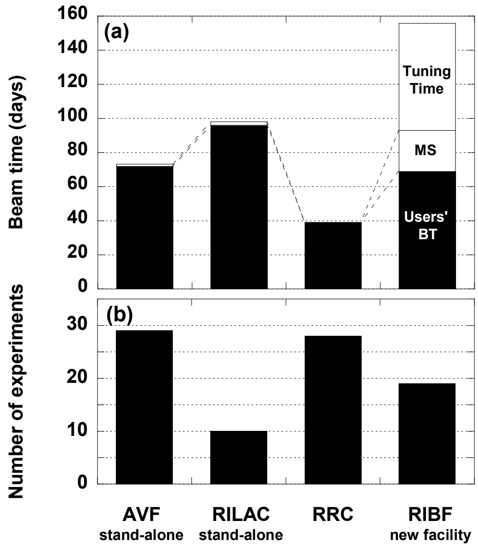

Fig. 1. Total (a) beam time and (b) number of users' experiments categorized by the accelerator operation mode. The beam time for machine studies of the facility, denoted by MS, and the tuning time of accelerator / BigRIPS are also shown for the RIBF new facility to indicate the total operation time.

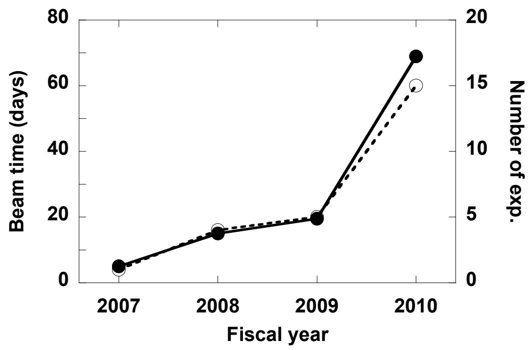

Fig. 2. The users' beam time (solid lines) and the number (dashed lines) of BigRIPS-based experiments as a function of fiscal year.

RIKEN Accel. Prog. Rep. 44 (2011)

Activities of the Industrial Cooperation Team

T. Kambara

The Industrial Cooperation team at RIKEN Nishina Center (RNC) handles non-academic activities at RIBF, i. e., industrial activities and public activities. A new project for the non-academic use of RIBF and the ongoing project of the fee-based distribution of radioisotopes are reported below.

In 2009 November, RNC started a new project that aims to make RIBF accelerators available to non-academic users in Japan. In the proposed project, RNC would open the old part of the RIBF facility, which includes the AVF cyclotron, RILAC, RIKEN Ring Cyclotron, and experimental instruments such as RIPS, to non-academic proposals from users, including private companies. Beam times are allocated to the approved proposals, and the users pay the beam time fee to RIKEN. The intellectual properties obtained by the use of RIBF belong to the users. In order to encourage the use of RIBF by those who are not familiar with the utilization of ion beams, the first two beam times in each proposal can be assigned free of charge, i. e., they would be trial uses. A new program advisory committee, industrial PAC, was set up in December 2009 to review the proposals.

The industrial PAC met for the first time in January 2010 and reviewed and approved two proposals as trial uses. One of the approved proposals, titled "Development of wear analysis technique of industrial materials with radioactive beam (Na-22)," was the implantation of a ^{22}Na beam produced at RIPS from a 63-MeV/nucleon ^{23}Na beam accelerated by RILAC and RIKEN Ring Cyclotron. The other, titled "Detection of Pr in multilayer foil on a Pd foil as a base," was trace-element analysis by accelerator mass spectroscopy (AMS) at RILAC. The beam times for both of these proposals were scheduled in February 2010, and the proposals were executed successfully. Reports of the results can be obtained from the project website (http://ribf.riken.jp/sisetu-kyoyo/reports/index.html, in Japanese). The second industrial PAC meeting was held in June 2010, where four proposals were reviewed and three of them were approved as trial uses. Two of the trials were continuations of those approved in the first industrial PAC meeting. The new proposal, titled "Irradiation test of PowerMOSFET for spacecraft," was successfully executed in December 2010 with a 36-MeV/nucleon Kr beam from the RIKEN Ring Cyclotron.

As the other project of the team, the radioisotopes (RIs) ^{65}Zn ($T_{1/2}$ = 244 days), ^{109}Cd ($T_{1/2}$ = 463 days), and ^{88}Y($T_{1/2}$ = 107 days), which are produced with a 14-MeV proton beam from the AVF cyclotron, are distributed for a fixed fee to users in Japan. This project, started in October 2007, is operated in collaboration with the Japan Radioisotope Association[1] (JRIA), which is an organization of RI users and research workers and maintains a complete system from the supply to the disposal of RIs in Japan. According to a Material Transfer Agreement (MTA) between JRIA and RIKEN, JRIA mediates the transaction of the RI distribution between RIKEN and the users. In 2010, we accepted four orders for ^{109}Cd and distributed a total amount of 30 MBq and 19 orders for ^{65}Zn and distributed 136.1 MBq; however we did not accept any order for ^{88}Y. The amount of ^{109}Cd distributed in 2010 was the same as that in 2009, but the amount of ^{65}Zn was 2.7 times higher (51.1 MBq in 2009 and 136.1 MBq in 2010). The final recipients of the RIs were eight universities and three research institutes.

Orders for RIs can be sent from inside of Japan through JRIA (FAX: 03-5395-8055, E-mail: gyomu1@jrias.or.jp). Normally, the RIs are dispatched 10 $\sim$ 16 days after the acceptance of the order.

References

1) http://www.jrias.or.jp/index.cfm/1,html (Japanese), http://www.jrias.or.jp/index.cfm/11,html (English).

Radiation Safety Management at RIBF

Y. Uwamino, H. Sakamoto, R. Hirunuma-Higurashi, H. Mukai[*1], A. Akashio, H. Fukuda, S. Fujita, T. Yamaki, K. Igarashi, K. Nakano and S. Iizuka

Residual radioactivities at the deflectors of cyclotrons have been measured regularly since 1986, and the variations in the dose rates are shown in Fig. 1. The beam intensity of AVF has been increased since 2006 for the radioisotope production, and the dose rate has also increased. In 2010, the residual radioactivity in the deflector of IRC was first measured 54 days after the end of operation with a 0.5-pμA 114-MeV/u ^{18}O beam, and the dose rate was found to be 220 μSv/h. We did not get an oppertunity to measure the deflectors of RRC and SRC in 2010.

The residual radioactivity was measured along the beam lines after almost every experiment. Spots 1–33, marked with solid circles in Fig. 2, are the locations where high dose rates were observed. Table 1 lists these dose rates and the measurement dates, beam conditions, and the decay periods after the end of operation. The maximum dose rate was found to be 12.6 mSv/h at point 21, which is the surface of the G01 Faraday cup located beyond the SRC.

We continuously monitor the radiation in and around the RIBF facility by using neutron and gamma area monitors. It is difficult to measure dose rates at the site boundary because of the existence of natural radiations. No accelerator was operated between August 9 and 25, and the dose rates at this period were assumed to be of the natural background. The net accumulated dose, i.e., the dose excluding that of the background, at the site boundary was smaller than the detection limit, which was assumed to be 8 μSv/y for gammas and 2 μSv/y for neutrons. In any case, the annual dose at the site boundary was considerably lower than the legal limit (1 mSv/y).

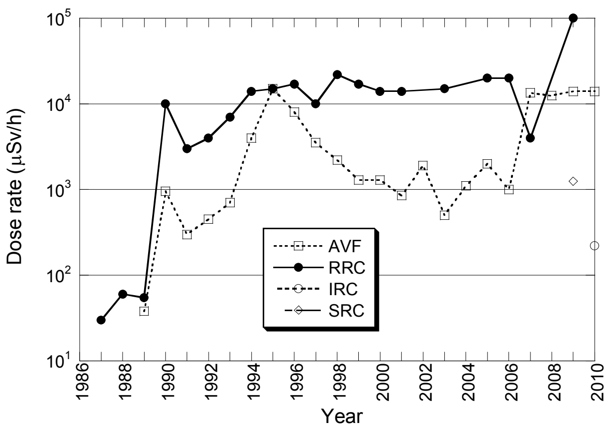

Fig. 1. Dose rates at the deflectors of AVF and RRC since 1986 and at the deflectors of SRC in 2009 and of IRC in 2010.

[*1] Japan Environment Research Corporation

Three monitors are placed at the boundary of the radiation-controlled area. One is in the computer room of the Nishina building, and two are on the roofs of the IRC and BigRIPS vaults of the RIBF accelerator building. The highest value was observed on the IRC roof as a result of the beam loss at the transport line between SRC and BigRIPS. The neutron dose was 126 ± 1.2 μSv/y, and the gamma dose was 77 ± 26 μSv/y. The dose in the computer room was 5.8 ± 1.1 μSv/y for neutrons, and 27 ± 1.4 μSv/y for gammas. The dose on the BigRIPS roof was below the detection limit of 3 μSv/y for neutrons and 4 μSv/y for gammas. The annual neutron dose at these locations since 1999 is shown in Fig. 3.

Table 1. Dose rates measured at beam lines in 2010. Points 1−33 indicate measured locations shown in Fig. 2.

Point	Dose rate (μSv/h)	Date (M/D)	Particle	Energy (MeV/u)	Intensity (pnA)	Decay period (h)
1	100	7/27	N-14	7.25	1300	31
2	3000	12/6	p	14	23000	5
3	1000	7/27	N-14	7.25	1300	31
4	120	7/22	C-13	100	666	31
5	3500	7/22	C-13	100	666	31
6	50	7/22	C-13	100	666	31
7	140	7/22	C-13	100	666	31
8	10	7/22	C-13	100	666	31
9	560	7/27	C-13	100	666	150
10	170	7/27	C-13	100	666	150
11	600	7/27	C-13	100	666	150
12	2500	7/27	C-13	100	666	150
13	130	7/27	C-13	100	666	150
14	250	6/3	N-14	135	500	797
15	25	7/22	C-13	100	666	31
16	800	10/26	d	250	100	77
17	500	10/26	d	250	100	77
18	150	7/6	O-18	345	250	130
19	110	12/21	Ca-48	345	475	100
20	240	7/6	O-18	345	250	130
21	12600	12/21	Ca-48	345	475	100
22	1500	7/6	O-18	345	250	130
23	230	7/6	O-18	345	250	130
24	800	7/6	O-18	345	250	130
25	50	7/6	O-18	345	250	130
26	33	7/6	O-18	345	250	130
27	1000	7/6	O-18	345	250	130
28	5800	12/22	Ca-48	345	475	124
29	7500	7/6	O-18	345	250	130
30	1000	12/22	Ca-48	345	475	124
31	100	12/22	Ca-48	345	475	124
32	35	12/22	Ca-48	345	475	124
33	40	12/22	Ca-48	345	475	124

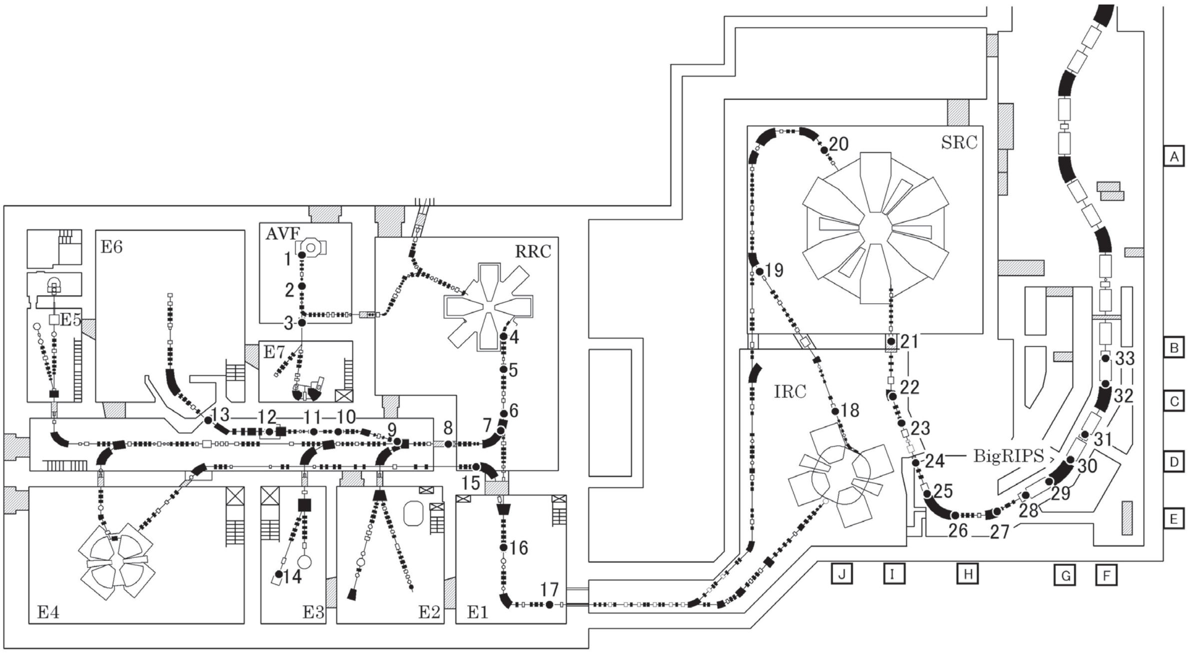

Fig. 2. Layout of beam lines at RIBF. Locations where high dose rate was observed are indicated by solid circles 1–33 and alphabets within squares A−J show the monitoring holes bored to the beam-line depth in the soil.

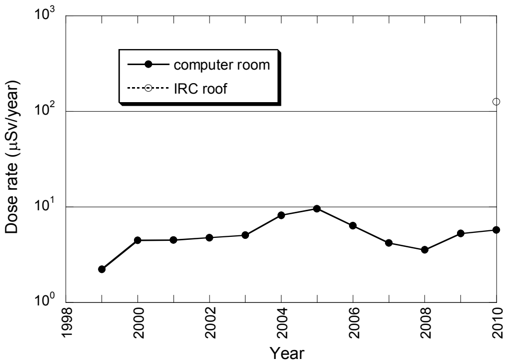

Fig. 3. Accumulated leakage radiation at the boundary of the radiation-controlled area.

Table 2. Radionuclide concentration in cooling water of BigRIPS at July 15, 2010 [a], and the allowable legal limits for drain water [b], and the ratio of the concentration to the allowable limit [a/b].

Cooling water	Nuclide	Concentration[a] (Bq/cm^3)	Limit[b] (Bq/cm^3)	Ratio to limit [a/b]
F0 target	H-3	1.9	60	3.1e-2[1)]
	Be-7	1.9e-2	30	6.4e-4
			summation	3.2e-2
Exit beam dump	H-3	5.3	60	8.8e-2
	Be-7	1.3e-2	30	4.3e-4
	Co-57	9.5e-4	4	2.4e-4
	Co-58	4.7e-3	1	4.7e-3
	Mn-54	1.1e-3	1	1.1e-3
			summation	9.5e-2
Side-wall beam dump	H-3	4.6	60	7.6e-2
	Be-7	1.5e-2	30	5.1e-4
			summation	7.6e-2

1) read as 3.1×10^{-2}

The water of closed cooling systems at BigRIPS was sampled after the operation with a 345-MeV/u 250-pnA ^{18}O beam in June, 2010, and radionuclide concentrations were measured by using a liquid-scintillation counter and a Ge detector. The results are shown in Table 2. In the case of the cooling water of the beam dumps, the summation of the ratios of the concentrations to the legal limits for the drain water of all the radionuclides was about 1/10, and the water was dumped into the drain tank. The water in the tank, which contained drain water from other places, was released after confirming that the concentration of radionuclides was lower than the legal limit. This confirmation is required by law.

We have 10 monitoring holes bored to the beam-line depth in the soil around the RIBF accelerator building, as shown in Fig. 2 by alphabets A−J, within squares. To measure the dose outside the building at the beam level, we inserted a QuIxel™ badge in it, which is the brand name of a combined personal dosimeter that includes an optically-stimulated luminescence dosimeter for photons and a solid-state track dosimeter for neutrons. The highest doses were observed in the hole I, 22 mSv for neutrons and 7.2 mSv for photons, during the beam time from October to December (3 months). A 250-MeV/u ^{14}N beam was accelerated in October and a 345-MeV/u ^{48}Ca beam was accelerated in November and December. The criterion for preventing excess activation of soil is an allowable dose of 1.3 mSv/h, which is considerably higher than the present value. During the same period, 0.05-mSv photon dose was detected in the hole J, and the doses in other holes were lower than the detection limit of 0.01 mSv.

X-ray and Residual γ-ray Monitor in SRC and IRC Vaults

H. Fukuda, Y. Uwamino, M. Kase, M. Nakamura, R. Koyama[*1] and M. Nishimura[*1]

Monitoring radiation doses of X-rays and γ-rays is a very important activity for radiation safety management. X-rays are emitted from RF cavities, and γ-rays are mainly produced by induced radioactivity. Even after a beam acceleration period is over, residual γ-rays are emitted from radio activated materials. In particular, residual γ-ray doses in SRC and IRC vaults are very high because heavy ions at high energies produce a large amount of radioactive materials. Commercially available radiation monitors, which have electric circuits at the detector head, cannot be used because the circuits are damaged by significant radiation levels during beam acceleration.

We developed ionization chambers with high sensitivity (Figs. 1 (a) and (b)) and installed them in the SRC and IRC vaults in order to monitor the radiation doses at all times. We installed two chambers in the SRC vault and one chamber in the IRC vault.

The radiation dose can be measured from electric signals received from the ionization chambers. The electric circuits of amplifiers and high-voltage power supplies are placed outside the SRC and IRC vaults. The output signals from the chambers are digitized by a data acquisition unit, and the dose rates of X-rays and γ-rays are shown by trend graphs and numerical data. Figure 2 shows a Web screen of the monitor. This screen can be seen from any computer connected to the accelerator EPICS LAN. This screen is also displayed at the entrance to the SRC vault. One can see the dose rate of residual γ-rays before entering and avoid excess exposure.

This system will be connected to the RIBF safety interlock system in the near future.

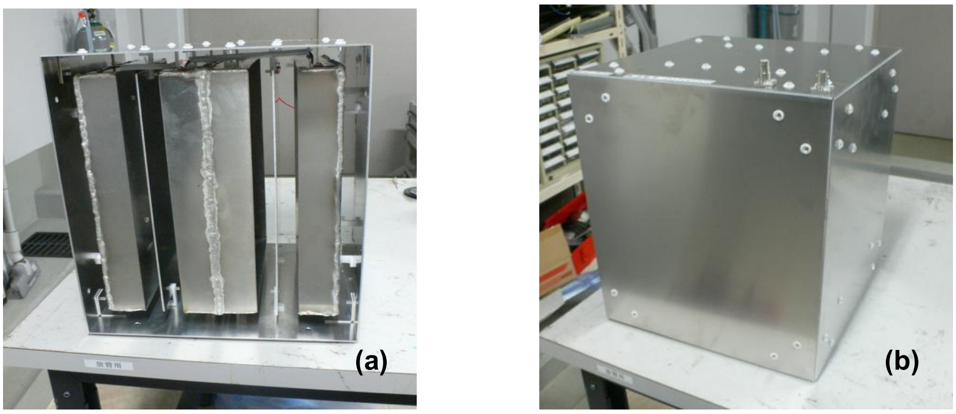

Fig. 1 View of the (a) interior and (b) exterior of the ionization chamber.

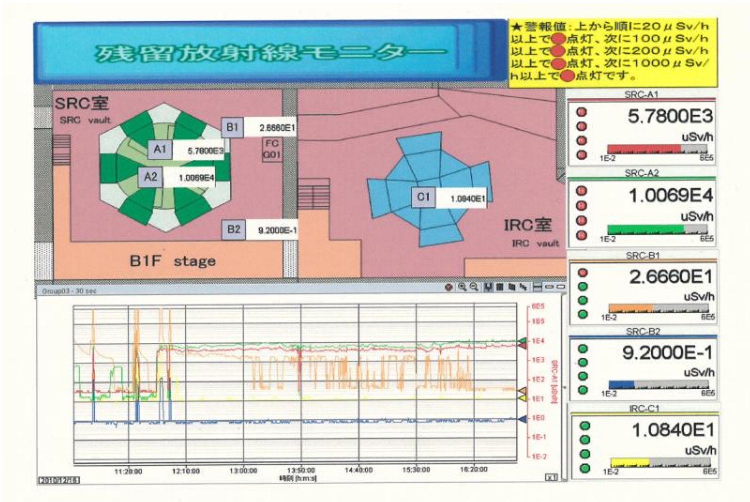

Fig. 2 The Web screen can be accessed from the accelerator EPICS LAN.

[*1] SHI Accelerator Service Ltd.

Radiation monitoring in the SRC using ionization chambers

M. Nakamura, N. Watanabe, N. Yamada, H. Okuno and M. Kase

The accelerators at the RIBF have been working well since their installation and many ion beams have been accelerated. However, beam losses in the accelerators have been a serious problem, and have restricted the intensity of ion beams.[1] For detecting such beam losses, we have constructed ionization chambers (ICs) and monitored radiations generated by the interactions between the ion beams and accelerator components. The monitoring results suggest that ICs can be used for beam-loss monitoring.[2),3] In this paper, we report the beam-loss monitoring of the SRC, which have been used for many frontier experiments. For the monitoring, we positioned seven ICs near the important components of the SRC.

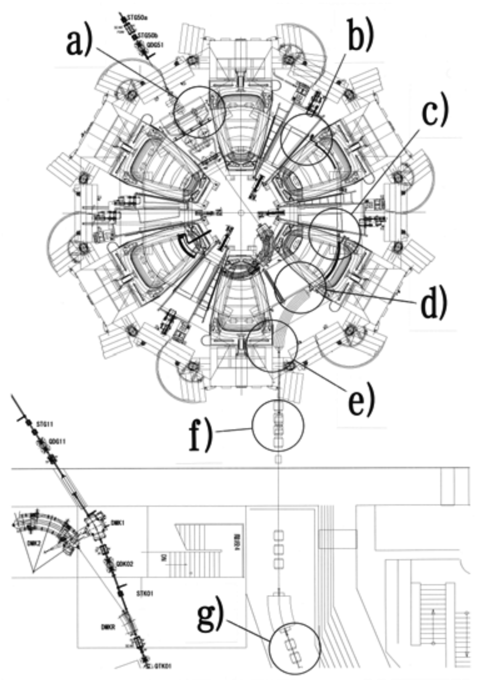

Fig. 1. Positions of ionization chambers in the SRC.

The positions of the ICs are shown in fig. 1 and are as follows: a) near the electrostatic deflection channel (EDC), b) near the entrance to the fifth superconducting magnet, c) near the entrance to the sixth superconducting magnet, d) near the entrance to the extraction bending magnet (EBM), e) near the exit of the EBM, f) near the quadrupole magnet of the SRC exit, and g) near the quadrupole magnet in BigRIPS room.

The size of the ICs and the electrodes in the ICs have been described in previous reports.[1,2,3] We used three similar amplifiers (AMPs) to detect signals from the ICs. The input resistance of these AMPs was 1 GΩ. A Matsusada HJPM-3P2-SP was used to supply power to the HV electrodes of the ICs. A Graphtec GL800 data logger was used for recording the signals, and a Yokogawa MX110 UNV-M10 data logger was used for real-time monitoring of the signals in the accelerator control room. We monitored radiations during the operation of the SRC from October 26 to December 17, 2010. During this period, $^{48}Ca^{20+}$ was accelerated to 345 MeV/nucleon. The voltage supplied to the HV electrodes of the ICs was 2 kV. Data were recorded at intervals of 5 s by the Graphtec data logger, and the data were monitored in the control room by using the Yokogawa data logger at all times.

Before we performed these measurements, we investigated the beam loss in the EDC, which is a serious problem that affects the SRC operation.[1] Ca-ion beam was attenuated to about 200 enA (1/10th the intensity under usual conditions) and the EDC was irradiated with the beam for a fairly short time for calibrating the beam loss in the EDC. When we measured the signal from IC(a) under these conditions, we could estimate the signal intensity when the beam loss was 10%. By using this result, we could calibrate the signal from IC(a) and exchange the signal intensity to beam loss. Consequently, in this experiment, the maximum voltage of IC(a) corresponding to a 10% beam loss was about 7 V. The details of this experiment have been reported in another paper.[1]

The signal from IC(a) detected by an AMP was sometimes quite strong and saturated (14 V). Therefore, for recording accurate signal values from IC(a), the input resistance of the AMP was changed

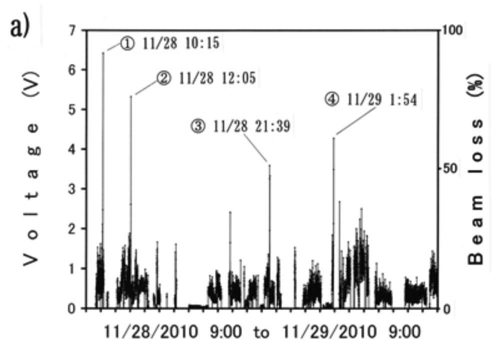

Fig. 2. Observation of the signal from the ionization chamber in position (a) in fig. 1.

to 100 MΩ. Figure 2 shows the data recorded from 9:00 on 11/28/2010 to 9:00 on 11/29/2010 as an example of the data measured by IC a).

The value of beam loss was estimated from the value of the maximum voltage in the previous calibration experiment. We can observe occasional strong signals in fig. 2. The instances when the value of beam loss was greater than 50% were compared with the records of accelerator operations. These results can be described as follows. Few minutes before ①, the state of resonator became unstable, and at ①, the temperature of the EDC suddenly increased. Moreover, a similar sudden increase in the temperature of the EDC was also observed at ②, ③, and ④. At ③ and ④, the ion-beam was stopped by an alarm signal from the EDC thermometer. We can presume that sometimes ion-beam adjustments were not suitable or these were other problems with the accelerators and that strong radiations were generated from the EDC at such instances. For other periods shown in the figure, the signals that correspond to the conditions for appropriate accelerator operation can be observed.

Figures 3(b)–(g) show the data recorded from 9:00 on 11/28/2010 to 9:00 on 11/29/2010 by the ICs at the positions (b)–(g), as shown in fig. 1. The signal from IC(g) was quite strong occasionally and was greater than 14 V. Hence, the input resistance of the AMP for IC(g) was changed to 100 MΩ. The resistance of the other ICs was 1 GΩ. The results showed that the signal from IC(b) was often strong and signals (d) and (f) were quite strong occasionally and reached close to 14 V. On the other hand, signal(c) was not so strong, and signal(e) was generally weak. Considering that the gain of signal(g) was set at 1/10, this signal was quite strong from 21:00 to 22:00 on 11/28/2010.

In this experiment, we performed simultaneous measurements of beam loss at seven important positions in the SRC. We can assume that these results reflected the SRC operations and beam transport to BigRIPS quite well. We can use the signals from the ICs to make changes to the SRC operation and to adjust the important parts such as EDC for ensuring the best operating conditions. When the signals that show beam loss increase in intensity, we can stop the SRC operation and protect the components from serious damage. For this purpose, we had input the feedback alarm signal from IC(a) (placed near the EDC) to the accelerator control room. We are now considering the alarm level that will be the most suitable for the SRC operation. However, in this study, the alarm level was set at 3 V which corresponds to about 40% of the beam loss, because as shown in fig. 2, some problems occurred in the EDC operation when the beam loss was greater than 50%. Next year, we will observe the progress of the SRC operation under these conditions and investigate the feedback alarm signals. The calibration of ICs(b)－(g) is under investigation.

References

1) M. Nakamura et al.: Proc. 7th Annual Meeting of Particle Accelerator Society of Japan, WEPS135, Himeji, Japan.
2) M. Nakamura et al.: RIKEN Accel. Prog. Rep. 42, 141 (2009).
3) M. Nakamura et al.: RIKEN Accel. Prog. Rep. 43, 138 (2010).

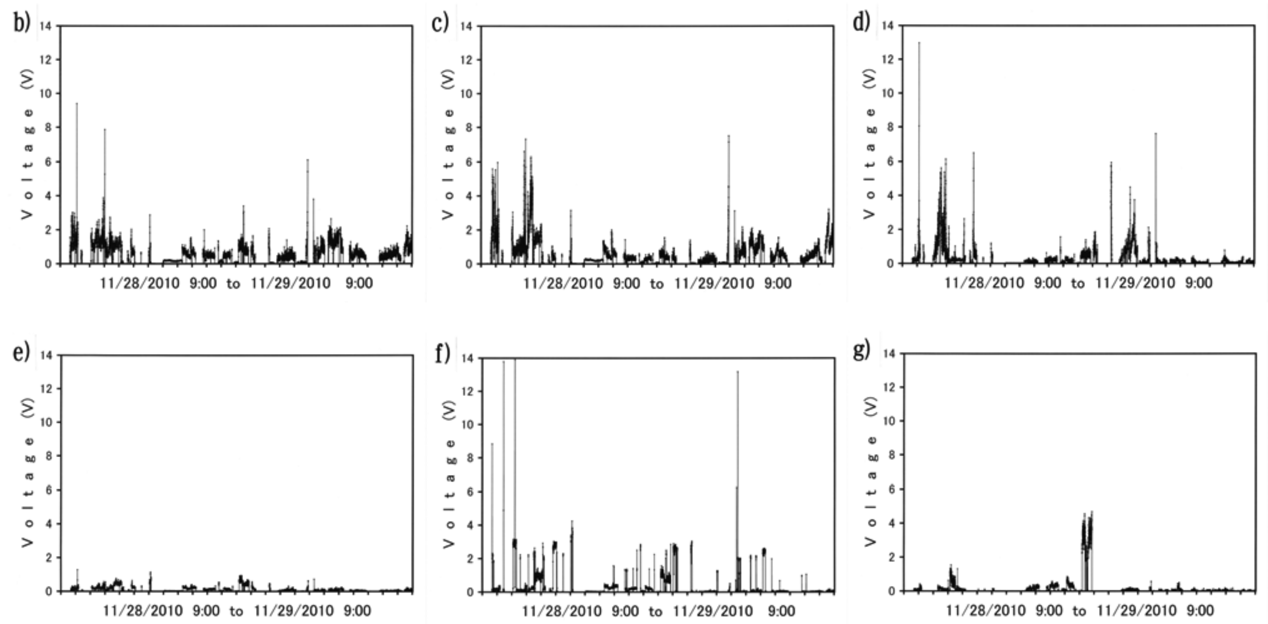

Fig. 2. Observations of signals from the ionization chambers from 9:00 on 11/28/2010to 9:00 on 11/289/2010.

Electrical activity in 2010

T. Fujinawa

1. Power supply and consumption

The RIKEN Wako campus received 134,365 MWh of electric power from TEPCO in 2010.

The RIKEN Nishina Center consumed 45,446 MWh of the received power throughout the year.

In addition, CGS supplied 22,670 MWh of electric power and 38,104 tons of saturated steam. The details are shown in Graphic 1 and Table 1.

We had three scheduled blackouts in 2010. The first one (Feb. 16 to 23) was for a new injector of the RIBF (RILAC2) cable connections; the second (Aug.11 to Aug. 20) for summer maintenance at Nishina Center; and the third (Oct. 23) for maintenance in the entire campus. CGS supplied power without interruption for important facilities such as the helium refrigerator system, ion source and buildings.

This was the first time that the ion source, SCRIT, and RRC received uninterrupted power simultaneously.

CGS showed the record highest efficiency of 68.02%, out of which the electrical efficiency was 32.02% and the thermal efficiency was 36.0%. This value was better than the efficiency of the world's latest MACC, 59%.

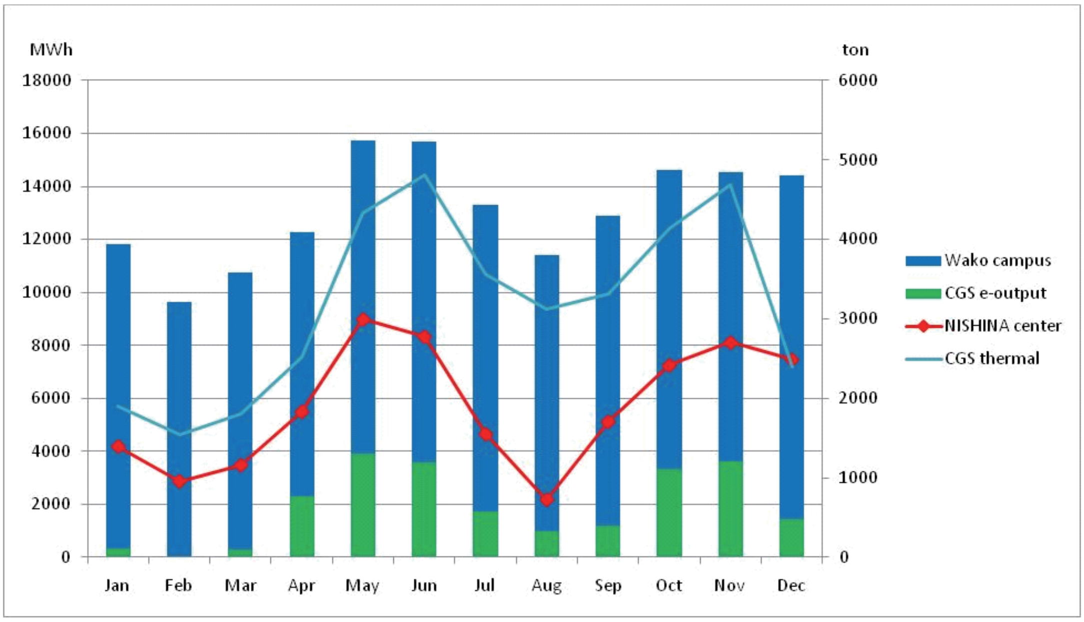

Graphic 1 Power consumptions and energy supply from CGS

	Jan	Feb	Mar	Apr	May	Jun	Jul	Aug	Sep	Oct	Nov	Dec	Total	Unit
Wako campus	11,457	9,634	10,463	9,974	11,825	12,140	11,600	10,389	11,710	11,270	10,925	12,978	134,365	MWh
NISINA center	3,846	2870	3,209	3,199	5,068	4,762	2,934	1,175	3,945	3,920	4,507	6,011	45,446	MWh
CGS e-output	343	0	269	2,297	3,921	3,569	1,716	999	1,173	3,333	3,603	1,447	22,670	MWh
NISHINA e tota	4,189	2,870	3,478	5,496	8,989	8,331	4,650	2,174	5,118	7,253	8,110	7,458	68,116	MWh
CGS thermal	1,895	1,541	1,803	2,515	4,326	4,810	3,558	3,127	3,308	4,142	4,681	2,398	38,104	tons
CGS chillers	441	358	419	585	1,006	1,118	827	727	769	963	1,088	558	8,859	kUSRT

Table 1 Power consumption of each month

CGS had a full overhaul and had its turbine blades changed. The gas turbine was sent to KAWASAKI Heavy Industry, which is located in Akashi City, Hyogo prefecture. Those tasks went on for more than one month; therefore, there was no electrical output in February.

CGS's compressor stalled twice, causing the exhaust gas temperature to rise and the system to trip. In Japan, we call this ENSUTO instead of engine stall.

These incidents occurred in July during the start time of the DSS operation, but the problem was soon solved.

We had eleven instant voltage drops in the TEPCO commercial line. All these were due to lightning strikes, and hence all of them ware force majeure. As a result, none of the equipments suffered physical damage.

2. Power supply system for RILAC2

We decided to use spare molded case circuit breakers (MCCBs) from our existing power sources instead of building an electric room and/or metal-clad switch gears for RILAC2.

This decision allowed us to save space,cost, and time.

Five distribution panels were newly constructed, and all of them were equipped with ELBs (earth leakage breakers).

The total cable length is 1,929 m and the cables run from the Ring Linac power source substation to the distribution panels. The shortest cables are from the cubicle to the RF power supply of RILAC2 on the same floor of the substation.

The longest cables are from the CGS bus and are meant for the uninterrupted power supply to the RILAC control computer, helium refrigerator, and a cooling water pump for RILAC2. For this purpose, the chilled-water supply pump for the RARF building, which is numbered 21 in the RIBF building, is equipped with a dual power supply; one from the CGS bus and the other from the commercial bus. We had four scheduled blackouts for the above construction; from Feb 16 to 23, 2010.

The contractor for this work is SHODEN-TECX Co, and as build drawings can be obtained from the archive of the RIKEN Nishina Center home page of the website.

Operation of SRC cryogenic system

H. Okuno, T. Dantsuka, Y. Mori,*[1], I. Tajima,*[1], M. Ohshima,*[1], R. Ise,*[1], T. Suzuki,*[1], K. Yamamoto,*[1] and S. Watanabe*[1]

[Superconducting ring cyclotron, cryogenic, He refrigerator]

The SRC cryogenic system, which consists of three compressors, a He refrigerator, and four He buffer tanks for cooling the 240-MJ superconducting magnets used for the SRC, has a cooling capacity of about 1 kW and an inventory of 5000 l of liquid He. The cooling system was operated for around 6 months in 2010, with a 2-month maintenance shutdown in summer (July–August), as shown Fig. 1. The trend observed for the main coil current of the SRC sector magnet is also shown in this figure. The operation in 2010 was very stable without any serious trouble or any need for stopping the operation of the cooling system. However, we identified three issues that could have caused serious problems: (1) malfunctioning of a limit switch for a low-temperature valve located in a wet environment; (2) insufficient cooling capacity for the second turbine in the He refrigerator; (3) stagnation of precooling of the superconducting magnets in the final stage of precooling.

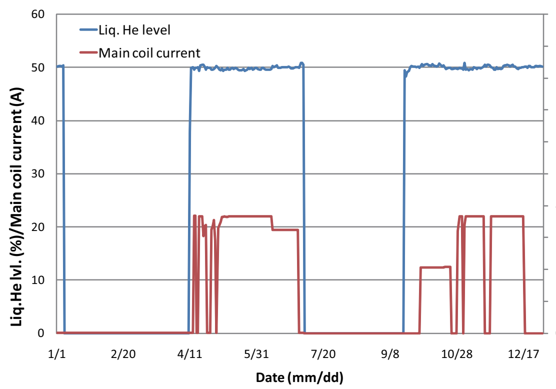

Fig. 1. Trend observed in liquid He level in the dewar and main coil current for the SRC superconducting sector magnet.

The first issue concerns the limit switch for the low-temperature valve in the control dewar on the top of the SRC magnets. On October 2, 2010, slow discharge of all the superconducting coils was triggered by the cryogenic control sequence in the beam time for the acceleration of ^{14}N. When using the cryogenic control system, we remembered the closure of the valve CV-M8501. This valve is installed for precooling the superconducting coil, and it must be left open in the excitation stage. Otherwise, He gas would accumulate in the He vessel of the main coil and cause quenching.

*[1] Nippon Kucho Service Co., Ltd

Therefore, the control sequence was so adjusted that the signal for the closure of the valve triggers slow discharge of all the superconducting coils. However, after checking the valve in the SRC room, we realized that the aforementioned signal was false and that the limit switch was soaked with water from the busbars, which are easily frozen, as shown in Fig. 2. In the next summer, we will fabricate a cover for the limit switch so that malfunctioning of the switch is prevented.

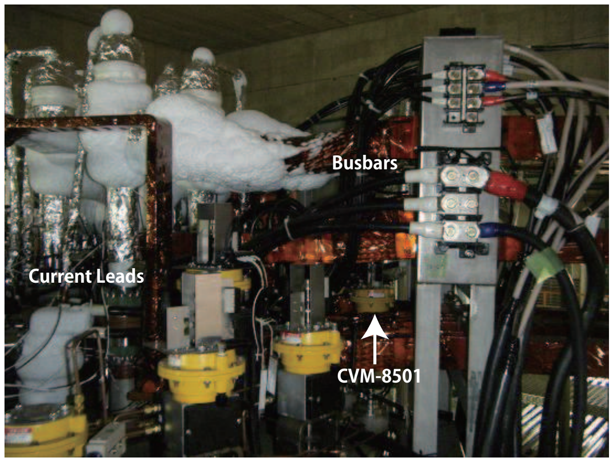

Fig. 2. Location of the CV-M8501 with busbars for the superconducting coils.

The second issue is regarding the brake gas temperature of the second turbine (T2). There are four turbines cooled by water. The water flow cools the brake gas and cartridge of the turbine. When the temperature of the brake gas reaches 89.5 ^{o}C, the turbine trips. Figure 3 shows that the brake gas temperature for T2 reaches about 80 ^{o}C of in June and July as the atmospheric temperature increases, suggesting that there is a high risk of T2 tripping because of the high temperature level; the current flow rate of the cooling water used for the break gas is not sufficient. Hence, we increased the pipe diameter for the cooling water supply from 25A to 40A. This enlargement helps in decreasing the brake gas temperature for T2 by 2–3 degree. We can thus reduce the risk of the aforementioned tripping of T2 during summer (June and July).

The third issue concerns the stagnation of the precooling of the superconducting magnets. Two precooling operations for the SRC were scheduled in April and September, 2010. In both cases, the cooling stagnated at around 16 K in the final stage of the precooling of the cold mass, as shown in Fig. 4. The T4 bypass

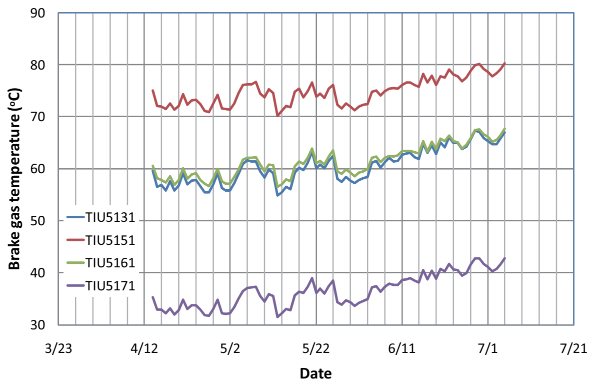

Fig. 3. Trend in the brake gas temperatures for the four turbines.

valve position is now automatically controlled to go to zero depending on the return temperature during precooling. However, we must change the mode to manual control to proceed with the precooling. In other words, the valve must be closed earlier than it would be under automatic control and hence, less He will be availavle for cooling the cold mass. In the next precooling operation in the autumn of 2011, we will try to optimize the CV value of the bypass valve in the final precooling stage to prevent stagnation and justify why the bypass valve setting should be changed to the automatic mode.

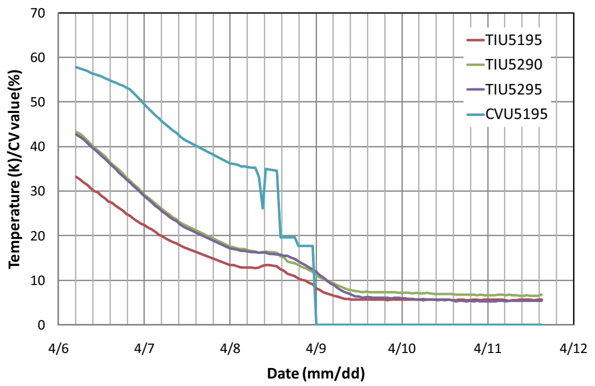

Fig. 4. Trend in the return and supply temperatures for the T4 bypass valve (CV3195) in the final stage of precooling of the SRC superconducting magnets.

In summary, operation of the He refrigerator system in 2010 was successful, although three issues that may cause serious problems were identified. The first issue, malfunctioning of the limit switch for the cryogenic valve, will be resolved in the next summer during the regular maintenance period. The second issue, insufficient cooling capacity for the second turbine, has already been resolved by increasing the diameter of the pipes used for cooling water supply. The third issue, stagnation of precooling of the superconducting magnets, will be resolved by changing the sequence program during the precooling operation.

Present status of the BigRIPS cryogenic plant

K. Kusaka, M. Ohtake, T. Kubo, K. Yoshida, A. Yoshida, T. Ohnishi, Y. Yanagisawa, N. Fukuda, Y. Yano,

Y. Mori*[1], I. Tajima*[1], R. Ise*[1], M. Ohshima*[1], T. Suzuki*[1], K. Yamamoto*[1], S. Watanabe*[1],

M. Nobutoki,*[2] M. Noguchi,*[3] N. Suzuki,*[3] H. Ito,*[4] T. Tsuchihasi,*[4] and K. Sato*[4]

Long-term (9-10 months) continuous operations of the BigRIPS cryogenic plant started in 2008, with an improved compressor unit[1]. Every year, we start the operation of the cryogenic plant with the purification of the helium gas after the summer maintenance. After the purification operation, the five superconducting triplet quadrupoles (STQ1-STQ5) are then cooled to 4 K in 2-3 weeks, and it takes few more days to fill the cryostats with liquid helium. The liquid helium level in the cryostats was kept constant in the steady-state operation in a refrigerator mode, and the STQs are excited according to the schedule of the experiments. The period of the steady-state operation is about 9 months, and we stop the turbines of the refrigerator in early summer for maintenance.

Before the improvement of the oil-removal module of the compressor unit, in the early summer of 2008, the periods of the steady-state operation in the refrigerator mode were less than 2 months[2,3]. The cooling capacity decreased gradually in each operation cycle, and we had to warm up the cold box to recover the cooling capacity. The reason for the decreasing cooling capacity was oil contamination in the heat exchangers, and therefore we improved the oil-removal module of the compressor unit. In ref. 3, the improvement and cleaning of oil-contaminated heat exchangers and high-pressure lines in the cold box have been reported in detail. After the improvement, we have carefully controlled the oil contamination level of the helium gas during operations. Here, we report our studies on oil contamination performed over the past 2 years.

The design of the improved compressor unit is schematically shown in Fig. 1. Our main compressor is of the 2-stage oil-flooded screw type, with a flow rate of 73.5 g/s and a discharge pressure of 1.60 MPaG. The improved 5-stage oil-removal module comprises an oil vessel with a demister that is used as a bulk oil separator (1SP), three coalescer vessels (2SP, 3SP, and, 3.5SP), and two adsorbent vessels (4SP and 5SP) that contain activated charcoal and molecular sieves. The oil-separation vessels newly introduced in 2008 are indicated as “New” in Fig. 1. The compressor lubricant applied to the screws is separated from the discharged helium gas by using the 5-stage oil-removal module, and the oil contamination is expected to be 0.008-0.02 ppm, on the basis of the manufacturer’s experience.

*1 Nippon Kucho Service Co., Ltd.
*2 Taiyo Nippon Sanso Corporation
*3 Mayekawa Mfg. Co., Ltd.
*4 Toshiba Corporation

Each coalescer vessel contains four coalescer filters, and the drain oil separated from the helium gas is sent to the compressor via a drain line with solenoid valves, depending on the oil level in the vessel. The coalescer filters, manufactured by Domnick Hunter, must be replaced every two years to maintain its oil-separation performance. We replaced all the coalescer filters during the summer maintenance in 2008 and 2010. The expected oil contamination levels at the entrance of the coalescer vessels are 2500, 15-50, and 0.75-1.25 weight ppm (wt. ppm) for 2SP, 3SP, and 3.5SP, respectively.

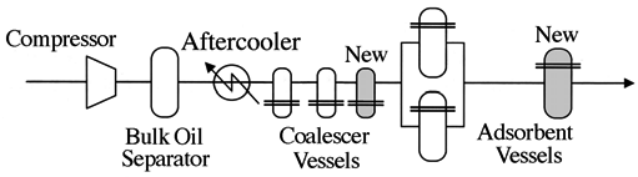

Fig. 1. Schematic diagram of the improved compressor unit.

Since 2008, we have repeatedly measured the oil contamination at the exit of the coalescer vessels with an oil check kit[1]. Figure 2 shows the contamination measured at the entrance of 3SP as a function of the coalescer operation time. An estimate from the oil drain from the 3SP is also shown in Fig. 2. We estimate the oil contamination level by measuring the operation interval of the solenoid valve installed in 3SP. The oil check kit values for the 2008 and 2009 operations, shown as open diamonds in Fig. 2, show an increase from 12.5 wt. ppm to 75 wt. ppm up to an operation time of 2500 h, and it then stays constant up to 13500 h. The estimates from the oil drain, shown as solid diamonds, also show a gradual increasing tendency of the oil contamination. On the other hand, the oil check kit values for the 2010 operation, shown as open triangles, start from 0.25 wt. ppm and increase to 25 wt. ppm up to an operation time of 3500 h (end of January 2011). The estimates from oil drain data for 2010, shown as solid triangles, are also around 30 wt. ppm and roughly 1/3 of the values for 2008 and 2009.

In Fig. 3, we show a similar analysis of the oil contamination at the entrance of the third coalescer vessel 3.5SP. The definition of the symbols in Fig. 3 is identical to that in Fig. 2. In 2008, since the solenoid valve caused to remove the drain oil attached to the 3.5SP vessel did not work, drain oil was manually removed and the amount of oil was measured. The solenoid valve was fixed during the summer maintenance in 2009 and the operation interval of the solenoid valve was recorded as well as 3SP case. The oil contamination level was then evaluated by measuring the amount of the drain oil in 2008 operation (from 1150 h to 6500 h in Fig. 3) and by counting the motion of the solenoid valve for the 2009 operation. Although data are scattered, both methods give similar results. The oil check kit results are also consistent. A gradual increasing tendency of the oil contamination is seen in the 2008 and 2009 operation. This tendency suggests that the performance of the coalescer filters declines after 10000 h of operation. Therefore, we have replaced all the coalescer filters during the summer maintenance of 2010. After the replacement, the oil contamination level was found to be significantly low (0.25 wt. pppm) up to an operation time of 3500 h, in both the oil check kit result and the oil drain estimation (shown as the open and solid triangles). We shall continue observations until we stop the compressor, to figure out the reason for the decline in the filter performance.

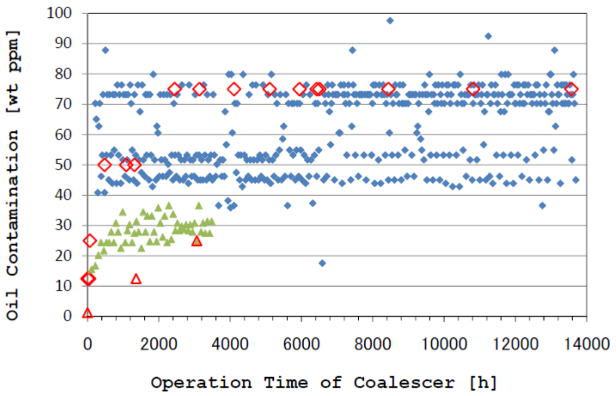

Fig. 2. Oil contamination at the entrance of the second coalescer vessel (3SP).

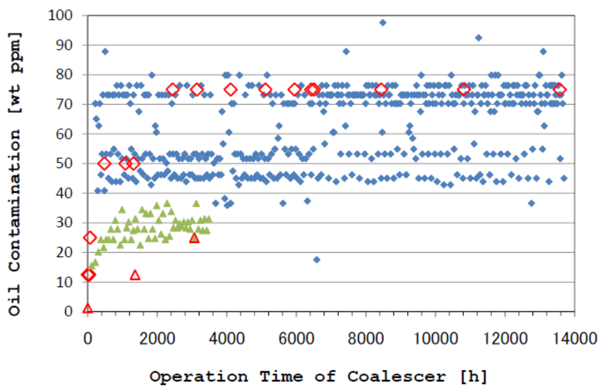

Fig. 3. Oil contamination at the entrance of the third coalescer vessel (3.5SP).

Although we have tried to measure the oil contamination at the exit of 3.5SP with the oil check kit several times, the values obtained have always been less than 0.25 wt. ppm, which is the lower measurement limit of the oil check kit. We applied a warm trap method instead[1]. The values obtained were less than 40 wt. ppb up to 6500 h and 0.7 wt. ppm at 11109 h of coalescer operation time. This also indicates a decline in the coalescer filter performance.

In addition to replacing the coalescer filters, we have replaced the adsorbent in 4SP and 5SP to maintain the performance of the oil-removal modules. The 4SP adsorbent vessel contains activated charcoal and molecular sieves, and they are replaced with new ones every year. On the other hand, the 5SP vessel contains activated charcoal only, which is scheduled to be replaced every 2 years.

The measurement of oil contamination at the final exit of the oil-removal module, namely, at the exit of 5SP, was also carried out by the cold trap method[1]. The measurements have been carried out twice so far. The first measurement was performed after 68 h of operation time from the improvement of the compressor unit and the value obtained was less than 10 wt. ppb. The second measurement was carried out after 13574 hours of coalescer operation time and after 7069 h of operation of the adsorbent of 4SP and 5SP, and the value obtained was 41 wt. ppb. We are planning the third measurement at the end of the 2010 operation, namely, in June 2011.

In addition to the maintenance of the oil-removal modules, we have serviced several compressor components during every summer shutdown period. The water line of the aftercooler was washed and the oil pump was serviced in 2009. In 2010, the main compressor unit was shipped to the manufacturer's factory. The compressor was disassembled and its interior, including screws, was cleaned (see Fig. 4). The mechanical seal and thrust and main side bearings were replaced with new ones. All the used components were checked carefully and no significant mechanical damage was found. All components were cleaned and reassembled at the factory, and the rebuilt compressor was successfully installed on site in July 2010.

The continuous operation of the cryogenic plant started on Sept. 9, 2010. After 12 days of precooling and 3 days of liquefaction operation, steady-state operation in the refrigerator mode started on Sept. 25, 2010, and we are planning to maintain continuous operation up to the end of June 2011.

Fig. 4. Disassembled compressor casing at the manufacturer's factory.

References
1) K. Kusaka et al.: RIKEN Accel. Prog. Rep. **43**, 309 (2010).
2) K. Kusaka et al.: RIKEN Accel. Prog. Rep. **41**, 244 (2008).
3) K. Kusaka et al.: RIKEN Accel. Prog. Rep. **42**, 309 (2009).

Present Status of Liquid-Helium Supply and Recovery System

T. Dantsuka, H. Okuno, Y. Odashima, M. Nakamura, T. Maie, K. Kato, K. Ikegami, M. Kase,
M. Ohshima*, R. Ise*, Nippon Air Conditioning Service K.K.*

The liquid-helium supply and recovery system[1)], which can produce liquid helium at a rate of 200 L/h from pure helium gas, has been stably operated since the beginning of April 2001. The volumes of liquid helium that were supplied each year from 2001-2009 are listed in Table 1 and also shown in Fig. 1. The volume gradually increased from 2001 to 2008, but decreased sharply in 2009. While the amount of liquid helium used by the Exploratory Materials Team increased, that used by other major laboratories decreased from 2008. In particular, the Laboratory for Human Brain Dynamics at the Brain Science Institute (BSI) had stopped using liquid helium by the end of September 2008.

We extended the recovery pipe at two places. First, a new recovery pipe was connected to the existing pipe at the Frontier Material Research Facilities at B1F. Next, new recovery pipes were connected to the existing pipe in the Main Research Building at B1F.

The control system of the compressor for liquefying helium gas tripped several times between December 2009 and February 2010. The cause was not well understood. It might have been related to the temperature of the cooling water.

The purity of helium gas recovered from laboratories gradually improved once the construction of the system was completed. The volume of helium gas recovered from each building in the Wako campus and the volume transported to the liquid-helium supply and recovery system were measured. The recovery efficiency, which is defined as the ratio of the amount of recovered helium gas to the amount of supplied liquid helium, was calculated. The recovery efficiency for the buildings on the south side of the Wako campus, such as the Cooperation Center building of the Advanced Device Laboratory, the Chemistry and Material Physics building, and the Nanoscience Joint Laboratory building, increased to a value above 90%. The average recovery efficiency from January 2008 to July 2010 is shown in Fig. 2. It increased to a value above over 90%.

References

1) K. Ikegami et al.: RIKEN Accel. Prog. Rep. 34, 349 (2001).

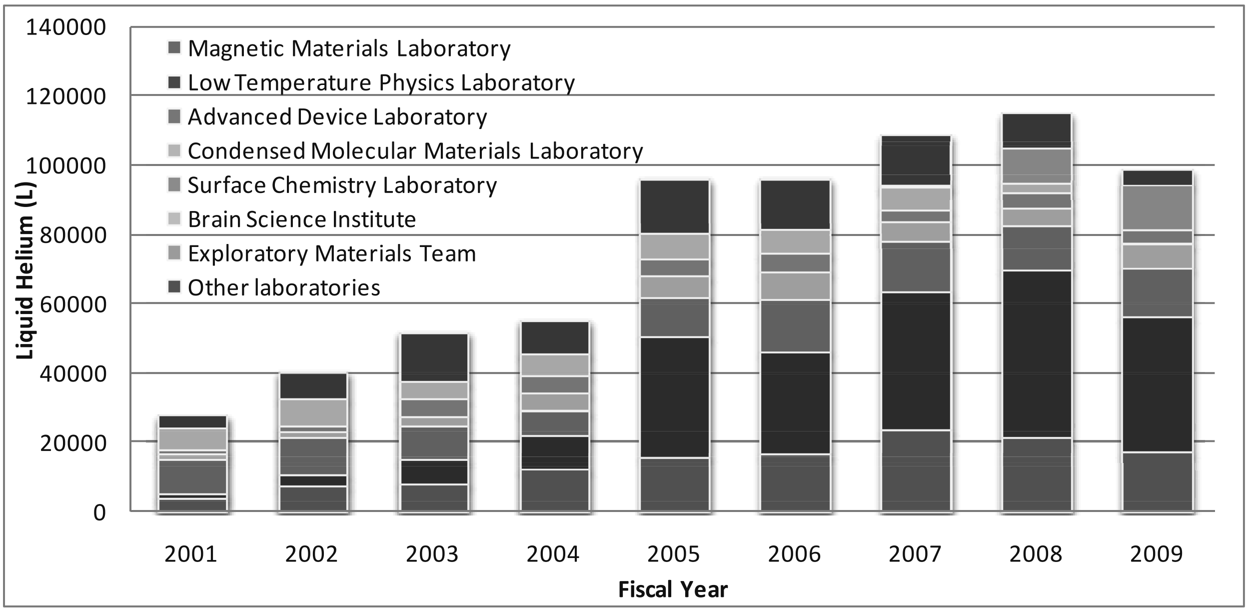

Fig.1. Volumes of liquid helium supplied to laboratories per year from fiscal 2001 to 2009

Table 1. Volumes of liquid helium supplied to laboratories per year from fiscal 2001 to 2009

Fiscal Year	2001	2002	2003	2004	2005	2006	2007	2008	2009
Laboratory / Institute	Amount of liquid helium supplied (L)								
Magnetic Materials Laboratory	3392	7024	7713	11829	15672	16512	23282	20899	16971
Low Temperature Physics Laboratory	1270	3090	6966	9515	34713	29520	39855	48756	38860
Advanced Device Laboratory	9977	10849	9726	7401	11264	15017	14733	12554.5	14306.5
Condensed Molecular Materials Laboratory	1939	1615	3079	5353	5912	7772	5331	5459.5	7015.5
Surface Chemistry Laboratory	1146	1676	4533	5007	5370	5486	3636	4080.5	3920.5
Brain Science Institute	6277	8144	5055	6292	7285	6956	6480	3226	0
Exploratory Materials Team							624.5	9853.5	13207
Other laboratories	3535	7730	14476	9487	15717	14767	14628.5	9862.5	4198.5
Total	27536	40182	51530	54884	95933	96030	109194	114691.5	98479

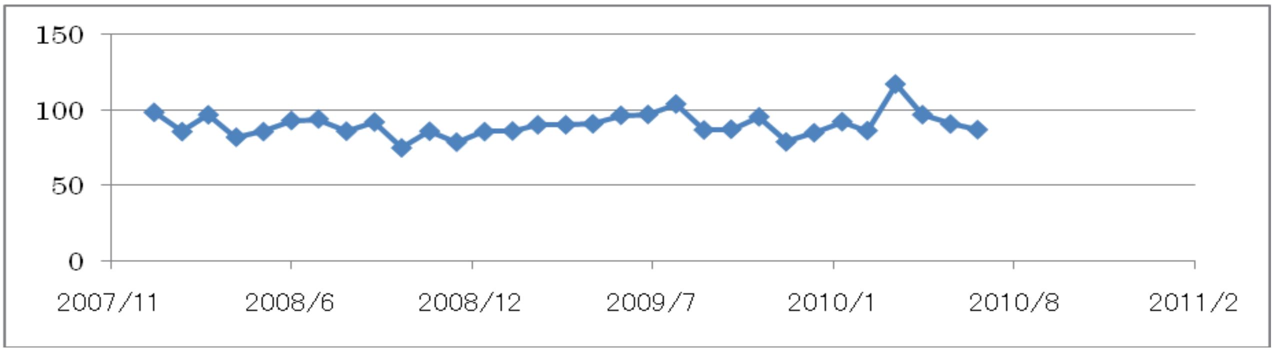

Fig.2. Average recovery efficiency measured from January 2008 to July 2010

Optimization of control sequences for He liquifier

H. Okuno, T. Dantsuka, Y. Odajima, S. Tsuruma, R. Ise,[*1] and M. Ohshima,[*1]

[Liquid He, control sequence]

It has been a decade since the operation of the He liquifier (TCF50, 200 L/s) at the Wako campus was started. Figure 1 shows a basic flow diagram of the liquefier with a liquid helium dewar. Supply of liquid He has increased over the past decade and has now reached 100000–110000 L/year. However, in this decade, we have encountered some problems such as blowing up of an emergency valve and tripping of the first turbine (T1) during pre-cooling of the liquefier. The loud noise due to the blow of the emergency valve frightens the people who are around the liquefier. The tripping of the turbine increases the risk of turbine damage and delays the start of the normal operation by about 20 min, and as a result, the time for producing liquid He in the routine operation (about 5 h) decreases. Table 1 shows the frequencies of the problems encountered before and after adopting three series of measures that mainly included changes in the sequence of operation of the liquifier. From Aug. 1, 2008 to Aug. 11, 2009, when no measures were implemented to prevent the problems, the emergency valve blew up at a frequency of 26% and T1 tripped at a frequency of 48%. The first series of measures implemented in August 2009 reduced the frequency of T1 trip to 6%. The emergency valve did not blow up after the second series of measures were implemented in November 2010, but the second turbine (T2) started tripping at a frequency of 8%. The third series of measures were implemented at the beginning of 2011 to stop the tripping of T2.

When the liquefier starts pre-cooling during routine operations, the dewar contains liquid helium that occupies 30–60% of the dewar volume. The parts of the liquefier are cooled by two turbine expanders by opening the JT bypass valve (CV3175), while the supply/return lines from/to the dewar remain warm. After the temperature of the outlet stream from T2 reaches 30–60 K, the liquifier comes in contact with the liquid helium dewar, and then, the warm gas between the liquifier and the liquid helium dewar will typically be at a temperature of 150–200 K, which will make the making the operation of the liquifier unstable. Figure 2 shows an example of trends of the temperature at the return valve from the dewar (TI3290) and at T2 outlet. The plot for TI3290 has the two peaks, while that for T2 decreases monotonically. The first peak that temporally reaches about 180 K can be attributed to the warm gas from the dewar when the return valve (CV3290) starts to control the pressure of the dewar to set the pressure at 0.024 MPa. In this operation, the initial pressure of the dewar is 0.032 MPa, which pushes the warm gas to the liquifier. The second peak can be attributed to the warm gas from the dewar when the JT valve (CV3170) and the throttle valve (CV3165) start opening to facilitate the flow between the liquifier and the dewar. We can easily imagine that the injection of the warm gas into the cooled liquifier will render the operation unstable. The three series of measures implemented to overcome the problems related to the liquifier focused on how to extract the heat of the pipes without affecting the pre-cooling of the liquifier. Furthermore, as a result of the various initial conditions (dewar pressure and temperature in the liquifier) during the routine operation, it becomes difficult to overcome the problems.

The first series of measures involved changing the rotation speed of T1 whose nominal speed and trip speed are 4650 rps and 4800 rps, respectively. Although the T1 rotation speed is controlled by the flow of the braking gas, the flow rate through the turbine and the temperature around the turbine easily change the real T1 rotation speeds. In most cases, the fluctuation of the rotation speed results in the tripping of the turbine. Therefore, we change the set value of the rotation speed from 4650 rps to 4300 rps during the pre-cooling. After the end of the pre-cooling of the liquifier, the turbine speed increases slowly from 4300 rps to 4650 rps. This change decreases the frequency of tripping of the first turbine from 48% to 6%. The reason why tripping was not completely avoided is that in rare cases, the turbine has such substantial disturbances that the rotation speed exceeds the set value by more than 1500 rps.

The second series of measures was to prevent the blow of the emergency valve located in the pipe be-

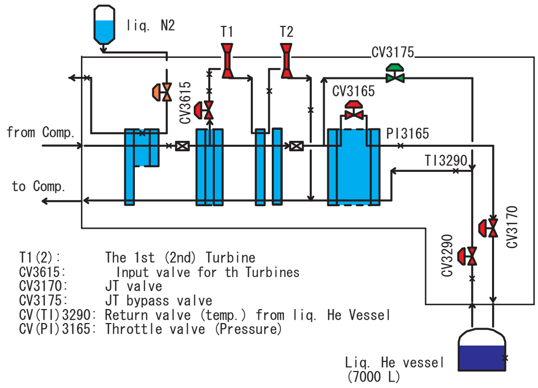

Fig. 1. Flow diagram of the liquifier.

[*1] Nihon Kuchou Service

Table 1. Frequencies of the problems encountered (blow of emergency valve and tripping of the turbines).

	2008/9/1 - 2009/8/11	Aug. 2009	2009/8/12 - 2010/11/1	Nov. 2010	2010/11/2 - 2010/12/28	Jan. 2011	2011/1/5 - 2011/1/19
E. V.	50/195 = 26%		59/238 = 25%		0/36 = 0%		0/8 = 0%
T1 trip	94/195 = 48%	Meas. 1	15/238 = 6%	Meas. 2	0/36 = 0%	Meas. 3	0/8 = 0%
T2 trip	0/195 = 0%		0/238 = 0%		3/36 = 8%		0/8 = 0%

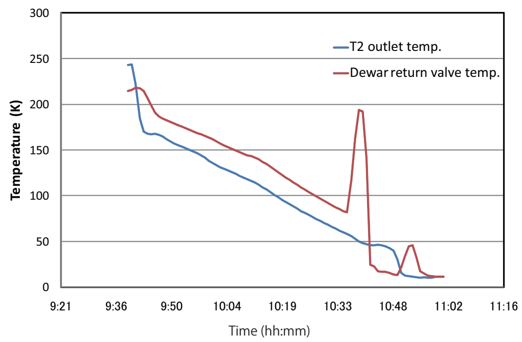

Fig. 2. Example of the temperature trend at T2 outlet and return valve of the dewar.

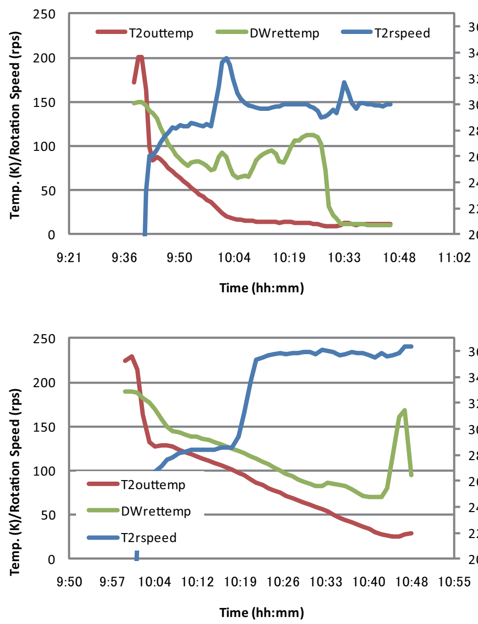

Fig. 3. Trends of the T2 outlet temperature, return valve temperature, and T2 speed. The upper (lower) graph shows the trends when CV3170 = 20(50)%

tween CV3165 and CV3170. The valve blows when the CV3165 starts controlling the pressure of PI3165 to be 0.4 MPa, thus facilitating the flow between the liquifier and the dewar. At that time, CV3170 is open up to 20%. After the pressure control starts, CV3165 starts opening and closes completely due to pressure rise. Although the CV3165 is fully closed, the rise in pressure does not stop until it reaches the pressure at which the emergency valve is set to blow up (1.6 MPa). After the valve blows 5–6 times on an average or a maximum of 10 times, the pressure starts to decrease and normal pressure control process starts working. This phenomena indicates that the temporal pressure increase is due to a type of “liquid close” because 20% opening of CV3165 is too small to facilitate the flow between the liquifier and dewar. We changed the opening value of CV3165 from 20% to 50% to prevent this rise in pressure. After this change, the blow of the emergency valve has never happened.

The second series of measures stopped the blow of the emergency valve. However, T2 started tripping at a frequency of about 8% after the measures were implemented. The T2 tripping occurred when the initial pressure was below 0.024 MPa. Figure 3 shows the temperature trends of T2 outlet and dewar return valve when the opening values of CV3170 were 20% and 50%. The upper graph in Fig. 3 shows the trends when the opening value of CV3170 was 20%. The flow between the liquifier and the dewar starts after T2 outlet temperature reaches 30 K. The flow is very slow, showing slow increase in the return-valve temperature. Such slow increase in the temperature does not affect the T2 outlet temperature. The set value of T2 rotation speed falls from 3600 rps to 3000 rps after T2 outlet temperature reaches 20 K. Because the rotation speed at which T2 trips is 3700 rps, after setting the speed to 3000 rps, the risk of tripping becomes very low. The lower graph shows the trends in the case of opening value of 50%. In this case, the flow of the warm gas is so fast that the return-valve gas temperature increase quickly up to 180 K. Such a quick increase affects the T2 outlet temperature. T2 temperature remains above 20 K and starts rising as shown in the graph. When the T2 rotation speed is set as 3600 rps, the actual rotation speed rises up to 3700 rps and causes tripping. This phenomena indicates that the warm gas should be extracted as soon as possible. We changed the temperatures at which the control of PI3165 (dewar pressure) starts from 30(60) K to 60(90) K to extract the warm gas at a higher-temperature stage. These changes were introduced at the beginning of 2011. We have not experienced the tripping of T1 and T2, and the blow of the emergency valve after these changes were introduced.

V. ORGANIZATION AND ACTIVITIES
OF RIKEN NISHINA CENTER
(Activities and Members)

2010/10/1

Organization Chart of Nishina Center for Accelerator-Based Science

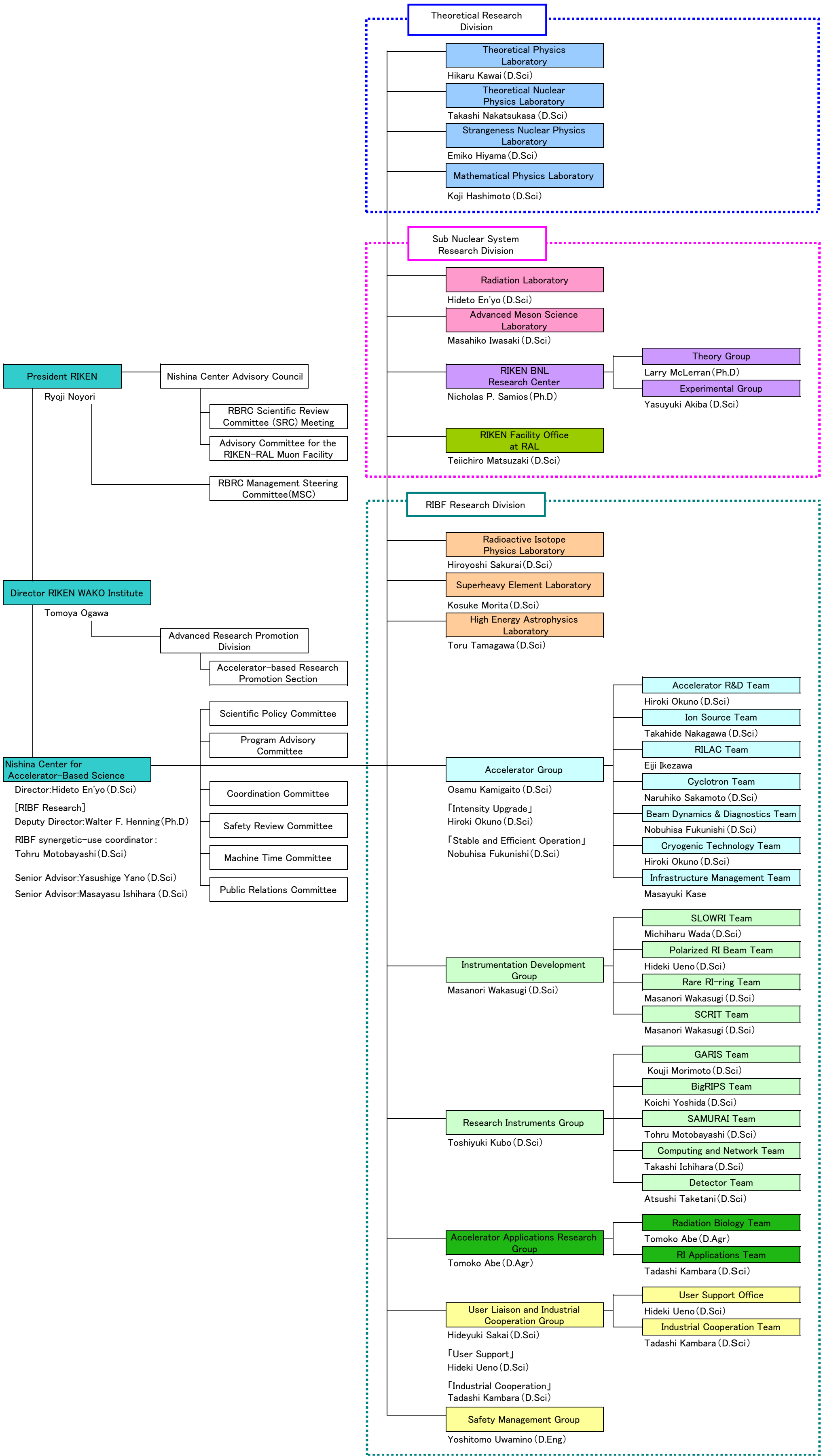

Members of Nishina Center for Accelerator-based Science

Executiv Members

Hideto EN'YO (Director)
Walter F. HENNING (Deputy Director)
Tohru MOTOBAYASHI (RIBF synergetic-use coordinator)
Yasushige YANO (Senior Advisor)
Masayasu ISHIHARA (Senior Advisor)
Minami IMANISHI (Secretary)

Research Promotion Section Members

Motohide YOKOTA (Director, Advanced Research Promotion Division)
Shigeki ASAKAWA (5/1～)
(Manager, Head of Accelerator-based Research Promotion Section)
Kyoji YAMADA
Hiroshi MIYAMOTO (～11/30)
Takamori SHIMANA
Mari AOKI (12/1 ～)
Masatoshi MORIYAMA
Yukiko SATO
Rie KUWANA
Yuko OKADA

Nishina Center's Committee Members

Scientific Policy Committee Members

July, 2010

(Chair) Shoji NAGAMIYA (J-PARC Center)
Yasuhiko FUJII (Comprehensive Research Organization for Science and Society)
Yoshiyuki FUJII (National Institute of Polar Research)
Shoji FUTATSUKAWA (Japan Radioisotope Association)
Osamu HASHIMOTO (Tohoku University)
Ryutaro HIMENO (RIKEN)
Ryosuke KADONO (KEK)
Tadafumi KISHIMOTO (RCNP of Osaka University)
Hitoshi NAKAGAWA (National Agriculture and Food Research Organization)
Mitsuaki NOZAKI (KEK)
Hideo OHNO (JASRI)
Takaharu OTSUKA (CNS)
Osamu SHIMOMURA (KEK)
Kazuo SHINOZAKI (RIKEN)
Kohei TAMAO (RIKEN)
Hirokazu TAMURA (Tohoku University)
Hirohiko TSUJII (NIRS)
Akira UKAWA (University of Tsukuba)

Program Advisory Committee meeting for Nuclear Physics Experiments at RI Beam Factory (NP-PAC) Members

June, 2010 / December, 2010

(Chair) Robert TRIBBLE (Texas A & M University, USA)
Brian FULTON (University of York, ENGLAND)
Thomas GLASMACHER (NSCL, USA)
Ikuko HAMAMOTO (Lund University, SWEDEN)
Mark HUYSE (Instituut voor Kern- en Stralingsfysica, BELGIUM)
Tadafumi KISHIMOTO (RCNP, Osaka University, JAPAN)
Karlheinz LANGANKE (GSI, GERMANY)
Marek LEWITOWICZ (GANIL, FRANCE)
Wei-ping LIU (CIAE, P.R. CHINA)
Takashi NAKAMURA (Tokyo Institute of Technology, JAPAN)
Testuo NORO (Kyushu University, JAPAN)
Alexey A. OGLOBLIN (Kurchatov Institute, RUSSIA)
Akira ONO (Tohoku University, JAPAN)
Tadashi SHIMODA (Osaka University, JAPAN)
Kazuhiro YABANA (University of Tsukuba, JAPAN)

Program Advisory Committee meeting for Materials and Life Science Researches at RIKEN Nishina Center (ML-PAC) Members

June, 2010 / January, 2011

(Chair) Jean-Michel POUTISSOU (TRIUMF, CANADA)
Alex AMATO (PSI, SWITZERLAND)
George A. BEER (University of Victoria, CANADA)
Fumio HANAOKA (Gakushuin University, JAPAN)
Reizo KATO (RIKEN, JAPAN)
Kenichiro KOMAKI (University of Tokyo, JAPAN)
Kenya KUBO (International Christian University, JAPAN)
Douglas E. MACLAUGHLIN (University of California, Riverside, USA)
Sadamichi MAEKAWA (Japan Atomic Energy Agency, JAPAN)
Kanetada NAGAMINE (University of California, Riverside, USA)
Nobuhiko NISHIDA (Tokyo Institute of Technology, JAPAN)
Kusuo NISHIYAMA (KEK, JAPAN)
Francis L. PRATT (RAL, STFC, UK)
Isamu YAMAGUCHI (Tokyo University of Agriculture, JAPAN)
Johann ZMESKAL (Stefan Meyer Institute For Subatomic Physics, AUSTRIA)

Industrial Program Advisory Committee (In-PAC) Members

June, 2010

(Chair) Akihiro IWASE (Osaka Prefecture University)
Toshiyuki AZUMA (RIKEN)
Kenya KUBO (International Christian University)
Toshinori MITSUMOTO (Sumitomo Heavy Industries, Ltd.)
Hitoshi NAKAGAWA (National Agriculture and Food Research Organization)
Nobuhiko NISHIDA (Tokyo Institute of Technology)

Theoretical Research Division
Theoretical Physics Laboratory

1. Abstract

The aim of this laboratory is to reveal the laws of nature ranging from elementary particles to the universe. More precisely, the following three issues are pursued with their mutual relations emphasized:(1) Understanding the microscopic fundamental law of nature. In particular, trying to give a consistent definition of superstring and derive all the fundamental laws from one principle. (2) Understanding many-body systems. Both of the following two aspects are considered. One is the universal laws such as thermodynamics and the universality of spin systems, and the other is specific properties of individual systems such as hadrons, condensed matter, and the universe. (3) Computational science. Besides numerical analyses as an important tool for the above mentioned (1) and (2), aspects of fundamental mathematics are also pursued.

2. Major Research Subjects

(1) Constructive Definition of String Theory as Fundamental law of Physics
(2) Fundamental aspects of Quantum Field Theory and its applications
(3) High precision inspection of experimental and observational data

3. Summary of Research Activity

The ability to understand nature at its most profound level is a basic human desire. Science is founded on accumulated and tremendous efforts driven by that aspiration. The objective of our laboratory is to participate in the endeavor to better understand nature by adding our contributions to theoretical physics. The present seems to be a particularly exciting time for this as many developments appear to be about to converge and allow formation of the ultimate theory of everything.
We organize our research activities into three segments: the pursuit of the microscopic fundamental laws of physics, the study of many-body systems, and the science and technology of computation. These three aspects have an inseparable interrelation and are investigated in an integrated manner throughout the research conducted within this laboratory.

(1) Understanding the fundamental law of nature through string theory.

1)Large N reduction on group manifolds
Large N reduction is the fundamental property behind the matrix model formulation as a non-perturbative formulation of string theory. It has been known quite sometime that large N reduction occurs in flat spacetime. Now we have established that large N reduction works for more general group manifolds.

2) Observational implication of string theory
It is considered to be very difficult finding any direct evidence for string theory or falsifying it. We studied what kind of signature in CMB could be traced back to the existence of string theory or derived effective field theory.

3) Chiral Magnetic Effect from Q-balls
We studied a non-topological solitonic object, a Q-ball, in a generic framework of linear sigma

models. It is found that the Q-ball can be an origin of the chiral magnetic effect in the quark-gluon plasma.

4) Deformation of half-BPS solution in ABJM model and instability of supermembrane
We studied Deformations of half-BPS solutions in world volume theories of an M2-brane and a D2-brane. The solution in the M2-brane theory describes intersecting M2-branes,
while the solution in the D2-brane case corresponds to a fundamental string ending on the brane. We found a difference between the deformations of these two solutions and discussed its possible interpretation as a difference in stabilities of the supermembrane and the string.

5) Study of certain solvable limit in string theory
We studied fluctuations around an M2-brane world-volume extending along $AdS_2 \times S^1$ in $AdS_4 \times S^7/Z_k$. Representing this seven-sphere as a U(1) fibration over CP^3 , we identify the S^1 direction as the U(1) fibre. We obtain the spectrum on AdS_2 after a KK-reduction of the S^1 and find that for k = 1, 2 it forms eight N = 1 scalar supermultiplets for each μ. It is also shown that among them sixteen bosonic modes can reach the boundary. Further, fluctuations around a D3-brane world-volume dual to a Wilson line in symmetric representation were studied. The shape of the world-volume extends along $AdS_2 \times S^2$ in AdS_5 and it carries string charge. It is shown that they are 6 massless scalars and a U(1) gauge field (and 8 massless spinors after κ-gauge fixing) propagating in $AdS_2 \times S^2$. This field content is the same as that of N = 4 U(1) Yang-Mills on $R^{1,3}$. To extract the spectrum on AdS_2 we perform a KK-reduction on S_2 and obtain 6 towers of (2l+1) massive scalars for each l≥0, a tower of (2l+1) massive scalars for each l≥1, a tower of (2l+1) massive vectors for each l≥1, and a U(1) gauge field propagating in AdS_2 .

(2) Quantum field theory and physics of many body systems
1)Lattice formulation of supersymmetric gauge theory
For lattice formulations of the two-dimensional N=(2,2) Wess-Zumino (2D N=(2,2) WZ) model on the basis of the Nicolai map, we show that supersymmetry (SUSY) and other symmetries are restored in the continuum limit without fine tuning, to all orders in perturbation theory. This provides a theoretical basis for these lattice formulations which are useful to numerically investigate the Landau–Ginzburg description of N=(2,2) supersymmetric conformal field theories.

2) Three-flavor quark mass dependence of baryon spectra in holographic QCD.
QCD is a fundamental theory of the strong interaction. Unfortunately, at low energy, it has been difficult to calculate QCD analytically so far. By contrast, holographic QCD has been proposed as an analytically calculable QCD-like model via gauge/string duality. We regard it as a first step to calculate real-world QCD analytically. We introduce the strange quark mass to the Sakai-Sugimoto model of holographic QCD. We compute mass shifts in the spectra of three-flavor baryons at the leading order in perturbation in quark masses. Comparison with experimental data shows an agreement only qualitatively.

(3) High precision calculation of field theory and computational science
1)High precision calculation of QED

The anomalous magnetic moment of electron, called $g-2$,plays a central role in testing the validity of Quantum Electrodynamics(QED). The direct comparison of the experimentally determined $g-2$ to its theoretical prediction, however, had been impossible because of insufficient accuracy of the known coupling constant of QED (the fine structure constant α). The situation was changed in the end of 2010. The new measurement of $h/m_{\rm Rb}$, the ratio of the Planck constant and the mass of Rb atom, provides α with a relative uncertainty of $6.6 X 10^{-10}$.Now that we need an actual value of the tenth-order term of QED $g-2$ calculation to realize a more stringent test of QED.
There are 12672 vertex Feynman diagrams that contribute to the tenth-order $g¥!-¥!2$.
They are divided into 32 gauge-invariant sets. The contributions from 17 sets, I(a--f), II(a,b), II(f), VI(a--c), VI(e,f), and VI(i--k), were previously determined.
The 10 more sets, I(j),II(e), I(g,h), VI(d,g,h), I(i), and II(c,d) have been recently reported. We are now performing the final check on set III(a,b) and set IV, and preparing for publication. Numerical evaluation of remaining two sets, set III(c) and V is on the final stage on RICC, RIKEN's supercomputer system.
Though they are still preliminary, we have now obtained the results from all 32 gauge-invariant sets of the tenth-order diagrams.

Head

Hikaru KAWAI

Members

Hiroshi SUZUKI
Tsukasa TADA

Postdoctoral Researchers

Daisuke KADOH
Ta-sheng TAI
Akitsugu MIWA
Michael ENDRES

Contract Researchers

Makiko MATSUKAWA

Visiting Scientists

Hajime AOKI (Fac. of Sci. and Eng., Saga Univ.)
Jiro ARAFUNE (National Inst. for Academic Degrees and Univ. Evaluation)
Zyun F. EZAWA (Grad. Sch. of Sci., Tohoku Univ.)
Kazuo FUJIKAWA (College of Sci. and Tech., Nihon Univ.)
Amihay HANANY (Massachusetts Inst. of Tech., USA)
Masashi HAYAKAWA (Grad. Sch. of Sci., Nagoya Univ.)
Takeo INAMI (Fac. of Sci. and Eng., Chuo Univ.)
Nobuyuki ISHIBASI (Grad. Sch. of Pure and Applied Sci., Univ. of Tsukuba,)
Satoshi ISO (High Energy Accelerator Res. Organization)
Hiroshi ITOYAMA (Grad. Sch. of Sci., Osaka City Univ.)
Toichiro KINOSHITA (Cornell Univ., USA)

Yoshihisa KITAZAWA (High Energy Accelerator Res. Organization)
Ivan KOSTOV (Service de Physique Theoreique, CNRS, FRANCE)
Didina SERBAN (Service de Physique Theoreique, CNRS, FRANCE)
Jnanadeva MAHARANA (Inst. of Phys., INDIA)
Avinash DHAR (Tata Institute of Fundamental Research,INDIA)
Jun NISHIMURA (High Energy Accelerator Res. Organization)
Fumihiko SUGINO (Okayama Inst. for Quantum Phys.)
Asato TSUCHIYA (Grad. Sch. of Sci., Osaka Univ.)
Tatsumi AOYAMA (KEK)
Shoichi MIDORIKAWA (Aomori Univ.)
Masanori HANADA (University of Washington, U.S.A.)
Yuuichiro SHIBUSA (Nagasaki Institute of Technology)
Issaku KANAMORI (University of Regensburg, GERMANY)
Muneto NITTA (Keio University)
Kazutoshi OHTA (Meiji Gakuin University)
Norisuke SAKAI (Tokyo Women's Christian University)
Isao KISHIMOTO (Niigata University)

Research Consultants

Keiji IGI
Hironari MIYAZAWA
Yoshio YAMAGUCHI
Masao NINOMIYA

Secretariy

Yumi KURAMITSU

Theoretical Research Division
Theoretical Nuclear Physics Laboratory

1. Abstract

Nuclei are finite many-particle systems composed of protons and neutrons. They are self-bound in femto-scale (10^{-15}m) by the strong interaction (nuclear force) whose study was pioneered by Hideki Yukawa. Uncommon properties of the nuclear force (repulsive core, spin-isospin dependence, tensor force, etc.) prevent complete microscopic studies of nuclear structure. There exist number of unsolved problems even at present. In addition, radioactive beam facilities reveal novel aspects of unstable nuclei. We are tackling these old problems and new issues in theoretical nuclear physics, developing new models and pursuing large-scale calculations of quantum many-body systems. We are also strongly involved in research on other quantum many-body systems, to resolve mysteries in the quantum physics

2. Major Research Subjects

(1) Nuclear structure and quantum reaction theories
(2) First-principle calculations with the density functional theory for many Fermion systems
(3) Computational nuclear physics

3. Summary of Research Activity

(1) Systematic analysis on pygmy dipole modes with the finite amplitude method
We studied the low-lying electric dipole mode, so-called the pygmy dipole resonances (PDR), with systematic calculation of the electric dipole responses up to mass A=110 region. In light neutron-rich nuclei, the PDRs emerge when the Fermi level is located in the loosely-bound low-angular-momentum orbital, which suggests their non-collective character. In heavier nuclei, the PDR seems to be more collective to be described by a superposition of particle-hole excitations to the loosely-bound orbitals. We also found that there is a linear correlation between the neutron skin thickness and the PDR transition strength. However, further analysis is needed to judge whether the PDR strength can be used for a measurement of the neutron skin thickness.

(2) Development of the finite amplitude method for superfluid nuclei
We have developed a new theoretical tool to apply the finite amplitude method (FAM) to nuclei with superfluidity. The implementation of the FAM on an existing spherically symmetric Hartree-Fock-Bogoliubov code (HFBRAD) in the coordinate-space representation has been carried out. This has become a new computer program for the quasi-particle-random-phase approximation (QRPA) which can be used for a variety of modes of excitation in superfluid nuclei. In addition, we expect the method can facilitate the developments of the QRPA codes for deformed nuclei.

(3) Roles of deformation and neuron excess on the giant monopole resonance
Roles of deformation on the giant monopole resonance (GMR), particularly the mixing of the giant quadrupole resonance (GQR) and the effects of the neutron excess in Zr isotopes were investigated by means of the deformed QRPA employing the Skyrme and the local pairing energy-density functionals. In the drip-line nuclei, the neutron excitation is dominant over the proton excitation. We found for an isovector excitation the GMR has a four-peak structure

due to the neutron excess as well as the mixing of the $K^{\pi}=0^{+}$ component of the isovector GQR.

(4) Giant dipole resonance in the rare-earth nuclei with shape changes
Photoabsorption cross sections of Nd and Sm isotopes from spherical to deformed even nuclei were systematically investigated by means of the QRPA based on the Hartree-Fock-Bogoliubov ground states using the Skyrme energy density functional. The gradual onset of deformation in the ground states as increasing the neutron number leads to characteristic features of the shape phase transition. The calculations well reproduce the isotopic dependence of broadening and emergence of a double-peak structure in the cross sections without any adjustable parameters.

(5) Application of the canonical-basis TDHFB method to calculation of the photoabsorption cross sections in heavy deformed nuclei
We proposed the Canonical-basis time-dependent Hartree-Fock-Bogoliubov (Cb-TDHFB) method for studies of nuclear dynamics of nuclei with superfluidity. The computer program with the Skyrme functional has been developed and applied it to heavy deformed nuclei for the first time. The linear-response calculation for ^{172}Yb indicates that the method can reproduce the result of the QRPA calculation and significantly saves the computational cost. Roughly speaking, it reduces the computational task by a factor of 1/1,000.

(6) Microscopic description of large-amplitude quadrupole collective dynamics in low-lying states
We studied the large-amplitude collective dynamics in low-lying states using the five-dimensional collective Hamiltonian constructed with the constrained-Hartree-Fock-Bogoliubov (CHFB) + local QRPA method. Various collective deformations associated with the deformed magic numbers appear in the sd-shell region. We analyzed the large-amplitude axial and triaxial quadrupole collective dynamics in low-lying states of 24Mg, 26Mg, 24Ne, and 28Si. We could reproduce well the prolate ground state and gamma vibrational band in 24Mg, oblate ground state and beta vibrational band in 28Si. We also analyzed the neutron and proton quadrupole transition matrix elements in 26Mg, and found an E2 transition where the proton matrix element is strongly suppressed by the large-amplitude collective dynamics in triaxial (gamma) direction. These results indicate the importance of the triaxial degree of freedom in low-lying states.

Neutron-rich Mg isotopes around 32Mg locates in the “island of inversion” where collective deformation develops, and the structure and dynamics in their low-lying states are an important current topic. Using the CHFB + local QRPA method, We successfully reproduced the excitation energies, B(E2)'s of the yrast bands. As neutron number increases, the structure of ground state changes from spherical to prolate shape. Especially in 32Mg, the potential energy surface shows spherical-prolate shape coexistence. Associated with the change of ground states, excited 0+ changes from shape coexistence to beta-vibration of a prolate ground states. We also showed that the potential energy surface becomes soft against the triaxial deformation as neutron number increases, and the energies of the excited 2^{+} state (gamma vibration) come down.

We have also applied the method to oblate-prolate shape coexistence phenomena in the low-lying states of proton-rich Se and Kr isotopes. The results of our calculation show that the inclusion of the time-odd components of mean field, which are ignored in the widely-used Inglis-Belyaev cranking formula, increases the inertial masses and yields a better agreement with experimental data. The results of the calculation also show the importance of large-amplitude shape fluctuation in the triaxial shape degree of freedom and rotational motion for the shape mixing dynamics. The calculation for neutron-rich Cr isotopes is under progress.

(7) Extra-push energy in heavy-ion fusion reaction studied with the TDHF simulation
It is known for a long time that the fusion probability is hindered for heavy ions. This is often referred to the extra-push energy, which means that the incident energy much higher than the Coulomb barrier height is necessary for heavy nuclei with $Z_1*Z_2 > 1800$ to fuse. We are investigating whether the microscopic time-dependent Hartree-Fock (TDHF) calculation quantitatively reproduces the extra-push energy for the fusion reaction, including the criterion for the mass combination of projectile and target. We study these issues in heavy-ion fusion reactions with TDHF theory employing the full Skyrme force and without any geometric symmetry restrictions. We found that for light systems the TDHF fusion threshold, interaction barrier with frozen-density energy density functional (FD-EDF) method and experimental Coulomb barrier have a quite good agreement, which imply extra push is not needed for light systems. However for heavy system, the TDHF fusion threshold is higher than the interaction barrier with FD-EDF method. One may make a conclusion that an extra push energy above the interaction barrier is needed in order to achieve the fusion for heavy systems. In order to give more confidential answers to those issues on the fusion dynamics, more systematic calculations for heavy systems are now under progress.

(8) Deformed and clustering states in ^{42}Ca
Characteristics of deformed states and alpha cluster correlations are studied using the anti-symmetrized molecular dynamics (AMD) and the generator coordinate method. A ground-state band and a deformed band built on the $J^{\pi}=2^{+}$ state are reproduced. A deformed band built on the $J^{\pi}=3^{+}$ contains significant clustering-structure components, which is consistent with experimental results of ^{38}Ar(^{6}Li, d) reactions. Combinations of particle-hole configurations that protons and neutrons cause those coexistence of various deformed states.

(9) Adiabatic inter-nucleus potentials and sub-barrier fusion
The inter-nucleus potential for the adiabatic nuclear reaction was investigated. A method to derive adiabatic inter-nuclear potentials is proposed using the AMD, and effects of valence neutrons are clarified using the potentials. Valence neutrons of ^{18,22}O gain additional attractive force, which enhance probability of tunneling effects and sub-barrier fusion.

(10) Chemical potential beyond the quasi-particle mean field
The effects of quantal and thermal fluctuations beyond the BCS quasi-particle mean field on the chemical potential are studied within a model, which consists of N particles distributed amongst doubly folded equidistant levels interacting via a simple pairing force. The results obtained at zero and finite temperatures T within several approaches, which include the fluctuations beyond the BCS theory, are compared with the exact results. The chemical potential, defined as the Lagrangian multiplier to preserve the average number of particles, is compared with the corresponding quantity, which includes the effect due to fluctuations of particle and quasi-particle numbers beyond the BCS quasi-particle mean field.

(11) Canonical ensemble treatment of pairing within BCS and quasi-particle random phase approximation

A description of pairing properties in finite systems is proposed within the canonical and microcanonical ensembles. The approach is derived by solving the BCS and self-consistent QRPA with the Lipkin-Nogami particle-number projection at zero temperature. The obtained eigenvalues are embedded into the canonical and microcanonical ensembles. The results obtained are found in quite good agreement with the exact solutions of the doubly-folded equidistant multilevel pairing model as well as the experimental data for ^{56}Fe nucleus. The merit of the present approach resides in its simplicity and its application to a wider range of particle number, where the exact solution is impracticable.

(12) Thermodynamic properties of hot nuclei within the self-consistent quasi-particle random-phase approximation

The thermodynamic properties of hot nuclei are described within the canonical and microcanonical ensemble approaches. These approaches are derived based on the solutions of the BCS and self-consistent quasi-particle random-phase approximation at zero temperature embedded into the canonical and microcanonical ensembles. The obtained results agree well with the recent data extracted from experimental level densities by Oslo group for ^{94}Mo, ^{98}Mo, ^{162} Dy and ^{172}Yb nuclei.

(13) Black-sphere model for total reaction cross sections

In the framework of the contemporary black-sphere model, we examine total reaction cross sections between heavy nuclei, such as ^{56}Fe+^{208}Pb (or ^{238}U) where the Coulomb dissociation may contribute. Along this study, we point out that several semi-empirical parameterizations in simulation codes may contain terms leading to different energy and/or mass-number dependence from the empirical behavior. Further study to pin them down is now in progress.

(14) Transparency parameter for total reaction cross sections

We propose a unified parameterization of the transparency parameter in the well-known Kox and Shen models, which are two of the popular semi-empirical parameterizations for total reaction cross sections in several simulation codes due to their good reproducibility of a variety of available data. This study is aiming at allowing these models to be used at energies below 30MeV per nucleon, where the parameterization of these models is missing. The transparency parameter is responsible for describing the energy dependence of the cross sections in the models. We also give the recommendation that the models should be used so that the lighter nucleus is always treated as projectile, no matter what the actual case might be, because these models contain the asymmetry in exchanging the mass number of target and projectile.

Head

Takashi NAKATSUKASA

Members

Akihisa KOHAMA

Special Postdoctoral Researchers

Yasutaka TANIGUCHI

Nobuo HINOHARA
Kenichi YOSHIDA
Gentaro WATANABE
Tsunenori INAKURA

Foreign Postdoctoral Researcher
Carlo BARBIERI

Contract Researchers
Paolo AVOGADORO
NguyenDinh DANG

Research Associate
Guo LU

Senior Visiting Scientists
Kenichi MATSUYANAGI
Hiroyuki SAKURAGI

Research Consultants
Kiyomi IKEDA
Syuhei YAMAJI
Kosai TANABE

Visiting Scientists
Takashi ABE (Univ of Tokyo)
Yasuhisa AB (RCNP)
Anatolijs AFANASJEVS (Mississippi State Univ.)
Shigeyoshi AOYAMA (Niigata Univ.)
Yoshihiro ARITOMO (JINR)
Simone BARONI (Univ. of Washington)
Carlos BERTULIANI (Texas A&M Univ.)
Satoshi CHIBA (Japan Atomic Energy Agency.)
TiebKhoa DAO (Inst. Nucl. Scie. Tech.)
Elisabeth ELSTER (Ohio Univ.)
Yoshiko ENYO (Yukawa Inst. Theoretical Phys.)
Hubert FLOCARD (INP-Orsay)
Yasuro FNAKI (Univ. Tsukuba)
Shinichiro FUJII (CNS)
Koichi HAGINO (Tohoku Univ.)
Ikuko HAMAMOTO (Lund Univ.)
Koji HIGASHIYAMA (Chiba Institute of Technology)
Michio HONMA (Aizu Univ.)
Takatoshi HORIBATA (Aomori Univ.)
Munetake ICHIMURA (The Open Univ of Japan)
Kei IIDA (Kochi Univ.)

Akitsu IKEDA (Shizuoka Inst. Scie. Tech.)
Tsunenori INAKURA (Grad. Sch. of Pure and Applied Sci., Univ. Tsukuba)
Naoyuki ITAGAKI (Univ of Tokyo)
Makoto ITO (Kansai Univ.)
Akira IWAMOTO (Japan Atomic Energy Agency)
Jie MENG (Peking Univ.)
Kaori KAKI (Shizuoka Univ.)
Kiyoshi KATO (Hokkaido Univ.)
Toshitaka KAJINO (NAOJ)
Masaaki KIMURA (Hokkaido Univ.)
Wenhui LONG (Peking Univ.)
Takuma MATSUMOTO (Hokkaido Univ.)
Peter MOLLER (Los Alamos National Lab.)
Kazuo MUTO (Tokyo Institute of Technology)
Kazusuke OGATA (Kyushu Univ.)
Makito OI (Univ of Surrey.)
Akira ONO (Tohoku Univ.)
Masahisa OTA (Konan Univ.)
Kazuhiro OYAMATSU (Aichi Shukutoku Univ.)
Hiroyuki SAGAWA (Aizu Univ.)
Badawy SARHAN (Cairo Univ.)
Ryoichi SEKI (California Univ.)
Noritaka SHIMIZU (Univ of Tokyo)
Yoshihumi SHIMIZU (Kyushu Univ.)
Kosuke SUMIYOSHI (Numazu National College of Technology)
Akihiro SUZUKI (Suzuki Corporation)
Yasuyuki SUZUKI (Niigata Univ.)
Toshio SUZUKI (Fukui Univ.)
Naoki TAJIMA (Univ of Fukui)
Masatoshi TAKANO (Waseda Univ.)
Masaaki TAKASHINA (RCNP)
Kazuo TAKAYANAGI (Sophia Univ.)
Noboru TAKIGAWA (Tohoku Univ.)
Kazuko TANABE (Otsuma Women's Univ.)
Jun TERASAKI (Univ. North Carolina)
Yutaka UTSUNO (Japan Atomic Energy Agency.)
Takahiro WADA (Kansai Univ.)
Kazuhiro YABANA (Grad. Sch. of Pure and Applied Sci., Univ. Tsukuba)
Taiichi YAMADA (Kanto Gakuin Univ.)
Masayuki YAMAGAMI (Aizu Univ.)
Naotaka YOSHINAGA (Saitama Univ.)
Yumin ZHAO (Shanghai Jiao Tong Univ.)

Students
Junior Research Associates
Shuichiro EBATA (Grad. Sch. of Pure and Applied Sci., Univ. Tsukuba)

Koichi SATO (Dept. Phys., Kyoto Univ.)

Intern

Bruno CHARRON (Ecole Polytechnique)

International Program Associate

Jia-Jie SHEN (Shanghai Jiao Tong Univ.)

Student Trainees

Wataru HORIUCHI (Niigata Univ.)

Secretaries

Noriko KIYAMA
Keiko SUZUKI

Theoretical Research Division
Strangeness nuclear physics Laboratory

1. Abstract

We proposed accurate few-body calculational method called "Infinitesimally shifted Gaussian lobe method". Recently, we developed this method to four-body systems and five-body systems. This method is applicable for various three- and four-body systems. For example, we applied it to hypernuclear physics and clarified what is important and impressed. In fact, we applied this method to three kinds of hypernuclear experiments (KEK-E419, BNL-E930, and –E929) in the past, and we contributed to these experiments by discussing with experimentalists, analyzing the data, and interpreting the data.

2. Major Research Subjects

(1) Hypernuclear structure from the view point of few-body problem

(2) Structure of exotic hadron system

(3) Baryon-baryon interaction based on lattice QCD

(4) Neutron-rich Λ hypernuclei from shell model approach

3. Summary of Research Activity

(1) Energy levels of the double Λ hypernucleus, ${}^{11}Be_{\Lambda\Lambda}$ are calculated within the framework of a $\alpha\alpha n\Lambda\Lambda$ five-body model. Two Λ separation energy of the ground state and bound excited states of ${}^{11}Be_{\Lambda\Lambda}$ are calculated with the Gaussian Expansion method. The Hida event, recently observed at KEK-E373 experiment, is interpreted as an observation of the ground state of the ${}^{11}Be_{\Lambda\Lambda}$.

(2) As one of the typical sd-shell hypernuclei, the positive- and negative-parity energy levels of ${}^{20}Ne_{\Lambda}$ are calculated to investigate structures of low-lying states within the shell model calculations. The production cross section of (π^+,K^+) and (K^-,π^-) reactions are estimated using the calculated shell-model wave functions.

(3) The study of the resonance energy of the strange dibaryons using two models with the energy-independent and energy-dependent potentials for the s-wave KN interaction, both of which are derived by certain reductions from the leading order term of the effective chiral Lagrangian. The model with energy-independent (energy-dependent) potential) potential predicts one (two) resonance pole in the Λ(1405) region, while they predicts one resonance pole of the strange dibaryons, whereas the energy-dependent potential model predicts two resonance poles.

Head

Emiko HIYAMA

Contract Researchers

Atsushi UMEYA

Yoichi IKEDA

Visiting Scientists

Takayuki MYO (Osaka Institute of Technology)
Qamar Usmani (University Malaysia Perlis)
Yasuo YAMAMOTO (Tsuru University)
Taiichi YAMADA (Kanto Gakuin University)
Tetsuo HYODO (Tokyo Institute of Technology)
Makoto OKA (Tokyo Institute of Technology)
Tomokazu FUKUDA (Osaka Electro-Communication University)
Daisuke JIDO (YITP, Kyoto University)
Hidekatsu NEMURA (Tohoku University)
Soichi ISHIKAWA (Hosei University)
Takenori FURUMOTO (Osaka City University)
Atsushi HOSAKA (RCNP, Osaka University)
Shoji SHINMURA (Gifu University)
Akinobu DOTE (HIGH ENERGY ACCELERATOR RESEARCH ORGANIZATION, KEK)
Thomas RIJKEN (Radboud University Nijmegen)
Kazuma NAKAZAWA (Gifu University)

Research Consultants

Kiyomi IKEDA

Secretary

Makiko OHISHI

Theoretical Research Division
Mathematical Physics Laboratory

1. Abstract

The aim of mathematical physics laboratory is to apply mathematical scheme to resolve long-standing issues in various subjects of physics. Mathematics, in particular that originates in superstring theory, has universal feature which is common to wide range of physics. This covers elementary particle physics, hadron physics, nuclear physics, cosmology, general relativity and condensed matter physics. We apply mathematical scheme such as superstring theory, D-branes, AdS/CFT correspondence, solitons, statistical mechanics and integrable systems. Topics which the laboratory covers currently include non-perturbative analysis of quantum chromo-dynamics, superstrings, and models beyond the standard model of particle physics, and soliton physics.

2. Major Research Subjects

(1) Application of Superstring Theory
(2) Non-perturbative analyses of strongly-coupled gauge theories
(3) Physics of Black Holes and Cosmology
(4) Solitons physics

3. Summary of Research Activity

Interplay between mathematics and physics is indispensable, as any physics law is described in terms of mathematics. However, the present status of various theoretical physics does not fully appreciate the usefulness of mathematics, as each topics goes into details and has less interaction with other subjects even nearby. We integrate various subjects of physics, by applying recent development of mathematics and mathematical physics, to solve long-standing issues in physics. In particular, mathematical methods in superstring theory has been developed and is mature enough to be applied to other physics. We put efforts on the application as described below, in addition to some other mathematical techniques such as numerical simulations, solitons and integrable systems.

(1) Application of superstring theory

AdS/CFT correspondence and nuclear physics
The renowned AdS/CFT correspondence, which was initiated in superstring theory, is a useful and powerful tool for analyzing strongly-coupled gauge theories. This has been applied to QCD, the dynamics of quarks. We studied how this powerful tool can have an impact on nuclear physics. We computed an effective action of multi-baryon systems, which should serve as a basic quantum action for nuclear physics. This turned out to reproduce nicely nuclear forces and baryon spectrum. In addition, three-body nuclear force was computed.

AdS/CFT correspondence and hadron mass
An approach to realize a hyperon as a bound-state of a two-flavor baryon and a kaon was considered in the context of holographic QCD. Pseudo-scalar kaon was considered as a fluctuation around a baryon. We found various bound states for hyperons.

Rapid thermalization of heavy ion collisions studied by string theory

Using the AdS/CFT correspondence for strongly coupled gauge theories, we calculated thermalization of mesons caused by a time-dependent change of a baryon number chemical potential. On the gravity side, the thermalization corresponds to a horizon formation on the probe flavor brane in the AdS throat. Since heavy ion collisions are locally approximated by a sudden change of the baryon number chemical potential, we discuss implication of our results to RHIC and LHC experiments, to find a rough estimate of rather rapid thermalization time-scale $t_{th} < 1$ [fm/c]. We also discussed universality of our analysis against varying gauge theories.

(2) Soliton techniques applied to various physics

1) Zero-modes on non-abelian vortices in 3 dimensions

We studied non-Abelian solitons of the Bogomol'nyi type in N=2 (d=2+1) supersymmetric Chern-Simons (CS) and Yang-Mills (YM) theory with a generic gauge group. In CS theory, we found topological, non-topological and semi-local (non-)topological vortices of non-Abelian kinds in unbroken, broken and partially broken vacua. We calculated the number of zero-modes using an index theorem and then we applied the moduli matrix formalism to realize the moduli parameters.

2) Symmetric nature on solitons

We investigated the structure of the moduli space of multiple BPS non-Abelian vortices in U(N) gauge theory with N fundamental Higgs fields, focusing our attention on the action of the exact global (color-flavor diagonal) SU(N) symmetry on it.

3) Confined monopoles in dense QCD

We analytically showed that mesonic bound states of confined monopoles appear inside a non-Abelian vortex-string in massless three-flavor QCD at large quark chemical potential μ.

4) Chiral magnetic effect

We applied a generic framework of linear σ models for revealing a mechanism of the mysterious phenomenon, the chiral magnetic effect, in quark-gluon plasma. An electric current arises along a background magnetic field, which is given rise to by Q-balls (non-topological solitons) of the linear σ model with axial anomaly. We found additional alternating current due to quark mass terms. The hadronic Q-balls, baby boson stars, may be created in heavy-ion collisions.

(3) Static interactions and stability of matter in Rindler space

Dynamical issues associated with quantum fields in Rindler space are addressed in a study of the interaction between two sources at rest generated by the exchange of scalar particles, photons and gravitons. These static interaction energies in Rindler space were shown to be scale invariant, complex quantities. The imaginary part will be seen to have its quantum mechanical origin in the presence of an infinity of zero modes in uniformly accelerated frames which in turn are related to the radiation observed in inertial frames. The impact of a uniform acceleration on the stability of matter and the properties of particles was discussed and estimates are presented of the instability of hydrogen atoms when approaching the horizon.

(4) Numerical simulation of strongly-coupled QCD

1) Transport coefficients of causal dissipative relativistic hydrodynamics in quenched lattice simulations

Transport coefficients of causal dissipative relativistic fluid dynamics (CDR) were studied in quenched lattice simulations. CDR describes the behavior of relativistic non-Newtonian fluids in which the relaxation time appears as a new transport coefficient besides the shear and bulk viscosities. We studied the transport coefficients with lattice simulations in pure SU(3) gauge theory. After defining the energy-momentum tensor on the lattice, we extracted a ratio of the shear viscosity to the relaxation time which is given only in terms of the static correlation functions.

2) Hadron properties at finite temperature and density with two-flavor Wilson fermions

Meson properties at finite temperature and density were studied in lattice QCD simulations with two-flavor Wilson fermions. For this purpose, we investigate screening masses of mesons in pseudo-scalar (PS) and vector (V) channels. We found that the temperature dependence of the screening masses normalized by temperature, shows notable structure, and approach 2π at high temperature in both channels, which is consistent with twice the thermal mass of a free quark in high temperature limit.

Head

Koji HASHIMOTO

Special Postdoctoral Researchers

Minoru ETO

Contract Researcher

Yu MAEZAWA
Hideaki IIDA

Visiting Researcher

Takaaki ISHII

Senior Visiting Scientist

Koichi YAZAKI

Visiting Scientists

Tamiaki YONEYA (The Open Univ. of Japan)
Frieder LENTZ (The Univ.Erlangen-Nurnberg)

Secretary

Noriko KIYAMA
Keiko SUZUKI

Sub Nuclear System Research Division
Radiation Laboratory

1. Abstract

Nucleons, such as protons and neutrons, are a bound state of constituent quarks glued together with gluons. The detail structure of nucleons, however, is not well understood yet. Especially the mechanism to build up the spin of proton, which is 1/2, is a major problem in physics of the strong force. The research goal of Radiation Laboratory is to solve this fundamental question using the world first polarized-proton collider, realized at RHIC in Brookhaven National Laboratory (BNL) in USA. RHIC stands for Relativistic Heavy Ion Collider, aiming also to create Quark Gluon Plasma, the state of Universe just after the Big Bang. RIKEN-BNL Research Center (RBRC) directed by N. Samios carries our core team at BNL for those exciting researches using the PHENIX detector. We have found that the proton spin carried by gluons is indeed small, which is a very striking finding beyond our expectations. Recently we successfully identified W boson in the electron/positron decay channel, with which we established the method to determine how much anti-quarks carry the proton spin. Other than the activities at RHIC we are preparing new experiments at SPring-8, J-PARC and Fermilab to study the nature of hadron. We are also performing technical developments such as novel ion sources, fine pitch pixel detectors and neutron optical devices.

2. Major Research subjects

1) Spin physics with relativistic polarized-proton collisions at RHIC
2) Study of nuclear matter at high temperature and/or at high density
3) Technical developments on radiation detectors and accelerators

3. Summary of Research Activity

(1) Experimental study of spin structure of proton using RHIC polarized proton collider

[See also RIKEN-BNL Research Center Experimental Group for the activities at BNL]

To study orbital motions of quarks and gluons in the proton, one of the key measurements is the Drell-Yan process(quark-antiquark annihilation) with a polarized beam or target. We are considering to perform such measurements with the PHENIX detector and/or with a new internal-target experiment at RHIC. As a pilot some of us are participating in the Fermilab-E906/SeaQuest experiment which measures muon pairs from Drell-Yan process using a 120-GeV unpolarized proton at Fermilab. One of the goals of the experiment is to reconfirm the flavor asymmetry of the antiquark distributions. This asymmetry can be related with the proton spin carried by antiquarks.

(2) Experimental study of quark-gluon plasma using RHIC heavy ion collider

[See also RIKEN-BNL Research Center Experimental Group for the activities at BNL]

In Wako we are operating a cluster computer system specialized to analyze huge data sets taken with the PHENIX detector. We have introduced a new type of cluster consisting of 18 nodes each of which has two quad-core CPUs and 10 sets of 1TB local disk for data repository. This configuration ensures fastest disk I/O when the jobs are assigned to the nodes where the required data sets are stored. The new system has in total 144 CPU cores and 180 TB disks, and can analyze 150 TB data within 9 hours, which is roughly 10 times faster than the usual scheme with a common data storage accessed from many nodes. It is also important that this scheme doesn't require expensive RAID system and network. Through this development we have established a fast and cost-effective solution in analyzing massive data.

(3) Study of properties of mesons and exotic hadrons with domestic accelerators

Preparation of the experiment E16 at J-PARC 50-GeV PS is underway with the Grant -in-Aid for Scientific Research on Innovative Areas (MEXT, No. 21105004) . The experiment aims to perform the systematic study of the mass modification of low-mass vector mesons in nuclei to explore the chiral symmetry in nuclear matter, i.e. the mechanism to create the mass. Gas Electron Multiplier (GEM) tracker and hadron-blind Cherenkov detector (HBD) are being developed for the experiment. Large GEM foils (30cm x 30cm, one of the largest in the world) for the tracker were developed and exhibited the position resolution of 0.1mm as required by the experiment. Another key element, GEM foil coated with CsI photocathode, for the HBD was also developed and the required photo-electron efficiency is almost achieved on the test bench and to be proven using a beam. The spectrometer construction is to be completed by the end of JFY 2012, to start detector commissioning with a primary beam at J-PARC.

(4) Detector development for PHENIX experiment

After 7 years of hard work, we finally completed and installed the silicon vertex tracker (VTX) into the PHENIX detector at RHIC on December 2010. It will enhance physics capability of the PHENIX by identifying charm and bottom quarks separately and by enlarging the acceptance for charged particles. Nobel pixel and stripixel technologies are introduced and the construction was accomplished by the proponents from Radiation Laboratory, the RIBF Detector team, RIKEN-BNL Research Center and other collaborating institutes.

We have also completed the momentum-sensitive trigger system for the PHENIX forward muon arms under the collaboration with KEK, Kyoto and Rikkyo University. Together with the newly-installed resistive plate chambers and the hadron absorbers, the new trigger system is about operational to indentify muons from W boson decays.

(5) Neutron optics

Cold or thermal neutron beam is a high-sensitivity probe to study not only the structure of condensed matter, but also fundamental physics. We have successfully observed interference of 67% with an interferometer using multilayer mirrors. Complete separation of the two paths of epithermal neutron is achieved for the first time. This device will be useful for tests of quantum mechanics and other fundamental physics.

We are also developing a new method to see an internal structure of a bulk by the differential phase image with neutrons. Using two neutron absorption gratings, we have demonstrated a crack in acrylic plate is observable.

(6) Development of beam source

Under the collaboration with BNL, we are developing a laser ion source (LIS) to produce a high current heavy-ion beam, which is useful for the next generation accelerators. We have demonstrated the instantaneous intensity of more than 70 mA for highly charged carbon and aluminum beams. This is the highest current heavy ion beam produced by any methods. We also discovered that, using a week magnetic field to confine the expanding laser plasma, the beam pulse length can be extended up to 4 micro seconds with keeping the same peak current. The number of accelerated carbon ions reached more than 10^{11} per single laser shot.

At Wako, the development of a next-generation electron beam source is underway using the novel photocathode based on a super-lattice semiconductor with a negative electron affinity (NEA) surface. We optimized GaAs/AlGaAs super-lattice based on theoretical energy-band calculations, and observed high quantum yield and small beam emittance.

(7) Theoretical study of hadron physics

We have been performing the theoretical study of hadron physics more than 10 years. This year such activity was transferred to newly established Mathematical Physics Laboratory (head: K. Hashimoto) to open a new horizon of theoretical QCD study.

Head

Hideto EN'YO

Members

Yasuyuki AKIBA
Yuji GOTO
Itaru NAKAGAWA
Yoshie OTAKE
Yasushi WATANABE
Satoshi YOKKAICHI
Ralf SEIDL

Special Postdoctoral Researchers

Kazuya AOKI
Kohei SHOJI
Yoshichika SEKI

Foreign Postdoctoral Researcher

Stephen BAUMGART

Contract Researchers

Yoshinori FUKAO
Tomohiro NISHITANI
Takashi HACHIYA

Postdoctoral Researcher

Yoshimitsu IMAZU

Contract Technical Scientist

Yohei NAKATSUGAWA

Research Consultant

Katsuya HIROTA

Senior Visiting Scientists

Ken-ichi IMAI (Grad. Sch. of Sci., Kyoto Univ.)
Toshiaki SHIBATA (Grad. Sch. of Sci. and Eng., Tokyo Inst. of Tech. Sch. of Sci.)
Hirohiko SHIMIZU (Inst. of Materials Structure Sci., KEK)
Ken-ichi AOKI (Grad. Sch. of Sci., Kanazawa Univ.)
Takashi NAKANO (RCNP, Osaka Univ.)

Visiting Scientists

Tomohiro ADACHI (DAI-ICHI KIDEN CO.,LTD)
Christine A. AIDALA (Univ. Massachusetts, Amherst, USA)
Alexander BAZILEVSKY (BNL, USA)
Wolfgang BENTZ (Tokai Univ.)
Mickey CHIU (Univ. of Illinois at Urbana, USA)
Ondrej CHVALA (Univ. of California at Riverside)
Takumi DOI (University of Kentucky)
Dipanwita DUTTA (Nuclear Physics Division, Bhabha Atomic Research Centre)
Hirotsugu FUJII (Grad. Sch./College of Arts and Sciences, Univ. of Tokyo)
Kenji FUKUSHIMA (YITP, Kyoto Univ.)
Haruhiko FUNAHASHI (Grad. Sch. of Sci., Kyoto Univ.)
Yuji HASEGAWA (Wien Inst. Tech.)
Tetsuo HATSUDA (Grad. Sch. of Sci., Univ. of Tokyo)
Toshiyuki HATTORI (Res. Lab. for Nuclear Reactors, Tokyo Inst. of Tech. Sch. of Sci.)
Masanori HIRAI (Grad. Sch. of Sci. and Eng., Tokyo Inst. of Tech.)
Kensuke HOMMA (Grad. Sch. of Sci., Hiroshima Univ.)
Takuma HORAGUCHI (Grad. Sch. of Sci., Hiroshima Univ.)
Ryo ICHIMIYA (KEK)
Katsuya ISHIGURO (Grad. Sch. of Natural Sci. & Tech., Kanazawa Univ.)
Noriyoshi ISHII (Grad. Sch. of Pure and Applied Sci., Univ. of Tsukuba)
Hirokazu ISHINO (Tokyo Inst.Tech.)
Robert JAMESON (Goethe Universitat Frankfurt, Germany)
Takeshi KANESUE (Kyushu Univ.)
Hirotsugu KASHIWAGI (Takasaki Advanced Radiation Res. Inst., JAEA)
Hiroyuki KAWAMURA (The Univ.of Liverpool)
Yuji KOIKE (Grad. Sch. of Sci. & Tech., Niigata Univ.)
Yoshiaki KOMA (Numazu National College of Technology)
Kotaro KONDO (Grad. Sch. of Sci. and Eng., Tokyo Inst. of Tech.)
Shunzo KUMANO (Inst. of Particle and Nuclear Studies, KEK)
Teiji KUNIHIRO (Grad. Sch. of Sci., Kyoto Univ.)
Makoto KUWAHARA (Nagoya Univ.)
Yoshikazu MAEDA (RCNP , Osaka Univ.)
Yajun MAO (Peking Univ., China)
Tsutomu MIBE (KEK)
Liu MING (LANL)
Kenji MISHIMA (KEK)
Yoshiyuki MIYACHI (Tokyo Inst. Tech.)
Yoshihiro MORI (Grad. Sch. of Sci., Kanazawa Univ.)
Norihito MURAMATSU (RCNP, Osaka Univ.)
Ryotaro MUTO (KEK)
Katsuro NAKAMURA (Grad. Sch. of Sci., Kyoto Univ.)
Yoshifumi NAKAMURA (DESY, Germany)
Atsushi NAKAMURA (Information Media Center, Hiroshima Univ.)
kenichi NAKANO (Tokyo Inst. Tech.)
Megumi NARUKI (KEK)

Masayuki NIIYAMA (Grad. Sch. of Sci., Kyoto Univ.)
Munehisa OHTANI (Inst. fuer Theoretische Physik, Universitact Regensburg, Germany)
Hiromi OKADA (KEK)
Masahiro OKAMURA (BNL, USA)
Kyoichiro OZAWA (Grad. Sch. of Sci., Univ. of Tokyo)
Petra RIEDLER (CERN, Switzerland)
Naohito SAITO (J-PARC, KEK)
Hiroyuki SAKO (JAEA)
Murad SARSOUR (Georgia State University)
Shoichi SASAKI (Grad. Sch. of Sci., Univ. of Tokyo)
Susumu SATO (JAEA)
Shin-ya SAWADA (Inst. of Particle and Nuclear Studies, KEK)
Michiko SEKIMOTO (Inst. of Particle and Nuclear Studies, KEK)
Kenta SHIGAKI (Grad. Sch. of Sci., Hiroshima Univ.)
Prashant SHUKLA (Nuclear Physics Division, Bhabha Atomic Research Centre)
Kazutaka SUDO (Inst. of Particle and Nuclear Studies, KEK)
Toru SUGITATE (Grad. Sch. of Sci., Hiroshima Univ.)
Mizuki SUMIHAMA (RCNP , Osaka Univ.)
Tsuneo SUZUKI (Grad. Sch. of Sci., Kanazawa Univ.)
Taneja SWADHIN (SUNY at Stony Brook)
Masao TABUCHI (Nagoya Univ.)
Junpei TAKANO (KEK)
Kiyoshi ANIDA (Seoul National Univ.)
Hisayuki TORII (Grad. Sch. of Sci., Hiroshima Univ.)
Xiaorong WANG (New Mexico State University)
Shizui WATANABE (Tokyo Metropolitan College of Aeronautical Engineering)
Imuran YOUNUS (Univ. of New Mexico, USA)

Students

Junior Research Associate

Ryoji AKIMOTO (CNS, Univ. Tokyo)
Hidemitsu ASANO (Fac. of Sci., Kyoto Univ.)
Yoki ARAMAKI (CNS, Univ. Tokyo)
Kimiaki HASHIMOTO (Fac. of Sci., Rikkyo Univ.)
Kenichi KARATSU (Fac. of Sci., Kyoto Univ.)
Masaya NIHASHI (Grad. Sch. of Sci., Hiroshima Univ.)
Dosatsu SAKATA (Univ. Tsukuba)
Satoshi SANO (CNS , Univ.Tokyo)
Takahito TODOROKI (Univ. Tsukuba)

International Program Associate

Ryu SUNYOUNG (RCNP,Osaka Univ.)

Student Trainees

Atsushi ERA (Nagoya Univ.)
Hikaru FKUSHIMA (Tokyo Univ. of Science)

Ciprian GAL (Dept. of Physics , SUNY at Stony Brook)
Masayasu HASEGAWA (Grad. Sch. of Sci., Kanazawa Univ.)
Kazuya HAYASE (Tokyo Univ. of Science)
Seiko HIROTA (Fac. Sci. , Univ. Tokyo)
Shouyang HU (China Inst. Atom. Energy)
Yuuji KATOU (RCNP , Osaka Univ.)
Kouki KANNO (Fac. Sci. , Univ. Tokyo)
Paul KLINE (Dept. of Physics , SUNY at Stony Brook)
Yusuke KOMATSU (Fac. Sci. , Univ. Tokyo)
Andrew MANION (Dept. of Physics , SUNY at Stony Brook)
Nathan MEANS (Dept. of Physics, SUNY at Stony Brook)
Shou MIYASAKA (Tokyo Inst. Tech.)
Shinji MOTOKI (Grad. Sch. of Biosphere Sci., Hiroshima Univ.)
Yoshihide NAKAMIYA (Grad. Sch. of Sci., Hiroshima Univ.)
Takahiro SAWADA (RCNP, Osaka Univ.)
Atsuko TAKAGI (Fac. Sci. , Univ. Tokyo)
Yosuke WATANABE (Fac. Sci. , Univ. Tokyo)
Ruizhe YANG (UIUC)

Technical Staff

Junpei KANAYA

Secretaries

Noriko KIYAMA
Keiko SUZUKI

Sub Nuclear System Research Division
Advanced Meson Science Laboratory

1. Abstract

Particles like muons, pions, and kaons have finite lifetimes, so they do not exist in natural nuclei or matters. Implanting these particles into nuclei/matters, exotic phenomena in varieties of objects can be studied from a new point of view.

Kaon is the second lightest meson which has strange-quark as a constituent quark. It is expected that if one embed a kaon into nuclei, the sizes of the nuclei become smaller and forms a high density object beyond the normal nuclear density. Study of this object could lead to better understanding of the origin of the mass of the matter, and may reveal the quark degree of freedom beyond the quark-confinement. Those properties can be studied by precise heavy pionic atom research in different angle. The other example is the weak interaction in nuclear matter. It can only be studied by the weak decay of hypernuclei, which have lambda particle in the nuclei.

Muon provides even wider variety of study ranging from particle physics to condensed matter and life sciences. For instance, stopping positively charged muon in a material, we obtain information on the magnetic properties or the local field at the trapped site. Injecting negatively charged muon to mixture of deuterium and tritium, muon attracts surrounding atoms and is known to cause d-t fusions.

As is already clear, in our research we introduce different kind of impurities into nuclei/matters, and study new states of matter, new phenomena, or the object properties.

2. Major Research Subjects

(1) Study of meson property and interaction in nuclei
(2) Origin of matter mass / quark degree of freedom in nuclei
(3) Condensed matter and material studies with muon
(4) Nuclear and particle physics studies via muon catalyzed fusion and ultra cold muon beam
(5) Materials science using Mössbauer spectroscopy

3. Summary of Research Activity

<u>Hadron physics at J-PARC and RIKEN-RIBF</u>

Kaon and pion will shed a new insight to the nuclear physics. The recent discovery of deeply bound pionic atom enables us to investigate the properties of mesons in nuclear matter. At RIKEN-RIBF, we are preparing precise experimental study of the pionic atom. We are intensively preparing another next generation kaon experiments (E15, E17 and E31) at J-PARC as day-one experiments. In these experiments, we are aiming at precise determination of the KN interaction, and clarify the nature of kaon in nuclei and $\Lambda(1405)$. By these experiments, we aim to be a world-leading scientific research group using these light meta-stable particles.

1) Deeply bound kaonic nuclei

We have performed experimental exploration of theoretically predicted deeply bound kaonic nuclear states in ^{3}He nucleus K^-ppn and K^-pnn. Akaishi and Yamazaki first calculated large binding energy and narrow width for the K^-ppn state. One of the most interesting features of the kaonic nucleus is that the strong attraction of the kaon is expected to contract the surrounding nucleons resulting in extremely high density of several times larger than normal nuclear density. Measurement of the kaon properties at such high energy density will provide precious information on the origin of hadron masses and the chiral symmetry breaking and its partial restoration.

The experimental principle adopted uses stopped K^- on suprefluid helium target, and we focus on emitted nucleon momenta measurement by Time-of-Flight (TOF) method. The last orbit of kaonic ^{4}He atom is 2p and the branching ratio from the last orbit to the nuclear kaon bound state accompanied with a nucleon emission was estimated to be 1 % at minimum.

The exploration was performed from 2002/September till 2005/December as series of experiments at the KEK-PS (E471, E549, E570) with almost common experimental setup. The obtained spectral shape was rather smooth and elaborate analysis showed uppper limit of the kaonic nucleus formation for both K^-ppn and K^-pnn states.

After the completion of above series of experiments, the KEK-PS was shut down to switch to a new facility J-PARC. Presently, we are preparing for an experiment to search for K^-pp nuclear system at the K1.8BR beamline of the J-PARC.

2) Deeply bound pionic atoms

We have made precision spectroscopy of pionic lead and tin atoms, and extracted information on the in-medium interaction between pion and nucleus, which leads to the exclusive quantitative evaluation of the chiral symmetry restoration in the nuclear matter.

Our collaboration which mainly consists of the RIKEN and the University of Tokyo group conducted throughout the experiments starting from R&D of pionic atom formation in nuclear reactions to its application to the precision spectroscopy.

The experiment was carried out in GSI, Darmstadt. Our first discovery was pionic 2p state in the lead 207 nucleus where the negative pion is accommodated in a delicate balance between the Coulomb attraction and the strong repulsion.

Following the discovery, we have performed experiments to measure 1s pionic lead 205 and ^{115}Sn, ^{119}Sn and ^{123}Sn isotopes.

We have analyzed the experimental spectra elaborately and extracted in-medium isovector interaction between pion and nucleus. In combination with experimental information on the pionic hydrogen and deuterium which gives the interaction in vacuum, we have accomplished evalution of the in-medium interaction modification. The modification is originating in the partial restoration of the chiral symmetry in the nucleus, and we have quantitatively evaluated for the first time the reduction of the chiral order parameter in the nuclear matter to be 33 %, which is consistent with theoretical prediction of 30 %.

Presently, we have been preparing for a sophisticated experimental setup of the pionic atom spectroscopy at the RIBF in the RIKEN. We expect about twice better experimental resolution with much smaller systematic errors.

3) Precision X-ray measurement of kaonic atom

Simultaneously with the above experiment (1), we have performed an X-ray spectroscopy of atomic $3d \rightarrow 2p$ transition of negatively charged K mesons captured by helium atoms. Many Kaonic atoms are known to be measured with various elements, however, there are very large deviations in the measured energy levels for the helium (and the oxygen) from the systematic expectations. The deviation originates in technical issues in old experiments, and new and high precision data have been long awaited for. Also, wave functions of the Kaonic atoms are expected to reflect the information on the existence of the inner structure, namely deeply bound Kaonic states. As a result of the experiment, we have succeeded in performing the spectroscopy and achieved the shift of 2 ± 2(stat.) ± 2(syst.) eV. The obtained results reject older data without any doubt, and the above deviation is dissolved. Presently, aiming at the determination of the level width and yield, we are analyzing the data. To clarify the KN interaction strength, we are preparing another x-ray measurement of the kaonic helium-3 atom, which is another day-one experiment at J-PARC.

Muon science at RIKEN-RAL branch

The research area ranges over particle physics to condensed matter studies and life science. Our core activities are based on the RIKEN-RAL Muon Facility located at the Rutherford Appleton Laboratory (UK), which provides intense pulsed-muon beam. We have variety of important research activities such as muon-catalyzed fusion (μCF) and condensed matter physics by muon spin rotation / relaxation / resonance (μSR).

(A) Condensed matter/materials studies with μSR

A new spectrometer named CHRONUS has been installed in Port-4 and commissioning works using real muon beam has also been completed to optimize the performance of the new spectrometer. The spectrometer has more than 600 detectors to minimize the counting loss and maximize the performance to measure tiny samples less than 20 mg. A platform of the Port-4 area is now being installed and will be completed after the summer time in 2011. After the completion of the Port-4 area, parallel experiment at both Port-2 and Port-4 will be planned.
There are three topics of material sciences studied by the muon-spin relaxation method at the RIKEN-RAL Muon facility in 2010.

1) Coherent soft-mode motion in a bond-disordered quantum spin system has been clarified from longitudinal-field μSR experiments. A shift of the spectral density of the spin fluctuations toward the low-frequency side was observed with decreasing temperature. It was shown from this result that the Bose-Einstein condensation of excited spin fluctuations at zero-degree is expected in quantum-spin systems.

2) A line node in the superconducting gap in the Fe-based superconducting oxide, KFe_2As_2, has been clarified. A change of a full-gap state to a nodal-gap state with changing the carrier concentration has been suggested.

3) A gapless state of the quantum spin-liquid state has been suggested to appear as the ground state of $EtMe_3Sb[Pd(dmit)_2]_2$ organic magnet. This result would suggest the appearance of a resonating valence bond state caused by an ideal triangular crystal structure.

(B) Nuclear and particle physics studies via muon catalyzed fusion and ultra cold muon beam

1) Muon catalyzed fusion (μCF)

We are studying the muon catalyzed fusion (μCF) processes in a wide range of hydrogen target conditions such as isotope mixtures and temperatures. This year the construction of a high pressure target was complete. We are testing the condition to keep D_2 target in solid state up to 30 K, thus we will be able to study μCF in high density and high temperature solid target, where the μCF is expected to occur much faster than in liquid.

2) Generation of ultra slow positive muon beam

Low energy muon beam, whose kinetic energy is variable from a few keV to a few tens of keV, will extend the scope of μSR technique from a bulk material to surfaces and multi-layered materials. It is also expected that a very sharp beam of low energy muon may enable a new way of precision measurement of muon's anomalous gyro-magnetic ratio (g-2). Following the successful generation of slow muon beam by laser ionization of thermally emitted muonium in vacuum, we plan to increase the slow muon beam intensity by more than 100 times. For this purpose, works are in progress on construction of a new intense laser system, search of materials for efficient muonium emission at room temperature, and design of new slow muon microscope optics. The new laser system was manufactured except the final amplifier. We successfully measured the muonium emission from material surface of silica aerogel in collaboration with TRIUMF.

Mössbauer spectroscopy at RIKEN-RIBF, HIMAC and CERN-ISOLDE

^{57}Fe Mössbauer spectroscopy following ion implantation of radioactive ^{57}Mn ($T_{1/2}$ = 1.45 min) has been applied to investigate the atomic jump processes of Fe impurity in semiconductors. ^{57}Mn is one of the useful nuclear probes to study the dynamic behavior and chemical states of dilute Fe atoms in solid. Iron impurities are known to degrade seriously electronic properties of silicon-based devices as well as solar cells. Generally, Fe atoms are thought to occupy only on interstitial sites in Si leading to a fast diffusion. In addition, substitutional Fe atoms were not found experimentally by standard evaluation techniques. Our investigation is to clarify the impurity diffusion of Fe atoms and the formation processes of “*substitutional Fe atoms*” in Si at high temperatures.

^{57}Mn implantation Mössbauer spectra from 800 K to 1200 K can be analyzed only by a broad singlet. The area intensities decreased with increasing temperatures, as explained by Debye model. The intensities suddenly decreased at 1000 K, but recovered again at 1100 K.

The relaxation behaviors observed in the present experiment can be interpreted in terms of a diffusion-reaction process of interstitial Fe atoms with vacancies within the time scale of 100 ns, leading to the formation of substitutional Fe atoms in the Si matrix. The process must be related to the recovery processes from non-equilibrium to the equilibrium states of the Si lattice around the ^{57}Fe nuclear probes.

^{57}Mn implantation Mössbauer studies were performed to study the defect formations induced by Fe/Mn implantation in ZnO, Al_2O_3, and MgO. These are attracting attention as dilute magnetic semiconductors. In the case of ZnO, the formation of Fe^{3+}–vacancy complexes is found to depend strongly on the implanted dose and to be faster and more efficient at higher temperatures. The results at these temperatures suggest the mobility of the Zn vacancy, together with vacancy trapping at the substitutional Mn/Fe impurities are responsible for the formation of Fe–V_{Zn} complexes. These experiments were carried out at CERN-ISOLDE and HIMAC.

The detection system for ^{57}Mn implantation Mössbauer studies was improved by using an anticoincidence method where a thin plastic scintillation counter was set between the detector and a sample in order to reject the β-rays from ^{57}Mn. The Mössbauer spectrum with sufficient signal-to-noise (S/N) ratio that is about 20 times higher than that in previous measurements was successfully obtained.

Head

Masahiko IWASAKI

Members

Katsuhiko ISHIDA
Kenta ITAHASHI
Yoshio KOBAYASHI
Teiichiro MATSUZAKI
Hiroaki OHNISHI
Haruhiko OUTA
Fuminori SAKUMA

Special Postdoctoral Researchers

Masami IIO
Kazuki OHISHI
Kazuki UENO

Foreign Postdoctoral Researcher

Risdiana

Contract Researchers

Yasuyuki ISHII
Takahisa KOIKE
Dai TOMONO
Kyo TSUKADA
Koji YOKOYAMA

Visiting Scientists

Tadashi ADACHI (Grad. Sch. Eng., Tohoku Univ.)
Jun AKIMITSU (Coll. Sci. Eng., Aoyama Gakuin Univ.)
Kunio AWAGA (Grad. Sch. Sci., Nagoya Univ.)
Pavel BAKULE (RAL, UK)
George BEER (Univ. of Victoria, Canada)
HyoungChan BHANG (Seoul National Univ., Korea)
N. Ludmila BOGDANOVA (ITEP, Russia)
Catalina CURCEANU (INFN, Italy)
Prasad Tara DAS (SUNY, USA)
Irwan DHARMAWAN (UNPAD, Indonesia)
Yasuaki EINAGA (Fac. Sci & Tech., Keio. Univ.)
Donald FLEMING (Univ. of British Columbia/TRIUMF)
Masaya ENOMOTO (Fac. Sci., Tokyo Univ. of Sci.)
Mark FAYFMAN (Kurchatov Inst., Russia)
Yutaka FUJII (Fac. Eng., Fukui Univ.)
Hiroyuki FUJIOKA (Grad. Sch. Sci., Univ. of Tokyo)

Masaki FUJITA (IMR, Tohoku Univ.)
Hideto FUKAZAWA (Grad. Sch. Sci., Chiba Univ.)
Takayuki GOTO (Fac. Sci. & Tech., Sophia Univ.)
Kazuo HAYAKAWA (Fac of Sci. & Tech., Shizuoka Inst. Sci. & Tech.)
Ryugo, S. HAYANO (Grad. Sch. Sci., Univ.of Tokyo)
Kazuto HIRATA (NIMS)
Satoru HIRENZAKI (Fac. Sci., Nara Women's Univ.)
Masahiko HIROI (Fac. Sci., Kagoshima Univ.)
Susumu IKEDA (IMSS, KEK)
Yutaka IKEDO (IMSS, KEK)
Rintaro INOUE (ICR, Kyoto Univ.)
Takayuki ISHIDA (Grad. Sch. Infor. & Eng., Univ. Elect. Commu.)
Fumihiro ISHIKAWA (Grad. Sch. Sci. & Tech., Niigata Univ.)
Shigeru ISHIMOTO (IPNS, KEK)
Tomoichi ISHIWATARI (SMI, Austria)
Ryosuke KADONO (IMSS, KEK)
Kazuya KAMAZAWA (Toyota Central R&D Labs.)
Toshiji KANAYA (ICR, Kyoto Univ.)
Motomi KATADA (Grad. Sch. Sci. & Eng., Tokyo Met. Univ.)
Mineo KATO (IMSS, KEK)
Roland KAWAKAMI (UC Riverside, USA)
Takayuki KAWAMATA (Grad. Sch. Sci. , Nagoya Univ.)
Naritoshi KAWAMURA (IMSS, KEK)
Seiko KAWAMURA (J-PARC, JAEA)
Hikomitsu KIKUCHI (Grad. Sch. Eng., Univ. of Fukui)
Jungho KIM (KRISS, Korea)
Yasushi KINO (Fac. Sci., Tohoku Univ.)
Wataru KOBAYASHI (Grad. Sch. Pure & Applied Sci., Univ. of Tsukuba)
Akihiro KODA (IMSS, KEK)
Yoh KOHORI (Fac. Sci., Chiba Univ.)
Yoji KOIKE (Grad. Sch. Eng., Tohoku Univ.)
Norimichi KOJIMA (Grad. Sch. Arts and Sci., Univ of Tokyo)
Kenya KUBO (Grad. Sch. Sci, ICU)
Shoko KUME (Grad. Sch. Sci., Univ.of Tokyo)
Yoshitaka KUNO (Grad. Sch. Sci., Osaka Univ.)
Takuya KURAHASHI (IMS)
Haruhiko KUROE (Fac. Sci. & Tech., Sophia Univ.)
Guido LANGOUCHE (NVAO, Netherlands)
Chow LEE (UCF, USA)
Shunsuke MAKIMURA (IMSS, KEK)
Hirotaka MANAKA (Grad. Sch. Sci. & Eng., Kagoshima Univ.)
Yasuyuki MATSUDA (Grad. Sch. Arts and Sci., Univ. of Tokyo)
Tsutomu MIBE (IPNS, KEK)
Yasuhiro MIYAKE (IMSS, KEK)
Hitoshi MIYASAKA (Grad. Sch. Sci., Tohoku Univ.)
Jun MIYAZAKI (Fac. Sci. Div., Nihon Univ.)

Soichiro MIZUSAKI (Coll.Sci. & Eng., Aoyama Gakuin Univ.)
Tomoyuki MOCHIDA (Grad. Sch. Sci., Kobe Univ.)
Kazuhiko MUKAI (Toyota Central R&D Labs.)
Yujiro NAGATA (Coll. Sci. Eng., Aoyama Gakuin Univ.)
Takashi NAGATOMO (Grad. Sch. Sci., ICU)
Hiroyuki NAKAMURA (Grad. Sch. Eng., Kyoto Univ.)
Jin NAKAMURA (Grad. Sch. Infor. & Eng., Univ. Elect. Commu.)
Kazutaka NAKAHARA (Univ. of Maryland. USA)
Satoshi NAKAMURA (Grad. Sch. Sci., Tohoku Univ.)
Takashi NAKAMURA (Grad. Sch. Sci. & Eng., Tokyo Tech.)
Takayoshi NAKAMURA (RIES, Hokkaido Univ.)
Takehito NAKANO (Grad. Sch. Sci., Osaka Univ.)
Saburou NASU (Grad, Sch. Eng. & Sci., Osaka Univ.)
Kazuhiko NINOMIYA (Advanced Sci. Res. Center, JAEA)
Nobuhiko NISHIDA (Fac. Sci., Tokyo Tech.)
Yoichi NISHIWAKI (Sch. Medi., TWMU)
Kusuo NISHIYAMA (IMSS, KEK)
Tatsuo NORITAKE (Toyota Central R&D Labs.)
Hiroyuki NOUMI (RCNP, Osaka Univ.)
Hiroshi NOZAKI (Toyota Central R&D Labs.)
Yasuo NOZUE (Grad. Sch. Sci., Osaka Univ.)
Agung NUGROHO (ITB, Indonesia)
Yoshitaka OHKUBO (KURRI, Kyoto Univ.)
Shinji OKADA (INFN, Italy)
Vassili PEREVOZCHIKO (VNIEF, Russia)
Leonid PONOMAREV (Kurchatov Institute, Russia)
Francis PRATT (RAL, UK)
Lusy SAFRIANI (UNPAD, Indonesia)
Shin-ichi SAKAMOTO (J-PARC, JAEA)
Naohito SAITO (IPNS, KEK)
Kazuhiko SATO (Grad. Sch. Sci. & Eng., Saitama Univ.)
Masaharu SATO (Grad. Sch. Sci., Univ.of Tokyo)
Ralph SCHEICHER (Michigan Tech. Univ., USA)
Ryoichi SEKI (California State Univ., Northridge, USA)
Kouichirou SHIMOMURA (IMSS, KEK)
Ichiro SHIRAKI (Grad. Sch. Medi. & Eng. Sci., Univ. of Yamanashi)
Vyacheslas STORCHAK (VNIIEF, Russia)
Patrick STRASSER (IMSS, KEK)
Hiroyuki SUGAI (Advanced Sci. Res. Center, JAEA)
Jun SUGIYAMA (Toyota Central R&D Labs.)
Ken SUZUKI (SMI, Austria)
Haruhiko SUZUKI (Grad. Sch. Nat. Sic. & Tech., Kanazawa Univ.)
Hiroyuki SUZUKI (NIMS)
Soh SUZUKI (CRC, KEK)
Takao SUZUKI (Grad. Sch. Sci., ICU)
Takatoshi SUZUKI (Grad. Sch. Sci., Univ.of Tokyo)

Yoshikazu TABATA (Grad, Sch. Eng. & Sci., Kyoto Univ.)
Shigeru TAKAGI (Grad, Sch. Sci., Tohoku Univ.)
Kazuyuki TAKAI (Grad. Sch. Sci. & Eng., Tokyo Tech.)
Nao TAKESHITA (NeRI, AIST)
Hiroyuki TAKEYA (NIMS)
Yoichi TANABE (WPI, Tohoku Univ.)
Manobu TANAKA (IPNS, KEK)
Hiroshi TANIDA (Grad. Sch. Adv. Sci. Matter, Hiroshima Univ.)
Akihiro TANIGUCHI (KURRI, Kyoto Univ.)
Harry TOM (UC Riverside, USA)
Eiko TORIKAI (Grad. Sch. Medi. & Eng. Sci., Univ. of Yamanashi)
Akihisa TOYODA (IPNS, KEK)
Satoshi TSUTSUI (JASRI)
Kazuo UEDA (ISSP, Univ. of Tokyo)
Masatomo UEHARA (Grad. Sch. Eng., Yokohama Natl.Univ.)
Helmut WEICK (GSI, Germany)
Zhuan XU (Zhejiang Univ. China)
Kazuyoshi YAMADA (IMR, Tohoku Univ.)
Yasuhiro YAMADA (Fac. Sci., Tokyo Univ. of Sci.)
Yutaka YOSHIDA (Fac of Sci. & Tech., Shizuoka Inst. Sci. & Tech.)
Arkady YUKHINCHUK (VNIIEF, Russia)
Johann ZMESKAL (SMI, Austria)

Visting Technician

Shinji KAI (Tanaka Kikinzoku Kogyo K.K.)
Kunihiro SHIMA (Tanaka Kikinzoku Kogyo K.K.)

Research Consultants

Yoshinori AKAISHI
Masayasu KAMIMURA
Atsuko ITO
Toshimitsu YAMAZAKI

Students

Junior Reserch Associates

Yuya FUJIWARA (Grad. Sch. Sci., Univ. of Tokyo)
Toshihiko HIRAIWA (Grad. Sch. Sci., Kyoto Univ.)
Satoshi ITOH (Grad. Sch. Sci., Univ. of Tokyo)
Yuta SADA (Grad. Sch. Sci., Kyoto Univ.)
Makoto TOKUDA (Grad. Sch. Sci. & Eng., Tokyo Tech.)

International Program Associate

Budi ADIPERDANA (UNPAD, Indonesia)

Intern

Hiroshi KOU (Grad. Sch. Sci. & Eng., Tokyo Tech.)

Student Trainees

Yuki AKIYAMA (Grad. Sch.Sci. & Eng., Shizuoka Inst. Sci. & Tech.)
Mika DOIZOE (Grad. Sch. Sci., Tokyo Univ. Sci.)
Shun ENOMOTO (Grad, Sch. Sci., Osaka Univ.)
Jafar ESMAILI (Isfahan Univ. Tech., Iran)
Masatoshi HIRAISHI (Sch. High Enegy Acce. Sci.,Sokendai)
Tadashi HASHIMOTO (Grad. Sch. Sci., Univ. of Tokyo)
Maryam HASSANVAND (Isfahan Univ. Tech., Iran)
Masahiro ICHINO (Grad. Sch.Sci. & Eng., Shizuoka Inst. Sci. & Tech.)
Naho IINUMA (Grad. Sch. Sci., Tokyo Univ. Sci.)
Miho ITO (Grad. Sch. Sci. & Eng., Saitama Univ.)
Naoki KASE (Grad. Sch. Sci.& Eng., Aoyama Gakuin Univ.)
Yu KAWAHARA (Grad. Sch. Sci., Tokyo Univ. Sci.)
Akio KAWASAKI (MIT, USA)
Jun KOBAYASHI (Fac. Sci., Saitama Univ.)
Takumi KOBAYASHI (Grad. Sch. Sci., Univ. of Tokyo)
Hiroto KUMABE (Grad. Sch.Sci. & Eng., Shizuoka Inst. Sci. & Tech.)
Daisuke KUNO (Grad. Sch. Sci., Tohoku Univ.)
Tatsuya MATSUE (Fac. Sci., Tokyo Univ. Sci.)
Masanori MIYAZAKI (Sch. Phys. Sci.,Sokendai)
Saori NAKAJIMA (Grad. Sch. Sci. & Tech., Sophia Univ.)
Masaki NAKAMURA (Grad. Sch. Sci. & Eng., Tokyo Tech.)
Takahiro NISHI (Grad. Sch. Sci., Univ. of Tokyo)
Yuki NOZAWA (Grad. Sch. Sci., Kyoto Univ.)
Noriaki OKABE (Grad. Sch. Sci. & Eng., Saitama Univ.)
ROGER PINK (SUNY at Albany, USA)
Manami SATAKE (Grad. Sch. Sci. & Eng., Tokyo Tech.)
Takaaki SHINKAWA (Grad. Sch. Sci. & Eng., Saitama Univ.)
Ryuichi SUEHIRO (Grad. Sch. Sci., Osaka Univ.)
Kensuke SUZUKI (Grad. Sch. Eng., Tohoku Univ.)
Kazuhiro TAKAHASHI (Grad. Sch. Sci., Univ. of Tokyo)
Tomonori TAKAHASHI (Grad. Sch. Sci., Univ. of Tokyo)
Hideyuki TATSUNO (Grad. Sch. Sci., Univ. of Tokyo)
Koichi TODOROKI (Grad. Sch. Sci., Univ. of Tokyo)
Natsuki TOMIDA (Grad. Sch. Sci., Kyoto Univ.)
Yoshinori TSUKAMOTO (Fac. Sci. & Eng., Shizuoka Inst. Sci. & Tech.)
Yoshiko TSUKIYAMA (Grad. Sch. Sci. & Eng., Saitama Univ.)
Tomotaka UEHARA (Fac. Sci., Saitama Univ.)
Riku YAMAGUCHI (Fac. Sci., Tokyo Univ. Sci.)
Mamoru YASUIKE (Fac. Sci., Tokyo Univ. Sci.)

Assistants

Yoko FUJITA
Yuri TSUBURAI

Sub Nuclear System Research Division
RIKEN-BNL Research Center
Theory Group

1. Abstract

The RIKEN BNL Research Center (RBRC) was established in April 1997 at Brookhaven National Laboratory in New York, USA. The Center is dedicated to study of strong interactions, including hard QCD/spin physics, lattice QCD and RHIC physics through nurturing of a new generation of young physicists. The Theory Group activities are closely and intimately related to those of the Nuclear Theory, High Energy Theory and Lattice Gauge Theory Groups at BNL. The RBRC theory group carries out research in three areas: numerical lattice QCD, perturbative QCD and phenomenological QCD. It pioneered the use of the domain-wall fermion method in lattice QCD and has investigated various aspects of hadron physics including the calculation of neutral Kaon CP-violations that is relevant for checking the Cabibbo-Kobayashi-Maskawa theory. The perturbative QCD effort has developed various new methods required for studying hadron structures, especially in spin physics research. The group has pioneered phenomenological QCD researches of color superconductivity, isospin density,and small-x phenomena in extreme hadronic matters.

2. Major Research Subjects

(1) Perturbative QCD
(2) Lattice QCD numerical research
(3) Phenomenological QCD

3. Summary of Research Activity

The RIKENBNL Research Center (RBRC) was established in 1997 to support the RIKEN activities at RHIC in BNL, and also to promote theoretical studies related to RHIC, i.e. theories of strong interaction. The center's first director was T. D. Lee (Columbia University), and in October 2003, the former director of BNL, N. P. Samios, succeeded to the post of director. The center consists of a theory group lead by L. Mclerran (BNL) and an experimental group lead by Y. Akiba of RIKEN.

Research in the RBRC theory group focuses on a wide variety of phenomena caused by the strong interaction, one of the four fundamental interactions in nature. The strong interaction is described theoretically by Quantum Chromodynamics (QCD), and the research projects in the RBRC theory group aim to elucidate various phenomena brought about by the strong interaction from the principles of QCD. Major subjects of our research include studies (a) based on lattice QCD, (b) on spin physics based on perturbative QCD, and (c) on QCD in extreme conditions such as high temperature, high density or high energy. RBRC offers RHIC Physics Fellowships, allowing joint appointments with universities. These Fellowships enable a talented researcher to maintain a tenure track position at his/her university as well as a Fellow position at RBRC for a certain period of time. This system was established in order to increase the research potential of RBRC and to disseminate its research activities and results.

At present, RBRC has cooperative agreements with Arizona State University, the City University of New York, Pennsylvania State University, the State University of New York at Stony Brook, Texas A&M University, as well as with BNL and with Lawrence Berkeley National Laboratory.

(1) Lattice QCD

QCDOC (QCD on chip), a second-generation lattice-QCD computer, was developed in the collaboration amongst the RBRC group, Columbia University and IBM. Three units of such a machine with 10 teraflops computing power are in operation since 2005; two in BNL (RBRC and DOE) and one in Edinburgh (UK-QCD), and formed a world-wide strong collaboration for the lattice QCD studies. Computations are also being performed on the IBM Blue Gene super computers located at ANL and BNL(NY Blue), on the the cluster computers at RIKEN(Japan), FNAL and JLAB.

Such computing power enables us to perform precise calculations with 3 quark flavors with proper handling on the chiral symmetry breaking. Several projects are ongoing: flavor physics for Kaon and B-meson, electro-magnetic properties of hadrons, proton decay, the nuclear force, nucleon form factors which relates to the proton spin problem, and QCD thermodynamics in finite temperature/density systems as is produced in RHIC heavy-ion collisions. The third generation supercomputer for QCD research, QCDCQ (QCD with Chiral Quarks), a successor to the QCDOC computer, (200Tflops peak / rack) is planed to be installed by the end of 2011. The major breakthrough to the important problems such as the direct CP violating process ($K \rightarrow \pi\pi$, ε'/ε) will be address on this computer.

(2) Perturbative QCD and spin physics

The ongoing RHIC spin experiments have motivated much of the parallel theoretical developments at RBRC. In the area of transverse spin physics, novel predictions have been obtained for the single transverse-spin asymmetry in open charm production in pp collisions at RHIC. This asymmetry probes three gluon correlations in polarized proton. In addition, radiative QCD corrections to single-spin observables were investigated, providing the relevant evolution equations. Further work focused on hyperon production at RHIC, and on azimuthal asymmetries in the Drell-Yan process.

In the spin and perturbative QCD program, a major contribution from the hadronization process to the single transverse spin asymmetry in inclusive hadron production was obtained, which is likely to explain the recent experimental anomaly between the eta and pi mesons. In addition, the evolution and the universality properties of the so-called naive time-reversal odd fragmentation function has been obtained. Other work includes the investigation of the universality properties of the unintegrated gluon distribution a small x .

(3) Phenomenological QCD -- QCD under extreme conditions --

To establish a detailed picture of relativistic heavy ion collisions, QCD-based theoretical approaches are in progress. Especially the idea of "color glass condensation (CGC)" can be a key to understand the initial condition of the heavy ion collision. Other phenomenological approaches are in progress to understand the characteristics of strongly interacting quark gluon plasma. A recent effort has been initiated to understand heavy ion elliptic flow in term s of viscous hydrodynamics. A new finite temperature effective field theory is being developed for the strongly interacting quark gluon plasma to explain the suppression of sheer viscosity in the region of the phase transition.

Efforts on RHIC phenomenology proceed on a broad front. Recent efforts include improving hydrodynamic computations using state of the art equations of state derived from lattice gauge theory. Understanding the nature of matter at high baryon number density has generated the idea of Quarkyonic Matter, that may have implications for an upcoming low energy run at RHIC and eventual experiments in the future at FAIR and NICA. An issue being studied is the nature of mass generation and the breaking of translational invariance. A central focus of work at RBRC, the Color Glass Condensate and the Glasma, matter that controls the high energy limit of QCD, is being realized in experiments at RHIC. A workshop held in May 2010 summarized activity in this field, and proceedings will come out as a special edition of Nuclear Physics A. Much activity focuses on the relation between observations at LHC and the implications made at RHIC.

Group Leader

Larry McLERRAN

Deputy Group Leader

Anthony J. BALTZ

Members

Yasumichi AOKI *1
Denes MOLNAR *2
Kirill TUCHIN *2
Rainer FRIES *2
Toru KOJO *4
Taku IZUBUCHI *1
Derek TEANEY *2
Adrian DUMITRU *2
Cecilia LUNARDINI *2
Anna STASTO *2
Zhongbo KANG *3
Eigo SHINTANI *3
Christoph LEHNER *3(RIKEN FPR)

Visiting Members

Miklos GYULASSY (Columbia Univ., USA)
Robert L. JAFFE (Massachusetts Inst. Technol., USA)
Robert MAWHINNEY (Columbia Univ., USA)
Edward HURYAK (State Univ. New York, Stony Brook, USA)
Testufumi HIRANO (U. Tokyo)
Shigemi OHTA (KEK)
Feng YUAN (LBNL)
Thomas BLUM (University of Connecticut)
Christopher DAWSON (The University of Virginia)
Tomomi ISHIKAWA (University of Connecticut)
Chulwoo JUNG (BNL)
Meifeng LIN (Yale U)

Yusuke TANIGUCHI (Tsukuba U)
Takeshi YAMAZAKI (Nagoya Univ)
Shumpei UNO (Nagoya Univ)
Ran ZHOU (University of Connecticut)

Secretarial Staff

Kerry ZENDZIAN (Secretary to Director N. P. Samios)
Pamela ESPOSITO (Theory Group Secretary)
Taeko ITO (Assistant to Account Manager for Administration)
Susan FOSTER (Experimental Group Secretary)

Administrative Staff / RIKEN Japan

Minoru Fujiki, Deputy Director, Nishina Center Research Promotion Office

Emiko ADACHI (RBRC Account Manager for Administration)
Keiko SUSUKI (Japan)

****1 RIKEN BNL Fellow   *2 RHIC Physics Fellow,***
****3 Research Associate,   *4 Special Postdoctoral Researcher,***
****5 RHIC visiting Fellow***

Sub Nuclear System Research Division
RIKEN-BNL Research Center
Experimental Group

1. Abstract

RIKEN BNL Research Center (RBRC) Experimental Group studies the strong interactions (QCD) using RHIC accelerator at Brookhaven National Laboratory, the world first heavy ion collider and polarized p+p collider. We have three major activities: Spin Physics at RHIC, Heavy ion physics at RHIC, and detector upgrades of PHENIX experiment at RHIC.

We study the spin structure of the proton using the polarized proton-proton collisions at RHIC. This program has been promoted by RIKEN's leadership. The first focus of the research is to measure the gluon spin contribution to the proton spin. Our recent data analysis has shown that the proton spin carried by the gluons is small, which is a very striking finding beyond our expectations.

The aim of Heavy ion physics at RHIC is to re-create Quark Gluon Plasma (QGP), the state of Universe just after the Big Bang. Two important discoveries, jet quenching effect and strong elliptic flows, have established that new state of dense matter is indeed produced in heavy ion collisions at RHIC. We are proceeding to understand the nature of the matter. Recently, we have measured direct photons in Au+Au collisions for $1<p_T<3$ GeV/c , where thermal radiation from hot QGP is expected to dominate. The comparison between the data and theory calculations indicates that the initial temperature of 300 MeV to 600 MeV is achieved. These values are well above the transition temperature to QGP, which is calculated to be approximately 170 MeV by lattice QCD calculations.

We has major roles in detector upgrades of PHENIX experiment, namely, the silicon vertex tracker (VTX) and muon trigger upgrades.

2. Major Research Subjects

(1) Experimental Studies of the Spin Structure of the Nucleon
(2) Study of Quark-Gluon Plasma at RHIC
(3) PHENIX detector upgrades

3. Summary of Research Activity

The RIKEN-BNL Research Center was established in 1997 to support the RIKEN activities at RHIC in BNL, and also to promote theoretical studies related to RHIC, i.e. theories of strong interaction. The center's first director was T. D. Lee (Columbia University), and in October 2003, the former director of BNL, N.P. Samios, succeeded to the post of the director. The center consists of a theory group lead by L. Mclerran (BNL) and an experimental group lead by Y. Akiba, a vice chief scientist of RIKEN in Wako.

We study the strong interactions (QCD) using the RHIC accelerator at Brookhaven National Laboratory, the world first heavy ion collider and polarized p+p collider. We have three major activities: Spin Physics at RHIC, Heavy ion physics at RHIC, and detector upgrades of PHENIX experiment.

(1) Experimental study of spin structure of proton using RHIC polarized proton collider

How is the spin of proton formed with 3 quarks and gluons? This is a very fundamental question in Quantum Chromodynamics (QCD), the theory of the strong nuclear forces. The RHIC Spin Project has been established as an international collaboration between RIKEN and Brookhaven

National Laboratory (BNL) to solve this problem by colliding two polarized protons for the first time in history. This project also has extended the physics capabilities of RHIC.

The first goal of the RHIC spin physics program is to elucidate a contribution of the gluon spin in the proton spin. We have measured double-helicity asymmetries of neutral pions to study gluon polarization in proton. Our most recent publication from 2006 run have shown that the gluon polarization in the proton is small, and only about half of proton spin can be accounted by gluon spin in the measured region of gluon momentum in proton. The remaining part must be carried by gluons in lower momentum region where the measurement is not sensitive, and/or reside in the orbital-angular momentum of quarks and gluons.

To finalize the smallness of the gluon-spin contribution, we need to measure double helicitiy asymmetry in direct photon production. This process is dominated by a single and the simplest process, gluon Compton scattering, in perturbative QCD, and is the golden channel to determine the gluon density and the gluon polarization in the proton. We published a paper on direct photon cross section in p+p collisions at RHIC. Preliminary results on double-helicity asymmetry of direct photon from the 2006 run have been obtained.

We have also accumulating transversely-polarized proton collision data to measure single transverse-spin asymmetries of processes which are predicted to be sensitive to the orbital-angular momentum of quarks and gluons. In 2006 and 2008, PHENIX recorded 2.7/pb and 4.5/pb, respectively, of transversely-polarized proton collisions data at 200 GeV to investigate single transverse-spin asymmetries. Several transverse spin analyses of these high statistics data are on going.

The 2009 run of RHIC is a major spin run. We had the first 500 GeV p+p run and a long p+p run at 200 GeV. The main purpose of the 500 GeV run is to measure anit-quark polarization from the single longitudinal asymmetry A_L in the W boson production. The 500 GeV part of RUN9 is an engineering run. The polarization is lower (~40%) than the 200 GeV run and the luminosity in the 5 weeks of data taking period is rather limited, at about 14/pb recorded in PHENIX. Yet we have observed the first signal of W→e decays in p+p collisions in PHENIX central arm. We measured the production cross section of the W boson and a large spin asymmetry A_L in the W production. These results have been recently published in Physical Review Letters.

In addition to the study of polarized p+p collisions at RHIC, we study quark fragmentation function. With collaboration with the BELLE experiment at High Energy Accelerator Research Organization (KEK), we discovered that the spin direction of a quark can be determined from its hadronic fragments. Precise data of the quark fragmentation function can be used to understand the cross sections and the spin dependences of particle production in polarized p+p collisions at RHIC. We continue the study of the quark fragmentation function at BELLE.

(2) Experimental study of Quark-Gluon Plasma using RHIC heavy-ion collider

The goal of high energy heavy ion physics at RHIC is study of QCD in extreme conditions i.e. at very high temperature and at very high energy density. Experimental results from RHIC have established that dense partonic matter is formed in Au+Au collisions at RHIC. The matter is very dense and opaque, and it has almost no viscosity and behaves like a perfect fluid. These conclusions are primarily based on the following two discoveries:

- Strong suppression of high transverse momentum hadrons in central Au+Au collisions (jet quenching)
- Strong elliptic flow

The focus of the research in heavy ion physics at RHIC is now to investigate the properties of the matter. RBRC have played the leading roles in some of the most important results from PHENIX in the study of the matter properties. These include (1) measurements of heavy quark production from the single electrons from heavy flavor decay (2) measurements of J/ψ production (3) measurements of di-electron continuum and (4) measurements of direct photons.

The most important recent result is the measurement of direct photons for $1<p_T<5$ GeV/c in p+p and Au+Au through their internal conversion to e^+e^- pairs. If the dense partonic matter formed at RHIC is thermalized, it should emit thermal photons. Observation of thermal photon is direct evidence of early thermalization, and we can determine the initial temperature of the matter. It is predicted that thermal photons from QGP phase is the dominant source of direct photons for $1<p_T<3$ GeV/c at the RHIC energy. We measured the direct photon in this pT region from measurements of quasi-real virtual photons that decays into low-mass e^+e^- pairs. Strong enhancement of direct photon yield in Au+Au over the scaled p+p data has been observed. Several hydrodynamical models can reproduce the central Au+A data within a factor of two. These models assume formation of a hot system with initial temperature of T_{init} = 300 MeV to 600 MeV. This is the first measurement of initial temperature of quark gluon plasma formed at RHIC. These results are recently published in Physical Review Letters.

(3) PHENIX detector upgrade

The group has major roles in several PHENIX detector upgrades, namely, the silicon vertex tracker (VTX) and muon trigger upgrades.

VTX is 4 layers of silicon tracker, jointly funded by RIKEN and the US DOE. The inner two layers are silicon pixel detectors and the outer two layers are silicon strip detectors. The detector has been completed in November 2010 and has been installed in PHENIX IR. With this new detector we can measure heavy quark (charm and bottom) production in p+p and heavy ion collisions.

Muon trigger upgrades are needed for W→ mu measurement at 500 GeV. New trigger electronics (Muon Trigger FEE) have been installed in the muon arms. New muon trigger detectors based on RPC technology have been also installed. With these new trigger systems, we can start measuring the W production in forward and backward direction.

Group Leader

Yasuyuki AKIBA

Deputy Group Leader

Abhay DESHPANDE

Members

Yuji GOTO
Itaru NAKAGAWA
Takashi ICHIHARA
Atsushi TAKETANI
Yasushi WATANABE
Satoru YOKKAICHI
Ralf-Christian SEIDL
Kensuke OKADA *1
Stefan BATHE *2

David KAWALL *2
Kieran BOYLE *3
John KOSTER (RIKEN FPR) *3
Kenichi KARATSU (Kyoto Univ)*5
Yoki ARAMAKI (CNS-U-Tokyo)*5
Akihisa TAKAHARA (CNS-U-Tokyo)*5
Ryoji AKIMOTO (CNS-U-Tokyo)*5
Hidemitsu ASANO (Kyoto Univ)*5
Masaya NIHASHI (Hiroshima Univ)*5
Takahito TODOROKI (Tsukuba Univ)*5

Visiting Members
Naohito SAITO (KEK)
Zheng LEE (BNL)
Kiyoshi TANIDA (Seoul Univ.)
Akio OGAWA (BNL)
Masahiro OKAMURA (BNL)
Rachid NOUICER (BNL)
Kotaro KONDO (BNL)
Ady HERSHCOVITCH (BNL)
Kohei SHOJI (Kyoto Univ.)*4
Seishi DAIRAKU (Kyoto Univ.)*7
Katsuro NAKAMURA (Kyoto Univ.)*6
Takeshi KANESUE (Kyusyu Univ.)*6
Yorito YAMAGUCHI (CNS-U-Tokyo)*7

***1RIKEN BNL Fellow, *2 RHIC Physics Fellow,**
***3 Research Associate, *4 Special Postdoctoral Researcher,**
***5 Junior Research Associate, *6 JSPS Student, *7 Student trainee**

RIBF Research Division
Radioactive Isotope Physics Laboratory

1. Abstract

This laboratory explores exotic nuclear structures and dynamics in exotic nuclei that have never been investigated before, such as those with largely imbalanced proton and neutron numbers. Our aim is to develop new experimental techniques utilizing fast RI beams to discover new phenomena and properties in exotic nuclei. Another important subject is the equation-of-state in asymmetric nuclear matter, and its association with the origin of elements and with neutron stars. For instance, we are making attempts to the better understand underlying mechanism for exotic stability-enhancements of very neutron-rich fluorine isotopes, the large deformation of the nucleus Mg-34 with N=22 in spite of its vicinity to the N=20 magic neutron number and anomalous collectivity in C-16. We are further extending these studies to medium- and heavy-mass regions by developing facilities, detectors and unique methods at RIBF, thereby leading on the challenging task to find new exotic phenomena. We also perform numerical simulations of nucleosynthesis under the environment of core-collapse supernovae, and moreover quest for footprints of supernovae and solar activities in the past, embedded in Antarctic ice core.

2. Major Research Subjects

(1) Study of structure and dynamics of exotic nuclei through developments of new tools in terms of reaction- and technique-based methodology
(2) Research on EOS in asymmetric nuclear matter via heavy-ion induced reactions
(3) Promotion of nuclear astrophysics in an interdisciplinary organization
(4) Detector developments for spectroscopy and reaction studies

3. Summary of Research Activity

(1) Missing mass method

Missing mass technique is promising for future radioactive isotope programs at RIBF. Detection of recoil particles from target is essential in excitation energy determination of particle unbound states without any assumption of particle- and gamma-decay processes, and also giving transfer angular momentum from the angular distribution measurement. We have developed a solid hydrogen target as well as a detector system called ESPRI for proton-(in)elastic scattering. In 2010, the ESPRI system was placed at GSI to measure proton elastic scattering from Ni isotopes. In addition, the first missing mass spectroscopy was performed at RIBF, where the start-of-art detector MUST2 was invited from France to investigate O-24 and its neighboring nuclei.

(2) In-beam gamma spectroscopy

In the medium and heavy mass region explored at RIBF, collective natures of nuclei are one of important subjects, which are obtained through production and observation of high excited and high spin states. To populate such states, heavy-ion induced reactions such as fragmentation, fission are useful. So far, we have developed two-step fragmentation method as an efficient method to identify and populate excited states, and lifetime measurements to deduce transition strength. At the end of 2008, the first spectroscopy on nuclei island-of-inversion region was performed and the result on the first excited state in Ne-32 was published in PRL in 2009. At the end of 2009, the second campaign of in-beam gamma spectroscopy was organized and backgrounds originating from atomic processes in heavy target were investigated. At the end of 2010, the island-of-inversion region was revisited and the region at N=28 was also investigated. A multitude of data via inelastic, nucleon knock-out, fragmentation channels were obtained. Analysis is now in progress.

(3) Decay spectroscopy

Beta- and isomer-spectroscopy is an efficient method for studying nuclear structure, especially for non-yrast levels. We had accumulated experimental techniques at the RIPS facility to investigate nuclear structure in light mass region via beta-gamma and beta-p coincidence. Concerning the medium and heavy mass region available at RIBF, we have developed two position-sensitive active-stoppers to achieve low-background via position correlation; strip-silicon detectors and a cylindrical active stopper called CAITEN. At the end of 2009, the first decay spectroscopy on neutron-rich nuclei with A~100 was performed at the new facility of RIBF. Half-lives for 18 neutron-rich nuclei were determined for the first time, and the results were published in PRL, where we discussed in comparison with theoretical predictions as well as in terms of the r-process path. At the same time, the CAITEN detector was successfully tested with fragments produced with a Ca-48 beam.

(4) Equation-of-state via heavy-ion central collisions

Equation-of-state in asymmetric nuclear matter is one of major subjects in physics of exotic nuclei. Concerning RIBF programs, a detector for pions produced in heavy-ion collisions is being tested at the HIMAC. In addition, a TPC for the SAMURAI spectrometer is being designed.

(5) Interdisciplinary study for nuclear astrophysics

To understand the origin of elements beyond ion, interdisciplinary works are important in linking data from nuclear physics program. We are promoting simulation of nucleosynthesis in the r-process path, and investigation of Antarctic ice core to search for footprints of supernovae as well as solar activity in the past via mass spectrometer, to link data obtained from nuclear physics program.

Head

Hiroyoshi SAKURAI

Members

Takashi ICHIHARA
Takashi KISHIDA
Yoichi NAKAI
Shunji NISHIMURA
Hideaki OTSU
Heiko SCHEIT
Tadaaki ISOBE

Nishina Center Research Scientist

Yuko MOTIZUKI

Research Associate

Hiroshi WATANABE

Satoshi TAKEUCHI
Mizuki NISHIMURA
Hiu Ching LEE

Contract Researcher
Maya TAKECHI

Special Postdoctoral Researcher
Satoshi SAKAGUCHI
Yasuhiro TOGANO

Foreign Postdoctoral Researcher
David STEPPENBECK
Zhihuan LI
Pieter DOORNENBAL

Senior Visiting Scientist
Wolfgang MITTING (Michigan State University, USA)
Kengo OGAWA (Chiba Univ.)
Igal TALMI (Weizmann Institute of Science, Israel)
Hisashi HORIUCHI (Kyoto Univ.)

Visiting Scientists
Sachiko AMARI (Washington Univ.,USA)
Koichiro ASAHI (Tokyo Institute of Technology)
Sudhee BANERJEE (Variable Energy Cyclotron Center, India)
Susan Jill BERRYMAN(Lawrence Berkeley National Laboratory, USA)
Nives BLASI (INFN(Istituto Nazionale di Fisica Nucleare)Italy)
Angela BRACCO (The University of Milano, Italy)
Franco CAMERA (The University of Milano, Italy)
Silivio CHERUBINI (University of Catania, Italy)
Alfred DEWALD (University of Cologne, Germany)
Adrian GELBERG (Universitat zu Koeln, Germany)
Hui HUA (Peking University, China)
DongXing JIANG (Peking University, China)
Reiner KRUECKEN (Technische Universitaet Muenchen, Germany)
Xiangqing LI (Peking University, China)
Chen LII (Peking University, China)
William LYNCH (Michigan State University, USA)
Bradley S. MEYER（Clemson University ,USA)
Evgueni NIKOLSKI (RRC Kurchatov Institute, Institute of General and Nuclear Physics, Russia)
Yuri PENIONZHKEVICH (Flerov Laboratory of Nuclear Reactions,Russia)
Zsolt Ferenc PODOLYAK (University of Surrey, England)
Simona SCHEIT (Tokyo Univ.)
Michael Scott SMITH (Oak Ridge National Laboratory,USA)
Oleg Borisovich TARASOV (Michigan State University, USA)

Betty ManYee TSANG (Michigan State University, USA)
Philip Malzard WALKER (University of Surrey, Indaia)
Oliver WIELAND (INFN(Istituto Nazionale di Fisica Nucleare)Italy)
Henrik Alojzy WITALA（Jagiellonian University, Poland)
Zhigang XIAO（Tsinghua University, China)
Furong XU (Peking University, China)
Shuangquan ZHANG (Peking Univ., China)
Hooi Jing ONG (RCNP)
Wei GUO (Shanghai Inst. Applied Physics, China)
Yucheng GE (Peking Univ., China)
Hideki MADOKORO (Mitsubishi Heavy Industries, Ltd)
Hidetomo YOSHIDA (Tohoku Univ.)
Takahiro TACHIBANA (Waseda High Sch., Waseda Univ.)
Kohji TAKAHASHI (Universite Libre de Bruxelles,Belgian)
Yasuo MIAKE (Tsukuba Univ.)
Satoru TERASHIMA (GSI, Germany)
Hiroyuki KOURA (JAEA)
Yohei MATSUDA (Tohoku Univ.)
Yoshihiro SHINBARA (Nigata Univ.)
Junsei CHIBA (Tokyo University of Science)
Juzo ZENIHIRO (RCNP)
Tetsuya MURAKAMI (Kyoto Univ.)
Jiro MURATA (Rikkyo Univ.)
Naohiko OTSUKA (International Atomic Energy Agency, Austria)
Toshiyuki SUMIKAMA (Tokyo University of Science)
Yugang MA (Shanghai Inst. Applied Physics, China)
Atsushi HATAKEYAMA (Tokyo University of Agriculture and Technology）
Takamasa MOMOSE（The University of British Columbia, Canada）
Deqing FANG (Shanghai Institute of Applied Physics, Chinese Academy of Science)
Akira HORI（Kitami Institute of Technology ）
Tetsuo NORO (Kyusyu Univ.)
Jianling LOU (Peking University, China)
Ryouichi WADA (Texas A&M Univ., USA)
Xiangzhou CAI (Shanghai Institute of Applied Physics, Chinese Academy of Science)

Contract Researcher

Yasuyuki GONO
Yasuo AOKI
Tateaki TORII

Junior Research Associate

Takamasa KUBOKI
Masami SAKO
Hiroshi TOKIEDA
Kenta YOSHINAGA
Masafumi MATSUSHITA

Kenjiro MIKI

Student Trainees

Tomoki ASAKA (Tohoku Univ.)
Yasushi ABE (Tsukuba.Univ.)
CheongSoo LEE (Saitama Univ.)
Yoko ISHIBASHI (Tsukuba Univ.)
Takumi IZUMO (Saitama Univ.)
Chisa ICHIKAWA (Saitama Univ.)
Takeshi ITO (Niigata Univ.)
Kei IMAMURA (Meiji Univ.)
Koudai IWAMOTO (Osaka Univ.)
Hidekazu UENISHI (Osaka Univ.)
Hiroto OOISHI (Tsukuba Univ.)
Junichi ONISHI (Rikkyo Univ.)
Toshiyuki OGURA (Niigata Univ.)
Yuki KATO (Meiji Univ.)
Kouki KAMEI (Tohoku Univ.)
Satomi KIKUCHI (Saitama Univ.)
Sunji KIM (Soul Univ., Korea)
Kota KOBAYASHI (Rikkyo Univ.)
Kaori SAITOH (Saitama Univ.)
Kanae SATO (Saitama Univ)
Zheng YU XU (Tokyo Univ)
Kenichi SUGIMOTO (The Tokyo University of Science)
Fumi SUZAKI (Saitama Univ)
Masanori DOZONO (Kyusyu Univ.)
Taro NAKAO (Tokyo Univ.)
Ryo NISHIKIORI (Tsukuba Univ.)
Takahiro NIWA (Tsukuba Univ.)
Shota FUKUOKA (Tsukuba Univ.)
Hirotaka FURUKI (Saitama Univ.)
Masahiro MAKUTA (Tokyo University of Agriculture and Technology)
Adrien Edouard MATTA (Tokyo Institute of Technology)
Yuichi MATSUURA (Meiji Univ.)
Syuu MIYAZAWA (Saitama Univ.)
Yuki MIYASHIATA (The Tokyo University of Science)
Masaki YAGUCHI (Osaka Univ.)
Yasuhiro YAMAGUCHI (Meiji Univ.)
Taku YAMADA (Tohoku Univ.)
Kazuyuki YOKOYAMA (Tsukuba Univ.)

IPA

Ruijiu CHEN (Peking Univ., China)
Xiaofei YANG (Peking Univ., China)
He WANG (Peking Univ., China)

Visiting Rsearcher

Giuseppe LORUSSO (JSPS)

Secretary

Tomoko FUJII

Yu NAYA

RIBF Research Division
Superheavy Element Laboratory

1. Abstract

The elements with their atomic number Z>103 are called as trans-actinide or superheavy elements. The chemical properties of those elements have not yet been studied in detail. Those elements does not exist in nature therefore, they must be produced artificially for scientific studies. In our laboratory, we have been studying the physical and chemical properties of the superheavy elements utilizing the accelerators in RIKEN and various methods of efficient production for the superheavy elements.

2. Major Research Subjects

(1) Search for new superheavy elements
(2) Decay spectroscopy of the heaviest nuclei
(3) Study of the chemical properties of the heaviest elements
(4) Study of the reaction mechanism of the fusion process (theory)

3. Summary of Research Activity

(1) Searching for new elements

To expand the periodic table of elements and the nuclear chart, we will search for new elements.

(2)Spectroscopic study of the nucleus of heavy elements

Using the high sensitivity system for detecting the heaviest element, we plan to perform a spectroscopic study of nuclei of the heavy elements.

(3) Chemistry of superheavy elements

Study of chemistry of the trans-actinide (superheavy element) has just started world-wide, making it a new frontier in the field of chemistry. Relativistic effects in chemical property are predicted by many theoretical studies. We will try to develop this new field.

(4) Study of a reaction mechanism for fusion process

Superheavy elements have been produced by complete fusion reaction of two heavy nuclei. However, the reaction mechanism of the fusion process is still not well understood theoretically. When we design an experiment to synthesize nuclei of the superheavy elements, we need to determine a beam-target combination and the most appropriate reaction energy. This is when the theory becomes important. We will try to develop a reaction theory useful in designing an experiment by collaborating with the theorists.

Head

Kosuke MORITA

Members

Hiromitsu HABA
Kouji MORIMOTO

Nishina Center Research Scientist

Daiya KAJI

Nishina Center Technical Scientist

Akira YONEDA

Postdoctoral Researcher

Hidetoshi KIKUNAGA (Osaka Univ.)

Contract Researcher

Yuki KUDOU

Kazutaka OHZEKI

Visiting Researcher

Tianheng HUANG

Visiting Technician

Yuichiro WAKITANI

Shinichi YAMAMOTO

Visiting Scientists

Kazuhiko AKIYAMA (Tokyo Metropolitan Univ.)

Masato ASAI (Japan Atomic Energy Agency)

Shin-ichi GOTO (Niigata Univ.)

Kentaro HIROSE (Tohoku Univ.)

Takatoshi ICHIKAWA (Yukawa Institute for Theotetical Physics, Kyoto Univ.)

Yoshitaka KASAMATU (Osaka Univ.)

Hisaaki KUDO (Fac. Sci., Niigata Univ.)

Yuichiro NAGAME (Japan Atomic Energy Agency)

Tsutomu OHTUKI (Tohoku Univ.)

Yasuji OURA

Minoru SAKAMA (Tokushima Univ.)

Nozomi SATO (Japan Atomic Energy Agency)

Tetsuya SATO (Japan Atomic Energy Agency)

Atsushi SHINOHARA (Osaka Univ.)

Keisuke SUEKI (Grad. Sch. Pure Appl. Sci., Univ. Tsukuba)

Koichi TAKAMIYA (Kyoto Univ Research Reactor Institute)

Fuyuki TOKANAI (Dept. Phys., Yamagata Univ.)

Atsushi TOYOSHIMA (Japan Atomic Energy Agency)

Kazuaki TSUKADA (Japan Atomic Energy Agency)

Akihiko YOKOYAMA (Dept. Chemi., Kanazawa Univ.)

Takashi YOSHIMURA (Osaka Univ.)

Research Consultants

Kenji KATORI

Toru NOMURA

Students

Junior Research Associate

Takayuki SUMITA (Tokyo Univ. of Science)

Student Trainees

Kazuhiro OOE (Osaka Univ.)
Shota KIMURA (Tohoku Univ.)
Aiko KINO (Osaka Uiv.)
Yukiko KOMORI (Osaka Univ.)
Ai KURIYAMA (Osaka Univ.)
Yuki KIKUTANI (Osaka Univ.)
Hideki KAIYA (Kanazawa Univ.)
Yuuka KOGAMA (Osaka Univ.)
Yuki TAKEDA (Kanazawa Univ.)
Reona TAKAYAMA (Osaka Univ.)
Kousuke TODA (Kanazawa Univ.)
Ryutaro SAKAI (Saitama Univ.)
Keita MAYAMA (Yamagata Univ.)
Mirei TAKEYAMA (Yamagata Univ.)
Saori NAMAI (Yamagata Univ.)
Masaki NISHIO (Kanazawa Univ.)
Megumi NISHIKAWA (Kanazawa Univ.)
Takahiro MASHIKO (Yamagata Univ.)
Masashi MURAKAMI (Niigata Univ.)
Norihiro Yamada (Kanazawa Univ.)
Takuya YOKOKITA (Osaka Uiv.)
Ayaka WADA (Tokyo Metropolitan Univ.)

Secretary

Shinko ODAI

RIBF Research Division
High Energy Astrophysics Laboratory

1. Abstract

In the immediate aftermath of the Big Bang, the beginning of the universe, only hydrogen and helium existed. However, nuclear fusion in the interior of stars and the explosion of supernovae in the universe over the course of 13.7 billion years led to the evolution of a world brimming with the many different elements we have today. By using man-made satellites to observe X-rays and gamma-rays emitted from celestial objects, we are observing the synthesis of the elements at their actual source. Our goal is to comprehensively elucidate the scenarios for the formation of the elements in the universe, together with our research on sub-atomic physics through the use of an accelerator.

2. Major Research Subjects

(1) Nucleosynthesis in Stars and Supernovae
(2) Particle Acceleration Mechanism in Astronomical Objects
(3) Physics in Extremely Strong Magnetism and Gravity
(4) Research and Development of Innovative X-ray and Gamma-ray detectors

3. Summary of Research Activity

High Energy Astrophysics Laboratory started on April 2010. The goal of our research is to reveal the mechanism of nucleosynthesis in the universe, and to observe exotic physical phenomena in extremely strong magnetic and/or gravitational field. We have observed supernova remnants, strongly magnetized neutron stars, pulsars, black holes and galaxies with X-ray astronomical satellites.

We showed that the expansion of ejecta in Tycho's supernova remnant was consistent with a spherically symmetric shell, based on Suzaku (Japanese X-ray observatory) measurements of the Doppler broadened X-ray emission lines. This is the first direct measurement of the expansion velocity of the elements produced in the thermonuclear expansion supernova. This information tells us the stratified structure of the elements, implying that the heavier elements such as Fe are produced deeper interior of the explosion.

We discovered the emission line of aluminum in supernova remnant G344.7-0.1 for the first time. Aluminum is produced in the neutron rich environment of supernova explosions. We also found manganese, which is enriched in the environment of neutron excess, in some supernova remnants. A systematic study of those lines emitted from the neutron rich elements will be a good tool to explore the nucleosynthesis in the interior of star explosions.

We detected gamma-ray emission from thunder cloud, and revealed that the gamma-ray energy spectra extended to 10 MeV, suggesting that the detected gamma-rays were produced by relativistic electrons via bremsstrahlung. Those relativistic electrons are probably accelerated through an electrical potential difference. This observation gives us a hint of the particle acceleration probably occurred near the neutron stars.

We continue to construct the Gravity and Extreme Magnetism Small Explorer (GEMS) under the collaboration with NASA Goddard Space Flight Center (USA). GEMS is the first dedicated satellite for the X-ray polarimetry, which is opening a new field in Astrophysics and Astronomy. The construction of an engineering model and basic performance studies of an X-ray polarimeter were carried out in FY2010. The satellite will be launched in 2014.

Head

Toru TAMAGAWA

Special Postdoctoral Researchers

Yujin NAKAGAWA
Rohta TAKAHASHI
Harufumi TSUCHIYA
Hiroya YAMAGUCHI

Visiting Scientists

Yukikatsu TERADA (Saitama Univ.)
Madoka KAWAHARADA (ISAS/JAXA)
Aya BAMBA (ISAS/JAXA)
Atsushi SENDA
Junko SATO
Poshak GANDHI (ISAS/JAXA)
Ken OHSUGA (NAOJ)
Naohisa INADA (Univ. of Tokyo)
Toru MISAWA (Shinshu Univ.)

Support Scientist / Technical Support Staff

Asami HAYATO
Hiroshi KATO

Research Collaborative Advisor

Masaharu OKANO

Students

Junior Research Associates

Atsushi HARAYAMA (Saitama Univ.)

Student Trainees

Takehiro KANEMARU (Tokyo Univ. of Science)
Takanori IWAHASHI (Tokyo Univ. of Science)
Saori KONAMI (Tokyo Univ. of Science)
Wataru IWAKIRI (Saitama Univ.)
Fumi ASAMI (Tokyo Univ. of Science)
Rie YOSHII (Tokyo Univ. of Science)
Akifumi YOSHIKAWA (Tokyo Univ. of Science)
Yoko TAKEUCHI (Tokyo Univ. of Science)
Kenichi IWATA (Shibaura Institute of Technology)

Secretary

Yu NAYA

RIBF Research Division
Accelerator Group

1. Abstract

The accelerator group, consisting of seven teams, pursues various upgrade programs of the new-generation heavy-ion accelerator facility, RI-Beam Factory (RIBF), to improve the accelerator performance and operation efficiency. The programs include the R&D of superconducting ECR ion source, charge stripping systems, beam diagnostic devices, radiofrequency systems, control systems, and beam simulation studies. We are also maintaining the large infrastructure to realize effective operation of the RIBF, and are actively promoting the applications of the facility to a variety of research fields.

Our primary mission is to supply intense, stable heavy-ion beams for the users through effective operation, maintenance, and upgrade of the RIBF accelerators and related infrastructure. The director members shown below govern the development programs that are not dealt with by a single group, such as intensity upgrade and effective operation. They also explore the future plans of RIBF accelerators along with other laboratories belonging to the RIBF research division.

2. Major Research Subjects

(1) Intensity upgrade of RIBF accelerators (Okuno)
(2) Effective and st able operation of RIBF accelerators (Fukunishi)
(3) Upgrade of AVF cyclotron (Goto)
(4) Installation and commissioning of RILAC2 injector (Kase, Kamigaito)
(5) Investigation of future projects (Kamigaito, Fukunishi, Okuno)

3. Summary of Activity

(1) Gas stripper systems based on hydrogen and helium were tested for the uranium beam, which was provided by the superconducting ECR ion source at 11 MeV/u. Favorable results were obtained.
(2) High intensity beams of deuterons, ^{14}N, ^{18}O, and ^{48}Ca were supplied for the users (Fig. 1).
(3) The beam energy and beam currents from the AVF cyclotron were increased owing to the modifications of the central region as well as the new beam monitor in the extraction region. This program was performed along with the staff members of CNS, the University of Tokyo.
(4) The commissioning of the RILAC2 was performed as scheduled by using the ^{124}Xe beam from the superconducting ECR ion source.
(5) Possible future plans were explored by taking the potential performance of RIBF accelerators and the world-wide activities in the rare-isotope beam facilities into account.

Group Director
Osamu KAMIGAITO

Deputy Group Director

Hiroki OKUNO (Intensity Upgrade)

Nobuhisa FUKUNISHI (Stable and Efficient Operation)

Members

Akira GOTO

Masayuki KASE

Secretary

Yoko SAKUMA

RIBF Research Division
Accelerator Group
Accelerator R&D Team

1. Abstract

We are developing the key hardware in upgrading the RIBF accelerator complex. Firstly we are developing the challenging superconducting coils for the new 28 GHz ECR ion source which is being developed in order to increase the intensity of uranium beam. We are designing LEBT (Low Energy Beam Transport) which transport the high power beam from the ion source to the next injector linac. Correct estimations of neutralization of space charge forces are hard task. Finally we are developing long-lived charge stripper foils which are installed to breed the ion charges for reduction of their magnetic rigidities. We are also developing gas strippers.

2. Major Research Subjects

(1) Development of superconducting technology in acceleration system.
(2) Development of the LEBT(Low Energy Beam Transport) and the new injector for the high power beams.
(3)Development of charge strippers for high power beams (foil, gas, liquid)

3. Summary of Research Activity

(1) Development of superconducting technology in acceleration system.
Ohnishi, J.
We are developing the challenging superconducting magnets for the 28GHz ECR ion source. We just started to study the possibility of the superconducting cavity in the RIBF accelerator complex.
(2) Development of the LEBT (Low Energy Beam Transport) and the new injector for the high power beams.
Ohnishi, J.
We are developing the LEBT for the ion beams from the new 28GHz ion source. We are also studying space charge effects in the new injector for the RIBF accelerator complex.
(3)Development of charge strippers for high power beams (foil, gas)
Hasebe, H., Imao, H., Kuboki, H., Yokouchi, S., Okuno, H.,
We are developing the long lived charge stripper for high power ion beams. Foils and for the strippers are being studied in parallel.

Team Leader
Hiroki OKUNO

Members
Jun-ichi OHNISHI
Hiroshi IMAO

Nishina center engineer
Hiroo HASEBE

Contract Researcher

Hironori KUBOKI

Visiting Scientists

Noriyosu HAYASHIZAKI (Tokyo Institute of Technology)
Mitsuhiro FUKUDA (RCNP, Osaka Univ.)
Andreas ADELMANN (PSI, Switzerland)

Research Consultants

Yoshiaki CHIBA
Shigeru YOKOUCHI

RIBF Research Division
Accelerator Group
Ion Source Team

1. Abstract

Our aim is to operate and develop the ECR ion sources for the accelerator-complex system of the RI Beam Factory. We focus on further upgrading the performance of the RI Beam Factory through the design and fabrication of a superconducting ECR heavy-ion source for production of high-intensity uranium ions.

2. Major Research Subjects

(1) Operation and development of the ECR ion sources
(2) Development of a superconducting ECR heavy-ion source for production of high-intensity uranium ions

3. Summary of Research Activity

(1) Operation and development of ECR ion sources

T. Nakagawa, M. Kidera, Y. Higurashi, H. Haba, T. Kageyama and A. Goto

We routinely produce and supply various kinds of heavy ions such as zinc and neon ions for the super-heavy element serach experiment as well as uranium ions for RIBF experiments. We also perform R&D's to meet the requirements for stable supply of high-intensity heavy ion beams.

(2) Development of a superconducting ECR ion source for use in production of a high-intensity uranium beam

T. Nakagawa, J. Ohnishi, M. Kidera, Y. Higurashi, Y. Sato and A. Goto

The RIBF is required to supply uranium beams with very high intensity so as to produce RI's. We have designed and are fabricating an ECR ion source with high magnetic field and high microwave-frequency, since the existing ECR ion sources have their limits in beam intensity. The coils of this ion source are designed to be superconducting for the production of high magnetic field. We are also designing the low-energy beam transport line of the superconducting ECR ion source.

Team Leader

Takahide NAKAGAWA

Members

Hiromitsu HABA

Contract Researcher

Yoshihide HIGURASHI
Masanori KIDERA

Special temporary employee

Tadashi KAGEYAMA

Part-time staff I

Michiko KITAGAWA

part-time staff II

Tsuyoshi NAGAMATSU

Visiting Scientists

Takehiro MATSUSE (Fac.Text. Sci. Technol.,Shinshu Univ.)

RIBF Research Division
Accelerator Group
RILAC Team

1. Abstract

The operation and maintenance of the RIKEN Heavy-ion Linac (RILAC) have been carried out. There are two operation modes: one is the stand-alone mode operation and the other is the injection mode operation. The RILAC has been used especially as an injector for the RIKEN RI- Beam Factory accelerator complex. The RILAC is composed of the ECR ion source, the frequency-variable RFQ linac, six frequency-variable main linac cavities, and six energy booster cavities (CSM).

2. Major Research Subjects

(1) The long term high stability of the RILAC operation.
(2) Improvement of high efficiency of the RILAC operation.

3. Summary of Research Activity

The RILAC was started to supply ion beams for experiments in 1981. Thousands hours are spent in a year for delivering many kinds of heavy-ion beams to various experiments.

The RILAC has two operation modes: one is the stand-alone mode operation delivering low-energy beams directly to experiments and the other is the injection mode operation injecting beams into the RRC. In the first mode, the RILAC supplies a very important beam to the nuclear physics experiment of “the research of super heavy elements”. In the second mode, the RILAC plays a very important role as upstream end of the RIBF accelerator complex.

The maintenance of these devices is extremely important in order to keep the log-term high stability and high efficiency of the RILAC beams. Therefore, improvements are always carried out for the purpose of more stable and more efficient operation.

Team Leader
Eiji IKEZAWA

Member
Yutaka WATANABE
Shigeaki ARAI

Research Consultants
Toshiya CHIBA
Masatake HEMMI
Yoshitoshi MIYAZAWA

RIBF Research Division
Accelerator Group
Cyclotron Team

1. Abstract

Together with other teams of Nishina Center accelerator division, maintaining and improving the RIBF cyclotron complex. The accelerator provides high intensity heavy ions. Our mission is to have stable operation of cyclotrons for high power beam operation. Recently stabilization of the rf system is a key issue to provide 10 kW heavy ion beam.

2. Major Research Subjects

(1) RF technology for Cyclotrons
(2) Operation of RIBF cyclotron complex
(3) Maintenance and improvement of RIBF cyclotrons
(4) Single turn operation for polarized deuteron beams
(5) Development of the rebuncher system for intermediate-energy heavy ion beams

3. Summary of Research Activity

Development of the rf system for a reliable operation
Development of highly stabilized low level rf system
Development of superconducting rebuncher cavity
Development of the intermediate-energy polarized deuteron beams.

Team Leader
Naruhiko SAKAMOTO

Research Ascociate
Kenji SUDA

RIBF Research Division
Accelerator Group
Beam Dynamics and Diagnostics Team

1. Abstract

In order to realize stable and efficient operations of RIBF accelerator complex, various improvements including beam diagnosis, computer control, power supplies have been performed. Our final goal is to establish simulation-based operation of RIBF accelerator complex.

2. Major Research Subjects

(1) Improvement on the beam transmission along the multi-stage accelerator system.
(2) Development of beam diagnosis.
(3) Development of computer control.
(4) Establishment of long-term stabilities of magnet and magnet power supplies.

3. Summary of Research Activity

(1) Development of the beam diagnostic technology

We have improved existing beam intensity monitors (Faraday cup) for precise measurements of heavy ions like uranium. In addition, non-destructive beam intensity monitor using SQUID have been developed. These modifications resulted in a great improvement of beam transmission efficiency.

(2) Development of the computer control system of accelerator

EPICS-based control system and a home-made beam interlock system have been stably operated. We also applied embedded EPICS system on F3RP61-2L to our new injector system RILAC2.

(3) Stability tests of old power supplies

We tested long-term stabilities of old power supplies used for more than twenty years to realize stable operation of accelerator complex.

(4) New injector system RILAC2

Team Leader

Nobuhisa FUKUNISHI

Members

Masaki FUJIMAKI
Sachiko ITO
Keiko KUMAGAI
Tamaki WATANABE

Contract Technical Scientist

Misaki KOBAYASHI-KOMIYAMA
Kazunari YAMADA
Hiroshi WATANABE
Makoto NAGASE

Visiting Scientists

Hiromichi RYUTO (Photonics and Electronics Science and Engineering Center, Kyoto University)

Jun-ichi ODAGIRI (Accelerator Laboratory, High Energy Accelerator Research Organization (KEK))

Yuichiro SASAKI

Research Consultants

Jiro FUJITA

RIBF Research Division
Accelerator Group
Cryogenic Technology Team

1. Abstract

We are operating the cryogenic system for the superconducting ring cyclotron in RIBF. We are also operating the helium cryogenic system in the south area of RIKEN Wako campus and delivering the liquid helium to users in RIKEN. We are trying to collect efficiently gas helium after usage of liquid helium.

2. Major Research Subjects

(1) Operation of the cryogenic system for the superconducting ring cyclotron in RIBF
(2) Operation of the helium cryogenic plant in the south area of Wako campus and delivering the liquid helium to users in Wako campus.

3. Summary of Research Activity

(1) Operation of the cryogenic system for the superconducting ring cyclotron in RIBF
Okuno, H., Dantsuka, T.,
(2) Operation of the helium cryogenic plant in the south area of Wako campus and delivering the liquid helium to users in Wako campus.
Dantsuka, T., Odashima, Y., Nakamura, M., Maie, T., Ikegami, K., Tsuruma, S., Okuno., H.

Team Leader
Hiroki OKUNO

Members
Masato NAKAMURA

Nishina Center Engineer
Takeshi MAIE

Technical Staff-I
Tomoyuki DANTSUKA

Research Consultant
Kumio IKEGAMI
Yutaka ODAJIMA
Ken-ici KATO

RIBF Research Division
Accelerator Group
Infrastructure Management Team

1. Abstract

The RIBF accelerators are an incomparable multi-stage accelerator complex. For the long and stable operations of these accelerators, their infrastructures become very important. Our team supports their infrastructure; buildings, electric facilities, cooling system, vacuum system and so on. It also concerns the regular operation and maintenance of all the accelerators, and improves or renews the old parts of the accelerators.

2. Major Research Subjects

Management of the RIBF accelerator infrastructure; buildings, electric facilities, cooling system, vacuum system and so on.

3. Summary of Research Activity

The current research subjects are summarized as follows:

(1) Operation and maintenance of infrastructure for RIBF accelerators.
(2) Improvement or renewal of the, especially old, accelerators.
(3) Support of accelerator operations.

Team Leader
Masayuki KASE

Members
Hiromi YAMASAWA

Temporary Employee
Tadashi FUJINAWA

RIBF Research Division

Instrumentations Development Group

1. Abstract

This group develops experimental installations for the RI Beam factory. Experimental installations currently planned include designs containing common elements enabling multiple use, as well as others that are highly program specific. All are designed to maximize the research potential of the world's most intense RI beams, made possible by the exclusive equipment available at the RI Beam Factory.

2. Major Research Subjects

(1) SCRIT Project
(2) SLOWRI Project
(3) Polarized RI Beam Project
(4) Rear RI Ring Project

3. Summary of Research Activity

We are developing beam manipulation technology in carrying out above listed project. They are the high-quality slow RI beam production (SCRIT and SLOWRI), the beam cooling and stopping (SCRIT and SLOWRI), the polarized and aligned RI beam production (Pol. RI Beam), and the beam accumulation technology (Rare RI Ring). The technological knowhow accumulated in our projects will play a significant role in the next generation RIBF. Future Plan for each project is described in subsections. SCRIT is now under construction and partially tested using stable isotopes. Design studies of SLOWRI and Rare RI Ring have been almost finished and they are ready for construction. A new technique to efficiently align nuclear spin of RI produced by Big RIPS has been developed by Pol. RI Beam project team. This will be powerful tool for nuclear structure study for short-lived unstable nuclei.

Group Leader
Masanori WAKASUGI

Secretary
Minami IMANISHI

RIBF Research Division
Instrumenttation Development Group
SLOWRI Team

1. Abstract

A next-generation slow radioactive nuclear ion beam facility (SLOWRI) which provides slow, high-purity and small emittance ion beams of all elements is being build as one of the principal facilities at the RIKEN RI-beam factory (RIBF). High energy radioactive ion beams from the projectile fragment separator BigRIPS are thermalized in a large gas catcher cell. The thermalized ions in the gas cell are guided and extracted to a vacuum environment by a combination of dc electric fields and inhomogeneous rf fields (rf carpet ion guide). From there the slow ion beam is delivered via a mass separator and a switchyard to various devices: such as an ion trap, a collinear fast beam apparatus, and a multi-reflection time of flight mass spectrometer. In the R&D works at the present RIKEN facility, an overall efficiency of 5% for a 100A MeV ^{8}Li ion beam from the present projectile fragment separator RIPS was achieved and the dependence of the efficiency on the ion beam intensity was investigated.

First spectroscopy experiment at the prototype SLOWI was performed on Be isotopes. Energetic ions of ^{7,10,11}Be from the RIPS were trapped and laser cooled in a linear rf trap and precision spectroscopy was performed. The evaluated ion temperature of <10 mK demonstrates that a reduction of more than 15 orders of magnitude for the kinetic energy of radioactive Be was achieved online. Precise investigation of the hyperfine structure will confirm the anomalous mean radius of the valence neutron of the so called neutron halo nucleus.

Other spectroscopy experiments using the slow RI-beams are also under progress in off-line setups. A collinear fast beam apparatus for nuclear charge radii measurements was build and tested with stable Ar+ ion beams. A multi-reflection time-of-flight mass spectrograph was build for precise and fast measurements of short-lived radioactive nuclei. A high mass resolving power of 140,000 for K and Rb ions has been achieved with a 5 ms measurement period.

An advanced SLOWRI facility is also proposed. The expected number of nuclides which can be investigated at SLOWRI is more than 3000, however, the realistic beam time for each experiment would be very limited. The advanced facility will parasitically provide slow RI-beams everyday as long as the fragment separator BigRIPS is operated. The parasitic beam can be produced from those nuclei dumped at the first focal plane slits of BigRIPS by placing a compact gas catcher cell. The thermalized and neutralized RI in the cell can be re-ionized at the exit of the cell by resonance laser ionization. Development the new method, named PALIS, is underway.

2. Major Research Subjects

(1) Development and construction of the next-generation slow RI-beam facility

(2) Laser spectroscopy of trapped radioactive Beryllium isotopes.

(3) Development of a multi-reflection time-of-flight mass spectrograph for precision mass measurements of short-lived nuclei.

(4) Development of collinear fast beam apparatus for isotope shift measurements.

(5) Development of parasitic slow RI-beam production method using resonance laser ionization.

3. Summary of Research Activity

(1) Development of universal slow RI-beam facility

WADA, Michiharu, SCHURY Peter, SONODA, Tetsu, ITO, Yuta, TAKAMINE, Aiko, OKADA, Kunihiro, KUBO, Toshiyuki, WOLLNIK, Hermann, SCHUESSLER, Hans, KATAYAMA Ichiro

A next-generation slow radioactive nuclear ion beam facility (SLOWRI) which provides slow, high-purity and small emittance ion beams of all elements is being build as one of the principal facilities at the RIKEN RI-beam factory (RIBF). High energy radioactive ion beams from the projectile fragment separator BigRIPS are thermalized in a large gas catcher cell. The thermalized ions in the gas cell are guided and extracted to a vacuum environment by a combination of dc electric fields and inhomogeneous rf fields (rf carpet ion guide). From there the slow ion beam is delivered via a mass separator and a switchyard to various devices: such as an ion trap, a collinear fast beam apparatus, and a multi-reflection time of flight mass spectrometer. In the R&D works at the present RIKEN facility, an overall efficiency of 5% for a 100*A* MeV ^{8}Li ion beam from the present projectile fragment separator RIPS was achieved and the dependence of the efficiency on the ion beam intensity was investigated.

(2) Laser spectroscopy of trapped radioactive beryllium isotope ions

WADA, Michiharu, TAKAMINE, Aiko, SCHURY Peter, SONODA Tetsu, OKADA, Kunihiro, KANAI, Yasuyuki, YOSHIDA, Atsushi, KUBO, Toshiyuki, YAMAZAKI, Yasunori, WOLLNIK, Hermann, SCHUESSLER, Hans, NODA, Koji, OHTANI, Shunsuke, KATAYAMA Ichiro

As a first application of the prototype SLOWRI setup, we applied hyperfine structure spectroscopy to the beryllium isotopes to determine in particular the anomalous radius of the valence neutron of the neutron halo nucleus ^{11}Be, and to determine the charge radii of these beryllium isotopes through laser-laser double resonance spectroscopy of laser-cooled ions. Laser cooling is an essential prerequisite for these planned experiments. The first laser spectroscopy experiments for beryllium isotopes were performed to measure the resonance frequencies of 2s $^{2}S_{1/2}$ - 2p $^{2}P_{3/2}$ transition of ^{7}Be+, ^{9}Be+, $^{10}Be^{+}$ and ^{10}Be+ ions and the nuclear charge radii of these isotopes were determined. The hyperfine structure of $^{11}Be^{+}$ and $^{7}Be^{+}$ ions using the laser-microwave double resonance spectroscopy were also performed and the magnetic hyperfine constants of $^{7}Be^{+}$ and $^{11}Be^{+}$ ions were determined with an accuracy of 10^{-7}

(3) Development of a multi-reflection TOF mass spectrograph for short-lived nuclei

WADA, Michiharu, SCHURY Peter, ITO, Yuta, NAIMI, Sarah, NAKAMURA, Sousuke, TAKAMINE, Aiko, SONODA Tetsu, OKADA, Kunihiro, WOLLNIK, Hermann,

The atomic mass is one of the most important quantity of a nucleus and has been studied in various methods since the early days of physics. Among many methods we chose a multi-reflection time-of-flight (MR-TOF) mass spectrometer. Slow RI beams extracted from the RF ion-guide are bunch injected into the spectrometer with a repetition rate of ~500 Hz. The spectrometer consists of two electrostatic mirrors between which the ions travel back and forth repeatedly. These mirrors are designed such that energy-isochrononicity in the flight time is guaranteed during the multiple reflections while the flight time varies with the masses of ions. A mass-resolving power of 140,000 has been obtained with a 5 ms flight time for K and Rb isotopes. It is equivalent to use a 90 T magnet for a Penning trap mass spectrometer. This mass-resolving power should allow us to determine ion masses with an accuracy of 10^{-7}. The advantages of the MR-TOF spectrometer are: 1) short measurement periods, typically 2 ms, which allows all neutron rich nuclei to be investigated, 2) the device is compact and its operation is simple, especially, it is independent from the all upstream devices, accelerators and fragment separators, 3) ions of more than isobars can be measured simultaneously, so that mass reference can easily be established in the mass spectra. In total, the number of measurable nuclides within a limited beam time would be larger than that can be achieved by other methods. It should be noted here also that this method can be used even during a low-duty parasite beam time. Online mass measurements of short-lived radioactive nuclei are planned in FY2011.

(4) Development of collinear fast beam apparatus for nuclear charge radii measurements
WADA, Michiharu, SCHUESSLER, Hans, IIMURA, Hideki, SONODA, Tetsu, SCHURY, Peter, TAKAMINE, Aiko, OKADA, Kunihiro, WOLLNIK, Hermann,

The root-mean-square charge radii of unstable nuclei have been determined exclusively by isotope shift measurements of the optical transitions of singly-charged ions or neutral atoms by laser spectroscopy. Many isotopes of alkaline, alkaline-earth, noble-gases and several other elements have been measured by collinear laser spectroscopy since these ions have all good optical transitions and are available at conventional ISOL facilities. However, isotopes of other elements especially refractory and short-lived ones have not been investigated so far.
In SLOWRI, isotopes of all atomic elements will be provided as well collimated mono-energetic beams. This should expand the range of applicable nuclides of laser spectroscopy. In the first years of the RIBF project, Ni and its vicinities, such as Ni, Co, Fe, Cr, Cu, Ga, Ge are planned to be investigated. They all have possible optical transitions in the ground states of neutral atoms with presently available laser systems. Some of them have so called recycle transitions which enhance the detection probabilities noticeably. Also the multistep resonance ionization (RIS) method can be applied to the isotopes of Ni as well as those of some other elements. The required minimum intensity for this method can be as low as 10 atoms per second.
We have built an off-line mass separator and a collinear fast beam apparatus with a large solid-angle fluorescence detector. A 617 nm transition of the metastable Ar+ ion at 20 keV was measured with both collinear and anti-collinear geometry that allowed us to determine the absolute resonant frequency of the transition at rest with more than 10^{-8} accuracy. Such high accuracy measurements for Ti and Ni isotopes are in progress.

(5) Development of parasitic slow RI-beam production scheme using resonance laser ionization
WADA, Michiharu, SONODA Tetsu, TAKAMINE, Aiko, OKADA, K., MATSUO Yukari, FURUKAWA, Takeshi, TIMITA, Hideki, KOBAYASHI T., MIYATAKE Hiroari, JEONG Sun Chan, ISHIYAMA, H., IMAI, N., HIRAYAMA Y., KATAYAMA I., TOMITA, H., IIMURA, H., SHINOZUKA T., WAKUI, T., HUYSE, M., VAN DUPPEN, P., KUDRYAVTSEV, Yu., SCHUESSLER, H., WOLLNIK, H.

More than 99.9% of RI ions produced in projectile fission or fragmentation are simply dumped in the first dipole magnet and the slits. A new scheme, named PALIS, to rescue such dumped precious RI using a compact gas catcher cell and resonance laser ionization was proposed. The thermalized RI ions in a cell filled with Ar gas can be quickly neutralized and transported to the exit of the cell by gas flow. Irradiation of resonance lasers at the exit ionizes neutral RI atoms efficiently and selectively. The ionized RI ions can be further selected by a magnetic mass separator and transported to SLOWRI experimental area for spectroscopy experiment. The resonance ionization scheme itself can also be a useful method to perform precision optical spectroscopy of RI of many elements.

An off-line setup for resonance ionization in gas cell is prepared. Extraction from 500 mbar Ar gas cell by resonance ionization method for Ni and Cu ions were demonstrated. A differential pumping from 500 mbar to 10-5 mbar using multiple small pumps and an rf sextupole ion beam guide (SPIG) has been achieved. Design of a gas cell which will be placed at the second focal plane (F2) of BigRIPS is in progress.

Head

Michiharu WADA

Members

Tetsu SONODA
Peter SCHURY
Aiko TAKAMINE
Sarah NAIMI
Yuta ITO
Sousuke NAKAMURA
Kunihiro OKADA
Ichiro KATAYAMA
Hideki IIMURA
Hideo TOMITA
Hans SCHUESSLER
Hermann WOLLNIK

.

RIBF Research Division
Instrumenttation Development Group
Polarized RI Beam Team

1. Abstract

The team conducts the research and development on the production of spin-oriented radioactive-isotope beams (RIBs), and applies it to the research on nuclear physics, fundamental physics, and material science. The microscopic investigation of physical and chemical processes is performed based on nuclear techniques which takes the advantage of intrinsic nuclear properties and phenomena (spins, electromagnetic moments, decay modes etc.). In particular, the precession/resonance of a polarized/aligned nuclear spin under an external field is observed through a change in the angular distribution of radiation, for the study of nuclear structures via nuclear moments. The experimental methods and devices for fundamental physics research with polarized nuclei have been also developed. The same method, as well as the Möessbauer technique, are used for the investigation of condensed matter such as semiconductor, ferromagnets, fullerenes, systems with dilute magnetic impurities etc. by capitalizing radioactive nuclei as microscopic probes into them. All these research activities are to be extended to wide variety of unstable nuclei which RI Beam Factory (RIBF) provides. A method to produce beams of highly polarized radioactive nuclei, taking full advantage of RIBF, is being developed.

2. Major Research Subjects

(1) Nuclear-moment measurements of unstable nuclei
(2) RIPS upgrade and the development of highly polarized slow RI beams
(3) Fundamental physics: Study of symmetry
(4) Condensed matter studies using radioactive nuclear probes

3. Summary of Research Activity

(1) Nuclear-moment measurements of unstable nuclei

It has been revealed in our earlier work that spin-oriented RIBs can be obtained as a function of their outgoing momentum in the projectile-fragmentation reaction. With the obtained spin-polarized nuclei, ground- and excited-state nuclear moments can be determined by means of the β-NMR and TDPAD methods, respectively. Based on these technique, we have recently been conducted the nuclear-moments measurement of neutron-rich *sd*-shell around the neutron magic number N=20. It has been proposed in this region that an inversion of amplitudes between the *sd* normal and the *pf* intruder configurations would lead to deformation of the ground states. Thus, the region of nuclei is called the *island of inversion*. The measured nuclear moments are expected to provide microscopic properties for those nuclei of interest. The sub-themes are the following:

- Nuclear structure study of neutron-rich aluminum isotopes $^{30\text{-}32}$Al on the border of the *island of inversion* and $^{33\text{-}34}$Al on/beyond it.
- Investigation of a new *island of inversion* around N=28, the nuclear-moment measurements of neutron-rich isotopes.
- Development of a new method to produce highly spin-aligned RIBs and the magnetic-moment measurement of isomeric state in ^{32}Al with the TDPAD method.
- The ground-state electric quadrupole moment measurements of ^{23}Al for the study of the

T=3/2 mirror symmetry.

- Study of nuclei around Fe region: isospin symmetry study by means of the magnetic moment of the 10^+ isomer in ^{54}Ni, and the study of magicity in the vicinity of ^{68}Ni through the quadrupole moment of the $13/2^+$ isomeric state in ^{69}Cu and isomeric state in ^{65}Fe.

(2) RIPS upgrade and the development of highly polarized slow RI beams

The upgrade of RIPS has been proposed in the phase-II programs. In the cyclotron-cascade acceleration scheme, beams are accelerated up to the energy of E = 115 A MeV with IRC. In this upgrade, the former fragment separator RIPS is equipped with a new beam line that delivers beams of 115 A MeV heavy ions from the IRC cyclotron. RI beams produced by the primary beams at such an intermediate energy are high enough to produce RIBs via projectile-fragmentation reactions and suitably low in energy to be stopped in a sample material of limited thicknesses. Compared with the production yield of RIBs in the present AVF-RRC acceleration scheme, they are drastically increased. The design study of the upgrade program is in progress in our team. We noted that RIBs produced at E = 115 A MeV can be spin-oriented so that the nuclear-moment measurements will be further conducted. Also, combining a new atomic-beam resonance method to combine with fragmentation-based RI beams, which is under development, to this program, highly spin-polarized RI beams will be produced in a low beam-energy region. Then, they could be useful not only for nuclear-moment measurements but also for spin-related subjects in nuclear physics, fundamental physics, and material sciences.

(3) Fundamental physics: Study of symmetry

Nuclear spins of stable and unstable isotopes sometimes play important roles in fundamental physics research. New experimental methods and devices have been developed for studies on the violation of time reversal symmetry (T-violation) using spin-polarized nuclei. These experiments aim detection of small frequency shift of the spin precession or measurement of the T-odd angular correlation in β-decay as T-violating signals arising from new mechanisms beyond the “Standard Model”. Sub-themes are the following:

- Precision measurement of spin-precession frequency with a new type of the nuclear spin maser for atomic EDM (Electric Dipole Moment) search.
- Development of high-sensitive atomic magnetometer for EDM experiments.
- Development of a new Mott polarimeter for T-violation experiment using β-decay of polarized unstable nuclei.

(4) Condensed matter studies using radioactive nuclear probes

Utilizing RI beams as a probe, online Mössbauer spectroscopy and online perturbed angular correlation experiments have been carried out through the γ-ray measurements. The microscopic structures, dynamics in ferromagnets, and properties of semiconductors have been investigated from the deduced internal local fields and the spin relaxation of the probe in materials. The β-NMR/NQR method is also utilized for these condensed matter studies. The methods and apparatus have been developed. Also, basic studies on the probe nuclei have been carried out. Sub-themes are the following:

- Study of Fe impurity in silicon solar cells with the online Mössbauer spectroscopy of implanted ^{57}Fe.
- Study of “exotic” chemical states and the fast atomic-jump processes in solid with the online Mössbauer spectroscopy of implanted ^{57}Fe

- Development of the on-line perturbed angular-correlation method with ^{19}O beams as a new probe
- Study of the diffusion and segregation of Fe impurity atoms in Si through in-beam Mössbauer experiment with a Coulomb excited, recoil implanted ^{57}Fe nuclei.
- Study of the fast diffusion of Cu impurity atoms in Si through β-NMR/NQR with implanted ^{58}Cu.

Team Leader

Hideki UENO

Members

Akihiro YOSHIMI
Yuichi ICHIKAWA
Yoshio KOBAYASHI

RIBF Research Division
Instrumenttation Development Group
Rare RI-ring Team

1. Abstract

We are developing the isochronous storage ring to measure the mass for rare radioactive isotopes (Rare RI ring). It is assumed that uranium is synthesized by neutron capture process after the supernovae explosion (r-process). To prove r-process, mass measurements for the rare RI are indispensable. To deduce the mass, we measure the circulation time (cyclotron frequency) for the rare RI inside the ring. RI beams produce in RIBF have some energy spread. To compensate the spread, isochronicity inside the ring is indispensable (isochronous storage ring). We will inject the rare RI one by one to the ring (individual injection) to identify the RI event-by-event.

2. Major Research Subjects

Developments of isochronous storage ring to measure mass of rare RI.

3. Summary of Research Activity

Developments of isochronous storage ring to measure mass of rare RI.

The conceptual design for an isochronous storage ring has been finalized in this year. To minimize construction cost, we plan to use the SHARAQ beam line as an injection beam transport line for the isochronous ring and re-use TARN-II bending magnets, which have been moved from KEK, as main components of the ring. A quick activated kicker magnet system required for one by one injection has been developed in this year. Another important item in the ring is schottoki beam monitor, which observes single ion circulating the ring. It is now under designing, and it will be manufactured in next year and installed in the HIMAC for test experiment.

Team Leader

Masanori WAKASUGI

Research Associate

Yoshitaka YAMAGUCHI

Visiting Scientists

Akira OZAWA (Inst. Phys., Univ.of Tsukuba)
Yusuke YASUDA (Inst. Phys., Univ.of Tsukuba)
Ichiro ARAI (Inst. Phys., Univ.of Tsukuba)
Takeshi SUZUKI (Saitama University)
Takayuki YAMAGUCHI (Saitama University)
Takashi KIKUCHI (Nagaoka University of Technology)
Daisuke NAGAE (Inst. Phys., Univ.of Tsukuba)

Junior Research Associate

Shinpei NAKAJIMA (Saitama University)
Tetsuaki MORIGUCHI (University of Tsukuba)

RIBF Research Division
Instrumenttation Development Group
SCRIT Team

1. Abstract

We aim at the investigation of internal nuclear structure of short-lived radioactive nuclei (RI) by means of electron scattering. Electron scattering for RI's has never been performed duo to inability to make target of these nuclei. An electron-RI collider system, which requires a huge accelerator complex, has so far been unique solution to overcome the difficulty. We have developed a novel internal target system named SCRIT (Self-Confining RI Ion Target) in an electron storage ring to make the experiment easier with much compact experimental system. The SCRIT device has been installed into an electron storage ring SR2 in this year, and the test experiment has been started. An RI ion source and an ISOL system, which will supply RI beams to the SCRIT, are now manufacturing.

2. Major Research Subjects

Development of the SCRIT technology and electron scattering for unstable nuclei.

3. Summary of Research Activity

Development of a novel internal target of unstable nuclei (SCRIT) in an electron storage ring for electron scattering experiment.
(Wakasugi, Miyashita, Kurita, Suda, Tamae, Hori, Hara)
We have finished the commissioning of the electron accelerator system, which has constructed in last year, and a SCRIT devices have been installed into the straight section of the storage ring (SR2). The test experiment using stable isotopes is planed in the beginning of next year. In this electron scattering facility, we will construct the U photo-fission ion source for RI production and an ISOL system for RI injection into the SCRIT device. They are now manufacturing. Detector system for scattered electrons from the SCRIT is under designing and it will be manufactured in next year. We plan to start the electron scattering experiment for unstable nuclei in 2012.

Team Leader
Masanori WAKASUGI

Special Postdoctoral Researcher
Yuji MIYASHITA

Research Consultant
Shin-ichi ICHIKAWA
Masahiro HARA
Toshitada HORI

Visiting Scientists
Toshimi SUDA (Research Center of Electron Photon Science, Tohoku Univ.)
Tadaaki TAMAE (Research Center of Electron Photon Science, Tohoku Univ.)
Kazuyoshi KURITA (Inst. Phys., Rikkyo Univ.)

RIBF Research Division
Research Instruments Group

1. Abstract

The research instruments group is the driving force at RI Beam Factory (RIBF) for continuous enhancement of activities and competitiveness of experimental research. Consisting of five teams, we are in charge of the design, construction, operation and improvement of the core research instruments at RIBF, such as BigRIPS separator, ZeroDegree spectrometer, GARIS spectrometer and SAMURAI spectrometer, and the related infrastructure and equipments. The group also conducts related experimental research as well as R&D studies on the research instruments.

2. Major Research Subjects

Design, construction, operation and improvement of the core research instruments at RIBF and related R&D studies. Experimental studies on exotic nuclei.

3. Summary of Research Activity

The current research subjects are summarized as follows:

(1) Design, construction, operation, and improvement of the core research instruments at RIBF and their related infrastructure and equipments for continuous enhancement of activities and competitiveness of experimental research

(2) R&D studies on technical issues of the core research instruments and related equipments at RIBF

(3) Experimental research on exotic nuclei using the core research instruments at RIBF

Group Director

Toshiyuki KUBO

Senior Visiting Scientist

Toshio KOBAYASHI (Tohoku University)

RIBF Research Division
Research Instruments Group
GARIS Team

1. Abstract

Development and maintenance of devices related to study of the superheavy elements.

2. Major Research Subjects

(1) Maintenance and development of a recoil separator and the related devices.

(2) Development of rapid chemistry devices.

3. Summary of Research Activity

(1) Maintenance and development of recoil separator

A gas-filled recoil separator has been used as a main experimental device for the study of superheavy elements. We will develop and maintain the related devices. We will also offer user-support if a researcher wishes to use the devices for his/her own research program.

(2) Development of devices for fast chemistry

We do research and development of devices for fast chemistry of superheavy elements. We also offer user-support for potential users.

Team Leader

Kouji MORIMOTO

Nishina Center Research Scientist

Daiya KAJI

Nishina Center Technical Scientist

Akira YONEDA

RIBF Research Division
Research Instruments Group
BigRIPS Team

1. Abstract

This team is in charge of design, construction, development and operation of BigRIPS in-flight separator and its related research instruments at RI beam factory (RIBF). They are employed not only for the production of RI beams but also the experimental studies using RI beams.

2. Major Research Subjects

Design, construction, development and operation of BigRIPS in-flight separator, RI-beam transport lines, and their related research instruments

3. Summary of Research Activity

This team is in charge of design, construction, development and operation of BigRIPS in-flight separator, RI-beam transport lines, and their related research instruments such as ZeroDegree spectrometer at RI beam factory (RIBF). They are employed not only for the production of RI beams but also various kinds of experimental studies using RI beams.

The research subjects may be summarized as follows:

(1) General studies on RI-beam production using in-flight scheme.
(2) Studies on ion-optics of in-flight separators, including particle identification of RI beams
(3) Simulation and optimization of RI-beam production.
(4) Development of beam-line detectors and their data acquisition system.
(5) Experimental studies on production reactions and unstable nuclei.
(6) Experimental studies of the limits of nuclear binding.
(7) Development of superconducting magnets and their helium cryogenic systems.
(8) Development of a high-power production target system.
(9) Development of a high-power beam dump system.
(10) Development of a remote maintenance and remote handling systems.
(11) Operation, maintenance and improvement of BigRIPS separator system, RI-beam transport lines, and their related research instruments such as ZeroDegree spectrometer and so on.
(12) Experimental research using RI beams.

Team Leader

Koichi YOSHIDA

Members

Naohito INABE
Atsushi YOSHIDA
Masao OHTAKE
Yoshiyuki YANAGISAWA

Contract Researchers

Kensuke KUSAKA
Tetsuya OHNISHI

Naoki FUKUDA
Hiroyuki TAKEDA

Research Associates
Daisuke KAMEDA
Kanenobu TANAKA

Part-time Staff
Hidekazu KUMAGAI

Visiting Scientist
Bradley SHERRILL (NSCL, Michigan State Univ., USA)
Daniel BAZIN (NSCL, Michigan State Univ., USA)
Anthony NETTLETON (NSCL, Michigan State Univ., USA)
Laura BANDURA (NSCL, Michigan State Univ., USA)
Hans GEISSEL (GSI, Germany)
Martin WINKLER (GSI, Germany)
Michael FAMIANO (Western Michigan Univ., USA)
Jerry NOLEN (Argonne National Lab., USA)
Shashikant MANIKONDA (Argonne National Lab., USA)
Yutaka MIZOI (Osaka Electro-Commnication Univ.)
Khiem LE HONG (IOP, Vietnamese Academy for Science and Technology)
Cuong PHAN VIET (IOP, Vietnamese Academy for Science and Technology)

RIBF Research Division
Research Instruments Group
SAMURAI Team

1. Abstract
In collaboration with research groups in and outside RIKEN, the team designs, develops and constructs the SAMURAI spectrometer and relevant equipment that will be used for reaction experiments using RI beams at RI Beam Factory. The team prepares for commissioning of SAMURAI planned in the year 2012. The team also provides basis for research activities by, for example, organizing workshops. SAMURAI consists of a large superconducting dipole magnet and a variety of detectors to detect charged particles and neutrons.

2. Major Research Subjects
Design, development and construction of the SAMURAI spectrometer and its related research instruments.

3. Summary of Research Activity
The current research activities are summarized as follows:

(1) Design, development and construction of a large superconducting dipole magnet that will be the main component of the SAMURAI spectrometer.

(2) Design, development and construction of various detectors that are used for nuclear reaction experiments at SAMURAI.

(3) Preparation for starting experiments using SAMURAI planned in 2012.

(4) Formation of a collaboration platform called "SAMURAI collaboration".

Team Leader
Tohru MOTOBAYASHI

Members
Hiromi SATO
Ken-ichiro YONEDA
Yohei SIMIZU

Senior Visiting Scientist
Toshio KOBAYASHI (Tohoku University)

RIBF Research Division
Research Instruments Group
Computing and Network Team

1. Abstract

This team is in charge of development, management and operation of the computing and network environment, mail and information servers and data acquisition system and management of the information security of the RIKEN Nishina Center.

2. Major Research Subjects

(1) Development, management and operation of the general computing servers
(2) Development, management and operation of the mail and information servers
(3) Development, management and operation of the data acquisition system
(4) Development, management and operation of the network environment
(5) Management of the information security

3. Summary of Research Activity

This team is in charge of development, management and operation of the computing and network environment, mail and information servers and data acquisition system and management of the information security. The details are described elsewhere in this progress report.

(1) Development, management and operation of the general computing servers

We are operating Linux/Unix NIS/NFS cluster system for the data analysis of the experiments and general computing. This cluster system consists of eight computing servers with 28 CPU cores and totally 20 TB RAID of highly-reliable Fibre-channel HDD. Approximately 500 user accounts are registered on this cluster system. We are adopting the latest version of the Scientific Linux (X86_64) as the primary operating system, which is widely used in the accelerator research facilities, nuclear physics and high-energy physics communities in the world.

(2) Development, management and operation of the mail and information servers

We are operating RIBF.RIKEN.JP server as a mail/NFS/NIS server. This server is a core server of RIBF Linux/Unix cluster system. We are preparing to replace this server and RAID file systems in the summer of 2011 since it passed more than five years from the installation. This Postfix is used for mail transport software and dovecot is used for imap and pop services. These software packages enable secure and reliable mail delivery. Sophos Email Security and Control (PMX) installed on the mail front-end servers tags spam mails and isolates virus-infected mails. The probability to identify the spam is approximately 95-99%. We are operating several information servers such as WWW servers, Wiki servers, Groupware servers, Windows Media and Quick Time streaming servers, and an anonymous FTP server (FTP.RIKEN.JP).

(3) Development, management and operation of the data acquisition system

We are developing a data-acquisition system for the RIBF. This system has functions of network-distributed data processing, hierarchical event building and parallel readout which are achieved with newly developed software and commodity hardware. This system is both versatile and scalable, allowing it to meet the various requirements for RIBF experiments. It has a maximum data processing capability of around 40 MB/s. We are also developing a time stamping system with 10 ns precision for the RIBF experiments.

(4) Development, management and operation of the network environment

We have been managing the network environment collaborating with Advanced Center for Computing and Communications (ACCC). All the Ethernet ports of the information wall sockets are capable of the Gigabit Ethernet connection (10/100/1000BT). Many wireless LAN access points have been installed to cover the almost entire area of Nishina Center.

(5) Management of the information security

It is essential to take proper information security measures for information assets.

We are managing the information security of Nishina Center collaborating with ACCC.

Team Leader

Takashi ICHIHARA

Member

Yasushi WATANABE

Hidetada BABA

RIBF Research Division
Research Instruments Group
Detector Team

1. Abstract

This team is in charge of development, fabrication, and operation of various detector for nuclear physics experiment in RIKEN Nishina center. Also the team organizes collaboration work for detector technology among related research groups in order to improve mutual share of knowledge and experience.

2. Major Research Subjects

(1) Construction of silicon pixel detector.
(2) Development of high dynamic range preamplifier for silicon strip detector
(3) Development of time projection chamber
(4) Development of the detector with high position resolution and high counting rate
(5) Search for extra dimensions by measuring short-range gravity

3. Summary of Research Activity

This team is presently focusing on developments of detectors for RHIC PHENIX experiments and RIBF nuclear experiments.

(1) Development of silicon pixel detector.
RIKEN, Rikkyo, KEK, and JAEA group is responsible for the pixel ladder fabrications for the RHIC PHENIX detector upgrade. The ladder is a module which is composed of pixel sensor modules, support frame, and readout bus. We completed the fabrication of ladders and installed them into the PHENIX apparatus in December 2010 and started commissioning with stripixel detector part.

(2) Development of high dynamic range preamplifier
Coulomb break up experiment at RIBF needs high dynamic range silicon strip detector in order to identify the charged particle from proton to Sn. We propose to use both high gain and low gain preamplifiers. Dual hybrid preamplifiers with discrete devices were developed and proofed the principal. Then an application specific integrated circuit was designed and fabricated by collaboration with KEK. It was confirmed having expected dynamic range. Second turn of design for fabrication was submitted.

(3) Development of time projection chamber
A time projection chamber will be used for SAMURAI spectrometer. RIKEN, Kyoto and MSU started to build TPC.

(4) Development of the detector with high position resolution and high counting rate
RIBF experiment must have high rate capability to explore low cross section events. We would like to develop such detector by using MICROMEGAS or GEM technology. RIKEN and Tokyo Met. Indust. Res. Institute was collaborated for low cross talk pad readout. We designed it and fabricated the trial readout pad and compared with simulation results.

(5)Short range gravity force is measured by using torsion pendulum. If the gravity force is deviated from the inverse square law, it will be the indication of the new physics. We are measuring the movement of the torsion pendulum by using CCD with online fashion analysis tools.

Team Leader
Atsushi TAKETANI

Contract Researcher
Maki KUROKAWA

Part-time Staff Ⅰ
Meiko UESAKA

Visiting Scientist
Kohei FUJIWARA (Tokyo Metropolitan Industrial Tehcnology Research Institute)

Research Consultant
Hiroyuki MURAKAMI

Students
Junior Research Associate
Kazufumi NINOMIYA

Student Trainees
Naruya OGAWA (Fac. of Sci., Rikkyo Univ.)
Hironori NISHIO (Fac. of Sci., Rikkyo Univ.)
Syuhei YOSHIDA (Fac. of Sci., Rikkyo Univ.)
Sei OKAYAMA (Fac. of Sci., Rikkyo Univ.)
Tatsuro KARAKI (Fac. of Sci., Rikkyo Univ.)
Ryo OGAWARA (Fac. of Sci., Rikkyo Univ.)
Manami OOKAWARA (Fac. of Sci., Rikkyo Univ.)
Akira TAKUMA (Fac. of Sci., Rikkyo Univ.)

RIBF Research Division
Accelerator Applications Research Group

1. Abstract

Accelerator Applications Research Group promotes various applications of ion beams from RI Beam Factory. Radiation Biology Team studies biological effects of fast heavy ions and develops heavy-ion breeding. RI Applications Team studies production and application of radioisotopes and develops new technologies of accelerator mass spectrometry for the trace-element analyses. Details of these activities are described by each team elsewhere. The group has also collaborated with research groups in and outside RIKEN in research and applications of heavy-ion irradiation effects on materials like polymers, superconductors and semiconductor devices. However, some of these activities are finished in FY 2010 and others will be continued by outside groups.

2. Major Research Subjects

Research and development in biology, chemistry and materials science utilizing heavy-ion beams from RI Beam Factory.

3. Summary of Research Activity

(1) Biological effects of fast heavy ions.
(2) Development of heavy-ion breeding.
(3) Production and application of radioisotopes.
(4) Developments of trace elements analyses.

Group Director

Tadashi KAMBARA（～9/30）
Tomoko ABE　(10/1～)

Secretary

Yoshiko SAKATA

RIBF Research Division
Accelerator Applications Research Group
Radiation Biology Team

1. Abstract

The radiation biology team carries out on studies various biological effects of fast heavy ions. It is also involved in the development of a new technique to breed plants by heavy-ion irradiation. Fast heavy ions can cause dense and localized ionization of matter along their tracks, in contrast to photons X-rays and γ-rays, which cause randomly distributed isolated ionization. The localized, dense ionization can cause double-strand DNA breaks in cells induced by; these breaks are not easily repaired, and they result in more effective mutation than that single-strand DNA breaks. A unique feature of our experimental facility at the RIKEN Ring Cyclotron (RRC) is that living bodies in helps them the atmosphere or bottles can be irradiated since the delivered heavy-ion beams have sufficiently high energy that penetrate matter to a significant depth. The radiation biology team utilizes a dedicated beam line (E5B) of the RRC to irradiate microbes, plants, and animals with a wide variety of ion beams, ranging from C to Fe. The research subjects include physiological studies on DNA repair, genome analyses of mutation, and mutation breeding of plants by heavy-ion irradiation. Some new cultivars have already been introduced in the market.

2. Major Research Subjects

(1) Biological effects caused by heavy-ion irradiation
(2) Ion-beam breeding and genome analysis
(3) Innovative applications of heavy-ion beams

3. Summary of Research Activity

The radiation biology team focuses on the biological effects of fast heavy ions from the RRC by using 135 MeV/u C, N, Ne ions, 95 MeV/u Ar ions, and 90 MeV/u Fe ions. It is also involved in the development of a breeding technique for microbes and plants. The main topics covered are as below:

(1) Biological effects caused by heavy-ion irradiation

Uniform dose distribution is the key to systematic studies and thus to the improvement of the mutation efficiency. Therefore, plants and microbes are treated using ions with a stable linear energy transfer (LET). The deletion size appears to depend on the LET: 43~203 bp for C ions (23~60 keV/μm) and 119-647 bp for Fe ions (640 keV/μm) in *Mesorhizobium loti*. Almost 90% deletions are less than 100 bp in *Arabidopsis* when using C ions (22.5~30 keV/μm).

(2) Ion-beam breeding and genome analysis

In contrast to X-rays and γ-rays, fast heavy ions are found to be useful for plant breeding since they only cause localized damage to DNA and induce mutations more effectively at a lower dosage. The radiation biology team utilizes beams of fast heavy ions from the RRC to develop heavy-ion breeding techniques. An LET of 30 keV/μm with C and N ions is the most effective for mutation induction in *Arabidopsis*. In the case of rice, the highest mutation is observed in the LET range 61 to 74 keV/μm, with C and Ne ions. Insertion and deletion mutation rates for Fe ions are higher than those for C ions in the case of *M. loti*. Thus, the LET of the ion beam is an important factor affecting mutagenesis. Many types of mutations that produce variegation, dwarf, early- or late-flowering, high-yielding, and salt-tolerant phenotypes are found in M_2

plants. Genome analyses are performed to reveal the relation between the genotype and the phenotype.

(3) Innovative applications of heavy-ion beams

An international heavy-ion breeding research consortium has been organized with 135 national user groups and 15 international institutes in 2010. The consortium includes agricultural experimental stations, universities, and seed and horticulture companies. The radiation biology team irradiated about 2000 different samples for a total beam time of 40 hours in a year. The advantages of heavy-ion mutagenesis include, low dose high with survival rates, induction of high mutation rates, and a wide range of variation. The ion beam used often changes only a single characteristic. Thus, a new variety can be obtained by selecting a mutant with modification to a target trait while retaining the existing valuable ones. This approach has been particularly successful in flower breeding. The international heavy-ion breeding research consortium produced *Dianthus* with a new color, "Olivia Pure White", and cherry blossom with a new color, "Nishina Zao", in 2008, the dwarf *Delosperma* "Reiko Rose" and "Reiko Pink Ring" in 2009, and the everblooming cherry blossom "Nishina Otome" in 2010. The development period for the aforementioned new varieties of plants was only three years. Thus, the consortium has added 18 new cultivars to the market in Japan, USA, Canada, and EU since 2002.

Team Leader

Tomoko ABE

Members

Tomonari HIRANO
Masako IZUMI
Ryouhei MORITA
Teruyo TSUKADA

Special Postdoctoral Researcher

Yusuke KAZAMA

Technical Staff I

Yoriko HAYASHI

Technical Staff II

Sumie OHBU

Part-time Staffs

Yuko HAYASHI
Sachiko KOGURE
Mayu NAKAGAWA
Yuki SHIRAKAWA
Hideo TOKAIRIN

Visiting Scientists

Ryutaro AIDA (Natl. Inst. Floricult. Sci.)

Mari AMINO (Tokai University Hospital)
Chang-Hyu BAE (Sunchon Natl. Univ., Korea)
Hiroyuki DAIMON (Osaka Pref. Univ.)
Ali FERJANI (Tokyo Gakugei Univ.)
Makoto FUJIWARA (Grad. Sch., Col. Arts Sci., Univ. of Tokyo)
Eitaro FUKATSU (Forest tree beeding Cet.)
Koji FURUKAWA (Mukoyama Orchids Co., Ltd.)
Yoshiya FURUSAWA (Natl. Inst. Radiol. Sci.)
Toshinari GODO (Botanic Gardens Toyama)
Misako HAMATANI (Hiroshima City Agric. Forest. Promot. Cen.)
Yasuhide HARA (Kanagawa Inst. Agric. Sci.)
Masanori HATASHITA (Wakasa Wan Energy Res. Cen.)
Atsushi HIGASHITANI (Grad. Sch. Life Sci., Tohoku Univ.)
Ryoichi HIRAYAMA (Natl. Inst. Radiol. Sci.)
Akiko HOKURA (Tokyo Denki Univ.)
Ichiro HONDA (Natl. Agric. Res. Cen.)
Mitsugu HORITA (Hokuren Agri. Res. Inst.)
Hiroyuki ICHIDA (Meiji Univ.)
Yuji ITO (Natl. Agric. Res. Cen., Hokkaido Region)
Akihiro IWASE (Grad. Sch. Engin., Osaka Pref. Univ.)
Hiroshi KAGAMI (Shizuoka Citrus Exp. Station)
Kensuke KAGEYAMA (Fac. Engin.,Saitama Univ.)
Takeshi KANAYA (Suntory Flowers, Ltd.)
Si-Yong KANG (Dep. Rad. Plant Breed. Genet., KAERI, Korea)
Tomojirou KOIDE (Riken Vitamin Co., Ltd.)
Tsutomu KUBOYAMA (Ibaraki Univ.)
Norihiko MISHIMA (Fukuda Denshi Co., Ltd.)
Yutaka MIYAZAWA (Grad. Sch. Life Sci., Tohoku Univ.)
Kazumitsu MIYOSHI (Fac. Bioresour. Sci., Akita Pref. Univ.)
Toshikazu MORISHITA (Inst. Rad. Breeding, Natl. Inst. Agric. Res.)
Koji MURAI (Fukui Pref. Univ.)
Francesco MUSUMECI (Catania Univ.)
Daisuke NAKADA (Ela Medical Japan Co. Ltd.)
Koichiro NISHIKAWA (FLORSAIKA CIA. LTDA.)
Norihiro OHTSUBO (Natl. Inst. Floricult. Sci.)
Tomo OOMIYA (Hokkaido Ornamental Plants Veg. Res. Cen.)
Kenji OSAWA (Nagano Agric. Res. Cen.)
Masaya SAKAI (Fukuda Denshi Co., Ltd.)
Kouichi SAKAMOTO (YUKIGUNI AGURI Co.,Ltd.)
Tadashi SATO (Grad. Sch. Life Sci., Tohoku Univ.)
Yoichi SATO (Riken Food Co., Ltd.)
Mikio SHIMADA (Kyoto Univ.)
Fumio SUGAWARA (Tokyo Univ. of Sci.)
Masao SUGIYAMA (Hokko Chem. Ind. Co., Ltd.)
Keita SUGIYAMA (Nat. Inst. Veg.Tea Sci.)
Ryuji SUGIYAMA (Ajinomoto, Co., INC.)

Kazunori SUZUKI (Plant Biotech. Inst. Ibaraki Agric. Cen.)
Masao SUZUKI (Natl. Inst. Radiol. Sci.)
Kenichi SUZUKI (Suntory Flowers, Ltd.)
Kunio SUZUKI (Technoflora, Co., Ltd.)
Hinako TAKEHISA (Natl. Inst. Agric. Sci.)
Sachie TANAKA (Tokai Univ.)
Teruhiko TERAKAWA (Hokko Chem. Ind. Co., Ltd.)
Ken TOKUHARA (Dogashima Orchid Cen.)
Masanori TOMITA (CRIEPI)
Hisashi TSUJIMOTO (Fac. Agri., Tottori Univ.)
Kozo TSUKADA (Nippon Veterinary and Life-sci. Univ.)
Makoto UBUKATA (Hokkaido Univ.)
Masao WATANABE (Fac. Agri., Tohoku Univ.)
Takuji YOSHIDA (Takii Seed Co., Ltd.)
Koichiro YOSHIOKA (Tokai University Hospital)
Yi XIE (Inst.of Modern Physics, Chinese Academy of Sciences.)

Research Fellows

Hideki ASAUMI (Ehime Agricultural Experiment Station)
Masataka CHAYA (Nagasaki Agr. Forest. Exp. Station)
Fumiko HIDAKA (Kagoshima Pref. Inst. for Agric. Dev.)
Shunsuke IMANISHI (Natl. Inst.Veg. and Tea Sci.)
Hiroaki KISAKA (Ajinomoto, Co., INC.)
Yuri KURUMATANI (Chiba Pref. Agr. Res. Cent.)
Chikara KUWATA (Chiba Pref. Agr. Res. Cent.)
Tadanori MINO (Wadomari Cho Agr. Exp. Station)
Miyuki NISHI (Saga Agricultural Experiment Station)
Kyousuke NIWA (Hyogo Pref. Res. Inst.)
Tadahito OOTUBO (Wadomari Cho Agr. Exp. Station)
Eikou OOYABU (Saga Pref. Agr. Res. Cen.)
Takenori SAITO (Shizuoka Tea Exp. Station)
Yoshihide SAKITA (Wadomari Cho Agr. Exp. Station)
Tsukasa SHIRAO (Kagoshima Biotechnology Inst.)
Keiichi TAKAGI (Wakasa-wan Energy Research Center)
Kei-ichiro UENO (Kagoshima Biotechnology Inst.)
Naoji WAKITA (Wadomari Cho Agr. Exp. Station)

Consultant

Hiroyuki SAITO

Students

Junior Research Associate

Liqiu MA (Grad. Sch. Sci. & Engin ., Saitama Univ.)
Kiyoshi NISHIHARA (Grad. Sch. Frontier Sci., Univ. of Tokyo)

Student trainees

Hiroki HANASHIMA (Tokyo Denki Univ.)
Saki HARADA (Tokyo Denki Univ.)
Fumihiro MASUYAMA (Tokyo Denki Univ.)
Tomomi MORISHIMA (Tokyo Denki Univ.)
Takuma NAGANO (Tokyo Denki Univ.)
Tetsuya OKABE (Fac. Sci., Tokyo Univ. of Sci.)
Hiroki TAOKA (Fac. Sci., Tokyo Univ. of Sci.)
Wakiko YAMAOKA (Fac. Sci., Tokyo Univ. of Sci.)
Yuichi YOSHII (Fac. Sci., Tokyo Univ. of Sci.)

RIBF Research Division
Accelerator Applications Research Group
RI Applications Team

1. Abstract

RI Applications Team performs following researches at the ion accelerators of RIBF: (1) With 14-MeV protons from the RIKEN AVF Cyclotron, we produce radioisotopes for research of chemistry, biology, medicine, pharmaceutical and environmental sciences. The nuclides Zn-65, Cd-109 and Y-88 are delivered to Japan Radioisotope Association for fee-based distribution to the general public in Japan. We also study the production and application of short-lived RI's. (2) We develop new technologies of mass spectrometry for the trace-element analyses using accelerator technology and apply them to the scientific research fields, such as cosmochemistry, environmental science, archaeology and so on.

2. Major Research Subjects

(1) Production of radioisotopes for research and distribution,
(2) Research and development for new RI production at AVF cyclotron and Ring cyclotron
(3) The development of trace element analysis, using the accelerator techniques, and its application to geo and environmental sciences

3. Summary of Research Activity

RI applications team utilizes RIBF heavy-ion accelerators for following research subjects:

(1) Production of radioisotopes

Using 14-MeV proton beam irradiations at the RIKEN AVF Cyclotron, we develop techniques of production and application of various radio-isotopes (RI's) for research in chemistry, biology, medicine, pharmaceutical and environmental sciences. We can produce RI's with wide range of lifetimes as short as seconds. Long-life (> a few days) RI's are produced in a target which is cooled by water and He gas, and short-life RI's are produced at a gas-jet system where RI atoms are recoiled out of thin foil targets, captured by KCl aerosols and transported to a hot laboratory by a flow of He carrier gas. These systems are in the same chamber in series and can operate simultaneously with the same beam. Among the long-life RI's, Zn-65 ($T_{1/2}$=244 days) and Cd-109 ($T_{1/2}$=463 days) have been delivered to Japan Radioisotope Association since October 2007 for fee-based distribution to the general public in Japan. In addition, we started to deliver Y-88 ($T_{1/2}$=107 days) in February 2010.

(2) R/D for RI production

We work to improve production procedure of the three RI species for the fee-based distribution. We also develop production techniques for other RI species like Sr-85 ($T_{1/2}$=64.8 days), Ce-139 ($T_{1/2}$=138 days), and W-181 ($T_{1/2}$=121 days) which are demanded but lack supply sources. The collection efficiency of gas-jet system has been optimized for Zr-89m ($T_{1/2}$=4.16m), Nb-90m ($T_{1/2}$=18.8s) and Nd-141m ($T_{1/2}$=62s) nuclides.

(3) Trace element analyses with accelerator technologies

We have developed two new technologies of mass spectrometry for the trace-element analyses as an application of accelerator technology to various fields such as cosmochemistry, environmental science, archaeology and so on. One is a new type Accelerator Mass Spectrometry (AMS) at the RILAC equipped with an ECR ion source. This system is available for the measurements of trace-elements (10^{-14}-10^{-15}level), and is expected to be especially effectible for the measurements of low electron-affinity elements such as ^{26}Al, ^{41}Ca, ^{53}Mn and so on. As a preliminary study, the ECR ion source system has been evaluated and the basic data have been obtained for the detection and quantitative analysis of trace nuclides in archaeological samples (cinnabar) and functional metals. As another technology, we have attempted to customize a mass spectrometer equipped with a stand-alone ECR ion source for analyses of elemental and isotopic abundances.

Team Leader
Tadashi KAMBARA

Members
Hiromitsu HABA
Kazuya TAKAHASHI
Shuichi ENOMOTO

Temporary Staff
Jumpei KANAYA

Visiting Scientists
Hiroshi HIDAKA (Fac. Sci., Hiroshima Univ.)
Hiroshi SHIMIZU (Fac. Sci., Hiroshima Univ.)
Miho TAKAHASHI (Tokyo Univ. Marine Sci. and Tech.)
Shigekazu YONEDA (Natl. Sci. Museum)
Tokuko WATANABE (Aoyama Gakuin Women's Junior College)
Masayoshi TODA (Tokyo Univ. Marine Sci. and Tech.)
Tatsuya URABE (Tokyo Univ. Marine Sci. and Tech.)
Tatsuo OKANO (Inst. Industrial Science, Univ. Tokyo)

Research Consultants
Kuniko MAEDA

Part-time Staff
Akihiro MURAOKA
Masashi WAKASUGI

RIBF Research Division
User Liaison and Industrial Cooperation Group

Abstract

The essential mission of the "User Liaison and Industrial Cooperation(ULIC) Group" is to maximize the research activities of RIBF by attracting users in various fields with a wide scope.

The ULIC Group consists of two teams.

The User Support Team provides various supports to visiting RIBF users. For this purpose, the User's Office has been set up. The Industrial Cooperation Team supports potential users in industries who use the beams for application purposes or for accelerator related technologies other than basic research. Production of various radioisotopes by the AVF cyclotron is also one of the important mission. The produced radioisotopes are distributed to researchers in Japan for a charge through the Japan Radioisotope Association.

Group Director

Hideyuki SAKAI

Deputy Group Director

Hideki UENO　(10/1～) (User Support)

Tadashi KAMBARA　(Industrial Cooperation)

Members

Mieko KOGURE

Secretary

Yoshiko SAKATA

Tomoko IWANAMI

Emiko ISOGAI

Katsura IWAI (10/1～)

RIBF Research Division
User Liaison and Industrial Cooperation Group
User Support Office

1. Abstract

The RIKEN RI Beam Factory is the world preeminent facility providing the greatest opportunities for scientific researches. The facility, completed its construction in 2007, has started its full-scale operation in the end of the year 2008. It is essential to promote a broad range of application and thus to maximize the facility importance in order to truly make RIBF to a world-class facility. Now, the installation of key devices for experiments is in progress. We consider intangible improvement is also important as well as such intangible ones. In 2010, we have opened RIBF users office for outside users and prepared a new position for visiting researchers called RIBF Independent Users, aiming at synergetic-use of the RIBF facility. We manage to facilitate the use of RI Beam Factory to the researchers both inside and outside of RIKEN.

2. Major Research Subjects

(1) Facilitation of the use of the RI Beam Factory
(2) Support of experiments in the RI Beam Factory
(3) Promotion of the RI Beam Factory to interested researchers

3. Summary of Research Activity

In order to facilitate the use of RI Beam Factory to the researchers both inside ad outside of RIKEN, we have organized international Program Advisory Committee, consisting of world leading scientists, to review proposals, purely based on their scientific merit and feasibility, in the fields of nuclear physics (NP) and material-and-life science (ML). The NP- and ML-PAC meetings are organized twice a year.
Another important activity is beam-time coordination of the PAC approved experiments and other development activities. The operation schedule of the RIBF accelerator complex is managed by our team taking into account strong demand of user's experiments.

Team Leader
Hideki UENO

Vice Team Leader
Yasushi WATANABE

Technical Staff I
Narumasa MIYAUCHI

RIBF Research Division
User Liaison and Industrial Cooperation Group
Industrial Cooperation Team

1. Abstract

The scope of the industrial cooperation team includes industrial application of RIBF facility and research and development for industrial application of accelerator associated technologies.

2. Major Subjects

Distribution of radioisotopes Zn-65, Cd-109 and Y-88 produced at RIKEN AVF Cyclotron and investigation of novel industrial applications of the accelerator beam and its related technologies

3. Summary of Research Activity

(1) Fee-based distribution of radioisotopes

At RIBF, various specific radioisotopes for research have been produced with the cyclotrons and used for research projects. This team handles fee-based distribution of radioisotopes Zn-65, Y-88 and Cd-109, which are produced by the RI application team at the AVF cyclotron, to nonaffiliated users under a Material Transfer Agreement between Japan Radioisotope Association and RIKEN. In 2010, total amount of 136.1MBq of Zn-65 and 30MBq of Cd-109 were distributed. In addition, we started distribution of Y-88 in February 2010.

(2) Industrial application of RIBF

This team manages and supports the non-academic applications of heavy ion and RI beams at the RIBF facility. In 2010, three private companies utilized the heavy-ion and RI beams.

Team Leader

Tadashi KAMBARA

Members

Tomoko ABE

Hiroshige TAKEICHI

Visiting Scientists

Akira NAGANO (S. H. I. Examination & Inspection, LTD.)

Ryuji UEMOTO (S. H. I. Examination & Inspection, LTD.)

Hiroyuki UNO (S. H. I. Examination & Inspection, LTD.)

Shuhei TATEMICHI (Fuji Electric Systems)

Masanori INOUE (Fuji Electric Systems)

RIBF Research Division
Safety Management Group

1. Abstract

The Nishina Center for Accelerator-Based Science possesses one of the biggest accelerator facilities in the world which consists of two heavy-ion linear accelerators and five cyclotrons. Uranium ions are accelerated here only in Japan. Electron accelerators of microtron and synchrotron-storage-ring are also possessed. Our function is to keep the radiation level in and around the facility below the allowable limit and to control the exposure on the workers as low as reasonably achievable. We are also involved in the safety management of the Radioisotope Center where many types of experiments are performed with sealed and unsealed radioisotopes.

2. Major Research Subjects

(1) Safety management at radiation facilities of Nishina Center for Accelerator-Based Science
(2) Safety management at Radioisotope Center
(3) Radiation shielding design and development of accelerator safety systems

3. Summary of Research Activity

Our most important task is to keep the personnel exposure as low as reasonably achievable, and to prevent an accident. Therefore, we daily patrol the facility, measure the ambient dose rates, maintain the survey meters, shield doors and facilities of exhaust air and wastewater, replenish the protective supplies, and manage the radioactive waste. Advice, supervision and assistance at major accelerator maintenance works are also our task.

We installed radiation safety interlock system at the newly built RIBF building, and are extending it along with the constructions of experimental facilities. The suffocation-safety interlock system was also installed at the BigRIPS tunnel of RIBF accelerator building where huge amount of liquid He is used for superconducting magnets. The radiation safety interlock system for Nishina building was extended since a new linear accelerator, RILAC2, was installed in the AVF cyclotron vault in 2010.

Head

Yoshitomo UWAMINO

Members

Hisao SAKAMOTO
Rieko HIGURASHI HIRUNUMA

Technical Staff I

Atsuko AKASHIO

Assistant

Tomomi OKAYASU

Contract Officer

Satoshi HASHIGUCHI
Hiroyuki FUKUDA

Hiroki MUKAI
Mamoru TAKEKOSHI

Special Temporary Employee
Shin FUJITA

Visiting Scientists
Koji OHISHI

Secretary
Tsutomu YAMAKI
Kazushiro NAKANO
Hiroko AISO
Kimie IGARASHI
Satomi IIZUKA

Center for Nuclear Study, Graduate School of Science, University of Tokyo

1. Abstract

The Center for Nuclear Study (CNS) aims to elucidate the nature of nuclear system by producing the characteristic states where the Isospin, Spin and Quark degrees of freedom play central roles. These researches in CNS lead to the understanding of the matter based on common natures of many-body systems in various phases. We also aim at elucidating the explosion phenomena and the evolution of the universe by the direct measurements simulating nuclear reactions in the universe. In order to advance the nuclear science with heavy-ion reactions, we develop AVF upgrade, CRIB and SHARAQ facilities in the large-scale accelerators laboratories RIBF. We promote collaboration programs at RIBF as well as RHIC-PHENIX and ALICE-LHC with scientists in the world, and host international meetings and conferences. We also provide educational opportunities to young scientists in the heavy-ion science through the graduate course as a member of the department of physics in the University of Tokyo and through hosting the international summer school.

2. Major Research Subjects

(1) Accelerator Physics
(2) Nuclear Astrophysics
(3) Nuclear spectroscopy of exotic nuclei
(4) Quark physics
(5) Spin Physics
(6) Nuclear Theory
(7) SHARAQ project

3. Summary of Research Activity

(1) Accelerator Physics

One of the Major tasks of the accelerator group is the AVF upgrade project which includes development of ion sources, upgrading the AVF cyclotron of RIKEN and the beam line to CRIB. Development of ECR heavy ion sources is to provide a new HI beams, higher and stable beams of metallic ions, and to improve the control system. Two CNS ECR sources now provide all the beams for the AVF cyclotron and support not only CRIB experiments but also a large number of RIBF experiments. A charge-breeding ECR source is also under development.

Three major works were advanced for upgrading the AVF cyclotron. The first is a design study of the central region of the cyclotron with harmonic number of 1. The second is installation of a new central module to increase the beam energy up to K78. The third is installation of a new beam deflector monitor to improve the transmission efficiency. Injection beam monitoring and control are being studied.

New ion-source beam diagnosis and monitoring system (ISDM) was designed. This new beam monitor will become a powerful tool for all the RIBF facility.

(2) Nuclear Astrophysics

Major program of the nuclear astrophysics group is to study nuclear reactions and structures under explosive conditions in the universe, and clarify the mechanism of stellar evolution and explosive phenomena such as supernovae. High-intensity RI beams of light nuclei from the CNS low-energy RI beam separator CRIB provide a good opportunity to study stellar nuclear reactions under explosive conditions both by the direct method as well as by indirect methods. The research programs include investigations of a-induced stellar reactions on 7Be, 18Ne, and 30S. The 12N(p,g) stellar reaction was also investigated indirectly using a 12N beam with the ANC method. Developments were also made for new RI beams, and an active target with GEM (GEM-MSTPC) has been developed and used successfully for direct measurements of (a,p) stellar reactions using 18Ne and 30S beams. This demonstrated that the GEM-MSTPC detector can measure efficiently stellar reactions with low-cross sections. Further technological development for the Wien-filter of CRIB was made in the past year.

(3) Nuclear structure of exotic nuclei

The NUSPEQ (NUclear SPectroscopy for Extreme Quantum system) group studies exotic structures in high-isospin and/or high-spin states in nuclei. The CNS GRAPE (Gamma-Ray detector Array with Position and Energy sensitivity) is a major apparatus for high-resolution in-beam gamma-ray spectroscopy. Missing mass spectroscopy using the SHARAQ is going to start as another approach on exotic nuclei. In 2010, the following progress has been made.

New high-spin states in $^{49-51}$Ti populated by fusion reactions of an RI beam have been found, which gives information on the N=28 shell gap and the single particle energies in the fp-shell. High-spin states in A～40 mass region were studied via ^{18}O+^{26}Mg fusion evaporation reactions. A superdeformed rotational band (β_2～0.5) was observed up to 12^+ state in ^{40}Ar. This finding indicates the presences of the N=22 and Z=18 superdeformed shell structure in this region. High-spin states of ^{107}In were studied via the ^{58}Ni(^{52}Cr, 3p) reaction. A rotational cascade consisting of ten gamma-ray transitions was observed. The band exhibits the features typical for smooth terminating bands in A～100 mass region.

Upgrade of the readout system of the CNS GRAPE has started, where digital pulse data taken by sampling ADCs are analyzed by FPGAs on boards.

Proposal for studying tetra neutron system using the double-charge exchange reaction ^{4}He(^{8}He,^{8}Be)4n at 200 A MeV was submitted to the NP-PAC and approved, which will be performed in near future.

(4) Quark Physics

Main goal of the quark physics group is to understand the properties of hot and dense nuclear matter created by colliding heavy nuclei at relativistic energies. The group has been involved in the PHENIX experiment at Relativistic Heavy Ion Collider (RHIC) at Brookhaven National Laboratory, and in the ALICE experiment at Large Hadron Collider (LHC) at CERN. A big news in this year was that LHC succeeded making Pb+Pb collisions in November of 2010, .

As for PHENIX, the group has been concentrating on the physics analysis involving leptons and photons, which include direct photon production at low transverse momentum using the virtual-gamma method, neutral pion production with high transverse momentum as a function of azimuthal angle from the reaction plane in Au+Au collisions, and J/y production in ultra-peripheral Au+Au collisions. The group has also been involved in the construction and commissioning of Si VTX detector subsystem.

As for ALICE, the group has been involved in the commissioning of the Transition Radiation Detector (TRD), and calibration and performance study of Time Projection Chamber (TPC). Efforts to analyze p+p and Pb+Pb data have been initiated. The group has also been playing a leading role in the development of forward calorimeter for future upgrade.

R&D of gas electron multiplier (GEM) and related techniques has been continuing.

Development of resistive GEM with resistive anodes has been progressing in collaboration with the Tamagawa group of RIKEN.

(6) Nuclear Theory
The nuclear theory group has been promoting the RIKEN-CNS collaboration project on large-scale nuclear structure calculations since 2001 and maintaining its parallel computing cluster. In 2009, we developed the effective interactions of various mass region based on the large-scale shell model calculation technique and discussed the "shell evolution" and the role of tensor force quantitatively in exotic nuclei, such as ^{17}C, ^{48}Ca, N=50 isotones, Sm isotopes and so on.

(7) SHARAQ project
The SHARAQ promoted momentum and angular dispersion matching (DM) technique for RI beams. We successfully achieved DM beam transport by using RI beams of ^{10}C and ^{12}N in BigRIPS, High-resolution beamline and SHARAQ spectrometer, following the achievement of DM transport with a primary ^{14}N beam in 2009. By using the DM beam transport, we performed two experiments to search the isovector spin monopole (IVSM) mode and the isovector spin-non-flip monopole (IVM) mode in nuclei: In the experiment for IVSM, we obtained an excitation function in $^{90}Zr(^{12}N, ^{12}C)$ reaction, which is exothermic and is possible to excite the target nucleus by IVSM mode with recoilless; The experiment for IVM aims at searching IVM mode of nuclear excitation. We observed the spectra in $^{90}Zr(^{10}C, ^{10}B$(Ex = 1740 keV)) channel, which is likely to be an effective probe for IVM excitation because of its feature of DT=1 and DS=0. The analyses of these experimental data are now in progress.

SHARAQ group developed two tracking detectors installed in the beam line especially in the point of high-rate operation. As a tracking detector for small beam spot and high intensity, we developed a stack of plastic scintillators (Plastic tracker). Hit positions are determined by light output from each plastic bar, its position resolution is 1 mm, corresponding to the plastic scintillator width.

Secondly, the low-pressure MWDC for beam tracking developed by study of its operation parameters. After optimization, the capability of beam tracking advanced up to 2×10^6 particles/sec and the detector stably operated by RI beam of 10^6 cps during 2 weeks.

Derector
Takaharu OTSUKA

Scientific Staff
Susumu SHIMOURA (Professor)
Shigeru KUBONO (Professor)
Hideki HAMAGAKI (Associate Professor)
Tomohiro UESAKA (Associate Professor)
Eiji IDEGUCHI (Lecturer)
Hidetoshi YAMAGUCHI (Research Associate)
Shin'ichiro MICHIMASA (Research Associate)
Taku GUNJI (Research Associate)

Shinsuke OTA (Research Associate)

Guest Scientists

Toshio SUZUKI (Guest Professor, Nihon Univ.)
Toshinori MITSUMOTO (Guest Associate Professor, Sumitomo Heavy Industries, Ltd.)

Technical Staff

Yukimitsu OHSHIRO
Norio YAMAZAKI

Techinical Assistants

Shin-ichi WATANABE
Hiroshi KUREI
Hideaki NINOMIYA
Akira YOSHINO
Shoichi YAMAKA

Post Doctoral Associates

Akito SAITO (-Mar/31, 2010)
Takashi HASHIMOTO
Yuji TSUCHIMOTO
Toru YOSHIDA
Hideaki MATSUBARA (Oct/1,2010-)
Masanori DOZONO (Oct/1, 2010-, JSPS fellow)

Post Doctoral Fellowship of Foreign Researcher

Silvio CHERUBINI (June/29, 2010-)

Graduate Students

Yoshiko SASAMOTO
Yorito YAMAGUCHI
Yoki ARAMAKI
Nguyen Binh DAM (-Sep/28, 2010)
Satoshi SANO
Seiya HAYAKAWA
David. M KAHL
Akihisa TAKAHARA
Hiroyuki MIYA
Ryoji AKIMOTO
Yasuto HORI
Hiroshi TOKIEDA
Tomoya TSUJI
Shintaro GO
Shoichiro KAWASE
ShinIchi HAYASHI (April/1, 2010-)
KeiIchi KISAMORI (April/1, 2010-)

Motonobu TAKAKI (April/1, 2010-)
Atsushi NUKARIYA (April/1, 2010-)
Yosuke KIKUCHI (April/1, 2010-)
Tang T. Leung (Oct/1/2010-)
Tomomi KAWAHARA
Anna SHIBUSAWA
Masaki TACHI

Administration Staff

Midori HIRANO
Ikuko YAMAMOTO
Takako ENDO
Yukino KISHI
Toshiko ITAGAKI
Yuko SOMA

TORIJIN (Todai-RIKEN Joint International Program for Nuclear Physics) Term

1. Abstract

University of Tokyo and RIKEN agreed to corporate with each other in the field of nuclear physics and established Todai-RIKEN Joint International Program for Nuclear Physics (TORIJIN) in June 2006. The aim of this organization is to promote the international collaborations, such as JUSTIPEN (Japan-US Theory Institute for Physics with Exotic Nuclei) and EFES (International Research Network for Exotic Femto Systems). JUSTIPEN was launched in June 2006 in order to facilitate collaborations between U.S. and Japanese scientists whose main research thrust is in the area of the physics of exotic nuclei. More than 67 nuclear scientists in U.S. have visited Japan in three years, and many collaborations are established. EFES was selected as one of the Core-to-Core Programs of Japan Society for the Promotion of Science (JSPS). This is the program to send Japanese nuclear scientists to U.S., Germany, France, Italy, Norway, and Finland and to promote the international collaborations in the field of nuclear study. Many joint workshops were held with the partner countries.

2. Main activities

Promote the international collaborations of both theoretical and experimental nuclear physicists under JUSTIPEN and EFES programs.

3. Summary of Research Activity

Under the JUSTIPEN program, many nuclear scientists visited in this fiscal year and collaborations are established. Under the EFES program, we have carried out four types of activities: initiating the collaboration projects, organizing seminars with partner courtiers, sending researchers abroad, and sending/inviting young scientists to the summer schools. Regarding the collaborative works, we have carried out six projects. Many experimentalists and theoreticians have been sent abroad. As for the joint workshops, we have organized seven workshops/symposia/conferences and all of them were quite fruitful. Also, young scientists have been sent to partner countries for educational purpose and starting collaborations. As for the summer school, Japanese graduate students have been sent to the summer schools in Germany and USA, and we have invited students to CNS-EFES summer school from the partner countries.

Leader

Takaharu TSUKA (University of Tokyo)

Vice leader

Hiroyoshi SAKURAI (RIKEN)

Members

Susumu SHIMOURA (University of Tokyo),
Takashi NAKATSUKASA (RIKEN),
Tomohiro UESAKA (University of Tokyo),
Shin'ichiro FUJII (University of Tokyo)
Tohru MOTOBAYASHI (RIKEN)

Events of Nishina Center & CNS from January 2010 to March 2011

2010	Jan. 5	Final Review of Theoretical Physics Laboratory
	Jan. 6	The 1st Industrial Program Advisory Committee
	Jan. 14	Press Release on "Nishina Otome" (New cherry blossom tree that blooms during all four seasons)
	Jan. 20-21	RIKEN Symposium on "Muon Science at the RIKEN-RAL Muon Facility 2009"
	Feb. 15	Press Release on "Perfect' Liquid Hot Enough to be Quark Soup" -Protons, neutrons melt to produce 'quark-gluon plasma' at RHIC-
	Feb. 26	Interim Review of Advanced Meson Science Laboratory
	Apr. 23	RIKEN Wako Institute's Open House
	May. 23	IPAC'10 Special Lectures to Commemorate the 120th Anniversary of the Birth of Yoshio Nishina: Yoshio Nishina's and Japanese pioneers' developments in particle accelerators and their applications
	Jun. 8	Press conference on the "Discovery of 45 New radioisotopes" at the MEXT
	Jun. 15-16	The 7th Program Advisory Committee for Nuclear Physics experiments at RI Beam Factory
	Jul. 2	An MOU extending the "Agreement between RIKEN and STCF concerning muon science" until March, 2018 was signed
	Aug. 18-24	The 9th CNS-EFES International Summer School（CNS-EFES10）
	Oct. 1	Registration for RIBF independent users begins
	Oct. 5-8	Nishina School
	Nov. 19-21	Science Agora 2010 at Odaiba
	Dec. 21	124Xe-beam acceleration up to the energy of 672 keV/A with the new linac, RILAC2
	Dec. 3-5	The 8th Program Advisory Committee for Nuclear Physics experiments at RI Beam Factory
2011	Jan. 11-12	The 7th Program Advisory Committee for Materials & Life Science experiments at RIKEN Nishina Center
	Feb. 1	"The world's first successful measurement of 18 new half-lives of very neutron-rich nuclei" - an evidence of nucleosynthesis in Supernova explosions faster than previously expected

Awards from April 2010 to March 2011

Awardee	Motizuki Yuko
Laboratory	Radioactive Isotope Physics Laboratory
Name of award	Best Oral Presentation Award at the XXXI SCAR (Scientific Committee on Antarctic Research) Open Science Conference, Buenos Aires, Argentina
Sponsoring organization	Scientific Committee on Antarctic Research
Date of award	Aug. 1, 2010

Awardee	Kinoshita Toichiro
Laboratory	Theoretical Physics Laboratory
Name of award	The Gian Carlo Wick 2010 Gold Medal Award
Sponsoring organization	World Federation of Scientists
Date of award	Aug. 20, 2010

Awardee	Ichikawa Yuichi
Laboratory	Polarized RI Beam Team
Name of award	The 16th Young Scientist Prize
Sponsoring organization	Nuclear Experimental Physics Forum
Date of award	Sep.13, 2010

Awardee	Takashi Kishida
Laboratory	Radioactive Isotope Physics Laboratory
Name of award	The Commendation by Chairman of the High Pressure Gas Association of Saitama
Sponsoring organization	The High Pressure Gas Association of Saitama
Date of award	Oct. 22, 2010

Awardee	Yamazaki Toshimitsu
Laboratory	Advanced Meson Science Laboratory
Name of award	The Order of the Sacred Treasure, Gold and Silver Star
Sponsoring organization	Cabinet Office
Date of award	Nov. 3, 2010

Awardee	Imao Hiroshi
Laboratory	Accelerator Group Accelerator R&D Team
Name of award	Physics World Breakthrough of the Year
Sponsoring organization	Institute of Physics
Date of award	Dec. 20, 2010

Awardee	Ohnishi Tetsuya
Laboratory	Research Instruments Group BigRIPS Team
Name of award	The 5th Young Scientist Award of the Physical Society of
Sponsoring organization	The Physical Society of Japan
Date of award	Mar. 26, 2011

Awardee	Imao Hiroshi
Laboratory	Accelerator Group Accelerator R&D Team
Name of award	The 22nd Young Scientist Award of the Society of Muon and Meson Science of Japan
Sponsoring organization	Society of Muon and Meson Science of Japan
Date of award	Mar. 9, 2011

VI. LIST OF PUBLICATIONS

& PRESENTATIONS

RIKEN Nishina Center for Accelerator-Based Science

Publications

[Journal]

(Original Papers) *Subject to Peer Review

Yano Y., Wakasugi M., and Suda T.: "A New Method for Electron-Scattering Experiments using a Self-Confining Radioacctive Ion Target in an Electron Storage Ring", Nucl. Instrum. Methods Phys. Res. A **532**, 216–223 (2004). ∗

Kameda D., Asahi K., Ueno H., Yoshimi A., Haseyama T., Watanabe H., Miyoshi H., Shimada K., Kijima G., Nagae D., Kato G., Emori S., Tsukui M., Kobayashi Y., and Ishihara M.: "Magnetic moments of ^{30}Al an ^{32}Al", Czech. J. Phys. **55 Suppl. A**, 327–332 (2005). ∗

Sugimoto T., Nakamura T., Kondo Y., Aoi N., Baba H., Bazin D. P., Fukuda N., Gomi T., Hasegawa H., Imai N., Ishihara M., Kobayashi T., Kubo T., Miura M., Motobayashi T., Otsu H., Saito A., Sakurai H., Shimoura S., A.M. V., Watanabe K., Watanabe Y., Yakushiji T., Yanagisawa Y., and Yoneda K.: "The first 2+ state of 14Be", Phys. Lett. B **654**, 160–164 (2007). ∗

Kondo Y., Nakamura T., Sato Y., Matsumoto T., Aoi N., Endo N., Fukuda N., Gomi T., Hashimoto Y., Ishihara M., Kawai S., Kitayama M., Kobayashi T., Matsuda Y., Matsui N., Motobayashi T., Nakabayashi T., Ogata K., Okumura T., Ong H., Onishi T., Otsu H., Sakurai H., Shimoura S., Shinohara M., Sugimoto T., Takeuchi S., Tamaki M., Togano Y., and Yanagisawa Y.: "One-neutron removal reactions of ^{18}C and ^{19}C on a proton target", Phys. Rev. C **79**, No. 014602, pp. 014602-1–014602-7 (2009). ∗

Aoi N., Kanno S., Takeuchi S., Suzuki H., Bazin D. P., Bowen M. D., Campbell C. M., Cook J. M., Dinca D. -., Gade A., Glasmacher T., Iwasaki H., Kubo T., Kurita K., Motobayashi T., Mueller W. F., Nakamura T., Sakurai H., Takashina M., Terry J. R., Yoneda K., and Zwahlen H.: "Enhanced collectivity in 74Ni", Phys. Lett. B **692**, 302–306 (2010). ∗

(Review)

Motobayashi T.: "New research opportunities at RIKEN RI Beam Factory", AIP Conf. Proc. **1224**, 454–460 (2010).

(Others)

Yasuda Y., Ozawa A., Arai I., Fujinawa T., Fukunishi N., Goto A., Ohnishi T., Sakurai H., Wakasugi M., Yamaguchi Y., Yano Y., Suzuki T., Yamaguchi T., Kikuchi T., and Ohtsubo T.: "Present status of rare-RI ring project in RIKEN RIBF", Int. J. Mod. Phys. E **18**, No. 2, pp. 459–464 (2009).

Arai I., Ozawa A., Yasuda Y., Fujinawa T., Fukunishi N., Goto A., Ohnishi T., Sakurai H., Wakasugi M., Yamaguchi Y., Yano Y., Suzuki T., Yamaguchi T., Kikuchi T., and Ohtsubo T.: "Beam optics simulation for rare-RI ring at RI beam factory in RIKEN", Int. J. Mod. Phys. E **18**, No. 2, pp. 498–504 (2009).

[Book・ Proceedings]

(Original Papers) *Subject to Peer Review

Kamigaito O., Arai S., Fujimaki M., Fujinawa T., Fujisawa H., Fukunishi N., Goto A., Higurashi Y., Ikezawa E., Kageyama T., Kase M., Komiyama M., Kuboki H., Kumagai K., Maie T., Nagase M., Nakagawa T., Ohnishi J., Okuno H., Sakamoto N., Sato Y., Suda K., Watanabe H., Watanabe T., Watanabe Y., Yamada K., Yamasawa H., Yano Y., and Yokouchi S.: "Intensity-upgrade plans of RIKEN RI-Beam Factory", Proceedings of 11th International Conference on Heavy Ion Accelerator Technology (HIAT09), Venezia, Italy, 2009–6, HIAT09 International Organizing Committee, Venice, pp. 21–25 (2009).

Kamigaito O., Ikezawa E., Kase M., Fujimaki M., Fujinawa T., Fukunishi N., Goto A., Haba H., Higurashi Y., Kidera M., Komiyama M., Koyama R., Kuboki H., Kumagai K., Maie T., Nagase M., Nakagawa T., Ohnishi J., Okuno H., Sakamoto N., Sato Y., Suda K., Watanabe T., Yamada K., Yokouchi S., and Yano Y.: "Present status of RIKEN heavy-ion linac", Proceedings of LINAC 08, Canada, Victoria, 2008–9〜10, TRIUMF, Vancouver, pp. 112–114 (2010).

上垣外修一, 藤巻正樹, 藤縄雅, 福西暢尚, 後藤彰, 長谷部裕雄, 日暮祥英, 池上九三男, 池沢英二, 影山正, 加瀬昌之, 木寺正憲, 込山美咲, 久保木浩功, 熊谷桂子, 眞家武士, 長瀬誠, 中川孝秀, 大西純一, 奥野広樹, 龍頭啓充, 坂本成彦, 佐藤洋一, 須田健嗣, 若杉昌徳, 渡辺博, 渡邉環, 山田一成, 横内茂, 矢野安重: "理研 RI ビームファクトリーの現状", 第 5 回日本加速器学会年会・第 33 回リニアック技術研究会論文集, 東広島, 2008–8, 日本加速器学会, 東広島, pp. 10–12 (2008).

(Others)

Okuno H., Fukunishi N., Goto A., Hasebe H., Kamigaito O., Kase M., Kuboki H., Imao H., Yano Y., and Hershcovitch A.: "A New Possibility of Low-Z Gas Stripper for High Power Uranium Beam Acceleration Alternative to C Foil", Proceedings of HB2010 (46th ICFA Advanced Beam Dynamics Workshop on High-Intensity and High-Brightness Hadron Beams), Morschach, Switzerland, ICFA, , pp. 600–604 (2011).

上垣外修一, 新井重昭, 藤巻正樹, 藤縄雅, 藤澤博, 福西暢尚, 後藤彰, 日暮祥英, 池沢英二, 影山正, 加瀬昌之, 込山美咲, 久保木浩功, 熊谷桂子, 眞家武士, 長瀬誠, 中川孝秀, 大西純一, 奥野広樹, 坂本成彦, 佐藤洋一, 須田健嗣, 渡辺博, 渡邉環, 渡邉裕, 山田一成, 山澤秀行, 矢野安重, 横内茂: "Intensity-upgrade plans of RIKEN RI-Beam Factory", 第 6 回日本加速器学会年会プロシーディングス, 東海村, 2009–8, 日本加速器学会, 東海村, pp. 38–41 (2010).

Oral Presentations

(International Conference etc.)

Kamigaito O., Ikezawa E., Kase M., Fujimaki M., Fujinawa T., Fukunishi N., Goto A., Haba H., Higurashi

Y., Kidera M., Komiyama M., Koyama R., Kuboki H., Kumagai K., Maie T., Nagase M., Nakagawa T., Ohnishi J., Okuno H., Sakamoto N., Sato Y., Suda K., Watanabe T., Yamada K., Yokouchi S., and Yano Y.: "Present status of RIKEN heavy-ion linac", 24th International Linear Accelerator Conference (LINAC08), (LINAC08 Organizing Committee), Victoria, Canada, Sept.–Oct. (2008).

Kamigaito O., Arai S., Fujimaki M., Fujinawa T., Fujisawa H., Fukunishi N., Goto A., Higurashi Y., Ikezawa E., Kageyama T., Kase M., Komiyama M., Kuboki H., Kumagai K., Maie T., Nagase M., Nakagawa T., Ohnishi J., Okuno H., Sakamoto N., Sato Y., Suda K., Watanabe H., Watanabe T., Watanabe Y., Yamada K., Yamasawa H., Yano Y., and Yokouchi S.: "Intensity-upgrade plans of RIKEN RI-Beam Factory", 11th International Conference on Heavy Ion Accelerator Technology (HIAT09), (HIAT09 International Organizing Committee), Venezia, Italy, June (2009).

Motobayashi T.: "Nuclear astrophysics at RIKEN RIBF", 5th European Summer School on Experimental Nuclear Astrophysics, (University of Catania), Santa Tecla, Italy, Sept. (2009).

Kamigaito O., Arai S., Dantsuka T., Fujimaki M., Fujinawa T., Fujisawa H., Fukunishi N., Goto A., Hasebe H., Higurashi Y., Ikegami K., Ikezawa E., Imao H., Kageyama T., Kase M., Kidera M., Komiyama M., Kuboki H., Kumagai K., Maie T., Nagase M., Nakagawa T., Nakamura M., Ohnishi J., Okuno H., Sakamoto N., Suda K., Watanabe H., Watanabe Y., Watanabe T., Yamada K., Yamasawa H., Yokouchi S., and Yano Y.: "Status of RIBF accelerators at RIKEN", 19th International Conference on Cyclotrons and their Applications (CYCLOTRONS 2010), (Cyclotrons2010 International Organizing Committee), Lanzhou, China, Sept. (2010).

Okuno H., Fukunishi N., Goto A., Hasebe H., Kamigaito O., Kase M., Kuboki H., Imao H., Yano Y., and Hershcovitch A.: "A New Possibility of Low-Z Gas Stripper for High Power Uranium Beam Acceleration Alternative to C Foil", 46th ICFA Advanced Beam Dynamics Workshop on High-Intensity and High-Brightness Hadron Beams, (Paul Scherrer Institut), Morschach, Switzerland, Sept.–Oct. (2010).

(Domestic Conference)

上垣外修一, 藤巻正樹, 藤縄雅, 福西暢尚, 後藤彰, 長谷部裕雄, 日暮祥英, 池上九三男, 池沢英二, 影山正, 加瀬昌之, 木寺正憲, 込山美咲, 久保木浩功, 熊谷桂子, 眞家武士, 長瀬誠, 中川孝秀, 大西純一, 奥野広樹, 龍頭啓充, 坂本成彦, 佐藤洋一, 須田健嗣, 若杉昌徳, 渡辺博, 渡邉環, 山田一成, 横内茂, 矢野安重: "理研 RI ビームファクトリーの現状", 第 5 回日本加速器学会年会/第 33 回リニアック技術研究会, (日本加速器学会), 東広島, 8 月 (2008).

上垣外修一, 新井重昭, 藤巻正樹, 藤縄雅, 藤澤博, 福西暢尚, 後藤彰, 日暮祥英, 池沢英二, 影山正, 加瀬昌之, 込山美咲, 久保木浩功, 熊谷桂子, 眞家武士, 長瀬誠, 中川孝秀, 大西純一, 奥野広樹, 坂本成彦, 佐藤洋一, 須田健嗣, 渡辺博, 渡邉環, 渡邉裕, 山田一成, 山澤秀行, 矢野安重, 横内茂: "理研 RIBF のビーム増強計画", 第 6 回日本加速器学会年会, (日本加速器学会), 茨城県東海村, 8 月 (2009).

小沢顕, 鈴木宏, 長江大輔, 新井一郎, 森口哲朗, 伊藤由太, 長谷部裕雄, 藤縄雅, 福西暢尚, 後藤彰, 大西哲哉, 櫻井博儀, 若杉昌徳, 山口由高, 矢野安重, 鈴木健, 山口貴之, 菊池崇志, 大坪隆, 安田裕介, 久保野茂: "RIBF における稀少 RI リング", RIBF に於ける測定器についての検討会, 和光, 12 月 (2009).

小沢顕, 新井一郎, 伊藤由太, 森口哲朗, 長江大輔, 鈴木宏, 藤縄雅, 福西暢尚, 後藤彰, 長谷部裕雄, 大西哲哉, 櫻井博儀, 若杉昌徳, 山口由高, 矢野安重, 鈴木健, 山口貴之, 菊池崇志, 大坪隆, 安田裕介, 久保野茂: "RIBF に於ける稀少 RI リング計画", 蓄積リング検討ミニワークショップ, (大阪大学　核物理研究センター), 茨木, 1 月 (2010).

鈴木宏, 新井一郎, 藤縄雅, 福西暢尚, 後藤彰, 菊池崇志, 久保野茂, 森口哲朗, 長江大輔, 大坪隆, 小沢顕, 櫻井博儀, 鈴木健, 若杉昌徳, 安田裕介, 山口貴之, 山口由高, 矢野安重: "理研稀少 RI リングの粒子軌道計算", 日本物理学会 2010 年秋季大会, (日本物理学会), 北九州, 9 月 (2010).

Theoretical Physics Laboratory

Publications

[Journal]

(Original Papers) *Subject to Peer Review

Aoyama T., Hayakawa M., Kinoshita T., and Nio M.: "Automated calculation of QED corrections to lepton $g-2$", Proceedings of Science **RAD COR 2007**, No. 025, pp. 1–6 (2007). *

Aoki S., Ishikawa K., Ishizuka N., Kadoh D., Kanaya K., Kuramashi Y., Murano K., Namekawa Y., Okawa M., Taniguchi Y., Ukawa A., Ukita N., and Yoshie T.: "Precicise determination of the strong coupling constant in Nf=2+1 lattice QCD with the Schrodinger functional scheme", J. High-Energy Phys. **10**, 053-0–053-22 (2008). *

Haba N., Sakamura Y., and Yamashita T.: "Weak boson scattering in Gauge-Higgs Unification", J. High Energy Phys. **0907**, 020-1–020-19 (2009). *

Azeyanagi T., Hanada M., Kawai H., and Matsuo Y.: "Worldsheet analysis of gauge/gravity dualities", Nucl. Phys. B **816**, 278–292 (2009). *

Azeyanagi T., Fukuma M., Kawai H., and Yoshida K.: "Universal description of viscoelasticity with foliation preserving diffeomorphisms", Phys. Lett. B **681**, 290–295 (2009). *

Kanamori I.: "Vacuum energy of two-dimensional N=(2,2) super Yang-Mills theory", Phys. Rev. D **79**, 115015-1–115015-6 (2009). *

Kawai H., Shimasaki S., and Tsuchiya A.: "Large N reduction on group manifolds", Int. J. Mod. Phys. A **25**, 3389–3406 (2010). *

Hatsuda Y. and Tanaka H.: "Scattering of Giant Magnons in CP^3", J. High Energy Phys. **1002**, 085-1–085-25 (2010). *

Haba N., Sakamura Y., and Yamashita T.: "Tree-level unitarity in Gauge-Higgs Unification", J. High Energy Phys. **1003**, 069-1–069-33 (2010). *

Hatsuda Y., Ito K., Sakai K., and Satoh Y.: "Thermodynamic Bethe Ansatz Equations for Minimal Surfaces in AdS3", J. High Energy Phys. **1004**, 108-1–108-23 (2010). *

Tai T.: "Uniformization, Calogero-Moser/Heun duality and Sutherland/bubbling pants", J. High Energy Phys. **1010**, 107-1–107-18 (2010). *

Hashimoto K., Iizuka N., Ishii T., and Kadoh D.: "Three-flavor quark mass dependence of baryon spectra in holographic QCD", Phys. Lett. B **691**, No. 1, pp. 65–71 (2010). *

Kawai H., Shimasaki S., and Tsuchiya A.: "Large N reduction on coset spaces", Phys. Rev. D **81**, 085019-1–085019-9 (2010). *

Blum T., Zhou R., Doi T., Hayakawa M., Izubuchi T., Uno S., and Yamada N.: "Electromagnetic mass splittings of the low lying hadrons and quark masses from 2+1 flavor lattice QCD+QED", Phys. Rev. D **82**, 094508-1–094508-47 (2010). *

Tai T.: "Triality in SU(2) Seiberg-Witten theory and Gauss hypergeometric function", Phys. Rev. D **82**, 105007-1–105007-9 (2010). *

Hanada M. and Kanamori I.: "Absence of sign problem in two-dimensional N = (2,2) super Yang-Mills on lattice", J. High Energy Phys. **1101**, 058-1–058-25 (2011). *

Kadoh D. and Suzuki H.: "Supersymmetry restoration in lattice formulations of 2D $\mathcal{N} = (2,2)$ WZ model based on the Nicolai map", Phys. Lett. B **696**, No. 1/2, pp. 163–166 (2011). *

Oral Presentations

(Domestic Conference)

鈴木博: "超対称ゲージ理論の格子シミュレーション", 次世代格子ゲージシミュレーション研究会, 和光, 9 月 (2010).

Theoretical Nuclear Physics Laboratory

Publications

[Journal]

(Original Papers) *Subject to Peer Review

Moller P., Ragnar B., Carlsson G., Olivius P., Ichikawa T., Sagawa H., and Iwamoto A.: "Axial and reflection asymmetry of the nuclear ground state", Atomic Data and Nuclear Data Tables **94**, 758–780 (2008). *

Ito M. and Itagaki N.: "Unified studies of nuclear reactions and exotic structures in ^{12}Be", Int. J. Mod. Phys. E **12**, No. 10, pp. 2061–2066 (2008). *

Kawashita Y., Yabana K., Noda M., Nobusada K., and Nakatsukasa T.: "Oscillator strength distribution of C_{60} in the time-dependent density functional theory", J. Mol. Struct.: Theochem **914**, 130–135 (2009). *

Ito M. and Itagaki N.: "Covalent, Ionic, and Atomic Structures in ^{12}Be", Mod. Phys. Lett. A **24**, No. 11-13, pp. 1005–1008 (2009). *

Avogadro P. and Nakatsukasa T.: "The finite amplitude method for the QRPA", Mod. Phys. Lett. A **25**, 1999–2000 (2009).

Kondo Y., Nakamura T., Sato Y., Matsumoto T., Aoi N., Endo N., Fukuda N., Gomi T., Hashimoto Y., Ishihara M., Kawai S., Kitayama M., Kobayashi T., Matsuda Y., Matsui N., Motobayashi T., Nakabayashi T., Ogata K., Okumura T., Ong H., Onishi T., Otsu H., Sakurai H., Shimoura S., Shinohara M., Sugimoto T., Takeuchi S., Tamaki M., Togano Y., and Yanagisawa Y.: "One-neutron removal reactions of ^{18}C and ^{19}C on a proton target", Phys. Rev. C **79**, No. 014602, pp. 014602-1–014602-7 (2009). *

Ichikawa T., Iwamoto A., and Moller P.: "Origin of the narrow, single peak in the fission-fragment mass distribution for ^{258}Fm", Phys. Rev. C **79**, 014305-1–014305-6 (2009). *

Yamada T., Funaki Y., Horiuchi H., Roepke G., Schuck P., and Suzuki A.: "Internal One-Particle Density Matrix for Bose-Einstein Condensates with Finite Number of Particles in a Harmonic Potential", Phys. Rev. C **79**, 054314-1–054314-11 (2009). *

Matuyanagi K., Matsuo M., Nakatsukasa T., Hinohara N., and Sato K.: "Open problems in the microscopic theory of large-amplitude collective motion", J. Phys. G **37**, No. 6, pp. 064018-1–064018-16 (2010). *

Yoshida K.: "COLLECTIVE MODES OF EXCITATION IN DEFORMED NEUTRON-RICH Mg ISOTOPES", Mod. Phys. Lett. A **25**, No. 21/23, pp. 1783–1786 (2010). *

Aoi N., Kanno S., Takeuchi S., Suzuki H., Bazin D. P., Bowen M. D., Campbell C. M., Cook J. M., Dinca D. -., Gade A., Glasmacher T., Iwasaki H., Kubo T., Kurita K., Motobayashi T., Mueller W. F., Nakamura T., Sakurai H., Takashina M., Terry J. R., Yoneda K., and Zwahlen H.: "Enhanced collectivity in 74Ni", Phys. Lett. B **692**, 302–306 (2010). *

Nguyen H. Q. and Nguyen D. D.: "Canonical and microcanonical ensemble descriptions of thermal pairing within BCS and quasiparticle random-phase approximation", Phys. Rev. C **81**, No. 5, pp. 057302-1–057302-4 (2010). *

Sarhan B. A. and Kohama A.: "Scaling properties of proton-nucleus total reaction cross sections", Phys. Rev. C **81**, No. 5, pp. 057601-1–057601-4 (2010). *

Oyamatsu K., Iida K., and Koura H.: "Neutron drip line and the equation of state of nuclear matter", Phys. Rev. C **81**, 027301-1–027301-4 (2010). *

Oyamatsu K. and Iida K.: "Symmetry energy at subnuclear densities deduced from nuclear masses", Phys. Rev. C **81**, 054302-1–054302-6 (2010). *

Yoshida K.: "Roles of deformation and neutron excess on the giant monopole resonance in neutron-rich Zr isotopes", Phys. Rev. C **82**, No. 3, pp. 034324-1–034324-6 (2010). *

Nguyen H. Q. and Nguyen D. D.: "Thermodynamic properties of hot nuclei within the self-consistent quasiparticle random-phase approximation", Phys. Rev. C **82**, No. 4, pp. 044316-1–044316-9 (2010). *

Hinohara N., Sato K., Nakatsukasa T., Matsuo M., and Matuyanagi K.: "Microscopic description of large-amplitude shape-mixing dynamics with inertial functions derived in local quasiparticle random-phase approximation", Phys. Rev. C **82**, No. 6, pp. 064313-1–064313-16 (2010). *

Ebata S., Nakatsukasa T., Inakura T., Yoshida K., Hashimoto Y., and Yabana K.: "Canonical-basis time-dependent Hartree-Fock-Bogoliubov theory and linear-response calculations", Phys. Rev. C **82**, No. 034306, pp. 034306-1–034306-13 (2010). *

Taniguchi Y., Enyo Y., Kimura M., Ikeda K., Horiuchi H., and Ideguchi E.: "Triaxial superdeformation in ^{40}Ar", Phys. Rev. C **82**, 011302-1–011302-5 (2010). *

Nguyen D. D. and Nguyen H. Q.: "Thermal nuclear pairing within the self-consistent quasiparticle RPA", J. Phys.: Con. Ser. **267**, No. 1, pp. 012049-1–012049-6 (2011). *

Sato K. and Hinohara N.: "Shape mixing dynamics in the low-lying states of proton-rich Kr isotopes", Nucl. Phys. A **849**, No. 1, pp. 53–71 (2011). *

Hinohara N. and Enyo Y.: "Triaxial quadrupole deformation dynamics in *sd*-shell nuclei around ^{26}Mg", Phys. Rev. C **83**, No. 1, pp. 014321-1–014321-15 (2011). *

Yoshida K. and Nakatsukasa T.: "Dipole responses in Nd and Sm isotopes with shape transitions", Phys. Rev. C **83**, No. 2, pp. 021304-1–021304-5 (2011). *

(Review)

吉田賢市: "スキルム型密度汎関数を用いた変形中性子過剰核における集団励起モード", 原子核研究 **55**, No. 1, pp. 23–32 (2010).

(Others)

Oyamatsu K. and Iida K.: "Equation of state of nuclear matter and nuclei in laboratories and neutron-star crusts", Nucl. Phys. A **805**, 585–587 (2008).

Hinohara N., Sato K., Nakatsukasa T., and Matsuo M.: "Microscopic derivation of five-dimensional collective Hamiltonian of large-amplitude quadrupole motion: application to shape coexistence in proton-rich Se isotopes", AIP Conf. Proc. **1235**, 96–100 (2010).

Hinohara N., Sato K., Nakatsukasa T., and Matsuo M.: "Large-amplitude quadrupole collective dynamics of shape coexistence phenomena in proton-rich Se and Kr isotopes", AIP Conf. Proc. **1238**, 286–289 (2010).

Taniguchi Y., Enyo Y., and Kimura M.: "α clustering and superdeformation of ^{28}Si", EPJ Web Conf. **3**, 06004-1–06004-7 (2010).

Hinohara N., Sato K., Nakatsukasa T., and Matsuo M.: "Microscopic approach to adiabatic large-amplitude quadrupole collective dynamics in Se isotopes", Mod. Phys. Lett. A **25**, No. 21-23, pp. 1796–1799 (2010).

Kohama A., Sarhan B. A., Horiuchi W., Iwasaki S., and Suzuki Y.: "Total reaction cross sections of light neutron-rich nuclei in the Glauber approximation", Mod. Phys. Lett. A **25**, No. 21-23, pp. 1963–1966 (2010).

Sato K., Hinohara N., Nakatsukasa T., and Matsuo M.: "Phenomenological analysis of the oblate-prolate symmetry breaking in triaxial deformation dynamics", Mod. Phys. Lett. A **25**, No. 21-23, pp. 2018–2019 (2010).

Sato K., Hinohara N., Nakatsukasa T., and Matsuo M.: "Microscopic analysis of shape mixing in low-lying states of proton-rich Kr isotopes", Mod. Phys. Lett. A **25**, No. 21-23, pp. 2020–2021 (2010).

Taniguchi Y.: "Triaxial superdeformation in ^{40}Ar", Mod. Phys. Lett. A **25**, 1915–1918 (2010).

[Book・Proceedings]

(Review)

Yabana K., Kawashita Y., Nakatsukasa T., and Iwata J.: "Time-dependent density-functional theory for oscillator strength distribution", Charged Particle and Photon Interactions with Matter, CRC Press, Taylor & Francis Group, Boca Raton, pp. 65–86 (2011).

Oral Presentations

(International Conference etc.)

Yoshida K.: "Low-lying Excitations and Giant Resonances in Deformed Mg Isotopes", 4th LACM-EFES-JUSTIPEN Workshop, Oak Ridge, USA, Mar. (2010).

Yoshida K.: "Collective modes of excitation in deformed neutron-rich Mg isotopes", International Symposium on Forefronts of Researches in Exotic Nuclear Structures (Niigata2010), (Niigata University), Niigata, Mar. (2010).

Kohama A.: "Total reaction cross sections of light neutron-rich nuclei in the Glauber approximation", International Symposium on Forefronts of Researches in Exotic Nuclear Structures (Niigata2010), (Niigata University), Tokamachi, Niigata Pref., Mar. (2010).

Nakatsukasa T.: "Time-dependent approaches to quantum dynamics of many-body systems", Workshop on Decoherence in Quantum Dynamical Systems, (ECT*), Trento, Italy, Apr. (2010).

Nguyen D. D. and Nguyen H. Q.: "Thermal nuclear pairing within the selfconsistent quasipartical RPA", 10th International Spring Seminar on Nuclear Physics: New Quests in Nuclear Structure, (University of Napoli), Vietri sul Mare, Italy, May (2010).

Taniguchi Y.: "Clustering correlations and triaxiality in sd-shell region", 2nd Workshop on "State of the Art in Nuclear Cluster Physics", (Universite Libre de Bruxelles), Bruxelles, Belgium, May (2010).

Ebata S., Nakatsukasa T., Inakura T., Hashimoto Y., and Yabana K.: "Linear Response Calculation using Canonical-basis TDHFB with a schematic pairing functional", 2nd EMMI-EFES Workshop on Neutron-Rich Nuclei (EENEN 10), (EFES), Wako, June (2010).

Hinohara N.: "Microscopic description of large-amplitude shape dynamics in neutron-rich Mg isotopes", 2nd EMMI-EFES Workshop on Neutron-Rich Nuclei (EENEN 10), (GSI, University of Tokyo), Wako, June (2010).

Yoshida K.: "Pygmy resonance and giant resonance in deformed nuclei", 2nd EMMI-EFES Workshop on Neutron-Rich Nuclei (EENEN 10), (EMMI-EFES), Wako, June (2010).

Sato K. and Hinohara N.: "Shape mixing dynamics in the low-lying states of proton-rich Kr isotopes", 2nd EMMI-EFES Workshop on Neutron-Rich Nuclei (EENEN 10), (GSI, University of Tokyo), Wako, June (2010).

Inakura T., Nakatsukasa T., and Yabana K.: "Systematic calculation of electric dipole mode with fully self-consistent Skyrme-HF+RPA", 2nd EMMI-EFES Workshop on Neutron-Rich Nuclei (EENEN 10), Wako, June (2010).

Barbieri C.: "Understanding one- and two-nucleon structure from (ab-initio) Green's function theory", 2nd EMMI-EFES Workshop on Neutron-Rich Nuclei (EENEN 10), Wako, June (2010).

Nakatsukasa T.: "Projects for computational fundamental physics in Japan and TD approaches to nuclear structure/reaction", Annual UNEDF Collaboration Meetings, (Michigan State University), East Lansing, USA, June (2010).

Sihver L., Lantz M. J., Takechi M., Kohama A., Ferrari A., Cerutti F., and Saito T.: "A comparison of total reaction cross section models used in particle and heavy ion transport codes", 38th COSPAR scientific assembly (COSPAR 2010), (The Committee on Space Research), Bremen, Germany, July (2010).

Nakatsukasa T.: "Linear response calculations using the Canonical-basis TDHFB with a schematic pairing functional", International Nuclear Physics Conference (INPC2010), (TRIUMF), Vancouver, Canada, July (2010).

Yoshida K.: "Exotic modes of excitation in deformed neutron-rich nuclei", Nuclear Structure 2010, (University of California Berkeley), Berkeley, USA, Aug. (2010).

Inakura T., Nakatsukasa T., and Yabana K.: "Systematic calculations of electric dipole responses with fully self-consistent Skyrme-RPA", Workshop on Gamma Strength and Level Density in Nuclear Physics and Nuclear Technology, (Dresden-Rossendorf), Dresden, Germany, Aug.–Sept. (2010).

Hinohara N.: "Local QRPA vibrational and rotational inertial functions for large-amplitude quadrupole collective dynamics", Zakopane Conference on Nuclear Physics Extremes of the Nuclear Landscape, (Institute of Nuclear Physics PAN), Zakopane, Poland, Aug.–Sept. (2010).

Nakatsukasa T.: "Self-consistent description of nuclear photoabsorption cross sections", Zakopane Conference on Nuclear Physics Extremes of the Nuclear Landscape, (Henryk Niewodniczanski Institute of Nuclear Physics PAN), Zakopane, Poland, Aug.–Sept. (2010).

Nakatsukasa T.: "Complex absorbing potential for the continuum in real-space calculations", JAPAN-ITALY EFES(-INFN) Workshop on Correlations in Reactions and Continuum, (University of Torino, JSPS), Torino, Italy, Sept. (2010).

Yoshida K.: "Skyrme energy-density functional approach to collective excitations in medium-mass to heavy nuclei", JAPAN-ITALY EFES(-INFN) Workshop on Correlations in Reactions and Continuum, (EFES, INFN), Turin, Italy, Sept. (2010).

Ebata S., Nakatsukasa T., Inakura T., Yoshida K., Hashimoto Y., and Yabana K.: "The research of E1 mode using Canonical-basis TDHFB", JAPAN-ITALY EFES(-INFN) Workshop on Correlations in Reactions and Continuum, (EFES), Torino, Italy, Sept. (2010).

Nakatsukasa T.: "Large-scale numerical simulations of nuclear many-body dynamics using the time-dependent density-functional theory", International Workshop Nuclear Structure: Recent Developments, (The Bogoliubov Laboratory of Theoretical Physics), Dubna, Russia, Oct. (2010).

Inakura T., Nakatsukasa T., and Yabana K.: "Systematic calculations of electric dipole response with fully self-consistent Skyrme-RPA", University of Aizu-JUSTIPEN-EFES Symposium on "Cutting-Edge Physics of Unstable Nuclei", Aizuwakamatsu, Oct. (2010).

Yoshida K.: "Nuclear density-functional theory for collective dynamics", International Symposium "From Quarks to Supernovae", (University of Tsukuba), Higashiizucho, Shizuoka Pref., Nov. (2010).

Yoshida K.: "Exotic modes of excitation in deformed neutron-rich nuclei", International Symposium New Faces of Atomic Nuclei, (EFES, OIST), Okinawa, Nov. (2010).

Hinohara N.: "Microscopic description of large-amplitude shape-mixing dynamics with local QRPA inertial functions", International Symposium New Faces of Atomic Nuclei, (University of Tokyo), Okinawa, Nov. (2010).

Nguyen D. D.: "Nuclear Thermodynamics Properties within Self-Consistent Quasiparticle Random-Phase Approximation", Invited seminar by Centre d'Etudes Nucleaires de Bordeaux-Gradignan, (Centre d'Etudes Nucleaires de Bordeaux-Gradignan), Bordeaux-Gradignan, France, Nov. (2010).

Hinohara N.: "Large-Amplitude Shape Mixing Dynamics with Local QRPA Inertial Functions", University of Aizu-JUSTIPEN-EFES Symposium on "Cutting-Edge Physics of Unstable Nuclei", (University of Aizu), Aizuwakamatsu, Nov. (2010).

Sato K., Hinohara N., Nakatsukasa T., Matsuo M., and Matuyanagi K.: "Microscopic study of development of quadruple deformation in neutron-rich Cr isotopes", University of Aizu-JUSTIPEN-EFES Symposium on "Cutting-Edge Physics of Unstable Nuclei", (University of Aizu, International Research Network for Exotic Femto Systems (EFES), Japan-US Theory Institute for Physics with Exotic Nuclei (JUSTIPEN)), Aizuwakamatsu, Nov. (2010).

Yoshida K.: "Skyrme-QRPA approach to collective modes of excitation in deformed nuclei", University of Aizu-JUSTIPEN-EFES Symposium on "Cutting-Edge Physics of Unstable Nuclei", (University of Aizu, JUSTIPEN, EFES), Aizuwakamatsu, Nov. (2010).

Taniguchi Y.: "Various deformed states and α clustering in ^{42}Ca", University of Aizu-JUSTIPEN-EFES Symposium on "Cutting-Edge Physics of Unstable Nuclei", (University of Aizu), Aizuwakamatsu, Nov. (2010).

Nguyen D. D.: "Nuclear Thermodynamics Properties within Self-Consistent Quasiparticle Random-Phase Approximation", Seminar at Centro de Fisica das Interaccoes Fundamentais, Instituto Superior Tecnico, Lisbon, Portugal (CFIF, IST), (CFIF, Instituto Superior Tecnico), Lisbon, Portugal, Nov.–Nov. (2010).

Kohama A.: "Interaction cross sections and the Glauber model", Halo2010 Symposium, (The Center for Nuclear Study (CNS), the University of Tokyo), Hayama, Dec. (2010).

Kohama A., Iida K., and Oyamatsu K.: "Black-sphere approximation to nuclei and its application to reactions with neutron-rich nuclei", French Japanese Symposium on Nuclear Structure Problems, (French Japanese Nuclear Structure Problems International Associated Laboratory and the JSPS core-to-core project), Wako, Jan. (2011).

Taniguchi Y.: "Coexistence of various deformed states and

α clustering in ^{42}Ca", French Japanese Symposium on Nuclear Structure Problems, Wako, Jan. (2011).

Hinohara N.: "Large-amplitude quadrupole collective dynamics in neutron-rich Mg and Cr isotopes", French Japanese Symposium on Nuclear Structure Problems, Wako, Jan. (2011).

Sato K., Hinohara N., Nakatsukasa T., Matsuo M., and Matuyanagi K.: "Microscopic desription of large-amplitude large-amplitude collective motions with local QRPA inertial masses", French Japanese Symposium on Nuclear Structure Problems, (FJNSP LIA , EFES), Wako, Jan. (2011).

Inakura T.: "Recent progress of nuclear density functional calculations -towards to next-generation supercomputer-", French-Japanese Symposium on Nuclear Structure Problems, Wako, Jan. (2011).

Nakatsukasa T.: "Density functional approaches to atomic nuclei -Historical review and recent developments-", International Symposium Nanoscience and Quantum Physics (nanoPHYS'11), (Tokyo Institute of Technology), Tokyo, Jan. (2011).

Yoshida K.: "Skyrme energy-density functional approach to collective dynamics", International EFES-IN2P3 Conference "Many body correlations from dilute to dense nuclear systems", (EFES, IN2P3, LIA), Paris, France, Feb. (2011).

Sato K., Hinohara N., Nakatsukasa T., Matsuo M., and Matuyanagi K.: "Microscopic approach to large-amplitude shape mixing dynamics with local QRPA inertial masses", 5th LACM-EFES-JUSTIPEN Workshop, (the Japan-US Theory Institute for Physics with Exotic Nuclei (JUSTIPEN), the Todai-RIKEN Joint International Program for Nuclear Physics (TORIJIN), the JSPS Core-to-Core program), Oak Ridge, USA, Mar. (2011).

(Domestic Conference)

吉田賢市: "Core polarization for the electric quadrupole moment of neutron-rich Aluminum isotopes", 日本物理学会第 65 回年次大会, 岡山, 3 月 (2010).

吉田賢市: "Skyrme density-functional approach to excitation modes in deformed neutron-rich nuclei", 日本物理学会第 65 回年次大会, 岡山, 3 月 (2010).

小濱洋央, 飯田圭, 親松和浩, 岩瀬広, 仁井田浩二: "重核＋重核反応の全反応断面積", 日本物理学会第 65 回年次大会, 岡山, 3 月 (2010).

谷口億宇: "Cluster correlations and triaxiality", 「少数粒子系物理の現状と今後の展望」研究会, 福岡, 8 月 (2010).

佐藤弘一, 日野原伸生, 中務孝, 松尾正之, 松柳研一: "中性子過剰 Cr 同位体における変形の発達", 日本物理学会 2010 年秋季大会, (日本物理学会), 北九州, 9 月 (2010).

日野原伸生, 佐藤弘一, 中務孝, 松尾正之, 松柳研一: "中性子過剰 Mg 核の大振幅変形ダイナミクスの微視的記述", 日本物理学会 2010 年秋季大会, (日本物理学会), 北九州, 9 月 (2010).

吉田賢市: "Pygmy dipole mode in deformed neutron-rich Mg isotopes close to the drip line", 日本物理学会 2010 年秋季大会, (日本物理学会), 北九州, 9 月 (2010).

江幡修一郎, 中務孝, 稲倉恒法, 橋本幸男, 矢花一浩: "CbT-DHFB による A=50 近辺までの E1 モードの研究", 日本物理学会 2010 年秋季大会, (日本物理学会), 北九州, 9 月 (2010).

小濱洋央, 飯田圭, 親松和浩, 岩瀬広, 仁井田浩二: "重核＋重核反応の全反応断面積：高エネルギー領域の振舞い", 日本物理学会 2010 年秋季大会, 北九州, 9 月 (2010).

谷口億宇: "Ar 同位体の超変形状態の非軸対称性", 日本物理学会 2010 年秋季大会, (日本物理学会), 北九州, 9 月 (2010).

佐藤 弘一: "Micoscopic description of shape coexistence/mixing phenomena as large-amplitude collective motions", Noyori summer school 2010, 播磨, 9 月 (2010).

中務孝: "核子多体系シミュレーション計算の現状と課題", 次世代格子ゲージシミュレーション研究会, 和光, 9 月 (2010).

吉田賢市: "Skyrme energy-density functional approach to collective excitations in medium-mass to heavy nuclei", 京都大学基礎物理学研究所セミナー, (基礎物理学研究所), 京都, 10 月 (2010).

谷口億宇, 延與佳子: "断熱近似核間ポテンシャルと低エネルギー核融合断面積", 基研研究会「大振幅集団運動の微視的理論」, (京都大学), 京都, 10 月 (2010).

佐藤弘一, 日野原伸生, 中務孝, 松尾正之, 松柳研一: "Constrained HFB + Local QRPA 法による大振幅集団運動の記述", 基研研究会「大振幅集団運動の微視的理論」, (京都大学基礎物理学研究所), 京都, 10 月 (2010).

日野原伸生: "断熱的自己無撞着集団座標法による集団経路の抜き出し", 基研研究会「大振幅集団運動の微視的理論」, (京都大学基礎物理学研究所), 京都, 10 月 (2010).

吉田賢市: "Skyrme energy-density functional approach to nuclear collective dynamics", 基研研究会「大振幅集団運動の微視的理論」, (基礎物理学研究所), 京都, 10 月 (2010).

江幡修一郎, 中務孝, 稲倉恒法, 吉田賢市, 橋本幸男, 矢花一浩: "Canonical-basis TDHFB を用いた線形応答計算", 基研研究会「大振幅集団運動の微視的理論」, (京都大学基礎物理学研究所), 京都, 10 月 (2010).

吉田賢市: "Pairing and deformation in nuclei around the island of inversion", 仁科センター研究会「電磁気モーメント・核力反応による Island of Inversion の理解にむけて」, 和光, 12 月 (2010).

日野原伸生: "Shape coexistence/mixing in Mg isotopes", 仁科センター研究会「電磁気モーメント・核力反応による Island of Inversion の理解にむけて」, 和光, 12 月 (2010).

佐藤 弘一: "Microscopic description of shape mixing dynamics in atomic nuclei with local quasiparticle RPA inertial masses", 次世代スーパーコンピューティング・シンポジウム 2010 および第 1 回戦略プログラム 5 分野合同ワークショップ, 神戸, 1 月 (2011).

佐藤 弘一: "Microscopic approach to large-amplitude collective dynamics in shape coexistence/mixing phenomena", GCOE シンポジウム「フロンティア開拓」, (京都大学), 京都, 2 月 (2011).

稲倉恒法: "ピグミー共鳴状態と他の物理量との相関につい

て", 日本物理学会第 66 回年次大会, (日本物理学会), 新潟, 3 月 (2011).

日野原伸生, 延與佳子: "^{26}Mg 付近の sd シェル核における大振幅非軸対称変形ダイナミクス", 日本物理学会第 66 回年次大会, (日本物理学会), 新潟, 3 月 (2011).

佐藤弘一, 日野原伸生, 中務孝, 松尾正之, 松柳研一: "中性子過剰 Cr 同位体における変形ダイナミクスの微視的解析", 日本物理学会第 66 回年次大会, (日本物理学会), 新潟, 3 月 (2011).

吉田賢市: "Roles of deformation and neutron excess on the giant monopole resonance in neutron-rich Zr isotopes", 日本物理学会第 66 回年次大会, (日本物理学会), 新潟, 3 月 (2011).

Strangeness Nuclear Physics Laboratory

Publications

[Journal]

(Original Papers) *Subject to Peer Review

Umeya A. and Harada T.: "Σ-admixture in neutron-rich Li Λ hypernuclei in a microscopic shell-model calculation", EPJ Web Conf. **3**, 07012-1–07012-4 (2010).

Ikeda Y., Kamano H., and Sato T.: "On the resonance energy of the strange dibaryon", Nucl. Phys. A **835**, 386–389 (2010). *

Umeya A. and Harada T.: "Shell-model study of Σ-mixing in neutron-rich $_{\Lambda}$Li hypernuclei", Nucl. Phys. A **835**, 426–429 (2010). *

Harada T., Hirabayashi Y., and Umeya A.: "Production of doubly strange hypernuclei via Ξ^- doorways in the ^{16}O(K^-, K^+) reaction at 1.8 GeV/c", Phys. Lett. B **690**, 363–368 (2010). *

Ikeda Y. and Iida H.: "The $\bar{q}$-q potential from Bethe-Salpeter amplitudes on lattice", Proceedings of Science **Lattice 2010**, No. 143, pp. 1–7 (2010). *

Ikeda Y., kamano h., and Sato T.: "Energy Dependence of $\bar{K}N$ Interactions and esonance Pole of Strange Dibaryons", Prog. Theor. Phys. **124**, No. 3, pp. 533–539 (2010). *

Inoue T., Ishii N., Aoki S., Doi T., Hatsuda T., Ikeda Y., Murano K., Nemura H., and Sasaki K.: "Baryon-Baryon Interactions in the Flavor SU(3) Limit from Full QCD Simulations on the Lattice", Prog. Theor. Phys. **124**, 591–603 (2010). *

Ikeda Y.: "KN potential and Θ^+ in Lattice QCD", Prog. Theor. Phys. Suppl., No. 186, pp. 228–233 (2010). *

Oral Presentations

(International Conference etc.)

Hiyama E.: "Four-body structure of S = -2 hypernuclei", 2nd Workshop on "State of the Art in Nuclear Cluster Physics", (University of Brussels), Brussels, Belgium, May (2010).

Ikeda Y. and Iida H.: "The $\bar{q}$-q potential from Bethe-Salpeter amplitudes on lattice", 28th International Symposium on Lattice Field Theory (Lattice 2010), Villasimius, Italy, June (2010).

Umeya A., Motoba T., and Harada T.: "Structures and productions of typical sd-shell hypernuclei in shell-model calculations", International Nuclear Physics Conference (INPC2010), (TRIUMF), Vancouver, Canada, July (2010).

Hiyama E.: "Recent progress in hypernuclear physics", 21st European Conference on Few-Body Problems in Physics, (University of Salamanca, Instituto de Estructura de la Materia), Salamanca, Spain, Aug.–Sept. (2010).

Hiyama E.: "Binding energies of few-body hypernuclear systems and CSB", Joint SPHERE and JSPS Meeting 2010, Prague, Czech, Sept. (2010).

Hiyama E.: "Few-body aspect of hypernuclear physics", 3rd International Conference on Nuclear and Particle Physics with CEBAF at Jefferson Lab, (NCCU, Jefferson Lab. , Ruder Boskovic Institute), Dubrovnik, Croatia, Oct. (2010).

Hiyama E.: "Five and four-body structure of S=-2 hypernuclei", ECT* European Centre for Theoretical Studies In Nucleaer Physics and Related Areas Strangeness in Nuclei, (European centre for theoretical studies in nuclear physics and related areas), Trento, Italy, Oct. (2010).

Hiyama E.: "Five-body aspect of hypernuclear physics", International Symposium on Nuclear Physics in Asia, (Beihang University), Beijing, China, Oct. (2010).

Hiyama E.: "Recent progress in hypernuclear physics", 2010 Fall Meeting of the APS Division of Nuclear Physics, (American Physical Society), Santa Fe, USA, Nov. (2010).

Hiyama E.: "Few-body aspects of hypernuclear physics", Seminar at Los Alamos National Laboratory, (Los Alamos National Laboratory), Los Alamos, USA, Nov. (2010).

Ikeda Y.: "Lattice QCD studies of s-wave meson-baryon interactions", International Conference on the Structure of Baryons (BARYONS' 10), Suita, Dec. (2010).

Hiyama E.: "Few-body aspects of hypernuclear physics", Seminar at Chinese academy of sciences, (Institute of Theoretical Physics, Chinese Academy of Sciences), Beijing, China, Jan. (2011).

Hiyama E.: "Five-body cluster structure of double Λ hypernucleus, 11ΛΛBe", Hadron-Nuclear Physics (HNP) 2011, Pohang, Korea, Feb. (2011).

Hiyama E.: "Three- and four-body structure of hypernuclei", Seminar at LNF-INFN, (LNF-INFN), Frascati, Italy, Feb. (2011).

Hiyama E.: "Structure of hypernuclei with double strangeness", Seminar at the University of Torino, (The University of Torino), Torino, Italy, Feb. (2011).

Hiyama E.: "Theory Status", Informal Meeting on Strangeness Nuclear Physics in Vienna, (Stefan-Meyer-Institut), Vienna, Austria, Mar. (2011).

Hiyama E.: "Few-body aspects of hypernuclear physics", SMI Seminar, (Stefan-Meyer-Institut), Vienna, Austria, Mar. (2011).

(Domestic Conference)

池田陽一: "3 体精密計算に基づくストレンジダイバリオン共鳴の研究", 日本物理学会第 65 回年次大会, 岡山, 3 月 (2010).

梅谷篤史, 元場俊雄, 原田融: "sd 殻ラムダハイパー核の構造分析および生成反応", 日本物理学会第 65 回年次大会, (日本物理学会), 岡山, 3 月 (2010).

池田陽一: "格子 QCD による K 中間子－核子相互作用の研究", 日本物理学会第 65 回年次大会, 岡山, 3 月 (2010).

飯田 英明, 池田 陽一: "Interquark potentials from qbar q

Bethe-Salpeter amplitudes on lattice", 東大セミナー, (東京大学), 東京, 6 月 (2010).

肥山詠美子: "Five-body cluster structure of double-Λ hypernucleus ${}^{11}_{\Lambda\Lambda}$Be", 京都大学基礎物理学研究所セミナー, (京都大学基礎物理学研究所), 京都, 7 月 (2010).

飯田英明, 池田陽一: "格子 QCD によるベーテ・サルピータ波動関数に基づくクォーク間ポテンシャルの導出", 「少数粒子系物理の現状と今後の展望」研究会, (九州大学、大阪大学 RCNP、理化学研究所・仁科加速器研究センター), 福岡, 8 月 (2010).

梅谷篤史: "中性子過剰ラムダハイパー核の構造", 「少数粒子系物理の現状と今後の展望」研究会, (九州大学), 福岡, 8 月 (2010).

池田陽一: "$\bar{K}N$ 相互作用とストレンジ・ダイバリオン", 原子核三者若手夏の学校 2010 原子核パート研究会, 長野県木島平村, 8 月 (2010).

飯田英明, 池田陽一: "Inter-quark potential based on Bethe-Salpeter amplitudes in lattice QCD", 日本物理学会 2010 年秋季大会, (日本物理学会), 北九州, 9 月 (2010).

池田陽一: "S 波メソン-バリオン相互作用の格子 QCD による研究", 日本物理学会 2010 年秋季大会, 北九州, 9 月 (2010).

梅谷篤史, 明孝之, 肥山詠美子: "中性子過剰ラムダハイパー核, ${}^{9}_{\Lambda}$He の構造", 日本物理学会 2010 年秋季大会, (日本物理学会), 北九州, 9 月 (2010).

池田陽一: "Study of Kbar N - pi Sigma interactions with accurate experimental data", KEK 理論センター研究会「ストレンジネス核物理 2010」, つくば, 12 月 (2010).

梅谷篤史, 明孝之, 肥山詠美子: "中性子過剰ハイパー核 ${}^{9}_{\Lambda}$He の構造", KEK 理論センター研究会「ストレンジネス核物理 2010」, (高エネルギー加速器研究機構), つくば, 12 月 (2010).

肥山詠美子: "大次元量子力学的少数多体系計算法とストレンジネス核物理への応用", KEK 大型シミュレーション研究シンポジウム「KEK 大型シミュレーション研究の 5 年間と今後」, (高エネルギー加速器研究機構), つくば, 1 月 (2011).

肥山詠美子: "軽いハイパー核の構造と YN, YY 相互作用", 研究会「バリオン物質と中性子星」, (岩手大学), 盛岡, 1 月 (2011).

肥山詠美子: "A=10 ラムダハイパー核の構造", 日本物理学会第 66 回年次大会, (日本物理学会), 新潟, 3 月 (2011).

Mathematical Physics Laboratory

Publications

[Journal]

（Original Papers） *Subject to Peer Review

Ishii T.: "Toward bound-state approach to strangeness in holographic QCD", Phys. Lett. B **695**, No. 1-4, pp. 392–396 (2011). *

Oral Presentations

(International Conference etc.)

Ikeda Y. and Iida H.: "The $\bar{q}$-q potential from Bethe-Salpeter amplitudes on lattice", 28th International Symposium on Lattice Field Theory (Lattice 2010), Villasimius, Italy, June (2010).

Ishii T.: "Baryon with massive strangeness in holographic QCD", Summer Institute 2010 (Cosmology & String), (Yukawa Institute for Theoretical Physics), Fujiyoshida, Aug. (2010).

Ishii T.: "Baryons with massive strangeness in holographic QCD", Crete Conference On Gauge Theories And The Structure Of Spacetime, (University of Crete), Kolymvari, Greece, Sept. (2010).

(Domestic Conference)

衛藤 稔: "Color superconductor vortex in high density QCD", 研究会「ソリトンと QCD」, 和光, 6 月 (2010).

飯田 英明, 池田 陽一: "Interquark potentials from qbar q Bethe-Salpeter amplitudes on lattice", 東大セミナー, (東京大学), 東京, 6 月 (2010).

石井 貴昭: "Baryon with massive strangeness in holographic QCD", 九州大学素粒子論研究室セミナー, (九州大学素粒子論研究室), 福岡, 7 月 (2010).

石井 貴昭: "Baryon with massive strangeness in holographic QCD", 大阪大学原子核理論研究室セミナー, (大阪大学原子核理論研究室), 豊中, 7 月 (2010).

石井 貴昭: "Baryon with massive strangeness in holographic QCD", 基研研究会「場の理論と超弦理論の最先端」, (京都大学基礎物理学研究所), 京都, 7 月 (2010).

衛藤稔: "高密度 QCD のカラー超伝導ボルテックスの最近の発展について", 基研研究会「場の理論と超弦理論の最先端」, (京都大学基礎物理学研究所), 京都, 7 月 (2010).

飯田英明, 池田陽一: "格子 QCD によるベーテ・サルピータ波動関数に基づくクォーク間ポテンシャルの導出", 「少数粒子系物理の現状と今後の展望」研究会, (九州大学、大阪大学 RCNP、理化学研究所・仁科加速器研究センター), 福岡, 8 月 (2010).

橋本幸士, 飯塚則裕, Yi P.: "Nuclear matrix model", Summer Institute 2010: Cosmology and String, (京都大学基礎物理学研究所), 富士吉田, 8 月 (2010).

飯田英明, 前沢祐, 矢崎紘一: "Screening masses of mesons at finite temperature and density on lattice with two-flavor Wilson fermion", 京都大学基礎物理学研究所研究会「熱場の量子論とその応用」, (京都大学), 京都, 8 月 (2010).

飯田英明, 池田陽一: "Inter-quark potential based on Bethe-Salpeter amplitudes in lattice QCD", 日本物理学会 2010 年秋季大会, (日本物理学会), 北九州, 9 月 (2010).

衛藤稔: "non-Abelian Chern-Simons ボルテックスのゼロモードについて", 日本物理学会 2010 年秋季大会, (日本物理学会), 北九州, 9 月 (2010).

石井 貴昭: "Baryon with massive strangeness in holographic QCD", KEK 理論セミナー, (KEK 理論センター), つくば, 9 月 (2010).

石井貴昭: "Toward Bound-State Approach to Strangeness in Holographic QCD", 理研シンポジウム「場と弦の理論の新展開に向けて」, 和光, 12 月 (2010).

衛藤稔: "non-Abelian Chern-Simons ボルテックスのゼロモードについて", 立教大学理論物理コロキウム, (立教大学), 東京, 12 月 (2010).

衛藤稔: "Chiral magnetic effect from Q-balls and baryons", 京都大学理学部素粒子論研究室セミナー, (京都大学), 京都, 2 月 (2011).

衛藤稔: "Chiral magnetic effect from Q-balls", 大阪大学素粒子論研究室セミナー, (大阪大学), 吹田, 2 月 (2011).

石井貴昭: "Toward Bound-State Approach to Strangeness in Holographic QCD", 日本物理学会第 66 回年次大会, (日本物理学会), 新潟, 3 月 (2011).

飯田英明, 前沢祐, 矢崎紘一: "ウィルソンフェルミオンを用いた格子 QCD による有限温度・密度下のメソン遮蔽質量の研究", 日本物理学会第 66 回年次大会, (日本物理学会), 新潟, 3 月 (2011).

Radiation Laboratory

Publications

[Journal]

(Original Papers) ∗*Subject to Peer Review

Ohno M., Sato H., Ikeda T., and Shimizu H.: "Development of a low energy particle detector using a superconducting transition edge sensor", Nucl. Instrum. Methods Phys. Res. A **559**, No. 2, pp. 573–575 (2006). ∗

Rodrigues T. E., Arruda-Neto J., Mesa J., Garcia C., Shtejer K., Cole P., Dale D., and Nakagawa I.: "Nuclear photoproduction of pseudoscalar mesons at forward angles up to 6.0 GeV", AIP Conf. Proc. **947**, 101–108 (2007). ∗

Stratmann M., Schafer A., and Riedl J.: "Prospects of Open Charm Production at GSI-FAIR and J-PARC", Eur. Phys. J. C **52**, No. 4, pp. 987–997 (2007). ∗

Digal S.: "Can the 2-flavor chiral transition be of first order?", Int. J. Mod. Phys. A **22**, 2395–2403 (2007). ∗

Iwashita Y., Nakamura S., Yamada K., Ogata A., Wada Y., and Hirota K.: "Possibility of a small neutron source by laser-plasma interaction", Int. J. Mod. Phys. B **21**, No. 3/4, pp. 600–608 (2007). ∗

Onuki Y.: "Pixel detector of Silicon Vertex Tracker for PHENIX at RHIC", Int. J. Mod. Phys. E **16**, No. 7 and 8, pp. 2509–2515 (2007).

Fukushima K.: "Light projectile scattering off the Color Glass Condensate", J. High Energy Phys. **0706**, 1–17 (2007). ∗

Stratmann M. and Vogelsang W.: "Exploring the Polarization of Gluons in the Nucleon", J. Phys.: Con. Ser., pp. 012035-1–012035-10 (2007). ∗

Stratmann M., de Florian D., and Sassot R.: "Global Analysis of Fragmentation Functions for Protons nd Charged Hadrons", Phys. Rev. D **76**, 074033 (2007). ∗

Stratmann M., Hendlmeier C., and Schafer A.: "Next-to-Leading Order QCD Corrections to Spin-Dependent Hadron-Pair Photoproduction", Eur. Phys. J. C **55**, No. 4, pp. 597–605 (2008). ∗

Stratmann M., de Florian D., Sassot R., and Vogelsang W.: "Global Analysis of Helicity Parton Densities and their Uncertainties", Phys. Rev. Lett. **101**, 072001-1–072001-4 (2008). ∗

Blum T., Zhou R., Doi T., Hayakawa M., Izubuchi T., Uno S., and Yamada N.: "Electromagnetic mass splittings of the low lying hadrons and quark masses from 2+1 flavor lattice QCD+QED", Phys. Rev. D **82**, 094508-1–094508-47 (2010). ∗

[Book・ Proceedings]

(Original Papers) *Subject to Peer Review

Ju J., Mishima K., Yamagata Y., Sunaga H., Hirota K., Iwashita Y., Shimizu H., Kiyanagai Y., and Makinouchi A.: "A plan for neutron radiography facility using a compact accelerator at RIKEN", PSI-Proceedings 10-01, Grindelwald, Switzerland, 2010–3, Paul Sherrer Institut, Villigen, pp. IP140-1–IP140-5 (2010).

Morita S., Yamagata Y., Hirota K., Mihara S., Dung D., Sunaga H., Sera T., Yokota H., Shinohara T., Metoki N., and Makinouchi A.: "Neutron radiography for the structual simulation using VCAD system", PSI-Proceedings 10-01, Grindelwald, Switzerland, 2010–3, Paul Sherrer Institut, Villigen, pp. IP141-1–IP141-5 (2010).

Oral Presentations

(International Conference etc.)

Ju J., Mishima K., Yamagata Y., Sunaga H., Hirota K., Iwashita Y., Shimizu H., Kiyanagai Y., and Makinouchi A.: "A plan for neutron radiography facility using a compact accelerator at RIKEN", 19th Meeting of the International Collaboration on Advanced Neutron Sources (ICANS-XIX), (Paul Sherrer Institut), Grindelwald, Switzerland, Mar. (2009).

Morita S., Yamagata Y., Hirota K., Mihara S., Dung D., Sunaga H., Sera T., Yokota H., Shinohara T., Metoki N., and Makinouchi A.: "Neutron radiography for the structual simulation using VCAD system", 19th Meeting of the International Collaboration on Advanced Neutron Sources (ICANS-XIX), (Paul Sherrer Institut), Grindelwald, Switzerland, Mar. (2009).

Yokkaichi S.: "Vector meson in nuclear medium, experiments at KEK and J-PARC", New Frontier in QCD 2010: Exotic Hadron Systems and Dense Matter, (YITP), Kyoto, Feb. (2010).

Hirota K.: "Instrumentation and Device Development at RIKEN", 1st Meeting of The Union for Compact Accelerator-driven Neutron Sources (UCANS-I), Beijing, China, Aug. (2010).

Morita S., Yamagata Y., Hirota K., Mihara S., Dinh T., Sunaga H., Sera T., Yokota H., Shinohara T., Metoki N., and Makinouchi A.: "Thermal neutron radiography and structural simulation using VCAD system software", 1st Meeting of The Union for Compact Accelerator-driven Neutron Sources (UCANS-I), Beijing, China, Aug. (2010).

Yokkaichi S.: "Vector meson measurements through dielectron: planned experiment at J-PARC", Electromagnetic Probes of Strongly Interacting Matter: Status and Future of Low-Mass Lepton-Pair Spectroscopy, (ECT*), Trento, Italy, Sept. (2010).

(Domestic Conference)

四日市悟: "primary beam を用いた有限密度 QCD の研究", 研究会「ハドロンホールの拡張によって展開する物理」, (ハドロンホールユーザー会/KEK/理研仁科センター), つくば, 3 月 (2010).

広田克也, 山形豊, 横田秀夫, 世良俊博, 大竹淑恵, 森田晋也, 朱正明, 牧野内昭武: "JRR-3 MUSASI における工業製品の中性子ラジオグラフィ測定", 日本中性子科学会第 10 回年会, 仙台, 12 月 (2010).

山形豊, 広田克也, 森田晋也, 朱正明, 世良俊博, 横田秀夫,

大竹淑恵, 須長秀行, 牧野内昭武, 岩下芳久, 北口雅暁, 川端祐司: “KUR E-2 ポートにおける工業製品の中性子ラジオグラフィー測定”, 日本中性子科学会第 10 回年会, 仙台, 12 月 (2010).
朱正明, 王盛, 森田晋也, 広田克也, 山形豊, 須長秀行, 牧野内昭武, 岩下芳久, 三島賢二, 清水裕彦, 鬼柳善明: “小型加速器ベース中性子源とラジオフラフィーのシミュレーション”, 日本中性子科学会第 10 回年会, 仙台, 12 月 (2010).
大竹淑恵, 関義親, 広田克也, 安達智宏, 山形豊, 朱正明, 森田晋也, 岩下芳久, 市川雅浩, 北口雅暁, 日野正裕, 高橋敏男, 吉沢英樹, Lee S., 矢代航, 百生敦: “中性子微分位相コントラスト干渉イメージングの開発研究”, 日本中性子科学会第 10 回年会, 仙台, 12 月 (2010).

Advanced Meson Science Laboratory

Publications

[Journal]

(Original Papers) ＊*Subject to Peer Review

Suzuki T., Bhang H., Chiba J., Choi S., Fukuda Y., Hanaki T., Hayano R. S., Iio M., Ishikawa T., Ishimoto S., Ishiwatari T., Itahashi K., Iwai M., Iwasaki M., Kienle P., Kim J. H., Matsuda Y., Okada S., Onishi H., Outa H., Sato M., Suzuki S., Tomono D., Widmann E., Yamazaki T., and Yim H.: "Λd correlations from the ^{4}He(stopped-K^-,d) reaction", Phys. Rev. C **76**, No. 6, pp. 068202-1–068202-4 (2007). ＊

Bakule P., Matsuda Y., Miyake Y., Nagamine K., Iwasaki M., Ikedo Y., Simomura K., Strasser P., and Makimura S.: "Pulsed source of ultra low energy positive muons for near-surface μSR studies", Nucl. Instrum. Methods Phys. Res. B **266**, 335–346 (2008). ＊

Adachi T., Oki N., Risdiana ., Yairi S., Koike Y., and Watanabe I.: "Effects of Zn and Ni substitution on the Cu spin dynamics and superconductivity in $La_{2-x}Sr_xCu_{1-y}(Zn,Ni)_yO_4$ (x=0.15-0.20): Muon spin relaxation and magnetic susceptibility study", Phys. Rev. B **78**, No. 13, pp. 134515-1–134515-11 (2008). ＊

Iwasaki M. and Ishida K.: "Development of new muon source for muon g-2 measurement and muon magnetic microscope", J. Phys.: Con. Ser. **225**, 012005-1–012005-8 (2010). ＊

Kawamura S., Tamura M., Kato R., Hiraki K., Takahashi T., and Iwasaki M.: "Muon spin relaxation studies on magnetic properties of organic conductors $Pd(dmit)_2$ salts and α-$(BETS)_2l_3$", J. Phys.: Con. Ser. **225**, 012041-1–012041-5 (2010). ＊

Tomono D., Kawamata T., Hirayama Y., Iwasaki M., Watanabe I., Ishida K., and Matsuzaki T.: "Progress in development of new μSR spectrometer at RIKEN-RAL", J. Phys.: Con. Ser. **225**, 012056-1–012056-5 (2010). ＊

Yagi E., Mori K., Miyahara K., Fukagai S., Koike S., Sakuma K., Yoshii M., Hagiwara S., Okada Y., Matsuba H., Sugawara T., Shishido T., and Ogiwara K.: "Site occupancy of hydrogen in a distorted bcc lattice in niobium alloyed with Mo atoms", J. Phys. Soc. Jpn. **79**, No. 4, pp. 044602-1–044602-9 (2010). ＊

Yagi E., Higami N., Takebayashi A., Hayashi T., Murakami Y., Koike S., and Ogiwara K.: "Formation of hydrogen-associated vacancy clusters in Nb as investigated from site occupancy change of hydrogen", J. Phys. Soc. Jpn. **79**, No. 11, pp. 114601-1–114601-9 (2010). ＊

Ishii Y., Nagasawa M., Suzuki T., Watanabe I., Matsuzaki T., Yamamoto H., and Kato R.: "Zero field- and longitudinal field-μSR studies of quasi-one-dimensional organic conductor, $TMTTF_2PF_6$", Physica B **405**, No. 11, pp. S98–S100 (2010). ＊

Oral Presentations

(International Conference etc.)

Ishii Y., Watanabe I., Kato R., and Matsuzaki T.: "μSR studies on organic triangular antiferromagnets, $(cation)[Pd(dmit)_2]_2$", International Conference on Science and Technology of Synthetic Metals (ICSM 2010), Kyoto, July (2010).

Ishii Y., Watanabe I., Kobayashi Y., Nagatomo T., Ito M., Matsuo T., and Tamao K.: "μSR Study of Linear Two-Coordinate Fe Complexes with Bulky Arylthiol Ligands", International Chemical Congress of Pacific Basin Societies (PACIFICHEM 2010), (Pacifichem 2010 Organizing Committee), Honolulu, USA, Dec. (2010).

Kobayashi Y., Nagatomo T., Ito M., Matsuo T., Shoji Y., Watanabe I., Ishii Y., and Tamao K.: "Mössbauer Studies of Linear Two-Coordinate Fe Complexes with Bulky Arylthiol Ligands", International Chemical Congress of Pacific Basin Societies (PACIFICHEM 2010), (Pacifichem 2010 Organizing Committee), Honolulu, USA, Dec. (2010).

(Domestic Conference)

伊藤幹直, 橋爪大輔, 石井康之, 小林義男, 渡邊功雄, 松尾司, 玉尾皓平: "ヒドロインダセン骨格を用いたかさ高い単座配位子を有する直線型二配位鉄錯体の合成と性質", 第 60 回錯体化学討論会, (錯体化学会), 大阪, 9 月 (2009).

小池貴久, 原田融: "K^--核間有効ポテンシャルの虚部のエネルギー依存性", 日本物理学会 2010 年秋季大会, (日本物理学会), 北九州, 9 月 (2010).

大石一城, 石井康之, 渡邊功雄, 齊藤拓, 深澤英人, 小堀洋, 宮沢喜一, 木方邦宏, Lee C. H., 伊豫彰, 永崎洋: "μSR による鉄砒素系超伝導体 KFe_2As_2 の磁束状態の研究", 日本物理学会 2010 年秋季大会, (日本物理学会), 堺, 9 月 (2010).

山岡人志, Jarrige I., 池田篤史, 筒井智嗣, Lin J. F., 竹下直, 宮沢喜一, 伊豫彰, 鬼頭聖, 永崎洋, 平岡望, 石井啓文, Tsuei K. D.: "$CeFeAsO_{1-y}$ における価数揺動の圧力・温度依存性", 日本物理学会 2010 年秋季大会, (日本物理学会), 堺, 9 月 (2010).

池田時浩, 小島隆夫, Meissl W., 金井保之, 小林知洋, 岩井良夫, 前島一博, 宮本聡, 友野大, 石田勝彦, 松崎禎市郎, 岩崎雅彦, 今本尚子, 山崎泰規: "ガラスキャピラリーを用いた量子ビーム応用", 第 3 回異分野交流の夕べ, 和光, 10 月 (2010).

Loutchev O. A., Bakule P., 斎藤徳人, 和田智之, 横山幸司, 石田勝彦, 岩崎雅彦: "Numerical modeling of Lyman-alpha radiation generation by a high-intensity laser four-wave mixing in Kr-Ar gas", シンポジウム「レーザーの新世代応用とレーザーの医療応用」, 和光, 2 月 (2011).

斎藤徳人, Loutchev O. A., 和田智之, 横山幸司, 石田勝彦, 岩崎雅彦: "超低速ミュオン発生のためのライマン α 共鳴光源", シンポジウム「レーザーの新世代応用とレーザーの医療応用」, 和光, 2 月 (2011).

小池貴久, 原田融: "ヘリウム 3 標的の (飛行 K^-, N) 反応の断面積について", 日本物理学会第 66 回年次大会, (日本物理学会), 新潟, 3 月 (2011).

小島隆夫, 友野大, 池田時浩, 石田勝彦, 岩崎雅彦, 岩井良夫,

金澤悠, 松田恭幸, 松崎禎市郎, 徳田真, 山崎泰規: “キャピラリー法によるミュオンビームの集束効果（I）”, 日本物理学会第 66 回年次大会, (日本物理学会), 新潟, 3 月 (2011).
大石一城, 石井康之, 渡邊功雄, 齊藤拓, 深澤英人, 小堀洋, 木方邦宏, Lee C. H., Shirage P. M., 鬼頭聖, 伊豫彰, 永崎洋: “μSR による鉄砒素系超伝導体 $Ba_{1-x}K_xFe_2As_2$ ($x=0.6, 0.7$) の磁束状態の研究”, 日本物理学会第 66 回年次大会, (日本物理学会), 新潟, 3 月 (2011).
小林義男, 伊藤幹直, 松尾司, 石井康之, 渡邊功雄, 玉尾皓平: “直線二配位 Fe 錯体の巨大内部磁場”, 日本化学会第 91 春季年会 (2011), (日本化学会), 横浜, 3 月 (2011).

RIKEN BNL Research Center

Publications

[Journal]

(Original Papers)　*Subject to Peer Review

Albertus C., Aoki Y., Boyle P. A., Christ N. H., Dumitrescu T. T., Flynn J. M., Ishikawa T., Izubuchi T., Loktik O., Sachrajda C. T., Soni A., Wennekers J., Van de Water R., and Witzel O.: "Neutral B-meson mixing from unquenched lattice QCD with domain-wall light quarks and static b-quarks", Phys. Rev. D **82**, 014505-1–014505-29 (2010). *

Blum T., Zhou R., Doi T., Hayakawa M., Izubuchi T., Uno S., and Yamada N.: "Electromagnetic mass splittings of the low lying hadrons and quark masses from 2+1 flavor lattice QCD+QED", Phys. Rev. D **82**, 094508-1–094508-47 (2010). *

Christ N. H., Dawson C., Izubuchi T., Jung C., Li Q., Mawhinney R. D., Sachrajda C. T., Soni A., and Zhou R.: "The η and η' Meson from Lattice QCD", Phys. Rev. Lett. **105**, 241601-1–241601-4 (2010). *

(Review)

Samios N. P.: "Murray and The Omega Minus", Int. J. Mod. Phys. A **25**, No. 21, pp. 4005–4013 (2010).

Oral Presentations

(International Conference etc.)

Aoki Y.: "NEUTRAL B MESON MIXING WITH 2+1 FLAVOR DOMAIN- WALL LIGHT AND STATIC HEAVY QUARKS", 28th International Symposium on Lattice Field Theory (Lattice 2010), Villasimius, Italy, June (2010).

(Domestic Conference)

青木保道: "SM/BSM matrix elements: heavy mesons and nucleons", 次世代格子ゲージシミュレーション研究会, 和光, 9 月 (2010).

Theory Group

Publications

[Journal]

(Original Papers) *Subject to Peer Review

Kepka O., Marquet C., Peschanski R., and Royon C.: "Next-to-leading BFKL phenomenology of forward-jet cross sections at HERA", Eur. Phys. J. C **55**, 259–272 (2008). *

McLerran L. and Pisarski R. D.: "Baryons and the phase diagram for a large number of colors and flavors", Nucl. Phys. A **808**, 117–123 (2008). *

Yuan F.: "Single spin asymmetry in inclusive hadron production in pp scattering from Collins mechanism", Phys. Lett. B **666**, No. 1, pp. 44–47 (2008). *

Yuan F. and Zhou J.: "Single spin asymmetries in heavy quark and antiquark productions", Phys. Lett. B **668**, No. 3, pp. 216–220 (2008). *

Yuan F.: "Collins asymmetry at hadron colliders", Phys. Rev. D **77**, No. 7, pp. 074019-1–074019-12 (2008). *

Yuan F.: "Heavy-quarkonium production in single-transverse-polarized high-energy scattering", Phys. Rev. D **78**, No. 1, pp. 014024-1–014024-6 (2008). *

Petreczky P., Cheng M., Datta S., van der Heide J., Huebner K., Karsch F., Kaczmarek O., Edwin L., Laermann E., Liddle J., Mawhiney R. D., Miao C., Petrov K., Schnidt C., Soeldner W., and Umeda T.: "The Spatial String Tension and Dimensional Reduction in QCD", Phys. Rev. D **78**, No. 3, p. 034506 (2008). *

Yuan F., Zhou J., and Liang Z.: "Hyperon polarization in unpolarized scattering processes", Phys. Rev. D **78**, No. 11, pp. 114008-1–114008-6 (2008). *

Yuan F., Kang Z., Qiu J., and Vogelsang W.: "Accessing trigluon correlations in the nucleon via the single spin asymmetry in open charm production", Phys. Rev. D **78**, No. 11, pp. 114013-1–114013-9 (2008). *

Yuan F., Avakian H., Schweitzer P., and Efremov A.: "Transverse momentum dependent distribution function h1T[perpendicular] and the single spin asymmetry AUTsin(3 phi-3S)", Phys. Rev. D **78**, No. 11, p. 114024 (2008). *

Lunardini C.: "Diffuse neutrinos from failed supernovae", AIP Conf. Proc. **1182**, 32–35 (2009).

Fries R.: "Hadron Chemistry at High P_T with Identified Particles", AIP Conf. Proc. **1182**, 751–754 (2009).

Molnar D. and Huovinena P. C.: "Applicability of viscous hydrodynamics at RHIC", Nucl. Phys. A **830**, 475c–478c (2009). *

Fries R., Kunihiro T., Muller B., Ohnishi A., and Shafer A.: "From 0 to 5000 in 2×10^{-24} seconds: Entropy production in relativistic heavy-ion collisions", Nucl. Phys. A **830**, 519c–522c (2009). *

Fries R. and Liu W.: "High-P(T) Physics with Identified Particles.", Nucl. Phys. A **830**, 693c–696c (2009). *

Fries R.: "High Momentum Probes of Nuclear Matter", Proceedings of Science **High-pT physics09**, No. 041, pp. 1–7 (2009). *

Shintani E., Aoki S., Hashimoto S., Matsufuru H., Noaki J., Onogi T., and Yamada N.: "Strong coupling constant and four-quark ondensates from vacuum polarization functions ith dynamical overlap fermions", Proceedings of Science **LATTICE 2008**, No. 134, pp. 1–7 (2009).

Stasto A. M. and Avsar E.: "Non-linear evolution in CCFM: the interplay between coherence and saturation", J. High-Energy Phys. **06**, 112-0–112-37 (2010). *

Tuchin K. L.: "Synchrotron radiation by fast fermions in heavy-ion collisions", Phys. Rev. C **82**, 034904-1–034904-5 (2010). *

He M., Fries R., and Rapp R.: "Scaling of elliptic flow, recombination, and sequential freeze-out of hadrons in heavy-ion collisions", Phys. Rev. C **82**, 034907-1–034907-9 (2010). *

Aoki Y., Blum T., Lin H., Ohta S., Sasaki S., Tweedie R. J., Zanotti J. M., and Yamazaki T.: "Nucleon isovector structure functions in (2+1)-flavor QCD with domain wall fermions", Phys. Rev. D **82**, 014501-1–014501-14 (2010). *

Albertus C., Aoki Y., Boyle P. A., Christ N. H., Dumitrescu T. T., Flynn J. M., Ishikawa T., Izubuchi T., Loktik O., Sachrajda C. T., Soni A., Wennekers J., Van de Water R., and Witzel O.: "Neutral B-meson mixing from unquenched lattice QCD with domain-wall light quarks and static b-quarks", Phys. Rev. D **82**, 014505-1–014505-29 (2010). *

Lund T., Marek A., Lunardini C., Janka H., and Raffeit G.: "Fast time variations of supernova neutrino fluxes and their detectability", Phys. Rev. D **82**, 063007-1–063007-13 (2010). *

Kojo T., Pisarski R. D., and Tsvelik3 A. M.: "Covering the Fermi surface with patches of quarkyonic chiral spirals", Phys. Rev. D **82**, 074015-1–074015-8 (2010). *

Dumitru A. and Jalilian-Marian J.: "Forward dijets in high-energy collisions: Evolution of QCD n-point functions beyond the dipole approximation", Phys. Rev. D **82**, 074023-1–074023-7 (2010). *

Golec-Biernat K., Lewandowska E., and Stasto A. M.: "Drell-Yan process at forward rapidity at the LHC", Phys. Rev. D **82**, 094010-1–094010-11 (2010). *

Blum T., Zhou R., Doi T., Hayakawa M., Izubuchi T., Uno S., and Yamada N.: "Electromagnetic mass splittings of the low lying hadrons and quark masses from 2+1 flavor lattice QCD+QED", Phys. Rev. D **82**, 094508-1–094508-47 (2010). *

Boer D., Kang Z., Vogelsang W., and Yuan F.: "Test of the Universality of Naive-Time-Reversal-Odd Fragmentation Functions", Phys. Rev. Lett. **105**, No. 20, pp. 202001-1–202001-4 (2010). *

Christ N. H., Dawson C., Izubuchi T., Jung C., Li Q., Mawhinney R. D., Sachrajda C. T., Soni A., and Zhou R.: "The η and η' Meson from Lattice QCD", Phys. Rev. Lett. **105**, 241601-1–241601-4 (2010). ∗

Gubler P., Jido D., Kojo T., Nishikawa T., and Oka M.: "S=+1 pentaquarks in QCD sum rules", Proceedings of Science **CD09**, No. 022, pp. 1–8 (2010). ∗

Izubuchi T.: "Studies of the QCD and QED effects on isospin breaking", Proceedings of Science **KAON09**, No. 034, pp. 1–9 (2010). ∗

Lehner C., Hashimoto S., and Wettig T.: "Geometry dependence of RMT-based method to extract the low-energy constatns Sigma and F", Proceedings of Science **Lattice 2010**, No. 088, pp. 1–7 (2010).

McLerran L. and Praszalowicz M.: "Saturation and Scaling of Multiplicity Mean pT and pT Distributions from 200 GeV $\leq \sqrt{s} \leq$ 7 TeV Addendum", Acta Phys. Pol. B **42**, No. 1, pp. 99–103 (2011). ∗

Dumitru A., Dusling K., Gelis F., Jalilian-Marian J., Lappie T., and Venugopalan R.: "The ridge in proton-proton collisions at LHC", Phys. Lett. B **697**, 21–25 (2011). ∗

Tuchin K. L.: "Photon decay in a strong magnetic field in heavy-ion collisions", Phys. Rev. C **83**, 017901-1–017901-3 (2011). ∗

Dumitru A., Yun G., Hidaka Y., Korthals Altes C. P., and Pisarski R. D.: "How wide is the transition to deconfinement?", Phys. Rev. D **83**, 034022-1–034022-9 (2011). ∗

(Review)

Aoki Y.: "Non-perturbative renormalization in lattice QCD", Proceedings of Science **LAT2009**, No. 012, pp. 1–20 (2010).

Oral Presentations

(International Conference etc.)

Molnar D.: "Hydro paradigm and covariant transport", Workshop on Critical Examination f RHIC Paradigms, (University of Texas at Austin), Austin, USA, Apr. (2010).

Dumitru A.: "Initial Conditions and Global Event Properties", Saturation, the Color Glass Condensate and Glasma: What Have we Learned from RHIC?, Upton, USA, May (2010).

Dumitru A.: "Color Glass Condensate in heavy-ion collisions", INT 10-2A Summer Program "Quantifying the Properties of Hot QCD atter - Initial conditions, low x", (Institute for Nuclear Theory, University of Washington), Upton, USA, May–June (2010).

Izubuchi T.: "Isospin Breaking Study on Lattice", 28th International Symposium on Lattice Field Theory (Lattice 2010), Villasimius, Italy, June (2010).

Lehner C.: "Low-energy constants from Dirac eigenvalue correlators at NNLO in the epsilon expansion", 28th International Symposium on Lattice Field Theory (Lattice 2010), Villasimius, Italy, June (2010).

Ohta S.: "Nucleon structure from RBC/UKQCD 2+1 flavor DWF dynamical ensembles at a nearly physical pion mass", 28th International Symposium on Lattice Field Theory (Lattice 2010), Villasimius, Italy, June (2010).

Shintani E.: "Two-photon decay of π^0 from two-flavor QCD", 28th International Symposium on Lattice Field Theory (Lattice 2010), Villasimius, Italy, June (2010).

Molnar D.: "Overview of Hydro", Hot Quarks 2010, La Londe les Maures, French Riviera, June (2010).

Kojo T.: "Quarkyonic Chiral Spirals", Hot Quarks 2010, La Londe les Maures, French Riviera, June (2010).

Izubuchi T.: "Lattice QCD+QED simulation", CERN Theory Institute, Future directions in lattice gauge theory - LGT10, (Cern), Meyrin, Switzerland, July–Aug. (2010).

Dumitru A.: "Quarkonium in a non-ideal QCD Plasma", One-day School and Three+Half-day Symposium on High Energy Strong Interactions (HESI2010),, (Yukawa Institute for Theoretical Physics), Kyoto, Aug. (2010).

Ohta S.: "Nucleon structure from 2+1 flavor domain wall QCD at a nearly physical pion mass", T(r)opical QCD II Workshop, (CSSM, Australia), Cairns, Australia, Sept.–Oct. (2010).

Kang Z.: "Scale Evolution for the Correlations", INT-10-3: Gluons and the Quark Sea at High Energies: Distributions, Polarization, Tomography,, (Institute for Nuclear Theory, University of Washington), Seattle, USA, Sept.–Nov. (2010).

Kang Z.: "Overview of DIS results, global fittings and DY predictions", Santa Fe Polarized Drell-Yan Workshop, Santa Fe, USA, Oct.–Nov. (2010).

Kang Z.: "Recent progress in spin physics", 2010 Fall Meeting of the APS Division of Nuclear Physics, (American Physical Society), Santa Fe, USA, Nov. (2010).

Experimental Group

Publications

[Book・ Proceedings]

(Others)

Okuno H., Fukunishi N., Goto A., Hasebe H., Kamigaito O., Kase M., Kuboki H., Imao H., Yano Y., and Hershcovitch A.: "A New Possibility of Low-Z Gas Stripper for High Power Uranium Beam Acceleration Alternative to C Foil", Proceedings of HB2010 (46th ICFA Advanced Beam Dynamics Workshop on High-Intensity and High-Brightness Hadron Beams), Morschach, Switzerland, ICFA, , pp. 600–604 (2011).

Oral Presentations

(International Conference etc.)

Okuno H., Fukunishi N., Goto A., Hasebe H., Kamigaito O., Kase M., Kuboki H., Imao H., Yano Y., and Hershcovitch A.: "A New Possibility of Low-Z Gas Stripper for High Power Uranium Beam Acceleration Alternative to C Foil", 46th ICFA Advanced Beam Dynamics Workshop on High-Intensity and High-Brightness Hadron Beams, (Paul Scherrer Institut), Morschach, Switzerland, Sept.–Oct. (2010).

RIKEN Facility Office at RAL

Oral Presentations

(Domestic Conference)

池田時浩, 小島隆夫, Meissl W., 金井保之, 小林知洋, 岩井良夫, 前島一博, 宮本聡, 友野大, 石田勝彦, 松崎禎市郎, 岩崎雅彦, 今本尚子, 山崎泰規: “ガラスキャピラリーを用いた量子ビーム応用”, 第 3 回異分野交流の夕べ, 和光, 10 月 (2010).

Radioactive Isotope Physics Laboratory

Publications

[Journal]

(Original Papers) *Subject to Peer Review

Yamaguchi Y., Suzuki T., Wu C., Ozawa A., Fang D., Fukuda M., Iwasa N., Izumikawa T., Ohnishi T., Ohtsubo T., Tanihata I., and Kanungo R.: "Density distribution of 17B from a reaction cross section measurement", Phys. Rev. C **70**, No. 5, p. 054320 (2004). *

Ideguchi E., Niikura M., Fukuchi T., Baba H., Iwasaki H., Kubo T., Komatsubara T., Uesaka M., Michimasa S., Morimoto K., Ohnishi T., Ota S., Ozawa A., Shimoura S., Suda T., Tanihata I., Wakabayashi Y., and Yoshida K.: "Study of high-spin states in the 48Ca region by using secondary fusion reactions", Eur. Phys. J. A **25**, No. s01, pp. 429–430 (2005). *

Guo W., Fang D., Ma. Y., Ma. C., Wang K., Yang T., Cai X., Shen W., Sun Z., Ren Z., Chen J., Chen J., Liu G., Ma E., Ma G., Shi Y., Su Q., Tian W., Wang H., Zhong C., Zuo J., Hosoi M., Izumikawa T., Kanungo R., Nakajima S., Ohnishi T., Ohtsubo T., Ozawa A., Suda T., Sugawara K., Suzuki T., Takisawa A., Tanaka K., Yamaguchi T., and Tanihata I.: "Measurements of reaction cross section and fragment momentum distribution for N=10 proton-rich isotones", Int. J. Mod. Phys. E **15**, 1523–1530 (2006). *

Tsang M., Lynch W., Friedman W. A., Mocko M., Sun Z., Aoi N., Cook J. M., Delaunay F., Famiano M., Hui H., Imai N., Iwasaki H., Motobayashi T., Niikura M., Onishi T., Rogers A., Sakurai H., Suzuki H., Takeshita E., Takeuchi S., and Wallace M.: "Fragmentation cross sections and binding energies of neutron-rich nuclei", Phys. Rev. C **76**, 041302-1–041302-4 (2007). *

Matsuta K., Mihara M., Nagatomo T., Matsumiya R., Momota S., Ohtsubo T., Izumikawa T., Hirano H., Takahashi S., Nishimura D., Komurasaki J., Kitagawa A., Kanazawa M., Torikoshi M., Sato S., Fukuda M., Minamisono T., Sumikama T., Tanaka K., Takechi M., Ishikawa D., Pahlovy S. A., Nagano M., Nojiri Y., Alonso J. R., Krebs G. F., and Symons T. J.: "Hyperfine interaction of ^{25}Al in α-Al_2O_3 and its quadrupole moment", Hyperfine Interact. **180**, 65–69 (2008). *

Nagatomo T., Matsuta K., Minamisono K., Sumikama T., Mihara M., Ozawa A., Tagisi Y., Ogura M., Matsumiya R., Fukuda M., Yamaguchi M., Yasuno T., Ohta H., Hashizume Y., Fujiwara H., Chiba A., and Minamisono T.: "β-Ray angular distribution from purely nuclear spin aligned ^{20}F", Hyperfine Interact. **180**, 75–78 (2008). *

Scheit H., Gade A., Glasmacher T., and Motobayashi T.: "On the analysis of intermediate-energy Coulomb excitation experiments", Phys. Lett. B **659**, 515–519 (2008). *

Sumikama T., Matsuta K., Nagatomo T., Ogura M., Iwakoshi T., Nakashima Y., Fujiwara H., Fukuda M., Minamisono K., Yamaguchi T., and Minamisono T.: "Search for the G-parity irregular term in weak nucleon currents extracted from mirror beta decays in the mass 8 system", Phys. Lett. B **664**, 235–240 (2008). *

Minamisono K., Matsuta K., Minamisono T., Levy C. D., Nagatomo T., Ogura M., Sumikama T., Behr J. A., Jackson K. P., Mihara M., and Fukuda M.: "Quadrupole moments of neutron-deficient ^{20,21}Na", Phys. Lett. B **672**, 120–125 (2009). *

Kondo Y., Nakamura T., Sato Y., Matsumoto T., Aoi N., Endo N., Fukuda N., Gomi T., Hashimoto Y., Ishihara M., Kawai S., Kitayama M., Kobayashi T., Matsuda Y., Matsui N., Motobayashi T., Nakabayashi T., Ogata K., Okumura T., Ong H., Onishi T., Otsu H., Sakurai H., Shimoura S., Shinohara M., Sugimoto T., Takeuchi S., Tamaki M., Togano Y., and Yanagisawa Y.: "One-neutron removal reactions of ^{18}C and ^{19}C on a proton target", Phys. Rev. C **79**, No. 014602, pp. 014602-1–014602-7 (2009). *

Ichikawa Y., Onishi T. K., Suzuki D., Iwasaki H., Kubo T., Naik V., Chakrabarti A., Aoi N., Brown A. B., Fukuda N., Kubono S., Motobayashi T., Nakabayashi T., Nakamura T., Nakao T., Okumura T., Ong J. H., Suzuki H., Suzuki M. K., Teranishi T., Yamada K., Yamaguchi H., and Sakurai H.: "Gamow-Teller transition of the proton-rich nucleus ^{24}Si", AIP Conf. Proc. **1235**, 265–269 (2010).

Ichikawa Y., Onishi T. K., Suzuki D., Iwasaki H., Kubo T., Naik V., Chakrabarti A., Aoi N., Brown A. B., Fukuda N., Kubono S., Motobayashi T., Nakabayashi T., Nakamura T., Nakao T., Okumura T., Ong J. H., Suzuki H., Suzuki M. K., Teranishi T., Yamada K., Yamaguchi H., and Sakurai H.: "Mirror asymmetry for B(GT) of ^{24}Si induced by Thomas-Ehrman shift", AIP Conf. Proc. **1238**, 290–293 (2010).

Nishimura M., Ando Y., Kobayashi T., Matsuo Y., Suzuki H., Hayashizaki Y., and Kawai J.: "Sequencing of Isotope-Labeled Small RNA Using Femtosecond Laser Ablation Time-of-Flight Mass Spectrometry", Appl. Phys. Express **3**, 047002-1–047002-3 (2010). *

Motizuki Y., Nakai Y., Takahashi K., and Dome F glaciologic a.: "Supernovae and solar cycles embedded in a Dome F ice core", Highlights of Astronomy **15**, 630–631 (2010). *

Furukawa T., Matsuo Y., Hatakeyama A., Fujikake K., Matsuura Y., Kobayashi T., and Shimoda T.: "Laser spectroscopy on exotic RI atoms in superfluid helium - OROCHI experiment -", Hyperfine Interact. **196**, 191–197 (2010). *

Ichikawa Y., Onishi T. K., Suzuki D., Iwasaki H., Kubo T., Naik V., Chakrabarti A., Aoi N., Brown A. B., Fukuda N., Kubono S., Motobayashi T., Nakabayashi T., Nakamura T., Nakao T., Okumura T., Ong J. H., Suzuki H., Suzuki M. K., Teranishi T., Yamada K., Yamaguchi H., and Sakurai H.: “Mirror asymmetry investigated by β decay of proton-rich ^{24}Si”, Mod. Phys. Lett. A **25**, 1895–1898 (2010).

Steppenbeck D., Deacon A. N., Freeman S. J., Janssens R. V., Carpenter M. P., Hoffman C. R., Kay B. P., Lauritsen T., Lister C. J., O'Donnell D., Ollier J., Seweryniak D., Smith J. F., Spohr K. -., Tabor S. L., Tripathi V., Wady P. T., and Zhu S.: “Cross-shell excitations in ^{30}Al and ^{30}Si at high spin”, Nucl. Phys. A **847**, No. 3/4, pp. 149–167 (2010). ∗

Aoi N., Kanno S., Takeuchi S., Suzuki H., Bazin D. P., Bowen M. D., Campbell C. M., Cook J. M., Dinca D. -., Gade A., Glasmacher T., Iwasaki H., Kubo T., Kurita K., Motobayashi T., Mueller W. F., Nakamura T., Sakurai H., Takashina M., Terry J. R., Yoneda K., and Zwahlen H.: “Enhanced collectivity in 74Ni”, Phys. Lett. B **692**, 302–306 (2010). ∗

Oyamatsu K., Iida K., and Koura H.: “Neutron drip line and the equation of state of nuclear matter”, Phys. Rev. C **81**, 027301-1–027301-4 (2010). ∗

Deacon A. N., Smith J. F., Freeman S. J., Janssens R. V., Carpenter M. P., Hadinea B., Hoffman C. R., Kay B. P., Lauritsen T., Lister C. J., O'Donnell D., Ollier J., Otsuka T., Seweryniak D., Spohr K. -., Steppenbeck D., Tabor S. L., Tripathi V., Utsuno Y., Wady P. T., and Zhu S.: “Cross-shell excitations near the “island of inversion”: Structure of ^{30}Mg”, Phys. Rev. C **82**, No. 3, pp. 034305-1–034305-7 (2010). ∗

Taniguchi Y., Enyo Y., Kimura M., Ikeda K., Horiuchi H., and Ideguchi E.: “Triaxial superdeformation in ^{40}Ar”, Phys. Rev. C **82**, 011302-1–011302-5 (2010). ∗

Kobayashi T. and Matsuo Y.: “Study on the carbon fragment anions produced by femtosecond laser ablation of solid C_{60}”, J. Chem. Phys. **134**, No. 6, pp. 064320-1–064320-4 (2011). ∗

Oral Presentations

(International Conference etc.)

Matsuo Y.: “Advanced atomic photon spectroscopy”, 4th Yamada Symposium on Advanced Photons and Science Evolution (APSE 2010), Osaka, June (2010).

Sihver L., Lantz M. J., Takechi M., Kohama A., Ferrari A., Cerutti F., and Saito T.: “A comparison of total reaction cross section models used in particle and heavy ion transport codes”, 38th COSPAR scientific assembly (COSPAR 2010), (The Committee on Space Research), Bremen, Germany, July (2010).

Ichikawa Y., Onishi T. K., Suzuki D., Iwasaki H., Kubo T., Naik V., Chakrabarti A., Aoi N., Brown A. B., Fukuda N., Kubono S., Motobayashi T., Nakabayashi T., Nakamura T., Nakao T., Okumura T., Ong J. H., Suzuki H., Suzuki M. K., Teranishi T., Yamada K., Yamaguchi H., and Sakurai H.: “Proton-rich nuclear structure and mirror asymmetry investigated by β-decay spectroscopy of ^{24}Si”, International Nuclear Physics Conference (INPC2010), (TRIUMF at the University of British Columbia), Vancouver, Canada, July (2010).

Ichikawa Y., Ueno H., Ishii Y., Furukawa T., Yoshimi A., Kameda D., Aoi N., Watanabe H., Asahi K., Iijima H., Suzuki K., Inoue T., Tsuchiya M., Hayashi H., Nanao T., Kubo T., Inabe N., Ohnishi T., Takeda H., Fukuda N., Ishihara M., Daugas J., Chevrier R., Georgiev G., Rajabali M. M., and Balabanski D. L.: “g-factor measurement for isomeric state of ^{32}Al using two-step fragmentation reaction with dispersion matching”, GCOE International Summer School: Hadrons and Nuclei under Extreme Conditions (HANEC2010), (Tokyo Institute of Technology), Tokyo, Sept. (2010).

Nakajima T., Kobayashi T., and Matsuo Y.: “Polarizing nuclear-spin by a sequence of short laser pulses: Application to polarize muonium and ytterbium”, 19th International Spin Physics Symposium (SPIN 2010), (The International Spin Physics Committee), Julich, Germany, Sept.–Oct. (2010).

Matsuo Y.: “Precision laser spectroscopy of atoms in superfluid helium”, 11th Asia Pacific Physics Conference (APPC11), Shanghai, China, Nov. (2010).

(Domestic Conference)

須田慎太郎, 中野祐司, 目時健一, 高野靖史, 畠山温, 中井陽一, 東俊行, 小牧研一郎, 山崎泰規, 高田栄一, 村上健: “コヒーレント共鳴励起にともなう電子放出”, 原子衝突研究協会第34回年会, (原子衝突研究協会), 八王子, 8月 (2009).

中野祐司, 須田慎太郎, 目時健一, 高野靖史, 畠山温, 中井陽一, 東俊行, 小牧研一郎, 山崎泰規, 高田栄一, 村上健: “コヒーレント共鳴励起にともなう電子放出の観測２”, 日本物理学会 2009 年秋季大会, (日本物理学会), 熊本, 9月 (2009).

須田慎太郎, 中野祐司, 目時健一, 高野靖史, 畠山温, 中井陽一, 東俊行, 小牧研一郎, 山崎泰規, 高田栄一, 村上健: “コヒーレント共鳴励起にともなう電子放出の観測　”, 日本物理学会 2009 年秋季大会, (日本物理学会), 熊本, 9月 (2009).

小沢顕, 鈴木宏, 長江大輔, 新井一郎, 森口哲朗, 伊藤由太, 長谷部裕雄, 藤縄雅, 福西暢尚, 後藤彰, 大西哲哉, 櫻井博儀, 若杉昌徳, 山口由高, 矢野安重, 鈴木健, 山口貴之, 菊池崇志, 大坪隆, 安田裕介, 久保野茂: “RIBF における稀少 RI リング”, RIBF に於ける測定器についての検討会, 和光, 12月 (2009).

小沢顕, 新井一郎, 伊藤由太, 森口哲朗, 長江大輔, 鈴木宏, 藤縄雅, 福西暢尚, 後藤彰, 長谷部裕雄, 大西哲哉, 櫻井博儀, 若杉昌徳, 山口由高, 矢野安重, 鈴木健, 山口貴之, 菊池崇志, 大坪隆, 安田裕介, 久保野茂: “RIBF に於ける稀少 RI リング計画”, 蓄積リング検討ミニワークショップ, (大阪大学　核物理研究センター), 茨木, 1月 (2010).

酒向正己, 村上哲也, 市川裕大, 今城想平, 鮫島玲, 村田次郎, 家城和夫, 松下昌史, 中井陽一, 西村俊二, 高田栄一: “中間エネルギー重イオン衝突における荷電パイオン生成 (III)”, 日本物理学会第65回年次大会, 岡山, 3月 (2010).

須田慎太郎, 中野祐司, 目時健一, 進藤大輝, 大月聡子, 高野靖史, 畠山温, 中井陽一, 東俊行, 小牧研一郎, 山崎泰規, 高田栄一, 村上健: “コヒーレント共鳴励起にともなう電子放出の観測３”, 日本物理学会第65回年次大会, (日本物理

学会), 岡山, 3 月 (2010).

松浦佑一, 古川武, 小林徹, 畠山温, 加藤裕樹, 立川真樹, 松尾由賀利: “超流動ヘリウム中での光ポンピング法による Au 原子の偏極生成”, 第 6 回停止・低速不安定核ビームを用いた核分光研究会, 東京, 3 月 (2010).

望月優子: “雪氷コアからさぐる天文・宇宙のサイエンス〜過去の超新星の爆発から宇宙のリズムまで〜”, 理工学概論特別講義, (慶応義塾大学), 横浜, 4 月 (2010).

加藤裕樹, 古川武, 松浦佑一, 小林徹, 畠山温, 立川真樹, 松尾由賀利: “光ポンピングへ向けた超流動ヘリウム中での III 族原子 Ga, In 原子の励起スペクトル測定”, 第 7 回 AMO 討論会, つくば, 6 月 (2010).

磯部忠昭: “SAMURAI-TPC のチェンバーと読出しパッドのデザイン”, 原子核ハドロン実験のための検出器と大規模読み出しに関するワークショップ, (日本原子力研究開発機構), 茨城県東海村, 6 月 (2010).

小林徹, 松尾由賀利: “固相 C_{60} のレーザーアブレーションによる負イオン生成”, 第 26 回化学反応討論会, (第 26 回化学反応討論会事務局), 東広島, 6 月 (2010).

須田慎太郎, 中野祐司, 目時健一, 進藤大輝, 大月聡子, 高橋聡樹, 森本航, 東俊行, 高野靖史, 畠山温, 中井陽一, 小牧研一郎, 高田栄一, 村上健: “ゼロ度放出電子測定によるコヒーレント共鳴励起の観測”, 原子衝突研究協会第 35 回年会, (原子衝突研究協会), 奈良, 8 月 (2010).

加藤裕樹, 古川武, 松浦佑一, 小林徹, 畠山温, 立川真樹, 松尾由賀利: “超流動ヘリウム中での III 族原子 In, Ga の励起スペクトル”, 日本物理学会 2010 年秋季大会, 堺, 9 月 (2010).

酒向正己, 村上哲也, 市川裕大, 今城想平, 鮫島玲, 村田次郎, 家城和夫, 松下昌史, 中井陽一, 西村俊二, 高田栄一: “中間エネルギー重イオン衝突における荷電パイオン生成 (IV)”, 日本物理学会 2010 年秋季大会, (日本物理学会), 北九州, 9 月 (2010).

市川雄一, 上野秀樹, 石井裕司, 古川武, 吉見彰洋, 亀田大輔, 青井考, 渡邉寛, 旭耕一郎, 飯島裕章, 鈴木都文, 井上壮志, 土屋真人, 林宏憲, 七尾翼, 久保敏幸, 稲辺尚人, 大西哲哉, 竹田浩之, 福田直樹, 石原正泰, Daugas J., Chevrier R., Georgiev G., Rajabali M. M., Balabanski D. L.: “分散整合二回散乱法による核スピン整列ＲＩビームの生成”, 日本物理学会 2010 年秋季大会, (日本物理学会), 北九州, 9 月 (2010).

磯部忠昭: “パイ中間子をプローブとしたハロー原子核の研究”, 第 17 回 ICEPP シンポジウム, (東京大学素粒子物理国際研究センター), 長野県白馬村, 2 月 (2011).

須田慎太郎, 中野祐司, 目時健一, 進藤大輝, 大月聡子, 森本航, 高橋聡樹, 高野靖史, 畠山温, 中井陽一, 東俊行, 小牧研一郎, 高田栄一, 村上健: “コヒーレント共鳴励起にともなう電子放出の観測 IV”, 日本物理学会第 66 回年次大会, (社団法人日本物理学会), 新潟, 3 月 (2011).

Superheavy Element Laboratory

Publications

[Journal]

(Original Papers) *Subject to Peer Review

Yamaguchi Y., Suzuki T., Wu C., Ozawa A., Fang D., Fukuda M., Iwasa N., Izumikawa T., Ohnishi T., Ohtsubo T., Tanihata I., and Kanungo R.: "Density distribution of 17B from a reaction cross section measurement", Phys. Rev. C **70**, No. 5, p. 054320 (2004). *

Ideguchi E., Niikura M., Fukuchi T., Baba H., Iwasaki H., Kubo T., Komatsubara T., Uesaka M., Michimasa S., Morimoto K., Ohnishi T., Ota S., Ozawa A., Shimoura S., Suda T., Tanihata I., Wakabayashi Y., and Yoshida K.: "Study of high-spin states in the 48Ca region by using secondary fusion reactions", Eur. Phys. J. A **25**, No. s01, pp. 429–430 (2005). *

Mazzocco M., Signorini C., Romoli M., Botteti R., De Francesco A., De Rosa A., Di Pietro M., Fortunato L., Glodariu T., Guglielmetti A., Inglima G., Ishikawa T., Ishiyama H., Kanungo R., Khai N., La Commara M., Jeong S., Martin B., Miyatake H., Motobayashi T., Nomura T., Pierroutsakou D., Sandoli M., Soramel F., Stroe L., Sugai I., Tanaka M., Vardaci E., Watanabe Y., Yoshida K., and Yoshida A.: "Elastic scattering for the system ^{11}Be+^{209}Bi at Coulomb barrier energies", Eur. Phys. J. Special Topics **150**, 37–40 (2007).

Moller P., Ragnar B., Carlsson G., Olivius P., Ichikawa T., Sagawa H., and Iwamoto A.: "Axial and reflection asymmetry of the nuclear ground state", Atomic Data and Nuclear Data Tables **94**, 758–780 (2008). *

Ichikawa T., Iwamoto A., and Moller P.: "Origin of the narrow, single peak in the fission-fragment mass distribution for ^{258}Fm", Phys. Rev. C **79**, 014305-1–014305-6 (2009). *

Haba H., Kaji D., Kasamatsu Y., Kikunaga H., Komori Y., Kudou Y., Morimoto K., Morita K., Ooe K., Ohzeki K., Sato N., Shinohara A., Toyoshima A., Yokoyama A., Yoneda A., and Yoshimura T.: "Superheavy Element Nuclear Chemistry at RIKEN", AIP Conf. Proc. **1235**, 356–362 (2010).

Toyoshima A., Kasamatsu Y., Tsukada K., Asai M., Ishii Y., Toume H., Nishinaka I., Sato T., Nagame Y., Schaedel M., Haba H., Goto S., Kudo H., Akiyama K., Oura Y., Ooe K., Shinohara A., Sueki K., and Kratz J. V.: "Extraction chromatographic behavior of Rf, Zr, and Hf in HCl solution with styrene-divinylbenzene copolymer resin modified by TOPO (trioctylphosphine oxide)", J. Nucl. Radiochem. Sci. **11**, No. 1, pp. 7–11 (2010). *

Asai M., Tsukada K., Haba H., Ishii Y., Ichikawa T., Toyoshima A., Ishii T., Nagame Y., Nishinaka I., Kojima Y., and Sueki K.: "Neutron one-quasiparticle states in 251Fm151 populated via the a decay of 255No", Phys. Rev. C **83**, No. 1, pp. 014315-1–014315-12 (2011). *

(Others)

Li Z., Toyoshima A., Asai M., Tsukada K., Sato T., Sato N., Kikuchi T., Liang X., Kasamatsu Y., Nagame Y., Goto S., Haba H., Takeda Y., Ikarashi S., Murakami M., Nishikawa M., Komori Y., Ooe K., Akiyama K., and Sueki K.: "Cation-exchange behavior of rutherfordium, 104Rf in H2SO4/HNO3 mixed solution ([H+] = 1.0 M)", JAEA-Review **2010-056**, 65–66 (2010).

Toyoshima A., Tsukada K., Asai M., Sato T., Li Z., Sato N., Kikuchi T., Kitatsuji Y., Nagame Y., Ooe K., Kasamatsu Y., Shinohara A., Haba H., and Even J.: "Reduction of mendelevium using an electrochemistry apparatus", JAEA-Review **2010-056**, 67–68 (2010).

Oral Presentations

(International Conference etc.)

Tsukada K., Kasamatsu Y., Asai M., Toyoshima A., Ishii Y., Li Z., Sato T., Nagame Y., Schaedel M., Goto S., Hasegawa T., Kudo H., Haba H., Kudou Y., Kikunaga H., Ooe K., Fujisawa H., Sato W., Shinohara A., Oura Y., Akiyama K., Nanri T., Araki M., Yokoyama A., and Sueki K.: "Anion-exchange behavior of Db in HF and HNO3 mixed solution using an on-line chemical apparatus", International Chemical Congress of Pacific Basin Societies (PACIFICHEM 2010), (American Chemical Society), Honolulu, USA, Dec. (2010).

Li Z., Toyoshima A., Tsukada K., Asai M., Kasamatsu Y., Sato T., Sato N., Kikuchi T., Liang X., Nagame Y., Haba H., Goto S., Akiyama K., Nishinaka I., Takeda Y., Murakami M., Ikarashi S., and Sueki K.: "Cation-exchange behavior of rutherfordium, 104Rf, in H2SO4/HNO3 mixed solutions ([H+] = 1.0 M)", International Chemical Congress of Pacific Basin Societies (PACIFICHEM 2010), (American Chemical Society), Honolulu, USA, Dec. (2010).

Goto S., Murakami M., Murayama H., Kudo H., Kaji D., Morimoto K., Haba H., Kasamatsu Y., Kudou Y., and Morita K.: "Decay properties of 261Rf and 262Rf", International Chemical Congress of Pacific Basin Societies (PACIFICHEM 2010), (American Chemical Society), Honolulu, USA, Dec. (2010).

Kikunaga H., Yoshimura T., Ooe K., Takahashi N., Haba H., Ezaki Y., Mitsugashira T., and Shinohara A.: "Development of a liquid scintillation detector coupled with a capillary-electrophoresis apparatus for analysis of spent nuclear fuel", International Chemical Congress of Pacific Basin Societies (PACIFICHEM 2010), (American Chemical Society), Honolulu, USA, Dec. (2010).

Komori Y., Ooe K., Fujisawa H., Kuriyama A., Takayama R., kikutani Y., Kikunaga H., Kasamatsu Y., Yoshimura T., Takahashi N., Haba H., Kudou Y., and Shinohara A.: "Development of an on-line liquid scintillation alpha-particle detection system for aqueous chemical studies of superheavy elements", International Chemical Congress of Pacific Basin Societies (PACIFICHEM 2010), (American Chemical Society), Honolulu, USA, Dec. (2010).

Toyoshima A., Tsukada K., Asai M., Kitatsuji Y., Ishii Y., Sato T., Li Z., Sato N., Kikuchi T., Nishinaka I., Nagame Y., Kasamatsu Y., Haba H., Ooe K., Shinohara A., Sato W., Akiyama K., Even J., and Schaedel M.: "Electrochemistry of the heaviest elements", International Chemical Congress of Pacific Basin Societies (PACIFICHEM 2010), (American Chemical Society), Honolulu, USA, Dec. (2010).

Ooe K., Komori Y., Fujisawa H., Kuriyama A., Takayama R., kikutani Y., Kikunaga H., Kasamatsu Y., Yoshimura T., Takahashi N., Haba H., Kudou Y., Ezaki Y., and Shinohara A.: "Electrolytic oxidation of nobelium with a microchannel-electrode chip", International Chemical Congress of Pacific Basin Societies (PACIFICHEM 2010), (American Chemical Society), Honolulu, USA, Dec. (2010).

Kudou Y., Haba H., Kasamatsu Y., and Morita K.: "FIA-based continuous extraction system for superheavy element chemistry", International Chemical Congress of Pacific Basin Societies (PACIFICHEM 2010), (American Chemical Society), Honolulu, USA, Dec. (2010).

Haba H., Kaji D., Kasamatsu Y., Kikunaga H., Komori Y., Kudo H., Kudou Y., Morimoto K., Morita K., Nagame Y., Ooe K., Ohzeki K., Sato N., Shinohara A., Sumita T., Toyoshima A., Tsukada K., Yokoyama A., Yoneda A., and Yoshimura T.: "Superheavy Element Nuclear Chemistry at RIKEN", International Chemical Congress of Pacific Basin Societies (PACIFICHEM 2010), (American Chemical Society), Honolulu, USA, Dec. (2010).

(Domestic Conference)

福地知則, 本村信治, 武田伸一郎, 金山洋介, 羽場宏光, 渡辺恭良, 榎本秀一, 渡辺房雄, 荒井陽一: "デジタル信号処理による半導体コンプトンカメラ GREI の高度化", 第 5 回日本分子イメージング学会総会・学術集会, (日本分子イメージング学会), 大津, 5 月 (2010).

小森有希子, 大江一弘, 栗山亜依, 山玲央奈, 菊谷有希, 菊永英寿, 笠松良崇, 吉村崇, 高橋成人, 篠原厚: "超重元素の溶液化学のための液体シンチレーション検出器の作成と評価", 2010 日本放射化学会年会・第 54 回放射化学討論会, (日本放射化学会), 吹田, 9 月 (2010).

森本幸司, 加治大哉, 馬場秀忠, 門叶冬樹: "極短寿命な超重元素探索実験のための信号処理装置開発", 2010 日本放射化学会年会・第 54 回放射化学討論会, (日本放射化学会), 吹田, 9 月 (2010).

大江一弘, 小森有希子, 藤沢弘幸, 栗山亜依, 山玲央奈, 菊谷有希, 菊永英寿, 笠松良崇, 吉村崇, 高橋成人, 羽場宏光, 工藤祐生, 江崎豊, 篠原厚: "電極マイクロチップを用いたノーベリウムの電解酸化", 2010 日本放射化学会年会・第 54 回放射化学討論会, (日本放射化学会), 吹田, 9 月 (2010).

菊谷有希, 大江一弘, 小森有希子, 藤沢弘幸, 栗山亜依, 山玲央奈, 菊永英寿, 笠松良崇, 吉村崇, 高橋成人, 篠原厚: "natLu(p,xn)175Hf 反応の励起関数測定", 2010 日本放射化学会年会・第 54 回放射化学討論会, (日本放射化学会), 吹田, 9 月 (2010).

村上昌史, 村山裕史, 後藤真一, 加治大哉, 森本幸司, 羽場宏光, 笠松良崇, 工藤祐生, 米田晃, 森田浩介, 工藤久昭: "261a,bRf の合成と崩壊特性", 2010 日本放射化学会年会・第 54 回放射化学討論会, (日本放射化学会), 吹田, 9 月 (2010).

羽場宏光, 大江一弘, 大関和貴, 笠松良崇, 加治大哉, 菊永英寿, 工藤久昭, 工藤祐生, 小森有希子, 佐藤望, 篠原厚, 住田貴之, 塚田和明, 森田浩介, 森本幸司, 米田晃: "248Cm(22Ne,5n)265Sg 反応による 265Sg の合成", 2010 日本放射化学会年会・第 54 回放射化学討論会, (日本放射化学会), 吹田, 9 月 (2010).

栗山亜依, 大江一弘, 小森有希子, 藤沢弘幸, 山玲央奈, 菊谷有希, 菊永英寿, 中井浩二, 高橋成人, 吉村崇, 笠松良崇, 篠原厚: "52Fe と 62Zn の製造と PET 用ヘマトポルフィリン錯体の合成", 2010 日本放射化学会年会・第 54 回放射化学討論会, (日本放射化学会), 吹田, 9 月 (2010).

山玲央奈, 大江一弘, 小森有希子, 藤沢弘幸, 栗山亜依, 菊谷有希, 菊永英寿, 笠松良崇, 吉村崇, 高橋成人, 斎藤直, 豊嶋厚史, 浅井雅人, 三頭聰明, 篠原厚: "HDEHP を用いた三価重アクチニドの溶媒抽出", 2010 日本放射化学会年会・第 54 回放射化学討論会, (日本放射化学会), 吹田, 9 月 (2010).

武田勇樹, 荒木幹生, 横山明彦, 羽場宏光, 菊永英寿: "マイクロカラム法による Rf 化学種解明のための逆相抽出クロマトグラフィーの検討", 2010 日本放射化学会年会・第 54 回放射化学討論会, (日本放射化学会), 吹田, 9 月 (2010).

Li Z., 豊嶋厚史, 浅井雅人, 塚田和明, 佐藤哲也, 佐藤望, 菊池貴宏, Schaedel M., 永目諭一郎, Liang X., 笠松良崇, 小森有希子, 大江一弘, 篠原厚, 後藤真一, 村山裕史, 村上昌史, 工藤久昭, 羽場宏光, 武田勇樹, 西川恵, 横山明彦, 五十嵐訓, 末木啓介, 秋山和彦: "Sulfate complexation of element 104, Rf, in H2SO4/HNO3 mixed solution ([H+] = 1.0 M)", 2010 日本放射化学会年会・第 54 回放射化学討論会, (日本放射化学会), 吹田, 9 月 (2010).

菊永英寿, 吉村崇, 篠原厚: "使用済核燃料の分析に向けた液体シンチレーション検出器のオンライン化の試み", 2010 日本放射化学会年会・第 54 回放射化学討論会, (日本放射化学会), 吹田, 9 月 (2010).

金山洋介, 羽場宏光, 榎本秀一: "理研における医学・薬学研究ＲＩ製造", 2010 日本放射化学会年会・第 54 回放射化学討論会, (日本放射化学会), 吹田, 9 月 (2010).

福地知則, 本村信治, 武田伸一郎, 金山洋介, 羽場宏光, 渡辺恭良, 榎本秀一: "半導体検出器における多重相互作用信号の分解法", 日本物理学会 2010 年秋季大会, (日本物理学会), 北九州, 9 月 (2010).

廣村信, 金山洋介, 本村信治, 五十嵐香織, 羽場宏光, 榎本秀一: "糖尿病モデル動物で変化する生体微量金属元素の統合的解析", 日本薬学会第 131 年会, (日本薬学会), 静岡, 3 月 (2011).

High Energy Astrophysics Laboratory

Publications

[Journal]

(Original Papers) *Subject to Peer Review

Kawaharada M., Makishima K., Kitaguchi T., Okuyama S., Nakazawa K., and Fukazawa Y.: "Suzaku Constraints on Soft and Hard Excess Emissions from Abell 2199", Publ. Astron. Soc. Jpn. **62**, No. 1, pp. 115–129 (2010). ∗

Nakahira S., Yamaoka K., Sugizaki M., Ueda Y., Negoro H., Ebisawa K., Kawai N., Matsuoka M., Tsunemi H., Daikyuji A., Eguchi S., Hiroi K., Ishikawa M., Ishiwata R., Isobe N., Kaawasaki K., Kimura M., Kohama M., Mihara T., Miyoshi S., Morii M., Nakagawa Y., Nakajima M., Ozawa H., Sotome T., Sugimori K., Serino M., Tomida H., Ueno S., Yamamoto T., Yoshida A., and MAXI team ..: "MAXI GSC observations of a spectral state transition in the black hole candidate XTE J1752-223", Publ. Astron. Soc. Jpn. **62**, L27–L32 (2010). ∗

Isobe N., Sugimori K., Kawai N., Ueda Y., Negoro H., Sugizaki M., Matsuoka M., Daikyuji A., Eguchi S., Hiroi K., Ishikawa M., Ishiwata R., Kaawasaki K., Kimura M., Kohama M., Mihara T., Miyoshi S., Morii M., Nakagawa Y., Nakahira S., Nakajima M., Ozawa H., Sotome T., Serino M., Tomida H., Tsunemi H., Ueno S., Yamamoto T., Yamaoka K., Yoshida A., and MAXI team ..: "Bright X-ray flares from the BL Lac object Markarian 421, detected with MAXI in 2010 January and February", Publ. Astron. Soc. Jpn. **62**, L55–L60 (2010). ∗

(Others)

Ueno S., Matsuoka M., Kaawasaki K., Tomida H., Serino M., Ishikawa M., Adachi Y., Itamoto Y., Mihara T., Kohama M., Sugizaki M., Nakagawa Y., Yamamoto T., Tsunemi H., Kimura M., Kawai N., Morii M., Sugimori K., Yoshida A., Yamaoka K., Nakahira S., Negoro H., Ishiwata R., Miyoshi S., Ozawa H., Nakajima M., Ueda Y., Isobe N., Eguchi S., Hiroi K., Katayama H., and Ebisawa K.: "The first light from MAXI", Proceedings of Science **extremesky2009**, 1–8 (2009).

Matsuoka M., Serino M., Kaawasaki K., Ueno S., Tomida H., Adachi Y., Ishikawa M., Itamoto Y., Takahashi D., Katayama H., Ebisawa K., Mihara T., Kohama M., Sugizaki M., Nakagawa Y., Yamamoto T., Tsunemi H., Kimura M., Kawai N., Morii M., Sugimori K., Yoshida A., Yamaoka K., Nakahira S., Takahashi I., Negoro H., Nakajima M., Ishiwata R., Miyoshi S., Ozawa H., Ueda Y., Isobe N., Eguchi S., Hiroi K., Yamauchi M., and Daikyuji A.: "The first light from MAXI on board JEM (Kibo)-EF on ISS", AIP Conf. Proc. **1248**, 531–536 (2010).

Matsuoka M., Mihara T., Sugizaki M., Serino M., Nakagawa Y., Yamamoto T., Sotome T., Kaawasaki K., Ueno S., Tomida H., Kohama M., Ishikawa M., Adachi Y., Itamoto Y., Kobayashi Y., Katayama H., Kawai N., Morii M., Sugimori K., Tsunemi H., Kimura M., Yoshida A., Yamaoka K., Nakahira S., Negoro H., Ozawa H., Suwa F., Nakajima M., Ueda Y., Isobe N., Eguchi S., Hiroi K., Ebisawa K., Daikyuji A., Yamauchi M., Uzawa A., Matsumura T., Yamazaki K., and Tsuboi Y.: "Early results of MAXI (Monitor of ALL-sky X-ray Image) on ISS", Proc. SPIE-Int. Soc. Opt. Eng. **7732**, 77320Y-1–77320Y-9 (2010).

Oral Presentations

(Domestic Conference)

芹野素子, 松岡勝, 三原建弘, 杉崎睦, 中川友進, 山本堂之, 五月女哲哉, 吉田篤正, 中平聡志, 山岡和貴, 小谷太郎, 冨田洋, 上野史郎, 小濱光洋, 根來均, 中島基樹, 小澤洋志, 諏訪文俊, 河合誠之, 森井幹雄, 杉森航介, 薄井竜一, 常深博, 木村公, 上田佳宏, 磯部直樹, 江口智士, 廣井和雄, 山内誠, 大休寺新, 坪井陽子, 鵜澤明子, 山崎恭平, 松村和典, 石川真木: "全天 X 線監視装置 MAXI による 1 年間のガンマ線バーストの観測と解析", 日本天文学会 2010 年秋季年会, (社団法人 日本天文学会), 金沢, 9 月 (2010).

三原建弘, 松岡勝, 杉崎睦, 芹野素子, 山本堂之, 中川友進, 冨田洋, 上野史郎, 小濱光洋, 河合誠之, 森井幹夫, 吉田篤正, 山岡和貴, 中平聡志, 根来均, 中島基樹, 上田佳宏, 磯部直樹, 常深博, 山内誠: "全天 X 線監視装置 MAXI：運用開始 1 年 7ヶ月の現状", 日本物理学会第 66 回年次大会, (日本物理学会), 新潟, 3 月 (2011).

Accelerator Group

Publications

[Journal]

(Others)

Okuno H., Dantsuka T., Yamada K., Kase M., Maie T., and Kamigaito O.: "Superconducting Ring Cyclotron for RIKEN RI Beam Factory in Japan", AIP Conf. Proc. **1218**, 1410–1417 (2010).

[Book・ Proceedings]

(Original Papers) *Subject to Peer Review

Kamigaito O., Arai S., Fujimaki M., Fujinawa T., Fujisawa H., Fukunishi N., Goto A., Higurashi Y., Ikezawa E., Kageyama T., Kase M., Komiyama M., Kuboki H., Kumagai K., Maie T., Nagase M., Nakagawa T., Ohnishi J., Okuno H., Sakamoto N., Sato Y., Suda K., Watanabe H., Watanabe T., Watanabe Y., Yamada K., Yamasawa H., Yano Y., and Yokouchi S.: "Intensity-upgrade plans of RIKEN RI-Beam Factory", Proceedings of 11th International Conference on Heavy Ion Accelerator Technology (HIAT09), Venezia, Italy, 2009–6, HIAT09 International Organizing Committee, Venice, pp. 21–25 (2009).

Kamigaito O.: "World-wide efforts on rare isotope and radioactive ion beams", Proceedings of IPAC'10, Kyoto, 2010–5, IPAC'10 Organizing Committee, Kyoto, pp. 16–20 (2010).

Kamigaito O., Ikezawa E., Kase M., Fujimaki M., Fujinawa T., Fukunishi N., Goto A., Haba H., Higurashi Y., Kidera M., Komiyama M., Koyama R., Kuboki H., Kumagai K., Maie T., Nagase M., Nakagawa T., Ohnishi J., Okuno H., Sakamoto N., Sato Y., Suda K., Watanabe T., Yamada K., Yokouchi S., and Yano Y.: "Present status of RIKEN heavy-ion linac", Proceedings of LINAC 08, Canada, Victoria, 2008–9〜10, TRIUMF, Vancouver, pp. 112–114 (2010).

上垣外修一, 藤巻正樹, 藤縄雅, 福西暢尚, 後藤彰, 長谷部裕雄, 日暮祥英, 池上九三男, 池沢英二, 影山正, 加瀬昌之, 木寺正憲, 込山美咲, 久保木浩功, 熊谷桂子, 眞家武士, 長瀬誠, 中川孝秀, 大西純一, 奥野広樹, 龍頭啓充, 坂本成彦, 佐藤洋一, 須田健嗣, 若杉昌徳, 渡辺博, 渡邉環, 山田一成, 横内茂, 矢野安重: "理研 RI ビームファクトリーの現状", 第 5 回日本加速器学会年会・第 33 回リニアック技術研究会論文集, 東広島, 2008–8, 日本加速器学会, 東広島, pp. 10–12 (2008).

池沢英二, 加瀬昌之, 渡邉裕, 大木智則, 藍原利光, 山内啓資, 内山暁仁, 小山田和幸, 田村匡史: "理研重イオンリニアックの現状報告", 第 6 回日本加速器学会年会プロシーディングス, 茨城県東海村, 2009–8, 日本加速器学会, 東京, pp. 622–624 (2010).

(Others)

Suda K., Arai S., Chiba Y., Kamigaito O., Kase M., Sakamoto N., and Yamada K.: "Drift Tube Linac Cavities with Space-Saving Amplifier Coupling of New Injector for RI-Beam Factory", Proceedings of of the 1st International Particle Accelerator Conference (IPAC'10), Kyoto, 2010–5, The IPAC'10 Organizing Committee and Asian Committee for Future Accelerators, Kyoto, pp. 3726–3728 (2010).

Okuno H., Fukunishi N., Goto A., Hasebe H., Kamigaito O., Kase M., Kuboki H., Imao H., Yano Y., and Hershcovitch A.: "A New Possibility of Low-Z Gas Stripper for High Power Uranium Beam Acceleration Alternative to C Foil", Proceedings of HB2010 (46th ICFA Advanced Beam Dynamics Workshop on High-Intensity and High-Brightness Hadron Beams), Morschach, Switzerland, ICFA, , pp. 600–604 (2011).

須田健嗣, 藤巻正樹, 福西暢尚, 逸見政武, 上垣外修一, 加瀬昌之, 小山亮, 熊谷桂子, 坂本成彦, 渡邉環, 山田一成: "理研 RIBF における高周波系およびビームの安定度", 第 6 回日本加速器学会要旨集, 茨城県東海村, 2009–8, 日本加速器学会, 東京, pp. 397–400 (2009).

上垣外修一, 新井重昭, 藤巻正樹, 藤縄雅, 藤澤博, 福西暢尚, 後藤彰, 日暮祥英, 池沢英二, 影山正, 加瀬昌之, 込山美咲, 久保木浩功, 熊谷桂子, 眞家武士, 長瀬誠, 中川孝秀, 大西純一, 奥野広樹, 坂本成彦, 佐藤洋一, 須田健嗣, 渡辺博, 渡邉環, 渡邉裕, 山田一成, 山澤秀行, 矢野安重, 横内茂: "Intensity-upgrade plans of RIKEN RI-Beam Factory", 第 6 回日本加速器学会年会プロシーディングス, 東海村, 2009–8, 日本加速器学会, 東海村, pp. 38–41 (2010).

Oral Presentations

(International Conference etc.)

Kamigaito O., Ikezawa E., Kase M., Fujimaki M., Fujinawa T., Fukunishi N., Goto A., Haba H., Higurashi Y., Kidera M., Komiyama M., Koyama R., Kuboki H., Kumagai K., Maie T., Nagase M., Nakagawa T., Ohnishi J., Okuno H., Sakamoto N., Sato Y., Suda K., Watanabe T., Yamada K., Yokouchi S., and Yano Y.: "Present status of RIKEN heavy-ion linac", 24th International Linear Accelerator Conference (LINAC08), (LINAC08 Organizing Committee), Victoria, Canada, Sept.–Oct. (2008).

Kamigaito O., Arai S., Fujimaki M., Fujinawa T., Fujisawa H., Fukunishi N., Goto A., Higurashi Y., Ikezawa E., Kageyama T., Kase M., Komiyama M., Kuboki H., Kumagai K., Maie T., Nagase M., Nakagawa T., Ohnishi J., Okuno H., Sakamoto N., Sato Y., Suda K., Watanabe H., Watanabe T., Watanabe Y., Yamada K., Yamasawa H., Yano Y., and Yokouchi S.: "Intensity-upgrade plans of RIKEN RI-Beam Factory", 11th International Conference on Heavy Ion Accelerator Technology (HIAT09), (HIAT09 International Organizing Committee), Venezia, Italy, June (2009).

Okuno H., Dantsuka T., Yamada K., Kase M., Maie T., and Kamigaito O.: "Superconducting Ring Cyclotron for RIKEN RI Beam Factory in Japan", Cryogenic Engineering Conference and the International Cryogenic Materials Conference (CEC/ICMC 2009), Tucson, USA, June–July (2009).

Suda K., Arai S., Chiba Y., Kamigaito O., Kase M., Sakamoto N., and Yamada K.: "Drift Tube Linac Cavities with Space-Saving Amplifier Coupling of New Injector for RIKEN RI-Beam Factory", 1st International Particle Accelerator Conference (IPAC'10), (Science Council of Japan, The Physical Society of Japan, Particle Accelerator Society of Japan, and Ato), Kyoto, May (2010).

Kamigaito O.: "World-wide efforts on rare isotope and radioactive ion beams", 1st International Particle Accelerator Conference (IPAC'10), (IPAC'10 Organizing Committee), Kyoto, May (2010).

Watanabe T., Fukunishi N., Sasaki Y., Kase M., Goto A., and Kamigaito O.: "Development of beam current monitor with high Tc SQUID at RIBF", 2010 Beam Instrumentation Workshop (BIW10), (Los Alamos National Laboratory), Santa Fe, USA, May (2010).

Watanabe T., Fujimaki M., Fukunishi N., Kase M., Komiyama M., Sakamoto N., Watanabe H., Yamada K., Kamigaito O., and Koyama R.: "Beam dignostics for RIBF in RIKEN", 19th International Conference on Cyclotrons and their Applications (CYCLOTRONS 2010), (Institue of Modern Physics , Lanzhou, China), Lanzhou, China, Sept. (2010).

Vorozhtsov S., Smirnov V. L., and Goto A.: "Modification of the center region in the RIKEN AVF cyclotron for acceleration at the h=1 RF harmonics", 19th International Conference on Cyclotrons and their Applications (CYCLOTRONS 2010), Lanzhou, China, Sept. (2010).

Goto A.: "Review of high-power cyclotrons for heavy ion beams", 19th International Conference on Cyclotrons and their Applications (CYCLOTRONS 2010), Lanzhou, China, Sept. (2010).

Suda K., Fujimaki M., Fukunishi N., Hemmi M., Kamigaito O., Kase M., Koyama R., Kumagai K., Sakamoto N., and Yamada K.: "Stable Operation of RF Systems for RIBF", 19th International Conference on Cyclotrons and their Applications (CYCLOTRONS 2010), (Institute of Modern Physics, Chinese Academy of Sciences), Lanzhou, China, Sept. (2010).

Kamigaito O., Arai S., Dantsuka T., Fujimaki M., Fujinawa T., Fujisawa H., Fukunishi N., Goto A., Hasebe H., Higurashi Y., Ikegami K., Ikezawa E., Imao H., Kageyama T., Kase M., Kidera M., Komiyama M., Kuboki H., Kumagai K., Maie T., Nagase M., Nakagawa T., Nakamura M., Ohnishi J., Okuno H., Sakamoto N., Suda K., Watanabe H., Watanabe Y., Watanabe T., Yamada K., Yamasawa H., Yokouchi S., and Yano Y.: "Status of RIBF accelerators at RIKEN", 19th International Conference on Cyclotrons and their Applications (CYCLOTRONS 2010), (Cyclotrons2010 International Organizing Committee), Lanzhou, China, Sept. (2010).

Okuno H., Fukunishi N., Goto A., Hasebe H., Kamigaito O., Kase M., Kuboki H., Imao H., Yano Y., and Hershcovitch A.: "A New Possibility of Low-Z Gas Stripper for High Power Uranium Beam Acceleration Alternative to C Foil", 46th ICFA Advanced Beam Dynamics Workshop on High-Intensity and High-Brightness Hadron Beams, (Paul Scherrer Institut), Morschach, Switzerland, Sept.–Oct. (2010).

(Domestic Conference)

上垣外修一, 藤巻正樹, 藤縄雅, 福西暢尚, 後藤彰, 長谷部裕雄, 日暮祥英, 池上九三男, 池沢英二, 影山正, 加瀬昌之, 木寺正憲, 込山美咲, 久保木浩功, 熊谷桂子, 眞家武士, 長瀬誠, 中川孝秀, 大西純一, 奥野広樹, 龍頭啓充, 坂本成彦, 佐藤洋一, 須田健嗣, 若杉昌徳, 渡辺博, 渡邉環, 山田一成, 横内茂, 矢野安重: "理研 RI ビームファクトリーの現状", 第 5 回日本加速器学会年会/第 33 回リニアック技術研究会, (日本加速器学会), 東広島, 8 月 (2008).

上垣外修一, 新井重昭, 藤巻正樹, 藤縄雅, 藤澤博, 福西暢尚, 後藤彰, 日暮祥英, 池沢英二, 影山正, 加瀬昌之, 込山美咲, 久保木浩功, 熊谷桂子, 眞家武士, 長瀬誠, 中川孝秀, 大西純一, 奥野広樹, 坂本成彦, 佐藤洋一, 須田健嗣, 渡辺博, 渡邉環, 渡邉裕, 山田一成, 山澤秀行, 矢野安重, 横内茂: "理研 RIBF のビーム増強計画", 第 6 回日本加速器学会年会, (日本加速器学会), 茨城県東海村, 8 月 (2009).

小沢顕, 鈴木宏, 長江大輔, 新井一郎, 森口哲朗, 伊藤由太, 長谷部裕雄, 藤縄雅, 福西暢尚, 後藤彰, 大西哲哉, 櫻井博儀, 若杉昌徳, 山口由高, 矢野安重, 鈴木健, 山口貴之, 菊池崇志, 大坪隆, 安田裕介, 久保野茂: "RIBF における稀少 RI リング", RIBF に於ける測定器についての検討会, 和光, 12 月 (2009).

小沢顕, 新井一郎, 伊藤由太, 森口哲朗, 長江大輔, 鈴木宏, 藤縄雅, 福西暢尚, 後藤彰, 長谷部裕雄, 大西哲哉, 櫻井博儀, 若杉昌徳, 山口由高, 矢野安重, 鈴木健, 山口貴之, 菊池崇志, 大坪隆, 安田裕介, 久保野茂: "RIBF に於ける稀少 RI リング計画", 蓄積リング検討ミニワークショップ, (大阪大学　核物理研究センター), 茨木, 1 月 (2010).

寺岡毅, 澤野郁夫, 中嶌輝子, 加々美裕, 神尾章子, 浜部直哉, 林依子, 龍頭啓充, 福西暢尚, 阿部知子: "重イオンビーム照射によるウンシュウミカンの形態変異の誘発", 第 7 回イオンビーム育種研究会大会, (イオン育種研究会), 鳥栖, 5–6 月 (2010).

渡邉裕, 池沢英二, 今尾浩士, 大西純一, 奥野広樹, 加瀬昌之, 上垣外修一, 熊谷桂子, 後藤彰, 込山美咲, 坂本成彦, 須田健嗣, 中川孝秀, 日暮祥英, 福西暢尚, 藤縄雅, 藤巻正樹, 眞家武士, 山田一成, 山澤秀行, 横内茂, 渡邉環, 渡辺博, 新井重昭, 佐藤洋一: "理研リニアック新入射器システム (RILAC2) の建設状況", 第 7 回日本加速器学会年会, (日本加速器学会), 姫路, 8 月 (2010).

渡邉環, 福西暢尚, 加瀬昌之, 若杉昌徳, 藤巻正樹, 山田一成, 坂本成彦, 小高康照, 小山亮, 仲村武志, 上垣外修一: "RIBF におけるビームエネルギーと縦方向のビームプロファイル測定システムの改良", 第 7 回日本加速器学会年会, (日本加速器学会), 姫路, 8 月 (2010).

池沢英二, 上垣外修一, 加瀬昌之, 渡邉裕, 大木智則, 藍原利光, 山内啓資, 内山暁仁, 小山田和幸, 田村匡史: "理研重イオンリニアックの現状報告", 第 7 回日本加速器学会年会, (日本加速器学会), 姫路, 8 月 (2010).

山田一成, 池沢英二, 今尾浩士, 大西純一, 奥野広樹, 加瀬昌之, 熊谷桂子, 込山美咲, 後藤彰, 坂本成彦, 須田健嗣, 中川孝秀, 日暮祥英, 福西暢尚, 藤縄雅, 藤巻正樹, 眞家武士, 山澤秀行,

横内茂, 渡邉環, 渡辺博, 渡邉裕, 新井重昭, 藤澤博, 佐藤洋一, 上垣外修一: “理研 RIBF 用の新しい重イオン入射ライナック RILAC2 の製作”, 第 7 回日本加速器学会年会, (日本加速器学会), 姫路, 8 月 (2010).

鈴木宏, 新井一郎, 藤縄雅, 福西暢尚, 後藤彰, 菊池崇志, 久保野茂, 森口哲朗, 長江大輔, 大坪隆, 小沢顕, 櫻井博儀, 鈴木健, 若杉昌徳, 安田裕介, 山口貴之, 山口由高, 矢野安重: “理研稀少 RI リングの粒子軌道計算”, 日本物理学会 2010 年秋季大会, (日本物理学会), 北九州, 9 月 (2010).

後藤彰: “サイクロトロンにおける空間電荷力による”round beam”生成のメカニズムについて”, ビーム物理研究会 2010, (仁科加速器研究センター), 和光, 11 月 (2010).

Accelerator R&D Team

Publications

[Journal]

(Original Papers) *Subject to Peer Review

Tominaka T.: "Current and field distributions of a superconducting power transmission cable composed of helical tape conductors", Supercond. Sci. Technol. **22**, 125025-1–125025-10 (2009). ∗

Yagi E., Mori K., Miyahara K., Fukagai S., Koike S., Sakuma K., Yoshii M., Hagiwara S., Okada Y., Matsuba H., Sugawara T., Shishido T., and Ogiwara K.: "Site occupancy of hydrogen in a distorted bcc lattice in niobium alloyed with Mo atoms", J. Phys. Soc. Jpn. **79**, No. 4, pp. 044602-1–044602-9 (2010). ∗

Yagi E., Higami N., Takebayashi A., Hayashi T., Murakami Y., Koike S., and Ogiwara K.: "Formation of hydrogen-associated vacancy clusters in Nb as investigated from site occupancy change of hydrogen", J. Phys. Soc. Jpn. **79**, No. 11, pp. 114601-1–114601-9 (2010). ∗

Enomoto Y., Kuroda N., Michishio K., Kim C., Higaki H., Nagata Y., Kanai Y., Torii H., Corradini M., Leali M., Lodi-Rizzini E., Mascagna V., Venturelli L., Zurlo N., Fujii K., Ohtsuka M., Tanaka K., Imao H., Nagashima Y., Matsuda Y., Juha'sz B., Mohri A., and Yamazaki Y.: "Synthesis of Cold Antihydrogen in a Cusp Trap", Phys. Rev. Lett. **105**, No. 24, pp. 243401-1–243401-4 (2010). ∗

(Others)

Okuno H., Dantsuka T., Yamada K., Kase M., Maie T., and Kamigaito O.: "Superconducting Ring Cyclotron for RIKEN RI Beam Factory in Japan", AIP Conf. Proc. **1218**, 1410–1417 (2010).

[Book・Proceedings]

(Original Papers) *Subject to Peer Review

Kamigaito O., Arai S., Fujimaki M., Fujinawa T., Fujisawa H., Fukunishi N., Goto A., Higurashi Y., Ikezawa E., Kageyama T., Kase M., Komiyama M., Kuboki H., Kumagai K., Maie T., Nagase M., Nakagawa T., Ohnishi J., Okuno H., Sakamoto N., Sato Y., Suda K., Watanabe H., Watanabe T., Watanabe Y., Yamada K., Yamasawa H., Yano Y., and Yokouchi S.: "Intensity-upgrade plans of RIKEN RI-Beam Factory", Proceedings of 11th International Conference on Heavy Ion Accelerator Technology (HIAT09), Venezia, Italy, 2009–6, HIAT09 International Organizing Committee, Venice, pp. 21–25 (2009).

Kamigaito O., Ikezawa E., Kase M., Fujimaki M., Fujinawa T., Fukunishi N., Goto A., Haba H., Higurashi Y., Kidera M., Komiyama M., Koyama R., Kuboki H., Kumagai K., Maie T., Nagase M., Nakagawa T., Ohnishi J., Okuno H., Sakamoto N., Sato Y., Suda K., Watanabe T., Yamada K., Yokouchi S., and Yano Y.: "Present status of RIKEN heavy-ion linac", Proceedings of LINAC 08, Canada, Victoria, 2008–9〜10, TRIUMF, Vancouver, pp. 112–114 (2010).

青木孝道, Stingelin L., 上垣外修一, 坂本成彦, 福西暢尚, 横内茂, 加瀬昌之, 後藤彰: "Rebuncher resonator between RRC and fRC in RIKEN", 第 3 回日本加速器学会年会・第 31 回リニアック技術研究会論文集, 仙台, 2006–8, Japan Accelerator Society, 仙台, pp. 801–803 (2006).

上垣外修一, 藤巻正樹, 藤縄雅, 福西暢尚, 後藤彰, 長谷部裕雄, 日暮祥英, 池上九三男, 池沢英二, 影山正, 加瀬昌之, 木寺正憲, 込山美咲, 久保木浩功, 熊谷桂子, 眞家武士, 長瀬誠, 中川孝秀, 大西純一, 奥野広樹, 龍頭啓充, 坂本成彦, 佐藤洋一, 須田健嗣, 若杉昌徳, 渡辺博, 渡邉環, 山田一成, 横内茂, 矢野安重: "理研 RI ビームファクトリーの現状", 第 5 回日本加速器学会年会・第 33 回リニアック技術研究会論文集, 東広島, 2008–8, 日本加速器学会, 東広島, pp. 10–12 (2008).

(Others)

Okuno H., Yang J., and Adelmann A.: "Possibility of Round Beam Formation in RIBF cyclotrons", Proceedings of ICAP09, San Francisco, USA, 2009–8〜9, Volker RW Schaa, , pp. 333–336 (2010).

Suda K., Arai S., Chiba Y., Kamigaito O., Kase M., Sakamoto N., and Yamada K.: "Drift Tube Linac Cavities with Space-Saving Amplifier Coupling of New Injector for RI-Beam Factory", Proceedings of of the 1st International Particle Accelerator Conference (IPAC'10), Kyoto, 2010–5, The IPAC'10 Organizing Committee and Asian Committee for Future Accelerators, Kyoto, pp. 3726–3728 (2010).

Okuno H., Fukunishi N., Goto A., Hasebe H., Kamigaito O., Kase M., Kuboki H., Imao H., Yano Y., and Hershcovitch A.: "A New Possibility of Low-Z Gas Stripper for High Power Uranium Beam Acceleration Alternative to C Foil", Proceedings of HB2010 (46th ICFA Advanced Beam Dynamics Workshop on High-Intensity and High-Brightness Hadron Beams), Morschach, Switzerland, ICFA, , pp. 600–604 (2011).

上垣外修一, 新井重昭, 藤巻正樹, 藤縄雅, 藤澤博, 福西暢尚, 後藤彰, 日暮祥英, 池沢英二, 影山正, 加瀬昌之, 込山美咲, 久保木浩功, 熊谷桂子, 眞家武士, 長瀬誠, 中川孝秀, 大西純一, 奥野広樹, 坂本成彦, 佐藤洋一, 須田健嗣, 渡辺博, 渡邉環, 渡邉裕, 山田一成, 山澤秀行, 矢野安重, 横内茂: "Intensity-upgrade plans of RIKEN RI-Beam Factory", 第 6 回日本加速器学会年会プロシーディングス, 東海村, 2009–8, 日本加速器学会, 東海村, pp. 38–41 (2010).

Oral Presentations

(International Conference etc.)

Kamigaito O., Ikezawa E., Kase M., Fujimaki M., Fujinawa T., Fukunishi N., Goto A., Haba H., Higurashi Y., Kidera M., Komiyama M., Koyama R., Kuboki H., Kumagai K., Maie T., Nagase M., Nakagawa T., Ohnishi J., Okuno H., Sakamoto N., Sato Y., Suda K., Watanabe T., Yamada K., Yokouchi S., and Yano Y.: "Present status of RIKEN heavy-ion linac", 24th International Linear Accelerator Conference (LINAC08), (LINAC08 Organizing Committee), Victoria, Canada, Sept.–Oct.

(2008).

Kamigaito O., Arai S., Fujimaki M., Fujinawa T., Fujisawa H., Fukunishi N., Goto A., Higurashi Y., Ikezawa E., Kageyama T., Kase M., Komiyama M., Kuboki H., Kumagai K., Maie T., Nagase M., Nakagawa T., Ohnishi J., Okuno H., Sakamoto N., Sato Y., Suda K., Watanabe H., Watanabe T., Watanabe Y., Yamada K., Yamasawa H., Yano Y., and Yokouchi S.: "Intensity-upgrade plans of RIKEN RI-Beam Factory", 11th International Conference on Heavy Ion Accelerator Technology (HIAT09), (HIAT09 International Organizing Committee), Venezia, Italy, June (2009).

Okuno H., Dantsuka T., Yamada K., Kase M., Maie T., and Kamigaito O.: "Superconducting Ring Cyclotron for RIKEN RI Beam Factory in Japan", Cryogenic Engineering Conference and the International Cryogenic Materials Conference (CEC/ICMC 2009), Tucson, USA, June–July (2009).

Okuno H., Yang J., and Adelmann A.: "Possibility of Round Beam Formation in RIBF cyclotrons", 10th International Computational Accelerator Physics Conference, (LBNL, SLAC), San Francisco, USA, Aug.–Sept. (2009).

Suda K., Arai S., Chiba Y., Kamigaito O., Kase M., Sakamoto N., and Yamada K.: "Drift Tube Linac Cavities with Space-Saving Amplifier Coupling of New Injector for RIKEN RI-Beam Factory", 1st International Particle Accelerator Conference (IPAC'10), (Science Council of Japan, The Physical Society of Japan, Particle Accelerator Society of Japan, and Ato), Kyoto, May (2010).

Kamigaito O., Arai S., Dantsuka T., Fujimaki M., Fujinawa T., Fujisawa H., Fukunishi N., Goto A., Hasebe H., Higurashi Y., Ikegami K., Ikezawa E., Imao H., Kageyama T., Kase M., Kidera M., Komiyama M., Kuboki H., Kumagai K., Maie T., Nagase M., Nakagawa T., Nakamura M., Ohnishi J., Okuno H., Sakamoto N., Suda K., Watanabe H., Watanabe Y., Watanabe T., Yamada K., Yamasawa H., Yokouchi S., and Yano Y.: "Status of RIBF accelerators at RIKEN", 19th International Conference on Cyclotrons and their Applications (CYCLOTRONS 2010), (Cyclotrons2010 International Organizing Committee), Lanzhou, China, Sept. (2010).

Okuno H., Fukunishi N., Goto A., Hasebe H., Kamigaito O., Kase M., Kuboki H., Imao H., Yano Y., and Hershcovitch A.: "A New Possibility of Low-Z Gas Stripper for High Power Uranium Beam Acceleration Alternative to C Foil", 46th ICFA Advanced Beam Dynamics Workshop on High-Intensity and High-Brightness Hadron Beams, (Paul Scherrer Institut), Morschach, Switzerland, Sept.–Oct. (2010).

(Domestic Conference)

上垣外修一, 藤巻正樹, 藤縄雅, 福西暢尚, 後藤彰, 長谷部裕雄, 日暮祥英, 池上九三男, 池沢英二, 影山正, 加瀬昌之, 木寺正憲, 込山美咲, 久保木浩功, 熊谷桂子, 眞家武士, 長瀬誠, 中川孝秀, 大西純一, 奥野広樹, 龍頭啓充, 坂本成彦, 佐藤洋一, 須田健嗣, 若杉昌徳, 渡辺博, 渡邉環, 山田一成, 横内茂, 矢野安重: "理研 RI ビームファクトリーの現状", 第 5 回日本加速器学会年会/第 33 回リニアック技術研究会, (日本加速器学会), 東広島, 8 月 (2008).

上垣外修一, 新井重昭, 藤巻正樹, 藤縄雅, 藤澤博, 福西暢尚, 後藤彰, 日暮祥英, 池沢英二, 影山正, 加瀬昌之, 込山美咲, 久保木浩功, 熊谷桂子, 眞家武士, 長瀬誠, 中川孝秀, 大西純一, 奥野広樹, 坂本成彦, 佐藤洋一, 須田健嗣, 渡辺博, 渡邉環, 渡邉裕, 山田一成, 山澤秀行, 矢野安重, 横内茂: "理研 RIBF のビーム増強計画", 第 6 回日本加速器学会年会, (日本加速器学会), 茨城県東海村, 8 月 (2009).

小沢顕, 鈴木宏, 長江大輔, 新井一郎, 森口哲朗, 伊藤由太, 長谷部裕雄, 藤縄雅, 福西暢尚, 後藤彰, 大西哲哉, 櫻井博儀, 若杉昌徳, 山口由高, 矢野安重, 鈴木健, 山口貴之, 菊池崇志, 大坪隆, 安田裕介, 久保野茂: "RIBF における稀少 RI リング", RIBF に於ける測定器についての検討会, 和光, 12 月 (2009).

小沢顕, 新井一郎, 伊藤由太, 森口哲朗, 長江大輔, 鈴木宏, 藤縄雅, 福西暢尚, 後藤彰, 長谷部裕雄, 大西哲哉, 櫻井博儀, 若杉昌徳, 山口由高, 矢野安重, 鈴木健, 山口貴之, 菊池崇志, 大坪隆, 安田裕介, 久保野茂: "RIBF に於ける稀少 RI リング計画", 蓄積リング検討ミニワークショップ, (大阪大学　核物理研究センター), 茨木, 1 月 (2010).

渡邉裕, 池沢英二, 今尾浩士, 大西純一, 奥野広樹, 加瀬昌之, 上垣外修一, 熊谷桂子, 後藤彰, 込山美咲, 坂本成彦, 須田健嗣, 中川孝秀, 日暮祥英, 福西暢尚, 藤縄雅, 藤巻正樹, 眞家武士, 山田一成, 山澤秀行, 横内茂, 渡邉環, 渡辺博, 新井重昭, 佐藤洋一: "理研リニアック新入射器システム (RILAC2) の建設状況", 第 7 回日本加速器学会年会, (日本加速器学会), 姫路, 8 月 (2010).

山田一成, 池沢英二, 今尾浩士, 大西純一, 奥野広樹, 加瀬昌之, 熊谷桂子, 込山美咲, 後藤彰, 坂本成彦, 須田健嗣, 中川孝秀, 日暮祥英, 福西暢尚, 藤縄雅, 藤巻正樹, 眞家武士, 山澤秀行, 横内茂, 渡邉環, 渡辺博, 渡邉裕, 新井重昭, 藤澤博, 佐藤洋一, 上垣外修一: "理研 RIBF 用の新しい重イオン入射ライナック RILAC2 の製作", 第 7 回日本加速器学会年会, (日本加速器学会), 姫路, 8 月 (2010).

奥野広樹: "RI ビームファクトリーの低エネルギーサイクロトロンにおけるラウンドビーム形成について", ビーム物理研究会 2010, (ビーム物理研究会), 和光, 11 月 (2010).

大塚未来, 永田祐吾, 榎本嘉範, 黒田直史, 満汐孝治, 金燦鉉, 檜垣浩之, 金井保之, 鳥居寛之, Corradini M., Leali M., Lodi-Rizzini E., Mascagna V., Venturelli V., Zurlo N., 藤居甲基, 田中香津生, 今尾浩士, 長嶋泰之, 松田恭幸, Juhasz B., 毛利明博, 山崎泰規: "反水素原子消滅信号の検出と検出効率の見積もり", 日本物理学会第 66 回年次大会, (日本物理学会), 新潟, 3 月 (2011).

田中香津生, 毛利明博, 榎本嘉範, 黒田直史, 永田祐吾, 満汐孝治, 金燦鉉, 檜垣浩之, 金井保之, 鳥居寛之, Corradini M., Leali M., Lodi-Rizzini E., Mascagna V., Venturelli V., Zurlo N., 藤居甲基, 大塚未来, 今尾浩士, 長嶋泰之, 松田恭幸, Juhasz B., 山崎泰規: "カスプトラップ中での陽電子温度測定", 日本物理学会第 66 回年次大会, (日本物理学会), 新潟, 3 月 (2011).

藤居 甲基, 榎本 嘉範, 金 燦鉉, 満汐 孝治, 檜垣 浩之, 黒田

直史, 鳥居寛之, 田中香津生, 金井保之, 今尾浩士, 永田祐吾, 吉良健太郎, Corradini M., Leali M., Lodi-Rizzini E., Mascagna V., Venturelli V., Zurlo N., 大塚未来, 長嶋泰之, 松田恭幸, Juhasz B., 毛利明博, 山崎泰規: "反水素合成に向けた前段陽電子蓄積装置での陽電子の準備", 日本物理学会第 66 回年次大会, (日本物理学会), 新潟, 3 月 (2011).

金燦鉉, 満汐孝治, 檜垣浩之, 榎本嘉範, 黒田直史, 藤居甲基, 田中香津生, 金井保之, 今尾浩士, 永田祐吾, 毛利明博, Lodi-Rizzini E., Venturelli L., Corradini M., Leali M., Zurlo V., Mascagna V., 鳥居寛之, 大塚未来, 長嶋泰之, 松田恭幸, 山崎泰規: "反水素合成実験における、反陽子入射による陽電子雲形状の変化", 日本物理学会第 66 回年次大会, (日本物理学会), 新潟, 3 月 (2011).

檜垣浩之, 満汐孝治, 金燦鉉, 藤居甲基, 田中香津生, 榎本嘉範, 金井保之, 黒田直史, 今尾浩士, 吉良健太郎, 大塚未来, 永田祐吾, 長嶋泰之, 毛利明博, 鳥居寛之, 松田恭幸, 山崎泰規: "カスプトラップ法による低エネルギー反水素合成と陽電子の輸送・制御", 日本物理学会第 66 回年次大会, (日本物理学会), 新潟, 3 月 (2011).

榎本嘉範, 黒田直史, 満汐孝治, 金燦鉉, 檜垣浩之, 永田祐吾, 金井保之, 鳥居寛之, Corradini M., Leali M., Lodi-Rizzini E., Mascagna V., Venturelli L., Zurlo N., 藤居甲基, 大塚未来, 田中香津生, 今尾浩士, 長嶋泰之, 松田恭幸, 毛利明博, 山崎泰規: "カスプトラップ中での反水素生成", 日本物理学会第 66 回年次大会, (日本物理学会), 新潟, 3 月 (2011).

永田祐吾, 毛利明博, 榎本嘉範, 黒田直史, 満汐孝治, 金燦鉉, 檜垣浩之, 金井保之, 鳥居寛之, Corradini M., Leali M., Lodi-Rizzini E., Mascagna V., Zurlo N., 藤居甲基, 大塚未来, 田中香津生, 今尾浩士, 長嶋泰之, 松田恭幸, Juhasz B., 山崎泰規: "基底状態反水素原子の偏極ビーム生成", 日本物理学会第 66 回年次大会, (日本物理学会), 新潟, 3 月 (2011).

満汐孝治, 金燦鉉, 檜垣浩之, 榎本嘉範, 黒田直史, 藤居甲基, 田中香津生, 金井保之, 今尾浩士, 鳥居寛之, 永田祐吾, 吉良健太郎, Corradini M., Leali M., Lodi-Rizzini E., Mascagna V., Venturelli L., Zurlo V., 大塚未来, 長嶋泰之, 松田恭幸, Juhasz B., 毛利明博, 山崎泰規: "反水素原子合成に向けたカストラップ中における高密度陽電子雲の生成", 日本物理学会第 66 回年次大会, (日本物理学会), 新潟, 3 月 (2011).

Ion Source Team

Publications

[Journal]

(Original Papers)　*Subject to Peer Review

Nakagawa T.: "New superconducting electron cyclotron resonance ion source for RIKEN RI beam factory project", Rev. Sci. Instrum. **79**, No. 2, pp. 02A327-1–02A327-4 (2008). *

Higashijima H. and Nakagawa T.: "Measurment of plasma potential of liquid-he-free superconducting electron cyclotron resonance ion source", Rev. Sci. Instrum. **79**, No. 2, pp. 02B505-1–02B505-3 (2008). *

Higurashi Y. and Nakagawa T.: "Production of U beam from riken 18ghz electron cyclotron resonance ion source", Rev. Sci. Instrum. **79**, No. 2, pp. 02C714-1–02C714-3 (2008). *

Kidera M., Seto Y., Takahashi K., Enomoto S., Kishi S., Makita M., Nagamatsu T., Tanaka T., and Toda M.: "New method for comprehensive detection of chemical warfare agents using an electron-cyclotron-resonance ion-source mass spectrometer", Spectrochim. Acta Pt. A **78**, 1215–1219 (2011). *

[Book・ Proceedings]

(Original Papers)　*Subject to Peer Review

Kamigaito O., Arai S., Fujimaki M., Fujinawa T., Fujisawa H., Fukunishi N., Goto A., Higurashi Y., Ikezawa E., Kageyama T., Kase M., Komiyama M., Kuboki H., Kumagai K., Maie T., Nagase M., Nakagawa T., Ohnishi J., Okuno H., Sakamoto N., Sato Y., Suda K., Watanabe H., Watanabe T., Watanabe Y., Yamada K., Yamasawa H., Yano Y., and Yokouchi S.: "Intensity-upgrade plans of RIKEN RI-Beam Factory", Proceedings of 11th International Conference on Heavy Ion Accelerator Technology (HIAT09), Venezia, Italy, 2009–6, HIAT09 International Organizing Committee, Venice, pp. 21–25 (2009).

Kamigaito O., Ikezawa E., Kase M., Fujimaki M., Fujinawa T., Fukunishi N., Goto A., Haba H., Higurashi Y., Kidera M., Komiyama M., Koyama R., Kuboki H., Kumagai K., Maie T., Nagase M., Nakagawa T., Ohnishi J., Okuno H., Sakamoto N., Sato Y., Suda K., Watanabe T., Yamada K., Yokouchi S., and Yano Y.: "Present status of RIKEN heavy-ion linac", Proceedings of LINAC 08, Canada, Victoria, 2008–9～10, TRIUMF, Vancouver, pp. 112–114 (2010).

上垣外修一, 藤巻正樹, 藤縄雅, 福西暢尚, 後藤彰, 長谷部裕雄, 日暮祥英, 池上九三男, 池沢英二, 影山正, 加瀬昌之, 木寺正憲, 込山美咲, 久保木浩功, 熊谷桂子, 眞家武士, 長瀬誠, 中川孝秀, 大西純一, 奥野広樹, 龍頭啓充, 坂本成彦, 佐藤洋一, 須田健嗣, 若杉昌徳, 渡辺博, 渡邉環, 山田一成, 横内茂, 矢野安重: "理研 RI ビームファクトリーの現状", 第 5 回日本加速器学会年会・第 33 回リニアック技術研究会論文集, 東広島, 2008–8, 日本加速器学会, 東広島, pp. 10–12 (2008).

(Others)

上垣外修一, 新井重昭, 藤巻正樹, 藤縄雅, 藤澤博, 福西暢尚, 後藤彰, 日暮祥英, 池沢英二, 影山正, 加瀬昌之, 込山美咲, 久保木浩功, 熊谷桂子, 眞家武士, 長瀬誠, 中川孝秀, 大西純一, 奥野広樹, 坂本成彦, 佐藤洋一, 須田健嗣, 渡辺博, 渡邉環, 渡邉裕, 山田一成, 山澤秀行, 矢野安重, 横内茂: "Intensity-upgrade plans of RIKEN RI-Beam Factory", 第 6 回日本加速器学会年会プロシーディングス, 東海村, 2009–8, 日本加速器学会, 東海村, pp. 38–41 (2010).

Oral Presentations

(International Conference etc.)

Kamigaito O., Ikezawa E., Kase M., Fujimaki M., Fujinawa T., Fukunishi N., Goto A., Haba H., Higurashi Y., Kidera M., Komiyama M., Koyama R., Kuboki H., Kumagai K., Maie T., Nagase M., Nakagawa T., Ohnishi J., Okuno H., Sakamoto N., Sato Y., Suda K., Watanabe T., Yamada K., Yokouchi S., and Yano Y.: "Present status of RIKEN heavy-ion linac", 24th International Linear Accelerator Conference (LINAC08), (LINAC08 Organizing Committee), Victoria, Canada, Sept.–Oct. (2008).

Kamigaito O., Arai S., Fujimaki M., Fujinawa T., Fujisawa H., Fukunishi N., Goto A., Higurashi Y., Ikezawa E., Kageyama T., Kase M., Komiyama M., Kuboki H., Kumagai K., Maie T., Nagase M., Nakagawa T., Ohnishi J., Okuno H., Sakamoto N., Sato Y., Suda K., Watanabe H., Watanabe T., Watanabe Y., Yamada K., Yamasawa H., Yano Y., and Yokouchi S.: "Intensity-upgrade plans of RIKEN RI-Beam Factory", 11th International Conference on Heavy Ion Accelerator Technology (HIAT09), (HIAT09 International Organizing Committee), Venezia, Italy, June (2009).

Kidera M., Takahashi K., Nagamatsu T., Seto Y., Toda M., Enomoto S., and Tanaka T.: "Study of potential application of compact ECRIS tp analytical system", 19th International Workshop on ECR Ion Sources (ECRIS 2010), (Laboratoire de Physique Subatomique et de Cosmologie), Grenoble, France, Aug. (2010).

Kamigaito O., Arai S., Dantsuka T., Fujimaki M., Fujinawa T., Fujisawa H., Fukunishi N., Goto A., Hasebe H., Higurashi Y., Ikegami K., Ikezawa E., Imao H., Kageyama T., Kase M., Kidera M., Komiyama M., Kuboki H., Kumagai K., Maie T., Nagase M., Nakagawa T., Nakamura M., Ohnishi J., Okuno H., Sakamoto N., Suda K., Watanabe H., Watanabe Y., Watanabe T., Yamada K., Yamasawa H., Yokouchi S., and Yano Y.: "Status of RIBF accelerators at RIKEN", 19th International Conference on Cyclotrons and their Applications (CYCLOTRONS 2010), (Cyclotrons2010 International Organizing Committee), Lanzhou, China, Sept. (2010).

Kidera M., Toda M., Makita M., Mitsubori Y., Tanaka T., and Takahashi K.: "Development of the mass spectrometer equipped with ECRIS and its application to the isotopic analyses", International Chemical Congress of

Pacific Basin Societies (PACIFICHEM 2010), Honolulu, USA, Dec. (2010).

(Domestic Conference)

上垣外修一, 藤巻正樹, 藤縄雅, 福西暢尚, 後藤彰, 長谷部裕雄, 日暮祥英, 池上九三男, 池沢英二, 影山正, 加瀬昌之, 木寺正憲, 込山美咲, 久保木浩功, 熊谷桂子, 眞家武士, 長瀬誠, 中川孝秀, 大西純一, 奥野広樹, 龍頭啓充, 坂本成彦, 佐藤洋一, 須田健嗣, 若杉昌徳, 渡辺博, 渡邉環, 山田一成, 横内茂, 矢野安重: "理研 RI ビームファクトリーの現状", 第 5 回日本加速器学会年会/第 33 回リニアック技術研究会, (日本加速器学会), 東広島, 8 月 (2008).

上垣外修一, 新井重昭, 藤巻正樹, 藤縄雅, 藤澤博, 福西暢尚, 後藤彰, 日暮祥英, 池沢英二, 影山正, 加瀬昌之, 込山美咲, 久保木浩功, 熊谷桂子, 眞家武士, 長瀬誠, 中川孝秀, 大西純一, 奥野広樹, 坂本成彦, 佐藤洋一, 須田健嗣, 渡辺博, 渡邉環, 渡邉裕, 山田一成, 山澤秀行, 矢野安重, 横内茂: "理研 RIBF のビーム増強計画", 第 6 回日本加速器学会年会, (日本加速器学会), 茨城県東海村, 8 月 (2009).

渡邉裕, 池沢英二, 今尾浩士, 大西純一, 奥野広樹, 加瀬昌之, 上垣外修一, 熊谷桂子, 後藤彰, 込山美咲, 坂本成彦, 須田健嗣, 中川孝秀, 日暮祥英, 福西暢尚, 藤縄雅, 藤巻正樹, 眞家武士, 山田一成, 山澤秀行, 横内茂, 渡邉環, 渡辺博, 新井重昭, 佐藤洋一: "理研リニアック新入射器システム (RILAC2) の建設状況", 第 7 回日本加速器学会年会, (日本加速器学会), 姫路, 8 月 (2010).

山田一成, 池沢英二, 今尾浩士, 大西純一, 奥野広樹, 加瀬昌之, 熊谷桂子, 込山美咲, 後藤彰, 坂本成彦, 須田健嗣, 中川孝秀, 日暮祥英, 福西暢尚, 藤縄雅, 藤巻正樹, 眞家武士, 山澤秀行, 横内茂, 渡邉環, 渡辺博, 渡邉裕, 新井重昭, 藤澤博, 佐藤洋一, 上垣外修一: "理研 RIBF 用の新しい重イオン入射ライナック RILAC2 の製作", 第 7 回日本加速器学会年会, (日本加速器学会), 姫路, 8 月 (2010).

RILAC Team

Publications

[Journal]

(Original Papers)　*Subject to Peer Review

春日博, 林偉民, 渡邉裕, 三島健稔, 土肥俊郎, 大森整: "4H-SiC（0001）面の高能率研削", 砥粒加工学会誌 **52**, No. 11, pp. 645–650 (2008). ＊

[Book o Proceedings]

(Original Papers)　*Subject to Peer Review

Kamigaito O., Arai S., Fujimaki M., Fujinawa T., Fujisawa H., Fukunishi N., Goto A., Higurashi Y., Ikezawa E., Kageyama T., Kase M., Komiyama M., Kuboki H., Kumagai K., Maie T., Nagase M., Nakagawa T., Ohnishi J., Okuno H., Sakamoto N., Sato Y., Suda K., Watanabe H., Watanabe T., Watanabe Y., Yamada K., Yamasawa H., Yano Y., and Yokouchi S.: "Intensity-upgrade plans of RIKEN RI-Beam Factory", Proceedings of 11th International Conference on Heavy Ion Accelerator Technology (HIAT09), Venezia, Italy, 2009–6, HIAT09 International Organizing Committee, Venice, pp. 21–25 (2009).

Kamigaito O., Ikezawa E., Kase M., Fujimaki M., Fujinawa T., Fukunishi N., Goto A., Haba H., Higurashi Y., Kidera M., Komiyama M., Koyama R., Kuboki H., Kumagai K., Maie T., Nagase M., Nakagawa T., Ohnishi J., Okuno H., Sakamoto N., Sato Y., Suda K., Watanabe T., Yamada K., Yokouchi S., and Yano Y.: "Present status of RIKEN heavy-ion linac", Proceedings of LINAC 08, Canada, Victoria, 2008–9～10, TRIUMF, Vancouver, pp. 112–114 (2010).

上垣外修一, 藤巻正樹, 藤縄雅, 福西暢尚, 後藤彰, 長谷部裕雄, 日暮祥英, 池上九三男, 池沢英二, 影山正, 加瀬昌之, 木寺正憲, 込山美咲, 久保木浩功, 熊谷桂子, 眞家武士, 長瀬誠, 中川孝秀, 大西純一, 奥野広樹, 龍頭啓充, 坂本成彦, 佐藤洋一, 須田健嗣, 若杉昌徳, 渡辺博, 渡邉環, 山田一成, 横内茂, 矢野安重: "理研 RI ビームファクトリーの現状", 第 5 回日本加速器学会年会・第 33 回リニアック技術研究会論文集, 東広島, 2008–8, 日本加速器学会, 東広島, pp. 10–12 (2008).

池沢英二, 加瀬昌之, 大木智則, 藍原利光, 山内啓資, 内山暁仁, 小山田和幸, 田村匡史: "理研重イオンリニアックの運転状況", 第 5 回加速器学会年会・第 33 回リニアック技術研究会プロシーディングス, 東広島, 2008–8, 日本加速器学会, 東京, pp. 265–267 (2009).

池沢英二, 加瀬昌之, 渡邉裕, 大木智則, 藍原利光, 山内啓資, 内山暁仁, 小山田和幸, 田村匡史: "理研重イオンリニアックの現状報告", 第 6 回日本加速器学会年会プロシーディングス, 茨城県東海村, 2009–8, 日本加速器学会, 東京, pp. 622–624 (2010).

(Others)

Suda K., Arai S., Chiba Y., Kamigaito O., Kase M., Sakamoto N., and Yamada K.: "Drift Tube Linac Cavities with Space-Saving Amplifier Coupling of New Injector for RI-Beam Factory", Proceedings of of the 1st International Particle Accelerator Conference (IPAC'10), Kyoto, 2010–5, The IPAC'10 Organizing Committee and Asian Committee for Future Accelerators, Kyoto, pp. 3726–3728 (2010).

須田健嗣, 藤巻正樹, 福西暢尚, 逸見政武, 上垣外修一, 加瀬昌之, 小山亮, 熊谷桂子, 坂本成彦, 渡邉環, 山田一成: "理研 RIBF における高周波系およびビームの安定度", 第 6 回日本加速器学会要旨集, 茨城県東海村, 2009–8, 日本加速器学会, 東京, pp. 397–400 (2009).

上垣外修一, 新井重昭, 藤巻正樹, 藤縄雅, 藤澤博, 福西暢尚, 後藤彰, 日暮祥英, 池沢英二, 影山正, 加瀬昌之, 込山美咲, 久保木浩功, 熊谷桂子, 眞家武士, 長瀬誠, 中川孝秀, 大西純一, 奥野広樹, 坂本成彦, 佐藤洋一, 須田健嗣, 渡辺博, 渡邉環, 渡邉裕, 山田一成, 山澤秀行, 矢野安重, 横内茂: "Intensity-upgrade plans of RIKEN RI-Beam Factory", 第 6 回日本加速器学会年会プロシーディングス, 東海村, 2009–8, 日本加速器学会, 東海村, pp. 38–41 (2010).

Oral Presentations

(International Conference etc.)

Kamigaito O., Ikezawa E., Kase M., Fujimaki M., Fujinawa T., Fukunishi N., Goto A., Haba H., Higurashi Y., Kidera M., Komiyama M., Koyama R., Kuboki H., Kumagai K., Maie T., Nagase M., Nakagawa T., Ohnishi J., Okuno H., Sakamoto N., Sato Y., Suda K., Watanabe T., Yamada K., Yokouchi S., and Yano Y.: "Present status of RIKEN heavy-ion linac", 24th International Linear Accelerator Conference (LINAC08), (LINAC08 Organizing Committee), Victoria, Canada, Sept.–Oct. (2008).

Kamigaito O., Arai S., Fujimaki M., Fujinawa T., Fujisawa H., Fukunishi N., Goto A., Higurashi Y., Ikezawa E., Kageyama T., Kase M., Komiyama M., Kuboki H., Kumagai K., Maie T., Nagase M., Nakagawa T., Ohnishi J., Okuno H., Sakamoto N., Sato Y., Suda K., Watanabe H., Watanabe T., Watanabe Y., Yamada K., Yamasawa H., Yano Y., and Yokouchi S.: "Intensity-upgrade plans of RIKEN RI-Beam Factory", 11th International Conference on Heavy Ion Accelerator Technology (HIAT09), (HIAT09 International Organizing Committee), Venezia, Italy, June (2009).

Suda K., Arai S., Chiba Y., Kamigaito O., Kase M., Sakamoto N., and Yamada K.: "Drift Tube Linac Cavities with Space-Saving Amplifier Coupling of New Injector for RIKEN RI-Beam Factory", 1st International Particle Accelerator Conference (IPAC'10), (Science Council of Japan, The Physical Society of Japan, Particle Accelerator Society of Japan, and Ato), Kyoto, May (2010).

Suda K., Fujimaki M., Fukunishi N., Hemmi M., Kamigaito O., Kase M., Koyama R., Kumagai K., Sakamoto N., and Yamada K.: "Stable Operation of RF Systems for RIBF", 19th International Conference on Cyclotrons and their Applications (CYCLOTRONS 2010), (Institute of Modern Physics, Chinese Academy of Sciences), Lanzhou, China, Sept. (2010).

Kamigaito O., Arai S., Dantsuka T., Fujimaki M., Fujinawa T., Fujisawa H., Fukunishi N., Goto A., Hasebe H., Higurashi Y., Ikegami K., Ikezawa E., Imao H., Kageyama T., Kase M., Kidera M., Komiyama M., Kuboki H., Kumagai K., Maie T., Nagase M., Nakagawa T., Nakamura M., Ohnishi J., Okuno H., Sakamoto N., Suda K., Watanabe H., Watanabe Y., Watanabe T., Yamada K., Yamasawa H., Yokouchi S., and Yano Y.: "Status of RIBF accelerators at RIKEN", 19th International Conference on Cyclotrons and their Applications (CYCLOTRONS 2010), (Cyclotrons2010 International Organizing Committee), Lanzhou, China, Sept. (2010).

(Domestic Conference)

上垣外修一, 藤巻正樹, 藤縄雅, 福西暢尚, 後藤彰, 長谷部裕雄, 日暮祥英, 池上九三男, 池沢英二, 影山正, 加瀬昌之, 木寺正憲, 込山美咲, 久保木浩功, 熊谷桂子, 眞家武士, 長瀬誠, 中川孝秀, 大西純一, 奥野広樹, 龍頭啓充, 坂本成彦, 佐藤洋一, 須田健嗣, 若杉昌徳, 渡辺博, 渡邉環, 山田一成, 横内茂, 矢野安重: "理研 RI ビームファクトリーの現状", 第 5 回日本加速器学会年会/第 33 回リニアック技術研究会, (日本加速器学会), 東広島, 8 月 (2008).

上垣外修一, 新井重昭, 藤巻正樹, 藤縄雅, 藤澤博, 福西暢尚, 後藤彰, 日暮祥英, 池沢英二, 影山正, 加瀬昌之, 込山美咲, 久保木浩功, 熊谷桂子, 眞家武士, 長瀬誠, 中川孝秀, 大西純一, 奥野広樹, 坂本成彦, 佐藤洋一, 須田健嗣, 渡辺博, 渡邉環, 渡邉裕, 山田一成, 山澤秀行, 矢野安重, 横内茂: "理研 RIBF のビーム増強計画", 第 6 回日本加速器学会年会, (日本加速器学会), 茨城県東海村, 8 月 (2009).

渡邉裕, 池沢英二, 今尾浩士, 大西純一, 奥野広樹, 加瀬昌之, 上垣外修一, 熊谷桂子, 後藤彰, 込山美咲, 坂本成彦, 須田健嗣, 中川孝秀, 日暮祥英, 福西暢尚, 藤縄雅, 藤巻正樹, 眞家武士, 山田一成, 山澤秀行, 横内茂, 渡邉環, 渡辺博, 新井重昭, 佐藤洋一: "理研リニアック新入射器システム (RILAC2) の建設状況", 第 7 回日本加速器学会年会, (日本加速器学会), 姫路, 8 月 (2010).

池沢英二, 上垣外修一, 加瀬昌之, 渡邉裕, 大木智則, 藍原利光, 山内啓資, 内山暁仁, 小山田和幸, 田村匡史: "理研重イオンリニアックの現状報告", 第 7 回日本加速器学会年会, (日本加速器学会), 姫路, 8 月 (2010).

山田一成, 池沢英二, 今尾浩士, 大西純一, 奥野広樹, 加瀬昌之, 熊谷桂子, 込山美咲, 後藤彰, 坂本成彦, 須田健嗣, 中川孝秀, 日暮祥英, 福西暢尚, 藤縄雅, 藤巻正樹, 眞家武士, 山澤秀行, 横内茂, 渡邉環, 渡辺博, 渡邉裕, 新井重昭, 藤澤博, 佐藤洋一, 上垣外修一: "理研 RIBF 用の新しい重イオン入射ライナック RILAC2 の製作", 第 7 回日本加速器学会年会, (日本加速器学会), 姫路, 8 月 (2010).

Cyclotron Team

Publications

[Book・ Proceedings]

(Original Papers) *Subject to Peer Review

Kamigaito O., Arai S., Fujimaki M., Fujinawa T., Fujisawa H., Fukunishi N., Goto A., Higurashi Y., Ikezawa E., Kageyama T., Kase M., Komiyama M., Kuboki H., Kumagai K., Maie T., Nagase M., Nakagawa T., Ohnishi J., Okuno H., Sakamoto N., Sato Y., Suda K., Watanabe H., Watanabe T., Watanabe Y., Yamada K., Yamasawa H., Yano Y., and Yokouchi S.: "Intensity-upgrade plans of RIKEN RI-Beam Factory", Proceedings of 11th International Conference on Heavy Ion Accelerator Technology (HIAT09), Venezia, Italy, 2009–6, HIAT09 International Organizing Committee, Venice, pp. 21–25 (2009).

Kamigaito O., Ikezawa E., Kase M., Fujimaki M., Fujinawa T., Fukunishi N., Goto A., Haba H., Higurashi Y., Kidera M., Komiyama M., Koyama R., Kuboki H., Kumagai K., Maie T., Nagase M., Nakagawa T., Ohnishi J., Okuno H., Sakamoto N., Sato Y., Suda K., Watanabe T., Yamada K., Yokouchi S., and Yano Y.: "Present status of RIKEN heavy-ion linac", Proceedings of LINAC 08, Canada, Victoria, 2008–9〜10, TRIUMF, Vancouver, pp. 112–114 (2010).

青木孝道, Stingelin L., 上垣外修一, 坂本成彦, 福西暢尚, 横内茂, 加瀬昌之, 後藤彰: "Rebuncher resonator between RRC and fRC in RIKEN", 第 3 回日本加速器学会年会・第 31 回リニアック技術研究会論文集, 仙台, 2006–8, Japan Accelerator Society, 仙台, pp. 801–803 (2006).

上垣外修一, 藤巻正樹, 藤縄雅, 福西暢尚, 後藤彰, 長谷部裕雄, 日暮祥英, 池上九三男, 池沢英二, 影山正, 加瀬昌之, 木寺正憲, 込山美咲, 久保木浩功, 熊谷桂子, 眞家武士, 長瀬誠, 中川孝秀, 大西純一, 奥野広樹, 龍頭啓充, 坂本成彦, 佐藤洋一, 須田健嗣, 若杉昌徳, 渡辺博, 渡邉環, 山田一成, 横内茂, 矢野安重: "理研 RI ビームファクトリーの現状", 第 5 回日本加速器学会年会・第 33 回リニアック技術研究会論文集, 東広島, 2008–8, 日本加速器学会, 東広島, pp. 10–12 (2008).

(Others)

Suda K., Arai S., Chiba Y., Kamigaito O., Kase M., Sakamoto N., and Yamada K.: "Drift Tube Linac Cavities with Space-Saving Amplifier Coupling of New Injector for RI-Beam Factory", Proceedings of of the 1st International Particle Accelerator Conference (IPAC'10), Kyoto, 2010–5, The IPAC'10 Organizing Committee and Asian Committee for Future Accelerators, Kyoto, pp. 3726–3728 (2010).

須田健嗣, 小山亮, 加瀬昌之, 上垣外修一, 坂本成彦, 福西暢尚, 藤巻正樹, 山田一成, 渡邉環: "RIBF における高周波系の安定度", 第 5 回日本加速器学会年会・第 33 回リニアック技術研究会論文集, 東広島, 2008–8, 日本加速器学会, 東京, pp. 379–381 (2008).

須田健嗣, 藤巻正樹, 福西暢尚, 逸見政武, 上垣外修一, 加瀬昌之, 小山亮, 熊谷桂子, 坂本成彦, 渡邉環, 山田一成: "理研 RIBF における高周波系およびビームの安定度", 第 6 回日本加速器学会要旨集, 茨城県東海村, 2009–8, 日本加速器学会, 東京, pp. 397–400 (2009).

上垣外修一, 新井重昭, 藤巻正樹, 藤縄雅, 藤澤博, 福西暢尚, 後藤彰, 日暮祥英, 池沢英二, 影山正, 加瀬昌之, 込山美咲, 久保木浩功, 熊谷桂子, 眞家武士, 長瀬誠, 中川孝秀, 大西純一, 奥野広樹, 坂本成彦, 佐藤洋一, 須田健嗣, 渡辺博, 渡邉環, 渡邉裕, 山田一成, 山澤秀行, 矢野安重, 横内茂: "Intensity-upgrade plans of RIKEN RI-Beam Factory", 第 6 回日本加速器学会年会プロシーディングス, 東海村, 2009–8, 日本加速器学会, 東海村, pp. 38–41 (2010).

Oral Presentations

(International Conference etc.)

Kamigaito O., Ikezawa E., Kase M., Fujimaki M., Fujinawa T., Fukunishi N., Goto A., Haba H., Higurashi Y., Kidera M., Komiyama M., Koyama R., Kuboki H., Kumagai K., Maie T., Nagase M., Nakagawa T., Ohnishi J., Okuno H., Sakamoto N., Sato Y., Suda K., Watanabe T., Yamada K., Yokouchi S., and Yano Y.: "Present status of RIKEN heavy-ion linac", 24th International Linear Accelerator Conference (LINAC08), (LINAC08 Organizing Committee), Victoria, Canada, Sept.–Oct. (2008).

Kamigaito O., Arai S., Fujimaki M., Fujinawa T., Fujisawa H., Fukunishi N., Goto A., Higurashi Y., Ikezawa E., Kageyama T., Kase M., Komiyama M., Kuboki H., Kumagai K., Maie T., Nagase M., Nakagawa T., Ohnishi J., Okuno H., Sakamoto N., Sato Y., Suda K., Watanabe H., Watanabe T., Watanabe Y., Yamada K., Yamasawa H., Yano Y., and Yokouchi S.: "Intensity-upgrade plans of RIKEN RI-Beam Factory", 11th International Conference on Heavy Ion Accelerator Technology (HIAT09), (HIAT09 International Organizing Committee), Venezia, Italy, June (2009).

Suda K., Arai S., Chiba Y., Kamigaito O., Kase M., Sakamoto N., and Yamada K.: "Drift Tube Linac Cavities with Space-Saving Amplifier Coupling of New Injector for RIKEN RI-Beam Factory", 1st International Particle Accelerator Conference (IPAC'10), (Science Council of Japan, The Physical Society of Japan, Particle Accelerator Society of Japan, and Ato), Kyoto, May (2010).

Watanabe T., Fujimaki M., Fukunishi N., Kase M., Komiyama M., Sakamoto N., Watanabe H., Yamada K., Kamigaito O., and Koyama R.: "Beam dignostics for RIBF in RIKEN", 19th International Conference on Cyclotrons and their Applications (CYCLOTRONS 2010), (Institue of Modern Physics , Lanzhou, China), Lanzhou, China, Sept. (2010).

Suda K., Fujimaki M., Fukunishi N., Hemmi M., Kamigaito O., Kase M., Koyama R., Kumagai K., Sakamoto N., and Yamada K.: "Stable Operation of RF Systems for RIBF", 19th International Conference on Cyclotrons and their Applications (CYCLOTRONS 2010), (Institute of Modern Physics, Chinese Academy of Sciences), Lanzhou, China, Sept. (2010).

Kamigaito O., Arai S., Dantsuka T., Fujimaki M., Fujinawa T., Fujisawa H., Fukunishi N., Goto A., Hasebe H., Higurashi Y., Ikegami K., Ikezawa E., Imao H., Kageyama T., Kase M., Kidera M., Komiyama M., Kuboki H., Kumagai K., Maie T., Nagase M., Nakagawa T., Nakamura M., Ohnishi J., Okuno H., Sakamoto N., Suda K., Watanabe H., Watanabe Y., Watanabe T., Yamada K., Yamasawa H., Yokouchi S., and Yano Y.: "Status of RIBF accelerators at RIKEN", 19th International Conference on Cyclotrons and their Applications (CYCLOTRONS 2010), (Cyclotrons2010 International Organizing Committee), Lanzhou, China, Sept. (2010).

(Domestic Conference)

上垣外修一, 藤巻正樹, 藤縄雅, 福西暢尚, 後藤彰, 長谷部裕雄, 日暮祥英, 池上九三男, 池沢英二, 影山正, 加瀬昌之, 木寺正憲, 込山美咲, 久保木浩功, 熊谷桂子, 眞家武士, 長瀬誠, 中川孝秀, 大西純一, 奥野広樹, 龍頭啓充, 坂本成彦, 佐藤洋一, 須田健嗣, 若杉昌徳, 渡辺博, 渡邉環, 山田一成, 横内茂, 矢野安重: "理研 RI ビームファクトリーの現状", 第 5 回日本加速器学会年会/第 33 回リニアック技術研究会, (日本加速器学会), 東広島, 8 月 (2008).

上垣外修一, 新井重昭, 藤巻正樹, 藤縄雅, 藤澤博, 福西暢尚, 後藤彰, 日暮祥英, 池沢英二, 影山正, 加瀬昌之, 込山美咲, 久保木浩功, 熊谷桂子, 眞家武士, 長瀬誠, 中川孝秀, 大西純一, 奥野広樹, 坂本成彦, 佐藤洋一, 須田健嗣, 渡辺博, 渡邉環, 渡邉裕, 山田一成, 山澤秀行, 矢野安重, 横内茂: "理研 RIBF のビーム増強計画", 第 6 回日本加速器学会年会, (日本加速器学会), 茨城県東海村, 8 月 (2009).

渡邉裕, 池沢英二, 今尾浩士, 大西純一, 奥野広樹, 加瀬昌之, 上垣外修一, 熊谷桂子, 後藤彰, 込山美咲, 坂本成彦, 須田健嗣, 中川孝秀, 日暮祥英, 福西暢尚, 藤縄雅, 藤巻正樹, 眞家武士, 山田一成, 山澤秀行, 横内茂, 渡邉環, 渡辺博, 新井重昭, 佐藤洋一: "理研リニアック新入射器システム (RILAC2) の建設状況", 第 7 回日本加速器学会年会, (日本加速器学会), 姫路, 8 月 (2010).

渡邉環, 福西暢尚, 加瀬昌之, 若杉昌徳, 藤巻正樹, 山田一成, 坂本成彦, 小高康照, 小山亮, 仲村武志, 上垣外修一: "RIBF におけるビームエネルギーと縦方向のビームプロファイル測定システムの改良", 第 7 回日本加速器学会年会, (日本加速器学会), 姫路, 8 月 (2010).

山田一成, 池沢英二, 今尾浩士, 大西純一, 奥野広樹, 加瀬昌之, 熊谷桂子, 込山美咲, 後藤彰, 坂本成彦, 須田健嗣, 中川孝秀, 日暮祥英, 福西暢尚, 藤縄雅, 藤巻正樹, 眞家武士, 山澤秀行, 横内茂, 渡邉環, 渡辺博, 渡邉裕, 新井重昭, 藤澤博, 佐藤洋一, 上垣外修一: "理研 RIBF 用の新しい重イオン入射ライナック RILAC2 の製作", 第 7 回日本加速器学会年会, (日本加速器学会), 姫路, 8 月 (2010).

Beam Dynamics & Diagnostics Team

Publications

[Journal]

(Original Papers) *Subject to Peer Review

Ichikawa Y., Onishi T. K., Suzuki D., Iwasaki H., Kubo T., Naik V., Chakrabarti A., Aoi N., Brown A. B., Fukuda N., Kubono S., Motobayashi T., Nakabayashi T., Nakamura T., Nakao T., Okumura T., Ong J. H., Suzuki H., Suzuki M. K., Teranishi T., Yamada K., Yamaguchi H., and Sakurai H.: "Gamow-Teller transition of the proton-rich nucleus ^{24}Si", AIP Conf. Proc. **1235**, 265–269 (2010).

Ichikawa Y., Onishi T. K., Suzuki D., Iwasaki H., Kubo T., Naik V., Chakrabarti A., Aoi N., Brown A. B., Fukuda N., Kubono S., Motobayashi T., Nakabayashi T., Nakamura T., Nakao T., Okumura T., Ong J. H., Suzuki H., Suzuki M. K., Teranishi T., Yamada K., Yamaguchi H., and Sakurai H.: "Mirror asymmetry for B(GT) of ^{24}Si induced by Thomas-Ehrman shift", AIP Conf. Proc. **1238**, 290–293 (2010).

Ichikawa Y., Onishi T. K., Suzuki D., Iwasaki H., Kubo T., Naik V., Chakrabarti A., Aoi N., Brown A. B., Fukuda N., Kubono S., Motobayashi T., Nakabayashi T., Nakamura T., Nakao T., Okumura T., Ong J. H., Suzuki H., Suzuki M. K., Teranishi T., Yamada K., Yamaguchi H., and Sakurai H.: "Mirror asymmetry investigated by β decay of proton-rich ^{24}Si", Mod. Phys. Lett. A **25**, 1895–1898 (2010).

(Others)

Yasuda Y., Ozawa A., Arai I., Fujinawa T., Fukunishi N., Goto A., Ohnishi T., Sakurai H., Wakasugi M., Yamaguchi Y., Yano Y., Suzuki T., Yamaguchi T., Kikuchi T., and Ohtsubo T.: "Present status of rare-RI ring project in RIKEN RIBF", Int. J. Mod. Phys. E **18**, No. 2, pp. 459–464 (2009).

Arai I., Ozawa A., Yasuda Y., Fujinawa T., Fukunishi N., Goto A., Ohnishi T., Sakurai H., Wakasugi M., Yamaguchi Y., Yano Y., Suzuki T., Yamaguchi T., Kikuchi T., and Ohtsubo T.: "Beam optics simulation for rare-RI ring at RI beam factory in RIKEN", Int. J. Mod. Phys. E **18**, No. 2, pp. 498–504 (2009).

Okuno H., Dantsuka T., Yamada K., Kase M., Maie T., and Kamigaito O.: "Superconducting Ring Cyclotron for RIKEN RI Beam Factory in Japan", AIP Conf. Proc. **1218**, 1410–1417 (2010).

[Book・ Proceedings]

(Original Papers) *Subject to Peer Review

Kamigaito O., Arai S., Fujimaki M., Fujinawa T., Fujisawa H., Fukunishi N., Goto A., Higurashi Y., Ikezawa E., Kageyama T., Kase M., Komiyama M., Kuboki H., Kumagai K., Maie T., Nagase M., Nakagawa T., Ohnishi J., Okuno H., Sakamoto N., Sato Y., Suda K., Watanabe H., Watanabe T., Watanabe Y., Yamada K., Yamasawa H., Yano Y., and Yokouchi S.: "Intensity-upgrade plans of RIKEN RI-Beam Factory", Proceedings of 11th International Conference on Heavy Ion Accelerator Technology (HIAT09), Venezia, Italy, 2009–6, HIAT09 International Organizing Committee, Venice, pp. 21–25 (2009).

Kamigaito O., Ikezawa E., Kase M., Fujimaki M., Fujinawa T., Fukunishi N., Goto A., Haba H., Higurashi Y., Kidera M., Komiyama M., Koyama R., Kuboki H., Kumagai K., Maie T., Nagase M., Nakagawa T., Ohnishi J., Okuno H., Sakamoto N., Sato Y., Suda K., Watanabe T., Yamada K., Yokouchi S., and Yano Y.: "Present status of RIKEN heavy-ion linac", Proceedings of LINAC 08, Canada, Victoria, 2008–9〜10, TRIUMF, Vancouver, pp. 112–114 (2010).

青木孝道, Stingelin L., 上垣外修一, 坂本成彦, 福西暢尚, 横内茂, 加瀬昌之, 後藤彰: "Rebuncher resonator between RRC and fRC in RIKEN", 第 3 回日本加速器学会年会・第 31 回リニアック技術研究会論文集, 仙台, 2006–8, Japan Accelerator Society, 仙台, pp. 801–803 (2006).

上垣外修一, 藤巻正樹, 藤縄雅, 福西暢尚, 後藤彰, 長谷部裕雄, 日暮祥英, 池上九三男, 池沢英二, 影山正, 加瀬昌之, 木寺正憲, 込山美咲, 久保木浩功, 熊谷桂子, 眞家武士, 長瀬誠, 中川孝秀, 大西純一, 奥野広樹, 龍頭啓充, 坂本成彦, 佐藤洋一, 須田健嗣, 若杉昌徳, 渡辺博, 渡邉環, 山田一成, 横内茂, 矢野安重: "理研 RI ビームファクトリーの現状", 第 5 回日本加速器学会年会・第 33 回リニアック技術研究会論文集, 東広島, 2008–8, 日本加速器学会, 東広島, pp. 10–12 (2008).

(Others)

Suda K., Arai S., Chiba Y., Kamigaito O., Kase M., Sakamoto N., and Yamada K.: "Drift Tube Linac Cavities with Space-Saving Amplifier Coupling of New Injector for RI-Beam Factory", Proceedings of of the 1st International Particle Accelerator Conference (IPAC'10), Kyoto, 2010–5, The IPAC'10 Organizing Committee and Asian Committee for Future Accelerators, Kyoto, pp. 3726–3728 (2010).

須田健嗣, 小山亮, 加瀬昌之, 上垣外修一, 坂本成彦, 福西暢尚, 藤巻正樹, 山田一成, 渡邉環: "RIBF における高周波系の安定度", 第 5 回日本加速器学会年会・第 33 回リニアック技術研究会論文集, 東広島, 2008–8, 日本加速器学会, 東京, pp. 379–381 (2008).

須田健嗣, 藤巻正樹, 福西暢尚, 逸見政武, 上垣外修一, 加瀬昌之, 小山亮, 熊谷桂子, 坂本成彦, 渡邉環, 山田一成: "理研 RIBF における高周波系およびビームの安定度", 第 6 回日本加速器学会要旨集, 茨城県東海村, 2009–8, 日本加速器学会, 東京, pp. 397–400 (2009).

上垣外修一, 新井重昭, 藤巻正樹, 藤縄雅, 藤澤博, 福西暢尚, 後藤彰, 日暮祥英, 池沢英二, 影山正, 加瀬昌之, 込山美咲, 久保木浩功, 熊谷桂子, 眞家武士, 長瀬誠, 中川孝秀, 大西純一, 奥野広樹, 坂本成彦, 佐藤洋一, 須田健嗣, 渡辺博, 渡邉環, 渡邉裕, 山田一成, 山澤秀行, 矢野安重, 横内茂: "Intensity-upgrade plans of RIKEN RI-Beam Factory", 第 6 回日本加速器学会年会プロシーディングス, 東海村, 2009–8, 日本加速器学会, 東海村, pp. 38–41 (2010).

Oral Presentations

(International Conference etc.)

Kamigaito O., Ikezawa E., Kase M., Fujimaki M., Fujinawa T., Fukunishi N., Goto A., Haba H., Higurashi Y., Kidera M., Komiyama M., Koyama R., Kuboki H., Kumagai K., Maie T., Nagase M., Nakagawa T., Ohnishi J., Okuno H., Sakamoto N., Sato Y., Suda K., Watanabe T., Yamada K., Yokouchi S., and Yano Y.: "Present status of RIKEN heavy-ion linac", 24th International Linear Accelerator Conference (LINAC08), (LINAC08 Organizing Committee), Victoria, Canada, Sept.–Oct. (2008).

Kamigaito O., Arai S., Fujimaki M., Fujinawa T., Fujisawa H., Fukunishi N., Goto A., Higurashi Y., Ikezawa E., Kageyama T., Kase M., Komiyama M., Kuboki H., Kumagai K., Maie T., Nagase M., Nakagawa T., Ohnishi J., Okuno H., Sakamoto N., Sato Y., Suda K., Watanabe H., Watanabe T., Watanabe Y., Yamada K., Yamasawa H., Yano Y., and Yokouchi S.: "Intensity-upgrade plans of RIKEN RI-Beam Factory", 11th International Conference on Heavy Ion Accelerator Technology (HIAT09), (HIAT09 International Organizing Committee), Venezia, Italy, June (2009).

Okuno H., Dantsuka T., Yamada K., Kase M., Maie T., and Kamigaito O.: "Superconducting Ring Cyclotron for RIKEN RI Beam Factory in Japan", Cryogenic Engineering Conference and the International Cryogenic Materials Conference (CEC/ICMC 2009), Tucson, USA, June–July (2009).

Suda K., Arai S., Chiba Y., Kamigaito O., Kase M., Sakamoto N., and Yamada K.: "Drift Tube Linac Cavities with Space-Saving Amplifier Coupling of New Injector for RIKEN RI-Beam Factory", 1st International Particle Accelerator Conference (IPAC'10), (Science Council of Japan, The Physical Society of Japan, Particle Accelerator Society of Japan, and Ato), Kyoto, May (2010).

Watanabe T., Fukunishi N., Sasaki Y., Kase M., Goto A., and Kamigaito O.: "Development of beam current monitor with high Tc SQUID at RIBF", 2010 Beam Instrumentation Workshop (BIW10), (Los Alamos National Laboratory), Santa Fe, USA, May (2010).

Ichikawa Y., Onishi T. K., Suzuki D., Iwasaki H., Kubo T., Naik V., Chakrabarti A., Aoi N., Brown A. B., Fukuda N., Kubono S., Motobayashi T., Nakabayashi T., Nakamura T., Nakao T., Okumura T., Ong J. H., Suzuki H., Suzuki M. K., Teranishi T., Yamada K., Yamaguchi H., and Sakurai H.: "Proton-rich nuclear structure and mirror asymmetry investigated by β-decay spectroscopy of ^{24}Si", International Nuclear Physics Conference (INPC2010), (TRIUMF at the University of British Columbia), Vancouver, Canada, July (2010).

Watanabe T., Fujimaki M., Fukunishi N., Kase M., Komiyama M., Sakamoto N., Watanabe H., Yamada K., Kamigaito O., and Koyama R.: "Beam dignostics for RIBF in RIKEN", 19th International Conference on Cyclotrons and their Applications (CYCLOTRONS 2010), (Institue of Modern Physics , Lanzhou, China), Lanzhou, China, Sept. (2010).

Suda K., Fujimaki M., Fukunishi N., Hemmi M., Kamigaito O., Kase M., Koyama R., Kumagai K., Sakamoto N., and Yamada K.: "Stable Operation of RF Systems for RIBF", 19th International Conference on Cyclotrons and their Applications (CYCLOTRONS 2010), (Institute of Modern Physics, Chinese Academy of Sciences), Lanzhou, China, Sept. (2010).

Kamigaito O., Arai S., Dantsuka T., Fujimaki M., Fujinawa T., Fujisawa H., Fukunishi N., Goto A., Hasebe H., Higurashi Y., Ikegami K., Ikezawa E., Imao H., Kageyama T., Kase M., Kidera M., Komiyama M., Kuboki H., Kumagai K., Maie T., Nagase M., Nakagawa T., Nakamura M., Ohnishi J., Okuno H., Sakamoto N., Suda K., Watanabe H., Watanabe Y., Watanabe T., Yamada K., Yamasawa H., Yokouchi S., and Yano Y.: "Status of RIBF accelerators at RIKEN", 19th International Conference on Cyclotrons and their Applications (CYCLOTRONS 2010), (Cyclotrons2010 International Organizing Committee), Lanzhou, China, Sept. (2010).

(Domestic Conference)

上垣外修一, 藤巻正樹, 藤縄雅, 福西暢尚, 後藤彰, 長谷部裕雄, 日暮祥英, 池上九三男, 池沢英二, 影山正, 加瀬昌之, 木寺正憲, 込山美咲, 久保木浩功, 熊谷桂子, 眞家武士, 長瀬誠, 中川孝秀, 大西純一, 奥野広樹, 龍頭啓充, 坂本成彦, 佐藤洋一, 須田健嗣, 若杉昌徳, 渡辺博, 渡邉環, 山田一成, 横内茂, 矢野安重: "理研 RI ビームファクトリーの現状", 第 5 回日本加速器学会年会/第 33 回リニアック技術研究会, (日本加速器学会), 東広島, 8 月 (2008).

上垣外修一, 新井重昭, 藤巻正樹, 藤縄雅, 藤澤博, 福西暢尚, 後藤彰, 日暮祥英, 池沢英二, 影山正, 加瀬昌之, 込山美咲, 久保木浩功, 熊谷桂子, 眞家武士, 長瀬誠, 中川孝秀, 大西純一, 奥野広樹, 坂本成彦, 佐藤洋一, 須田健嗣, 渡辺博, 渡邉環, 渡邉裕, 山田一成, 山澤秀行, 矢野安重, 横内茂: "理研 RIBF のビーム増強計画", 第 6 回日本加速器学会年会, (日本加速器学会), 茨城県東海村, 8 月 (2009).

寺岡毅, 澤野郁夫, 中嶌輝子, 加々美裕, 神尾章子, 浜部直哉, 林依子, 龍頭啓充, 福西暢尚, 阿部知子: "重イオンビーム照射によるウンシュウミカンの形態変異の誘発", 第 7 回イオンビーム育種研究会大会, (イオン育種研究会), 鳥栖, 5–6 月 (2010).

渡邉裕, 池沢英二, 今尾浩士, 大西純一, 奥野広樹, 加瀬昌之, 上垣外修一, 熊谷桂子, 後藤彰, 込山美咲, 坂本成彦, 須田健嗣, 中川孝秀, 日暮祥英, 福西暢尚, 藤縄雅, 藤巻正樹, 眞家武士, 山田一成, 山澤秀行, 横内茂, 渡邉環, 渡辺博, 新井重昭, 佐藤洋一: "理研リニアック新入射器システム (RILAC2) の建設状況", 第 7 回日本加速器学会年会, (日本加速器学会), 姫路, 8 月 (2010).

渡邉環, 福西暢尚, 加瀬昌之, 若杉昌徳, 藤巻正樹, 山田一成, 坂本成彦, 小高康照, 小山亮, 仲村武志, 上垣外修一: "RIBF におけるビームエネルギーと縦方向のビームプロファイル測定システムの改良", 第 7 回日本加速器学会年会, (日本加速器学会), 姫路, 8 月 (2010).

山田一成, 池沢英二, 今尾浩士, 大西純一, 奥野広樹, 加瀬昌之, 熊谷桂子, 込山美咲, 後藤彰, 坂本成彦, 須田健嗣, 中川孝秀, 日暮祥英, 福西暢尚, 藤縄雅, 藤巻正樹, 眞家武士, 山澤秀行, 横内茂, 渡邉環, 渡辺博, 渡邉裕, 新井重昭, 藤澤博, 佐藤洋一, 上垣外修一: "理研 RIBF 用の新しい重イオン入射ライナック RILAC2 の製作", 第 7 回日本加速器学会年会, (日本加速器学会), 姫路, 8 月 (2010).

Cryogenic Technology Team

Publications

[Journal]

（Others）

Okuno H., Dantsuka T., Yamada K., Kase M., Maie T., and Kamigaito O.: "Superconducting Ring Cyclotron for RIKEN RI Beam Factory in Japan", AIP Conf. Proc. **1218**, 1410–1417 (2010).

[Book・ Proceedings]

（Original Papers） *Subject to Peer Review

Kamigaito O., Arai S., Fujimaki M., Fujinawa T., Fujisawa H., Fukunishi N., Goto A., Higurashi Y., Ikezawa E., Kageyama T., Kase M., Komiyama M., Kuboki H., Kumagai K., Maie T., Nagase M., Nakagawa T., Ohnishi J., Okuno H., Sakamoto N., Sato Y., Suda K., Watanabe H., Watanabe T., Watanabe Y., Yamada K., Yamasawa H., Yano Y., and Yokouchi S.: "Intensity-upgrade plans of RIKEN RI-Beam Factory", Proceedings of 11th International Conference on Heavy Ion Accelerator Technology (HIAT09), Venezia, Italy, 2009–6, HIAT09 International Organizing Committee, Venice, pp. 21–25 (2009).

Kamigaito O., Ikezawa E., Kase M., Fujimaki M., Fujinawa T., Fukunishi N., Goto A., Haba H., Higurashi Y., Kidera M., Komiyama M., Koyama R., Kuboki H., Kumagai K., Maie T., Nagase M., Nakagawa T., Ohnishi J., Okuno H., Sakamoto N., Sato Y., Suda K., Watanabe T., Yamada K., Yokouchi S., and Yano Y.: "Present status of RIKEN heavy-ion linac", Proceedings of LINAC 08, Canada, Victoria, 2008–9〜10, TRIUMF, Vancouver, pp. 112–114 (2010).

上垣外修一, 藤巻正樹, 藤縄雅, 福西暢尚, 後藤彰, 長谷部裕雄, 日暮祥英, 池上九三男, 池沢英二, 影山正, 加瀬昌之, 木寺正憲, 込山美咲, 久保木浩功, 熊谷桂子, 眞家武士, 長瀬誠, 中川孝秀, 大西純一, 奥野広樹, 龍頭啓充, 坂本成彦, 佐藤洋一, 須田健嗣, 若杉昌徳, 渡辺博, 渡邉環, 山田一成, 横内茂, 矢野安重: "理研 RI ビームファクトリーの現状", 第 5 回日本加速器学会年会・第 33 回リニアック技術研究会論文集, 東広島, 2008–8, 日本加速器学会, 東広島, pp. 10–12 (2008).

（Others）

上垣外修一, 新井重昭, 藤巻正樹, 藤縄雅, 藤澤博, 福西暢尚, 後藤彰, 日暮祥英, 池沢英二, 影山正, 加瀬昌之, 込山美咲, 久保木浩功, 熊谷桂子, 眞家武士, 長瀬誠, 中川孝秀, 大西純一, 奥野広樹, 坂本成彦, 佐藤洋一, 須田健嗣, 渡辺博, 渡邉環, 渡邉裕, 山田一成, 山澤秀行, 矢野安重, 横内茂: "Intensity-upgrade plans of RIKEN RI-Beam Factory", 第 6 回日本加速器学会年会プロシーディングス, 東海村, 2009–8, 日本加速器学会, 東海村, pp. 38–41 (2010).

Oral Presentations

(International Conference etc.)

Kamigaito O., Ikezawa E., Kase M., Fujimaki M., Fujinawa T., Fukunishi N., Goto A., Haba H., Higurashi Y., Kidera M., Komiyama M., Koyama R., Kuboki H., Kumagai K., Maie T., Nagase M., Nakagawa T., Ohnishi J., Okuno H., Sakamoto N., Sato Y., Suda K., Watanabe T., Yamada K., Yokouchi S., and Yano Y.: "Present status of RIKEN heavy-ion linac", 24th International Linear Accelerator Conference (LINAC08), (LINAC08 Organizing Committee), Victoria, Canada, Sept.–Oct. (2008).

Kamigaito O., Arai S., Fujimaki M., Fujinawa T., Fujisawa H., Fukunishi N., Goto A., Higurashi Y., Ikezawa E., Kageyama T., Kase M., Komiyama M., Kuboki H., Kumagai K., Maie T., Nagase M., Nakagawa T., Ohnishi J., Okuno H., Sakamoto N., Sato Y., Suda K., Watanabe H., Watanabe T., Watanabe Y., Yamada K., Yamasawa H., Yano Y., and Yokouchi S.: "Intensity-upgrade plans of RIKEN RI-Beam Factory", 11th International Conference on Heavy Ion Accelerator Technology (HIAT09), (HIAT09 International Organizing Committee), Venezia, Italy, June (2009).

Okuno H., Dantsuka T., Yamada K., Kase M., Maie T., and Kamigaito O.: "Superconducting Ring Cyclotron for RIKEN RI Beam Factory in Japan", Cryogenic Engineering Conference and the International Cryogenic Materials Conference (CEC/ICMC 2009), Tucson, USA, June–July (2009).

Kamigaito O., Arai S., Dantsuka T., Fujimaki M., Fujinawa T., Fujisawa H., Fukunishi N., Goto A., Hasebe H., Higurashi Y., Ikegami K., Ikezawa E., Imao H., Kageyama T., Kase M., Kidera M., Komiyama M., Kuboki H., Kumagai K., Maie T., Nagase M., Nakagawa T., Nakamura M., Ohnishi J., Okuno H., Sakamoto N., Suda K., Watanabe H., Watanabe Y., Watanabe T., Yamada K., Yamasawa H., Yokouchi S., and Yano Y.: "Status of RIBF accelerators at RIKEN", 19th International Conference on Cyclotrons and their Applications (CYCLOTRONS 2010), (Cyclotrons2010 International Organizing Committee), Lanzhou, China, Sept. (2010).

(Domestic Conference)

上垣外修一, 藤巻正樹, 藤縄雅, 福西暢尚, 後藤彰, 長谷部裕雄, 日暮祥英, 池上九三男, 池沢英二, 影山正, 加瀬昌之, 木寺正憲, 込山美咲, 久保木浩功, 熊谷桂子, 眞家武士, 長瀬誠, 中川孝秀, 大西純一, 奥野広樹, 龍頭啓充, 坂本成彦, 佐藤洋一, 須田健嗣, 若杉昌徳, 渡辺博, 渡邉環, 山田一成, 横内茂, 矢野安重: "理研 RI ビームファクトリーの現状", 第 5 回日本加速器学会年会/第 33 回リニアック技術研究会, (日本加速器学会), 東広島, 8 月 (2008).

上垣外修一, 新井重昭, 藤巻正樹, 藤縄雅, 藤澤博, 福西暢尚, 後藤彰, 日暮祥英, 池沢英二, 影山正, 加瀬昌之, 込山美咲, 久保木浩功, 熊谷桂子, 眞家武士, 長瀬誠, 中川孝秀, 大西純一, 奥野広樹, 坂本成彦, 佐藤洋一, 須田健嗣, 渡辺博, 渡邉環, 渡邉裕, 山田一成, 山澤秀行, 矢野安重, 横内茂: "理研 RIBF のビーム増強計画", 第 6 回日本加速器学会年会, (日本加速器学会), 茨城県東海村, 8 月 (2009).

渡邉裕, 池沢英二, 今尾浩士, 大西純一, 奥野広樹, 加瀬昌之, 上垣外修一, 熊谷桂子, 後藤彰, 込山美咲, 坂本成彦, 須田健嗣, 中川孝秀, 日暮祥英, 福西暢尚, 藤縄雅, 藤巻正樹,

眞家武士, 山田一成, 山澤秀行, 横内茂, 渡邉環, 渡辺博, 新井重昭, 佐藤洋一: “理研リニアック新入射器システム (RILAC2) の建設状況”, 第 7 回日本加速器学会年会, (日本加速器学会), 姫路, 8 月 (2010).

山田一成, 池沢英二, 今尾浩士, 大西純一, 奥野広樹, 加瀬昌之, 熊谷桂子, 込山美咲, 後藤彰, 坂本成彦, 須田健嗣, 中川孝秀, 日暮祥英, 福西暢尚, 藤縄雅, 藤巻正樹, 眞家武士, 山澤秀行, 横内茂, 渡邉環, 渡辺博, 渡邉裕, 新井重昭, 藤澤博, 佐藤洋一, 上垣外修一: “理研 RIBF 用の新しい重イオン入射ライナック RILAC2 の製作”, 第 7 回日本加速器学会年会, (日本加速器学会), 姫路, 8 月 (2010).

Instrumentation Development Group

Publications

[Book・ Proceedings]

(Original Papers) *Subject to Peer Review

Kamigaito O., Arai S., Fujimaki M., Fujinawa T., Fujisawa H., Fukunishi N., Goto A., Higurashi Y., Ikezawa E., Kageyama T., Kase M., Komiyama M., Kuboki H., Kumagai K., Maie T., Nagase M., Nakagawa T., Ohnishi J., Okuno H., Sakamoto N., Sato Y., Suda K., Watanabe H., Watanabe T., Watanabe Y., Yamada K., Yamasawa H., Yano Y., and Yokouchi S.: "Intensity-upgrade plans of RIKEN RI-Beam Factory", Proceedings of 11th International Conference on Heavy Ion Accelerator Technology (HIAT09), Venezia, Italy, 2009–6, HIAT09 International Organizing Committee, Venice, pp. 21–25 (2009).

Kamigaito O., Ikezawa E., Kase M., Fujimaki M., Fujinawa T., Fukunishi N., Goto A., Haba H., Higurashi Y., Kidera M., Komiyama M., Koyama R., Kuboki H., Kumagai K., Maie T., Nagase M., Nakagawa T., Ohnishi J., Okuno H., Sakamoto N., Sato Y., Suda K., Watanabe T., Yamada K., Yokouchi S., and Yano Y.: "Present status of RIKEN heavy-ion linac", Proceedings of LINAC 08, Canada, Victoria, 2008–9〜10, TRIUMF, Vancouver, pp. 112–114 (2010).

上垣外修一, 藤巻正樹, 藤縄雅, 福西暢尚, 後藤彰, 長谷部裕雄, 日暮祥英, 池上九三男, 池沢英二, 影山正, 加瀬昌之, 木寺正憲, 込山美咲, 久保木浩功, 熊谷桂子, 眞家武士, 長瀬誠, 中川孝秀, 大西純一, 奥野広樹, 龍頭啓充, 坂本成彦, 佐藤洋一, 須田健嗣, 若杉昌徳, 渡辺博, 渡邉環, 山田一成, 横内茂, 矢野安重: "理研 RI ビームファクトリーの現状", 第 5 回日本加速器学会年会・第 33 回リニアック技術研究会論文集, 東広島, 2008–8, 日本加速器学会, 東広島, pp. 10–12 (2008).

(Others)

上垣外修一, 新井重昭, 藤巻正樹, 藤縄雅, 藤澤博, 福西暢尚, 後藤彰, 日暮祥英, 池沢英二, 影山正, 加瀬昌之, 込山美咲, 久保木浩功, 熊谷桂子, 眞家武士, 長瀬誠, 中川孝秀, 大西純一, 奥野広樹, 坂本成彦, 佐藤洋一, 須田健嗣, 渡辺博, 渡邉環, 渡邉裕, 山田一成, 山澤秀行, 矢野安重, 横内茂: "Intensity-upgrade plans of RIKEN RI-Beam Factory", 第 6 回日本加速器学会年会プロシーディングス, 東海村, 2009–8, 日本加速器学会, 東海村, pp. 38–41 (2010).

Oral Presentations

(International Conference etc.)

Kamigaito O., Ikezawa E., Kase M., Fujimaki M., Fujinawa T., Fukunishi N., Goto A., Haba H., Higurashi Y., Kidera M., Komiyama M., Koyama R., Kuboki H., Kumagai K., Maie T., Nagase M., Nakagawa T., Ohnishi J., Okuno H., Sakamoto N., Sato Y., Suda K., Watanabe T., Yamada K., Yokouchi S., and Yano Y.: "Present status of RIKEN heavy-ion linac", 24th International Linear Accelerator Conference (LINAC08), (LINAC08 Organizing Committee), Victoria, Canada, Sept.–Oct. (2008).

Kamigaito O., Arai S., Fujimaki M., Fujinawa T., Fujisawa H., Fukunishi N., Goto A., Higurashi Y., Ikezawa E., Kageyama T., Kase M., Komiyama M., Kuboki H., Kumagai K., Maie T., Nagase M., Nakagawa T., Ohnishi J., Okuno H., Sakamoto N., Sato Y., Suda K., Watanabe H., Watanabe T., Watanabe Y., Yamada K., Yamasawa H., Yano Y., and Yokouchi S.: "Intensity-upgrade plans of RIKEN RI-Beam Factory", 11th International Conference on Heavy Ion Accelerator Technology (HIAT09), (HIAT09 International Organizing Committee), Venezia, Italy, June (2009).

Fujinawa T.: "The 7th Internatinal Workshop on Accelerator Opration: Training syllabus for NISHINA center", 7th International Workshop on Accelerator Operations, (KAERI), Daejeon, Korea, Apr. (2010).

Watanabe T., Fujimaki M., Fukunishi N., Kase M., Komiyama M., Sakamoto N., Watanabe H., Yamada K., Kamigaito O., and Koyama R.: "Beam dignostics for RIBF in RIKEN", 19th International Conference on Cyclotrons and their Applications (CYCLOTRONS 2010), (Institue of Modern Physics , Lanzhou, China), Lanzhou, China, Sept. (2010).

Kamigaito O., Arai S., Dantsuka T., Fujimaki M., Fujinawa T., Fujisawa H., Fukunishi N., Goto A., Hasebe H., Higurashi Y., Ikegami K., Ikezawa E., Imao H., Kageyama T., Kase M., Kidera M., Komiyama M., Kuboki H., Kumagai K., Maie T., Nagase M., Nakagawa T., Nakamura M., Ohnishi J., Okuno H., Sakamoto N., Suda K., Watanabe H., Watanabe Y., Watanabe T., Yamada K., Yamasawa H., Yokouchi S., and Yano Y.: "Status of RIBF accelerators at RIKEN", 19th International Conference on Cyclotrons and their Applications (CYCLOTRONS 2010), (Cyclotrons2010 International Organizing Committee), Lanzhou, China, Sept. (2010).

(Domestic Conference)

上垣外修一, 藤巻正樹, 藤縄雅, 福西暢尚, 後藤彰, 長谷部裕雄, 日暮祥英, 池上九三男, 池沢英二, 影山正, 加瀬昌之, 木寺正憲, 込山美咲, 久保木浩功, 熊谷桂子, 眞家武士, 長瀬誠, 中川孝秀, 大西純一, 奥野広樹, 龍頭啓充, 坂本成彦, 佐藤洋一, 須田健嗣, 若杉昌徳, 渡辺博, 渡邉環, 山田一成, 横内茂, 矢野安重: "理研 RI ビームファクトリーの現状", 第 5 回日本加速器学会年会/第 33 回リニアック技術研究会, (日本加速器学会), 東広島, 8 月 (2008).

上垣外修一, 新井重昭, 藤巻正樹, 藤縄雅, 藤澤博, 福西暢尚, 後藤彰, 日暮祥英, 池沢英二, 影山正, 加瀬昌之, 込山美咲, 久保木浩功, 熊谷桂子, 眞家武士, 長瀬誠, 中川孝秀, 大西純一, 奥野広樹, 坂本成彦, 佐藤洋一, 須田健嗣, 渡辺博, 渡邉環, 渡邉裕, 山田一成, 山澤秀行, 矢野安重, 横内茂: "理研 RIBF のビーム増強計画", 第 6 回日本加速器学会年会, (日本加速器学会), 茨城県東海村, 8 月 (2009).

小沢顕, 鈴木宏, 長江大輔, 新井一郎, 森口哲朗, 伊藤由太, 長谷部裕雄, 藤縄雅, 福西暢尚, 後藤彰, 大西哲哉, 櫻井博儀, 若杉昌徳, 山口由高, 矢野安重, 鈴木健, 山口貴之, 菊池崇志, 大坪隆, 安田裕介, 久保野茂: "RIBF における稀

少 RI リング", RIBF に於ける測定器についての検討会, 和光, 12 月 (2009).

小沢顕, 新井一郎, 伊藤由太, 森口哲朗, 長江大輔, 鈴木宏, 藤縄雅, 福西暢尚, 後藤彰, 長谷部裕雄, 大西哲哉, 櫻井博儀, 若杉昌徳, 山口由高, 矢野安重, 鈴木健, 山口貴之, 菊池崇志, 大坪隆, 安田裕介, 久保野茂: "RIBF に於ける稀少 RI リング計画", 蓄積リング検討ミニワークショップ, (大阪大学　核物理研究センター), 茨木, 1 月 (2010).

渡邉裕, 池沢英二, 今尾浩士, 大西純一, 奥野広樹, 加瀬昌之, 上垣外修一, 熊谷桂子, 後藤彰, 込山美咲, 坂本成彦, 須田健嗣, 中川孝秀, 日暮祥英, 福西暢尚, 藤縄雅, 藤巻正樹, 眞家武士, 山田一成, 山澤秀行, 横内茂, 渡邉環, 渡辺博, 新井重昭, 佐藤洋一: "理研リニアック新入射器システム (RILAC2) の建設状況", 第 7 回日本加速器学会年会, (日本加速器学会), 姫路, 8 月 (2010).

山田一成, 池沢英二, 今尾浩士, 大西純一, 奥野広樹, 加瀬昌之, 熊谷桂子, 込山美咲, 後藤彰, 坂本成彦, 須田健嗣, 中川孝秀, 日暮祥英, 福西暢尚, 藤縄雅, 藤巻正樹, 眞家武士, 山澤秀行, 横内茂, 渡邉環, 渡辺博, 渡邉裕, 新井重昭, 藤澤博, 佐藤洋一, 上垣外修一: "理研 RIBF 用の新しい重イオン入射ライナック RILAC2 の製作", 第 7 回日本加速器学会年会, (日本加速器学会), 姫路, 8 月 (2010).

鈴木宏, 新井一郎, 藤縄雅, 福西暢尚, 後藤彰, 菊池崇志, 久保野茂, 森口哲朗, 長江大輔, 大坪隆, 小沢顕, 櫻井博儀, 鈴木健, 若杉昌徳, 安田裕介, 山口貴之, 山口由高, 矢野安重: "理研稀少 RI リングの粒子軌道計算", 日本物理学会 2010 年秋季大会, (日本物理学会), 北九州, 9 月 (2010).

藤縄雅: "理研仁科加速器研究センター RI ビームファクトリーの電力供給方式", 日本大学生産工学部第 43 回学術講演会, 習志野, 12 月 (2010).

Instrumentation Development Group

Publications

[Journal]

(Others)

Yasuda Y., Ozawa A., Arai I., Fujinawa T., Fukunishi N., Goto A., Ohnishi T., Sakurai H., Wakasugi M., Yamaguchi Y., Yano Y., Suzuki T., Yamaguchi T., Kikuchi T., and Ohtsubo T.: "Present status of rare-RI ring project in RIKEN RIBF", Int. J. Mod. Phys. E **18**, No. 2, pp. 459–464 (2009).

Arai I., Ozawa A., Yasuda Y., Fujinawa T., Fukunishi N., Goto A., Ohnishi T., Sakurai H., Wakasugi M., Yamaguchi Y., Yano Y., Suzuki T., Yamaguchi T., Kikuchi T., and Ohtsubo T.: "Beam optics simulation for rare-RI ring at RI beam factory in RIKEN", Int. J. Mod. Phys. E **18**, No. 2, pp. 498–504 (2009).

Oral Presentations

(Domestic Conference)

小沢顕, 鈴木宏, 長江大輔, 新井一郎, 森口哲朗, 伊藤由太, 長谷部裕雄, 藤縄雅, 福西暢尚, 後藤彰, 大西哲哉, 櫻井博儀, 若杉昌徳, 山口由高, 矢野安重, 鈴木健, 山口貴之, 菊池崇志, 大坪隆, 安田裕介, 久保野茂: "RIBF における稀少 RI リング", RIBF に於ける測定器についての検討会, 和光, 12 月 (2009).

小沢顕, 新井一郎, 伊藤由太, 森口哲朗, 長江大輔, 鈴木宏, 藤縄雅, 福西暢尚, 後藤彰, 長谷部裕雄, 大西哲哉, 櫻井博儀, 若杉昌徳, 山口由高, 矢野安重, 鈴木健, 山口貴之, 菊池崇志, 大坪隆, 安田裕介, 久保野茂: "RIBF に於ける稀少 RI リング計画", 蓄積リング検討ミニワークショップ, (大阪大学　核物理研究センター), 茨木, 1 月 (2010).

森口哲朗, 小沢顕, 伊藤由太, 鈴木宏, 長江大輔, 鈴木健, 山口貴之, 大坪隆, 大西哲哉, 山口由高, 金澤光隆: "RI ビーム粒子識別検出器の開発", 平成 21 年度 HIMAC 共同利用研究成果発表会, (独立行政法人放射線医学総合研究所), 千葉, 4 月 (2010).

渡邉環, 福西暢尚, 加瀬昌之, 若杉昌徳, 藤巻正樹, 山田一成, 坂本成彦, 小高康照, 小山亮, 仲村武志, 上垣外修一: "RIBF におけるビームエネルギーと縦方向のビームプロファイル測定システムの改良", 第 7 回日本加速器学会年会, (日本加速器学会), 姫路, 8 月 (2010).

鈴木宏, 新井一郎, 藤縄雅, 福西暢尚, 後藤彰, 菊池崇志, 久保野茂, 森口哲朗, 長江大輔, 大坪隆, 小沢顕, 櫻井博儀, 鈴木健, 若杉昌徳, 安田裕介, 山口貴之, 山口由高, 矢野安重: "理研稀少 RI リングの粒子軌道計算", 日本物理学会 2010 年秋季大会, (日本物理学会), 北九州, 9 月 (2010).

SLOWRI Team

Oral Presentations

(International Conference etc.)

Wada M.: "Precision measurements of the hyper ne constants and optical isotope shifts of ^{7,9,10,11} Be^{+}ions in an online ion trap", 5th conference on Trapped Charged Particles and Fundamental Physics (TCP2010), (University of Jyvaskylan), Saariselka, Finland, Apr. (2010).

Meissl W., Clever M., Maeshima K., Meissl E., Ikeda T., Tokesi K., Schury P. H., Miyamoto S., Kojima T., Kanai Y., Ogiwara K., Hamagaki M., Kobayashi T., Imamoto N., and Yamazaki Y.: "Precise micro-irradiation of individual living targets using MeV ion beams", 24th International Conference on Atomic Collisions in Solids (ICACS 24), Krakow, Poland, July (2010).

Meissl W., Ikeda T., Kobayashi T., Schury P. H., Meissl E., Ogiwara K., Hamagaki M., Clever M., Maeshima K., Kojima T., Kanai Y., Imamoto N., and Yamazaki Y.: "Towards three-dimensional ion beam confinement inside the cell", 9th International Microbeam Workshop, Darmstadt, Germany, July (2010).

Meissl W., Ikeda T., Clever M., Meissl E., Tokesi K., Schury P. H., Maeshima K., Miyamoto S., Kobayashi T., Kojima T., Kanai Y., Ogiwara K., Hamagaki M., Wada M., Imamoto N., and Yamazaki Y.: "CLOSED-TIP TAPERED GLASS CAPILLARIES AS A NOVEL TOOL FOR MICRO-IRRADIATION OF LIVING CELLS BY MeV ION BEAMS", 18th International Workshop on Inelastic Ion-Surface Collisions (IISC-18), (IISC), Gatlinburg, USA, Sept.–Oct. (2010).

(Domestic Conference)

小沢顕, 鈴木宏, 長江大輔, 新井一郎, 森口哲朗, 伊藤由太, 長谷部裕雄, 藤縄雅, 福西暢尚, 後藤彰, 大西哲哉, 櫻井博儀, 若杉昌徳, 山口由高, 矢野安重, 鈴木健, 山口貴之, 菊池崇志, 大坪隆, 安田裕介, 久保野茂: "RIBF における稀少 RI リング", RIBF に於ける測定器についての検討会, 和光, 12 月 (2009).

小沢顕, 新井一郎, 伊藤由太, 森口哲朗, 長江大輔, 鈴木宏, 藤縄雅, 福西暢尚, 後藤彰, 長谷部裕雄, 大西哲哉, 櫻井博儀, 若杉昌徳, 山口由高, 矢野安重, 鈴木健, 山口貴之, 菊池崇志, 大坪隆, 安田裕介, 久保野茂: "RIBF に於ける稀少 RI リング計画", 蓄積リング検討ミニワークショップ, (大阪大学　核物理研究センター), 茨木, 1 月 (2010).

森口哲朗, 小沢顕, 伊藤由太, 鈴木宏, 長江大輔, 鈴木健, 山口貴之, 大坪隆, 大西哲哉, 山口由高, 金澤光隆: "RI ビーム粒子識別検出器の開発", 平成 21 年度 HIMAC 共同利用研究成果発表会, (独立行政法人放射線医学総合研究所), 千葉, 4 月 (2010).

Polarized RI Beam Team

Publications

[Journal]

(Original Papers) *Subject to Peer Review

Ichikawa Y., Onishi T. K., Suzuki D., Iwasaki H., Kubo T., Naik V., Chakrabarti A., Aoi N., Brown A. B., Fukuda N., Kubono S., Motobayashi T., Nakabayashi T., Nakamura T., Nakao T., Okumura T., Ong J. H., Suzuki H., Suzuki M. K., Teranishi T., Yamada K., Yamaguchi H., and Sakurai H.: "Gamow-Teller transition of the proton-rich nucleus ^{24}Si", AIP Conf. Proc. **1235**, 265–269 (2010).

Ichikawa Y., Onishi T. K., Suzuki D., Iwasaki H., Kubo T., Naik V., Chakrabarti A., Aoi N., Brown A. B., Fukuda N., Kubono S., Motobayashi T., Nakabayashi T., Nakamura T., Nakao T., Okumura T., Ong J. H., Suzuki H., Suzuki M. K., Teranishi T., Yamada K., Yamaguchi H., and Sakurai H.: "Mirror asymmetry for B(GT) of ^{24}Si induced by Thomas-Ehrman shift", AIP Conf. Proc. **1238**, 290–293 (2010).

Furukawa T., Matsuo Y., Hatakeyama A., Fujikake K., Matsuura Y., Kobayashi T., and Shimoda T.: "Laser spectroscopy on exotic RI atoms in superfluid helium - OROCHI experiment -", Hyperfine Interact. **196**, 191–197 (2010). *

Ichikawa Y., Onishi T. K., Suzuki D., Iwasaki H., Kubo T., Naik V., Chakrabarti A., Aoi N., Brown A. B., Fukuda N., Kubono S., Motobayashi T., Nakabayashi T., Nakamura T., Nakao T., Okumura T., Ong J. H., Suzuki H., Suzuki M. K., Teranishi T., Yamada K., Yamaguchi H., and Sakurai H.: "Mirror asymmetry investigated by β decay of proton-rich ^{24}Si", Mod. Phys. Lett. A **25**, 1895–1898 (2010).

(Review)

市川雄一: "陽子過剰核 ^{24}Si のベータ崩壊とその鏡映対称性", 原子核研究 **55**, No. 1, pp. 33–42 (2010).

Oral Presentations

(International Conference etc.)

Ichikawa Y., Onishi T. K., Suzuki D., Iwasaki H., Kubo T., Naik V., Chakrabarti A., Aoi N., Brown A. B., Fukuda N., Kubono S., Motobayashi T., Nakabayashi T., Nakamura T., Nakao T., Okumura T., Ong J. H., Suzuki H., Suzuki M. K., Teranishi T., Yamada K., Yamaguchi H., and Sakurai H.: "Proton-rich nuclear structure and mirror asymmetry investigated by β-decay spectroscopy of ^{24}Si", International Nuclear Physics Conference (INPC2010), (TRIUMF at the University of British Columbia), Vancouver, Canada, July (2010).

Ichikawa Y., Ueno H., Ishii Y., Furukawa T., Yoshimi A., Kameda D., Aoi N., Watanabe H., Asahi K., Iijima H., Suzuki K., Inoue T., Tsuchiya M., Hayashi H., Nanao T., Kubo T., Inabe N., Ohnishi T., Takeda H., Fukuda N., Ishihara M., Daugas J., Chevrier R., Georgiev G., Rajabali M. M., and Balabanski D. L.: "g-factor measurement for isomeric state of ^{32}Al using two-step fragmentation reaction with dispersion matching", GCOE International Summer School: Hadrons and Nuclei under Extreme Conditions (HANEC2010), (Tokyo Institute of Technology), Tokyo, Sept. (2010).

Ueno H.: "Spin-oriented radioactive-isotope beams at RIBF", 19th International Spin Physics Symposium (SPIN 2010), (Forschungszentrum Juelich), Juelich, Germany, Sept.–Oct. (2010).

Tsukada K., Kasamatsu Y., Asai M., Toyoshima A., Ishii Y., Li Z., Sato T., Nagame Y., Schaedel M., Goto S., Hasegawa T., Kudo H., Haba H., Kudou Y., Kikunaga H., Ooe K., Fujisawa H., Sato W., Shinohara A., Oura Y., Akiyama K., Nanri T., Araki M., Yokoyama A., and Sueki K.: "Anion-exchange behavior of Db in HF and HNO3 mixed solution using an on-line chemical apparatus", International Chemical Congress of Pacific Basin Societies (PACIFICHEM 2010), (American Chemical Society), Honolulu, USA, Dec. (2010).

Toyoshima A., Tsukada K., Asai M., Kitatsuji Y., Ishii Y., Sato T., Li Z., Sato N., Kikuchi T., Nishinaka I., Nagame Y., Kasamatsu Y., Haba H., Ooe K., Shinohara A., Sato W., Akiyama K., Even J., and Schaedel M.: "Electrochemistry of the heaviest elements", International Chemical Congress of Pacific Basin Societies (PACIFICHEM 2010), (American Chemical Society), Honolulu, USA, Dec. (2010).

(Domestic Conference)

松浦佑一, 古川武, 小林徹, 畠山温, 加藤裕樹, 立川真樹, 松尾由賀利: "超流動ヘリウム中での光ポンピング法による Au 原子の偏極生成", 第 6 回停止・低速不安定核ビームを用いた核分光研究会, 東京, 3 月 (2010).

加藤裕樹, 古川武, 松浦佑一, 小林徹, 畠山温, 立川真樹, 松尾由賀利: "光ポンピングへ向けた超流動ヘリウム中での III 族原子 Ga, In 原子の励起スペクトル測定", 第 7 回 AMO 討論会, つくば, 6 月 (2010).

市川雄一: "陽子過剰核 ^{24}Si のベータ崩壊とその鏡映対称性", 日本物理学会 2010 年秋季大会, (日本物理学会), 北九州市, 9 月 (2010).

加藤裕樹, 古川武, 松浦佑一, 小林徹, 畠山温, 立川真樹, 松尾由賀利: "超流動ヘリウム中での III 族原子 In, Ga の励起スペクトル", 日本物理学会 2010 年秋季大会, 堺, 9 月 (2010).

市川雄一, 上野秀樹, 石井裕司, 古川武, 吉見彰洋, 亀田大輔, 青井考, 渡邉寛, 旭耕一郎, 飯島裕章, 鈴木都文, 井上壮志, 土屋真人, 林宏憲, 七尾翼, 久保敏幸, 稲辺尚人, 大西哲哉, 竹田浩之, 福田直樹, 石原正泰, Daugas J., Chevrier R., Georgiev G., Rajabali M. M., Balabanski D. L.: "分散整合二回散乱法による核スピン整列ＲＩビームの生成", 日本物理学会 2010 年秋季大会, (日本物理学会), 北九州, 9 月 (2010).

Rare RI-ring Team

Publications

[Journal]

(Original Papers)　*Subject to Peer Review

Yamaguchi Y., Suzuki T., Wu C., Ozawa A., Fang D., Fukuda M., Iwasa N., Izumikawa T., Ohnishi T., Ohtsubo T., Tanihata I., and Kanungo R.: "Density distribution of 17B from a reaction cross section measurement", Phys. Rev. C **70**, No. 5, p. 054320 (2004). *

(Others)

Yasuda Y., Ozawa A., Arai I., Fujinawa T., Fukunishi N., Goto A., Ohnishi T., Sakurai H., Wakasugi M., Yamaguchi Y., Yano Y., Suzuki T., Yamaguchi T., Kikuchi T., and Ohtsubo T.: "Present status of rare-RI ring project in RIKEN RIBF", Int. J. Mod. Phys. E **18**, No. 2, pp. 459–464 (2009).

Arai I., Ozawa A., Yasuda Y., Fujinawa T., Fukunishi N., Goto A., Ohnishi T., Sakurai H., Wakasugi M., Yamaguchi Y., Yano Y., Suzuki T., Yamaguchi T., Kikuchi T., and Ohtsubo T.: "Beam optics simulation for rare-RI ring at RI beam factory in RIKEN", Int. J. Mod. Phys. E **18**, No. 2, pp. 498–504 (2009).

Oral Presentations

(Domestic Conference)

小沢顕, 鈴木宏, 長江大輔, 新井一郎, 森口哲朗, 伊藤由太, 長谷部裕雄, 藤縄雅, 福西暢尚, 後藤彰, 大西哲哉, 櫻井博儀, 若杉昌徳, 山口由高, 矢野安重, 鈴木健, 山口貴之, 菊池崇志, 大坪隆, 安田裕介, 久保野茂: "RIBF における稀少 RI リング", RIBF に於ける測定器についての検討会, 和光, 12 月 (2009).

小沢顕, 新井一郎, 伊藤由太, 森口哲朗, 長江大輔, 鈴木宏, 藤縄雅, 福西暢尚, 後藤彰, 長谷部裕雄, 大西哲哉, 櫻井博儀, 若杉昌徳, 山口由高, 矢野安重, 鈴木健, 山口貴之, 菊池崇志, 大坪隆, 安田裕介, 久保野茂: "RIBF に於ける稀少 RI リング計画", 蓄積リング検討ミニワークショップ, (大阪大学　核物理研究センター), 茨木, 1 月 (2010).

森口哲朗, 小沢顕, 伊藤由太, 鈴木宏, 長江大輔, 鈴木健, 山口貴之, 大坪隆, 大西哲哉, 山口由高, 金澤光隆: "RI ビーム粒子識別検出器の開発", 平成 21 年度 HIMAC 共同利用研究成果発表会, (独立行政法人放射線医学総合研究所), 千葉, 4 月 (2010).

鈴木宏, 新井一郎, 藤縄雅, 福西暢尚, 後藤彰, 菊池崇志, 久保野茂, 森口哲朗, 長江大輔, 大坪隆, 小沢顕, 櫻井博儀, 鈴木健, 若杉昌徳, 安田裕介, 山口貴之, 山口由高, 矢野安重: "理研稀少 RI リングの粒子軌道計算", 日本物理学会 2010 年秋季大会, (日本物理学会), 北九州, 9 月 (2010).

Research Instruments Group

Publications

[Journal]

(Original Papers)　*Subject to Peer Review

Sugimoto T., Nakamura T., Kondo Y., Aoi N., Baba H., Bazin D. P., Fukuda N., Gomi T., Hasegawa H., Imai N., Ishihara M., Kobayashi T., Kubo T., Miura M., Motobayashi T., Otsu H., Saito A., Sakurai H., Shimoura S., A.M. V., Watanabe K., Watanabe Y., Yakushiji T., Yanagisawa Y., and Yoneda K.: "The first 2+ state of 14Be", Phys. Lett. B **654**, 160–164 (2007). *

Ichikawa Y., Onishi T. K., Suzuki D., Iwasaki H., Kubo T., Naik V., Chakrabarti A., Aoi N., Brown A. B., Fukuda N., Kubono S., Motobayashi T., Nakabayashi T., Nakamura T., Nakao T., Okumura T., Ong J. H., Suzuki H., Suzuki M. K., Teranishi T., Yamada K., Yamaguchi H., and Sakurai H.: "Gamow-Teller transition of the proton-rich nucleus ^{24}Si", AIP Conf. Proc. **1235**, 265–269 (2010).

Ichikawa Y., Onishi T. K., Suzuki D., Iwasaki H., Kubo T., Naik V., Chakrabarti A., Aoi N., Brown A. B., Fukuda N., Kubono S., Motobayashi T., Nakabayashi T., Nakamura T., Nakao T., Okumura T., Ong J. H., Suzuki H., Suzuki M. K., Teranishi T., Yamada K., Yamaguchi H., and Sakurai H.: "Mirror asymmetry for B(GT) of ^{24}Si induced by Thomas-Ehrman shift", AIP Conf. Proc. **1238**, 290–293 (2010).

Ichikawa Y., Onishi T. K., Suzuki D., Iwasaki H., Kubo T., Naik V., Chakrabarti A., Aoi N., Brown A. B., Fukuda N., Kubono S., Motobayashi T., Nakabayashi T., Nakamura T., Nakao T., Okumura T., Ong J. H., Suzuki H., Suzuki M. K., Teranishi T., Yamada K., Yamaguchi H., and Sakurai H.: "Mirror asymmetry investigated by β decay of proton-rich ^{24}Si", Mod. Phys. Lett. A **25**, 1895–1898 (2010).

Aoi N., Kanno S., Takeuchi S., Suzuki H., Bazin D. P., Bowen M. D., Campbell C. M., Cook J. M., Dinca D. -., Gade A., Glasmacher T., Iwasaki H., Kubo T., Kurita K., Motobayashi T., Mueller W. F., Nakamura T., Sakurai H., Takashina M., Terry J. R., Yoneda K., and Zwahlen H.: "Enhanced collectivity in 74Ni", Phys. Lett. B **692**, 302–306 (2010). *

Oral Presentations

(International Conference etc.)

Ichikawa Y., Onishi T. K., Suzuki D., Iwasaki H., Kubo T., Naik V., Chakrabarti A., Aoi N., Brown A. B., Fukuda N., Kubono S., Motobayashi T., Nakabayashi T., Nakamura T., Nakao T., Okumura T., Ong J. H., Suzuki H., Suzuki M. K., Teranishi T., Yamada K., Yamaguchi H., and Sakurai H.: "Proton-rich nuclear structure and mirror asymmetry investigated by β-decay spectroscopy of ^{24}Si", International Nuclear Physics Conference (INPC2010), (TRIUMF at the University of British Columbia), Vancouver, Canada, July (2010).

Ichikawa Y., Ueno H., Ishii Y., Furukawa T., Yoshimi A., Kameda D., Aoi N., Watanabe H., Asahi K., Iijima H., Suzuki K., Inoue T., Tsuchiya M., Hayashi H., Nanao T., Kubo T., Inabe N., Ohnishi T., Takeda H., Fukuda N., Ishihara M., Daugas J., Chevrier R., Georgiev G., Rajabali M. M., and Balabanski D. L.: "g-factor measurement for isomeric state of ^{32}Al using two-step fragmentation reaction with dispersion matching", GCOE International Summer School: Hadrons and Nuclei under Extreme Conditions (HANEC2010), (Tokyo Institute of Technology), Tokyo, Sept. (2010).

(Domestic Conference)

市川雄一, 上野秀樹, 石井裕司, 古川武, 吉見彰洋, 亀田大輔, 青井考, 渡邉寛, 旭耕一郎, 飯島裕章, 鈴木都文, 井上壮志, 土屋真人, 林宏憲, 七尾翼, 久保敏幸, 稲辺尚人, 大西哲哉, 竹田浩之, 福田直樹, 石原正泰, Daugas J., Chevrier R., Georgiev G., Rajabali M. M., Balabanski D. L.: "分散整合二回散乱法による核スピン整列ＲＩビームの生成", 日本物理学会 2010 年秋季大会, (日本物理学会), 北九州, 9 月 (2010).

GARIS Team

Publications

[Journal]

(Original Papers)　*Subject to Peer Review

Ideguchi E., Niikura M., Fukuchi T., Baba H., Iwasaki H., Kubo T., Komatsubara T., Uesaka M., Michimasa S., Morimoto K., Ohnishi T., Ota S., Ozawa A., Shimoura S., Suda T., Tanihata I., Wakabayashi Y., and Yoshida K.: "Study of high-spin states in the 48Ca region by using secondary fusion reactions", Eur. Phys. J. A **25**, No. s01, pp. 429–430 (2005). *

Oral Presentations

(Domestic Conference)

森本幸司, 加治大哉, 馬場秀忠, 門叶冬樹: "極短寿命な超重元素探索実験のための信号処理装置開発", 2010 日本放射化学会年会・第 54 回放射化学討論会, (日本放射化学会), 吹田, 9 月 (2010).

村上昌史, 村山裕史, 後藤真一, 加治大哉, 森本幸司, 羽場宏光, 笠松良崇, 工藤祐生, 米田晃, 森田浩介, 工藤久昭: "261a,bRf の合成と崩壊特性", 2010 日本放射化学会年会・第 54 回放射化学討論会, (日本放射化学会), 吹田, 9 月 (2010).

羽場宏光, 大江一弘, 大関和貴, 笠松良崇, 加治大哉, 菊永英寿, 工藤久昭, 工藤祐生, 小森有希子, 佐藤望, 篠原厚, 住田貴之, 塚田和明, 森田浩介, 森本幸司, 米田晃: "248Cm(22Ne,5n) 265Sg 反応による 265Sg の合成", 2010 日本放射化学会年会・第 54 回放射化学討論会, (日本放射化学会), 吹田, 9 月 (2010).

BigRIPS Team

Publications

[Journal]

(Original Papers)　*Subject to Peer Review

Aoi N., Kanno S., Takeuchi S., Suzuki H., Bazin D. P., Bowen M. D., Campbell C. M., Cook J. M., Dinca D. -., Gade A., Glasmacher T., Iwasaki H., Kubo T., Kurita K., Motobayashi T., Mueller W. F., Nakamura T., Sakurai H., Takashina M., Terry J. R., Yoneda K., and Zwahlen H.: "Enhanced collectivity in 74Ni", Phys. Lett. B **692**, 302–306 (2010). *

[Book・Proceedings]

(Original Papers)　*Subject to Peer Review

Ariyoshi S., Taino T., Dobroiu A., Sato H., Matsuo H., and Otani C.: "Evaluation of a Terahertz Detector based on a Superconducting Tunnel Junction Coupled to a Thin Superconductor Film", Proceedings of 35th International Conference on Infrared, Millimeter and Terahertz Waves (IRMMW-THz 2010), Rome, Italy, 2010–9, IRMMW-THz 2010, Rome, pp. Mo-P.18–Mo-P.18 (2010).

Oral Presentations

(International Conference etc.)

Ariyoshi S., Taino T., Dobroiu A., Sato H., Matsuo H., and Otani C.: "Evaluation of a Terahertz Detector based on a Superconducting Tunnel Junction Coupled to a Thin Superconductor Film", 35th International Conference on Infrared, Millimeter and Terahertz Waves (IRMMW-THz 2010), Rome, Italy, Sept. (2010).

SAMURAI Team

Publications

[Journal]

(Original Papers) *Subject to Peer Review

Kameda D., Asahi K., Ueno H., Yoshimi A., Haseyama T., Watanabe H., Miyoshi H., Shimada K., Kijima G., Nagae D., Kato G., Emori S., Tsukui M., Kobayashi Y., and Ishihara M.: "Magnetic moments of ^{30}Al an ^{32}Al", Czech. J. Phys. **55 Suppl. A**, 327–332 (2005). *

Ideguchi E., Niikura M., Fukuchi T., Baba H., Iwasaki H., Kubo T., Komatsubara T., Uesaka M., Michimasa S., Morimoto K., Ohnishi T., Ota S., Ozawa A., Shimoura S., Suda T., Tanihata I., Wakabayashi Y., and Yoshida K.: "Study of high-spin states in the 48Ca region by using secondary fusion reactions", Eur. Phys. J. A **25**, No. s01, pp. 429–430 (2005). *

Guo W., Fang D., Ma. Y., Ma. C., Wang K., Yang T., Cai X., Shen W., Sun Z., Ren Z., Chen J., Chen J., Liu G., Ma E., Ma G., Shi Y., Su Q., Tian W., Wang H., Zhong C., Zuo J., Hosoi M., Izumikawa T., Kanungo R., Nakajima S., Ohnishi T., Ohtsubo T., Ozawa A., Suda T., Sugawara K., Suzuki T., Takisawa A., Tanaka K., Yamaguchi T., and Tanihata I.: "Measurements of reaction cross section and fragment momentum distribution for N=10 proton-rich isotones", Int. J. Mod. Phys. E **15**, 1523–1530 (2006). *

Mazzocco M., Signorini C., Romoli M., Botteti R., De Francesco A., De Rosa A., Di Pietro M., Fortunato L., Glodariu T., Guglielmetti A., Inglima G., Ishikawa T., Ishiyama H., Kanungo R., Khai N., La Commara M., Jeong S., Martin B., Miyatake H., Motobayashi T., Nomura T., Pierroutsakou D., Sandoli M., Soramel F., Stroe L., Sugai I., Tanaka M., Vardaci E., Watanabe Y., Yoshida K., and Yoshida A.: "Elastic scattering for the system ^{11}Be+^{209}Bi at Coulomb barrier energies", Eur. Phys. J. Special Topics **150**, 37–40 (2007).

Kondo Y., Nakamura T., Sato Y., Matsumoto T., Aoi N., Endo N., Fukuda N., Gomi T., Hashimoto Y., Ishihara M., Kawai S., Kitayama M., Kobayashi T., Matsuda Y., Matsui N., Motobayashi T., Nakabayashi T., Ogata K., Okumura T., Ong H., Onishi T., Otsu H., Sakurai H., Shimoura S., Shinohara M., Sugimoto T., Takeuchi S., Tamaki M., Togano Y., and Yanagisawa Y.: "One-neutron removal reactions of ^{18}C and ^{19}C on a proton target", Phys. Rev. C **79**, No. 014602, pp. 014602-1–014602-7 (2009). *

Ichikawa Y., Onishi T. K., Suzuki D., Iwasaki H., Kubo T., Naik V., Chakrabarti A., Aoi N., Brown A. B., Fukuda N., Kubono S., Motobayashi T., Nakabayashi T., Nakamura T., Nakao T., Okumura T., Ong J. H., Suzuki H., Suzuki M. K., Teranishi T., Yamada K., Yamaguchi H., and Sakurai H.: "Gamow-Teller transition of the proton-rich nucleus ^{24}Si", AIP Conf. Proc. **1235**, 265–269 (2010).

Ichikawa Y., Onishi T. K., Suzuki D., Iwasaki H., Kubo T., Naik V., Chakrabarti A., Aoi N., Brown A. B., Fukuda N., Kubono S., Motobayashi T., Nakabayashi T., Nakamura T., Nakao T., Okumura T., Ong J. H., Suzuki H., Suzuki M. K., Teranishi T., Yamada K., Yamaguchi H., and Sakurai H.: "Mirror asymmetry for B(GT) of ^{24}Si induced by Thomas-Ehrman shift", AIP Conf. Proc. **1238**, 290–293 (2010).

Ichikawa Y., Onishi T. K., Suzuki D., Iwasaki H., Kubo T., Naik V., Chakrabarti A., Aoi N., Brown A. B., Fukuda N., Kubono S., Motobayashi T., Nakabayashi T., Nakamura T., Nakao T., Okumura T., Ong J. H., Suzuki H., Suzuki M. K., Teranishi T., Yamada K., Yamaguchi H., and Sakurai H.: "Mirror asymmetry investigated by β decay of proton-rich ^{24}Si", Mod. Phys. Lett. A **25**, 1895–1898 (2010).

Aoi N., Kanno S., Takeuchi S., Suzuki H., Bazin D. P., Bowen M. D., Campbell C. M., Cook J. M., Dinca D. -., Gade A., Glasmacher T., Iwasaki H., Kubo T., Kurita K., Motobayashi T., Mueller W. F., Nakamura T., Sakurai H., Takashina M., Terry J. R., Yoneda K., and Zwahlen H.: "Enhanced collectivity in 74Ni", Phys. Lett. B **692**, 302–306 (2010). *

(Others)

Yasuda Y., Ozawa A., Arai I., Fujinawa T., Fukunishi N., Goto A., Ohnishi T., Sakurai H., Wakasugi M., Yamaguchi Y., Yano Y., Suzuki T., Yamaguchi T., Kikuchi T., and Ohtsubo T.: "Present status of rare-RI ring project in RIKEN RIBF", Int. J. Mod. Phys. E **18**, No. 2, pp. 459–464 (2009).

Arai I., Ozawa A., Yasuda Y., Fujinawa T., Fukunishi N., Goto A., Ohnishi T., Sakurai H., Wakasugi M., Yamaguchi Y., Yano Y., Suzuki T., Yamaguchi T., Kikuchi T., and Ohtsubo T.: "Beam optics simulation for rare-RI ring at RI beam factory in RIKEN", Int. J. Mod. Phys. E **18**, No. 2, pp. 498–504 (2009).

Oral Presentations

(International Conference etc.)

Yoshida A.: "The BIGRIPS production target at RIBF", Stripper and Target Technology for High Power Heavy Ion Beams Workshop, (Facility for Rare Isotope Beams (FRIB) at MSU), East Lansing, USA, Dec. (2009).

Ichikawa Y., Onishi T. K., Suzuki D., Iwasaki H., Kubo T., Naik V., Chakrabarti A., Aoi N., Brown A. B., Fukuda N., Kubono S., Motobayashi T., Nakabayashi T., Nakamura T., Nakao T., Okumura T., Ong J. H., Suzuki H., Suzuki M. K., Teranishi T., Yamada K., Yamaguchi H., and Sakurai H.: "Proton-rich nuclear structure and mirror asymmetry investigated by β-decay spectroscopy of ^{24}Si", International Nuclear Physics Conference (INPC2010), (TRIUMF at the University of British Columbia), Vancouver, Canada, July (2010).

Ichikawa Y., Ueno H., Ishii Y., Furukawa T., Yoshimi A., Kameda D., Aoi N., Watanabe H., Asahi K., Iijima H., Suzuki K., Inoue T., Tsuchiya M., Hayashi H., Nanao T., Kubo T., Inabe N., Ohnishi T., Takeda H., Fukuda N., Ishihara M., Daugas J., Chevrier R., Georgiev G., Rajabali M. M., and Balabanski D. L.: "g-factor measurement for isomeric state of ^{32}Al using two-step fragmentation reaction with dispersion matching", GCOE International Summer School: Hadrons and Nuclei under Extreme Conditions (HANEC2010), (Tokyo Institute of Technology), Tokyo, Sept. (2010).

(Domestic Conference)

小沢顕, 鈴木宏, 長江大輔, 新井一郎, 森口哲朗, 伊藤由太, 長谷部裕雄, 藤縄雅, 福西暢尚, 後藤彰, 大西哲哉, 櫻井博儀, 若杉昌徳, 山口由高, 矢野安重, 鈴木健, 山口貴之, 菊池崇志, 大坪隆, 安田裕介, 久保野茂: "RIBF における稀少 RI リング", RIBF に於ける測定器についての検討会, 和光, 12 月 (2009).

小沢顕, 新井一郎, 伊藤由太, 森口哲朗, 長江大輔, 鈴木宏, 藤縄雅, 福西暢尚, 後藤彰, 長谷部裕雄, 大西哲哉, 櫻井博儀, 若杉昌徳, 山口由高, 矢野安重, 鈴木健, 山口貴之, 菊池崇志, 大坪隆, 安田裕介, 久保野茂: "RIBF に於ける稀少 RI リング計画", 蓄積リング検討ミニワークショップ, (大阪大学　核物理研究センター), 茨木, 1 月 (2010).

森口哲朗, 小沢顕, 伊藤由太, 鈴木宏, 長江大輔, 鈴木健, 山口貴之, 大坪隆, 大西哲哉, 山口由高, 金澤光隆: "RI ビーム粒子識別検出器の開発", 平成 21 年度 HIMAC 共同利用研究成果発表会, (独立行政法人放射線医学総合研究所), 千葉, 4 月 (2010).

上蓑義朋, 向井弘樹, 日暮利江子, 赤塩敦子, 福田弘幸, 坂本久雄, 吉田敦, 吉田光一: "理研 RIBF・BigRIPS 周辺における 2 次放射線測定", 日本原子力学会 2010 年秋の大会, (日本原子力学会), 札幌, 9 月 (2010).

市川雄一, 上野秀樹, 石井裕司, 古川武, 吉見彰洋, 亀田大輔, 青井考, 渡邉寛, 旭耕一郎, 飯島裕章, 鈴木都文, 井上壮志, 土屋真人, 林宏憲, 七尾翼, 久保敏幸, 稲辺尚人, 大西哲哉, 竹田浩之, 福田直樹, 石原正泰, Daugas J., Chevrier R., Georgiev G., Rajabali M. M., Balabanski D. L.: "分散整合二回散乱法による核スピン整列ＲＩビームの生成", 日本物理学会 2010 年秋季大会, (日本物理学会), 北九州, 9 月 (2010).

Computing and Network Team

Oral Presentations

(International Conference etc.)

Kobayashi T., Baba H., and Andrzejewski R. A.: "Three-dimensional medium-energy ion scattering", Professor Leszek Wojtczak Colloquium, (University of Lodz), Lodz, Poland, Sept. (2009).

Kobayashi T., Baba H., Maehara M., Shimoda S., Andrzejewski R. A., Ueno S., Kuwahara Y., and Sato T.: "Development of a compact system for three-dimensional medium-energy ion scattering", 5th International Workshop on High-Resolution Depth Profiling, (The Japan Society of Applied Physics), Kyoto, Nov. (2009).

(Domestic Conference)

森本幸司, 加治大哉, 馬場秀忠, 門叶冬樹: "極短寿命な超重元素探索実験のための信号処理装置開発", 2010 日本放射化学会年会・第 54 回放射化学討論会, (日本放射化学会), 吹田, 9 月 (2010).

Detector Team

Publications

[Journal]

(Original Papers)　*Subject to Peer Review

Matsuta K., Mihara M., Nagatomo T., Matsumiya R., Momota S., Ohtsubo T., Izumikawa T., Hirano H., Takahashi S., Nishimura D., Komurasaki J., Kitagawa A., Kanazawa M., Torikoshi M., Sato S., Fukuda M., Minamisono T., Sumikama T., Tanaka K., Takechi M., Ishikawa D., Pahlovy S. A., Nagano M., Nojiri Y., Alonso J. R., Krebs G. F., and Symons T. J.: "Hyperfine interaction of ^{25}Al in α-Al_2O_3 and its quadrupole moment", Hyperfine Interact. **180**, 65–69 (2008). *

Accelerator Applications Research Group

Oral Presentations

(Domestic Conference)

柳生田英徳, 仲島康行, 為ヶ井強, 神原正, 金井保之: “2.6 GeV の U 照射した Co ドープ $BaFe_2As_2$ における臨界電流密度と磁束ダイナミクス”, 日本物理学会 2010 年秋季大会, (社団法人日本物理学会), 堺, 9 月 (2010).

田縁俊光, 仲島康行, 為ヶ井強, 岡安悟, 神原正, 金井保之, 北村尚, 村上健: “重イオン照射した $FeTe_xSe_{1-x}$ における磁束ダイナミクスと核種依存性”, 日本物理学会 2010 年秋季大会, (社団法人日本物理学会), 堺, 9 月 (2010).

眞鍋理一郎, Arner E. A., 平野智也, 渋川登美子, 市田裕之, 川島麗, 荒川貴博, Daub C. O., 河合純, 阿部知子: “Whole genome sequencing of salt-tolerant mutant of rice by next generation sequencing technology”, 第 33 回日本分子生物学会年会・第 83 回日本生化学会大会合同大会 (BMB2010), (日本分子生物学会), 神戸, 12 月 (2010).

榎本嘉範, 黒田直史, 満汐孝治, 金燦鉉, 檜垣浩之, 永田祐吾, 金井保之, 鳥居寛之, Corradini M., Leali M., Lodi-Rizzini E., Mascagna V., Venturelli L., Zurlo N., 藤居甲基, 大塚未来, 田中香津生, 今尾浩士, 長嶋泰之, 松田恭幸, 毛利明博, 山崎泰規: “カスプトラップ中での反水素生成”, 日本物理学会第 66 回年次大会, (日本物理学会), 新潟, 3 月 (2011).

Radiation Biology Team

Publications

[Journal]

(Original Papers) *Subject to Peer Review

Yatagai F., Umebayashi Y., Suzuki M., Abe T., Suzuki H., Shimazu T., Ishioka N., Iwaki M., and Honma M.: "Influence of low-dose and low-dose-rate ionizing radiation on mutation induction in human cells", Adv. Space Res. **40**, No. 4, pp. 470–473 (2007). ∗

Nishiyama R., Ishii K., Kifune E., Kazama Y., Nishihara K., Matsunaga S., Shinozaki K., and Kawano S.: "Sex chromosome evolution revealed by physical mapping of SlAP3X/Y in the dioecious plant Silene latifolia", Cytologia **75**, No. 3, pp. 319–325 (2010). ∗

Ishii K., Amanai Y., Kazama Y., Ikeda M., Kamada H., and Kawano S.: "Analysis of BAC clones containing homologous sequences on the end of the Xq arm and on chromosome 7 in the dioecious plant *Silene latifolia*", Genome **53**, No. 4, pp. 311–320 (2010). ∗

Kashiwabara T., Mitsuo S., Hokura A., kitajima N., Abe T., and Nakai I.: "In vivo micro X-ray analysis utilizing synchrotron radiation of the gametophytes of three arsenic accumulating ferns, Pteris vittata L., Pteris cretica L. and Athyrium yokoscense, in different growth stages", Metallomics **2**, 261–270 (2010). ∗

Nakano M., Amano J., Watanabe Y., Nomizu T., Suzuki M., Mizunashi K., Mori S., Kuwayama S., Han D., Saito H., Ryuto H., Fukunishi N., and Abe T.: "Morphological variation in Tricyrtis hirta plants regenerated from heavy ion beam-irradiated embryogenic calluses", Plant Biotechnol. **27**, 155–160 (2010). ∗

Koizumi A., Yamanaka K., Nishihara K., Kazama Y., Abe T., and Kawano S.: "Two separate pathways including *SlCLV1*, *SlSTM* and *SlCUC* that control carpel development in a bisexual mutant of *Silene latifolia*", Plant Cell Physiol. **51**, No. 2, pp. 282–293 (2010). ∗

Nakano M., Watanabe Y., Nomizu T., Suzuki M., Mizunashi K., Mori S., Amano J., Han D., Saito H., Ryuto H., Fukunishi N., and Abe T.: "Promotion of somatic embryo production from embryogenic calluses of monocotyledonous and dicotyledonous plants by heavy-ion beam irradiation", Plant Growth Regul. **60**, 169–173 (2010). ∗

Fujiwara M., Hashimoto H., Kazama Y., Hirano T., Yoshioka Y., Aoki S., Sato N., Itoh R. D., and Abe T.: "Dynamic morphologies of pollen plastids visualised by vegetative-specific FtsZ1-GFP in Arabidopsis thaliana", Protoplasma **242**, 19–33 (2010). ∗

古川浩二, 岩澤洋樹, 阿部知子, 松山知樹: "DNA マーキングによるシンビジウムの品種内判別", DNA 多型 **18**, 81–84 (2010). ∗

森下敏和, 六笠裕治, 鈴木達郎, 清水明美, 山口博康, 出花幸之介, 相井城太郎, 長谷純宏, 鹿園直哉, 田中淳, 宮沢豊, 林依子, 阿部知子: "ガンマ線およびイオンビーム照射によって得られたダッタンソバ半矮性系統の形態および遺伝特性", 育種学研究 **12**, 39–43 (2010). ∗

山岡和希子, 高田沙織, 竹久妃奈子, 林依子, 保倉明子, 寺田靖子, 阿部知子, 中井泉: "放射光マイクロビーム蛍光 X 線分析と X 線吸収微細構造解析を用いたイネのカドミウム蓄積機能に関する研究", 分析化学 **59**, No. 6, pp. 463–475 (2010). ∗

(Review)

阿部知子, 風間裕介, 平野智也: "重イオンビーム育種技術の実用化 10 年", 植物の生長調節 **45**, 58–63 (2010).

(Others)

阿部知子: "世界に初めての花を咲かせる", エネルギーレビュー **30**, 44 (2010).

[Book・ Proceedings]

(Review)

平野智也, 茶谷正孝, 林依子, 阿部知子: "ランの新たな品種改良：重イオンビーム育種による挑戦", 第 3 回智のシンポジウム：文明・文化と科学技術 論文集, 東京, 2010–11, 「智のシンポジウム」組織員会, 東京, pp. 31–34 (2010).

森田竜平, 西村実, 阿部知子: "突然変異を利用した品種改良：作物のポテンシャルを引き出す", 第 3 回智のシンポジウム：文明・文化と科学技術 論文集, 東京, 2010–11, 「智のシンポジウム」組織委員会, 東京, pp. 35–38 (2010).

風間裕介, 河野重行, 阿部知子: "マルチ蛍光標識プローブを用いた植物巨大 Y 染色体の構造解析", 第 3 回智のシンポジウム：文明・文化と科学技術 論文集, 東京, 2010–11, 「智のシンポジウム」組織員会, 東京, pp. 39–42 (2010).

Oral Presentations

(International Conference etc.)

Nishihara K., Kazama Y., Hirano T., Ohbu S., Matsuyama T., Kawano S., and Abe T.: "LET-dependent effects of ionizing radiation on deletion mutants in *Arabidopsis thaliana*", Molecular aspects of plant development 2010, (Vienna International Plant Conference Association), Vienna, Austria, Feb. (2010).

Kazama Y., Ishii K., Nishihara K., Torii C., Aonuma W., Kawano S., and Abe T.: "Molecular Aspects of Sexual Flower Differentiation in the Dioecious Plant *Silene latifolia*", Molecular aspects of plant development 2010, (Vienna International Plant Conference Association), Vienna, Austria, Feb. (2010).

Ma L., Kazama Y., Ichida H., Hayashi Y., Abe T., Tanaka S., Inoue H., and Hatakeyama S.: "Research of mutation of ion beam irradiation in *Neurospora*", Neurospora 2010, (Neurospora Policy Committee), Asilomar, USA, Apr. (2010).

Manickavelu A., Kawaura K., Sakakibara H., Kamiya Y., Abe T., Shinozaki K., and Ogihara Y.: "Dwarf mutant characterization in heavy ion-beam mutated diploid wheat (*Triticum Monococcum*L)", 21st International Conference on Arabidopsis Research (ICAR 2010), Yokohama, June (2010).

Nishihara K., Kazama Y., Hirano T., Ohbu S., Kawano S., and Abe T.: "Dynamic rearrangement induced by Fe-

ions in *Arabidopsis thaliana*", 21st International Conference on Arabidopsis Research (ICAR 2010), (Scientific Organizing Committee for ICAR2010), Yokohama, June (2010).

Hirano T., Kazama Y., Nishihara K., Ohbu S., Liu Y., Hayashi Y., and Abe T.: "LET dependent effect on DNA damage in irradiation of heavy-ion beam to Arabidopsis thaliana", 21st International Conference on Arabidopsis Research (ICAR 2010), (Scientific Organizing Committee for ICAR2010), Yokohama, June (2010).

Hayashi Y., Kazama Y., Hirano T., Tokairin H., Ohbu S., Sato T., and Abe T.: "LET-dependent effect of heavy-ion beam irradiation on mutation induction in rice", 21st International Conference on Arabidopsis Research (ICAR 2010), (Scientific Organizing Committee for ICAR2010), Yokohama, June (2010).

Abe T., Hayashi Y., Kazama Y., Nishihara K., and Hirano T.: "New innovative technology for mutation breeding using heavy-ion beams", 21st International Conference on Arabidopsis Research (ICAR 2010), (Scientific Organizing Committee for ICAR2010), Yokohama, June (2010).

Kazama Y., Hirano T., Ohbu S., Liu Y., Hayashi Y., and Abe T.: "*Arabidopsis* deletion mutant collection produced by heavy-ion beam irradiation", 21st International Conference on Arabidopsis Research (ICAR 2010), Yokohama, June (2010).

Hokura A., Yoshii Y., Nakai I., Abe T., Itouga M., and Sakakibara H.: "Study on lead and copper stroage mechanism of copper moss,*Scopelophila cataractae*,by Micro-XRF imaging and XAFS analyses using synchrotron radiation", 5th International Conference on Ion Exchange, (Japan Association of Ion Exchange), Melbourne, Australia, July (2010).

(Domestic Conference)

阿部知子, 斉藤宏之, 竹之下佳久, 長谷健, 大江正和: "イオンビーム照射によるイチゴ品種「さつまおとめ」早生優良系統の作出", 第 6 回イオンビーム育種研究会大会, 和光, 5 月 (2009).

古川浩二, 岩澤洋樹, 阿部知子, 松山知樹: "DNA マーキングによるシンピジウムの品種内識別", 第 6 回イオンビーム育種研究会大会, (イオンビーム育種研究会), 和光, 5 月 (2009).

高城啓一, 畑下昌範, Trieu L., 鈴木勝久, 阿部知子, 風間裕介, 塚田晃代: "プロトンビーム照射の斑入りペチュニアに対する内部摘芽効果", 第 6 回イオンビーム育種研究会大会, 和光, 5 月 (2009).

今西俊介, 野口有里紗, 横谷尚起, 風間裕介, 平野智也, 林依子, 本多一郎, 阿部知子: "重イオンビーム照射によるトマトの効率的変異固定を目指した基盤研究", 第 7 回イオンビーム育種研究会大会, (イオンビーム育種研究会), 鳥栖, 5–6 月 (2010).

佐々木克友, 山口博康, 間竜太郎, 四方雅仁, 阿部知子, 大坪憲弘: "重イオンビーム照射により第 2 ウォールが萼化したトレニア変異表現型の原因遺伝子の解明", 第 7 回イオンビーム育種研究会大会, (イオン育種研究会), 鳥栖, 5–6 月 (2010).

西美友紀, 石地耕太朗, 阿部知子, 吉田桂一郎, 宮　雄太, 木下剛仁, 中島寿亀: "シンクロトロン光を用いた突然変異誘発技術の開発に向けた取り組み", 第 7 回イオンビーム育種研究会大会, (イオン育種研究会), 鳥栖, 5–6 月 (2010).

西原潔, 風間裕介, 平野智也, 大部澄江, 河野重行, 阿部知子: "シロイヌナズナを用いた Fe イオン誘発 DNA 突然変異の解析", 第 7 回イオンビーム育種研究会大会, (イオンビーム育種研究会), 鳥栖, 5–6 月 (2010).

寺岡毅, 澤野郁夫, 中嶌輝子, 加々美裕, 神尾章子, 浜部直哉, 林依子, 龍頭啓充, 福西暢尚, 阿部知子: "重イオンビーム照射によるウンシュウミカンの形態変異の誘発", 第 7 回イオンビーム育種研究会大会, (イオン育種研究会), 鳥栖, 5–6 月 (2010).

森田竜平, 草場信, 山口博康, 横田裕一郎, 長谷純宏, 西村実: "イオンビーム・ガンマ線照射によるイネ突然変異体の解析", 第 7 回イオンビーム育種研究会大会, (イオンビーム育種研究会), 鳥栖, 5–6 月 (2010).

井上忍, 東谷篤志, 惠郷博文, 高橋直, 大竹雄次: "X 線自由電子レーザー計画における電子ビームスリット", 第 7 回日本加速器学会年会, (日本加速器学会), 姫路, 8 月 (2010).

吉井 雄一, 保倉 明子, 中井 泉, 阿部 知子, 井藤賀 操, 榊原均, 寺田 靖子: "ホンモンジゴケ *Scopelophila cataractae*(Mitt.)Broth. に蓄積している銅の分布と化学形態", 日本蘚苔類学会第 39 回山口大会, (日本蘚苔類学会), 岩国, 8 月 (2010).

平野智也, 風間裕介, 西原潔, 大部澄江, 白川侑希, 林祐子, 林依子, 阿部知子: "シロイヌナズナ変異体を用いた重イオンビーム変異領域の特性解析", 日本植物形態学会第 22 回総会・大会, (日本植物形態学会), 春日井, 9 月 (2010).

風間 裕介, 平野 智也, 西原 潔, 大部 澄江, 白川 侑希, 林 祐子, 阿部知子: "重イオンビーム LETmax の検証とシロイヌナズナ形態変異体ラインの作出", 日本植物形態学会第 22 回総会・大会, (日本植物形態学会), 春日井, 9 月 (2010).

風間 裕介, 石井公太郎, 鳥居千尋, 藤田尚子, 河野重行, 阿部知子: "重イオンビーム照射で作出した無性花変異体を用いて明らかにする Y 染色体雄性決定領域", 日本植物学会第 74 回大会, ((社) 日本植物学会), 春日井, 9 月 (2010).

藤田尚子, 青沼航, 清水祐史, 鳥居千寛, 石井公太郎, 風間裕介, 阿部知子, 河野重行: "雄性決定機能領域の特定を目指した新規 Y 染色体特異的 STS マーカーの探索", 日本植物学会第 74 回大会, ((社) 日本植物学会), 春日井, 9 月 (2010).

青沼航, 清水祐史, 鳥居千寛, 藤田尚子, 石井公太郎, 風間裕介, 阿部知子, 河野重行: "ヒロハノマンテマの先熟後熟花粉と雌蕊成熟から見た欠失突然変異体獲得の照射タイミング", 日本植物学会第 74 回大会, ((社) 日本植物学会), 春日井, 9 月 (2010).

石井公太郎, 風間裕介, 西山りゑ, 阿部知子, 河野重行: "ヒロハノマンテマの XY 性染色体の対立遺伝子 *APETARA3* の構造とその周辺領域", 日本植物学会第 74 回大会, ((社) 日本植物学会), 春日井, 9 月 (2010).

森田竜平, 阿部知子: “重イオンビームによる有用微生物育種技術の開発”, デジタル加速器ユーザーズフォーラム（10-9-14）, (高エネルギー加速器研究機構), つくば, 9 月 (2010).

西原潔, 風間裕介, 平野智也, 大部澄江, 河野重行, 阿部知子: “鉄イオン照射により誘導されたシロイヌナズナ染色体のダイナミックリアレンジメント”, 日本遺伝学会第 82 回大会, (日本遺伝学会), 札幌, 9 月 (2010).

古川浩二, 岩澤洋樹, 阿部知子, 松山知樹: “DNA マーキングによるシンビジウムの品種内判別（第３報）”, 園芸学会平成 22 年度秋季大会, (園芸学会), 大分, 9 月 (2010).

平野智也, 茶谷正孝, 林依子, 阿部知子: “ランの新たな品種改良:重イオンビーム育種による挑戦”, 第 3 回智のシンポジウム：文明・文化と科学技術, (第 3 回智のシンポジウムー文明・文化と科学技術ー組織委員会), 東京, 11 月 (2010).

風間裕介, 河野重行, 阿部知子: “マルチ蛍光プローブを用いた植物巨大 Y 染色体の構造解析”, 第 3 回智のシンポジウム：文明・文化と科学技術, (第 3 回智のシンポジウムー文明・文化と科学技術ー組織委員会), 東京, 11 月 (2010).

阿部知子, 林依子, 石井重久: “重イオンビームで日本のサクラが変わる”, 第 3 回智のシンポジウム：文明・文化と科学技術, (第 3 回智のシンポジウム：文明・文化と科学技術 - 組織委員会), 東京, 11 月 (2010).

古川浩二, 岩澤洋樹, 阿部知子, 松山知樹: “シンビジウム品種内系統判別のための DNA マーク開発”, 日本 DNA 多型学会第 19 回学術集会, (日本 DNA 多型学会), 三島, 11 月 (2010).

眞鍋理一郎, Arner E. A., 平野智也, 渋川登美子, 市田裕之, 川島麗, 荒川貴博, Daub C. O., 河合純, 阿部知子: “Whole genome sequencing of salt-tolerant mutant of rice by next generation sequencing technology”, 第 33 回日本分子生物学会年会・第 83 回日本生化学会大会合同大会 (BMB2010), (日本分子生物学会), 神戸, 12 月 (2010).

泉雅子, 柳憲一郎, 水野武, 杉村和人, 今本尚子, 奥村克純, 花岡文雄: “ヒト Mcm10 の機能ドメインの解析”, 第 33 回日本分子生物学会年会・第 83 回日本生化学会大会合同大会 (BMB2010), (日本分子生物学会、日本生化学会), 神戸, 12 月 (2010).

田畑哲之, 松山知樹, 古川浩二, 室田有里: “放射線利用による栄養繁殖作物の品種内識別法「DNA マーキング」の開発”, NIRS テクノフェア 2010：放射線科学に通じる健康と安全・安心に関する技術, (独立行政法人放射線医学総合研究所), 千葉, 12 月 (2010).

風間裕介, 石井公太郎, 藤田尚子, 青沼航, 清水祐史, 河野重行, 阿部知子: “重イオンビーム照射で得た無性花変異体を用いた植物 Y 染色体雄性決定領域の解析”, 日本育種学会第 119 回講演会, (日本育種学会), 横浜, 3 月 (2011).

丸山大輔, 笠原竜四郎, 風間裕介, 阿部知子, 東山哲也: “受精を完了した後にも胚珠が花粉管を誘引してしまうシロイヌナズナ多精拒否変異体の解析”, 第 52 回日本植物生理学会年会, (日本植物生理学会), 仙台, 3 月 (2011).

藤原誠, 風間裕介, 阿部知子, 伊藤竜一: “Plastid Replication in Leaf Epidermis: Insights from the *atminE1* Mutant of *Arabidopsis thaliana*”, 第 52 回日本植物生理学会年会, (日本植物生理学会), 仙台, 3 月 (2011).

久永哲也, Ferjani A., 堀口吾郎, 石田喬志, 杉本慶子, 塚谷裕一: “DNA 損傷応答が fugu2 の補償作用に果たす役割”, 第 52 回日本植物生理学会年会, (日本植物生理学会), 仙台, 3 月 (2011).

RI Applications Team

Publications

[Journal]

（Original Papers） *Subject to Peer Review

Motizuki Y., Nakai Y., Takahashi K.: "Supernovae and solar cycles embedded in a Dome F ice core", The Dome Fuji Glaciological Astoronomy Collaboration : Highlights of Astronomy **15**, 630–631 (2010). ∗

Kidera M., Seto Y., Takahashi K., Enomoto S., Kishi S., Makita M., Nagamatsu T., Tanaka T., and Toda M.: "New method for comprehensive detection of chemical warfare agents using an electron-cyclotron-resonance ion-source mass spectrometer", Spectrochim. Acta Pt. A **78**, 1215–1219 (2011). ∗

[Book・ Proceedings]

（Original Papers） *Subject to Peer Review

Kamigaito O., Ikezawa E., Kase M., Fujimaki M., Fujinawa T., Fukunishi N., Goto A., Haba H., Higurashi Y., Kidera M., Komiyama M., Koyama R., Kuboki H., Kumagai K., Maie T., Nagase M., Nakagawa T., Ohnishi J., Okuno H., Sakamoto N., Sato Y., Suda K., Watanabe T., Yamada K., Yokouchi S., and Yano Y.: "Present status of RIKEN heavy-ion linac", Proceedings of LINAC 08, Canada, Victoria, 2008–9〜10, TRIUMF, Vancouver, pp. 112–114 (2010).

Oral Presentations

(International Conference etc.)

Kamigaito O., Ikezawa E., Kase M., Fujimaki M., Fujinawa T., Fukunishi N., Goto A., Haba H., Higurashi Y., Kidera M., Komiyama M., Koyama R., Kuboki H., Kumagai K., Maie T., Nagase M., Nakagawa T., Ohnishi J., Okuno H., Sakamoto N., Sato Y., Suda K., Watanabe T., Yamada K., Yokouchi S., and Yano Y.: "Present status of RIKEN heavy-ion linac", 24th International Linear Accelerator Conference (LINAC08), (LINAC08 Organizing Committee), Victoria, Canada, Sept.–Oct. (2008).

Kidera M., Takahashi K., Nagamatsu T., Seto Y., Toda M., Enomoto S., and Tanaka T.: "Study of potential application of compact ECRIS tp analytical system", 19th International Workshop on ECR Ion Sources (ECRIS 2010), (Laboratoire de Physique Subatomique et de Cosmologie), Grenoble, France, Aug. (2010).

Kikunaga H., Yoshimura T., Ooe K., Takahashi N., Haba H., Ezaki Y., Mitsugashira T., and Shinohara A.: "Development of a liquid scintillation detector coupled with a capillary-electrophoresis apparatus for analysis of spent nuclear fuel", International Chemical Congress of Pacific Basin Societies (PACIFICHEM 2010), (American Chemical Society), Honolulu, USA, Dec. (2010).

Kidera M., Toda M., Makita M., Mitsubori Y., Tanaka T., and Takahashi K.: "Development of the mass spectrometer equipped with ECRIS and its application to the isotopic analyses", International Chemical Congress of Pacific Basin Societies (PACIFICHEM 2010), Honolulu, USA, Dec. (2010).

Toyoshima A., Tsukada K., Asai M., Kitatsuji Y., Ishii Y., Sato T., Li Z., Sato N., Kikuchi T., Nishinaka I., Nagame Y., Kasamatsu Y., Haba H., Ooe K., Shinohara A., Sato W., Akiyama K., Even J., and Schaedel M.: "Electrochemistry of the heaviest elements", International Chemical Congress of Pacific Basin Societies (PACIFICHEM 2010), (American Chemical Society), Honolulu, USA, Dec. (2010).

Ooe K., Komori Y., Fujisawa H., Kuriyama A., Takayama R., kikutani Y., Kikunaga H., Kasamatsu Y., Yoshimura T., Takahashi N., Haba H., Kudou Y., Ezaki Y., and Shinohara A.: "Electrolytic oxidation of nobelium with a microchannel-electrode chip", International Chemical Congress of Pacific Basin Societies (PACIFICHEM 2010), (American Chemical Society), Honolulu, USA, Dec. (2010).

Kudou Y., Haba H., Kasamatsu Y., and Morita K.: "FIA-based continuous extraction system for superheavy element chemistry", International Chemical Congress of Pacific Basin Societies (PACIFICHEM 2010), (American Chemical Society), Honolulu, USA, Dec. (2010).

(Domestic Conference)

大江一弘, 小森有希子, 藤沢弘幸, 栗山亜依, 山玲央奈, 菊谷有希, 菊永英寿, 笠松良崇, 吉村崇, 高橋成人, 羽場宏光, 工藤祐生, 江崎豊, 篠原厚: "電極マイクロチップを用いたノーベリウムの電解酸化", 2010 日本放射化学会年会・第 54 回放射化学討論会, (日本放射化学会), 吹田, 9 月 (2010).

廣村信, 金山洋介, 本村信治, 五十嵐香織, 羽場宏光, 榎本秀一: "肥満、糖尿病モデル動物のメタロミクス研究", 第 2 回メタロミクス研究フォーラム, (京都薬科大学), 京都, 11 月 (2010).

User Liaison and Industrial Cooperation Group

Publications

[Journal]

(Original Papers)　*Subject to Peer Review

Aoi N., Kanno S., Takeuchi S., Suzuki H., Bazin D. P., Bowen M. D., Campbell C. M., Cook J. M., Dinca D. -., Gade A., Glasmacher T., Iwasaki H., Kubo T., Kurita K., Motobayashi T., Mueller W. F., Nakamura T., Sakurai H., Takashina M., Terry J. R., Yoneda K., and Zwahlen H.: "Enhanced collectivity in 74Ni", Phys. Lett. B **692**, 302–306 (2010). *

User Support Office

Publications

[Journal]

(Original Papers) *Subject to Peer Review

Ichikawa Y., Onishi T. K., Suzuki D., Iwasaki H., Kubo T., Naik V., Chakrabarti A., Aoi N., Brown A. B., Fukuda N., Kubono S., Motobayashi T., Nakabayashi T., Nakamura T., Nakao T., Okumura T., Ong J. H., Suzuki H., Suzuki M. K., Teranishi T., Yamada K., Yamaguchi H., and Sakurai H.: "Gamow-Teller transition of the proton-rich nucleus ^{24}Si", AIP Conf. Proc. **1235**, 265–269 (2010).

Ichikawa Y., Onishi T. K., Suzuki D., Iwasaki H., Kubo T., Naik V., Chakrabarti A., Aoi N., Brown A. B., Fukuda N., Kubono S., Motobayashi T., Nakabayashi T., Nakamura T., Nakao T., Okumura T., Ong J. H., Suzuki H., Suzuki M. K., Teranishi T., Yamada K., Yamaguchi H., and Sakurai H.: "Mirror asymmetry for B(GT) of ^{24}Si induced by Thomas-Ehrman shift", AIP Conf. Proc. **1238**, 290–293 (2010).

Ichikawa Y., Onishi T. K., Suzuki D., Iwasaki H., Kubo T., Naik V., Chakrabarti A., Aoi N., Brown A. B., Fukuda N., Kubono S., Motobayashi T., Nakabayashi T., Nakamura T., Nakao T., Okumura T., Ong J. H., Suzuki H., Suzuki M. K., Teranishi T., Yamada K., Yamaguchi H., and Sakurai H.: "Mirror asymmetry investigated by β decay of proton-rich ^{24}Si", Mod. Phys. Lett. A **25**, 1895–1898 (2010).

Aoi N., Kanno S., Takeuchi S., Suzuki H., Bazin D. P., Bowen M. D., Campbell C. M., Cook J. M., Dinca D. -., Gade A., Glasmacher T., Iwasaki H., Kubo T., Kurita K., Motobayashi T., Mueller W. F., Nakamura T., Sakurai H., Takashina M., Terry J. R., Yoneda K., and Zwahlen H.: "Enhanced collectivity in 74Ni", Phys. Lett. B **692**, 302–306 (2010). *

Oral Presentations

(International Conference etc.)

Ichikawa Y., Onishi T. K., Suzuki D., Iwasaki H., Kubo T., Naik V., Chakrabarti A., Aoi N., Brown A. B., Fukuda N., Kubono S., Motobayashi T., Nakabayashi T., Nakamura T., Nakao T., Okumura T., Ong J. H., Suzuki H., Suzuki M. K., Teranishi T., Yamada K., Yamaguchi H., and Sakurai H.: "Proton-rich nuclear structure and mirror asymmetry investigated by β-decay spectroscopy of ^{24}Si", International Nuclear Physics Conference (INPC2010), (TRIUMF at the University of British Columbia), Vancouver, Canada, July (2010).

Ichikawa Y., Ueno H., Ishii Y., Furukawa T., Yoshimi A., Kameda D., Aoi N., Watanabe H., Asahi K., Iijima H., Suzuki K., Inoue T., Tsuchiya M., Hayashi H., Nanao T., Kubo T., Inabe N., Ohnishi T., Takeda H., Fukuda N., Ishihara M., Daugas J., Chevrier R., Georgiev G., Rajabali M. M., and Balabanski D. L.: "g-factor measurement for isomeric state of ^{32}Al using two-step fragmentation reaction with dispersion matching", GCOE International Summer School: Hadrons and Nuclei under Extreme Conditions (HANEC2010), (Tokyo Institute of Technology), Tokyo, Sept. (2010).

(Domestic Conference)

小沢顕, 鈴木宏, 長江大輔, 新井一郎, 森口哲朗, 伊藤由太, 長谷部裕雄, 藤縄雅, 福西暢尚, 後藤彰, 大西哲哉, 櫻井博儀, 若杉昌徳, 山口由高, 矢野安重, 鈴木健, 山口貴之, 菊池崇志, 大坪隆, 安田裕介, 久保野茂: "RIBF における稀少 RI リング", RIBF に於ける測定器についての検討会, 和光, 12 月 (2009).

小沢顕, 新井一郎, 伊藤由太, 森口哲朗, 長江大輔, 鈴木宏, 藤縄雅, 福西暢尚, 後藤彰, 長谷部裕雄, 大西哲哉, 櫻井博儀, 若杉昌徳, 山口由高, 矢野安重, 鈴木健, 山口貴之, 菊池崇志, 大坪隆, 安田裕介, 久保野茂: "RIBF に於ける稀少 RI リング計画", 蓄積リング検討ミニワークショップ, (大阪大学　核物理研究センター), 茨木, 1 月 (2010).

森口哲朗, 小沢顕, 伊藤由太, 鈴木宏, 長江大輔, 鈴木健, 山口貴之, 大坪隆, 大西哲哉, 山口由高, 金澤光隆: "RI ビーム粒子識別検出器の開発", 平成 21 年度 HIMAC 共同利用研究成果発表会, (独立行政法人放射線医学総合研究所), 千葉, 4 月 (2010).

鈴木宏, 新井一郎, 藤縄雅, 福西暢尚, 後藤彰, 菊池崇志, 久保野茂, 森口哲朗, 長江大輔, 大坪隆, 小沢顕, 櫻井博儀, 鈴木健, 若杉昌徳, 安田裕介, 山口貴之, 山口由高, 矢野安重: "理研稀少 RI リングの粒子軌道計算", 日本物理学会 2010 年秋季大会, (日本物理学会), 北九州, 9 月 (2010).

酒向正己, 村上哲也, 市川裕大, 今城想平, 鮫島玲, 村田次郎, 家城和夫, 松下昌史, 中井陽一, 西村俊二, 高田栄一: "中間エネルギー重イオン衝突における荷電パイオン生成 (IV)", 日本物理学会 2010 年秋季大会, (日本物理学会), 北九州, 9 月 (2010).

市川雄一, 上野秀樹, 石井裕司, 古川武, 吉見彰洋, 亀田大輔, 青井考, 渡邉寛, 旭耕一郎, 飯島裕章, 鈴木都文, 井上壮志, 土屋真人, 林宏憲, 七尾翼, 久保敏幸, 稲辺尚人, 大西哲哉, 竹田浩之, 福田直樹, 石原正泰, Daugas J., Chevrier R., Georgiev G., Rajabali M. M., Balabanski D. L.: "分散整合二回散乱法による核スピン整列ＲＩビームの生成", 日本物理学会 2010 年秋季大会, (日本物理学会), 北九州, 9 月 (2010).

Industrial Cooperation Team

Publications

[Journal]

(Original Papers) *Subject to Peer Review

Inoue Y., Inagaki M., Gunji A., Furushima W., Okada H., Sasaki H., Omori T., Takeichi H., and Kaga M.: "Altered effect of preceding response execution on inhibitory processing in children with AD/HD: An ERP study", Int. J. Psychophysiol. **77**, No. 2, pp. 118–125 (2010). *

Takeichi H., Mitsudo T., Nakajima Y., Remijn G. B., Goto Y., and Tobimatsu S.: "A neural decoding approach to auditory temporal assimilation", Neural Comput. Appl., pp. 1–9 (2010). *

Oral Presentations

(International Conference etc.)

Takeichi H., Mitsudo T., Nakajima Y., Remijn G. B., Goto Y., and Tobimatsu S.: "Electrophysiological Correlate of Auditory Temporal Assimilation between Two Neighboring Time Intervals: A Principal Component Analysis", 29th International Congress of Clinical Neurophysiology (ICCN 2010), (International Federation of Clinical Neurophysiology), Kobe, Oct.–Nov. (2010).

(Domestic Conference)

竹市博臣: "ベイズ的知覚と事前確率の表現", 日本心理学会第 74 回大会, (日本心理学会), 豊中, 9 月 (2010).

竹市博臣: "チュートリアル招待講演：奥行き知覚の諸問題", 第 15 回日本バーチャルリアリティ学会大会, (日本バーチャルリアリティ学会), 石川県野々市町, 9 月 (2010).

眞鍋理一郎, Arner E. A., 平野智也, 渋川登美子, 市田裕之, 川島麗, 荒川貴博, Daub C. O., 河合純, 阿部知子: "Whole genome sequencing of salt-tolerant mutant of rice by next generation sequencing technology", 第 33 回日本分子生物学会年会・第 83 回日本生化学会大会合同大会 (BMB2010), (日本分子生物学会), 神戸, 12 月 (2010).

中島祥好, 竹市博臣: 日本音響学会聴覚研究会, 柳川, 12 月 (2010).

軍司敦子, 竹市博臣, 井上祐紀, 岡田浩之, 大森隆司, 稲垣真澄, 加我牧子: "Single one-minute trial assessment of speech processing in school age children", 日本音響学会聴覚研究会, 柳川, 12–12 月 (2010).

中島祥好, 竹市博臣: "時間知覚の精神物理学と脳科学", 日本音響学会 2011 年春季研究発表会, 東京, 3 月 (2011).

Safety Management Group

Publications

[Book・ Proceedings]

（Technical Document）

Ipe N., Fehrenbacher G., Gudowska I., Paganetti H., Schippers J. M., Roesler S., and Uwamino Y.: "Shielding design and radiation safety of charged particle therapy facilities", Shielding design and radiation safety of charged particle therapy facilities, Particle Therapy Co-Operative Group, Villigen, (2010).

Oral Presentations

(International Conference etc.)

Hagiwara M., Sanami T., Iwamoto Y., Matsuda N., Sakamoto Y., Nakane Y., Nakashima H., Masumoto K., and Uwamino Y.: "Spectrum measurement of neutrons and gamma-rays from thick $H_2{}^{18}O$ target bombarded with 18 MeV protons", International Conference on Nuclear Data for Science and Technology, (Korean Nuclear Society), Jeju Island, Korea, Apr. (2010).

(Domestic Conference)

上蓑義朋, 向井弘樹, 日暮利江子, 赤塩敦子, 福田弘幸, 坂本久雄, 吉田敦, 吉田光一: "理研 RIBF・BigRIPS 周辺における 2 次放射線測定", 日本原子力学会 2010 年秋の大会, (日本原子力学会), 札幌, 9 月 (2010).

萩原雅之, 佐波俊哉, 松田規宏, 中根佳弘, 岩元洋介, 中島宏, 坂本幸夫, 桝本和義, 上蓑義朋: "陽子 18MeV 入射における厚いターゲットからの中性子・γ線スペクトルの系統的測定", 日本原子力学会 2010 年秋の大会, (日本原子力学会), 札幌, 9 月 (2010).

CNS (Center for Nuclear Study, Graduate School of Science, University of Tokyo)

Publications

[Journal]

(Original Papers) *Subject to Peer Review

Uesaka T., Sakaguchi S., Iseri Y., Amos K., Aoi N., Hashimoto Y., Hiyama E., Ichikawa M., Ichikawa Y., Ishikawa S., Itoh K., Itoh M., Iwasaki H., Karataglidis S., Kawabata T., Kawahara T., Kuboki H., Maeda Y., Matsuo R., Nakao T., Okamura H., Sakai H., Sasamoto Y., Sasano M., Satou Y., Sekiguchi K., Shinohara M., Suda K., Suzuki D., Takahashi Y., Tanifuji M., Tamii A., Wakui T., Yako K., Yamamoto Y., Yamaguchi M.: "Analyzing power for the proton elastic scattering from neutron-rich 6He nucleus", Phys. Rev. C**82** (2010) 021602(R).*

Ideguchi E., Cederwall B., Ganioğlu E., Hadinia B., Lagergren K., Bäck T., Johnson A., Wyss R., Eeckhaudt S., Grahn T., Greenlees P., Julin R., Juutinen S., Kettunen H., Leino M., Leppanen A.-P., Nieminen P., Nyman M., Pakarinen J., Rahkila P., Scholey C., Uusitalo J., Joss D.T., Paul E.S., Wiseman D.R., Wadsworth R., Afanasjev A.V., Ragnarsson I.: "High-spin intruder band in ^{107}In", Phys. Rev. C **81**, (2010) 034303,*

Scholey C., Andgren K., Bianco L., Cederwall B., G. I., Eeckhaudt S., Ertürk S., GomezHornillos M.B., Grahn T., T. P., Hadinia B., Ideguchi E., Jones P., T. D., Julin R., Juutinen S., Ketelhut S., Leino M., Leppänen A.-P., Nieminen P., Niikura M., Nyman M., O'Donnell D., D. R., Pakarinen J., Rahkila P., Sarén J., Sandzelius M., Simpson J., Sorri J., Thomson J., Uusitalo J., Venhart M.: "Isomeric and ground-state properties of $^{171}_{78}$Pt, $^{167}_{76}$Os,and $^{163}_{74}$W", Phys. Rev. C **81**, (2010) 014306,*

Ideguchi E., Ota S., Morikawa T., Oshima M., Koizumi M., Toh Y., Kimura A., Harada H., Furutaka K., Nakamura S., Kitatani F., Hatsukawa Y., Shizuma T., Sugawara M., Miyatake H., Watanabe Y.X., Hirayama Y., Oi M.: "Superdeformation in asymmetric $N > Z$ nucleus ^{40}Ar", Phys. Lett. B **686**,(2010) 18–22.*

Tanaka K., Yamaguchi T., Suzuki T., Ohtsubo T., Fukuda M., Nishimura D., Takechi M., Ogata K., Ozawa A., Izumikawa T., Aiba T., Aoi N., Baba H., Hashizume Y., Inafuku K., Iwasa N., Kobayashi K., Komuro M., Kondo Y., Kubo T., Kurokawa M., Matsuyama T., Michimasa S., Motobayashi T., Nakabayashi T., Nakajima S., Nakamura T., Sakurai H., Shinoda R., Shinohara M., Suzuki H., Takeshita E., Takeuchi S., Togano Y., Yamada K., Yasuno T., Yoshitake M.: "Observation of a Large Reaction Cross Section in the Drip-Line Nucleus ^{22}C", Phys. Rev. Lett. **104**, (2010) 062701,*

Ideguchi E., Ota S., Morikawa T., Oshima M., Koizumi M., Toh Y., Kimura A., Harada H., Furutaka K., Nakamura S., Kitatani F., Hatsukawa Y., Shizuma T., Sugawara M., Miyatake H., X. Y., Hirayama Y., Oi M.: "Superdeformation in asymmetric N>Z nucleus ^{40}Ar", Phys. Lett. B **686** (2010) 18–22,*

Baba H., Ichihara T., Ohnishi T., Takeuchi S., Yoshida K., Watanabe Y., Ota S., Shimoura S.: "New Data Acquisition System for the RIKEN Radioactive Isotope Beam Factory", Nucl. Instrum. Methods. A **616** (2010) 65–68.*

Kondo Y., Nakamura T., Satou Y., Matsumoto T., Aoi N., Endo N., Fukuda N., Gomi T., Hashimoto Y., Ishihara M., Kawai S., Kitayama M., Kobayashi T., Matsuda Y., Matsui N., Motobayashi T., Nakabayashi T., Okumura T., Ong H.J., Onishi T.K., Ogata K., Otsu H., Sakurai H., Shimoura S., Shinohara M., Sugimoto T., Takeuchi S., Tamaki M., Togano Y., Yanagisawa Y.: "Low-lying intruder state of the unbound nucleus ^{13}Be", Phys. Lett. B **690**, 245–249 (2010).*

Ohnishi T., Kubo T., Kusaka K., Yoshida A., Yoshida K., Ohtake M., Fukuda N., Takeda H., Kameda D., Tanaka K., Inabe N., Yanagisawa Y., Gono Y., Watanabe H., Otsu H., Baba H., Ichihara T., Yamaguchi Y., Takechi M., Nishimura S., Ueno H., Yoshimi A., Sakurai H., Motobayashi T., Nakao T., Mizoi Y., Matsushita M., Ieki K., Kobayashi N., Tanaka K., Kawada Y., Tanaka N., Deguchi S., Satou Y., Kondo Y., Nakamura T., Yoshinaga K., Ishii C., Yoshii H., Miyashita Y., Uematsu N., Shiraki Y., Sumikama T., Chiba J., Ideguchi E., Saito A., Yamaguchi T., Hachiuma I., Suzuki T., Moriguchi T., Ozawa A., Ohtsubo T., Famiano M.A., Geissel H., Nettleton A.S., Tarasov O.B., Bazin D.P., Sherrill B.M., Manikonda S.L., Nolen J.A.: "Identification of 45 New Neutron-Rich Isotopes Produced by In-Flight Fission of a ^{238}U Beam at 345 MeV/nucleon", J. Phys. Soc. Jpn. **79**, 073201 (2010).*

Rudolph D., Ragnarsson I., Reviol W., Andreoiu C., Bentley M.A., Carpenter M.P., Charity R.J., Clark R.M., Cromaz M., Ekman J., Fahlander C., Fallon P., Ideguchi E., Macchiavelli A.O., Mineva M.N., Sarantites D.G., Seweryniak D., Williams S.J., "Rotational bands in the semi-magic nucleus $^{57}_{28}$Ni$_{29}$", J. Phys. G **37**, 075105 (2010).*

Taniguchi Y., Kanada-Enyo Y., Kimura M., Ikeda K., Horiuchi H., Ideguchi E.: "Triaxial superdeformation in ^{40}Ar, Phys. Rev. C **82**, 011302 (2010).*

Kim A., Lee N.H, Hahn I.S, Yoo J.S, Han M.H, Kubono S., Yamaguchi H., Hayakawa S., Wakabayashi Y., Binh D.N., Hashimoto H., Kawabata T., Kahl D., Kurihara Y., K. Kwon Y., Teranishi T., Kato S., Komatsubara T., Guo B., Bing G., Liu W.P., Wang Y.: "Direct Measurement of the ^{14}O(α,p)^{14}O Cross Section for Astrophysically Important ^{14}O + α Resonances", J. Korean Phys. Soc., **57** (2010) 40 - 43.*

Aamodt K. *et al* for the ALICE Collaboration: "First proton+proton collisions at the LHC as observed with the

ALICE detector-Measurement of the charged-particle pseudorapidity density at $\sqrt{s} = 900$ GeV", Eur. Phys. J. **C65**, 111-125, 2010,*

Aamodt K. *et al* for the ALICE Collaboration: "Alignment of the ALICE Inner Tracking System with cosmic-ray tracks", JINST, 5, PO3003, 2010,*

Adare A. *et al* for the PHENIX Collaboration: "Enhanced production of direct photons in Au+Au collisions at $\sqrt{s_{NN}}$ =200 GeV and implications for the initial temperature", Phys. Rev. Lett. 104, 132301, 2010,*

Adare A. *et al* for the PHENIX Collaboration: "Detailed measurement of the e^+e^- pair continuum in $p+p$ and Au+Au collisions at $\sqrt{s_{NN}} = 200$-GeV and implications for direct photon production", Phys. Rev. C 81, 034911, 2010,*

Adare A. *et al* for the PHENIX Collaboration: "Double Helicity Dependence of Jet Properties from Dihadrons in Longitudinally Polarized $p+p$ Collisions at $\sqrt{s} =$ 200-GeV", Phys. Rev. D81, 012002, 2010,*

Aamodt K., *et al.*, for the ALICE Collaboration, "Elliptic flow of charged particles in Pb-Pb collisions at 2.76 TeV", Phys. Rev. Lett. **105**, 252302 (2010).*

Aamodt K., *et al.*, for the ALICE Collaboration, "Charged-particle multiplicity density at mid-rapidity in central Pb-Pb collisions at $\sqrt{s_{NN}} = 2.76$ TeV", Phys. Rev. Lett. **105**, 252301 (2010).*

Aamodt K., *et al.*, for the ALICE Collaboration, "Transverse momentum spectra of charged particles in proton-proton collisions at $\sqrt{s} = 900$ GeV with ALICE at the LHC", Phys. Lett. B **693** (2010) 53-6.*

Aamodt K., *et al.*, for the ALICE Collaboration, "Transverse momentum spectra of charged particles in proton-proton collisions at $\sqrt{s} = 900$ GeV with ALICE at the LHC", Phys. Lett. B **693** (2010) 53-6.*

Aamodt K., *et al.*, for the ALICE Collaboration, "Two-pion Bose-Einstein correlations in pp collisions at $\sqrt{s} =$ 900 GeV", Phys. Rev. D **82**, 052001 (2010).*

Aamodt K., *et al.*, for the ALICE Collaboration, "Midrapidity Antiproton-to-Proton Ratio in pp Collisions at $\sqrt{s}$ = 0.9 and 7 TeV Measured by the ALICE Experiment", Phys. Rev. Lett. **105**, No.7, (2010).*

Aamodt K., *et al.*, for the ALICE Collaboration, "Charged-particle multiplicity measurement in proton collisions at $\sqrt{s} = 7$ TeV with ALICE at LHC", Eur. Phys. J. C **68**, (2010), 345-5.*

Aamodt K., *et al.*, for the ALICE Collaboration, "Charged-particle multiplicity measurement in proton-proton collisions a $\sqrt{s}$ =0.9 and 2.36 TeV with ALICE at LHC ", Eur. Phys. J. C **68**, (2010), 89-10.*

Adare A., *et al.*, for the PHENIX Collaboration, "Measurement of Transverse Single-Spin Asymmetries for J/ψ Production in Polarized p+p Collisions at $\sqrt{s} =$ 200 GeV", Phys. Rev. D **82**, 112008 (2010).*

Adare A., *et al.*, for the PHENIX Collaboration, "High p_T Direct Photon and π^0 Triggered Azimuthal Jet Correlations in $\sqrt{s}$=200 GeV p+p Collisions", Phys. Rev. D **82**, 072001 (2010).*

Adare A., *et al.*, for the PHENIX Collaboration, "Azimuthal anisotropy of neutral pion production in Au+Au collisions at $\sqrt{s_{NN}} = 200$ GeV: Path-length dependence of jet quenching and the role of initial geometry", Phys. Rev. Lett. **105**, 142301 (2010).*

Adare A.,*et al.*, for the PHENIX Collaboration, "Elliptic and hexadecapole flow of charged hadrons in Au+Au collisions at $\sqrt{s_{NN}} = 200$ GeV", Phys. Rev. Lett. **105**, 062301 (2010).*

Adare A.,*et al.*, for the PHENIX Collaboration, "Transverse momentum dependence of eta meson suppression in Au+Au collisions at $\sqrt{s_{NN}} = 200$ GeV", Phys. Rev. C **82**, 011902 (2010).*

Adare A.,*et al.*, for the PHENIX Collaboration, "Transverse momentum dependence of J/ψ polarization at mid-rapidity in p+p collisions at $\sqrt{s}$=200 GeV", Phys. Rev. D **82**, 012001 (2010).*

Adare A.,*et al.*, for the PHENIX Collaboration, "Transition in yield and azimuthal shape modification in dihadron correlations in relativistic heavy ion collisions", Phys. Rev. C **82**, 011902 (2010).*

Otsuka T., Suzuki T., Holt J.D., Schwenk A., Akaishi Y.: "Three-Body Forces and the Limit of Oxygen Isotopes", Phys. Rev. Lett. **105** (2010), 032501.*

Otsuka T., Suzuki T., Honma M., Utsuno Y., Tsunoda N., Tsukiyama K., Hjorth-Jensen M., "Novel features of nuclear forces and shell evolutions in exotic nuclei", Phys. Rev. Lett. **104** (2010) 012501/1-4,*

[Book・ Proceedings]

(Original Papers)　*Subject to Peer Review

Uesaka T., Michimasa S., Ota S., Saito A., Nakanishi K., Sasamoto Y., Miya H., Tokieda H., Kawase S., Shimizu Y., Shimoura S., Miki K., Noji S., Sakai H., Yako K., Itoh S., Kawabata T., Yanagisawa Y., Ohnishi T., Takeda H., Kameda D., Kubo T., Sasano M., Baba H., Itahashi K., Ichihara T., Berg G.P.A., Roussel-Chomaz P., Bazin D., Shimbara Y., Nagashima M.: "SHARAQ Spectromete-Current status and future experimental plans-", AIP Conference Proceedings **1224** (2010) 573.

Uesaka T., Michimasa S., Ota S., Saito A., Nakanishi K., Sasamoto Y., Miya H., Tokieda H., Kawase S., Shimizu Y., Shimoura S., Miki K., Noji S., Sakai H., Yako K., Itoh S., Kawabata T., Yanagisawa Y., Ohnishi T., Takeda H., Kameda D., Kubo T., Sasano M., Baba H., Itahashi K., Ichihara T., Berg G.P.A., Roussel-Chomaz P., Bazin D., Shimbara Y., Nagashima M.: "Current status and future experimental program of the SHARAQ spectrometer", AIP Conference Proceedings **1235** (2010) 308.

Zhou P., Fang DQ., Ma YG., Cai XZ., Chen JG., Guo W., Sun XY., Tian WD., Wang HW., Zhang GQ., Cao XG., Fu Y., Hu ZG., Wang JS., Wang M., Togano Y., Aoi N., Baba H., Honda T., Okada K., Hara Y., Ieki K., Ishibashi Y., Itou Y., Iwasa N., Kanno S., Kawabata T., Kimura H., Kondo Y., Kurita K., Kurokawa M., Moriguchi T., Murakami H., Oishi H., Ota S., Ozawa A., Sakurai H., Shimoura S., Shioda R., Takeshita E., Takeuchi S., Yamada K., Yamada Y., Yasuda Y., Yoneda K., Motobayashi T., "Measurement of two-proton correlation from the break-up of ^{23}Al", Proc. of International Conference on Nuclear Reactions on Nucleons and Nuclei, Oct. 5–9, 2009, Messina, Itally, International Jounal of Modern Physics E Nuclear Physics **19** (2010) 957–964

Togano Y., Motobayashi T., Aoi N., Baba H., Bishop S., Doornenbal P., Furukawa T., Kanno S., Kondo Y., Kurokawa M., Matsuo Y., Murakami H., Takeuchi S., Yamada K., Yoneda K., Cai X., Fang D., Ma YG., Tian W., Wang H., Ieki K., Kurita K., Matsushita M., Okada K., Shioda R., Yamada Y., Iwasa N., Kume N., Kawabata T., Ota S., Shimoura S., Kobayashi N., Nakamura T., Satou Y., Tanaka K., Kuboki T., Wang J.: "Experimental investigation of the stellar reaction ^{30}S(p,γ)^{31}Cl via coulomb dissociation", Proc. of International Symposium on Forefronts of Researches in Exotic Nuclear Structures, Mar. 1– 4, 2010, Tokamachi, JAPAN, Mod. Phys. Lett. A **25** (2010) 1763–1766

Morikawa T., Ideguchi E., Ota S., Oshima M., Koizumi M., Toh Y., Kimura A., Harada H., Furutaka K., Nakamura S., Kitatani F., Hatsukawa Y., Shizuma T., Sugawara M., Miyatake H., Watanabe Y.X., Hirayama Y., Oi M.: "Superdeformed band in asymmetric $N > Z$ nucleus ^{40}Ar", Proc. of International Symposium on Forefronts of Researches in Exotic Nuclear Structures, Mar. 1–4, 2010, Tokamachi, JAPAN, Mod. Phys. Lett. A **25** (2010) 1792–1795

Sun XY., Chen JG., Fang DQ., Ma YG., Cai XZ., Guo W., Tian WD., Wang HW., Zhou P., Zhang GQ., Cao XG., Fu Y., Hu ZG., Wang JS., Wang M., Togano Y., Aoi N., Baba H., Honda T., Okada K., Hara Y., Ieki K., Ishibashi Y., Itou Y., Iwasa N., Kanno S., Kawabata T., Kimura H., Kondo Y., Kurita K., Kurokawa M., Moriguchi T., Murakami H., Oishi H., Ota S., Ozawa A., Sakurai H., Shimoura S., Shioda R., Takeshita E., Takeuchi S., Yamada K., Yamada Y., Yasuda Y., Yoneda K., Motobayashi T., "Measurement of the proton-proton correlation function from the break-up of ^{22}Mg and ^{20}Ne", Proc. of International Workshop on Nuclear Dynamics in Heavy-Ion Reactions and the Symmetry Energy (IWND2009), Aug. 23–25, 2009, Shnghai, Peoples R CHINA, International Jounal of Modern Physics E Nuclear Physics **19** (2010) 1823–1828

Satou Y., Nakamura T., Fukuda N., Sugimoto T., Kondo Y., Matsui N., Hashimoto Y., Nakabayashi T., Okumura Y., Shinohara M., Motobayashi T., Yanagisawa Y., Aoi N., Takeuchi S., Gomi T., Togano Y., Kawai S., Sakurai H., Ong H.J., Onishi T.K., Shimoura S., Tamaki M., Kobayashi T., Otsu H., Endo N., Kitayama M., Ishihara M., "Invariant mass spectroscopy of ^{19,17}C and ^{14}B using proton inelastic and charge-exchange reactions", Proceedings of the 10th International Conference on Nucleus-Nucleus Collisions (NN2009), Aug. 17–21, 2009, Beijing, China, Nucl. Phys. **A834**, 404c–407c (2010).

Zhou P., Fang D.Q., Ma Y.G., Cai X.Z., Chen J.G., Guo W., Sun X.Y., Tian W.D., Wang H.W., Zhang G.Q., Cao X.G., Fu Y., Hu Z.G., Wang J.S., Wang M., Togano Y., Aoi N., Baba H., Honda T., Okada K., Hara Y., Ieki K., Ishibashi Y., Itou Y., Iwasa N., Kanno S., Kawabata T., Kimura H., Kondo Y., Kurita K., Kurokawa M., Moriguchi T., Murakami H., Oishi H., Ota S., Ozawa A., Sakurai H., Shimoura S., Shioda R., Takeshita E., Takeuchi S., Yamada K., Yamada Y., Yasuda Y., Yoneda K., Motobayashi T., "Measurement of two-proton correlation from the break-up of ^{23}Al", Proceedings of International Workshop on Nuclear Dynamics in Heavy-ion Reactions and the Symmetry Energy, Aug. 23–25, 2009, Shanghai, China, Int. J. Mod. Phys. **E19**, 957–964 (2010).

Sun X.Y., Chen J.G., Fang D.Q., Ma Y.G., Cai X.Z., Guo W., Tian W.D., Wang H.W., Zhou P., Zhang G.Q., Cao X.G., Fu Y., Hu Z.G., Wang J.S., Wang M., Togano Y., Aoi N., Baba H., Honda T., Okada K., Hara Y., Ieki K., Ishibashi Y., Itou Y., Iwasa N., Kanno S., Kawabata T., Kimura H., Kondo Y., Kurita K., Kurokawa M., Moriguchi T., Murakami H., Oishi H., Ota S., Ozawa A., Sakurai H., Shimoura S., Shioda R., Takeshita E., Takeuchi S., Yamada K., Yamada Y., Yasuda Y., Yoneda K., Motobayashi T., "MEASUREMENT OF THE PROTON-PROTON CORRELATION FUNCTION FROM THE BREAK-UP OF ^{22}Mg AND ^{20}Ne", Proceedings of International Workshop on Nuclear Dynamics in Heavy-ion Reactions and the Symmetry Energy, Aug. 23–25, 2009, Shanghai, China, Int. J. Mod. Phys. **E19**, 1823–1828 (2010).

Togano Y., Motobayashi T., Aoi N., Baba H., Bishop S., Doornenbal P., Furukawa T., Kanno S., Kondo Y., Kurokawa M., Matsuo Y., Murakami H., Takeuchi S., Yamada K., Yoneda K., Cai X., Fang D., Ma Y.G., Tian W., Wang H., Ieki K., Kurita K., Matsushita M., Okada K., Shioda R., Yamada Y., Iwasa N., Kume N., Kawabata T., Ota S., Shimoura S., Kobayashi N., Nakamura T., Satou Y., Tanaka K., Kuboki T., Wang J., "EXPERIMENTAL INVESTIGATION OF THE STELLAR REACTION ^{30}S(p,γ)^{31}Cl VIA COULOMB DISSOCIATION", Proceedings of International Symposium on Forefronts of Researches in Exotic Nuclear Structures (Niigata 2010), Mar. 1–4, 2010, Niigata, Japan, Mod. Phys. Lett. A. **25**, 1763–1766 (2010).

Saito A., Shimoura S., Minemura T., Matsuyama Y.U., Baba H., Aoi N., Gomi T., Higurashi Y., Ieki K., Imai N., Iwasa N., Iwasaki H., Kanno S., Kubono S., Kunibu

M., Michimasa S., Motobayashi T., Nakamura T., Ryuto H., Sakurai H., Serata M., Takeshita E., Takeuchi S., Teranishi T., Ue K., Yamada K., Yanagisawa Y., "THE ^{6}He+^{6}He AND α+^{8}He CLUSTER STATES IN ^{12}Be VIA α-INELASTIC SCATTERING", Proceedings of International Symposium on Forefronts of Researches in Exotic Nuclear Structures (Niigata 2010), Mar. 1–4, 2010, Niigata, Japan, Mod. Phys. Lett. A. **25**, 1858–1861 (2010).

Kubono S., Binh D.N., Hayakawa S., Hashimoto H., M. D., Wakabayashi Y., Yamaguchi H., Teranishi T., Iwasa N., Komatsubara T., Kato S., Khiem L.H.: "Nuclear Clusters in Astrophysics", Proc. of the 10th International Conference on Nucleus-Nucleus Collisions (NN2009), August 16-21, 2009, Beijing, China Nucl. Phys. A **834**, (2010) 647c – 650c,

Satou Y., Nakamura T., Fukuda N., Sugimoto T., Kondo Y., Matsui N., Hashimoto Y., Nakabayashi T., Okumura Y., Shinohara M., Motobayashi T., Yanagisawa Y., Aoi N., Takeuchi S., Gomi T., Togano Y., Kawai S., Sakurai H., Ong H.J., Onishi T.K., Shimoura S., Tamaki M., Kobayashi T., Otsu H., Endo N., Kitayama M., Ishihara M., "Invariant mass spectroscopy of ^{19,17}C and ^{14}B using proton inelastic and charge-exchange reactions", Proc. the 10th International Conference on Nucleus-Nucleus Collisions (NN2009), Beijing, China, 16–21 August 2009, Nucl. Phys. A **834** (2010) 404c–407c,

Kubono S., Binh D.N., Hayakawa S., Hashimoto T., Kahl D.M., Yamaguchi H., Wakabayashi Y., Teranishi T., Iwasa N., Komatsubara T., Kato S., and , Khiem L.H.: "Nuclear Astrophysics Programs with Low-Energy RI Beams at CRIB", Proc. of the International Symposium on Exotic Nuclei (EXON), Sochi, Russia, October, 2009, AIP Conf. Proc. vol. 1224 (2010) 475 - 481 (2010),*

Kubono S.: "Nuclear Cluster Aspects in Astrophysics", Proc. of the 5th European Summer School on Nuclear Astrophysics, Sept. 20 - 27, 2009, Santa Tecla, Italy, AIP Conf. Proc. vol. 1213 (2010) 107 - 111,*

Morikawa T., Ideguchi E., Ota S., Oshima M., Koizumi M., Toh Y., Kimura A., Harada H., Furutaka K., Nakamura S., Kitatani F., Hatsukawa Y., Shizuma T., Sugawara M., Miyatake H., Watanabe Y.X., Hirayama Y., Oi M.: "SUPERDEFORMED BAND IN ASYMMETRIC N ¿ Z NUCLEUS ^{40}Ar", Proceedings of International Symposium on Forefronts of Researches in Exotic Nuclear Structures (Niigata 2010), Mar. 1–4, 2010, Niigata, Japan, Mod. Phys. Lett. A. **25**, 1792–1795 (2010).

Odahara A., Takahima A., Suga M., Tajiri K., Kurata K., Takatsu J., Ito Y., Kenmoku Y., Yamaguchi K., Kazato M., Kura K., Shimoda T., Suzuki T., Watanabe H., Nishimura S., Gono Y., Ideguchi E., Go S., Wakabayashi Y., Morikawa T., Petrache C., Beaumel D.: "ISOMER SPECTROSCOPY AT RI BEAM LINE IN RCNP", Proceedings of International Symposium on Forefronts of Researches in Exotic Nuclear Structures (Niigata 2010), Mar. 1–4, 2010, Niigata, Japan, Mod. Phys. Lett. A. **25**, 1951–1954 (2010).

Uesaka T., Michimasa S., Ota S., Saito A., Nakanishi K., Sasamoto Y., Miya H., Tokieda H., Kawase S., Shimizu Y., Shimoura S., Miki K., Noji S., Sakai H., Yako K., Itoh S., Kawabata T., Yanagisawa Y., Ohnishi T., Takeda H., Kameda D., Kubo T., Sasano M., Baba H., Itahashi K., Ichihara T., Berg G.P.A., Roussel-Chomaz P., Bazin D., Shimbara Y., Nagashima M.: "SHARAQ Spectrometer-Current Status and Future Eexperimental Plans", Proc. Intern. Symposium Exotic Nuclei, Sochi, (Russia), 28 Sept.–2 Oct. 2009, Yu.E.Penionzhkevich, S.M.Lukyanov, Eds., p.573–581 (2010); AIP Conf.Proc. 1224 (2010).

Yamaguchi H., Hashimoto T., Hayakawa S., N. Binh D., Kahl D., Kubono S.: "Nuclear Astrophysics and Structure Studies Using Low-energy RI Beams at CRIB", 7th Japan-China Joint Nuclear Physics Symposium, Nov. 9–13, 2009, Tsukuba University, Tsukuba, Japan. AIP conference proceeding **1235** (2010) 247–252 .

Yamaguchi H., Hashimoto T., Hayakawa S., N. Binh D., Kahl D., Kubono S.: "Studies of alpha-induced astrophysical reactions at CRIB", The 10th International Symposium on Origin of Matter and Evolution of Galaxies: OMEG–2010, March 8–10, 2010, RCNP, Osaka University, Osaka, Japan AIP conference proceeding **1269** (2010) 262–267 .

Hayakawa S., Kubono S., Hashimoto T., Yamaguchi H., N. Binh D., Kahl D., Wakabayashi Y., Iwasa N., Kume N., Miura I., Teranishi T., J. He J., K. Kwon Y., Komatsubara T., Kato S., Wanajo S.: "Direct measurement of the ^{11}C$(\alpha,p)^{14}$N stellar reaction at CRIB", AIP Conference Proceedings Volume 1269 (2010) pp104–109, The 10th International Symposium on Origin of Matter and Evolution of Galaxies (OMEG2010).

Aramaki Y., *et al.*, for the PHENIX Collaboration, "Neutral pion production with respect to reaction plane in Au+Au collisions at RHIC-PHENIX", Proc. of the 20th International Conference in Ultra-Relativistic Nucleus-Nucleus Collisions (QM2008), Indian Journal of Physics 84, pp1669-1673, 2010

Akimoto R.: "Development of a Time Projection Chamber (TPC) Using Gas Electron Multiplier (GEM) for Use as an Active Target", Proc. of 2010 IEEENuclear Science Symposium Conference Record, Oct. 30 - Nov. 6, 2010

Akimoto R., Hamagaki H., Gunji T., Yamaguchi Y.L., Hori Y.: "Measurement of the basic features of Thick-GEM and Resistive GEM", Proc. of the 1st International conference on Micro Pattern Gaseous Detectors, Jun. 12–15, 2009, Crete, Greece, Journal of Instrumentation, **5** (2010)

Oral Presentations

(International Conference etc.)

Uesaka T.: "Polarization Study of Unstable Nuclei", ECT* Wrokshop on Reactions and Nucleon Properties in Rare Isotpe, 6-10, April 2010, Trento, Italy

Uesaka T.: "High-resolution SHARAQ Spectrometer at RI Beam Factory", International Nuclear Physics Conference 2010, 4-9 July 2010, Vancouver, Canada

Uesaka T.: "SHARAQ Spectromete", 4th International Expert Meeting on In-flight Separators and Related Issues, 15-17 December 2010, Darmstadt, Germany

Uesaka T.: "Spin-isospin studies with the SHARAQ Spectromete", University of Aizu-JUSTIPEN-EFES Symposium on Cutting-Edge Physics of Unstable Nuclei, 10-13 November 2010, Aizu, Japan

Matsubara H., Takaki M., Uesaka T., for E358 collaboration (Poster): "Spectroscopy of ^{9}He via the (^{18}O,^{18}Ne) reaction by high resolution spectrograph Grand Raiden at RCNP", HALO2010, Dec. 7–9, 2010, Shonan international village, Kanagawa, Japan.

Shimoura S.: "Direct reactions populating continuum states of exotic nuclei", Japan-Italy EFES Workshop, Sept. 6–8, 2010, Istituti di Fisica, Torino, Italy.

Shimoura S.: "Single-particle wave functions near the threshold — coupled-channel effects on spectroscopic factors —", ECT* Workshop on Reactions and Nucleon Properties in Rare isotopes, April 6–10, 2010, Trento, Italy.

Uesaka T.: "Polarization study of unstable nuclei", ECT* Workshop on Reactions and Nucleon Properties in Rare isotopes, April 6–10, 2010, Trento, Italy.

Shimoura S.: "Nuclear Physics Research at CNS", The International Symposium on Nuclear Physics in Asia, Oct. 13–15, 2010, Beihang University, Beijing, China.

Kubono S.: " Experimental Approach to Explosive Nucleosynthesis with Low-Energy RI beams", The International Symposium on Nuclear Physics in Asia, Oct. 13–15, 2010, Beihang University, Beijing, China.

Ideguchi E.: "Superdeformed band in asymmetric N¿Z nucleus, ^{40}Ar", Nuclear Sturucture 2010 conference, August 8–13, 2010, Clark-Kerr Campus, U.C. Berkeley, CA, USA.

Ideguchi E.: "Superdeformed Band in Asymmetric N¿Z Nucleus, ^{40}Ar, and High-Spin Studies in A=30∼40 Nuclei", University of Aizu-JUSTIPEN-EFES symposium on 'utting-Edge Physics of Unstable Nuclei, November 10–13, 2010, University of Aizu, Fukushima, Japan.

Kubono S.: "Experimental Approach to Hydrogen Burning at Extremely High-Temperatures – The αp-Process–", Pan-American Advanced Studies Institute on Rare Isotopes (PASI), invited talk, Joao Pessoa, 2010.8.2-13

Kubono S.: "Nuclear Astrophysics with Low-Energy, High-Intensity RI Beams at CRIB", International Symposium on Asian Nuclear Science (ISANS) Beijing, 2010.10.14-15

Kubono S.: "Experimental Approach to Hydrogen Burning at Extremely High-Temperatures - Cluster and the αp-Process -", Korea-Japan Workshop on Nuclear Physics and Nuclear Astrophysics, Seoul, 2010.10.26

Kubono S.: "Experimental Approach to Explosive Phenomena in the Universe with Low-Energy RI Beams", Topical Conference on Nuclear Physics, High Energy Physics, and Astrophysics, Hanoi, 2010.10.8-12

Yamaguchi H., Hashimoto T., Hayakawa S., Binh D.N., Kahl D., Kubono S.: "Alpha-resonance-scattering measurements at CRIB", Second EMMI-EFES workshop on neutron-rich nuclei (EENEN10), June 16–18, 2010, RIKEN, Wako, Japan.

Yamaguchi H., Hashimoto T., Hayakawa S., Binh D.N., Kahl D., Kubono S.: "Alpha-induced astrophysical reactions studied at CRIB", 11th Symposium on Nuclei in the Cosmos (NIC XI), Jul. 19–23, 2010, Heidelberg, Germany.

Yamaguchi H.: "Experimental techniques with RIB – Introduction of CRIB facility–", Korea-Japan joint workshop for the nuclear physics and the nuclear astrophysics, Oct. 26, 2010, Seoul National University, Seoul, Korea.

Yamaguchi H., Hashimoto T., Hayakawa S., Binh D.N., Kahl D., Kubono S.: "Studies for alpha-induced astrophysical reactions at CRIB", University of Aizu-JUSTIPEN-EFES Symposium on Cutting-Edge Physics of Unstable Nuclei, Nov. 10–13, 2010, University of Aizu, Fukushima, Japan.

Hayakawa S., Kubono S., Hashimoto T., Yamaguchi H., Binh D.N., Kahl D., Wakabayashi Y., Iwasa N., Kume N., Miura Y., Teranishi T., He J.J., Kwon Y.K., Komatsubara T., Kato S., Wanajo S.: "Direct determination of the ^{11}C$(\alpha,p)^{14}$N reaction rate with CRIB: an alternative synthesis path to the CNO elements", at 11th Symposium on Nuclei in the Cosmos, Jul. 19–23, 2010, Heidelberg, Germany.

Gunji T.: "W+Si Forward tracking calorimeter for the ALICE upgrade", Workshop on the PHENIX decadal plan, Dec. 12-14, 2010, BNL, USA

Akimoto R.: "Development of a Time Projection Chamber (TPC) Using Gas Electron Multiplier (GEM) for Use as an Active Target", 2010 Nuclear Science Symposium and Medical Imaging Conference (IEEE), 10/30- 11/6, 2010, Knoxville, USA

Takahara A., for the PHENIX Collaboration,: "Measurement of the Ultra-peripheral J/ψ Cross Section in Au+Au Collisions with the PHENIX Detector", The Third Asian Triangle Heavy-Ion Conference (ATHIC 2010), 10/18-20, 2010, Wuhan, China

Hamagaki H., for the ALICE Collaboration,: "The first results from ALICE", Workshop on High Energy Strong Interactions 2010, 8/10-8/13, 2010, Yukawa Institute for Theoretical Physics, in Kyoto, Japan,

Gunji T.: "Heavy quark and quarkonia production in high energy nucleus-nucleus collisions at RHIC and LHC", Workshop on High Energy Strong Interactions 2010, 8/10-8/13, 2010, Yukawa Institute for Theoretical

Physics, in Kyoto, Japan,

Hori Y.: "Simulation study of Forward Calorimeter in LHC-ALICE experiment", 14th International Conference on Calorimetry in High Energy Physics, 5/10-5/14, 2010, Peking, China

Suzuki T.: "Electron capture reactions in fp-shell nuclei and beta decays in rare isotones", ECT* Workshop on Reactions and Nucleon Properties in Rare Isotopes, April 2010, Torento, Italy.

Suzuki T., Honma M., Yoshida T., Mao H., Kajino T., Otsuka T.: "Gamow-Teller and First-forbidden Transition Strengths in Astrophysical Processes", International Nuclear Physics Conference 2010 (INPC2010), July 9, 2010, Vancouver, Canada.

Suzuki T., Honma M., Mao H., Yoshida T., Kajino T., Otsuka T.: "Electron capture reactions and beta decays in astrophysical environments", The 3rd International Conference on Frontiers in Nuclear Structure, Astrophysics and Reactions (FINUSTAR3), August 23, 2010, Rhodos, Greece.

Suzuki T.: "Nuclear weak processes in stars", Japan-Italy EFES Workshop on Correlations in REactions and Continuum, Sept. 8, 2010, Torino, Italy.

Suzuki T., Honma M., Yoshida T., Mao H., Kajino T., Otsuka T.: "Spin dependent nuclear weak processes and nucleosynthesis in stars", International School of Physics, 32nd Cource, Particle and Nuclear Astrophysics, Sept. 22, 2010, Erice, Italy.

Suzuki T., Otsuka T.: "Spin modes in nuclei and nuclear forces", Internationa Symposium on New Faces of Atomic Nuclei, Nov. 15, 2010, Okinawa, Japan.

Suzuki T., "Beta decays and isobaric analog states of exotic light nuclei", Internationa Symposium on HALO 2010, Dec. 8, 2010, Zushi, Japan.

Yoshida T., Itagaki N., Kato K.: " $Sp(2,R)_z$ structure and monopole strength in ^{12}C", Halo2010, Dec. 6–9, 2010, Shonan Village Center, Hayama, Japan.

Saito A.: "The ^{6}He+^{6}He and α+^{8}He cluster states in ^{12}Be via inelastic scattering", International Symposium on Forefronts of Researches in Exotic Nuclear Structures (Niigata2010), March 1–4, 2010, Tokamachi, Niigata, Japan.

Uesaka T.: "The SHARAQ Spectrometer", ICHOR-EFES International Symposium on New Facet of Spin-Isospin Responses 2010, Feb. 18–21, 2010, University of Tokyo, Tokyo, Japan

Sasamoto Y., Uesaka T., Sakai H., Shimoura S., Noji S., Yako K., Michimasa S., Ota S., Saito A., Miki K., Tokieda H., Miya H., Kawase S., Kubo T., Yoshida K., Ohnishi T., Yanagisawa Y., Fukuda N., Takeda H., Kameda D., Aoi N., Takeuchi S., Ichihara T., Baba H., Sakaguchi S., Shimizu Y., Schiet H., Doornembal P., Kawabata T., Itoh K., Kawahara T., Maeda Y., Saitoh T., Itoh M., Zegers R.G.T., Sasano M., Roussel-Chomaz P., Berg G.P.A.: "The super-allowed Fermi type charge exchange reaction for studies of isovector non-spin-flip monopole resonance", ICHOR-EFES International Symposium on New Facet of Spin-Isospin Responses (SIR2010) , Feb. 18–21, 2010, Koshiba Hall, University of Tokyo, Japan.

Ota S.: "Active Target Development in CNS", GET-ACTAR General Meeting, Jan. 11–15, 2010, Ferme de la Rançonnière, Crepon, France.

Ota S.: "Study of giant resonances in unstable nuclei with CNS Active Target", ICHOR-EFES International Symposium on New Facet of Spin-Isospin Responses (SIR2010) , Feb. 18–21, 2010, Koshiba Hall, University of Tokyo, Japan.

Miki K., Sakai H., Uesaka T., Baba H., Berg G.P.A., Fukuda N., Kameda D., Kawabata T., Kawase S., Kubo T., Kusaka K., Michimasa S., Miya H., Noji S., Ohnishi T., Ota S., Saito A., Sasamoto Y., Sasano M., Shimoura S., Takeda H., Tokieda H., Yako K., Yanagisawa Y., Yoshida A., Yoshida K., and , Zegers R.G.T.: "Search for the Isovector Spin Monopole Resonance via the ^{208}Pb,^{90}Zr$(t,^{3}$He) Reactions at 300 MeV/u", The 4th LACM-EFES-JUSTIPEN Workshop, Mar. 15–17, 2010, Oak Ridge National Laboratory, Tennessee, USA

Miki K., Sakai H., Uesaka T., Baba H., Berg G.P.A., Fukuda N., Kameda D., Kawabata T., Kawase S., Kubo T., Kusaka K., Michimasa S., Miya H., Noji S., Ohnishi T., Ota S., Saito A., Sasamoto Y., Sasano M., Shimoura S., Takeda H., Tokieda H., Yako K., Yanagisawa Y., Yoshida A., Yoshida K., and , Zegers R.G.T.: "Measurement of the ^{208}Pb and ^{90}Zr$(t,^{3}$He) reactions at 300 MeV/u – the first physics measurement with SHARAQ –", ICHOR-EFES International Symposium on New Facet of Spin-Isospin Responses (SIR2010), Feb. 18–21, 2010, University of Tokyo, Tokyo, Japan

Yamaguchi H., Hashimoto T., Hayakawa S., Binh D.N., Kahl D., Kubono S.: "Status of the studies on nuclear reactions and structures at CRIB", The 6th International Workshop on "Physics with Stopped and Slow Radioisotope Beams (SSRI)", Mar 1–2, 2010, Tokyo Institute of Technology, Tokyo, Japan.

Yamaguchi H., Hashimoto T., Hayakawa S., Binh D.N., Kahl D., Kubono S.: "Studies for alpha-induced astrophysical reactions at CRIB", The 10th. International Symposium on. Origin of Matter and Evolution of the Galaxies (OMEG10), March 8–10, 2010, RCNP, Osaka University, Osaka, Japan.

Suzuki T.: "Shell Model Study of Spin Modes in Ni and Ca Isotopes", EFES-NSCLWorkshop on Perspectives on the Modern Shell Model and Related Experimental Topics, Feb. 2010, Michigan State University, U.S.A.

Suzuki T.: "Nuclear Weak Processes and Nucleosynthesis in Stars", ICOR-EFES International Symposium on New Facet of Spin-isospin Responses (SIR2010), Feb. 2010, Koshiba Hall, Univ. of Tokyo, Japan

Suzuki T., Yoshida T., Utsuno Y.: "Half-lives of N=126

Isotones and the r-Process", 10th International Symposium on Origin of Matter and Evolution of the Galaxies (OMEG10), Mar. 2010, RCNP, Osaka, Japan

Suzuki T.: "GT and FF Transitions in Astrophysical Processes", The 4th LACM- EFES-JUSTIPEN Workshop, Mar. 2010, Oak Ridge, USA

(Domestic Conference)

Uesaka T.: "Heavy-ion charge exchange reactions with transitions within supermultiplet members", RCNP workshop on Nuclear Reaction, 2-4 August 2010, Osaka, Japan

Uesaka T.: "Tensor force effects in few-body reactions with large momentum transfer", RCNP 研究会核構造の真の理解に向けて－テンソル力と高運動量成分－戦略会議, 25-26 November 2010, Osaka, Japan

Ideguchi E., "Gamma-ray spectroscopy at storage ring", RCNP Workshop on Physics of heavy-ion strage ring, September 24–25, RCNP, Osaka university, Japan.

Kubono S.: "Experimental Approach to Explosive Nucleosynthesis in pp and CNO regions at CRIB", Workshop on Impact of new $\alpha\alpha\alpha$ reaction rate on stellar evolution and nucleosynthesis, RIKEN, 2010.12.17-18

Yamaguchi H., Hashimoto T., Hayakawa S., Binh D.N., Kahl D., Kubono S.: "Studies on 7Li/7Be+alpha resonant scatterings", RIBF-ULIC Symposium on Impact of the new $\alpha\alpha\alpha$ reaction rate on stellar evolution and nucleosynthesis, Dec. 17–18, 2010, RIKEN Nishina Center, Wako, Japan.

Yamaguchi H., "Experiments on alpha resonance state", Mini-workshop for resonance elastic scattering in inverse kinematics, Dec. 17, 2010, RIKEN Nishina Center, Wako, Japan.

Hayakawa S., Kubono S., Hashimoto T., Yamaguchi H., Binh D.N., Kahl D., Wakabayashi Y., Iwasa N., Kume N., Miura Y., Teranishi T., He J.J., Kwon Y.K., Komatsubara T., Kato S., Wanajo S.: "Direct measurement of the $^{11}\mathrm{C}(\alpha,p)^{14}\mathrm{N}$ reaction $\sim$ pp to CNO $\sim$", at Impact of New Triple Alpha Reaction Rate on Stellar Evolution and Nucleosynthesis, Dec. 19–23, 2010, RIKEN, Wako, Japan.

Kawahara T., Uesaka T., Shimizu Y., Sakaguchi S., Shibusawa A., Wakui T.：“Pulse structure dependence of the proton polarization rate", at the JPS Fall meeting,Sep. 11-14,2010,Kyushu Institute of technology university, Kyushu ,Japan.

Sasamoto Y., Uesaka T., Shimoura S., Michimasa S., Ota S., Tokieda H., Miya H., Kawase S., Kikuchi Y., Kisamori K., Takaki M., Dozono M., Mathubara H., Noji S., Miki K., Yako K., Sakai H., Kubo T., Yanagisawa Y., Yoshida K., Ohnishi T., Fukuda N., Takeda H., Kameda D., Inabe N., Aoi N., Takeuchi S., Ichihara T., Baba H., Sakaguchi S., Doornembal P., He W., Ruijiu C., Shimizu Y., Kawahara T., Kawabata T., Yokota N., Maeda Y., Miyasako H., Berg G.P.A.：“Studies for isovector non-spin-flip monopole resonances via the super allowed Fermi type charge exchange reaction" at the JPS Spring meeting, Mar. 25–28, Niigata university, Niigata, Japan

Miya H., Shimoura S., Saito A., Miki K., Sasano M., Kawabata T., Kawase S., Ota S., Uesaka T., Sakai H.：“Performance evaluation of Low-Pressure Multi-Wire Drift Chamber", at the JPS Autumn meeting, Sep. 11–14, 2010, Kyushu institute of techonogy University, Fukuoka, Japan.

Sasamoto Y., Uesaka T., Shimoura S., Michimasa S., Ota S., Tokieda H., Miya H., Kawase S., Kikuchi Y., Kisamori K., Takaki M., Dozono M., Mathubara H., Noji S., Miki K., Yako K., Sakai H., Kubo T., Yanagisawa Y., Yoshida K., Ohnishi T., Fukuda N., Takeda H., Kameda D., Inabe N., Aoi N., Takeuchi S., Ichihara T., Baba H., Sakaguchi S., Doornembal P., He W., Ruijiu C., Shimizu Y., Kawahara T., Kawabata T., Yokota N., Maeda Y., Miyasako H., Berg G.P.A.：“Studies for isovector non-spin-flip monopole resonances via the super allowed Fermi type charge exchange reaction" at the JPS Spring meeting, Mar. 25–28, Niigata university, Niigata, Japan.

Gunji T.：“Future perspectives and plans of the ALICE experiment", at the JPS Autumn meeting, September 11-14, 2010, Kyusyu Institute of Technology, Kitakyushu, Japan.

Aramaki Y., for the PHENIX Collaboration：“Study of parton energy loss with high-pT pi0 in Au+Au collisions at PHENIX", at the JPS Autumn meeting, September 11-14, 2010, Kyusyu Institute of Technology, Kitakyushu, Japan.

Sano S., for the ALICE Collaboration, "The Status and the results in measurement of charged particles" at the JPS Autumn meeting, September 11-14, 2010, Kyusyu Institute of Technology, Kitakyushu, Japan.

Hori Y., for the ALICE-TPC Collaboration, "LHC-ALICE 実験における TPC の ExB ディストーション" at the JPS Autumn meeting, September 11-14, 2010, Kyusyu Institute of Technology, Kitakyushu, Japan.

Tsuji T.：“LHC-ALICE 実験のアップグレードに向けた前方カロリーメーターの研究" at the JPS Autumn meeting, September 11-14, 2010, Kyusyu Institute of Technology, Kitakyushu, Japan.

Uesaka T., Akimoto R., Ota S., Michimasa S., Gunji T., Yamaguchi H., Hashimoto T., Tokieda H., Tsuji T., Kawase S., Hamagaki H., Kubono S., Kawabata T., Isobe T., Ozawa A., Suzuki H., Nagae D., Moriguchi T., Ito Y., Ishibashi Y., Oishi H., Abe Y., Kamiguchi N.: "CNS active targets for Missing Mass Spectroscopy with RI beams", Detector Workshop for RIBF Experiments, Dec. 21–22, 2010, RIKEN, Saitama, Japan

Gunji T., "J/ψ Production in High energy heavy ion collisions at RHIC", at the JPS Spring meeting, Mar. 20–23, 2010, Okayama University, Okayama, Japan.

Sano S., for the ALICE Collaboration: "LHC-ALICE 実験

における粒子多重度測" at the JPS Spring meeting, Mar. 20–23, 2010, Okayama University, Okayama, Japan.

Takahara A., for the PHENIX Collaboration: "Study of J/ψ photoproduction in ultra-peripheral Au+Au collisions at the PHENIX experiment", at the JPS Spring meeting, Mar. 20–23, 2010, Okayama University, Okayama, Japan.

Akimoto R., Ota S., Michimasa S., Gunji T., Yamaguchi H., Hashimoto T., Tokieda H., Tsuji T., Kawase S., Hamagaki H., Uesaka T., Kubono S., Isobe T., Kawabata T., Ozawa A., Suzuki H., Nagae D., Moriguchi T., Ito Y., Ishibashi Y., Ooishi H., Abe Y.: "Performance evaluation of active target GEM-TPC" at the JPS Spring meeting, Mar. 20–23, 2010, Okayama University, Okayama, Japan.

Tsuji T., Hamagaki H., Gunji T., Hori Y., Kistenev E., Chiu M., Sukhanov A., Seto R.: "Study of basic properties of the Forward Calorimeter for PHENIX upgrade", at the JPS Spring meeting, Mar. 20–23, 2010, Okayama University, Okayama, Japan.

Go S., Shimoura S., Ideguchi E., Ota S., Miya H., Baba H.: "New method of digital pulse shape analysis of signals from segmented Ge detectors by using moments", JPS Spring Meeting, March 20-23, 2010, Okayama University, Okayama, Japan.

Michimasa S., Tokieda H., Noji S., Ota S., Shimoura S., Uesaka T., Sakai H., Roussel-Chomaz P., Libin J-F., Gangnant P., Spetaels C.: "Performance of Detectors Installed at SHARAQ Final Focal Plane", JPS Spring Meeting, March 20-23, 2010, Okayama University, Okayama, Japan.

Kawase S., Ota S., Baba H., Shimoura S., Uesaka T.: "Performance Evaluation of Charge-to-Time-Converter (QTC)", the 65th JPS Annual Meeting, Mar. 20–23, 2010, Okayama University, Okayama, Japan.

Ota S., Shimoura S., Aoi N., Takeshita E., Takeuchi S., Suzuki H., Baba H., Fukuchi T., Fukui T., Hashimoto Y., Ideguchi E., Ieki K., Iwasa N., Iwasaki H., Kanno S., Kondo Y., Kubo T., Kurita K., Minemura T., Michimasa S., Motobayashi T., Murakami T., Nakabayashi T., Nakamura T., Niikura M., Okumura T., Onishi T.K., Sakurai H., Shinohara M., Suzuki D., Suzuki M., Tamaki M., Tanaka K., Togano Y., Wakabayashi Y., Yamada K.："High Resolution Gamma-ray Spectroscopy of N=20 Neutron-rich Nuclei via Direct Reactions", the 65th JPS Annual Meeting, Mar. 20–23, 2010, Okayama University, Okayama, Japan.

Miki K., Sakai H., Uesaka T., Baba H., Berg G.P.A., Fukuda N., Kameda D., Kawabata T., Kawase S., Kubo T., Kusaka K., Michimasa S., Miya H., Noji S., Ohnishi T., Ota S., Saito A., Sasamoto Y., Sasano M., Shimoura S., Takeda H., Tokieda H., Yako K., Yanagisawa Y., Yoshida A., Yoshida K., and , Zegers R.G.T.: "Measurement of the the isovector spin monopole resonance via the ^{208}Pb,^{90}Zr(t,^{3}He) reactions at 300 MeV/u", at the JPS Spring meeting, Mar. 20–23, 2010, Okayama University, Okayama, Japan.

Suzuki T.: "Beta decay modes of nuclei in the third peak region of the r-process", at the 65th JPS Annual meeting, Mar. 20–23, 2010, Okayama University, Okayama, Japan

Yoshida T., Kato K.: Study of ^{12}C structure based on Sp(2,R) algebra", at the JPS meeting, Mar. 20-23, 2010, Okayama University, Okayama, Japan.

TORIJIN (Todai-RIKEN Joint International Program for Nuclear Physics) Term)

Publications

[Journal]

(Original Papers)　*Subject to Peer Review

Suzuki T., Honma M., Yoshida T., Mao H., Kajino T., Otsuka T.: “Spin-Dependent Nuclear Weak Processes and Nucleosynthesis in Stars”, Prog. in Part and Nucl. Phys. **66**, 385–389 (2011). *

Ebata S., Nakatsukasa T., Inakura T., Yoshida K., Hashimoto Y., Yabana K.: “Canoical-Basis Time-Dependent Hartree-Fock-Bogoliubov Theory and Linear-Response Calculations”, Phys. Rev. C **82**, 034306 1-13 (2010). *

Itagaki N., Ploszaiczak M., Cseh J.: “Simplified Modeling of Cluster-shell Competition in ^{20}Ne and ^{24}Mg”, Phys. Rev. C **83**, 014302 1-12 (2011). *

Iwata Y., Otsuka T., Maruhn J.A., Itagaki N.: “Suppression of Charge Equilibration Leading to the Synthesis of Exotic Nuclei”, Phys. Rev. Lett. **104**, 252501 1-4 (2011). *

Khan E., Margueron J., Colo G., Hagino K., Sagawa H.: “Effect of Pairing Correlations on Incompressibility and Symmetry Energy in Nuclear Matter and Finite Nuclei”, Phys. Rev. C. **82**, 24322 1-9 (2010). *

Matic A. et al.: “High-precision (p,t) Reaction to Determne 25Al(p,gamma)26Si Reaction Rates”, Phys. Rev. C. **82**, 025807 1-12 (2010). *

Hinohara N., Kanada-Enyo Y.: “Triaxial Quadrupole Deformation Dynamics in sd-shell Nuclei Around 26Mg”, Phys. Rev. A. **849**, 53-71 (2011). *

Nomura K., Shimizu N., and Otsuka T.: “Formulating the Interaction Boson Model by Mean field Methods”, Phys. Rev. C. **81**, 44307 1-20 (2010). *

VII. LIST OF PREPRINTS

RIKEN-NC-NP

(2010 April ～2011 March)

1 P. Doornenbal, H. Scheit, N. Kobayashi, N. Aoi, S. Takeuchi, K. Li, E. Takeshita, Y. Toganao, H. Wang, S. Deguchi, Y. Kawada, Y. Kondo, T. Motobayashi, T. Nakamura, Y. Satou, K. N. Tanaka, and H. Sakurai "Exploring the "Island of Inversion" by in-beam gamma-ray spectroscopy of the neutron-rich sodium isotopes 31,32,33Na" May, 2010

2 T. Ohnishi, T. Kubo, K. Kusaka, A. Yoshida, K. Yoshida, M. Ohtake, N. Fukuda, H. Takeda, D. Kameda, K. Tanaka, N. Inabe, Y. Yanagisawa, Y. Gono, H. Watanabe, H. Otsu, H. Baba, T. Ichihara, Y. Yamaguchi, M. Takechi, S. Nishimura, H. Ueno, A. Yoshimi, H. Sakurai, T. Motobayashi, T. Nakao, Y. Mizoi, M. Matsushita, K. Ieki, N. Kobayashi, K, Tanaka, Y. Kawada, N. Tanaka, S. Deguchi, Y. Satou, Y. Kondo, T. Nakamura, K. Yoshinaga, C. Ishii, H. Yoshii, Y. Miyashita, N. Uematsu, Y. Shiraki, T. Sumikama, J. Chiba, E. Ideguchi, A. Saito, T. Yamaguchi, I. Hachiuma, T. Suzuki, T. Moriguchi, A. Ozawa, T. Ohtsubo, M. A. Famiano, H. Geissel, A. S. Nettleton, O. B. Tarasov, D. P. Bazin, B. M. Sherrill, S. L. Manikonda, and J. A. Nolen "Identification of 45 New Neutron-Rich Isotopes Produced by In-Flight Fission of a 238U Beam at 345 MeV/nucleon" May, 2010

3 E. Yu. Nikolski, A. A. Korsheninnikov, H. Otsu, H. Suzuki, K. Yoneda, H. Baba, K. Yamada, Y. Kondo, N. Aoi, A. S. Denikin, M. S. Golovkov, A. S. Fomichev, S. A. Krupko, M. Kurokawa, E. A. Kuzmin, I. Martel, W. Mittig, T. otobayashi, T. Nakamura, M. Niikura, S. Nishimura, A. A. Ogloblin, P. Roussel-Chomaz, A. Sanchez-Benitez, Y. Sato, S. I. Sidorchuk, T/ Suda, S. Takeuchi, K. Tanaka, G. M. Ter-Akopian, Y. Toganao, and M. Yamaguchi "Search for 7H in 2H + 8He collisions" May, 2010

4 Y. Kondo, T. Nakamura, Y. sato, T. Matsumoto, N. Aoi, N. Endo, N. Fukuda, T. Gomi, Y. Hashimoto, M. Ishihara, S. Kawai, M. Kitayama, T. Kobayashi, Y. Matsuda, N. Matsui, T. Motobayashi, T. Nakabayashi, T. Okumura. H. J. Ong, T. K. Onishi, K. Ogata, H. Otsu, H. Sakurai, S. Shimoura, M. Shinohhara, T. Sugimoto, S. Takeuchi, M. Tamaki, Y. Togano, and Y. Yanagisawa "Low-Lying intruder state of the unbound nucleus 13Be" June, 2010

5 S. Ebata, T. Nakatsukasa, T. Inakura, K. Yoshida, Y. Hashimoto, and K. Yabana "Canonical-basis time-dependent Hartree-Fock-Bogoliubov theory and linear-response calculations" July, 2010

6 K. Yoshida, and T. Nakatsukasa "Dipole responses in Nd and Sm isotopes with shape transitions" August, 2010

7 Kenichi Yoshida "Roles of deformation and neutron excess on the giant monopole resonance in neutron-rich Zr isotopes" August, 2010

8 N. Aoi, S. Kanno, S. Takeuchi, H. Suzuki, D. Bazin, M. D. Bowen, C. M. Campbell, J. M. Cook, D. -C. Dinca, A. Gade, T. Glasmacher, H. Iwasaki, T. Kubo, K. Kurita, T. Motobayashi, W. F. Mueller, T. Nakamura, H. Sakurai, M. Takashina, J. R. Terry, K. Yoneda, and H. Zwahlen "Enbannced collectivity in 74Ni" August, 2010

9 Shuichiro Ebata, Takashi Nakatsukasa, and Kazuhiro Obana "Linear response calculation using the canonical-basis TDHFB with aschematic pairing functional" September, 2010

10 N. Hinohara, K. Sato, T. Nakatsukasa, M. Matsuo, and K. Matsuyanagi "Microscopic description of large-amplitude shape-mixing dynamics with local QRPA inertial functions" September, 2010

11 Nobuo Hinohara and Yoshiko Kanada-En'yo "Triaxial quadrupole deformation dynamics in sd-shell nuclei around 26Mg" September, 2010

12 T. Nakatsukasa, P. Avogadro, S. Ebata, T. Inakura, and K. Yoshida "Self-consistent description of nuclear photoabsorption cross sections" January, 2011

13 K. Yoshida and N. Hinohara "Shape changes and large-amplitude collective dynamics in neutron-rich Cr isotopes" March, 2011

CNS-REP

1 S. Mitimasa "CNS Annual Report 2008" February, 2010

2 T. Uesaka, S. Sakaguchi, Y. Iseri, K. Amos, N. Aoi, Y. Hashimoto, E. Hiyama, M. Ichikawa, Y. Ichikawa, S. Ishikawa, K. Itoh, M. Itoh, H. Iwasaki, S. Karataglidis, T. Kawabata, T. Kawahara, H. Kuboki, Y. Maeda, R. Matsuo, T. Nakao, H. Okamura, H. Sakai, Y. Sasamoto, M. Sasano, Y. Satou, K. Sekiguchi, M. Shinohara, K. Suda, D. Suzuki, Y. Takahashi, M. Tanifuji, A. Tamii, T. Wakui, K. Yako, Y. Yamamoto, and M. Yamaguchi "Analyzing power for the proton elastic scattering from neutron-rich 6He nucleus" July, 2010

3 S. Watanabe, S. Kubono, Y. Ohshiro, H. Yamaguchi, M. Kase, M. Wada, and R. koyama, "Simple, High-Sensitive and Non-Destructive Beam Monitor for RI Beam Facilities" December, 2010

VIII. LIST OF SYMPOSIAS

(2010 April ～2011 March)

1 Workshop on P- and CP-odd Effects in Hot and Dense Matter
Apr. 26-30, RBRC

2 Workshop on Saturation, the Color Glass Condensate and Glasma:What Have we Learned from RHIC?
May 10-12, RBRC

3 Workshop "Study of plant sexual differentiation using heavy-ion irradiation."
May 13, Radiation Biology Team

4 Special Lectures to Commemorate the 120th Anniversary of Birth of Yoshio Nishina
May 23, RIKEN Nishina Center

5 A Space-Time Odyssey
May 26-28, RBRC

6 Workshop 6 High-Energy and Nuclear Physics in the Far Future
Jun. 8, RBRC

7 Strangeness in Nuclei
Jun. 12, Strangeness Nuclear Physics Laboratory

8 Second EMMI-EFES workshop on neutron-rich exotic nuclei EENEN 10 Neutron-rich nuclear matter, nuclear structure and nuclear astrophysics
Jun. 16-18, JUSTIPEN (Theoretical Nuclear Physics Laboratory)

9 The Physics of W and Z Bosons
Jun. 24-25, RBRC

10 OMEG Institute on SNe and the r-process, RIKEN
Jul. 15, CNS

11 Japan-Italy EFES workshop on “Correlations in reactions and continuum”
Sept.6-8, INFN, EFES

12 LHC-Theory Initiative Workshop
Oct. 7-8, RBRC

13 OMEG Institute on the C12(a,g) reaction rate, RIKEN
Nov. 1, CNS

14 Cutting-Edge Physics of Unstable Nuclei
Nov. 10-13, University of Aizu-JUSTIPEN-EFES Symposium

15 Beam Physics Meeting 2010
Nov. 11-12, Accelerator Group

16 International Symposium “New Faces of Atomic Nuclei An EFES/OIST contribution”
Nov. 15-17, OIST, Onna, Japan, Oslo Univ., EFES, OIST, RIKEN

17 International Symposium "From Quarks to Supernovae"
Nov. 28-30, University of Tsukuba, Universeity of Tokyo, RIKEN(Strangeness Nuclear Physics Laboratory)

18 The Symposium of 25th Anniversary of the Discovery of Halo Nuclei (Halo2010)
Dec. 6-9, RNC and CNS

19 Workshop on Impact of new aaa reaction rate on stellar evolution and nucleosynthesis RIKEN
Dec. 17-18, CNS

20 Towards New Developments in Field and String Theories, 2010
Dec. 17-19, Theoretical Physics Laboratory

21 French-Japanese Symposium on Nuclear Structure Problems-organized in the framework of FJNSP LIA and EFES
Jan. 5-8, JUSTIPEN

22 Initial State Fluctuations and Final-State Particle Correlations
Feb. 2-4, RBRC

23 International EFES-IN2P3 Conference “Many-body correlations from dilute to dense nuclear systems”
Feb. 15-18, IN2P3, EFES, RIKEN

24 "New Hadrons" Workshop 2010
Feb. 28-Mar. 1, Radiation Laboratory

25 The 2nd Workshop on KEK Isotope Separator System (KISS)
Mar. 5, KEK, SLOWRI Team

26 eRHIC, ePHENIX, eSTAR, EIC TF, eRHIC-CAD: Meeting
Mar. 10-11, RBRC

27 Workahop on "Future Vision of the Nucleon Structure Study
Mar. 14, Radiation Laboratory

28 The 5th LACM-EFES-JUSTIPEN Workshop
Mar. 15-17, Oakridge National Lab., USA, EFES, JUSTIPEN, Oak Ridge National Labl.

IX. LIST OF SEMINARS

(2010 April ～2011 March)

Theoretical Research Division

1 Akitsugu Miwa (RNC) Apr. 12 "A non-relativistic limit of 2 dimensional conformal field theory"

2 Shinya Aoki (University of Tsukuba) Apr. 20 "Application of the operator product expansion to the short distance behavior of nuclear potentials"

3 Tetsuo Hatsuda (University of Tokyo) Apr. 24 "Towards New Developments in Field and String Theories, 2010"

4 Makoto Sakaguchi (RNC) Apr. 26 "Semiclassical analysis of M2-brane in AdS_4 x S^7/Z_k"

5 Shigehiro Yasui (High Energy Accelerator Research Organization) May 10 "Fermion structure in non-Abelian vortices in high density QCD"

6 Ryoichi Seki (California State University) May 13 "J/y-nucleon interaction and J/y- nuclei"

7 Keiji Igi (RNC) May 17 "Universal rise of hadronic total cross sections based on forward pi p, K p and p bar p, p p scatterings"

8 Fumihiko Sugino (Okayama Institute for Quantum Physics) May 19 "Two-dimensional lattice for four-dimensional N=4 supersymmetric Yang-Mills"

9 Seth Waldecker (Washington Univ.) May 19 "Extensions of the Dispersive Optical Model"

10 Mihai Horoi (Central Michigan Univ.) May 20 "Novel Computational Aspects of the Shell Model Nuclear Level Densities and Reaction Rates"

11 Yuzuru Sato (Hokkaido University) May 24 "Computability, complexity and dynamical systems"

12 Eigo Shintani (RBRC) May 25 "Precision measurement of Standard Model via lattice QCD"

13 Yoichi Kazama (University of Tokyo) May 31 "An overture to quantum superstring in AdS5 x S5"

14 Tadashi Takayanagi (University of Tokyo) Jun. 14 "Mini Black Holes and Quantum Quench from AdS/CFT"

15 Takahiro Fukui (Ibaraki University) Jun. 25 "Stability of Majorana zero modes in superconductor-topological insulator systems"

16 Koichi Yazaki (RIKEN) Jun. 28 "Quantum effects in accelerated systems"

17 Nobuyuki Sawado (Tokyo University of Science) Jul. 5 "Soliton solutions in the extended Skyrme-Faddeev model"

18 Toru Takahashi (Gunma National College of Technology) Jul. 7 "Lattice QCD study of spin-1/2 Lambda baryons"

19 Masato Taki (Yukawa Institute for Theoretical Physics) Jul. 8 "AGT relation, conformal symmetry, and topological string duality"

20 Hiroki Kawai (University of Tokyo) Jul. 12 "A lattice study of N=2 Landau-Ginzburg model using a Nicolai map"

21 T. Yamazaki (University of Tsukuba) Jul. 12 "Calculation of Helium nuclei in quenched lattice QCD"

22 Tamiaki Yoneya (Open University of Japan) Oct. 4 "M(atrix) Theory and the Gauge/Gravity Correspondence"

23 Muneto Nitta (Keio University) Oct. 4 "Topological Solitons and D-branes in Bose-Einstein Condensates"

24 Washington Taylor (Massachusetts Institute of Technology) Oct. 8 "Supergravity and string vacua in 6 dimensions"

25 Elias Kiritsis (Crete University) Oct. 8 "AdS/QCD from Tachyon Condensation"

26 Shuichiro Ebata (RNC) Oct. 19 "Canonical-basis Time-Dependent Hartree-Fock-Bogoliubov Theory and Systematic Calculation of Linear Response"

27 Kenji Fukushima (Keio univ.) Oct. 29 "QCD Phase Transitions and Chiral Magnetic Effect"

28 Frieder Lenz (Univ. of Erlangen-Nuernberg) Nov. 1 "The peculiar kinematics of quantum fields in Rindler space and their dynamical implications"

29 Carlos Bertulani (Texas A&M Univ.) Nov. 8 "The nucleus-nucleus interaction between boosted nuclei"

30 Toshihiro Matsuo (Okayama Institute for Quantum Physics) Nov. 11 "Gravitational string-membrane hedgehog and internalstructure of black holes"

31 Nodoka Yamanaka (Osaka University) Nov. 15 "One-loop level analysis of R-parity violating supersymmetric contribution to the neutron beta decay and atomic EDM"

32 Ken-Ichi Ishikawa (Hiroshima University) Nov. 22 "A review on algorithms and techniques for lattice QCD simulations"

33 Kenji Fukushima (Keio University) Nov. 29 "QCD Phase Transitions and Chiral Magnetic Effect"

34 Pawel Danielewicz (Michigan State University) Dec. 1 "Towards Quantum Transport for Central Nuclear Reactions"

35 Ken Suzuki (Stefan Meyer Institute for Subatomic Physics) Dec. 14 "Kaonic nuclear search in the pp $\rightarrow$ pΛ K+ reaction"

36 Fumihiko Sugino (Okayama Institute for Quantum Physics) Dec. 21 "Spontaneous supersymmetry breaking in matrix models from the viewpoints of localization and Nicolai"

37 Issaku Kanamori (Institut fur Theoretische Physik Universitaet Regensburg) Jan. 7 "Getting rid of fermions on link:SU(N)SYM on 2-dimensional lattice"

38 Wojciech Satula (University of Warsaw) Jan. 14 "Isospin mixing and isospin-symmetry-breaking corrections to the superallowed beta decay"

39 Yutaka Ookouchi (IPMU) Jan. 17 "Cosmological aspects of direct gauge mediation"

40 Sanefumi Moriyama (Nagoya University) Jan.25 "An Algebraic Model for the su(2|2) Light-Cone String Field Theory"

41 Norihiro Iizuka (CERN) Jan. 28 "Holographic description of quantum Hall effect"

42 Hiroaki Abuki (Tokyo univ. os Sci.) Jan. 31 "Nambu-Goldstone boson in color superconducting 2SC state under charge neutrality constraint"

43 Ting-Wai Chiu (National Taiwan University) Feb. 1 "Simulation of unquenched QCD with the optimal domain-wall fermion"

44 Naoto Yokoi (Tohoku University) Feb. 10 "Operator formulation of Green-Schwarz superstring in the semi-light-cone conformal gauge"

45 Koichi Murakami (Okayama Institute for Quantum Physics) Feb. 21 "Light-cone gauge superstring field theory and dimensional regularization"

46 TAKASHINA Masaaki (Osaka University) Feb. 23 "Researches in medical physics using particle transport simulation"

47 Hirotaka Hayashi (University of Tokyo) Feb. 28 "Phenomenological Aspects of Global F-theory Compactifications"

48 Walter Vinci (University of Minnesota, School of Physics and Astronomy) Mar. 3 "Non-Abelian Monopoles in the Higgs Phase"

49 Kazunori Itakura (KEK) Mar. 7 "High-Energy Heavy-Ion Collisions: from CGC to Glasma"

50 Hidenori Sonoda (Kobe University) Mar. 11 "Phase structure of a 3 dimensional Yukawa model"

Sub Nuclear System Research Division

1 Peter Petreczky (BNL) Apr. 1 "Chiral and confinement transition in finite temperature QCD"

2 Andrei Belitsky (Arizona State University) Apr. 2 "Joint HET/ATLAS Lunch Seminar"

3 Lisa Goodenough (New York University) Apr. 7 "HET/RIKEN Seminar"

4 Giorgio Torrieri (JW Goethe Universitaet) Apr. 9 "Nuclear Theory/RIKEN Seminar"

5 Daniel Feldman (University of Michigan) Apr. 14 "SUSY and Hidden Sector Extensions with Dark Matter and LHC Signatures"

6 Jack Laiho (Univ. of Glasgow) Apr. 15 "The neutral kaon mixing parameter from lattice QCD"

7 Koji Yokoyama (RNC) Apr. 16 "Muon Probes of Spin-polarized Electrons in GaAs"

8 Burak Alver (MIT) Apr. 16 "Collision geometry fluctuations and triangular flow in heavy-ion collisions"

9 David Lin (NCTS & National Chiao-Tung University) Apr. 21 "Walking Step by Step on the Lattice"

10 Massimo D'Elia (Genoa University) Apr. 22 "QCD Phase Structure and Imaginary Endpoints"

11 Subhir Sachdev (Harvard University) Apr. 28 "Quantum criticality and the cuprate superconductors"

12 Bumhoon Lee (Sogang University) Apr. 30 "Holographic approach for the effects of nuclear density and gluon condensation"

13 Christoph Lehner (RBRC) May 6 "Low-energy constants from Dirac eigenvalue correlators at NNLO in the epsilon expansion"

14 Oliver Witzel (BNL) May 14 "Viscosity of Strongly Interacting Fermi Gases"

15 Henri Kowalski (DESY) May 20 "Using HERA Data to Determine the Infrared Behaviour of the BFKL Amplitude"

16 Ryoichi Seki (California State University) May 26 "Physics and experimental feasibility of J/ψ- nuclei"

17 Shoji Hashimoto (KEK) Jun. 2 "Spontaneous chiral symmetry breaking on the lattice"

18 Juhee Hong (SUNY Stony Brook) Jun. 4 "Spectral Densities for Hot QCD Plasmas in a Leading-Log Approximation"

19 Yasushi Kino (Tohoku University) Jun. 7 "Stau atomic collisions and big-bang nucleosynthesis"

20 Edward Shuryak (SBU) Jun. 30 "W-Z-top bags and baryogenesis"

21 Bronislav Zakharov (Landau Institute) Jul. 2 "Induced gluon radiation in QCD matter and jet quenching"

22 Joyce Meyers (Swansea University) Jul. 9 "QCD with chemical potential in a small hyperspherical box"

23 Takashi Nagatomo (ICU) Jul. 12 "β detected NMR method (β-NMR) and its application ~Measurement of the nuclear Q moment and test of the G-parity symmetry in weak decay~"

24 Jingyi Chao (NCSU) Jul. 23 "Thermal Conductivity Of Quark Matter In The CFL Phase"

25 Eigo Shintani (RBRC) Jul. 29 "pi0 to two photon decay on the lattice"

26 Zuowei Liu (YITP, SBU) Jul. 30 "Multicomponent Dark Matter"

27 Giorgio Torrieri (Columbia University) Jul. 30 "The nuclear liquid-gas phase transition at large N_c in the Van der Waals approximation"

28 Taichi Kawanai (Univ. of Tokyo) Aug. 5 "Charmonium-nucleon interaction from lattice QCD"

29 Rajamani Narayanan (Florida International University) Aug. 6 "Strong to weak coupling transition in large Nc QCD"

30 Meifeng Lin (Yale University) Aug. 19 "Nucleon physics on the lattice"

31 David Lin (NCTS) Aug. 20 "Taiwan-Zeuthen project on lattice simulations for large Yukawa-coupling systems."

32 Bjoern Schenke (McGill University) Aug. 27 "Monte-Carlo simulation of heavy-ion collisions"

33 Jan Steinheimer-Froschauer (Goethe University Frankfurt) Sep. 3 "An effective chiral Equation of State including hadronic and quark degrees of freedom"

34 Esmaili Jafar (Isfahan University of Technology) Sep. 3 "Resonant formation of ¥ Lambda (1405) by stopped-K- absorption in deuteron"

35 Shoichi Sasaki (Univ. of Tokyo) Sep. 9 "Lattice study of flavor SU(3) breaking in hyperon beta decays"

36 Tracy Slatyer (IAS) Sep. 15 "Constraining Dark Matter Annihilation with the Cosmic Microwave Background"

37 Kai Wang (IPMU, The University of Tokyo) Sep. 22 "BSM theory review of solutions to the Top quark forward-backward asymmetry anomaly at Tevatron"

38 Alex Kovner (University of Connecticut) Sep. 22 "Better understanding the relation between the JIMWLK Hamiltonian and the BFKL limit"

39 Kevin Dusling (BNL) Sep. 28 "Observation of a ridge in proton--proton collisions at the LHC"

40 Fabio Dominguez (Columbia University) Oct. 1 "k_t-factorization for hard processes in nuclei"

41 Alexander Friedland (Los Alamos National Laboratory) Oct. 6 "Oscillations of supernova neutrinos (and what they are good for)"

42 Brock Tweedie (Boston University) Oct. 14 "Improving and Expanding Searches for TeV-Scale Z' Bosons Decaying to WW and Zh"

43 Hans Pirner (Univ. of Heidelberg) Oct. 15 "The dilemma with AdS/QCD"- String Theory meets Quantum Chromo Dynamics"

44 Walter Goldberger (Yale) Oct. 20 "Sum rules and the OPE for non-relativistic conformal theories"

45 Daniel Fernandez-Fraile (BNL) Oct. 21 "Bulk viscosity of QCD mater"

46 Can Kılıç (Rutgers) Nov. 3 "The dark matter–LHC connection: a few model-independent statements"

47 Jinfeng Liao (BNL) Nov. 4 "The geometry of Jet Quenching"

48 Ron Longacre (Brookhaven National Lanoratory) Nov. 5 "pi deuteron effective mass correlation as a probe hadron gas density"

49 Erich Poppitz (University of Toronto) Nov. 10 "Monopoles, bions, and other oddballs in confinement or conformality"

50 Florian Goertz (Mainz) Nov. 12 "Higgs Physics and Precision Tests in Warped Extra Dimensions"

51 Kimiko Sekiguchi (Tohoku Univ.) Nov. 15 "Three Nucleon Force and Few Nucleon Scattering"

52 David Shih (Princeton) Nov. 17 "Prospects for Early Discovery of General Gauge Mediation at the LHC"

53 Abhijit Majumdar (Ohio State Univ.) Nov. 18 "Jet quenching in DIS and heavy-ion collisions"

54 Shaouly Bar-Shalom (Technion) Nov. 19 "A 4th generation paradigm: from LEPI to LHC"

55 A. deGouvea (Northwestern) Dec. 1 "Looking for The Origin of Neutrinos Masses: from neV to YeV"

56 Ho-Ung Yee (Stony Brook) Dec. 2 "Waves of anomaly in QGP"

57 Hung-Ming Tsai (Duke Univ.) Dec. 3 "Thermal Quark and Gluon Distributions in the PNJL model"

58 Yang Bai (SLAC) Dec. 8 "Heavy octets and Tevatron signals with 3b or 4b"

59 Lusy Safriani (Universitas Padjadjaran) Dec. 14 "Fabrication and emission property of functional inverse opal TiO2 waveguide"

60 Daekyoung Kang (Ohio State University) Jan. 11 "Universal relation for strong interacting atoms"

61 Patrick Meade (Stony Brook) Jan. 14 "SUSY as a model independent search tool for experimentalists"

62 David Adams (BNL) Jan. 14 "Discussion on model independent limits and cross section measurements in limited phase space"

63 Heng-Tong Ding (BNL) Jan. 20 "Estimating thermal dilepton rate and electrical conductivity in quenched QCD"

64 Bjoern Schenke (BNL) Jan. 27 "Anisotropic flow in event-by-event viscous hydrodynamics"

65 Atsushi Oshiyama (University of Tokyo) Feb. 2 "Current Status of First-Principle Calculations that may Clarify Physics of Imperfection in Materials"

66 Robert Mawhinney (Columbia University) Feb. 9 "Exploring 8 and 12 Flavor QCD"

67 Jacobus Verbaarschot (Stony Brook University) Feb. 10 "Spectrum of the Wilson Dirac Operator"

68 Kaustubh Agashe (Maryland) Feb. 16 "Exotic Dark Matter at Colliders from Proton Stability"

69 Eugene Levin (Tel Aviv University) Feb. 17 "Long range rapidity correlations in azimuthal angle for pp and AA"

70 Tianjun Li (Chinese Academy of Science) Feb. 23 "No-Scale F-SU(5)"

71 Huey-Wen Lin (University of Washington) Feb. 24 "Beyond the Standard Model with Nucleons"

72 Shamayita Ray (Cornell) Feb. 25 "2540 km: Bimagic Baseline for Neutrino Oscillation Parameters"

73 Monika Blanke (Cornell) Mar. 2 "A new perspective on CP violation in three-body decays"

74 Li Yan (Stony Brook University) Mar. 3 "The anisotropy flows in viscous hydrodynamics"

75 Herman Verlinde (Princeton) Mar. 9 "String Theory and the Real World"

76 Tomer Volansky (UC Berkeley) Mar. 16 "Asymmetric Dark Matter from Leptogenesis"

77 Ikuto Kawasaki (Japan Atomic Energy Agency) Mar. 29 "(1)Band structure and Fermi surface of heavy fermion compound URu2Si2 (2)Magnetic clustering and non-Fermi-liquid behavior accompanying"

RIBF Research Division

1 Marek Lewitowicz, Marcel Jacquemet (GANIL) Apr. 2 "SPIRAL2 - towards the high intensity frontier both for stable heavy ions and Radioactive Ion Beams"

2 Immanuel Gfall HEPHY (Institute of High Energy Physics of Vienna) Apr. 5 "Mechanics and cooling of Belles SuperSVD silicon vertex trackers"

3 Hiroyuki Murakami (RNC) Apr. 12 "1st Lectures of analog electronics for radiation measurement 2010"

4 K. Yoshida (RNC) Apr. 13 "Skyrme density-functional approach to excitation modes in deformed neutron-rich nuclei"

5 Y. Ikeda (RNC) Apr. 13 "Strange dibaryoon resonance in Kbar N N -- pi Y N coupled-channel system"

6 S. Takeuchi (RNC) Apr. 13 "Low-lying states in 32Mg studied by proton inelastic scattering"

7 Hiroyuki Murakami (RNC) Apr. 26 "2nd Lectures of analog electronics for radiation measurement 2010"

8 Meiko Kurokawa (RNC) Apr. 26 "Development of the wide dynamic range charge sensitive preamplifier and ASCI."

9 Hiroyuki Murakami (RNC) May 10 "3rd Lectures of analog electronics for radiation measurement 2010"

10 Carsten P. Welsch (Univ. of Liverpool) May 20 "Development of Beam Instrumentation for Particle Accelerators within DITANET and the QUASAR Group"

11 Mihai Horoi (Central Michigan Univ.) May 20 "Novel Computational Aspects of the Shell Model Nuclear Level Densities and Reaction Rates"

12 Hiroyuki Murakami (RNC) May 24 "4th Lectures of analog electronics for radiation measurement 2010"

13 Dario Vretenar (Univ. of Zagreb, Croatia) May 25 "Nuclear Energy Density Functionals"

14 Newcomers (RNC) Jun. 1 "Newcomer Seminar"

15 Valery Zagrebaev (JINR, Russia) Jun. 4 "New ideas and prospects for production of heavy and superheavy neutron rich nuclei"

16 Hiroyuki Murakami (RNC) Jun. 9 "5th Lectures of analog electronics for radiation measurement 2010"

17 Wolfram Weise (PTechnical Univ. of Munich) Jun. 10 "CHIRAL SYMMETRY IN STRONGLY INTERACTING MATTER"

18 Hiroyuki Murakami (RNC) Jun. 21 "6th Lectures of analog electronics for radiation measurement 2010"

19 Ikuko Hamamoto (Lund University) Jun. 22 - 23 "One-particle motion in nuclear many-body problem"

20 T. Otsuka (U. Tokyo) Jun. 29 "Unstable Nuclei and the Nuclear Force"

21 Hiroyuki Murakami (RNC) Jul. 5 "7th Lectures of analog electronics for radiation measurement 2010"

22 Koji Hashimoto (RNC) Jul. 13 "Superstrings and Nuclear forces"

23 A. Ohnishi (YITP, Kyoto U) Jul. 20 "Nuclear matter equation of state and hyperons"

24 Tetsuo Sawada (Tokyo Institute of Technology) Jul. 26 "Plutonium as seen from science"

25 Makoto Minowa (University of Tokyo) Jul. 26 "Anti-neutrino detection to monitor reactor operations"

26 Hiroyuki Murakami (RNC) Jul. 26 "8th Lectures of analog electronics for radiation measurement 2010"

27 Hiroyoshi Sakurai (RNC) Jul. 26 "New generation of physics with exotic nuclei at RIBF"

28 Hiroyuki Murakami (RNC) Aug. 30 "9th Lectures of analog electronics for radiation measurement 2010"

29 Augusto O. Macchiavelli (LBNL) Sep. 16 "Some Aspects of the Structure of Exotic Nuclei"

30 Federic Chautard (GANIL) Sep. 17 "GANIL Operation status and developments"

31 Hiroyuki Murakami (RNC) Sep. 22 "10th Lectures of analog electronics for radiation measurement 2010"

32 Yuri Batygin (LANL) Sep. 22 "Status and Future Plans of LANSCE Accelerator Facility"

33 Vaishali Naik (VECC, India) Sep. 27 "VECC/TRIUMF Injector for the e-Linac Project"

34 Yuri A. Litvinov (Max Planck Institute for Nuclear Physics) Sep. 27 "At the borderline between atomic and nuclear physics: two-body nuclear decay of highly-charged ions"

35 Hiroyuki Murakami (RNC) Sep. 29 "11th Lectures of analog electronics for radiation measurement 2010"

36 K. Kaki (Shizuoka U) Oct. 12 "Relativistic Impulse Approximation Analysis of Unstable Calcium & Nickel Isotopes: 60-74Ca & 48-82Ni"

37 Hiroyuki Murakami (RNC) Oct. 13 "12th Lectures of analog electronics for radiation measurement 2010"

38 A. Ukawa (Tsukuba University) Oct. 19 "Lattice QCD at the Turning Point"

39 Xie Yi (Institute of Modern Physics, Chinese Academy of Sciences) Oct. 22 "My research life in China"

40 Hiroyuki Murakami (RNC) Oct. 27 "13th Lectures of analog electronics for radiation measurement 2010"

41 Jens Volker Kratz (U. Mainz) Oct. 28 "Recent of future research in superheavy elements at Mainz/GSI"

42 Juan Esposito (INFN-LNL) Nov. 8 "The accelerator-driven TRASCO-BNCT project at INFN Legnaro labs"

43 Fritz Nolden (GSI) Nov. 10 "The FAIR Accelerator and Storage Ring Facility"

44 Hiroyuki Murakami (RNC) Nov. 17 "14th Lectures of analog electronics for radiation measurement 2010"

45 Igal Talmi (Weizmann Institute of Science) Nov. 24 "On single nucleon wave functionsfiles"

46 Hiroyuki Murakami (RNC) Dec. 1 "15th Lectures of analog electronics for radiation measurement 2010"

47 Pawel Danielewicz (Michigan State University) Dec. 1 "Towards Quantum Transport for Central Nuclear Reactions"

48 Peter Muller (Argonne National Laboratory) Dec. 6 "Atom trap experiments with RIBs: from fundamental studies to applications"

49 Jean-Marc Richard (University of Lyon) Dec. 13 "Hadronic interactions, and the stability of multiquarks"

50 K. Kondo (JAEA) Dec. 21 "High intensity laser and charged particle acceleration"

51 Yasuyuki Suzuki (NiigataUniversity) Dec. 22 "Introduction to the Glauber approximation and its application"

52 T. Nakatsukasa (RNC) Dec. 27 ""Time-saving" theory for quantum simulation of superfluid nuclei"

53 T. Abe (RNC) Jan. 18 "Biological effects of fast heavy ions on DNA damage amd mutation induction"

54 Y. Akiba (RNC) Jan. 24 "Direct photons from Au+Au collisions and initial temperature of the Quark Gluon Plasma at RHIC"

55 T. Myo (Osaka Inst. Tech.) Jan. 25 "Tensor correlation in light nuclei studied with the tensor optimized shell model"

56 S. Nishimura (RNC) Feb. 8 "β-Decay Half-lives of Very Neutron-rich Kr to Tc Isotopes on the Boundary of the r-process Path : An Indication of Fast r-Matter Flow"

57 M. Takechi (RNC) Feb. 15 "Measurements of Interaction cross sections at RIBF"

58 Toshio Sano (Hosei University) Mar. 3 "Utility of tobacco BY-2 cells"

59 Akiko Hokura (Tokyo Denki University) Mar. 3 "Study on accumulation mechanism of Cd in cultured tobacco BY-2 cells by micro-XRF imaging utilizing high-energy synchrotron radiation"

60 K. Oyama (University of Heidelberg) Mar. 4 "ALICE, the high energy heavy ion experiment at LHC"

61 Takayuki Yamaguchi (Saitama Univ.) Mar. 8 "Reaction cross sections of neutron-rich carbon isotopes and related topics"

CNS

1 D. N.~Bihm (CNS, University of Tokyo) Mar. 30 "The measurement of 21Na+alpha in inverse kinematics and the 21Na(alpha,p) stellar reaction rate"

2 A.~Stolz (NSCL, MSU) Apr. 22 "Development of diamond detectors for heavy ion beam tracking"

3 Augusto O. Macchiavelli (Lawrence Berkeley National Laboratory) Sep. 16 "Some Aspects of the Structure of Exotic Nuclei"

4 S. Wanajo (TUM/MPA) Oct. 29 "Uncertainties in the nu p-process: supernova dynamics vs. nuclear physics"

AUTHOR INDEX

RIKEN Accelerator Progress Report *vol.* **44**

独立行政法人理化学研究所加速器年次報告　第44巻 (2011)

印　刷　平成23年（2011）9月30日
発　行　平成23年（2011）9月30日

発行者　独立行政法人理化学研究所　仁科加速器研究センター
代表者　延　與　秀　人
〒351-0198　埼玉県和光市広沢2番1号
電話（048）462-1111

編集者　独立行政法人理化学研究所　仁科加速器研究センター
加速器年次報告編集委員会

印刷所　株式会社　プライムステーション
〒160-0005　東京都新宿区愛住町19-16　富士ビル4F